

# Sunday Afternoon, November 5, 2023

## AVS Quantum Science Workshop

Room B110-112 - Session AQS-SuA

### AVS Quantum Science Workshop: Materials & Surface Science of Quantum Sensing

**Moderators:** Philippe Bouyer, University of Amsterdam – Technical University Eindhoven, Charles R. Eddy, Jr., Office of Naval Research Global - London

2:00pm **AQS-SuA-1 Single Ion Implantation for Quantum Devices and Materials using Focused Ion Beam Irradiation**, Edward Bielejec, Sandia National Laboratories **INVITED**

We will present an overview of Sandia's Ion Beam Laboratory (IBL) and its ongoing efforts to develop single ion implantation capability using a range of accelerators and detection techniques. The IBL operates seven focused ion beam (FIB) systems that range in ion energy from less than 1 keV to greater than 70 MeV, including a wide range of ion species from protons (H) to lead (Pb) over a range of spot sizes from nm to mm. This presentation will cover three topics:

(1) Novel liquid metal alloy ion source development (LMAIS) where we will concentrate on the development of LMAIS for our two mass filtered FIB systems, the A&D nanoplantier (A&D FIB100NI) and the Raith Velion, both of which include high spatial resolution with CAD based patterning to enable the formation of arbitrary patterned implantation in a wide range of substrates.

(2) In-situ counting and in-situ photoluminescence (PL) to enable single defect center creation in wide bandgap materials such as diamond and silicon carbide. Using counting we demonstrate a seven-fold improvement on the expected ion implantation error over timed implantation. Using PL we enable real-time error correction on the formation of low yield optically active defect centers. The combination of counting and PL is a promising pathway towards deterministic formation of these defect centers.

(3) The development of ultra-low energy ( $\ll 1$  keV) focused ion implantation capability based on a biased sample holder configuration. This enables ultra-low energy implantation while maintaining an expected implantation resolution of between 100-300 nm.

Sandia National Laboratories is a multimission laboratory managed and operated by National Technology & Engineering Solutions of Sandia, LLC, a wholly owned subsidiary of Honeywell International Inc., for the U.S. Department of Energy's National Nuclear Security Administration under contract DE-NA0003525.

2:40pm **AQS-SuA-3 On the Relevance of Avalanche Phenomenon in Wide Bandgap Technology**, Srabanti Chowdhury, Stanford University **INVITED**

Wide bandgap (WBG) materials like Silicon Carbide (SiC) and Gallium Nitride (GaN) have shown remarkable adaptability in fields ranging from optics to power electronics and radio technology. Their flexibility has led to a wide range of applications and a growing presence in the market. What makes them stand out is their exceptional ability to perform well in tough, high-temperature conditions. The progress in WBG materials has also sparked interest in a newer category of semiconductors known as ultrawide-bandgap (UWBG) materials, which have even wider bandgaps. Both WBG and UWBG materials are resilient to electric field issues due to their generous bandgap dimensions, offering advantages like improved efficiency, the ability to operate in high-temperature environments, smaller device sizes, simpler system designs, and energy savings. These technologies have the potential for broader positive impacts, including reducing carbon emissions. In terms of specific applications, GaN is currently a standout in lighting technology and has made significant contributions to radar and telecommunications. GaN has also found its way into power electronics. On the other hand, SiC excels in medium to high-power electronics and serves as an excellent foundation for GaN RF technology. As a result, SiC and GaN both complement and compete in different areas, shaping the landscape of applications and markets.

In our research focus on electronic device technology, we place particular emphasis on enhancing the efficiency of GaN through the phenomenon of avalanche multiplication. Avalanche, a fundamental occurrence in semiconductors, initiated by the impact ionization phenomenon, holds pivotal significance in various electronic devices, especially those designed for high-power and high-frequency applications. Our recent investigations have unveiled that beyond its traditional applications, avalanche can serve as a valuable tool for assessing material quality and refining device design. While achieving avalanche in GaN has become more common, attaining

uniform avalanche behavior remains challenging. The relevance and intriguing observations associated with uniform avalanche will be discussed in our presentation. Concurrently, we are studying emerging technologies like AlGaIn/AlN, Diamond, and  $\beta$ -Ga<sub>2</sub>O<sub>3</sub>, which have not yet demonstrated avalanche characteristics. The absence of avalanche phenomena prompts us to investigate the challenges faced by these materials. Our thorough examination covers different aspects of these materials, such as their properties, growth, and essential doping techniques. These factors are crucial in enabling avalanche capabilities in UWBG materials.

3:40pm **AQS-SuA-6 Interfacing Biomolecules with Coherent Quantum Sensors**, Peter Maurer, University of Chicago **INVITED**

Quantum metrology enables some of the world's most sensitive measurements. When applied to biophysical systems, diamond-based quantum sensors have the potential to probe processes that cannot be accessed by conventional technologies. Examples of such processes range from cancer research to neuroscience to developmental biology. However, interfacing coherent qubit sensors with fragile biological target systems has remained an outstanding challenge that has severely limited applications. In this talk, I will discuss a novel approach that combines single-molecule biophysics technology with quantum engineering to interface intact biomolecules on a diamond quantum sensor without impacting qubit coherence and bio-functionality. In a second part, I will discuss our recent work on engineering highly coherent quantum sensors based on diamond nanocrystal. Such nanosensors can readily be taken up by cells and integrated into intact organisms. However, coherence in these nanocrystal sensors is limited by surface noise, which severely reduces the sensor's sensitivity. In our work we developed a new approach to engineer spin coherence in core-shell nanostructures which leads to a 50-fold improvement in qubit sensitivity. Finally, potential future applications of quantum sensing to biophysics and diagnostics will be discussed.

4:20pm **AQS-SuA-8 Scale-Invariant Lasers Beyond the Schawlow-Townes Two-Mirror Strategy**, Boubacar Kanté, University of California at Berkeley **INVITED**

Lasers play a fundamental role in science and technology from quantum computing, to communications, sensing, and imaging. The scaling of lasers and in-particular of surface emitting lasers is a multi-decade long question that has been investigated since the invention of lasers in 1958. In the first part of the talk, I will argue that a surface emitting laser that remains single mode irrespective of its size, a scale-invariant laser, should of necessity also waste light at the edge. This is a fundamental departure from the Schawlow-Townes two-mirror strategy that preserves gain and minimizes loss by keeping light away from mirrors. The strategy was implemented in our recent discovery of the Berkeley Surface Emitting Laser (BerkSEL) [1]. In the second part of this talk, I will discuss our invention of functional topological lasers: integrable non-reciprocal coherent light sources as well as compact bound state in continuum sources [2-3].

#### References.

- 1- R. Contractor, W. Noh, W. Redjem, W. Qarony, E. Martin, S. Dhuey, A. Schwartzberg, and B. Kanté, "Scalable single-mode surface emitting laser via open-Dirac singularities," *Nature* 608, 692–698 (2022).
- 2- B. Bahari, A. Ndao, F. Vallini, A. El Amili, Y. Fainman, B. Kanté, "Nonreciprocal lasing in topological cavities of arbitrary geometries," *Science* 358, 636-640 (2017).
- 3- A. Kodigala, T. Lepetit, Q. Gu, B. Bahari, Y. Fainman, and B. Kanté, "Lasing Action from Photonic Bound States in Continuum," *Nature* 541, 196 – 199 (2017).

5:00pm **AQS-SuA-10 Panel Discussion**,

# Sunday Afternoon, November 5, 2023

## Biomaterials Plenary Session (ALL-INVITED)

Room B117-119 - Session BP-SuA

### Coupled Phenomena in Biomaterial Systems (ALL-INVITED SESSION)

Moderators: Kenan Fears, U.S. Naval Research Laboratory, Markus Valtiner, Vienna University of Technology, Austria

4:00pm **BP-SuA-7 BID Early Career Awardee Talk: Large-Scale Vascularized Polymers Enable Continuous Sensing of and Responding to Bacteria at Interfaces**, B. Dixon, A. Briley, K. Marquis, B. Chasse, **Caitlin Howell<sup>1</sup>**, University of Maine

INVITED

Large-scale, non-destructive detection and active response to cellular layers at interfaces is crucial for the scale-up of controlled biointerfaces. One way Nature accomplishes this passive detection and active response process is through the use of complex vascular systems that aid in transporting signals and responding accordingly. In this work, we embedded vascular networks in polymeric hydrogels using 3D printing to create a non-destructive detect-and-respond system for living bacteria at the material surface. Tests with *E. coli* as a model system showed that bacteria-specific signals could be detected through the vascular network. The cells could then be precisely targeted at the surface by introducing gentamicin into specific sections of the vascular channels. Theoretical models of the system were developed to permit the rational design of the detect-and-respond system suitable for other applications. This work lays the foundation for the fabrication and use of vascularized polymers as an adaptive system for the early detection of and response to bacteria or other cells at interfaces.

4:40pm **BP-SuA-9 Learning from Nature to Tackle Adhesion in Wet and Challenging Conditions**, **Ali Dhinojwala**, University of Akron

INVITED

A small magnitude of roughness and wetness can disrupt interfacial bonding and reduce adhesion. I will discuss how roughness affects both dry and wet adhesion, and the lack of our current theoretical framework to explain these results. Particularly in the case of underwater adhesion, the presence of trapped water can accentuate the challenges in creating molecular contact with rough surfaces. The drainage of confined water is a function of both roughness and surface chemistry. I will describe how nature has developed strategies to stick to rough and wet surfaces: fibrillar structures used by geckos and insects to create molecular contact and improve water drainage; the use of hygroscopic salts by spiders to reduce the water next to hydrophilic surfaces; or the use of catechol groups by mussels to bind to polar surfaces. I will discuss how these strategies have inspired new synthetic adhesives (with emphasis on sustainability) for improving adhesion to wet and rough surfaces with an impact on biomedical and engineering applications.

5:20pm **BP-SuA-11 Mechanoresponsive Proteins - from Molecular Mechanisms Towards Applications in Biology and Materials Science**, **Kerstin G. Blank**, Johannes Kepler University Linz, Austria

INVITED

Mechanoresponsive proteins undergo structural and functional changes when experiencing mechanical stimuli. These proteins play crucial roles in various cellular processes, including cell adhesion, tissue development, and mechanotransduction. Moreover, they are essential building blocks for biogenic materials where they determine the structure-mechanics relationships of these materials from the molecular to the macroscale. In our research, we aim to engineer mechanoresponsive proteins to understand their fundamental structure-mechanics relationships and to utilize them as molecular force sensors and programmable building blocks for smart bioinspired materials. Coiled coils are prototype mechanoresponsive protein building blocks that are highly abundant in mammalian tissues. Using single-molecule force spectroscopy, we have uncovered key factors that determine the stability of these structures against shear forces [1-5]. We have then employed this knowledge to establish a library of synthetic and mechanically calibrated coiled coils. These building blocks are currently being developed as molecular force sensors to measure cell-generated traction forces at the cell-material interface and as mechanoresponsive hydrogel crosslinks [2,6,7]. Another example are proteins from the arthropod cuticle that interact with chitin. We have started with chitin-binding domains as the basic molecular building block and determined their binding strength to chitin fibers. Single-molecule force spectroscopy shows bond lifetimes on the second to minute timescale, indicating that these proteins may act as sacrificial bonds that facilitate energy dissipation and cuticle self-healing. Our next goal is to explore the application of engineered chitin-binding domains in chito-

protein composite materials, where they can serve to crosslink chitin fibers or chitosan polymers. In conclusion, these examples demonstrate the potential of protein building blocks with tunable and calibrated mechanical properties. These building blocks allow for the bottom-up control of smart materials and interfaces that can sense and respond to external forces, with potential applications in biomedicine, robotics, and nanotechnology.

- [1] Goktas et al. (2018) Chem. Sci. 9:4610
- [2] Tunn et al. (2018) Nanoscale 10:22725
- [3] López-García et al. (2019) Phys. Chem. Chem. Phys. 21:9145
- [4] López-García et al. (2021) Angew. Chem. Int. Ed. 60:232
- [5] Tsigoni et al. (2023) Macromol. Biosci. 2200563
- [6] Tunn et al. (2019) Biomimetics 4: 25
- [7] Grad et al. (2020) Front. Chem 8:536

## Nanoscale Science and Technology Plenary Session (ALL-INVITED)

Room B113 - Session NSP-SuA

### Nanoscience and Technology Division Plenary Session (ALL-INVITED SESSION)

Moderators: Georg Fantner, EPFL, Adina Luican-Mayer, University of Ottawa, Canada

2:00pm **NSP-SuA-1 Bits to Atoms and Atoms to Bits: Atomic Fabrication in Electron Microscopy**, **Sergei Kalinin**, University of Tennessee Knoxville

INVITED

The last note left by Richard Feynman stated “*What I cannot create, I do not understand.*” Building solid state quantum computers, creating nanorobots, and designing new classes of biological molecules and catalysts alike requires the capability to manipulate and assemble matter atom by atom, probe the resulting structures, and connecting them to macroscopic world. Until now, the only viable approach for atomic fabrication was the Scanning Tunneling Microscopy, often integrated with the bespoke surface science techniques. Over the last decade, it has been shown that electron beams in Scanning Transmission Electron Microscopy can be used not only to probe structure and electronic properties of materials on atomic level, but also to modify materials on the atomic level. Harnessing electron beam changes for direct atomic fabrication however requires synergy between machine learning methods and microscope control. In this presentation, I will illustrate the progression of automated electron microscopy from real-time data analysis to physics discovery to atomic manipulations. Here, the applications of classical deep learning methods in streaming image analysis are strongly affected by the out of distribution drift effects, and the approaches to minimize though are discussed. The robust approach for real-time analysis of the scanning transmission electron microscopy (STEM) data streams, based on the ensemble learning and iterative training (ELIT) of deep convolutional neural networks, is implemented on an operational microscope, enabling the exploration of the dynamics of specific atomic configurations under electron beam irradiation via an automated experiment in STEM. Combined with beam control, this approach allows studying beam effects on selected atomic groups and chemical bonds in a fully automated mode. We demonstrate atomically precise engineering of single vacancy lines in transition metal dichalcogenides and the creation and identification of topological defects graphene. The ELIT-based approach opens the pathway toward the direct on-the-fly analysis of the STEM data and engendering real-time feedback schemes for probing electron beam chemistry, atomic manipulation, and atom by atom assembly. We further illustrate how deep kernel learning (DKL) methods allow to realize both the exploration of complex systems towards the discovery of structure-property relationship, and enable automated experiment targeting physics (rather than simple spatial feature) discovery. The latter is illustrated via experimental discovery of the edge plasmons in STEM/EELS. Jointly, these developments open the pathway for creation and characterization of designed defect configurations and artificial molecules in 2D materials.

3:00pm **NSP-SuA-4 NSTD Early Career Competition Finalist Talks: N. Hosseini, Y. Liu, S. Challa**,

3:40pm **NSP-SuA-6 NSTD Graduate Competition Finalist Talks: N. Asmari, L. Kuo**,

<sup>1</sup> BID Early Career Researchers Award  
Sunday Afternoon, November 5, 2023

# Sunday Afternoon, November 5, 2023

4:20pm **NSP-SuA-8 Co-Localizing Atomic Force Microscopy with Other Microscopies and Spectroscopies: Elucidating Material Composition, Structure, and Properties at the Nanoscale**, *B. Bailey, O. Maryon, J. Tenorio*, Boise State University; *D. Cintron Figuero*, Pennsylvania State University; *J. Benzing*, National Institute for Science and Technology (NIST); *F. DelRio*, Sandia National Laboratories; *J. Robinson*, Pennsylvania State University; *M. Hurley, S. Hues, E. Graugnard, Paul Davis*, Boise State University

A wide variety of scanning probe microscopy (SPM) modes based on atomic force microscopy (AFM) have been developed to probe the nanoscale electrical, electrochemical, magnetic, mechanical, and thermal properties of surfaces. As a result, AFM and associated SPM modes enjoy widespread use in the surface characterization of materials. However, AFM typically does not directly report on chemical composition or optical properties. This talk will show how this limitation can be overcome through sub-micron precision co-localization of AFM and associated advanced SPM modes with other analytical techniques such as scanning electron microscopy (SEM), Raman microscopy, and/or fluorescence-based super-resolution optical microscopy. In particular, co-localization of Kelvin probe force microscopy (KPFM) with SEM, energy dispersive spectroscopy (EDS), and electron backscatter diffraction (EBSD) has enabled correlation of surface Volta potentials with the composition and/or orientation of microstructural phases present in metal alloys. Additionally, the recently developed technique of photothermal AFM-IR, which simultaneously couples AFM and infrared spectroscopy to enable chemical identification at the nanoscale, has been applied to the study of few-layer atomic layer deposited and etched (ALD/ALE) transition metal dichalcogenides (TMDCs).

4:40pm **NSP-SuA-9 Electron Paramagnetic Resonance of Individual Rare-Earth Atoms**, *Gregory Czap, C. Lutz*, IBM Almaden Research Center; *H. Brune*, EPFL, Switzerland

Lanthanide series atoms are promising candidates for realizing single molecule magnets which remain magnetically stable at elevated temperatures. They are also being explored for their use as qubits both in the solid state and within molecules due to the long phase coherence time of the magnetic *f*-electrons and especially their nuclear spins. Recently, Electron Spin Resonance combined with the Scanning Tunneling Microscope (ESR-STM) has been developed into a powerful tool to address individual atomic spins on surfaces. However, driving and sensing spin resonance in lanthanide atoms with ESR-STM has remained a challenge due to *f*-electron shielding by the nonmagnetic valence electrons, which inhibits magnetoresistive sensing required for the technique. On the other hand, rare earths with an open valence shell have been shown to facilitate stronger interactions with tunneling electrons through intraatomic exchange coupling between the *f* electrons and valence shell. Here we demonstrate the detection of spin resonance in two different open-shell rare earth elements adsorbed on a thin insulating film using the STM. In one case, our measurements reveal an unexpectedly rich spectral structure which arises from the combination of a large electronic manifold of states and nuclear hyperfine interactions which can all be accessed at GHz energy scales. In the other case, a relatively large *g* factor presents opportunities for magnetic sensing at the atomic scale. Our results demonstrate the ability to drive and sense spin resonance of individual rare earth atoms with atomic resolution while providing a route to studying uncommon open valence shell lanthanide species.

## Atomic Scale Processing Mini-Symposium Room A107-109 - Session AP+PS+TF-MoM

### Thermal Atomic Layer Etching and Deposition

Moderator: Jean-Francois de Marneffe, IMEC, Belgium

8:20am **AP+PS+TF-MoM-1 Atomic Layer Etching of Aluminum and Aluminum Oxide for Optical Applications**, *John Hennessy, R. Rodriguez, A. Jewell*, Jet Propulsion Laboratory

**INVITED**

Thermal atomic layer etching can be utilized for the surface preparation of aluminum in order to improve its optical performance at ultraviolet wavelengths. In this work we report on the use of trimethylaluminum and anhydrous hydrogen fluoride to remove the native oxide of aluminum prior to encapsulation with fluoride dielectric materials. This ALE/ALD process is used for the fabrication of reflective coatings and bandpass filters operating at wavelengths shorter than 200 nm. The etch rate of aluminum oxide is observed to be dependent on chamber conditioning with a significant enhancement in etch rate observed when the cyclic etching is performed in the presence of alkali halide materials. This enhancement can reduce the temperature threshold where etching dominates the reaction cycle over deposition.

The reduction of the overall processing temperature can enhance the compatibility of the full coating process with some temperature-sensitive substrates, and limit the amount of etch damage experienced by aluminum surfaces. Etching into the aluminum surface is generally observed to result in non-conformal etching which greatly increases the surface roughness of films and degrades the optical performance of resulting structures. Reducing the etch temperature can mitigate this effect by increasing the selectivity of the native oxide removal over the underlying metal. Optimization of these processes may provide insight into achieving conformal ALE of aluminum surfaces. The extension of these atomic layer processing methods towards the fabrication of meter-class mirror coatings is also discussed in the context of future large UV space observatories for NASA astrophysics applications.

9:00am **AP+PS+TF-MoM-3 Thermal Etching of First Row Transition Metal Oxides using Acetylacetone and O<sub>3</sub>: Pathway for Atomic Layer Etching**, *Jonathan Partridge<sup>1</sup>, S. George*, University of Colorado at Boulder

Etching metal oxides with halogen-free methods is important during processing to avoid corrosion. Acetylacetone (Hacac) is an organic hydrocarbon. Hacac can supply acac ligands that can form volatile metal complexes with most transition metals. Consequently, Hacac can spontaneously etch metal oxides to form  $M(\text{acac})_x$  and  $\text{H}_2\text{O}$ . One difficulty is that Hacac can also decompose on the metal oxide surface and block the spontaneous etching. However, this surface poisoning also leads to a self-limiting reaction. The  $\text{O}_3$  exposure can then remove the carbonaceous decomposition species and produce a pathway for atomic layer etching.

Thermal etching of first row metal oxides was demonstrated using Hacac and  $\text{O}_3$  at pressures of 2.5 Torr at 250 °C. A quadrupole mass spectrometer (QMS) reactor with molecular beam expansion and line-of-sight to the ionizer was employed to detect etch species with high sensitivity. Metal oxide nanopowders were used to maximize the surface area and signal intensity of the etch products. The reactant sequence used five sequential Hacac exposures, one  $\text{O}_3$  exposure, and one final Hacac exposure to check for etch product enhancement after  $\text{O}_3$  exposure. Etching was monitored by the production of  $M(\text{acac})_x$  etch products.

$M(\text{acac})_x$  etch products were observed for  $\text{Sc}_2\text{O}_3$ ,  $\text{V}_2\text{O}_5$  and  $\text{VO}_2$ ,  $\text{Cr}_2\text{O}_3$ ,  $\text{Mn}_2\text{O}_3$  and  $\text{MnO}$ ,  $\text{Fe}_2\text{O}_3$  and  $\text{Fe}_3\text{O}_4$ ,  $\text{Co}_3\text{O}_4$  and  $\text{CoO}$ ,  $\text{CuO}$  and  $\text{Cu}_2\text{O}$ , and  $\text{ZnO}$ . No etching was observed for  $\text{TiO}_2$ ,  $\text{MnO}_2$ , and  $\text{NiO}$ . The metal oxides that etched either displayed (1) spontaneous etching by Hacac with no self-limiting behavior or (2) etching that limited itself versus Hacac exposure. The metal oxides that were spontaneously etched by Hacac were  $\text{Mn}_2\text{O}_3$  and  $\text{MnO}$ ,  $\text{Co}_3\text{O}_4$  and  $\text{CoO}$ , and  $\text{ZnO}$ . The metal oxides that displayed self-limiting behavior were  $\text{Sc}_2\text{O}_3$ ,  $\text{V}_2\text{O}_5$  and  $\text{VO}_2$ ,  $\text{Cr}_2\text{O}_3$ ,  $\text{Fe}_2\text{O}_3$  and  $\text{Fe}_3\text{O}_4$ , and  $\text{CuO}$  and  $\text{Cu}_2\text{O}$ . ALE processes for these metal oxides that displayed self-limiting reactions are possible using Hacac and  $\text{O}_3$ .

A comparison between the  $M(\text{acac})_x$  etch products and the metal oxide also provided information about oxidation state changes during etching. The  $x$  in  $M(\text{acac})_x$  is both the number of acac ligands and the oxidation state of the  $M$  metal center.  $\text{Sc}_2\text{O}_3$ ,  $\text{Cr}_2\text{O}_3$ ,  $\text{MnO}$ ,  $\text{Fe}_2\text{O}_3$ ,  $\text{CoO}$ ,  $\text{CuO}$ , and  $\text{ZnO}$  all formed  $M(\text{acac})_x$  etch products with the same oxidation state as the metal oxide. In

contrast, the other metal oxides all displayed evidence for reduction during etching. This reduction may occur by oxygen loss during the combustion of Hacac.

9:20am **AP+PS+TF-MoM-4 Selectivity between Silicon-Based Materials for Thermal Atomic Layer Etching and Spontaneous Etching**, *Marcel Junige, S. George*, University of Colorado at Boulder

Sub-10-nm technology nodes must overcome the limits of photolithography. This requires selectivity between various Si-based materials for thermal atomic layer etching (ALE) and spontaneous etching. This work examined selectivity between silicon dioxide ( $\text{SiO}_2$ ) and silicon nitride ( $\text{Si}_3\text{N}_4$ ) for thermal ALE using trimethylaluminum (TMA) and hydrogen fluoride (HF), as well as for spontaneous etching using HF alone, at 275 °C. Distinct etch rates between  $\text{SiO}_2$  and  $\text{Si}_3\text{N}_4$  achieved inherent selectivity.

Experiments were conducted in a hot-wall, viscous-flow vacuum reactor with good control over the pressure during static reactant dosing to ensure reproducibility. *In situ* spectroscopic ellipsometry (iSE) was utilized to study etch-per-cycle (EPC), synergy, and selectivity characteristics. Sodium bifluoride ( $\text{NaHF}_2$ ) was tested as an alternative HF source.  $\text{NaHF}_2$  is a solid salt with negligible HF vapor pressure at room temperature, making  $\text{NaHF}_2$  safer to handle than HF-pyridine.  $\text{NaHF}_2$  delivered HF pressures up to 15 Torr when heated to 150 °C without releasing sodium. During thermal ALE of alumina ( $\text{Al}_2\text{O}_3$ ),  $\text{NaHF}_2$  exhibited diffusion-limited fluorination and EPC characteristics comparable with HF-pyridine.

For thermal ALE of  $\text{SiO}_2$  alternating TMA and HF, the EPC and synergy were  $-0.2 \text{ \AA}$  and 88%, indicating minor spontaneous etching by HF alone. This moderate synergy for  $\text{SiO}_2$  thermal ALE improved to 95% by ensuring water-free conditions during fluorination. On the other hand, the EPC for  $\text{Si}_3\text{N}_4$  thermal ALE was  $-1.1 \text{ \AA}$ . The EPC for  $\text{Si}_3\text{N}_4$  was expected to be much lower than for  $\text{SiO}_2$  because no oxygen reactant was employed to oxidize  $\text{Si}_3\text{N}_4$ . However, iSE experiments revealed that repeated exposures of HF alone spontaneously etched  $\text{Si}_3\text{N}_4$ . Anhydrous HF vapor might form  $\text{F}^-$  species at the surface that have been attributed to dominate  $\text{Si}_3\text{N}_4$  etching. Spontaneous etching using static exposures of 45 s at 3 Torr HF alone obtained a high selectivity of  $\sim 50:1$  for  $\text{Si}_3\text{N}_4$  removal over  $\text{SiO}_2$  retention.

For thermal ALE alternating TMA and HF in co-dose with ammonia ( $\text{NH}_3$ ), the selectivity inverted to  $\sim 9,000:1$  for  $\text{SiO}_2$  over  $\text{Si}_3\text{N}_4$ .  $\text{HF}+\text{NH}_3$  co-dosing led to rapid spontaneous etching of  $\text{SiO}_2$ .  $\text{NH}_3$ , similar to water, might facilitate the dissociation of HF into  $\text{H}^+$  and  $\text{F}^-$ , where the increased  $\text{F}^-$  concentration immediately produces  $\text{HF}_2^-$  species.  $\text{HF}_2^-$  species have been attributed to dominate  $\text{SiO}_2$  etching.

In conclusion, this work demonstrated conditions for inherently selective gas-phase etching of either  $\text{SiO}_2$  or  $\text{Si}_3\text{N}_4$ .

9:40am **AP+PS+TF-MoM-5 Thermal Atomic Layer Etching of  $\text{SnO}_2$  by Fluorination and Ligand-Exchange Using HF and  $\text{Al}(\text{CH}_3)_3$** , *C. Li*, University of Colorado Boulder, China; *J. Partridge, Steven George*, University of Colorado Boulder

Thermal atomic layer etching (ALE) can be achieved with sequential, self-limiting surface reactions. One mechanism for thermal ALE is based on fluorination and ligand-exchange reactions. For metal oxide ALE, fluorination converts the metal oxide to a metal fluoride. The ligand-exchange reaction then removes the metal fluoride by forming volatile products. Previous studies have successfully applied this thermal ALE strategy for  $\text{Al}_2\text{O}_3$ ,  $\text{HfO}_2$ , and  $\text{ZrO}_2$  ALE. However, no previous investigations have explored the thermal ALE of  $\text{SnO}_2$  films.

This study demonstrated the thermal ALE of  $\text{SnO}_2$  thin films using sequential, self-limiting thermal reactions with hydrogen fluoride (HF) and trimethylaluminum ( $\text{Al}(\text{CH}_3)_3$ , TMA) as the reactants. The initial  $\text{SnO}_2$  films were grown by atomic layer deposition (ALD) using tetrakis(dimethylamino) tin and  $\text{H}_2\text{O}_2$ . The thermal  $\text{SnO}_2$  ALE process was then studied using various techniques including quartz crystal microbalance (QCM), spectroscopic ellipsometry (SE), and quadrupole mass spectrometry (QMS).

*In situ* QCM experiments monitored  $\text{SnO}_2$  ALE at temperatures from 250 to 300 °C. The  $\text{SnO}_2$  etching was linear versus the number of HF and TMA reaction cycles. The QCM studies also showed that the sequential HF and TMA reactions were self-limiting versus reactant exposures. The  $\text{SnO}_2$  etching rates increased at higher temperatures. The QCM analysis measured mass change per cycle (MCPC) values that varied from  $-44.32 \text{ ng}/(\text{cm}^2 \text{ cycle})$  at 250 °C to  $-123.5 \text{ ng}/(\text{cm}^2 \text{ cycle})$  at 300 °C. These MCPCs correspond to  $\text{SnO}_2$  etch rates from  $0.64 \text{ \AA}/\text{cycle}$  at 250 °C to  $1.78 \text{ \AA}/\text{cycle}$  at 300 °C.

SE measurements confirmed the linear removal of  $\text{SnO}_2$  and the etching rates. QMS analysis also revealed the volatile etching products during the

<sup>1</sup> TFD James Harper Award Finalist

# Monday Morning, November 6, 2023

sequential HF and TMA exposures on SnO<sub>2</sub> at 300 °C. These QMS investigations observed Sn(CH<sub>3</sub>)<sub>3</sub><sup>+</sup>, indicating Sn(CH<sub>3</sub>)<sub>4</sub> as the etch product during TMA exposures. Al<sub>x</sub>F<sub>y</sub>(CH<sub>3</sub>)<sub>z</sub> dimer and trimer species were identified as the ligand-exchange products. QMS analysis during multiple sequential TMA doses before HF/TMA cycling also revealed that fluorination was necessary for Sn(CH<sub>3</sub>)<sub>4</sub> etch product evolution. This observation indicated that TMA does not convert SnO<sub>2</sub> to Al<sub>2</sub>O<sub>3</sub>. The results indicate that thermal SnO<sub>2</sub> ALE using sequential HF and TMA exposures occurs by fluorination and ligand-exchange reactions.

10:40am **AP+PS+TF-MoM-8 Reactivity and Volatility as Key Metrics for Classifying the Substrate Selectivity of Ligands in Atomic Level Processing**, Hadi Abroshan, Schrödinger, Inc.; S. Lim, Schrödinger, Inc., Republic of Korea; A. Chandrasekaran, Schrödinger, Inc.; S. Elliott, Schrödinger, Inc., Germany; H. Kwak, M. Halls, Schrödinger, Inc.

One of the main challenges in the area-selective deposition or etch for semiconductor processing is finding a single reagent that undergoes different chemistry on different substrates. The reagent may be an organometallic complex containing a particular ligand or may be the protonated version of that ligand. In this work we propose that examining just two properties of the organometallic complex across a series of metal cations is sufficient to give an indication of the area-selectivity that can be achieved with reagents based on the particular ligand chemistry.

The first property is reactivity towards the hydrolysis reaction, which gives information about oxide formation versus surface passivation or etching, and the second property is volatility of the organometallic reagent or etch by-product. Figure 1a shows the four limiting cases of the combination of these two properties. Using quantum chemical and machine learning methods to predict the properties, such reactivity-volatility maps can be plotted quickly for a wide range of ligands and metal-containing substrates. We validate our results on the chloro ligand (Figure 1b), thd, RCp and NR2 against area-selective experiments, including those using HCl as etchant [1], ruthenocene and ferrocene [2] as metal sources and β-diketones as inhibitors [3]. While approximate, this approach provides a starting point for designing and understanding atomic-level processes that are area-selective with respect to a wide variety of substrates.

[1] M.F.J. Vos et al., Chem. Mater. 31, 3878 (2019).

[2] H. Nadhom et al., J. Phys. Chem. Lett. 12, 4130 (2021).

[3] A. Mameli et al., ACS Nano 11, 9303 (2017).

11:00am **AP+PS+TF-MoM-9 Etching of Silicon Nitride Using Vapor-Phase HF Exposures at Various Temperatures: Role of Ammonium Hexafluorosilicate Salt**, Vahid Ghodsi, S. George, University of Colorado Boulder

The etching of silicon nitride (SiN<sub>x</sub>) was explored using vapor-phase HF exposures at various temperatures. The investigations were performed using *in situ* quadrupole mass spectrometry (QMS) and *ex situ* attenuated total reflectance Fourier transform infrared (ATR-FTIR) spectroscopy to detect the volatile and non-volatile etch products, respectively. These QMS and ATR-FTIR studies provide valuable understanding of the SiN<sub>x</sub> atomic layer etching (ALE) process employing hydrofluorocarbon plasma to form (NH<sub>4</sub>)<sub>2</sub>SiF<sub>6</sub> salt at low temperatures and then thermal annealing at higher temperatures to desorb the salt [N. Miyoshi et al., Jpn. J. Appl. Phys. 56, 06HB01 (2017)].

At low temperatures, T≤60°C, QMS detected the evolution of SiF<sub>4</sub> from HF exposure at 0.5 Torr on SiN<sub>x</sub>. SiF<sub>4</sub> formed concurrently with the formation of a (NH<sub>4</sub>)<sub>2</sub>SiF<sub>6</sub> salt layer on the SiN<sub>x</sub> surface according to: Si<sub>3</sub>N<sub>4</sub> + 16HF(g) → 2(NH<sub>4</sub>)<sub>2</sub>SiF<sub>6</sub> + SiF<sub>4</sub>(g). To verify the presence of the salt, the temperature could be ramped up to 200°C in the absence of HF exposure. During this temperature ramp, QMS detected SiF<sub>4</sub> at higher temperatures T≥80°C corresponding to the thermal decomposition of the (NH<sub>4</sub>)<sub>2</sub>SiF<sub>6</sub> salt according to: (NH<sub>4</sub>)<sub>2</sub>SiF<sub>6</sub> → 2NH<sub>3</sub>(g) + 2HF(g) + SiF<sub>4</sub>(g).

When the HF exposure was performed at higher temperatures T≥120°C, SiF<sub>4</sub> was again observed as an etch product. However, no secondary rise of SiF<sub>4</sub> was detected by QMS during the temperature ramp to 200°C in the absence of HF exposure. This behavior indicated that the (NH<sub>4</sub>)<sub>2</sub>SiF<sub>6</sub> salt did not form on the surface at temperatures T≥120°C. The spontaneous etching of SiN<sub>x</sub> with no salt on the SiN<sub>x</sub> surface is possible at these higher

temperatures. ATR-FTIR studies corroborated the salt formation at lower temperatures and the salt decomposition at higher temperatures.

To demonstrate that HF exposures could achieve high SiN<sub>x</sub> etch rates without salt formation, experiments were conducted at T≥140°C with higher HF pressures. A four-fold increase in HF pressure to 2.0 Torr led to a ~five-fold increase in SiF<sub>4</sub> signal intensity measured by QMS. At these higher temperatures T≥140°C, SiN<sub>x</sub> etching can proceed with no inhibition from the salt.

11:20am **AP+PS+TF-MoM-10 Crystal Phase Transformations During Thermal Atomic Layer Etching of Hafnium–Zirconium Oxide (HZO) Using Hydrogen Fluoride and Dimethylaluminum Chloride**, Aziz Abdullagatov, J. Partridge, University of Colorado at Boulder; M. Surman, ASM Microchemistry Ltd., Finland; S. George, University of Colorado at Boulder  
Thermal atomic layer etching (ALE) of Hf<sub>0.5</sub>Zr<sub>0.5</sub>O<sub>2</sub> (HZO) was previously demonstrated using hydrogen fluoride (HF) and dimethylaluminum chloride (DMAC) [1]. This current work focused on crystallographic transformations of HZO during ALE. Grazing incidence x-ray diffraction (GIXRD) analysis of initial 10 nm thick HZO film on 20 nm thick TiN on Si revealed orthorhombic (o-phase), tetragonal (t-phase), and monoclinic phases (m-phase). *Ex situ* spectroscopic ellipsometry and X-ray reflectivity (XRR) measurements showed that sequential exposures of HF and DMAC at 250 °C resulted in a linear decrease in film thickness with an HZO etch rate of ~0.45 Å/cycle.

GIXRD studies observed that the peaks associated with the o- and t-phases decreased faster in intensity than the m-phase peaks. As the number of ALE cycles increased, only the m-phase remained before the majority of the HZO film was removed by etching. Interestingly, as o- and t-phases were removed, the grain size of the m-phase crystallites increased in size according to the Scherrer equation. XRR investigations also monitored a decrease in the film density with ALE. In addition, atomic force microscopy (AFM) measurements observed that the density decrease was accompanied by an increase in film roughness.

Powder diffraction (PXRD) studies were also conducted to investigate the phase transformation of crystalline ZrO<sub>2</sub> powder at 250 °C. ZrO<sub>2</sub> powder was used as a model system since the chemical properties of HfO<sub>2</sub> and ZrO<sub>2</sub> are very similar. PXRD analysis of as-received ZrO<sub>2</sub> powder showed crystallographic planes of mostly m-phase with some cubic (c-phase) and t-phase. As expected, the etching of ZrO<sub>2</sub> powder resulted in a mass loss. PXRD also observed the loss of c- and t-phases and an increase in grain size of m-phase crystallites. The results for the HZO films and ZrO<sub>2</sub> powder are similar. There are crystal phase transformations that occur with loss of o- and t-phases and growth of m-phase during thermal ALE.

[1] J. A. Murdzek and S. M. George, J. Vac. Sci. Technol. A 38, 022608 (2020)

11:40am **AP+PS+TF-MoM-11 Novel Conversion Half-Cycle for Thermal ALD of High-Density HfO<sub>2</sub> and Its Use in HfO<sub>2</sub>/Al<sub>2</sub>O<sub>3</sub> Nanolaminate Dielectric Barriers**, Dane Lindblad, Forge Nano

Hafnium dioxide, HfO<sub>2</sub>, is an attractive material for use as a dielectric barrier in high-power SiC and GaN electronics, both MOSFET and HEMT, due to its high dielectric constant and thermal stability. Current techniques for depositing HfO<sub>2</sub> by thermal atomic layer deposition (ALD) tend to produce low density and performing films. While plasma enhanced ALD (PEALD) is employed to improve the performance, the high field and fast switching requirements of the device can make the barriers insufficient. In addition, not all applications can accommodate plasma. As such, a novel conversion process, referred to as the “CRISP” process, for the deposition of HfO<sub>2</sub> via thermal ALD has been explored. Utilizing the tool’s unique ability to introduce a small amount of non-metal catalyst during the conversion half-cycle, the CRISP process employs surface catalysis to increase growth per cycle, improve stoichiometry, increase density, and modify crystal morphology compared to HfO<sub>2</sub> films grown with conventional conversion methods, O<sub>3</sub>, as shown in Figure 1 and Table 1 below. A comparison of the HfO<sub>2</sub> films grown using the CRISP process and the conventional O<sub>3</sub> process, both deposited at 250°C, will be presented. Furthermore, due to the layer-by-layer growth of ALD, this deposition technique lends itself well to the fabrication of nanolaminate materials. Specifically, HfO<sub>2</sub>/Al<sub>2</sub>O<sub>3</sub> laminate stacks can be precisely manufactured to alter the bulk material properties and curate device performance, allowing one to choose improvements in leakage current or dielectric breakdown in the nanolaminate film. An initial investigation into the performance of various HfO<sub>2</sub>/Al<sub>2</sub>O<sub>3</sub> laminate stacks is presented, and this work, coupled with higher quality HfO<sub>2</sub> films, gives insight into the use of these materials for the next generation of high-power electronic devices.

## Biomaterial Interfaces Division

### Room B117-119 - Session BI1+PS-MoM

#### Microbes and Fouling at Surfaces

**Moderators:** Kenan Fears, U.S. Naval Research Laboratory, Sally M. McArthur, Deakin University, Australia

8:20am **BI1+PS-MoM-1 Amphiphilic Coatings for Marine Low-Fouling Applications**, *Axel Rosenhahn*, Ruhr University Bochum, Germany **INVITED**  
Manmade materials in contact with ocean water become rapidly colonized by living matter like bacteria, diatoms, barnacles, or mussels. Increased fuel consumption, failure of devices, and substantial maintenance costs are among the penalties associated with marine biofouling. As the historical paradigm to combat fouling by biocide releasing coatings is increasingly challenged by legal restrictions, environmentally benign low-fouling materials for marine applications are intensively explored [1]. While several hydrophilic and hydrophobic materials show promising properties, their combination into amphiphilic coatings unites the best of the two worlds [2]. As hydrophilic compound, zwitterionic materials with different molecular architectures were developed and their structure-function relationship against different fouling organisms have been studied [3]. Amphiphilic coatings based on zwitterionic polymers have been designed and their antipolyelectrolyte properties have been characterized by several methods including AFM and SPR. Their antifouling properties against a range of marine fouling species and in short term field exposures have been assessed and the results will be discussed under consideration of the interaction of the organic coatings with inorganic particulate matter in the ocean [4,5,6]. Based on the obtained data, design criteria for optimized zwitterionic building blocks for fouling-release technologies will be discussed.

[1] M. Callow, J. Callow, *Nature Communications* 2011, 2, 244

[2] S. Krishnan, C. Weiman, C. Ober, *J. Materials Chemistry* 2008, 18, 3405

[3] A. Laschewsky, A. Rosenhahn, *Langmuir* 2018, 35, 1056

[4] F. Koschitzki, R. Wanka, L. Sobota, J. Koc, H. Gardner, K.Z. Hunsucker, G.W. Swain, A. Rosenhahn, *ACS Applied Materials & Interfaces* 2020, 12(30), 134148

[5] J. Koc, E. Schönemann, R. Wanka, N. Aldred, A.S. Clare, H. Gardner, G.W. Swain, K. Hunsucker, A. Laschewsky, A. Rosenhahn, *Biofouling* 2020, 36(6), 646

[6] L. Schardt, A.M. Guajardo, J. Koc, J.L. Clarke, J.A. Finlay, A.S. Clare, H. Gardner, G.W. Swain, K. Hunsucker, A. Laschewsky, A. Rosenhahn *Macromolecular Rapid Communications* 2021, 43(12), 2100589

9:00am **BI1+PS-MoM-3 Bio-Informed Interface Design and Synthesis to Manipulate Microbial Behavior**, *Rong Yang*, Cornell University **INVITED**

Biofilm is often considered detrimental, which needs to be minimized as it can cause infections and fouling in healthcare, food and water manufacturing, and underwater civil and military activities. Nevertheless, we also believe such naturally occurring biofilm can be desirable, upon appropriate programming via precise control over the surface they inhabit, as building blocks for self-actuated and self-repairing "living" coatings. To gain insight into the biointerface, research in the past two decades has unraveled the fundamental thermodynamics and hydrodynamics that have guided the design of numerous antifouling/antimicrobial surfaces. However, the biological effects of insoluble materials remain elusive. Recent advances in vacuum-based synthesis have enabled well-defined material properties at length scales relevant to microbes' biochemical and biophysical activities, enabling a bio-informed materials design approach. Motivated by the unmet needs for antifouling materials and living materials, our recent research has advanced our current understanding of the biointerface in three critical ways: (i) leveraging dynamic surface chain reorientation to achieve antifouling at the air-liquid-solid interface, the importance of which has been overlooked in past research; (ii) recognizing bacteria to be complex microorganisms with dynamic structure and metabolism and sophisticated chemical communication systems and leveraging the recent breakthroughs in microbiology to guide the design of bio-active polymer coatings; (iii) enabling living materials by performing polymerization directly on living organisms, which overcomes the limited tunability of the native microbial extracellular scaffolds and preserves the function and viability of coated organisms by avoiding harmful synthesis conditions. We seek to underscore the importance of understanding detailed microbe-material interactions and provide an outlook on extending

the material-bacteria interactions beyond "kill or repel" towards signaling and control.

9:40am **BI1+PS-MoM-5 Using Flow-Cells to Culture Microbial Biofilms for Improved Secondary Ion Mass Spectral Imaging**, *Yuchen Zhang*, Oak Ridge National Laboratory, USA; *X. Yu*, Oak Ridge National Laboratory

Bacterial biofilms are a main player in organic processing in the environment. Therefore, characterization and understanding of the biofilm interactions with groundwater and soil components is important in deepening our knowledge in the biosphere and rhizosphere. We present two approaches to prepare the bacterial biofilms suitable for time-of-flight secondary ion mass spectrometry (ToF-SIMS). *Shewanella* MR-1 was used as the model bacteria biofilm due to their known traits in subsurface, surface, and soil microbiology. A mixture of silica, alumina, and iron oxide was used as the model soil system. In the static culture, the bacteria were inoculated in a multi-well cell culture dish at their log phase. Then minerals were added to the culturing well. The mixture of the bacteria biofilms and minerals were scratched off carefully and deposited onto the clean silicon (Si) wafers before ToF-SIMS analysis. Second, we used a microfluidic cell to culture biofilms. We made a modification of the system for analysis at the liquid vacuum interface (SALVI) microfluidics for biofilm attachment in the growth and detection chamber. The mineral components were mixed to the growth media at a ratio of 1:1 by volume as nutrients to support the biofilm's growth. During static culturing, a series of Si wafers were used to capture the temporal progression of the biofilms and the soil components over days. In dynamic cultures, effluents were collected onto clean Si substrates. The time intervals were chosen based on the growth curve of the strain. Distinctive fatty acids peaks of *Shewanella* biofilms, such as myristic acid ( $m/z$  227,  $C_{14}H_{27}O_2^-$ ), palmitic acid ( $m/z$  255,  $C_{16}H_{31}O_2^-$ ), and arachidic acid ( $m/z$  311,  $C_{20}H_{39}O_2^-$ ), and the biomarker riboflavin peak ( $m/z$  241,  $C_{12}H_9N_4O_2^-$ ) are observed in the dynamic results. In contrast, the static results do not provide as much information. This finding indicates that static culture is not optimal for studying biofilms using ToF-SIMS. Our results demonstrate that sample preparation is quite critical in microanalysis of bacteria biofilms, specifically in surface analysis like ToF-SIMS. The microfluidic growth chamber is more flexible in microbial culture and media tuning, both are important in simulating a variety of conditions to understand microbes and soil interactions at the microscale. Additionally, characteristic signals of biofilms are not buried under the mineral components in the dynamic setup, which is imperative in understanding the role of biofilms in soil aggregation and bioremediation occurring at the microbial interface.

10:00am **BI1+PS-MoM-6 Role of Microbial Biofilms in the Settlement of Macrofoulers on Antifouling Marine Coatings**, *Sara Tuck*, *M. Kardish*, US Naval Research Laboratory; *B. Orihuela*, Duke University; *G. Vora*, US Naval Research Laboratory; *D. Rittschof*, *K. Franz*, Duke University; *K. Fears*, US Naval Research Laboratory

Accumulation of biofouling on submerged surfaces is a foundational problem for maritime transport and human health. Biofouling build-up increases the drag coefficient, fuel consumption, exhaust emissions, and operational costs. Traditionally, biofouling is inhibited by the application of antifouling coatings, the most popular of which, contain copper. Copper-based antifouling coatings can contain up to ~75% CuO, by weight, in attempt to release sufficient levels of copper to deter the settlement of fouling organisms. Despite these high loadings, the efficacy of these antifouling coatings has been declining with the emergence and spread of copper tolerant species. Microbial communities resistant to copper have been found to form mature biofilms on these coatings, which could be altering the interfacial properties to create more favorable conditions for the settlement of a broader biofouling community. To gain an understanding of the mechanisms responsible for the loss in antifouling performance, coated and uncoated polyvinyl chloride panels were submerged at estuarine and marine field test sites and microbial communities were harvested. Collected biofouling communities were cultured and individual species were collected and identified. Copper tolerance was assessed by re-exposing cells to copper-containing coatings and traditional antimicrobial assays to determine susceptibility to an array of biocides. Finally, resistant biofilms were formed on marine coatings to assess the effect of their presence on the settlement of acorn barnacle larvae.

# Monday Morning, November 6, 2023

## Biomaterial Interfaces Division

### Room B117-119 - Session BI2+AS+HC+SS-MoM

#### Energy Transfer and Light Induced Phenomena in Biologic Systems

**Moderators:** Morgan Alexander, University of Nottingham, UK, Tobias Weidner, Aarhus University, Denmark

10:40am **BI2+AS+HC+SS-MoM-8 Electrochemically Conducting Lipid Bilayers: Q-Lipid-Containing Membranes Show High in-Plane Conductivity Using a Membrane-on-a-Chip Setup**, U. Ramach, TU Wien, Austria; J. Andersson, IST Austria; **Markus Valtiner**, TU Wien, Austria

The light-driven reactions of photosynthesis as well as the mitochondrial powersupply are located in specialized membranes containing a high fraction of redox-active lipids. In-plane charge transfer along such cell membranes is currently thought to be facilitated by the diffusion of redox lipids and proteins.

Using a membrane on-a-chip setup, we show here that redox-active model membranes can sustain surprisingly high currents (mA) in-plane at distances of 25 nm. We also show the same phenomenon in free-standing monolayers at the air-water interface once the film is compressed such that the distance between redox centers is below 1 nm. Our data suggest that charge transfer within cell walls hosting electron transfer chains could be enabled by the coupling of redox-lipids via simultaneous electron and proton in-plane hopping, similar to conductive polymers. This has major implications for our understanding of the role of lipid membranes, suggesting that Q-lipid-containing membranes may be essential for evolving the complex redox machineries of life.

[1] U. Ramach, J. Andersson, R. Schöfbeck and M. Valtiner, *Iscience* 26 (2), 2023.

11:00am **BI2+AS+HC+SS-MoM-9 Light Responsive Cyclic Peptide Polymer Nanomaterials**, O. Atoyebi, M. Beasley, W. Maza, M. Kolel-Vetil, A. Dunkelberger, **Kenan Feares**, US Naval Research Laboratory

Cyclic peptides are capable of self-assembling into supramolecular peptide nanostructures, via hydrogen bonding along the backbone of the peptide rings. To improve upon this molecular architecture, we designed and synthesized cyclic peptide polymers by covalently linking the cyclic peptides into a linear polymer chain, and demonstrated the conformation of the polymer chain could be transitioned from an unfolded state into rigid, peptide nanorods by varying solution pH. Here we present an alternate way to control the self-assembly via photo-isomerization. We capitalize on azobenzene's photo-actuable nature using a di-carboxylic acid azobenzene to covalently crosslink the cyclic peptide rings into a linear cyclic peptide polymer via terminal amines present in the ring. Self-assembly of the cyclic peptide nanotube occurs by exposing the polymerized cyclic peptide to ultraviolet radiation causing a trans- to -cis transition of the azobenzene and thus assembling the cyclic peptide nanotube. Furthermore, we fluorescence donor/acceptor pairs can be displayed from these materials, at highly controlled separation distances, to alter the optical response of these materials as a function of polymer conformation.

11:20am **BI2+AS+HC+SS-MoM-10 Programmable Biomimetic Light-Harvesting Systems based on Strong Coupling of Synthetic Peptides and Dye-Functionalised Polymer Brushes to Plasmon Modes**, **Graham Leggett**, University of Sheffield, UK

Excitation transfer in molecular photonic materials is dominated by incoherent hopping processes; consequently, exciton diffusion lengths are short (~10 nm) placing severe constraints on device design. A grand challenge for the past two decades has been to discover how to achieve efficient long-range transfer of excitation in molecular systems. We have developed a new approach to the design of materials for solar energy capture that combines biomimetic design, inspired by structures used in photosynthesis, with strong light-matter coupling.

Photosynthetic pigment-protein light-harvesting antenna complexes (LHCs) from plants and bacteria are strongly coupled to the localised surface plasmon resonances (LSPRs) in arrays of metal nanostructures leading to the formation of macroscopically extended excited states. Modelling of data indicates that the coupling results from linear combinations of plasmon and exciton states. For example, wild-type and mutant LH1 and LH2 from *Rhodospirillum rubrum* containing different carotenoids yield different coupling energies; the methods of synthetic biology enable strong light-matter coupling to be programmed.

However, proteins are not suitable for putative applications of molecular photonic materials. Instead, we have designed programmable biomimetic

pigment-peptide and pigment-polymer antenna complexes, in which surface-grafted peptide and polymer scaffolds organise excitons within localised surface plasmon resonances to achieve strong light-matter coupling. In these systems, delocalised excited states (plexcitons) extend across at least 1000s of pigments. In synthetic peptide and protein systems, we find that the plasmon mode couples to states not seen under weak-coupling, providing evidence for the formation of macroscopically-extended excited states that facilitate coherent transfer of excitation across long distances. In pigment-polymer systems, the dye concentration in the film can be increased to ~2M, significantly exceeding the concentration of chlorophyll in biological light-harvesting complexes, by optimisation of the polymer grafting density and the dye-scaffold coupling chemistry. Fitting of spectra for these plexcitonic antenna complexes yields Rabi energies up to twice as large as those achieved with biological LHCs. Moreover, synthetic plexcitonic antenna complexes display pH- and temperature-responsiveness, enabling active control of strong plasmon-exciton coupling via regulation of the polymer conformation.

These biomimetic quantum-optical brush systems offer great promise for the design of new types of molecular photonic device.

## Chemical Analysis and Imaging of Interfaces Focus Topic

### Room A105 - Session CA1+AS+LS+NS+SS+VT-MoM

#### Modeling, AI, and Machine Learning Applied to Interfaces

**Moderators:** J. Trey Diulus, NIST, Kateryna Artyushkova, Physical Electronics

8:20am **CA1+AS+LS+NS+SS+VT-MoM-1 Topological and Geometric Descriptors of Complex Self-assembly at Liquid Interfaces**, **Aurora Clark**, University of Utah **INVITED**

Amphiphilic surfactants at liquid/liquid interfaces can form complex self-assembled architectures that underpin interfacial reactivity and transport. This has been demonstrated by surface sensitive spectroscopies and molecular dynamics simulations within the domain of liquid/liquid extraction, which involves solute adsorption, complexation reactions and transport across the phase boundary. Being able to quantify surfactant organization is a significant challenge because the distribution of species is broad and highly heterogeneous. As such, in the analysis of molecular dynamics data, there is significant need to develop descriptors that allow statistical analysis of surface organization. This work presents recent developments based upon geometric measure theory and topological data analysis that are able to identify surface assemblies and their dynamic evolution. These methods are revealing intricate dependencies of surface assembly upon solution composition and the impact this has upon transport mechanisms.

References:

Kumar, N.; Clark, A. E. Persistent Homology Descriptors for Surface Image Analysis in Complex Chemical Systems, *Journal of Chemical Theory and Computation*, **2023**, In Press. ChemArXiv: <https://doi.org/10.26434/chemrxiv-2023-vwrwxj>

Zarayeneh, N.; Kumar, N.; Kalyanaraman, A.; Clark, A. E. Dynamic Community Detection Decouples Hierarchical Timescale Behavior of Complex Chemical Systems, *Journal of Chemical Theory and Computation*, **2022**, 18, 7043 – 7051. DOI:10.1021/acs.jctc.2c00454

Kumar, N.; Clark, A. E. Unexpected Inverse Correlations and Cooperativity in Ion-pair Phase Transfer, *Chemical Science*, **2021**, 12, 13930-13939. DOI: 10.1039/D1SC04004A

Liu, Z.; Clark, A. E. An Octanol Hinge Opens the Door to Water Transport, *Chemical Science*, **2021**, 12, 2294 – 2303. DOI: 10.1039/D0SC04782A.

Alvarado, E.; Liu, Z.; Servis, M. J.; Krishnamoorthy, B.; Clark, A. E. A Geometric Measure Theory Approach to Identify Complex Structural Features on Soft Matter Surfaces, *Journal of Chemical Theory and Computation*, **2020**, 16, 4579-4587. DOI: 10.1021/acs.jctc.0c00260,

9:00am **CA1+AS+LS+NS+SS+VT-MoM-3 Machine Learning and the Future of Surface Analysis**, J. Jones, M. Caouette, **Kateryna Artyushkova**, Physical Electronics **INVITED**

Machine learning can potentially revolutionize all areas of material science and engineering, including surface analysis, by automating and accelerating data acquisition and analysis. The application of machine learning and artificial intelligence (ML/AI) has been actively evaluated and used in scanning probe microscopic methods<sup>1-2</sup>, while the application of AI in

8:20 AM

# Monday Morning, November 6, 2023

surface analysis methods such as AES, XPS, and TOF-SIMS is in the very early stages.<sup>3</sup> In this talk, I will discuss the potential areas where AI will change how we do surface analysis.

With recent instrumental development yielding improvements in sensitivity and throughput, the data acquisition stage of surface analysis has become much faster than the experimental planning or data analysis stages, which both require significant operator time and human-based decisions. Using a spectrometer still requires a human operator with instrument-specific knowledge and experience in how to operate it. More importantly, the operator uses physical and chemical knowledge to decide on what specific data must be obtained and from which locations on the sample, depending on the analytical question being addressed by the experiment. Experienced scientists make these decisions effortlessly during the experiment, but it is a very challenging task for ML algorithms that rely on training data with explicit descriptors.

Initial AI applications to analytical surface analysis will focus on instrument optimization and performance inherent in the analytical workflow. Unlike acquisition parameters based on chemical or material science requiring broader context, tuning, and standardizing the spectrometer can be easily cast into numerical terms processable by AI.

Machine learning can also be utilized as a live data integrity monitoring service during acquisition, recognizing and rejecting "bad data". Systemically erroneous data caused by charging or sample damage are often not discovered until the experiment is complete and the data analyzed by a human. Catching it automatically during the experiment saves valuable operator and instrument time. Here, I will present an initial application wherein ML was used to identify whether ToF-SIMS spectra were correctly calibrated.

1. S.V. Kalinin, *ACS Nano* 2021, 15, 8, 12604–12627.

2. S.V. Kalinin, arXiv:2304.02048

3. G. Drera *et al* 2020 *Mach. Learn.: Sci. Technol.* 1 015008

9:40am **CA1+AS+LS+NS+SS+VT-MoM-5 Complexity to Clarity: Detecting, Identifying and Analyzing Complex Materials with Machine Learning**, **Paul Pigram**, *W. Gardner, S. Bamford, D. Winkler, B. Muir, R. Sun, S. Wong*, La Trobe University, Australia

Our ability to analyze and understand any physical, chemical, or biological material relies on accurately determining its structure, characteristics, and responses. Contemporary analytical techniques produce large volumes of data from pointwise sample analyses (one dimensional (1D) data), maps of compositional distributions (two dimensional (2D) data), and depth profiles showing composition throughout a sample volume (three dimensional (3D) data).

Correlative analyses linking data from the same sample, obtained by different analytical techniques or different operating parameters, are becoming critically important. Different analytical perspectives on the same sample enhance the richness and depth of the conclusions that can be drawn from it.

Recent advances in analytical science have resulted in an overwhelming avalanche of data – the “big data” problem. In our lab a single time-of-flight secondary ion mass spectrometry (ToF-SIMS) experiment might collect a map (512 x 512 pixels) with 2000 mass spectral peaks of significant intensity in 2 – 10 minutes. These half a billion data points all have differing degrees of significance.

In many cases, only a small number of peaks, 10 – 200, may be judged to be characteristic of a specific sample, and the rest of the data may be discarded. However, there are significant risks that such analyses are biased, and may miss important but subtle trends.

There is a very substantial knowledge gap in our ability to find and make full use of the information and knowledge contained in large scale data sets. This gap is driving rapid international progress in the application of materials informatics and machine learning to analytical surface science.

This presentation will highlight our work on applying artificial neural network approaches to analysis of a variety of very large hyperspectral data sets to better understand complex materials and their interactions.

## Chemical Analysis and Imaging of Interfaces Focus Topic Room A105 - Session CA2+AS+LS+NS+SS+VT+MoM

### Environmental and Energy Interfaces

**Moderators:** Xiao-Ying Yu, Oak Ridge National Laboratory, USA, **Musahid Ahmed**, LBNL

10:40am **CA2+AS+LS+NS+SS+VT+MoM-8 Probing hydrogen bonding in aerosols, and solutions with X-Ray and vibrational spectroscopy**, **Musahid Ahmed**, LBNL

INVITED

Hydrogen and non-covalent bonding drive myriad processes which have enormous ramifications in molecular growth in soft systems. For instance, subtle changes in pH can drive dramatic changes in assembly processes relevant to biology, while a few degrees of change in temperature leads to enormous changes in plastic crystals, a phase change material (PCM) -- systems of significant importance in thermal science. At Berkeley lab, we have developed an integrated suite of both synchrotron (X-Ray) and non-synchrotron-based (vibrational-THz, IR, Raman) spectroscopic techniques coupled with micro-reactors and aerosol beams to establish a molecular-level understanding of bonding & dynamics in heterogeneous systems.<sup>1-3</sup>

Deep eutectic solvents (DESs), an important class of solutions, are considered as alternatives to conventional organic solvents and ionic liquids in many applications because they are highly biodegradable and renewable. DESs consist of a hydrogen bond donor and an acceptor and the ability to tune these hydrogen bonds to target required properties is what makes them attractive. At specific compositions, these forms a eutectic mixture which resemble many characteristics of ionic liquids and organic solvents thanks to its complicated inter and intramolecular hydrogen bonding network. Connecting PCM's and DES's are hydrogen bond networks and the changes impacted on it by including inorganic salts, which can be extended to build hydrogen bonded organic frameworks (HOF). Beyond enormous potential for new materials for energy storage, transport, and carbon capture, the study of HOF dynamics may also answer fundamental and controversial questions on the nature of hydrogen bonding, such as the invocation of anti-electrostatic forces in their formation. In this talk, I will describe new results using Raman spectroscopy coupled to aerosol-based X-Ray spectroscopy to probe such dynamics in choline chloride/glycerol, phosphoric acid and ammonium sulfate systems. These results also benefit from electronic structure calculations particularly for X-Ray photoelectron and absorption spectroscopy in providing exquisite insight at the molecular level on structural changes on the nanoscale.

1 Lu, W. *et al.* *Cell Reports Phys. Sci.* **3**, doi:10.1016/j.xcrp.2022.100988 (2022).

2 Weeraratna, C., Amarasinghe, C., Lu, W. C. & Ahmed, M. *JPC Lett* **12**, 5503-5511, doi:10.1021/acs.jpcl.1c01383 (2021).

3 Weeraratna, C. *et al.* *JPC Lett* **14**, 1279-1287, doi:10.1021/acs.jpcl.2c03748 (2023).

11:20am **CA2+AS+LS+NS+SS+VT+MoM-10 The Investigation of Degraded Historic Glass Samples Using X-ray Photoelectron Spectroscopy**, **G. Verhaar**, Rijksmuseum, Netherlands; **J. Vienes**, **N. Tennent**, University of Texas at Dallas, United States Minor Outlying Islands (the); **Amy Walker**, University of Texas at Dallas

The atmospheric deterioration of glass is a well-known phenomenon and is often referred to as glass disease, weeping or crizzling. Understanding this process and the underlying chemical mechanisms are important for a number of industries from preserving historic glass objects in museums to the long-term evaluation of nuclear waste glasses. In this talk we shall discuss the use of x-ray photoelectron spectroscopy (XPS), or electron spectroscopy for chemical analysis (ESCA), to examine two fragments of heavily degraded, historic glass objects.

The two glass fragments studied originated from French wineglasses and were made available for destructive analysis by the Corning Museum of Glass. The first fragment originated from c. 1750 and is a potassium rich glass (CMG449). The second fragment was dated c. 1600-1650 and is a sodium rich glass (CMG1050). Using SEM, the thickness of the alteration layers were 60-75  $\mu\text{m}$  and  $\sim 30 \mu\text{m}$  for CMG449 and CMG1050, respectively.

Two types of XPS experiments were made. In the first, the surface composition of the glass fragments was examined. Second, a non-destructive cross-section analysis was performed by rotating the sample by 90° and data taken across the fracture surface providing a depth profile through the degradation layer. For example, for CMG449 an increase in the abundance of K, Na and was observed in the first  $\sim 100 \mu\text{m}$  in agreement with other studies. For CMG1050, the atomic concentration of Na also

# Monday Morning, November 6, 2023

increased as a function of depth. Little, or no, K was observed as expected for a sodium rich glass.

Further, the CMG1050 surface composition did not vary across the sample. However, for CMG449 the surface composition did vary across the sample. Three different areas were identified. The outer rim of the glass contained more K compared to the inside of the foot. The middle portion contained less Na, K and Ca overall. This is a result of the manufacture of the glass. During production, the outer rim of the foot was folded over leading to the formation of a thicker rim than the inner foot region. These changes in glass thickness and stress likely lead to the observed changes in chemical composition.

Surprisingly, we also observed carbonates and formates present in the glass; their concentration varied with position and depth across the sample. There are two potential reasons for this observation. First, during the glass manufacturing process the glass melt was not completely calcined and so some carbonate was incorporated into the glass structure. Second these species are the result of aging of the glass and form in a similar manner to the formation of carbonate salts on glass surfaces. Studies are on-going to determine the origin.

11:40am **CA2+AS+LS+NS+SS+VT+MoM-11 Studying Oil-in-Water Emulsion Interfacial Changes Using Static and in Situ Imaging**, *Xiao-Ying Yu*, Oak Ridge National Laboratory

Bilgewater emulsion formed from the shipboard is regarded as a major pollutant in the marine environment. Bilgewater exists in a stable oil-in-water (O/W) emulsion form. However, little is known about the O/W liquid-liquid (L-L) interfacial evolution. Although some compositional information can be acquired, traditional bulk characterization approach is not capable of capturing the chemical changes at the O/W L-L interface. Surfactants are deemed essential in droplet formation, however, their roles in bilgewater stabilization are not fully understood. We have employed both static and novel in situ scanning electron microscopy (SEM) and time-of-flight secondary ion mass spectrometry (ToF-SIMS) to study the evolving O/W interface using a NAVY bilge model for the first time. Optical microscopy was also used to confirm droplet size distribution (DSD) measurements. Our results show that the DSD of bilgewater does not change significantly without the addition of X-100 surfactants at static or rocking conditions. The in situ SEM results show that droplets coagulate even as freshly prepared emulsions. The mean DSD becomes bigger over a short course of twenty-four hours. Furthermore, both oil components and water clusters are shown to evolve over time at the O/W droplet interface by in situ liquid SIMS imaging. Of particular interest to droplet stabilization, the contribution of surfactants to the aged bilge droplets becomes more significant as the droplet size increases. The higher mass surfactant component does not appear on the droplet surface immediately while many lower mass surfactants are solvated inside the droplet. However, such interfacial information is lost when using static SIMS, because the solvent cage is collapsed during sample drying. We have provided the first three-dimensional images of the evolving O/W interface and demonstrated that in situ surface chemical mapping is powerful to reveal the complex and dynamic L-L interface in the liquid state. Our observational insights suggest surfactants are important in mediating droplet growth and facilitating effective separation of bilgewater emulsion. To conclude, our recent findings demonstrate the importance of using in situ molecular imaging to study the evolving L-L interface and offer new insights into the physicochemical changes of emulsions.

## Spectroscopic Ellipsometry Technical Group Room C124 - Session EL1-MoM

### Big Data, AI and Analytical Methods

Moderators: **David Aspnes**, North Carolina State University, **Tino Hofmann**, University of North Carolina at Charlotte

8:20am **EL1-MoM-1 Ellipsometry Analysis Overview: Things We Can't Ignore**, *Nikolas Podraza*, A. Bordoalvos, University of Toledo; *P. Dulal*, N. Jayswal, M. Mainali, E. Miller, B. Shrestha, M. Tumusange, R. Collins, A. Shan, University of Toledo, United States Minor Outlying Islands (the

INVITED

Most spectroscopic ellipsometry measurements are relatively straightforward to make (but still must be done with care), however the analyses may not be straightforward even for seemingly simple samples. Appropriate and justifiable structural and optical property models must be developed to obtain meaningful information from measured

ellipsometric spectra. However, even after substantial time spent analyzing data all of us in the field ask: "Is this the correct model?" More complicated measurement configurations and simultaneous analysis of multiple sets of spectra can either help answer that question or make the situation even more challenging and uncertain. A follow up question also becomes "When do I stop?" Many of us have also spent long amounts of time (sometimes far more time than we should in retrospect) trying to describe small, nuanced features in our measured spectra that we simply can't ignore. To answer those questions, there are also things we can't ignore in the analyses of ellipsometric spectra including if the structural model makes sense; if the complex optical properties obtained are Kramers-Kronig consistent and appropriate for the type of material and spectral range measured; the extent of surface or interfacial layer effects and our ability to describe them meaningfully; and of course the parameters of interest to be extracted from our models, quality of fit, confidence limits, and correlation matrices. These considerations will be discussed for metallic, semiconducting, and dielectric thin film and bulk materials characterized by spectroscopic ellipsometry spanning the ultraviolet (UV) to terahertz (THz) range. This will include strategies for analyzing thin films with unknown optical properties, samples with complicated structures (and knowing when to stop), mapping spectroscopic ellipsometry data, and in situ real time spectroscopic ellipsometry data. Most examples we will discuss are materials used in thin film polycrystalline solar cells based on hybrid organic inorganic lead halide based perovskites, cadmium telluride, and copper indium gallium diselenide absorbers as well as spectroscopic ellipsometry characterization of complete, functional solar cells.

9:00am **EL1-MoM-3 Noise Reduction Using Linear and Nonlinear Filtering**, *Long V. Le*, Institute of Materials Science, Vietnam Academy of Science and Technology, Viet Nam

INVITED

If lineshape distortion and loss of information are not factors, linear low-pass filters are very effective at eliminating noise from spectra. However, achieving the balance among lost information, leaked noise, and Gibbs oscillations (ringing) can be difficult. Many linear filters are available that operate with direct-(spectral) space (DS) convolution. This approach is convenient, and endpoint discontinuities in value or slope have only local effects. However, intelligent linear filtering requires assessments in reciprocal-(Fourier) space (RS), capitalizing on the separation of information and noise into low- and high-index Fourier coefficients, respectively. Comparing the information content of the data to the RS transfer function of the filter is necessary if filtering is to be performed intelligently.

We recently quantified the tradeoff between reducing noise and preserving information by capitalizing on Parseval's Theorem to cast two DS measures of performance, mean-square error (MSE) and noise, into RS. This provides quantitative insight not only into the effectiveness of the various linear filters but also information on how they can be improved. The best practical linear filter was found to be the Gauss-Hermite filter introduced about 20 years ago by Hofmann and co-workers.

Nonlinear filters have an interesting history, which is reviewed briefly. Originally designed to "whiten" (sharpen) structure in spectra, a recent solution of Burg's equations allows the trend established by low-index Fourier coefficients to be extrapolated into the white-noise region in a model-independent way. This corrected-maximum-entropy (CME) filter achieves all 3 goals: information is left intact, noise is eliminated, and by eliminating apodization, ringing is also eliminated. Recent progress includes adapting the theory to filter general lineshapes. By introducing an enhancement factor in the ME equations, weak features can be discovered and structures enhanced without the complications inherent in Burg's original result. Examples will be provided throughout, along with MATLAB programs that perform the processes discussed.

9:40am **EL1-MoM-5 Numerical Ellipsometry: Artificial Intelligence Methods for Solving Ellipsometer Data**, *Frank Urban*, D. Barton, Florida International University

Ellipsometry is a material analytical method which works by measuring the change in polarization state of light reflecting from or transmitting through the material of interest. Desired parameters, such as thin film thickness and optical properties, are related by mathematical models to the measurements themselves. In the beginning those parameters were obtained by lookup using a printed table provided along with a commercial ellipsometer. This was followed by solution methods using a calculator and this evolved to the personal computer based programs that are in use today. Because a single ellipsometer measurement provides two real numbers, typically  $\Psi$  and  $\Delta$ , it can provide for determination of only two unknowns associated with the reflecting surface regardless of whether

# Monday Morning, November 6, 2023

other measurement modes are employed such as Mueller matrix forms. As a consequence it usually became necessary to make use of more than a single measurement at a single wavelength to obtain more than two parameters. Two of the ways forward are to take multiple measurements at each wavelength of interest to obtain data sufficiency and the other way is to take spectroscopic measurements with the aim of solving for optical constants as represented as various functions (fitting functions) of wavelength. For the spectroscopic approach the match to the Maxwell equations and to the selected "fitting functions" by which the number of unknowns is reduced hugely by the small number typically three or four per fitting function. Thus data sufficiency is achieved at the cost of requiring good selections of fitting functions which might not be unique. We have found, following earlier work, that current Artificial Intelligence methods in the form of Deep Learning or Artificial Neural Networks offers a new way to obtain solutions or at least to provide very accurate initial estimates from which numerical method solutions can reliably and accurately be determined. The work presented here both covers a two measurement method AI network at single wavelengths and spectroscopic measurements (a thousand or more) using fitting functions. Accuracy, speed, and ease of use will be demonstrated.

10:00am **EL1-MoM-6 Modeling Many-body Effects in Ge Using Pump-Probe Time-Resolved Spectroscopic Ellipsometry**, *Carlos A. Armenta*, New Mexico State University; *M. Zahradnik, M. Rebarz*, ELI Beamlines Facility, The Extreme Light Infrastructure ERIC, Czechia; *S. Espinoza*, ELI Beamlines Facility, The Extreme Light Infrastructure ERIC; *S. Vazquez-Miranda*, ELI Beamlines Facility, The Extreme Light Infrastructure ERIC, Czechia; *J. Andreasson*, ELI Beamlines Facility, The Extreme Light Infrastructure ERIC; *S. Zollner*, New Mexico State University

We analyze the transient dielectric function (TDF) of Ge at very high electron-hole pair densities via time-resolved spectroscopic ellipsometry. Through a pump-probe technique, the bulk Ge is photoexcited up to densities of around  $\sim 3 \times 10^{21} \text{ cm}^{-3}$ . We specifically focus on the  $E_1$  and  $E_1 + \Delta_1$  critical points and how their parameters such as energy and broadening change as a function of delay time.

Our analysis aims to model the TDF of Ge and describe its behavior at different carrier concentrations. In particular, it addresses phase-filling singularities that are usually difficult to study in implanted and annealed samples due to defects. High-power laser induced carriers can achieve density levels on undoped samples that are ideal for the study of many-body phenomena. The model also addresses other effects taking place during the excitation and relaxation of electrons, such as excitonic screening and acoustic phonon oscillations produced by the transferring of energy to the lattice.

## Spectroscopic Ellipsometry Technical Group

### Room C124 - Session EL2-MoM

#### Industrial Applications of Spectroscopic Ellipsometry

**Moderators:** *Andy Antonelli*, Nanometrics, *Stefan Zollner*, New Mexico State University

10:40am **EL2-MoM-8 Spectroscopic Ellipsometry and Reflectometry for Advanced Semiconductor Metrology**, *Shankar Krishnan*, KLA Corporation  
**INVITED**

This presentation will provide an overview of Spectroscopic Ellipsometry (SE) and Spectroscopic Reflectometry (SR) and how they enable KLA to provide advanced metrology solutions in the semiconductor industry. It will focus on both Film and Critical Dimension (CD) Metrology and provide an in-depth look into the latest hardware, algorithms and selected applications in Logic/Foundry and Flash/DRAM. Key hardware innovations including simultaneous multi-AOI ellipsometry, Vacuum Ultraviolet (VUV) – Infrared (IR) broadband ellipsometry, small-spot and ultra-high resolution optical designs will be discussed. We will show how a multi-Angle-of-incidence (AOI) SE contains unique spectral signatures in each AOI and in selected Mueller matrix elements to enable detailed measurements in shape and profiles in the Gate-All-Around (GAA) structures. We will demonstrate how a high-resolution optical system and a combined SE+SR signal are needed in order to be sensitive to changes within small regions (zones) of a 3D-NAND film stack. The value of Deep UV/VUV photons and the enhanced sensitivity to film thickness and film composition of high-K dielectric and threshold voltage layers will be described. This presentation will also touch on the use of SE/SR to measure emerging applications involving very large-pitch structures and on transparent substrates and waveguides. Lastly we will also

present a summary of recent advances in algorithms using model-based and model-assisted machine learning to solve critical metrology problems like GAA, hybrid bonding and focus-dose measurements.

11:20am **EL2-MoM-10 Ellipsometry in Industrial Applications**, *Andre Miller*, Intel  
**INVITED**

Optical Critical Dimension (OCD) metrology, the use of spectroscopic ellipsometry on patterned structures, is the dominant inline shape metrology technique in the semiconductor industry. The technique is used to output geometric parameters for the device patterns on the wafer. This information is used to control the line, to determine processing conditions at subsequent steps and to establish correlations to predict and improve performance and yield. The primary limitations are internal model parameter correlations and requirement for a periodic structure that may not accurately represent the structures of the device.

## Laboratory-Based Ambient-Pressure X-ray Photoelectron Spectroscopy Focus Topic

### Room B116 - Session LX+AS+HC+SS-MoM

#### Laboratory-Based AP-XPS: Advances in Instrumentation and Applications

**Moderators:** *Sylwia Ptasinska*, University of Notre Dame, *Heath Kersell*, Oregon State University

8:20am **LX+AS+HC+SS-MoM-1 Instrumentation for Electron Microscopy and Spectroscopy in Plasma Environment**, *Andrei Kolmakov*, NIST-Gaithersburg  
**INVITED**

Plasma-assisted processes are of principal importance for modern semiconductors microfabrication technology, catalysis, environmental remediation, medicine, etc. Understanding the chemical and morphological evolutions of the surfaces and interfaces under a plasma environment requires *operando* metrologies that have a high spatial, temporal, and spectroscopic resolution. Combining the APXPS system with ambient pressure scanning electron microscopy would, in principle, meet these needs. Here we review the status of the field and discuss the prospective designs as well as application examples of ambient pressure scanning electron microscopy and spectroscopy for *in situ* analysis and processing of the surfaces under plasma environments

9:00am **LX+AS+HC+SS-MoM-3 Scienta Omicron HiPPLab - A Lab-based APXPS Instrument for Probing Surface Chemical Reactions**, *Peter Amann*, Scienta Omicron, Germany

Investigating reaction intermediates, oxidation states, solid-liquid interfaces and buried interfaces under near ambient pressure conditions is highly desired in materials science applications. Ambient pressure X-ray photoelectron spectroscopy (APXPS) is a powerful method to investigate the chemical nature of surfaces and interfaces and has undergone a tremendous improvement in the last years. The development of the HiPP analysers allowed to overcome the one bar pressure regime without using pressure separating membranes. [1] [2]

During the past decade, increased attention has been shown to laboratory based APXPS system solutions, which is motivated by the 24/7 access capability and possibility for highly customized sample environments. Drawing on extensive experience in the fields of photoelectron spectroscopy, UHV technology, and system design, Scienta Omicron has designed the HiPPLab as an easy-to-use system that encourages user creativity through flexibility, modularity and an innovate chamber design. [3] It combines a state-of-the-art HiPP analyser with a high flux, variable focus X-ray source. Multiple options complement the HiPPLab offer, including a gas reaction cell, a preparation chamber, laser heating, or options for mass-spectroscopy. Using automated gas-flow controllers, experiments can be conducted in a controlled way. Future upgrade possibilities are given.

The HiPP-3 analyser features a 2D detector allowing for spatial resolved measurements with customer proven results down to 2.8  $\mu\text{m}$  resolution. The swift acceleration mode allows for high electron transmission without applying a sample bias. A sophisticated pre-lens design in which efficient pumping between two close-by apertures is implemented, allows dragging out corrosive gases or moisture, which would otherwise be detrimental to the instrument.

In this presentation, I will give an overview on our APXPS product portfolio focusing on laboratory based solutions and present application examples.

# Monday Morning, November 6, 2023

[1] Amann, et al. *Review of Scientific Instruments*, 2019 90(10)

[2] Takagi, et al. X-ray photoelectron spectroscopy under real ambient pressure conditions. *Applied Physics Express*, 2017, 10(7), 8–11.

[3] Scienta Omicron HiPPLab <https://scientaomicron.com/en>

9:20am **LX+AS+HC+SS-MoM-4 Using Microheaters for Time-Resolved APXPS and Correlated ETEM, Ashley Head**, Brookhaven National Laboratory; *B. Karagoz*, Diamond Light Source, UK; *J. Carpena-Nuñez*, Air Force Research Laboratory; *D. Zakharov*, Brookhaven National Laboratory; *B. Maruyuma*, Air Force Research Laboratory; *D. Stacchiola*, Brookhaven National Laboratory

With a rise in the number of lab-based APXPS systems, these instruments afford an opportunity to continue the development of multimodal and correlated capabilities for more comprehensive information of reactions at surfaces. Here I will discuss the methods of using an ETEM commercial microheater for collecting APXPS data on the same sample under identical conditions. A specialized holder was fabricated to use commercial microheaters on MEMS chips in a lab-based APXPS instrument. The rapid heating of the microheater enables a time-zero for collecting APXPS data with a time resolution of 500 ms. Proof-of-principle measurements following the oxidation and reduction of a Pd film demonstrate correlative experiments with TEM. The specialized holder was fabricated with the possibility of dosing gases locally to the sample surface while confined by a graphene membrane. Using the gas lines, the Pd film was oxidized under a partial pressure of air (~0.4 mbar). Overall, using this microheater in APXPS offers chemical information complementary to structural changes seen in ETEM. The rapid heating enables new opportunities in time-resolution and increased pressure for APXPS experiments.

9:40am **LX+AS+HC+SS-MoM-5 NAP-XPS Instrumentation Came a Long Way - Where Will Applications Lead Us from Here?**, *P. Dietrich, F. Mirabella, K. Kunze, O. Schaff, Andreas Thissen*, SPECS Surface Nano Analysis GmbH, Germany **INVITED**

Over the last fifty years significant developments have been done in photoelectron spectroscopy instrumentation and thus opened new fields of application. Especially XPS or ESCA developed into the most important standard surface analytical method in many laboratories for surface and materials characterization.

For the last fifteen years XPS under near ambient pressure conditions (NAP-XPS) has gained significant attention. Although invented as a laboratory method it initially started to grow at synchrotrons. The development of more efficient and sensitive electron analyzers and high-brilliance monochromated laboratory X-ray and UV sources running at pressures of up to 100 mbar finally brought it back to the individual laboratories. The reasons are the availability of individual infrastructure for sample preparation and handling, safety regulations and easier access to measurement time on a daily basis. Nowadays the vast majority of instruments worldwide are laboratory-based.

It opened the method XPS to liquids, solid-liquid interfaces, gas-solid-interfaces, gas-liquid-interfaces and many more. The development of instrumentation followed the important applications and besides the "active" components, mainly excitation sources and electron analyzers, a lot of developments have been done in the fields of sample environments, sample handling, system setup and automation and combination with other techniques and even in quantification of data. There are only a few applications left where experiments at synchrotron based beamlines and end stations offer the only solution.

The market driving applications nowadays are catalysis, electrochemistry, behaviour of liquid phases, biological samples and surface chemistry. Along these applications this presentation will show the existing instrumentation, discuss its limits and the perspective for near future developments to further increase the user base of laboratory based NAP-XPS systems to turn it into an integral part of the large routine analysis community.

10:40am **LX+AS+HC+SS-MoM-8 Evolution of Metal-Organic Frameworks in the Presence of a Plasma by AP-XPS and IRRAS**, *J. Anibal Boscoboinik*, Brookhaven National Laboratory and State University of New York at Stony Brook; *M. Ahmad*, Stony Brook University/Brookhaven National Laboratory; *M. Dorneles de Mello*, Brookhaven National Laboratory; *D. Lee*, Johns Hopkins University; *P. Dimitrakellis*, University of Delaware; *Y. Miao*, Johns Hopkins University; *W. Zheng*, University of Delaware; *D. Nykypanchuk*, Brookhaven National Laboratory; *D. Vlachos*, University of Delaware; *M. Tsapatsis*, Johns Hopkins University **INVITED**

Zeolitic imidazolate frameworks (ZIF), a class of metal-organic frameworks, are promising materials for various applications, including the separation and trapping of molecules and catalysis. Recent work has shown that exposure to plasma can result in the functionalization of the framework for tailored applications. This talk will report in-situ plasma studies of ZIF-8 as a model system. We will study the framework's evolution in the presence of N<sub>2</sub>, O<sub>2</sub>, and H<sub>2</sub> plasmas by combining lab-based ambient pressure XPS and infrared reflection absorption spectroscopy.

11:20am **LX+AS+HC+SS-MoM-10 Surface Degradation and Passivation in Perovskite Solar Cells**, *Wendy Flavell*, The University of Manchester, UK **INVITED**

There is an urgent requirement to make better use of the 120,000 TW of power provided by the Sun, by using it to generate power, or by using its energy directly to make useful chemical feedstocks. Around the world, there is an explosion of research activity in new systems for harvesting solar energy, including solar cells based organometal halide perovskites. Issues of key importance are the interfacial energy level line-up of the cell components, and the influence of the surface properties of these materials on charge separation in the devices. Indeed, the deployment of perovskites in solar cells is currently limited by their high reactivity and rate of surface oxidation. Thus, a key problem is to develop an understanding of the interface chemistry of solar heterojunctions in order to develop passivation strategies. I show how a combination of techniques including near-ambient pressure X-ray photoelectron spectroscopy (NAP-XPS) and hard X-ray photoelectron spectroscopy (HAXPES) may be used to investigate surface ageing and the surface degradation reactions[1-7], chemical composition as a function of depth[4,5], and to develop passivation strategies for perovskite solar cell heterojunctions[2,3,5-7].

## References

1. J C-R Ke, A S Walton, A G Thomas, D J Lewis, *et al.*, *Chem Commun* **53**, 5231 (2017).
2. J C-R Ke, D J Lewis, A S Walton, B F Spencer, *et al.*, *J Mater Chem A*, **6**, 11205 (2018).
3. C-R Ke, D J Lewis, A S Walton, Q Chen, *et al.*, *ACS Applied Energy Materials* **2**, 6012 (2019).
4. B F Spencer, S Maniyarasu, B P Reed, D J H Cant *et al.*, *Applied Surface Science* **541**, 148635 (2021).
5. S Maniyarasu, J C-R Ke, B F Spencer, A S Walton *et al.*, *ACS Applied Energy Materials* **13**, 43573 (2021).
6. S Maniyarasu, B F Spencer, H Mo, A S Walton *et al.*, *J Mater Chem A*, **10**, 18206 (2022).
7. D Zhao, T A Flavell, F Aljuaid, S Edmondson *et al.*, *ACS Applied Materials and Interfaces*, submitted.

## Nanoscale Science and Technology Division

### Room B113 - Session NS1+2D+BI+SS-MoM

#### Combined Nanoscale Microscopy

**Moderators:** *Adina Luican-Mayer*, University of Ottawa, Canada, *Sergei Kalinin*, Oak Ridge National Laboratory

8:20am **NS1+2D+BI+SS-MoM-1 Combined Metrology at the Nanoscale: Advanced Scanning Probe Microscopy to Evaluate Complex Semiconductors**, *Fernando A. Castro*, National Physical Laboratory, UK **INVITED**

The performance of semiconductors is strongly affected by spatial variations that can be introduced during manufacturing or due to degradation processes. In addition to the impact of microstructure and defects on electrical and optical properties, complex semiconductors, such as some compound semiconductors, perovskites or 2D materials, can present dynamic changes in properties during operation. Combining metrology methods is critical to better understand and characterise such

# Monday Morning, November 6, 2023

complex samples as individual methods provide insufficient information. Ideally these combined measurements should be either co-localised or simultaneous in order to reduce uncertainty associated with post process image registration, spatial heterogeneity, or sample contamination. NPL has been developing a suite of spatially resolved measurement methods to understand critical factors that impact semiconductor performance and reliability. In this presentation, we'll focus on nanoscale methods under controlled operational or environmental conditions, including advanced modes of scanning probe microscopy (SPM) such as time-resolved scanning kelvin probe (tr-SKPM) and tip enhanced optical microscopy (TEOS). After introducing the challenges and recent results from the European project PowerELEC, we'll present two examples of how these combined measurements are applied. First, we'll describe the application of SPM to understand degradation mechanisms in state-of-the-art perovskite solar cells (PSCs). Time-resolved SKPM can be used to distinguish the impact of ionic and electronic charges on dynamic processes and in-situ co-localised measurements under controlled environmental conditions can identify nucleation of nanoscale grains on the perovskite film surface at the start of the degradation process, allowing us to link degradation to the local electrostatic environment. The second example will focus on 2D transition metal dichalcogenide (TMD), which present promise for optoelectronic applications but are often limited by Fermi level pinning effects and consequent large contact resistances upon contacting with bulk metal electrodes. A potential solution for near-ideal Schottky–Mott behavior and concomitant barrier height control has been proposed in the literature by contacting TMDs and (semi-)metals in van der Waals heterostructures. We will show how combined nanoscale measurements allows to directly access interface parameters relevant to the Schottky–Mott rule on a local scale and how we use SKPM and TEOS measurements under simulated operational conditions (e.g. electrostatic doping induced Fermi levels) to enable decoupling and quantification of contributions from the interface dipole and electrode work function.

9:00am **NS1+2D+BI+SS-MoM-3 Correlated Functional Imaging of Printed and Ferroelectric 2D Devices for Ubiquitous Sensing and Neuromorphic Computing**, J. Kim, Z. Zhu, T. Chu, H. Choi, M. Moody, **Lincoln Lauhon**, Northwestern University

The unique properties of 2D materials stimulate the design of devices that exhibit useful new behaviors. However, the correspondence of expected and actual operating principles of devices cannot always be established from simple analysis of temperature-dependent current-voltage characteristics. As a result, the rational optimization of even simple devices such as thin-film transistors, as well as the successful realization of novel neuromorphic devices, benefits from spatially resolved characterization of nanoscale structure and properties to discern the relative contributions of device geometry and 2D material structure and chemistry to device performance. This talk will describe case studies in which Kelvin probe force microscopy (KPFM) and scanning photocurrent microscopy (SPCM) are used to investigate the operating principles of thin-film transistors (TFTs) and source-gated transistors (SGTs) fabricated from MoS<sub>2</sub> and In<sub>2</sub>Se<sub>3</sub>. In the case of n-type semiconducting 2H MoS<sub>2</sub>, model devices constructed from overlapping exfoliated flakes are analyzed to identify factors limiting the performance of printed thin-film transistors (*ACS Nano* 2023, **17**, 575). KPFM analysis is used to isolate the contact, channel, and junction resistances and calibrate a resistor network model of printed thin films. Simulations of the effective mobility and on-current dependence on flake thickness, size, and degree of overlap suggest that the performance of printed TFTs are limited by resistance arising from unpassivated edge states.

In the second use case, KPFM, SPCM, and piezoresponse force microscopy (PFM) are used to pinpoint the origin of resistance modulation in  $\alpha$ -In<sub>2</sub>Se<sub>3</sub> transistors that exhibit tunable non-volatile channel conductance. Memristive behavior in In<sub>2</sub>Se<sub>3</sub> TFTs has been attributed to switching of the channel polarization, but the lack of an obvious threshold for switching raises questions about the evolution of domain structure and the contribution of trap states. Furthermore, the presumed modulation of the Schottky barrier has yet to be confirmed experimentally. We address this gap in understanding through correlated PFM, KPFM, and SPCM measurements. We then fabricate MoS<sub>2</sub>-In<sub>2</sub>Se<sub>3</sub> transistors with a geometry that induces depletion at the source electrode, i.e. a source-gated transistor, and observe non-volatile switching of the low output current. KPFM, SPCM, and finite element simulations are used to confirm source pinch-off and non-volatile multi-level modulation of the effective source resistance. The quantitative correlation of device behaviors with the changes in channel potential at key interfaces usefully constrains the

interpretation of the operating principles and builds a foundation for rational design of novel neuromorphic devices and systems.

9:20am **NS1+2D+BI+SS-MoM-4 A Unique New Correlative Microscopy Platform for Combined Nanoscale Microscopy by Combination of AFM and SEM**, **Chris Schwab**, Quantum Design Microscopy GmbH, Germany; K. Arat, Quantum Design, Inc.; H. Alemansour, A. Alipour, Quantum Design, Inc., Iran (Islamic Republic of); A. Amann, Quantum Design, Inc., Germany; L. Montes, Quantum Design, Inc., Colombia; J. Gardiner, Quantum Design, Inc.; H. Frerichs, L. Stuehn, S. Seibert, Quantum Design Microscopy GmbH, Germany; S. Spagna, Quantum Design, Inc.

The combination of different analytical methods into one instrument is a powerful technique for the contemporaneous acquisition of complementary information. This is especially true for the in-situ combination of atomic force microscopy (AFM) and scanning electron microscopy (SEM), two of the most powerful microscopy techniques available. This combination gives completely new insights into the nanoscale.

In this work, we introduce a highly integrated new correlative microscopy platform, the FusionScope, that seamlessly combines AFM and SEM within a unified coordinate system. The self-sensing piezoresistive cantilever technology used for the AFM scanner results in a purely electrical measurement of the cantilever deflection signal. This allows for concurrent, correlated acquisition of both SEM and AFM images at the region of interest. In addition, a three-axis sample stage and a trunnion provide unique experimental capabilities such as profile view – an 80-degree tilt of the combined sample stage and AFM giving full SEM access to the cantilever tip region.

We will present a variety of novel case studies to highlight the advantages of this new tool for interactive, correlative, in-situ nanoscale characterization for different materials and nanostructures. First results will focus on hard-to-reach samples. FusionScope allows for fast and easy identification of the area of interest and precise navigation of the cantilever tip for correlative SEM and AFM measurements. We demonstrate that approach for analysis of blade radius of razor blades and the characterization of lacunae structures on bone surfaces.

In addition, we will present first results for the in-situ characterization of individual nanowires that will be used for energy harvesting applications. The SEM enables the easy location of individual or multiple nanowires, whereas the in-situ AFM allows the characterization of topography, surface roughness, mechanical, and electrical properties of the nanowire.

Based on the broad variety of applications regarding the inspection and process control of different materials and devices, we anticipate that this new inspection tool to be one of the driving characterization tools for correlative SEM and AFM analysis in the future.

9:40am **NS1+2D+BI+SS-MoM-5 Correlative *in-Situ* Nanoscale Microscopy Using AFM and FIB-SEM for Nanomechanical Property Mapping Throughout a 3D Volume**, **Prabhu Prasad Swain**, M. Penedo, N. Hosseini, M. Kangül, S. Andany, N. Asmari, G. Fantner, Ecole Polytechnique Fédérale de Lausanne (EPFL), Switzerland

In this work, we present results obtained with an atomic force microscope (AFM) integrated in a focused ion beam- scanning electron microscope (FIB-SEM). The FIB-SEM is a powerful instrument, capable of automated structural analysis and prototyping at nanometer resolution, while the AFM is a well-established versatile tool for multiparametric nanoscale characterization. Combining the two techniques allows unprecedented *in-situ* correlative analysis at the nanoscale. Nanoprototyping and enhanced multiparametric analysis can be performed without contamination of the sample or environmental changes between the subsequent processing steps. The power of the combined tool lies in the complementarity of the two techniques. The AFM offers nanomechanical property mapping with electrical and magnetic characterization of the sample, while SEM offers elemental analysis and FIB enables thin slicing of the sample for block face imaging. This enables 3D tomographic imaging of complex samples mapping composition and mechanical properties throughout the 3D volume. Controlling both these instruments with open-hardware controller (OHC), allows us to perform automated *in-situ* AFM-FIB-SEM characterization. The setup is aimed to provide true 3D correlative information and mapping, with increased resolution for a larger volume. We will demonstrate the capabilities of correlative AFM/SEM/FIB imaging through a series of correlative experiments on polymers, 2D materials, nanowires and rock sediments.

# Monday Morning, November 6, 2023

10:00am **NS1+2D+BI+SS-MoM-6 Anisotropic Friction Effects of Perovskite Nanoplatelets on a vdW Substrate**, *Sidney Cohen, N. Itzhak, I. Rosenhek-Goldian, O. Brontvein, E. Joselevich*, Weizmann Institute of Science, Israel

Interest in 2D materials can be attributed to their unique properties such as electrical, optical, and mechanical characteristics, which can be harnessed in small devices. Assembly of these materials can be challenging. vdW epitaxy is a promising approach, in which nano-sized crystalline structures are grown on a 2D vdW substrate which has minimal interaction energy, resulting in low strain. The epitaxial growth still provides sufficient interaction to favor specific geometries according to lattice directions. In this presentation, the system is CsPbBr<sub>3</sub> platelets grown on vdW ReSe<sub>2</sub>. This combination is of fundamental and applied interest due to special optoelectronic properties of these 2D-3D mixed semiconductor systems. The mechanism of the nanoplatelet growth leading to their shape and orientation on the surface remains to be fully revealed. Here, we present tribological studies performed by monitoring the force required to push the platelets along the surface. We observed a significant directional effect expressed in the lateral forces required to slide the platelets along the surface. In particular, forces 4-5 times those required to push rectangular platelets along the ReSe<sub>2</sub> surface along the long axis were insufficient to move the same platelets along their short axis. STEM images showed that this correlated with commensurability of the two lattice structures. Some of the experiments were performed in an ambient AFM system. Because sliding along the surface can be hindered by atomic steps and defects, unbiased analysis of this effect requires searching for small steps of atomic height along the sliding path. Scanning electron microscopy is a convenient way to search for these defects: thus, comparative experiments were performed in-situ in a combined AFM-SEM system. This combination had the additional advantage of allowing rapid overview of the surface to locate regions of interest.

In the process of evaluating the measurements, those performed in vacuum required much higher (by as much as an order of magnitude) forces to support pushing along the surface in comparison with comparable measurements made in the ambient AFM system. These measurements will be presented in the context of the characterization of the 2D substrate and platelet nanostructure as revealed by the two correlative measurement techniques.

## Nanoscale Science and Technology Division Room B113 - Session NS2+2D+BI+EL+SS-MoM

### Chemical Identification with Scanning Probe Microscopy

**Moderators:** *Sidney Cohen*, Weizmann Institute of Science, Israel, *Harald Plank*, Graz University of Technology

10:40am **NS2+2D+BI+EL+SS-MoM-8 Nanoscale imaging with photo-induced force microscopy**, *Eric Potma*, University of California Irvine  
**INVITED**

Imaging with molecular contrast at the nanoscale is important for a myriad of applications, yet it remains a technical challenge. Over the past two decades, various flavors of optical spectroscopy combined with atomic force microscopy have been developed, each offering hope for a more routine nanospectroscopy technology. One of these approaches is photo-induced force microscopy (PiFM), a non-contact scan probe technique that is sensitive to the light-induced polarization in the material. PiFM has been used to generate molecular maps with 5 nm resolution, based on absorption contrast or on contrast derived from nonlinear optical interactions. Nonetheless, questions remain about the origin of the signal, in particular the possible contribution of forces that result from the thermal expansion of the sample. In this presentation, we will discuss various physical mechanisms that contribute to the PiFM signal and highlight several applications that are unique to the PiFM technique.

11:20am **NS2+2D+BI+EL+SS-MoM-10 Near-field Optical Microscopy Imaging and Spectroscopy at 10nm Spatial Resolution**, *Artem Danilov*, Attocube Systems Inc.

Fourier-transform infrared (FTIR) spectroscopy is an established technique for characterization and recognition of inorganic, organic and biological materials by their far-field absorption spectra in the infrared fingerprint region. However, due to the diffraction limit conventional FTIR spectroscopy is unsuitable for measurements with nanoscale spatial resolution. Scattering-type Scanning Near-field Optical Microscopy (s-SNOM) allows to overcome the diffraction limit of conventional light microscopy or spectroscopy enabling optical measurements at a spatial resolution of

10nm, not only at IR frequencies but also in the whole spectral range from visible to terahertz. s-SNOM employs an externally-illuminated sharp metallic AFM tip to create a nanoscale hot-spot at its apex. The optical tip-sample near-field interaction is determined by the local dielectric properties (refractive index) of the sample and detection of the elastically tip-scattered light yields nanoscale resolved near-field images simultaneous to topography. Use of material-selective frequencies in the mid-IR spectral range can be exploited to fully characterize polymer blends or phase change polymers with nanometer-scale domains. Quantification of free-carrier concentration and carrier mobility in doped semiconductor nanowires, analysis of 2D (graphene) nanostructures, or study phase propagation mechanisms in energy storage materials is achieved by amplitude- and phase-resolved near-field imaging. Furthermore, here we introduce correlative tip-enhanced nanoscopy, enables complete colocal vibrational analysis of both IR- and Raman-active modes at the same spatial scale. Our instrument allows for a straight-forward implementation of nano-PL measurements using background suppressing provided by the demodulation of detector signal utilized in nano-FTIR detection scheme. Combining Raman, TERS, nano-FTIR and nano-PL measurements in the same instrument significantly reduces the effort of correlating the resulting datasets, enabling complete optical analysis at nanoscale, which has not been possible so far.

11:40am **NS2+2D+BI+EL+SS-MoM-11 Correlative Nanoscale Chemical, Mechanical and Electrical Property Mapping on a Single AFM-IR Platform**, *C. Li, Martin Wagner, C. Phillips*, Bruker Nano Surfaces Division

Chemical identification on the nanoscale is a long sought after capability from the inception of AFM. AFM-IR has proven to be uniquely successful in achieving this among all other attempts. It uses a mid-IR laser that is focused onto the AFM tip. Light absorption by the sample results in photothermal expansion that causes a detectable cantilever deflection change of the AFM probe. The obtained IR spectra correlate with conventional FTIR spectroscopy but are associated with sub-10nm spatial resolution.

However, a single data set rarely tells the full story and multiplexed analysis is essential to fully understand a material. We use an AFM-IR microscope with image registration and overlay capability to return to the same position on a sample when changing AFM probes, enabling extensive multimodal analysis. Data on a two-component polymer sample PS-LDPE comprising polystyrene and polyethylene reveals nanoIR spectra that correlate well with FTIR, while nanoIR maps at different IR wavenumbers provide the spatial distribution of each component. Further, we show that they are directly correlated at the nanometer level through PeakForce QNM elastic modulus and adhesion maps, as well as work function (surface potential) and dielectric maps with FM-KPFM (frequency-modulated Kelvin probe force microscopy). Many of the properties can be conveniently obtained simultaneously, while others are preferably obtained sequentially in a colocalized manner with the optimal probe choice and parameter settings for each AFM mode. Data on real-world industrial samples is then discussed, e.g. SBR (styrene-butadiene rubber) with carbon-black additives for car tires, exemplifying how ratio-map and multimodal property mapping unravel information not seen through one technique alone. In another use case chemical identification is complemented by nDMA, a mode where viscoelastic nanoscale sample properties are measured that match bulk dynamic mechanical analysis (DMA) data.

## Plasma Science and Technology Division Room A106 - Session PS+TF-MoM

### Plasma Processing for Advanced Emerging Memory Technologies

**Moderators:** *Harutyun Melikyan*, Micron Technology, *Jeffrey Shearer*, TEL

8:20am **PS+TF-MoM-1 IBE Patterning and Characterization of High Density STT-MRAM at Pitch 50nm and MTJ CD 20nm**, *Romuald Blanc, L. Souriau, K. Wostyn, S. Couet, F. Lazzarino*, IMEC, Belgium

Spin Transfer Torque Magnetic Random Access Memory (STT-MRAM) is a promising non-volatile memory technology that offers high-density storage, low power consumption, and fast read/write operations. One potential application of STT-MRAM is as a last level cache (LLC) in computer systems, since it can offer higher performance, lower power consumption, and higher scaling potential than traditional SRAM. However, the patterning of STT-MRAM with Ion Beam Etching (IBE) at CD 20nm and pitch 50nm presents several challenges such as high aspect ratio, damaged magnetic-

tunneling junction (MTJ) and sidewall shorts[1,2]. IBE relies on physical ion sputtering which does not allow high selectivity to the hard mask, therefore the choice of the hard mask stack is crucial to avoid excessively high aspect ratio[3]. In this study, we use a hybrid hard mask composed of high-density diamond-like carbon (DLC) to increase etch selectivity and TiN which becomes the STT-RAM top electrode.

In this talk, we present the magnetic and electrical results obtained for STT-MRAM at pitch 50nm using multiple process conditions of IBE main etch, sidewall clean and post-oxidation. We demonstrate that the etch parameters have a significant impact on device yield, with the best condition leading to a wafer-level yield of 95% functional devices with Tunnel Magnetoresistance (TMR) higher than 100%. On the best devices, we measure a TMR of 170% which corresponds to the TMR value before MTJ patterning. Finally, we report a switching current of 20 $\mu$ A with low dependence on pulse width from 5 to 20ns which is consistent with a MTJ CD of 20nm.

## References:

[1] Lei Wan et al, *Fabrication and Individual Addressing of STT-MRAM Bit Array With 50 nm Full Pitch*, IEEE TRANSACTIONS ON MAGNETICS, VOL. 58, NO. 5, MAY 2022

[2] Murat Pak et al, *Orthogonal Array Pillar Process Development for High Density 4F2 Memory Cells at 40nm Pitch and Beyond*, SPIE Advanced Lithography 2022, Paper 12051-45

[3] Kuniaki Sugiura et al, *Ion Beam Etching Technology for High-Density Spin Transfer Torque Magnetic Random Access Memory*, Japanese Journal of Applied Physics 48 (2009) 08HD02

8:40am **PS+TF-MoM-2 Cryogenic Etching by Physisorption of Neutrals for High-Aspect-Ratio Contact**, *Masahiko Yokoi, R. Suda, K. Tanaka, M. Tomura, K. Matsushima, Y. Ohya, M. Honda, Y. Kihara*, Tokyo Electron Miyagi Limited, Japan

The most crucial challenge in High-Aspect-Ratio (HAR) dielectric etching is supplying both ions and etchants [1] at the same rate to the etch front. If a large amount of etchant supplied to bottom of the feature is consumed by sufficient ion bombardment, higher aspect ratio etching with superior etching rate can be achieved. Conventional HAR processes which rely on the formation of radicals utilize fluorocarbon and hydrofluorocarbon gases combined with high-applied bias power. However, the stable chemisorption of radicals on feature sidewalls decreases the radical flux at the etch front, which results in a lack of radical supply and a drastic etch rate attenuation in the high aspect region. A technological breakthrough has long been required to solve this problem.

In this work, we focus on neutral physisorption at cryogenic temperatures. There have been several reports on plasma etching in the cryogenic temperature regime [2, 3], but the mechanism has not yet been well understood nor implemented for HAR dielectric etching. We have evaluated a novel etchant in cryogenic temperature and discovered a synergy between hydrogen fluoride (HF) as the etchant and HAR etching process. The dielectric etch rate strongly correlates with the physisorption of the HF, enhanced in the cryogenic temperature regime. The direct injection of HF as the process gas yields higher partial pressure and increased flux compared to radical flux formed by plasma reaction in vapor phase. Furthermore, we confirmed that the phosphorous-containing gas acts as an effective catalyst in the HF reaction. The phosphorous-containing gas stabilizes the HF or etchant physisorption on the SiO<sub>2</sub> film, which provides an etch rate enhancement at cryogenic temperature. In this conference, we will present a detailed surface reaction model.

Applying this innovative process to HAR etching enables a higher etch rate, higher selectivity, and higher aspect ratio etching capability. This novel process will enable the manufacturing of next-generation 3D NAND flash memory devices.

[1] K. Ishikawa, et al., Jpn. J. Appl. Phys. Vol. 57, No. 6S2, 06JA01, (2018).

[2] T. Ohiwa, et al., Jpn. J. Appl. Phys. Vol. 31, p.405, (1992).

[3] R. Dussart, et al., J. Phys. D: 47123001, (2014).

9:00am **PS+TF-MoM-3 Plasma Etching Processes Challenges in Emerging Non-Volatile Memories**, *C. Boixaderas, T. Magis, C. Socquet, A. Roman, B. Martin, CEA-LETI, France; B. Fontaine, P. Gouraud, STMicroelectronics, France; J. Dubois, STMicroelectronics, France; N. Posseme, STMicroelectronics, France; L. Grenouillet, C. Jahan, G. Navarro, G. Bourgeois, M. Cyrille, Thierry Chevolleau, CEA-LETI, France* **INVITED**

Since the appearance of flash memory in 1980s, the non-volatile memory (NVM) market is in constant evolution. Nowadays the random access memory (RAM) market is divided into two categories: standalone memories and embedded memories that are integrated into the core CMOS. Since the 2010s, new non-volatile embedded memories are emerging to achieve specific performances in terms of storage, speed, endurance and retention. Such advanced memories are based on resistive (RRAM), material phase change (PCRAM), magnetic (MRAM) and ferroelectric (FeRAM) properties. An overview of the main advanced memory technologies will be presented (operation principles, materials and investigated multilayers stacks).

We will address the patterning challenges that we are facing for the integration of the advanced non-volatile memories. We will mainly focus on the etching and stripping development in terms of scaling down, profile control and plasma induced damages on features sidewalls. The etch process optimization to control the profile and potential technological solutions to minimize plasma damages will be also presented and discussed in terms of plasma surface-interaction.

9:40am **PS+TF-MoM-5 Principle and Application of Etching Lag Mitigation in High Aspect Ratio Contact Process**, *Kyungsoo Chung, H. Kim, S. Park, J. Min, K. Yoon, B. Kuh*, Samsung Electronics, Republic of Korea

High Aspect Ratio Contact (HARC) etching is associated with various defects, such as random bending, global tilting, hole distortion, and vertical CD reduction. Depth loading, in particular, is significant and is intricately linked to all these issues. The implementation of a cryogenic process with specific gases has been verified to increase the initial etch rate by nearly threefold compared to the high-temperature process. Furthermore, this procedure has also amplified the patterned aspect ratio where etching lag is observable, in addition to increasing the etch rate. We engage in a comprehensive review and investigation of the mechanisms contributing to the improvement of etching lag. Firstly, it is essential to attain a substantial physisorption amount of neutrals, including radicals, while concurrently delivering highly directional ion energy to activate the surface. Additionally, the transport of neutrals within the hole is crucial for the etchant to be effectively adsorbed up to the etch front. We argue that elements such as a cryogenic environment, low-molecular-weight etchants, compounds that facilitate surface reactions, and a distribution of highly energetic ions are vital for overcoming depth loading. Ultimately, we propose advanced strategies for next-generation HARC etching, based on the lag reduction mechanisms.

10:00am **PS+TF-MoM-6 Etching Selectivities of SiO<sub>2</sub> and SiN Against  $\alpha$ -C Films Using CF<sub>4</sub>/H<sub>2</sub> with a Pseudo-Wet Plasma Etching Mechanism**, *Yusuke Imai, S. Hsiao, M. Sekine, T. Tsutsumi, K. Ishikawa*, Nagoya University, Japan; *M. Iwata, M. Tamura*, Tokyo Electron Ltd., Japan; *Y. Iijima*, Tokyo Electron, Japan; *T. Gohira, K. Matsushima, Y. Ohya*, Tokyo Electron Ltd., Japan; *M. Hori*, Nagoya University, Japan

With the advancement of cloud computing and AI technology, there is a growing demand for high-speed processing of large amounts of data and high-capacity storage. To manufacture 3D NAND, it is necessary to etch the layer structure where SiO<sub>2</sub> and SiN layers are alternately stacked, utilizing the amorphous C layer as a mask. A continuous increase of interest using cryogenic etching for high aspect ratio structure can be observed. Recently, etch selectivities among SiO<sub>2</sub>, SiN and poly-Si with CHF<sub>3</sub>/Ar and an ultra-high speed etch process at cryogenic temperature for 3D NAND have also been reported.<sup>[1,2]</sup> However, the cryogenic etching on variation of selectivities among SiN and SiO<sub>2</sub> over  $\alpha$ -C have not been discussed yet. In this study, the etching selectivity among SiO<sub>2</sub>, SiN and  $\alpha$ -C was investigated by varying the hydrogen content (20 to 60 %) in CF<sub>4</sub>/H<sub>2</sub> plasma at substrate temperature ( $T_s$ ) of -60 and 20 °C. A capacitively coupled plasma reactor was used in the experiments. The total flow rate of gas mixture of CF<sub>4</sub> and H<sub>2</sub> was set at 150 sccm and the pressure during process was fixed at 4 Pa. As shown in the supplementary file, at  $T_s = 20$  °C, the both ER of SiO<sub>2</sub> and SiN films decreased with increasing the hydrogen content, which is consistent with previous studies. Contrarily, for  $T_s = -60$  °C the ER of SiO<sub>2</sub> reached its maximum at around 30-40% hydrogen additives, while the ER value of SiN decreased by nearly half compared to that at 20 °C. As a

# Monday Morning, November 6, 2023

consequence, the etching selectivity of SiO<sub>2</sub>/SiN at 20 °C was found to be less than 1 for all hydrogen contents, indicating that SiN was preferentially etched. For T<sub>s</sub> = -60 °C it exhibited values greater than unity with the same process. This demonstrates that surface reactions and etching mechanism were changed when substrate was cooled. On the other hand, for *α*-C films increasing the hydrogen content in the CF<sub>4</sub>/H<sub>2</sub> plasma results in a transition from etching to deposition. The transition point was found to be H<sub>2</sub> additive of around 50% at 20 °C and around 30% at -60 °C, indicating a wider process window with infinite etching selectivities of SiO<sub>2</sub>/SiN over *α*-C mask at low T<sub>s</sub>. The etching characteristics at low temperature is correlated to the surface reactions between the films and neutral HF, based on the results of HF molecular density during plasma discharge using FTIR. A pseudo-wet etching mechanism was proposed to explain the obtained results. The bias power was also varied to investigate the etching behavior further at cryogenic temperature.

[1] R. Dussart *et al.*, *J. Appl. Phys.* **133**, 113306 (2023).

[2] Y. Kihara *et al.*, VLSI symposium T3-2 (2023)

## 10:40am PS+TF-MoM-8 Enhancing Etching Processes at Lower Wafer Temperatures: New Insights into Chemical and Physical Mechanisms, Thorsten Lill, Clarycon Nanotechnology Research, Inc. INVITED

Lower temperatures hold significant importance for etching advanced memory devices. In this presentation, we provide a comprehensive overview of the chemical and physical processes involved in etching at lower wafer temperatures. Traditionally, plasma etching techniques heavily rely on the generation of radicals that readily chemisorb onto the surface. However, at low temperatures, molecules tend to adsorb through physisorption, lacking the necessary energy to overcome the energy barrier required for a chemical reaction. However, the concentration of neutrals in typical plasma used for semiconductor manufacturing is notably higher (by one to two orders of magnitude) than that of radicals. At lower temperatures, the physisorption of neutrals becomes significant, increasing their concentration on the surface and contributing to the etching process once chemically activated by energy from the plasma<sup>1</sup>.

Etching of high aspect ratio structures utilizes ions and neutral reactive species that must effectively traverse through high aspect ratio features to reach the etch front. We present computational results on neutral transport within such features, exploring the influence of aspect ratio, profile shape, and surface processes including adsorption, desorption, and diffusion of neutral species. Our findings indicate a substantial increase in the steady-state transmission probability with the introduction of surface diffusion<sup>2</sup>. While spontaneous and collision-induced desorption of adsorbed neutrals alone do not alter the steady-state transmission probability, they do impact the time required to reach it. However, in the presence of surface diffusion, spontaneous desorption enhances the transmission probability, whereas desorption resulting from collisions with co-flowing nonreactive gas reduces it. These results unveil the potential for enhancing neutral transport at low surface temperatures, facilitated by physisorption and surface diffusion mechanisms.

By shedding light on the intricate interplay between chemical and physical phenomena during etching processes at lower temperatures, this presentation provides insights into the optimization of etching techniques for advanced memory devices.

<sup>1</sup>T. Lill, I. L. Berry, M. Shen, J. Hoang, A. Fischer, T. Panagopoulos, J. P. Chang, and V. Vahedi, *J. Vac. Sci. Technol. A* **41**, 023005 (2023).

<sup>2</sup>T. Panagopoulos, T. Lill, *J. Vac. Sci. Technol. A* **41**, 033006 (2023)

## 11:20am PS+TF-MoM-10 High Selectivity Etching via Pulsed Selective Deposition, André Amend, M. Yakushiji, K. Kuwahara, Hitachi High-Tech, Japan

Semiconductor device structures are shrinking and increasing in verticality, thus requiring novel plasma dry-etching processes to manufacture high Aspect-Ratio (AR) profiles on nanometer scales. Fabrication of such devices requires hard masks (HM) with high etching resistance that have small Critical Dimension (CD) and large height, corresponding to the needs of the device dimensions. As a result, creating the HMs themselves becomes more expensive and requires costly multi-layer processes to deal with the relatively low etching resistance of the C-rich photomask, which transfers the device pattern via photolithography. HM fabrication could be significantly simplified by an etching process that selectively etches hard materials, such as SiO<sub>2</sub>, even under soft C-rich masks.

Here, a Phase Mask Reconstruction Process (P-MRP) is introduced, that drastically increases the SiO<sub>2</sub> etching selectivity and is compatible with

small CD structures. P-MRP allows control of the C-based mask shape while etching SiO<sub>2</sub> via a time-modulated bias voltage, that tunes separate selective mask deposition and sample etching phases with a frequency up to above 1000 Hz. While a high voltage is applied to the sample, high-energy ions promote etching, whereas deposition occurs during the low voltage phase. Preferential deposition on the mask is achieved via chemical selectivity and radical shading due to the mask AR.

By precise control of the time-modulated sample bias voltage to adjust etching and deposition phases, the etching selectivity, as well as the mask shape and stability, can be controlled, which is critical to processing small patterns. To achieve high selectivity, the net etching rate on top of the mask can be decreased by reducing average ion energy, while controlling the mask side-deposition rate via the maximum ion energy and duration of the deposition phase. Since P-MRP rapidly alternates mask etching and mask passivation (during the deposition phases) low pattern roughness is achieved as well. For Line/Space and Hole patterns with CD 16-26 nm, etching selectivity as high as 10 was demonstrated while etching a depth of up to 200 nm of SiO<sub>2</sub>, with AR of up to about 10.

This result indicates that P-MRP could be used to simplify and accelerate HM fabrication. Furthermore, since deposition selectivity is also achieved through AR shading, it can be adopted to process materials other than C-masks and SiO<sub>2</sub> etching targets, as well.

## Quantum Science and Technology Mini-Symposium Room B110-112 - Session QS+EM+TF-MoM

### Materials for Quantum Computation and Quantum Information

**Moderators:** Robert Grubbs, IMEC Belgium, Dave Pappas, Rigetti Computing

### 8:20am QS+EM+TF-MoM-1 High Stability Metal-Based Single Electron Transistors for Silicon Quantum Dot Charge Sensors, Runze Li, University of Maryland College Park; P. Namboodiri, NIST-Gaithersburg; Y. Hong, N. Ebadollahi, University of Maryland College Park; J. Pomeroy, NIST-Gaithersburg

Extremely stable metal-based single electron transistors (SETs) are fabricated using a plasma oxidation technique, resolving the time stability problem that has been a major disadvantage for metal-based SETs. Metal-based SETs were studied extensively ~20 years ago, but were abandoned due to the much worse instability in the charge sensing results compared to Si-based SETs. The most severe instability was a low-frequency noise called "charge offset drift," which causes random and unreproducible readout. Our goal is to produce high stability aluminum-based SETs using plasma oxidation and couple them to Si-based QDs as the charge sensor. The plasma oxidation reduces the two-level defects in the tunnel junction, and we consequently gain a significantly lower charge offset drift of  $\Delta Q_0 = 0.13 e \pm 0.01 e$  in 7 days compared to  $\Delta Q_0 > 1 e$  in 1 day for thermally oxidized Al-SETs in the literature. However, we are only able to get an output current of ~4 pA during our measurements, which is insufficient as a charge sensor. Our current goal is to increase the output current to ~100 pA (similar to the level of Si-based SETs) by lowering the resistance of the AlOx tunnel junctions. Increasing the tunnel junction area will decrease the resistance, but also increase capacitance, so we are reducing the oxidation time from 7 seconds (which is the oxidation duration for the stabilized SETs being made) to 3 seconds, to reduce the resistance of the tunnel junction by ~10 times.

### 8:40am QS+EM+TF-MoM-2 High-quality and High Deposition Rate Atomic Layer Deposition of NbN and TiN for Superconducting Quantum Applications, H. Knoops, Oxford Instruments Plasma Technology, Netherlands; L. Bailey, D. Besprozvanny, M. Powell, Oxford Instruments Plasma Technology, UK; Russ Renzas, Oxford Instruments Plasma Technology

Due to the potential of excellent film control, uniformity, and conformality, atomic layer deposition (ALD) is seen as very promising for quantum devices where interface and material quality and their uniformities are a big challenge. Furthermore, for superconducting circuits, the deposition rate of ALD can be an issue, since a high enough film thickness (> 50 nm) is needed to minimize kinetic inductance effects on resonator frequency and where the shielding effectiveness of superconducting vias for crosstalk mitigation depends on film thickness and film conformality in the 3D structures. The challenge here is to deliver sufficiently fast processes while maintaining the desired film properties.

# Monday Morning, November 6, 2023

Here, we will share our recent development of a high-quality superconducting NbN and TiN for quantum applications, such as resonators and interconnects, capable of depositing > 50 nm film thickness in two hours. The RF-driven remote plasma source design and chamber of our system is optimized for ALD and allows for deposition rates which are > 3x faster than conventional substrate-biased plasma ALD deposition of similar materials.

The quality of the deposited films was demonstrated to be excellent, as measured by four-point probe electrical resistivity, conformality (100% on 8:1 trench for NbN, verified by SEM), and superconducting transition temperature ( $T_c$ ). Good superconductive properties of the film were demonstrated by SQUID measurements. Thickness uniformity of  $< \pm 5\%$  across a 150 mm Si wafer was achieved with good repeatability. We will also show how stress can be tuned as a function of process parameters, such as the RF source power.

Emerging quantum technologies based on superconducting nitride materials are showing great promise and will benefit not only from the uniformity of the deposition, conformality and film quality, but also from the speed and control provided by this ALD process.

**9:00am QS+EM+TF-MoM-3 Navigating MBE Growth of Atomically Precise Complex Oxides using Source Chemistry, Bharat Jalan, University of Minnesota, USA**

**INVITED**

From its beginnings as a successful method for III-V semiconductor growth to today for the growth of many contenders for next-generation electronics, spintronics and quantum devices, molecular beam epitaxy (MBE) has been very successful. However, several challenges exist for metal oxide growth where a metal is hard-to-oxidize and/or difficult to evaporate/sublimate. In this talk, I will review these issues and will present my group's effort to address these challenges using a novel solid-source metal-organic MBE approach. We show, for the first time, controlled synthesis of metal and metal oxides of these "stubborn" elements with the *same ease and control* as afforded by III-V MBE. We will present detailed growth study utilizing chemistry of source materials as a controlling knob to navigate synthesis. With the goal to understand and control electronic ground states in defect-managed complex oxide films and nano-membranes, we will discuss how chemistry of source materials can be used to navigate synthesis on-demand.

**9:40am QS+EM+TF-MoM-5 Atomic Layer Deposition of Superconducting Titanium Nitride for Through-Silicon-Via Structures and Photon Detection, John Femi-Oyetero, H. LeDuc, P. Day, M. Dickie, F. Greer, Jet Propulsion Laboratory (NASA/JPL)**

Superconducting detectors (SDs) play a crucial role in solving various problems in astronomy and cosmology, including dark matter, exoplanet transit spectroscopy, quantum computing and information. An example of such devices is the microwave kinetic inductance devices (MKIDs). This device has been employed in answering questions about the first light emitted after the big bang approximately 14 billion years ago. SDs make use of thin films of superconducting materials, such as titanium nitride (TiN), because of their high intrinsic kinetic inductance (KI) and large London penetration depth, which makes them particularly interesting and useful. In this study, we demonstrate the atomic layer deposition (ALD) of high-quality TiN with high transition temperature ( $T_c$ ) and KI suitable for large photon detector arrays and high-density through-silicon-via (TSV) structures. ALD-TiN provides an alternative and reliable source of high-quality films for scarce high-quality sputtering targets. Additionally, these films are expected to be more uniform than reactive sputtered films, which is crucial for cm-scale detector arrays, increasing the absolute detector yield on each wafer. We explored various precursors, gas chemistries, techniques, and deposition conditions, including temperatures as low as 200°C. In particular, we also employed ion bombardment via RF biasing for our deposition process. This is a unique method for removing oxygen impurities, a major contributor to low-quality and high-resistivity films. Furthermore, this energy supply facilitates film densification, efficient elimination of precursor ligand residues, and surface adatom diffusion. We are able to repeatedly deposit a film of ~ 54 nm on a planar 6-inch wafer that transitions and superconducts at  $T_c = \sim 4.35$  K. Overall, our goal is to produce SC films with spatial uniformity, highly conformal, and high  $T_c$  to overcome the challenges of large detector arrays and interconnect density using 3D integration. The results aiding these efforts will be discussed further.

**10:40am QS+EM+TF-MoM-8 Molecular Beam Epitaxy of Superconducting ZrN Thin Films on GaN Substrates, Brelon May, K. Vallejo, D. Hurley, K. Gofryk, Idaho National Laboratory**

Group III-Nitride materials have found applications in optoelectronics and photonic devices due to the large variation in direct bandgap spanning from the infrared to the deep ultraviolet. Recent research has pursued the integration of this well-established material system with transition-metal nitrides to create complex heterostructures with additional magnetic or superconducting functionality. ZrN is a well-known refractory conductor with high oxidation resistance, high hardness, and has been shown to be a superconductor at low temperatures. The estimated lattice mismatch of ZrN with InN, GaN, and AlN is 8.5%, -1.5%, and -4.2%, respectively, suggesting strain free as well as strain-tunable growth on the ternary III-Ns. This work focuses on the epitaxial growth of ZrN on c-plane GaN substrates via molecular beam epitaxy. An electron beam evaporation source and an RF-plasma source were used to supply the Zr and active nitrogen, respectively. Reflection high energy electron diffraction (RHEED) and X-ray diffraction (XRD) did not reveal any crystallographic texture of ZrN deposited on fused silica at temperatures >700°C. However, growth of ZrN on c-plane GaN substrates at similar temperatures was epitaxial. RHEED revealed that the ZrN maintains the symmetry of the underlying GaN throughout the entire deposition, and post-growth examination via XRD showed (111) oriented ZrN thin films. RHEED patterns during the regrowth of GaN directly on thicker layers of higher symmetry ZrN suggest a preference for twin formation and a slight degree of surface faceting. A physical property measurement system was used to measure electrical transport as a function of temperature and magnetic field. Initial results of uncapped ZrN thin films reveal a superconducting phase with a critical temperature of <10 K and a critical field of 2 T. Because the critical temperature is lower than expected, the presence of off stoichiometry or structural disorder is suspected. These results pave the way for integration of superconductors and quantum phenomena in existing III-N photonic systems.

**11:00am QS+EM+TF-MoM-9 Enhancing Quantum Circuits Through Biased Plasma-Enhanced ALD of Ultrathin Superconducting Ta<sub>x</sub>N<sub>1-x</sub>, Silke Peeters, Eindhoven University of Technology, Netherlands; C. Lennon, V. Seferai, R. Hadfield, M. Weides, University of Glasgow, UK; M. Verheijen, E. Kessels, Eindhoven University of Technology, Netherlands; H. Knoops, Eindhoven University of Technology, Oxford Instruments, Netherlands**

Superconducting quantum circuits are one of the leading architectures in quantum computing platforms. Recent experiments [1,2] demonstrating up to 0.5 ms coherence time in superconducting Ta transmon qubits mark a six order of magnitude improvement in superconducting qubit coherence over the past two decades [3,4]. However, major material challenges, such as uncontrolled oxides and disordered interfaces, still stand in the way of realizing large-scale, fault-tolerant quantum computers.

In this contribution, material properties of ultrathin Ta<sub>x</sub>N<sub>1-x</sub> are extensively characterized and coupled to cryogenic superconducting quantum device performance. In this way, we aim to clarify the roles of various processing aspects in achieving high-quality-factor devices. Ta<sub>x</sub>N<sub>1-x</sub> films with thicknesses of 7 – 40 nm were prepared by plasma-enhanced atomic layer deposition (PEALD) with radiofrequency substrate bias. Because of its atomic-scale growth control PEALD is a promising technique for growth of thin films with high-quality interfaces. Ion energy control in the ~25 – 250 eV range is provided by the substrate bias.

We have observed that energetic ions can counteract oxygen impurity incorporation and promote a larger grain size, while minimizing ion-induced material damage. Increasing the ion energy from ~25 eV to ~150 eV yields a hundredfold decrease in room-temperature resistivity to 239 μΩ cm for an 18 nm film. Smooth, dense, polycrystalline Ta<sub>x</sub>N<sub>1-x</sub> films of the fcc crystal structure are obtained, which are stable in ambient atmosphere. These films maintain a high critical temperature of superconductivity ( $T_c$ ) of 7 K down to 11 nm film thickness.

The high ultrathin-film quality achieved by PEALD with substrate bias is promising for ultrathin, low-loss superconducting quantum devices. Specifically, superconducting resonators were fabricated from 20 - 35 nm Ta<sub>x</sub>N<sub>1-x</sub> films on high-quality silicon and sapphire substrates, with preliminary measurements showing internal quality factors of at least  $2 \times 10^5$  in the single-photon regime. Furthermore, we provide practical pointers for quantum device compatibility of ultrathin superconducting films. Through

# Monday Morning, November 6, 2023

the high level of control in PEALD with substrate bias, this work contributes to the understanding of material loss mechanisms in superconducting quantum circuits.

## References

8. P. M. Place *et al.* Nat. Commun. **12**, 1779 (2021).
9. C. Wang *et al.* npj Quantum Inf. **8**, 3 (2022).
10. W. D. Oliver and P. B. Welander *MRS Bulletin* **38**, 816 (2013).
11. D. Gill and W. M. J. Green *IEEE ISSCC* 30 (2020).

11:20am **QS+EM+TF-MoM-10 Characterization of Ultra-Thin Superconducting TaN Nanowires with Integrated Heatsink Capabilities for SNSPD Applications**, *Ekta Bhatia*, NY CREATES; *T. Nanayakkara*, *C. Zhou*, Center for Functional Nanomaterials, Brookhaven National Laboratory; *T. Vo*, American Institute for Manufacturing Integrated Photonics; *W. Collison*, *S. Schujman*, *A. Biedron*, *J. Nalaskowski*, *S. Olson*, NY CREATES; *S. Kar*, American Institute for Manufacturing Integrated Photonics; *H. Frost*, College of Nanoscale Sci. & Eng., SUNY Polytechnic Institute; *J. Mucci*, *B. Martinick*, *I. Wells*, *T. Murray*, *C. Johnson*, *V. Kaushik*, NY CREATES; *C. Black*, *M. Liu*, Center for Functional Nanomaterials, Brookhaven National Laboratory; *S. Papa Rao*, NY CREATES

Tantalum nitride (TaN) has emerged as a promising candidate for superconducting nanowire single-photon detectors (SNSPD) due to its favorable properties such as lower  $T_c$  that enables easier Cooper-pair breaking and a longer wavelength cut-off [1]. TaN is also attractive because it is widely used in the CMOS IC industry enabling TaN SNSPDs to be readily made at a large scale, on 300 mm wafers. While the body of knowledge about superconducting TaN has been growing, its knowledge at 300 mm scale is limited. In this work, we report on the superconducting properties of 300 mm scale TaN and its dependence on process variables. We then discuss the impact of novel integration schemes on the thermal characteristics of TaN nanowires for SNSPD applications.

Copper encapsulated damascene TaN nanowires (with a N/Ta ratio of 0.53 set by room temperature reactive sputtering conditions) have a coherence length of  $\sim 8$  nm. This is in rough agreement with prior literature on TaN thin films deposited at 750°C on sapphire substrates [2]. Extracted values of effective penetration depth, critical magnetic field, and critical current density are reported. We also studied the  $T_c$ ,  $I_c$  dependence on varying thicknesses and line widths (100 nm to 3000 nm). Our TaN nanowires exhibit a  $T_c$  of  $\sim 3.45$  K (at a thickness of  $\sim 35$  nm) with  $< 5\%$  variation across the 300 mm wafer. Sheet resistance (at 300 K) and  $I_c$  vary by  $< 5\%$  across the 300 mm wafer for all the line widths measured, similar to the  $< 5\%$  cross-wafer non-uniformity of thickness (XRR) and N/Ta ratio (SIMS & XPS). We also investigated the superconducting properties of different in-film N/Ta ratios varying from 0.35 to 0.7 using 20 nm thick nanowires.

We explored the efficacy of Cu as a heat transport material that is integrated with TaN nanowires in various schemes (damascene Cu above the nanowire, and a blanket underlayer of Cu) and compared to a control case with no Cu. We used the ratio of retrapping current to  $I_c$  as the metric of heat transfer efficiency. This study demonstrates a novel way to increase heat transport away from the nanowire, hence improving the reset times of SNSPDs. We discuss one possible design of a focal plane array of fast SNSPDs based on the findings of this work. This study further strengthens the case for scalable fabrication of TaN nanowires using state-of-the-art 300 mm process tools, with applications ranging from arrayed detectors for cosmology to single photon detection in photonic quantum computing and superconducting optoelectronic neuromorphic computing.

- [1] A. Engel *et al.* Appl. Phys. Lett. **100**, 062601 (2012).  
[2] K. Il'in *et al.* Physica C **470**, 953–956 (2010).

Authors 1 and 2 contributed equally.

11:40am **QS+EM+TF-MoM-11 Cryogenic Microwave Loss Measurements of Metal-Oxides using 3D Superconducting Cavities**, *Nicholas Materise*, Colorado School of Mines, USA; *J. Pitten*, University of Colorado Boulder; *W. Strickland*, *J. Shabani*, New York University; *C. McRae*, University of Colorado Boulder/National Institute for Science and Technology (NIST)

Reports of high performance tantalum-based qubits has stimulated interest in comparing the quality of tantalum pentoxide with niobium pentoxide and suboxides of niobium. Here, we present a high participation cavity capable of resolving differences in losses due to oxides grown on Ta and Nb

thin films. We distinguish losses of the oxide from the other interfaces using in a multi-step measurement process, first measuring the substrate with its native oxide, then repeating the measurement with the film deposited on the same substrate with oxide grown on the surface. Participation ratio calculations estimate the losses due to each interface, with their thicknesses measured by cross-sectional transmission electron microscopy. This measurement capability opens possibilities to screen candidate materials, and their oxides, for use in superconducting qubits and devices.

## Advanced Surface Engineering Division Room C123 - Session SE1+TF-MoM

### Advanced Multi-Functional Thin Film Materials

Moderator: Suneel Kumar Kodambaka, Virginia Tech

8:20am **SE1+TF-MoM-1 AVS John A. Thornton Memorial Award Talk: Low Temperature Thin Film Growth Using Metal-ion/Surface Interactions**, *Lars Hultman*<sup>1</sup>, *G. Greczynski*, Linköping University, Sweden; *I. Petrov*, University of Illinois, Urbana-Champaign

#### INVITED

Ion irradiation is a key tool for controlling epitaxy-to-nanostructure, phase content, and properties of refractory ceramic thin films grown by magnetron sputtering, as described in extended Thornton's structure-zone diagrams. Until recently, film growth relied on enhancing adatom mobility by inert and/or reactive gas ion irradiation to obtain dense layers at low deposition temperatures. The development of high-power pulsed magnetron sputtering (HiPIMS), which provides metal-ion plasmas with tunable degree of ionization, enabled systematic studies of the effects of metal-ion irradiation on refractory ceramic thin films. Metal ions are film constituents, hence they provide the benefits of ion-mixing without causing the high compressive stresses associated with trapping of gas ions.

This presentation reviews our growth experiments of pseudobinary TM nitride model systems including TiAlN, TiSiN, VAlN, TiTa<sub>n</sub>, TiAlTa<sub>n</sub>, and TiAlWN [1] carried out in a hybrid configuration with one target powered by HiPIMS, and the other operated in direct current magnetron sputtering (DCMS) mode. [2] A substrate bias potential  $V_s$  is synchronized with the metal-ion-rich portion of the HiPIMS pulses to allow for a control of metal-ion energy. Essential input is provided by time-resolved mass spectrometry analyses performed at the substrate position, which reveals the temporal evolution of metal- and gas-ion fluxes. This enables us to suppress the role of gas ion irradiation and study the influence of intense  $M_1^{(n+)}$  and  $M^{(n+)}_2$  metal-ion fluxes ( $n = 1, 2$ ) on film growth kinetics over a wide range of  $M_1M_2N$  alloy compositions.

The effects of metal-ion irradiation depend on the mass of incident ion with respect to that of film constituents. Irradiation with lower-mass metal-ions (Al<sup>+</sup> or Si<sup>+</sup>) results in near-surface trapping with the depth determined by  $V_s$  amplitude. This enables growth of NaCl-structure Me1Me2N solid solutions far above the Me1N concentration range achieved with DCMS.[3] At the other extreme, bombardment of the growing film surface with pulsed high-mass metal ion fluxes (W<sup>+</sup> or Ta<sup>+</sup>) during hybrid HiPIMS/DCMS high-rate deposition of dilute Ti<sub>1-x</sub>Ta<sub>x</sub>N, Ti<sub>1-x-y</sub>Al<sub>y</sub>Ta<sub>x</sub>N, and Ti<sub>1-x-y</sub>Al<sub>x</sub>W<sub>y</sub>N alloys provides fully-dense/low-stress films without intentional substrate heating (temperature  $\leq 130$  oC). The high metal-ion mass irradiation leads to low-energy recoil generation that provide sufficient adatom mobility, necessary to obtain high-quality fully-dense films, in the absence of resistive heating. Such energy-efficient PVD contributes to a sustainable development.

For cubic-TiAlWN, we recently discovered that Guinier-Preston (GP) zone hardening- known from soft light-metal alloys - can operate also in refractory ceramics. [4] The present GP hardening at 1000 °C is by the formation of atomic-plane-thick W islands populating {111} planes.

- [1] G. Greczynski, I. Petrov, J.E. Greene, L. Hultman, J. Vac. Sci. Technol. A **37** (2019) 060801  
[2] G. Greczynski, J. Lu, M. Johansson, J. Jensen, I. Petrov, J.E. Greene, L. Hultman, Surf. Coat. Technol. **206** (2012) 4202  
[3] G. Greczynski, S. Mráz, J.M. Schneider, L. Hultman, J. Appl. Phys. **127** (2020) 180901  
[4] O.Pshyk, X.Li, I.Petrov, D.G.Sangiovanni, J.Palisaitis, L.Hultman, G.Greczynski (Submitted 2023)

<sup>1</sup> John A. Thornton Memorial Award Winner

# Monday Morning, November 6, 2023

9:00am **SE1+TF-MoM-3 Multi-Component Materials – Bonding, Disorder and Possibilities**, *Erik Lewin*, Uppsala University, Sweden **INVITED**

Multi-component, often referred to as high-entropy, materials have received a large amount of attention during the past two decades. There are several reasons for this, including applicable properties and the fundamental design aspects connected to the large compositional space available, as well as the so-called core effects. The first research in the field was concerned with bulk alloys, but the concept has been expanded to compounds of metals and p-elements, e.g. nitrides, carbides, oxides, borides. Today, much of the research is on coating materials. In the field of coating research, popular properties and potential applications include hard materials, diffusion barriers, as well as corrosion or radiation resistant coatings.

This presentation will focus on solid solution phases with simple crystal structures where at least five different metallic elements share a crystalline sub-lattice. Recent results on the chemical bonding in multi-component alloy, nitride, and carbide coatings based on the early transition metals Ti, V, Zr, Nb and Hf will be presented. These results are based on the combination of *ab-initio* DFT simulations and electron spectroscopy using, both in-house XPS and synchrotron-based methods, and show that there is a charge transfer between the different metal atoms in a multi-component alloy, and that this effects the size of the atoms. Similar effects are also observed in corresponding nitrides and carbides, despite that all metal atoms have a first coordination of nitrogen or carbon. The results illustrate that chemical bonding matters, and that to fully understand and exploit the possibilities of multi-component materials this need to be considered. The results also show that the variation in local chemical environment effect the local electronic structure, giving rise to a range of chemically different sites.

This leads to a forward looking discussion on the fundamental understanding of the multi-component materials, and the possibilities that may arise from understanding and designing the chemical bonding (charge transfer) in multi-component materials. This will include the both the array of different chemical sites, as well as the intriguing combination of order (the crystalline lattice) and disorder, in the form of unordered occupation of the lattice points by different metals, as well as displacive disorder where the atoms are not on the lattice points (commonly called lattice distortion).

9:40am **SE1+TF-MoM-5 High-k Gate Dielectrics for InAlN and ScAlN Barrier GaN HEMT Structures**, *Neeraj Nepal, B. Downey, M. Hardy, D. Meyer, V. Wheeler*, U.S. Naval Research Laboratory

InAlN and ScAlN-barrier GaN high electron mobility transistors (HEMTs) have shown the ability to generate larger two dimensional electron gas (2DEG) densities for a given barrier thickness, leading to improved frequency and power performance in these devices [1-2]. However, HEMT devices utilizing these thin barriers often suffer from higher leakage current [2,3] and premature electric field breakdown, requiring the integration of gate dielectrics in order to realize the full potential of novel InAlN and ScAlN-barrier HEMTs by reducing leakage current, maintaining high electric field breakdown, and mitigating dc-RF dispersion.

In this talk, we report growth optimization and electrical properties of atomic layer deposition (ALD) grown TiO<sub>2</sub> gate dielectric on InAlN and ScAlN HEMTs structures. ALD process windows were initially monitored and optimized on Si substrates using *in-situ* ellipsometry. Films were deposited using tetrakis(dimethylamino)titanium (TDMAT) at 75 °C and an Ar/O<sub>2</sub> plasma at 300 W. Optimization of TiO<sub>2</sub> films was done by varying the typical growth parameters, such as TDMAT pulse duration and growth temperature, as well as the plasma gas chemistry. Optimum films were then deposited and characterized on HEMT structures to determine electrical performance for device applications.

Atomic force microscopy on HEMT structures measured before and after ALD deposition showed minimal change in roughness as a result of the conformal TiO<sub>2</sub> deposition. Contactless resistivity measurements performed before and after ALD showed negligible change, indicating that no plasma induced damage was occurring during ALD gate deposition. Vertical current-voltage and capacitance-voltage measurements were made on a Schottky-contacted HEMT structure and compared to devices with TiO<sub>2</sub> gate dielectrics deposited at different temperatures to discern the full electrical impact of the ALD process. As an example, an extracted dielectric constant of TiO<sub>2</sub> layer deposited on ScAlN surface at 200°C with O<sub>2</sub> flow of 20 sccm was 50 with no significant change in 2DEG density ( 2.6-2.7x10<sup>13</sup> cm<sup>-2</sup>). Using only a 7 nm gate TiO<sub>2</sub> film, the off-state gate leakage in InAlN/GaN HEMTs was reduced by ~10<sup>4</sup> compared to a Schottky gate. Additional electrical HEMT characterization and the band alignment of an optimum

ALD TiO<sub>2</sub> on ScAlN structure will be discussed to show the full potential of these films in novel structures.

References:

12. Li et al., *IEEE Electron Device Lett.* 41, 689 (2020).
13. Hardy et al., *Appl. Phys. Lett.* 110, 162104 (2017).
14. Green et al., *IEEE Electron Device Lett.* 40, 1056 (2019).

10:00am **SE1+TF-MoM-6 Molecular Layer Deposition for Alumina Gas Separation Membranes**, *Lucie Badouric, C. Charmette, J. Cartier, M. Drobek, A. Julbe, M. Bechelany*, University of Montpellier, France

Making hydrogen a reliable energy vector in future decades requires the implementation of complex technologies related namely to its production, storage or transport. Intensive research is also underway to optimize its use by increasing its purity and to ensure the safety of hydrogen facilities.

Techniques such as cryogenic distillation, pressure swing adsorption (PSA) or membrane processes can be used to purify hydrogen. Both cryogenic distillation and PSA are used at commercial scale although these techniques are energy intensive. In comparison, membrane processes appear as a promising technology to separate H<sub>2</sub> from gas mixtures, by consuming less energy and operating in a continuous way. They can be either dense or porous, and made of polymers, metals, carbon, ceramics, hybrids or composite materials. Different gas transport and separation mechanisms are involved depending on the type of membrane. In microporous membranes (pore sizes < 2 nm) the separation of gas molecules might occur by molecular sieving, difference in diffusivity and/or competitive adsorption. Molecular sieving is an efficient thermally activated separation mechanism, particularly attractive for gas mixtures with different kinetic diameters. A good compromise between selectivity and permeability values can be reached with pore sizes smaller than the kinetic diameters of the molecules to be retained.

This work is dedicated to the development of a new type of alumina microporous membrane using the Molecular Layer Deposition (MLD) technique. As Atomic Layer Deposition (ALD), MLD allows to synthesize hybrid organic-inorganic materials by conformal coatings on various substrates using both organic and inorganic precursors. We developed a MLD process able to coat uniformly the pores (size~ 5-8 nm) of an alumina tubular support with alucone (aluminum alkoxide). Then, the film was calcined to transform the organic layer into a microporous alumina frame. Maximum pore sizes around 0.3 nm are targeted to obtain a molecular sieve membrane able to extract H<sub>2</sub> from mixtures with larger gas.

The MLD parameters have been optimized to obtain homogenous layers. Then, we investigated the influence of post-synthesis parameters to improve the membrane selectivity and permeability, as well as its stability. Single gas permeance measurements with He (H<sub>2</sub> simulant) and N<sub>2</sub> were used to validate the membrane quality and molecular sieving performance before testing them with gas mixtures under various working conditions (e.g., temperature, transmembrane pressure).

This project was partially supported by the French national research agency (ANR, program ALD4MEM-ANR-20-CE09-0008-01) and the Occitanie Region (React-Eu Défi clé Hydrogène Vert).

## Advanced Surface Engineering Division

### Room C123 - Session SE2+TF-MoM

#### Surface Engineering by Deposition of Protective Coatings

Moderator: *Suneel Kumar Kodambaka*, Virginia Tech

10:40am **SE2+TF-MoM-8 Advanced Surface Engineering Coating Technologies for Automotive Applications**, *Jianliang Lin*, Southwest Research Institute, San Antonio Texas **INVITED**

The pursuit of the automotive industry for more efficient engines to reduce fuel consumption and improve fuel economy continues. One means is to reduce the coefficient of friction (COF) of critical moving parts in engines, e.g. piston rings and camshafts using advanced surface engineering coating technologies. The presentation presents an overview of a series of efforts in the development of advanced low friction nanocomposite coatings, diamond like carbon (DLC) based coatings, and their hybrid for automotive applications. The coatings were designed and deposited using different surface engineering coating technologies, including plasma enhanced magnetron sputtering (PEMS), plasma immersion ion deposition (PIID), and high power impulse magnetron sputtering (HiPIMS). The chemistry and

structure of the coatings were tailored to achieve a multi-functionality of good adhesion, low friction, low wear rate, and sufficient thickness. The coatings were iteratively optimized for its tribological performance in a series of tests including pin-on-disc test, Plint TE77 test, and block-on-ring test in engine lubricants (e.g. 10W-30) to narrow down the selection of the coatings. The nanocomposite coating showed superior performance in engine lubricants due to its unique structure and surface characteristics. Sets of piston rings were tested in a heavy-duty diesel engine to determine their wear and reliability. Finally, a full set of coated rings was tested robotically in a 4-cylinder gasoline engine on a commercial vehicle using the EPA standard method to determine the fuel economy in city driving and high way driving. This coating technology has been demonstrated to reduce COF and wear between piston rings and cylinder liners, and improve engine fuel economy. Other technical examples of tailoring the nanocomposite coating technology for improving performance of other moving parts in an IC engine (e.g., camshaft and tappets, etc) and applications in auto racing will also be presented.

11:20am **SE2+TF-MoM-10 Thin Film Materials Design & Some Thoughts on Complexity and Sustainability**, **Jochen M. Schneider**, Materials Chemistry RWTH Aachen University, Germany

**INVITED**

Designing the next generation of thermally stable thin films without utilizing trial and error-based methodologies requires truly predictive computational approaches. Important design criteria for protective thin film materials are, besides phase formation, mechanical behavior as well as thermal stability. Examples of predictions thereof showcasing so-called MAB phases [1], transition metal nitrides [2], and transition metal aluminum nitrides [3] which are chemically modified will be presented. Furthermore, the generation of point defects in transition metal aluminum nitrides by ion bombardment is predicted [4,5]. All aforementioned predictions are critically appraised by experimental data. Implications for future design efforts will be discussed also in the context of (chemical and structural) complexity as well as sustainability.

## Surface Science Division

### Room D136 - Session SS1+HC-MoM

#### Electrochemistry

**Moderators: Jan Balajka**, TU Wien, **Sefik Suzer**, Bilkent University, Turkey

8:20am **SS1+HC-MoM-1 Surface Inhomogeneities and Ordering Phenomena of (Pr,Ba)CoO<sub>3-δ</sub> Thin Film Electrocatalysts Induced by High Temperatures and Oxygen Partial Pressures**, **David Mueller**, **M. Giesen**, **T. Duchon**, **C. Schneider**, Forschungszentrum Jülich GmbH, Germany

Complex transition metal oxides are used ubiquitously in (electro-)catalysis, ternary and quaternary compounds of the perovskite structure showing especial promise for increasing the efficacy of a plethora of redox reactions. The perovskite structure ABO<sub>3</sub> being able to accommodate a huge range of elements on both A- and B-site allows to tune the electronic and physicochemical properties and tailor those towards a certain catalytic application by careful design of the chemistry. This rational design paradigm has led to the identification of simple descriptors that offer structure-property-activity predictions. These descriptors, mostly derived from the electronic states near the Fermi level, can, for example, be elucidated through X-Ray absorption (XAS) or photoemission spectroscopy.<sup>1</sup>

The catalyst surfaces, however, are dynamic in technologically relevant conditions. Design rules thus have to consider structural, chemical and electronic rearrangements at the surface during catalysis or catalyst processing. Adding to this complexity, spatial inhomogeneities may arise from decomposition pathways that are not found in the bulk, and occur on length scales that can not be resolved by standard electrochemical or spectroscopic techniques.

Here, we investigate (Pr,Ba)CoO<sub>3-δ</sub> (PBCO) as a prototypical example material that exhibits both promising catalytic properties towards the oxygen evolution reaction in solid electrochemical cells<sup>2</sup> as well as a rich structural and chemical complexity depending on oxygen content.<sup>3</sup> Exposing epitaxial thin films grown by pulsed laser deposition to elevated temperatures and oxygen partial pressures typically present in operation, we could identify severe chemical rearrangements at the nanoscale using X-Ray absorption photoelectron microscopy (X-PEEM). We employ principal component analysis on the spatially resolved XAS spectra of all constituents to unambiguously identify correlations of chemical and electronic inhomogeneities.<sup>4,5</sup> Even though PBCO has been found to be thermodynamically stable in the cubic phase over a wide range

temperature and oxygen partial pressures in the bulk, our data suggests a Cahn Hillard type decomposition process confined to the surface after mere hours of exposure. The decomposition products show a considerable lateral inhomogeneity of both A-site chemistry and the electronic structure at the surface, emphasizing that activity descriptors derived from this through spatially averaging techniques have to be heavily scrutinized.

<sup>1</sup>J. Suntivich *et al.*, *Science* **334**, 1383–1385 (2011); <sup>2</sup>A.Grimaud *et al.*, *Nat. Commun.* **4**,2439 (2013); <sup>3</sup>C. Frontera, *Chem. Mater.*, **17**, 5439-5445 (2005); <sup>4</sup>M. Giesen *et al.*, *Thin Solid Films***665**, 75-84(2018). <sup>5</sup>D. N. Mueller *et al.*, *J. Phys. Chem. C* **125**, 2021, 10043-10050

8:40am **SS1+HC-MoM-2 Understanding the Influence of Electrolyte and the Buried Interface on the Stability of Hybrid Systems: A Spectro-Electrochemical Approach**, **Tom Hauffman**, **N. Madelat**, **B. Wouters**, **A. Hubin**, **H. Terryn**, Vrije Universiteit Brussel, dept. Materials and Chemistry, Belgium

The stability of the interface between (organic) coatings and metal (oxides) is of crucial importance for the durability and efficiency of hybrid structures in numerous applications, e.g. in food packaging, automotive, ... This interface is a challenging zone to analyze: from both sides covered with micro- to millimeter thick layers, surface sensitive spectroscopic techniques cannot unravel its characteristics in a non-destructive way. Moreover, the change of this interface due to environmental influences remains challenging to reveal.

In this work, we propose the use of a combined electrochemical and spectroscopic method: Odd Random Phase Multisine Electrochemical Impedance Spectroscopy in combination with Infrared Spectroscopy in a Kretschmann geometry. This fusion allows to correlate the global electrochemical characteristics of the system – such as water uptake and ion diffusion – with enhanced interfacial information.

The concept of this approach is proven on ultrathin PAA and PMMA layers on aluminium oxide<sup>1</sup>, clearly elucidating the surface sensitivity of the Kretschmann geometry and unravelling the enhanced adhesion effect of water on short time scales.

The combined characterization tool has been employed on “industrial-like” organic coatings on model engineering metals. Here, the influence of water uptake, the possibility to make a distinction between water ingress and water diffusion, the influence of both species on delamination and corrosion and the influence of the tuned buried interface will be presented<sup>2,3,4</sup>.

15. Pletincx S. et al., An in situ spectro-electrochemical monitoring of aqueous effects on polymer/metal oxide interfaces, *Journal of Electroanalytical Chemistry* 848 (2019).
16. Wouters B. et al., Monitoring initial contact of UV-cured organic coatings with aqueous solutions using odd random phase multisine electrochemical impedance spectroscopy, *Corrosion Science* 190 (2021).
17. Madelat N. et al., Differentiating between the diffusion of water and ions from aqueous electrolytes in organic coatings using an integrated spectro-electrochemical approach, *Corrosion Science* 212 (2022).
18. Madelat N. et al., An ORP-EIS approach to distinguish the contribution of the buried interface to the electrochemical behaviour of coated aluminium, *Electrochimica Acta* 455 (2023).

9:00am **SS1+HC-MoM-3 Controlling CO<sub>2</sub> Reduction and Electrocatalysis Reactivity Using Alloy and Polymer-modified Electrodes**, **Andrew Gewirth**, University of Illinois at Urbana Champaign

**INVITED**

This talk addresses the reactivity associated with CO<sub>2</sub> and nitrate electroreduction. Electrodeposition of metals from plating baths containing 3,5-diamino-1,2,4-triazole (DAT) as an inhibitor yields highly porous materials exhibiting enhanced activity for electrochemical reactions. Electrodeposition of Cu or CuAg and CuSn, alloy films from such plating baths yields high surface area catalysts for the active and selective electroreduction of CO<sub>2</sub> to multi-carbon hydrocarbons and oxygenates. Alloy films containing Sn exhibit the best CO<sub>2</sub> electroreduction performance, with the Faradaic efficiency for C<sub>2</sub>H<sub>4</sub> and C<sub>2</sub>H<sub>5</sub>OH production reaching nearly 60 and 25%, respectively, at a cathode potential of just -0.7 V vs. RHE and a total current density of ~300 mA/cm<sup>2</sup>. *In-situ* Raman and electroanalysis studies suggest the origin of the high selectivity towards C<sub>2</sub> products to be a combined effect of the enhanced destabilization of the Cu<sub>2</sub>O overlayer and the optimal availability of the CO intermediate due to the Ag or Sn

# Monday Morning, November 6, 2023

incorporated in the alloy. Sn-containing films exhibit less Cu<sub>2</sub>O relative to either the Ag-containing or neat Cu films, likely due to the increased oxophilicity of the admixed Sn. A related effect is found for nitrate reduction on alloy-modified Cu electrodes. Modification of the Cu electrode with certain polymers yields substantially enhanced CO<sub>2</sub> reduction reactivity, due in part to control of the Cu<sub>2</sub>O layer and elevated surface pH. Polymer-composite electrodes exhibit enhanced reactivity over a wide range of proton-involved electrochemical reactions. As an example, methanol oxidation reactivity is substantially enhanced with polymer-modified Pt electrodes.

9:40am **SS1+HC-MoM-5 Enhancement of CO<sub>2</sub> Reduction Reaction Activity and Selectivity of Sub-2 nm Ag Electrocatalysts by Electronic Metal-Carbon Interactions**, *Xingyi Deng, D. Alfonso, T. Nguyen-Phan, D. Kauffman*, National Energy Technology Laboratory

We show that the activity and selectivity of sub-2 nm Ag electrocatalysts for electrochemical CO<sub>2</sub> to CO conversion is drastically improved by electronic metal-support interactions (EMSIs). The EMSIs between Ag and carbon support, created by deposition of Ag onto heavily sputtered, highly oriented pyrolytic graphite (HOPG), were revealed by X-ray photoelectron spectroscopy (XPS), and supported by computational modeling based on density functional theory (DFT). While sub-2 nm Ag electrocatalysts lack of EMSIs showed selectivity (CO Faradaic efficiency  $FE_{CO} < 2\%$ ) toward the electrochemical CO<sub>2</sub> reduction reaction (CO<sub>2</sub>RR), similar sized Ag electrocatalysts with EMSIs demonstrated  $\sim 100\%$   $FE_{CO}$  and more than 15-fold increase of CO turnover frequency (TOF<sub>CO</sub>). Our calculations elucidated that the electronic Ag-C interactions led to a significant charge transfer (1.02 e) from Ag to carbon support and subsequently lowered the potential-limiting step in CO<sub>2</sub>RR by 0.41 eV. Our results provide the direct evidence of improving CO<sub>2</sub>RR performances of electrocatalysts through EMSIs, particularly between metal and carbon. The EMSIs help break the limit of size-dependent CO<sub>2</sub>RR activity in Ag nanoparticles, hinting at a new approach for creating active and selective electrocatalysts.

10:00am **SS1+HC-MoM-6 Super Structure and Surface Reconstructions with High-Energy Surface X-Ray Diffraction**, *Gary Harlow*, University of Oregon; *D. Gajdek*, University of Malmo, Sweden; *G. Abbondanza*, *A. Grespi*, Lund University, Sweden; *H. Wallander*, University of Malmo, Sweden; *A. Larsson*, University of Lund, Sweden; *L. Merte*, University of Malmo, Sweden; *E. Lundgren*, Lund University, Sweden

The performance of an electrocatalyst (its activity, selectivity, and stability) is strongly dependent on the electrode structure and composition, particularly in the near surface region. A successful approach in trying to understand the impact of structure is the use of well-defined model electrodes such as single crystals, to isolate how various changes in structure and composition impact upon the catalyst behavior. Surface x-ray diffraction gives the average surface structure of an isolated facet, whereas real catalysts often contain multiple facets and edge sites. This contribution will discuss the application of high energy surface x-ray scattering to quickly map out large volumes of 3D reciprocal space and then extract crystal truncation rods. These truncation rods can then be used to determine atomic coordinates of surface atoms, in operando.

Examples during methanol oxidation on both Pt(111) and Au(111) surfaces will be presented. As well as measurements on the the stability of ultra-thin Fe oxide layers on Pt(111) after transfer from vacuum to our in situ electrochemical cell.

## Surface Science Division

### Room D136 - Session SS2-MoM

#### Liquid-Solid Interfaces

Moderators: *Jan Balajka*, TU Wien, *Sefik Suzer*, Bilkent University, Turkey

10:40am **SS2-MoM-8 Local Potential Determinations by XPS Provides the Missing Link about Charge Dynamics of Ionic Liquid Devices**, *Sefik Suzer*, Bilkent University, Chemistry Department, Turkey

Ionic liquid materials show rich dynamic responses on electrified surfaces. A long-standing question is why these materials exhibit very different time responses, ranging from microseconds to several hours, which are attributed to the complex interplay of chemical and physical factors, including steric and molecular interactions. However, experimental observations and theoretical predictions do not always match in IL based devices. Particularly considering the overall electrode capacitance resulting from asymmetric ion size effects, the local voltage levels can show large differences, and drift-diffusion process of ions generally fails to account for

them. To clarify this point, we have utilized a combination of electrochemical devices with different chemical make-up, geometry and dynamic XPS analysis and modelling, and were able to probe the spatiotemporal voltage profiles directly from the shifts in the binding energy positions of the ionic core levels, within IL based devices. Results from a number of single and mixed ILs, as well as different device geometries will be presented and discussed.

11:00am **SS2-MoM-9 Interactions at the Solid-Liquid Interface of Microcrystalline ZnO and Bacterial Growth Environments**, *Dustin Johnson*, *J. Reeks*, *A. Caron*, *M. Smit*, Texas Christian University; *T. McHenry*, Texas Christian University; *S. McGillivray*, *Y. Strzemechny*, Texas Christian University

Despite the prevalence of traditional antibiotics, new threats are posed by bacterial infections due to the rise of antibiotic resistant strains. As such, development of novel antibacterial agents is a critical area of research. In this regard nano- and microscale ZnO have been found to be particularly promising. ZnO at these scales has been shown to exhibit selective toxicity and growth inhibition for a wide range of both Gram-positive and Gram-negative bacteria as well as for microbial strains resistant to traditional antibiotics. The abundance of constituent elements and inexpensive synthesis methods in combination with the aforementioned antimicrobial properties have led ZnO based antibacterial agents to be implemented in biomedical, water treatment, food storage and various other industries. Refinement of current techniques and development of novel bactericidal applications are limited by incomplete descriptions of the fundamental interactions responsible for the observed antibacterial behaviors. In particular, the role and nature of interactions of ZnO with bacterial growth media is not well understood. Herein, we investigate environmental influences relevant to the antibacterial action of ZnO through the interactions with both bacteria and the bacterial environments on the physicochemical and optoelectronic properties of the free crystalline surface of ZnO microparticles (MPs). We expose hydrothermally grown ZnO MPs to phosphate-buffered saline (PBS) media both with and without the presence of Newman strain *Staphylococcus Aureus* (*S. aureus*) bacteria. Surface electronic structure and charge dynamics are probed via both time- and energy-dependent surface photovoltage (SPV) conducted prior to and following biological assays. We observe significant changes in the characteristic timescales under varying conditions, indicating, among other, a possibility of a significant phosphate adsorption at the free crystalline surface. This is further supported by the suppression of spectral signatures of the oxygen-rich defects after exposure to PBS media.

11:20am **SS2-MoM-10 Towards Understanding Interfacial Thermodynamics: Visualizing and Quantifying Competitive Adsorption on Muscovite Mica with AFM**, *Matteo Olgiati*, *J. Dziadkowiec*, *A. Celebi*, *L. Mears*, *M. Valtiner*, Technische Universität Wien, Austria

Given its peculiar crystal structure and inherent surface charge, the (001) plane of muscovite mica has served as an excellent model system to study the hydration and electric double layer (EDL) forces at solid-liquid interfaces [1]. So far, force spectroscopies, which measure along the direction perpendicular to the surface, as well as molecular dynamics (MD) simulations, have demonstrated a certain ion-specificity towards the strength of hydration forces on mica surfaces [2-5]. These deviations are mainly attributed to the different properties of individual ions (e.g., hydration shell, size, valency, etc.), which ultimately determine their adsorption character on mica, as well as the interfacial hydration structure [5]. Nevertheless, lateral distribution and arrangement of cations adsorbed on mica was experimentally investigated only to a lesser extent [6], although unravelling the ions' organisation directly at the surface is crucial to elucidate the structure and properties of EDLs.

In the present contribution, we discuss how high-resolution atomic force microscopy (AFM) imaging enables us to visualize the lateral distribution of individual mono- and multi-valent ions on the surface of mica. Thanks to this approach, we are able not only to resolve the crystal structure of mica immersed in aqueous solution, but also to transiently picture the population of adsorbed ions from the salt-rich solutions at different concentrations. By using an automated triangulation algorithm, the ion adsorption coverage as a function of concentration can be quantified in a first order approximation. This methodology highlights the possibility to outline a certain competitive behaviour of charged species at the surface. Understanding such competition as a function of type and concentration of ions allows us to unravel the interfacial thermodynamics directly from AFM data, which has been so far mainly exclusive to MD simulations. To further support our findings, we use surface force apparatus and MD simulations to

# Monday Morning, November 6, 2023

characterise the structure and mechanical properties of EDLs on mica for different cation species.

## References

- [1] R. M. Pashley, *J. Colloid Interface Sci.* **83**, 2, 531-546 (1981).
- [2] T. Baimpos, B. R. Shrestha, S. Raman and M. Valtiner, *Langmuir* **30**, 4322-4332 (2014).
- [3] Z. Zachariah, R. M. Espinosa-Marzal and M. P. Heuberger, *J. Colloid Interface Sci.* **506**, 263-270(2017).
- [4] I. C. Bourg, S. S. Lee, P. Fenter and C. Tournassat, *J. Phys. Chem. C* **121**, 9402-9412(2017).
- [5] S. R. van Lin, K. K. Grotz, I. Siretanu, N. Schwierz and F. Mugele, *Langmuir* **35**, 5737-5745 (2019).
- [6] M. Ricci, P. Spijker and K. Voitchovsky, *Nat. Commun.* **5**, 4400 (2014).

## Vacuum Technology Division

### Room C120-122 - Session VT-MoM

#### Vacuum Measurement, Partial Pressure, and Gas Analysis

**Moderators:** James Fedchak, National Institute of Standards and Technology, Yev Lushtak, Lawrence Berkeley Lab

#### 8:20am VT-MoM-1 30 Years of Active and Combination Cold-Cathode Gauges, Martin Wüest, INFICON Ltd., Liechtenstein

It is 30 years since the first high vacuum active total pressure gauges appeared on the market.

Previously the sensors were operated via a cable by a controller. Due to miniaturization of electronics, it became possible to reduce the size of the electronics box such that it could be mounted directly on the feedthrough of the sensor. Not long after the active gauges, the first high vacuum combination sensors appeared on the market, where two different sensors were combined in one package.

We will trace the development of inverted magnetron gauges from their invention in the 1950s, to the active and combination sensors available since 1993/1994 to today's self plasma optical emission spectroscopy gauges.

#### 8:40am VT-MoM-2 Enabling Vacuum Process Monitoring with Time-of-Flight Spectroscopy, Kristian Kirsch, VACOM Vakuumkomponenten & Messtechnik GmbH, Germany

The increasing complexity of industrial vacuum processes requires broader and deeper knowledge of the vacuum itself. A crucial aspect for increasing quality demands is the necessity of in-situ monitoring and control of pressure and residual gas composition within vacuum processes. A consequence of advanced process control is the reduction of production errors, prevention of failures or major damage in combination with increased operating time. Traditional monitoring devices like hot cathodes or quadrupole mass spectrometers are both only able to measure either pressure or residual gas composition. Therefore, these devices are only conditionally suited for complete process control of vacuum processes. With our novel wide-range vacuum monitor NOVION® industrially available pressure and gas analysis is possible.

In this talk we present the fundamental principles of the novel vacuum monitor and explain the compact combination of well-known time-of-flight spectroscopy with our own patented ion trap. Within different application cases we discuss advantages and limits of this technology and demonstrate with one single device wide range gas analysis, simultaneous measurement of total and partial pressures, leak detection for Helium and detection of air leaks. With these combined capabilities the novel vacuum monitor is able to quickly capture the complete pressure and gas composition measurement at various stages of the vacuum process chain.

#### 9:00am VT-MoM-3 Remote (100 meters) RGA Operation for High Energy Physics Experiments, W. Fletcher, A. Nikitin, D. RioPousa, M. Aitken, J. Leslie, G. Johnson, G. Jennings, MKS Instruments, Inc. Mass Spectrometry Solutions Group, UK; Gerardo Brucker, MKS Instruments, Inc. Mass Spectrometry Solutions Group

Residual gas analyzers(RGA) are widely considered essential vacuum monitoring instrumentation for both high and ultra-high vacuum processes. High Energy Physics vacuum installations sometimes place RGA sensors within ionizing radiation environments, which can degrade the semiconductor and other components of their control/analysis subsystems.

To protect all vulnerable components from such harsh conditions, the electronics control unit (ECU) must be remotely located with respect to the quadrupole mass filter (QMF) subsystem. In such a configuration, the QMF and ECU may be connected via long transmission cables. Bridge cable assemblies include mixed communication paths for conveying (1) information (mass and ion currents), (2) control signals (electrode biases) and (3) power (filament current supply and quadrupole RF drive). The cable assembly must also comprise a coaxial transmission line as required for efficient RF delivery. Critical to the operation is the delivery of precisely controlled two phase RF supply signals to the quadrupole subsystem, as required to generate repeatable mass spectra. The RF supply signal amplitude is of the order of hundreds of volts peak ( $V_{pk}$ ) and its frequency is typically a few MHz. With modern vacuum installation projects demanding cable lengths exceeding 50 meters, our engineering team recently developed a patented methodology for (1) conveying a time-varying voltage signal from ECU to QMF including (2) monitoring and adaptively controlling an amplitude of the time-varying voltage signal at the QMF. A physical length of the transmission line configured to correspond to an electrical length substantially equal to a positive integer multiple of one-half wavelength of the time-varying voltage signal allows the transmission line to operate resonantly and adaptively control the amplitude of the time-varying voltage signal from the ECU for cable lengths exceeding 100 meters.

#### 9:20am VT-MoM-4 Prospects for Wide-Range, Primary Pressure Sensing with Tethered Optomechanics, Daniel S. Barker, Y. Bao, J. Lawall, J. Gorman, J. Scherschligt, National Institute of Standards and Technology

We present our initial tests of the pressure sensing performance of silicon nitride membranes and trampolines. The damped motion of these micromechanical systems is calculable using the kinetic theory of gases and can be measured with optical interferometry. We assess the accuracy at which kinetic theory predicts the sensor response via comparison with a capacitance diaphragm gauge transfer standard. The intrinsic thermomechanical damping of our current devices restricts their linear operation to the medium vacuum range (0.1 Pa to 100 Pa). Refinements to both the device design and optical readout system will allow field-deployable, chip-scale sensors with range extending below  $10^{-4}$  Pa.

#### 9:40am VT-MoM-5 Novel Diaphragm Vacuum Gauge: Q'zGauge (QZG), Masatoshi Ono, S. Goto, H. Motoyama, H. Hojoh, Vacuum Products Co., Japan

**INVITED**

Among practical gauges, only diaphragm gauges give the pressure independent of gas species. Highly accurate (error of 0.2 %) capacitance diaphragm gauges (CDG) are used for process control of semiconductor fabrication, for example. The gauges have several problems, such as (a) Limited pressure range of two decades, (b) Possible measurement error of about 3% in molecular flow region due to thermal transpiration effect, (c) Startup time of a few hours, and (d) Necessity of stable room environment.

For overcoming these problems, we developed an accurate diaphragm gauge for wider pressure range, by using twin diaphragms and a quartz crystal oscillator, and named Q'zGauge (QZG). The head of the gauge, alike a drum in shape, consisted of a hollow metal barrel with a Inconel diaphragm welded at each end. The diaphragms, of 12 mm in diameter and 100  $\mu$ m in thickness, were bridged at their centers with the oscillator, called "dual tuning fork resonator", which showed large frequency change for longitudinal stress caused by deflection of the diaphragms. The inside of the head was kept at high vacuum. The resonant frequency was about 40 kHz without stress, and changed about 6% for the stress corresponding to pressure of 100 kPa which gave 3.5  $\mu$ m of deflection of the diaphragms.

Through optimized design, taking into account of the temperature characteristics of the oscillator and gage head material, the sensitivity of the gauge, the ratio of change in pressure reading to that of the frequency, was almost constant, but shows slight temperature dependence. This dependence was measured with a thermistor attached to the head and used in the pressure calculation which made it possible to give an accurate pressure without a constant temperature oven.

The uncertainty of reading was 0.001 Pa for pressure range of 100 kPa to 0.1 Pa. This range was equivalent to that of more than two CDGs gauges.

Problems:

- (a) Pressure range of QZG was more than four decade,
- (b) and (c) problems peculiar to a constant temperature oven were unrelated to QZG.
- (d) Influence of AC circuits of the controller in the ambient temperature and humidity was negligibly small on QZG's resonant frequency.

# Monday Morning, November 6, 2023

These performances of QZG were realized mainly by extremely high Q of the oscillator.

The deflection of the diaphragm was far smaller than the plastic deformation. This fact eliminated necessity of a cut off valve for protecting the damages of the diaphragms. This valve was essential to CDGs with maximum pressure of less than 10 kPa.

The similar tuning fork quartz oscillators have been used widely for wrist watches. This fact also made us expect reliable long life of Q'z Gauges.

**10:40am VT-MoM-8 A Demonstration of the Portable Cold Atom Vacuum Standard as a Pressure Sensor, *Stephen Eckel, D. Barker, J. Fedchak, J. Scherschligt, NIST***

We will demonstrate, live, the use of the portable cold atom vacuum standard as a pressure sensor. Cold atom vacuum standards use the loss rate of cold atoms from a conservative trap to measure the vacuum pressure. Because the collision cross section between a cold atom and a background gas particle can be calculated from first principles, such gauges are also primary standards. We will describe and show how these pressure readings are taken, including the preparation of the cold atom cloud, readout, and the conversion between loss rate and pressure. We will also describe the known specifications of this cold-atom-based vacuum gauge, including its range of operation, readout time, and overall precision. Our live demonstration will hopefully convince a skeptical audience of the ability of the portable cold atom vacuum standard to supplant ionization gauges for pressure sensing in the ultra-high vacuum.

**11:00am VT-MoM-9 Update on Construction of the Vacuum Fixed Length Optical Cavity Pressure Standard, *Jacob Ricker, K. Douglass, J. Hendricks, NIST***

Over the past few years, NIST has constructed and tested several Fixed Length Optical Cavity (FLOC) Pressure Standards for measuring gas pressure using refractometry. This refractometry technique has been shown to have similar uncertainty to the best primary standards in the world. NIST is currently constructing the next generation FLOC which will aim to have a resolution of below 5e-8 Torr. This FLOC will help span the gap in quantum traceable pressure standards between the Cold Atom Vacuum Standard and the existing FLOC performance.

Critical to our goals is construction of a high reflectance/narrow linewidth optical cavity. This presentation will update on the construction and fabrication of components for this next generation FLOC. Additionally, we will discuss the temperature control systems and temperature stability as it directly relates to our ultimate performance. Lastly, the goals and next steps to this project will be outlined.

**11:20am VT-MoM-10 Mfig a Mass Filtered Ion Gauge, *Freek Molkenboer, H. Bekman, T. Mechelsen, D. Elstgeest, Y. Westland, J. Emmelkamp, M. Haye, H. Lensen, TNO Science and Industry, the Netherlands***

In 2008, TNO introduced a sensor capable of detecting heavy hydrocarbons in vacuum systems at extremely low concentrations. In 2019, TNO embarked on the development of the third generation of this sensor, known as the Mass Filtering Ion Gauge (MFIG). To optimize the MFIG sensor's design, COMSOL modeling was utilized. The modeling allowed for the precise optimization of specific elements' geometric layout and size within the sensor, making it unique in its performance capabilities.

Through this approach, a highly sensitive sensor has been developed that is capable of measuring volatile organic compounds (VOC) contamination in high vacuum systems. The sensor operates in both transient and continuous regimes, outperforming state-of-the-art RGA technology in detecting a wide range of contamination. Additionally, the MFIG sensor exhibits the ability to detect ultra-short bursts of VOC contamination. These unique selling points offer distinct advantages that are valuable to industries where VOC contamination is a critical concern. Ultimately, this advanced sensor technology has the potential to increase yield and productivity in such sensitive fields.

To validate the performance claims of the MFIG sensor, extensive testing was conducted in laboratory environments both internally at TNO and by external companies, as part of the European ECSEL MADEin4 program which facilitated the development of this third generation sensor.

During the presentation, a detailed overview of the MFIG sensor's general concept will be provided, followed by a presentation of the experimental results obtained from the testing process.

## Atomic Scale Processing Mini-Symposium

Room A107-109 - Session AP+PS-MoA

### Plasma Enhanced Atomic Layer Etching

Moderators: Robert Bruce, IBM Research, T. J. Watson Research Center, Scott Walton, Naval Research Laboratory

1:40pm **AP+PS-MoA-1 Chemical Contrast by Nitridation for Improving Atomic Layer Etching Selectivity in Interconnect and EUV Absorber Applications**, Taylor G. Smith<sup>1</sup>, University of California, Los Angeles; J. de Marneffe, V. Philippen, IMEC, Belgium; J. Chang, University of California, Los Angeles

As extreme ultraviolet lithography (EUVL) dominates the fabrication of future integrated circuits, advanced EUV photomask absorber materials such as Ni and Ni-Al alloys are needed. As Ru emerges as the capping layer for EUV absorber and a potential supplementary material for backend interconnects, the fact that Ru etches rapidly in oxygen requires a different approach (e.g., nitridation) to create the needed chemical contrast for atomic layer etching. In this work, we present a plasma-thermal atomic layer etching (ALE) approach to etch Ni that relies on nitriding the metal surface using nitrogen plasma, then removing the surface metal nitride with formic acid (FA) vapor. Previous work relied on oxygen plasma as the modification step to form a surface NiO<sup>1</sup>. However, oxygen plasma is known to etch Ru, the standard capping material in EUVL masks. Here we explore a nitrogen plasma-based ALE process to increase the selectivity of the Ni etch to the Ru capping layer. An additional motivation for exploring nitridation-based ALE is that metal nitrides, unlike metal oxides, do not form spontaneously in air, making it possible to ascertain that all surface metal nitride formation must be a result of the plasma processing.

The composition of the metal nitride layer is measured by X-ray photoelectron spectroscopy (XPS) and is controlled by varying the plasma power, pressure, and exposure time. Ni films nitridized in a 500 W, 35 mTorr nitrogen plasma for 5 min have a surface composition of Ni<sub>2.8</sub>N, close to the stoichiometric Ni<sub>3</sub>N composition. XPS also confirmed the removal of the surface Ni<sub>3</sub>N after exposure to FA vapor at 80°C as manifested by the disappearance of the metal nitride N 1s peak at 397.6 eV. The thickness of the Ni films as a function of ALE cycles is measured by scanning electron microscopy (SEM) and spectroscopic ellipsometry (SE), with the etch rate measured by SE being 0.49 ± 0.20 nm/cycle. We also determine the selectivity of the plasma nitridation ALE process to common hardmasks and to Ru. Finally, we extend this plasma nitridation ALE chemistry to Ni-Al alloys, determining both the etch rate and the stoichiometry changes in the film as a function of ALE cycles.

1. X. Sang and J. P. Chang, J. Vac. Sci. Technol. A **38** (4), 042603 (2020).

2:00pm **AP+PS-MoA-2 Anisotropic and Selective Atomic Layer Etching of Ruthenium**, Owen Watkins, University of California at Los Angeles; H. Simka, Samsung; J. Chang, University of California at Los Angeles

Ruthenium has been proposed as a replacement for copper in sub-10 nm interconnects, where it has a lower resistivity and does not need as thick of a diffusion or adhesion layer. Ruthenium is known to be etched aggressively in an oxygen plasma by the formation of RuO<sub>4</sub>. A reactive ion etching process using plasma with both O<sub>2</sub> and Cl<sub>2</sub> is a direct, high etch rate method, but there is a need to achieve better control and selectivity in order for Ru to be a viable interconnect material. In this work, a thermodynamic approach was first taken to determine viable chemistries. It confirmed that Ru and RuO<sub>2</sub> react with atomic O spontaneously to form RuO<sub>4</sub>, and with atomic N to form a metastable RuN layer. RuN reacts with atomic O, but the reaction is less favorable, and can be reduced by H and H<sub>2</sub> into metallic Ru. The thermodynamic assessment led to a novel three-step process to control the etching of ruthenium where a nitrogen plasma forms RuN on the surface of the ruthenium thin film, a hydrogen plasma reduces some of the RuN, creating a surface layer of Ru, then an oxygen plasma etches this topmost layer of Ru but is unable to etch into the RuN. Experimental validation was first realized by exposing blanket Ru film to the sequential process. Compared to a baseline of continuous O<sub>2</sub> plasma with equal conditions and total exposure time as the O<sub>2</sub> plasma step, the three-step process shows an increase in RMS surface roughness of 0.05 nm/cycle and a post-etching resistivity of 30 μΩ-cm, whereas continuous O<sub>2</sub> plasma shows an increase of 0.2 nm/30s of exposure and a post-etching resistivity of 280 μΩ-cm.

Finally, using a SiO<sub>2</sub>-patterned Ru structure, a highly anisotropic etch profile was obtained: the nitrogen plasma exposure forms RuN on the exposed surface and sidewalls. Hydrogen plasma with an applied bias anisotropically reduces RuN. Then, an oxygen plasma selectively etches Ru while leaving RuN on the sidewall intact. By creating the anisotropy in the previous steps, a gentler O<sub>2</sub> plasma exposure can be used, which results in an etch rate of 4 nm per cycle and a selectivity of Ru vs. SiO<sub>2</sub>/Si<sub>3</sub>N<sub>4</sub> of 15, compared to conventional O<sub>2</sub> + Cl<sub>2</sub> RIE plasma etching in literature that reports etch rates in excess of 40 nm per minutes and selectivities around 6.

2:20pm **AP+PS-MoA-3 Mechanisms and Benefits of Cryogenic Processes in Silicon Based Material Atomic Layer Etching**, Remi Dussart, R. Ettouri, J. Nos, G. Antoun, P. Lefauchaux, T. Tillocher, GREMI CNRS/Université d'Orléans, France

INVITED

Since its introduction in 1988, plasma cryogenic processing has been applied to deep etching of silicon for microelectronics and MEMS devices. High aspect ratio structures can be obtained at very low temperature (typically -100°C) of the substrate in SF<sub>6</sub>/O<sub>2</sub> plasma. The mechanism is based on a passivation SiO<sub>x</sub>F<sub>y</sub> layer, which forms at low temperature only. The formation of this passivation layer has been characterized by in-situ diagnostics such as ellipsometry, mass spectrometry and XPS. SiF<sub>4</sub> molecules which correspond to the main by products of silicon etching by fluorine can also participate in the passivation layer formation and reinforce it. The composition of the SiO<sub>x</sub>F<sub>y</sub> layer formed in SiF<sub>4</sub>/O<sub>2</sub> plasma strongly depends on temperature. In particular, the fluorine content significantly increases below a temperature threshold between -60°C and -100°C. However, this threshold is reached at higher temperature if we process a Si<sub>3</sub>N<sub>4</sub> surface instead of a Si surface.

We can take advantage from these interesting properties at cryogenic temperature to develop new cryo-ALE processes. In this presentation, two different types of cryo-ALE will be introduced. The first one is based on the physisorption of C<sub>6</sub>F<sub>8</sub> molecules without plasma followed by an argon plasma step to etch SiO<sub>2</sub> at the atomic scale. The second one consists in alternating SiF<sub>4</sub>/O<sub>2</sub> plasma interacting with a cooled substrate with argon plasma. During the SiF<sub>4</sub>/O<sub>2</sub> plasma, the passivation layer composition can be tuned depending on temperature and substrate material surface. In particular, we will show that a very good etch selectivity between Si<sub>3</sub>N<sub>4</sub> and Si can be obtained at a temperature of -65°C for which a very low etch rate is obtained for Si while Si<sub>3</sub>N<sub>4</sub> surface is etched at a higher rate. This property can be explained by the chemical analysis of the two surfaces at low temperature. Finally, some experiments of cryoetching in CHF<sub>3</sub>/Ar plasma will be presented showing some interesting trends at low temperature on different silicon based materials.

3:00pm **AP+PS-MoA-5 Damage Formation Analyses of Steady Plasma-Enhanced Atomic Layer Etching for Silicon Nitride with Molecular Dynamics Simulations**, Jomar U. Tercero<sup>2</sup>, Osaka University, Japan; A. Hirata, Sony Semiconductor Solutions Corporation, Japan; M. Isobe, K. Karahashi, Osaka University, Japan; M. Fukasawa, Sony Semiconductor Solutions Corporation, Japan; S. Hamaguchi, Osaka University, Japan

Molecular dynamics (MD) simulations were performed to study the etching mechanisms and surface damage formations during the plasma-enhanced atomic layer etching (PEALE) of silicon nitride (SiN). PEALE is a thin-layer etching technique to achieve a uniform and precisely etched material surface. The typical ALE process consists of alternating self-limiting adsorption and desorption steps. In the adsorption step, the material is exposed to reactive species, which modifies the surface layer. In contrast, in the desorption step, the modified surface is bombarded with low-energy inert ions, resulting in the removal of the modified layer. A recent report on SiN PEALE processes with hydrofluorocarbon (HFC) radical adsorption and Ar ion impacts has shown that C tends to accumulate on the surface, which causes an etch stop [1]. Our simulations of an ideal PE-ALE system with CH<sub>2</sub>F radical adsorption and Ar ion bombardment have revealed that the remaining C atoms from the initial ALE cycle can trigger the C accumulation. The surface damage was also observed due to the ion bombardment. Due to the formation of a C layer, high-density Si-C bonds were found to remain on the surface after several ALE cycles, causing further accumulation of C atoms. Therefore, we introduced a short O<sub>2</sub> plasma irradiation process after the desorption step to help remove the problematic C atoms [2]. Our simulations agree with the experimental observations that the additional O<sub>2</sub> plasma irradiation step can prevent the etching from stopping. The Si-C bonds were minimized since O atoms reacted with the C atoms, forming CO

<sup>1</sup> PSTD Coburn & Winters Student Award Finalist  
Monday Afternoon, November 6, 2023

<sup>2</sup> PSTD Coburn & Winters Student Award Finalist

# Monday Afternoon, November 6, 2023

and CO<sub>2</sub> species. Regardless, Ar ions with sufficient incident energy are still needed for the etching to proceed, which can cause damage to the etched surface. To understand the effect of the energetic ions in the desorption step, we also performed SiN PEALE with heavier inert gas ions such as Kr. It has been observed that, while Kr ions have shallow penetration depths than Ar ions and therefore cause less surface damage, Ar ions remove C atoms from the surface more efficiently than Kr ions.

## References

- [1] A. Hirata, M. Fukasawa, K. Kugimiya, K. Nagaoka, K. Karahashi, S. Hamaguchi, and H. Iwamoto, *JVST A*, **38**, 062601 (2020).
- [2] A. Hirata, M. Fukasawa, J.U. Tercero, K. Kugimiya, Y. Hagimoto, K. Karahashi, S. Hamaguchi, and H. Iwamoto, *JJAP* (2022).

**3:20pm AP+PS-MoA-6 Orientation Dependent Etching of Silicon: A Computational Chemistry Study, Yuri Barsukov, O. Dwivedi, S. Jubin, J. Vella, I. Kaganovich, Princeton University Plasma Physics Lab**

Orientation dependent etching of silicon is a phenomenon, when etch rate of silicon surface depends on the surface orientation. It was experimentally established that Si(111) surface is slower etched than Si(100) and Si(110). In this case the etch profile becomes anisotropic (without plasma and ions) and the surface is textured with micro- and nano-scale pits. In other words, anisotropy of the etching determines surface roughness. Plasma-less atmospheric dry etching is one of the applications of this processing in technology of black silicon production for photovoltaic solar cell manufacturing, where F<sub>2</sub> gas makes silicon surface rougher. On the other hand, rough surface is unwanted during manufacturing of integrated circuits, because it leads to degradation of device characteristics. Thus, basic understanding of this phenomenon is needed to better control surface structure during the etching.

We performed modeling of Si(100), Si(110) and Si(111) etching by F<sub>2</sub> molecule combined with DFT (density functional theory), TST (transition state theory) and MD (molecular dynamics) approaches like it was done in [1,2]. The combination of DFT and TST enables us to calculate probabilities of gas-surface reactions and perform kinetic modeling of the etching, while under MD approach evolution of the surface at different temperatures at ns time-scale is considered.

We assumed that F<sub>2</sub> dissociative chemisorption leading to Si-Si bond breaking is rate-determining step of whole etching process and reproduce the experimental measurements that the barrier of F<sub>2</sub> dissociation on Si(111) is significantly higher than on Si(100) and Si(110). We established that the value of the barrier is determined by the charge distribution on the surface, and the charge distribution in turn is determined by the number of F atoms incorporated into the surfaces.

Our modeling was validated and well reproduced experimental data such as values of activation barrier and etch rate as a function of temperature.

Based on our mechanism of the etching we will perform similar modeling aimed to design new etchants for Si etching to better control roughness and surface texturing.

## References:

19. S Jubin et al, *Frontiers in Physics* 10, (2022) DOI: 10.3389/fphy.2022.908694.
20. Y Barsukov et al, *Nanotechnology* 32, 475604 (2021) DOI: 10.1088/1361-6528/ac1c20.

**4:20pm AP+PS-MoA-9 Process Drift of SiO<sub>2</sub> Atomic Layer Etching in HFC and FC/Ar Chemistries by Optical Spectroscopy and Surface Chemistry Analysis, Antoine Ronco<sup>1</sup>, F. Boulard, N. Posseme, Univ. Grenoble Alpes, CEA, Leti, France**

Manufacturing new semiconductor devices requires atomic scale control of etching processes in order to decrease their dimensions. Atomic Layer Etching (ALE) allows such thin control of the processes [1][2]. One of the challenges is tuning the durations of the deposition and activation steps to obtain a process with a stable amount of material etched per cycle. If not tuned correctly the fluorocarbon (FC) film can accumulate on the sample's surface causing a drift in the amount of material etched per cycle (EPC)[3]. In this paper, we investigate the use of Optical Emission Spectroscopy (OES) to monitor the drift of a quasi-ALE process. Then, we study the impact of the gas chemistry on the appearance of the drift. Finally, we optimize contact hole etching and especially the landing on the etch stop layer.

The samples studied consist of 100 nm SiO<sub>2</sub> on Si blanket wafers. The experiments are carried out in a 300 mm capacitively coupled plasma reactor. The wafers are etched using C<sub>4</sub>F<sub>8</sub>, C<sub>6</sub>F<sub>6</sub>, or CH<sub>3</sub>F/Ar based chemistry in a two steps approach, namely deposition and activation. The reactor is cleaned using an O<sub>2</sub> plasma before and after etching each wafer.

We observe a decrease in EPC of a quasi-ALE process when increasing the number of cycles. The examination of the evolution of the intensities of OES spectra through deposition and activation steps reveals that the line at 251 nm, which could correspond to CF/CF<sub>2</sub> radicals, is an indicator of the drift of the process [4]. The decreasing intensity observed during the activation step suggests the accumulation of a carbon film on the sample's surface. This is confirmed through XPS analysis showing an increase in carbon content on the sample's surface when increasing the number of cycles. The correlation between XPS analysis, OES observation, and EPC evolution with the number of cycle shows that the EPC drift can be monitored in real time using OES.

We use this method to study the impact of gas chemistry on the drift of our etching process for SiO<sub>2</sub> and SiN etching. The effect of the FC gas used on the selectivity and uniformity of our process is also reported.

Finally, the impact of gas chemistry and number of cycles on pattern etching is characterized using a Scanning Electron Microscope (SEM). Particular interest is paid to the conformality of the FC film deposited on patterns and etching at the bottom of the contact.

- [1] K. J. Kanarik et al., *JVSTA* **33**, no 2, 020802, 2015
- [2] G. S. Oehrlein, et al., *ECS J. Solid State Sci. Technol.* **4**, no 6, N5041–N5053, 2015
- [3] C. M. Huard, et al., *JVSTA* **36**, no 6, 06B101, 2018
- [4] R. W. B. Pearse, et al., *The identification of molecular spectra*, 4th ed. London: Chapman & Hall, 1976.

**4:40pm AP+PS-MoA-10 Atomic Layer Etching of Superconducting Titanium Nitride Thin Films Using Molecular Oxygen and H<sub>2</sub>/SF<sub>6</sub> Plasma, Azmain Hossain, A. Minnich, California Institute of Technology**

Microwave loss in superconducting titanium nitride (TiN) films is attributed to two-level systems in various interfaces arising in part from oxidation and microfabrication-induced damage. Atomic layer etching (ALE) is an emerging subtractive fabrication method which is capable of etching with Angstrom-scale etch depth control and potentially less damage. However, while ALE processes for TiN have been reported, they either employ HF vapor, incurring practical complications; or the etch rate lacks the desired control. Further, the superconducting characteristics of the etched films have not been characterized. Here, we report an isotropic plasma-thermal TiN ALE process consisting of sequential exposures to molecular oxygen and an SF<sub>6</sub>/H<sub>2</sub> plasma. For certain ratios of SF<sub>6</sub>:H<sub>2</sub> flow rates, we observe selective etching of TiO<sub>2</sub> over TiN, enabling self-limiting etching within a cycle. Etch rates were measured to vary from 1.1 Å/cycle at 150 °C to 3.2 Å/cycle at 350 °C using ex-situ ellipsometry. We demonstrate that the superconducting critical temperature of the etched film does not decrease beyond that expected from the decrease in film thickness, highlighting the low-damage nature of the process. The ALE-treated films were also studied using XPS and AFM. These findings have relevance for applications of TiN in microwave kinetic inductance detectors and superconducting qubits. (arXiv:2307.02821)

**5:00pm AP+PS-MoA-11 Quasi-Atomic Layer Etching of X-Cut MgO-Doped Lithium Niobate Using Sequential Exposures of H<sub>2</sub> and SF<sub>6</sub> Plasma, Ivy Chen, J. Solgaard, R. Sekine, A. Hossain, A. Ardizzi, D. Catherall, A. Marandi, California Institute of Technology; F. Greer, Jet Propulsion Laboratory (NASA/JPL), California Institute of Technology; A. Minnich, California Institute of Technology**

Lithium niobate (LiNbO<sub>3</sub>, LN) is an emerging platform for integrated photonics. Recent demonstrations of record on-chip quantum states, >100 GHz electro-optic modulators with CMOS compatible voltages, and multi-octave frequency combs with ~100 fJ pump pulse energies highlight the potential of this platform to enable novel on-chip photonic functionalities. However, thin-film lithium niobate (TFLN) devices suffer from large scattering losses resulting from the surface roughness left by Ar<sup>+</sup> milling, the standard technique used for nanophotonic LN waveguide fabrication, negatively impacting device performance. Atomic layer etching (ALE) can potentially mitigate scattering losses due to its ability to smooth surfaces to sub-nanometer length scales, but no ALE process has been reported for TFLN. Here, we report an anisotropic quasi-ALE process for X-cut MgO-doped LN using sequential exposures of H<sub>2</sub> and SF<sub>6</sub> plasma. We observe etch rates up to 2.1 nm/cycle with a synergy of ~97% and characterize the

# Monday Afternoon, November 6, 2023

etched surfaces using X-ray photoelectron spectroscopy, secondary ion mass spectrometry, and atomic force microscopy. This process has the potential to serve as a post-processing step to smooth patterned TFLN surfaces which may both increase the performance of existing TFLN devices and enable novel devices not attainable in other integrated photonic platforms.

## Biomaterial Interfaces Division

### Room B117-119 - Session B11-MoA

#### SIMS and Orbi-SIMS Characterization of Biological and Biomaterials Surfaces

**Moderators:** Axel Rosenhahn, Ruhr-University Bochum, Markus Valtiner, Vienna University of Technology, Austria

##### 1:40pm B11-MoA-1 Mixing Things Up to Reduce Mix Ups in Lipid and Fatty Acid Analysis, Daniel Graham, H. Lei, L. Gamble, University of Washington

Each ToF-SIMS spectrum can contain a combination of molecular species, fragments of these species, rearranged fragments, cluster ions (combinations of molecules and atoms) and atomic species. The complexity of the spectral information increases with the complexity of the surface being analyzed. This is particularly true when analyzing cells and tissues. Each of these systems contain a rich mixture of molecules including proteins, sugars, lipids and fatty acids. The lipids are typically arranged in well-ordered layers that can contain a wide variety of lipid molecules. While ToF-SIMS has been shown to provide detailed chemical information from the lipids and fatty acids from cells and tissues, this information is complex and can be difficult to uniquely interpret. Recently, it has been shown that the fragmentation pattern in ToF-SIMS spectra contains similar information to an MS/MS experiment and that this information can be used to uniquely identify lipids without doing MS/MS.<sup>1</sup> However, additional work needs to be done to better understand which fragments will show up and whether the relative intensity of these fragments might also encode information about the mixture of molecules which are present.

In order to better understand these complex systems we have taken a reductive approach and started by looking at mixtures of fatty acids. Fatty acids make up a large part of lipids and generate unique signals within ToF-SIMS spectra. This presentation will focus on our work looking at binary mixtures of fatty acids with ToF-SIMS. ToF-SIMS spectra were compared with simulated mixture spectra generated using a custom built graphical user interface (GUI) in Matlab. This GUI allows the user to create spectra of mixtures of two molecules based on the peak intensities of pure component spectra from each chosen fatty acid. Peak areas from the simulated spectra were compared with peak areas from experimental data. It was found that the experimental data deviated from the expected intensities of the simulated spectra. These deviations provide insight into mechanisms that enhance or reduce the yield of certain fatty acid peaks in the mixtures. Insights from these studies will be used to look at increasingly complex surfaces simulating mixtures seen in cells and tissues.

1 T.B. Angerer, D. Velickovic, C.D. Nicora, J.E. Kyle, D.J. Graham, C. Anderton, and L.J. Gamble, *Anal Chem.* **91**, no. 23, pp. 15073–15080, (2019).

##### 2:00pm B11-MoA-2 Native State Physicochemical Characterisation of Drug Delivery Hydrogels using Cryo-OrbiSIMS and SEM, Julie Watts, D. Scurr, University of Nottingham, UK

Supramolecular hydrogel formulations have the potential to increase topical delivery of active agents and are well suited being biocompatible, with facile gel formation from cationic surfactant bis-imidazolium salts and combination with anionic, cationic or neutral drugs [Limón et. al., *Eur J Pharm Biopharm.* 2015]. Although the potential of hydrogels for improved topical skin permeation analysis has been demonstrated using time of flight secondary ion mass spectrometry (ToF-SIMS) [Starr et. al., *Int. J. Pharm.* 2019] the chemistry of the systems themselves have not been chemically characterised in their native state. This is primarily due to ion beam induced fragmentation and limitations of mass resolving power, as well as the obscuring of the spectra of frozen hydrated samples with water fragment ions.

In this work we investigate the application of cryo-OrbiSIMS in the molecular characterisation of supramolecular hydrogels loaded with two different porphyrins (0.1% w/v). Skin permeation studies were performed to evaluate the delivery of 5,10,15,20-Tetrakis(4-hydroxyphenyl)porphyrin (TPPOH) and 5,10,15,20-Tetrakis(4-carboxylatephenyl)porphyrin (TCPP). It was observed that in *ex vivo* porcine skin permeation studies the TPPOH appeared to have permeated the skin whereas the TCPP had not. Gel

monomer skin permeation was below detectable levels in all cases. In order to understand this difference in delivery, cryo-OrbiSIMS and SEM were performed to determine if there were any variations in the physicochemical properties of the gels.

In native state gels as well as those loaded with porphyrin, the cryo-OrbiSIMS spectra show the detection of a range of secondary ions attributable to the gel, [M-H]<sup>+</sup> at m/z 901, TPPOH[M-4H]<sup>+</sup> at m/z 677, and TCPP [M-4Na]<sup>+</sup> at m/z 788. Ions detected include molecular and fragments ions. The data suggests that the chemistry of the supramolecular gel is confirmed and that the porphyrins have been successfully loaded into the gels and are uniformly distributed. Using a controlled sample sublimation approach to expose the fibrous microstructure of the frozen hydrated gels, cryo-SEM images indicate structural differences between gels with and without porphyrins, with longer, more interconnected fibres present in gels systems without porphyrins. However, the two porphyrin containing systems are comparable, as such the release behaviour is proposed to relate to a difference in their affinity to the gel fibres.

##### 2:20pm B11-MoA-3 Molecular Characterization of Cells and Bio-interfaces using SIMS: The Foreign Body Reaction, Morgan Alexander, The University of Nottingham, UK

INVITED

New biomaterials are necessary to tackle the challenges of medical device centred infection combined with antimicrobial resistance and the foreign body reaction (FBR). Together, these cause unacceptably high rates of device failure, rejection, mortality and morbidity.

Novel polymers have been discovered which reduce bacterial biofilm formation, infection, and control host immune response.<sup>1,2,3</sup> To understand their mode of action and improve these cell-instructive biomaterials requires detailed characterisation of the biointerface that plays a central role in their achieving homeostasis. Recently lipids have been proposed as critical in controlling FBR using ToF SIMS data;<sup>4</sup> this finding is intriguing since it offers an alternative to the prevalent protein adsorption paradigm.

Whilst ToF SIMS is excellent for imaging metabolites present at sufficient abundance, it struggles in identifying endogenous species in complex biological systems due to its relatively poor mass resolving power when faced with myriad possible peak assignments for each secondary ion peak.<sup>5</sup> The 3D OrbiSIMS approach addresses that by combining an OrbiTrap with a time-of-flight SIMS instrument to undertake direct analysis of solid samples.<sup>6</sup> The 3D OrbiSIMS has been able to undertake single cell metabolomics for primary macrophages<sup>7</sup> which orchestrate the body's response to implanted medical devices. This has been used to help interpret the complex spectra acquired from the tissue interface with novel implanted novel biomaterials.<sup>8</sup> The outlook for this approach in medical device characterisation, and more widely using unbiased assignment procedures for SIMS will be discussed.<sup>9</sup>

- Immune-Instructive Polymers Control Macrophage Phenotype and Modulate the Foreign Body Response In Vivo **Matter (Cell Press)** Rostam2020
- Combinatorial hydrogel library enables identification of materials that mitigate the foreign body response in primates **Nature Biotechnology** Vegas2016
- Combinatorial discovery of polymers resistant to bacterial attachment **Nature Biotechnology** Hook2012
- Lipid deposition profiles influence foreign body responses **Advanced Materials** Schreib 2023
- Mass Spectrometry and Informatics **Anal Chem** Green2011
- The 3D OrbiSIMS: Label-free metabolic imaging with subcellular lateral resolution and high mass-resolving power **Nature Methods** Passarelli2017
- Single cell metabolomics of macrophages using 3D OrbiSIMS: correlations with phenotype **Anal Chem** Suvannapruk 2022
- Spatially resolved molecular analysis of host response to subcutaneous medical device implantation achieved using the 3D OrbiSIMS *UnderReview*.
- Molecular formula prediction for chemical filtering of 3D OrbiSIMS Datasets **Anal Chem** Edney2022

3:00pm **B11-MoA-5 Elucidating of Native Macromolecule Structure in Cryo-OrbiSIMS**, *Anna Kotowska, M. Alexander, D. Scurr*, University of Nottingham, UK

Analysis of proteins in SIMS has historically been limited due to fragmentation caused by the energetic analysis beam, resulting in only single amino acid secondary ions. In previous work, we successfully demonstrated that the combination of a GCIB with an Orbitrap analyser can return primary structure information from proteins [1]. This was achieved through *de novo* peptide sequencing, with sequence coverage up to 50%.

The presence of water is known to increase ionisation of the sample components, particularly high molecular weight compounds [2]. Analysis of frozen-hydrated samples, spraying water above the sample or using water clusters as primary ion beams have been found to increase the  $[M+H]^+$  signals as well as fragments and  $[M+Na]^+$  and  $[M+K]^+$  adducts [2]. In this work, focusing on macromolecules, this enhancement enabled us to map proteins in human skin and in bacterial biofilm. The additional benefit of analysing large biomolecules in cryogenic conditions is preserving the native state of the molecule, which may enable acquisition of 3D structural information in addition to primary structure.

The extent of chemical information available from cryo-OrbiSIMS analysis is expansive and can be difficult to deconvolute. We have developed a molecular formula prediction (MFP) and level of molecule saturation (double bond equivalents) process to chemically filter multidimensional SIMS data [3]. Chemical filtering is particularly beneficial for the assignment of poorly ionisable molecules (e.g. protein fragments). Here, in addition to filtering protein fragments, we generated a protein fragment database, which facilitates rapid assignment and classification of protein ions and could pave the way for the development of a proteomics-like approach for OrbiSIMS analysis of large biomolecules.

In this work we demonstrate the potential of combining *de novo* sequencing with using cryogenic conditions and advanced data analytics approaches to identify unknown protein samples and obtain structural information from macromolecules.

[1] Anna M. Kotowska *et al.*, *Nat. Comms.*, 2020

[2] Sheraz Née Rabbani *et al.*, *Anal. Chem.*, 2015

[3] Max K. Edney *et al.*, *Anal. Chem.*, 2022

3:20pm **B11-MoA-6 Comparing Desalination Methods of Bacterial Biofilms for Static ToF-SIMS Analyses**, *Gabriel Parker*, University of Illinois - Chicago; *X. Yu*, Oak Ridge National Laboratory; *A. Plymale, J. Dhas, Z. Zhu*, Pacific Northwest National Laboratory; *L. Hanley*, University of Illinois - Chicago

Time-of-flight secondary ion mass spectrometry (ToF-SIMS) is a central technique for imaging of intact bacterial biofilms. Sample preparation in ToF-SIMS is simpler compared with gas chromatography - mass spectrometry (GC-MS) or liquid chromatography mass spectrometry (LC-MS) for biofilm analysis. Nevertheless, sample desalination is crucial to successful measurements from the native environment of biofilms consisting of complex salt and organic matrices. Without desalination, salt and other undesirable signals could dominate biofilm mass spectra and obscure acquisition of useful signals. Matrix effects in high salt environment can also affect the ion yield by enhancing disproportionate ion signals and nonlinear concentration correlations. This work compares desalination methods for ToF-SIMS of planktonic bacterial cells and biofilms on hard surface substrates. *Paenibacillus* sp. 300A biofilms are grown over the course of one week via static cell incubation at room temperature. Two methods of desalination, water submersion (WS) and centrifugal spinning (CS) of bacterial samples, are compared against each other and against samples with no desalination treatment. Water submersion samples are prepared by plating drops of biomaterial solution (planktonic cells or biofilm) onto a substrate, drying the sample, then submerging it in a water bath, and drying again prior to static SIMS analysis. Centrifugal spinning samples are prepared by centrifuging biomaterial, discarding the supernatant, resuspending biomaterial with deionized water, then plating biomaterial solution on substrate and drying under nitrogen prior to SIMS analysis. Results show that non-desalinated samples have the highest salt signal that arises in part from bacteria growth media with signal suppression of biologically relevant ions. By contrast, both WS and CS desalination display well defined peaks with high signal to noise that correspond to metabolites, amino acids, lipids, fatty acids, and salt adducts up to  $m/z$  800. WS displays similar peak intensities compared to CS, but in some cases, the signal is higher for WS samples. Overall, experimental results show that the simple WS method for desalination lowers matrix effects in biofilms for ToF-SIMS analysis while keeping the biofilm structure

intact. Centrifugal spinning proves to be a reliable method to reduce matrix effects in ToF-SIMS analyses of biofilms.

## Biomaterial Interfaces Division Room B117-119 - Session BI2-MoA

### Functional Biomaterials I: Fabrication and Application

**Moderators:** *Pierluigi Bilotto*, CEST GmbH, *Caitlin Howell*, University of Maine

4:00pm **BI2-MoA-8 Low Fouling Marine Coatings Based on Nitric Oxide-Releasing Polysaccharide-Based Hybrid Materials**, *Samantha Muhring-Salamone, R. Wanka, A. Rosenhahn*, Ruhr University Bochum, Germany

Biofouling describes the undesired accumulation of bioorganisms on surfaces which is a ubiquitous problem and has a severe environmental and ecological impact.<sup>[1-3]</sup> Increasing restrictions for biocide-releasing coating result in a growing need for environmentally friendly, sustainable, and biodegradable approaches.<sup>[1,4,5]</sup> Here, we developed a hybrid material coating based on the polysaccharides alginate and heparin and combined them with amine-containing compounds through sol-gel chemistry. The high amine concentration enables the hybrid material to bind nitric oxide when exposed to high pressure NO. The NO binding was characterized by UV-Vis and ATR-IR spectroscopy, and the NO-releasing kinetics by Griess-assays. Dynamic attachment assays with the marine diatom *N. perminuta* revealed a significant reduction in attachment compared to coatings without NO release capabilities. All coatings readily suppressed the attachment of the marine bacterium *C.marina*. The binding of nitric oxide and the release of nitrogen monoxide species was found to be a promising mechanism to add additional fouling-inhibiting functionalities. All building blocks are environmentally friendly, biodegradable, and biocompatible which makes these protective coatings interesting for environmentally benign marine applications.

[1] J. A. Callow, M. E. Callow, *Nat. Commun.* **2011**, 2, 244. [2] V. Eyring, H. W. Köhler, J. Van Aardenne, A. Lauer, *J. Geophys. Res. D Atmos.* **2005**, 110, 171–182. [3] M. P. Schultz, J. A. Bendick, E. R. Holm, W. M. Hertel, *Biofouling* **2011**, 27, 87–98. [4] D. M. Yebra, S. Kiil, K. Dam-Johansen, *Prog. Org. Coatings* **2004**, 50, 75–104. [5] A. Rosenhahn, S. Schilp, H. J. Kreuzer, M. Grunze, *Phys. Chem. Chem. Phys.* **2010**, 12, 4275–4286.

4:20pm **BI2-MoA-9 Underwater Adhesives Through Chemically-Induced Protein Aggregation**, *M. Wilson*, Purdue University; *Q. Lu*, Naval Research Laboratory, Chemistry Division; *K. Nachtrieb, J. Fuller, C. Skogg, E. Yates*, United States Naval Academy; *M. Thum, Christopher So*, Naval Research Laboratory, Chemistry Division

The common strategy to develop bioinspired underwater adhesives is the incorporation of specific chemistries into synthetic polymers or proteins. However, many organisms—including barnacles—use amyloid-like materials to produce successful adhesives, relying on the aggregation of proteins rather than extraordinary chemistry to achieve durable underwater bonding. Inspired by such systems, we control the aggregation of a commercially available protein, bovine serum albumin, to develop waterborne adhesives that cure underwater. For this, we investigate the action of added chemicals using gel inversion tests, differential scanning calorimetry, rheometry, and infrared spectroscopy. We find that added chemical constituents influence the unfolding, aggregation kinetics, and final structure of the solid protein material in different ways. Multiple chemicals can be added to a formulation to provide synergistic effect, forming a solid material within minutes at room temperature underwater. These adhesives produce bond strengths comparable to many synthetic bioinspired adhesives when tested by lap shear after exposure to dry and wet conditions. The ease with which these glues can be fabricated paves the way for opportunities with other commercial proteins and curing agents as a new avenue to produce scalable underwater adhesives.

4:40pm **BI2-MoA-10 Analysis of a Pharmaceutical Formulation using Orbitrap-SIMS**, *Birgit Hagenhoff*, Tascon GmbH, Germany; *J. van Rüschen*, University of Muenster, Germany; *D. Breitenstein*, Tascon GmbH, Germany; *A. Pirkel*, IONTOF GmbH, Germany; *G. Winkler*, Tascon GmbH, Germany  
Pharmaceutical formulations are subject to high quality standards which must be checked at regular intervals. A pharmaceutical review of the composition of the active ingredients is part of the quality assurance of

# Monday Afternoon, November 6, 2023

pharmaceutical companies. For this purpose, also mass spectrometric methods are applied.

Orbitrap-SIMS ("3D-Orbi-SIMS") is a comparably new mass spectrometric technique introduced in 2016 [1]. It is a powerful tool to identify organic as well as inorganic components on the surface of a solid sample. Furthermore, it allows the detection of the lateral distribution of these analytes with high mass resolving power. To perform Orbitrap-SIMS on a sample, typically no pre-separation of analytes is necessary.

In Orbitrap-SIMS, a primary ion beam is directed at the sample surface, causing the sample to emit secondary ions. These ions are then mass separated and detected by an Orbitrap mass analyzer. By rastering the surface with the primary ion beam, 2D images reveal the lateral distribution of the molecules.

In this study, the application of Orbitrap-SIMS on selected pharmaceutical samples is tested. The focus is set to the mass spectrometric identification of the active agents as well as on the revealing of their lateral distribution in a cross-sectioned tablet.

One type of sample examined was composed of two active ingredients: Hydrochlorothiazide and Candesartancilexetil. Both active agents belong to the group of antihypertensives: Hydrochlorothiazide is a thiazide diuretic, whereas Candesartancilexetil is an angiotensin receptor blocker [2].

Identification was performed by the acquisition of full mass spectra of the sample followed by data evaluation using Principal Component Analysis (PCA). The detected SIMS-induced fragmentation pattern was in line with the fragmentation behaviour of the active agents determined by tandem mass spectrometry.

At last, mass spectrometric imaging of the sample was performed in order to reveal the lateral distribution of the active components within the sample.

The results give a glimpse into the potential of Orbitrap-SIMS to solve analytical questions in pharmaceutical industry.

Sources:

[1] Passarelli MK, Pirkl A, Moellers R et. al. The 3D OrbiSIMS-label-free metabolic imaging with subcellular lateral resolution and high mass-resolving power. *Nat Methods*. 2017 Dec;14(12):1175-1183.

[2] Carey RM, Moran AE, Whelton PK. Treatment of Hypertension: A Review. *JAMA*. 022;328(18):1849-1861.

## Chemical Analysis and Imaging of Interfaces Focus Topic

### Room A105 - Session CA+AS+LS+NS+SS+VT-MoA

#### Environmental and Energy Interfaces

**Moderators:** Musahid Ahmed, LBNL, Xiao-Ying Yu, Oak Ridge National Laboratory, USA

1:40pm **CA+AS+LS+NS+SS+VT-MoA-1 In situ Spectroscopies of Interfacial Reactions and Processes in Batteries, Feng Wang**, Argonne National Laboratory **INVITED**

The performance and lifetime of batteries, whether they are traditional lithium-ion, solid-state, or other types, strongly depend on the effectiveness and stability of electrochemical interfaces within the devices. To design battery materials and interfaces with desired functionality, it is crucial to have a mechanistic understanding of the interfacial reactions and processes occurring during battery operation. This necessitates developing advanced techniques capable of characterizing local structures and capturing *non-equilibrium* dynamics at electrochemical interfaces, with the relevant spatial, time resolution and chemical sensitivity, both to light elements (H, Li, O) and heavy ones. Herein, we present the development and application of *in situ* spectroscopies specialized for probing interfacial reaction and processes in lithium-ion and solid-state batteries. With specific examples from our recent studies, we will show how to correlate the structure and function of electrochemical interfaces through *in situ* spectroscopy characterization, thereby gaining insights into the design and processing of battery materials, electrolytes and other components. Towards the end of this talk, we will discuss emerging opportunities in data-driven experimentation, analysis, and modeling for closed-loop battery development to accelerate the transition from lab discovery to commercial deployment.

2:20pm **CA+AS+LS+NS+SS+VT-MoA-3 Novel Strategies for the Characterization of the Next-Generation Energy Storage Materials by ToF-SIMS: From an in-Situ Exploration to an Operando Measurement, Tanguy Terlier, Q. Ai, S. Sidhik, A. Mohite, J. Lou**, Rice University **INVITED**

Recently, advances in instrumentation and sample preparation have permitted a rapid development for characterizing a wide range of applications such as next-generation energy storage materials. Developing new materials is one of the most crucial topics for emerging technologies. However, the complexity of these materials in their structures makes them particularly challenging for numerous characterization and analytical techniques. Exploring chemical composition and the potential chemical reactions such as degradation, diffusion, or doping is crucial to understand advanced materials and to transfer the new technologies to the industry. Among the most suitable characterization tool, time-of-flight secondary ion mass spectrometry (ToF-SIMS) is a very sensitive surface analytical technique providing detailed elemental and molecular information about the surface, thin layers, interfaces, and full three-dimensional analysis of the samples.

Thanks to the advances in ToF-SIMS characterization, understanding of the chemical composition and the different components in the complex structures, permit a deeper exploration and a better knowledge in the next-generation energy storage materials such as batteries, perovskites, and 2D materials.

Firstly, we will focus on the characterization of batteries. Initially, we will discuss the sample preparation and our specific setup for transferring the specimens from the inert atmosphere in the glovebox to the ultra-high vacuum chamber of our instrument. We will illustrate the possibility to study the reversibility of the chemical composition between pristine, charged, and discharged batteries using surface mass spectrometry by ToF-SIMS in operando conditions. Then we will compare three methods of cross-sectioning used to identify the interfacial species in a composite cathode.

Secondly, we will show a study of an in-depth distribution of the 3D/2D heterostructures for perovskite solar cells where we have been able to identify individually the 3D and 2D heterostructures along with the depth of the film. Then, we will illustrate the characterization of interdiffusion in quasi-2D perovskite light-emitting diodes as a function of the organic ligand layer inserted into the perovskite crystals.

Finally, we will demonstrate how the retrospective analysis using ToF-SIMS can be very powerful and useful for exploring any single feature in 2D materials. Typically, ToF-SIMS acquisition is recording a full mass range spectrum per pixel (or voxel), which permits to isolate and to decorrelate specific regions of interest for resolving interfaces, diffusion, and doping in thin 2D structures. We will present how to treat a 3D volume image of a multilayer perovskite device for extracting useful information.

3:00pm **CA+AS+LS+NS+SS+VT-MoA-5 Advanced In-Situ and Ex-Situ S/TEM Probing of Interfacial Process in Rechargeable Batteries, Chongmin Wang**, Pacific Northwest National Laboratory

In-situ diagnosis appears to be one of the essential methods for gaining insights as how an electrode material failure, therefore feeding back for designing and creating new materials with enhanced battery performances. In this presentation, I will highlight recent progress on ex-situ, in-situ and operando S/TEM for probing into the structural and chemical evolution of interfacial process in energy storage materials. Both ex-situ and In-situ high resolution imaging enables direct observation of structural evolution, phase transformation and their correlation with mass, charge and electron transport, providing insights as how active materials failure during the cyclic charging and discharging of a battery. In perspective, challenges and possible direction for further development of the in-situ S/TEM imaging and spectroscopic methods for energy storage materials and other field will also be discussed. Most importantly, integration of different analytical tools appear to be the key for capturing complementary information.

3:20pm **CA+AS+LS+NS+SS+VT-MoA-6 Investigating  $sp^2$  and  $sp^3$  Carbon Ratios by XPS: A Study of the D-Parameter and a New Second Plasmon Loss (2PL) Parameter, Alvaro Lizarbe, G. Major, B. Clark**, Brigham Young University; *D. Morgan*, Cardiff University, UK; *M. Linford*, Brigham Young University

The D-parameter provides a useful estimate of the ratio of the  $sp^2$  and  $sp^3$  carbon in a sample. It is the energy difference between the maximum and minimum of the derivative of the C KLL Auger peak. The D-parameter can be an important analytical resource for diamond samples, as the quality of diamond depends on the  $sp^3$  to  $sp^2$  carbon ratio and any lattice impurities.

# Monday Afternoon, November 6, 2023

For example, the highly sought after type 2a diamonds, which are colorless and free from impurities, consist almost entirely of  $sp^3$  carbon. According to the universal curve for XPS, electrons with different kinetic energies have different mean free paths. Thus, electrons with different kinetic energies sample materials at different depths. In the case of carbon, the KLL Auger peak comes shallower in a material compared to the C 1s signal, which is a result of electrons with much higher kinetic energies. That is, a limitation of the D-parameter is that it is based on the C KLL Auger peak, found at around 1220 eV, while it is often related to the C 1s peak located at approximately 284.8 eV. Thus, the D-parameter is much more sensitive to adventitious carbon contamination. In an effort to derive a parameter that will be more representative of the amounts of  $sp^2$  and  $sp^3$  carbon in a material, we have examined the plasmon loss peaks of the zero-loss C 1s peak of direct current chemical vapor deposition (DC-CVD) diamonds, carbon nanotubes, and graphitic materials such as HOPG. By analyzing the second plasmon loss signal of the C 1s narrow scan, we obtain a new parameter for analyzing carbonaceous materials: the 2PL parameter. The 2PL parameter is the difference in energy between the second plasmon loss signal and the C 1s peak. We compare the traditional D-parameter with the 2PL parameter for various materials. They correlate quite well. We have also investigated various mathematical methods of deriving the 2PL parameter, including via a weighted average of the second plasmon loss and C 1s signals. Ultimately, because the 2PL parameter involves signals that are closer to the C 1s photoemission binding energy, we believe it may be more representative of the full chemistry of carbonaceous materials.

4:00pm **CA+AS+LS+NS+SS+VT-MoA-8 Solid-Liquid Interfaces for Energy-efficient Chemical Separation of Critical Minerals and CO<sub>2</sub> Conversion, Manh-Thuong Nguyen, V. Prabhakaran, D. Heldebrant, G. Johnson, Pacific Northwest National Laboratory**

**INVITED**

Chemical separations consume around 15% of the energy used by industry today. It is thus critical to develop energy- and material-efficient approaches for large-scale separations. In the first part of this presentation, I will illustrate how we employ modified 2-dimensional materials and solvents to separate critical minerals including rare earth elements. Polar functional groups present at the interface of graphene oxide laminate membranes are demonstrated to improve the selectivity of metal cations separated by both adsorption and sieving. Hydrophobic ionic liquid molecules including 1-ethyl-3-methylimidazolium chloride, when used as a minor solvent component, are shown to increase the energy efficiency of the desolvation of aqueous lanthanide cations in electrochemical separations. In the second part, I will present studies exploring the use of functionalized hexagonal boron nitride (h-BN) membranes to separate CO<sub>2</sub> from multicomponent gas mixtures. Strategies for improving CO<sub>2</sub> separation selectivity and efficiency, such as chemical functionalization and engineering the dimensions of interlayer transport channels, will be discussed. Finally, I will present studies on the electrochemical conversion of CO<sub>2</sub> into value added chemical feedstocks such as methanol on membrane-supported catalysts. Insights into the effects of local structure modification and confinement on catalytic processes will be presented.

4:40pm **CA+AS+LS+NS+SS+VT-MoA-10 Buried Interfaces of Ir Photodetector Devices Analyzed with Lab-Based Xps/Haxpes, Roman Charvior, M. Juhel, STMicroelectronics, France; O. Renault, Univ. Grenoble-Alpes, CEA, Leti, France; A. Valery, D. Guiheux, L. Mohgouk Zouknak, STMicroelectronics, France; B. Domenichini, ICB UMR 6303 CNRS-Université de Bourgogne, France**

The development of new IR photodetectors should respond to challenges in order to reach best performances. A major objective is to understand critical interfaces that play an important role in the final device properties. This work addresses to chemical analysis of molybdenum oxide (MoO<sub>3-x</sub>) used as hole transport material which is deposited between a photosensitive material and top electrode often made of indium-tin oxide (ITO). Such critical interfaces are typically located under 20 to 50 nm under the surface.

In the case of MoO<sub>3-x</sub>, the stoichiometry is generally controlled by X-ray photoelectron spectroscopy (XPS) which is well-known to obtain chemical data close to the material surface (analysis depth < 10 nm). Two methods can be used to analyse deeper buried layers: (i) the use of hard X-rays to perform Hard X-ray PhotoElectron Spectroscopy (HaXPES) and thus generate photoelectrons having a kinetic energy able to go through several tens of nm; (ii) the etching of the surface by means of an Ar<sup>+</sup> beam (having an energy from 0.5 to 3 keV) in order to remove the superficial layers giving access to the underlying layers. In the former case, the analyzed thickness remains far below 100 nm while in the latter case, the chemistry of the

surface atoms are often modified by argon ion beam. It is then necessary to mix the two approaches to allow the chemical analysis of buried interfaces. This analysis way is used here to characterize the stoichiometry of MoO<sub>3-x</sub> thin films buried under 50 nm of ITO using chromium K $\alpha$  hard-X-ray from lab-based HaXPES.

5:00pm **CA+AS+LS+NS+SS+VT-MoA-11 Detection and Discrimination of Aquatic Toxins Targeting Voltage Gated Sodium Channels Using Static ToF-SIMS Imaging, Jiyoung Son, K. Engbrecht, J. Mobberley, PNNL**

Neurotoxins from aquatic microorganisms, such as cyanobacteria and algae, have been a public health concern due to their harmful impacts on the nervous systems of animals, including humans. A subset of these neurotoxins, including saxitoxin and brevetoxin, bind to and alter the function of voltage-gated sodium channels, which are essential to generating the cell membrane action potential. Existing detection and categorization methods, such as PCR and antibody-based enzyme-linked immunosorbent assays, are too specific and they require live animals like the mouse bioassay. They also require time-consuming and expensive sample preparation for analysis using LC-MS/MS and HPLC. In this project, we developed a method to detect the activity of the aquatic sodium channel neurotoxins, brevetoxin and saxitoxin, using a cell-based process. We specifically examined the impact of these two neurotoxins on HEK-293 cells, a robust cell line that has been transfected with a voltage-gated sodium channel gene, SCN1A, in order to better study neurotoxins. We cultured a layer of cells onto disinfected silicon chips, exposed the cells to neurotoxins, performed chemical fixation, and then air-dried the chips. We also prepared mock exposed samples where the cells on the silicon chips were not exposed to neurotoxins, but just the solutions each neurotoxin was resuspended in, either a 3mM HCl solution (mock saxitoxin) or a 50:50 ACN: water solution (mock brevetoxin). Control samples, which just exposed cells to cell culture media only, gave us a baseline reference. Dried samples were analyzed with mass spectral imaging using time-of-flight secondary ion mass spectrometry (ToF-SIMS). After collecting a series of spectral data, we utilized an in-house MATLAB tool to run principal component analysis (PCA) as previously described (Yu et al., 2020). Our initial statistical analysis of SIMS spectral data using PCA shows a noticeable difference in peak trends between neurotoxin and mock-exposed cells as well as neurotoxin-exposed and control cells. Our approach utilizes chemical imaging to develop a threat-agnostic model system for detecting and classifying neurotoxin activity. The technology and protocols developed from this work could transition to other rapid cellular assays for pathogenic and chemical threats.

Reference

Yu, J., Zhou, Y., Engelhard, M. et al. *In situ* molecular imaging of adsorbed protein films in water indicating hydrophobicity and hydrophilicity. *Sci Rep* 10, 3695 (2020). <https://doi.org/10.1038/s41598-020-60428-1>

## Spectroscopic Ellipsometry Technical Group Room C124 - Session EL1+TF-MoA

### Thin Films & Novel Materials

**Moderators: Mathias Schubert**, University of Nebraska - Lincoln, **Megan Stokey**, Milwaukee School of Engineering

1:40pm **EL1+TF-MoA-1 Enhancement of Electron Effective Mass in Semiconductor Materials and 2DEGs Revealed by THz Optical Hall Effect, Nerijus Armakavicius**, Linköping University, Sweden; *S. Knight*, Linköping University; *P. Kuhne, H. Zhang, R. Carrascon*, Linköping University, Sweden; *S. Richter*, Linköping University, Lund University, Sweden; *V. Stanishev*, Linköping University, Sweden; *M. Schubert*, Linköping University, Sweden, University of Nebraska-Lincoln; *P. Paskov*, Linköping University, Sweden; *V. Darakchieva*, Lund University, Sweden

**INVITED**

Progress in semiconductor material technology continues to enable significant advances in nearly all scientific endeavors and lies at the heart of modern information and communication networks. Wide band gap semiconductors, such as GaN and SiC transpire as key materials to address the demands of next-generation quantum technology and green electronics. Understanding transport in semiconductor materials is a prerequisite for their implementation in advanced device architectures with improved functionalities. Electron effective mass is a fundamental material parameter defining the free charge carrier transport but it is very challenging to be directly determined at high temperatures and frequencies relevant for device operation.

With the advent of the optical Hall effect (OHE), which consists of performing generalized spectroscopic ellipsometry at long wavelengths in magnetic field the determination of the electron effective mass tensor at variable temperatures has become possible without the need to invoke any additional electrical measurements [1,2]. The OHE describes the external magnetic field induced anisotropic charge displacement in materials when interacting with electromagnetic waves and allows for the determination of the charge carrier sign, concentration, mobility and effective mass parameters [2].

In this work, we present a comprehensive investigations of the electron effective mass parameters in GaN bulk and epitaxial layers, as well as in two-dimensional electron gas (2DEG) in GaN based high-electron mobility transistor structures [3,4] by THz and MIR OHE [5]. OHE analysis allows to extract the free charge carrier concentration and mobility in the various structures as a function of temperature and the results are found to be in a good agreement with the respective parameters obtained by electrical Hall effect and capacitance-voltage measurements. In addition, the electron effective mass parameter is determined from the OHE at temperatures from 10K to 370K. At low temperatures (< 100 K) an electron effective mass of approximately  $0.20m_0$  is obtained in agreement with the well accepted value. Unusual enhancement of the electron effective mass is discovered with increasing temperatures to room temperature and above for both bulk, epitaxial and 2DEG GaN systems. We evaluate and discuss various mechanisms such as band gap nonparabolicity, magnetic field, strain and polaron effects, that could potentially contribute to the observed increase. We propose a frequency-dependent scattering time to be at the origin of the effective mass enhancement. We also discuss possible deviations of the free electron behavior from the classical Drude model and its implications for transport and devices operating at high temperatures (room temperature and above) and frequencies (100 GHz to 1THz).

## References

- [1] M. Schubert et al., J. Opt. Soc. Am. A 20, 347 (2003).
- [2] M. Schubert et al., J. Opt. Soc. Am. A 33, 1553 (2016).
- [3] A. Papamichail et al., Appl. Phys. Lett. 122, 153501 (2023).
- [4] P. Kühne et al., Appl. Phys. Lett. 121, 253102 (2022).
- [5] P. Kühne et al., IEEE Trans. Terahertz Sci. Technol. 8, 257 (2018).

## 2:20pm EL1+TF-MoA-3 In Situ and Real Time Spectroscopic Ellipsometry of Polycrystalline CuInSe<sub>2</sub> Co-Evaporation for Narrow Bandgap Photovoltaic Absorbers, D. Sapkota, Balaji Ramanujam, M. Alaani, A. Shan, N. Podraza, R. Collins, University of Toledo

Deposition processes for narrow bandgap ( $E_g = 1.02$  eV) polycrystalline CuInSe<sub>2</sub> (CIS) thin films with intended applications as photovoltaic (PV) absorbers have been developed and studied using various techniques of in situ and real time spectroscopic ellipsometry (SE). Real time SE analyses of two series of sequentially deposited Cu and In<sub>2</sub>Se<sub>3</sub> thin films on the same substrates, but at different Cu and In evaporation source temperatures, serves as an accurate source calibration method. This calibration enables co-evaporation of CIS films at independently controllable deposition rates and compositions, the latter characterized by the [Cu]/[In] molar ratio which establishes their p-type character as PV absorbers. In situ SE analyses of the starting crystalline Si substrates provide an accurate substrate temperature calibration, and real time SE of CIS co-evaporation on such substrates provides insights into polycrystalline nucleation and grain coarsening processes. In contrast to earlier studies of hydrogenated amorphous silicon PV absorbers, the highest device quality CIS absorbers are obtained in processes leading to the most extensive increases in the surface roughness layer thickness with bulk layer thickness, characteristic of crystallites of increasing size protruding from the film surface. Real time SE provides the time evolution of the surface roughness layer, bulk layer, and effective thicknesses for the deposited film, where the effective thickness is the volume per planar area of substrate and, thus, includes the surface roughness contribution. The effective thickness is used to evaluate the deposition rate for the desirable situation in which the roughness thickness increases continuously with bulk layer thickness. For substrate temperatures of 500°C and below in CIS co-evaporation, the roughness thickness is relatively stable with increasing bulk layer thickness at values controlled by the initial nucleation. At higher temperatures, in contrast, the surface roughness thickness increases rapidly and continuously with bulk layer thickness, well above that observed in the initial nucleation process. Such grain growth enhancement is also reflected in the following variations in the final film properties with increasing substrate temperature: (i) an increased grain size as determined by the widths of the peaks in the X-ray

diffraction pattern, (ii) a reduction in the bandgap critical point broadening parameter from ex situ SE, consistent with an increase in the grain boundary scattering time for excited carriers, (iii) a steeping of the Urbach tail, and (iii) higher performance PV devices for absorbers incorporated into cell structures.

## 2:40pm EL1+TF-MoA-4 Anisotropic Optical Properties of GdScO<sub>3</sub>, Prabir Dulal, E. Miller, University of Toledo; D. Sotir, M. Barone, D. Schlom, Cornell University; N. Podraza, University of Toledo

GdScO<sub>3</sub> is a wide-band gap semiconductor with a high dielectric constant, the potential to replace SiO<sub>2</sub> in silicon-based transistors, and use as a substrate for epitaxial thin film growth. It has an orthorhombic crystal structure resulting in crystallographic and optical anisotropy. The optical properties in the form of complex dielectric function ( $\epsilon = \epsilon_1 + i\epsilon_2$ ) spectra for each principal direction of single crystal GdScO<sub>3</sub> are investigated using generalized spectroscopic ellipsometric spectra collected over the photon energy range from 0.70 to 8.50 eV. Multiple sets of generalized ellipsometric spectra are collected from (001) and (110) surface plane oriented single crystals of GdScO<sub>3</sub> as a function of rotation about the surface normal. A divided spectral range analysis is used to determine the structural parameters of the GdScO<sub>3</sub> including bulk and surface layer thicknesses and the azimuthal Euler angle for each measurement while the remaining Euler angles are fixed based on known lattice parameters and the respective surface plane cut. In divided spectral range analysis, the full measured spectra range is subdivided into nominally transparent, weakly absorbing, and highly absorbing regions. A common structural model is used to describe the transparent and the highly absorbing spectral region to obtain common structural parameters while separate physically realistic models are applied to describe spectra in  $\epsilon$  in each direction and both of these spectral regions. The weakly absorbing region is initially ignored as the line shape describing  $\epsilon$  is not initially known. After obtaining structural parameters, numerical inversion is then used to extract  $\epsilon$  corresponding to electric fields oscillating parallel to each crystallographic axis over the full spectral range, including the initially ignored weakly absorbing region. Critical points transition in  $\epsilon$  corresponding to each direction are identified by simultaneously fitting each numerically inverted spectra in  $\epsilon_2$  and  $d\epsilon_2/dE$  using a sum of critical point parabolic band (CPPB) oscillators. A piecewise parameterization is developed that includes an Urbach tail below the band gap energy and CPPB behavior at and above the band gap energy to parameterize the numerically inverted optical response. The lowest direct transition is identified at 6.46 eV for electric fields oscillating parallel to a-axis, and above gap critical transitions at 6.72, 6.78, 6.95, 7.40, 7.92, and 8.25 eV are identified from all spectra in  $\epsilon$ .

## 3:00pm EL1+TF-MoA-5 Combined Density Functional Theory and Spectroscopic Ellipsometry Studies of Anisotropic Materials, Rafal Korlacki, M. Hilfiker, M. Stokey, M. Schubert, University of Nebraska-Lincoln INVITED

The ability of spectroscopic ellipsometry (SE) to resolve all components of the dielectric tensor combined with the predictive power of density functional theory (DFT) and related first-principles methods, is a particularly useful combination of techniques to study anisotropic materials. In recent years, a wide-bandgap gallium oxide Ga<sub>2</sub>O<sub>3</sub> is a promising candidate for applications in high-power electronic devices. The most stable  $\beta$  phase, which can be grown as a high-quality bulk crystal is highly anisotropic, thanks to the low-symmetry monoclinic lattice [1,2]. In order to further increase the bandgap, the alloys of gallium oxide and aluminum oxide, (Al<sub>x</sub>Ga<sub>1-x</sub>)<sub>2</sub>O<sub>3</sub>, can be epitaxially grown on gallium oxide substrates. Heteroepitaxial films are inherently strained. The dependence of material properties on the components of the strain tensor for monoclinic crystals have been obtained from symmetry analysis [3], and the linear deformation potentials for energies of phonon modes and band to band transitions in Ga<sub>2</sub>O<sub>3</sub> - from DFT calculations [3,4]. The same principle can be applied to the monoclinic phase of Al<sub>2</sub>O<sub>3</sub>, and Vegard's rule can then be used to construct a simple universal model of strain and composition dependencies of various material properties, including band-to-band transitions, refractive indices, components of the dielectric tensors, and effective mass parameters. Thus, these dependencies can be fully resolved for actual heterostructures under specific strain patterns [5,6].

- [1] M. Schubert et al., Phys. Rev. B 93, 125209 (2016)
- [2] A. Mock, R. Korlacki, C. Briley, V. Darakchieva, B. Monemar, Y. Kumagai, K. Goto, M. Higashiwaki, and M. Schubert, Phys. Rev. B 96, 245205 (2017)
- [3] R. Korlacki, M. Stokey, A. Mock, S. Knight, A. Papamichail, V. Darakchieva, and M. Schubert, Phys. Rev. B 102, 180101(R) (2020)

# Monday Afternoon, November 6, 2023

[4] R. Korlacki, J. Knudtson, M. Stokey, M. Hilfiker, V. Darakchieva, and M. Schubert, *Appl. Phys. Lett.* **120**, 042103 (2022)

[5] R. Korlacki, M. Hilfiker, J. Knudtson, M. Stokey, U. Kilic, A. Mauze, Y. Zhang, J. Speck, V. Darakchieva, and M. Schubert, *Phys. Rev. Appl.* **18**, 064019 (2022)

[6] M. Stokey, R. Korlacki, J. Knudtson, A. Mock, M. Hilfiker, A. Mauze, Y. Zhang, J. Speck, A. Papamichail, S. Knight, V. Darakchieva, and M. Schubert, Phonon modes and strain effects in  $\beta$ -(Al<sub>x</sub>Ga<sub>1-x</sub>)<sub>2</sub>O<sub>3</sub>, in preparation

## Spectroscopic Ellipsometry Technical Group Room C124 - Session EL2-MoA

### Instrumentation

**Moderators:** Alain Diebold, SUNY Polytechnic Institute, Nikolas Podraza, University of Toledo

4:00pm **EL2-MoA-8 Advancing Metrology in Semiconductor Manufacturing: Challenges and Novel Ellipsometry Techniques**, M. Lee, *Wookrae Kim*, Samsung Electronics Co., Inc., Republic of Korea **INVITED**  
Manufacturers of semiconductor devices must ensure uniformity in the critical dimension (CD) for proper device functionality. Precision and accuracy in semiconductor metrology and inspection are crucial to accurately measure even the smallest details of semiconductor structures. Minor imperfections in the CDs can result in device malfunctions, highlighting the importance of maintaining high levels of precision.

Ellipsometry has been a powerful method used in high volume manufacturing to provide 3D information on sample structures and achieve high measurement throughput. However, the continuous evolution of semiconductor devices with new designs, high aspect ratio contacts, and smaller cell sizes has given rise to new metrology requirements, presenting various technical challenges. As a result, further advancements in standard ellipsometry techniques are needed to meet these requirements and overcome the challenges they pose.

There are several specific challenges that need to be addressed. Firstly, the decreasing cell size in DRAM and SRAM makes smaller metrology spot sizes critically important. Secondly, the required metrology sensitivity and precision specifications become more stringent in high volume manufacturing (HVM). In the case of VNAND devices, the new cell-on-peri architecture restricts the use of the full wavelength of light from the tool, and the increasing aspect ratio of contacts limits the application of critical angle illumination in spectroscopic ellipsometry. Additionally, the number of measurement points on a wafer increases exponentially for advanced devices, necessitating innovative solutions to enable massive measurements. Finally, the time required to develop regression models is a significant drawback, particularly during the research and development (R&D) period.

To overcome these challenges, researchers have been developing various innovative techniques. These include high throughput imaging ellipsometry for massive measurements, highly sensitive pupil ellipsometry, infrared (IR) ellipsometry, and small spot ellipsometry, among others. I will present an overview of the challenges faced by ellipsometry techniques in semiconductor manufacturing and review the recently introduced novel ellipsometry techniques.

4:40pm **EL2-MoA-10 Mid-Infrared Ellipsometry for High Aspect Ratio Semiconductor Process Control Applications**, *Troy Ribaud*, Onto Innovation **INVITED**

Optical critical dimension metrology (OCD) has been a critical process control tool in the semiconductor industry for many years. Traditional OCD measurement platforms operate within the ultraviolet to near infrared spectral range and combine Mueller Matrix spectroscopic ellipsometry spectra with RCWA simulations of complex 3-dimensional models to effectively measure subwavelength geometrical properties. In recent years, challenges regarding sensitivity and parameter correlation performance

metrics have reduced the efficacy of the technique, specifically for some key VNAND technology applications with high aspect ratio structures. This situation has been remedied through the development of a spectroscopic ellipsometer which operates in the mid-infrared part of the electromagnetic spectrum. In both the lab and the field, it has been proven to outperform the existing OCD technologies for a number of those important applications.

In this talk, we shall describe the theoretical considerations that led to the change of spectral range on this unique OCD platform. We will also show a performance comparison of the two classes of OCD systems on the already explored high aspect ratio applications as well as simulations showing performance estimates as VNAND technology continues to evolve. Finally, a description of the technology roadmap for the product line will be described.

## Laboratory-Based Ambient-Pressure X-ray Photoelectron Spectroscopy Focus Topic Room B116 - Session LX+AS+BI+HC+SS+TH-MoA

### Laboratory-Based AP-XPS: Surface Chemistry and Biological/Pharmaceutical Interfaces

**Moderators:** Gregory Herman, Argonne National Laboratory, Ashley Head, Brookhaven National Laboratory

1:40pm **LX+AS+BI+HC+SS+TH-MoA-1 The Role of Co-Adsorbed Water in Decomposition of Oxygenates**, H. Nguyen, K. Chuckwu, *Líney Árnadóttir*, Oregon State University **INVITED**

The decomposition of oxygenates in the presence of water finds various applications in chemical processes, such as biomass conversion. The presence of co-adsorbates and solvents affects both the reaction rate and selectivity. In this study, we used NAP-XPS and DFT to investigate the decomposition of acetic acid on Pd(111) as a model system for the decomposition of small oxygenates in the absence and presence of water. The decomposition of acetic acid occurs through two main reaction pathways, decarboxylation, and decarbonylation, forming CO<sub>2</sub> or CO, respectively. Our DFT calculations indicate that the two pathways have similar barriers without water. However, in the presence of water, the decarboxylation path becomes. Similarly, our AP-XPS experiments show an increase in the CO<sub>2</sub>/CO ratio as well as a decrease in the CO/acetate-acetic acid and acetic acid/acetate ratios when water is present. The shift in selectivity is not due to a single reaction step, but rather the decreasing barrier in general for OH scissoring and the increasing barrier for C-O scissoring. This shift favors the formation of CO<sub>2</sub>, as demonstrated by our microkinetic model.

2:20pm **LX+AS+BI+HC+SS+TH-MoA-3 Integrating First-principles Modeling and AP-XPS for Understanding Evolving Complex Surface Oxides in Materials for Hydrogen Production and Storage**, B. Wood, *Tuan Anh Pham*, Lawrence Livermore Laboratory **INVITED**

Chemical processes occurring at solid-gas, solid-liquid, and solid-solid interfaces critically determine the performance and durability of hydrogen production and storage technologies. While directly probing behavior of these interfaces under actual operating conditions remains challenging, modern surface science approaches such as ambient-pressure X-ray photoelectron spectroscopy (AP-XPS) can provide insight into the evolution of surface chemistry in approximate environments. However, interpretation of these spectra can be complicated: standards for complex surface chemical moieties are often unavailable, and bulk standards can be unreliable. First-principles computations are emerging as an important companion approach, offering the ability to directly compute spectroscopic fingerprints. This has the advantage of aiding interpretation of the experiments, while simultaneously using the experiment-theory comparison to inform construction of more accurate interface models. In this talk, I will show how computation has been combined with laboratory-based AP-XPS measurements to understand the evolving chemistry of complex native surface oxides. Two examples will be drawn from activities within the U.S. Department of Energy HydroGEN and HyMARC consortia, which focus on renewable hydrogen production and materials-based hydrogen storage, respectively. First, I will discuss the application to surface oxidation of III-V semiconductors for photoelectrochemical hydrogen production, which demonstrates transitions between kinetically and thermodynamically controlled oxidation regimes with implications for device performance. Second, I will also show how the same approach has been applied to understand the rate-determining role of surface oxides in

the dehydrogenation performance of  $\text{NaAlH}_4$  for solid-state hydrogen storage.

This work was performed under the auspices of the U.S. Department of Energy by Lawrence Livermore National Laboratory under Contract DE-AC52-07NA27344.

3:00pm **LX+AS+BI+HC+SS+TH-MoA-5 Particle Encapsulation on Reducible Oxides Under Near-Ambient Pressures**, *F. Kraushofer, M. Krinninger, P. Petzoldt, M. Eder, S. Kaiser, J. Planksy, T. Kratky, S. Günther, M. Tschurl, U. Heiz, F. Esch, Barbara A. J. Lechner*, TUM, Germany **INVITED**

Catalysts on reducible oxide supports often change their activity significantly at elevated temperatures due to the strong metal-support interaction (SMSI), which induces the formation of an encapsulation layer around the noble metal particles. However, the impact of oxidizing and reducing treatments at elevated pressures on this encapsulation layer remains controversial, partly due to the 'pressure gap' between surface science studies and applied catalysis.

In the present work, we employ near-ambient pressure X-ray photoelectron spectroscopy (NAP-XPS) and scanning tunneling microscopy (NAP-STM) to study the effect of reducing and oxidizing atmospheres on the SMSI-state of well-defined oxide-supported Pt catalysts at pressures from UHV up to 1 mbar. On a  $\text{TiO}_2(110)$  support, we can either selectively oxidize the support or both the support and the Pt particles by tuning the  $\text{O}_2$  pressure.<sup>[1]</sup> We find that the growth of the encapsulating oxide overlayer is inhibited when Pt is in an oxidic state. Our experiments show that the Pt particles remain embedded in the support once encapsulation has occurred. On  $\text{Fe}_3\text{O}_4(001)$ , the encapsulation stabilizes small Pt clusters against sintering.<sup>[2]</sup> Moreover, the cluster size and thus footprint lead to a change in diffusivity and can therefore be used to tune the sintering mechanism. Very small clusters of up to 10 atoms even still diffuse intact after encapsulation.

[1] P. Petzoldt, P., M. Eder, S. Mackewicz, M. Blum, T. Kratky, S. Günther, M. Tschurl, U. Heiz, B.A.J. Lechner, Tuning Strong Metal-Support Interaction Kinetics on Pt-Loaded  $\text{TiO}_2(110)$  by Choosing the Pressure: A Combined Ultrahigh Vacuum/Near-Ambient Pressure XPS Study, *J. Phys. Chem. C* 126, 16127-16139 (2022).

[2] S. Kaiser, J. Planksy, M. Krinninger, A. Shavorskiy, S. Zhu, U. Heiz, F. Esch, B.A.J. Lechner, Does Cluster Encapsulation Inhibit Sintering? Stabilization of Size-Selected Pt Clusters on  $\text{Fe}_3\text{O}_4(001)$  by SMSI, *ACS Catalysis* 13, 6203-6213 (2023).

4:00pm **LX+AS+BI+HC+SS+TH-MoA-8 Applications of NAP XPS in Pharmaceutical Manufacturing: Surface Analysis, Hydrogen Bonds, and Solute-Solvent Interactions**, *Sven Schroeder*, University of Leeds, UK **INVITED**

The availability of laboratory-based NAP XPS creates novel interface research opportunities for scientific disciplines and technology areas that deal with materials incompatible with traditional ultra-high vacuum XPS. This is, for example, the case for many organic and/or pharmaceutical materials and formulations, whose characterization by XPS has hitherto been restricted by their vapour pressures. NAP XPS permits for the first time systematic and detailed analysis of the light element photoemission lines (especially C/N/O 1s) in these materials. In conjunction with elemental analysis by survey XP spectra they provide quantitative information on composition and speciation both in the bulk and at the surfaces of pure organic solids, in their formulations with other components and in solutions. Especially of interest are studies of the solid/liquid interface with water, which is of high relevance for understanding and controlling drug release profiles from tablets. To illustrate these points I will present various examples of research on pharmaceutical materials. Moreover, near-ambient pressure core level spectroscopy turns out to be an extremely powerful probe for the structure and dynamics of hydrogen bonding and proton transfer in materials, both in the solid state and in solutions. NAP XPS measurements provide unique insight into proton dynamics in noncrystalline solids and liquids, where traditional characterisation by crystallography and nuclear magnetic resonance fails or provides ambiguous information on proton locations.

4:40pm **LX+AS+BI+HC+SS+TH-MoA-10 The Change of DNA and Protein Radiation Damage Upon Hydration: In-Situ Observations by Near-Ambient-Pressure XPS**, *Marc Benjamin Hahn*, Bundesanstalt für Materialforschung und -prüfung (BAM), Germany **INVITED**

X-ray photoelectron-spectroscopy (XPS) allows simultaneous irradiation and damage monitoring. Although water radiolysis is essential for radiation damage, all previous XPS studies were performed in vacuum. [1] Here we

present near-ambient-pressure XPS experiments to directly measure DNA damage under water atmosphere. They permit in-situ monitoring of the effects of radicals on fully hydrated double-stranded DNA. Our results allow us to distinguish direct damage, by photons and secondary low-energy electrons (LEE), from damage by hydroxyl radicals or hydration induced modifications of damage pathways. The exposure of dry DNA to x-rays leads to strand-breaks at the sugar-phosphate backbone, while deoxyribose and nucleobases are less affected. In contrast, a strong increase of DNA damage is observed in water, where OH-radicals are produced. In consequence, base damage and base release become predominant, even though the number of strand-breaks increases further. Furthermore, first data about the degradation of single-stranded DNA binding-proteins (GSP / GV5 and hmtSSB) under vacuum and NAP-XPS conditions are presented.

[1] Hahn, M.B., Dietrich, P.M. & Radnik, J. In situ monitoring of the influence of water on DNA radiation damage by near-ambient pressure X-ray photoelectron spectroscopy. *Commun Chem* 4, 50, 1-8 (2021). <https://doi.org/10.1038/s42004-021-00487-1>

## Nanoscale Science and Technology Division Room B113 - Session NS+EM+MN-MoA

### Nanoscale Devices, Structures and Materials

**Moderators: Aubrey Hanbicki**, Laboratory for Physical Sciences, **Deep Jariwala**, University of Pennsylvania

1:40pm **NS+EM+MN-MoA-1 Integrated Nanophotonics Temperature Metrology Platform**, *Nikolai N. Klimov, K. Douglass, D. Barker, T. Bui, S. Robinson, T. Herman, K. Quelhas*, National Institute of Standards and Technology (NIST)

Temperature, being, perhaps, the second most measured physical property after time and frequency plays a crucial role in various aspects of modern technology ranging from medicine and Earth's climate to semiconductor industry and advanced manufacturing process control. While there have been great strides in developing novel thermometry approaches, resistance-based thermometry remains the standard method for disseminating the SI unit of temperature at the highest level of precision. The fundamental limitations of resistance thermometry, as well as the desire to reduce sensor ownership cost, have ignited a substantial interest in the development of alternative technologies such as photonics-based temperature sensors.

At the National Institute of Standards and Technology (NIST), we are developing a new photonics-based temperature measurement solution that has the potential to revolutionize how temperature is realized and disseminated to customers. One of the key elements of our Photonic Thermometry program is an ultra-Sensitive Photonic Thermometer (SPoT) – an on-chip integrated silicon nanophotonic resonator, whose optical resonance frequency shifts with temperature due to high thermo-optic coefficient of silicon and can be used to trace temperature variations with high precision. Our goal is to evolve SPoT into a robust, field-deployable device that is on par or better than the state-of-the-art resistance thermometer.

In this work, we describe the performance of SPoT thermometer, as well as a new photonic readout for SPoT. In our new read-out scheme, we employ a novel offset-locking technique for reading out the resonance wavelength of the SPoT. This method provides extremely high accuracy for relative temperature changes on a short time scale (<< 1s). Our results indicated that the packaged on-chip integrated SPoT can detect temperature fluctuations as small 2  $\mu\text{K}$  over 200 ms integration time. This methodology as well as other proposed methods will be discussed. We also show a benchmark comparison of SPoT thermometer to Standard Platinum Resistance Thermometer (SPRT) – the best-in-class resistance thermometer, in various fixed-point cells of ITS-90, evaluating temperature resolution and repeatability

2:00pm **NS+EM+MN-MoA-2 AVS Dorothy M. and Earl S. Hoffman Scholarship Recipient Talk: Breaking the Efficiency Bottleneck of Micro-LEDs Through Nanoscale and Excitonic Engineering**, *Yixin Xiao<sup>1</sup>, R. maddaka, Y. Wu, Y. Malholtra, Y. Guo, S. Yang, K. Sun, A. Pandey, J. Min, Z. Mi*, University of Michigan, Ann Arbor

The performance of conventional optoelectronic devices, such as LEDs and laser diodes, is extremely sensitive to the presence of defects and

<sup>1</sup> AVS Dorothy M. and Earl S. Hoffman Scholarship Recipient

# Monday Afternoon, November 6, 2023

dislocations. For these reasons, it has remained challenging to achieve high efficiency nanoscale LEDs and laser diodes. For example, while conventional broad area LEDs can exhibit external quantum efficiency (EQE) in the range of 80-100%, the EQE of submicron scale LEDs is often <1%, due to the dominant nonradiative surface recombination. The operation of conventional LEDs involves the radiative recombination of free electrons and holes in the active region. It is known that an exciton, a bound state of an electron and hole through strong Coulomb interaction, can drastically enhance the radiative recombination efficiency, which can be potentially exploited to make micro and nanoscale LEDs relatively immune from the presence of defects/traps. Recent studies have shown that the exciton oscillator strength can be increased by nearly two orders of magnitude in small size InGaN nanowires, due to efficient strain relaxation. Here we demonstrate that the efficiency bottleneck of  $\mu$ LEDs can be fundamentally addressed by utilizing bottom-up III-nitride nanostructures. We report on the demonstration of micrometer scale green and red LEDs with an external quantum efficiency of 25% and 8%, respectively, which are the highest values ever reported to the best of our knowledge. We employ selective area plasma-assisted molecular beam epitaxy as the material synthesis platform. Due to efficient strain relaxation, such bottom-up nanostructures are largely free of dislocations. By exploiting the large exciton binding energy and oscillator strength of quantum-confined InGaN nanostructures, we show that the external quantum efficiency of a green-emitting micrometer scale LED can be dramatically improved from ~4% to >25%. The dramatically improved efficiency is attributed to the utilization of semipolar planes in strain-relaxed nanostructures to minimize polarization and quantum-confined Stark effect and the formation of nanoscale quantum-confinement to enhance electron-hole wavefunction overlap. We have further developed a new approach that included an InGaN/GaN short period superlattice together with an InGaN quantum dot active region to achieve high efficiency red emission. A maximum quantum efficiency of >7% was measured. Our studies offer a viable path to achieve high efficiency micrometer scale LEDs for a broad range of applications including mobile displays, virtual/augmented reality, biomedical sensing, and high-speed optical interconnects, that were difficult for conventional quantum well based LEDs.

**2:20pm NS+EM+MN-MoA-3 Modeling Gas Phase Etching in High Aspect Ratio Stacked Nanostructures for Semiconductor Processing: Stacked SiGe Layer Etching, Zach Zajo, Stanford University; D. Mui, J. Zhu, M. Kawaguchi, Lam Research Corp.; E. Shaqfeh, Stanford University**

Gate all around (GAA) nano-transistors offer better channel control and increased current carrying capacity compared to FinFETs (Field Effect Transistor) which are currently the standard in the semiconductor industry. However, the need for precise control of their nanoscale features poses a challenge in manufacturing such GAA nano-transistors. The high material selectivity required in fabricating these transistors makes gas phase etching much more appealing in comparison to liquid phase and plasma-based etching techniques. An etching configuration that is of particular interest is one consisting of alternating layers of Si and SiGe from which the SiGe layers are selectively etched by fluorine gas. In the etching of these structures, it is important to have a uniform etch-rate for SiGe layers from top to bottom, to maintain consistency of the etched features. This consistency is essential for the superior performance of the GAA devices. The key gas phase processing challenge then is to determine and maximize the number of SiGe-Si layers that can be stacked in a single structure while still maintaining a nearly uniform etch-rate from top to bottom in the stack. While experiments have offered insights in terms of the effect of layer thickness, number of layers, gas pressure etc. on the viability of the process, such experiments are quite expensive and tedious. We propose and develop computer simulations as a tool to predict the etch profile evolution over time in a gas phase etching process. The tool is based on a mathematical model which considers the transport processes and surface interactions involved in the gas phase etching process – which at the nanoscale is primarily governed by Knudsen diffusion in the free molecular flow regime. Thus, the transport model is formulated as a boundary integral equation which takes into account the direct flux of etchant molecules that any given point on the exposed surface receives from the bulk gas phase as well as the re-emission flux from other parts of the structure itself. We compared the applicability of two different surface reaction models - a model where the local etch rate is linear in the flux at a point and a Langmuir adsorption/reaction model- to connect the net flux received at a point on the surface to the local etch rate. Our results show that the re-emission of etchants at the etching interface plays a vital role in determining the differential etch rates observed across layers at different depths in the stacked feature. In addition, we have characterized the effect

Monday Afternoon, November 6, 2023

of layer thickness and the spacing between adjacent stacks as these impact the etch rates observed from layer to layer.

**2:40pm NS+EM+MN-MoA-4 Fabrication of Silicon Microfluidic Gratings for Neutron Imaging, S. Robinson, R. Murphy, National Institute of Standards and Technology (NIST); Y. Kim, National Institute of Standards and Technology (NIST)/ University of Maryland, College Park; J. LaManna, C. Wolf, K. Weigandt, D. Hussey, Nikolai N. Klimov, National Institute of Standards and Technology (NIST)**

In this work, we describe the development of a spatial modulator for x-ray and neutron beams. Current technology for x-ray and neutron phase imaging uses individual source gratings with a fixed period to modulate the beams. Each fixed-period, or “static” source grating, has a limited range in spatial resolution at a specific length scale, thus, a relatively larger set of individual static source gratings is required to achieve high-resolution imaging. Our team is developing a neutron imaging technique that will probe heterogeneous samples across multiple length scales. To address the need for a large variability of source grating periods, we are building a silicon microfluidic-based device, DynAmic ReconfigURable Source grating (DARIUS), that itself is capable to adjust, with high resolution, the grating period from 20  $\mu$ m to 20,000  $\mu$ m. With such on-demand tunability, a single DARIUS has the potential to replace more than 500 static source gratings, minimizing the need of fabricating, installing, and aligning a new source grating for the required period. To achieve such functionality, DARIUS features over 5,000 microfluidic grating channels that are etched on both the front and back sides of a 100 mm silicon wafer. Each of these grating channels can be selectively infilled with a neutron and/or x-ray absorbing fluid, and provide real-time reconfigurable spatial modulations for neutron and x-ray beams. In this work, we present updates on the double-sided deep silicon etch (on the front and the back of the wafer), as well as the front-to-back alignment of the silicon channels. We also describe the progress towards wafer bonding to seal the front and back sides of DARIUS device. Due to the challenges of both the microfluidic control and tight fabrication tolerances, we are evaluating the design specifics to address larger grating periods.

**3:00pm NS+EM+MN-MoA-5 The Small Shift Matters – Submilliradian Tilt Goniometry in Scanning Electron Microscopy, Andrew Madison, J. Villarrubia, D. Westly, R. Dixon, C. Copeland, National Institute of Standards and Technology (NIST); J. Gerling, K. Cochran, A. Brodie, L. Muray, KLA-Tencor; J. Liddle, S. Stavis, National Institute of Standards and Technology (NIST)**

Electron optical aberrations degrade the accuracy and reliability of scanning electron microscopy. Among multiple aberrations of potential concern, an axial tilt of the electron beam shifts the apparent positions and deforms the intensity profiles of features in scanning electron micrographs. Measurement of the beam tilt can enable either a physical correction of beam deflection or an analytical correction in a measurement function. In this study, we report a novel reference structure and image analysis method to measure such shifts, among other key effects. Our new concept has the potential to improve accuracy in scanning electron microscopy, with multifunctional standards enabling integrative calibrations of beam tilt and beyond. Such advances will be of particular interest in semiconductor manufacturing metrology, where even the small shift matters.

We explore conical frustum arrays as multifunctional reference structures, using physical theory to guide ongoing experiments. For a tilt inclination  $\vartheta$ , a centroid shift  $s$  between the top and bottom edges of a conical frustum shows the effect of tilt. For a frustum height  $h$ , the measurement function is simply  $\vartheta = \sin^{-1}(s/h) \approx s/h$ , yielding a null-tilt sensor and self-calibrating goniometer. To understand the limiting random effect of shot noise, we simulate frustum images using a physical model of electron scattering and emission. At a dose of 60 electrons per  $\text{nm}^2$ , model shifts show the possibility of submilliradian accuracy for sidewall angles greater than approximately 40 mrad. In experimental measurements, charge accumulation and hydrocarbon contamination may limit the achievable electron dose, while conical asymmetry among other systematic effects will ultimately limit accuracy. In initial experiments, we fabricate submicrometer frustum arrays in silicon using electron-beam lithography and reactive ion etching and demonstrate use of the reference structure in calibrations of a typical scanning electron microscope.

In an integrative calibration, frustum arrays are optimal structures for correlative atomic force, super-resolution optical, and scanning electron microscopy. This workflow yields reference heights and positions that allow calibration of scale factor and correction of scanfield distortion, improving

# Monday Afternoon, November 6, 2023

the accuracy of centroid shifts to show electron beam tilt and spatial variation thereof across the imaging field.

**4:00pm NS+EM+MN-MoA-8 On Point – Accurate Integration of Quantum Dots and Bullseye Cavities, Craig Copeland, A. Pintar, R. Dixon, A. Chanana, K. Srinivasan, D. Westly, B. Ilic, M. Davanco, S. Stavis, NIST-Gaithersburg**

Self-assembled quantum dots are promising light sources for quantum networks and sensors. These emerging technologies require the accurate integration of quantum dots and photonic structures, but epitaxial growth forms quantum dots at random positions in semiconductor substrates. Optical localization of these random positions can guide the placement of photonic structures by electron-beam lithography. This integration process requires the reliable registration of position data across microscopy and lithography systems. However, large errors can result from multiple sources, including lithographic and cryogenic variation of reference dimensions for microscope calibration, as well as localization errors from optical distortion. Such errors tend to increase across an imaging field, presenting a critical impediment to exploiting the throughput and scalability of widefield microscopy. In this study, we target this problem and show how our solution enables accurate integration to improve device performance and process yield. We develop our methods of traceable localization to calibrate a cryogenic localization microscope – an optical microscope with the sample and objective lens inside of a cryostat, and custom optics outside of the cryostat. We fabricate and characterize arrays of submicrometer pillars in silicon, creating microscopy standards with both traceable reference positions and traceable reference data for thermal expansion coefficient. We image these arrays with the cryogenic microscope at approximately 1.8 K, localize the pillar positions, and use the reference data to calibrate the microscope. Our calibration determines the scale factor of the imaging system and corrects position errors due to complex distortion, among other aberration effects. We combine the results of this cryogenic calibration with our previous assessment of fabrication accuracy by electron-beam lithography, introducing a comprehensive model of the effects of registration errors on Purcell factor. This performance metric quantifies the radiative enhancement that occurs upon integration of a quantum dot into a bullseye resonator. The Purcell factor reaches a maximum value of approximately 11 for error-free registration of the quantum dot and resonator center. Our model demonstrates the possibility of greatly improving Purcell factor across a wide field. Depending on the Purcell factor threshold, on-point integration can increase yield by one to two orders of magnitude. This foundation of accuracy will enable a transition from demonstration devices to efficient processes, leading to the reliable production and statistical characterization of quantum information systems.

**4:20pm NS+EM+MN-MoA-9 Nanostructured Gas Sensors for the Detection of Meat Spoilage, Ken Bosnick, National Research Council of Canada**

The sustainability of the food industry will remain a key societal challenge in the decades ahead. In North America, over 20% of meat produced is wasted, mostly at the later stages in the supply chain [1]. When meat begins to degrade, it releases biogenic amines (e.g., putrescine,  $H_2N-(CH_2)_4-NH_2$ ) for which early detection provides a means to sense the onset of spoilage [2]. Early detection of meat spoilage through the sensing of such amines can proactively assure quality in the food production process and potentially eliminate the need for food recalls and other waste. At the heart of these envisioned quality assurance strategies are portable devices that are capable of rapid detection of low levels of biogenic amines and that can be easily deployed at various stages in the production process. New material technologies with a selective response to low levels of biogenic amines are needed to enable these envisioned devices.

The use of MOS-type gas sensing technology represents a promising avenue for portable gas sensors with many advantages over competing sensing technologies and over more traditional analysis methods. We have investigated the application of Pd-decorated ZnO nanoflowers in a chemiresistive sensing mechanism and found an excellent response of 99.5% at 250 °C towards 400 ppm methylamine [3]. The device also shows a promising response of 45% at room temperature, making it a candidate sensing material for early detection of spoilage in meat-based products. Towards improved performance at room temperature, ZnO nanocantilevers [4] are being investigated for amine sensing and will also be discussed.

[1]FAO. 2011. “Global food losses and food waste – extent, causes and prevention”

[2]Fernanda Galgano, Fabio Favati, Malvina Bonadio, Vitina Lorusso, Patrizia Romano, “Role of biogenic amines as index of freshness in beef meat packed with different biopolymeric materials”, *Food Res. Int.*, 42 (2009) 1147

[3]Jennifer Bruce, Ken Bosnick, Elham Kamali Heidari, “Pd-decorated ZnO nanoflowers as a promising gas sensor for the detection of meat spoilage”, *Sens. Actuators B Chem.* 355 (2022) 131316

[4]Kissan Mistry, Viet Huong Nguyen, Mohamed Arabi, Khaled H. Ibrahim, Hatameh Asgarimoghaddam, Mustafa Yavuz, David Muñoz-Rojas, Eihab Abdel-Rahman, and Kevin P. Musselman, “Highly Sensitive Self-Actuated Zinc Oxide Resonant Microcantilever Humidity Sensor”, *Nano Lett.* 22 (2022) 3196

**4:40pm NS+EM+MN-MoA-10 From Natural to Fabricated Gas Sensing Photonic Nanostructures: Unexpected Discoveries and Societal Impact, Baokai Cheng, J. Brewer, B. Scherer, R. Potyraiolo, GE Research Center**

Existing gas sensors often degrade their performance in complex backgrounds. Thus, new sensing approaches are required with improved sensor selectivity, accuracy, and stability for demanding applications ranging from homeland security, to industrial process monitoring and safety, and to monitoring of outdoor and indoor pollutants and volatile biomarkers.

In this talk, first, we will demonstrate and analyze capabilities of natural photonic nanostructures as sensors for detection of different gases and the origins of these capabilities. Next, we will demonstrate that this new acquired knowledge from studies of natural nanostructures allowed us to develop design rules to fabricate nanostructures for needed gas selectivity and stability for numerous gas monitoring scenarios at room and high temperatures. These design rules for selective gas sensors bring a multivariable perspective for sensing, where selectivity is achieved within a single nanostructured sensing unit, rather than from an array of separate sensors. We fabricated bioinspired nanostructures using several contemporary technologies and have achieved several new functionalities beyond Nature. By utilizing individual nanostructured sensors rather than sensor arrays we also have improved sensor stability by eliminating independent aging factors in separate sensors and their arrays. The use of existing and our new machine learning (a.k.a. multivariate analysis, chemometrics) tools further advanced our sensor designs and performance in detection of multiple gaseous species. The achieved performance capabilities of our developed bio-inspired photonic gas sensors complete with the capabilities of existing commercially available gas sensors and their arrays. These colorimetric sensors can be tuned for numerous gas sensing scenarios in ambient and high temperatures, in confined areas or as individual nodes for distributed monitoring.

**5:00pm NS+EM+MN-MoA-11 Argon-Plasma Dry Etch of sub-Micron Feature-Size Waveguides in Thin-Film Lithium Niobate, Sessa Challa, N. Klimov, P. Kuo, NIST-Gaithersburg**

Lithium Niobate (LN) possesses exceptional properties such as a wide transparency range, large non-linear coefficient, and high-electro-optic efficiency. These properties along with successful implementation of periodic poling in LN have spurred the development of devices finding applications in spectroscopy, remote sensing, and quantum communications.

Despite these valuable properties and possessing large second-order non-linearity, LN has taken a backseat to compete integrated photonic platforms, such as silicon, which has no second-order nonlinearity. This was due to difficulties in fabrication of a low-loss LN waveguides (WGs), integration, as well as processing on a wafer-scale.

With commercial TFLN wafers now being accessible, in parallel with the rapid advancement of scalable micro-/nano fabrication techniques, TFLN photonic devices are steadily emerging. By offering tighter confinement compared to ion-exchanged WGs, TFLN WGs boost the performance of devices such as EOMs to have bandwidth with smaller power consumption.

Etching LN is however challenging, hence, making it difficult to fabricate low-loss WGs. In particular poor etch induces substantial roughness and non-vertical side-wall angles contributing to high propagation losses in the WGs. Low-loss LN WGs have been demonstrated over the past several years. Most of these WGs were fabricated using argon gas inductively

coupled reactive ion plasma (ICP-RIE) etching. Etch recipe optimization is of utmost importance to reduce optical losses. Initial demonstrations have shown that TFLN devices can match or exceed the performance of traditional silicon or indium phosphide devices. However, low-loss TFLN waveguides are not widely available.

As a part of the effort to develop low-loss TFLN devices, we perform a systematic study of fabrication high-quality LN WGs. The main goal of this investigation is to reduce the WG's surface roughness while keeping an optimum side-wall angle profile that minimizes light propagation loss. In particular, our efforts are focused on three criteria: (1) selecting appropriate mask materials to reduce the transfer of mask defects into LN WGs, (2) establishing the optimal plasma chemistry by detailed study of various ICP-RIE etch parameters, and, (3) determining the optimum chemical cleaning protocol to remove the redeposited during ICP-RIE etch material on the WG's side-wall. In this presentation, we discuss the details of all three fabrication aspects to make high-quality TFLN devices and structures.

## Plasma Science and Technology Division Room A106 - Session PS+SE-MoA

### Plasma Sources, Diagnostics, Sensors and Control

**Moderators:** Michael Gordon, University of California at Santa Barbara, Yohei Ishii, Hitachi High Technologies America Inc.

1:40pm **PS+SE-MoA-1 On the Influence of the Target Material on the Discharge Properties of the High Power Impulse Magnetron Sputtering Discharge**, Jon Tomas Gudmundsson, K. Barynova, University of Iceland; M. Rudolph, Leibniz Institute of Surface Engineering (IOM), Germany; J. Fischer, Linköping University, Sweden; S. Suresh Babu, University of Iceland; M. Raadu, N. Brenning, KTH Royal Institute of Technology, Sweden; D. Lundin, Linköping University, Sweden

High power impulse magnetron sputtering (HiPIMS) operation results in increased ionization of the sputtered species and lower deposition rate than the dc magnetron sputtering discharge, when operated at the same average power. We have applied the ionization region model (IRM) [1] to model HiPIMS discharges in argon with a number of different targets [2,3], to study various processes, such as working gas rarefaction and refill processes, the electron heating mechanisms, ionization probability and back-attraction of the sputtered species, and recycling mechanisms. The HiPIMS discharge can contain a large fraction of ionized sputtered material and often a significant fraction, of the ions involved in the sputter process are ions of the target material. This also implies that a large fraction of the ions of the sputtered species can be attracted back to the target and are not deposited on the substrate to form a film or coating. Self-sputtering and the self-sputter yield are therefore expected to play a significant role in HiPIMS operation, and have a decisive impact on the film deposition rate, at least for metal targets. We explore the relationship between the self-sputter yield and deposition rate as well as the ionization and back attraction probabilities. The back-attraction probability appears to decrease with increased self-sputter yield. The various contributions to working gas rarefaction including electron impact ionization, kick-out by the sputtered species, and diffusion, are evaluated and compared for the different target materials, over a range of discharge current densities. For all cases the working gas rarefaction is found to be significant, and to be caused by several processes, and that their relative importance varies between different target materials. In the case of a graphite target, electron impact ionization is the dominating contributor to the working gas rarefaction, with 55 - 64 % contribution, while the kick-out, or sputter wind, has negligible influence, whereas in the case of tungsten target, the kick-out dominates, with 39 - 48 % contribution. The relative role of kick-out by the sputtered species increases and the relative role of electron impact ionization decreases with increased mass of the target atoms.

[1] Huo et al., Journal of Physics D: Applied Physics 50, 354003 (2017)

[2] Gudmundsson et al., Surface and Coatings Technology 442, 128189 (2022).

[3] Babu et al., Plasma Sources Science and Technology 31, 065009 (2022)

2:00pm **PS+SE-MoA-2 Numerical Analysis of Curling Probe Designing for an Effective Electron Density Measurement in Plasma**, Daisuke Ogawa, S. Kato, H. Sugai, K. Nakamura, Chubu University, Japan

Electrons make a main contribution to generating reactive species in a low-temperature plasma. Optical emission is often utilized to monitor plasma, but it should be noted that the ultimate origin of the emission is due to collisions with the electrons in the plasma. This means that electron monitoring could be the primary information of the plasma. A curling probe is one of the probes that enable an electron density measurement in the plasma. The probe measures the density derived from a shift of the fundamental resonant frequency that the probe holds. Therefore, the probe measures the density even in an environment where the plasma makes a dielectric film deposition. The probe utilizes a slot antenna to make the electromagnetic resonance, which is equipped on the top surface of the probe. This antenna structure gives an advantage in directional electron density measurement. This directionality is useful, particularly when the probe desires to be embedded into a wall and/or an electrode. Recently, we have also developed a technique with the curling probe that enables one to make in-situ measurements of electron density in plasma and the film thickness deposited on the probe surface. The technique requires two different-sized curling probes, so we named it the double curling probe method. This technique is potentially powerful in a plasma-processing reactor with electron density monitoring. However, we noticed that the technique requires further improvement in their measurement resolution; the frequency shift is not always noticeable, especially when the deposited film thickness is small. The frequency resolution depends on the quality factor of an inverted peak in the reflectance spectrum. According to the circuit theory, the factor depends on antenna configuration, such as the antenna's resistance, inductance and capacitance. These parameters depend on the antenna design, so we have researched how curling probe design affects the factor with an electromagnetic wave simulator, CST microwave studio. Our recent result showed that the factor depends on the antenna material, the antenna length, and the antenna thickness. In particular, the long antenna helps stabilize the factor even when increasing electron density in plasma. In this presentation, we will show our recent analysis to suggest what antenna design a curling probe ought to have to improve electron density measurement with a curling probe.

2:20pm **PS+SE-MoA-3 Annular Beam Confocal Laser-Induced Fluorescence Diagnostic for Measurements of Ion Velocity Distribution Function in Industrial Plasmas**, Ivan Romadanov, Y. Raitses, Princeton Plasma Physics Laboratory

Laser-Induced Fluorescence (LIF) is a powerful diagnostic tool for analyzing ion velocity distribution functions (VDFs) in plasma [1]. However, the requirement for two-sided access to plasma for beam injection and fluorescence collection in conventional LIF configuration is not always practical. Confocal LIF configurations, which are widely used in various fields such as biology and medicine, have been developed for several plasma diagnostic applications [2]. The primary advantage of confocal LIF configurations is the coincidence of the laser beam injection and fluorescence collection branches, enabling measurements in systems with limited optical access or complex geometries. This study introduces a novel variation of confocal LIF - Annular Beam Confocal Laser-Induced Fluorescence (ABC-LIF) configuration [3]. The proposed LIF configuration utilizes a structured Laguerre-Gaussian laser beam with an annular intensity profile, generated by diffractive axicons. This approach facilitates LIF signal collection along the main optical axis within the ring region while controlling spatial resolution through laser beam parameters, such as annulus thickness and beam diameter. Consequently, all enclosed fluorescence light is collected, maximizing the signal-to-noise ratio (SNR). This method achieves a spatial resolution of approximately 5 mm at a 300 mm focal distance, with the potential for 1 mm resolution, comparable to conventional LIF. The ABC-LIF configuration benefits from a small depth of field (DOF), typically achieved by Gaussian beams of large diameter, while the Laguerre-Gaussian beam allows for maintaining spatial separation between fluorescence and laser lights at comparable DOF values. Additionally, the configuration circumvents issues with beam back reflection. The ABC-LIF configuration was experimentally verified in industrial DC plasma source measurements of argon ion VDFs. Comparisons between confocal and conventional LIF revealed good agreement in determining plasma parameters, such as ion temperature, flow velocities, and ion density profiles. Applicable to various plasma processing equipment and sources, including hollow cathodes, microplasmas, and electric propulsion, the ABC-LIF configuration presents a promising diagnostic tool for industrial plasmas.

## References

- [1] Bachet G et al 1998 Phys. Rev. Lett. 80 3260  
[2] Thompson D et al 2017 Rev. Sci. Instrum. 88 103506  
[3] I. Romadanov, Y. Raitses, arXiv preprint arXiv:2303.12580. (2023)  
Funding Acknowledgement: This work was performed under the U.S. Department of Energy through contract DE-AC02-09CH11466.

### 2:40pm **PS+SE-MoA-4 Control of Electron Energy Distribution Function in Electron Beam Generated ExB Plasma**, *Nirbhav Chopra, Y. Raitses*, Princeton Plasma Physics Laboratory

Electron beam (e-beam) generated plasmas are promising for low pressure, low damage threshold material processing applications requiring efficient generation of ions and radical species [1,2]. The production of reactive species generated by electron impact is controlled by the electron energy distribution function (EEDF). In this work, we investigate the EEDF and plasma parameters of a partially magnetized plasma generated by e-beam in low pressure (0.1-10 mTorr) argon and nitrogen. The e-beam (energy < 100 eV) is extracted from a negatively biased thermionic filament and injected into a cylindrical vacuum chamber with applied axial magnetic field. The EEDF is measured using electrostatic probes. Results show the presence of e-beam electrons with energies comparable with the applied cathode voltage and a group of warm electrons (10-30 eV). Mechanisms of the formation of this intermediate group of electrons will be discussed. In addition, we will present and discuss the effect of the addition of nitrogen gas to the argon plasma on the EEDF.

- [1] Zhao F et al C G 2021 *Carbon* **177** 244–51  
[2] Walton S G et al 2015 *ECS J. Solid State Sci. Technol.* **4** N5033–40

### 3:00pm **PS+SE-MoA-5 Expanding the Capabilities of Microwave Hairpin Resonator Probes**, *Steven Shannon*, North Carolina State University

**INVITED**

Microwave hairpin resonator probes are a common diagnostic for measuring electron density in plasmas. They are particularly effective in low temperature plasmas, RF driven plasmas, reactive (particularly depositing) plasma chemistries, and other plasma environments that can challenge the effective use of comparable probe diagnostics such as Langmuir probes or emissive probes. Efforts to increase the utility of these probes through both innovative probe design (such as biasing and curling probe design) and combination of the hairpin probe with other diagnostic techniques (such as laser photodetachment studies in electronegative discharges) have increased the utility of hairpin probes in the field of experimental plasma science. This work presents efforts to expand on the measurement capabilities of these probes in two ways. First, the analysis of resonance data is expanded to account for plasma contributions to the Q-factor of the loaded resonance circuit. From this, additional plasma parameters such as electron neutral collision frequency can be estimated. Second, the time resolution of these probes are expanded to provide insight into the time modulation of plasma discharges including pulsed RF discharges, and can be extended to time resolved measurements within the period of an RF driven system, complementing the growing area of phase resolved plasma characterization. The methods for expanding the capabilities of these probes are presented in this talk as well as examples of where this extension of probe capability has provided insight into basic plasma phenomena including moderate pressure operation of RF discharges, sheath heating, probe perturbation effects on density measurement, electronegative plasma instabilities, and the role of plasma edge uniformity on power coupling in inductively coupled plasma reactors. This work has been supported by the National Science Foundation, U.S. Department of Energy, Samsung Electronics, Applied Materials Inc. MKS Instruments and the state of North Carolina.

### 4:00pm **PS+SE-MoA-8 Time-Resolved Electron Energy Distribution in a Multi-Frequency Capacitively Coupled Plasma Reactor**, *C. Kelly, Md. Amzad Hossain, D. Kapelyan, D. Ruzic*, University of Illinois at Urbana-Champaign

This work uses a time-resolved Langmuir probe to measure the electron energy distribution function (EEDF) in a capacitively-coupled parallel-plate (CCP) plasma reactor. The EEDF completely determines the plasma chemistry in a low-temperature plasma, and that is why it is so important to obtain. By seeing how the EEDF changes throughout an RF cycle, both as a function of time and position, one then knows the extent by which altering the RF waveform can affect the energy of the electrons. Often industry mixes RF frequencies to alter the plasma -- particularly the ion energy distribution at the substrate. Here we add a second frequency in a

systematic manner and examine the changes in the instantaneous EEDF. We also examine the turn on and turn off times of the RF generator itself.

Specialized circuits were designed for this work to ensure high frequency fidelity so digitization at 1.5 GHz is possible and accurate. A set of experiments were conducted to show how only altering circuit parameters affect the results, and steps were taken to eliminate those effects. Spatial variations of the resulting EEDFs were investigated, especially near the edge of the CCP reactor, to see which aspects change the most with radius.

### 4:20pm **PS+SE-MoA-9 Mass Spectral Characterization and Control of Plasma Etch Processes**, *L. Shoer, P. Heil, S. Pursel*, Intel Corporation; *N. Salovich*, Edwards Vacuum; *David Shykind*, Intel Corporation

As semiconductor critical dimensions have reached the single-digit nanometer scale, reproducible control of etch processes has become critically dependent on consistent wafer-to-wafer processing. Nanometer feature sizes and atomically thin layers have led to a regime where traditional bulk plasma characterization techniques no longer give insight into the chemical processes occurring on the wafer. Furthermore, the number of moles of reactants on the walls of an etch chamber are greater than or equal to the quantity of reactants intended to be etched on a wafer itself. Uncontrolled, this situation complicates etch processes, introducing hysteretic behavior even assuming an ideal input stream of identical wafers, and exacerbates actual wafer-to-wafer variation effects. We show how high-speed (subsecond time resolution), non-invasive mass spectrometry of plasma cleaning, seasoning and actual etch steps themselves leads to improved performance and enhanced mechanistic understanding of plasma etch processes.

### 4:40pm **PS+SE-MoA-10 Development of a Catalytic Probe for the Detection of Fluorine Radicals with Applications to Semiconductor Manufacturing**, *Nicholas Connolly, J. Mettler, R. Garza, R. Sankaran, D. Ruzic*, University of Illinois Urbana-Champaign

Plasma processing is an essential part of integrated circuit manufacturing, with plasma etching, plasma strip, and chamber cleaning being three critical steps. All of these steps rely on radicals, highly reactive neutral species created in the plasma, to drive the desired etching reactions. Because of the importance of radical species in etching reactions and rates, quantification of the densities of these species is important for understanding plasma etching dynamics. Additionally, spatial resolution of radical densities allows specific knowledge of etch dynamics at a substrate or a chamber component of interest.

One technique that has been developed to detect and quantify radical species is a catalytic probe, which consists of two thermocouples each coated with a different metal. The different metals catalyze the recombination of radical species at different rates, leading to a temperature difference between the thermocouples. This temperature difference is proportional to the density of radical species, and so a radical density can be determined. The catalytic probe technique provides in-situ, spatially resolved radical densities. This has advantages over techniques which gather a line-averaged signal, such as optical emission spectroscopy (OES), and measurement methods that require ex-situ analysis, such as coupon etch rates.

Previous studies have applied catalytic probes to the detection of hydrogen (H), oxygen (O), and nitrogen (N) radicals.<sup>1</sup> To our knowledge, a catalytic probe for fluorine (F) has yet to be reported. Here, we present a thermocouple-based catalytic probe to determine spatially resolved fluorine radical densities in SF<sub>6</sub>/Ar plasmas. The catalytic activity of zinc, copper, and gold is reported. The radical densities determined from the radical probes are compared to those determined via actinometry and coupon etch rates. These methods also provide verification of the recombination coefficient of the probe material and thereby confirm the quantitative results of the radical probe.

- [1] D. Qerimi, I. Shchelkanov, G. Panici, A. Jain, J. Wagner, and D.N. Ruzic. *J. Vac. Sci. Technol.* A 39, 023003 (2021).

### 5:00pm **PS+SE-MoA-11 Multi-Diagnostic Investigation of Etching Plasma Species in an Industry-Grade Inductively-Coupled Plasma Etcher**, *Jeremy Mettler<sup>1</sup>, N. Connolly, S. Dubowsky, D. Ruzic*, University of Illinois at Urbana-Champaign

Plasma etching kinetics and reaction mechanisms often involve complex interactions between radical, neutral, and charged species. Optimization of etch rate and selectivity for a given process can be tedious without a

<sup>1</sup> PSTD Coburn & Winters Student Award Finalist

# Monday Afternoon, November 6, 2023

detailed mechanistic understanding of the etching mechanisms, which in turn can be difficult to determine without accurate measurements of all relevant plasma species. Many diagnostics exist which are able to measure some of these species, but each has their own tradeoffs, and none are able to measure all species under all conditions.

In this work we discuss the development of a suite of plasma diagnostics for measuring the environment in an etching system, including neutral, charged, and radical species. To accurately measure each component of the etch process, results from appearance energy mass spectroscopy, optical emission spectroscopy, fluorine radical probe analysis, and Langmuir probe analysis are combined, with overlap in the sensing capabilities of each diagnostic used for cross-validation. The use of multiple independent diagnostics with different spatial resolutions and species sensitivities provides flexibility and increased confidence in quantitative results. This work will present a comparison of results obtained by the individual diagnostics across several  $\text{CF}_4$  based etching conditions in an industry-grade inductively-coupled plasma etching tool. Further comparison will be made between experimental etching results and 0-D plasma modeling of the etching system.

## Quantum Science and Technology Mini-Symposium Room B110-112 - Session QS-MoA

### Systems and Devices for Quantum Computing

Moderators: Ekta Bhatia, NY CREATES, Dave Pappas, Rigetti Computing

**1:40pm QS-MoA-1 Hole-Based, Atomic-Scale Quantum Devices in Silicon, Robert Butera**, Laboratory for Physical Sciences **INVITED**  
 $\delta$ -doped Si provides a novel frontier to explore quasi-2D electronic transport of an extremely high concentration of carriers ( $> 10^{14} \text{ cm}^{-2}$ ) through a highly-disordered potential. These carriers can be further confined using atomic-precision advanced manufacturing (APAM) techniques to generate a variety of atomic-scale quantum devices [1]. Over the past two decades these techniques have been used to realize and characterize atomic-scale wires, single atom and single electron transistors, as well as single atom qubits based on P [2-5], the quintessential electron donor dopant for Si. In contrast, atomic-scale quantum devices have only recently begun to be explored with B [6, 7], the archetypal acceptor dopant in silicon.

Under standard conditions, a single B atom in Si has an associated hole that forms a promising single qubit platform on its own right [8], but with sufficiently high concentrations of B, Si has been shown to exhibit superconductivity [9]. Motivated by these intriguing possibilities, we developed an APAM-compatible process for B to ultimately explore single acceptor qubits and atomic-scale, superconducting Si devices. Here we discuss the fabrication and initial characterization of the resulting hole-based, atomic-scale quantum devices in which we observe weak anti-localization and universal conductance fluctuations in magnetotransport measurements, and demonstrate Coulomb oscillations in a single hole transistor.

[1] Bussmann, E., Butera, R.E., Owen, J.H.G. *et al.*, Atomic-precision advanced manufacturing for Si quantum computing. *MRS Bulletin* **46**, 607–615 (2021).

[2] B. Weber, S. Mahapatra, H. Ryu, *et al.*, Ohm's Law survives to the atomic scale. *Science* (2012).

[3] Fuechsle, M., Miwa, J., Mahapatra, S. *et al.*, A single-atom transistor. *Nature Nanotech* **7**, 242–246 (2012).

[4] Wang, X., Wyrick, J., Kashid, R. *et al.*, Atomic-scale control of tunneling in donor-based devices. *Commun Phys* **3**, 82 (2020).

[5] Y. He, S.K. Gorman, D. Keith, *et al.*, A two-qubit gate between phosphorus donor electrons in silicon. *Nature* (2019).

[6] K. Dwyer, S. Baek, A. Farzaneh, *et al.*, B-doped  $\delta$ -Layers and nanowires from area-selective deposition of  $\text{BCl}_3$  on  $\text{Si}(100)$  *ACS Appl. Mater. Interfaces*, **13** (34) (2021), pp. 41275–41286.

[7] Škereň, T.; Köster, S. A.; Douhard, B.; *et al.*, A. *Bipolar Device Fabrication Using a Scanning Tunnelling Microscope*. *Nat. Electron* **2020**, *3*, 524–530.

[8] Kobayashi, T., Salfi, J., Chua, C. *et al.*, Engineering long spin coherence times of spin-orbit qubits in silicon. *Nat. Mater.* **20**, 38–42 (2021).

[9] Bustarret, E., Marcenat, C., Achatz, P. *et al.* Superconductivity in doped cubic silicon. *Nature* **444**, 465–468 (2006).

**2:20pm QS-MoA-3 Interface Loss Engineering for High Coherence Aluminium Qubits, Janka Biznarova**, J. Bylander, Chalmers University of Technology, Gothenburg, Sweden

Superconducting qubits are current hot candidates for delivering on the promise of quantum computation. However, their implementation is not without challenges. Quantum information stored in a qubit has a finite lifetime before it loses coherence. For superconducting qubits to be able to sustain the fragile quantum information in a coherent state sufficiently long so that a meaningful number of logical gates can be executed, it is vital to examine the sources of decoherence and to eliminate them. In this work, we show how improvements in device fabrication can enable  $T_1$  times of up to  $500 \mu\text{s}$  in aluminium-based transmon qubits.

The nature of the sources of coherence loss in quantum circuits is a topic of ongoing debate. In this work we investigate the parasitic two-level systems (TLS) that compete with our devices for photons, as well as uncover other losses that may limit performance once TLS loss has been mitigated.

This problem can be approached from two angles - through optimizing device geometry, and through surface engineering. Manipulating device geometry, we can quantify the relative effect each interface of the CPW resonator has on the total loss, and minimize the participation of the lossiest interfaces. With surface engineering, we can target a given interface in order to mitigate the specific type of loss it entails.

In this work, we design, fabricate and characterize resonators and qubits using aluminium on silicon in order to further investigate the nature of TLS. We vary the deposition conditions of the metal, as well as surface treatments, and draw conclusions for the participation of TLS loss to the total loss of the circuits at low temperatures. Varying the absolute size of the CPWs, as well as the ratio of the CPW center conductor to its gap to ground, we can get a more accurate picture of the various loss contributions. Once a fabrication recipe is optimized for a resonator proxy, the recipe is extended to qubit fabrication. We show that aluminium-based transmon qubits fabricated with the optimized recipe can reach  $T_1$  values up to  $500 \mu\text{s}$ , with mean  $T_1$  values exceeding  $200 \mu\text{s}$ .

**2:40pm QS-MoA-4 Examine the Electrical Transport Properties of Superconducting Quantum Devices Based on PtSi, Tharanga Nanayakkara**, A. Bollinger, R. Li, M. Liu, C. Black, Brookhaven National Laboratory

Quantum information systems have the potential to revolutionize many fields, including health, defense, and finance. Despite their vast potential, practical applications of quantum information systems face numerous challenges that must be addressed to fully realize their benefits. Fabricating nano-scaled superconducting qubits for quantum information systems is a highly challenging process. One of the primary remaining challenges is identifying suitable superconducting materials with sufficient coherence times in their qubits. Therefore, it is essential to investigate novel materials, such as platinum silicide (PtSi), to recognize their potential candidacy in quantum information science. PtSi is a transition metal silicide, formed by

# Monday Afternoon, November 6, 2023

reacting silicon with platinum. PtSi finds extensive use in semiconductor microelectronics since its ability to create low resistance electrical contacts to silicon. Significantly, PtSi exhibits superconducting properties, and it is a potential material for integrating quantum computation with silicon technology.

In this study, Pt thin films were deposited onto silicon substrates using magnetron sputtering technique. Subsequently, the Pt on the silicon wafer was thermally annealed in a rapid thermal processor to form PtSi thin films, which were confirmed by X-ray diffraction measurements. We patterned PtSi thin films on Si substrate using electron-beam lithography to fabricate superconducting devices, including constriction type Josephson junctions (JJs), and Superconducting Quantum Interference Devices (SQUIDs). The fabrication process for constriction-type devices involves a single-step electron-beam lithography, which is simpler than the conventional tunneling junction fabrication process. After patterning the device structure onto the PtSi, a reactive ion etching technique was used to carve the device shape by selectively etching away the surrounding PtSi.

We performed low-temperature electrical transport measurements on constriction type JJs and SQUIDs to evaluate the material characteristics for high-quality superconducting quantum circuit fabrication. The parameters extracted from the PtSi devices, including critical temperature, normal-state resistance, coherence length, critical current density, and critical field values, will be comprehensively discussed in this work.

## 3:00pm **QS-MoA-5 Two Architectures for Superconducting Quantum Processors with Tunable Couplers**, *Stefano Poletto*, Rigetti Computing **INVITED**

Superconducting quantum processor units (QPUs) with 10s to 100s of physical qubits are now commercially available from multiple companies and institutions. However, to build and operate a high performance superconducting QPU several physics and engineering challenges must still be addressed.

In this talk, I will focus on the implementation of tunable qubit-qubit interactions as a promising alternative to fixed coupling schemes from both a scalability and performance point of view. I will present two types of floating tunable coupler architectures as well as two different methods to implement two-qubit gates. I show how floating tunable couplers allow increased physical separation between qubits; making it an ideal candidate for scalability. Additionally, the two-qubit parametric resonance gate can also help reduce the incoherent errors per operation by performing the gate at its maximum speed. I will give a side-by-side comparison of the different architectures to highlight the benefits of the proposed approaches.

## 4:00pm **QS-MoA-8 Quantum Device Formation in Silicon via Ion Implantation**, *Jeffrey McCallum*, School of Physics, Australia **INVITED**

Spin qubits based on impurities such as phosphorus, P, in isotopically pure silicon  $^{28}\text{Si}$ , have attractive attributes for development of quantum computing devices.[1] Very long coherence times can be achieved for donor-based qubits when the  $^{29}\text{Si}$  atoms, that otherwise lead to decoherence, are removed from the active region of the device. Standard semiconductor-industry ion implantation techniques can be used to fabricate well-behaved donor qubits in Si. Exceptionally long coherence times greater than 30 s have been demonstrated for nuclear spin qubits. Conditional quantum operation of a pair of exchange coupled single P-donor spin qubits in an ion implanted  $^{28}\text{Si}$  epi-layer device has also been recently demonstrated.[2] While many key achievements have been obtained for P donor qubits in Si, other donor qubit systems such as antimony, Sb, and bismuth, Bi, are also starting to be developed and have potential to offer new degrees of freedom and new qubit control functionalities. The crucial next stage is to develop suitable scale-up pathways that allow patterned arrays of donor qubits to be controllably coupled and that are robust against the inherent donor placement tolerances and material processing constraints that exist. Here, we will review progress on the fabrication and measurement of ion implanted donor-based qubits in silicon and discuss the pathway to deterministically implanted single donor arrays with inter-donor spacings suitable for available coupling protocols.

Silicon is also an attractive platform for the development of devices that contain both superconducting and semiconducting components on a single chip for emerging quantum technologies. Recently, we have investigated superconductivity in nanowire devices fabricated using an Al-Si exchange process in silicon-on-insulator wafers.[3] The Al-exchange-transformed material is conformal with predefined device patterns. Magneto-transport measurements on nanoring structures formed by this process exhibit

periodic features in the differential resistance and in the critical current resulting from fluxoid quantization. The devices can be operated in temperature/magnetic-field regimes where some components of the device are in the superconducting state while others are in resistive states. The details of the Al-Si exchange process suggest that it could allow a range of new nanoscale superconducting-semiconducting device structures to be formed. Here, we will also briefly introduce our preliminary exploration of these superconducting nanowire devices and their promise for quantum technologies development.

[1] J. C. McCallum, et al., Appl. Phys. Rev. 8, 031314 (2021).

[2] M. T. Madzik, et al., Nat. Commun. 12, 181 (2021).

[3] B. C. Johnson, et al., Nano Lett. 23, 17–24, (2023).

## 4:40pm **QS-MoA-10 Quantum Technology Manufacturing Roadmap v1.0**, *Jonathan Felbinger*, SRI International

This roadmap effort, led by SRI International and its team of industry, national lab and academic partners, will identify pre-competitive development work and supply chain gaps to support scaling up quantum technology and help maintain U.S. dominance in quantum-related fields, rather than focus on scientific discovery or a specific application.

Quantum information science and technology are rapidly advancing and have potential applications in computing, sensing, communications and security. The development of quantum technology and a U.S.-based quantum industry is a key strategic priority of the U.S. government. To achieve its full potential, novel materials, devices, structures and systems must be developed and manufactured. Though still emerging, the quantum industry is taking shape, products are beginning to emerge and companies are developing internal roadmaps for more complex systems, such as error-corrected quantum computers.

To support the development of technology critical to the quantum industry, SRI and its team of industry, national lab and academic partners propose to develop a technology roadmap focused on supply chain gaps and barriers to advanced manufacturing capability. SRI currently manages the Quantum Economic Development Consortium [<https://quantumconsortium.org/>] (QED-C), an industry-led consortium supported by the U.S. government and 170+ industry, academic and national lab members. The mission of QED-C is to enable and grow the U.S. quantum industry and supply chain. SRI proposes to leverage ties with QED-C members to establish a separate consortium to develop the roadmap that will guide development across the emerging industry and identify the necessary manufacturing technologies and capabilities. This new consortium will include QED-C members and non-QED-C members across the stakeholder spectrum.

## 5:00pm **QS-MoA-11 Cryogenic Properties of Discrete Electronic Components for Use in Quantum Measurement Circuits**, *Nikki Ebadollahi*, National Institute of Standards and Technology (NIST)/ University of Maryland, College Park; *P. Shrestha*, National Institute of Standards and Technology (NIST); *D. Krymski*, University of Maryland, College Park; *Y. Hong*, *E. Rissanen*, *J. Pomeroy*, National Institute of Standards and Technology (NIST)

The changes in transistors, capacitors and resistors when they are cooled to cryogenic temperatures are measured to enable the design and fabrication of quantum control and readout circuits. Quantum devices, and eventual quantum computers, function at cryogenic temperatures, and achieving high efficiency requires that the classical and quantum components are positioned closely together within a circuit. Before discrete classical components can be integrated into basic auxiliary circuits for a quantum system, it is essential to understand the properties of these components at 4 K. While the cold temperatures yielded predictable changes for resistor properties, capacitors and transistors underwent significant and unpredictable changes. For the capacitors, the changes in capacitance were largely dependent on the material, dielectric constant, and surface area. The dielectric constant decreases as cryogenic temperatures are reached for some materials. For some capacitors, the capacitances decreased by a factor of 20 in response to the temperature drop. For the transistors, the threshold voltage, transconductance, and transfer curves all notably changed from room temperature to 4 K. Both the threshold voltage as well as the slope of the transfer curve increased significantly at 4 K compared to the behavior at room temperature. Due to the temperature-dependent characteristics of discrete electronic components, circuits must be designed with operating parameters suited for cryogenic temperatures in order to function.

## Advanced Surface Engineering Division

### Room C123 - Session SE+TF-MoA

#### Mechanics and Tribology of Thin Films and Coatings

**Moderators:** Rebecca Cai, Virginia Tech, Suneel Kumar Kodambaka, Virginia Tech

**1:40pm SE+TF-MoA-1 Mini-Module Stress Testing to Assess 'Fatigue-Like' Failure Mode of Gridlines on Silicon Solar Cells, A. Chavez, Sang Han, University of New Mexico; S. Huneycutt, A. Ebong, University of North Carolina at Charlotte; D. Harwood, N. Azpiroz, D2Solar**

Microcracks in solar cells can eventually propagate through metal gridlines and busbars, leading to PV module power loss over time. With the latest glass/glass PV module construction – in which the glass is only heat-treated (not tempered) and its thickness is reduced from 3.2 mm to 2.0 mm – along with ever-increasing module size, the stress-induced cell cracks are rapidly becoming one of the main degradation modes. In this study, we compare how metal matrix composite gridlines fare in comparison to standard silver gridlines against three-point-bending stress test. We have fabricated two-cell, mini-modules with full-size Passivated Emitter and Rear Contact (PERC) cells. The backside of each cell is laser-scribed prior to encapsulation to initiate cell cracks. The completed mini-modules are then placed on a three-point-bending setup and flexed until the cells crack, and the cracks propagate through the gridlines to cause electrical discontinuity. The mini-modules are then subjected to cyclic mechanical stress on the three-point-bending setup up to the sub-critical fracture stress level to simulate the field operation and to characterize the long-term 'fatigue-like' wear-out failure. The results show that enhanced ductility and compliance of composite gridlines lead to their increased durability compared to standard silver gridlines, strongly suggesting increased lifetime of PV modules against cell cracks.

This material is based upon work supported by the U.S. Department of Energy's Office of Energy Efficiency and Renewable Energy (EERE) under the Solar Energy Technologies Office Award Number DE-EE0009013.

**2:00pm SE+TF-MoA-2 Relating Stress in Thin Films to the Underlying Kinetic Processes: Experiments and Modeling, E. Chason, Tong Su, Brown University**

Stress in thin films can have a significant impact on their performance and reliability. Since stress is affected by many parameters (growth rate, temperature, microstructural evolution, composition, particle energy for sputter deposition, etc.), a fundamental understanding of its origins stress would allow it to be predicted and optimized. We describe a model for we have developed to explain stress evolution during deposition in terms of the underlying kinetic processes. The model includes mechanisms related to non-energetic growth kinetics, microstructural evolution and energetic particle bombardment. Examples are discussed that use the model to explain the dependence of stress on the growth rate, grain growth kinetics and sputter pressure. A user-friendly computer program based on the model is described that is available to interested users to analyze wafer curvature measurements.

**2:20pm SE+TF-MoA-3 Tailoring the Tribocorrosion Resistance of Al-based Metallic Thin Films via Alloying and Nanolayering, Wenjun (Rebecca) Cai, Virginia Tech**

INVITED

The increasing complexity and severity of service conditions in areas such as aerospace and marine industries, nuclear systems, microelectronics, batteries, and biomedical devices etc., imposes great challenge on the reliable performance of metallic thin films subjected to simultaneous surface stress and corrosion. However, the design of strong and corrosion-resistant coatings, especially those containing passivating elements such as Al are challenged by the tradeoff between strength and corrosion resistance. Towards this end, this talk will focus on the development of novel microstructure design strategies for metallic thin films to mitigate the combined attack of wear and corrosion (i.e. tribocorrosion) under harsh conditions. Two design strategies will be discussed to overcome this long-standing dilemma: by forming solid solution alloys and nanostructured multilayers. These studies provide insights for general design guidelines to engineer more robust, high-performance metals for use under harsh conditions.

**3:00pm SE+TF-MoA-5 Tribological Properties of Conversion Layers and Carbon-based PVD Coatings for Rolling Bearing Applications, Esteban Broitman, A. Ruellan, R. Meeuwenoord, D. Nijboer, SKF B.V. - Research and Technology Development, Netherlands**

In this study, different coatings and conversion layers have been compared in terms of friction performance based on a single-contact oil-lubricated tribometer and on a grease-lubricated double row bearing friction test rig ran under relevant operating conditions for a railway application. Conversion layers like zinc-calcium-phosphate, manganese-phosphate and black-oxide have been compared on friction performance to that of an uncoated steel surface and to a proprietary diamond-like-carbon base coating.

Results demonstrate that the optimum conversion layer can reduce friction by more than 25% on rolling/sliding raceway contacts (ball-on-disk) and up to 80% on the sliding flange contacts (roller-on-disk), which share a significant portion of power losses in roller bearing units. Results at the bearing level demonstrate that the same optimum conversion layer can reduce the running torque by approximately 30% compared to the current products both at low and intermediate speeds relevant to intercity trains.

**3:20pm SE+TF-MoA-6 The Tribological Behaviour of TiAlN Coating Under High-Temperature Conditions, Aljaž Drnovšek, Jozef Stefan Institute, Slovenia; P. Šumandl, Faculty of Natural Sciences and Engineering, University of Ljubljana, Slovenia; Ž. Gostenčnik, Jozef Stefan Institute, Slovenia; M. Čekada, Jozef Stefan Institute, Slovenia**

TiAlN coating is a popular hard coating for high-temperature applications such as high-speed cutting and cutting of new, hard-to-cut materials. However, the most commonly used method for depositing this coating on cutting tools, cathodic arc evaporation, can result in a relatively rough surface due to the emission of micro-droplets. This roughness and the presence of embedded droplets in the coating matrix can significantly affect the coating's wear and friction properties

Our objective was to assess the wear and friction properties of the TiAlN coating during both the running-in and steady-state periods under varying temperature conditions. To evaluate the performance of the TiAlN hard coating, we conducted tribological tests using a high-temperature pin-on-disc tribometer. The tests were carried out with an Al<sub>2</sub>O<sub>3</sub> ball as a counter body at different temperatures: room temperature, 250 °C, 500 °C, and 700 °C. We varied the test duration at specific temperatures, ranging from 50 up to 140,000 cycles, to examine the effect of test length on the coating's wear and friction properties. After each tribological test, we analysed the coatings.

The results indicated that the coating experienced the highest wear during the room temperature test. Conversely, the wear during the running-in phase and steady-state friction was the lowest at 250 °C. As the temperature increased, the wear rate rose, which we attributed to tribo-oxidation and fatigue caused by the high test lengths. Ultimately, the coating delaminated from the WC-C substrate at the highest temperature. The asperities on the surface of the coating due to micro-droplets played a significant role in friction and wear behaviour, as they were a primary source of wear particles and the first spots of oxidation on the coating.

We conducted detailed 3D profilometry, SEM and FIB analyses on numerous samples to determine the wear mechanisms at different stages of high-temperature wear. In addition to tribological evaluation, we performed high-temperature mechanical tests at the same temperatures as the tribological tests.

The combination of these analyses allowed us to gain a comprehensive understanding of the wear mechanisms and behaviour of the TiAlN coating at high temperatures. By analysing the samples at different stages of wear, we were able to identify the dominant wear mechanisms and how they evolved over time.

**4:00pm SE+TF-MoA-8 Atomic Layer Deposition Coatings on Micron-Sized Iron Powders for Increased Oxidation Resistance, Chris Gump, J. Burger, T. Porcelli, J. Travis, B. Boeyink, T. Champ, Forge Nano**

The physical, electrical, and magnetic properties of micron-sized and smaller metal powders make them useful for a variety of applications, including additive manufacturing, electronic components, metal injection molding, microwave absorption, and powder metallurgy. As the particle size of these metals becomes smaller, oxidation of the particle surface becomes a larger issue. In the case of flammable metal powders like iron and titanium, this can have severe safety implications, as the rapid oxidation of the powder can result in a metal fire or dust explosion. However, even the slower oxidation reactions that occur in salty, foggy, or typical ambient conditions can reduce shelf life and have other negative effects on the

properties of products made from these feedstocks. The desirable properties of these materials can be preserved by encapsulating the powders with a barrier film. To minimize the effects on the properties of the composite particles, the barrier film should be as thin as possible.

Atomic Layer Deposition (ALD), long used in the semiconductor industry for coating wafers, has in recent years been applied to a wider range of application spaces, including the surface modification of powders with nanometer-scale films. We studied the deposition of thin, nanoscale alumina ALD barrier films onto metal powders, using carbonyl iron powder (CIP) as a model substrate that has a range of applications. Coatings were performed on 30 g batches of powder in a highly scalable fluidized bed reactor. The barrier properties of the films were studied as a function of deposition temperature (80 – 230°C) and film thickness (1 – 8 nm), using thermogravimetric analysis in oxygen as the performance metric. Optimal barrier performance, in terms of the shift in onset temperature for oxidation, occurred for the middle range of deposition temperatures. The thickest films were able to shift the onset temperature for oxidation by as much as 300°C (from 250°C to 550°C). The barrier performance as a function of temperature was found to correlate with previously published studies of the film density and growth per cycle (GPC) of Al<sub>2</sub>O<sub>3</sub> ALD deposited as a function of temperature. Although not characterized in this case, the barrier films are also expected to decrease electrical conductivity while maintaining magnetic susceptibility. The deposition process has been successfully demonstrated at the 1-5 kg scale, and the 100 kg scale for similar metal powders, with the potential for even higher throughputs on established coating tools.

**4:20pm SE+TF-MoA-9 Characterizing the Composition, Structure, and Mechanical Properties of Titanium Silicon Nitride Erosion Resistant Coatings, Gilad Zorn, P. Shower, S. Weaver, R. Rose, J. Her, J. Salisbury, GE Research Center**

Titanium nitride (TiN) coatings have a wide range of applications due to their practical properties such as high hardness, good corrosion resistance, heat resistance and excellent wear resistance. They have been widely used in various industries including decorative coatings, diffusion barriers and hard coatings. The properties of TiN can be greatly enhanced by addition of other elements, such as Si [1-2]. Incorporation of Si in the TiN cubic structure leads to formation of TiSiN coatings characterized by high hardness and high oxidation resistance up to 800 °C. This enables synthesizing coatings and designing materials with a broad range of applications, especially as materials that should perform under harsh environments. The ternary TiSiN system is formed due to the total miscibility of Si, which creates a solid solution while preserving the crystalline structure B1 of TiN. Si is also believed to create nanocomposite structure of TiSiN coatings consisting of nanocrystalline TiN grains encapsulated by an amorphous silicon nitride (Si<sub>3</sub>N<sub>4</sub>) matrix. To achieve high hardness TiN films, significant bonding strength between Ti and N must be achieved. If the bonding is too weak, the surface of the coating can oxidize, forming titanium oxynitride and eventually TiO<sub>2</sub> even at room temperature conditions [3]. The oxynitride and oxide forms are known to exhibit a lower hardness than TiN and experience oxidation propagation.

This study is focused on the characterization of TiSiN hard coatings. For example, X-ray Photoelectron Spectroscopy (XPS) was used to study the compositions and high resolution XPS was used to determine the surface oxide to nitride ratios. Mechanical tests were performed with nano indenter to determine the hardness of these coatings. Figure 1 shows the correlation between the hardness of the films and the percentage of the XPS titanium oxide component. X-ray diffraction confirmed the formation of titanium nitride cubic phase and different crystallographic orientations were observed depending on the composition of each film. The results of this study show that adding Si and reducing the oxygen level improved the performance of the nitride films as erosion resistant coatings.

30. Akhte, Rumana; Zhou, Zhifeng; Xie, Zonghan, Munroe, Paul *Surface and coating technology* 425 (2021) 127687.
31. Greczynski, G.; Bakhit, B.; Hultman, L.; Odén, M. *Surface and coating technology* 398 (2020) 126087.
32. Logothetidis, S.; Meletis, E.I.; Stergioudis, G.; Adjaottor, A.A. *Thin Solid films* 338 (1999) 304.

This material is based upon work supported by the U.S. Department of Energy, Office of Fossil Energy and Carbon Management under Award Number FE0031911.

## Surface Science Division

### Room D136 - Session SS+AS+TF-MoA

#### Mechanisms at Surfaces and Interfaces

**Moderators: Florencia C. Calaza**, Instituto de Desarrollo Tecnológico para la Industria Química, **Jun Nakamura**, UEC Tokyo

**1:40pm SS+AS+TF-MoA-1 Spin- and Alignment-Controlled O<sub>2</sub> Chemisorption and Catalytic CO Oxidation on Stepped Pt and Pt/Co Alloy Surfaces, Mitsunori Kurahashi**, National Institutes for Materials Science, Japan

**INVITED**

O<sub>2</sub> chemisorption and catalytic oxidation on Pt and its alloy surfaces have been studied intensively due to the relevance to important processes such as car exhaust gas purification and oxygen reduction reaction (ORR) in fuel cell. Since O<sub>2</sub> is a linear diatomic molecule with an electron spin, the alignment of the O<sub>2</sub> axis relative to the surface local structure is a key to understand the elementary processes of O<sub>2</sub> chemisorption. If the surface is magnetic, the spin correlation between O<sub>2</sub> and the surface also plays an important role. A single spin-rotational state-selected [(J,M)=(2,2)] O<sub>2</sub> beam allows us to investigate the effects of molecular alignment and spin on O<sub>2</sub>/surface interactions [1].

In this talk, I will firstly present the alignment-controlled O<sub>2</sub> chemisorption and CO oxidation on curved Pt(111). The use of a curved crystal surface and a local probe allows us to monitor the step-density dependence in surface properties or reactivity[2,3]. In this study, by scanning the aligned O<sub>2</sub> beam with a dimension of 0.2mmW x 2mm across a curved Pt(111) surface, the step-density and structure dependence in alignment-resolved O<sub>2</sub> chemisorption probability and CO oxidation rate were measured. The results indicate that step affects the reactivity of the neighboring terraces, and that the low temperature CO oxidation rate at step site is much lower than at (111) terrace.

Secondly, I will present the spin-dependent catalytic CO oxidation on Pt/Co/Pt(111). Pt/Co alloy has attracted much attention since it shows a higher ORR activity than pure Pt [4]. The higher reactivity has been attributed to the charge transfer from the subsurface Co to the surface Pt layer while how the spin of the subsurface Co affects the reactivity of the surface Pt remains unclear. Spin-resolved O<sub>2</sub> chemisorption and CO oxidation experiments on a perpendicularly-magnetized Pt/Co(2ML)/Pt(111) film indicate that the O<sub>2</sub> chemisorption probability and the catalytic oxidation rate depend strongly on the spin orientation between O<sub>2</sub> and the Pt surface. The magnitude of the spin orientation dependence was larger than that observed for O<sub>2</sub>/Ni [1,5]. An SPMDS measurement and DFT calculation show that the surface Pt layer is spin-polarized at around E<sub>F</sub>. The present experiments indicate that the catalytic activity of Pt is strongly affected by the magnetism of neighboring atoms.

- [1] M. Kurahashi, *Prog. Surf. Sci.*, **91**, 29 (2016).
- [2] A. Walter et al., *Nat. Comm.*, **6**, 1 (2015); S. Auras, L. Juurlink, *Prog. Surf. Sci.*, **96**, 100627 (2021).
- [3] K. Cao, R. Lent, A. W. Kleyn, M. Kurahashi, and L. B. F. Juurlink, *PNAS* **116**, 13862 (2019).
- [4] V. Stamenkovic et al., *J. Phys. Chem. B*, **106**, 11970 (2002).
- [5] M. Kurahashi, *J. Chem. Phys.*, **157**, 124707 (2022).

**2:20pm SS+AS+TF-MoA-3 Atomic-Scale Insights Into the Sintering Resistance and Oxidation of Single-Atom Alloys, Audrey Dannar<sup>1</sup>**, Tufts University; *J. Finzel*, University of California, Santa Barbara; *V. Cinar*, *E. Sykes*, Tufts University

Copper-based catalysts are used in a wide range of heterogeneous catalytic processes that can take place in oxidizing environments, where Cu is known to readily oxidize to form CuOx, and reducing environments, where Cu is known to deactivate via sintering. Single-atom alloys (SAAs) are a new type of catalyst in which isolated atoms of dilute reactive dopants such as Pt and Rh are present in more inert host metals such as Cu. Despite their great promise for hydrogenation and dehydrogenation reactions, there exists limited understanding of these materials under oxidizing conditions. Similarly, SAAs have shown exceptional long-term stability with anecdotal reports of sintering resistance in industrial conditions that are not presently fundamentally understood. This work aims to develop atomic-scale structure-function relationships for Cu-based catalysts that span oxidizing and reducing conditions and understand how single dopant atoms stabilize the undercoordinated Cu atoms responsible for sintering and involved in CuOx formation upon O<sub>2</sub> exposure.

First, we used a specialized method for measuring the surface diffusion of metal atoms that leads to sintering with scanning tunneling microscopy (STM) experiments which reveals that single Pt atoms in a Cu(110) surface

<sup>1</sup> SSD Morton S. Traum Award Finalist

# Monday Afternoon, November 6, 2023

significantly reduce the rate of Cu atom detachment from undercoordinated surface sites. Thus, the origin of sintering resistance exhibited by SAA is hypothesized to be due to dopant atom stabilization of undercoordinated Cu atoms at the step edge. This is validated by DFT and paired with collaborator work that shows PtCu/SiO<sub>2</sub> dilute alloy catalysts are significantly more stable than monometallic Cu/SiO<sub>2</sub> in methanol synthesis experiments via EXAFS and TEM.

Next we used STM experiments to elucidate atomic-scale details of the oxidation processes of both PtCu(111) and RhCu(111) SAAs. STM images reveal that on Cu(111), oxidation occurs below Cu step edges, consistent with literature reports. Interestingly, for the RhCu(111) SAA, oxidation occurs both below the step edges and also above, where the Rh atoms are located, but this is not the case for the Pt brim on PtCu(111). For both Rh and Pt SAAs the oxidation below the step edge is reduced compared to Cu, which we hypothesize is due to the stabilization of Cu step edge atoms, which are required to restructure during CuOx formation below the step. The reduced rates of sintering and oxidation of PtCu SAAs compared to Cu originate from Cu step edge atoms being kinetically stabilized by dilute dopants. Together, these results begin to shed light on the role of single dopant atoms in the mechanisms Cu nanoparticle sintering and Cu oxidation.

**2:40pm SS+AS+TF-MoA-4 Visualization of the Local Dipole Moment at the Si(111)-(2x2) Surface Using DFT Calculations, Akira Sumiyoshi, J. Nakamura, The University of Electro-Communications (UEC Tokyo), Japan**

Understanding the polarization state of a sample is essential in the development of devices and functional materials. Recently, the spatial distribution of the surface polarization has been observed using new microscopy techniques, such as SNDM[1-3]. However, there have yet to be any reports regarding the theoretical simulation of surface polarization. Here, we focused on the dipole moment (DM), an essential aspect of polarization, and developed a method to visualize the distribution of surface DM using theoretical calculations. In this study, we report on the surface DM distribution of Si(111)-(2x2) with the characteristic motif of the Si(111)-(7x7) DAS structure. Furthermore, we confirmed that the surface dipole distribution can be explained consistently with the surface stabilization mechanism.

We defined and calculated the DM using the following formula;

$$\mu_{(x,y,z)} = \int \rho_{(x,y,z)} * (z' - z_0) dz'$$

Here,  $\mu$  is the DM,  $\rho_{(x,y,z)}$  is the total charge density, and  $z_0$  is the origin in the vertical direction. In order to eliminate the effect of the backside surface of the Si(111) slab, we adopted the midpoint of the deepest bulk layer of the slab as the origin and integrated the above formula from  $z_0$  to the vacuum position  $z$  sufficiently far from the topmost surface. The total charge density was calculated using DFT-based first-principles calculations.

Upon optimizing the structure, the restatom was lifted compared to the original bulk position, suggesting the larger orbital electronegativity[4] of the surface orbital of the restatom[5]. This change in orbital electronegativity leads to an electron transfer from the adatom to the restatom, resulting in no surface dangling bond. We calculated the electron localization function (ELF) map and the band diagram to confirm the surface electron transfer. We confirmed the presence of the electron pair on the restatom from ELF. It was revealed that the Si(111)-(2x2) surface has a finite energy gap. As a result, it was clearly shown that the electron transfer occurs from the adatom to the restatom, emptying the dangling bond at the adatom and forming a lone pair at the restatom.

Furthermore, we simulated the surface DM distribution. As a result, an upward DM was observed at the adatom position, which is explained by the depletion of electrons just above the adatom due to the electron transfer at the surface.

[1] Yasuo Cho et al., Phys. Rev. Lett. 99, 186101(2007)

[2] Kohei Yamasue et al., Appl. Phys. Lett. 105, 121601(2014)

[3] Yasuo Cho, Scanning Nonlinear Dielectric Microscopy, Wood. Pub.(2020)

[4] Jun Nakamura et al., J. Phys. Soc. Jpn. 66, 1656(1997)

[5] Akihiro Ohtake, Jun Nakamura et al., Phys. Rev. B 64, 045318(2001)

**3:00pm SS+AS+TF-MoA-5 Mechanism Study of a Chemisorbed O<sub>2</sub> Molecule on Ag(110) Induced by High-Order Overtone Excitation Using STM, Minhui Lee, E. Kazuma, The University of Tokyo, Japan; C. Zhang, Tongji University, China; M. Trenary, University of Illinois at Chicago; J. Takeya, The University of Tokyo, Japan; J. Jung, University of Ulsan, Republic of Korea; Y. Kim, The University of Tokyo, Japan**

The dissociation pathway of chemisorbed O<sub>2</sub> on Ag(110) was elucidated by single-molecule microscopic and spectroscopic studies using a scanning tunneling microscope (STM). The dissociation reaction was found to be predominantly triggered by inelastically tunneled holes from the STM tip due to the significantly distributed density of states below the Fermi level of the substrate. A combination of action spectroscopy with the STM and density functional theory calculations revealed that the O<sub>2</sub> dissociation reaction is caused by direct ladder-climbing excitation of the high-order overtones of the O-O stretching mode arising from anharmonicity enhanced by molecule-surface interactions.

**3:20pm SS+AS+TF-MoA-6 Characterization of Oxygen Evolution from Rh(111), Maxwell Gillum, E. Jamka, F. Lewis, D. Killelea, Loyola University Chicago**

Due to the importance of oxide surfaces in heterogeneously catalyzed reactions, it is critical to gain a fundamental understanding of the reactivity and behavior of oxygen on these transition metal surfaces. In previous studies we have been able to establish that the reactivity and thermodynamic stability of oxygen on Rh(111) relies in part on the concentration of oxygen present in the subsurface. However, more research needs to be conducted in order to gain a better understanding of the relationship between surface reactivity and subsurface concentration. In addition to the techniques used in our previous studies, namely temperature programmed desorption (TPD) and scanning tunneling microscopy (STM), the experiments herein will include simultaneous infrared (IR)/TPD techniques to gain more information on these critical interactions.

**4:00pm SS+AS+TF-MoA-8 Spin-Polarized VLEED from Au(111): Surface Sensitivity of the Scattering Process, Christoph Angrick, A. Reimann, University of Münster, Germany; J. Braun, Ludwig-Maximilians-University of Munich, Germany; M. Donath, University of Münster, Germany**

Low-energy electron diffraction from Au(111) shows the well-known threefold symmetry of the diffracted electron beams despite the sixfold symmetry of the surface layer. This is due to the influence of the second and deeper layers and the probing depth of the electrons. In this work, we investigated Au(111) with spin-polarized very-low-energy electron diffraction (VLEED) [1,2,3] experimentally and theoretically. We monitor the reflected specular beam at a fixed polar angle of incidence of  $\Theta=45^\circ$  while the azimuthal orientation of the crystal is varied. This puts the surface sensitivity of the VLEED scattering process to a test.

Our results show that the electron reflection and the spin-orbit-induced reflection asymmetry along  $\Gamma M$  and  $\Gamma M'$  are equivalent. The observed sixfold symmetry suggests a sensitivity to one atomic layer only. At azimuth angles deviating from the high-symmetry directions  $\Gamma M$  and  $\Gamma M'$ , however, the VLEED signal from Au(111) shows a threefold symmetry. To reveal the origin of this effect, we varied the parameters in the calculation. The results indicate a non-negligible influence of the second atomic layer in the VLEED scattering process.

[1] Burgbacher *et al.*, Phys. Rev. B **87**, 195411 (2013).

[2] Thiede *et al.*, Phys. Rev. Applied **1**, 054003 (2014).

[3] Angrick *et al.*, J. Phys.: Condens. Matter **33**, 115001 (2020).

**4:20pm SS+AS+TF-MoA-9 Unravelling the Chemisorption Mechanism of Epoxy-Amine Coatings on Zr-Based Converted Galvanized Steel by Combined Static XPS/ToF-SIMS Approach, Vanina Cristaudo, K. Baert, P. Laha, Research Group Electrochemical and Surface Engineering (SURF), Vrije Universiteit Brussel, Belgium; M. Lim, L. Steely, D. Clingerman, E. Brown-Tseng, Coatings Innovation Center, PPG; H. Terryn, T. Hauffman, Research Group Electrochemical and Surface Engineering (SURF), Vrije Universiteit Brussel, Belgium**

In the automotive industry, the corrosion protection of hot-dip galvanized (HDG) steel is of primary importance. To this purpose, a Zr oxide-based conversion pre-treatment of the metal surface for passivation and improved adhesion [1], in combination with the application of a polymeric primer coating is often performed. Usually, organic and inorganic additives

are used in the acidic conversion bath for a large variety of purposes. For instance, Cu(II) salts are employed to accelerate the deposition of zirconium oxide [1]. Recently, the heterogeneity and multi-metal nature of the resulting surface has been demonstrated in our laboratory [2]. Now, it is of pivotal importance to study the efficiency and durability of such hybrid (hydr)oxide-polymer systems, which depend on the formation and degradation of the chemical bonds at the buried interface.

This work aims at the elucidation of the interfacial interactions established between an epoxy-amine coating and HDG steel [3]. The influences of the Zr-based conversion treatment of the substrate and the use of Cu(II) additive on interfacial bonding will be studied [3]. To this purpose, an amine-functionalized molecule – diethylenetriamine (DETA), a common curing agent – will be adsorbed and used as an indicator of the acid-base properties of the metal oxide surface. The complex multi-metal oxide surface of the Cu-modified Zr-based converted substrate will be decomposed in derivative (simpler) systems, such as pure Zn, Zr, and Cu. The resulting DETA-adsorbed model and multi-metal surfaces will be investigated by X-ray photo-electron spectroscopy (XPS), and by examination of the N 1s peak, the interfacial bond densities will be determined. Time-of-flight secondary ion mass spectrometry (ToF-SIMS) will be performed to discriminate between the different metal oxide contributions present on the substrate surface. Preferential adsorption of the DETA molecule on the zinc atoms is found on converted substrates. SIMS also points out the interfacial bonding with the Cu cationic sites when the copper additive is used, highlighting the extreme usefulness of this analytical technique in the assessment of interfacial interactions of “diluted” adsorption sites.

## References

- [1] I. Milošev, *et al.* Conversion coatings based on zirconium and/or titanium. *J. Electrochem. Soc.* (2018), 165, p.C127.
- [2] V. Cristaudo, *et al.* A combined XPS/ToF-SIMS approach for the 3D compositional characterization of Zr-based conversion of galvanized steel. *Appl. Surf. Sci.* (2021), p.150166.
- [3] V. Cristaudo, *et al.* Unravelling the chemisorption mechanism of epoxy-amine coatings on Zr-based converted galvanized steel by combined static XPS/ToF-SIMS approach. *Appl. Surf. Sci.* (2022), 599, p.153798.

**4:40pm SS+AS+TF-MoA-10 Fermi Surface Emergence and Valence Band Maximum Formation During Li<sub>x</sub>CoO<sub>2</sub> Insulator-to-Metal Transition, Elena Salagre**, Dpto Física Materia Condensada, Universidad Autónoma de Madrid, Spain; *P. Segovia*, Dpto Física Materia Condensada, Universidad Autónoma de Madrid. IFIMAC (Condensed Matter Physics Center), Spain; *M. González-Barrio*, Dpto Física de Materiales, Universidad Complutense de Madrid, Spain; *J. Pearson, I. Takeuchi*, Materials Science and Engineering, Univ. Of Maryland; *E. Fuller, A. Talin*, Sandia National Laboratories; *M. Jugovac, P. Moras*, Istituto di Struttura della Materia, Consiglio Nazionale delle Ricerche, Italy; *A. Mascaraque*, Dto. Física de Materiales, Univ. Complutense de Madrid, Spain; *E. Garcia Michel*, Dto. Física Materia Condensada, Univ. Autonoma de Madrid, IFIMAC (Condensed Matter Physics Center), Spain

Despite the great interest in LiCoO<sub>2</sub> (LCO) and related materials for their applications in batteries, catalysis and resistive memory devices, uncertainties regarding the valence band structure, charge compensation and the nature of the insulator-to-metal transition (IMT) remain controversial [1][2]. In addition, the use of chemical and electrochemical methods on heterogeneous materials, including cathode binders and solid electrolyte interfaces, pushes research further away from a fundamental understanding of the processes involved in ion deintercalation.

We have developed a surface science-based approach to vary the Li content, based on Ne<sup>+</sup> sputtering and performed entirely in situ under ultra-high vacuum (UHV) conditions on epitaxial LCO thin films, without interactions between the material and any electrolyte.

This has allowed us to obtain high-resolution angle-resolved photoemission (ARPES) data of the valence band structure in LCO for a wide range of Li molar fractions, directly observing the IMT at x=0.95 and the regions of phase coexistence and phase dominance. X-ray photoelectron spectroscopy (XPS) and X-ray absorption spectroscopy (XAS) were used to characterize the material during Li deintercalation and to investigate the mechanisms of charge compensation in the absence of electrolyte. Li removal is accompanied by the formation of Co<sup>4+</sup> from the initial Co<sup>3+</sup> in the LCO structure. Oxygen holes were also observed, related to the hybridization of Co 3d and O 2p orbitals. The valence band was interpreted using reported theoretical calculations [3] and limited previous experimental work [4]. We

identify the Co 3d t<sub>2g</sub> energy levels as those involved in the IMT and locate the valence band maxima (VBM) with a clear 3-fold symmetry and band renormalization, suggesting a Mott character of the transition.

- [1] C. A. Marianetti, G. Kotliar, y G. Ceder, «A first-order Mott transition in Li<sub>x</sub>CoO<sub>2</sub>», *Nat. Mater.*, vol. 3, n.º 9, pp. 627-631, 2004
- [2] A. Milewska *et al.*, «The nature of the nonmetal-metal transition in Li<sub>x</sub>CoO<sub>2</sub> oxide», *en Solid State Ionics, Elsevier*, 2014, pp. 110-118
- [3] S. K. Radha, W. R. L. Lambrecht, B. Cunningham, M. Grüning, D. Pashov, y M. Van Schilfgaarde, «Optical response and band structure of LiCoO<sub>2</sub> including electron-hole interaction effects», *Phys. Rev. B*, vol. 104, n.º 11, p. 115120, 2021
- [4] Y. Okamoto *et al.*, «Electronic structure and polar catastrophe at the surface of Li<sub>x</sub>CoO<sub>2</sub> studied by angle-resolved photoemission spectroscopy», *Phys. Rev. B*, vol. 96, n.º 12, p. 125147, 2017

**5:00pm SS+AS+TF-MoA-11 Nanoscale Hydrogen Detection Using Time-of-Flight Secondary Ion Mass Spectrometry, B. Paudel, J. Dhas, M. Choi, Y. Du, Zihua Zhu**, Pacific Northwest National Laboratory

Hydrogen in materials attracts tremendous interest as its incorporation leads to significant alterations in structure, composition, and chemistry, which in turn impacts functional properties. Additionally, it has been integral to nuclear fusion reactors and is regarded as the major source of clean energy. However, nanoscale manipulation and characterization of hydrogen in materials are challenging as only a selected few analytical technique can readily detect hydrogen, among which time-of-flight secondary ion mass spectrometry (ToF-SIMS) is a unique and powerful technique due to its excellent detection limit along with decent spatial and depth resolutions. In our lab, ToF-SIMS has been used for hydrogen detection for more than 15 years, and it became more and more important in the last several years. In this presentation, we will discuss, using selected examples, how the detection and quantification of hydrogen in materials by ToF-SIMS has been utilized to reveal the hydrogenation/protonation-induced novel functional states in different classes of materials along with some tricks on sample preparation, optimized experimental conditions to achieve reasonable detection limits of hydrogen, and future prospects. We emphasize the unique capabilities of ToF-SIMS which can potentially unlock new functional states and answer some outstanding scientific questions in materials science.

## Vacuum Technology Division Room C120-122 - Session VT-MoA

### Leaks, Flows, and Material Outgassing

**Moderators: Giulia Lanza**, SLAC National Accelerator Laboratory, **Chandra Romel**, Consultant

**1:40pm VT-MoA-1 Cesium Intercalation of Graphene: A 2D Protective Layer on Alkali Antimonide Photocathode, Mengjia Gaowei**, Brookhaven National Laboratory

**INVITED**

Alkali antimonide photocathodes have wide applications in free-electron lasers and electron cooling. The short lifetime of alkali antimonide photocathodes necessitates frequent replacement of the photocathodes during a beam operation. Furthermore, exposure to mediocre vacuum causes loss of photocathode quantum efficiency due to the chemical reaction with residual gas molecules. Theoretical analyses have shown that covering an alkali antimonide photocathode with a monolayer graphene or hexagonal boron nitride protects it in a coarse vacuum environment due to the inhibition of chemical reactions with residual gas molecules. Alkali antimonide photocathodes require an ultra-high vacuum environment, and depositing a monolayer 2D material on it poses a serious challenge. In the present work, we have incorporated a novel method known as intercalation, in which alkali atoms pass through the defects of a graphene thin film to create a photocathode material underneath. Initially, Sb was deposited on a Si substrate, and a monolayer graphene was transferred on top of the Sb film. Heat cleaning around 550–600 °C effectively removed the Sb oxides, leaving metallic Sb underneath the graphene layer. Depositing Cs on top of a monolayer graphene enabled the intercalation process. Atomic force microscopy, Raman spectroscopy, x-ray photoelectron spectroscopy, low energy electron microscopy, and x-ray diffraction measurements were performed to evaluate photocathode formation underneath the monolayer graphene. Our analysis shows that Cs penetrated the graphene and reacted with Sb and formed Cs<sub>3</sub>Sb.

# Monday Afternoon, November 6, 2023

2:20pm **VT-MoA-3 On Ground and In-Orbit Decontamination Strategies for Space Hardware**, *Delphine Faye*, Centre National d'Etudes Spatiales, France **INVITED**

Lessons learnt from the past have led to anticipating space equipment failures that may be caused by the presence of chemical contaminants resulting mainly from outgassing of polymer materials under vacuum<sup>[1]</sup>.

Nowadays, when on-board instruments are becoming more and more sophisticated, when constraints are becoming more and more stringent in terms of quality and reliability for an extended mission duration, controlling both molecular and particulate contamination levels is a necessity and must be applied throughout the various phases of development and operation of a spacecraft. In order to maintain optimum performance of all equipment until the end of the mission, it is of paramount importance to mitigate the risks of degradation. This requires basic precautions not only in design and manufacturing but also and above all in integration and testing where a clean environment is highly recommended<sup>[2]</sup>.

However, if there are very strict rules for selecting space materials, if thermal pre-treatments under ultra-high vacuum are performed at different stages of assembly, a residual outgassing potential of some materials often remains to be considered. As a result, undesirable matter may be deposited on sensitive surfaces and evolve depending on in-orbit environmental conditions. Thus decontamination strategies must be foreseen whether on ground or in orbit, at the very beginning of life or when anomaly occurs. To do this, there are conventional cleaning processes but interesting alternatives are also being studied e.g. for cleaning especially with non-contact techniques or for trapping contaminants under vacuum<sup>[3]</sup>.

After a brief reminder of contamination issues for space sub-systems, this talk will present feedback from several use cases on specific projects. Different methodologies and associated techniques will be described as preventive or corrective actions as well as recent Research and Technologies developments<sup>[4]</sup>.

## references

- 1.A.C. Tribble, "fundamentals of contamination control", SPIE Press, 2000
- 2.ECSS-Q-70-01C, "Space Product Assurance, Cleanliness and contamination control", 2008
- 3.ECSS-Q-70-54C, "Space Product Assurance, Ultracleaning of flight hardware", 2017
- 4.D. Cheung, D. Faye, "Evaluation of decontamination processes adapted to large optical components" International Symposium on Contamination Control 2018, The Hague, Netherlands, 23-26/09/18

3:00pm **VT-MoA-5 Helium Permeation Through Zerodur Glass**, *Sefer Avdiaj*, University of Prishtina, Albania

In the pursuit of a new optical pressure standard [1], Ultra-Low Expansion (ULE) glass cavities were proposed as a means of measuring helium refractivity. However, the utilization of ULE glass gave rise to certain complications, with the pumping effect on helium being a significant issue [2]. As a solution, Zerodur glass was suggested as an alternative material for the cavity. To estimate the flow of helium gas through Zerodur glass, knowledge of the permeation constant K and the diffusion constant D is necessary. These parameters are related through the solubility S of helium in glass, as  $K = S \cdot D$ . In this research work, we experimentally measured the permeation of helium gas in Zerodur over a temperature range of 27 – 120 °C. Our results indicate that Zerodur has potential as a material for the new quantum standard of pressure.

3:20pm **VT-MoA-6 Improvement and Verification of Modified Knudsen Equation to Calculate the Gas Flow Rate through a Cylindrical Tube in Various Flow Regimes**, *Hajime Yoshida*, AIST, NMIJ, Japan

Calculating the gas flow rate through a cylindrical tube of known geometry might seem to be a simple problem but is actually rather complicated. This is because the characteristics of the gas flow depend on pressure, gas species, temperature, tube diameter, and tube length. There are at least six

flow regimes to explain the characteristics of the gas flow, such as molecular flow, viscous laminar flow, turbulent flow, critical flow, subcritical flow, and their intermediates including slip flow.

In recent, we have developed the modified Knudsen equation which is applicable to the whole flow regime for arbitrary length of the tubes [1,2]. This equation has two advantages; one is that this equation is used without considering Knudsen number, Reynolds number, Mach number and the length-to-diameter ratio of tube, and the other is that it can be solved in straight forward without an iterative procedure although the other equations sometimes need it. This equation is especially useful when one does not know which flow regime the gas flow is in.

The solution of the modified Knudsen equation agreed with typical previous studies within 20 % - 30 %, but more study was still needed to confirm if this equation would be truly used for "whole" flow range. 70 literatures reported so far were compared with the modified Knudsen equation. The results reveal the conditions that the relatively large differences between them were observed. The author improved the modified Knudsen equation so that the agreements became within 20 % by introducing the effective length of turbulent flow. On the other hand, it was also found that significant differences around 50 % were observed at the high Reynolds number flow of short tubes. The improvement of modified Knudsen equation and comparison of the calculations of improved modified Knudsen equation with 70 literatures will be presented.

[1] H. Yoshida, Y. Takei and K. Arai, Vacuum and Surface Science 63 (2020) 373.

[2] H. Yoshida, M. Hirata, T. Hara, Y. Higuchi, Packag Technol Sci. 34 (2021) 557.

4:00pm **VT-MoA-8 Dirty Vacuums - To Contamination and Beyond**, *Rod Boswell*, C. Charles, M. Davoodianidalik, J. Richmond, M. Shadwell, Australian National University, Australia

With the recent global interest in space centred around the moon and Mars there is a real need for environmental test facilities that closely mimic lunar and Martian conditions. The challenges centre around two phenomena: vacuum and dust and both challenge mechanical sliding and rotating mechanisms, thermal control, space suits, interaction with charged particle and photon radiation.

Our group and Boswell Technologies has embarked on a number of projects aimed at investigating the basic physics and engineering problems posed by these environmental conditions and also to make available large dirty vacuum systems for research and industry to test systems in a dirty aggressive environment. In particular the lunar regolith comprises sharp edged dust with dimensions down to micrometres what can wreak havoc with moving systems especially human space suits where the dust apparently "burrows" into the material spurning all attempts to remove it. It is considered that photo-electrons generated by Lyman Alpha from the sun results in charged dust levitating from the surface and coating everything.

We have constructed a 3 metre diameter concrete dome and successfully vacuum tested it down to conditions close to that found on Mars. The design was inspired by habitats fabricated for those who, believing the arrival of imminent Armageddon, desired to protect themselves in these structures buried in the Australian sub-soil..... Smaller vacuum systems of a few hundred litres are being used to approach lunar conditions with pressures around  $10^{-6}$ Torr. For both chambers care needed to be taken with the structural integrity, dust and vacuum pumps and the onerous conditions of Work Health and Safety.....

A Lyman Alpha source has been developed and tested using rf energised hydrogen plasmas and magnesium fluoride windows. Initial tests have demonstrated the generation of photo-electrons by VUV radiation and absolute calibrations are being carried out with a commercially available VUV spectrometer and a VUV Deuterium source.

4:20pm **VT-MoA-9 Outgassing Studies of A36 Mild Steel**, *James Fedchak*, E. Newsome, D. Barker, S. Eckel, J. Scherschligt, NIST-Gaithersburg

We present our most recent outgassing results for A36 mild steel. Mild or low-carbon steel is commonly used for structural applications and for piping. Modern secondary refining processes reduce the hydrogen content in mild steel, thus making these steels excellent candidates as low-outgassing materials for the construction of ultra-high vacuum chambers. Indeed, results from a 2016 paper by Park et al.<sup>1</sup> show H<sub>2</sub> outgassing rates for three Korean mild steels to be much lower than those from untreated stainless steel. Stainless steels such as 316L or 304L are commonly used for

# Monday Afternoon, November 6, 2023

vacuum chamber construction, but for ultra-high vacuum or extreme-high vacuum applications, these steels must typically be heat-treated by vacuum-firing (nominally a 950 °C bake under vacuum for several hours) or subjected to a medium heat treatment (>400 °C bake in vacuum or air for several days) to achieve the required H<sub>2</sub> outgassing rate. However, untreated mild steel has the potential to achieve similar outgassing rates as heat-treated stainless steel. This could significantly impact the construction of future gravity wave detectors and other large vacuum systems because of the potential to reduce the cost compared to vacuum systems constructed of stainless steel which is both more expensive and must be heat-treated. We present results for both H<sub>2</sub> and H<sub>2</sub>O outgassing. The former is measured after most of the water has been removed from the vacuum system by low-temperature bake (150 °C or less) with the system under vacuum. The water outgassing rate is measured during the system pump down prior to the baking the system to remove water, and is critical to many large vacuum system users as this affects the time and cost of commissioning.

<sup>1</sup> C. Park, T. Ha, and B. Cho, J. Vac. Sci. Technol. A Vacuum, Surfaces, Film. **34**, 021601 (2016).

## 2D Materials Technical Group

### Room C123 - Session 2D-TuM

#### 2D-Materials: Heterostructures and Functionalization

Moderators: Xiangfeng Duan, UCLA, Kai Xiao, Oak Ridge National Laboratory

8:00am **2D-TuM-1 A Wafer Scale Approach to Synthesize Targeted Metastable Heterostructures**, *David Johnson*, University of Oregon INVITED  
Heterostructures consisting of two or more compounds with different crystal structures interleaved with targeted layer thicknesses and sequences of constituents have been the focus of intense interest due to the discovery of emergent properties of interest for a number of applications. My group has pioneered a synthesis approach to these materials based on repeated deposition of a sequence of elemental layers where the number of atoms in each layer correspond to the amount need to form each of the targeted constituent structures. These designed layered precursors self-assemble at low temperatures into the targeted heterostructures because phase segregation into separated bulk constituents is disfavored by low interdiffusion rates. Since this self-assembly is independent of the substrate structure, this synthesis approach is compatible with lithography. The ability to precisely control constituent layer thicknesses and layer sequences provides opportunities to systematically probe structure-function relationships. We discovered that monolayers of  $VSe_2$  in  $(MSe)_m(VSe_2)_n$  heterostructures have a charge density wave whose onset temperature depends on both the identity and the thickness of the  $MSe$  ( $m$ ) constituent. We found that the chemical potential difference between constituent layers is compensated by charge donation, leading to systematic changes in electrical transport properties as the relative thickness of constituent layers are varied. We have also discovered that the interaction between constituent layers can stabilize constituent layer structures that are not known as isolated compounds. We have prepared magnetic  $Pb_2MnSe_3$  layers in  $(Pb_2MnSe_3)(VSe_2)_n$  heterostructures and a new 1T structured transition metal dichalcogenide,  $FeSe_2$ , in  $(PbSe)_1(FeSe_2)_n$ . Since this synthesis approach is compatible with lithography, we have been able to develop an approach to measure both cross plane and in plane electrical properties on the same structure. The ability to prepare families of heterostructures with a variety of constituent layers from designed precursors creates a new "thin film metallurgy" where nanostructure, interfacial phenomena and interlayer interactions can be systematically exploited to manipulate physical properties.

8:40am **2D-TuM-3 Simple Approach to Demonstrate the Van Der Waals Heterostructure Composed of Different Kinds of  $MoS_2$  Phase for Photodetector Application**, *K. Aydin, T. Kim*, Sungkyunkwan University (SKKU), Republic of Korea; *Chisung Ahn*, Korea Institute of Industrial Technology, Republic of Korea

The 2D materials have considered as noticeable candidates to demonstrate photodetector because of their excellent optical and electronic properties. Especially, inherent phase dependent tunable optical band gap properties of 2D- $MoS_2$  (Molybdenum Disulfide) have significant advantages for versatile optoelectronic applications. Therefore, development the easy phase controlling methodology of 2D- $MoS_2$  could be considered as an important factor to figure out its applicability for photodetector. In this study, innovative procedure is suggested to synthesis the Van der Waals heterostructure by stacking the different phase of  $MoS_2$  (1T and 2H) based on plasma assisted sulfurization process through only process temperature control under the optimized other variables. It allowed to prepare 4 kinds of different  $MoS_2$  structures (1T/2H, 1T/1T, 2H/1T and 2H/2H) by stacking the homo or hetero phase, and photocurrents for each also measured to explore the relevant correlation.

9:00am **2D-TuM-4  $Ta_x$  Prepared by Atomic Layer Deposition: Two-Dimensional Crystalline Films as Cu Diffusion Barrier**, *Sanne Deijkers, H. Thepass*, Eindhoven University of Technology, The Netherlands; *H. Sprey, J. Maes*, ASM, Belgium; *E. Kessels, A. Mackus*, Eindhoven University of Technology, The Netherlands

As transistors in leading-edge nanoelectronics are becoming smaller and smaller, the challenge of scaling the interconnect becomes very prominent. In this scaling, we need a replacement for the Cu diffusion barrier in the back-end-of-line, since conventionally used TaN/Ta barriers fail if they are thinner than 3 nm [1]. Tantalum sulfide ( $Ta_x$ ) is a versatile Ta-based two-dimensional transition metal dichalcogenide (2D-TMD) that can function as Cu diffusion barrier as has been recently shown for films prepared by chemical vapor deposition [2]. In this work we report on the diffusion barrier performance of  $Ta_x$  synthesized by atomic layer deposition (ALD).

ALD offers the desired control and conformality required for thin layers in demanding structures. In our previous work, we have shown that 2D-TMD  $MoS_2$  films synthesized by ALD can outperform  $MoS_2$  films deposited by other techniques [3].

$Ta_x$  films were deposited using a plasma-enhanced ALD process using tert-butyliminotrisdimethylaminotantalum (TBDTMT) as Ta precursor and an  $H_2S / Ar / H_2$  plasma mixture as co-reactant at 300 °C. It is demonstrated that the crystallinity and stoichiometry can be altered by changing the plasma composition. Addition of  $H_2$  to the Ar and  $H_2S$  plasma mixture leads to crystalline  $Ta_2$  films, instead of amorphous  $Ta_3$  films, as measured by x-ray diffraction and x-ray photoelectron spectroscopy.

The barrier performance of the  $Ta_x$  films against Cu diffusion was characterized by time-dependent dielectric breakdown (TDDB) tests. Amorphous  $Ta_3$  films do not function as Cu diffusion barrier, while the crystalline  $Ta_2$  films show a median time to failure ( $TTF_{50\%}$ ) of  $530 \pm 14$  s, where the longest observed breakdown time is 93 hours. This is a substantial improvement compared to barrierless structures ( $TTF_{50\%} = 201 \pm 5$  s), which reveals the potential of ALD-grown  $Ta_x$  as Cu diffusion barrier.

[1] Li *et al.*, *Materials* **13**, 5049 (2020)

[2] Lo *et al.*, *J. Appl. Phys.* **128**, 080903 (2020)

[3] Deijkers *et al.*, *Adv. Mater. Interfaces* **10**, 2202426(2023)

9:20am **2D-TuM-5 Hybrid Epitaxial Heterostructures for Topological Spintronics**, *Nitin Samarth*, Pennsylvania State University INVITED

The confluence of fundamental symmetries and spin-orbit coupling is known to produce emergent electronic states in crystalline solids that are accurately described using the language of topology [1]. This talk describes how recent developments in the synthesis and study of epitaxially grown topological quantum materials and their heterostructures yield new insights into the interplay between spin and charge transport, providing an attractive path toward topological spintronic technologies that work under ambient conditions [2-9].

Sponsored by SMART, a funded center of nCORE, an SRC program sponsored by NIST, the Institute for Quantum Matter under DOE EFRC grant DE-SC0019331, the Penn State Two-Dimensional Crystal Consortium-Materials Innovation Platform (2DCC-MIP) under NSF Grant No. DMR-2039351, and the Penn State MRSEC Center for Nanoscale Science via NSF award DMR2011839

33. Nitin Samarth, "Quantum materials discovery from a synthesis perspective," *Nature Mater*, **16**, 1068-1076 (2017).

34. A. R. Mellnik, *et al.*, "Spin-transfer torque generated by a topological insulator," *Nature* **511**, 449 (2014).

35. Hailong Wang *et al.*, "Surface-state-dominated spin-charge current conversion in topological-insulator-ferromagnetic-insulator heterostructures," *Phys. Rev. Lett.* **117**, 076601 (2016).

36. Hailong Wang *et al.*, "Fermi level dependent spin pumping from a magnetic insulator into a topological insulator," *Phys. Rev. Res.* **1**, 012014 (R) (2019).

37. W. Yanez *et al.*, "Spin and charge interconversion in Dirac semimetal thin films," *Phys. Rev. Appl.* **16**, 054031 (2021).

38. Y. Ou *et al.*, "ZrTe<sub>2</sub>/CrTe<sub>2</sub>: an epitaxial van der Waals platform for spintronics," *Nature Comm.* **13**, 2972 (2022).

39. W. Yanez *et al.*, "Giant dampinglike-torque efficiency in naturally oxidized polycrystalline TaAs thin films," *Phys. Rev. Appl.* **18**, 054004 (2022).

40. W. Yanez *et al.*, "Thin film growth of the Weyl semimetal NbAs," arXiv:2304.13959

41. A. Vera, W. Yanez, et al., "Emergent spin phenomena in air-stable, atomically thin lead," arXiv:2205.06859

11:00am **2D-TuM-10 Designer Quantum Matter in Van Der Waals Heterostructures**, *Peter Liljeroth*, Aalto University, Finland INVITED

Van der Waals (vdW) heterostructures have emerged as a playground for realizing and engineering exotic quantum states not found in naturally occurring materials. Materials with very different physical properties can be combined essentially at will. As the layers interact only through weak vdW forces, the individual layers retain their intrinsic properties. However, proximity effects cause properties to "leak" between the adjacent layers and allow creating exotic quantum mechanical phases that arise from the interactions between the layers. These key features have recently made it possible to realize exotic quantum phases by design.

# Tuesday Morning, November 7, 2023

I will highlight these concepts through our results on realizing topological superconductivity and heavy-fermion physics in vdW heterostructures [1-3]. We use molecular-beam epitaxy (MBE) in ultra-high vacuum for the sample growth and characterize the resulting samples using low-temperature scanning tunneling microscopy (STM). Topological superconductivity requires combining out of plane ferromagnetism, Rashba-type spin-orbit interactions and s-wave superconductivity, and we use monolayer ferromagnet CrBr<sub>3</sub> on a superconducting NbSe<sub>2</sub> substrate to realize this [1,2]. I will discuss how the moiré pattern due to the lattice mismatch between CrBr<sub>3</sub> and NbSe<sub>2</sub> is an essential ingredient in this system as it profoundly modifies the topological phase diagram and enables the realization of a topological superconducting state that would not be accessible in the absence of the moiré. As another example of a designer system, I will introduce 1T-TaS<sub>2</sub> / 1H-TaS<sub>2</sub> heterostructures as a platform for realizing heavy fermion physics in a vdW heterostructure [3]. These results highlight the versatility of vdW heterostructures in realizing quantum states that are difficult to find and control in naturally occurring materials.

## References

[1] S. Kezilebieke, M.N. Huda, V. Vaño, M. Aapro, S.C. Ganguli, O.J. Silveira, S. Głodzik, A.S. Foster, T. Ojanen, P. Liljeroth, Topological superconductivity in a van der Waals heterostructure, Nature 588, 424 (2020).

[2] S. Kezilebieke, V. Vaño, M.N. Huda, M. Aapro, S.C. Ganguli, P. Liljeroth, J.L. Lado, Moiré-enabled topological superconductivity, Nano Lett. 22, 328 (2022).

[3] V. Vaño, M. Amini, S.C. Ganguli, G. Chen, J.L. Lado, S. Kezilebieke, P. Liljeroth, Artificial heavy fermions in a van der Waals heterostructure, Nature 599, 582 (2021).

11:40am **2D-TuM-12 2D Hybrids Based on Graphene Oxide and Palladium Nanozymes for Multimodal Theranostics**, A. Foti, L. Cali, S. Petralia, A. Fraix, G. Forte, R. Fiorenza, S. Scirè, L. D'Urso, C. Bonaccorso, C. Fortuna, **Cristina Satriano**, University of Catania, Italy

Graphene oxide (GO)/palladium (Pd) nanocomposites have shown a great potential as multifunctional nanoparticles with plasmonic, photothermal and enzyme-like behavior for multimodal theranostics.

In this work, different types of hybrid 2D GO/Pd nanosystems were synthesized, with the size of the 2D nanomaterials being controlled by the precursor concentrations as well as different chemical functionalities, including GO vs. reduced-thiolated GO (rGOSH), N-doped reduced GO (rGO-N<sub>x</sub>), mixed organic/inorganic matrix. The physicochemical properties were scrutinized by using UV-visible and Raman spectroscopies, atomic force microscopy, zeta-potential and hydrodynamic light scattering. Theoretical DFT calculations paralleled the experimental studies. The GO/Pd hybrids were tested in terms of photocatalysis experiments of H<sub>2</sub> evolution and photothermal response.

The assessment of nanozyme features for the GO/Pd nanoplateforms unveiled a strong enhancement of hydrogen evolution and broad antioxidant activities, as scrutinized respectively by photocatalysis experiments and MitoSOX and SOD-like activity, respectively. The bio-interface response of systems was evaluated on both tumor cells and healthy cells. Proof-of-work in vitro cell experiments on human prostate cancer cells (PC-3 line) and mouse embryonic fibroblast cells (3T3 line) cells were carried out in terms of cytotoxicity (MTT assay), inhibition of cell migration (wound scratch test) and organelle perturbation (colocalization studies by confocal microscopy). The MTT assay and wound scratch test confirmed the antitumor efficiency of all Pd-based samples in inhibiting tumor growth and monitoring cell migration, respectively. In particular, cells treated with GO-PdNP hybrids with larger sizes showed higher cell viability and migration rate in healthy cells (3T3 line). This makes them promising candidates as nanozyme-theranostic platforms for cancer treatment. The results pointed to a significant reduction of tumor growth and thus the promising potential of the developed GO/Pd hybrid nanozymes in cancer therapy.

This work has been partially funded by the European Union (NextGeneration EU), through the MUR- PNRR project SAMOTHRACE (ECS0000022) and by the University of Catania (PIA no di inCentivi per la Ricerca di Ateneo 2020/2022 GRABIO\_Linea di intervento 2).

12:00pm **2D-TuM-13 Hybrid Molecule/Quantum Material van Der Waals Heterostructures**, **Emanuele Orgiu**, Institut national de la recherche scientifique (INRS), Canada

2D materials are held together by weak interplanar van der Waals (vdW) interactions. The incorporation of molecules in such materials holds an

Tuesday Morning, November 7, 2023

immense potential to understand and modify the fundamental physical properties of the pristine materials while creating new *artificial materials*. Whilst nature offers a finite number of 2D materials, an almost unlimited variety of molecules can be designed and synthesized with predictable functionalities. The possibilities offered by systems in which continuous molecular layers are interfaced with inorganic 2D materials to form hybrid organic/inorganic van der Waals heterostructures (H-vdWH) are emphasized. Similar to their inorganic counterpart, the hybrid structures have been exploited to suggest novel device architectures. Moreover, specific molecular groups can be employed to modify intrinsic properties and confer new capabilities to 2D materials. In particular, I will highlight how molecular self-assembly at the surface of 2D materials can be mastered to achieve precise control over position and density of (molecular) functional groups, paving the way for a new class of hybrid functional materials.

In particular, within such vdW heterostructures, currently assembled by mechanical superposition of different layers, *periodic potentials* naturally occur at the interface between the 2D materials. These potentials significantly modify the electronic structure of the individual 2D components within the stack and their alignment, thus offering the possibility to build up hybrid and novel materials with unique properties.

Also, I will show how the presence of ordered supramolecular assemblies bearing different functional groups can *modify the pristine Shubnikov-De Haas oscillations* occurring in graphene.

## Actinides and Rare Earths Focus Topic

### Room C124 - Session AC+MI+TH-TuM

#### Magnetism, Electron Correlation, and Superconductivity in the Actinides/Rare Earths

**Moderators:** Edgar Buck, PNNL, Tomasz Durakiewicz, Idaho National Laboratory, Krzysztof Gofryk, Idaho National Laboratory

8:00am **AC+MI+TH-TuM-1 Uranium and Cerium Based Systems Probed with High-Pressure XANES and XMCD**, **Fabrice Wilhelm**, A. Roagel, ESRF, France

This talk reviews recent advances in use of polarized x-rays to study local magnetic properties and electronic structure of uranium and cerium based compounds such as the ferromagnetic UGe<sub>2</sub>, the heavy-fermion paramagnet UTe<sub>2</sub> and the nanolamellar ferromagnetic Kondo lattice Mo<sub>4</sub>Ce<sub>4</sub>Al<sub>7</sub>C<sub>3</sub> system.

8:40am **AC+MI+TH-TuM-3 Searching for New Uranium-Based Arsenides**,

**Eteri Svanidze**, Max Planck Institute for Chemical Physics of Solids, Germany

As new classes of superconducting materials emerge, puzzles of high-temperature superconductivity continue to be one of the pressing issues in condensed matter physics and solid-state chemistry. In particular, iron pnictide superconductors still pose many open questions. Surprisingly, very few actinide-based analogues of iron pnictide high temperature superconductors have been reported so far, perhaps as a result of synthesis complications imposed by toxicity, reactivity, and high vapor pressure of constituent elements. In this work, we revisit the U-Fe-As ternary, in which only one compound has been reported to exist so far – UFeAs<sub>2</sub> (*P4/nmm* space group) [1]. By implementing flux synthesis, we were able to grow large single crystals of UFe<sub>5</sub>As<sub>3</sub> compound, which adopts UCr<sub>5</sub>P<sub>3</sub> structure type [2] (*P2<sub>1</sub>/m*, *mP18*) with lattice parameters  $a = 7.0501(17) \text{ \AA}$ ,  $b = 3.8582(9) \text{ \AA}$  and  $c = 9.6342(13) \text{ \AA}$ ,  $\beta = 100.2(8)^\circ$  [3]. The refined composition agrees well with the elemental ratio established by the EDX analysis – U<sub>9.9(2)</sub>Fe<sub>58.7(2)</sub>As<sub>31.4(2)</sub>. The magnetic behavior of UFe<sub>5</sub>As<sub>3</sub> was studied by magnetic susceptibility measurements in the temperature range 1.8 - 600 K and an antiferromagnetic ordering below T<sub>N</sub> = 56 K was established. The Sommerfeld coefficient  $\gamma = 138 \text{ mJ/mol K}^2$  indicates enhanced effective electron mass. More in-depth investigations of this and other U-Fe-As ternary compounds are currently underway.

#### References:

[1] D. Kaczorowski, J. Alloys. Compd. 186, 333-338 (1992).

[2] W. Jeitschko, R. Brink, P.G. Pollmeier, Z. Naturforsch. (1993) 48b, p. 52-57.

[3] N.Zaremba, M. Krnel, Yu. Prots, A. Leithe-Jasper, Yu. Grin, E. Svanidze, in preparation (2023)

# Tuesday Morning, November 7, 2023

9:00am **AC+MI+TH-TuM-4 5f Magnetism at an Extreme**, *Ladislav Havela*, Charles University, Faculty of Mathematics and Physics, Czechia; *V. Buturlim*, Idaho National Laboratory; *F. Honda*, Tohoku University, Japan; *D. Kaczorowski*, Institute of Low Temperature and Structure Research, Wrocław, Poland

Specific features of 5f magnetism in U-based systems, namely the strong spin-orbit coupling and very strong magnetic anisotropy or giant magnetoresistance, are degraded by low temperatures of magnetic ordering. The variability of  $T_C$  or  $T_N$  in intermetallics has been explored and it turns out that involvement of magnetic *d*-metals such as Fe or Co does not help, unless very high fraction of the transition metals turns a compound in fact a regular *d*-magnet, in which the unique 5f features are suppressed. The reason is the 5f-*d* hybridization with a destabilizing action on both *d* and 5f moments.

Seeking additional degrees of freedom we turned towards compounds with more polar character of bonding, which drives U to the verge of metallicity. Interesting alternative to intermetallics is provided by Zintl phases, typically ternary compounds with one cation (e.g. an *f*-metal) and a complex covalently bond anion, stabilized by a charge transfer from the cation. An excellent insight is provided by such compounds with layered crystal structures, which leads to strongly anisotropic electronic properties. Our research focuses on Zintl phases with the trigonal  $\text{CaAl}_2\text{Si}_2$  type (*P*-3*m*), formed by alternating cationic (Ca) and anionic (Al-Si) layers. Those without *f*-metals or with 4f metals tend to be narrow-gap semiconductors. U-based phases such as  $\text{UCu}_2\text{P}_2$  are semi-metallic. The prominence of this compound dwells in ferromagnetism with high Curie temperature  $T_C = 216$  K, which is further enhanced by pressure application to the vicinity of room temperature. Ab-initio calculations reveal it this material is actually a half-metal, with spin-split 5f band bringing spin-up only states to the Fermi level. The conduction electron states remain hybridized with the 5f states, which causes also the non-*f* electrons to be fully spin polarized. The magnetism is of local moment type, with magnetic entropy exceeding  $R \ln 2$ , but arising from 5f bands.  $\text{UCu}_2\text{P}_2$  can be compared with  $\text{EuZn}_2\text{P}_2$ . Here the  $\text{Eu}^{2+}$  moments are organized in an AF structure. The field alignment of the moments impacts the width of the gap seen in transport data, but the material remains semiconducting.

This work was supported by the Grant Agency of the Czech Republic under the grant No. 21-09766S.

9:20am **AC+MI+TH-TuM-5 Valence-to-Core RIXS in Insulating Compounds with 4f and 5f Elements**, *Jindrich Kolorenc*, Institute of Physics, Czech Academy of Sciences, Czechia

In the first part, we investigate the electronic structure of europium sulfide ( $\text{EuS}$ ) with the aim to understand the valence-to-core resonant inelastic x-ray scattering (RIXS) spectra measured at the  $\text{Eu L}_3$  edge. We show that the main part of the observed signal comes from the direct RIXS: an  $\text{Eu 2p}$  core electron is excited to an empty  $\text{Eu 5d}$  band above the Fermi level, and then another electron from an  $\text{Eu 5d}$  state hybridized with the  $\text{S 3p}$  bands (located below the Fermi level and hence occupied) fills back the core hole. Besides this straightforward channel, the measured RIXS spectra display two satellite features. After considering several candidates (such as excitations of the 4f shell excited by indirect RIXS processes, that is, by the interaction with the core hole in the intermediate state), we arrive at the conclusion that the satellites are excitons formed by a 4f hole and an 5d electron localized at the same  $\text{Eu}$  atom. Such excitons were suggested in the context of optical absorption a long time ago [1], but the concept is not widely accepted. It was argued that existence of these excitons is incompatible with photoconductivity measurements [2]. Our observations indicate that these arguments may need to be revisited.

In the second part, we simulate valence-to-core RIXS at the actinide  $M_5$  edge in selected actinide oxides starting from the dynamical mean-field electronic structure obtained earlier [3] and using techniques similar to [4]. This investigation is motivated by the recent experimental study of  $\text{UO}_2$  and  $\text{UF}_4$  [5]. Our preliminary results suggest that the feature observed at an energy loss of roughly 10 eV above the white line is likely a charge-transfer excitation, the intensity of which is sensitive to the hybridization between the actinide 5f states and the ligand 2p states.

This work was supported by the Czech Science Foundation under the grant No. 21-09766S.

[1] T. Kasuya and A. Yanase, Rev. Mod. Phys. 40 (1968) 684, <https://doi.org/10.1103/RevModPhys.40.684>

[2] P. Wachter and B. Bucher, Physica B 408 (2013) 51, <https://doi.org/10.1016/j.physb.2012.09.018>

[3] J. Kolorenc, A. Shick, A. I. Lichtenstein, Phys. Rev. B 92 (2015) 085125, <https://doi.org/10.1103/PhysRevB.92.085125>

[4] J. Kolorenc, Physica B: Condensed Matter 536 (2018) 695, <https://doi.org/10.1016/j.physb.2017.08.069>

[5] J. G. Tobin et al., J. Phys.: Condens. Matter 34 (2022) 505601, <https://doi.org/10.1088/1361-648X/ac9bbd>

9:40am **AC+MI+TH-TuM-6 Magnetism of Binary Actinide Oxides**, *Binod Rai*, A. Bretaña, Savannah River National Laboratory; *G. Morrison*, University of South Carolina, Columbia; *R. Greer*, Savannah River National Laboratory; *K. Gofryk*, Idaho National Laboratory; *H. zur Loye*, University of South Carolina, Columbia

Historically, the bulk of actinide oxide research has focused on the properties of various uranium and plutonium compounds as they impact their use in the nuclear fuel industry. While the fundamental understanding of compounds such as  $\text{UO}_2$  has improved, a fundamental grasp of the physical properties of other actinide oxides remains elusive. In actinide systems, the 5f electrons experience a uniquely delicate balance of effects and interactions having similar energy scales, which are often difficult to properly disentangle. The interplay of factors such as the dual character of 5f-states, competing interactions, and strong spin-orbit coupling results in magnetically unusual and intriguing behavior: multi-*k* antiferromagnetic ordering, multipolar ordering, mixed valence configurations, and more. In this presentation, I will provide an overview of the available synthesis techniques for selected binary actinide oxides. I will also show the current state of knowledge on their crystal structures and magnetic properties. Moreover, I will talk about the future opportunities that are vital for a fundamental understanding of these systems.

11:00am **AC+MI+TH-TuM-10 N-Point Saddle-Band Model for the Hidden Order Phase of  $\text{URu}_2\text{Si}_2$** , *J. D. Denlinger*, Lawrence Berkeley National Laboratory; *J. Kang*, The Catholic University of Korea; *L. Dudy*, SOLEIL, France; *J. Allen*, University of Michigan; *L. Wray*, New York University; *A. Gallagher*, R. Baumbach, National High Magnetic Field Laboratory; *N. Butch*, University of Maryland; *M. Maple*, University of California, San Diego

The 5f heavy fermion system of  $\text{URu}_2\text{Si}_2$  is famous for an unconventional hidden order (HO) phase transition at  $T_0=17.5$ K and the various related doping phase diagrams explored to elucidate the nature of this unknown transition. A new model of an extended U 5f saddle-point dispersion at the N-point is proposed for the underlying physics of this 35-year old puzzle. With a 10X DFT energy renormalization suggested by angle resolved photoemission (ARPES) measurements in comparison to DMFT calculations [1], this feature lies only a few meV below  $E_F$  and thus is thermally active at  $T_0$ . ARPES reveals a distinct temperature-dependent evolution of incommensurate 5f nesting hotspots lying along Z-N-Z [1], whose origins are found in electronic susceptibility calculations of intraband q-scattering for thermal occupations in the temperature range of  $T_0$ . Tuning of the N-point region f-band energetics with chemical doping is thus naturally proposed to unify our understanding of the various phase diagrams. ARPES is presented which confirms the existence of N-point spectral and dichroic changes for ferromagnetic Re/Ru-substitution, for (001) antiferromagnetic Fe and Os/Ru-substitution, and for (1/2,1/2,1/2) antiferromagnetic P/Si-substitution, thus further demonstrating experimentally the key relevance of the N-point electronic structure to the HO phase. [1] J. D. Denlinger et al., Electron. Struct. 4, 013001 (2022).

11:20am **AC+MI+TH-TuM-11 Magnetoelastic Properties of 5f Ferromagnet  $\text{UCu}_2\text{P}_2$** , *Volodymyr Buturlim*, Idaho National Laboratory; *P. Doležal*, O. Koloskova, J. Prchal, Charles University, Czechia; *I. Turek*, Charles university, Czechia; *M. Martinez Celis*, CRISMAT Laboratory, France; *F. Honda*, Kyushu University, Japan; *M. Divis*, Charles University, Czechia; *D. Kaczorowski*, Polish Academy of Sciences, Poland; *K. Gofryk*, Idaho National Laboratory; *L. Havela*, Charles University, Czechia

$\text{UCu}_2\text{P}_2$ , a Zintl phase with the trigonal  $\text{CaAl}_2\text{Si}_2$  structure type, is a 5f ferromagnet with a record-high Curie temperature among U compounds,  $T_C = 216$  K [1]. While the size of the magnetic moment  $2.0 \mu_B/\text{U}$  is not surprising due to U-U spacing exceeding the Hill limit, the reasons for the high  $T_C$  are less understood. Ab-initio calculations reveal only very weak hybridization of the U-5f states with the 6d states as well as with electronic states of Cu and P. It seems that a transfer of U-6d states to the P-3p states is an important ingredient, which was highlighted by a rapid increase of  $T_C$  under hydrostatic pressure so that a room-temperature 5f ferromagnetism could be demonstrated. Besides magnetization, transport, and heat capacity studies on single crystals we performed also characterization of a polycrystalline material, which has  $T_C = 219$  K. Thermal expansion study revealed a moderate increase of both lattice parameters just below  $T_C$ , so

we can exclude that the pressure enhancement of  $T_c$  is driven simply by thermodynamics (via the Ehrenfest relation). Hence the reasons have to be attributed to the enhancement of specific U-U couplings upon compression. Indeed, ab initio calculations probing the energy enhancement upon moments reversal gave a semi-quantitative account of the observed tendency of  $T_c$ .

[1] D. Kaczorowski, R. Troc, Magnetic and transport properties of a strongly anisotropic ferromagnet  $UCu_2P_2$ , *J. Phys. Condens. Matter*, 1990, 2, 4185.

\*This work was supported by the Czech Science Foundation under the grant No. 21-09766S.

11:40am **AC+MI+TH-TuM-12 Density Functional Theory Calculations of the Phonons in Gamma and Delta Phase Pu**, *Sven P. Rudin*, Los Alamos National Laboratory

The thermodynamics of plutonium challenges both theory and experiment. The challenge arises from the multiple structural phase transitions, the nature of the 5f electrons, and the effects due to the material's self-irradiation. Density functional theory calculations have made steady progress toward clarifying experimental measurements. Recently, for the delta phase a non-collinear 3Q spin structure was shown to make all structurally equivalent bonds equivalent in their bonding character. This results in elastic constants and phonons with the correct symmetry, and the calculated phonon dispersion agrees well with experiment. Extending the calculations into the gamma phase of Pu now provides a prediction for the phonons of that phase.

12:00pm **AC+MI+TH-TuM-13 The 5f UDOS of the Actinide Dioxides: Why Pu is  $n = 5$  in  $PuO_2$** , *James Tobin*, University of Wisconsin-Oshkosh; *H. Ramanantoanina*, KIT, Germany; *C. Daul*, U. Fribourg, Switzerland; *S. Yu*, LLNL; *P. Roussel*, AWE, UK; *S. Nowak*, *R. Alonso-Mori*, *T. Kroll*, *D. Nordlund*, *T. Weng*, *D. Sokaras*, SSRL

The Unoccupied Density of States (UDOS) of  $ThO_2$ ,  $UO_2$  and  $PuO_2$  have been investigated with a combined experimental and theoretical approach.<sup>1,2</sup> Ligand field density functional theory calculations of the dioxides of thorium, uranium, and plutonium have been combined with high-energy-resolution fluorescence detection (HERFD) in x-ray absorption spectroscopy and inverse photoelectron spectroscopy (IPES) measurements to provide powerful insight into the underlying composition of the unoccupied 5f electronic structure in these 5f localized systems. Fine structure in the  $5f_{5/2}$  transitions in HERFD can be directly correlated with the fine structure in the leading edge of the IPES. The shapes, intensities, and systematics in HERFD and IPES are explained in a consistent and rigorous fashion in terms of the j-specific 5f electronic structure. Additionally, an actinide  $N_{4,5}$  branching ratio analysis of  $PuO_2$  and  $UO_2$  has been performed, including measurements with a scanning transmission electron microscope at the Advanced Light Source and simulation with FEFF. It is shown that the 5f occupation of the Pu in plutonium dioxide is  $n = 5$ .

## References

42. J. G. Tobin, H. Ramanantoanina, C. Daul, S.-W. Yu, P. Roussel, S. Nowak, R. Alonso-Mori, T. Kroll, D. Nordlund, T.-C. Weng, D. Sokaras, "The Unoccupied Electronic Structure of Actinide Dioxides," *Phys. Rev. B* 2022, **105**, 125129. <https://doi.org/10.1103/PhysRevB.105.125129>
43. J. G. Tobin and S.-W. Yu, "Pu5f Occupation in Plutonium Dioxide," *Inorg. Chem.* 2023, **62**, 6, 2592–2598, <https://doi.org/10.1021/acs.inorgchem.2c03202>

## Atomic Scale Processing Mini-Symposium Room A107-109 - Session AP+EM+PS+TF-TuM

### Area Selective Processing and Patterning

**Moderators:** *Eric A. Joseph*, IBM Research Division, T.J. Watson Research Center, *Adrie Mackus*, Eindhoven University, Netherlands

8:00am **AP+EM+PS+TF-TuM-1 Area-Selective Deposition in Nanoscale Patterns**, *Annelies Delabie*, Imec Belgium, and KU Leuven Belgium; *J. Clerix*, IMEC Belgium; *K. Van Dongen*, IMEC, Belgium; *J. Sinha*, IMEC Belgium; *L. Nyns*, IMEC, Belgium; *R. Nye*, LAM Research; *G. Parsons*, North Carolina State University; *J. Swerts*, IMEC Belgium

**INVITED**  
Manufacturing nano-electronic devices becomes more and more complex as the device dimensions reach the nanoscale and a wide range of new materials is being implemented to achieve high device performance. Additional complexity comes from the use of three dimensional (3D) structures to reduce the active footprint. Area-Selective Deposition (ASD) provides a promising avenue to assist and/or even simplify device manufacturing processes. ASD is a technique to deposit material only on a pre-defined area of a patterned surface (the growth area), while no deposition is intended on other areas of the same surface (the non-growth area). As such, ASD can be used to replicate patterns on 3D substrates and to (partly) fill narrow trenches or holes from the bottom up. ASD can be achieved by tuning the adsorption and diffusion kinetics in atomic layer deposition (ALD) and chemical vapor deposition (CVD) processes. Insight in the chemical and physical processes is essential to enable rational design of new ASD processes for nano-electronic device manufacturing for advanced technology nodes.

This presentation will discuss the growth mechanisms during ASD on substrates that contain nanoscale patterns, where the geometry of the nanopatterns can affect the growth behavior, selectivity and uniformity. An aminosilane small molecule inhibitor can enable ASD on a wide range of materials with  $SiO_2$  as the non-growth surface [1]. The selectivity of  $TiO_2$  ALD relies mainly on adsorption. Selectivity loss during  $TiO_2$  ALD occurs via a nucleation site generation mechanism: small  $TiO_2$  nanoparticles are continuously generated during ALD by slow, unintentional adsorption on the passivated non-growth surface area [2]. ASD super cycles consisting of inhibitor adsorption,  $TiO_2$  ALD and etch effectively improve the selectivity, but may compromise the height uniformity in nanoscale patterns. The selectivity of Ru and  $Ge_2Sb_2Te_5$  ALD relies on a complex interplay of adsorption, diffusion and aggregation. We reveal a pattern-dependent selectivity for Ru ALD, which is explained by aggregation of Ru adspecies at the pattern edges [3]. We conclude that the selectivity and uniformity of ALD processes can change when pattern dimensions reach the nanoscale.

[1] K. Van Dongen et al, *J. Vac. Sci. Technol. A* 2023, 41, 032404.

[2] R. A. Nye et al, *Appl. Phys. Lett.* 2022, 121, 082102.

[3] J.-W. J. Clerix et al, *Appl. Surf. Sci.* 2023, 626, 157222.

8:40am **AP+EM+PS+TF-TuM-3 N-Heterocyclic Carbenes as Small Molecule Inhibitors in AS-ALD**, *Cathleen Crudden*, Queen's University, Canada

**INVITED**  
A unique carbon-based SMI, called an N-heterocyclic carbene (NHC), has been developed as a small molecule inhibitor using carbon as the heteroatom. NHCs have been used in organometallic and catalysis chemistry for decades, where they are renowned for their ability to form strong bonds to metal surfaces. We have developed a suite of organic SMIs with high volatility and thermal stability enabling deposition in an ALD tool. We demonstrated strong binding of the SMI to Ru, Co, Mo and Cu and selectivity for binding to metal surfaces in the presence of insulators. These results are informed by surface science studies including microscopy and spectroscopy.

9:20am **AP+EM+PS+TF-TuM-5 Unraveling Precursor Blocking Mechanisms in Area-Selective Atomic Layer Deposition Using Small Molecule Inhibitors**, *Olaf Bolkenbaas*, *M. Merckx*, Eindhoven University of Technology, Netherlands; *P. Yu*, Eindhoven University of Technology, Netherlands; *T. Sandoval*, Universidad Tecnica Federico Santa Maria, Chile; *E. Kessels*, *A. Mackus*, Eindhoven University of Technology, Netherlands

Area-selective atomic layer deposition (ALD) has garnered significant attention as a potential technique for enabling the further miniaturization of semiconductor devices. One method for achieving area-selective ALD is through the use of small molecule inhibitors (SMIs) that selectively block deposition on certain materials. Previous research has indicated that precursor blocking by SMIs involves two components: the chemical removal of reactive surface sites and the physical blocking of the surface, also

referred to as chemical passivation and steric shielding respectively [1]. However, it is difficult to differentiate between these two factors as they occur simultaneously. In this work we attempt to unravel the steric shielding and the chemical passivation contributions by the SMI acetylacetone (Hacac) with the use of reflection adsorption infra-red spectroscopy (RAIRS) on dehydroxylated Al<sub>2</sub>O<sub>3</sub> surfaces obtained through annealing.

When comparing Hacac adsorption on an as-prepared and an annealed Al<sub>2</sub>O<sub>3</sub> surface using RAIRS, a lower amount of Hacac adsorbates was observed on the annealed surface. Furthermore, a higher fraction of the Hacac adsorbates was present in the more strongly bonded chelate configuration. This difference in the distribution of the binding configurations demonstrates that the density of surface sites affects the SMI adsorption behavior. We expect that this different adsorption behavior is caused by a lower amount of steric hindrance between the SMIs on the annealed Al<sub>2</sub>O<sub>3</sub> surface. Furthermore, the increase in the amount of adsorbates in the chelate configuration will result in a higher contribution of chemical passivation on the dehydroxylated surface, since only the adsorbates in the chelate configuration chemically passivate the surface [2]. From this we can conclude that the removal of surface sites can be used to obtain a better understanding of the two precursor blocking mechanisms. This better understanding will create opportunities for the development of new area-selective ALD strategies involving the removal of reactive surface sites before the functionalization with SMIs to improve selectivity.

[1] Merckx, et al., *Chem. Mater.* **32**, 3335–3345 (2020).

[2] Mameli et al., *ACS Nano* **11**, 9303–9311 (2017).

9:40am **AP+EM+PS+TF-TuM-6 Topographically-Selective Deposition Using Amorphous Carbon as Inhibition Layer**, *Thijs Janssen, M. Merckx, W. Kessels, A. Mackus*, Eindhoven University of Technology, The Netherlands

To accommodate the increasing complexity of device architectures in nanoelectronics, new nanoscale processing techniques are required. Selective deposition techniques have been developed in recent years to enable bottom-up and self-aligned processing<sup>12</sup>. While traditional area-selective deposition distinguishes between areas depending on their chemical character, topographically-selective deposition (TSD) distinguishes between areas based on their orientation within a 3D structure<sup>2,3</sup>. Such TSD approaches offer new fabrication opportunities, for example when the growth and non-growth areas possess similar material properties, or when too many different materials are present within the device structure. Previously reported TSD methods have been demonstrated only for specific materials.

In our work, we develop a versatile TSD strategy that is potentially suitable for a broad range of materials. Our approach utilizes a pulsed Ar/CH<sub>4</sub> plasma to selectively apply an amorphous carbon (aC) inhibition layer on horizontally-oriented surfaces by relying on the directional ions from the plasma. The vapor-phase selective deposition of aC is integrated together with existing ALD processes and plasma treatments into a TSD supercycle recipe.

The highly inert surface of aC lacks suitable adsorption sites for ALD precursors and co-reactants, making it an effective inhibition layer. It was found that only the horizontally-oriented surfaces are covered by the aC layer, thus subsequent ALD of target materials proceeds exclusively on vertically-oriented surfaces.

Successful ALD inhibition on the aC surface is established for several different target materials such as TiO<sub>2</sub> using TDMAT and H<sub>2</sub>O, Nb<sub>2</sub>O<sub>5</sub> using TBTDEN and H<sub>2</sub>O, and NiO<sub>x</sub> using Ni(BuAMD)<sub>2</sub> and H<sub>2</sub>O. In particular 90% selectivity was maintained for 35 cycles TiO<sub>2</sub> deposition (1.09 ± 0.01 nm selective growth), 70 cycles Nb<sub>2</sub>O<sub>5</sub> deposition (4.38 ± 0.02 nm) and 40 cycles of NiO<sub>x</sub> deposition (1.28 ± 0.01 nm). It is demonstrated for NiO<sub>x</sub> that the supercycle can be repeated, which effectively resets the nucleation delay, such that a thicker film (nominally ~5 nm after 4 supercycles) can be deposited selectively.

44. Mackus, A. J. M., Merckx, M. J. M. & Kessels, W. M. M. From the Bottom-Up: Toward Area-Selective Atomic Layer Deposition with High Selectivity. *Chem. Mater.* **31**, 2–12 (2019).
45. Parsons, G. N. & Clark, R. D. Area-Selective Deposition: Fundamentals, Applications, and Future Outlook. *Chem. Mater.* **32**, 4920–4953 (2020).
46. Chaker, A. et al. Topographically selective deposition. *Appl. Phys. Lett.* **114**, (2019).

11:00am **AP+EM+PS+TF-TuM-10 A ReaxFF Study for Hacac Interaction on Al<sub>2</sub>O<sub>3</sub> Surface in Area-Selective ALD**, *Naoya Uene*, Tohoku University, Japan; *I. Tezsevin, W. Kessels, A. Mackus*, Eindhoven University of Technology, Netherlands; *A. van Duin*, Pennsylvania State University; *T. Tokumasu*, Tohoku University, Japan

An area-selective ALD process of SiO<sub>2</sub> was developed comprising acetylacetone inhibitor (Hacac), bis(diethylamino)silane precursor (BDEAS), and O<sub>2</sub> plasma reactant pulses. Hacac inhibitors lead to delayed SiO<sub>2</sub> growth on the Al<sub>2</sub>O<sub>3</sub> surface for about 15 ALD cycles, after which the selectivity is lost. Two chemisorption configurations of Hacac inhibitors on Al<sub>2</sub>O<sub>3</sub> surfaces have been reported: monodentate and chelate configurations. (Merckx et al. 2020) Density functional theory (DFT) calculations have shown that the monodentate configuration is relatively reactive with incoming BDEAS, causing the loss of selectivity due to precursor-inhibitor reactions. Therefore, exploration of the relative densities of the chelate/monodentate configurations on the surface is crucial for the understanding of the selectivity loss mechanism. We aim to understand the reaction mechanisms of Hacac inhibitor adsorption on Al<sub>2</sub>O<sub>3</sub> surfaces at the atomic scale.

Up to now, the investigation of the adsorption of inhibitor molecules has been studied via DFT calculations. Thereactive force-field molecular dynamics (ReaxFF MD), which can simulate chemical reactions and physical dynamics at the atomic scale, has been used for gas-surface systems. (van Duin et al. 2001) We performed ReaxFF MD simulations to consider the chemical reactions of Hacac inhibitor molecules with dislocation effects on the surface. An initial force field has been developed for the Hacac interaction on Al<sub>2</sub>O<sub>3</sub> surface based on the two existing force fields: Li/Si/Al/O force field for Al<sub>2</sub>O<sub>3</sub> structure and protein force field for carbohydrate interactions. (Kim et al. 2016; Monti et al. 2013) The initial force field is trained for Hacac geometry, and their reaction on an OH-terminated Al<sub>2</sub>O<sub>3</sub> surface is also modeled.

We performed ReaxFF MD simulations using the developed force field. The simulation consists of three steps. First, the Al<sub>2</sub>O<sub>3</sub> surface is pre-thermally relaxed. Then, the Hacac inhibitor is supplied on the relaxed surface, followed by post-thermal relaxation of the Hacac-adsorbed surface. We first confirmed the temperature stability of the Al<sub>2</sub>O<sub>3</sub> surface with different temperatures. Our force field can control the temperature of the Al<sub>2</sub>O<sub>3</sub> surface ranging from 300 K to 1500 K. Next, sequential adsorption of 20 Hacac inhibitor molecules was simulated on the temperature-controlled Al<sub>2</sub>O<sub>3</sub> surface, as shown in the supplemental document. The findings from our ReaxFF simulations provide in-depth insights into the mechanisms of Hacac adsorption and saturation on the surface. These insights will be used for the investigation of precursor blocking and blocking selectivity loss in our future work.

11:20am **AP+EM+PS+TF-TuM-11 Enhancement of TMSDMA Passivation on SiO<sub>2</sub> by Surface Fluorination**, *Anthony Valenti*, SUNY College of Nanoscale Science and Engineering; *C. Vallée*, SUNY College of Nanoscale Science and Engineering, France; *C. Ventrice*, SUNY College of Nanoscale Science and Engineering; *K. Tapily, K. Yu, S. Consiglio, C. Wajda, R. Clark, G. Leusink*, TEL Technology Center, America, LLC, USA

With the ever-shrinking scale of semiconductor devices, area-selective atomic layer deposition (AS-ALD), a bottom-up and self-aligned patterning process with atomic-scale control has been in development in order to meet the demands of industry. This technique is typically conducted by promoting growth on specific surface termination types, while inhibiting growth on the other surface types of the substrate via selective chemisorption of molecules that are inert to the deposition process. With its affinity for chemisorbing to hydroxylated oxide surfaces, specifically SiO<sub>2</sub>, but not on Si or non-oxidized metal surfaces, N-(trimethylsilyl)dimethylamine (TMSDMA) has been of recent interest for its use as a small molecule inhibitor (SMI) for area selective deposition (ASD). Upon interaction with a surface hydroxyl group, the TMSDMA molecule dissociates, resulting in a trimethylsilyl group bonded to the chemisorbed oxygen atom of the hydroxyl group. Although TMSDMA-passivated SiO<sub>2</sub> typically remains inert over several ALD cycles, nucleation of the growth precursor can eventually occur. This may be due to hydroxyl groups on the surface that did not interact with TMSDMA molecules and/or non-hydroxylated sites that were not passivated by trimethylsilyl groups. For instance, surface siloxane bridges do not dissociate TMSDMA and can act as nucleation sites for the ALD growth precursor. In order to enhance the passivation of SiO<sub>2</sub> surfaces, the use of co-passivants has been explored. In particular, a remote NF<sub>3</sub> plasma has been studied as a means for forming a co-inhibitor. Dosing before or after TMSDMA treatment has been investigated. The deposition of the small molecules were carried out on 10 Å SiO<sub>2</sub>/Si(100) substrates. Water contact angle measurements were taken

# Tuesday Morning, November 7, 2023

to determine relative surface passivation of each sample. Angle-resolved X-ray photoelectron spectroscopy and attenuated total reflection/Fourier transform infrared spectroscopy were performed in order to characterize the chemical state of each surface. Our results indicate that exposure of the substrate to the NF3 plasma after passivation with TMSDMA, results in damage to the passivating layer. However, exposure of the surface to the NF3 plasma before TMSDMA exposure maintains the passivation of the SiO<sub>2</sub> surface. In addition, temperature programmed desorption (TPD) measurements are being conducted to assess the relative coverage of the inhibiting film on each sample and its thermal stability.

**11:40am AP+EM+PS+TF-TuM-12 A Study of Elucidation and Improvement of TiO<sub>2</sub> Selectivity by First-Principles Based Thermodynamic Simulation, Yukio Kaneda, Sony Semiconductor Solutions Corporation, Japan; E. Marques, S. Armini, A. Delabie, M. van Setten, G. Pourtois, imec, Belgium**

**INVITED**

Area-selective deposition (ASD) enables the deposition of materials in a targeted area, typically a pre-patterned surface, while preventing the growth on adjacent surfaces.[1] The technique is appealing for both academia and industry as it offers a vehicle to simplify material developments in nanoelectronics. Consequently, numerous efforts have been dedicated to investigate the factors driving the selectivity mechanisms and to identify optimal process deposition conditions, including surface treatments, that enable highly selective processes.

The “selectivity” dimension results from the identification of the right combination of precursors (including co-agents), surface treatments, and reactor operating conditions. This is typically a complex and laborious process that requires many systematic and tightly controlled experiments. As a result, the development of highly selective ASD processes is often a slow and challenging task where any form of guidance provided by modeling insights can be precious.

In this context, we studied, by combining thermodynamic considerations and first principle simulations, the reactivities of complex surface chemical reaction networks and the factors impacting on selectivity. In this talk, we will discuss the case of the ASD of TiO<sub>2</sub> on SiO<sub>2</sub> substrates terminated with either “reactive” (-OH) or “passivated” alkyl-silyl groups. First, we will first briefly discuss the validation of our approach by comparing our model prediction with experimental measurements for the case of the ALD of TiO<sub>2</sub> using the precursors TiCl<sub>4</sub> and Ti(OMe)<sub>4</sub> and then report the insights gained for the identification of optimum Ti precursor and inhibitor for the ASD of TiO<sub>2</sub>. We will then extend the discussion to the case of the ASD supercycles of TiO<sub>2</sub>, where the interaction of some Ti precursors (or of their ligands) leads to the degradation of the surface “passivation” and then requires restoring the surface by injecting of alkyl-silyl functional groups. We will review the strategies that worked with their drawbacks.

[1] Gregory N. Parsons and Robert D. Clark, *Chem. Mater.* **2020**, *32*, 12, 4920–4953

[2] Job Soethoudt, *et al., The Journal of Physical Chemistry C* **2020** *124* (13), 7163–7173

[3] Janne-Petteri Niemelä *et al., Semicond. Sci. Technol.* **2017** *9* (32), 093005

## Biomaterial Interfaces Division

### Room B117-119 - Session BI+AS+PS-TuM

#### Biomolecules and Biophysics at Interfaces

**Moderators: Christopher So, Naval Research Laboratory, Markus Valtiner, Vienna University of Technology, Austria**

**8:00am BI+AS+PS-TuM-1 Probing Protein Structure on Nanoplastic Surface by Sum Frequency Scattering, Akriti Mishra, T. Weidner, Aarhus University, Denmark**

The safe use of nanoparticle protein conjugates in biomedical applications like disease diagnosis, drug delivery, biosensing, etc. depends on the efficacy and stability of these conjugates in body fluids. To date, several analytical techniques like UV-Vis, dynamic light scattering, Fourier transform infrared spectroscopy, circular dichroism, nuclear magnetic resonance, etc. have been used to study the interaction of proteins on nanoparticle surface. Since most of the techniques can not differentiate between the surface bound and the free proteins in solution, it becomes impossible to gather any information about the interfacial proteins. The

confirmation of a protein after adsorption on nanoparticle surface can be drastically different from that in solution, which may hamper or amend the activity and function of proteins. Surface sensitive sum frequency scattering (SFS) stands out best in this case since it selectively probes the vibrational modes of the adsorbed analytes on any interface. Sum frequency generation from flat interfaces has been successfully shown to provide rich information about the structure, order, and composition of molecules at the interface. Recently, our group has shown that SFS can effectively probe the structure and orientation of model peptides at nanoscopic oil particle surfaces.<sup>1</sup> We will here discuss how also complex human corona proteins can be probed on particle surfaces. We focus on alpha synuclein (aS) interactions with nanoparticles relevant for medical applications and environmental nanoplastics. aS is a 14 kDa intrinsically disordered protein known to form amyloids called Lewy bodies, which can propagate across the neurons to induce Parkinson’s disease (PD). Using SFS we follow how aS binds and folds on polymer nanoparticle surfaces. SFS spectra in the amide I region strongly suggest that aS folds into beta sheet and fibrillated structures at the nanointerfaces This is in contrast with flat surfaces, where monomers and helical folds dominate based on reflection SFG experiments.<sup>2</sup> We believe, aS binding to the nanoparticles leads to close packing of aS monomers, which leads to the formation of beta sheet and fibrillar type structures.

Fig 1. Schematic of the SFS experiments to follow the binding of aS to polymer nanoparticles particles and the corresponding SFS spectrum

References:

1.) Thaddeus W. Golbeck, Kris Strunge, Adam S. Chatterly, and Tobias Weidner\* *J. Phys. Chem. Lett.* **2022**, *13*, 10858-62.

2.) Kris Strunge, Tucker Burgin, Thaddeus W. Golbek, Steven J. Roeters, Jim Pfaendtner and Tobias Weidner\* Umbrella-like helical structure of alpha-synuclein at the air-water interface observed with experimental and theoretical sum frequency generation spectroscopy, in preprint.

**8:20am BI+AS+PS-TuM-2 The Structure of Alpha-Synuclein at Lipid Interfaces Determined by Experimental and Theoretical Sum Frequency Generation Spectroscopy, K. Strunge, K. Pedersen, T. Golbek, M. Brngenhøj, D. Otzen, B. Schiøtt, Tobias Weidner, Aarhus University, Denmark**

The aberrant folding of  $\alpha$ -synuclein ( $\alpha$ S) into amyloid aggregates is associated with Parkinson’s disease. It has been shown that the refolding into oligomers and harmful fibrils can be catalyzed by lipid-membrane surfaces. Despite the importance of lipid interactions, the 3D-structure of lipid-membrane bound  $\alpha$ S, and thereby, the mechanism of the catalysis process, is still not known at the molecular level. Here, we report interface-specific sum-frequency generation (SFG) experiments revealing how monomeric  $\alpha$ S binds, folds and orients at anionic lipid membranes. Since SFG is inherently surface specific and unbound proteins are not detected, the experiments can be performed at high  $\alpha$ S concentrations, far beyond previous structural studies. To interpret the experimental SFG data and develop a high fidelity structural model of the aS binding motif, we developed an analysis method in which out-of-equilibrium molecular-dynamics (MD) simulations are linked to excitonic amide-I SFG spectra calculations. 10s of thousands of theoretical spectra calculated for frames of extensive MD simulations are evaluated pooled for their experimental fitness to determine the structure of aS binding at low, physiological and pathological aS concentrations. We find that at low and physiological aS concentrations, the protein binds in a flat geometry, while at elevated, pathological concentrations, a transition to an upright aS binding pose occurs. This upright conformation promotes lateral interactions and likely explains how protein concentrations can catalyze the formation of aS amyloids.

**8:40am BI+AS+PS-TuM-3 Lubricant Viscosity Affects the Antifouling Activity of PFPE Based SLIPS Coatings, Onur Özcan, J. Karthäuser, R. Kopeck, A. Gelhar, A. Rosenhahn, Ruhr-Universität Bochum, Germany**

Settlement of organisms on submerged surfaces can enhance the spread of life-threatening infections.[1] Therefore it is desired to identify methods for the prevention of biofilm formation. The omniphobic properties of slippery liquid infused porous surfaces (SLIPS) have been shown to provide outstanding protection against biofouling, icing, corrosion and to be repellent against complex liquids like blood.[2] In this study, we examine the fouling behavior of *E. coli*, *P. fluorescens*, and *B. subtilis* on seven different superhydrophobic perfluoropolyether (PFPE) urethane methacrylate-based SLIPS with varying lubricant viscosities. The polymers were fabricated following our previously published grafting-through protocol by which superhydrophobic micro-structured porous PFPE matrices could be obtained by adding cyclohexanol as pore forming agent to the

# Tuesday Morning, November 7, 2023

monomer mixture.[3,4] The coatings were incubated in an excess of seven different lubricants of varying viscosities to obtain SLIPS. In dynamic attachment assays we were able to show the antifouling capabilities of these SLIPS with organism reductions of up to 90% compared to the dry, smooth, and hydrophobic butyl methacrylate references. Our results further revealed critical species-specific settlement on the coatings that depended on the viscosity of the incorporated liquid, highlighting the relevance of the choice of the lubricant in the design of low-fouling SLIPS.

[1] M.V. Horton, J. E. Nett, *Curr. Clin. Microbiol. Rep.* 2020, 7, 51-56. [2] T.-S. Wong, S. H. Kang, S. K. Y. Tang, E. J. Smythe, B. D. Hatton, A. Grinthal, J. Aizenberg, *Nature* 2011, 477, 443-447. [3] F. Koschitzki, R. Wanka, L. Sobota, J. Koc, H. Gardner, K. Z. Hunsucker, G. W. Swain, A. Rosenhahn, *ACS Appl. Mater. Interfaces.* 2020, 12, 34148-34160. [4] N. Keller, J. Bruchmann, T. Sollich, C. Richter, R. Thelen, F. Kotz, T. Schwartz, D. Helmer, B. E. Rapp, *ACS Appl. Mater. Interfaces,* 2019, 11, 4480-4487.

9:00am **BI+AS+PS-TuM-4 Orientation of the Dysferlin C2A Domain is Responsive to the Composition of Lipid Membranes**, *A. Carpenter*, Oregon State University; *S. Roeters*, *T. Weidner*, Aarhus University, Denmark; *Joe Baio*, Oregon State University

Dysferlin is a 230 kD protein that plays a critical function in the active resealing of micron-sized injuries to the muscle sarcolemma by recruiting vesicles to patch the injured site via vesicle fusion. Muscular dystrophy is observed in humans when mutations disrupt this repair process or dysferlin is absent. While lipid binding by dysferlin's C2A domain (dysC2A) is considered fundamental to the membrane resealing process, the molecular mechanism of this interaction is not fully understood. By applying nonlinear surface-specific vibrational spectroscopy, we have successfully demonstrated that dysferlin's N-terminal C2A domain (dysC2A) alters its binding orientation in response to a membrane's lipid composition. These experiments reveal that dysC2A utilizes a generic electrostatic binding interaction to bind to most anionic lipid surfaces, inserting its calcium binding loops into the lipid surface while orienting its  $\beta$ -sheets 30–40° from surface normal. However, at lipid surfaces, where PI(4,5)P2 is present, dysC2A tilts its  $\beta$ -sheets more than 60° from surface normal to expose a polybasic face, while it binds to the PI(4,5)P2 surface. Both lipid binding mechanisms are shown to occur alongside dysC2A-induced lipid clustering. These different binding mechanisms suggest that dysC2A could provide a molecular cue to the larger dysferlin protein as to signal whether it is bound to the sarcolemma or another lipid surface.

9:20am **BI+AS+PS-TuM-5 Probing the Interfacial Action of *Thermomyces lanuginosus* Lipase at Lipid Surfaces with Vibrational Sum Frequency Spectroscopy – from Monolayers to Emulsions**, *Khezlar Saeed*, *K. Strunge*, *T. Golbek*, *T. Weidner*, Aarhus University, Denmark

Lipases are a diverse class of biologically important enzymes with a key role in the digestion of dietary fats. The general ability to catalyse triacyl glyceride hydrolysis also enables their application to a wide variety of systems outside of the digestive tract, including transesterification, enantioselective synthesis and as an additive to laundry detergents. Key to their efficacy is the phenomenon of interfacial activation. For lipases this almost universally involves the “opening” of a lid domain upon interaction with a lipid surface, revealing a hydrophobic region containing the active site. The lipase derived from the *Thermomyces lanuginosus* fungus (TLL) is used extensively on an industrial scale as an additive to laundry detergents. As such significant effort has been expended to genetically engineer improvements to the lipase function, with particular attention paid to this lid region. Gaining a deeper understanding of the interfacial activation mechanisms of such lipases could inform the design of improved enzymes in the future.

The inherent surface sensitivity of vibrational sum frequency generation (VSFG) spectroscopy can provide the required molecular level information to further our understanding of the interfacial activation of TLL. VSFG spectroscopy relies on the selection rules associated with frequency mixing of high power visible and infrared laser beams, resulting in a vibrational spectrum of solely the interfacial region. Three key results are presented here:

(i)The TLL-catalysed reaction at the air/triglyceride/water interface can be monitored by reflection VSFG spectroscopy, showing loss of ester carbonyl modes and appearance of carboxylate stretching modes of the fatty acid products.

(ii)Comparison of experimental and predicted VSFG spectra of the amide I band are used to interpret structural changes in the lid domain of TLL upon interaction with a hydrophobic surface.

(iii)Specially formulated emulsions allow further analysis using our new angle-resolved sum frequency scattering spectrometer, showing the first example of reaction dynamics at a particle surface probed by vibrational sum frequency scattering spectroscopy.

This work highlights the utility of VSFG spectroscopy for studying interfacial reactions. Not only does it offer a label-free method of following surface reactions, but it also provides structural and orientational information on interfacial species when combined with appropriate simulations. Furthermore, the results from the sum frequency scattering spectrometer open the door to studying a whole new class of chemical systems at particle surfaces with as yet unseen levels of molecular detail for such systems.

11:00am **BI+AS+PS-TuM-10 An *in Situ* Look at Interfacial Controls on Nucleation, Self-Assembly, and Crystal Growth in Biomolecular and Biomimetic Systems**, *Jim De Yoreo*, Pacific Northwest National Laboratory

INVITED

From harvesting solar energy to capturing CO<sub>2</sub> to purifying water, living organisms have solved some of the most vexing challenges now faced by humanity. They have done so by creating a vast library of proteins and other macromolecules that can assemble into complex architectures and direct the mineralization of inorganic components to produce materials characterized by a hierarchy of structure. While the high information content contained within the intricate sequences of the proteins is crucial for accomplishing these tasks, self-assembly and mineralization are nonetheless constrained to proceed according to the physical laws that govern all such processes, even in synthetic systems. An understanding of the mechanisms by which biological systems successfully manipulate those laws to create hierarchical materials would usher in an era of materials design to address our most pressing technological challenges. In this talk, I will present the results of recent research using *in situ* atomic force microscopy and *in situ* transmission electron microscopy to directly observe interfacial structure, protein self-assembly, and nanocrystal formation in biomolecular and biomimetic systems, including protein-directed nucleation of calcium carbonate and calcium phosphate and mineral-directed nucleation of two-dimensional protein assemblies. The results elucidate the mechanisms by which the interface between biomolecules and materials directs nucleation, self-assembly and crystal growth, leading to unique materials and morphologies. The results reveal the importance of surface charge, facet-specific binding, solvent organization near interfaces, and, more generally, the balance of protein-substrate-solvent interactions in determining how ordered materials emerge in these systems.

11:40am **BI+AS+PS-TuM-12 the Surface Chemistry of Gecko Toe Pads**, *Mette Heidemann Rasmussen*, *K. Holler*, Department of Chemistry, Aarhus University, Denmark; *J. Baio*, School of Chemical, Biological and Environmental Engineering, Oregon State University; *C. Jaye*, *D. Fischer*, National Institute of Standards and Technology, Gaithersburg; *S. Garb*, Functional Morphology and Biomechanics, Zoological Institute, Kiel University, Germany; *T. Weidner*, Department of Chemistry, Aarhus University, Denmark

Geckos can climb nearly all surface and are able to cling to walls and ceilings using their toe pads. The gecko adhesion mechanism has been debated over the past years. Current models include van der Waals, hydrophobic and acid-base interactions. Even though the adhesion mechanism of the spatulas has been studied in detail, the surface chemistry involved in the gecko adhesion mechanism is unclear. What is the structure of the supporting proteins within the spatula at the very tips of the setae within the gecko toe pad? What is the role of lipids in the adhesion process? Understanding the surface chemistry of the adhesion of the gecko toe pads gives insight into this highly specialized biological interface, and give clues for materials scientists aiming at mimicking the gecko adhesion mechanisms. Using near edge X-ray absorption fine structure (NEXAFS) imaging and spectroscopy we have studied the structure and order of the molecules at the outermost surface layer of gecko toe pads. We show that the keratin molecules within the spatulas are highly organized and adopt a flat, strand-like geometry, which may support the stability and adaptability of gecko setae (1). We will also discuss evidence showing that a nanometer-thin ordered lipid layer is covering the beta proteins (2).

47. Structure of Keratins in Adhesive Gecko Setae Determined by Near-Edge X-ray Absorption Fine Structure Spectromicroscopy. *J Phys Chem Lett.* 2022 Mar 10;13(9):2193–6.

48. Evidence that gecko setae are coated with an ordered nanometre-thin lipid film. *Biology Letters.* 18(7):20220093.

12:00pm **BI+AS+PS-TuM-13 All-Atom Simulations of Peptide Aggregation: Understanding and Predicting Biopolymeric Morphologies**, *A. Kwansa, A. Cannon*, North Carolina State University; *Yaroslava Yingling*, 911 Partners Way, Engineering Building I, Campus Box 7907

The self-assembly and aggregation of partly or completely disordered peptides have emerged as crucial areas of research with broad implications in therapeutics, supramolecular assembly, and functional biomaterials. Understanding the intricate processes underlying the self-assembly and aggregation of these proteins is essential for harnessing their functional properties and expanding their applications. Simulations can be used to isolate the importance of the interplay between aggregate morphology and secondary structure formation. However, most of the simulation's studies investigate either single peptide in solution or several short peptide analogues. We used large-scale all-atom MD simulations to investigate the structure of hydrated peptide aggregates in detail. Two example systems were investigated, reflectin and elastin-like peptides (ELP). Reflectin proteins, found in cephalopods, play a pivotal role in dynamic coloration for camouflage and communication. On the other hand, ELP proteins possess unique thermoresponsive properties, making them attractive for drug delivery systems, tissue engineering, and biomaterial design. We found significant differences between the structure of a single polypeptide in water and the structure of peptide within the aggregate. Overall, the aggregation process is driven by the formation of peptide-peptide interactions whereas the average hydration of peptides remains almost the same between dissolved and aggregated states. Even though the aggregation is driven by hydrophobic interactions, aggregate has no hydrophobic core and contains many water molecules. Overall, our findings provide an insight into the sequence-dependent structure of aggregates and molecular behavior of individual peptides during aggregation.

## Chemical Analysis and Imaging of Interfaces Focus Topic Room A105 - Session CA+AS+LS+LX+MN+SE+SS-TuM

### Novel Developments and Applications of Interfacial Analysis

**Moderators:** *Andrei Kolmakov*, National Institute of Standards and Technology (NIST); *Slavomir Nemsak*, Advanced Light Source, Lawrence Berkeley National Laboratory

8:00am **CA+AS+LS+LX+MN+SE+SS-TuM-1 Hypervelocity Nanoprojectile Impacts on Graphene, Graphene-Solid/Liquid Interphases: From Mechanisms of Interaction/Ejection to Practical Applications**, *Dmitriy Verkhoturov*, Texas A&M University; *S. Lee*, Mayo Clinic; *M. Eller*, California State University Northridge; *M. Goluński, S. Hrabar*, Jagiellonian University, Poland; *S. Verkhoturov*, Texas A&M University; *Z. Postawa*, Jagiellonian University, Poland; *A. Kolmakov*, National Institute for Science and Technology (NIST); *A. Revzin*, Mayo Clinic; *E. Schweikert*, Texas A&M University

#### INVITED

Presented here are the experiment and theory on processes accompanying the impacts of  $C_{60}$  and  $Au_{400}$  projectiles ( $\sim 1$  keV/atom) on graphene/matter interphases. A variety of targets were used: a) free standing graphene, b) molecules and extracellular vesicles (EVs) deposited on free standing graphene, c) interphases graphene-solids/liquids, d) EVs deposited on functionalized monocrystals.

Two custom-built Cluster ToF secondary ion mass spectrometry (SIMS) devices with similar parameters were used. The experiments were run in the event-by-event bombardment/detection mode where the regime of bombardment is super-static<sup>1</sup>. The analyzed surfaces were bombarded at the rate of  $\sim 1000$  impacts/sec with  $1-6 \times 10^5$  impacts collected on a surface area of 50-500  $\mu m$  in diameter. This regime allows acquisition of individual mass spectra for each impact, thus allowing the comparison of experimental data with MD simulations at the level of single projectile impacts. The method allows detection of ejecta in reflection (3D case) and transmission (2D case) directions.

The mechanisms of ejection from 2D and 3D materials (including graphene-solid/liquid interphase) are different. For example, in the case of  $C_{60}$  impacts on a molecular layer deposited on graphene (2D case) the mechanism of ejection is described with the "trampoline" model<sup>2</sup>. For the 3D case of graphene-solid/liquid interphase, graphene suppresses the ejection of molecules. The compression of matter in the excitation volume around the impact is not sufficient to destroy the graphene<sup>3</sup>.

Our method allows to test individual nano-objects. A biological example is EVs. There were anchored on functionalized Si and graphene substrates, with the EVs labeled with antibodies carrying lanthanide tags (Ab@Ln) for normal hepatic and liver cancer markers. Up to four Ab@Ln tags could be detected simultaneously, enabling analysis of population heterogeneity with single EV resolution and to distinguish between normal and cancer EVs based on surface marker expression. Using co-localization of cancer biomarkers, it is possible to find small subpopulation of EVs originating from cancerous cells potentially allowing for early cancer detection. The sensitivity of the method can be increased several folds via transmission configuration where ejecta are emitted and detected in the forward direction. In this case nano-objects, such as EVs, are anchored on graphene oxide, a 2D material.

<sup>1</sup>S.V. Verkhoturov et al. J. Chem. Phys. 150 (2019)

<sup>2</sup>R.D. Rickman et al. Phys. Rev. Lett. 92, 047601 (2004)

<sup>3</sup>D.S. Verkhoturov et al. Biointerphases 11, 02A324 (2016)

Acknowledgements: NSF Grant CHE-1308312, NIH Grant R01 GM123757-01,

Polish National Science Center 2019/33/B/ST4/01778, PLGrid Infrastructure Grant

8:40am **CA+AS+LS+LX+MN+SE+SS-TuM-3 Applying *in Situ* Bias During TOF-SIMS Analysis to Investigate Ion Migration in Perovskite Devices**, *Steven Harvey*, National Renewable Energy Laboratory; *I. Gould*, University of Colorado, Boulder; *D. Morales, M. McGehee*, University of Colorado Boulder; *A. Palmstrom*, National Renewable Energy Laboratory

Metal Halide Perovskite Photovoltaics have the potential to be a game-changing technology in photovoltaics, with low cost solution processing inherent to the technology and a rapid progress in device efficiency and stability. Understanding ion migration in these materials has led to improvements in both efficiency and reliability, and further understanding of these phenomena is of great importance.

Time of flight secondary ion mass spectrometry is well suited to provide unique insight for this class of materials, as it can reveal the distribution of both the organic and inorganic components of a device stack (both through the depth as well as laterally with 2-D and 3-D imaging). We will briefly cover our past work on technique development for this class of materials, before presenting new work where an *in situ* electrical bias was placed on a perovskite device while under investigation with TOF-SIMS. This was completed with simple commercial off the shelf components in an ION-TOF TOF-SIMS V instrument and could be easily implemented on other instruments. A device stack of glass / ITO / Me-4PACz / DMA0.1FA0.6Cs0.3Pb(I0.8Br0.2)3 / LiF (1 nm) / C60 (30 nm) / SnOx (15 nm)/Au (20 nm) was used for this study. An electrical bias was applied between the top gold contact and the bottom ITO contact during TOF-SIMS measurements. By applying a +0.75V and -0.75V forward and reverse bias to the device, a driving force for negatively charged halide ions is created to migrate towards the back or front of the device, respectively. The *in-situ* data shows the halide ion migration towards the back ITO contact after the forward bias is applied. The negative bias was then applied and the halide ions migrate back towards the front of the device and return to the original unbiased state. In both cases the formamidineum and lead traces do not show similar migration, showing only the charged species in the device are affected by the bias. The results show a framework that can be used for further study. Potential complications with the analysis of this type of data will be discussed.

9:00am **CA+AS+LS+LX+MN+SE+SS-TuM-4 Oxidation of a Single Fe Nanoparticle at the Nanoscale and Real-Time by Operando Atom Probe**, *Sten V. Lambeets*, Pacific Northwest National Laboratory; *N. Cardwell, I. Onyango*, Washington State University; *T. Visart de Bocarmé*, Université libre de Bruxelles, Belgium; *J. McEwen*, Washington State University; *D. Perea*, Pacific Northwest National Laboratory

Physics governing surface chemical reactions and interfaces involved in heterogeneous catalysts fundamentally depends on the synergistic interactions between reactive gases and specific surface structures. Surface science techniques are continuously evolving to help bridge knowledge gaps between fundamental research and real-world applications. In the past decade, an increasing number of analytical techniques successfully achieved their evolution towards an *in situ* and operando version of themselves, and recently such approaches are being developed for atom probe microscopy (APM) techniques. In this work, we will present the recent advances in the conversion of Atom Probe Tomography (APT) to study surface dynamics of  $O_2/Fe$  using two different APM techniques and

# Tuesday Morning, November 7, 2023

modifications: Field Ion Microscopy (FIM), and Operando Atom Probe (OAP).

APM techniques are capable of imaging the apex of sharp needles with nanometric lateral resolution, which can be seen as model nanoparticles. FIM is used to image such needles with atomic resolution and to identify the crystal orientation along with the local surface reaction dynamics during oxygen interaction with Fe. The resulting FIM image corresponds to a stereographical projection of the apex and allows the identification of the crystal orientations with atomic resolution. Regular APT, from which the OAP derives, relies on the thermally assisted field evaporation of positively charged ions from a needle shaped specimen. In regular use, the APT is performed in an Ultra High Vacuum ( $<10^{-11}$  mbar) while the sample is cooled at 50K. The OAP modification consists of performing the atom probe analysis in the presence of reactive gas at 300 K.

Once the FIM characterization is complete the sample is maintained at 300K before starting APT analysis and introducing  $1.1 \times 10^{-7}$  mbar of pure  $O_2$ . As soon as the  $O_2$  is introduced, we can measure the surface formation of Fe oxides by monitoring the local concentration of  $Fe_2O^{n+}$  ion species extracted from the surface over time. We can track the local concentration over the different surface regions in real time. We observe the progressive surface oxidation starting from open facets structures, such as Fe{222} and Fe{112}, towards the central Fe{011} and the Fe{024} which show significantly higher resistance toward oxidation. The combination of the different concentrations allows us to reconstruct the full movie of the surface oxidation in real-time. However, since the measurements are performed in the presence of very strong electric fields ( $>10$  V/nm), it is necessary to discuss the potential influences of it on the system as well.

9:20am **CA+AS+LS+LX+MN+SE+SS-TuM-5 Reporting Interfaces: Unconventional Excitation of Interfaces Enables Exquisite Gas Sensing Toward Our Sustainable Future, Radislav Potyrailo, GE Research INVITED**

As our society is developing solutions for more sustainable types of energy, the need for reliable, yet affordable tools for monitoring of emissions of greenhouse and other gases in urban and industrial environments is a substantial undertaking for two main reasons. First, to achieve a desired accuracy, existing gas monitoring solutions in complex backgrounds utilize traditional analytical instruments. While their mathematical design principles provide needed independent response outputs, their hardware design principles do not allow cost-effective ubiquitous implementations. Second, all gas sensors based on interface-driven interactions between gases of interest and sensing materials are single-output devices. By their original design principles from early last century, these sensors operate well only when levels of interfering gases are low. Once levels of interfering gases increase, existing sensors lose their accuracy because of competing interactions between the sensor interface and numerous interfering gases versus a gas of interest.

In this talk, we will present gas sensors that we built following mathematics of traditional analytical instruments but with our own different types of independent variables for detection of multiple gases with enhanced accuracy and stability. These sensors are multivariable gas sensors where independent response outputs are provided by our unconventional methodologies of excitation of interfaces between a sensing material and different ambient gases. We will show that our approach results in a reliable differentiation of one or more analyte gases in complex backgrounds of interfering gases with an individual multivariable gas sensor. This exquisite (i.e., accurate and reliable) gas sensing provides an affordable technical solution for monitoring of emissions of greenhouse and other gases in urban and industrial environments. Such technical solution is mathematically not feasible using conventional single-output sensor designs. We will also show that such multivariable gas sensors have the ability for self-correction for sensor drift. Our approach for the multi-gas detection and drift self-correction should allow implementations of gas sensors in diverse applications that cannot afford weekly, monthly, or quarterly periodic maintenance, typical of traditional analytical instruments.

11:00am **CA+AS+LS+LX+MN+SE+SS-TuM-10 A "Simple" Approach to Combine Electrochemistry and Operando Near Ambient Pressure XPS Studies, F. Mirabella, Paul Dietrich, A. Thissen, SPECS Surface Nano Analysis GmbH, Germany INVITED**

Electrochemical water splitting is an environmentally friendly technology to store renewable energy in the form of chemical fuels. Among the Earth-abundant, first-row transition metal-based catalysts, Ni and Fe oxides have shown promising performances as effective and low-cost catalysts of the oxygen evolution reaction (OER) in alkaline media. Notably, their structure evolves under oxygen evolution operating conditions with respect to the as-prepared catalysts but these changes and consequently the active sites have not been identified yet due to the difficulties associated with surface analysis measurement under working conditions (*operando*).

In this presentation, we will demonstrate the enormous potential of laboratory NAP-XPS for investigations of solid-liquid interfaces in electrochemical systems at elevated pressures ( $\leq 25$  mbar), also illustrating the ease of use of this specific setup. We will show a versatile three-electrodes electrochemical setup that allows for operando studies of solid-electrolyte interfaces, i.e., of nickel oxide foils as cathode for OER in alkaline environment as a simple laboratory NAP XPS experiment.

11:40am **CA+AS+LS+LX+MN+SE+SS-TuM-12 Recent Developments in Probing Buried Interfaces Using Standing-Wave Photoelectron Spectroscopy, Slavomir Nemsak, Lawrence Berkeley Lab**

Standing-wave photoelectron spectroscopy of multi-layer structures proved to be a very powerful technique for probing solid/solid, but also solid/liquid and solid/gas interfaces. Its superior depth selectivity and non-destructive nature were crucial to answer key questions in problems spread over several scientific fields, such as emergent phenomena at complex oxide interfaces [1], artificial multiferroics [2], adsorption mechanisms in liquids [3], corrosion [4], and electrocatalysis [5]. These achievements were only possible thanks to innovative approaches both in experiments and analyses, including development of X-ray optical simulations package [6] and its coupling with the black-box optimizer [7]. In this talk I will introduce novel tools and approaches for standing-wave experiments and I will highlight some of the recent applications [8,9,10].

[1] S. Nemsak et al., *Physical Review B* **93** (24), 245103 (2016).

[2] H. P. Martins et al., *arXiv preprint arXiv:2012.07993*.

[3] S. Nemsak et al., *Nature Communications* **5**, 5441 (2014).

[4] O. Karslioglu et al., *Faraday Discussions* **180**, 35 (2015).

[5] C. Baeumer et al., *Nature Materials* **20**, 674 (2021).

[6] S.-H. Yang et al., *Journal of Applied Physics* **113**, 073513 (2013).

[7] O. Karslioglu et al., *Journal of Electron Spectroscopy and Related Phenomena* **230**, 10 (2019).

[8] M. Scardamaglia, et al., *Journal of Electron Spectroscopy and Related Phenomena* **262**, 147281 (2023).

[9] G. Conti et al., *Journal of Micro/Nanopatterning, Materials, and Metrology* **20**, 034603 (2021).

[10] H.P. Martins et al., *Journal of Physics D: Applied Physics* **56**, 464002 (2021).

12:00pm **CA+AS+LS+LX+MN+SE+SS-TuM-13 The Influence of Surface Structure and Electrostatics on Measuring Unoccupied Electronic States via Low Energy Inverse Photoemission Spectroscopy (LEIPS), James Johns, Physical Electronics USA**

A material's energetic distribution of electronic states near the Fermi level is a key physical property for determining how it behaves in electronic, chemical, and optical applications. Photoemission has long been the gold standard for measuring the occupied electronic states below the Fermi level and is one of the most common surface science techniques worldwide. Inverse photoemission (IPES), the related process whereby an electron is absorbed at the surface and a photon is emitted, is similarly a very powerful tool for measuring the unoccupied electronic states. Unfortunately, the intrinsically lower rate for IPES and technical hurdles related to relevant photodetectors has historically necessitated the use of electron sources with sufficient energy to damage all but the most chemically robust surfaces.

The availability of narrow bandpass optical filters at UV photon energies between 3.5 and 6 eV over the past decade have enabled the development

and commercialization of Low Energy Inverse Photoemission Spectroscopy (LEIPS)<sup>1,2</sup>. Efficient detection of low energy UV photons (lower than traditional IPES at 9-10 eV) enables the use of low energy electrons (below 5 eV) which avoid damaging sensitive materials including organics. This key innovation has revitalized interest in IPES because the technique can now be applied to molecular materials and interfaces relevant to wide range of applications e.g. batteries, photovoltaics, organic semiconductors and OLEDs, chemical sensors. Furthermore, optical UV filters also improve the energy resolution, further enhancing the appeal of LEIPS over traditional IPES.

Like any surface science technique, the quality of LEIPS data depends on both the instrumentation and sample preparation. Here, I will discuss the material requirements and limitations for successful LEIPS measurements, several of which differ from more common techniques such as XPS, SPM, or electron microscopy. I will also present LEIPS data from taken at the interface between two metals and explain those results using calculated trajectories of the electron beam. Finally, I will illustrate a key difference between LEIPS, which probes the true unoccupied electronic density of states, and optical methods, such as optical spectroscopy or EELS which measure the joint density of states, by presenting LEIPS spectra of an excitonic 2D material.

<sup>1</sup> Yoshida, H; "Near-ultraviolet inverse photoemission spectroscopy using ultra-low energy electrons" *Chem. Phys. Lett.* **539-540**, 180-185, (2012)

<sup>2</sup> Lida, S.; Terashima, M; Mamiya, K; Chang, H. Y.; Sasaki, S; Ono, A; Kimoto, T; Miyayama, T; "Characterization of cathode-electrolyte interface in all-solid-state batteries using TOF-SIMS, XPS, and UPS/LEIPS" *J. Vac. Sci. & Tech. B*, **39**, 044001, (2021)

## Nanoscale Science and Technology Division Room B113 - Session NS+2D+EM+MN+SS-TuM

### Scanning Probe Microscopy

**Moderators:** **Aubrey Hanbicki**, Laboratory for Physical Sciences, **Fernando Castro**, National Physical Laboratory, U.K.

8:00am **NS+2D+EM+MN+SS-TuM-1 AVS Medard W. Welch Award Talk: Microscopy is All You Need: The Rise of Autonomous Science**, **Sergei Kalinin**<sup>1</sup>, University of Tennessee Knoxville **INVITED**

Making microscopes automated and autonomous is a North Star goal for areas ranging from physics and chemistry to biology and materials science – with the dream applications of discovering structure-property relationships, exploring physics of nanoscale systems, and building matter on nanometer and atomic scales. Over the last several years, increasing attention has been attracted to the use of AI interacting with physical system as a part of active learning – including materials discovery and optimization, chemical synthesis, and physical measurements. For these active learning problems, microscopy arguably represents an ideal model application combining aspects of materials discovery via observation and spectroscopy, physical learning with relatively shallow priors and small number of exogenous variables, and synthesis via controlled interventions. I introduce the concept of the reward-driven experimental workflow planning and discuss how these workflows can be implemented via domain-specific hyper languages. The applications of classical deep learning methods in streaming image analysis are strongly affected by the out of distribution drift effects, and the approaches to minimize though are discussed. The real-time image analysis allows spectroscopic experiments at the predefined features of interest and atomic manipulation and modification with preset policies. I further illustrate ML methods for autonomous discovery, where the microstructural elements maximizing physical response of interest are discovered. Complementarily, I illustrate the development of the autonomous physical discovery in microscopy via the combination of the structured Gaussian process and reinforcement learning, the approach we refer to as hypothesis learning. Here, this approach is used to learn the domain growth laws on a fully autonomous microscope. The future potential of Bayesian active learning for autonomous microscopes is discussed. These concepts and methods can be extended from microscopy to other areas of automated experiment.

<sup>1</sup> Medard W. Welch Award Winner  
Tuesday Morning, November 7, 2023

8:40am **NS+2D+EM+MN+SS-TuM-3 Dielectric Constant Measurement Sensitivity in Electrostatic Force and Force Gradient Microscopy-Based Modes**, **Gheorghe Stan**, National Institute of Standards and Technology (NIST); **C. Ciobanu**, Colorado School of Mines

Understanding of the nanoscale electrostatic interaction between a conductive atomic force microscopy (AFM) probe and a dielectric film is central to the operation of various nanoscale dielectric microscopies and determination of dielectric properties of the film. There is no simple analytical description of the electrostatic interaction generated in the confined probe-sample geometry of neither the static nor dynamic AFM modes used for dielectric measurements. An accurate description of the involved physics is obtained only by means of a finite element analysis modeling of the system. However, the alternative of using numerical analysis is not very popular being slower and requiring relatively high computation resources. In this work we revised the contributions from different parts of the AFM probe to the probe-sample capacitance by both analytical and numerical methods. We tried to reconcile the two approaches and observed the differences as a function of geometry and material parameters. Under various noise levels, the efficiency of an analytical model was tested against finite element analysis that captures in detail the electrostatic interaction in AFM-based dielectric measurements. The investigation was performed in both spectroscopic force-distance curves and constant height scans with measurements for the deflection and frequency of the AFM probe. The obtained measurement sensitivities are relevant in selecting the optimal scanning mode and its operational parameters for given film thicknesses and dielectric constants but are also showing the critical role of the numerical analysis to the correct interpretation of the measurements.

9:00am **NS+2D+EM+MN+SS-TuM-4 Measuring and Understanding the Nanomechanical Properties of Halide Perovskites and Their Correlation to Structure**, **I. Rosenhek-Goldian**, Dept. of Chemical Research Support, Weizmann Inst. of Science, Israel; **I. Buchine**, **N. Prathibha Jasti**, Bar-Ilan Inst. for Adv. Mater. and Nanotechnol & Dept. of Chem. Bar-Ilan Univ., Israel; **D. Ceratti**, Dept. of Mol. Chem. & Materials Science, Weizmann Inst. of Science, Israel & CNRS, UMR 9006, IPVF, Institut Photovoltaïque d'Ile-de-France; **S. Kumar**, Bar-Ilan Inst. for Adv. Mater. and Nanotechnol & Dept. of Chem. Bar-Ilan Univ. Ramat Gan Israel. & Dept. of Mol. Chem. & Materials Science, Weizmann Inst. of Science, Israel; **D. Cahen**, Bar-Ilan Inst. for Adv. Mater. and Nanotechnol & Dept. of Chem. Bar-Ilan Univ. & Dept. of Mol. Chem. & Materials Science, Weizmann Inst. of Science, Israel; **Sidney R. Cohen**, Dept. of Chemical Research Support, Weizmann Inst. of Science., Israel

Halide perovskites, HaP, and especially Pb-based ones exhibit a plethora of remarkable properties. Of these, their photovoltaic properties are the most widely studied due to the proven potential these materials hold for significant technological impact. In addition to photoresponse, this material class is characterized by interesting physical properties, of which mechanical properties enjoy special attention, not only because of potential use in flexible devices, but also from a fundamental science point of view. The mechanical response can shed light on the materials' behavior including dynamic processes and strain-related effects on optoelectronic behavior.

In the context of these studies, particular emphasis has been placed on environmental factors which can alter, especially degrade, material functionality and device performance. Exposure to humidity, light, and oxygen rank prominently amongst these factors.

In this study we measure the humidity influence on the mechanical properties, i.e., elastic modulus (E) and hardness (H), for two series of lead halide perovskite single crystals, varying either by cation or by anion type. Our conclusions are based on comparing results obtained from several different nano-indentation techniques, which separate surface modulus from that of the bulk, and probe different manifestations of the hardness. These studies reveal the different crystalline parameters governing influence of humidity on the mechanics at the surface and in the bulk.

An atypical inverse correlation between E and H was measured (as seen in the supplementary figure a). Furthermore, humidity influenced these two properties in opposite fashion – humidity exposure led to lower H, but to higher E (supplementary figure b). This trend is opposite to that found in most materials where hydration lowers both E and H. We suggest a link between dynamic disorder, self-healing, and the intriguing relation between E and H.

# Tuesday Morning, November 7, 2023

9:20am **NS+2D+EM+MN+SS-TuM-5 3D Nanoprinting of Advanced AFM Nano-Probes**, *Herald Plank, M. Brugger-Hatzl, R. Winkler, L. Seewald*, Graz University of Technology, Austria

The demand for correlative microscopy is still increasing, as it enables a superior ensemble of information by using various methods to combine individual strengths. The highest level of that approach are hybrid microscopes, which enable individual characterization at the very same spot in a consecutive or even parallel way. With that, however, comes the demand of a conflict-free integration of different microscopes, which require a radical redesign of the instrumentation. A major step in that direction is a recently introduced dual system called FUSIONScope, which is a deeply integrated scanning electron microscopy (SEM) and atomic force microscopy (AFM) solution. While the former enables high-resolution guidance towards the region of interest, the latter complements SEM capabilities by true quantitative 3D surface information, which together exploit their full potential by the possibility to precisely land the AFM tip on highly exposed regions. Even more importantly, advanced AFM modes such as conductive AFM (CAFM), magnetic force microscopy (MFM), electrostatic / Kelvin force microscopy (EFM/KFM), scanning thermal microscopy (SthM) or mechanical mapping, provide functional information beyond SEM capabilities. For that, special nano-probes are required, which typically achieve their intended functionality by additional thin film coatings, which contains two main disadvantages. First, they increase the apex radii and limit the lateral resolution, which is in conflict with the still decreasing feature sizes. Secondly, coatings are prone to delamination during operation, which affects resolution, lateral correlation and reliability. Therefore, to exploit the full potential of advanced AFM modes, it is of great interest to develop new approaches for the fabrication of functional nano-probes. Following that motivation, we joined forces with industry and apply the additive direct-write technology focused electron beam induced deposition (FEBID) for the development of novel 3D nano-probe concepts with industrial relevance. In this contribution, we briefly discuss the 3D nano-printing process and then go through a variety of advanced, FEBID-based tip concepts for CAFM, EFM, MFM and SthM. The joint element for all probes is the coating-free character, which eliminates the aforementioned risks during operation. Additionally, the apex regions are routinely in the sub-10 nm regime, which allows for high-resolution imaging. Aside of comparisons to traditionally used nano-probes, which reveal the superior performance of FEBID-based nano-tips, we discuss on currently ongoing research towards multi-functional AFM tips, based on FEBIDs flexibility.

11:00am **NS+2D+EM+MN+SS-TuM-10 Chemical, Mechanical, and Morphological Evolution of Nanostructures on the Surfaces of Asphalt Binders**, *L. Lyu, J. Pei*, Chang'an University, China; *E. Fini*, Arizona State University; *L. Poulikakos*, EMPA (Swiss Federal Laboratories for Materials Science and Technology), Switzerland; *Nancy Burnham*, Worcester Polytechnic Institute

Bitumen (asphalt binder) holds roads together. It is a complex, dynamic, nanostructured material that comes from the bottom of an oil refinery stack—a non-renewable resource. It ages, and it ages more quickly under the influence of heat and light. Can additives made from waste materials increase the longevity of bitumen, and thus roads?

In this study, atomic force microscopy (topography, phase imaging, PF-QNM) and its combination with infrared spectroscopy (AFM-IR) were used to explore the chemical, mechanical, and morphological evolution of the surface of bitumen without and with additives. Aging is assumed to begin at the surface.

Samples of bitumen were made with and without introducing bio-modified rubber additives. Each sample was exposed to several thermal and UV aging protocols. Evolution of surface under aging was studied. Depending on the additive and type of aging (thermal, UV, or combined), the nanostructures changed their chemistry, mechanical properties, and size. Furthermore, the matrices and phases immediately surrounding the nanostructures evolved differently upon aging than the included nanodomains. In general, carbonyl and sulfoxide IR bands became more prevalent, the samples became stiffer and less adhesive, and the phase immediately surrounding the nanostructures became smaller. One additive made from two different waste materials was found to enhance the stability of the surfaces.

By understanding the evolution of asphalt binders and which additives promote their stability, longer lasting roads might be designed and built, thereby lowering the need for a non-renewable resource.

11:20am **NS+2D+EM+MN+SS-TuM-11 Identifying Potential Carbon Sources for Direct Carbon Material Production by AI Assisted HR-AFM**, *Percy Zahl*, Brookhaven National Laboratory; *Y. Zhang*, ExxonMobil Technology and Engineering Company; *S. Arias*, Brookhaven National Laboratory

High-resolution Atomic Force Microscopy (HR-AFM) has proven to be a valuable and uniquely advantageous tool for studying complex mixtures such as petroleum, biofuels/chemicals, and environmental or extraterrestrial samples. However, the full potential of these challenging and time-consuming experiments has not yet been fully realized. To overcome these bottlenecks and enable further research into solutions for the energy transition and environmental sustainability, automated HR-AFM in conjunction with machine learning and artificial intelligence will be crucial [1].

In this study, we focus on identifying potential carbon sources suitable for more direct carbon material production by analyzing various pitch fractions based on their solubility in toluene. Specifically, we present the first comprehensive AI-assisted study of hydrocarbon fractions derived from petroleum and coal tar pitch, using and refining our previously introduced "Automated HR-AFM" tools. We explored four classes derived from Petroleum Pitch (PP) and Coal Pitch Tar (CPT), separated into toluene soluble (TS) and toluene insoluble (TI) fractions. Our analysis revealed differences in the structural characteristics of the molecules, which we binned based on the number of aromatic rings.

(Please see also the in our supplemental document included figures 1 and 2)

Overall, our results demonstrate the potential of automated HR-AFM and AI-assisted analysis for understanding complex mixtures and identifying potential carbon sources for direct carbon material production. This work represents an important step towards more sustainable and environmentally-friendly energy solutions.

Reference:

[1] Yunlong Zhang, *Energy & Fuels* 35(18), 14422 (2021)

11:40am **NS+2D+EM+MN+SS-TuM-12 Automated Microscopy for Physics Discovery: From High-Throughput to Hypothesis Learning-Driven Experimentation**, *Yongtao Liu, R. Vasudevan, M. Ziatdinov, S. Kalinin*, Oak Ridge National Laboratory

In this work, we explore the ferroelectric polarization switching in relation to the applied pulse bias including bias voltage and time in scanning probe microscopy (SPM). We perform two types of automated and autonomous experiments. First, we conduct automated high-throughput experimentation to gain a comprehensive understanding of the relationship between pulse biases and ferroelectric domain growth. Second, we employ an autonomous experimentation driven by machine learning (ML) algorithm to optimize experimental conditions based on real-time experiment results.

SPM has proven to be a powerful tool for manipulating and visualizing ferroelectric domains at the nanoscale. Investigations of ferroelectric domain size and stability can advance our knowledge of ferroelectrics application in memory devices, such as operating time, retention time, and bit size. However, conventional SPM measurements have been time-intensive and dependent on experienced researchers to perform repetitive tasks and make real-time decisions regarding measurement parameters. For example, researchers determine and manually tune the parameters for next iteration of experiment according to the previous results. Here, we perform automated and autonomous experiments in SPM to explore the mechanism of ferroelectric polarization. The first experiment is a high-throughput experiment of applying various bias pulse conditions to write ferroelectric domains followed by imaging domain structure using piezoresponse force microscopy. In this automated experiment, we systematically adapt the bias pulse parameters to gain a comprehensive understanding of their relationship with the resulting domain structures. We discovered different polarization states that show up upon different bias conditions. In the second experiment, we implement a hypothesis active learning (HypoAL) algorithm based on structured Gaussian process to control the SPM for ferroelectric domain writing. The HypoAL analyzes the relationship between the bias pulse conditions and the written domain size in real-time experiments, and determines the bias pulse parameters for the next iteration. The goal of HypoAL is to establish the best physical hypothesis for the material's behaviour within the smallest number of experiment step. The HypoAL identifies that the domain growth in a BaTiO<sub>3</sub> film is governed by kinetic control. The approaches developed here have the potential to be extended to other experiments beyond SPM in the future to

accelerate the discovery of new materials and advances in physics.

## Plasma Science and Technology Division Room A106 - Session PS-TuM

### Plasma Processing for Advanced Logic Device Fabrications

**Moderators:** John Arnold, IBM Research Division, Albany, NY, Tetsuya Tatsumi, Sony Semiconductor Solutions Corporation

8:00am **PS-TuM-1 Chemical Role of a Small Amount of Cl<sub>2</sub> in O<sub>2</sub>/Cl<sub>2</sub> Plasma for Ru Etching Reaction**, Masaya Imai, M. Matsui, R. Sugano, Hitachi, Ltd., Japan; T. Shiota, K. Takasaki, Hitachi High Technologies, Japan; Y. Ishii, Hitachi High Technologies America Inc.; M. Miura, K. Kuwahara, Hitachi High Technologies, Japan

Ruthenium (Ru) is an attractive candidate as an interconnect metal for future semiconductor devices which can replace conventional copper (Cu). This is because the Ru interconnect below 20-nm-pitch shows a lower resistivity and a higher electromigration reliability than Cu one. Especially, direct patterning of Ru is expected to maximize those advantages. In the patterning process of Ru, the dry etching with oxygen-based plasma is applied because Ru tetraoxides (RuO<sub>4</sub>) are volatile. Several reports using reactive ion etching (RIE) showed that the etch rate of Ru is the highest using a O<sub>2</sub>/Cl<sub>2</sub> plasma with a 10–20% amount of Cl<sub>2</sub>, while it is lower when using pure O<sub>2</sub>. The etch rate is also lower when Cl-rich plasma is applied due to the formation of non-volatile Ru chlorides. However, it has not been clarified why a small amount of Cl<sub>2</sub> in the plasma promotes the etching reaction and why the Ru is not etched by pure O<sub>2</sub> plasma.

In this work, the etching reaction mechanism on the Ru surface using a O<sub>2</sub>/Cl<sub>2</sub> plasma was investigated by experiments and simulations. Our electron cyclotron resonance (ECR) etcher is unique in that only radicals in the plasma reach the wafer by removing reactive ions using an ion shield plate. Applying this etching technique, we found that Ru can be etched by only radicals in O<sub>2</sub>/Cl<sub>2</sub> plasma and that the etch rate was the highest with a ~10% amount of Cl<sub>2</sub>. Therefore, a small amount of Cl-based radicals in the plasma explicitly contributes to the chemical reactions to form volatile Ru products, such as RuO<sub>4</sub> and RuCl<sub>x</sub>O<sub>y</sub>.

Using density functional theory (DFT) simulation, we modeled the atomic configuration on Ru surfaces where O and Cl radicals react. In our unit cell, there are nine chemisorption sites for O and Cl. We prepared three surface models where (1) all nine chemisorption sites were covered by O, (2) one chemisorption site was covered by Cl atom and the other eight were covered by O atoms, and (3) two adjacent chemisorption sites were covered by two Cl atoms and the other seven were covered by O atoms. Subsequently, we assumed that the volatile Ru products are formed by the oxidation reactions of the surface Ru atoms. Using nudged elastic band (NEB) method, we calculated the activation energies to desorb the volatile Ru products depending on the surface coverage of chemisorbed O and Cl. Comparing the activation energy among the three surface models, we revealed that it decreases as the number of chemisorbed Cl increases. We concluded that a small amount of Cl<sub>2</sub> in the O<sub>2</sub>/Cl<sub>2</sub> plasma contributes to decreasing the activation energy to form volatile Ru products on the surface, resulting in increasing the etching rate of Ru.

8:20am **PS-TuM-2 Coupling of Deposition and Etching to Achieve Selective Removal of TaN with Respect to Ultra Low-k Dielectric**, Ivo Otto IV, SUNY Polytechnic Institute; C. Vallée, SUNY Polytechnic Institute, France

The transition from silicon oxide and aluminum in the back-end-of-the-line (BEOL) to ultra low-k dielectric (ULK) and copper improved RC delay, but came with key challenges, one of which was copper diffusion into the ULK. Diffusion barriers are required in current integration schemes in order to mitigate copper diffusion, and TaN is a key diffusion barrier candidate because of strong dielectric adhesion and low in-plane resistivity properties at sub-5 nm thicknesses. Creation of the BEOL interconnect superstructure is completed in a cyclical fashion, requiring the repeated selective removal of not only copper, but the TaN diffusion barrier selective to the ULK. The TaN diffusion barrier directly contacts the ULK, making selectivity to the ULK of primary importance for this step. ULK films are susceptible to radical-dominated, fluorine-based etching because of the weak bond strength of methyl groups, high porosity allowing high accessibility, and high volatility of SiF<sub>2</sub>, SiF<sub>4</sub>, and CF<sub>x</sub> etch byproducts. The inherent fluorine-based etching pathways make selective fluorine etching of TaN with respect to ULK challenging but may be overcome by coupling of etching and deposition regimes. Plasma-assisted chemical vapor deposition of Si, SiO<sub>2</sub>,

and SiOF films have been previously explored with Si-containing precursors such as SiF<sub>4</sub> and SiCl<sub>4</sub>, with additives such as O<sub>2</sub> and H<sub>2</sub> used to manipulate deposited film stoichiometry and film properties. In this work, we explore the use of aforementioned Si-precursors and additives injected directly into an inductively-coupled discharge to perform a protective deposition on the ULK film, while etching the TaN film. The discharge is maintained without applied biasing and at a pressure to remove ion bombardment and allow deposition and etching mechanisms to be radical dominated and isotropic in nature. The focus is mainly the modulation of SiF<sub>4</sub> regimes by exploration of the addition of O<sub>2</sub> or H<sub>2</sub> with modulation of electrostatic chuck temperature, plasma discharge power, and injected species concentration. Ex-situ spectroscopic ellipsometry is utilized with support of scanning electron microscopic imaging to characterize film thickness changes. In-situ optical emission spectroscopy is utilized to better understand the plasma discharge species concentrations and the relevance to observed film thickness modulation. Ex-situ X-ray photoelectron spectroscopy is additionally used to probe the sample surface environment to characterize surface film properties. Through this investigation the possibility of selective deposition on ULK while simultaneously etching TaN is found to be possible by modulation of the aforementioned regimes.

8:40am **PS-TuM-3 Using Metal-Based Photoresists and Hard Masks for Patterning Process Window Expansion**, Joe Lee, Y. Mignot, S. Sieg, C. Penny, K. Motoyama, K. Petrillo, IBM Research Division, Albany, NY; E. Liu, S. Thibaut, C. Cole, Tokyo Electron Ltd.

Scaling of critical dimensions calls for greater control of processing conditions for smaller nodes. As such, materials with greater etch selectivity are required to successfully pattern with a healthy process window. Plasma etch tuning can only stretch so far as current schemes face an increasingly heavy burden of walking a tightrope to balance the conservation of photoresist or masking layers while ensuring good clearance of underlying materials. The introduction of metal-containing masking layers, including metalorgano resists (MOR) and metal hard masks, greatly alleviate the burden of traditional soft-mask layers that are more easily deformed during etching. We show schemes that implement its usage, yielding a vast array of benefits, such as reduction of defectivity and roughness in lines, increased flexibility of processing conditions, and a larger process window for structures with aggressive aspect ratios that would otherwise be extremely challenging to produce. Such metal-containing masking layers provide a great benefit to the integrity of multipatterned mandrel structures where pitch doubling is required. As dimensions grow more aggressive, any techniques to alleviate patterning challenges and reduce cycles of learning would be greatly welcome.

9:00am **PS-TuM-4 Understanding Etching of Nanoscale Structures Using Molecular Dynamics and Plasma Modeling**, Xingyi Shi, S. Rauf, J. Wang, J. Kenney, Applied Materials; J. Booth, LPP-CNRS, France; Y. Azamoum, Helmholtz Institute Jena, Germany; M. Foucher, LPP-CNRS, France

Pulsed plasmas are widely used in the semiconductor industry because of the flexibility they offer in controlling etch and deposition processes. Pulsed plasmas allow one to modulate the flux of energetic ions and neutral radicals to the substrate on a millisecond or faster timescale. As the semiconductor industry transitions to sub-5 nm technology nodes, pulsed plasma processes are becoming exceedingly complex due to the need to control surface processes with atomic precision. In this paper, we examine a pulsed chlorine plasma and its interaction with silicon substrates through a combination of fluid plasma simulations, molecular dynamics modeling, and feature scale flux calculations. First, we model the inductively coupled Cl<sub>2</sub> plasma for a range of pressures and powers. The plasma modeling results are compared to experimental measurements of electron density (by microwave hairpin resonator probe) and Cl density (by TALIF with absolute calibration [1]). The validated plasma model is also used to compute the ion angular and energy distribution with pulsed DC bias at low frequency.

From the plasma simulations, we obtain the fluxes and ion angular and energy distributions for the dominant etch species at different pulsing conditions. Cl radicals and Cl<sub>2</sub><sup>+</sup> ions are the primary species in inductive coupled Cl<sub>2</sub> plasma. We then compute the flux distributions for these species inside trench shaped features with aspect ratios ranging from 1 to 100. Due to the directionality of the charged ion species, the ion flux at the bottom of the feature is nearly the same as that at the top of the feature. In contrast, with increasing aspect ratio, fewer radicals can reach the bottom of the feature, resulting in a decrease in the radical to ion flux ratio.

The impact of the change in the flux ratio is examined through molecular dynamics simulations. Based on the flux ratios from the previous analysis,

# Tuesday Morning, November 7, 2023

different combinations of chlorine radicals and  $\text{Cl}_2^+$  ions at 100eV bombard a bare silicon surface. We observe that the silicon etch yield increases at low  $\text{Cl}/\text{Cl}_2^+$  flux ratio and plateaus at large flux ratios.

[1] Booth, J. P., Azamoum, Y., Sirse, N., & Chabert, P. (2012). Absolute atomic chlorine densities in a  $\text{Cl}_2$  inductively coupled plasma determined by two-photon laser-induced fluorescence with a new calibration method. *Journal of Physics D: Applied Physics*, 45(19), 195201.

9:20am **PS-TuM-5 Technology Options to Enable Logic Scaling in Advanced BEOL from Patterning to Metal Interconnect Formation**, *Eric Liu, A. Ko, N. Joy, S. Rogalskyj, S. Grzeskowiak, A. Krawicz, K. Kanzo, L. Huli, P. Biolsi*, TEL Technology Center, America, LLC

INVITED

The Back-End-Of-Line (BEOL) process is a crucial step in manufacturing advanced semiconductor logic devices. Recent advancements in EUV lithography, self-aligned multi-patterning, and ruthenium subtractive interconnect formation have led to the developing of more powerful and efficient devices.

EUV lithography employs shorter wavelengths of light to create finer and more complex circuit patterns, enabling the fabrication of smaller interconnects and vias with reduced edge-placement-error and line roughness. This technology has significantly contributed to extending the roadmap of device scaling and reducing the process/design complexity. Self-aligned multi-patterning is another key technique that uses several steps to create a single layer of patterned material with multiple, smaller patterns. This approach enables the self-alignment technique to fabricate more precise and complex circuits with manageable pattern placement and overlay accuracy. Finally, ruthenium subtractive interconnect formation is a novel process that has created interconnects with lower resistance, improved reliability, and overcome the fundamental challenge of RC delay from the conventional damascene approach with copper.

In this presentation, we examine several technology options and innovations to realize the formation of metal interconnects in a critical layer. These innovations include:

49. Advancements in EUV lithography and self-aligned multi-patterning.
50. Patterning consideration between CAR (chemically amplified resist) and MOR (metalorganic resist).
51. Plasma etch interaction to the interconnect material and pattern fidelity.

Meeting the physical and electrical requirements is essential to continuous scaling in advanced BEOL.

11:00am **PS-TuM-10 Direct Ru Etching Mechanism for Advanced Interconnect**, *Miyako Matsui*, Hitachi, Ltd., Japan; *Y. Ishii, L. Kovatch, K. Majer*, Hitachi High Tech America Inc.; *M. Miura, K. Kuwahara*, Hitachi High Tech, Japan

Logic devices are being continuously scaled by fabricating three-dimensional structures. The recent scaling has been achieved by both pitch scaling and various boosting technologies, such as design technology co-optimization. With the device scaling, alternative metal integrations are also required that enable shrinkage of metal pitch at the back end of the line. Ru is a candidate for interconnect material with metal pitches of 20 nm and beyond, because the Ru interconnect is expected to have lower effective resistance than the Cu interconnect at such small pitches. In addition, Ru is expected to be etched directly, which leads to new scaling boosters, such as semi-damascene patterning. To realize such patterning technology, Ru patterns need to be vertically etched with high selectivity for hard masks. In addition, roughness or other damage should be suppressed to reduce interconnect resistance. In this study, we investigated a Ru etching mechanism using a microwave-ECR etching system. The composition of the etched surface was analyzed by using X-ray photoelectron spectroscopy (XPS), and roughness was measured by using atomic force spectroscopy (AFM).

Ru was etched with high selectivity using  $\text{Cl}_2/\text{O}_2$  plasma in regard to various materials used for hard masks, which were TiN, Poly-Si,  $\text{SiO}_2$ , and  $\text{Si}_3\text{N}_4$ . The Ru etch rate was the highest when 20% of  $\text{Cl}_2$  gas was added to the  $\text{Cl}_2/\text{O}_2$  plasma. In that condition, Ru surface was etched by forming volatile  $\text{RuO}_4$  or  $\text{RuCl}_x\text{O}_y$ , and a smooth surface was obtained after etching. However, when using  $\text{O}_2$ -rich plasma, nonvolatile  $\text{RuO}_2$  was formed, which seems to cause the surface roughness. When using  $\text{Cl}_2$ -rich plasma, formation of

nonvolatile  $\text{RuCl}_x$  reduced the Ru etch rate and generated the surface roughness by forming micro masks.

We also evaluated a line-and-space Ru pattern with 32-nm-pitch using  $\text{Cl}_2/\text{O}_2$ -based plasma. Selectivity over the  $\text{Si}_3\text{N}_4$  mask and the Ru sidewall roughness were changed by ion flux, which was adjusted by the duty cycle of wafer bias power using  $\text{Cl}_2/\text{O}_2$  plasma. When the wafer bias was applied continuously, the  $\text{Si}_3\text{N}_4$  hard mask widened due to the Si containing by-product. When the ion flux was decreased by reducing a duty cycle of wafer bias, the Ru pattern was vertically etched, but larger sidewall roughness was formed. The roughness was thought to be formed because the sidewalls, on which non-volatile  $\text{RuO}_x$  and  $\text{RuCl}_y$  were formed, were etched by O and Cl radicals during the off period of the wafer bias power. We suggested adding a passivation gas to the  $\text{Cl}_2/\text{O}_2$  plasma to reduce sidewall roughness. Sidewall roughness was thought to be reduced because the sidewalls were uniformly protected from the etching.

11:20am **PS-TuM-11 Study and Characterization of Thick Beol Dual Damascene Self- Aligned via Indenting Etch for Bcd Smart Power Technology Node**, *Pietro Petruzza*, ST Microelectronics, Italy

Development and characterization of plasma etching processes of manufacturing dielectric self-aligned dual damascene etch for thick Cu BEOL metallization. DD process is carried out by a new reactive ion etching (RIE) employing with RF capacitive-coupled parallel plate plasma (CCP) for BCD smart power 110 nm technology node. The method is accomplished by providing a first inter-level dielectric, SiN via etch (indenting), depositing a second inter-level dielectric layer on the silicon nitride layer; finally selective patterning of line on second inter-level dielectric layer and vias on first inter-level dielectric. These applications require fine patterning of dielectric films by reactive ion etching (RIE) process. Precise control of critical dimensions (CD), etch profile and higher aspect ratio of DD etch are essential factors. Via first DD self-aligned approach increasingly require etching the trench without a stop layer. This place exacting demands on etch uniformity, etch front control and sidewall profile, angle control, micro-trenching effect and it becomes difficult to satisfy high selectivity with minimal small micro-loading at same time. The impact of these issues is crucial when the aspect ratio is very high and on the device are present several patterning structures, typical of smart power technology: ISO and dense with different wide and space. The results show that the loading can be improved and kept at same level when the recess depth increasing. We investigated the DD etching in terms of etching process parameters such as pressure, gas: polymerization gas / $\text{O}_2$  mixed, C to F ratio, gas flux directionality, increasing the upper frequency, power. At the same time also the multilayer stack of DD was modulated to meet the requirements of dry etching in terms of robustness and reliability. Using the obtained result, we have provided an etching process with suitable process parameters in order to realize high performance and low-cost semiconductor devices.

11:40am **PS-TuM-12 Process Development of Selective ICP Etching of  $\text{Si}_3\text{N}_4$  over  $\text{SiO}_2$  and of  $\text{SiO}_2$  over  $\text{Si}_3\text{N}_4$  to Produce Dense Arrays of 50 nm Patterns**, *Andréa Fassion, A. Sarrazin, T. Chevolleau*, Univ. Grenoble Alpes, CEA, Leti, France

The transition of silicon spin qubits from 1D (Dimension) devices to 2D ones demands to produce new architectures and develop dedicated patterning processes [1]. To produce the 2D silicon spin qubits devices developed at CEA-Leti, dense and low dimension arrays of patterns are required. 50 nm-wide square-based holes have to be obtained on a thin layer of Silicon On Insulator (SOI) using a crossbar Litho-Etch-Litho-Etch (LELE) scheme. It combines two thin (i.e. 10-40 nm thick) hard mask layers consisting of  $\text{SiO}_2$  on  $\text{Si}_3\text{N}_4$ . This patterning scheme requires the anisotropic etching of  $\text{Si}_3\text{N}_4$  with a high selectivity over  $\text{SiO}_2$  and vice-versa.

A previous study showed that a  $\text{CH}_3\text{F}/\text{O}_2$  based plasma allows the etching of  $\text{Si}_3\text{N}_4$  with a high selectivity over  $\text{SiO}_2$  [2]. Regarding the selective etching of  $\text{SiO}_2$  over  $\text{Si}_3\text{N}_4$ , a recent work presents a process using a  $\text{BCl}_3/\text{Ar}$  based plasma reaching a selectivity of about 4:1 [3]. The work presented here aims to further characterize the selectivity mechanisms of both  $\text{CH}_3\text{F}/\text{O}_2$  and  $\text{BCl}_3/\text{Ar}$  based processes.

Etching is performed in an industrial ICP (Inductively Coupled Plasma) reactor. The etching mechanisms are discussed in terms of plasma-surface interactions. These interactions are characterised using in-situ Optical Emission Spectroscopy (OES) and interferometry, ex-situ Spectroscopic Ellipsometry (SE), X-Ray Reflectometry (XRR), Atomic Force Microscope (AFM) and quasi in-situ X-Ray Photoelectron Spectrometry (XPS).

Our study shows that  $\text{CH}_3\text{F}/\text{O}_2$  based processes reach an etching selectivity higher than 15:1 and that it strongly relies on the use of F-poor fluorinated gas, high amount of  $\text{O}_2$  and high-pressure conditions (figures enclosed). Our

# Tuesday Morning, November 7, 2023

work also reveals that  $\text{BCl}_3/\text{Ar}$  based processes selectivity relies on both bias voltage and the operating pressure (figures enclosed). It also shows that  $\text{BCl}_3/\text{Ar}$  based process enable a  $\text{SiO}_2$  etching ranging from 2 to 15  $\text{nm}\cdot\text{min}^{-1}$  with a selectivity over  $\text{Si}_3\text{N}_4$  of 7:1 and 3:1, respectively.

According to these selective and low etch rate processes, alternative integration strategies are proposed and applications to patterns will be presented.

## References

- [1] M. Vinet, *Nature nanotechnology* **16**, 1296 (2021).
- [2] H. Ohtake et al. *Jpn. J. Appl. Phys.* **55**, 086502 (2016).
- [3] M. Matsui, K. Kuwahara *Jpn. J. Appl. Phys.* **57**, 06JB01 (2018).

12:00pm **PS-TuM-13 Plasma etch study of  $\text{Nb}_x\text{Ti}_{(1-x)}\text{N}$  metal lines for Superconducting Digital Logic**, **Yann Canvel**, L. Souriau, V. Renaud, A. Pokhrel, A. Gupta, M. Kim, J. Soulie, S. Sarkar, IMEC, Belgium; A. Herr, Q. Herr, IMEC; F. Lazzarino, Z. Tokei, IMEC, Belgium

In the development of next-generation logic devices, an attractive complement to CMOS technology would be to leverage the superconducting technology which operates at a low temperature. Superconducting Digital Logic (SDL) devices are attractive as they are inherently faster and have much less power dissipation than their CMOS counterpart. Although SDL devices have existed for decades now, there have been fundamental challenges to scale down its main components and related interconnects. To provide groundwork for exploring SDL device integration, and a possible hybrid integration of SDL/CMOS circuits, one of the key patterning challenges is the backend fabrication of superconducting metal lines using direct metal etch (DME) approach at relatively small CD/pitch dimension.

In this communication, an in-depth plasma etch investigation is reported to demonstrate the patterning of  $\text{Nb}_x\text{Ti}_{(1-x)}\text{N}$  wires. Using the Reactive Ion Etching (RIE) technique, the study has firstly consisted of screening the plasma chemistry and the tool-related parameters. It has provided some solid learnings to roll out a process optimization, leading to the successful fabrication of  $\text{Nb}_x\text{Ti}_{(1-x)}\text{N}$  metal lines at CD of 50 nm and pitch of 200 nm. Finally, some electrical measurements at room and cryogenic temperatures will complete the investigation validating the fabrication of the smallest superconducting interconnects ever produced.

Pokhrel, A. *et al.* Towards Enabling Two Metal Level Semi-Damascene Interconnects for Superconducting Digital Logic: Fabrication, Characterization and Electrical Measurements of Superconducting  $\text{Nb}_x\text{Ti}_{(1-x)}\text{N}$ . *IEEE International Interconnect Technology Conference (IITC)*, (2023).

Holmes, D. S. *et al.* Energy-Efficient Superconducting Computing - Power Budgets and Requirements. *IEEE Transactions on Applied Superconductivity* **23**, 1701610–1701610 (2013).

Herr, Q. P. *et al.* Ultra-low-power superconductor logic. *Journal of Applied Physics* **109**, 103903 (2011).

## Quantum Science and Technology Mini-Symposium Room B110-112 - Session QS+EM-TuM

### SiC, Diamond and Related Materials for Quantum Information Sciences

**Moderators:** Erin Cleveland, U.S. Naval Research Laboratory, Cheng Gong, University of Maryland

8:40am **QS+EM-TuM-3 Topology, Superconductivity and Unconventional Quantum Criticality in Monolayer  $\text{WTe}_2$** , **Sanfeng Wu**, Princeton University **INVITED**

Quantum critical points associated with quantum phase transitions are highly intriguing states of matter; yet they are difficult to study. An example is the superconductor to insulator or metal transition in two dimensions (2D), a topic that has a long history in condensed matter research, but many problems remain unsolved. In this talk, I will discuss our recent experimental finding of a quantum critical point in monolayer tungsten ditelluride ( $\text{WTe}_2$ ), a unique 2D crystal in which topology, strong correlations and superconductivity all occur in a single material. We directly measure superconducting quantum fluctuations, whose behaviors are so anomalous that an unusual explanation beyond the conventional Landau-Ginzburg-Wilson paradigm is required.

9:20am **QS+EM-TuM-5 Robust Cavity Emitter Coupled System Based on Lifetime-Limited Emission in h-BN**, **Sanchaya Pandit**, Department of Mechanical and Material Engineering, University of Nebraska - Lincoln; Y. Wang, Department of Electrical and Computer Engineering, University of Nebraska - Lincoln

In the field of quantum information technology, it is essential to reach a strong coupling regime, where the coupled systems exhibit quantum coherent oscillations. The ability to control the interactions between the single photon emitter and the cavity mode allows for the manipulation of the photon's quantum state, which is crucial for many quantum applications. Quantum emitters based on defect centers in hexagonal boron nitride (h-BN) have emerged as prominent light sources for integrated quantum photonic applications. Especially, the defect centers with single photon emission around 635 nm have been demonstrated to exhibit lifetime-limited linewidth even at room temperature. This work explores the monolithic integration of this type of h-BN emitters with the whispering gallery mode (WGM) in the microdisk cavity. By optimizing the cavity design, strong coupling between the emitter and cavity has been predicted analytically. Furthermore, coherent manipulation of photon based on cavity-emitter detuning, and spatial position of emitter has been explored and visualized as vacuum Rabi splitting and Rabi oscillation through the Quantum toolbox in Python (Qutip) simulation. The robust cavity design and methodology developed will provide valuable guidelines for the realization of scalable and integrated quantum photonic circuits based on h-BN defect centers.

11:00am **QS+EM-TuM-10 Collective Excitations in Topological Materials**, **Stephanie Law**, Pennsylvania State University **INVITED**

Topological insulators (TIs) are materials that have a bulk band gap crossed by surface states with linear dispersion. These surface states are present at the physical boundaries of the material, and host two-dimensional, massless electrons that are spin-momentum locked. When they couple to a photon, these electrons form the basis of Dirac plasmon polaritons (DPPs) with resonances in the THz spectral range.

In this talk, I will first discuss our efforts to grow TI materials by molecular beam epitaxy (MBE). The TI materials of interest are  $\text{Bi}_2\text{Se}_3$ ,  $\text{Bi}_x\text{Sb}_{1-x}$ , and  $\text{MnBi}_2\text{Se}_4$ . These are all two-dimensional materials, meaning that they exhibit a layered structure with van der Waals (vdW) bonding between each layer. Due to the relatively weak interlayer bonding, these materials grow by van der Waals epitaxy, which has unique opportunities and challenges. I will show our results on growing these materials on passivated substrates (e.g.  $\text{Al}_2\text{O}_3$ ) and unpassivated substrates (e.g. GaAs and Si).

I will then discuss our efforts to excite plasmonic excitations in these materials. The frequencies of the DPPs are predicted to depend both on the wavevector of the excitation as well as on the film thickness when the film is much thinner than the wavelength of light. In this regime, a DPP is excited on the top surface and on the bottom surface of the film simultaneously. These excitations couple, leading to an acoustic and an optical mode. By mapping this relationship, we have shown conclusively that we are able to excite DPPs in TI thin films. These resonances have mode indices of a few hundred, much higher than what is observed in traditional plasmonic systems, implying that light is strongly confined in these materials. We attribute the large mode index to the fact that we are exciting a coupled optical mode and that the bulk permittivity of the TI is also large. Unlike most materials, the large mode index does not lead to a decrease in lifetime. Instead, the lifetime of the mode determined by the full width at half maximum is a few hundred femtoseconds. We attribute this relatively long lifetime to the spin-momentum locking of the surface state electrons, which reduces their probability of scattering. We have also demonstrated coupling of the DPPs in the plane using a stripe array as well as coupling out of plane by growing a layered structure. Finally, we have created a multilayer structure comprising alternating layers of a TI and a normal insulator, leading to a Dirac hyperbolic metamaterial in the THz.

11:40am **QS+EM-TuM-12 Novel Particles in 2D Materials Detected with Quantum Interference and Raman**, **Kenneth Burch**, Boston College **INVITED**

The pursuit of new quasi-particles is driven by the quest to uncover novel phases of matter, emergent phenomena. These may also serve as a foundation for future technological innovations. In this presentation, I will elaborate on our utilization of Raman spectroscopy to identify emergent particles in 2D materials. Firstly, I will delve into our endeavors to identify fractional spin excitations in  $\text{RuCl}_3$ . Subsequently, I will highlight our recent

# Tuesday Morning, November 7, 2023

breakthrough in discovering the Axial Higgs mode, which results from Quantum Geometry and a charge density wave. This discovery was facilitated by Raman's unique ability to detect the particle's symmetry and employ quantum interference to unveil its Axial properties.

## Surface Science Division

### Room D136 - Session SS+2D+AS+HC-TuM

#### Oxide and Chalcogenide Surfaces and Interfaces

Moderators: Rachael Farber, University of Kansas, Gareth Parkinson, TU Wien

8:00am **SS+2D+AS+HC-TuM-1 ViPerLEED: LEED- $I(V)$  Made Easy**, Alexander Michael Imre<sup>1</sup>, TU Wien, Austria; F. Kraushofer, TU Munich, Germany; T. Kijßlinger, L. Hammer, Friedrich-Alexander-University Erlangen-Nürnberg (FAU), Germany; M. Schmid, U. Diebold, M. Riva, TU Wien, Austria

Most surface science laboratories are equipped with a low-energy electron diffraction (LEED) setup. LEED patterns provide quick, qualitative insight into surface structure and ordering. However, the diffracted electron beams contain a large amount of additional structural information which is often ignored. By studying the diffraction intensities as a function of incident electron energy [LEED- $I(V)$ ], it is possible to quantitatively compare experimentally observed surfaces with structural models.

Despite the clear need for such a direct experiment-to-theory comparison, LEED- $I(V)$  is only routinely used by few specialized groups. A main obstacle for widespread adoption is that existing solutions for LEED- $I(V)$  analysis and simulation are time-consuming and hard to use for scientists who are not already experts in the field.

To resolve this issue, we have developed the Vienna Package for Erlangen LEED (ViPerLEED) – a package of three independent but complementary tools for easy LEED- $I(V)$  acquisition and analysis. All parts of ViPerLEED will be released as open source at the time of publishing:

- **Electronics:** We provide schematics and control software for electronics, which allows users to easily and cheaply upgrade most existing LEED setups for acquiring high-quality LEED- $I(V)$  data. These ViPerLEED electronics are based on an Arduino microcontroller and can be home-built from off-the-shelf components. The associated control software synchronizes with the camera and automates the experiment.
- **Spot-tracker:** ViPerLEED provides a plugin for the public-domain image processing program ImageJ, for spot tracking and extraction of LEED- $I(V)$  spectra from series of raw diffraction images. The automatically extracted  $I(V)$  curves can be used for further analysis or as a fingerprint of the surface surface. The plugin package also provides user-friendly options for examination, selection and smoothing of the  $I(V)$  data.
- **Simulation software:** For structure analysis, we introduce a Python package for calculation of LEED- $I(V)$  spectra and structure optimization. This software is based on the established TensErLEED package and extends its functionality while still making it easy for new users to get started with the technique. It uses standard file formats for the surface structure, provides automated symmetry detection, and requires just a handful of parameters for running a structure determination.

8:20am **SS+2D+AS+HC-TuM-2 Quasicrystal-like Ordering of the  $\text{La}_{0.8}\text{Sr}_{0.2}\text{MnO}_3(001)$  Surface**, Erik Rheinfrank, G. Franceschi, L. Lezuo, M. Schmid, U. Diebold, M. Riva, TU Wien, Austria

Lanthanum-strontium manganite ( $\text{La}_{0.8}\text{Sr}_{0.2}\text{MnO}_3$ , LSMO) is a perovskite oxide used as a cathode material in solid oxide fuel cells, which convert chemical energy to electrical energy. To gain deeper insights into the reaction mechanisms, it is important to understand the structure of the surface at the atomic scale. To this end, we grow atomically flat single-crystalline LSMO thin films on Nb-doped  $\text{SrTiO}_3$  (STO) substrates via pulsed laser deposition (PLD). Previously, this has been achieved for the (110) orientation.<sup>1,2</sup> Here, we use a similar approach on the (001) surface that is commonly used for oxide-based electronics and spintronics. The as-grown films have a  $\text{MnO}_x$  terminated surface that shows a 4-fold symmetric structure in low-energy electron diffraction (LEED), best explained by a set

of four basis vectors reminiscent of quasicrystals. Scanning tunnelling microscopy (STM) and Q+ non-contact atomic force microscopy (nc-AFM) reveal an aperiodic arrangement of tiles with rotation angles of  $\pm 26.6^\circ$  and  $90 \pm 26.6^\circ$ , and a Fourier transform consistent with the LEED pattern. As for quasicrystals, the surface has a sharp diffraction pattern despite the lack of translational symmetry.

[1] Franceschi *et al.*, J. Mater. Chem. A, 2020, **8**, 22947-22961

[2] Franceschi *et al.*, Phys. Rev. Materials, 2021, **5**, L092401

8:40am **SS+2D+AS+HC-TuM-3 AVS Graduate Research Awardee Talk: The Selective Blocking of Potentially Catalytically-Active Sites on Surface-Supported Iron Oxide Catalysts**, Dairong Liu<sup>2,3</sup>, N. Jiang, University of Illinois - Chicago

The extensive research on ultrathin ferrous oxide (FeO) islands and films over the last few decades has significantly contributed to the understanding of their structural and catalytic properties. One important aspect that has been investigated is the surface properties of ultrathin FeO islands, particularly the role played by the edges of these islands in catalytic reactions, such as CO oxidation. So far, two different types of edge, Fe-terminated edge and O-terminated edge, have been identified in the well-growth FeO island. However, despite this significant progress, the local chemical properties of these two types of edges, including their metal affinity, have remained largely unexplored. Here, we used scanning tunneling microscopy (STM) to study the interaction of Pd and Pt with FeO grown on Au(111). Different Fe affinities for Pd and Pt are demonstrated by the preferential growth of Pd on the Fe-terminated edge and Pt on the O-terminated edge of FeO nanoislands, resulting in selectively blocked FeO edges. In addition to revealing the different metal affinities of FeO edges, our results provide new insights into the edge reactivity of FeO/Au(111) and suggest an approach for controlling the selectivity of FeO catalysts. By comparing the behavior of different edges in the catalysis reaction, the catalytic activity of these edges can be studied solely, thereby sheds light into the future modification of ferrous-based catalysts.

9:00am **SS+2D+AS+HC-TuM-4 Unraveling Surface Structures of Ga-Promoted Transition Metal Catalysts in  $\text{CO}_2$  Hydrogenation**, Si Woo Lee, S. Shaikhutdinov, B. Roldan Cuenya, Fritz Haber Institute of the Max Planck Society, Germany

Gallium-containing alloys with transition metals (TM) have recently been reported to be reactive in the selective hydrogenation of  $\text{CO}_2$  for methanol synthesis. However, a full understanding of the Ga-promoted catalysts is still missing due to the lack of information about the *surface* structures formed under reaction conditions. In this respect, studies using surface-sensitive techniques applied to well-defined model systems can provide key information to elucidate the reaction mechanism and provide the basis for the rational design of Ga-promoted catalysts.

In this work, we employed *in-situ* Near Ambient Pressure Scanning Tunneling Microscopy (NAP-STM) and X-ray Photoelectron Spectroscopy (NAP-XPS), which make it possible to study surfaces in the reaction conditions, for monitoring the structural and chemical evolution of the Ga-covered Cu surfaces in the  $\text{CO}_2$  hydrogenation reaction. NAP-STM images recorded in the reaction mixture revealed temperature- and pressure-dependent de-alloying of the initially formed, well-ordered ( $\sqrt{3} \times \sqrt{3}$ )R30°-Cu(111) surface alloy and the formation of Ga-oxide islands embedded into the Cu(111) surface, exposing  $\text{GaO}_x/\text{Cu}(111)$  interfacial sites. Notably, in our atomically-resolved STM image of Ga-oxide/Cu(111), it is clearly observed that Ga-oxide grows into an ultrathin oxide layer form with ( $4\sqrt{3} \times 4\sqrt{3}$ )R30° superstructure. From NAP-XPS studies on Ga/Cu(111) in the presence of  $\text{CO}_2$  and  $\text{H}_2$ , the formation of formate was observed, and this reaction intermediate was eventually transformed into methoxy at elevated temperatures, representing the final surface-bound intermediate for methanol synthesis. In contrast to Ga-containing Cu catalyst, on the other hand, there was no reaction intermediate at high temperature on the Ga-free Cu(111) surface, demonstrating that further reactions do not occur anymore from chemisorbed  $\text{CO}_2^{2-}$  on Cu surface alone. Therefore, the  $\text{GaO}_x/\text{Cu}$  interface formed under reaction conditions may expose catalytically active sites never considered for this reaction before. We believe that our experimental results shed light on the complex surface structure of Ga-containing catalytic systems, which is only possible to obtain using state-of-the-art experimental techniques under reaction conditions. Only by establishing the atomic structure of the Ga-oxide

<sup>1</sup> SSD Morton S. Traum Award Finalist

Tuesday Morning, November 7, 2023

<sup>2</sup> AVS Graduate Research Awardee

<sup>3</sup> SSD Morton S. Traum Award Finalist

# Tuesday Morning, November 7, 2023

layer(s) and its interface to the transition metal under working conditions can one bring insight into the reaction mechanism of this methanol synthesis catalyst.

9:20am **SS+2D+AS+HC-TuM-5 Ultrathin Metal Oxide, Nitride and Sulfide Films: Bringing the Well-Known Compounds to a Unit-Cell Thickness**, **Mikołaj Lewandowski**, NanoBioMedical Centre, Adam Mickiewicz University in Poznań, Poland **INVITED**

Bringing the well-known materials from bulk size to a unit-cell thickness may significantly influence their structure and physicochemical properties. As an example, ultrathin (< 1-nanometer-thick) films of metal/non-metal compounds, such as metal oxides, nitrides or sulfides epitaxially grown on single-crystal supports, are characterized by unique electronic, catalytic and magnetic properties not observed for their bulk counterparts. Such films also exhibit superior structural flexibility, undergoing phase transitions upon exposure to external factors (such as reactive gases or high temperatures) [1,2]. All this makes them promising candidates for applications in various technological fields, including nanoelectronics, spintronics and heterogeneous catalysis.

Within the lecture, I will address the growth, structure and properties of ultrathin metal oxide, nitride and sulfide films, with compounds of iron as exemplary cases. The scanning tunneling microscopy and spectroscopy (STM/STS), low energy electron diffraction (LEED), X-ray photoelectron spectroscopy (XPS), low energy electron microscopy (LEEM) and density functional theory (DFT) results – obtained by my group and our collaborators – provide universal guidelines for designing ultrathin films with desired structure and properties [1–3].

[1] Y. Wang, G. Carraro, H. Dawczak-Dębicki, K. Synoradzki, L. Savio, M. Lewandowski, *Applied Surface Science* 528 (2020) 146032.

[2] N. Michalak, T. Ossowski, Z. Miłosz, M. J. Prieto, Y. Wang, M. Werwiński, V. Babacic, F. Genuzio, L. Vattuone, A. Kiejna, Th. Schmidt, M. Lewandowski, *Advanced Materials Interfaces* 9 (2022) 2200222.

[3] P. Wojciechowski, W. Andrzejewska, M.V. Dobrotvorska, Y. Wang, Z. Miłosz, T. Ossowski, M. Lewandowski, submitted (2023).

The author acknowledges financial support from the National Science Centre of Poland (through SONATA 3 2012/05/D/ST3/02855, PRELUDIUM 11 2016/21/N/ST4/00302 and M-ERA.NET 2 2020/02/Y/ST5/00086 projects), as well as the Foundation for Polish Science (First TEAM/2016-2/14 (POIR.04.04.00-00-28CE/16-00) project co-financed by the European Union under the European Regional Development Fund).

11:00am **SS+2D+AS+HC-TuM-10 Optimized Infrared Reflection Absorption Spectroscopy for Metal Oxides: Overcoming Challenges of Low Reflectivity and Sub-Monolayer Coverage**, **Jiri Pavelec, D. Rath, M. Schmid, U. Diebold, G. Parkinson**, Vienna University of Technology, Austria

Infrared reflection absorption spectroscopy (IRAS) is a wide-spread technique in heterogeneous catalysis, and it is an ideal tool for the comparison of real and model catalysts [1]. Most surface science groups perform IRAS studies either directly on metal single crystals, or on (ultra-)thin metal oxide films grown directly on such samples [2]. Achieving high-quality data from metal-oxide single crystal surfaces is difficult because their low reflectivity necessitates averaging many individual measurements with long acquisition times [3]. The goal of this work was to develop an IRAS setup for studying the adsorption of molecules on model “single-atom” catalysts. Here, the low reflectivity of oxide support is exacerbated by the sub-monolayer coverage of adsorbates on single adatoms. In the contribution, I will present the novel IRAS system we have developed to overcome these two challenges.

The main improvements over commonly-used setups are a high numerical aperture, an optimized optical path, control of the incidence angle range, and high mechanical stability. The high numerical aperture of the optical system leads to an increase in the amount of light reflected from a small single crystal sample. This is achieved by placing both the illumination and collector mirrors inside the UHV chamber close to the sample. To minimize the loss of signal, optimization of the optical path was performed using a ray tracing program. The other limit is the small area on the sample that is covered with adsorbates: in our setup, a molecular beam delivers adsorbates with a spot diameter of 3.5 mm [4]. Infrared light is reflected only from this area.

The reflectivity and absorbance of non-metallic samples varies strongly with incidence angle, and can even change a sign, leading to cancellation. The optimum angle ranges are different for every material. As our setup has a large range of incident angles, we can use this to our advantage: Using

two adjustable aperture plates, we can vary the minimum and maximum incidence angle from 49° to 85° to maximize the signal for each single crystal sample. Angle control also allows us to optimize the signal for both p-polarized and s-polarized light independently.

We successfully executed and compared D<sub>2</sub>O and CO absorbance measurements on a rutile TiO<sub>2</sub>(110) surface, and our results agree with the established literature [3]. By properly selecting the incidence angle range, we achieved a signal-to-noise ratio of ~16 for 1 ML CO adsorbed on TiO<sub>2</sub> with only 150 seconds of measurement time.

[1] F. Zaera, *Chem. Soc. Rev.*, 43, 2014

[2] J. Libuda et al., *J. Chem. Phys.*, 114, 10, 2001

[3] N. G. Petrik et al., *The Journal of Physical Chemistry C*, 126 (51), 2022

[4] J. Pavelec et al., *J. Chem. Phys.*, 146, 2017

11:20am **SS+2D+AS+HC-TuM-11 VO Cluster-Stabilized H<sub>2</sub>O Adsorption on a TiO<sub>2</sub> (110) Surface at Room Temperature**, **Xiao Tong**, Brookhaven National Laboratory

We probe the adsorption of molecular H<sub>2</sub>O on a TiO<sub>2</sub> (110)-(1 × 1) surface decorated with isolated VO clusters using ultrahigh-vacuum scanning tunneling microscopy (UHV-STM) and temperature-programmed desorption (TPD). Our STM images show that preadsorbed VO clusters on the TiO<sub>2</sub> (110)-(1 × 1) surface induce the adsorption of H<sub>2</sub>O molecules at room temperature (RT). The adsorbed H<sub>2</sub>O molecules form strings of beads of H<sub>2</sub>O dimers bound to the 5-fold coordinated Ti atom (5c-Ti) rows and are anchored by VO. This RT adsorption is completely reversible and is unique to the VO-decorated TiO<sub>2</sub> surface. TPD spectra reveal two new desorption states for VO stabilized H<sub>2</sub>O at 395 and 445 K, which is in sharp contrast to the desorption of water due to recombination of hydroxyl groups at 490 K from clean TiO<sub>2</sub>(110)-(1 × 1) surfaces. Density functional theory (DFT) calculations show that the binding energy of molecular H<sub>2</sub>O to the VO clusters on the TiO<sub>2</sub> (110)-(1 × 1) surface is higher than binding to the bare surface by 0.42 eV, and the resulting H<sub>2</sub>O-VO-TiO<sub>2</sub> (110) complex provides the anchor point for adsorption of the string of beads of H<sub>2</sub>O dimers.

11:40am **SS+2D+AS+HC-TuM-12 Synthesis and Multimodal Characterization of Thin-Film Oxides**, **Dario Stacchiola**, Brookhaven National Laboratory

Thin films of metal oxides exhibit a variety of unique physical and chemical properties leading to broad applications in optics, microelectronics, optoelectronics, superconducting circuits, gas sensors, thermal catalysis, electrocatalysis, and solar energy harvesting. Many metal oxides can form stoichiometric and non-stoichiometric alloys and compounds with each other, commonly known as complex metal oxides. Alloy and compound formation, including growth and process conditions, offer great flexibility for manipulating the lattice, atomic scale structure motifs, and electronic structure to realize desired properties. In order to exploit this potential, knowledge about fundamental processes and atomic level structural information is required. We present here the synthesis and multimodal characterization of mixed-oxide films based on silica and titania, from single layers to complex metal oxides.

1. “Deciphering phase evolution in complex metal oxide thin films via high-throughput materials synthesis and characterization”, *Nanotechnology* 34, 125701 (2023)

2. “Resolving the evolution of atomic layer deposited thin film growth by continuous in situ X-ray absorption spectroscopy”, *Chem. Mat.* 33, 1740-1751 (2021)

3. “First-Principles Study of Interface Structures and Charge Rearrangement at the Aluminosilicate / Ru(0001) Heterojunction” *J. Phys. Chem. C* 123, 7731–7739 (2019)

12:00pm **SS+2D+AS+HC-TuM-13 Atomic Structure of Reconstructed Al<sub>2</sub>O<sub>3</sub>(0001) Surface**, **J. Hütner, A. Conti**, TU Wien, Austria; **D. Kugler**, CEITEC, Czechia; **F. Mittendorfer, U. Diebold, M. Schmid, Jan Balajka**, TU Wien, Austria

Corundum α-Al<sub>2</sub>O<sub>3</sub> is an important ceramic widely used in electronics, optical applications, or as catalyst support. Despite its importance, the atomic structure of the most stable (0001) termination has not been conclusively determined. Detailed studies of Al<sub>2</sub>O<sub>3</sub> surfaces have been stymied by its insulating nature, preventing the use of many surface science methods.

Structural models based on surface X-ray diffraction (SXRD) [1], and atomic force microscopy (AFM) [2], concluded the (√31 × √31)R±9°-reconstructed Al<sub>2</sub>O<sub>3</sub>(0001) surface formed upon high-temperature annealing is terminated

# Tuesday Morning, November 7, 2023

by one or two layers of metallic Al strained to lattice-match the oxide substrate.

We imaged the reconstructed  $\text{Al}_2\text{O}_3(0001)$  surface with noncontact AFM (nc-AFM) using specifically functionalized tips for chemically-sensitive contrast. In particular,  $\text{CuO}_x$  terminated tips [3], enabled us to directly identify oxygen and aluminum atoms in the topmost layer.

With the aid of *ab-initio* calculations, we propose a structural model of the  $(\sqrt{31} \times \sqrt{31})R\pm 9^\circ$ -reconstructed  $\text{Al}_2\text{O}_3(0001)$  surface consistent with atomically resolved nc-AFM images and area-averaging spectroscopic data. Unlike prior models, the surface does not contain a metallic Al layer but consists of oxygen and aluminum atoms arranged in similar structural units as reported in thin  $\text{AlO}_x$  films [4,5].

[1] G. Renaud, et al., *Phys. Rev. Lett.* **73**, 13 (1994)

[2] J. V. Lauritsen, et al., *Phys. Rev. Lett.* **103**, 076103 (2009)

[3] B. Shulze Lammers, et al., *Nanoscale* **13**, 13617 (2021)

[4] G. Kresse, et al., *Science* **308**, 1440 (2005)

[5] M. Schmid, et al., *Phys. Rev. Lett.* **99**, 196104 (2007)

## Theory for Surface Processes and Spectroscopies Focus Topic

### Room B116 - Session TH1+AS+SS-TuM

#### Introduction and Core-Level Spectroscopies I

**Moderators:** Gianfranco Pacchioni, Università degli Studi di Milano-Bicocca, John Rehr, University of Washington

8:00am **TH1+AS+SS-TuM-1 X-Ray Photoelectron Spectroscopy as a Useful Tool to Study Surfaces and Model Systems for Heterogeneous Catalysts, Hans-Joachim Freund**, Fritz-Haber-Institut der Max-Planck-Gesellschaft, Germany

INVITED

After a brief introduction into the concepts of photoemission, including multielectron excitations, and a discussion of ways how to extract information on the chemical state of atoms in the non-ionized ground state from the chemical shift in XPS spectra, as well as from the evaluation of the so-called Auger parameter, we present several examples on how appropriate theoretical calculations may be crucial to properly interpret the spectra in terms of initial and final state effects. Four studies on systems representing model systems for heterogeneous catalysts are discussed. The first two refer to simple thin film oxide systems of  $\text{MgO}(100)/\text{Ag}(100)$  supported on metal single crystals. We interpret line widths in terms of vibrational excitations, depending on the thickness of the oxide film, and compare surface core level chemical shifts with those in the bulk, and discuss the differences on the basis of *ab-initio* cluster calculations. The third example refers to chemical shifts of metal/(Pd) atoms adsorbed on bilayer silica films on  $\text{Ru}(0001)$ , and illustrates the use of the Auger parameter to extract initial state chemical shifts. The last example deals with  $\text{CeO}_2(111)$  surfaces and exemplifies the influence of open shell on the complexity of core level spectra.

8:40am **TH1+AS+SS-TuM-3 X-Ray Absorption and Emission Spectroscopy of Actinide Materials: Electronic Structure Questions from the Experimental Viewpoint, Bianca Schacherl**, Karlsruhe Institute of Technology (KIT), Institute for Nuclear Waste Disposal (INE), Germany

INVITED

Understanding the electronic structure of one of the most complex element groups in the periodic table, the actinides, has been topic of extensive research in the last decades.

Spectroscopic tools for these investigations are provided by X-ray absorption spectra. Especially the An  $M_{4,5}$ -edge high-resolution X-ray absorption and emission spectroscopy has proven to be a powerful tool for electronic structure investigations.<sup>1,2</sup>

In this talk it will be demonstrated how newly revealed spectral features can be used for in-depth analyses of the actinide-ligand chemical bond. For model systems, one focus will lie on how the spectra change upon changes in the electronic structure of the actinide compound. It will be highlighted how several theoretical methods can give a valuable input to understand the origin of the spectral features.<sup>3-7</sup>

*This work is supported by the ERC Consolidator Grant "The Actinide Bond" (N°101003292) under the European Union's Horizon 2020 research and*

*innovation program. The Institute for Beam Physics and Technology (IBPT), KIT is acknowledged for the operation of the storage ring, the Karlsruhe Research Accelerator (KARA).*

(1) Vitova, T.; Pidchenko, I.; Fellhauer, D.; Bagus, P. S.; Joly, Y.; Prößmann, T.; Bahl, S.; Gonzalez-Robles, E.; Rothe, J.; Altmaier, M.; Denecke, M. A.; Geckeis, H. *Nat. Commun.* **2017**, *8* (May), 1–9.

(2) Vitova, T.; Pidchenko, I.; Fellhauer, D.; Prößmann, T.; Bahl, S.; Dardenne, K.; Yokosawa, T.; Schimmelpfennig, B.; Altmaier, M.; Denecke, M.; Rothe, J.; Geckeis, H. *Chem. Commun.* **2018**, *54* (91), 12824–12827.

(3) Polly, R.; Schacherl, B.; Rothe, J.; Vitova, T. *Inorg. Chem.* **2021**, *60* (24), 18764–18776.

(4) Bagus, P. S.; Schacherl, B.; Vitova, T. *Inorg. Chem.* **2021**, *60* (21), 16090–16102.

(5) Schacherl, B.; Trumm, M.; Beck, A.; Vitova, T. **2024**, *submitted*.

(6) Schacherl, B.; Bowes, E.; Adelman, S. L.; Dardenne, K.; DiMucci, I.; Kozimor, S. A.; Long, B. N.; Müller, N.; Pace, K.; Pruessmann, T.; Rothe, J.; Xu, L.; Kasper, J. M.; Batista, E. R.; Yang, P.; Vitova, T. **2023**, *submitted*.

(7) Schacherl, B.; Tagliavini, M.; Popa, K.; Beck, A.; Walter, O.; Pruessmann, T.; Vollmer, C.; Kaufmann, H.; Mazzanti, M.; Haverkort, M.; Vitova, T. **2023**, *submitted*.

#### 9:20am TH1+AS+SS-TuM-5 Towards New Spectroscopic Tools for Detection of Bonding Properties in Radiopharmaceuticals: Application on La Used as a Homolog of Ac, Tonya Vitova

Karlsruhe Institute of Technology (KIT), Institute for Nuclear Waste Disposal, Germany; B. Schacherl, H. Ramanantoanina, Karlsruhe Institute of Technology (KIT), Institute for Nuclear Waste Disposal (INE), Germany; M. Benesova, German Cancer Research Center, Im Neuenheimer Feld 280, 69120 Heidelberg, Germany; J. Göttlicher, Karlsruhe Institute of Technology, Institute for Photon Science and Synchrotron Radiation (IPS), P.O. Box 3640, D-76021 Karlsruhe, Germany; R. Steininger, Karlsruhe Institute of Technology, Institute for Photon Science and Synchrotron Radiation (IPS), Germany; M. Haverkort, Heidelberg University, Institute for Theoretical Physics, P.O. Box 105760, 69047 Heidelberg, Germany; A. Kovac, European Commission, Joint Research Centre Karlsruhe, P.O. Box 2340, 76125 Karlsruhe, Germany

In recent years the use of radiopharmaceuticals based on alpha-particle emitting radionuclides has seen a considerable growth. In pre-clinical research and first clinical trials targeted alpha therapy has shown great potential. However, there are still many challenges in this field, one being the need for tight chelating of the alpha-emitting radionuclides and their daughters. We aim to understand relations between bonding properties and bond stability of such compounds.

High-energy resolution X-ray absorption near edge structure (HR-XANES) spectroscopy is a valuable tool for the electronic structure study of actinides and lanthanides.<sup>1,2</sup> Here we employ it first to probe the bonding properties of La, a homolog of Ac, with different ligands in discussion as nuclide binding site in radiopharmaceuticals for targeted alpha treatment.

$[\text{La}(\text{H}_2\text{O})_9]^{3+}$ ,  $[\text{La}(\text{TRIS})(\text{H}_2\text{O})_6]^{3+}$ ,  $[\text{La}(\text{TRIS})_2(\text{H}_2\text{O})_3]^{3+}$  (buffer media),  $[\text{La}(\text{DOTA})(\text{H}_2\text{O})]^{2+}$ ,  $[\text{La}(\text{MACROPA})]^{1+}$  and  $[\text{La}(\text{PSMA-617})(\text{H}_2\text{O})]$  have been prepared and characterized. We measured La  $L_2$ -edge HR-XANES spectra at the Synchrotron Laboratory for Environmental Studies (SUL-X) beamline and La  $L_3$ -edge extended X-ray absorption fine structure spectroscopy (EXAFS) at the INE-Beamline at the KIT Light Source. Additionally, density functional theory (DFT) and FDMNES calculations were performed to compute the spectra. Bonding interactions were evaluated using natural orbitals for chemical valence (NOCV) and quantum theory of atoms in molecules (QTAIM) which describes the topology (i.e., shape and magnitude) of the electron density between two bonded atoms.

Several tools (spectroscopic and theoretical) to determine the covalency of the La-ligand bond were developed. One example of this measure can be the comparison of position and shape of the pre- and main absorption edges. EXAFS and HR-XANES analysis gave insights into the coordination environment. With QTAIM bond analysis the covalent from the ionic part of the bonding was differentiated. Combined these results are the first steps towards developing new spectroscopic tools that will help understand the electronic structure and the bonding and will potentially help designing new chelating ligands for use in radiopharmaceuticals for targeted alpha therapy.

References

1. T. Pruessmann et al., *J Synchrotron Radiat* **2022**, *29*, 53-66.

# Tuesday Morning, November 7, 2023

2. T. Vitova *et al.*, *Commun Chem* **2022**, 5 (1).

9:40am **TH1+AS+SS-TuM-6 Potential Energy Curves of Core-Excited States and Vibrational Broadening of X-Ray Adsorption Spectra of Uranyl**, **Robert Polly**, Karlsruhe Institute of Technology (KIT), Germany; **P. Bagus**, University of North Texas

It is well known that vibrational excitations lead to an observable broadening of the features in the X-Ray Photoelectron Spectroscopy, XPS, in ionic compounds. This broadening is described as a Franck-Condon, FC, broadening since it arises because there is a change in the equilibrium geometry of the ionized system from that in the initial, ground, state of the system. Studies have shown how the FC broadening is sensitive to coordination of the ionized atom [1] and to the covalent character of the cation – anion interaction [2]. For Uranyl  $\text{UO}_2^{2+}$  the different potential energy curves of the relevant core-excited states of the U  $M_{4,5}$ -edge manifold differ significantly and cause different broadenings for the three peaks which characterize the U  $M_{4,5}$ -edge X-Ray Adsorption Near Edge Spectroscopy, XANES. Thus, FC broadening effects affect the features as they do for XPS. This should be of particular importance in determining the resolution possible with High-Resolution XANES, HR-XANES [3-4]. However, to our knowledge, the possibility of different FC broadening in XANES or HR-XANES has not been considered previously and theoretical modeling of the spectra has used the same geometry for the initial and excited configurations [4-5]. In the present work, we examine vibrational excitations for the representative case of uranyl,  $\text{UO}_2^{2+}$ . The U  $M_{4,5}$ -edge HR-XANES spectra reveal three distinct peaks which are assigned to excitations into different 5f valence orbitals. The corresponding core-excited states differ significantly depending on the 5f valence orbital occupation and so does the FC broadening. Based on rigorous *ab initio* calculations of the wavefunctions, WFs, for the  $M_4$  and  $M_5$ -edge XANES, we show that there are considerable changes in the geometry and we provide reliable estimates of the FC broadening due to these geometry changes. We also explain the linear behavior of the observed peak splittings with the internuclear distance, but we can not confirm a relation of the peak splittings with the covalence of the Uranium-Oxygen bond lengths.

[1] C. J. Nelin *et al.*, *Angew. Chem. Int. Ed.*, 2011, **50**, 10174-10177.

[2] P. S. Bagus and C. J. Nelin, "Computation of Vibrational Excitations in XPS Spectroscopy", in *Rare Earth Elements and Actinides: Progress in Computational Science Applications*, edited by D. A. Penchoff, et al. (American Chemical Society, 2021), Vol. 1388, p. 181.

[3] T. Vitova *et al.*, *Nat. Commun.*, 2017, **8**, 16053.

[4] R. Polly *et al.*, *Inorg. Chem.*, 2021, **60**, 18764-18776.

[5] P. S. Bagus *et al.*, *Inorg. Chem.*, 2021, **60**, 16090.

## Theory for Surface Processes and Spectroscopies Focus Topic

### Room B116 - Session TH2+AS+SS-TuM

#### Core-Level Spectroscopies II

**Moderators:** **Ria Broer**, University of Groningen, **Bianca Schacherl**, Karlsruhe Institute of Technology

11:00am **TH2+AS+SS-TuM-10 Cumulant Green's Function Approaches for Satellites and Multiplets in X-Ray Spectra**, **John J. Rehr**, Dept of Physics, University of Washington; **J. Kas**, Department of Physics, University of Washington

**INVITED**

The treatment of electronic correlations in open-shell systems is one of the most challenging problems in atomic, molecular, and condensed matter physics. Their importance is particularly evident in x-ray spectra, where the single particle theory breaks down and many-body effects such as satellites and atomic multiplet effects are observed. Conventional approximations are only partly successful. Ligand-field multiplet theory and dynamical mean field theory can describe intra-atomic correlation effects well but typically ignore long range correlation effects. The real-time cumulant Green's function method can describe shake-up effects well [1] but ignores multiplets. We have found, however, that separating the dynamic Coulomb interactions into local and longer-range parts with *ab initio* parameters yields a combined multiplet-plus-cumulant approach that can account for both local atomic multiplets and satellite excitations [2]. The approach is illustrated for transition metal oxides and explains the multiplet peaks, charge-transfer satellites, and distributed background features observed in XPS experiment. In an alternative approach for molecular systems, we have found that a real-time equation of motion coupled-cluster (RT-EOM-CC)

cumulant approach can also describe both correlation effects at the CCSD level and intrinsic losses in x-ray spectra, including orthogonality corrections that enhance XAS at the edge [3]. Comparisons with other approaches [4] are also discussed.

[1] Strengths of plasmon satellites in XPS: Real-time cumulant approach: J. J. Rehr and J. J. Kas, *J. Vac. Sci. Technol. A* **39**, 060401 (2021).

[2] *Ab Initio* Multiplet-Plus-Cumulant Approach for Correlation Effects in X-Ray Photoelectron Spectroscopy, J. J. Kas, J. J. Rehr, and T. P. Devereaux, *Phys. Rev. Lett.* **128**, 216401 (2022).

[3] Equation of motion coupled-cluster cumulant approach for intrinsic losses in x-ray spectra, J. Chem. Phys. J.J. Rehr, F.D. Vila, J.J. Kas, N.Y. Hirshberg, K. Kowalski, and B. Peng **152**, 174113 (2020).

[4] Analysis of the Fe 2p XPS for hematite  $\text{Fe}_2\text{O}_3$ : Consequences of covalent bonding and orbital splittings on multiplet splittings, P.S. Bagus, C. J. Nelin, C. R. Brundle, N. Lahiri, E. S. Ilton, and K. M. Rosso, *J. Chem. Phys.* **152**, 014704 (2020).

11:40am **TH2+AS+SS-TuM-12 Understanding Multiplets in the XPS of Transition Metal Oxides: Experiment and Theory and the Effects on Quantitation Procedures**, **Christopher Richard Brundle**, C. R. Brundle and Associates; **B. Christ**, XPS library; **P. Bagus**, Center for Advanced Scientific Computing and Modeling (CASCAM) Department of Chemistry University of North Texas

**INVITED**

Atoms with open valence shells suffer splitting to their XPS core-levels owing to the different spin-spin coupling possibility between the remaining unpaired core electron and the electrons in the open shell (1). This results in a spectrum with two components of unequal intensity, separated by an *ev* or two. Gupta and Sen (2) expanded the multiplet splitting theory to include spin-orbit coupling (angular momentum coupling), providing highly cited predictions for the 2p spectra of TM cations (eg  $\text{Ni}^{2+}$ ). Bagus, et al (3), and others, using rigorous *ab initio* MO calculations on clusters, have expanded theory further to allow XPS predictions for solid TM compounds (eg  $\text{Ni}^{2+}$  in NiO,  $\text{Fe}^{3+}$  in  $\text{Fe}_2\text{O}_3$ ) which include both ligand field and bonding effects. Finally, they included shake-up effects (excitation of valence electrons in addition to core level ionization), which can substantially alter the distribution of intensities across the complete core-level spectrum, for example Ni 2p for NiO (4). This progression in the understanding of the origin of the features of TM core-level spectra is discussed, as is also the effects on requirements for providing quantitation of TM compounds using core level intensity ratios or peak fitting. Comparison is then made to alternative theory approaches to modeling the spectra, such as the freely available semi-empirical charge transfer method, CTM4XAS, (5), and the many-body cumulative theory of Rehr and Kass (6). We examine how these agree/differ in the interpretation/understanding of the XPS features, usefulness in ascribing chemical states, and quantitation aspects.

52. C. S. Fadley, D. A. Shirley, A. J. Freeman, P. S. Bagus, and J. V. Mallow, *Phys. Rev. Lett.*, 1969, **23**, 1397-1401.

53. R. P. Gupta and S. K. Sen, *Phys. Rev. B*, 1974, **10**, 71-77; P. Gupta and S. K. Sen, *Phys. Rev. B*, 1975, **12**, 15-19.

54. P. S. Bagus, C. J. Nelin, C. R. Brundle, B. V. Crist, N. Lahiri, and K. M. Rosso, *Phys. Chem. Chem. Phys.*, 2022, **24**, 4562-4575.

55. P. S. Bagus, C. J. Nelin, C. R. Brundle, B. V. Crist, E. S. Ilton, N. Lahiri, and K. M. Rosso, *Inorganic Chemistry*, 2022, **61**, 18077

56. F. De Groot and A. Kotani, *Core level spectroscopy of solids. CRC Press, Boca Raton*, 2008.

57. J. J. Kas, J. J. Rehr and T. P. Devereaux, *Phys. Rev. Lett.* 2022, **128**, 216401

## Vacuum Technology Division

### Room C120-122 - Session VT-TuM

#### Particle Accelerators and Large Vacuum Systems

**Moderators:** **Julia Scherschligt**, National Institute of Standards and Technology, **Steven Wulfsberg**, SAES Getters USA

8:00am **VT-TuM-1 Study on a Pressure Anomaly Detection Method Applying Machine Learning in SuperKEKB Accelerator Vacuum System**, **Yusuke Suetsugu**, High Energy Accelerator Research Organization (KEK), Japan

A large-scale vacuum system of the SuperKEKB accelerator has been running well since the first commissioning in 2016. However, owing to the

# Tuesday Morning, November 7, 2023

large beam currents and the high frequency of beam loss and re-injection, air leaks from connection flanges due to thermal cycles caused by the intense synchrotron radiation etc., and irregular pressure rises due to discharging etc. have been often observed. Sometimes, they resulted in serious troubles which interrupt the beam operation. If any signs of abnormal pressure are detected before a usual alarm is issued or before machine operators notice the abnormality, quick countermeasures can be taken before the major troubles occurs. We are proposing and studying an anomaly detection method applying machine learning to detect the signs of pressure anomalies and call attention to operators as early as possible. First, a typical beam-filling cycle is defined as the period from the beam (re-)injection, storage, and abort. For each of the approximately 600 vacuum gauges in the main ring, the measured values for three days from eight days before the beam-filling cycle to be checked are defined as the "standard data", which include several beam-filling cycles. Then the regression curve for the behaviors of pressures during a beam-filling cycle is derived using the standard data against beam current (beam injection and storage) or time (just after beam abort). Second, for every beam-filling cycle to be checked, the standard errors are calculated from the measured pressure values during the cycle ("measured data") using the obtained regression curves. Using the ratio of the standard error of the measured data to that of the standard data and so on as feature quantities, the behavior of pressure is judged to be "normal" and "abnormal" (2 class classification) utilizing a two-layer neural network. The classification criteria are previously learned from actual abnormal behaviors of pressures when vacuum troubles occurred since 2016. A simulation test using the actual beam abort events from May 2022 showed that signs of pressure anomalies can be detected. Here we report on the status of the study on this pressure anomaly detection method.

**8:20am VT-TuM-2 NEG Coating for PETRA IV: Resistivity and Sticking Probability Measurements, Ruta Sirvinskaite, L. Lilje, S. Lederer, R. Boespflug, N. Plambeck, S. Antipov, M. Schroeder, A. Winiarska, DESY, Germany**

Non-Evaporable Getter (NEG) development at DESY has been ongoing to accommodate PETRA IV machine requirements. While most of the PETRA IV beam vacuum chambers will be manufactured from oxygen-free silver-bearing (OFS) copper and coated with NEG, getter film performance on these substrates has not been tested as extensively as on the stainless-steel. In order to investigate pumping and impedance properties of the columnar NEG films, TiZrV and Zr layers with varying thicknesses were sputtered on four Cu-OFS tubes. The 1  $\mu\text{m}$  films were activated at temperatures ranging from 140 to 250  $^{\circ}\text{C}$  to determine how the sticking probability as well as CO pumping capacity develops over time after multiple saturations prior to increasing the activation temperature. By measuring the attenuation of the RF signal along the four tubes, resistivity of both NEG materials was calculated. The results were then compared to previously reported findings for columnar NEG films.

**8:40am VT-TuM-3 Vacuum System for Cornell Brookhaven Energy Recovery Linac Test Accelerator, Yulin Li, D. Burke, Cornell University**

A novel electron accelerator, Cornell Brookhaven Cornell Energy Recovery LINAC Test Accelerator (CBETA) has been successfully designed, constructed, installed and commissioned by collaboration between CLASSE and Brookhaven National Laboratory. Many unique accelerator technologies are implemented in CBETA, including photo-cathode electron injector, 4-turn superconducting RF (SRF) Energy Recover LINAC (ERL), non-scaling Fixed-Field Alternating Gradient (NS-FFAG) optics with 4x energy acceptance. The CBETA layout consists of an existing photo-cathode injector with an SRF cryomodule (ICM) as well as a main LINAC cryomodule (MLC), a NS-FFA return loop (that transports electron beams at four energies, 42, 78, 114 and 150 MeV in a single bore beam pipe), and two splitter sections where the four energy beams are separated and combined. The total circumference of the CBETA loop is about 80-m. The basic requirement of the CBETA vacuum system is to achieve an adequate level of vacuum and physical aperture for transporting electron beams at four different energies. Furthermore, by the nature of this test accelerator, the vacuum system engineering must accommodate a very high density of beam diagnostics tools, such as over 150 beam position monitors, and insertable beam profile viewers. Beam path length change of up to 20 $^{\circ}$  RF-phase are achieved in the splitter sections via one set of three RF-shielded sliding joints mounted on a pair of motorized stages in each of the eight-splitter beam lines. Aluminum alloy was chosen as primary beam pipe construction material because of its good electric conductivity (resistive-wall), no residual radioactivity (from beam losses), low magnetization (from cold work and welding etc.) as well as its low cost of fabrication (machining,

extrusion, etc.). Compact non-evaporable getter (NEG) pumps are used due to the space constraints. To preserve the high performance of the superconducting RF cavities in the MLC, all vacuum beam line components were constructed and assembled in strict particulate-controlled condition, and installed using portable clean rooms. The CBETA vacuum system installation was completed in the summer of 2019 and the entire CBETA accelerator system was commissioned shortly after. All CBTA milestones were successfully achieved, including full beam energy recovery after 8 turns of beam circulations through the SRF cavities and the NS-FFA return loop. We present the CBETA vacuum component construction and installation, and the vacuum system operational experiences.

**9:00am VT-TuM-4 Operational Experiences of NEG Dominated Pumping System at CHESS-U, Leila Aboharb, Cornell University**

Successful operations of the Cornell High Energy Synchrotron Source Upgrade (CHESS-U) have proven the in-service reliability of the compact non-evaporable getter (NEG) pumps in a new experimental vacuum system predominantly pumped with distributed NEG-strips and modular high-capacity NEG pumps. The 80-meter section improvement in the Cornell Electron Storage Ring (CESR) is composed of 6 double-bend achromats operating with a single positron beam up to 200 mA. After a successful commissioning period, a vacuum level of 10 $^{-9}$  Torr was achieved with minimal maintenance and NEG re-activations.

The CHESS-U vacuum system experienced a catastrophic failure when a beam steering error created a pinhole leak in an undulator vacuum chamber (0.6-mm wall). The installed NEG-dominated pumping system had demonstrated an adequate pumping performance, which allowed a quick recovery and reconditioning of the affected 20+ meter vacuum section. With the hard work of the technical staff, X-ray user operations were able to resume after 10 days of recovery efforts (chamber fabrication and replacement, vacuum conditioning). The accidental air-exposure to the NexTorr pumps (combination of ion pump and NEG) resulted in minor Argon instability issues that required mitigation. Corrective actions were developed in areas such as thermal monitoring, chamber construction, and beam steering while also granting the opportunity to test the pumping integrity of the effected NEG pumps after the exposure.

The 3-year operational experiences of the NEG pumping system will be presented.

**9:20am VT-TuM-5 ALS-U Vacuum Systems Production QA/QC Process, Sol Omolayo, Lawrence Berkeley Lab, University of California, Berkeley**

The Advanced Light Source at Lawrence Berkeley National Lab is in the process of being upgraded to a 4th generation light source. The upgrade requires thousands of vacuum components to be procured, fabricated, inspected, assembled and installed. QA/QC is paramount concerned in ensuring the vacuum system meets requirement. A process was developed to manage QA/QC from the design phase to the installation and commissioning

**9:40am VT-TuM-6 Exploring Large Vacuum Systems at LIGO: A Brief Introduction to the Vacuum Challenges of the Cosmic Explorer, Melina Fuentes-Garcia, LIGO Laboratory, California Institute of Technology; J. Feicht, California Institute of Technology**

The Laser Interferometer Gravitational-Wave Observatory (LIGO) consists of a set of multi-kilometer-scale gravitational wave detectors able to detect major events in our universe, such as black hole pair collisions. Because of stringent noise requirements, LIGO operates in an ultra-high-vacuum environment to minimize disturbance to the laser, optics, and other equipment inside the chambers. Factors such as material outgassing, contamination control, seal integrity, and pumping must all be optimized for minimal disturbance to the detectors. Cosmic Explorer (CE) aims to increase LIGO's sensitivity tenfold by scaling LIGO's 4 km long vacuum arms to 40 km, which amounts to a 90-million-liter vacuum system nominally sustained at 1E-9 Torr. This next-generation detector will significantly enhance our ability to detect gravitational waves, but will require greater challenges to the design and construction of its large vacuum system. Here we introduce some of the major challenges currently being studied, with an emphasis on the selection of alternate beam tube materials and elimination of high temperature bakeouts to reduce outgassing.

# Tuesday Morning, November 7, 2023

11:00am **VT-TuM-10 Exploring the Gravitational Wave Universe: Vacuum Systems for LIGO A+ and Beyond**, *Michael Zucker*, LIGO Laboratory, Caltech and MIT **INVITED**

LIGO, the Laser Interferometer Gravitational-wave Observatory, recently completed the first phase of an upgrade called A+. This has improved sensitivity to gravitational waves from distant colliding black holes, neutron stars and other astrophysical phenomena by effectively circumventing the Heisenberg uncertainty principle, using a new quantum engineering technique called *Frequency-Dependent Squeezing* (FDS). An extension of both LIGO vacuum systems was required to enable this new technique. FDS is also an important step toward realizing vastly improved next-generation gravitational wave instruments, such as the *Einstein Telescope* and *Cosmic Explorer*, planned for the next two decades. These instruments will extend the realm of gravitational wave observations to the edge of the observable universe. Such new facilities will rely on ultrahigh vacuum at unprecedented scale, up to an order of magnitude larger than present instruments, presenting novel design and engineering challenges.

11:40am **VT-TuM-12 A Cryogenically Cooled Water Trap for ITER's Vacuum System**, *Jared Tippens, C. Smith III*, Oak Ridge National Laboratory

The ITER project has the goal to demonstrate the feasibility of fusion and to advance the scientific and engineering understanding of fusion for future commercial reactors. The vacuum systems that are under development for the tokamak and supporting systems are expected to be dominated by one-of-a-kind devices due to their scale and varying operating environments. One specific challenge for these devices is the ability to process and recycle tritium, a radioactive hydrogen isotope in the fuel that is necessary for the fusion reaction to occur but is rare on Earth. Additionally, several of the vacuum systems are sensitive to water vapor which has the capability to inhibit pump performance if not removed from the gas stream. A custom designed water trap can enable both requirements to be met, and four of them are planned for the ITER vacuum system.

Due to vacuum operating pressures (as low as 1 Pa), a desiccant such as Zeolite cannot be efficiently used to adsorb and retain water vapor, so an alternative approach was chosen to utilize a cryogenically cooled water trap to desublimates water vapor from the process gas. The temperature must be lowered enough to remove the water vapor from the stream, but not so low as to remove the helium and gaseous hydrogen isotopes. With helium at a temperature of 80K available in ITER's vacuum pumping room, this cooling load was selected as source for the water trap cooling.

To comply with the nuclear requirements, the tritium content inside the trap must be continuously monitored and removed to exhaust processing. The water trap must also be a double contained vacuum vessel with safety switches to mitigate the risk of tritium exposure to the vacuum pumping room. The tritiated water stored within must be removed batchwise to exhaust processing using heaters and inert purge gas. The capacity of the trap must be large (up to 5 kg of water) to account for the unlikely event of gross system water leaks, but in practice will accumulate water vapor at a low and steady rate of 1 Pa.m<sup>3</sup>/s. Each trap must fit within a 1 meter diameter by 1 meter tall space reservation and include embedded tubes that enable heat transfer between the cryogenic helium and the process gas.

In summary, a cryogenically cooled water trap has been designed to meet the unique requirements of ITER and its vacuum systems. Four of these traps will protect sensitive vacuum equipment from water vapor as well as enable the recycling of tritium back into the fuel.

12:00pm **VT-TuM-13 Photon Stimulated Desorption Beamline at NSLSII**, *M. Ferreira*, ESS, Sweden; *S. Hulbert, P. Palecek, I. Saleh, M. Seegitz, T. Shaftan, O. Tchoubar, Robert Todd*, Brookhaven National Laboratory

Understanding the expected gas desorption of an accelerator is critical in the proper design of accelerator vacuum systems and can have a major impact on the machine design and cost. From some of the earliest work on the subject for the Cambridge Electron Accelerator up through and including LHC, desorption measurements have played an important role in predicting vacuum behavior of large accelerators susceptible to synchrotron radiation. Much of this early work served well the machines they applied to and other machines with similar parameters and material choices. But as machines continue to be developed with higher energy, beam current, stability and susceptibility to e-cloud, novel materials need to be investigated to improve vacuum, and in some cases reduce SEY (Secondary Electron Yield). Part of these investigations require careful study of their desorption yields. This would benefit future upgrades to the existing NSLS-II facility as well as other synchrotrons facilities with stringent design

specifications. Additionally, such a beamline could have a major impact on the selection and validation of proposed materials and components for EIC, including possible coatings for the electron storage ring, IRs (Interaction Regions) and the beam screen of the Hadron/Ion ring. Desorption rates of these newly proposed materials would be used as inputs to advanced modeling tools such as Molflow and SynRad for accurate predictions of vacuum behavior. A beamline at NSLS-II, dedicated to the PSD/ESD study of novel and proposed vacuum materials has been constructed and commissioned to advance further research into desorption behavior. The PSD of stainless steel and OFHC copper to be used for the Rapid Cycling Synchrotron of EIC have been measured and compared to prior work to baseline the system, with plans to evaluate the NEG coated chambers for the EIC electron storage ring. The layout of the experimental line and the commissioning measurements will be presented.

# Tuesday Afternoon, November 7, 2023

## Exhibitor Technology Spotlight Workshops

### Room Exhibit Halls A-B Booth 1003 - Session EW-TuL

#### Exhibitor Technology Spotlight Session I

Moderator: Christopher Moffitt, Kratos Analytical Inc

#### 12:00pm EW-TuL-1 Challenges and Solutions for Ion Energy and Ion Flux Measurements in Plasma-Assisted Etching and Deposition Processes, Angus McCarter, Impedans

This work demonstrates the role of energetic ions in plasmas and how they affect the properties of materials etched or deposited in thin-film plasma processing. We will show how to use measured ion flux, ion energies and ion-neutral fractions to optimize industrial plasma-assisted processes. For this purpose, ion energy and ion flux measurements were carried out using fully automated advanced Retarding Field Energy Analyzers (RFEA's) by Impedans Ltd [1, 2]. The Semion RFEA measures the ion energies hitting a surface, the ion flux, negative ions and bias voltage at any position inside a plasma chamber using an array of integrated sensors. On the other hand, the Quantum system is an energy resolving gridded quartz crystal microbalance (QCM), used to measure the ion-neutral fraction hitting a surface inside a plasma reactor. This instrument also measures the etching/deposition rate, ion energy, ion flux and bias voltage.

Firstly, this talk will give general insights into how ions behave under different chamber and bias conditions. Then we will present a review of thin-film applications, particularly focusing on plasma-assisted Atomic Layer Deposition (ALD) and Atomic Layer Etching (ALE) processes is presented in detail [3-5]. This will include discussion on the impact of substrate biasing on the ion energy distribution (IED), impact of ion impingement on the chemical and microstructural properties of thin-films. The continuously decreasing feature sizes and aspect ratio dependent profiles need special techniques to control precisely the ion energies and flux of ions and neutrals responsible for the undergoing process. Pulsing the source and/or the bias voltages, or applying tailored voltage waveforms as biases, are techniques used to control the ion bombardment energy as well as for precise ion energy control. We will highlight the successful measurements done by Semion in such applications enabling accurate and precise control of etching profiles on different materials and various plasma chemistries.

#### References

- [1] Impedans Ltd, Dublin, Ireland [www.impedans.com]
- [2] S. Sharma et al., Ph.D. Thesis, Dublin City University (2016)
- [3] H. B. Profijt et al., J. Vac. Sci. Technol. A 31, 1 (2013)
- [4] M. H. Heyne et al., 2D Mater. 6, 035030 (2019)
- [5] S. Karwal et al., Plasma Chemistry and Plasma Processing 40, 697–712 (2020)

12:20pm EW-TuL-2 Advance in Momentum Microscopy with NanoESCA MARIS, Marten Patt, N. Weber, M. Escher, T. Kühn, FOCUS GmbH, Germany  
Since its introduction in 2005, the energy-filtered photoelectron microscope NanoESCA [1,2] has been used for various application including work-function mapping, imaging XPS and in the last years more prominently for imaging the reciprocal space, i.e., momentum microscopy or orbital tomography (e.g., at the NanoESCA at synchrotron Elettra, Trieste [3]).

The latest revision of the analyzer, called NanoESCA MARIS, has a new microscope lens. It was designed to achieve a better angular / momentum resolution while keeping the same good real space resolution < 35 nm from its predecessor. In momentum space mode, the instrument achieves a resolution of 0.005 Å<sup>-1</sup>. We will show the performance on the Rashba split surface state of a Au (111) single crystal.

In addition, new working modes, like off-axis zoom, double dispersive imaging mode and an energy dispersion snapshot mode were introduced with the new analyzer and will be presented. Developments in the Imaging Spin Filter for NanoESCA [4] will be discussed.

#### References

- [1] M. Escher et al., J. Phys. Cond. Matter 17 (2005)

[2] B. Krömker et al., Rev. Sci. Instrum. 79 (2008)

[3] M. Wießner et al., Nature Comm. 5(2014) 4156

[4] M. Escher et al., Ultramicroscopy 253 (2023) 113814

#### 12:40pm EW-TuL-3 New Developments for Surface Analysis from Thermo Fisher Scientific, Adam Bushell, T. Nunney, P. Mack, R. Simpson, H. Tseng, Thermo Fisher Scientific, UK

In this presentation we will present the latest innovations in instrumentation for Surface analysis and materials analysis from Thermo Fisher Scientific.

#### 1:00pm EW-TuL-4 Driving Discoveries Through Surface Analysis, J. Mann, Greg Fisher, Physical Electronics

Physical Electronics (PHI) is the only manufacturer offering surface analysis products for all three main analytical techniques – X-ray photoelectron spectroscopy (XPS), Auger electron spectroscopy (AES) and time-of-flight secondary ion mass spectrometry (TOF-SIMS). This presentation will discuss recent developments in TOF-SIMS and XPS, including the power of artificial intelligence for fast and reliable identification of species, unattended analysis for high throughput, and combining photoemission spectra from different analysis depths for thin film analysis. Our fully automated XPS system offers unprecedented value not found in conventional XPS instruments, by using multiple techniques covering a full range of energy - from conduction band with low energy inverse photoemission spectroscopy (LEIPS) to core-level excitation with hard X-ray photoelectron spectroscopy (HAXPES). The PHI TOF-SIMS instruments are optimized for the highest sensitivity elemental and molecular analysis, allowing detection of species in the ppm range. Our scanning AES instrument is optimized for high magnification chemical imaging and has increased versatility with multiple optional technique add-ons and accessories for specialized experiments.

#### 1:20pm EW-TuL-5 EnrivoMETROS – Advanced Surface Hybrid Metrology, Stefan Böttcher, SPECS Surface Nano Analysis GmbH, Germany

The SPECS EnrivoMETROS is a new generation hybrid surface metrology system for precise surface analysis and quantification. The correct stoichiometric, chemical and dimensional analysis of surfaces and layered materials is a highly relevant task in modern device development and fabrication. In addition, information on electronic properties provides a comprehensive picture of the sample under investigation. We present the latest technological advances in tool design and discuss key applications in scientific and industrial environments, focusing on correct layer analysis, electronic structure analysis for semiconductor characterization, and handling of technologically relevant sample formats under various conditions.

#### 1:40pm EW-TuL-6 Kratos Axis Supra+ -- Automated, Quantitative HAXPES for Advanced Materials Development, Chris Moffitt, Kratos Analytical Inc.

The automation of modern instrumentation allows for broader access to more robust analysis over larger sample sets with advanced approaches. Kratos Axis Supra+ incorporates automated sample handling with automated analysis of XPS, UPS, depth profiling and others, including higher energy Ag-L $\alpha$  generated, quantitative HAXPES, for increased depth analysis.

The Axis Supra+ allows more samples to be analyzed with the full capabilities of the highest-performing XPS instrument, without intervention. Once samples are physically loaded, analyses are submitted through the computer interface, utilizing multiple cameras for location identification, which can be done remotely. This follows on for utilizing the HAXPES mono source, so that analysis by standard Al-K $\alpha$  monochromatic x-rays can be automatically followed by analysis with the higher energy Ag-La monochromatic source and the results automatically processed and quantified using new Data Dependent Acquisition software features.

The Axis Supra+ is uncompromised in its ability to analyze the wide range of new advanced materials, including operando surface analysis measurement of battery materials while biasing or flowing current and heating. The multi-contact stage in the Axis Supra+ spectrometer accommodates the specialized holders for the operando analysis, supplying 4 electrical contacts to be used for these analyses, while still accepting all the standard sample platens for high throughput analysis. An inert sample transfer version of these multi-contact holders has also been developed, which allows the sample to be loaded and electrical connections made in a glove box and then loaded into the spectrometer without exposure to atmosphere.

Soft materials analysis has greatly expanded in the last several years since the introduction of argon gas cluster ion sources (GCIS), with the Kratos

# Tuesday Afternoon, November 7, 2023

dual mode cluster source also able to perform traditional monoatomic argon profiling of hard inorganic materials. The cluster mode is able to profile light ion materials without the artifacts inherent in monoatomic sputter-etching of these materials.

Additional analytical techniques, such as Ag-L $\alpha$  HAXPES, ISS, UPS, AES, REELS and IPES are all possible on the Supra<sup>+</sup>, and additional sample preparation chambers can be easily added, such as a station for deposition or the high-pressure, high-temperature gas reaction cell for catalysis experiments and measurement.

2:00pm **EW-TuL-7 VON ARDENNE: Shaping the Future of Coating Technologies to tackle Today's Challenges in Global Industries**, *Daniel Radach, B. Coll, B. Cohen, J. Rajan, P. Burke*, VON ARDENNE North America, Inc.

Since its inception in 1928, VON ARDENNE has grown into the world-renowned VON ARDENNE Group. As a family-owned entity headquartered in Dresden, Germany, the organization boasts a vast global footprint spanning more than 50 countries and harnessing the talents of over 1,000 dedicated employees. With a remarkable portfolio of over 650 patents worldwide, the company's innovative prowess has led to the successful installation of over 550 advanced coating systems worldwide.

VON ARDENNE's unique coating skills are at the forefront of tackling pressing global challenges, within energy, mobility, and connectivity sectors. The company's innovative capabilities extend to diverse industries, from solar cells and modules to smart glass and touch screens, batteries, fuel cells and electrolysis systems, and even the aerospace industry with turbine blade coating requirements. VON ARDENNE's success is based on key technologies perfected over half a century. These include expertise in electron beam and vacuum coating processes, encompassing magnetron sputtering, double rotary magnetrons, high-power electron beam guns, and thermal evaporation technologies. These capabilities translate into a comprehensive range of equipment, designed to meet a variety of needs – from small-scale laboratory tools for R&D, to medium-sized pilot tools, to large-scale mass production systems with very high throughput. We have acquired excellent process know-how based on the numerous coating systems which we have installed over the years.

VON ARDENNE's global activities are supported by a strong network of engineering, production, sales, and service centers located in key regions such as North America, Japan, China, India, Malaysia, Vietnam, and the company's German headquarters. The company's strengths include the ability to provide customized solutions ('Engineering to Order'), comprehensive qualification and ramp-up support, scalability and reproducibility, and a strong global service network. Concrete case studies illustrating VON ARDENNE's solutions, particularly in the field of crystalline silicon and thin-film photovoltaic cell technologies, highlight the company's technical skills, adaptability, and unwavering commitment to serving its global customer base with state-of-the-art high productivity and low Cost of Ownership (CoO) solutions.

As VON ARDENNE's legacy continues to fuel innovative breakthroughs in vacuum, plasma, sputtering and electron beam technologies, the company stands as a catalyst for significant contributions to global industries, ready to tackle the challenges of a rapidly changing world.

## 2D Materials Technical Group

Room C123 - Session 2D+TF-TuA

### 2D-Materials: Synthesis

Moderators: David Johnson, University of Oregon, Peter Liljeroth, Aalto University

#### 2:20pm 2D+TF-TuA-1 High-Order Van Der Waals Superlattices and Artificial Quantum Solid Beyond Mechanical Exfoliation and Restacking, *Xiangfeng Duan*, UCLA

INVITED

The advent of two-dimensional atomic crystals (2DACs) and van der Waals heterostructures (vdWHs) has inspired a new thinking on heterostructure construction beyond the limits of lattice matching requirement. However, the vdWHs explored to date have been largely limited to relatively simple systems with a small number of building blocks. The preparation of high-order vdW superlattices with a larger number of alternating units is exponentially more challenging due to the limited yield and scalability of the commonly used exfoliation-and-restacking strategy. Here I will discuss strategies to create high-order vdW superlattices (vdWSLs). First, by exploiting a capillary-force-driven rolling-up process, we show a series of synthetic VDWHs can be transformed into high-order vdWSLs with alternating atomic layers of widely variable material compositions, electronic band offset dimensions, chirality and topology. Alternatively, we further discuss a molecular intercalation approach to prepare a new family of hybrid superlattices consisting of alternating layers of covalently bonded 2D atomic layers and self-assembled molecular layers, which opens the door to exploit highly versatile molecular design strategies to tailor solid-state materials, enabling artificial materials with designable structural motifs and tunable electronic properties beyond the reach of conventional crystalline solids. We will particularly highlight a recent example of a new class of chiral molecular intercalation superlattices with robust chiral-induced spin selectivity. The formation of high-order vdW superlattices defines a rich artificial materials platform to unlock previously inaccessible physical limits and enable new device concepts beyond the reach of the existing materials.

#### 3:00pm 2D+TF-TuA-3 Understanding the Sequential Growth of Bilayer MoS<sub>2</sub> on SiO<sub>2</sub> Substrate by Mo Isotope Labeling, *Kai Xiao*, Center for Nanophase and Materials Sciences Oak Ridge National Laboratory; *Y. Yu*, School of Physics and Technology, Wuhan University, China; *J. Hachtel*, Center for Nanophase and Materials Sciences Oak Ridge National Laboratory; *M. Yoon*, Material Science and Technology Division, Oak Ridge National Laboratory; *A. Puzetzyk*, *A. Ievlev*, *C. Rouleau*, *D. Geohagan*, Center for Nanophase and Materials Sciences Oak Ridge National Laboratory

Bilayer 2D materials and heterostructures with different stacking configurations have attracted interest due to their emerging optical and quantum properties. Usually, it can be synthesized by the two-step chemical vapor deposition (CVD) method. Here we utilized isotope labeling method to study the CVD growth of bilayer MoS<sub>2</sub> on SiO<sub>2</sub>/Si substrates. The stacking configuration and growth sequence were characterized by Raman spectroscopy, time-of-flight second ion mass spectroscopy (ToF-SIMS), and scanning transmission electron microscopy (STEM). We found that the growth of bilayer MoS<sub>2</sub> follows a sequential growth process which the second growth layer of MoS<sub>2</sub> goes underneath the first growth layer. The AB and AA stacked bilayer MoS<sub>2</sub> are formed by templating the first growth single crystal MoS<sub>2</sub> layers. The embedded antiphase grain boundaries were characterized by atomic-resolution z-contrast STEM. Density functional theory (DFT) with molecular dynamic (MD) simulation were performed to understand the sequence growth pathway of bilayer MoS<sub>2</sub>. This new understanding of the growth mechanism for bilayer MoS<sub>2</sub> can provide a new strategy for synthesis of 2D materials with controllable layer numbers and stackings.

Synthesis science was supported by the U.S. Dept. of Energy, Office of Science, Materials Science and Engineering Division. This work was performed at the Center for Nanophase Materials Sciences, which is a DOE Office of Science User Facility.

#### 4:20pm 2D+TF-TuA-7 The Transformation from Dendritic to Triangular WS<sub>2</sub> Growth via NaCl-Assisted Low-Pressure Chemical Vapor Deposition, *Himal Pokhrel*, *J. Duncan*, *S. Pollard*, The University of Memphis

Monolayer tungsten disulfide (WS<sub>2</sub>) is one of the promising two-dimensional materials in the transition metal dichalcogenide family due to its remarkable optical, electronic, and electrocatalytic behavior. However, the structure of this material varies significantly with growth conditions. In this work, we use the salt-assisted low-pressure chemical vapor deposition

(LPCVD) method to grow monolayer WS<sub>2</sub> crystals reaching over 50 μm in size on the SiO<sub>2</sub>/Si substrates. We observe a transition from large, dendritic to triangular growth by systematically varying the amount of promoter material (NaCl), growth temperature, and source-substrate distance. The synthesized material is characterized by Raman spectroscopy, scanning electron microscopy, and X-ray photoemission spectroscopy in order to understand the role of each parameter during the growth process. The results of this work provide a framework for the synthesis of large-area WS<sub>2</sub> growth with variable morphology through salt-assisted LP-CVD.

Key words: Chemical vapor deposition, dendrites, WS<sub>2</sub>

#### 4:40pm 2D+TF-TuA-8 Hybrid Pulsed Laser Deposition Growth of Layered Chalcogenides, *Mythili Surendran*, *H. Chen*, *J. Ravichandran*, University of Southern California

Mythili Surendran<sup>1</sup>, Huandong Chen<sup>1</sup>, Shantanu Singh<sup>1</sup>, Boyang Zhao<sup>1</sup> and Jayakanth Ravichandran<sup>1</sup>

58. Mork Family Department of Chemical Engineering and Materials Science, University of Southern California

Chalcogenides, especially layered transition metal dichalcogenides, have emerged as an exciting class of materials that host several novel physical phenomena suitable for a broad range of electronic and photonic applications. High-quality thin film growth of these chalcogenides is critical to enable investigations into their fundamental properties and also for device applications. The thin films of layered chalcogenides are mostly grown using chemical vapor deposition, although molecular beam epitaxy, metal-organic vapor deposition, pulsed laser deposition (PLD) and several other techniques have been exploited. However, large area and high-quality growth with precise and uniform thickness control and low defect densities still remain a challenge due to a large cation-chalcogen vapor pressure mismatch, corrosive and reactive nature of most chalcogen precursors, high synthesis temperatures and the propensity to oxidize easily in the presence of oxygen at these high temperatures. In case of metal disulfides, most growth techniques utilize H<sub>2</sub>S as the sulfur source. However, H<sub>2</sub>S is a toxic, hazardous, and flammable gas and require high temperatures for efficient decomposition and sulfurization, resulting in high defect densities.

Here, we report an alternative hybrid PLD approach wherein we employed organo-sulfur precursors as sulfur source to grow chalcogenide thin films. This novel method enables low temperature growth (~500°C) of chalcogenides as the precursors decompose at a lower temperature (~250-400°C) to provide dissociated sulfur species. To demonstrate the efficacy of this approach, we have demonstrated large area epitaxial growth of Group IV 2D chalcogenides such as TiS<sub>2</sub> (metallic), ZrS<sub>2</sub> and HfS<sub>2</sub> (semiconducting). Structural and electrical characterization, along with low temperature transport studies reveal low defect densities and high carrier mobilities in these thin films. These results emphasize the importance of development of low temperature growth techniques for high mobility refractory metal-based chalcogenides for electronic applications, especially with back-end-of-line (BEOL) compatibility. The potential of these chalcogenides as suitable candidates for transparent and conducting layers in chalcogenide-based optoelectronic devices will be discussed. Further, we will also briefly discuss about the epitaxial growth of a variety of other chalcogenides such as 3D metal chalcogenides, chalcogenide perovskites, thus establishing the versatility of this novel method to grow chalcogenides for next-generation electronics and photonics.

#### 5:00pm 2D+TF-TuA-9 Effect of Several Growth Parameters on Graphene Growth on Four Types of Supported Cu Films Using Cold Wall Cvd and Perspective on Growth Mechanism of Graphene from Scaling Functions of Graphene Island Size Distribution, *Shantanu Das*, Intel Corporation

Graphene growth was explored on solid electrodeposited, recrystallized, sputter deposited and liquid Cu films supported on W or Mo refractory substrates under ambient pressure using Ar, H<sub>2</sub> and CH<sub>4</sub> mixtures using a custom-automated LabVIEW controlled graphene growth method in a custom-modified multi-chamber UHV chamber transformed into a cold wall CVD system. Among these films, electrodeposited Cu film was chosen to study the effect of total flow rate, CH<sub>4</sub>:H<sub>2</sub> ratio and dilution of the CH<sub>4</sub>/H<sub>2</sub> mixture by Ar at a fixed substrate temperature of 1000 °C and total pressure of 700 Torr, on the nucleation density and average size of graphene crystallites. The resulting morphological changes correspond with those that would be expected if the precursor deposition rate was varied at a fixed substrate temperature for physical deposition using thermal evaporation. The evolution of graphene crystallite boundary morphology

# Tuesday Afternoon, November 7, 2023

with decreasing effective C deposition rate indicates the role of edge diffusion of C atoms along the crystallite boundaries, in addition to H<sub>2</sub> etching on graphene crystallite shape. The results indicate that graphene grown on Cu films using cold wall CVD follows a classical two-dimensional nucleation and growth mechanism. Following nucleation at the earliest growth stages, isolated crystallites grow, impinge and coalesce to form a continuous layer. During the pre-coalescence growth regime, the size distributions of graphene crystallites exhibit scaling which is a function of island area, graphene coverage, average island area and areal density. For graphene grown on Cu surfaces that have been annealed in a reducing Ar+H<sub>2</sub> ambient, excellent data collapse onto a monotonically decreasing universal Avrami scaling function is observed irrespective of graphene coverage, surface roughness or Cu grain size. This result is interpreted to indicate attachment limited growth and desorption of C-containing species. Graphene grown on Cu surfaces that were annealed in a nonreducing environment exhibits a qualitatively different bimodal scaling function indicating diffusion-limited growth with a lower attachment barrier combined with C detachment from the graphene edges. Graphene growth on molten Cu films supported on custom-designed Mo substrates demonstrate a similar 2D nucleation and growth mechanism. The roles of temperature gradient, chamber pressure and rapid thermal heating in C precursor-rich environment on graphene growth morphology on thin sputtered Cu films are explained. I anticipate that applying the study of pre-coalescence size distribution method to other 2D material systems may be useful for elucidating atomistic mechanisms of film growth that are otherwise difficult to obtain.

5:20pm **2D+TF-TuA-10 Decoupling of Graphene from Metal Substrate via Interface Epitaxy**, *Abdullah Al-Mahboob, J. Sadowski*, Center for Functional Nanomaterials, Brookhaven National Laboratory

The research on two-dimensional quantum materials (2DQM) received significant attention in both, theoretical and experimental physics. Among 2DQM systems, graphene (Gr) remains a material of special interest since its discovery three decades ago. The interest in 2DQM research further evolved beyond Gr and its analogs (called Xenex) as these materials have potential for technological applications including quantum computing and quantum information.

The interest on Gr originated not only from well-known Gr stability in ambient conditions, massless Dirac carrier characteristics and feasibility of roll-to-roll production, but also successful use of Gr as a template for other 2DQMs. Despite the interest in Xenex other than Gr, such as silicene, antimonene, borophene, these materials are generally unstable at ambient conditions. In order to protect reactive Xenex and stabilizing their structure, Gr can also be used as a protective inert coating. In the present study we explored a method of interfacial 2D growth under the inert overlayer, graphene.

We employed in-situ real-time low-energy electron/photoemission electron microscopy (LEEM/PEEM), micro-beam LEED, XPS/UPS and micro-spot ARPES for the study of interface chemistry of silicon allotropes and 2D silica structures grown at the Gr/Ru interface.

In this report, we show how the Si interface epitaxy can decouple Gr electronically from the catalyst Ru substrate, and a successful scalable synthesis of Gr/V<sub>3</sub>-Silicene and Gr/Si/SiO<sub>2</sub> heterostructures can be realized. Tuning the growth conditions also provided means to control the growth of 2DQM at large scale. The strategy of interface epitaxy could be more general and opens the avenue of growing and stabilizing other atomically thin 2D materials.

Research was carried out at the Center for Functional Nanomaterials and the National Synchrotron Light Source II at Brookhaven National Laboratory under Contract No. DE-SC0012704.

5:40pm **2D+TF-TuA-11 Wafer-Scale, Phase-Selective Growth of Two-Dimensional Indium Selenides by Metal-Organic Chemical Vapor Deposition**, *Seunguk Song, S. Jeon, M. Rahaman, J. Lynch, D. Rhee, P. Kumar, S. Chakravarthi, G. Kim, X. Du*, University of Pennsylvania; *E. Blanton*, KBR Inc.; *K. Kisslinger*, Brookhaven National Laboratory; *M. Snure*, Air Force Research Laboratory, Sensors Directorate; *N. Glavin*, Air Force Research Laboratory, Materials and Manufacturing Directorate, USA; *E. Stach, R. Olsson III, D. Jariwala*, University of Pennsylvania

The two-dimensional (2D) indium selenides (InSe and In<sub>2</sub>Se<sub>3</sub>) have garnered attention as a highly desirable ultrathin III-VI semiconductor, possessing favorable qualities akin to III-V semiconductors and 2D van der Waals transition metal dichalcogenides. However, due to the complexity of the In-Se system and challenges related to promoting lateral growth, large-area, *Tuesday Afternoon, November 7, 2023*

phase-selective synthesis of 2D InSe and In<sub>2</sub>Se<sub>3</sub> has proved difficult. Here, our work presents a successful method for the growth of high-quality and thickness-controlled 2D InSe and In<sub>2</sub>Se<sub>3</sub> thin films using vertical, cold-walled metal-organic chemical vapor deposition. By interrupting the Se source periodically, we create an environment deficient in Se that favors the nucleation of InSe over In<sub>2</sub>Se<sub>3</sub>. Additionally, pulsing the Se precursor promotes lateral growth of InSe at low temperatures (360-500 °C), allowing us to produce highly stoichiometric, crystalline thin films on 2-inch sapphire substrates. Importantly, these growth temperatures are compatible with back-end-of-line integration in Si microelectronics. The resulting 2D domains are oriented along the crystal structure of the substrate, and the thickness can be controlled by growth time. We also demonstrate the fabrication of few-layer InSe transistors with high on-to-off current ratios (~10<sup>4</sup>-10<sup>5</sup>) and field-effect mobility (~2.8 cm<sup>2</sup>V<sup>-1</sup>s<sup>-1</sup>) comparable to that of mechanically exfoliated single crystals of InSe. In the case of a few-layer In<sub>2</sub>Se<sub>3</sub>, its inherent ferroelectric nature allows us to evaluate its potential as a ferroelectric semiconductor field-effect transistor with non-volatile memory. Our work offers a promising approach for creating phase-pure 2D InSe and In<sub>2</sub>Se<sub>3</sub> films at the wafer scale, which can be adapted for other material systems with multiple polymorphs.

## Actinides and Rare Earths Focus Topic Room C124 - Session AC+MI+TH-TuA

### Chemistry and Physics of the Actinides/Rare Earths

**Moderators:** *Ladislav Havela*, Charles University, Czech Republic, *Eteri Svanidze*, Max Planck Institute for Chemical Physics of Solids, *Gertrud Zwiznagl*, Technical University Braunschweig

2:20pm **AC+MI+TH-TuA-1 Electronic Structure Methods for f-Block Elements: Are We There Yet?**, *X. Li, Chad Hoyer*, University of Washington  
**INVITED**

The computational modeling of rare-earth and heavy-element complexes requires an accurate treatment of spin-orbit and electron correlation effects to fully understand the physical underpinnings of their chemical properties. The fully correlated frequency-independent Dirac-Coulomb-Breit Hamiltonian in a multireference framework provides the most accurate description of electron-electron interaction before going to a genuine relativistic quantum electrodynamics theory of many-electron systems. Our recent studies using many-body multireference methods suggest that there is a significant correlation effect of inner-valence electrons in rare-earth and heavy-element complexes. Ignoring this effect could lead to inaccurate descriptions of molecular properties, such as covalency, bonding, and spectroscopic response. In this talk, we will examine how the correlation effect of inner-valence electrons is manifested in molecular properties with a focus on the covalency in rare-earth and heavy-element complexes.

3:00pm **AC+MI+TH-TuA-3 Structures and Electronic States of Actinide and Lanthanide Complexes with Phenanthroline Derivatives**, *Tsuyoshi Yaita*, Japan Atomic Energy Agency, Japan  
**INVITED**

Actinides and lanthanides are f-electron elements, and thus their chemical behavior is very similar if they have the same valence. Recently, the demand for lanthanides, especially specific lanthanides such as Nd, Tb, and Dy, is increasing with the realization of a carbon-neutral society and the shift to EVs for vehicle, and there is a growing need to find new resources and recycle them from urban mines. On the other hand, in the case of geological disposal of radioactive waste generated from nuclear power generation, separation of minor actinides such as Am, which are long-lived  $\alpha$ -nuclides, is very important from the viewpoint of recycling in a geological repository in a small country like Japan, and the establishment of separation and transmutation technology is desired. This means that the need for separation of specific f elements from solutions such as high-level liquid waste containing a wide variety of lanthanides and actinides will, needless to say, increase more and more.

Here, we have been newly synthesized phenanthroline amide derivatives (phenanthroline amide: PTA) with N and O as donor elements for these purposes. These ligands achieve separation of a special f-element by recognizing slight size differences or utilize differences in their interactions with the donor elements.

In this talk, the chemical bonding properties of phenanthroline ligands to actinides and lanthanides by XAS/XES and RIXS using soft X-rays, the structural properties of tridentate and tetradentate PTA derivatives by single crystal structural analysis and EXAFS, respectively, will be presented.

# Tuesday Afternoon, November 7, 2023

Taken together, the mechanisms governing ion recognition of PTA derivatives will be reported.

4:20pm **AC+MI+TH-TuA-7 Unraveling the Unique Properties of *f*-Element Terpyridyl Complexes**, *Alyssa Gaiser*, Michigan State University; *C. Celis-Barras*, Colorado School of Mines; *F. White*, Oak Ridge National Laboratory; *T. Albrecht-Schoenert*, Colorado School of Mines **INVITED**

A terpyridine derivative was synthesized with the lanthanides and several trivalent actinides targeted at probing differences between americium and curium. In addition to investigating high quality structural data on both the americium and curium concluding in a slight increase in covalent character in the americium system, the cerium and berkelium analogs proved to be even more interesting, exhibiting enhanced covalent character in the system. This terpyridyl system continues to provide novel behavior throughout the *f*-elements exemplifying the inverse trans influence throughout the series with the interaction between the terpyridyl and the nitrate molecule in the same plane.

5:00pm **AC+MI+TH-TuA-9 Electronic Properties of Plutonium Oxycarbide**, *Paul Roussel*, AWE plc, UK

Plutonium is both electropositive and highly reactive, such that an oxide film of varying thickness is always present on metal samples. It is of interest from a safety point of view (reduced handling/processing) to investigate methods that either prevent or slow down the rate of the corrosion reaction of the metal. This can be achieved by alloying with a suitable quantity of gallium [1] or via the formation of a surface film of plutonium oxycarbide, PuO<sub>x</sub>C<sub>y</sub> (where x+y ≤ 1) [2]. Plutonium oxycarbide films have the NaCl structure and were initially called plutonium monoxide, PuO. Plutonium oxycarbide films are formed from the bulk to surface diffusion of the ubiquitous carbon impurity in the metal [3]. However, to date, there is little understanding of the electronic properties of plutonium oxycarbide films. The aim of this work is to investigate the electronic structure of plutonium oxycarbide surface films using X-ray photoelectron spectroscopy (XPS), ultraviolet photoelectron spectroscopy (UPS) and inverse photoemission spectroscopy (IPES). XPS measurements have been acquired at elevated temperature following the Pu 4f, O 1s and C 1s / Pu 5p<sub>1/2</sub> spectral regions on both alloyed and pure plutonium samples following sputter cleaning and oxidation at room temperature. UPS and IPES were acquired at room temperature following the formation of the surface plutonium oxycarbide film. All three spectroscopic measurements display a two peak structure consistent with a partially localized and itinerant *f* electronic structure for plutonium oxycarbide. Finally, the Auger parameter (Pu N<sub>7</sub>O<sub>5</sub>V – Pu 4f<sub>7/2</sub>) for plutonium oxycarbide films of varying carbon and oxygen stoichiometries are compared to the recently reported values for plutonium metal and the homoleptic plutonium oxides [1].

[1] XPS characterization of a PuGa-7 at. % alloy, P. Roussel, S. C. Hernandez, J. J. Joyce, K. S. Graham, T. Venhaus, J. Vac. Sci. Technol. A 41, 023204 (2023).

[2] Retardation of plutonium oxidation by a PuO surface film, D. T. Larson, D. L. Cash, J. Vac. Sci. Technol. 9, 800 (1972).

[3] Initial studies of plutonium corrosion, P. Roussel, D. S. Shaw, D. A. Geeson, J. Nucl. Sci. Technol. 39:sup3, 78 (2002).

5:20pm **AC+MI+TH-TuA-10 Exploring the Surface and Subsurface Behavior of Hydrogen in δ-Pu(100) and Bulk δ-Pu Through Density Functional Theory**, *Charles Fricke*, *S. Hernandez*, Los Alamos National Laboratory

The corrosion of plutonium to form its hydride creates significant challenges in handling, researching, and storing of the metal. Plutonium hydrides rapidly, much faster than most metals, and the kinetics are less well understood. Significant questions remain, including the energetics of hydrogen formation in different lattice sites, such as the tetrahedral, octahedral, and vacancy sites, as well as its reactive behavior on and in the surface of metallic plutonium. As such, this work aims to explore how hydrogen behaves within face-centered-cubic δ-plutonium from the surface into the subsurface and into the bulk through density functional theory. We find that hydrogen is energetically favored to remain on the surface, but that the energetics of hydrogen in the first subsurface remains thermodynamically favorable for both the subsurface tetrahedral and octahedral sites when compared to the referenced gas-phase hydrogen molecule. We also find that the octahedral site remains thermodynamically favorable for hydrogen species to fill from the 2<sup>nd</sup> subsurface to the bulk in δ-Pu(100). In addition, we find we have subsurface to bulk formation energy convergence at the 3<sup>rd</sup> sublayer of δ-Pu(100). Finally, we will discuss the energetics differences of hydrogen between the surface, subsurface, and bulk within δ-Pu.

5:40pm **AC+MI+TH-TuA-11 Nanoscale Nuclear Materials: Synthesis and Advanced X-Ray Characterization of Uranium Oxide Nanoparticles**, *Liane Moreau*, Washington State University, US

Nanostructures (particularly with sizes below 10 nm) are inherently challenging to characterize on the atomic scale, due to broadening which occurs in diffraction-based characterization methods, and the high concentration of surface defects and energy-minimization effects. Characterization challenges compound when investigating nanoscale actinide oxides, such as uranium oxide, due to radioactive sample constraints and rich electronic structure which can potentially stabilize a wide range of crystallographic arrangements. To address these challenges, x-ray spectroscopic and scattering based methods are used to probe challenging nanoscale systems in detail over multiple length scales. In particular, synthetic developments are paired with robust characterization, in order to improve knowledge of nanoparticle growth and transformation, as well as develop ways to make advanced x-ray characterization analysis more informed and accessible, in tandem.

Nanoscale uranium oxides are of interest towards the development of accident-tolerant nuclear fuels and are also relevant to the migration of actinides in environmental systems. Synthetic methods will be presented, which have enabled preliminary investigation into the size and morphology-dependent properties of uranium oxides. Specifically, the synthesis of UO<sub>2</sub> anisotropic nanoparticles and the deposition of uranium onto iron nanoparticles will be highlighted. These synthetic pursuits have been paired with x-ray spectroscopy and x-ray scattering to create new analysis strategies for decoupling surface vs. interior chemistry of nanoparticles and to interrogate the in-depth structural and electronic properties of uranium oxide as a function of particle size and morphology. The studies presented give a glimpse into the interesting fundamental and behavioral differences between actinide nanomaterials and their counterparts elsewhere on the periodic table.

6:00pm **AC+MI+TH-TuA-12 A Statistical Mechanics Treatment of Multiconfigurational Ground States in Isolated Neutral Atoms**, *Miles Beaux*, Los Alamos National Laboratory

Janoschek, et al. described the ground state of plutonium (Pu) as being, “governed by valence fluctuations, that is, a quantum mechanical superposition of localized and itinerant electronic configurations.” [*Science Advances*, 1, 6 (2015)]. However, a casual internet search of the electronic structure of Pu gives [Rn]7s<sup>2</sup>5f<sup>6</sup> which is wholly insufficient to describe the complex nature of its multiconfigurational ground state as described by Janoschek, et al. A better description might be given by



where  $\gamma_{s,\text{Pu}}$ ,  $\gamma_{f,\text{Pu}}$ ,  $\gamma_{d,\text{Pu}}$ ,  $\gamma_{p,\text{Pu}}$  represent potentially non-integer deviations from the integer electron occupancies of their respective orbitals. By judiciously selecting bounding conditions for how the eight valence electrons can distribute themselves within the given orbitals, a limited number of occupancy configurations can be identified with an identifiable number of cumulative allowable electron permutations. For example, the bounding conditions

$$-2 \leq \gamma_{s,\text{Pu}} \leq 0,$$

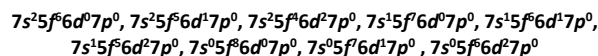
$$-2 \leq \gamma_{f,\text{Pu}} \leq 2,$$

$$0 \leq \gamma_{d,\text{Pu}} \leq 2,$$

$$\gamma_{p,\text{Pu}} = 0, \text{ and}$$

$$\gamma_{s,\text{Pu}} + \gamma_{f,\text{Pu}} + \gamma_{d,\text{Pu}} + \gamma_{p,\text{Pu}} = 0$$

result in nine possible occupancy configurations



with 487,630 cumulative possible electron permutations. With the specific number of permutations identified, principles of statistical mechanics can be applied to multiconfigurational ground states.

Similar generalized representations of ground state electronic structures will be described for each element in the periodic table. Classical Boltzmann's entropies for the respective electronic structures will be calculated by considering the possible electron permutations as statistical mechanics microstates. These entropies will then be compared to known standard molar entropies.

LA-UR-23-24803

# Tuesday Afternoon, November 7, 2023

## Atomic Scale Processing Mini-Symposium

Room A107-109 - Session AP1+2D+EM+PS+TF-TuA

### Atomic Layer Processing: Integration of Deposition and Etching

Moderator: John F. Conley, Jr., Oregon State University

2:20pm **AP1+2D+EM+PS+TF-TuA-1 Combination of Plasma-Based Atomic-Scale Deposition and Etching Processes for Advanced Patterning**, **Marceline Bonvalot**, LTM - MINATEC - CEA/LETI, France; **C. Vallée**, SUNY College of Nanoscale Science and Engineering; **r. gassilloud**, **T. Chevolleau**, CEA/LETI-University Grenoble Alpes, France; **N. Possémé**, STmicroelectronics, France

INVITED

Selective Deposition processes have gained increased research interest in recent years, because they enable the accurate placement of a thin film on a specific substrate surface (in the case of area selective deposition ASD) or on specifically oriented surfaces (in the case of topographical selective deposition TSD). Such processes require atomic-scale precision, and usually involve Atomic Layer Deposition techniques, with possibly plasma assistance. Several pathways have been proposed in the literature for ASD, most commonly implying surface inhibition treatments with dedicated chemical treatments (self-assembled molecules or small molecule inhibitors for instance) to increase the nucleation delay during the subsequent ALD growth. However, the dedicated inhibition behavior eventually deteriorates when exposed to a few ALD cycles, which requires that on the one hand, nuclei formed on non-growth surfaces be removed and on the other hand, the inhibitor be systematically regenerated.

In this presentation, we will show how the insertion of an *in situ* etching step in the overall ALD process can serve as an effective corrective treatment for this purpose. The etching periodicity in conventional deposition/etching duty cycles will be investigated in details. We will show that the etching step should preferentially be carried out before the transition from the Volmer-Weber 1D island growth mode to the 2D layer by layer growth mode on non-growth surfaces, to limit plasma-induced surface defects. Moreover, the 1D island growth mode seems to coincide with the onset of degradation for the surface inhibition treatment. In this context, it will be shown that the etching periodicity is a determining parameter for the successful development of a selective bottom-up growth strategy.

3:00pm **AP1+2D+EM+PS+TF-TuA-3 Application of Etching Reaction Models to Deposition Processes**, **Nobuyuki Kuboi**, Sony Semiconductor Solutions Corporation, Japan

INVITED

Advanced CMOS devices require highly intricate 3D stacked structures with varying aspect ratios such as FinFETs and GAAs [1]. Understanding the process properties of plasma etching [2] and deposition [3] processes based on their mechanism and combinations has become increasingly important in addressing this challenge. Additionally, microfabrication properties should be stably suppressed within a specific range during mass production. However, the monitoring system equipped in the process chamber is limited for mass production. Therefore, we propose predictive models for plasma etching and deposition that consider the physical and chemical aspects of the plasma and surface.

First, we briefly introduce simulations for fluctuations in the SiN etching rate influenced by the chamber wall condition, critical dimensions during Si gate etching caused by SiBr<sub>x</sub> by-products dependent on open area ratios on wafer/chip/local-pattern levels, damage distribution affected by local-pattern structure, ion energy, and hydrogen concentration in the SiO<sub>2</sub> and SiN films, and selectivity during SiO<sub>2</sub>-ALE [4][5][6].

We then present a modeling and simulation of the deposition process as a motif of the SiN-PECVD process using a 3D voxel method that can be associated with the previous process, such as plasma etching [7]. The model can predict film properties as well as the coverage on a large-scale pattern. Reactions among voxels are considered pseudo treatments for atomistic interactions on the surface. A statistical ensemble method involving probabilities is used to express physical and chemical phenomena such as sticking, migration, and bond formation on the deposited surface. The sticking and bond probabilities are affected by surface damage and IEADFs, respectively. Our model can successfully reproduce the experimental characteristic relationship between the morphology and film density dependent on the SiH<sub>4</sub> flow rate during the low temperature (120 °C) SiN-PECVD process considering different gas residence times that affect surface reactions. Furthermore, we discuss the issue of modeling the ALD process.

These simulation technologies can aid in optimizing the chamber wall condition, pattern design, and etching/deposition combination process.

- [1] N. Singh *et al.*, IEEE Electron Device Lett. **27**, 383 (2006).
- [2] T. Tatsumi *et al.*, Jpn. J. Appl. Phys. **61**, SA0804 (2022).
- [3] H. C. M. Knoop *et al.*, J. Vac. Sci. Technol. A **37**, (2019) 030902.
- [4] N. Kuboi *et al.*, Appl. Phys. Express **5**, (2012) 126201.
- [5] N. Kuboi *et al.*, J. Vac. Sci. Technol. A **35**, (2015) 061306.
- [6] N. Kuboi *et al.*, J. Vac. Sci. Technol. A **37**, (2019) 051004.
- [7] N. Kuboi *et al.*, Jpn. J. Appl. Phys. **62**, (2023) S11006.

4:20pm **AP1+2D+EM+PS+TF-TuA-7 Recent Advancements for Atomic Layer Advanced Manufacturing Processes: Microreactor Direct Atomic Layer Processing (μDALP™)**, **Maksym Plakhotnyuk**, **A. Varga**, **I. Kundrata**, ATLANT 3D Nanosystems, Denmark; **J. Bachmann**, ATLANT 3D Nanosystems; Friedrich-Alexander Universität Erlangen-Nürnberg, Denmark

INVITED

As the demand for miniaturized and complex devices continues to grow across various industries, the need for innovative and precise atomic layer advanced manufacturing (ALAM) technologies becomes increasingly apparent<sup>[1]</sup>. Our company, utilizing proprietary Microreactor Direct Atomic Layer Processing (μDALP™), is at the forefront of pushing sALD's capabilities and broadening its application horizons. The μDALP™ process undergoes the same cyclic ALD process but only in a spatially localized area.<sup>[2]</sup> The microreactor or micronozzle confines the flows of gases used for ALD within a defined μm-scale centric area on the substrate to deposit the desired material.<sup>[3]</sup>

ATLANT 3D's recent advancements in our novel μDALP™ technology have enabled innovation within the thin film deposition field ranging from ALD material development to rapid prototyping and manufacturing. The μDALP™ process enables multiple depositions e.g., depositions with varying film thicknesses, to be deposited onto a single wafer used to calculate a given processes growth rate within only a few hours, compared to days for a traditional ALD process. In Addition, innovation of applications including optics and photonics, quantum devices, MEMS, RF electronics, emerging memory technologies, advanced packaging, and energy storage are possible and have been demonstrated using μDALP™ technology.

Discussing the improvements to the μDALP™ process, we have decreased the process resolution, increased material compatibility, and accessible morphologies. Giving one example of the recent development in morphologies, films deposited with μDALP™ have conformal coverage of gratings, microchannels, and trenches up to a depth of 25 μm using a Platinum deposition process. **Fig. 1** demonstrates how a given ALD material process (in this case, Pt) can be used with ATLANT 3D technology to deposit localized area conformal coatings of complex surfaces with an aspect ratio of 1:25. Hence demonstrating the versatility and potential of our technology for achieving inherently selective ALD for processing on complex surface morphologies.

This talk aims to shed light on how our breakthroughs in spatial ALD and μDALP™ technology contribute to the advancement of ALAM and scale-up. Fostering a deeper understanding of our technology's capabilities and exploring the possibilities it opens up for various industries.

- [1] Poedt P., *JVSTA.*, **2012**, *30*, 010802
- [2] Kundrata I., *et al.*, *Small Methods.*, **2022**, *6* (5), 2101546
- [3] Plakhotnyuk M, *et al.*, *ALD/ALE 2022 [Int. Conf.]*, **2022**

## Atomic Scale Processing Mini-Symposium Room A107-109 - Session AP2+PS+TF-TuA

### Energy Enhanced ALD

Moderator: John F. Conley, Jr., Oregon State University

5:00pm **AP2+PS+TF-TuA-9 Atomic Layer Annealing with Radio Frequency Substrate Bias for Control of Grain Morphology in Gallium Nitride Thin Films**, **A. McLeod**, **P. Lee**, University of California, San Diego; **S. Yun**, **S. Ueda**, University of California, San Diego, USA; **Z. Devereaux**, **C. Winter**, Wayne State University; **J. Spiegelman**, RASIRC; **R. Kanjolia**, **M. Moinpour**, EMD Electronics, USA; **Andrew Kummel**, University of California, San Diego

INVITED

Low temperature GaN deposition is critical for passivation layers on nitride power FET as low as templating and capping layers on sputtered AlN films for heat spreader. A method of performing atomic layer annealing with RF substrate bias on insulating and amorphous substrates is demonstrated for

# Tuesday Afternoon, November 7, 2023

GaN deposition at 275 °C. GaN is typically deposited by MOCVD or MBE at >600 °C, resulting in strain upon cooling; this makes low temperature process alternatives desirable. Tris(dimethylamido) gallium (III) and hydrazine served as precursors while Ar and Kr were used for ion bombardment. Optimization of substrate bias potential is demonstrated by GI-XRD and XRR. Reference films were deposited by thermal ALD and non-substrate biased ALA processes. XPS surface and depth-profiling studies show that applied RF bias decreases film oxygen and carbon content relative to the reference films; these films also show crystallites broadening with increasing film thickness by TEM in contrast to the reference films. In summary, ALA with RF substrate bias is demonstrated as an effective method to deposit GaN thin films at a low deposition temperature on insulators. This technique has recently been expanded to growth of InGaN films which applications in microLEDs.

5:40pm **AP2+PS+TF-TuA-11 Atomic Layer Annealing for sub-10 nm, Wake-up Free Ferroelectric Hf<sub>0.5</sub>Zr<sub>0.5</sub>O<sub>2</sub> Thin Films**, *Yu-Sen Jiang*, National Taiwan University, Taiwan; *T. Chang, S. Yi*, Taiwan Semiconductor Manufacturing Company, Taiwan; *M. Chen*, National Taiwan University, Taiwan

Conventional annealing techniques pose significant challenges in nanoscale fabrication. One prominent issue involves the heating depth, which typically exceeds the critical dimension of nanoscale devices. Consequently, conventional annealing methods introduce excessive thermal budget, resulting in performance degradation of the devices. Atomic layer annealing (ALA) is capable of adjusting the film quality at the atomic level during low-temperature (300°C) deposition without the need for any post-annealing process, which tremendously lowers the thermal budget and can tailor the film properties as required. In this report, the ALA technique was used to realize sub-10 nm wake-up free ferroelectric Hf<sub>0.5</sub>Zr<sub>0.5</sub>O<sub>2</sub> (HZO) thin films with high remnant polarization and low thermal budget. The HZO thin films have also been used as gate dielectrics in junctionless transistors, demonstrating steep subthreshold swing (< 60 mV/decade) in nanoscale devices. The outcome manifests the remarkable capabilities of ALA in enabling precise engineering and fabrication of nanoscale materials and devices.

6:00pm **AP2+PS+TF-TuA-12 A System for Predicting the Area Selective Deposition of Titanium: Plasma State Diagnostics Using Electrical Simulation**, *Kyoungmi Choi, T. Hong, H. Kim, Y. Oh*, Samsung Electronics Co., Inc., Republic of Korea

The selective deposition of thin films in specific areas is crucial for achieving the desired size and low resistance of semiconductors. Due to differences in chemistry between molecule/surface and molecule/vapor interactions, thin films are selectively deposited on pre-patterned substrates. Although simulations have been used to predict Ti film thickness using plasma simulation and surface reaction models, the effect of selective deposition on the pattern was not studied. In this study, an electrical simulation was used to predict the selectivity of the area selective deposition process on the patterned wafer.

To identify the main factors affecting selectivity, we reviewed the plasma temperature and density. Plasma density can be indirectly inferred from the output current of the matcher. Another factor that influences selectivity is plasma temperature, specifically the electron temperature [eV]. The sheath voltage is proportional to the electron temperature. Therefore, we established an electric simulation system (Fig. 1) to estimate the sheath voltage. The CCP consists of an RF generator, a matcher, and a chamber. We identified the matcher parameters ( $C_{\text{tune}}/C_{\text{load}}/L$ ) using the maximum power transmission theory, assuming that the chamber was  $Z_{\text{chamber}}$  (Fig 2). The model was verified using MATLAB and the sheath voltage was derived using the matcher and bottom currents. The simulations and evaluations of pressure/RF power/impedance were performed. The validity of the electrical model was confirmed by comparing the simulation and the experimental current.

To verify the simulation, Ti deposition experiments were conducted on Si/SiO wafers under 7 conditions (Table 1). The simulation results for sheath voltage and the experimental results for deposition rate showed a correlation of 0.77, and the Si/SiO selectivity showed a correlation of 0.92 (Fig 3).

Through the correlation result, it was derived as the following conclusion. The correlation results between sheath voltage and the area selective deposition explains the difference in the activation energy of the Si/SiO surfaces: The Si-Si bonding energy is 3.39 eV and the Si-O bonding energy is 8.29 eV (Fig 4). Since there are regions where the plasma temperature is active on Si and inert on SiO, they are selectively deposited. Therefore, a sheath voltage simulation can be used to predict the selectivity. With

further development, this simulation can be applied to other deposition equipment that uses plasma, and trends in process results for other process parameters that are sensitive to plasma temperature can be inferred.

## Biomaterial Interfaces Division

### Room B117-119 - Session BI+AS+EM+NS+SE+TF-TuA

#### Functional Biomaterials II: Sensing and Diagnostics

**Moderators:** Joe Baio, Oregon State University, Caitlin Howell, University of Maine

2:20pm **BI+AS+EM+NS+SE+TF-TuA-1 AVS Nellie Yeoh Whetten Awardee Talk: Detection of SARS-CoV-2 using Surface-enhanced Raman Spectroscopy and Deep Learning Algorithms**, *Yanjun Yang<sup>1</sup>*, University of Georgia; *H. Li*, Chongqing University, China; *L. Jones, J. Murray, D. Luo, X. Chen, H. Naikare, Y. Mosley, R. Tripp*, University of Georgia; *B. Ai*, Chongqing University, China; *Y. Zhao*, University of Georgia

A rapid and cost-effective method to detect the infection of SARS-CoV-2 is crucial in the fight against COVID-19 pandemic. This study presents three strategies to detect SARS-CoV-2 from human nasopharyngeal swab (HNS) specimens using a surface-enhanced Raman spectroscopy (SERS) sensor with deep learning algorithms. The first strategy is to use DNA probes modified silver nanorod array (AgNR) substrate to capture SARS-CoV-2 RNA. SERS spectra of HNS specimens have been collected after RNA hybridization, and a recurrent neural network (RNN)-based deep learning (DL) model is developed to classify positive and negative specimens. The overall classification accuracy was determined to be 98.9%. For the blind test of 72 specimens, the RNN model gave 97.2% accuracy in the prediction of the positive specimens, and 100% accuracy for the negative specimens. The second strategy is to use a human angiotensin-converting enzyme 2 protein (ACE2) functionalized SERS sensor to capture the intact viruses. Such a method can differentiate different virus variants, including SARS-CoV-2, SARS-CoV-2 B1, and CoV-NL63. A convolutional neural network (CNN) deep learning model for classification and regression has been developed to simultaneously classify and quantify the coronavirus variants based on SERS spectra, achieving a differentiation accuracy of > 99%. Finally, a direct SARS-CoV-2 detection on SiO<sub>2</sub> coated AgNR substrate is tested. SERS spectra of HNS specimens from 120 positive and 120 negative specimens are collected. The HNS specimens can be accurately distinguished as positive or negative with an overall 98.5% accuracy using an RNN-based deep learning model, and the corresponding Ct value can be predicted accurately by a subsequent RNN regression model. In addition, 99.04% accuracy is achieved for blind SARS-CoV-2 diagnosis for 104 clinical specimens. All the detections are accomplished in 25 min. These results indicate that the SERS sensors combined with appropriate DL algorithms could serve as a potential rapid and reliable point-of-care virus infection diagnostic platform.

2:40pm **BI+AS+EM+NS+SE+TF-TuA-2 Wafer-Scale Metallic Nanotube Arrays: Fabrication and Application**, *Jinn P. Chu*, National Taiwan University of Science and Technology, Taiwan

This presentation reports on the wafer-scale fabrication of metallic nanotube arrays (MeNTAs) with highly ordered periodicity. Various metals and alloys have been used to prepare MeNTAs via sputtering over a contact-hole array template created in the photoresist. We have used ferrous (stainless steel) and nonferrous (Cu-, Ni-, Al-, and Ti-based) alloys, as well as elemental metals (Cu, Ag, and Au), to form MeNTAs. The proposed nanotubes can be fabricated over a wide range of heights and diameters (from a few hundred nm to 20 μm) in various shapes, including tall cylinders and dishes. In addition, after combining with other nanomaterials (e.g., ZnO nanowires, graphene oxide, or Au nanoparticles), MeNTAs become nanohybrids suitable for many applications. These applications include thermal emitters, triboelectric nanogenerators, SERS-active biosensors, microfluidics, and anti-icing devices.

3:00pm **BI+AS+EM+NS+SE+TF-TuA-3 Low-Cost, Continuous Spectroscopic Monitoring of Chemical and Biological Contamination in Liquids**, *Liza White, C. Howell*, University of Maine

Traditional UV-visible spectroscopic testing of liquids to assess contamination typically involves manual collection and measurement in a dedicated instrument at discreet time intervals. Here, we describe how low-cost, mass-produced diffraction gratings can be used to approach the functionality of traditional UV-visible spectroscopic readouts under

<sup>1</sup> AVS Nellie Yeoh Whetten Awardee

continuous flow conditions. We designed and built a flow chamber setup that permitted uninterrupted monitoring of the diffraction pattern as water with different contaminants was passed over it. Various chemical dyes as well as biological contaminants such as bacteria and algae at varying concentrations in water were tested using standard LEDs as a light source. Information was extracted from the diffraction patterns by analyzing changes in the transmitted wavelengths as well as changes in scattering. Our results showed that the system permitted reasonable detection of each of the contaminants tested within a subset of the concentration range of a standard UV-vis instrument. Tests using the toxic dye methylene blue showed accurate detection well below the toxic limit (5 µg/mL), although the limit of detection for *E. coli* was higher at  $\sim 10^7$  cells/mL. Our results demonstrate how mass-produced diffraction gratings can be used as low-cost detection systems for the continuous detection of contamination in liquids, opening the door for autonomous monitoring for a range of different applications.

3:20pm **BI+AS+EM+NS+SE+TF-TuA-4 Clickable Cerium Oxide Nanoparticles with Gadolinium Integration for Multimodal Micro- and Macroscopic Targeted Biomedical Imaging**, Anna du Rietz, C. Brommesson, K. Roberg, Z. Hu, K. Uvdal, Linköping University, Sweden

Multimodal and easily modified nanoparticles enable targeted biomedical imaging at both the macro- and micro level. Computed tomography and magnetic resonance imaging are biomedical imaging techniques used daily in clinical practice all over the world. These non-invasive techniques can identify more medical conditions if contrast and sensitivity are increased. Commonly, targeted imaging is realized by conjugating biomolecular recognition elements such as antibodies to the contrast agent.

Herein, we present a clickable nanoparticle of our own design, consisting of a Cerium oxide nanoparticle core with integrated Gadolinium, coated with polyacrylic acid and functionalized with both a clickable moiety and a fluorophore. Click chemistry is a versatile toolbox of conjugation reactions that can be performed under gentle conditions enabling facile tailoring of the nanoparticles. Results from XRD and TEM studies clearly show that the cores are mono-crystalline and approximately 2 nm in diameter, the hydrodynamic radius of <5 nm is measured by DLS. The soft coat of the nanoparticles is characterized by IR spectroscopy as well as zeta potential measurements. We have verified the presence of azide-groups on the finished particles and the carboxylic groups of polyacrylic acid are firmly bound to the nanoparticle core. The nanoparticles have high colloidal stability even in physiological ionic strength environments with a zeta potential of -48 mV. We have proven direct anchoring of monoclonal antibody cetuximab to the nanoparticles enabling targeting of epidermal growth factor receptor, a common target in many cancer types. Fluorescence spectroscopy and relaxivity measurements were used to evaluate and optimize the properties for future imaging applications of tumors. The nanoparticles provide high MRI contrast with a  $T_1$  relaxivity of  $42 \text{ s}^2\text{mM}^{-1} \text{ Gd}$ , more than two times higher than currently used contrast agents. The finished antibody functionalized nanoparticles are efficiently purified using size exclusion chromatography, separating them from unbound nanoparticles and antibodies. Finally, the cellular uptake of the nanoparticles was evaluated using fluorescence microscopy as well as live/dead assays. We show that the nanoparticles are taken up by cell lines of head- and neck squamous cell carcinoma, in a lysosomal pattern. The nanoparticles are visualized at the nm scale inside the lysosomes using TEM. In conclusion, we have designed and synthesized a versatile nanoparticle with functionalized capping that enables facile fabrication of tailored nanoprobe for biomedical imaging.

4:20pm **BI+AS+EM+NS+SE+TF-TuA-7 Molecularly Imprinted Polymers (MIPs): Rising and Versatile Key Elements in Bioanalytics**, J. Völkle, A. Feldner, Center for Electrochemical Surface Technology, Wiener Neustadt, Austria; P. Lieberzeit, University of Vienna, Faculty for Chemistry, Department of Physical Chemistry, Vienna, Austria; Philipp Fruhmann, Center for Electrochemical Surface Technology, Wiener Neustadt, Austria

INVITED

Molecularly imprinted polymers (MIPs) are specific materials with tailored binding cavities complementary to a specific target molecule. Although the first example of artificial materials with molecular recognition were already described 80 years ago, they experienced a surge of popularity since the late 1990s due to improved synthetic methods and their great potential as recognition element in (biomimetic) sensors. MIPs can achieve similar selectivity and sensitivity as antibodies<sup>1</sup>, while their robustness and stability is superior compared to biomolecules. They can also be used under non-

physiological conditions, are suitable for long-term storage and accessed by scalable synthetic methods. These properties make them highly promising candidates for a wide range of applications, from biomimetic receptor layers to nanomaterials or artificial antibodies.

Despite this versatility, their design and optimization towards a specific analyte is probably the most challenging task in the development of a sensor. In general, MIP based sensors either rely on electrochemical, mass sensitive or optical transducers and are commonly used as thin film or nanoparticle (nanoMIP). While there is a considerable amount of literature on electrochemical sensors with MIPs available, new developments such as the improvement of conductive MIPs<sup>2</sup>, optimized epitope imprinting<sup>3</sup>, or the development of novel synthetic techniques such as the solid-phase synthesis of nanoMIPs<sup>4</sup> are highly important for the further development of MIPs in sensing.

For this reason, this presentation will provide an overview about different MIP types, their synthesis, application, and challenges. Furthermore, their potential in future applications will be addressed to give a wholistic impression of the numerous possibilities of this versatile compound class.

## References

- [1]Chianella, I., et al., Direct Replacement of Antibodies with Molecularly Imprinted Polymer Nanoparticles in ELISA, Development of a Novel Assay for Vancomycin. *Anal. Chem.* **2013**, 85, 17, 8462–8468
- [2]Feldner, A., et al., Conductive Molecularly Imprinted Polymers (cMIPs): Rising and Versatile Key Elements in Chemical Sensing, *Submitted to Chemosensors (in Revision)*, **2023**
- [3] Pasquardini, L, Molecularly imprinted polymers by epitope imprinting: a journey from molecular interactions to the available bioinformatics resources to scout for epitope templates, *Anal Bioanal Chem*, **2021**, 413, 6101–6115. <https://doi.org/10.1007/s00216-021-03409-1>
- [4]Canfarotta F., et al. Solid-phase synthesis of molecularly imprinted nanoparticles, *Nat Protoc.* **2016** Mar;11(3):443-55. doi: 10.1038/nprot.2016.030. Epub 2016 Feb 11. PMID: 26866789.

#equal contribution

5:00pm **BI+AS+EM+NS+SE+TF-TuA-9 X-ray Fluorescence Analysis of Metal Containing Cytostatics in HeLa Cells using the Ultra-compact Cryo-vacuum Chamber  $\mu$ -HORST**, Lejla Jusufagic, C. Rumancev, A. Rosenhahn, A. Steinbrück, N. Metzler-Nolte, Ruhr-University Bochum, Germany

Synchrotron-based X-ray fluorescence spectroscopy (XRF) is an excellent method for investigating elemental distributions and metal concentrations in biological systems.<sup>[1-4]</sup> The method provides a high sensitivity down to the detection of trace elements with high spatial resolution and penetration depth.<sup>[3,4]</sup> We introduced an ultra-compact cryogenic vacuum chamber called “ $\mu$ -HORST” at the P06 nanoprobe beamline at PETRA III, DESY to measure 2D-XRF elemental distribution maps and concentrations in cryogenically fixated cells treated with cytostatic metal complexes with varying ligand sphere.<sup>[1,2]</sup> The cells are grown on silicon nitride membranes and treated with a 10 µM solution of the metal complexes for different durations and all physiological processes were stopped by rapid cryo-fixation. Cryogenic fixation is a non-destructive method that keeps the cells as close as possible to their biologically hydrated state. The frozen cell samples can be transferred into the  $\mu$ -HORST setup and maintained in a frozen state throughout the nano-XRF measurements. The acquired data show that the concentration of the metal complexes and their intracellular location can be correlated to the one of physiologically relevant ions such as potassium and zinc as well as associated changes in the metal homeostasis. The developed chamber can not only be used for the analysis of intracellular cytostatic metal complexes, but also to the accumulation of antimicrobial metal complexes or of anthropogenic metals in environmental samples.

## References

- [1] C. Rumancev, T. Vöpel, S. Stuhr, A. von Gundlach, T. Senkbeil, S. Ebbinghaus, J. Garrevoet, G. Falkenberg, B. De Samber, L.Vincze, A. Rosenhahn, W. Schroeder, *Biointerphases* **2021**, 16, 011004.
- [2] C. Rumancev, T. Vöpel, S. Stuhr, A. von Gundlach, T. Senkbeil, J. Garrevoet, L. Jolmes, B. König, G. Falkenberg, S. Ebbinghaus, W. Schroeder, A. Rosenhahn, *J. Synchrotron Rad.* **2020**, 27, 60-66.
- [3] M. J. Pushie, I. J. Pickering, M. Korbas, M. J. Hackett, G. N. George, *Chem. Rev.* **2014**, 114, 8499-8541.

# Tuesday Afternoon, November 7, 2023

[4] A. Sakdinawat, D. Attwood, *Nature photonics* **2010**, *4*, 840-848.

5:20pm **BI+AS+EM+NS+SE+TF-TuA-10 Hemocompatibility Analysis of Novel Bioinspired Coating**, *AnneMarie Hasbrook, R. Faase, M. Hummel, J. Baio*, Oregon State University

Surface-induced thrombosis is a critical concern in medical device development. To minimize thrombosis, current extracorporeal circulation units require systemic anticoagulation. However, systemic anticoagulants can cause adverse effects such as thrombocytopenia, hypertriglyceridemia, and hyperkalemia. To address this issue, we combine the technology of polydopamine (PDA) functionalization with slippery liquid infused porous surfaces (SLIPS) to potentially enhance the biocompatibility of medical devices. PDA readily coats a wide variety of surfaces and can be functionalized with a thiolated fluoropolymer, via Michael Addition, to form a pseudo self-assembled monolayer (pSAM) which serves as the porous surface component of SLIPS. Liquid perfluorodecalin can then be added to complete the SLIPS coating. We hypothesized that the PDA SLIPS coating provides enhanced hemocompatibility due to its omniphobic properties and composition of compounds currently used in medical applications. Surface modifications were confirmed using contact angle and X-ray photoelectron spectroscopy (XPS) which revealed significant changes to the surface chemistry after the addition of each subsequent layer of PDA SLIPS. The coatings were evaluated for thrombogenicity via quantification of Factor XII (FXII) activation under static and dynamic settings, fibrin formation, platelet adhesion, and clot morphology. The PDA SLIPS coating activated 50% less FXII than glass and 100% more FXII than bovine serum albumin (BSA) coated substrates. PDA SLIPS had similar plasma clotting time to BSA and plasma clotted two times slower on PDA SLIPS than on glass. Platelet adhesion was increased two-fold on SLIPS compared to BSA and decreased two-fold on SLIPS compared to glass. PDA SLIPS had approximately 20% higher fiber diameter and 25% lower clot density than glass and was significantly different in fiber diameter and density than BSA.

5:40pm **BI+AS+EM+NS+SE+TF-TuA-11 Signal Enhancement for Gravimetric Biomimetic Detection – Conjugation of Molecularly Imprinted Polymer Nanoparticles to Metal Nanoparticles**, *Julia Völkle*, CEST GmbH, University of Vienna, Austria; *A. Weiß, P. Lieberzeit*, University of Vienna, Austria; *P. Fruhmann*, CEST GmbH, Austria

Over the past decades, the field of biosensors and -diagnostics has been increasingly dominated by a growing demand for non-centralized point-of-care devices that do not rely on extensive laboratory infrastructure and trained personnel. Recently, the COVID-19 pandemic has emphasized the crucial role of such fast, reliable, and affordable diagnostic tools. Novel, tailor-made nanomaterials are considered a key component for tackling the upcoming challenges of miniaturization and cost-efficiency in the field of biosensing.

One emerging class of such biomimetic nanomaterials are molecularly imprinted polymer nanoparticles (nanoMIPs). nanoMIPs are artificial receptors that can mimic the highly selective binding capabilities of biological recognition units, such as antibodies and enzymes. Unlike their natural counterparts however, they are stable under a wide range of non-physiological conditions, suitable for long-term storage, and can be derived from a straightforward, rapid synthesis procedure without the need for cell culturing or animal experimentation. Thus, they are ideal candidates for the development of sensitive, robust and inexpensive bioanalogous sensors.

While impressive results regarding their high selectivity and low non-specific binding have been reported [1], nanoMIP-based gravimetric (quartz crystal microbalance, QCM) assays are restricted with regards to the achievable limit of detection by their comparatively low overall mass. This project therefore is focused on the synthesis of well-defined nanoMIP-metal nanoparticle (NP) conjugates, which would result in a larger change in mass upon binding of the recognition units to the QCM transducer. Moreover, conjugation to gold-NPs would allow the incorporation of nanoMIPs into other analytical techniques such as lateral flow devices (LFDs). Experiments therefore are focused on the incorporation of suitable functional groups for further conjugation into the nanoMIP polymer network, the surface functionalization of metal NPs with complementary linker moieties and a suitable coupling procedure. In the poster, nanoMIPs selective for various biologically relevant species are coupled to metal NPs and the performance of the conjugates in QCM-based detection is presented in detail and discussed.

[1] Park, et al. „Recent Advances of Point-of-Care Devices Integrated with Molecularly Imprinted Polymers-Based Biosensors: From Biomolecule Sensing Design to Intraoral Fluid Testing“. *Biosensors* **12**, Nr. 3 (22. Februar 2022): 136. <https://doi.org/10.3390/bios12030136>.

**Nanoscale Science and Technology Division**

**Room B113 - Session NS1+2D+EM+MN-TuA**

**Nanofabrication and Characterization of Low-Dimensional Materials**

**Moderator: Georg Fantner, EPFL**

2:20pm **NS1+2D+EM+MN-TuA-1 Atomic-Scale Design and Defect Networks at the 2D/3D Interface**, *Kate Reidy*, MIT **INVITED**

‘Mixed dimensional’ 2D/3D van der Waals heterostructures, where 3D metallic nanostructures are integrated with suspended two-dimensional (2D) van der Waals materials, show unique functionalities including light-matter coupling, charge transfer, and enhanced catalytic activity. To enable such integration, an understanding of how structure and defects at the 2D/3D interface affect heterostructure properties is required. Moreover, 2D/3D heterostructures display fluctuations of opto-electronic properties in nanometer spatial range; and it is advantageous to probe position-dependent properties at the same spatial scales. In this seminar, I will share work exploring the local properties of the 2D/3D interface using a combination of atomic resolution scanning transmission electron microscopy (STEM), in situ ultra-high vacuum (UHV) TEM, and monochromated high-energy resolution electron energy-loss spectroscopy (EELS). We demonstrate epitaxial, single-crystalline metallic nanoisland growth of technologically relevant metals (Au, Ti and Nb) with ultra-low defect density interfaces and faceted morphologies on several thin suspended 2D materials. We then explore the key parameters of 2D/3D growth, including the role of temperature, defects, moiré, surface chemistry, and thermodynamic equilibrium shapes. Lastly, we fabricate more complex heterostructure stacks with defect densities controlled by the compliance of the 2D material substrate. Through fundamental understanding of the structure-property-performance relationship, we suggest that future electronic, magnetic, and optical nanodevices will utilize versatile fabrication of 2D/3D heterostructures with well-characterized interfaces and morphologies.

3:00pm **NS1+2D+EM+MN-TuA-3 Highly Asymmetric Doping of Epitaxial Bilayer Graphene by Targeted Bonding of the Intercalated Gadolinium**, *Marek Kolmer*, Ames National Laboratory; *J. Hall*, Ames National Laboratory and Department of Physics and Astronomy, Iowa State University; *S. Chen, M. Tringides*, Ames National Laboratory, Department of Physics and Astronomy, Iowa State University

Heterostructures consisting of vertically stacked two-dimensional (2D) materials have recently gained large attention due to their highly controllable electronic properties. Particularly, mechanically stacked multilayered systems offer exceptional control over a stacking sequence or interlayer twist angles. On the other hand, epitaxially grown 2D materials express unprecedented quality and stability over wafer-scale lengths. In both cases controlling the interlayer coupling can generate novel electronic and topological phases and its effective implementation is commonly done with a transverse electric field. However, phases generated by high displacement fields are elusive.

Here, we introduce an exceptionally large displacement field by structural modification of a model system: AB-stacked epitaxial bilayer graphene (BLG) on a SiC(0001) surface. We show that upon intercalation of gadolinium with two specific interlayer locations, electronic states in the top two graphene layers exhibit a significant difference in the on-site potential energy (~1 eV), which effectively breaks the interlayer coupling between them. As a result, for energies close to the corresponding Dirac points, the BLG system behaves like two electronically isolated single graphene layers. We prove this fact by a comprehensive multi-technique methodology based on low-temperature scanning tunneling microscopy/spectroscopy (STM/S) and angle-resolved photoelectron spectroscopy, which are corroborated by density functional theory, tight binding, surface diffraction and multiprobe STM transport. The work presents charge transfer from intercalated metal atoms as a promising approach for the synthesis of 2D graphene heterostructures with electronic phases generated by giant displacement fields.

## References

[1]M. Kolmer, B. Schruck, M. Hupalo, J. Hall, S. Chen, J. Zhang, C.-Z. Wang, A. Kaminski, M.C. Tringides, "Highly Asymmetric Graphene Layer Doping and Band Structure Manipulation in Rare Earth–Graphene Heterostructure by Targeted Bonding of the Intercalated Gadolinium", *J. Phys. Chem. C* **126**, 6863 (2022). <https://doi.org/10.1021/acs.jpcc.2c01332>.

# Tuesday Afternoon, November 7, 2023

[2] M. Kolmer, W. Ko, J. Hall, S. Chen, J. Zhang, H. Zhao, L. Ke, C.-Z. Wang, A.-P. Li, M.C. Tringides, "Breaking of Inversion Symmetry and Interlayer Electronic Coupling in Bilayer Graphene Heterostructure by Structural Implementation of High Electric Displacement Fields", *J. Phys. Chem. Lett.* 13, 11571 (2022). <https://doi.org/10.1021/acs.jpcclett.2c02407>.

4:20pm **NS1+2D+EM+MN-TuA-7 AVS Dorothy M. and Earl S. Hoffman Scholarship Recipient Talk: Exfoliated 2D Nanosheets for Large-Area, Solution-Processed Optoelectronics**, *Lidia Kuo*<sup>1</sup>, *S. Rangnekar*, *V. Sangwan*, *M. Hersam*, Northwestern University

Two-dimensional (2D) materials exhibit thickness-dependent optoelectronic properties due to their atomically thin nature, unlike their bulk layered crystalline counterparts. In particular, semiconducting MoS<sub>2</sub> undergoes an indirect to direct bandgap transition as the thickness is decreased to the monolayer limit, leading to enhanced optical absorption and emission at the atomically thin scale. Liquid-phase exfoliation (LPE) is a scalable and cost-effective method for obtaining 2D materials from bulk crystals. However, the yield of monolayer sheets by LPE has been impractically low in previous work. The resulting LPE-processed optoelectronic devices have fallen short compared to nanosheets derived from mechanical exfoliation or chemical vapor deposition. Here, we demonstrate that LPE coupled with megasonic exfoliation – i.e., processing at megahertz frequencies compared to the kilohertz frequencies commonly utilized for LPE – yields an unprecedentedly high fraction of monolayer MoS<sub>2</sub>. As a result, megasonic exfoliation enables ultrahigh responsivity in printed MoS<sub>2</sub> photodetectors as well as the first demonstration of electroluminescence for large-area, solution-processed MoS<sub>2</sub> films. This work establishes megasonic exfoliation as a scalable and generalizable approach for achieving optoelectronic-grade 2D semiconductors via LPE.

## Nanoscale Science and Technology Division

### Room B113 - Session NS2+2D+EM-TuA

#### Light-Matter Interactions at the Nanoscale

Moderator: *Nancy Burnham*, Worcester Polytechnic Institute

4:40pm **NS2+2D+EM-TuA-8 Highly Tunable Room-Temperature Exciton-Polariton Strong Coupling from Monolayer WSe<sub>2</sub> in Nanocavities**, *P. Schuck*, *Thomas Darlington*, Columbia University **INVITED**

In the interaction of light and matter, strong coupling occurs when exchange between a photon and electronic transitions exceeds the relative loss rate leading to hybridization of the optical and electronic states. The behavior is well known in cavity quantum electrodynamics (QED), and is a fundamental ingredient in single photon quantum logic gates. In solid-state systems, many strong coupling phenomena have been explored between different material excitations. Plasmons in particular have attracted great interest owing to their small mode volumes, allowing for strong coupling of a plasmon and single quasi-particles excitations such as excitons, potentially recreating in the solid-state, at the nanoscale, and at elevated temperatures many of the phenomena previously studied in traditional trapped atom QED.

Here, I describe our investigations of strong coupling between TMD excitons and a tunable plasmonic nanocavity formed between a plasmonic tip and gold substrate. Strong coupling between plasmons and excitons has been observed in exciton systems: e.g., J-aggregates, and colloidal quantum-dots. While these systems offer large coupling strengths, the exciton transition energies are largely fixed, and vary randomly depending on variations in growth conditions. By contrast, TMDs offer strong exciton emission and large tunability of exciton energy by applied strain. We utilized this tunability to control coupling strengths in nanocavities in a proof-of-principle nano-electro-mechanical system (NEMS) platform, demonstrating the ability to continuously tune, between weak and strong coupling conditions where we observe both upper and lower polariton bands.

5:20pm **NS2+2D+EM-TuA-10 Surface Plasmon Characterization in Ag Nanotriangles for Evaluation of Fano Resonance Conditions**, *Nabila Islam*, Department of Physics, Portland State University; *R. Word*, Department of Physics, Portland State University, Portland, Oregon; *E. Abdul*, *S. Rananavare*, Department of Chemistry, Portland State University; *R. Könenkamp*, Department of Physics, Portland State University

Surface plasmon resonances in metal nanostructures allow confinement of the electromagnetic field well below the light diffraction limit and have

attracted research interest for a broad range of sensing applications [1]. The comparably broad spectral width of surface plasmon based sensors can be improved by coupling the plasmon resonance to other resonances to generate Fano resonances with the distinctive and sharp asymmetric Fano line-shape. We used photoemission electron microscopy to explore the spectral and spatial behavior of plasmon resonances in structures consisting of a single nanoscale triangular platelet on a substrate providing coupling to a waveguide layer or to an optically active excitonic layer. In our experiments stationary and propagating surface plasmons are optically excited in the nano-triangle at wavelengths around 820-900nm, and multi-photon electron-emission is used to obtain images of the lateral surface plasmon distribution. An aberration-corrected photoemission microscope allowed us to obtain a spatial resolution of ~15nm and a femtosecond pulsed Ti-sapphire laser provided the photon intensities needed for the 3-photon photoemission imaging process [2]. The analysis of the obtained images is done in optical simulations of the same experimental set-up and by calculating the plasmon electric field distribution which is then used to analyze and interpret the photoemission micrographs. The analysis allows to identify the prominent surface plasmon modes and to analyze their interaction to form stationary resonance patterns and propagating modes. Fano-resonances are established in the simulation by placing the triangles in the vicinity of an optical waveguide using an appropriate spacer layer [3]. The simulation then allows to optimize this type of arrangement and to determine locations where the Fano-resonance amplitudes are most pronounced. Simulations of this kind were also applied to the case of gold triangles on substrates provided with exciton and spacer layers. Our results indicate that both the high plasmon field strengths typical for single nanoparticle structures and the sharp spectral features available in Fano-resonances can be combined in these single nano-particle structures, thereby allowing improved resolution in sensor applications.

#### References

- [1] Kumar, D., Kumar Sharma, G., & Kumar, M. (2023). *Materials Today: Proceedings*, 74, 259–262. <https://doi.org/10.1016/j.matpr.2022.08.149>
- [2] Stenmark, T., & Könenkamp, R. (2019). *Physical Review B*, 99(20). <https://doi.org/10.1103/physrevb.99.205428>
- [3] Hayashi, S., Nesterenko, D. V., & Sekkat, Z. (2015). *Applied Physics Express*, 8(2), 022201. doi:10.7567/apex.8.022201

5:40pm **NS2+2D+EM-TuA-11 Interconnected Plasmonic Nanogap Antennas for Photodetection via Hot Carrier Injection**, *John Grasso*, *R. Raman*, *B. Willis*, University of Connecticut

Modern integrated circuits have active elements on the order of nanometers; however, optical devices are limited by diffraction effects with dimensions measured in wavelengths. Nanoscale photodetectors capable of converting light into electrical signals are necessary for the miniaturization of optoelectronic applications. Strong coupling of light and free electrons in plasmonic nanostructures efficiently confines light into sub-wavelength volumes with intense local electric fields. Localized electric fields are amplified in nanogap regions between nanostructures where enhancements can reach over 1000. Hot carriers generated within these high field regions from nonradiative decay of surface plasmons can be injected into the conduction band of semiconductors at room temperature, enabling sub-bandgap photodetection. The optical properties of these plasmonic photodetectors can be tuned by modifying antenna materials and geometric parameters like size, thickness, and shape. Electrical interconnects provide connectivity to convert light into electrical signals. In this paper, we will describe the optical properties of plasmonic nanostructures with electrical interconnects and compare experiment and theory using finite-difference time-domain (FDTD) simulations. We will present experimental extinction data and FDTD simulations to elucidate how geometric structure and dielectric properties influence optical properties. We will present sub bandgap photodetection for nanostructures integrated with ALD deposited TiO<sub>2</sub>, and investigate both wavelength and

<sup>1</sup> AVS Dorothy M. and Earl S. Hoffman Scholarship Recipient

# Tuesday Afternoon, November 7, 2023

polarization dependence. We will also discuss how plasmonic heating effects contribute to photocurrent generation. These plasmonic nanogap antennas are subwavelength, tunable photodetectors with sub-bandgap responsivity for a broad spectral range.

## Plasma Science and Technology Division Room A106 - Session PS+MS-TuA

### Modelling of Plasmas and Plasma Driven Processes

Moderators: Mingmei Wang, Lam Research Corporation, Jinyu Yang, University of Notre Dame

2:20pm PS+MS-TuA-1 Towards Completing Chemistry Sets for Plasma Simulations, Sebastian Mohr, G. Armstrong, K. Lemishko, Quantemol Ltd., UK; A. Owens, W. Wu, J. Tennyson, University College London, UK

Plasma simulations are widely used in both academic and industrial settings to gain insights into fundamental plasma physics and optimise plasmas processes. Their success not only hinges on a robust physical model but also on the availability of data describing the chemical processes in a discharge. These data can be in the form of

Collision cross-sections, mostly for electron processes

Rate coefficients, mostly for heavy particle processes

Lifetimes and de-excitation channels of excited states

Probabilities for surface reactions

Species properties such as the enthalpy of formation

For rather simple or common gas mixtures such as argon or oxygen, sufficient data can usually be found in existing publications or databases; however, for more complex gas mixtures, especially ones including gases which have not been extensively studied yet, these data are usually not available for all species and reactions of interest. Furthermore, even in quite well known gas mixtures so far unknown or neglected phenomena can become important under specific process conditions. Hence, it is of vital importance to generate new data in a timely fashion.

We have developed a series of software tools to address the issue of missing data for plasma simulation purposes and to give easy access to existing data. These include:

The calculation of missing electron – molecule collision cross sections [1].

An online database QDB [2] of existing plasma chemistry data including both cross-sections and rate coefficients as well as some surface chemistry data

Machine learning algorithms for the quick estimation of species and reaction data [3]

A database of radiative lifetimes for excited states tailored to the needs of plasma modellers [4].

A global plasma model with additional tools such as a chemistry set reduction [5] to tailor a chemistry set to specific process conditions.

A collisional-radiative model to calculate the emission spectrum of a plasma discharge based on the densities of the excited states and the neutral gas temperature.

We will present the latest additions to these tools and examples to showcase their use and their impact on plasma simulations such as adding

reactions with formerly unknown cross-sections or rate coefficients to chemistry sets or the impact of adding the radiative decay of vibrational states to a plasma model.

[1] B Cooper et al 2019 *Atoms* **7** 97

[2] J Tennyson et al 2022 *Plasma Sources Sci. Technol.* **31** 095020

[3] M Hanicinec et al 2023 *J Phys D*, in press, doi:10.1088/1361-6463/acd390

[4] A Owens et al 2023 *Plasma Sources Sci. Technol.*, submitted

[5] M Hanicinec et al 2020 *Plasma Sources Sci. Technol.* **29** 125024

2:40pm PS+MS-TuA-2 Particle-in-Cell Monte Carlo Collision Modeling of Low-Pressure Plasma Discharges, Ken Hara, Y. Yamashita, Stanford University

Predictive modeling of partially ionized gases plays a critical role for applications such as semiconductor manufacturing, plasma processing, spacecraft propulsion, hypersonic flows, and high-energy density plasmas. However, plasma modeling remains challenging due to the nonlinear coupling of different physical and chemical processes. In particular, when operating the plasma sources at low pressure, the plasma constituents are not in equilibrium and their velocity distribution functions may become a non-Maxwellian due to the lack of collisions. Conventional fluid approaches cannot capture such rarefied flow physics and thus kinetic methods are needed. In this talk, we will present the development of particle-in-cell (PIC) Monte Carlo collision (MCC) models for low-pressure plasma discharges. The in-house PIC/MCC models are applied to various phenomena, including DC/RF breakdown, cylindrical sheath, capacitively coupled plasmas, and plasma instabilities. In particular, the effects of macroparticle (MP) weights on the plasma behavior are studied using a cylindrical (axisymmetric) PIC/MCC model. As the cell center volume is small near the symmetry line compared to the periphery, the numerical noise due to the lack of MPs can artificially generate plasmas near the centerline, leading to numerical plasma nonuniformity. The numerical heating is mitigated by modifying the MP weight. Acceleration of the PIC/MCC simulations and applications to DC/RF breakdown will be discussed in the talk.

3:00pm PS+MS-TuA-3 Radio-frequency Hollow Cathode Discharge Characterization using Plasma and Machine Learning Models, Kallol Bera, A. Verma, S. Ganta, S. Rauf, Applied Materials, Inc. **INVITED**

Low to moderate pressure radio-frequency (RF) hollow cathode discharges (HCDs) have gained significance for advanced plasma processing in the semiconductor industry. HCDs form in cylindrical cavities in the cathode. One can use an array of such HCDs to create uniformly dense large-area plasma. In the HCD, RF sheath heating as well as secondary electron acceleration play an important role. For modeling low-pressure RF HCDs, where kinetic effects are important, particle-in-cell Monte Carlo collision (PIC-MCC) modeling scheme has been used. In this PIC-MCC model, using charge density of particles, Poisson equation is solved for electric potential, which yields the electric field. Using this electric field, all charged particles are moved. The code considers particle collisions with each other and with neutral fluid using a Monte Carlo model. The single HCD behavior is studied over a range of pressure, RF voltage, frequency, and secondary electron emission coefficient. A strong positive power deposition region is observed within the hollow-cathode hole. The plasma penetrates inside the hollow-cathode hole with an increase in pressure and frequency, leading to plasma density enhancement. Higher secondary electron emission coefficient has a stronger impact on the plasma penetration into the hole at higher frequency. However, the effect of increasing RF voltage on plasma penetration into the hole is limited. Large area plasma using an array of HCDs is coupled to electromagnetic fields in the process chamber. Multiphysics modeling of an array of RF HCDs is difficult due to the geometrical complexity, which makes the simulations computationally prohibitive. This precludes development and utilization of these models in scenarios where the computations need to be performed rapidly and repeatedly. To overcome these challenges, we developed a deep learning based non-linear model order reduction method for plasma process in HCDs. A space-filling method is used to design computational experiments at different voltages at the fundamental frequency and at the second harmonic along with their phase difference. The temporal voltage-current characteristics of the HCD are used to train the reduced order model based on modified recurrent neural network. Our model predictions match well with the plasma simulation results within and outside the training range at a significantly smaller computational time. Further, an electromagnetic model is developed with coupled non-linear voltage-current characteristics

# Tuesday Afternoon, November 7, 2023

from the neural network model. The coupling of electromagnetic field to non-linear discrete discharges characterizing an array of HCDs for large area plasma is in progress.

**4:20pm PS+MS-TuA-7 Experimental Characterization and Modeling of the Spatial Afterglow of Plasmas, *Nabiel Hilmy Abuyazid***, University of Illinois at Urbana Champaign; *N. Uner*, Middle East Technical University, Turkey; *S. Peyres, R. Sankaran*, University of Illinois at Urbana Champaign

There has been recent interest in the spatial afterglow of plasmas because of its potential role in charging and agglomeration of aerosol particles as well as neutralization and dosing of surfaces. In general, the spatial afterglow is analogous to a temporal afterglow, characterized by a decay of charge resulting from a change in the applied power, except that the charge decay occurs in space rather than in time. However, the nature of the charge decay has been much less studied than temporal afterglows, perhaps because of the challenge of performing experiments at higher pressures and in smaller dimensions.

Here, we performed double Langmuir probe (DLP) measurements, which enable spatial measurements of the plasma density, and developed a one-dimensional advection-diffusion-recombination model that describes the charge decay in the spatial afterglow. Our results show excellent agreement between experimental measurements and model outputs over different pressures. Experimental measurements were limited to a pressure of 300 Torr at which point the DLP traces no longer exhibited known shapes and could not be analyzed to extract plasma parameters. By validating the model at the lower pressures, we were then able to extend the model to predict behavior at higher pressures, up to atmospheric. At pressures above ~75 Torr, the rate of charged species decay is primarily influenced by pressure, as three-body recombination becomes increasingly dominant over diffusional losses, and is secondarily influenced by gas flow velocity and temperature. Importantly, our findings reveal a transition from ambipolar diffusion to free diffusion at some distance from the bulk plasma within the spatial afterglow. First studied in temporal afterglows, apparent diffusivities of charged species vary as the plasma decays, eventually reaching a critical point where the ambipolar field becomes too weak and charged species begin to diffuse freely. The shift to free diffusion could lead to negatively-charged electrons being lost and positively-charged ions remaining, which has been previously reported to explain how aerosol particles that leave a bulk plasma negatively charged become neutralized or even positively charged after their transit through the spatial afterglow.

**4:40pm PS+MS-TuA-8 Circuit-based Reduced Order Model for Fluid Plasma Simulation of Capacitively Coupled Plasma Reactors, *Sathya Ganta***, *A. Verma, K. Bera, S. Rauf*, Applied Materials, Inc.

Fluid plasma simulations are essential for the design of radio frequency (RF) driven capacitively coupled plasma (CCP) reactors used for plasma-based deposition/etching processes. One can assess on-wafer performance using the computed ion/neutral fluxes, sheath potentials, and ion energies. These plasma parameters are directly related to process parameters like deposited film thickness, film stress, wet etch rate, uniformity etc. Hence, the fluid plasma simulations are vital to the semiconductor industry. To predict the ideal process parameters required to meet the on-wafer specifications, one needs to run a large number of simulations in the multi-dimensional process space, which requires enormous computational resources. A key aid in such scenarios would be fast and reliable reduced-order surrogates to the computationally cumbersome plasma fluid simulations. This paper explores one such reduced-order surrogate model based on a circuit-based estimation of the RF sheath. Here, the RF sheath is estimated to be a circuit consisting of a constant current source predicting ion current, a diode predicting electron current and a capacitor predicting the displacement current where these three circuit elements are in parallel to each other. First, a small set of 1D plasma fluid simulations are run corresponding to a set of process parameters that span the entire process space. The results from these plasma simulations, specifically the sheath voltage and current characteristics, are used to fit the parameters of the current source, diode and capacitor that form the RF sheath using a non-linear regression model. Once the circuit parameters are fitted, the resulting RF sheath circuit is coupled to an electromagnetic finite difference time-domain (FDTD) simulation making it a reduced-order surrogate of the plasma fluid simulation. The reduced order model is finally run corresponding to a new set of process parameters within the process space and its performance is compared to that of fluid plasma simulations and analyzed.

**5:00pm PS+MS-TuA-9 Fully Kinetic Modeling of Wafer Processing Chambers in CCP and coupled ICP/CCP Systems Using VSim, *Daniel Main, E. Lanham, J. Cary, T. Jenkins, J. Leddy, S. Kruger***, Tech-X Corporation

Inductively Coupled Plasmas (ICPs) are extensively used for materials processing in the semiconductor industry, typically with the addition of an RF bias [1]. For these reactors, it is assumed that the majority of plasma generation comes from the inductive power while the bias can independently control the flux and energy of ions needed for processing. In reality, the interaction between the multiple power sources is difficult to isolate and computational modeling becomes a necessity. Typically ICPs are modeled using a fluid approach, which does not correctly model the collision processes at lower pressures (~1-10 mTorr) nor the sheath that forms near the wafer. In this work, we discuss multiple techniques using the particle-in-cell software package VSim [2,3] that can be used for reactor-scale modeling of mixed inductive and capacitive discharge systems to accurately characterize the ion energies impacting a wafer for processing. One method is to use a global model to first compute a near-steady-state system composed of neutrals and plasma. The fluxes and densities from the global model serve as initial conditions for a high-resolution electrostatic capacitively coupled plasma (CCP) simulation to correctly model the sheath near the wafer and ion fluxes onto the wafer. Another approach is to model both the inductive and capacitive power sources in one simulation using a newly developed implicit electromagnetic scheme. We discuss differences between the CCP-only and coupled ICP/CCP systems found in ion energies, ion fluxes and the ion distribution function impacting the wafer, as well as the computational costs of the two methods.

[1] M. A. Lieberman and A. J. Lichtenberg, Principles of Plasma Discharges and Materials Processing, John Wiley & Sons, Inc. (2005).

[2] C. Nieter and J. R. Cary, J. Comp. Phys. 196, 448 (2004).

[3] www.txcorp.com

**5:20pm PS+MS-TuA-10 Hybrid Particle-in-Cell + Fluid Model of Multi-Frequency Capacitively Coupled Plasma with Tailored Voltage Waveform Bias, *Shahid Rauf, X. Shi, T. Wang, S. Ganta***, Applied Materials, Inc.

Multi-frequency capacitively coupled plasmas (CCPs) are widely used for thin film etching and deposition in the semiconductor industry. When operated at low pressures, kinetic effects dominate electron dynamics and, therefore, fluid assumptions are inaccurate for electrons in plasma models. Most industrial applications are, however, done using complicated gas mixtures with a variety of ions and neutral species. These plasmas are often electronegative with large concentrations of negative ions. Kinetic modeling for all the species, e.g., by solving the Boltzmann equation or using particle-based techniques, is impractical due to the high computational cost. A hybrid model for multi-frequency CCPs is described in this paper where the electrons are modeled as particles (using the particle-in-cell technique) while the ions and neutral species are treated as a fluid. The equations governing the kinetics of electron pseudo-particles, continuity and momentum equations for ions, Poisson equation for the electric field, and the continuity equations for neutral species are coupled at each time-step, with the time-step typically governed by the light electrons. This model is used to examine plasmas of Ar/CF<sub>4</sub> and c-C<sub>4</sub>F<sub>8</sub>/O<sub>2</sub> in a parallel plate CCP reactor with a high frequency (40 MHz sinusoidal) and a low frequency (400 kHz tailored voltage waveform) source. A combination of 1-dimensional, 2-dimensional (2D) Cartesian geometry, and 2D axisymmetric cylindrical geometry simulations is used to examine the effect of the low-frequency duty cycle on plasma chemistry and spatial structure of the plasma. The relative flows of the gases in the mixture are varied to understand the dynamics of both electropositive and electronegative discharges. Due to the long electron mean free path (relative to the inter-electrode gap), the plasma spreads out far from the region where the electrons absorb energy. This has major consequences on plasma uniformity in the 2-dimensional model. It is also found that, at a lower duty cycle, the time-averaged sheath at the powered electrode is thinner and the plasma occupies a larger volume. Consequently, for a given HF power and LF voltage, charged and neutral specie densities are higher at a lower duty cycle.

**5:40pm PS+MS-TuA-11 Wafer Edge and Focus Ring Effects on Ion Energy Distributions and Har Features During Plasma Etching Using Low Bias Frequencies, *Evan Litch***, University of Michigan; *H. Lee, S. Nam*, Samsung Electronics Co., Inc., Republic of Korea; *M. Kushner*, University of Michigan

Current microelectronic device architectures are continuing to trend towards 3-dimensional devices for higher functionality. A consequence of

# Tuesday Afternoon, November 7, 2023

fabricating 3D devices is the need to plasma etch high aspect ratio (HAR) features of ARs > 100. An example of HAR plasma etching is deep trench isolation (DTI) which is used to isolate 3D logic structures and imaging cells from interfering with each other. These DTI etches are performed in halogen-based mixtures (e.g., HBr/Cl<sub>2</sub>) for a Si wafer in inductively coupled plasma (ICP) reactors.

At HARs, the primary etch mechanisms deep within the profile are ion/hot neutral chemical and physical sputtering. In order to reduce the etch time for these features while maintaining critical dimensions, plasma etching with narrow-angular distributions of incident ions is required. By lowering the bias frequency (100s kHz), ion transit through the sheath is in the thin-sheath limit. (The thin sheath limit refers to ions being able to transit the sheath in a fraction of the RF period.) While this is helpful for ions incident across the majority of the wafer, ion distributions are typically broader and perhaps skewed at these lower frequencies near the edge of the wafer. This is primarily due to charging of the focus ring (FR) due to the longer period exceeding the RC time constant for such charging leading to greater sheath curvature at the edge of the wafer. To maintain critical dimensions of HAR structures at the wafer edge, modifying the FR geometry and/or electrical properties may be necessary to take advantage of lower bias frequencies.

In this work, results from a computational investigation of an ICP using very low bias frequencies for different FR parameters will be discussed. The simulations were conducted with the Hybrid Plasma Equipment Model (HPEM), investigating an ICP sustained in Ar/O<sub>2</sub>/Cl<sub>2</sub>. IEADs, uniformity of fluxes to the wafer and sheath structure for these systems will be discussed. Consequences on etch profiles will also be discussed.

Work was supported by Samsung Electronics Co. and the US National Science Foundation.

6:00pm **PS+MS-TuA-12 Plasma Dynamics During Synchronous RF Pulsing in Dual Frequency Capacitively Coupled Plasma**, *Abhishek Verma, S. Rauf, K. Bera*, Applied Materials, Inc.; *D. Sydorenko*, University of Alberta Edmonton, Canada; *A. Khrabrov, I. Kaganovich*, Princeton Plasma Physics Laboratory

Low-pressure multi-frequency capacitively coupled plasmas (CCP) are used for numerous etch and deposition applications in the semiconductor industry. Pulsing of the radio-frequency (RF) sources enables control of neutral and charged species in the plasma on a millisecond timescale. In this work, the synchronous (i.e., simultaneous, in-phase) pulsing of both power sources in a dual frequency CCP is examined. To resolve kinetic effects at low gas pressure, modeling has been done using the electrostatic Particle-in-cell/Monte Carlo collision method. The objective of this work is to investigate the sensitivity of the plasma properties to small changes in timing during synchronous pulsing of the 2 RF sources. It is demonstrated that small deviations in the on and off times of the 2 RF sources can lead to major changes in the plasma characteristics. In the simulations, the pulsing parameters (on and off times and ramp rates) are varied and the temporal evolution of plasma characteristics such as electron density, ion energy, ion energy flux, species current at the electrode, and electron temperature are examined. It is demonstrated that if the low-frequency (LF) source is turned on (or off) a few  $\mu$ s before (or after) the high-frequency source, plasma density during the off-state (or on state) undergoes sharp variations due to the frequency coupling effect. Similarly, turning on the LF source with a small delay results in a sharp increase in the plasma density when the HF source is turned on. The study demonstrates the importance of synchronization of RF pulsing in dual frequency CCPs and discusses methods to finetune plasma properties further.

## Quantum Science and Technology Mini-Symposium Room B110-112 - Session QS+SS-TuA

### The Quantum Metrology Revolution

Moderators: *Luxherta Buzi*, IBM, *Petra Reinke*, University of Virginia

2:20pm **QS+SS-TuA-1 Quantum Sensing Enabled by Spin Qubits in Diamond**, *Fedor Jelezko*, Institute of Quantum Optics, Ulm University, Germany

INVITED

Synthetic diamond has recently emerged as a candidate material for a range of quantum-based applications including quantum information processing and quantum sensing. In this presentation we will show how single nitrogen-vacancy (NV) colour centres can be created with a few nanometers accuracy and coherent dipole-dipole coupling was employed to generate their entanglement. Single NV centers and clusters of entangled spins created close to the diamond surface can be employed as nanoscale

sensors of electric and magnetic fields. We will show nanoscale NMR enabled by single NV centers and discuss sensitivity and spectral resolution limits of nanoscale NMR. We will also discuss applications of NV centres for hyperpolarization of nuclear spins and application of optical spin polarization in MRI.

3:00pm **QS+SS-TuA-3 Tunneling Andreev Reflection - New Quantitative Microscopy of Superconductors with Atomic Resolution**, *W. Ko*, University of Tennessee Knoxville; *S. Song, J. Yan*, Oak Ridge National Laboratory; *C. Lane*, Los Alamos National Laboratory; *J. Lado*, Aalto University, Finland; *Petro Maksymovych*, Oak Ridge National Laboratory

Andreev reflection is an established method to probe the existence of superconductivity, and, crucially, the symmetry of the superconducting order parameter. In its conventional implementation of the point contact Andreev reflection (PCAR), the technique relies on so-called directional contacts, which inject quasiparticles into superconductors with well-defined momentum. However, good momentum resolution requires a trade-off for essentially no spatial resolution, which has limited the applicability of PCAR to atomic-scale properties of superconductors, including inhomogeneities and interfaces.

In this talk, we will present our latest developments in Tunneling Andreev Reflection - a new experimental approach which we recently introduced to quantify Andreev reflection through atomic-scale tunnel junction [1]. Similar to PCAR, TAR exhibits direct sensitivity to the superconducting order parameter in both conventional and unconventional superconductors [2]. Recently, we used TAR to unambiguously confirm the sign-changing order parameter in paradigmatic FeSe, and further revealed suppression of superconductivity along the nematic twin boundaries above 1.2 K [2]. Locally suppressed superconductivity, in turn, explains the peculiar vortex templating effect exerted by twin boundaries - essentially causing recrystallization of the vortex glass phase [3]. However, due to atomic-spatial resolution TAR lacks momentum resolution - the opposite of PCAR. Therefore, the measurements, observables and their interpretation are fundamentally distinct from PCAR as well. We will discuss our present understanding of this technique, relevant methods of data analysis needed to reveal Andreev signal, and specific effects of band structure on TAR. These effects are crucially important for robust characterization of unconventional superconductivity, while also enabling TAR to complement tunneling spectroscopy and quasiparticle imaging in search for exotic quantum materials. Research sponsored by Division of Materials Science and Engineering, Basic Energy Sciences, Office of Science, US Department of Energy. SPM experiments were carried out as part of a user project at the Center for Nanophase Materials Sciences, Oak Ridge National Laboratory, a US Department of Energy Office of Science User Facility.

1. W. Ko, J. Lado, P. Maksymovych, *Nano Lett.* 22 (2022) 4042.

2. W. Ko, S. Y. Song, J. Lado, P. Maksymovych, arXiv:2303.05301 [https://arxiv.org/abs/2303.05301].

3. S. Y. Song, C. Hua, L. Bell, W. Ko, H. Fangohr, J. Yan, G. B. Halász, E. F. Dumitrescu, B. J. Lawrie, P. Maksymovych, *Nano Lett.* 23(2023)2822.

3:20pm **QS+SS-TuA-4 Patterned-Stress-Induced Compositional Manipulation of Epitaxially Grown Semiconductors for Quantum Applications**, *Leonid Miroshnik*, University of New Mexico; *B. Rummel*, Sandia National Laboratories; *M. Patriotis*, University of New Mexico; *A. Li, T. Sinno*, University of Pennsylvania; *M. Henry*, Sandia National Laboratories; *G. Balakrishnan, S. Han*, University of New Mexico

We have previously demonstrated compositional patterning of epitaxially grown compound semiconductors, using lithographically patterned nanoscale pillars as a mechanical press.<sup>1-3</sup> The elastically introduced strain from the press, at elevated temperatures, steers large atoms out of the compressed region of compound semiconductors (e.g., indium in InGaAs) to form quantum confined structures. This approach allows forming quantum structures at desired locations in an addressable manner. In this work, we describe a new approach to introduce a patterned stress field to semiconductor films, using Surface Acoustic Waves (SAW) generated by Interdigitated transducers (IDTs). We fabricate SAW devices on GaAs(100) substrate and demonstrate that we can image standing surface acoustic waves using 2D Raman spectroscopy as well as atomic force microscopy.<sup>4</sup> The magnitude of these waves, upon optimization of SAW devices<sup>5</sup>, reaches greater than 5 nm, introducing 100s of MPa stress. We will share the stress characterization and optimization approach in this presentation and assess the likelihood of using the stress field to induce compositional patterning.

This material is based upon work supported by the National Science Foundation under Grant No. DMR-1809095

# Tuesday Afternoon, November 7, 2023

1. S. Ghosh, D. Kaiser, J. Bonilla, T. Sinno, and S. M. Han, "Stress-Directed Compositional Patterning of SiGe Substrates for Lateral Quantum Barrier Manipulation," *Applied Physics Letters***107**, 072106-1:5 (2015)

2. D. Kaiser, S. Ghosh, S. M. Han, and T. Sinno, "Modeling and simulation of compositional engineering in SiGe films using patterned stress fields," *Molecular Systems Design and Engineering***1**, 74-85 (2016)

3. D. Kaiser, S. Ghosh, S. M. Han, and T. Sinno, "Multiscale Modeling of Stress-Mediated Compositional Patterning in SiGe Substrates," *High Purity and High Mobility Semiconductors***75**, 129-141 (2016)

4. B. D. Rummel, L. Miroshnik, M. Patriotis, A. Li, T. R. Sinno, M. D. Henry, G. Balakrishnan, and S. M. Han, "Imaging of surface acoustic waves on GaAs using 2D confocal Raman microscopy and atomic force microscopy," *Applied Physics Letters***118**, 031602-1:6 (2021) <https://doi.org/10.1063/5.0034572>.

5. B. D. Rummel, L. Miroshnik, A. B. Li, G. D. Heilman, G. Balakrishnan, T. Sinno, and S. M. Han, "Exploring electromechanical utility of GaAs interdigitated transducers; using finite-element-method-based parametric analysis and experimental comparison," *Journal of Vacuum Science & Technology B***41**, 013203-1:8 (2023) <https://doi.org/10.1116/6.0002169>.

4:20pm **QS+SS-TuA-7 Atomic Tunneling Defects in Superconducting Quantum Circuits: Origins and Remedies**, **Jürgen Lisenfeld**, Karlsruhe Institute of Technology (KIT), Germany **INVITED**

Parasitic two-level systems formed by defects in the materials of superconducting qubits are a major source of decoherence. I will review the defects' origins, and discuss possible ways to mitigate their detrimental impacts. A focus will be set on recent experiments in Karlsruhe, where we develop novel methods to in-situ control defect properties by applied mechanical strain and electric fields. E-field tuning of defects provides a possibility to mitigate energy loss of qubits due to resonant defects. It also allows us to identify the locations of defects in a given quantum circuit which helps to guide the way towards better qubit fabrication.

5:00pm **QS+SS-TuA-9 Mechanistic Investigations of Superconducting Film Growth: Substrate-Mediated Sn Diffusion on a Niobium Oxide**, **Sarah Willson**, University of Chicago; **R. Farber**, University of Kansas; **S. Sibener**, University of Chicago

Niobium is the highest temperature elemental superconductor, making it the standard material for superconducting radiofrequency (SRF) cavities in next-generation linear accelerators. These facilities require cryogenic operating temperatures (< 4 K) to limit the formation of superconductivity-quenching hot spots in the near-surface region of the cavity. Widespread efforts are underway to increase the accelerating fields and reduce the cryogenic burden by improving SRF surfaces.

A promising solution is to coat the Nb SRF surface with a Nb<sub>3</sub>Sn thin film via Sn vapor deposition. The higher critical temperature and critical field makes Nb<sub>3</sub>Sn an ideal candidate for capping Nb surfaces. However, the persistence of defects, stoichiometric inhomogeneities, and excessive surface roughness in formed these Nb<sub>3</sub>Sn films nucleate quenching sites – limiting the SRF performance.

As part of a widespread interdisciplinary effort to optimize SRF accelerating capabilities, this work aims to develop a comprehensive growth model for pristine Nb<sub>3</sub>Sn films. We aim to understand the interplay between the underlying Nb oxide morphology, Sn coverage, and Nb deposition temperature on Sn wettability and Nb<sub>3</sub>Sn growth mechanisms. Alloy films are grown on single crystal and polycrystalline Nb surfaces terminated with a diverse range of morphologies and analyzed using both *in situ* and *ex situ* techniques.

Characterization of initial Sn/Nb<sub>2</sub>O<sub>5</sub> phases provide insight towards the dynamic and reactive interface that templates Nb<sub>3</sub>Sn films. Complementary experiments of Nb<sub>3</sub>Sn films grown at higher Sn coverages further illustrate how the diverse underlying Nb oxide surface morphologies impact the quality, and ultimately the accelerating performance, of these SRF surfaces.

5:20pm **QS+SS-TuA-10 Revealing Pairing Symmetry of Superconductors by Tunneling Andreev Reflection**, **Wonhee Ko**, University of Tennessee, Knoxville; **S. Song, J. Yan**, Oak Ridge National Laboratory; **J. Lado**, Aalto University, Finland; **P. Maksymovych**, Oak Ridge National Laboratory

Andreev reflection (AR) is an electronic transport process at the junction of a normal metal and a superconductor, where the electrons in the normal metal transform to the Cooper pairs by retroreflecting holes and conducts current across the junction. The process is highly sensitive to the superconducting order parameters and functions as a tool to directly probe the superconductivity. Based on AR, we developed a new technique,

tunneling Andreev reflection (TAR), by applying AR to the tunnel junction in scanning tunneling microscope (STM) [1,2]. Specifically, we precisely tune the STM tip-sample distance to systematically study the AR as a function of the tunneling barrier height. Since the AR is a higher order tunneling process compared to the normal electron tunneling, the relative decay rate of the tunneling conductance increases inside the superconducting gap, whose specific shape depends on the nature of the superconductivity [3]. By comparing the decay rate spectra with the theoretical calculations, we identify the pairing symmetry of various kinds of superconductors, from conventional s-wave ones to the unconventional high-T<sub>c</sub> ones such as iron-based or cuprate superconductors.

This research was performed at the Center for Nanophase Materials Sciences which is a DOE Office of Science User Facility.

[1] W. Ko, E. Dumitrescu, and P. Maksymovych, *Phys. Rev. Res.***3** 033248 (2021)

[2] W. Ko, J. L. Lado, and P. Maksymovych, *Nano Lett.***22** 4042 (2022)

[3] W. Ko, S. Y. Song, J. Yan, J. L. Lado, and P. Maksymovych, *arXiv:2303.05301*

5:40pm **QS+SS-TuA-11 Single-nm-Resolution Gate Fabrication for Top-Gated Quantum Dot Qubits**, **J. Owen, Joshua Ballard, E. Fuchs, J. Randall, Zyvex Labs; F. Beaudoin**, Nanoacademic Technologies, Canada; **A. Sigillito**, U. Pennsylvania

Top gated semiconductor quantum dot qubits represent an attractive path to quantum computing. However, variations in the physical dimensions of the top gates create significant variations in the electrostatic confinement and therefore the energy levels in the qubit. The variation in gate dimensions complicates the design of multi qubit systems and the required tuning of the biases on the gates for multiple qubits is so complex that machine learning is employed.

Multiple modeling runs of a generic top gated multi-qubit system carried out with the spin-qubit computer-aided design tool QCAD has found that a variation in the gate dimensions of ~2 nm causes a factor of 2 change in the tunneling rates, or a factor of 4 in the Exchange Interaction strength. This level of precision is not achievable using e-beam lithography where the proximity can cause an increase in the written feature width by 15 nm compared to the pattern.

We describe an alternative path which uses Atomic Precision Lithography[1] to create far more precise gates. Two methods to transfer the pattern into the gate structures are described; either saturate the patterns with dopant precursors to make dopant-based gate structures or growing area-selective etch mask material. The former will preserve the precision, but is less compatible with CMOS processes. Otherwise, area-selective atomic layer deposition and reactive ion etching can be used to make nanoimprint templates[2]. The accuracy of templates thus produced, and the precision of Jet and Flash Nanoimprint lithography will produce far more uniform top gates with a scalable manufacturing technique.

1. Bussmann, E.; Butera, R. E.; Owen, J. H. G.; Randall, J. N.; Rinaldi, S. M.; Baczewski, A. D.; Misra, S. Atomic – Precision Advanced Manufacturing for Si Quantum Computing. *MRS Bull.***2021**, *46*, 1–9.

2. Ballard, J.; McDonnell, S.; Dick, D.; Owen, J.; Mordi, G.; Azcatl, A.; Campbell, P.; Chabal, Y.; Randall, J.; Wallace, R., Patterned atomic layer deposition on scanning tunneling microscope constructed templates. *Technical Proceedings of the 2013 NSTI Nanotechnology Conference and Expo, NSTI-Nanotech 2013* **2013**,*2*, 481-484.

6:00pm **QS+SS-TuA-12 The Changing Role of National Metrology Institute with Quantum-Based Standards and the Nist on a Chip Program**, **Jay Hendricks, B. Goldstein**, NIST

This oral presentation covers a bit of metrology history of how we got to where we are today and gives a forward-looking vision for the future of measurement science. The role of NIST as a National Metrology institute (NMI) is briefly described considering the world-wide redefinition of units that occurred on May 20<sup>th</sup>, 2019. The re-definition of units is now aligned with physical constants of nature and fundamental physics which opens new realization routes with quantum-based sensors and standards. The NIST on a Chip program (NOAC) is briefly introduced in this context. The re-definition of the SI units enables new ways to realize the units for the pascal and the kelvin. These quantum-based systems; however exciting, do raise new challenges and several important questions: Can these new realizations enable the size and scale of the realization to be miniaturized to the point where it can be imbedded into everyday products? What will be

# Tuesday Afternoon, November 7, 2023

the role of metrology institutes in the is new ecosystem of metrology and measurement? What will be the NMI role for quality systems and measurement assurance for these new quantum-based systems? This talk will begin to explore these important philosophical questions.

## Surface Science Division

### Room D136 - Session SS+HC-TuA

#### Photochemistry

**Moderators:** Erik Jensen, University of Northern British Columbia, Ahmad Nawaz, Hebrew University of Jerusalem

**2:20pm SS+HC-TuA-1 Pt Nanoclusters on GaN Nanowires for Solar-Assisted Seawater Hydrogen Evolution, Victor Batista, W. Dong, Y. Xiao, K. Yang, Z. Ye, P. Zhou, I. Navid, Z. Mi, Yale University** **INVITED**

Seawater electrolysis provides a viable method to produce clean hydrogen fuel. To date, however, the realization of high-performance photocathodes for seawater hydrogen evolution reaction has remained challenging. Here, we introduce n+p Si photocathodes with dramatically improved activity and stability for hydrogen evolution reaction in seawater, modified by Pt nanoclusters anchored on GaN nanowires (Fig 1). We find that Pt-Ga sites at the Pt/ GaN interface promote the dissociation of water molecules and spilling H\* over to neighboring Pt atoms for efficient H<sub>2</sub> production. Pt/GaN/Si photocathodes achieve a current density of -10 mA/cm<sup>2</sup> at 0.15 and 0.39 V vs. RHE and high applied bias photon-to-current efficiency of 1.7% and 7.9% in seawater (pH = 8.2) and phosphate-buffered seawater (pH = 7.4), respectively. We further demonstrate a record-high photocurrent density of ~169 mA/cm<sup>2</sup> under concentrated solar light (9 suns). Moreover, Pt/GaN/Si can continuously produce H<sub>2</sub> even under dark conditions by simply switching the electrical contact. This work provides valuable guidelines to design an efficient, stable, and energy- saving electrode for H<sub>2</sub> generation by seawater splitting.

**3:00pm SS+HC-TuA-3 Photoreactivity of Single Micro-Sized TiO<sub>2</sub> Crystals, H. Zhu, W. Lu, K. Park, Zhenrong Zhang, Baylor University**

Understanding the reactivity of TiO<sub>2</sub> particles with different polymorphs and morphologies is important for many photocatalytic applications. Here, the reactivity of individual anatase TiO<sub>2</sub> microcrystals with a large percentage of (001) facet was monitored and studied using operando photoluminescence microscopy. The photoreduction of resazurin on anatase microcrystals shows that the photoreduction rate on each microcrystal was different although the microcrystals had comparable sizes and exposed the same facets. The reaction rate changes from no reactivity to higher than that of the anatase (001) bulk single crystal. The reaction rate of the anatase microcrystals depends on the morphology and the structure of each particle. The reactivities of the microcrystals with mixed anatase-rutile phases and after the anatase-to-rutile phase transformation have also been monitored.

**3:20pm SS+HC-TuA-4 Electron Induced Photochemistry of Nitrous Oxide-Water Co-Absorbed Film (N<sub>2</sub>O@H<sub>2</sub>O) as a Model Study of Astrochemistry in the Interstellar Medium, Ahmad Nawaz, The Hebrew University of Jerusalem, Israel**

The desorption kinetics of N<sub>2</sub>O@H<sub>2</sub>O film deposited on a Ru (0001) surface under ultra-high vacuum (UHV) environment (2x10<sup>-10</sup> Torr) has been investigated as a model study for electrons-induced reactivity that takes place in the interstellar medium, using temperature-programmed desorption (TPD) measurements, at substrate temperature of 35K. The TPD spectra of all the prominent product masses were well detected by the QMS, employing a 3D-TPD analysis. The N<sub>2</sub>O molecules, embedded within ASW as the host matrix, decompose upon exposure to electrons at kinetic energies of 10eV and 50 eV. This leads to the formation of new molecular products at m/z values of 28 (N<sub>2</sub>) and 30 (NO) as the primary products. Typical TPD spectra of the parent N<sub>2</sub>O molecules, while embedded in ASW layer (15 ML) are shown in Figure 1a and product formation is shown in Figure 1b. Here, the primary N<sub>2</sub>O TPD peaks appear at ~82K, while some of these molecules are trapped within the water film and desorb together with the main ASW film at ~160K.

**4:20pm SS+HC-TuA-7 Structure and Chemistry of Aqueous Oxide Interfaces from Molecular Simulations, A. Selloni, A. Raman, Princeton University; Marcos Calegari Andrade, Lawrence Livermore National Laboratory; B. Wen, Henan University, China** **INVITED**

Photo-electrocatalysis involving complex oxide-water interfaces is a highly promising technology for the sustainable production of fuels. However,

probing these complex interfaces and gaining atomistic insights is still very challenging for current experimental methods, and is often only possible through accurate computational simulations. In this talk I will discuss some of our recent work on the application of ab-initio based molecular simulations to understand the structure and dynamics of interfacial water on photoelectrochemically relevant oxide surfaces. Specific topics will include proton transfer at the aqueous TiO<sub>2</sub> and IrO<sub>2</sub> interfaces and the influence of surface atomic structure on the water dissociation fraction and hydroxyl lifetimes at the interface.

**5:00pm SS+HC-TuA-9 Photodissociation of an Adsorbate via Coadsorbate Photon Absorption: Electronic Energy Transfer in Heterogeneous Molecular Thin Films, Erik Jensen, University of Northern B.C., Canada**

The photophysics of many small aromatics and related molecular systems has been studied intensely and widely for many years, both in understanding the molecular origins of natural phenomenon such as photosynthesis, as well as in areas of technological interest. Although the UV photosensitization of CH<sub>3</sub>I dissociation in gas-phase mixtures with benzene was noted many years ago[1], we can find no subsequent examples of studies of the photochemical dynamics of this process. We have studied a set of thin film molecular systems on a metal substrate using UHV surface science techniques and time-of-flight spectroscopy on neutral photofragments.

In the present work, we have studied the dynamics of the near-UV photodissociation of CH<sub>3</sub>I adsorbed on thin films (1–10ML) of benzene[2] and a variety of fluorinated benzenes grown on a Cu(100) substrate. Using polarized 248nm light, we find that the kinetic energies of the CH<sub>3</sub> photofragments point to significantly altered CH<sub>3</sub>I dissociation dynamics when adsorbed on C<sub>6</sub>H<sub>6</sub>, C<sub>6</sub>H<sub>5</sub>F and C<sub>6</sub>H<sub>4</sub>F<sub>2</sub> thin films, with progressive changes in the observed dynamics as higher fluorobenzenes are used (up to C<sub>6</sub>F<sub>6</sub>). The altered CH<sub>3</sub>I photodissociation dynamics and coincidently increased effective photodissociation cross sections are ascribed to a new pathway with initial photoabsorption in the aromatic thin film, and the excitation energy being efficiently transported to the CH<sub>3</sub>I adsorbed on top. There is evidence that excitons in the aromatic thin film play a significant role in the transport and transfer of the electronic excitation to the CH<sub>3</sub>I top layer.

#### References

[1] Dubois, J.T. and Noyes Jr., W.A., *Photochemical Studies XLVI: Photosensitization by Benzene and Pyridine Vapours*, J. Chem. Phys. **19**, 1512 (1951).

[2] Jensen, E.T., *Contrasting Mechanisms for Photodissociation of Methyl Halides Adsorbed on Thin Films of C<sub>6</sub>H<sub>6</sub> and C<sub>6</sub>F<sub>6</sub>*. Phys. Chem. Chem. Phys. **23**, 3748 (2021).

**5:20pm SS+HC-TuA-10 UV-Induced Oxidation of Aluminum, Robert Berg, C. Tarrío, T. Lucatorto, National Institute of Standards and Technology (NIST); F. Eparvier, A. Jones, Laboratory for Atmospheric and Space Physics**

Aluminum oxide films are usually grown on aluminum metal by anodization in a liquid electrolyte (thick films) or heating in the presence of oxygen gas (thin films). A third way is to expose the aluminum to ultraviolet radiation (UV) in the presence of water vapor. We devised a model of such oxidation that combined descriptions of photoemission from the Al metal, electron-phonon scattering in the oxide, Al<sup>3+</sup> ion transport in the oxide, and the adsorption and ionization of H<sub>2</sub>O on the oxide surface. It also accounted for UV-induced desorption of H<sub>2</sub>O and the effect of the Al<sup>3+</sup> ion flux on the surface reactions.

The model's five free parameters were fit to our measurements of UV-induced oxidation of aluminum. The UV, which was produced by filtering synchrotron radiation, comprised wavelengths from 150 nm to 480 nm, and the H<sub>2</sub>O pressure was varied between 3 × 10<sup>-8</sup> mbar and 1 × 10<sup>-4</sup> mbar. Exposures lasted from 3 hours to 20 days. An exposure with oxygen instead of water caused oxidation consistent with the background H<sub>2</sub>O pressure; the oxygen caused no additional oxidation.

The parameter values fitted to our measurements allowed us to describe the oxidation of aluminum membranes that were used to filter extreme UV wavelengths on the Solar Dynamics Observatory, a sun-observing satellite. This new understanding will help prevent similar problems on future satellites. These results are the first experimental confirmation of a model of UV-induced oxidation.

# Tuesday Afternoon, November 7, 2023

5:40pm **SS+HC-TuA-11 Self-Induced and Progressive Photo-Oxidation of Organophosphonic Acid Grafted Titanium Dioxide**, *Nick Gys*, Vrije Universiteit Brussel, Belgium; *B. Pawlak*, Hasselt University, Belgium; *K. Marcoen*, Vrije Universiteit Brussel, Belgium; *G. Reekmans*, Hasselt University, Belgium; *L. Fernandez Velasco*, Royal Military Academy, Belgium; *R. An*, University of Antwerp, Belgium; *K. Wyns*, Flemish Institute for Technological Research, Belgium; *K. Baert*, Vrije Universiteit Brussel, Belgium; *K. Zhang*, *L. Lufungula*, University of Antwerp, Belgium; *A. Piras*, Hasselt University, Namur University, Belgium; *L. Siemons*, University of Antwerp, Belgium; *B. Michielsen*, Flemish Institute for Technological Research, Belgium; *S. Van Doorslaer*, *F. Blockhuys*, University of Antwerp, Belgium; *T. Hauffman*, Vrije Universiteit Brussel, Belgium; *P. Adriaensens*, Hasselt University, Belgium; *S. Mullens*, Flemish Institute for Technological Research, Belgium; *V. Meynen*, University of Antwerp, Belgium

The introduction of organic molecules onto the surface of metal oxides through surface grafting provides the ability to tailor the surface properties towards an increased specificity and control of interactions. In the field of hybrid organic-inorganic materials, organophosphonic acid (PA) grafted metal oxides are becoming increasingly more prominent given their versatility in surface tuning and their specific merits in applications ranging from supported metal catalysis<sup>(1)</sup>, hybrid (photo)-electric devices<sup>(2)</sup>, biosensing<sup>(3)</sup> and sorption and separation processes.<sup>(4)</sup> While synthesis-properties-performance correlations are being studied for organophosphonic acid grafted TiO<sub>2</sub>, their stability and the impact of exposure conditions on possible changes in the interfacial surface chemistry remain unexplored. In addition, a differentiation in the stability of the organic group (carbon chain) and the M-O-P bonds is missing. In this study<sup>(5)</sup>, the impact of different ageing conditions on the evolution of the surface properties of propyl- and 3-aminopropylphosphonic acid grafted mesoporous TiO<sub>2</sub> over a period of 2 years is reported, using solid-state <sup>31</sup>P and <sup>13</sup>C NMR, ToF-SIMS, EPR and XPS as main techniques. In humid conditions under ambient light exposure, PA grafted TiO<sub>2</sub> surfaces initiate and facilitate photo-induced oxidative reactions, resulting in the formation of phosphate species and degradation of the grafted organic group with a loss of carbon content ranging from 40 to 60 wt%. Since exposure under dry air does not result in ageing phenomena, humidity and more specifically, the interactions of adsorbed water with the grafted surface, play a fundamental role in the ageing process. By revealing the underlying ageing mechanism, solutions were provided to prevent degradation. This work creates critical awareness in the research community working on hybrid titania materials and other possible photo-active materials to evaluate changes in photo-activity and stability after surface grafting.

1. F. Forato et al., Chem. - A Eur. J. 24, 2457–2465 (2018).
2. H. Chen, W. Zhang, M. Li, G. He, X. Guo, Chem. Rev. 120, 2879–2949 (2020).
3. N. Riboni et al., RSC Adv. 11, 11256–11265 (2021).
4. G. A. Seisenbaeva et al., RSC Adv. 5, 24575–24585 (2015).
5. N. Gys et al., Chempluschem. 88 (2023), doi:10.1002/cplu.202200441.

6:00pm **SS+HC-TuA-12 "Laser-XPS" invented 1989 in Japan, Patented 1997**, *B. Vincent Crist*, XPS Library

In 1989, a novel technique, Laser-XPS, was developed. Laser-XPS uses XPS to probe the core level surface chemical physics of various solid state materials while the materials are held in an ultra-high vacuum (UHV) chamber and irradiated with CW tunable organic dye or argon ion lasers. These two tunable CW lasers provide energy in the 1.9-3.5 eV range (655-351 nm, 44-81 Kcal/mol) with power levels ranging from 100-1,000 mW. A dynamic mode of operation uses XPS to directly measure the electronic nature of the photo-excited states, the photo-thermal effects, and the lifetimes of the associated initial and final states produced by the tunable CW laser irradiation. Several reversible phenomena, which are wavelength or power level dependent, were observed via the dynamic mode. These phenomena include: energy shifts in XPS signals, changes in XPS peak widths, charge control quality, and phosphorescence during XPS. A sequential mode of operation makes it possible to study the non-reversible effects of irradiating materials under UHV conditions with CW lasers. Non-reversible phenomena observed via the sequential mode include: surface chemical reactions, elimination of adventitious carbon contamination, elimination of oxygen species associated with the presence of water, hydroxides, or carbonates, color changes, outgassing, and melting. The initially expected energy shifting of a specific XPS signal within a complex spectrum of XPS signals from very similar chemical species due to narrow, selective photo-excitation of specific valence bands, was, however, not realized in this preliminary study.

Thin Film Division

Room A105 - Session TF1-TuA

Catalytic and Active Materials

Moderators: **Mark Losego**, Georgia Institute of Technology, **Richard Vanfleet**, Brigham Young University

2:20pm **TF1-TuA-1 MLD as a Sandbox for Photoactive Hybrid Materials**, *Ola Nilsen*, University of Oslo, Norway **INVITED**

To an experimental chemist, the MLD approach is a desirable tool to explore chemical reactivity and to create structures that otherwise would not be possible. So, what are its limitations? And why should you use this approach? These, and other questions will be covered during this presentation where we will focus on volatilization of precursors, challenges with surface limited reactions when your material is porous, how to influence the growth during growth, and more. The MLD approach is highly effective in combining material classes that naturally do not combine. We use this approach to combine highly absorbing organic molecules with fluorides and oxides to design photoactive structures. By such manner, we have achieved complete energy transfer from the organic molecules to lanthanides without quenching. We also show drastic suppression of concentration quenching of multilayered structures of lanthanides as compared to solid solutions by confining energy migration in 2D planes. The flexibility of the MLD approach allows for exploration of exotic combinations of absorbers and emitters, but how far can you go with MLD?

3:00pm **TF1-TuA-3 Dry Pathways to Synthesize Thin Films of Covalent Organic Frameworks**, *Syed Ibrahim Gnani Peer Mohamed*, *S. Nejati*, *M. Bavarian*, University of Nebraska - Lincoln

Covalent organic frameworks (COFs) are porous materials with potential applications in gas storage, catalysis, and electronics. However, traditional COF synthesis methods are limited by low solubility and poor processability. In contrast, oxidative chemical vapor deposition (oCVD) and oxidative Molecular Layer Deposition (oMLD) provide versatile and scalable approaches to deposit COFs on different surfaces. Porphyrins and their derivatives have attracted the attention of many researchers as precursors for COF preparation. Porphyrin and its metal complexes can serve as electrocatalysts, especially for oxygen reduction, nitrate reduction, and carbon dioxide reduction reactions. In addition, these materials have also been explored for photocatalysis, separation, optical switches, and other applications. Polymerization of porphyrins to create frameworks and networks increases the stability of these materials. Thus, preparing porphyrin-based COFs is essential for their widespread application. COFs are commonly synthesized via the solvothermal method, which involves a very long reaction time and the use of toxic organic solvents. Therefore, a dry synthetic pathway is highly desirable. Herein, we report the one-step, solvent-free synthesis of crystalline and porous porphyrin-based COFs. Both 5,10,15,20-tetra(4-aminophenyl)porphyrin (TAPP) or its transition metal complex (MPOR-COF, M = H<sub>2</sub>, Cu<sup>2+</sup>, Co<sup>2+</sup>, Zn<sup>2+</sup>) in the presence of antimony pentachloride (SbCl<sub>5</sub>), as an oxidant, polymerized. The monomer TAPP undergoes polymerization via phenazine link formation (pTAPP) in the presence of SbCl<sub>5</sub>, leading to the formation of well-ordered MPOR-COFs. Here, we describe the bottom-up and dry assembly of pTAPP and its derivatives to create active materials. We also report on the control achieved over the reaction selectivity and separation performance of the thin films deposited through the oxidative vapor phase polymerization pathway and explore various strategies to control the film structure and properties. The resulting materials were characterized using various techniques such as spectroscopy, microscopy, and gas adsorption. We also investigated the effect of substrate, deposition conditions, and post-synthesis treatment on the structure and properties of the resulting COFs. Our results show that oCVD and oMLD are promising methods for synthesizing COFs with tunable properties and potential applications in various fields.

3:20pm **TF1-TuA-4 Vapor Phase Infiltration of Titanium Oxide into P3HT to Create Organic-Inorganic Hybrid Photocatalysts**, *Li Zhang*, *S. Gregory*, *M. Losego*, Georgia Institute of Technology

Chemical doping using vapor phase infiltration (VPI) of metal halide precursors and water has been shown to dope conjugated polymers (CP). The reacted product – metal oxide clusters – remain trapped within the CP and are often thought to just act as scattering centers that lower the electronic mobility of the CP. However, in this talk we will show how these metal oxides can be used as catalytic sites for photocatalytic reactions. Metal oxides such as TiO<sub>x</sub> have been well documented for their good photocatalytic properties, with the drawback that they do not absorb in the

# Tuesday Afternoon, November 7, 2023

visible region. In hybrid CP-MO<sub>x</sub> systems, the CP can act as a sensitizer absorbing light in the visible regime and then injecting the photo-excited electrons into the MO<sub>x</sub> to perform the catalysis. In this talk we will discuss our work in exploring the vapor phase infiltration of the CP poly(3-hexylthiophene-2,5-diyl) [P3HT] with TiCl<sub>4</sub> and H<sub>2</sub>O to form P3HT-TiO<sub>2</sub> hybrid photocatalysts. Specifically, we examine how these photocatalysts perform in degrading the dye methyl blue in aqueous solutions, fitting the degradation to a first-order reaction and extracting the rate constant. XPS analysis of the VPI treated P3HT confirms that the inorganic infiltrants dope the polymer, which is confirmed by electrical measurements, and leave behind TiO<sub>2</sub> clusters. Photocatalytic measurements reveal that the P3HT-TiO<sub>x</sub> hybrid material outperforms pure P3HT and pure TiO<sub>2</sub> by at least a factor of 4.5x, but only when illuminated. These results show a synergistic photosensitizing effect between the P3HT and TiO<sub>2</sub>. To confirm that the electronic doping is not the sole source of enhanced photocatalytic activity, we also examined P3HT films doped with common oxidative dopants. While these doped P3HT show significantly higher electrical conductivity than the VPI treated P3HT, they had significantly lower photocatalytic activity (at least 3x lower). Doping of the P3HT-TiO<sub>2</sub> hybrids to reduce conductivity also did not eliminate the photocatalytic performance of these hybrids, providing further evidence that this photocatalytic effect is not simply due to higher electrical conductivity. To explore how catalytically active VPI could make the P3HT, the polymer was exposed to differing number of VPI cycles. It was found that the catalytic activity increased until 5 cycles, where the surface S:Ti ratio was 3, and then proceeded to gradually decrease for more cycles. Based on subsequent characterization, we will discuss why this design is optimal and to what extent the infiltrated TiO<sub>x</sub> species need to be near the surface of the hybrid material. We will also demonstrate how this catalyst is amongst the best performing CP-MO<sub>x</sub> photocatalysts to have been reported in the literature.

## Thin Film Division

### Room A105 - Session TF2-TuA

#### Thin Films for Battery and Photovoltaic Applications

**Moderators:** Richard Vanfleet, Brigham Young University, Matthias Young, University of Missouri

4:40pm **TF2-TuA-8 Optimization and Structural Characterization of ITO Thin Films for Photovoltaic Applications**, F. Ali, Metallurgical and Materials Engineering, The University of Alabama; D. Li, Electrical and Computer Engineering, The University of Alabama; **Subhadra Gupta**, Metallurgical and Materials Engineering, The University of Alabama

We have optimized the processing and annealing of sputtered indium-tin oxide (ITO) thin films for solar cell applications by DC magnetron sputtering. The effects of process parameters such as deposition power, reactive gas flow percentage, annealing temperature and time, as well as film thickness, on the sheet resistance and transmission of the ITO films was systematically studied, using a Design of Experiments. Additionally, structural characterization of the deposited films was performed using various techniques, including X-ray diffraction (XRD), transmission electron microscopy (TEM), scanning electron microscopy (SEM), four-point probe, UV-VIS spectrometry, and atomic force microscopy (AFM). TEM analysis revealed grain boundaries, crystallinity, and d-spacing of ITO thin film. The grain size was calculated with the help of the Scherrer equation. The XRD spectra of the ITO films revealed a polycrystalline structure with preferred (222) orientation of the ITO film. The SEM image of the ITO target gives information about the morphology of the racetrack after sputtering. The topography and surface roughness were evaluated by atomic force microscopy (AFM). A sheet resistance of 10 ohms/sq. and transmission of over 90% over 400-700 nm wavelengths was achieved. Perovskite solar cells fabricated with these optimized ITO electrodes showed promising properties.

5:00pm **TF2-TuA-9 Isolating Battery Components to Understand How Processing Affects Interface Formation**, **Victoria Castagna Ferrari**<sup>1</sup>, G. Rubloff, D. Stewart, University of Maryland, College Park

Interfaces dominate the performance of electrochemical systems, from interphase formation to charge transfer impedances, and they require careful study to understand. We have undertaken a broadly applicable approach to isolating components of a solid-state battery (SSB) to analyze them using non-destructive electrochemical impedance spectroscopy (EIS), and systematically build up to the full device. We then apply this knowledge

to the matter of spontaneous Li transfer from LiPON to V<sub>2</sub>O<sub>5</sub> during the sputtering process, which was also seen in other electrode/electrolyte pairs but is poorly studied.

Using sputtering and *in vacuo* shadow mask exchange, we fabricated an array of 16 batteries (Si/LiPON/LiV<sub>2</sub>O<sub>5</sub>) in parallel with auxiliary devices with isolated materials and interfaces on a single 3 in Si wafer. The reproducibility of the SSBs was confirmed by electrochemical testing, and the interfaces were evaluated from EIS measurements of the auxiliary devices. Equivalent circuit models for each device were built, ensuring that the components were all physically correlated to a material property or to (non)faradaic reactions of the interface. Interface reaction dynamics were evaluated as the applied voltage was swept over the normal working range of the SSB. The parameters obtained from these auxiliary circuit models were used to build a complete and accurate electric circuit for the SSB.

To evaluate the effect of the sputtering process on the interfaces, two model systems were used offering different conditions. Ultra-thin layers (10-20 nm) of either Li<sub>2</sub>O or LiPON were sputtered on top of V<sub>2</sub>O<sub>5</sub> using a non-reactive Ar working gas, or reactive N<sub>2</sub>, respectively. EIS measurements of the models revealed the presence of an electron blocking LiPON layer, and the absence of a Li<sub>2</sub>O layer above the V<sub>2</sub>O<sub>5</sub>. Furthermore, the properties of the Li<sub>2</sub>O/V<sub>2</sub>O<sub>5</sub> sample were similar to the lithiated LiV<sub>2</sub>O<sub>5</sub> previously measured. An XPS depth profile confirmed that the V<sub>2</sub>O<sub>5</sub> was fully lithiated after sputtering Li<sub>2</sub>O, while only a fractional lithiation occurred after sputtering LiPON. DC polarization measurements and spectroscopy ellipsometry showed that the interfaces have distinct optical and electronic properties that might indicate interphase formation.

This work presents a materials-agnostic platform for investigating the interfaces in a SSB using non-destructive electrochemical techniques. The auxiliary devices are created in parallel with the SSB, ensuring a 1:1 comparison. Overall, this work presents a comprehensive approach to investigate the interfaces in SSBs, including chemical and physical reactions, and provides insights into improving the interfaces of thin films in SSBs.

5:20pm **TF2-TuA-10 Towards Dual Lithium-Ion and Electronically Conductive Polymer Coatings by MLD**, **Nikhila Paranamana**<sup>2</sup>, A. Datta, X. He, M. Young, University of Missouri, Columbia

Lithium ion batteries (LIBs) employing solid electrolyte offer potential advantages in safety and shelf life over current LIBs made with liquid electrolyte. However, undesired reactions occur between electrode active materials and the solid electrolyte, forming interphase layers that block Li<sup>+</sup> ion transport and degrade cell performance. To prevent these interphase reactions while maintaining battery operation, protective coatings are of interest which provide both electronic conductivity and Li<sup>+</sup> ion conductivity. Recent work has demonstrated the use of molecular layer deposition (MLD) to form electrically conducting poly(3,4-ethylenedioxythiophene) (PEDOT), anion-conducting polypyrrole (PPy), and cation conducting lithicone-glycerol (LiGL). However, MLD coatings that conduct both lithium ions and electrons have proven challenging to synthesize. In this work, we report on recent efforts to form MLD films of polyhydroquinone that are cation-conductive and electronically-conductive. We employ in-situ quartz crystal microbalance (QCM) studies during MLD growth to understand the growth mechanisms, as well as ex-situ spectroscopic ellipsometry (SE), electrochemical impedance spectroscopy (EIS), and electrochemical characterization to identify the material properties. We also report early work applying these coatings to nickel rich LiNi<sub>0.6</sub>Co<sub>0.2</sub>Mn<sub>0.2</sub>O<sub>2</sub> (NMC) cathode material to be used in solid electrolyte LIBs with the Li<sub>10</sub>GeP<sub>2</sub>S<sub>12</sub> (LGPS) solid electrolyte to understand how these protective coatings affect interphase layer formation in this system.

5:40pm **TF2-TuA-11 Initiated Chemical Vapor Deposition Stabilized Current Collectors for Anode-Free Lithium Metal Batteries**, **Ramsay Blake Nuwayhid**, J. Yeom, G. Waller, R. Carter, C. Love, U.S. Naval Research Laboratory

Anode-free Li-metal batteries (AFLBs) offer a substantial enhancement in energy density over conventional graphite anodes. However, their realization is hindered by heterogeneous and irreversible Li plating/stripping from the Cu current-collector, resulting in the buildup of resistive solid-electrolyte interphase (SEI) species leading to poor cycling efficiencies. In this work, we employ initiated chemical vapor deposition (iCVD) polymeric coatings to create a stable interface between the Cu and liquid-electrolyte. The capability to deposit conformal polymer films at the nanoscale makes iCVD an attractive technique to passivate the reactive and complex Cu/liquid-electrolyte interface. We apply nanoscale coatings (5-

<sup>1</sup> TFD James Harper Award Finalist

Tuesday Afternoon, November 7, 2023

<sup>2</sup> TFD James Harper Award Finalist

# Tuesday Afternoon, November 7, 2023

100 nm) of poly(1,3,5,7-tetravinyl-1,3,5,7-tetramethylcyclotetrasiloxane) (pV4D4) to Cu current-collectors and evaluate their electrochemical performance in Li/Cu coin-cells. The cycling behavior reveals an overall cycling enhancement dependent on pV4D4 thickness. Moderate thicknesses (20 nm) resulted in a coulombic efficiency >90% for 100 cycles, more than double that of uncoated Cu. Through SEM and XPS analysis, it is determined that the cycling improvement is attributed to the uniform plating morphology of Li and the prevention of deleterious SEI component growth from the liquid-electrolyte. For ultrathin coatings (5 nm), a marginal improvement to bare Cu is observed and thick coatings (>100 nm) suffer from poor kinetics due to pronounced insulating effects of the dielectric pV4D4 film. Two distinct mechanisms are observed for Li plating/stripping for sufficient pV4D4 passivation; (1) moderate coatings (20 nm) function as a solid-electrolyte with Li plating beneath the layer and (2) thick coatings (>100 nm) function as a nucleation layer with Li plating on top of it. Overall, this work provides the mechanistic understanding of iCVD pV4D4 layers on Li plating/stripping and demonstrates the promising capability of iCVD to operate as stable interlayers in Li metal batteries.

## Theory for Surface Processes and Spectroscopies Focus Topic

### Room B116 - Session TH1-TuA

#### Electronic Structure Theory

**Moderators:** Robert Polly, Karlsruhe Institute of Technology, Sefik Suzer, Bilkent University, Turkey

2:20pm TH1-TuA-1 **Non-Orthogonal Configuration Interaction for the Study of Ground and Excited State Properties of Materials**, *Ria Broer*, University of Groningen, Netherlands; *C. de Graaf*, Universitat Rovira i Virgili and ICREA, Spain; *A. Sanchez-Mansilla*, Universitat Rovira i Virgili, Spain; *C. Sousa*, University of Barcelona, Spain; *T. Straatsma*, Oak Ridge National Laboratory, USA

INVITED

The properties of materials including their interfaces and surfaces can be studied by a variety of advanced experimental techniques. The technique of choice depends on the material and on the property of interest. Likewise, a variety of theoretical/computational methods exist for the study of their ground and excited state properties and the method of choice again depends on the specific problem. In many cases progress in the understanding of the properties has leaped forward thanks to productive interaction between experimentalists and theorists. For such understanding the accurate computational reproduction or prediction of data is necessary but not sufficient, we need also interpretation in terms of (preferably simple) physical/chemical concepts.

This presentation introduces the non-orthogonal configuration interaction (NOCI) method, where the wave function of a molecular electronic state is written as an expansion in terms of a small number of many-electron basis functions (MEBFs), each representing a leading electronic configuration that is expressed in terms of its own, optimized orbitals. The MEBFs are single- or multi-configuration self-consistent field (SCF or MCSCF) wave functions. The orbital sets of different MEBFs are neither identical nor mutually orthogonal and this non-orthogonality complicates the computation of off-diagonal hamiltonian elements in the CI matrix. NOCI can be used to study isolated molecules, but also, when combined with the embedded cluster material model, to describe (rather) localized processes, like core excitations, in materials.

In the past decade we have extended the NOCI method to enable application to *ensembles* of molecules or fragments: NOCI-F. [1] The MEBFs are then spin-adapted linear combinations of anti-symmetrised *products* of MCSCF wavefunctions for each molecule/fragment in the ensemble. NOCI-F allows for the study of processes where inter-molecular (or inter-fragment) electron transfer or excitation transfer plays a role.

NOCI and NOCI-F are not computationally simple, but since the final wave functions are short expansions in terms of well-defined molecular states, a clear interpretation in terms of local excitations, charge transfer, etc. can still be given. It is shown how NOCI-F can be used to study multi-exciton generation and magnetic interactions in molecular crystals and electronic excitations involving (molecules on) surfaces.

[1] T. P. Straatsma, R. Broer, A. Sánchez-Mansilla, C. Sousa, and C. de Graaf, GronOR: Scalable and Accelerated Nonorthogonal Configuration Interaction for Molecular Fragment Wave Functions, *J. Chem. Theory Comput.* 18, 3549–3565 (2022)

3:00pm TH1-TuA-3 **Enabling Long Time-scale Quantum Molecular Dynamics Simulation for 5f-elements**, *P. Yang, Enrique Batista, M. Cawkwell, D. Perez*, Los Alamos National Laboratory

INVITED

5f-element chemistry in solution is very intricate in nature. There is a pressing need to develop molecular dynamics (MD) methods that can describe quantum mechanical behavior, such as bond breaking and forming, at long timescales. Current first-principle MD methods can only reach tens of picoseconds, while classical force fields cannot accurately describe bond breaking and forming. To achieve this goal, we developed semiempirical density functional theory tight-binding (DFTB) parameters for 5f-elements that enable MD simulations at long time scales. Such simulations will be instrumental in understanding the evolution of speciation and reaction mechanisms. In this talk, we will share our recent development on a hybrid model that combines modern machine learning approaches with physics-based methods. We will demonstrate the transferability of this hybrid model on prediction of molecular structural parameters of various molecular clusters and a variety of chemical reaction free energies. Using these parameters, we also demonstrate microsecond-long quantum-MD simulations of nanoparticle systems for complex f-elements, shedding light on their dynamics and kinetics.

## Theory for Surface Processes and Spectroscopies Focus Topic

### Room B116 - Session TH2-TuA

#### Electronic Structure and Reactivity

**Moderators:** Paul S. Bagus, University of North Texas, C. Richard Brundle, CR Brundle and Associates

4:20pm TH2-TuA-7 **Interaction of Hydrogen Species with  $\gamma$ -Al<sub>2</sub>O<sub>3</sub> Surfaces**, *Anne Chaka, K. Khivantsev, T. Ahmed, B. Schmitt, J. Szanyi, L. Kovarik*, Pacific Northwest National Laboratory

INVITED

The interaction of hydrogen species with active sites in transition aluminas such as  $\gamma$ -Al<sub>2</sub>O<sub>3</sub> is responsible for performance of these materials in important applications such as heterogeneous catalysis and hydrogen permeation barriers. Understanding these active sites and their interactions with hydrogen species has been inhibited by a lack of a clear crystal structure, let alone surface terminations, for these aluminas. Theoretical studies have had to make assumptions regarding surface terminations and the structure of active sites, leading to ambiguous spectroscopic interpretation and uncertainty in reaction mechanisms. Recent experimental investigation of hydrothermally synthesized  $\gamma$ -Al<sub>2</sub>O<sub>3</sub> rhombus-platelets utilizing state-of-the-art FTIR, high-field solid state <sup>27</sup>Al NMR, high resolution TEM, and CO/N<sub>2</sub> activation probes have clarified the nature of the active sites on (100) segments of highly reconstructed (110) faces and irrational surfaces. (Khivantsev *et al.*, *Angew. Chem. Int. Ed.* 2021, 60, 17522–17530.) High resolution FTIR and *ab initio* thermodynamics and molecular dynamics based on density-functional theory are utilized to characterize the structure and reactivity of these sites as well as surface and bulk transport as a function of temperature and partial pressures of H<sub>2</sub>, D<sub>2</sub>, H<sub>2</sub>O, and D<sub>2</sub>O.

5:00pm TH2-TuA-9 **Elucidating the Effects of Oxygen Vacancies and Electric Fields on the Adsorption of Species on La-Based Perovskites**, *Ariel Whitten, J. McEwen*, Washington State University; *E. Nikolla*, University of Michigan, Ann Arbor; *R. Denecke*, University of Leipzig, Germany

Perovskite materials can be used in electrochemical CO<sub>2</sub> reduction processes due to their higher stability than metal catalysts such as Nickel but are limited by their catalytic activity towards CO<sub>2</sub> reduction. For perovskites to be an alternative catalyst for this process, the surface chemistry of perovskites needs to be augmented by the introduction of active sites on the surface such as oxygen vacancies or by applying electric fields. We propose using La-based perovskites (LaNiO<sub>3</sub>, LaCoO<sub>3</sub> and LaFeO<sub>3</sub>) which are known to be highly active in CO<sub>2</sub> reduction to reduce CO<sub>2</sub> on the surface and we investigate these surfaces using both experimental and theoretical methods. While this proposal specifically focuses on the theoretical nature of the project, we use experimental methods to ground our theoretical calculations. Our first study explored experimental XPS spectra with theoretical calculations that predict the core level binding energy shifts of various adspecies on the surface (H, O, OH, H<sub>2</sub>O and CO<sub>2</sub>). Adsorption of species on the surface was favorable with considerable charge transfer occurring between the surface and the adspecies. This study is imperative for understanding the surface chemistry of our system before we augment it with oxygen vacancies and electric fields. We found

# Tuesday Afternoon, November 7, 2023

that the higher energy peak for both LaCoO<sub>3</sub> and LaNiO<sub>3</sub> corresponds to water adsorption while the lower energy peak is due to lattice oxygen. The other species correspond to intermediate satellite peaks. Figure 1 shows the XPS spectra generated for LaNiO<sub>3</sub>. Literature results and temperature dependent XPS spectra confirmed our results were accurate. We will also investigate the effects of coverage and oxygen vacancies on the XPS spectra for several of our surfaces (LaNiO<sub>3</sub> and LaCoO<sub>3</sub>). Finally, we investigate the effects of oxygen vacancies and electric fields on the surface activity and adsorption. Our preliminary studies show that oxygen vacancies can increase the adsorption of CO<sub>2</sub> on the surface and electric fields change the plane wave averaged potential of the surface. We expect that the influence of electric fields will strengthen the adsorption of CO<sub>2</sub> due to the increase electrons stabilizing the surface. Further work will be completed to explore the effects of electric fields on adsorption strength of CO<sub>2</sub> as well as the formation of oxygen vacancies.

5:20pm **TH2-TuA-10 Theory of Magnetic Impurities in Oxides. Complex Problem, Pragmatic Solutions, Gianfranco Pacchioni**, Università di Milano-Bicocca, Italy

Dopants in insulating and semiconducting oxides are of fundamental importance for the design of new materials and often lead to the presence of holes or trapped electrons in particular sites. The correct identification of these paramagnetic centers is crucial for understanding the optical, magnetic, photocatalytic and transport properties of oxides. The nature of magnetic impurities can be investigated by comparing DFT calculations using hybrid functionals with electron paramagnetic resonance, EPR, measurements. We will provide a historical perspective on the description of holes in the O 2p valence band of SiO<sub>2</sub> as a paradigmatic example of interaction between theory and experiment. Then we will discuss N-dopants in TiO<sub>2</sub>, ZnO, SnO<sub>2</sub>, ZrO<sub>2</sub> and MgO. A comparison with the EPR data allows one to evaluate the accuracy of the DFT calculations. At high N-dopant concentrations the presence of magnetic ordering in some of these materials has been suggested, implying the existence of magnetic interactions between the isolated defects. The use of hybrid functionals allows to adequately describe the nature of the isolated magnetic defects in the oxides, and shows that no magnetic ordering is expected for the dopant concentrations used in the experiments. Problems related to the theoretical treatment in DFT of magnetic impurities in insulating and semiconductor oxides are discussed.

5:40pm **TH2-TuA-11 Dynamics of Electrical Potential Distribution in Ionic Liquid Based Electrochemical Systems at Extended Time and Length Scales, Observed by Myriad of Experimental Techniques Awaits for Theoretical Attention, Pinar Aydogan Gokturk**, Koc University, Turkey; S. Suzer, Bilkent University, Turkey

Ionic liquid systems exhibit rich dynamic responses on electrified surfaces. A long-standing question is why these materials display widely different time constants, ranging from nanoseconds to several hours, which can be attributed to the complex interplay of chemical and physical factors, including steric and molecular interactions. Recent theoretical approaches have concentrated in the faster temporal- and shorter lateral-variations. Although a collection of experimental evidences have been reported the presence of longer length and time-dependent processes, understanding of the molecular nature of them is still elusive. Our group use X-ray photoelectron spectroscopy to directly probe the local electrical potential variations, extracted from the binding energy shifts of the corresponding core levels, for obtaining lateral- and temporal-responses on electrified cells in non-invasive and chemically-resolved fashion<sup>1</sup>. Others have used electrochemical, microscopic, terahertz imaging, X-ray and Neutron scattering techniques. Use of electrochemical force microscopy have given new input into the dynamics of charge screening at the solid-aqueous interfaces by identifying multiple time constants and relatively larger length scales of up to 10 microns<sup>2</sup>. But again, such distances are still small to represent real-life electrochemical devices. Moreover, information not only at the interfaces but in the bulk electrolyte covering the entire electrochemical cell is needed. Recent theoretical progress has shed new light on the time dependency, particularly nonlinear response of thin double layer in a parallel plate configuration, where Bazant et al., using a modified version of the Poisson-Nernst-Planck (PNP) equation, had identified different time scales controlled by geometric and ionic diffusion properties of the chemical moieties within such devices<sup>3</sup>. Most of these approaches have been developed and tested for small electrical potentials and relatively dilute aqueous solutions, while extension to higher voltages and highly concentrated electrolytes, as in the case of ionic liquids, still remains a challenging task due to the high interaction energy and long-range Coulombic forces. We will review some of the recent experimental

findings, including those from our own work, and the theoretical work mentioned above and highlight some of issues waiting for attention.

1. Aydogan Gokturk, P.; Suzer, S., J. Phys. Chem. C 2021, 125, 17, 9453–9460.

2. Collins, L.; Kilpatrick, J. I.; Kalinin, S. V.; Rodriguez, B. J., Rep. Prog. Phys. 2018, 81 (8), 086101.

3. Bazant, M. Z.; Thornton, K.; Ajdari, A., Phys. Rev. E 2004, 70 (2), 021506

6:00pm **TH2-TuA-12 Sub-eV Electron Inelastic Mean Free Path: A Second Inverted Trend ?, Hagai Cohen**, The Weizmann Institute, Israel

The dependence on kinetic energy of the electron inelastic mean free path (IMFP) parameter has already been studied extensively, showing a drastic qualitative difference between the high-energy regime (above e.g. 100 eV) and the low-energy regime (below e.g. 40 eV). In fact, definitely opposite energy dependencies are exhibited by the two ‘arms’ of the corresponding  $\lambda(E_k)$  universal curve. Extension of these studies to very low energies, below e.g. 5 eV, is by far more challenging experimentally. Hence, only few works have addressed this challenge so far.

Here, a new technique is applied, resulting in an interesting observation. XPS-based experiments with nanometrically thin self-assembled monolayers (SAMs) systematically indicate on a second *inversion* in the derivative of energy dependence, appearing as a common general feature of the sub-eV regime. Using a simple theoretical model, these results are explained and further propose interesting applications for future studies of hot-electron interactions with dielectric layers.

## Vacuum Technology Division

### Room C120-122 - Session VT-TuA

#### Novel Vacuum Instrumentation

Moderators: Jason Carter, Argonne National Laboratory, Yulin Li, Cornell University

2:20pm **VT-TuA-1 Saving Energy of Subfab Equipment for Semiconductor Manufacturing, Yohei Yoda**, EBARA, Japan **INVITED**

Since the semiconductor industry has achieved continuous high growth in terms of both technology and commerce due to the spread of IACCS \* 1, the market will be doubled to 100 trillion yen in 2030 is a consensus in that industry. To pursue miniaturization of devices based on Moore's Law, nanometer-order processing technology and three-dimensional processing technology are being researched and developed in various fields. Therefore, the increase in load and complexity of processes accompanied by the evolution of semiconductor manufacturing technology is remarkable. On the one hand, with an awareness of packaging technology, the diversification of processes and the increase in the number of processes will be further promoted in the future. On the other hand, as long as the increase in the production volume of semiconductor manufacturing and the number of processes, energy reduction and high efficiency during the manufacturing process are necessary issues in order to achieve a sustainable society in 2030.

In this report, we will discuss environmental technology development trends and roadmaps for 2030, which regarding exhaust systems centered on dry vacuum pumps for manufacturing equipment that uses a large amount of energy in semiconductor manufacturing and exhaust gas treatment equipment which is responsible for reducing greenhouse gases.

#### Environmental Technology Development Trends for Exhaust Systems and 2030 Roadmap

The energy consumption ratio in semiconductor manufacturing can be roughly divided into consumption in equipment such as air conditioning, DI water and cooling water in clean rooms, and equipment in manufacturing equipment. Among these, the energy consumption ratio in the exhaust system including the dry vacuum pump in the manufacturing equipment is about half, which accounts for a huge proportion. Furthermore, to consume greenhouse gases such as CF<sub>4</sub> and NF<sub>3</sub> which produced during semiconductor manufacturing, exhaust gas treatment equipment is used to reduce the gases emission. The equipment used in the exhaust system uses utilities such as electric power, circulating cooling water, nitrogen, city water, fuel, and oxygen. Technological development for reducing usage and recycling / reuse will be an important performance index for 2030, along

# Tuesday Afternoon, November 7, 2023

with achieving process performance and improving equipment availability. The latest technological trends regarding energy-saving technologies and on-demand control for each device will be reported and our environmental technology roadmap for 2030 will be explained.

**3:00pm VT-TuA-3 The Transfer of R&D Vacuum Products to Series Production - When Cleanliness and Quality Control Becomes Critical, Klaus Bergner, C. Worsch, F. Haidu, K. Marschall, M. Flaemmich, VACOM Vakuum Komponenten & Messtechnik GmbH, Germany**

Today's research in the field of vacuum technology is an essential enabler for lithography, measurement and correction of the smallest and most novel chip structures. This lays a foundation for future applications in medicine, communication or consumer electronics.

After a successful release, a market-driven transition from the R&D phase to volume production with short time-to-market cycles takes place. However, the ramp-up process can be challenging and could lead to several production errors or even destruction of substrates or modules. Troubleshooting is then often costly as personally supported prototypes leave the R&D status and obvious but uncommunicated details are overlooked. This is particularly crucial for ultra-clean vacuum systems, which require careful attention to design, production, cleaning, assembly and maintenance to prevent failure due to contamination.

Quality and process control of individual components and modules becomes critical to ensure the performance and reliability of the final system. In this talk, we will explore the challenges associated with ramping up individual components of ultra-clean vacuum systems and the measures that can be taken to reduce ramp-up time while maintaining quality.

We show how surface contamination can be reduced from a double-digit  $\mu\text{g}/\text{cm}^2$  value to a single-digit  $\text{ng}/\text{cm}^2$  value. We highlight the most essential steps in the design phase, the right choice of cleaning technologies, appropriate analyze methods and constant process monitoring.

In summary, we provide a decided insight into process chain for the realization of ultra-clean vacuum components in all stages of "cleanliness". True to the motto: Design clean, Plan clean, Make clean, Prove clean, Keep clean.

**3:20pm VT-TuA-4 High Temperature Inlet of Residual Gas Analyzers for Atomic Layer Deposition Process Monitoring, Chenglong Yang, MKS Instruments, Inc. Mass Spectrometry Solutions Group; J. Leslie, G. Jennings, MKS Instruments, Inc. Mass Spectrometry Solutions Group, UK; U. Meissner, MKS Instruments, Inc. Mass Spectrometry Solutions Group, Germany; M. Aitken, A. Wallace, MKS Instruments, Inc. Mass Spectrometry Solutions Group, UK; G. Brucker, MKS Instruments, Inc. Mass Spectrometry Solutions Group**

Residual gas analyzers (RGA) are used widely in the semiconductor industry for in-situ leak detection. Although RGAs can monitor contaminants, precursors and process byproducts in Atomic layer deposition (ALD), they are just used for process optimization/troubleshooting and are not yet ready for in-situ process monitoring owing to their short lifetime and less persuasive value for process monitoring. As an example, RGAs for ALD are challenged by harsh physico-chemical conditions including (1) chemical compatibility, (2) sensor contamination, (3) sensitivity degradation and (4) high measurement speed requirements. Many ALD precursors are liquid or solid at room temperature and can condense on cold surfaces, leading to blockage of the gas inlet system if the sampling pipes and valves are not at the required temperature conditions. MKS recently redesigned the popular UniBloc™ inlet system featured in most of its Process Analyzers to address the specific requirements of ALD. In its latest design, inlet components are uniformly heated (up to 200 °C) in order to avoid undesired reactions and/or deposition of byproducts prior to mass analysis. High sample flow rates, via bypass pumping, reduce sample transfer lag and improve sampling speeds as required for short pulse monitoring. Field replaceable valve seats and sampling orifices improve the lifetime and serviceability of the inlet system. Built-in calibration bottles, localized pressure measurement (Baratron® capacitance manometer) and sniffer tubes complete the new design and provide the performance and compatibility demanded by modern ALD processes. The improved Unibloc™ RGA design offers the opportunity to monitor ALD process in-situ, increase throughput and yield valuable process insights that will unlock future efficiencies in thin film growth.

**4:20pm VT-TuA-7 Improved Reliability of High Sensitivity Leak Testing of Large Chambers, Brad Shaw, Leak Testing Specialists, Inc. INVITED**

This paper will present practices that have been of great value in successful leak testing operations for very large high vacuum, and ultrahigh vacuum

projects. *Successful* in this context refers to the delivery of technically reliable leak testing with consistent schedule durations at an efficient cost.

This list of practices is the accumulation of lessons learned through the leak testing of a number of large projects, including the leak testing of the Laser Interferometer Gravitational Observatory (LIGO) beam tubes, the development and implementation of the leak testing of the National Ignition Facility (NIF) beam path clusters, space simulation chamber shroud replacement, and a series of large, double wall, vacuum insulated spheres for liquid hydrogen.

Some practices described in this paper have been of sufficient value across an array of applications that they have been added to industry codes and standards for leak testing. Use of vacuum pumping the calibrated leaks for system calibration is an example of a practice developed on a large project, that is now included in ASTM Standard Practice E1603/1603M. Another example is the calculation of the Test Quality Factor (TQF) in each leak test and evaluating the test reliability against a double bound requirement. This refined TQF practice has been added to the revised ASME Mandatory Appendices for helium hood and helium filled object leak testing.

Some practices in this paper are "best practices" that are frequently neglected, but that have historically been of great value. One example is the neglect of leak testing new components at receiving inspection. Failing to perform leak testing upon receipt is a common source of project schedule and cost over-run. The successful builders of large high and ultrahigh vacuum systems are among the most consistent in leak testing components at Receiving, without regard to the source of the component or assurances that the product was leak tested by the manufacturer.

Many practices discussed in this paper offer innovative ways of doing common, but difficult leak testing tasks by simpler, faster, more consistent and reliable means. The use of helium receivers for rapid filling of large hoods is one example. There are also details for helium hood leak testing that are not commonly used but that can be a significant source of savings. Another example involves the use of the Test Quality Factor (TQF) as a sensor for predictive maintenance of leak testing systems.

For each of the practices discussed, we will present cases that illustrate the benefits derived from implementation, or cases of non-implementation and the resulting consequences.

We hope the paper will contribute to future successful leak testing of large, high-vacuum and ultra-high vacuum systems.

**5:00pm VT-TuA-9 An Alternative to Helium Leak Checking, Kieran Massey, J. Brindley, V. Bellido-Gonzalez, D. Monaghan, Gencoa Limited, UK**

The vacuum leak detection market is dominated by helium detection using quadruple-based mass spectroscopy. These detectors offer high sensitivity and have become the industry standard. Helium, which enables these leak checkers to function so effectively, has an uncertain future with a critically short supply and prices on the rise. Leak checkers based on this technology are also costly to buy and have high ongoing maintenance costs.

What is required is a detector that functions with a cheap, readily available and safe gas but can still offer detection levels relevant for the particular industry. An alternative gas sensor built around plasma emission monitoring enables detection of gases using a small remote plasma which can be converted into a helium equivalent leak rate. This sensor is based on RPEM technology (remote plasma emission monitoring) which offers greater robustness and reduced maintenance relative to traditional mass spectrometer-based gas detection.

The presentation will cover the technology of RPEM and how it has been adapted for leak checking of vacuum systems and components using argon and carbon dioxide gas as opposed to Helium.

**5:20pm VT-TuA-10 Reference Leaks for Traceable Outgassing Rate Measurements of Hydrocarbons and Water, Annas Bin Ali, M. Bernien, Physikalisch-Technische Bundesanstalt (PTB), Germany; J. Setina, Institute of Metal Technology (IMT), Ljubljana, Slovenia; K. Jousten, Physikalisch-Technische Bundesanstalt (PTB), Germany**

Outgassing from components built into vacuum process chambers remains a pertinent issue for the semiconductor industry and has gained much attention as in Extreme Ultra-Violet Lithography (EUVL) where vacuum cleanliness is requisite. Too high outgassing can cause reflectivity loss in optical tools due to reactions of the light with adsorbed molecules stemming from outgassing of both photoresist and internal surfaces. Water and hydrocarbons are the major outgassing species affecting EUVL reflectivity as they trigger the diffusion and carbon growth on the optical

# Tuesday Afternoon, November 7, 2023

surfaces resulting in lifetime issues of the optics. Quadrupole mass spectrometers are widely employed to identify such outgassing species and quantify outgassing rates. However, quantitative gas rate measurements using quadrupole mass spectrometers lack the necessary metrological quality, and the measured quantity is not traceable. This could result in either underestimation or overestimation of outgassing rates. In this work, samples are developed and characterized to serve as reference and transfer standard for water and dodecane outgassing rates. Dodecane serves as a model contaminant for hydrocarbon outgassing. Reference samples are realized by using a silicone rubber as a permeate sandwiched between two CF16-sized stainless-steel discs having a hole on both sides which define the open area. The outgassing flow can be tuned by choosing the permeate thickness and the open area of the holes. The partial pressure calibration system of PTB was used to characterize the reference samples. The gas flow from a reference sample was compared with a gas flow of dodecane/water generated by means of a calibrated capillary. In this way the outgassing rate can be measured traceable to the international systems of units. The reference samples demonstrated stable permeation rates of dodecane/water with a relative standard deviation of  $\sim 3\%$  over the period of a year. The design of the reference sample offers the possibility to refill the reservoir without completely disassembling the permeation part.

**5:40pm VT-TuA-11 Anti-Deposition Sensor Diaphragm Structures of Sapphire-Based Capacitance Manometer for Semiconductor Manufacturing Processes, Takuya Ishihara, Y. Mastugi, M. Soeda,** Azbil Corporation, Japan

Recently, various new manufacturing processes are put into practical use in the semiconductor industry. Especially, Atomic layer processes such as Atomic Layer Deposition (ALD) and Atomic Layer Etching (ALE) are essential in the fine pattern processing. These processes are mainly used in high aspect ratio holes, narrow trenches, or complex 3D structures with micro to nano meter scale orders because of the excellent uniformity or step coverage based on the surface chemical reactions. On the other hand, because the film deposition could occur in any surface inside the process chamber, capacitance manometers used for pressure monitoring receive bad influences from these process with undesirable film depositions on the sensor diaphragm. These depositions often cause sensor output drifts which can lead to the process halt and need zero-point adjustments or the replacement of manometers. In the viewpoint of the productivity, this is crucial for any device manufactures. Similar problems are sometimes occurred in some kinds of conventional CVD (chemical vapor deposition) processes.

Authors have developed entirely sapphire-based capacitive pressure sensor chips (Fig.1) utilizing MEMS (Micro-Electro-Mechanical Systems) processes, which are packaged in capacitance manometers for semiconductor manufacturing (Fig.2). In fact, most of troubles we have in these applications are above mentioned depositions on the sensor diaphragm. In this paper we will present some improvement on sensor structure to resolve these issues, in which sensor output drift could be depressed even if deposition on the sensor diaphragm is occurred.

We take two of measures to correspond to properties of deposited films.

Structure1: For soft or fragile films which is often deposited during conventional CVD process.

These films tend to deposit mainly on open surface and not so much on the side wall or bottom of narrow trench structures. We used this property to divide films, which can weaken mechanical influence on the sensor diaphragm. Fig.3 shows the actual trench structure we fabricated on the sensor diaphragm surface.

Structure2: For hard or unformal films deposited in atomic layer processes.

These films deposited on any surface on diaphragms, so above-mentioned trench structure cannot be effective. Therefore, we improved sensor diaphragm edge structures to suppress diaphragm deformations accompanied with unformal film depositions based on mechanical simulation (Fig.4).

Finally, we have confirmed the effectiveness of these improvements in actual process. Fig.5 and Fig.6 are sensor output signals of improved sensors during the CVD process and the ALD process respectively compared with which of conventional sensors. These exhibit excellent anti-depo property of the improved manometers.

**6:00pm VT-TuA-12 Overview of the Vacuum Pumping Systems for the SPARC Tokamak, Matt Fillion, A. Kuang,** Commonwealth Fusion Systems; *C. Day,* Karlsruhe Institute of Technology (KIT), Germany; *O. Mulvaney, F. Ravelli,* Commonwealth Fusion Systems

Commonwealth Fusion Systems (CFS) is a spin-off of the Massachusetts Institute of Technology aiming to bring fusion energy to the grid. To accomplish this, CFS is developing and commercializing the ARC fusion power plant. To achieve this, CFS is currently building the SPARC tokamak—a superconducting, high-field, deuterium-tritium fueled tokamak that is designed for  $Q>1$ .

The Vacuum Pumping System of SPARC consists of three primary subsystems. The cryostat pumping system generates and maintains vacuum insulation of the cryostat to support the superconducting magnets. The leak detection system provides vacuum guarding for the tritium secondary interspaces and double seals in SPARC. Lastly, the torus pumping system is responsible for four main functions: the containment of tritium, reaching and maintaining the primary vacuum vessel base pressure, the recovery of the inter-pulse pressure, and providing particle control during the plasma discharge by pumping from the divertor. Each of the three vacuum pumping subsystems has an independent set of two dry screw pumps to provide rough vacuum and fore line pumping, mag-lev turbomolecular pumps for achieving ultrahigh vacuum, and a residual gas analyzer for leak detection and analysis of the plasma exhaust composition. The cryostat and torus pumping systems each contain custom tritium compatible closed loop refrigerator cooled cryogenic pumps to provide temporary enhanced pumping speeds.

Divertor pumping is a key aspect of tokamak particle transport control and an important area of study for ARC and other fusion power plants. The divertor is where neutral pressures are the highest ensuring the most efficient pumping for helium removal (a fusion byproduct). However, high divertor neutral pressure is crucial for divertor heat exhaust mitigation. To provide better control, CFS is developing a variable conductance louver system for active control over the divertor pumping speed. SPARC would provide much-needed data on desired neutral pressures and particles throughputs for steady state operations on next step devices.

The high throughputs required—along with the need to pump tritium—means a commercial solution for divertor pumping is unavailable. Thus, CFS is working with a commercial partner to develop an all-metal sealed cryogenic pump to meet the divertor pumping requirements. Utilizing added thermal mass on the lowest temperature stage, together with a proprietary charcoal, this pump can provide pumping at throughputs of  $10.6 \text{ Pa m}^3/\text{s}$  for the 10 second flattop duration of a SPARC pulse.

This talk will provide a general overview of the SPARC vacuum pumping systems and associated challenges, with a focus on the torus pumping system and the design of a custom cryogenic pump required by this system.

## Actinides and Rare Earths Focus Topic

### Room Oregon Ballroom 203-204 - Session AC-TuP

#### Actinides and Rare Earths Poster Session

**AC-TuP-2 Magnetic Properties of Lu doped Ce-Fe-B Magnets, Alex Bretaña, B. Raj, C. Housley, H. Aja, SRNL; G. Morrison, H. zur Loye, University of South Carolina**

Permanent magnets are integral components needed for future clean energy technologies, however the growing demand for Nd-Dy and Sm-Co based permanent magnets is exacerbating the current critical materials shortage. Designing, developing, and optimizing critical material free permanent magnets is essential for the future economy.  $\text{Ce}_2\text{Fe}_{14}\text{B}$ , based on  $\text{Nd}_2\text{Fe}_{14}\text{B}$  permanent magnets, is an attractive low-cost alternative due to the highly abundant rare-earth Ce, however, it displays several drawbacks, a rather low Curie temperature  $T_c$ , as well as a low magnetocrystalline anisotropy. Chemical substitutions have been shown to improve both  $T_c$  and the magnetic properties; Co, La, Ni, and Si have been shown to improve  $T_c$ , while La and Co have also been shown to improve the saturation magnetization,  $M_s$ , while Hf, Ga, Ge, Ti, and Zr doping improved the magnetic properties through microstructure and grain refinement. We prepared Lu doped  $(\text{Lu}_x\text{Ce}_{2-x})\text{Fe}_{14}\text{B}$  ( $x = 0.05, 0.1, \text{ and } 0.15$ ) alloys and studied their microstructure and magnetic properties before and after heat treatment. In this presentation, we will present X-ray diffraction, scanning electron microscopy and energy dispersive X-ray spectroscopy measurements, as well as temperature dependent magnetization and isothermal magnetization measurements on Lu doped  $\text{Ce}_2\text{Fe}_{14}\text{B}$ .

**AC-TuP-3 A Novel Approach to the FTA Procedure for Nuclear Forensics, Itzhak Halevy, Ben Gurion uni., Israel; R. Babayew, Y. Yehuda-Zada, N. Elgad, Engineering and Physics Department, Nuclear Research Centre Negev, Beer-Sheva, Israel; J. Lorincik, Nuclear Fuel Cycle Department, Research Centre Rez, Czech Republic; I. Orion, Unit of Nuclear Engineering, Faculty of Engineering Sciences, Ben-Gurion University of the Negev, Israel; A. Weiss, Faculty of Engineering, Bar Ilan University, Israel; G. Katarivas Levy, Department of Biomedical Engineering, Faculty of Engineering Sciences, Ben-Gurion University of the Negev, Israel**

Our laboratory has created a novel approach to the FTA procedure.

The query posed pertains to the presence of supplementary data within the detector image, beyond the star's spatial coordinates. Are there any further physical factors that hold forensic significance?

The acquisition of these novel findings was made possible through the creation of a state-of-the-art simulation tool, known as Trainer, specifically designed for the examination of fission stars.

The simulator in question is utilized for conducting a comprehensive examination of an individual fission star, as well as for generating an image that closely resembles the image acquired by a standard light microscope.

One significant initial finding is the feasibility of identifying the specific fissile isotope by an analysis of the trace lengths observed in the Lexan detectors. Another significant outcome is the capacity to examine individual fission traces arising from minuscule particles of fissile material ( $D < 0.1 \mu\text{m}$ ), which cannot be individually quantified using instrumentation like ICPMS-MC or comparable devices.

One notable finding is the relatively poor efficacy associated with the detection of individual fission traces. This phenomenon can be attributed to multiple sources. The acquisition of a fission trace is contingent upon the presence of a minimum angle between the fission trace and the lexan detector, which varies for each isotope. If this angle falls below the specified threshold, no fission trace will be observed. The circular trace produced by the fission product at an angle near 90 degrees exhibits a diameter of approximately one micron, posing challenges in its identification and differentiation from the surrounding background noise.

The newly developed "Trainer" simulator provides a platform for novice employees to engage in practical exercises aimed at facilitating their journey towards certification. This simulator also incorporates an evaluative component, enabling the assignment of a performance grade to individuals based on their simulated performance. Currently, there exists the capability to generate a substantial repository of images that can be utilized as a foundational resource for machine learning through the implementation of artificial intelligence techniques.

The coloring of traces in the Lexan detector is a novel product that is dependent on their depth. Initial investigations conducted using a fluorescent microscope have indicated the potential viability of this novel approach.

Our objective is to minimize the extensive etching of the Lexan detector, both in terms of temperature and duration, in order to enhance traceability in the Lexan.

## Atomic Scale Processing Mini-Symposium

### Room Oregon Ballroom 203-204 - Session AP-TuP

#### Atomic Scale Processing Poster Session

**AP-TuP-2 in-Situ Laser Diagnostics of Plasma Surface Interactions by fs-TALIF, Mruthunjaya Uddi, Advanced Cooling Technologies; A. Dogariu, Texas A&M University; E. Kudlanov, Advanced Cooling Technologies; G. Urdaneta, Texas A&M University; Y. Xiao, D. Jensen, C. Chen, Advanced Cooling Technologies**

Plasma surface interaction has been a critical area of research for many applications such as Plasma-Enhanced Atomic Layer Deposition (PEALD). To meet the demanding needs of more advanced atomically controlled microfabrication methods, the physics of PEALD needs to be better understood to enable high quality, repeatable and controllable deposition process. Several challenges that need to be addressed regarding PEALD include damage to the substrate from highly energetic species and UV radiation, need for precise amorphous/crystalline modulated selective layer deposition, conformality in coating non-uniform substrates, achieving an aspect ratio of  $>100$ , repeatability and controllability of the finish. To address these challenges, we are developing laser diagnostics methods to measure species over substrates by advanced laser diagnostics such as femtosecond- Two-Photon Absorption Laser Induced Fluorescence (fs-TALIF) to image atomic species over substrates. Here we present measurements of N atom densities over a substrate with high spatial ( $< 10$  microns) and temporal resolution ( $< 1$  ns) using fs-TALIF at pressures of 5-150 mTorr.

**AP-TuP-3 Characteristics of Hydrogenated Amorphous Carbon Thin Films Fabricated by Plasma-Enhanced Chemical Vapor Deposition of Cyclohexane Precursor, T. Poche, R. Chowdhury, Seonhee Jang, University of Louisiana at Lafayette**

The characteristics of the hydrogenated amorphous carbon (a-C) films can be determined by the composition of  $sp^3$ ,  $sp^2$ , and  $sp$  hybridized structures depending on the bond type of four valence electrons. The C-C bonds with  $sp^3$ ,  $sp^2$ , and  $sp$  correspond to diamond, graphite/graphene, and carbyne, respectively. Mixed hybridization determines different carbon allotropes such as graphyne ( $sp$  and  $sp^2$ ), nanotube and graphene quantum dots ( $sp^2$  with  $sp^3$ ), fullerene ( $sp^2$  and  $sp^3$ ), carbon dots ( $sp^3$  with  $sp^2$ ), and yne-diamond ( $sp$  and  $sp^3$ ). Different mechanical, electrical, chemical, and optical properties are obtained depending on the mixture of  $sp^3$ ,  $sp^2$ , and  $sp$ . For example, the  $sp^3$  bond shows some advantages including mechanical strength, wide band gap, and chemical and electrochemical inertness, however it is unfavorable for a strip process after etching. The a-C films are characterized according to the composition ratios among a  $sp^3$ ,  $sp^2$ , and hydrogen. When the hydrogen content is large, polymer-like a-C films can be formed with low film density due to high content of  $sp^3$ . When the hydrogen content is small, the content of  $sp^3$  becomes low, resulting in a diamond-like a-C with high film density and hardness. When the hydrogen content becomes smaller, the content of  $sp^2$  is high and a graphite-like a-C can be obtained. Depending on the deposition conditions, the  $sp^2/sp^3$  hybridization ratio can vary over a wide range of values. The a-C thin films were fabricated by plasma-enhanced chemical vapor deposition (PECVD) of cyclohexane ( $\text{CHex}$ ,  $\text{C}_6\text{H}_{12}$ ) precursor. The a-C films were deposited at room temperature of  $25^\circ\text{C}$  with a pressure of 26.7 Pa. The RF plasma power with 13.56 MHz was chosen from 20 to 80 W. The thickness, refractive index, and extinction coefficient of the a-C films were measured by ellipsometer. Surface morphology and roughness of the films were observed by atomic force microscopy (AFM). The functional groups of the films were identified using Fourier transform infrared (FTIR) spectroscopy. The FTIR spectrum consisted of C-H stretching, C-C stretching, and C-H bending modes. The C-H<sub>x</sub> stretching peak at  $3100\text{-}2800\text{ cm}^{-1}$  was deconvoluted to determine the bonding structure of hydrogen in the a-C films and the fractions of  $sp^3$   $\text{CH}_2$  stretching and  $sp^3$   $\text{CH}_3$  stretching modes was investigated depending on deposition parameters. The structural arrangement of the carbon bonds was analyzed by Raman spectroscopy and showed  $E_{2g}$  G and  $A_{1g}$  D breathing modes. The chemical composition of the films was determined by X-ray photoelectron spectroscopy (XPS). The deconvoluted C1s revealed  $sp^2$  C=C and  $sp^3$  C-C bonding peaks along with oxygen functional groups of C-O, C=O, and O-C=O.

# Tuesday Evening, November 7, 2023

**AP-TuP-4 Fabrication Related Impurities Study of Aluminum Transition Edge Sensors, Ghadendra Bhandari**, West Virginia University; *T. Stevenson, E. Barrentine, NASA; M. Holcomb*, West Virginia University

Superconducting aluminum-based microwave kinetic inductance detectors (MKID) are being developed to be used in space technology. These detectors operate at extremely low temperature regime which improves signal to noise ratio. We have studied the residues and adsorbates during different stages of the device preparation processes using x-ray absorption spectroscopy (XAS). We have observed oxidation and fluorination of aluminum during the fabrication process. We have observed aluminum oxidize as  $\alpha\text{-Al}_2\text{O}_3$  phase and fluorination at  $\text{AlF}_3$ . Additionally, we studied the effectiveness of residue removal processes with the help of reference samples.

**AP-TuP-5 Plasma-Induced Surface Defects and Their Impact on the Surface Chemistry of Silicon Nitride and Silicon Carbonitride, Ting-Ya Wang, G. Hwang**, University of Texas at Austin

As integrated circuits continue to shrink, the challenge of resistive-capacitive (RC) delay is becoming increasingly prevalent. Implementing low- $\kappa$  dielectric materials using techniques such as atomic layer deposition (ALD) has become a popular approach to decreasing capacitance and improving film conformality. However, there are still many technical challenges that need to be addressed. Although plasma is widely used in semiconductor processing, it can negatively impact the achievement of high-quality low- $\kappa$  materials.

A thorough understanding of surface structure and reactivity is essential. Currently available experimental methods are rather limited in their ability to study reaction mechanisms and non-invasively observe surfaces at the atomic level. Therefore, we have utilized computational methods, such as density functional theory (DFT) and Monte Carlo (MC), to investigate the underlying mechanisms of ALD, with a focus on silicon nitride (SiN) and silicon carbonitride (SiCN) thin films.

Based on DFT calculations, we have identified several active sites induced by plasma irradiation. For  $\text{N}_2$  plasma treatment, previous studies are mainly focused on under-coordinated sites such as  $>\text{Si}=\text{N}$ - site, while other potential surface sites remain incompletely understood. Our work demonstrates that  $\text{N}_2$  dimers can also act as reactive sites towards Si precursors. Moreover, we have found that under-coordinated Si and N defects can exhibit different electronic states and thus significantly different reactivity. In addition, plasma treatment can trigger bridging reactions that produce  $\text{Si}-\text{N}=\text{C}=\text{N}-\text{Si}$  bridges, which could also be active sites.

Different types of precursors, depending on the presence of carbon and chlorine, are commonly used to grow SiN or SiCN thin films. However, experimental studies have shown that precursors have different favorability over the reactive surfaces created by different plasmas. To better understand the phenomena, we have investigated the mechanisms underlying the reactions between various surface defects and these precursors. Moreover, we will also briefly touch our recent efforts of using DFT results as input data for MC simulations to investigate the coverage of these surface defects and how they affect the surface chemistry involved in plasma-enhanced ALD.

**AP-TuP-6 Electron Heating Mode Changes in Plasma Sources Used for Atomic Precision Processing, David Boris**, U.S. Naval Research Laboratory; *M. Johnson*, Huntington Ingalls Industries; *J. Woodward, V. Wheeler, S. Walton*, U.S. Naval Research Laboratory

The inclusion of plasma in plasma enhanced atomic layer deposition (PEALD) applications generally offers the benefit of substantially reduced process temperatures, greater flexibility in tailoring the gas-phase chemistry to produce desired film characteristics, and the ability to affect film crystallinity and phase.

Many PEALD systems use inductively coupled plasma (ICP) sources in materials synthesis. These sources can undergo changes in electron heating modes which can be induced by changes in applied power, pressure, or gas phase chemistry. Generally, these mode changes cause substantial variations in the electron energy distribution function and plasma density, which can impact the delivery of reactive and energetic species to substrates. This presentation explores the effects of heating mode changes on reactive species production and downstream plasma parameters (electron temperature, plasma potential, and plasma density). We discuss the use of probes and optical emission spectroscopy to characterize changes in the plasma parameters and how these changes affect the delivery of reactive and energetic species to the material surface. The discussion will include the results from select processing applications,

where changes in plasma properties are linked to differences in material properties. This work supported by the Naval Research Laboratory Base program

**AP-TuP-7  $\text{NaHF}_2$  as an Alternative Hydrogen Fluoride (HF) Source for Thermal Atomic Layer Etching and Deposition, Marcel Junge, R. Hirsch, V. Ghodsi, S. George**, University of Colorado Boulder

Thermal atomic layer etching (ALE) and deposition (ALD) are defined by an alternating sequence of separate, self-limiting surface reactions. ALE modifies and volatilizes a thin film surface, thereby removing ultra-thin layers of material. ALD adsorbs a precursor and, depending on the co-reactant, adds ultra-thin layers of film material. ALE and ALD processes have been developed for a wide range of film materials, including metals and semiconductors, as well as their oxides, nitrides, and fluorides. ALE and ALD provide precise control of shrinking critical dimensions, conformality in complex 3D structures, and wafer-scale uniformity.

A vital step for ALE and ALD is the fluorination reaction using hydrogen fluoride (HF). For example, thermal ALE of alumina ( $\text{Al}_2\text{O}_3$ ) cycles between HF to fluorinate and trimethylaluminum (TMA) to ligand exchange at elevated temperatures. Thermal ALD of aluminum fluoride ( $\text{AlF}_3$ ) also cycles between TMA adsorption and HF to remove methyl groups and form  $\text{AlF}_3$  below  $250^\circ\text{C}$ . One problem with HF is that its toxicity presents a challenge to health and safety. To address safety concerns, solvents may reduce the HF vapor pressure. For example, a 70% HF in 30% pyridine solution, commonly known as Olah's reagent, is used by organic chemists for fluorination reactions.

Other thermal ALE processes have also widely employed HF-pyridine. However, care is required during handling in a glovebox. Further difficulties are encountered in cleanup and waste management. To address these issues, this study tested sodium bifluoride ( $\text{NaHF}_2$ ), a salt that was safer to handle because  $\text{NaHF}_2$  exhibits negligible HF vapor pressure at room temperature. When heated to  $150^\circ\text{C}$ ,  $\text{NaHF}_2$  delivered HF vapor pressures up to 15 Torr. In addition, this solid salt was easier to clean up and reduced waste.

HF volatilization was observed by temperature-ramped quadrupole mass spectrometry. ALE experiments were conducted in a hot-wall, viscous-flow vacuum reactor equipped with an *in situ* spectroscopic ellipsometer. Thermal  $\text{Al}_2\text{O}_3$  ALE using sequential HF/TMA exposures served as a standard reference to evaluate  $\text{NaHF}_2$ . HF from  $\text{NaHF}_2$  exhibited diffusion-limited fluorination of  $\text{Al}_2\text{O}_3$  and an etch per cycle consistent with previous results using HF-pyridine. X-ray photoelectron spectroscopy detected no sodium on the surface after ALE, indicating that sodium fluoride remained in the source cylinder. These studies indicated that  $\text{NaHF}_2$  can be considered as an alternative HF source for fluorination reactions in thermal ALE or ALD on the laboratory scale.

## Biomaterial Interfaces Division

### Room Oregon Ballroom 203-204 - Session BI-TuP

#### Biomaterial Interfaces Flash Poster Session

**BI-TuP-1 Spacer Length Variations in Sulfo- and Sulfobetaines Affecting the Resistance Against Pathogenic Bacteria, Regina Kopeck, J. Karthäuser**, Ruhr University Bochum, Germany; *E. Schönemann, A. Martínez Guajardo, A. Laschewsky*, University Potsdam, Germany; *A. Rosenhahn*, Ruhr University Bochum, Germany

Zwitterionic polymers are characterized by their positively and negatively charged groups and their overall neutral net charge. The typically highly hydrophilic polymers are classified into several groups. Beside the well-studied phosphatidylcholine-, carboxybetaine-, and sulfobetaine-, also more recently developed sulfobetaine-based polymers were found to form fouling-resistant coatings.<sup>[1]</sup> Out of the large variety of possible geometric arrangements of zwitterionic functional groups, only very few have been explored. Following recent studies demonstrating the importance of the precise molecular polymer structure of sulfobetaines on their marine fouling resistance<sup>[2]</sup>, we synthesized sulfo- and sulfobetaines with varying chain lengths of inter-charge and backbone spacers to investigate the effect of the structural change on the resistance against proteins and pathogenic bacteria. The study included six different zwitterionic polymers synthesized by free radical polymerization of monomers with varying ethyl, propyl, and a long undecyl backbone-betaine spacer in combination with ethyl, propyl, and butyl inter-charge spacers. All zwitterionic polymers consistently exhibited very good wettability determined by contact angle goniometry. The non-specific attachment of proteins on the different coatings was

analyzed by surface plasmon resonance spectroscopy and the resistance against bacterial fouling was determined by dynamic attachment assays with the freshwater pathogens *E. coli*, *P. fluorescens*, and *B. subtilis*. The highest resistance exhibited the combination of propyl backbone betaine spacers with sulfonate functional groups.

[1] E. Schönemann, A. Laschewsky, E. Wischerhoff, J. Koc, A. Rosenhahn, *Polymers* (Basel). 2019,11, 1014. [2] J. F. Karthäuser, J. Koc, E. Schönemann, R. Wanka, N. Aldred, A. S. Clare, A. Rosenhahn, A. Laschewsky, *Adv. Mater. Interfaces* 2022, 9, [2200677] 1-9.

## BI-TuP-2 Frequency-Dependent Mechanical Characterization of Hygroscopic Biological Materials, *Saima Sumaiya, B. Sejour, O. Sahin*, Columbia University

Hygroscopic biological materials constitute a significant portion of the biological world, encompassing a diverse range of biomass from wood to bacterial spores. These materials respond to external stimuli by changing their size, shape, and mechanical properties. This responsiveness allows them to play critical roles in important natural processes such as growth of plants, distribution of seeds etc. Apart for their natural significance, these materials have also demonstrated promising applications in fields such as energy harvesting, development of biohybrid devices, and drug delivery. Our recent results show that these hygroscopic materials can exhibit a jamming-driven transition in mechanical properties at short timescales that differs from glassy and poroelastic behaviors (1). To this end, we have developed an atomic force microscopy (AFM)-based setup that can probe the nanomechanical properties of hygroscopic biological materials across a wide range of frequencies. With this setup, we study the frequency-dependent stiffness of the hygroscopic spores of *Bacillus subtilis* under varying load and humidity levels. We perform frequency sweeps over multiple decades and, alternatively, probe response at a single frequency at varying indentation forces. We interpret the response of the spores in terms of amplitude and phase differences between the applied modulation and cantilever response signal. Through this study, we aim to shed light on the jamming-driven transition in hygroscopic bacterial spores.

[1] Harrellson, S. G., DeLay, M., et al. Hydration Solids. *Nature*, in press, doi: 10.1038/s41586-023-06144-y.

## BI-TuP-4 Gas Sensing via Conductive Molecularly Imprinted Polymers (cMIPs), *Adriana Feldner*, CEST GmbH/University of Vienna, Austria; *P. Lieberzeit*, University of Vienna, Austria; *P. Fruhmam*, CEST GmbH, Austria

Molecularly imprinted polymers (MIPs) are synthetic materials that contain binding sites for selectively rebinding the target analyte. [1] Herein, cMIP blends serve as receptor layers on quartz crystal microbalances (QCMs) and chemiresistors. QCMs are mass-sensitive sensors based on the piezoelectric properties of quartz. [2] Chemiresistors can detect volatile organic compounds (VOCs) in the gas phase through thin conductive polymeric films. [3] The analytes in this case are volatile organic compounds (VOCs) that are known breath biomarkers of breast cancer patients. [4] Those sensors could be preliminary work towards applications in non-invasive early detection of diseases via breath analysis. Alternatively, they could serve as a stepping stone to other conductive MIP systems for VOC monitoring purposes

This work presents the results obtained with cMIPs as sensor materials for detecting 2-propanol, heptanal and acetophenone, respectively. MIPs for the detection of 2-propanol are based on polyurethane. For heptanal detection an acrylamide-based MIP was developed. The acetophenone MIP relies on an acrylate-based system. cMIPs were obtained by blending MIPs with a conductive material. The blends were applied to QCMs and chemiresistors. All sensors were tested in gas flow containing the respective analytes.

All described QCMs sensors react to the desired analyte in gas flow with concentration dependency. The cMIPs have also proven suitable for chemiresistors where binding of the analyte leads to a reversible concentration dependent change in the electric resistance. Detailed results for all analytes including selectivity studies with other VOCs will be presented on the poster.

## References

[1]Haupt, K. et al., Molecularly Imprinted Polymers. *Molecular Imprinting. Topics in Current Chemistry* **2011**, 325, 1-28.

[2]Alassi, A.et al., Quartz Crystal Microbalance Electronic Interfacing Systems: A Review. *Sensors* **2017**, 17 (12), 2799.

[3]Yan, S. et al., Inexpensive, Versatile and Robust USB-Driven Sensor Platform **2017**, 1 (6), 1-4.

[4]Phillips, M. et al., Prediction of breast cancer using volatile biomarkers in the breath. *Breast Cancer Research and Treatment* **2006**, 99 (1), 19-21.

## BI-TuP-7 3d Mass Imaging of Bacterial Biofilm Composition Using Water Cluster Sims, *Kate McHardy, N. Sano*, Ionoptika Ltd., UK; *N. von Jeinsen, D. Ward*, University of Cambridge, UK

Here we present recent work related to the study of biofilms; Microbial communities embedded in a 3D extracellular matrix. The matrix is composed of a complex array of extracellular polymeric substances that contribute to the unique attributes of biofilm lifestyle. Samples of bacteria and the biofilms they evolve are prepared and the growth arrested after a set period, with the resulting sample analysed with two distinct imaging techniques. We present data from water gas cluster ion beam secondary ion mass spectrometry (Water Cluster SIMS) which offers a mass and depth resolution to aid understanding of the spatial composition of the biofilm by visualising the 3D structures within.

One of the key benefits of Water Cluster SIMS is its ability to achieve high depth resolution due to the low kinetic energy of the water clusters which allows for the analysis of surface and subsurface structures with a high degree of precision. The use of water clusters as the primary ion source enhances secondary ion sensitivities of high mass molecules, in addition, it also minimises sample damage and fragmentation of high mass molecules which are common issues with other cluster ion beams. The water cluster beam was used in Ionoptika's J105 Cluster SIMS system with a beam spot size of 1.5um.

The results here show species consistent with biofilms and tracing masses through the sample in 3D, allows the differentiation between known surface features, for example, biofilm components, fixative residue, growth medium and substrate.

Despite the work being at an early stage, a significant step forward has been made in delivering new methods for the study of highly topical bio-samples that are of wide interest and application.

## BI-TuP-8 Characterization of Commercial Catheter Surfaces with Bio-Inspired Liquid-Infused Surfaces, *Evan Leonard*, University of Maine

Hospital-acquired infections (HAIs) affect over 1.7 million patients annually and are often treated with antibiotics, which can contribute to antibiotic resistance. Catheter-associated urinary tract infections (CAUTIs) are the most common type of HAI, resulting in an estimated \$390-450 million in treatment and increased length of stay-associated costs annually. Previously, a bio-inspired coating on commercial catheter surfaces has demonstrated the ability to reduce the need for antibiotics by minimizing both protein and bacterial adhesion to the catheter surface as well as the spread of bacteria to other organs. In this work, we treated commercial catheters with the bio-inspired liquid-infused coating to investigate changes in properties such as length, mass, and French size. Confocal microscopy was used to examine the catheter and coating interface, while material tensile testing was conducted to quantify bulk material properties after coating application. Through the development of liquid-infused treatments for commercial catheters, we aim to create a widely available, cost-effective solution for preventing CAUTI and reducing the need for antibiotic use in patients who need indwelling catheters.

## BI-TuP-9 Multi-Component Liquid-Infused Systems: A New Approach to Functional Coatings for Biomaterials, *Zachary Applebee, C. Howell*, University of Maine

Liquid-infused surfaces (LIS) have found utility across the globe due to their diverse applications including bactericidal functionality, ice adhesion prevention, and medical diagnostic equipment enhancement. Recent research has started exploring the broader potential of LIS by incorporating additional components into the liquid matrix. In this work, we present the concept of multi-component liquid-infused systems (MCLIS), in which the coating liquid consists of a primary liquid and a secondary component and review recent examples. At the molecular scale, MCLIS consisting of silicone oils infused with bacterial quorum sensing inhibitor compounds have been shown to stop bacterial biofilms not only from adhering but also from forming. At the nanoscale, MCLIS made from ferrous magnetic nanoparticles within fluorocarbon-based fluids or silicone oil can change their shape upon exposure to magnetic fields, making them useful for the active removal of adherent fouling organisms. Alternatively, MCLIS fabricated by first adding free particulates to the surface of a spherical droplet, then allowing the decorated droplet to be coated with an immiscible liquid, results in a 3D-coated MCLIS system. At the microscale, microdroplet arrays using more than one liquid in a defined pattern have been fabricated and used for high-throughput detection of compounds. By

introducing an additional element into the liquid matrix of liquid-infused systems, a diverse spectrum of attributes can be imbued into these materials, creating novel opportunities for applications within the biomedical realm and beyond.

**BI-TuP-10 Subcellular Detection of PEBCA Particles in Macrophages: Combining Darkfield Microscopy, Confocal Raman Microscopy, and ToF-SIMS Analysis, Elke Tallarek**, Tascon GmbH, Germany; *A. Vennemann*, IBE gGmbH, Germany; *M. Wiemann*, IBE gGmbH, Germany; *D. Breitenstein*, B. Hagenhoff, Tascon GmbH, Germany

The detection of biomedical organic nanocarriers in cells and tissues is still an experimental challenge. Here we developed an imaging strategy for the label-free detection of poly (ethylbutyl cyanoacrylate) (PEBCA) particles. Experiments were carried out with phagocytic NR8383 macrophages exposed to non-toxic and non-activating concentrations of fluorescent (PEBCA NR668 and PEBCA NR668/IR), non-fluorescent (PEBCA), and cabazitaxel-loaded PEBCA particles (PEBCA CBZ). Exposure to PEBCA NR668 revealed an inhomogeneous particle uptake similar to what was obtained with the free modified Nile Red dye (NR668). In order to successfully identify the PEBCA-loaded cells under label-free conditions, we developed an imaging strategy based on enhanced darkfield microscopy (DFM), followed by confocal Raman microscopy (CRM) and time-of-flight secondary ion mass spectrometry (ToF-SIMS). Nitrile groups of the PEBCA matrix and PEBCA ions were used as suitable analytes for CRM and ToF-SIMS, respectively. Masses found with ToF-SIMS were further confirmed by Orbitrap-SIMS. The combined approach allowed to image small (<1  $\mu\text{m}$ ) PEBCA-containing phagolysosomes, which were identified as PEBCA-containing compartments in NR8383 cells by electron microscopy. The combination of DFM, CRM, and ToF-SIMS is a promising strategy for the label-free detection of PEBCA particles.

We thank SINTEF, Norway for providing the samples.

**BI-TuP-11 Removal of Free Liquid Layer from Liquid-Infused Silicone Catheters Reduces Silicone Loss into the Environment while Maintaining Adhesion Resistance, Chun Ki Fong**, University of Maine; *M. Andersen*, University of Notre Dame; *E. Kunes*, *E. Leonard*, *D. Durand*, *R. Coombs*, University of Maine; *A. Flores-Mireles*, University of Notre Dame; *C. Howell*, University of Maine

Silicone catheters infused with silicone liquid are an effective alternative to antibiotic coatings in reducing the adhesion and dissemination of bacteria. However, free silicone liquid on the surface of catheters *in vivo* can be lost into the host system, potentially causing complications. To reduce the potential for liquid loss, free silicone liquid was removed from the surface of liquid-infused catheters and the effects on protein and bacterial adhesion were explored. Absorption of the surface liquid from fully saturated catheter surfaces removed the most if not all of the free liquid layer but preserved the slippery properties. As anticipated, significantly less oil could be forcibly removed from the surface of the samples with the free silicone liquid removed than samples that retained their liquid layer. Tests using the catheter infection-associated protein fibrinogen and bacterium *Enterococcus faecalis* revealed no significant differences in adhesion between the material with or without the free liquid layer. To better understand what point infusing liquid saturation becomes important to resisting adhesion, catheter samples were infused to between 5–100% of maximum liquid uptake values then tested for their ability to resist adhesion by fibrinogen and *E. faecalis*. The results revealed that samples infused with ~80% of their performed statistically similarly to fully infused materials. Together, the results suggest that eliminating free liquid layers through either mechanical means or partial infusion can reduce oil loss from liquid-infused catheters into the host system while preserving functionality, improving the safety of liquid infusion as alternatives to antibiotic coatings in catheters.

## Chemical Analysis and Imaging of Interfaces Focus Topic Room Oregon Ballroom 203-204 - Session CA-TuP

### Chemical Analysis and Imaging of Interfaces Poster Session

**CA-TuP-1 Combined Spectro-Electrochemical Methods to Investigate Electrochemical Corrosion in Real-Time, Matteo Olgiati**, CEST GmbH, Austria

Many engineering alloys, ranging from the aerospace grade aluminium alloys 2024 and 7075 to stainless steels, are vulnerable to localised corrosive degradation under certain environmental conditions.

The local nature of corrosion is most of the time dictated by the intrinsic features of the microstructure. The intermetallic second phases in age-hardened aluminium alloys, for example, are known to act as nucleation points for local corrosive attack [1]. Similarly, pitting corrosion in stainless steels was found to initiate in the vicinity of MnS inclusions [2]. Furthermore, the time-dependent evolution and further propagation of corrosive events depends on the local changes in chemistry of the microstructure [3-4], which will ultimately determine the mechanism and rate of such propagation.

For these reasons, characterising and, consequently, understanding the degradation mechanism of these alloys is not only complex, but must also rely on in-situ and highly spatio-temporally resolved techniques [5].

In this contribution, we present a recently developed spectro-electrochemical scanning flow cell, which enables to study corrosive degradation phenomena, as well as corrosion prevention with the use of corrosion inhibitors. Such scanning flow cell allows to induce local corrosion by electrochemically controlling the polarization of the working electrode immersed in 10 mM NaCl solution. Simultaneously, we can characterize the time-dependent appearance of micro- to macroscopic surface features by means of in-situ optical microscopy. This information can be further supported by the online identification and quantification of dissolved mass currents by means of online inductively coupled plasma mass spectrometry (ICP-MS). The combination of this techniques allows us to estimate not only the typical surface-initiated corrosion mechanisms, but also the characteristic corrosion rates of different metal alloys.

#### References:

- [1] A. Boag *et al.*, *Corrosion Science* **53** (1), 17-26 (2011)
- [2] D. Li *et al.*; *Corrosion Science* **211**, 110860 (2023)
- [3] A. Kosari *et al.*, *Corrosion Science* **177**, 108947 (2020)
- [4] A. Kosari *et al.*, *Corrosion Science* **177**, 108912 (2020)
- [5] M. Olgiati *et al.*, *Corrosion Science* **192**, 109836 (2021)

**CA-TuP-2 Diamond Hydrogenation Using a Compact and Cost-Effective Low-Power Plasma, J. Trey Diulus**, NIST Center for Nanoscale Science and Technology; *F. Yi*, NIST-Gaithersburg; *E. Strelcov*, NIST Center for Nanoscale Science and Technology; *D. LaVan*, NIST-Gaithersburg; *A. Kolmakov*, NIST Center for Nanoscale Science and Technology

Device fabrication of field effect transistors (FET)s and other electronic devices are still largely dependent on silicon, which has been the core semiconductor material for over seven decades.<sup>1,2</sup> Newer materials, like SiC and GaN, offer wide-bandgap alternatives to silicon that are required for high power electronics with improved carrier mobility, carrier density, and high operation temperatures.<sup>2,3</sup> Alternatively, diamond is another promising semiconductor material, with its ultra-wide bandgap (5.5 eV), unmatched thermal conductivity, breakdown voltage, and high charge carrier mobility (~4000 cm<sup>2</sup> V<sup>-1</sup> s<sup>-1</sup>).<sup>3</sup> Recently, advances in diamond growth through techniques like chemical vapor deposition (CVD) have demonstrated wafer size of diamond single crystals,<sup>4</sup> overcoming the primary challenge towards industrial implementation. However, hydrogenation of the diamond surface is a necessary process to fabricate high-mobility diamond FETs. The H-terminated surface, however, is sensitive to ambient adsorbates that deteriorate the stability of surface conductivity when using modern device manufacturing processes. The present method for H-terminating a diamond surface is via a high-power (> 1 kW) microwave plasma that typically utilizes a specially designed chamber for high pressure (tens of kPa) exposures at elevated temperatures (>700 °C).<sup>5</sup> Due to the high cost required for such a system, a roadblock exists that prevents broader research community efforts for diamond related devices that is imperative for improving high-power/frequency electronics. Thus, we have developed a recipe for H-terminating diamond based on an H<sub>2</sub> plasma generated by a simple low-power (75 W), low pressure (tens of Pa) RF plasma cleaner for a cost-effective diamond hydrogenation method. Furthermore, we have developed a relevant plasma characterization metrology for H-termination by real time monitoring of the radical flux using catalytically activated and reference metal film samples loaded in a nano-calorimeter,<sup>6</sup> in conjunction with standard optical spectroscopy. We have tested our hydrogenation method on diamond samples by characterizing the surface before and after plasma treatment with *in situ* x-ray photoelectron spectroscopy and *ex situ* 4-point probe measurements. Our efforts will provide researchers a facile route towards diamond research and will broaden the diamond research community.

<sup>1</sup>Alberi, K. *et al.*, *J Phys D Appl Phys*, **52**, 013001, (2019)

<sup>2</sup>Donato, N. *et al.*, *J Phys D Appl Phys*, **53**, (2019)

<sup>3</sup>Sasama, Y. *et al.*, *APL Mater*, **6**, (2018)

<sup>4</sup>Schreck, M. *et al.*, *MRS Bull*, **39**, 504-510, (2014)

<sup>5</sup>Geis, M. W. *et al.*, *Phys Status Solidi A*, **215**, (2018)

<sup>6</sup>Yi, F. *et al.*, *J Therm Anal Calorim*, **138**, 3367-3373, (2019)

**CA-TuP-3 A Study of the D-Parameter: Evaluating Measurement Techniques in X-ray Photoelectron Spectroscopy (XPS), Alvaro Lizarbe, G. Major, B. Clark, Brigham Young University; D. Morgan, Cardiff University; M. Linford, Brigham Young University**

When looking at carbonaceous material analysis, the D-parameter plays a pivotal role in determining the  $sp^2/sp^3$  ratio via X-ray photoelectron spectroscopy (XPS). Despite its utility, the methodological inconsistency in generating the peak envelope introduces uncertainty in the D-parameter analysis. This study investigates two distinct approaches to measuring the D-parameter, a modified b-spline method and a polynomial regression line fit. The b-spline method entails the creation of synthetic Gaussian peaks in the carbon KLL Auger peak, maintaining a consistent full width at half maximum (FWHM) and equal distance apart but varying areas. The polynomial regression approach, on the other hand, fits the curve by manipulating the degree of the polynomials. Both techniques strive to generate a fit that mirrors the raw data as closely as possible, thereby facilitating a more precise derivative from which the D-parameter can be computed. To evaluate the efficacy of these methods, a comparative analysis was conducted using different carbonaceous materials such as direct current chemical vapor deposition (DC-CVD) diamonds, carbon nanotubes, and highly oriented pyrolytic graphite (HOPG). The results are compared against the traditional D-parameter values for these materials. This research not only contributes to improving the reliability and reproducibility of D-parameter measurements but also offers valuable insights into the optimization of envelope creation methods in XPS.

**CA-TuP-4 Proton and Hydroxide Diffusion Within Supercooled Water, Megan Dunlap, Pacific Northwest National Lab; L. Kringle, R. Smith, B. Kay, G. Kimmel, Pacific Northwest National Laboratory**

The molecular mechanisms for the diffusion of protons and hydroxides within liquid water are controversial. To elucidate these processes, we examine proton and hydroxide diffusion within water films under ultra-high vacuum that are heated to temperatures spanning 110-140 K. At these temperatures, the water molecules are arrested, but the charged species move rapidly through the ~40 nm thick films. Their progress is monitored with reflection absorption infrared spectroscopy (RAIRS) via the exchange of the ion with isolated  $D_2O$  'probe' molecules within the film to form HDO. We have investigated the exchange rate as a function of the distance that the ions must travel to reach the  $D_2O$ , the temperature, the total thickness of the film, and the ion type. Based on the temporal evolution of the  $D_2O$ , we have found that both diffusion and trapping of the ion within the film are required to describe the observations.

## Spectroscopic Ellipsometry Technical Group Room Oregon Ballroom 203-204 - Session EL-TuP

### Spectroscopic Ellipsometry Poster Session

**EL-TuP-1 Dielectric Function of Tantalum Nitride Formed by Atomic Layer Deposition on 300 mm Wafers, Aaron Lopez Gonzalez, Y. Hettige, J. Love, S. Zollner, New Mexico State University; E. Bhatia, T. Vo, S. Papa Rao, NY CREATES**

In this undergraduate student poster, we describe the dielectric function of atomic layer deposition (ALD) tantalum nitride (TaN) from 0.03 eV to 6.6 eV determined from spectroscopic ellipsometry.

First, thermal oxides with about 50 nm thickness were grown on B-doped 10  $\Omega$ cm Si (100) 300 mm diameter wafers. Tantalum nitride layers with 12 nm and 25 nm thickness were then formed by atomic layer deposition using 300 mm process tools. The TaN layer thicknesses were confirmed by x-ray reflectance (XRR). The TaN surface roughness (also derived from XRR) was on the order of 0.5 nm. On a vertical J.A. Woollam variable angle of incidence rotating-analyzer ellipsometer (V-VASE), the ellipsometric angles  $\psi$  and  $\Delta$  were acquired at room temperature at incidence angles from 50° to 80° and photon energies from 0.5 to 6.6 eV with 0.02 eV steps. We used a Berek wave plate compensator and measured with both positive and negative polarizer angles to improve accuracy. We selected a broad range of

incidence angles, because the Brewster angle of  $SiO_2$  (55°) is much smaller than that of Si (75°). We also acquired the infrared ellipsometric spectra at the same angles of incidence from 0.03 to 0.70 eV with 8  $cm^{-1}$  resolution on a J.A. Woollam Fourier-transform infrared ellipsometer.

We first developed an ellipsometry model for the optical constants of the thermal oxide, using three Gaussian oscillators at 56, 132, and 146 meV in the infrared spectral region to describe the silicon-oxygen vibrations and a pole at 11 eV (fixed) with variable amplitude to model the visible and ultraviolet dispersion. The TaN layers were described with a Tauc-Lorentz oscillator centered at 3.2 eV with a band gap at 1.7 eV, one UV pole, and one Gaussian in the UV. The fit could be improved with an infrared Gaussian between 0.7 and 1.1 eV, but this peak could be an artifact arising from the uncertainty of the precise layer thicknesses. Across wafer uniformity of the band gap was determined for both thicknesses by performing spectroscopic ellipsometry on coupons from the wafer center, mid radius, and wafer edge. We will perform ellipsometry measurements at low temperatures to investigate the temperature dependence of the optical constants and oscillators.

**EL-TuP-2 A Generalized Maximum-Entropy Approach for Eliminating Apodization and Associated Errors in Noise Reduction, L. V. Le, Institute of Materials Science, Vietnam Academy of Science and Technology, Viet Nam; Y. Kim, Department of Physics, Kyung Hee University, Republic of Korea; D. Aspnes, North Carolina State University**

In linear filtering, apodization requires compromises to be made among noise leakage, information loss, and Gibbs oscillations (ringing). This problem, inherent in linear filtering, is avoided with the corrected maximum-entropy (CME) procedure. In CME, apodization and associated errors are eliminated by projecting trends established by low-order coefficients into the white-noise region in a model-independent, most-probable way. However, CME cannot be applied to structures that contain an appreciable dispersion-curve component. Capitalizing on Hilbert transforms, we develop a generalized maximum-entropy (GME) approach that can be applied to any lineshape, thereby allowing white noise to be eliminated completely with no deleterious side effects. Endpoint-discontinuity removal and a Hilbert transform can reversibly convert any segment consisting of a Lorentz/dispersion combination into an absorption spectrum, thus allowing any spectrum to be processed by CME. As an added benefit, Hilbert transforms are exact Kramers-Kronig (KK) transforms of these segments, providing new opportunities for analysis in spectroscopy.

**EL-TuP-3 Intelligent Linear Filters for Noise Reduction in Spectroscopy, Young Dong Kim, Kyung Hee University, Republic of Korea; L. Le, Vietnam Academy of Science and Technology, Viet Nam; D. Aspnes, North Carolina State University**

A linear filter must strike a balance among reducing noise, preserving lineshapes, and minimizing or eliminating ringing. While nonlinear methods offer superior performance, direct- (spectral-) space (DS) convolution is convenient and may be sufficient in many applications. However, optimization requires reciprocal- (Fourier-) space (RS) considerations. This follows because information appears as point-to-point correlations and noise as point-to-point fluctuations, thereby concentrating information and noise in low- and high-order Fourier coefficients, respectively. For optimum performance, the transfer function of any filter must be consistent with the Fourier transform of the spectrum.

Using Parseval's Theorem, we project typical DS performance measures such as mean-square error (MSE) into RS. The resulting expressions are simpler and more informative than their DS counterparts, providing quantitative insight not only into the effectiveness of different linear filters, but also how they can be improved. Surprisingly, the rectangular ("ideal" or "brick wall") filter is found to be nearly optimal, a consequence of its complete elimination of distortion in low-order coefficients. When ringing is taken into account, the best practical filter is the Gauss-Hermite. Capitalizing on the information provided by these calculations, we develop a version that is demonstrably superior to both brick-wall and Gauss-Hermite filters.

**EL-TuP-4 Temperature Dependence of the Fine Structure of the NiO Critical Points, Yoshitha Hettige, C. Armenta, J. Love, S. Zollner, New Mexico State University; M. Veis, Charles University, Prague, Czech Republic**

Nickel oxide (NiO) is a cubic charge-transfer insulator. Its valence band consists of Ni 3d and O 2p states. The Ni 3d states split into  $t_{2g}$  and  $e_g$  bands. The valence band maximum is a hybridized mixture of O 2p and Ni

$e_g$  states. The excited  $e_g^*$  band is about 4 eV above the  $e_g$  band. Optical interband transitions from  $e_g$  into  $e_g^*$  give rise to a strong absorption peak near 4 eV known as the charge transfer gap. The location of the Ni 4s band is not clear.

In addition to the strong charge transfer gap at 4 eV, there are two other features in the optical spectra of NiO. (1) There is a small amount of absorption between 1 and 4 eV (similar to the indirect absorption of Si) in the pseudodielectric function, which cannot be explained with surface roughness. It is possible that this absorption is due to defects, such as excess oxygen. (2) There are several weak peaks between 1.5 and 4.0 eV. They might be due to interatomic transitions between the Ni 3d orbitals. The temperature dependence of these weak peaks (which we call fine structure) is the topic of this abstract.

In this presentation, we will discuss the temperature dependence of the smaller peaks in these spectra and attribute them to features in the band structure of NiO.

## EL-TuP-5 Characterization of Hybrid Organic-Inorganic Perovskite Semiconductors and Solar Cells, *Bailey Frye, E. Miller, N. Podraza*, University of Toledo

Hybrid organic-inorganic lead-halide based perovskite semiconductors (ABX<sub>3</sub>) are absorber layers in high efficiency single junction and tandem thin film solar cells. The ability to modify the bandgap energies over a wide range is required for these applications, with typical components consisting of an organic molecule A-cation such as methylammonium (MA) or formamidinium (FA), metal B-cation such as Pb or Sn, and a halogen X-anion such as I or Br. Spectroscopic ellipsometry is the ideal characterization technique for determining the complex dielectric function ( $\epsilon = \epsilon_1 + i\epsilon_2$ ) spectra and thickness of these perovskites as thin films or within solar cell device structures. Various oscillator models have been used to describe  $\epsilon$  for these direct-gap, polycrystalline semiconductors. Many models may generate an approximate line shape for  $\epsilon$ , but unfortunately lack physically meaningful parameters, are not Kramers-Kronig (KK) consistent — and therefore not physically realistic, or require numerical integration of the KK-integral that is often prohibitively time consuming. A KK-consistent parametric model that uses excitonic critical point parabolic band (CPPB) oscillators and an Urbach tail is presented in this work. CPPBs represent the band-to-band transitions of a semiconductor, including the bandgap, while the Urbach tail describes subgap absorption features.  $\epsilon_2$  is described by a series of CPPB oscillators with an Urbach tail and then  $\epsilon_1$  is determined from the analytic solution to the KK-integral of  $\epsilon_2$ . This parametric model is thus KK-consistent with physically meaningful parameters relevant to direct gap crystalline semiconductors and is shown to model experimental ellipsometric spectra and describe the line shape of  $\epsilon$  accurately and quickly for various compositions of hybrid organic-inorganic lead-based perovskite semiconductors. This model may be of great use for analyses of perovskite semiconductors that require many data sets, such as real time spectroscopic ellipsometry and ellipsometric spatial mapping. Applications of this CPPB and Urbach tail model to the analysis of  $\epsilon$  for polycrystalline (FASnI<sub>3</sub>)<sub>1-x</sub>(MAPbI<sub>3</sub>)<sub>x</sub>, spatial mapping of FA<sub>0.8</sub>Cs<sub>0.2</sub>Pb(I<sub>0.65</sub>Br<sub>0.35</sub>)<sub>3</sub> and FA<sub>0.8</sub>Cs<sub>0.2</sub>Pb(I<sub>0.6</sub>Br<sub>0.4</sub>)<sub>3</sub> films including those in the partial and full device structures, and through-the-glass ellipsometry of full solar cells containing perovskite absorber layers are presented in this work.

## EL-TuP-6 Many-Body Effects in the Mid-Infrared Dielectric Function of InSb from 80 to 800 K, *M. Rivero Arias, C. Armenta*, New Mexico State University; *C. Emminger*, Leipzig University, Germany; *C. Zamarripa*, New Mexico State University; *N. Samarasingha*, Nova Measuring Instruments; *J. Love, S. Yadav, Stefan Zollner*, New Mexico State University

We describe measurements of the mid-infrared dielectric function of bulk InSb near the direct band gap using Fourier-transform infrared spectroscopic ellipsometry from 80 to 800 K in an ultra-high vacuum cryostat. Indium antimonide is the zinc blende compound semiconductor with the smallest direct band gap ( $E_0=0.18$  eV at 300 K) due to its heavy elements and the large resulting spin-orbit splitting and Darwin shifts. The band gap is extracted from the dielectric function by fitting with a parametric oscillator model. It decreases from 80 to 450 K following a Bose-Einstein model, then remains constant up to 550 K, and increases again at the highest temperatures. This is explained with a thermal Burstein-Moss shift: The onset of optical absorption increases as electron-hole pairs are thermally excited at the highest temperatures. The intrinsic carrier concentration determined from the Drude tail in the ellipsometry spectra agrees qualitatively with temperature-dependent Hall experiments and calculations based on degenerate Fermi-Dirac statistics.

## EL-TuP-8 Film-Side Versus Through-the-Glass Ellipsometry Measurements of Wide Band Gap Perovskites, *Emily Amonette, K. Dolia, B. Frye, Y. Yan, Z. Song, N. Podraza*, University of Toledo

Wide band gap FA<sub>0.8</sub>Cs<sub>0.2</sub>Pb(I<sub>1-x</sub>Br<sub>x</sub>)<sub>3</sub> ( $x = 0.3, 0.35, 0.4$ ) perovskite thin films are examined via spectroscopic ellipsometry in both the film-side mapping configuration and as part of complete superstrate photovoltaic (PV) devices. Complex dielectric function ( $\epsilon = \epsilon_1 + i\epsilon_2$ ) spectra of the perovskite and all layer thicknesses are determined for all measured samples. Film-side measurements are more commonly performed, and it is often assumed that the resulting  $\epsilon$  spectra represent a layer in a complete device, but this work examines variations in perovskite  $\epsilon$  and associated characteristics such as the band gap and Urbach energies that may only be apparent when considering data from a complete PV device taken in the through-the-glass configuration. Measurements of partial device-like structures consisting of glass superstrate / indium tin oxide / hole transport layer / perovskite reveal spatial variations in band gap energies ranging from 1.77 to >1.80 eV in the case of FA<sub>0.8</sub>Cs<sub>0.2</sub>Pb(I<sub>0.6</sub>Br<sub>0.4</sub>)<sub>3</sub> as well as variations in Urbach energies, while those of complete PV devices consisting of the same structure and perovskite composition but completed with the electron transport layer and metal back contact exhibit less spatial variation, where band gap energies vary only between 1.75 to 1.77 eV. This behavior indicates that atmospheric exposure amplifies perovskite material spatial uniformity. Optical property and thickness information from through-the-glass ellipsometry is used to simulate external quantum efficiency (EQE) spectra, and by comparing these simulations to experimental EQE, information about both optical and electronic loss in PV is obtained. These data sets comprised of many similar but slightly different samples and measurement configurations are used to develop methods for streamlining the analyses, such as considering which parameters may be kept common to multiple samples and how to deal with outliers resulting in substantially different optical properties and PV device performance. These patterns in parameter values may also predict success in accurately calculating PV device performance parameters from EQE simulations as well as develop strategies for analyzing large amounts of data sets.

## EL-TuP-9 Determination of the Optical Constants and Thickness of Ultrathin Thermally Evaporated Iron Catalyst Films Using Spectroscopic Ellipsometry, *Nicholas Allen, M. Linford, R. Vanfleet, R. Davis*, Brigham Young University

Vertically aligned carbon nanotube (VACNT) forest growth is a catalytic chemical vapor deposition process that uses a thin-film iron catalyst on an alumina support. Iron catalyst thickness for VACNT growth is typically from ~1-10 nm and thickness strongly affects forest morphology. Transmission electron microscopy has been used to directly measure the thicknesses of thin iron/iron oxide films but is destructive and not easily used for routine process monitoring. Atomic force microscopy has also been used but requires the creation of an abrupt step edge in the film. Here we describe the use of spectroscopic ellipsometry for characterization of these very thin iron films. However, in this thickness range, the optical constants and thickness are not easily separated. The absorptive nature of the iron/iron oxide films adds further difficulty. In this study, a multi-sample ellipsometry analysis was performed using iron films of various thicknesses to obtain the optical constants of thermally evaporated iron. We also explored contrast enhancement by incorporating a silicon dioxide layer under the film being analyzed to enhance sensitivity to the optical constants.

## EL-TuP-10 Elevated Temperature Model Dielectric Function of InAs Determined by Spectroscopic Ellipsometry, *Preston Sorensen, U. Kilic, R. Korlacki, M. Schubert*, University of Nebraska - Lincoln

We report a model dielectric function approach to determine and predict the elevated temperature (30-250°C) dielectric function of InAs across the spectral range of the near infrared to deep ultraviolet (0.73eV to 5.0eV). InAs is a III-V zincblende structure semiconductor with low-energy direct bandgap of 0.355eV and is of interest in long wavelength optoelectronic devices [1,3,4]. Determining accurately the thermal evolution of its optical properties, such as its complex index of refraction, bandgap energy, and band to band transitions permits for improved prediction of its thermal behavior in devices under operation. Also, knowledge of the dielectric function variation with temperature enables model-based analysis of spectroscopic ellipsometry data of InAs-based layer structures. Thermal perturbation of a crystal results in a small increase in the lattice constant of the material, altering the band structure, and therefore its dielectric function [4]. Spectroscopic ellipsometry permits measurement of the dielectric function of InAs. Measurements were taken from 30 °C to 250 °C at a single angle of incidence utilizing the temperature-controlled sample compartment of an atomic layer deposition system. The sample was also

# Tuesday Evening, November 7, 2023

measured at room temperature at multiple angles of incidence in normal ambient to identify surface over layer effects. All ellipsometry data were modeled using a critical-point model dielectric function approach with implemented temperature dependencies of all the critical point model parameters [2,3]. We find linear evolutions of all critical-point model parameters versus temperature for the investigated temperature range. The obtained model parameters permit accurate prediction of the dielectric function of InAs at any temperature in the investigated range. Our result can be useful for model-based quantitative analysis of in-situ ellipsometry data obtained during atomic layer deposition growth of layer structures on InAs substrates.

## References:

- [1] S. T. Schaefer, et al. "Absorption edge characteristics of GaAs, GaSb, InAs, and InSb" *Journal of Applied Physics* (2020).
- [2] E. Montgomery, et al. "Temperature dependent model dielectric function of highly disordered Ga<sub>0.52</sub>In<sub>0.48</sub>P" *Thin Solid Films* (2010).
- [3] S. Adachi. "Optical dispersion relationships for GaP, GaAs, GaSb, InP, InAs, InSb, Al<sub>x</sub>Ga<sub>1-x</sub>As and In<sub>1-x</sub>Ga<sub>x</sub>As<sub>y</sub>P<sub>1-y</sub>." *Journal of Applied Physics* (1989).
- [4] P. T. Webster, et al. "Measurement of InAsSb bandgap energy and InAs/InAsSb band edge positions using spectroscopic ellipsometry and photoluminescence spectroscopy" *Journal of Applied Physics* (2015).

**EL-TuP-11 Numerical Ellipsometry: Artificial Intelligence for Real-Time, *in Situ* Absorbing Film Process Control**, Frank Urban, Florida International University; D. Barton, Florida International University Retired

Ellipsometry is a material analytical method in which the desired parameters, for example film thickness and index of refraction, are related to the instrument measurements through Maxwell's equations, light wavelength, and measurement geometry. Consequently, obtaining the desired parameters has required solving the model equations using a wide variety of methods. A commonly used method is least squares curve fitting, frequently the Levenberg-Marquardt method. This numerical method depends upon not only the model but also the initial estimates of solution, the possible interference of local minima, and the algorithm stopping conditions. Being iterative, it also can take significant time. The work here demonstrates the use of Artificial Intelligence in the form of a multilayer perceptron artificial neural network to avoid these problems and find solutions in the microsecond time scale. This non-iterative, stable, and fast performance lends itself to real-time, *in situ* monitoring of thin film growth. Examples for thin (up to 30 nm) films will be given using a multilayer perceptron configuration consisting of 4 input and 4 output neurons with two hidden layers of up to 20 neurons each. Solutions are performed at each wavelength independently and do not rely on fitting functions for optical properties.

**EL-TuP-12 Massive Data Collection With A Pupil Plane Imaging Polarized White Light Interferometer**, Alexander Boosalis, Y. Wang, Onto Innovation; P. Vagos, Onto Innovation, France; Y. Liu, Onto Innovation, Singapore; G. Antonelli, N. Smith, Onto Innovation

We present novel instrumentation capable of measuring the Jones matrix response of a sample across a large range of incident angles (0-55 degrees), sample rotation angles (0-360 degrees), and wavelengths (400-1000 nm) in less than 10 seconds. The result is a massive data set with over 600,000 individual data points. Development of this tool was spurred by the requirements of commercial chip manufacturing to collect and process a large amount of data for optical critical dimension (OCD) metrology in the smallest possible time and within a shrinking measurement area. However, this instrument is increasingly applicable to the research community where development of metasurfaces, biaxial thin films, and other complex nanostructures requires measurement over a range of azimuth angles to properly characterize. The instrument also has a small measurement spot size – less than 10 μm in diameter – which is useful for both OCD metrology and prototype research nanostructures which tend to be hard to produce over large areas. We will demonstrate a prototype tool measuring an industry standard calibration scatterometry target with a 10 μm box size.

The white light interferometer is in a Linnik configuration with high numerical aperture objectives. By imaging the back focal plane of the sample objective to a camera we can collect a white light interferogram at every pixel that contains both reflection amplitude and phase information over a wide array of incidence angles. In this configuration the instrument lies somewhere between the capabilities of a polarized reflectometer and a rotating analyzer ellipsometer at each individual angle of measurement, with sensitivity to the entire Jones matrix but not the ability to measure the

Jones elements specifically. We will show that rotating the system polarizer allows determination of the individual Jones matrix elements.

**EL-TuP-13 Fast Spectroscopic Mueller Matrix Ellipsometry in the THz Range**, Alexander Ruder, University of Nebraska - Lincoln; S. Richter, Lund University, Sweden; P. Kuhne, Linköping University, Sweden; V. Rindert, Lund University, Sweden; V. Stanishev, Linköping University, Sweden; R. Korlacki, J. Olander, University of Nebraska - Lincoln; V. Darakchieva, Lund University, Sweden; M. Schubert, University of Nebraska - Lincoln

We demonstrate a spectroscopic Mueller matrix ellipsometer in the THz wavelength range using rotating anisotropic optical components for polarization state generation and analysis. A solid state source and detector allow for time division multiplexing of individual wavelengths at kHz rates. Synchronous modulation of the source wavelength, polarization state generator, and polarization state analyzer allows for rapid acquisition of 4x4 Mueller matrix spectra. Calibration procedures and initial results for isotropic and anisotropic samples are discussed.

**Laboratory-Based Ambient-Pressure X-ray Photoelectron Spectroscopy Focus Topic**  
Room Oregon Ballroom 203-204 - Session LX-TuP

**Laboratory-Based AP-XPS: Poster Session**

**LX-TuP-1 Multimodal Liquid Cell for Lab-based APXPS: Investigating Ruthenium-based Organometallic Molecules in Various Environments**, Youngseok Yu, A. Vidal Muller, Brookhaven National Laboratory; Z. Xi, Stony Brook University/Brookhaven National Laboratory; M. Liu, E. Stavitski, J. Concepcion, A. Head, Brookhaven National Laboratory

Dye-sensitized photo-electrosynthesis cells (DSPECs) hold great promise as sustainable and renewable energy sources. To enhance the adsorption efficiency, chromophores are anchored onto oxide surfaces to absorb visible light, as transition metal oxides typically possess band gaps within the range of 2-3 eV. In this research, we have developed a multimodal liquid cell for ambient-pressure X-ray photoelectron spectroscopy (APXPS) to investigate the solid/liquid interface of these systems. The cell design utilizes a graphene-covered holey SiNx membrane with deposited metal oxide and catalyst as the working electrode. Our study focuses on examining the electronic structure of a dye molecule, (bis-2,2'-bipyridine)[(4,4'-bis(diethyl phosphonate)-2,2'-bipyridine)]ruthenium(II) (or RuP), under various conditions, including being anchored on TiO<sub>2</sub>, anchored on IrO<sub>2</sub>, and in a 1mM NaOH solution. Our findings indicate that the electron density of the Ru metal center varies with its environment.

**LX-TuP-2 Investigating Solvation with Liquid Jet Photoelectron Spectroscopy**, Jared Bruce, University of Nevada, Las Vegas; A. Haines, F. Furche, University of California, Irvine; R. Seidel, Helmholtz-Zentrum Berlin für Materialien und Energie, Germany; B. Winter, Fritz Haber Institute of the Max Planck Society, Germany; J. Hemminger, University of California, Irvine

The local chemical structure around solutes in aqueous solution is challenging to characterize on a molecular scale given the amount of hydrogen bonding interactions that occur in solution. Liquid jet photoelectron spectroscopy (LJ-XPS) can be a critical tool providing valuable chemical information both near the surface and in the bulk of the solution.

In this talk, we will explore the solvation of acetic acid in aqueous solution both near the interface and into the bulk of the solution. The difference in binding energy between the methyl and carboxyl carbons ( $\Delta BE$ ) was used to compare electronic structure calculations coupled with molecular dynamics simulations to the results from the LJ-XPS. Experiment and theory were found to overlap when a single water molecule was added to the first solvation shell of acetic acid calculation, whereas 20 water molecules were required to reproduce the experiment for acetate. Building on these results, liquid jet work at the synchrotron was used to explore the difference in solvation near the interface at lower probe depths compared to those in the bulk of the solution and in the lab-based experiments.

**LX-TuP-4 Evaluation of AlCoCrFeNiMnTi High Entropy Alloys for CO<sub>2</sub> Hydrogenation, Chiezugolum Odilinye, H. Kersell, School of Chemical, Biological, and Environmental Engineering, Oregon State University; X. Fan, Department of Materials Science and Engineering, University of Tennessee, Knoxville; Z. Lyu, P. Liaw, Department of Materials Science and Engineering, University of Tennessee; G. Herman, School of Chemical, Biological, and Environmental Engineering, Oregon State University**

Carbon dioxide (CO<sub>2</sub>) hydrogenation is of considerable interest due to the ability to chemically recycle carbon dioxide with renewably generated hydrogen. A wide range of catalysts have been used for hydrogenation of CO<sub>2</sub> where methanation, Fischer-Tropsch, and methanol synthesis reactions are the most investigated. We are interested in evaluating high-entropy alloys (HEAs) for CO<sub>2</sub> hydrogenation, where we can take advantage of the multifunctional sites that exist at HEA surfaces. Indeed, certain HEAs recently showed promise for altering the selectivity and stability for CO<sub>2</sub> hydrogenation catalysts.<sup>[1]</sup> In this study, we have used laboratory-based ambient pressure X-ray photoelectron spectroscopy (APXPS) to investigate the reaction of CO<sub>2</sub> and CO<sub>2</sub>/H<sub>2</sub> mixtures with an AlCoCrFeNiMnTi HEA. For these experiments, the as-cast alloy was homogenized at 1100 °C, polished, and then sputter-cleaned in ultrahigh vacuum to remove adventitious carbon and native oxides. This clean surface was then exposed to 1 mTorr of CO<sub>2</sub>, while we monitored the chemical state of the adsorbed carbon species, as well as the oxidation state of the surface metal atoms. We have performed similar experiments with CO<sub>2</sub>/H<sub>2</sub> mixtures and will contrast the observed surface chemistries with only CO<sub>2</sub>. These studies demonstrate that APXPS is a powerful technique to monitor reactions on complex alloy surfaces.

Reference:

[1] K. Mori, N. Hashimoto, N. Kamiuchi, H. Yoshida, H. Kobayashi, and H. Yamashita, Hydrogen spillover-driven synthesis of high-entropy alloy nanoparticles as a robust catalyst for CO<sub>2</sub> hydrogenation, *Nat. Commun.*, 2021, 12, 3884

## Nanoscale Science and Technology Division Room Oregon Ballroom 203-204 - Session NS-TuP

### Nanoscale Science and Technology Poster Session

**NS-TuP-1 AVS Dorothy M. and Earl S. Hoffman Awardee Talk: Scalable and Sustainable Synthesis of ZnO Nanowires via Hot Water Treatment for Photocatalytic Applications, Ranjitha K. Hariharalakshmanan<sup>1</sup>, F. Watanabe, T. Karabacak, University of Arkansas at Little Rock**

There is growing interest in developing cost-effective and sustainable methods to synthesize photocatalysts that can be immobilized on substrates. In this study, we present a novel and ultra-scalable method for synthesizing ZnO nanowires that are immobilized on the surface of Zn plates using a hot water treatment (HWT) technique. This straightforward synthesis method involves immersing Zn coupons in deionized water at 75 °C without any chemical additives or precursors. SEM, TEM, EDS, XRD, XPS, and UV-Vis spectroscopy analysis on the surface of Zn after 5 hours of HWT showed the formation of well-developed, hexagonally-faceted, stoichiometric, and crystalline ZnO nanowires with a bandgap of 3.26 eV. To evaluate the photocatalytic activity of these ZnO nanowires, we performed methylene blue degradation tests under UV light. 93% of methylene blue was degraded in 120 minutes with a reaction rate constant of 0.021 min<sup>-1</sup>. Overall, our findings demonstrate the potential of HWT as a scalable and environmentally-friendly method for synthesizing ZnO nanostructures with excellent photocatalytic properties.

**NS-TuP-2 Nanopore Arrays Patterned by Thermal Scanning Probe Lithography for Electrochemical Biosensing, Ken Bosnick, J. Canlas, E. Kamali, National Research Council of Canada**

The use of nanopore arrays for electrochemical sensing represents an exciting avenue for improved detection of biomolecules. Through chemically modifying the nanopore arrays, sensitive and selective platforms can be engineered that exploit a transport-modulation-based amplification, whereby one analyte molecule can block multiple electrochemical reporter molecules [1]. This poster will report on the fabrication of such nanopore arrays using thermal scanning probe lithography in ultrathin dielectric layers on electrochemically active conductors (e.g., ALD SiO<sub>2</sub> on ITO).

[1] Róbert E. Gyurcsányi, "Chemically-modified nanopores for sensing", *Trends Analyt. Chem.* 27 (2008) 627-639

**NS-TuP-3 Tunable Gold- and Aluminum-Nanocrescents as a Platform for Circular Dichroism Spectroscopy, Anh Nguyen, University of Utah**

Gold (Au) has been a common material for plasmonic nanostructures studies. Although aluminum (Al) has several advantages over gold and is a promising material for nanoscience studies, the complication of the ubiquitous alumina film in Al nanostructures' fabrication limits its use. With the copper mask nanosphere template lithography fabrication method, our group has successfully fabricated both Au- and Al-nanocrescents (NCs) despite the challenges that arise from the native oxide layer of Al. Both Au- and AlNCs exhibit multimodal, polarization-dependent plasmons that can be tuned in different spectral regions. However, AuNCs' plasmon resonances are red-shifted compared to AlNCs due to the difference in surface properties. Moreover, chiral plasmonics is recently an area of particular interest in the rich and diverse field of plasmonic nanostructure studies. The fundamental focus of chiral plasmonics is to probe the difference in the nanostructures' ability to absorb left vs. right circularly polarized light. Au- and AlNCs have shown the properties of extrinsic chiral nanostructures, which have CD response when tilted to out-of-plane incident angles with respect to the incident circularly polarized light. At  $\theta = \pm 30^\circ$  out-of-plane incident, the Au- and AlNCs' true CD responses are equal in ellipticity but opposite in handedness. In addition, the Au- and AlNCs exhibit the opposite chiral response when rotated 180° relative to the sample's orientation at  $\theta = \pm 30^\circ$ . There is no handedness response for true CD of both Au- and AlNCs at normal incidence, which confirms the extrinsic chiral optical properties of the system. Conversely, there is negligible handedness response for the birefringence of Au- and Al-NCs at both normal and out-of-plane incident angles. These optical phenomena define that the nanocrescents system is an isotropic orientation averaging where there is little to no change in the original substrate surface forward/backward CD response as well as exhibits true CD behavior. These results have produced novel insight into understanding the chiral optical and resonant plasmonic support in nanostructures and opens further investigation into the use of Au- and Al-nanostructures in sensing and detection.

**NS-TuP-4 Towards Artifact-Free Atomic Force Microscopy Images, Nancy Burnham, Worcester Polytechnic Institute; L. Lyu, Chang'an University, China; L. Poulikakos, Empa, Swiss Federal Laboratories for Materials Science and Technology, Switzerland**

Atomic force microscopy (AFM) is based upon a simple operational principle. However, the presentation and interpretation of AFM images can easily suffer from consequential artifacts that are easily overlooked. Here we discuss results from AFM and its companion variations PF-QNM (peak-force quantitative nano-mechanical mapping) and AFM-IR (AFM combined with infrared spectroscopy) by imaging "bee" structures in asphalt binder (bitumen) as examples. We show how common problems manifest themselves, with the intent that authors can present their results clearly and avoid interpreting artifacts as true physical properties, thereby raising the quality of AFM research.

**NS-TuP-5 Probing Metal Substrate Effects on the Adsorbate Conformations of a Nonplanar Tetrabenzoporphyrin Molecule by Ultra-high Vacuum Tip-Enhanced Raman Spectroscopy, Soumyajit Rajak, N. Jiang, D. Liu, L. Li, University of Illinois - Chicago**

Tetrabenzoporphyrin molecules are one of the most widely studied model biomolecules in organic optoelectronics for modern-age electronic device applications and catalysis. Opto-electronic properties in the nanoscale are controlled by the local nanostructures of a molecular arrangement. The local nanostructures are determined by the real-space molecular conformations. It is really challenging to determine the real-space surface adsorbed conformations of a molecule using ensemble-averaged surface science techniques. The molecular structure and the 2-dimensional crystalline arrangements of the tetrabenzoporphyrins are primarily defined by the symmetry of the porphyrin molecule and the steric and electronic nature of the groups linked at meso-positions and  $\beta$ -positions of the ring. The flexibility of the  $\sigma$ -bonded peripheral groups in the meso-positions can induce dynamic behavior in the porphyrin molecule and may give rise to different binding configurations on different metal substrates or sometimes even on one substrate. Herein we present a combined topographical and chemical analysis of different surface-adsorbed conformations and surface-sensitive arrangements of a symmetric tetrabenzoporphyrin molecule using

<sup>1</sup> AVS Dorothy M. and Earl S. Hoffman Awardee

angstrom-scale resolution scanning tunneling microscopy (STM) and ultra-high vacuum tip-enhanced Raman spectroscopy (UHV-TERS). Low temperature (77K) scanning tunneling microscopic images and localized surface plasmon resonance enhanced Raman signals reveal different adsorbate conformations of single molecule entities and a fundamental view of adsorbate-substrate binding interactions.

**NS-TuP-6 Studies of Chemistry and Materials Approaching the Atomic Scale with Cryogenic Ultrahigh Vacuum Scanning Near-Field Optical Microscopy Methods, Jeremy F Schultz**, National Institute of Standards and Technology (NIST); *L. Li, S. Mahapatra, N. Jiang*, University of Illinois Chicago; *A. Centrone*, National Institute of Standards and Technology (NIST) Optical spectroscopies can be used to probe and characterize the composition as well as the physical and electronic structure of molecules and materials. By confining light-matter interactions into the near-field of a scanning probe microscope (SPM) the diffraction limit of light can be circumvented and the resulting measurements can consider composition and subtle local phenomena down to the nanoscale. In ultrahigh vacuum (UHV) and at cryogenic temperatures the spatial resolution of these methods can be pushed towards the atomic scale.

Scanning tunneling microscopy (STM) and tip-enhanced Raman spectroscopy (TERS) were used to investigate the behavior and chemistry of molecular adsorbates with surfaces. Spectroscopic imaging provides the ability to visualize highly localized phenomena, while vibrational fingerprints can be used to understand their effects on a molecule's or material's structure. This yields insight into adsorbate-substrate interactions crucial to the growth of nanostructures through surface chemistry, as well as the functionalization or modification of 2D materials.

Moving beyond UHV-STM-TERS, ongoing work focuses on the development of a new versatile cryogenic UHV-SPM platform for other measurements of light-matter interactions, specifically STM-induced luminescence (STML) and coupling pulsed infrared light into the tip-sample junction. STML leverages the atomically sharp STM tip as a probe to locally excite light emission and captures spectra that can be used to characterize excitonic behavior and vibronic structure. On the other hand, many relevant quantum phenomena occur in the infrared regime, which remains relatively unexplored with atomic scale near-field microscopy. Together, these capabilities are expected to result in a platform capable of studying properties of materials that would otherwise be inaccessible.

**NS-TuP-7 Novel Air Spacer Technology for Parasitic Bit-Line Capacitance Reduction, Dongmin Han**, Department of Semiconductor and Display Engineering The Graduate School Sungkyunkwan University, Republic of Korea; *B. Choi*, Department of Electrical and Computer Engineering, Sungkyunkwan University, Republic of Korea

In this study, a novel air spacer using plasma nitridation (PN) technique for dynamic random access memory (DRAM) device is investigated to minimize parasitic bit-line capacitance (Cb). The ratio of Cb to cell capacitance (Cs) is increasing due to smaller cell size. Thus, DRAM development faced great difficulties due to the decrease in bit-line sensing margin [1]. The Cb/Cs is a key factor in determining the bit-line sensing margin. In addition, Cs is expected to continue to decrease due to the physical limitations of cell capacitor technology, so technology that can lower Cb has become a key technology [2]. 20nm DRAM developed bit-line air spacer technology and greatly improved Cb [1]. However, Cb still needs additional improvements due to the continued reduction in bit-line spacer dimension. We improved the Si<sub>3</sub>N<sub>4</sub> transition layer by using the plasma nitridation techniques before the deposition of the outer Si<sub>3</sub>N<sub>4</sub> film. The pre-plasma nitriding treatment process forms an inter-diffusion and additional protective layer and improves the surface properties of the deposited film [3]. We used this technology to the air spacer. As shown in figure 1, it was expected to maximize the air layer thickness formed in the subsequent process by reducing the thickness of the transition layer formed during outer Si<sub>3</sub>N<sub>4</sub> deposition. The Cb was measured using the test element group, which can measure air spacer pattern and non-air spacer pattern. the Cb improved by 2%, as shown in figure 2. It is considered that the portion of air thickness is increased through surface transition layer improvement. This is a simple and innovative approach to improve the characteristics of DRAM. This study proposed a new direction to improve the Cb/Cs Characteristic for a sub 20 nm DRAM device.

Reference

[1] Park, J. M., et al. IEEE International Electron Devices Meeting (IEDM) (2015)

[2] Hwang, Yoosang, et al. Solid State Devices and Materials (2012)

[3] Bashir, M. I., et al. Surface and Coatings Technology Vol.327, pg 59-65 (2017)

**NS-TuP-8 Understanding Interaction Forces at Silicon Wafer Interfaces to Optimize Nanoscale Cleaning Processes, D. Miano**, CEST GmbH, Austria; *L. Palla, A. Seltenhammer*, TU Wien, Austria; **Pierluigi Bilotto**, CEST GmbH, Austria; *B. Loidl, S. Garvey*, Lam Research Corp., Austria; *M. Valtiner*, TU Wien, Austria

Miniaturization of electronics at the wafer surface is a possible answer to the growing demand of fast, cheap, and environmentally friendly devices. This strategy arises a question on how nanometer size particles, which could impact the yield of nanoscale electronics, could be removed from the wafer surface. The current state-of-the-art in wafer cleaning processes is based on subsequent streams of solvents (e.g., mega-sonic cavitation[1]) on rotating disks,[2] but such protocols can alter the surface to a level which is significant for nanoscale electronics, and do not affect nanoscale level particles. More than ten years ago, it was discussed that surface nanobubbles can remove nano particles,[3] but the understanding is still limited to a qualitative description of the phenomenon. In this project, we aim to shed light on the interaction between surface nanobubbles and nanoparticles, in order to finally clarify the physical-chemical interaction at the interface which can lead to a nanoscale-cleaning-process.

In this poster, I will show our innovative design of a microfluidic system applied to an atomic force microscope. We utilize thiol functionalization to define model systems and mimic the different interaction forces, explaining according to the DLVO theory, and that might take place onto a wafer surface during its industrial cleaning process.

In parallel we also cover with different size nanoparticles our surfaces, that should reproduce the possible impurity of a real Si surface, we study if it is possible to use the solvent exchange for remove these objects and we try to understand how to implement the cleaning process protocol. I will display our results and comments on what are the possible key elements participating in the nanoscale-cleaning-process.

The finding of this work are not only relevant from a fundamental point of view, but have a clear industrial application which is why we collaborate with top industrial partners in the field of semiconductor and wafer cleaning.

References:[1] Ahmed A. Busnaina et al 1995 J. Electrochem. Soc. 142 2812[2] D. Prieling, H. Steiner, International Journal of Heat and Mass Transfer 65, 10-22, 2013[3] Shangjiong Yang and Anton Duisterwinkel; Langmuir 2011, 27, 11430-1

**NS-TuP-9 The Design of Thermal Cloak Using Nanoporous Thin Films, Yue Xiao**, Advanced Cooling Technologies, Inc.; *Q. Chen, Q. Hao*, University of Arizona

In recent years, nanoporous thin films are widely studied as an effective way to manipulate the thermal transport within thin-film-based devices. In practice, nanoporous patterns can effectively cut off the heat flow and thus guide the thermal transport along the desired direction. However, a better design of these thermal devices is not addressed, such as thermal cloaking as the thermal counterpart for optical invisibility cloaks. In existing designs based on the Fourier's law, composite materials with varied structures are often introduced to achieve the required location-dependent thermal conductivities to distort the heat flux. At the micro-to nano-scale, such designs are difficult to be implemented and factors such as the interfacial thermal resistance must be further considered. In this work, inverse thermal designs of a nanoporous material are used to achieve the thermal cloaking effect for 2D materials or 3D thin films, without introducing any other variation of the composition or material to tune the local thermal conductivity. This simple approach can be widely used for thin-film-based devices to protect heat-sensitive regions or function as thermal camouflaging devices. The proposed nanoporous structures can also be used to tune the local properties of a thin film for general applications, such as graded thermoelectric materials.

**NS-TuP-11 Control and Manipulation of Superconducting Vortex Lattices from Nano to Mesoscales**, S. Song, J. Yan, Oak Ridge National Laboratory; W. Ko, University of Tennessee Knoxville; E. Dumitrescu, G. Halasz, Oak Ridge National Laboratory; H. Fangohr, Max Planck Institute for Structure and Dynamics of Matter, Germany; C. Ha, B. Lawrie, **Petro Maksymovych**, Oak Ridge National Laboratory

When a magnetic field larger than a lower critical field is applied to a type-II superconductor, magnetic fluxes will pass through the volume of the superconducting material, creating a vortex state. Vortices exhibit a rich structural diagram, with the possibility of vortex liquid, glass, and lattice states determined by the material properties and external parameters. On a fundamental level, single and few vortex manipulation opens a pathway to understand vortex properties and to tailor their dynamics to prospective applications in quantum computing.

We will discuss two experiments using scanning tunneling microscopy (STM) which demonstrate direct control over vortex positions in FeSe superconductor. First, we observed that the twin boundary in the FeSe superconductor traps a relatively high density of vortices and acts as a barrier that aligns the vortices on the terrace parallel to the twin boundary. The alignment effect causes various phases of vortex lattice structures such as rectangular and one-dimensional vortex lattices – both with ordering qualitatively different from the commonly observed vortex glass. The analysis of these interactions also reveals further clues regarding vortex dynamics, inter vortex interaction, and vortex pinning, and directly points to strain fields as possible effective approach for accurate control over vortex structures. Second, we found that the vortex shape can be controllably varied with the imaging conditions in STM, particularly at the extreme limit of very large local current density. We attribute the observations as direct evidence of vortex manipulation, by contrasting the behaviors of various types of vortices in proximity to twin boundaries on FeSe. Altogether we suggest that precise control over the high tunneling current, combined with specific structural topological defects, can translate into an effective strategy for vortex manipulation approach without destruction of the superconducting state, enabling STM to become a quantitative nanoscale probe of vortex dynamics and a platform to explore vortex manipulation in the context of topological quantum computing.

Work supported by the U.S. Department of Energy, Office of Science, Materials Sciences and Engineering Division. Experiments were carried out as part of the user project at the Center for Nanophase Materials Sciences, Oak Ridge National Laboratory, which is a US Department of Energy Office of Science User Facility.

S. Y. Song, C. Hua, L. Bell, W. Ko, H. Fangohr, J. Yan, G. B. Halász, E. F. Dumitrescu, B. J. Lawrie, P. Maksymovych, *Nano Lett.* 23(2023)2822.

**NS-TuP-12 Exploring the Complex Chemistry and Degradation of Ascorbic Acid in Aqueous Nanoparticle Synthesis**, **Debashree Roy**, L. Moreau, Washington State University

While ascorbic acid (AA) has been the ubiquitous choice as a mild reductant in the aqueous synthesis of noble metal nanoparticles (NPs), its role beyond the reducing powers has been mostly overlooked. Despite the fact that reduction kinetics of metal salt precursors are most susceptible to modifications by reducing agents, it has frequently been relegated to concentration and pH variations for AA, without delving into the more complex chemistry associated with the latter. The mechanism behind AA-mediated reduction is often stymied by an oversimplified presentation in literature wherein the diprotic acid is assumed to undergo consecutive oxidations via a radical intermediate to form dehydroascorbic acid (DHA). In reality, these assumptions may not accurately describe the aqueous behaviour of AA in a wide array of synthetically relevant conditions.

We show that facile degradation of ascorbic acid has considerable impacts on the formation and properties of aqueous silver NPs and discuss implications for the use of ascorbic acid in NP synthesis. Briefly, experimental evidence shows that the alkaline degradation of AA at no point converges to yield DHA, which follows an independent degradation pathway altogether. While DHA at different stages of degradation consistently results in the formation of spherical/quasi-spherical Ag NPs, it is interesting to note that AA aged for > 12h gives rise to anisotropic plate-like morphology, furthering the hypothesis that a different degradation pathway is followed for both. The role of various plausible degradation products has been additionally studied to inform AA's assumed behaviour in NP synthesis. These findings have profound implications for the understanding of AA in NP systems, and the mechanisms behind its role as a reductant and surfactant.

**NS-TuP-13 Exploiting Mixed-Dimensionality in Hybrid Van Der Waals Heterostructures**, **Emanuele Orgiu**, Institut National de la Recherche Scientifique / University of Quebec, Canada

2D Quantum Materials are held together by weak interplanar van der Waals (vdW) interactions. The incorporation of molecules in such materials holds an immense potential to understand and modify the fundamental physical properties of the pristine materials while creating new artificial materials. Whilst nature offers a finite number of 2D materials, an almost unlimited variety of molecules can be designed and synthesized with predictable functionalities. The possibilities offered by systems in which continuous molecular layers are interfaced with inorganic 2D materials to form hybrid organic/inorganic van der Waals heterostructures (H-vdWH) are emphasized. Similar to their inorganic counterpart, the hybrid structures have been exploited to suggest novel device architectures. Moreover, specific molecular groups can be employed to modify intrinsic properties and confer new capabilities to 2D materials. In particular, I will highlight how molecular self-assembly at the surface of 2D materials can be mastered to achieve precise control over position and density of (molecular) functional groups, paving the way for a new class of hybrid functional materials.

In particular, I will show how the presence of ordered supramolecular assemblies bearing different functional groups can modify the pristine Shubnikov-De Haas oscillations [1] occurring in graphene or tune the magnetoresistance in a given transition metal dichalcogenide [2].

[1] A. Pezeshki, A. Hamdi, Z. Yang *et al.*, *ACS Appl. Mat. Interf.* 13, 26152 (2021).

[2] A. Hamdi, A. Pezeshki, .. E. Orgiu, *Manuscript in preparation.*

**NS-TuP-14 Circuit-Level Device Modeling for Framework Analyzing Hot Carrier Injection Failure in Gate-All-Around (GAA) Charge Trapping Flash (CTF) Memory Devices Based on New Experimental Methodology**, **Sunghwan Cho**, Samsung Electronics Co., Inc., Republic of Korea

To overcome the limitation of conventional planar flash memory in scaling down, gate-all-around (GAA) charge trapping flash (CTF) memory gradually become the most promising alternative due to remarkably larger storage and less disturbance. However, as stacking more layers vertically and getting smaller in feature size, it is inevitable that device failures attributed to interference or leakage such as band-to-band tunneling (BTBT) and hot carrier injection (HCI) increase rapidly. Furthermore, a suitable framework to analyze failure mechanisms and optimize design by using circuit simulation is insufficient. In this paper, we proposed circuit-level device modeling as a framework focused on HCI failure analysis in GAA CTF, which is achieved by establishing new method in measuring HCI effect and optimizing model parameters by derived formula. As shown in Fig. 1, threshold voltages in non-programmed memory cell can be increased unexpectedly by HCI effect, which results in critical failure and degradation of performance. In conventional junction-less GAA CTF memory devices, electrons generated by BTBT in a large gap in boosted channel potential and high electric field in vertical direction contribute to HCI effect. As a result, circuit-level modeling for accurate calculation of boosted channel potential and determination of gate voltages in a cell string is essential in analyzing HCI effect. Fig. 2(a) and (b) illustrate single modeling structure and equivalent circuit attaching voltage-controlled-current sources which execute essential current flow in GAA CTF such as Fowler-Nordheim (FN) tunneling, BTBT and HCI leakage by using derived formula in our work. By connecting single modeling units serially as shown in Fig. 2(c), circuit-level modeling structure with a cell string unit is proposed which makes prediction of boosted channel potential and BTBT/HCI current more accurate. Fig. 3 presents mechanisms of HCI in the proposed experimental method. Since the amount of HCI leakage is determined by 2 dominant conditions which are potential difference in lateral direction generating BTBT and electric field in vertical direction, we separated 2 measurement conditions, as shown in Fig. 3(a) and (b), to extract model parameters compactly by breaking down 2 terms. Furthermore, since HCI failure commonly occurs at the end of channel, we enhanced experimental progress by measuring near gate select line (GSL) transistor, as shown in Fig. 3(c). Finally, the fitting results show good agreement with experimental data, as shown in Fig. 4, which means the proposed model would equip

# Tuesday Evening, November 7, 2023

circuit designer of GAA CTF by analyzing failure mechanism and optimizing the performance.

**NS-TuP-15 Statistic Analysis of Nanoscale Tunneling Electrical Contacts Based on Transmission Line Model, *Bingqing Wang, P. Zhang***, Michigan State University

The rising interest in innovative electronic circuits utilizing low-dimensional materials, like carbon nanotubes (CNTs), has made nanoscale contact engineering increasingly important. This study investigates the influence of contact resistances between carbon nanotubes (CNTs) on electron transport and electrical conductivity of carbon nanofibers (CNFs), which profoundly impacts the performance of CNT thin film field effect transistors (FETs)[1]. Utilizing a self-consistent contact model, we integrate a transmission line model with tunneling current model [2] to calculate the plethora of parallel CNT-CNT contacts within individual fibers. A statistical analysis is conducted, using Gaussian distributions to account for variations in contact lengths, gap distances, and single CNT aspect ratios, and producing data on CNT-CNT contact resistance and the overall resistance of CNT fiber. By scaling our model to a macroscopic level, our results are in significant alignment with experimental measurements [3]. Our calculation suggests that while increasing overlap length diminishes individual CNT-CNT contact resistance, it paradoxically increases macroscopic CNT fiber resistance, given a constant CNF mass density. Similarly, greater gap distance also increases both individual and fiber resistance. This research provides a tool for exploring CNT fiber electrical properties, promoting advancement in low-dimensional material-based electronic circuit development. Future work could leverage machine learning for establishing the correlations between different parameters and identify the optimal parameter values that most accurately represent the experimental results.

1. S. B. Fairchild, et al., Morphology dependent field emission of acid-spun carbon nanotube fibers, *Nanotechnology* 26, 105706 (2015).

2. Banerjee, S., Luginsland, J. & Zhang, P. A Two Dimensional Tunneling Resistance Transmission Line Model for Nanoscale Parallel Electrical Contacts. *Sci Rep* 9, 14484 (2019)

3. D. Tsentelovich, et al, Influence of Carbon Nanotube Characteristics on Macroscopic Fiber Properties, *ACS Appl. Mater. Interfaces*, 9, 36189 (2017)

\* Work is supported by the Air Force Office of Scientific Research (AFOSR) Award No. FA9550-22-1-0523.

**NS-TuP-16 Instrumentation of Ptychographic Microscopy at the Atomic Scale, *Chien-Nan Hsiao, F. Chen***, Taiwan Instrument Research Institute, National Applied Research Laboratories, Taiwan; *T. Chung*, Department of Materials Science and Engineering, National Yang Ming Chiao Tung University, Taiwan; *C. Chen*, Department of Engineering and System Science, National Tsing Hua University, Taiwan

Ptychographic electron microscopy at atomic-scale resolution had been established. A hybrid pixelated detector and remote controlled electron beam scanning coil were integrated on an aberration corrected scanning transmittance electron microscopy with a circular C2 aperture of 10  $\mu\text{m}$ . Experimental results shown that the 128 $\times$ 128 steps of electron probe interval (1  $\text{\AA}$ ) in real space with the size of each diffraction pattern is 512 $\times$ 512 pixels in high dynamical range. The 4D cube data of sampling areas were stable acquired at 200 kV with high diffraction space resolution. In addition, phase retrieval algorithms were developed to improve the point resolution of coherent diffraction imaging. Moreover, the lattice strain mapping was simultaneously interpreted with the high angle annual dark field image in nanostructural characterization by analysis the convergent beam electron diffraction patterns.

**NS-TuP-17 Influence of Defects on Oxidation of Rhodium, *Allison Kerr, M. Gillum, D. Killelea***, Loyola University Chicago

Due to the importance of oxide surfaces in heterogeneously catalyzed oxidation reactions, it is necessary to gain a fundamental understanding and behavior of oxygen on transition metal surfaces. Additionally, the atomic arrangement of the metal surface plays an important role in the behavior of the oxygen on the surface, which provides a need to study high defect density surfaces that are more akin to industrial catalysts. The research presented herein utilizes a curved rhodium crystal c-Rh(111) with two different well-defined defects on either side to conduct a systematic

study of the influence of defect geometry on the kinetics and dynamics of different oxygen species present on the surface. Scanning tunneling microscopy (STM), low energy electron diffraction (LEED), temperature programmed desorption (TPD), and Meitner-Auger electron spectroscopy (MAES) will be used to look at the surface on an atomic scale and to observe what chemical species are on the surface after introducing oxygen into the vacuum environment.

**Plasma Science and Technology Division  
Room Oregon Ballroom 203-204 - Session PS-TuP**

**Plasma Science and Technology Poster Session**

**PS-TuP-1 Sidewall Polymer Removal Challenges by Wet-Etching and the Proposal of High-Density Radical Flux (HDRF™) as a Dry-Etch Solution, *Sabrina Rosa Ortiz, J. Tressler, D. Meisner***, Plasma-Therm LLC

Addressing challenges in semiconductor industry often faced by advanced packaging, sensors, and MEMS by promoting cost-effective solutions has been the ultimate challenge throughout the years. This study explores the use of Plasma Dicing technologies such as plasma singulator systems (MDS-100 & MDS-300 SINGULATOR®) to facilitate and promote an increase in die count per wafer establishing a higher production volume with performance. Plasma dicing offers several advantages, including an improved die surface area per wafer promoting an increase in yield per wafer to be processed. The ability to navigate the incorporation of smooth sidewalls, and achievement of street sizes  $\leq 10\mu\text{m}$  promotes new advantages in the semiconductor industry. Plasma dicing not only removes material in dicing streets by Bosch process implementation but also prevents any physical impact on each die while performed using polymer deposition to facilitate the protection of sidewalls during etching. To enable several applications in the semiconductor industry, including increased device performance, absorption, and electrical conductivity throughout devices, polymer removal and post-etch cleaning are required which has been mainly performed by wet-etching procedures. Wet clean polymer removal has been tested for our standard Plasma-Therm wafer by using both 3M™ Novec™ 7100 Engineered Fluid and EKC265™ separately and analyzed using Energy Dispersive X-Ray Spectroscopy (EDX) to investigate the removal of residues of Carbon and Fluoropolymer. Although successful removal of polymer from the sidewalls was achieved, the amount of liquid required may increase the cost but also the residual waste, preventing proper process control, causing direct damage to the samples due to chemical nature, and handling issues. To address these limitations, we propose the introduction and implementation of dry plasma cleaning solutions that can perform the removal of polymers and photoresist materials without any device damage. At Plasma-Therm, LLC photoresist can be removed by a dry-etching step performed after completion of the Bosch process in a singulator system but also it can be accomplished by using a High-Density Radical Flux (HDRF™) process tool, which not only enables polymer removal but also is designed to perform photoresist strip allowing smoothing of sidewalls for several applications without causing device damage. This tool not only allows us to move from wet-etching by eliminating contamination of samples by particles or residues but also provides a more efficient and effective alternative to wet-etching processes for the removal of polymer and photoresist.

**PS-TuP-2 Mass Spectrometric Study of Ar-Diluted Ammonia Borane Plasma for h-BN 2D Film Formation, *Takeshi Kitajima, T. Nakano***, National Defense Academy, Japan

Ammonia borane is used as a relatively safe source of BN for the rapid synthesis of h-BN, an important insulating material<sup>1</sup> in the field of two-dimensional electronics<sup>2</sup>. Ammonia borane plasma attracts attention when aiming at high-speed film formation, and analysis of active species in the plasma is necessary. In this study, active species generated from ammonia borane powder irradiated with Ar plasma were analyzed by mass spectrometry.

Parallel plate type 100MHz driven capacitively coupled plasma generated in a high vacuum chamber is used. After placing 0.1 g of ammonia borane ( $\text{BH}_3\text{NH}_3$ ) powder on the RF electrode and evacuating, a 10 W glow discharge was formed with an Ar gas flow rate of 30 sccm. A copper sample heated to 800°C was placed downstream, and when BN radicals were supplied at a pressure of 800 Pa, an h-BN atomic film was formed over 30 minutes as shown in the SEM image and Raman spectrum of Fig. 1(a,b). Radical analysis in space was performed with a mass spectrometer at a pressure of 10 Pa. Figure 1(c) shows the difference in the mass spectrum

# Tuesday Evening, November 7, 2023

when the plasma is turned on and off.  $\text{BNH}_5(30)$  is increased by plasma lighting.  $\text{O}_2(32)$  is produced by plasma decomposition of  $\text{H}_2\text{O}(18)$ .

Radicals generated from ammonia borane raw material leading to formation of h-BN atomic film are presumed to be  $\text{BNH}_5$  generated by decomposition of  $\text{BNH}_6$ . Dangling bonds of  $\text{BNH}_5$  are thought to generate chemical reaction activity on the substrate.

- 1 K.H. Lee, et.al. Nano Letters 12, 714 (2012).
- 2 L. Song, et.al. Nano Letters 10, 3209 (2010).

**PS-TuP-3 Plasma Degradation of PTFE Channel in a DBD/Plasma Jet Configuration for Endoscopes Use in Plasma Medicine, Juliette Zveny, T. Serra, A. Remy, A. Nonclercq, J. Deviere, A. Delchambre, F. Reniers, Université Libre de Bruxelles, Belgium**

As plasma medicine is more and more developed and studied for treatment of pathologies such as skin cancer (Terefinkoet al. 2021) or tumorous intestinal cells (Hadeffi et al. 2022, Bastin et al. 2020) as well as for decontamination (Deng et al. 2007), the question of the effect of plasma on medical devices rises.

In this work, we are interested in endoscopes and the way plasma could damage them. Indeed, endoscopes working channels could be used to carry plasma inside a body to a desired target, but the effect of the plasma on the endoscope itself must be investigated. As the surfaces of the channels of endoscopes are coated with PTFE, mainly for its lubricating properties, we studied the plasma-induced degradation of a PTFE tube in a setup that mimics the characteristics of an endoscope device already described in previous work (Bastin et al. 2019). XPS was used to study the chemical and roughness modifications of the PTFE surface and FTIR was used to study the species ejected to the gas phase.

Given the preliminary nature of current exploratory studies in this field, we employed diverse parameters for our investigation. Different plasma compositions were used: He, He- $\text{O}_2(3\%\text{O}_2)$ , He- $\text{H}_2\text{O}$ , Ar, Ar- $\text{O}_2(3\%\text{O}_2)$ , Ar- $\text{H}_2\text{O}$ , and air with flow rates of 1,5 L/min. The AC electrical power varied from 10 W to 70 W.

Depending on the plasma treatment applied, variable amounts of gaseous fluorinated compounds like  $\text{COF}_2$  and HF have been detected. They result from the degradation of the PTFE polymeric chains by energetic species created in the plasma. In a pure helium plasma, these species are mainly metastable helium and high energy electrons, capable of breaking C-C and C-F bonds, hence creating carbon and fluorine radicals on the surface. Those radicals will then react with surrounding gas species.

The addition of oxygen containing molecules in the gas mixture ( $\text{H}_2\text{O}$ ,  $\text{O}_2$ ) creates higher amount of  $\text{COF}_2$  than without. The amounts observed of those three species is a direct measurement of the ability of the discharge to degrade the PTFE. The  $\text{COF}_2$  is believed to originate directly from the PTFE degradation by atomic oxygen ( $\text{O}^*$ ) (Vandecasteele et al.), whereas the HF should be formed by hydrolysis of  $\text{COF}_2$ . With pure gases (He and Ar) plasma, some water and air impurities could still introduce oxygen atoms, hydroxyl groups and nitrogen containing groups.

We observed a drastic increase of the concentrations of fluorine species with the Ar- $\text{H}_2\text{O}$  plasma compared to the He- $\text{H}_2\text{O}$  plasma.

The XPS analyses show a defluorination of the PTFE surface that depends on the plasma composition and power, and in agreement with the production of  $\text{COF}_2$  and HF detected by gas phase IR.

Acknowledgements:

This work is funded by the ARC project "COSMIC" and by the Michel Cremer foundation

**PS-TuP-4 Effect of Additive Gas on Etch Profile Improvement during Dielectric Etching, Hyun Woo Tak, S. Kim, C. Choi, S. Kim, S. Lee, M. Park, D. Park, D. Kim, ., Yeom, Sungkyunkwan University (SKKU), Republic of Korea**

As the memory device sizes reach scaling limit, the device structures are changing from 2D to 3D device structure. For 3D device structures, it has been known that improving high aspect ratio (HAR) etching process is one of the most important processes in device manufacturing as it determines the density of the devices. To improve the etch properties such as selectivity and etched profiles, various etch techniques have been widely studied including changing process schemes and equipment. But still, changing etch gas is known to be one of the essential solutions in improving plasma etching results. Recently, it has been reported that the etch profiles

of HAR etching can be improved by using  $\text{WF}_6$  as an additive material, but no detailed results and etch mechanism on the effect of metal-halide containing additive gas have not been reported. Therefore, in this study, the effects of metal-halide containing additives including  $\text{WF}_6$  on etching characteristics were investigated. It was found that HAR etch properties can be controlled and improved by using various additive gases containing carbon or fluorine. Therefore, the effect of various additive materials on dielectric etch properties will be reported for next generation HAR etching.

**PS-TuP-5 Etch Characteristics IGZO and Chamber Cleaning using  $\text{C}_x\text{H}_y\text{F}_z$  Gases, Jong Woo Hong, D. Kim, Sungkyunkwan University (SKKU), Republic of Korea; Y. Jeong, H. Cho, D. Jung, Y. Yeo, Samsung, Republic of Korea; G. Yeom, Sungkyunkwan University (SKKU), Republic of Korea**

Indium gallium zinc oxide (IGZO) is used in next-generation semiconductors and displays and requires anisotropic etch profile, fast etch rate, and high mask selectivity. In particular, as IGZO is used for gates in semiconductors and displays, the CD (critical dimension) is getting smaller and smaller, so highly anisotropic etching is crucial. Additionally, it is important to completely clean the etch residue in the chamber after IGZO is etched. In this study, IGZO was etched, and chamber cleaning was performed using various HFC-type gases ( $\text{C}_x\text{H}_y\text{F}_z$ ) in an ICP etcher. The results showed that mixing H and F-based gases was more effective in increasing the etch rate and etch selectivity of IGZO than using them alone. In fact, it is difficult to etch IGZO because zinc is easily etched by halogen gases, but it is found that the gases combined with C, H, and F make it easier to etch zinc.  $\text{C}_3\text{H}_x\text{F}_y$  ( $x+y=8$ ) gas was found to be better than  $\text{CH}_x\text{F}_y$  ( $x+y=4$ ) gas, as it lowers the binding energy. In addition, by using a  $\text{H}_2/\text{Ar}$  plasma, the etch by-products formed on the chamber sidewall by the etching using HFC-type gases ( $\text{C}_x\text{H}_y\text{F}_z$ ) could be effectively removed.

**PS-TuP-6 Molecular Dynamics Simulation of Vapor-Phase Nucleation of Metal Nanoparticles in a Reactive Plasma Atmosphere, Louis Hoffenberg, D. Graves, Princeton University; I. Kaganovich, Princeton Plasma Physics Laboratory**

Metallic nanoparticles (NPs) offer a wide range of applications in electronics, energy, biology, catalysis, and the production of carbon nanomaterials like carbon nanotubes (CNTs). Synthesis of NPs from the vapor phase using plasma methods such as spark discharge generation is promising for industrial scalability. The behavior of nucleating systems in reactive environments, especially reactive plasma environments, is understudied. Moreover, charge-induced dipole interactions between ions and neutrals are thought to play a key role in the nucleation, coalescence, and aggregation of NPs in dusty plasmas [1]. Because the lengthscales and timescales associated with vapor-phase NP formation are too small to effectively probe experimentally, a promising alternative is molecular dynamics (MD) simulation. MD can give strong insight into the nanoparticle formation process with its atomic resolution. In this work, we use MD simulations with a reactive forcefield to study iron vapor nucleation in the presence of ions, radicals, and molecular species relevant to the production of CNTs (i.e., H,  $\text{H}_2$ , C, CH,  $\text{CH}_2$ ,  $\text{CH}_3$ ,  $\text{CH}_4$ ,  $\text{C}_2$ ,  $\text{C}_2\text{H}$ ,  $\text{C}_2\text{H}_2$ , and ions). The effects of atomic-scale phenomena on metal vapor nucleation and nanoparticle behavior in a plasma environment will be discussed.

[1] Girshick, Steven L. "Particle nucleation and growth in dusty plasmas: On the importance of charged-neutral interactions." *Journal of Vacuum Science & Technology A: Vacuum, Surfaces, and Films* 38.1 (2020): 011001.

**PS-TuP-7 Elementary Surface Reactions During F- and CF- Based Plasma Cryoetching of Si and  $\text{SiO}_2$ : A Molecular Dynamics Study, Jonathan Romero Cedillo, G. Cunge, E. Despiou-Pujo, Univ. Grenoble Alpes, CNRS, LTM, France**

Introduced in the early 90s to achieve silicon deep etching, plasma cryoetching consists of using highly reactive plasmas, such as  $\text{SF}_6$ , to etch materials cooled down to temperatures below  $-100^\circ\text{C}$  with a high anisotropy. The addition of low amounts of oxygen allows to form a temperature sensitive  $\text{SiO}_x\text{F}_y$  passivation layer on the sidewalls of the trench, which prevents spontaneous lateral etching and fully desorbs when the substrate is brought back to room temperature. Cryogenic processes have the advantage to be polymer-free and clean (no deposition at the reactor walls since passivation layers only form on cooled surfaces), which avoids process drift and makes them suitable to new applications where smooth sidewalls or reduced plasma-induced damage (PID) are required. These characteristics are attractive for porous low-K materials etching in the back-end-of-line (BEOL) of advanced CMOS technology; applications to atomic layer etching (ALE) of conventional materials (Si, Ge, GaN, InP) or emerging 2D materials (graphene,  $\text{MoS}_2$ ) are also envisaged. Even though the understanding and control of plasma cryoetching have been improved

over the years, the fundamental mechanisms of the formation and desorption of the SiO<sub>2</sub>F<sub>x</sub> passivation layer are not well understood. And little is known about the differences between elementary plasma-surface interactions at cryogenic and room temperature processes. In this paper, Molecular Dynamics (MD) simulations are performed to study the interaction between F- and CF- based plasmas with Si and SiO<sub>2</sub> materials. The objective is to study the impact of given plasma parameters (nature, dose, energy of plasma species) on the modification of exposed materials, both at room and cryogenic temperatures. Quantitative information on surface reaction probabilities (sticking, thermal desorption, surface diffusion, sputtering yields) will be compared and discussed, to better understand the key mechanisms behind cryoetching and cryo-ALE processes.

**PS-TuP-9 Synthesis and Characterization of Antiviral (Doped)-TiO<sub>2</sub> Coatings by an Atmospheric Pressure Dielectric Barrier Discharge**, A. Chauvin, Université libre de Bruxelles/University of Mons, Belgium; M. Galais, L. Sauvage, C. Van Lint, A. Op De Beeck, Université libre de Bruxelles, Belgium; R. Snyders, University of Mons, Belgium; **Francois Reniers**, Université libre de Bruxelles, Belgium

The recent COVID pandemic raised the necessity to develop strategies to limit the contamination of human populations by viruses. Amongst the routes explored, the development of antiviral and antimicrobial surfaces is an elegant approach as it could represent a long term, passive (no need of chemicals or human action) and sustainable solutions. Although the antimicrobial action of copper surfaces is well known and documented (even in history books), it represents an expensive solution, and the potential toxicity of copper ions for cells can not be neglected. Titanium oxide, in its anatase phase, is known to possess strong oxidative properties, and is used as coating for “self cleaning” or “easy to clean” surfaces. It possesses strong antimicrobial properties. However, the main drawback is that anatase is only active when irradiated with UV light, which prevents the use of such surfaces in interiors. To circumvent this, nitrogen doped TiO<sub>2</sub> coatings were developed using an atmospheric pressure dielectric barrier discharge, and exposed to a variety of coronaviruses, including the SarsCOV2.

Coatings were deposited by PACVD from TTIP in an Ar/O<sub>2</sub>/NH<sub>3</sub> discharge (variable O<sub>2</sub> and NH<sub>3</sub> concentrations) at various substrate temperatures [1], using a new type of heating device [2,3]. They were characterized by XPS, Tauc plot (for the bandgap), and by SEM. Selected coatings were then put in contact with solutions containing coronaviruses and exposed to white light. Negative and positive controls were realized on fully inactive surfaces (plastic), or fully active surfaces (copper), respectively. It is shown that some surfaces exhibit an antiviral activity.

References :

- [1] A. Chauvin et al, Surf.Coat.Technol, submitted
- [2] A. Remy et al, Thin Solid Films (2019), 137437
- [3] A. Remy, F. Reniers, EP3768048A1

Acknowledgements :

This work is funded by the special research program of the FNRS-Belgium “PER-Virusurf”, and by the ULB special COVID fund

**PS-TuP-11 Stability Criteria for Radiofrequency Plasmas at Low Pressure\***, **Omar Alsaed**, A. Lietz, North Carolina State University; B. Yee, C. Qu, M. Mamunuru, B. Scheiner, Lam Research Corporation

Uniformity is critical in the plasma processing of semiconductors, and instabilities can give rise to destructive arcing, striations, and plasmoids that can permanently damage equipment or lead to scrapped wafers. The formation of self-organized striations in the direction parallel to the radiofrequency current in low-pressure, high-voltage plasmas has been experimentally reported<sup>1</sup>. We use a fluid description, typically called the nonlocal moment model<sup>2</sup>. The description uses the drift-diffusion approximation and importantly includes the thermoelectric electron energy transport coefficient which proves essential in describing the pattern formation mechanism<sup>3</sup> and is shown to be critical for the evolution of plasmoids in planar capacitively coupled plasmas (CCPs)<sup>4</sup>. The operating conditions under which these striations occur are analyzed in a planar inductively and capacitively coupled argon plasma. This analysis will be extended to Ar with CF<sub>4</sub> gas admixtures. The ionization rates and electron transport coefficients are derived from an electron energy distribution function calculated as a function of the reduced electric field using a multi-term Boltzmann equation solver, MultiBolt<sup>5</sup>. A key assumption of the nonlocal moment model is that transport coefficients and collision frequencies in the inhomogeneous 1D model are a function of the average

and bear the same relation as they do in a homogenous 0D Boltzmann equation solution at different values of the reduced electric field<sup>2</sup>. A linear stability analysis is performed to derive a stability criterion on the allowed values of the thermoelectric electron energy transport coefficient as a function of discharge parameters for stable plasma processing. Instability is more likely at higher electron temperatures which leads to the thermoelectric electron energy transport coefficient having positive enough values to destabilize the plasma. The application to practical plasma conditions and system operating parameters, such as pressure and power, is explored to identify process windows.

59. Désangles, V., Jean-Luc R., Alexandre P., Pascal C., and Nicolas P., Phys. Rev. Lett. **123**, 265001 (2019).
60. Ingold, J. H. Phys. Rev. E **56**, 5932 (1997).
61. Mackey, D., L. Plantié, and M.M. Turner. Appl. Math. Lett. **18**, 865 (2005).
62. Bera, Kallol, Shahid Rauf, John Forster, and Ken Collins. J. of Appl. Phys. **129**, 053304 (2021).
63. Stephens, J. J. of Appl. Phys. **51**, 125203 (2018).
64. Flynn, M, A Neuber, and J Stephens. J. of Appl. Phys. **55**, 015201 (2022).

\* Work funded by the Lam Research Foundation.

**PS-TuP-12 Cyclic Isotropic Etching of SiO<sub>2</sub> using NF<sub>3</sub>/H<sub>2</sub> Remote Plasma and Methanol Vapor**, **Ji Yeon Lee**, H. Gill, D. Kim, Y. Jang, H. Kwon, G. Kim, D. Kim, G. Yeom, Sungkyunkwan University (SKKU), Republic of Korea

The wet etching which has been mainly used for the isotropic etching presents challenges in nano-patterns due to the inability to etch the bottom of the pattern or pattern leaning by surface tension. Therefore, the development of a dry etching process for next-generation semiconductor devices is necessary. Currently, the most widely used isotropic dry etching processes of SiO<sub>2</sub> are the HF/NH<sub>3</sub> vapor process and the NF<sub>3</sub>/NH<sub>3</sub> plasma process. The conversion of SiO<sub>2</sub> to an ammonium salt such as (NH<sub>4</sub>)<sub>2</sub>SiF<sub>6</sub> occurs in these processes, and the desorption of the reacted compounds is achieved through a heating process. However, the formation of ammonium salts during NH<sub>3</sub>-based processes can produce solid powders that may contaminate the substrate and become particle sources in the chamber. Therefore, in this study, gas combinations without NH<sub>3</sub> were used for the cyclic dry etching of SiO<sub>2</sub> over Si<sub>3</sub>N<sub>4</sub>. HF was formed using an NF<sub>3</sub>/H<sub>2</sub> remote plasma, and methanol vapors were injected outside the plasma discharge region to eliminate F radicals produced by NF<sub>3</sub> dissociation and induce spontaneous etching of Si-based materials. Under the optimized conditions, the etching depth per cycle of SiO<sub>2</sub> was about ~13 nm/cycle, and the selectivity with Si<sub>3</sub>N<sub>4</sub> was over 50 and the selectivity with Si was over 20. Surface composition and bonding state were analyzed to confirm surface damage and to investigate the etching mechanism.

**PS-TuP-13 Etching Characteristics of SiON Films Using C<sub>2</sub>F<sub>4</sub>O/C<sub>2</sub>H<sub>2</sub>F<sub>2</sub> with a Low Global Warming Potential**, **Seul Ki Kim**, H. Tak, S. Kim, C. Choi, D. Kim, G. Yeom, Sungkyunkwan University (SKKU), Republic of Korea

In the semiconductor industry, perfluorocarbon and hydrofluorocarbon gases are widely used as etching gases. However, some currently commercialized gases have a negative impact on the global environment due to their high GWP (global warming potential) values. Therefore, it is essential to replace those with gases with a low GWP and similar characteristics. In this study, evaluation was conducted to replace existing perfluorocarbon and hydrofluorocarbon gases with high GWP, such as CF<sub>4</sub> and CHF<sub>3</sub>, with C<sub>2</sub>F<sub>4</sub>O and C<sub>2</sub>H<sub>2</sub>F<sub>2</sub>, which have a relatively high boiling point for easy recovery in a liquid state at room temperature and a low GWP, respectively. In the experiment, SiON (silicon oxynitride) film was etched using C<sub>2</sub>F<sub>4</sub>O/C<sub>2</sub>H<sub>2</sub>F<sub>2</sub> plasmas in a CCP (capacitively coupled plasma) equipment and the etch rates of PR (photoresist) and SiON films, and PR/SiON selectivity were measured. The etch profiles were observed by SEM (scanning electron microscopy) and XPS (X-ray photoelectron spectroscopy) was used to analyze the surface characteristics of the sample after etching. The results showed that the plasma etching characteristics with mixed gases of C<sub>2</sub>F<sub>4</sub>O/C<sub>2</sub>H<sub>2</sub>F<sub>2</sub> showed a higher PR/SiON selectivity and anisotropic SiON etching profile compared to those with conventional mixed gases of CF<sub>4</sub>/CHF<sub>3</sub>. Therefore, selective and anisotropic etching of SiON film masked with PR could be achieved with low global warming gas combination of C<sub>2</sub>F<sub>4</sub>O/C<sub>2</sub>H<sub>2</sub>F<sub>2</sub>. Details of experiments and analysis data will be reported in the presentation.

**PS-TuP-14 Isotropic Dry Etching of SiO<sub>2</sub> using NF<sub>3</sub>/H<sub>2</sub> Pulsed Remote Plasma and NH<sub>3</sub> Gas Injection, DaeWhan Kim, H. Gil, H. Kwon, D. Kim, Y. Jang, G. Kim, D. Kim, G. Yeom, Sungkyunkwan University (SKKU), Republic of Korea**

These days, for the isotropic etching of nanoscale device fabrication, due to the problems such as pattern collapse to surface tension, difficulty in controlling etch depth, nonuniform etching, etc., dry isotropic etching technology that can replace wet etching is actively investigated. For high selectivity SiO<sub>2</sub> isotropic dry etching, NF<sub>3</sub>/NH<sub>3</sub> remote plasma is generally used to react with SiO<sub>2</sub> to form (NH<sub>4</sub>)<sub>2</sub>SiF<sub>6</sub> which is sublimated and removed through a heating process of 100°C or higher. However, the process forming (NH<sub>4</sub>)<sub>2</sub>SiF<sub>6</sub> on the surface of a wafer by NF<sub>3</sub>/NH<sub>3</sub> remote plasma has the disadvantage of lowering selectivity of SiO<sub>2</sub> over Si or Si<sub>3</sub>N<sub>4</sub> because Si and Si<sub>3</sub>N<sub>4</sub> are etched by F radicals transported to the wafer from the remote plasma source. In this study, the F radicals transporting to the wafer surface was controlled by inducing to form HF by discharging NF<sub>3</sub>/H<sub>2</sub> in a pulsed remote plasma. (NH<sub>4</sub>)<sub>2</sub>SiF<sub>6</sub> was formed on the surface of SiO<sub>2</sub> by supplying NH<sub>3</sub> to the outside of the plasma discharge region, and then (NH<sub>4</sub>)<sub>2</sub>SiF<sub>6</sub> was removed through heat treatment. Through this method, SiO<sub>2</sub> could be selectively etched at a higher etching rate than Si and Si<sub>3</sub>N<sub>4</sub>. Etching mechanism by the pulsed remote plasma source was identified through plasma analysis and surface analysis, and possible surface damage during the etching process was also analyzed.

**PS-TuP-15 Etched Characteristics of Nanoscale TiO<sub>2</sub> Using C<sub>4</sub>F<sub>8</sub>-Based and BCl<sub>3</sub>-Based Gases, Nam Il Cho, J. Hong, H. Kim, D. Ji, D. Kim, G. Yeom, Sungkyunkwan University (SKKU), Republic of Korea**

TiO<sub>2</sub> is a material used in various fields such as electronics, optics, environment, etc. For the application to electronic and optical devices, TiO<sub>2</sub> needs to be patterned using reactive ion etching using halogen-based gases. In this study, a TiO<sub>2</sub> masked with ACL pillar pattern was etched using two types of gases such as C<sub>4</sub>F<sub>8</sub>-based (C<sub>4</sub>F<sub>8</sub>/SF<sub>6</sub>/Ar) and BCl<sub>3</sub>-based (BCl<sub>3</sub>/CF<sub>4</sub>/Ar), and the effect of etch gas and asynchronous pulsing (separated source power ON time and bias power ON time in a pulse period) on the etch properties such as etch rates, etch selectivity, and aspect ratio dependent etching (ARDE) were investigated. The use of asynchronous pulsing with decreased bias pulsing ratio (high source power ON time and low bias ON time in a pulse period) improved the etch selectivity and ARDE possibly due to the more similar etch environment among different aspect ratio TiO<sub>2</sub> features. The use of BCl<sub>3</sub>-based plasma showed higher etch selectivity over ACL compared to C<sub>4</sub>F<sub>8</sub>-based plasma, however, it showed the lower etch rate and more severe ARDE due to the higher stickiness of Cl compared to F to the sidewall during the etching of high aspect ratio TiO<sub>2</sub>.

**PS-TuP-16 Study on Atomic Layer Etching of Molybdenum by Formation of MoCl<sub>x</sub>/MoO<sub>x</sub>Cl<sub>y</sub>, Do Seong Pyun, J. Lee, D. Kim, Y. Jang, D. Kim, H. Kwon, H. Gil, G. Kim, J. Kim, G. Yeom, Sungkyunkwan University (SKKU), Republic of Korea**

Do Seong Pyun<sup>1</sup>, Ji Yeon Lee<sup>1</sup>, Dae Whan Kim<sup>1</sup>, Yun Jong Jang<sup>2</sup>, Doo San Kim<sup>2</sup>, Hae In Kwon<sup>2</sup>, Hong Seong Gil<sup>2</sup>, Gyoung Chan Kim<sup>2</sup>, Ju Young Kim<sup>2</sup> and Geun Young Yeom<sup>2,3</sup>

<sup>1</sup>Department of Semiconductor Display Engineering, Sungkyunkwan University, Suwon 16419, Korea

<sup>2</sup>School of Advanced Materials Science and Engineering, Sungkyunkwan University, Suwon, Gyeonggi-do 16419, Republic of Korea.

<sup>3</sup>SKKU Advanced Institute of Nano Technology (SAINT), Sungkyunkwan University, Suwon, Gyeonggi-do 16419, Republic of Korea.

To improve the integrity and performance and to reduce the power consumption of semiconductor, the line width between patterns of interconnects has been shrunk continuously. In order to solve this challenge, Cu is currently used as an interconnect material with a barrier material in a damascene structure because it has low resistivity. However, Cu also shows a rapid increase of resistivity in a critical dimension (CD) of less than 10 nm due to long mean free path in addition to a limitation in scaling down due to the requirement of a barrier material. Therefore, the importance of new materials such as Mo, Ru, Co, etc. to substitute Cu has been increased to solve this problem. In this experiment, atomic layer etching (ALE) of Mo has been carried out by using O<sub>2</sub>/Cl<sub>2</sub> gases as adsorption process and Ar<sup>+</sup> ion beam for desorption process. By using ICP-type ion beam for desorption step, fine control of the ion energy was possible during the ALE. In the adsorption step, by using O<sub>2</sub>/Cl<sub>2</sub> plasmas, the Mo surface was modified into MoCl<sub>x</sub> and MoO<sub>x</sub>Cl<sub>y</sub>. In the desorption step, the modified Mo surface such as MoCl<sub>x</sub> and MoO<sub>x</sub>Cl<sub>y</sub> was removed using an

Ar<sup>+</sup> ion beam. After the ALE process, physical and chemical analysis of the Mo surface was performed using X-ray photoelectron spectroscopy (XPS), atomic force microscope (AFM), etc.

**PS-TuP-17 Modeling the Impact of Electronegativity in Capacitively Coupled Argon/Oxygen Discharges with Tailored Voltage Waveforms, Sk Azmaeen Bin Amir, S. Zulqarnain, North Carolina State University; J. Prager, T. Ziemba, Eagle Harbor Technologies; A. Lietz, North Carolina State University**

Recent developments in power supply technology have made a greater variety of custom waveforms achievable at a scale relevant to semiconductor processing. These custom waveforms provide additional degrees of freedom that can be used to control the ion energy distributions. Dual-frequency capacitively coupled plasmas (CCPs) are often used with a sinusoidal high frequency to generate the plasma and a low-frequency custom waveform to accelerate the ions. Many etching processes use electronegative gases, introducing negative ions which have much lower mobility than electrons and altering the plasma dynamics and sheath behavior.

In this work, we explore the impact of oxygen and the resulting negative ions on the plasma dynamics and the control of the ion energy distribution for dual-frequency CCPs. The focus is on regimes of interest for atomic layer etching (ALE), where the desired ion energy is relatively low (< 100 eV), but must be more precisely controlled. EDIPIC, a particle-in-cell Monte Carlo Collision (PIC-MCC) model, is used to model the plasma in a one-dimensional simulation. A high-frequency (60 MHz) sinusoidal voltage is applied to the upper electrode, and the tailored voltage waveform is applied to the lower electrode at 400 kHz. In this case, the tailored waveform is a triangular positive pulse, with a negative voltage applied in the interpulse period.

The changing plasma dynamics with the varying Ar/O<sub>2</sub> mixtures will be discussed, as well as the impact of the amplitude of the custom waveform. Variations in the waveform, such as the duration of the positive pulse and the magnitude of the negative voltage, may also be explored. The impact on the ion angular and energy distribution, as well as the electric field dynamics in the sheath during the pulse and the role of secondary electron emission, are discussed. In particular, narrow ion energy distributions with a tunable energy are desirable for ALE, with a minimum flux of high energy ions, as these may cause etching that is not self-limiting and destroy the atomic precision.

**PS-TuP-18 Kinetic Modeling of Dual-Frequency Capacitively Coupled Argon Discharges Using Tailored Voltage Waveforms, Syed M. Zulqarnain, North Carolina State University; J. Prager, T. Ziemba, Eagle Harbor Technologies; A. Lietz, North Carolina State University**

As microelectronics technologies become more advanced, high aspect ratio (HAR) etching has become more challenging in recent years. In this work, plasma simulations are used to better understand industrial capacitively coupled plasmas (CCPs) with the goal of controlling ion energies and ion-radical flux ratios using tailored voltage waveforms. The use of a dual-frequency CCP enables high-quality HAR etching by controlling the ion energy and angular distributions. A regime in which ion flux and energy can be more independently controlled is accessed by applying two different frequencies of applied voltage, and tailoring the voltage waveforms can control ion energy and angular distributions. To achieve narrow ion energy and angular distributions, high voltages and low pressures are typically applied. As a result, fluid and hybrid models become inaccurate, and a kinetic approach is required. We investigate the dynamics of low-pressure (7 mTorr) dual-frequency argon plasmas in a 5 cm gap between electrodes using EDIPIC, a Monte Carlo collision-based particle-in-cell (PIC/MCC) simulation. In this work, we introduce the electrical asymmetry effect by tailoring voltage waveforms at the lower electrode (i.e., the wafer). The triangular pulsed tailored voltage waveform of low frequency (400 kHz) is applied to the lower electrode and sinusoidal high frequency (60 MHz) on the upper electrode. The effects of changing the peak-to-peak voltage of the driving voltage waveforms on the ion average energy, ion velocity, and secondary electron yields at the surface of the electrode are discussed. We found that increasing the amplitude of the low-frequency waveforms (100-1000 V) resulted in a tens of eV increase in the average ion energy in bulk regions and a significant increase in ion energy reaching the electrode surface (100-500 eV). Conversely, increasing the peak-to-peak voltage of high-frequency waveforms led to an increased density of bulk plasma but did not significantly change the average ion energy. Furthermore, inclusion of secondary electron emissions (SEE), using energy-dependent SEE yields,

# Tuesday Evening, November 7, 2023

resulted in increased electron collisions with the electrodes due to the low-energy electrons emitted from the electrodes. Additionally, during the positive pulse from the low-frequency voltage waveform, electrons only collided with the low-frequency electrode with a slight decrease in ion collisions, which springs back as the positive cycle relaxes.

**PS-TuP-19 Patterning of Magnetic Tunnel Junction (MTJ) using RF-biased Reactive Ion Beam Etching, *Kyoung Chan Kim, D. Kim, Y. Jang, H. Gil, H. Kwon, J. Kim, G. Yeom***, Sungkyunkwan University, Republic of Korea

Materials such as CoFeB and MgO are used in the Magnetic Tunnel Junction (MTJ) layer of MRAM devices. These materials are mostly used to make small-sized MRAM devices, and ion beam etching (IBE) is used to etch these materials. However, when using the ion beam etching method is used to etch the MTJ layer, hard mask materials or/and materials in the MTJ layer are also etched, leading to the re-deposition of byproducts on the side walls between nano-sized patterns as well as problems with non-vertical etching. To remove these problems, the MTJ layer of the MRAM device is generally etched at a slant angle by tilting the substrate from the ion beam to remove the redeposited layer on the side of the MTJ structure. However, as the distance between the MTJ structures is decreased to nanoscale, it is difficult to tilt the substrate for the removal of the redeposited sidewall byproducts due to the narrow width of the nanoscale patterns. To solve these issues, in this study, H<sub>2</sub>/NH<sub>3</sub> reactive ion etching with RF biasing was introduced to etch MTJ layer without tilting the substrate. The MTJ layer was etched through an RF-biased ion beam, and the etch profile, sidewall re-deposition, and etch characteristics were compared with a general reactive ion beam.

**PS-TuP-21 Production of Argon Metastable Species in an Electron Beam Generated Plasma, *Vighneswara Siva Santosh Kumar Kondeti, N. Chopra, S. Yatomi, Y. Raiteses***, Princeton University Plasma Physics Lab

Electron beam (e-beam) generated plasmas can produce desirable species for material processing applications by leveraging control of electron energy, while simultaneously maintaining a low electron temperature.<sup>1</sup> In particular, e-beam generated plasmas can be used to produce low energy ions in the periphery of the primary electron beam.<sup>2</sup> This production is enabled by the presence of metastable species in the discharge periphery. In this work, we measured the absolute density of argon (1s<sub>5</sub>) metastable density in an e-beam generated ExB secondary electron emission plasma source by laser induced fluorescence. We used a Langmuir probe to obtain the electron temperature and density. The measured electron density and Ar(1s<sub>5</sub>) densities were on the order of 10<sup>16</sup> m<sup>-3</sup>, while the electron temperature was less than 1eV. The electron density and the Ar(1s<sub>5</sub>) density reduced, while the electron temperature remained constant as a function of distance from the center of the discharge. A one-dimensional continuity equation model showed that there is continuous production of argon metastables even outside the core plasma region. Two distinct regions were identified in the spatial profile of Ar(1s<sub>5</sub>) level inside and outside the core plasma region. These results suggest that there is an additional source of production of Ar(1s<sub>5</sub>) in the core of the plasma in addition to the direct excitation by electrons from the ground state of argon.

Acknowledgement: This work was supported by the U.S. Department of Energy through contract DE-AC02-09CH11466.

<sup>1</sup> Lock E, Fernsler R and Walton S, Plasma Sources Science and Technology, 17 025009 (2008).

<sup>2</sup> Walton S G, Boris D R, Hernández S C, Lock E H, Petrova T B, Petrov G M and Fernsler R F, ECS Journal of Solid State Science and Technology, 4(6) N5033 (2015).

**PS-TuP-22 Effect of Plasma Nitrided Layer on the Deflection of Biopsy Needles, *Hideaki Kuwabara, T. Yamauchi, P. Abraha***, Meijo University, Japan

Biopsy needle deflection refers to the bending or flexing behavior exhibited by biopsy needles when subjected to external forces during medical procedures. The extent of deflection is influenced by various factors,

including needle diameter, length, material, geometry, and applied forces. The addition of a nitride layer, such as titanium nitride (TiN) or silicon nitride (Si<sub>3</sub>N<sub>4</sub>), has been reported to alter material properties, such as modulus of elasticity and hardness, impacting the deflection characteristics of biopsy needles. The objective of this research is to treat biopsy needles in an electron beam-induced plasma and diffuse neutral species of nitrogen into the needle surface creating a nitrided layer and investigating its effect on the deflection of biopsy needles. Both experimental testing and finite element analysis (FEA) are utilized in this study. In our experiments, we used neutral nitrogen species from electron beam-induced plasma to diffuse into the stainless steel surface of the biopsy needle, resulting in the formation of the nitrided layer. This process did not involve adding any material to the needle's surface. Additionally, FEA was employed to create a virtual model and analyze the deflection behavior of the biopsy needles under different loading scenarios. The results of our parametric studies, focusing on the impact of nitrided layer thickness on needle deflection, will be presented. These findings will be compared to the experimental testing conducted using a custom-designed setup. By combining experimental and numerical approaches, we aim to gain a comprehensive understanding of the effects of the nitride layer on biopsy needle deflection.

**PS-TuP-24 Understanding 3D Grayscale Pattern Transfer: A Plasma Etching Parametric Study for Optoelectronic Devices, *Assia SELMOUNI, A. TAVERNIER, A. WARSONO, S. BERARD-BERGERY, N. POSSEME***, Univ. Grenoble Alpes, CEA, Leti, France

The latest promising optoelectronic devices require increasingly complex three-dimensional structures made of specific materials that meet optical, mechanical and ageing requirements. These structures are diverse, for instance: microlenses are needed for image sensing devices in the visible and infrared range [1] while multi-height structures are used in diffractive optics [2]. In this study, these different shapes are patterned in a photoresist layer before being transferred into a non-photosensitive polymer layer by plasma etching. This can cause profile deformation and roughness that may affect device performances.

The experimental setup consists of a low contrast photoresist patterned using Grayscale I-Line lithography [3]. This innovative technique uses a binary mask to allow spatial variation of the light intensity transmitted on the resist surface during the exposure step. Exposing a low contrast resist at different doses results in different thicknesses in the resist film. This allows industrial production of various 3D shapes through a single lithography step. The resist structures are transferred into a non-photosensitive polymer layer using CF<sub>4</sub> chemistry in a 300 mm Capacitively Coupled Plasma (CCP) industrial chamber (Tokyo Electron Vigus™). Samples are characterized using ellipsometry, X-ray Photoelectron Spectroscopy (XPS), 2D and 3D Atomic Force Microscopy (AFM), Scanning Electron Microscopy (SEM) and Transmission Electron Microscopy Energy-Dispersive X-ray spectroscopy (TEM EDX).

To understand the impact of plasma etching on roughness and profile deformation, a parametric study is conducted focusing on multi height and microlens structures.

First, we propose etching mechanisms based on the variation of RF power, pressure and plasma chemistry. For instance, our study revealed that increasing high frequency power led to a rougher surface and shape deformation of microlenses as shown by SEM images displayed in [figure 1](#). XPS analysis on etched blanket wafers show a fluorocarbon layer with significant increase in fluorine content at high power. TEM EDX and 3D AFM analysis will also be discussed to support proposed etching mechanism.

Finally, a second part presents means for process optimisation to achieve smooth and conform shapes. For example, chuck temperature increase during microlens etching, illustrated through SEM images in [figure 2](#), has proved to be a simple way to limit edge roughness without significant shape deformation.

[1] L. C. P. Gouveia and B. Choubey, Sensor Review 36(3), pp. 231-239

(2016)

[2] N. Gerges et al., *J. Vac. Sci. Technol. B*, 39 (6), pp.062602 (2021)

[3] P. Chevalier et al., *Proc. SPIE*, 109581E (2019)

## **PS-TuP-25 Monocrystalline III-Nitride Films Grown on Sapphire Substrates at 200 °C via Hollow-Cathode Nitrogen Plasmas, *Narmin Ibrahimli, I. Saidjafarzoda, A. Mohammed, N. Biyikli*, University of Connecticut**

Research efforts on low-temperature ( $T < 300$  °C) synthesis of crystalline GaN thin films using plasma-assisted ALD utilized various reactor configurations featuring different plasma sources. While our early GaN growth experiments using quartz-based ICP sources resulted in nanocrystalline/amorphous films with elevated oxygen impurities, stainless-steel based hollow-cathode plasma sources revealed polycrystalline GaN films on Si(100) and sapphire substrates. Upon further modification of the hollow-cathode plasma source and reactor chamber design, in this work, we share our experimental findings on the epitaxial growth efforts of GaN, AlN, and InN using hollow-cathode plasma-assisted ALD (HCP-ALD) at 200 °C.

The films were deposited using metal-alkyl precursors (triethylgallium, trimethylaluminum, trimethylindium) and various nitrogen plasmas (N<sub>2</sub>/H<sub>2</sub>, N<sub>2</sub>-only, N<sub>2</sub>/Ar, and N<sub>2</sub>/H<sub>2</sub>/Ar) at 200 °C substrate temperature and 50 – 150 W RF-power range. In-situ Ar-plasma annealing cycles were also employed and tested for the binary III-nitride films to enhance the surface crystallization process. In-situ ellipsometry and optical emission spectroscopy (OES) were employed to monitor the surface ligand-exchange reactions, plasma surface interactions, and reaction byproducts in real-time. Ex-situ spectroscopic ellipsometry measurements revealed the growth-per-cycle (GPC) and optical properties of the III-nitride films. When compared to reference films grown on Si(100) substrates, GPC values obtained for III-nitride films on sapphire substrates showed a notable increase. For GaN samples, grazing-incidence XRD (GIXRD) measurements revealed single-phase hexagonal polycrystalline films on Si(100) substrates while GaN/sapphire samples exhibited no crystal peaks at all. Rocking curve XRD scans displayed a strong single (002) peak, confirming the monocrystalline epitaxial character of the synthesized GaN films on sapphire substrates. We attribute this significant improvement in crystal quality to the synergistic impact of a customized HCP-ALD reactor, large-diameter third-generation hollow-cathode plasma source, and optimized growth conditions (plasma gas mixture, rf-power). With further improvement in film properties, we aim to achieve device-quality electrical properties that can be used for logic, memory, power, and sensing applications.

## **PS-TuP-26 Plasma Delayering for Non-Selective Precision Etching, *Leonid Miroshnik, S. Han*, University of New Mexico; *T. Stevens, J. Duree, R. Shul, C. Nakakura*, Sandia National Laboratories**

For defect and reliability analysis of microdevices, we have begun investigating precision, non-selective delayering of microdevices where all materials are etched ideally at the same rate, resulting in a planar surface. The desired etch uniformity and precision over the wafer exceed what can be achieved by chemical etching and/or chemical mechanical planarization. In this poster, we will share preliminary results from methyl-acetate and ethyl-acetate-based plasmas in which we can relatively retard the etch rate of dielectric films compared to metal exposed to the same plasma. The surface analysis by spectroscopic ellipsometry and x-ray photoelectron spectroscopy suggests that the polymer films on dielectric and conductor materials are different in nature and likely responsible for relatively retarding or accelerating the etch rate for non-selective delayering.

This research was developed with funding from the Defense Advanced Research Projects Agency (DARPA). The views, opinions and/or findings expressed are those of the author and should not be interpreted as

representing the official views or policies of the Department of Defense or the U.S. Government.

Distribution Statement "A" (Approved for Public Release, Distribution Unlimited)

## **PS-TuP-27 Ion Energy Control in a Capacitively Coupled Plasma with a High Voltage Custom Waveform Bias, *Timothy Ziemba, J. Prager, J. Perry, K. Muggli*, Eagle Harbor Technologies, Inc.**

Producing high-aspect-ratio (HAR) features with plasma etching is becoming increasingly important as the market demands solid-state non-volatile memory storage. In order to minimize bowing and twisting defects in HAR features, precision control of the ion energy distribution (IED) is required. Eagle Harbor Technologies (EHT), Inc. has previously developed a Rapid Capacitor Charger power system that can charge capacitance to high voltage in tens of nanoseconds and operate at 400 kHz. In this work, EHT is investigating ion energy control with these high-voltage custom waveforms. The experimental test chamber includes a 60 MHz capacitively coupled plasma source and a pedestal that can be biased using the Rapid Capacitor Charger waveforms. EHT will present the chamber modifications, retarding field energy analyzer details, and IED measurements. Based on these measurements, the next steps will be discussed.

## **PS-TuP-28 Cryogenic Aspect Ratio Etching of SiO<sub>2</sub> at CF<sub>4</sub>/H<sub>2</sub>/Ar Plasma in a Cryogenic Reactive Ion Etch System, *H. Kwon, In Young Bang, J. Kim, H. Kim, S. Lim, S. Kim, S. Jo, J. Kim, W. Kim, G. Shin, G. Kwon*, Kwangwoon University, Republic of Korea**

In the manufacturing processes of 3D NAND, the high aspect ratio contact (HARC) etching process, which is one of the most critical steps, has encountered a significant challenge. HARC, typically performed at room temperature, has become increasingly difficult to achieve the desired high aspect ratio while maintaining high productivity. This challenge is expected to become harder when considering devices with highly stacked alternating layers of silicon-containing materials, such as SiO<sub>2</sub> and SiN. Therefore, cryogenic HARC technology has emerged as a promising solution to overcome this challenge, as it offers advantages in terms of productivity and better etch profile. Consequently, we conducted cryogenic aspect ratio etching of SiO<sub>2</sub> at CF<sub>4</sub>/H<sub>2</sub>/Ar plasma in a cryogenic reactive ion etch system. Overall, our results revealed that cryogenic aspect ratio etching of SiO<sub>2</sub> showed a higher etch rate and a higher aspect ratio under the experimental conditions. With these conditions, we conducted the cryogenic aspect ratio contact etching of SiO<sub>2</sub> for the comparison with the etching of SiO<sub>2</sub> at RT as well.

## **PS-TuP-29 In-Situ Electron Density Measurement in Inductively Coupled Plasma Using Microwave Reflectometer, *Jae Hyeon Kim, W. Kim, G. Shin, H. Kwon, J. Kim, I. Bang, S. Lim, H. Kim, S. Kim, S. Jo, G. Kwon*, Kwangwoon University, Republic of Korea, Korea (Democratic People's Republic of)**

Low temperature plasma has been widely used in semiconductor manufacturing process. The characteristics of low temperature plasma that are important in semiconductor manufacturing include electron density, electron temperature and electron energy distribution. Specifically, electron density is important to understand plasma physics and plasma process. The electron density is commonly measured using a Langmuir probe. The probe inserts a tip into plasma and voltage is applied to the probe. Charged particles in plasma move to the probe and current generated by the movement is measured to determine plasma density. However, the measured signals interfere with radio frequency and plasma perturbation by the probe distorts the plasma characteristics.

In this study, plasma density was measured using microwave reflectometer without plasma perturbation. The microwave signal radiated by Wi-Fi antenna is reflected by the plasma and collected through the antenna. The electron density measured by analyzing a phenomenon arising from the correlation between the microwave and plasma angular frequencies. The plasma angular frequency is derived using the reflection or transmission phenomenon of microwaves, which depends on the refractive index of the plasma. The refractive index of a plasma  $N$  is related to the microwave angular frequency  $\omega$  and the plasma angular frequency wave  $\omega_p$ , i.e.  $N = (1 - \omega_p/\omega)^{1/2}$ . The plasma angular frequency depends only on the plasma density as  $\omega_p = (n_e e^2 / \epsilon_0 m_e)^{1/2}$ . When the microwave frequency is equal to plasma frequency, the refractive index of the plasma becomes zero and the reflection becomes maximum. The  $S_{11}$  parameter is calculated by measuring the intensity of the reflected signals on the frequency sweep. The reflectivity was analyzed by measuring the difference between the  $S_{11}$  parameter before and after plasma discharge.

In this experiment, 13.56 MHz RF power source was used in a 300 mm inductively coupled plasma chamber. The applied RF power was 200, 400 and 600 W. The intensity of the reflected signal from the plasma was measured using mixer and RMS to DC converter.

**PS-TuP-30 Localized Deposition of Coatings Using Immobilized Streamers of a DBD: Interplay between the Electrode Gap and the Precursor Flow on the Coating Chemistry, Marie Brabant, Université libre de Bruxelles, Belgium; A. Demaude, D. Petitjean, F. Reniers, Université Libre de Bruxelles, Belgium**

Deposition of patterned coatings to generate hybrid surface properties often require a multi-step process, such as the use of masks or lithography [1]. We proposed recently a simple scalable method for the deposition of patterned coatings (morphological and chemical contrasts) [2]. As a case study, the deposition of propargyl methacrylate (PMA) based-coatings was realized, as, due to its structure (one double and one triple bond), this molecule allows very fast deposition, and can lead to hydrophobic coatings, without the need of fluorinated atoms. Moreover, we showed that, depending on the deposition conditions, one could obtain hybrid hydrophilic/hydrophobic patterns. In a recent paper, we showed that pulsing the power (in the ms range) leads to more localized filaments, to a global change in the plasma behaviour and to a change in the coating chemistry [3].

In this poster, we investigate the interplay between the interelectrode gap and the precursor gas flow on the overall plasma discharge and on the resulting (localized) coating. The plasma discharge is characterized by a high speed camera, and mass spectrometry, whereas the coating is characterized using micro-XPS and infrared spectroscopy in IRRAS mode. We show that increasing the gap necessitates an overall higher power to sustain the plasma, resulting in a higher voltage (according to Paschen Law) that leads to a global higher electron energy in the filaments. Such higher power injected into the discharge induces surface discharges between the immobilized filaments. In parallel, increasing the precursor gas flow leads to a higher luminosity in the inter-filament space. The coating thickness and chemistry is similarly influenced by the gap and the precursor flow. Increasing the gap and precursor flow lead to an increase in the coating diameter under the filaments but the thickness of the spots decreases when increasing too much gap. A better preservation of the chemical functionalities of the precursor inside the coating deposits is obtained for higher gas flows and low gaps, which is correlated with the mass spectroscopy analysis of the plasma phase. Results are interpreted in terms of the evolution of the Yasuda parameter.

References :

[1]. A. Demaude, C. Poleunis, E. Goormaghtigh, P. Viville, R. Lazzaroni, A. Delcorte, M. Gordon, and F. Reniers, *Langmuir*, 2019, 35, 9677–9683.

[2] A. Demaude, K. Baert, D. Petitjean, J. Zveny, E. Goormaghtigh, T. Hauffman, M. Gordon, and F. Reniers, *Advanced Science*. 2022, 2200237.

[3] A. Demaude, M. Brabant, D. Petitjean, M. Gordon, F. Reniers, *Plasma Chemistry and Plasma Processing*, 2023. <https://doi.org/10.1007/s11090-023-10355-6>

**PS-TuP-31 the Effect of Rf Bias Frequency on the Ion Energy Distribution in Ultra-Low Electron Temperature Plasma, Chang-Min Lim, M. Kim, J. Park, C. Chung, Department of Electrical Engineering, Hanyang University, Republic of Korea**

The ion energy distributions in an ultra-low electron temperature (ULET) plasma ( $T_e < 0.5$  eV) are expected as follows: The mean ion energy is closed to  $V_{dc}$  since  $V_p$  is nearly 0, and the energy dispersion of the ion energy distribution ( $\Delta E_i$ ) is much narrower. In this study, we measured the ion energy distributions in ULET plasma and ICP at bias frequencies of 27.12 MHz and 60 MHz. It is observed that when  $V_{dc}$  ranged from 0 to -40 V, the mean ion energy of ULET plasma is slightly greater than  $V_{dc}$ . Furthermore, the ion energy distributions in the ULET plasma have narrower  $\Delta E_i$ , which is a monoenergetic distribution compared to those in a conventional bias ICP.

**PS-TuP-32 Changes in Ion Density and Electron Temperature Over Time Due to Bias Power, Park Sung-Joon, E. Hyundong, C. Chin-Wook, Department of Electrical Engineering, Hanyang University, Republic of Korea**

In an inductively coupled plasma (ICP), we measured the electron temperature and ion density over time while applying RF bias power. We observed rapid temporal changes on the order of seconds using a higher time resolution probe (approximately 0.2 seconds). The experiment involved adjusting the antenna power and bias power. Additionally, we installed two types of probes for measurement, one at the plasma bulk and

the other at the biased electrode. We noticed that density changes occurred very rapidly, within a few seconds, due to the electron charging effect in response to the bias power. Furthermore, the trends in electron temperature and ion density are similar when the RF bias powers are changed at both positions.

**PS-TuP-33 On the Method of Dielectric Thickness Measurement by Using Three Frequencies, Hyeon ho Nahm, H. Lee, B. Seo, C. Chung, Department of Electrical Engineering, Hanyang University, Republic of Korea**

Optical emission spectroscopy (OES) is a widely used technique for noninvasive plasma measurement. However, the deposition of polymers on the viewport can lead to a reduction in light intensity, even under the same experimental conditions (e.g., pressure, power). It can be useful to measure the thickness of the deposition layer to compensate for the reduction in light intensity.

We applied three different voltages to an electrical probe to obtain deposition layer impedance. In an equivalent circuit model, the plasma sheath can be regarded as a parallel circuit of sheath resistance and sheath capacitance, representing displacement current and conduction current, respectively. The deposition layer can be considered as a dielectric film. By solving three equations derived from three voltages of different frequencies, we calculated the capacitance of the dielectric and determined its thickness.

However, two problems arose. First, due to the voltages applied to the probe, the floating potential shifted, distorting the plasma sheath resistance. Second, a significantly high impedance ratio between the plasma sheath and deposition layer made it challenging to obtain the thickness of the deposition layer. Therefore, we modulated the amplitude of the applied voltages to minimize distortion and decreased the frequencies to increase the dielectric impedance. Consequently, the error in the measured deposition layer thickness could be greatly reduced.

**PS-TuP-34 Etching Characteristics of  $NF_3$  and  $F_3NO$  at Reactive Ion Etching Plasma for Silicon Oxide, W. Kim, Seong Hee Jo, H. Kwon, G. Shin, J. Kim, I. Bang, S. Lim, J. Kim, H. Kim, S. Kim, G. Kwon, Kwangwoon University, Republic of Korea**

Nitrogen-trifluoride ( $NF_3$ ) is mainly used as a reactive gas in cleaning and etching process in the semiconductor and display fabrication. However,  $NF_3$  is a greenhouse gas with a high potential for global warming. As regulations related to the green index are getting stronger worldwide, the need for gas to replace  $NF_3$  is increasing.

In this study, an experiment was conducted on  $F_3NO$  gas as a gas to replace  $NF_3$ . The plasma etching process was similarly diagnosed by RGA and OES, and the etch rate was calculated by measuring the reflection. The etch rate of silicon oxide during  $F_3NO/Ar$  plasma etching is approximately 94% of that for  $NF_3/Ar$  plasma etching. The RGA and OES measurements confirmed that more  $O^+$ ,  $NO^+$ , and  $O_2^+$  ions were generated in the  $F_3NO$  plasma than in the  $NF_3$  plasma.

**PS-TuP-35 Investigation of Transient Phenomena of Electron Heating in Low-Frequency Pulse-Driven Capacitively Coupled Ar Plasmas Using a Particle-in-Cell Simulation, Seoi Choi, H. Lee, Pusan National University, Republic of Korea**

Pulsed capacitive RF plasma is demanded for the semiconductor etching because it mitigates plasma-induced damage. Repeating pulse-on and pulse-off time lowers ion energy and electron temperature compared to a continuous wave plasma, resulting in less wafer damage. This study performed a pulse-driven two-dimensional (2D) particle-in-cell (PIC) simulation parallelized with a graphics processing unit (GPU) to investigate the plasma dynamics for the time duration of ms. We investigated the effects of a 2D electrode structure empowered low-frequency (LF) pulsed voltage added to a high-frequency (HF) sinusoidal wave on the plasma potential, electron density, and electron temperature by varying frequency and pressure conditions. Plasmas diffuse for a sufficiently long afterglow period in the LF pulse and re-ignited from a lower electron density when the pulse is on again. The electron heating mechanisms are reported for the ramp-up and ramp-down phases at different frequencies.

**PS-TuP-37 An Arrival Time Difference-Based Elimination Method of Cavity Resonances for Crossing Frequency Determination of the Cutoff Probe,** *Chulhee Cho, S. Kim, W. Lee*, Chungnam National University, Republic of Korea; *B. Na*, Korea Institute of Fusion Energy, Republic of Korea; *Y. Seol, Y. Lee, I. Seong, W. Jeong, M. Choi, B. Choi, S. Seo, S. You*, Chungnam National University, Republic of Korea

The crossing frequency method of the cutoff probe, which is composed of radiating and detecting tips, has been recently developed for electron density measurement. However, this method faces challenge in accurately deducing electron density due to cavity resonances, which is caused by the standing wave resonance between the chamber wall and the cutoff probe. In this research, we propose an arrival time difference-based elimination method. As the cavity resonance occurs later in time compared to the directly transmitted between two tips, cavity resonance can be eliminated by adjusting the signal detection time. On the contrary with a conventional frequency sweeping system, we established a ns-pulse radiation and detection system, which can convert signals in time domain to that in frequency domain, so-called  $S_{21}$  by using Fast Fourier transform. As a result, by adjusting the detection time, the cavity resonance peaks in  $S_{21}$  spectrum were eliminated. By using this method, the crossing frequency can be clearly determined under wide range of chamber pressure and plasma density environments. This research not only addresses the challenges associated with high-pressure plasma measurements but also presents a reliable technique for obtaining precise electron density insides a cavity structure such as a vacuum chamber.

**PS-TuP-38 A Global Model with Monte Carlo Collision Method in Sheath for Capacitively Coupled Ar Plasma,** *Inho Seong, S. Kim, Y. Lee, Y. Seol, C. Cho, W. Jeong, M. Choi, B. Choi, S. Seo, W. Lee, S. You*, Chungnam National University, Republic of Korea

In conventional a global model, ion losses have been considered as the average of sheath voltages, without accounting for the ion energy distribution, making it inaccurate. In this research, we propose a global model with Monte Carlo Collision (GM/MCC) method for Ar capacitively coupled plasma (CCP). The input parameters in the GM/MCC are voltage and current waveforms of the powered electrode. Referenced on a 13.56 MHz Ar CCP source, we compared the electron density calculated through the GM/MCC with that measured by the cutoff probe and as a result, the discrepancy ranges from 30% to 70%. Hence, the GM/MCC is a simple-and-accurate model to analyze a conventional CCP source. Besides, the GM/MCC can be employed as a plasma monitoring sensor accompanied with voltage/current probe of the powered electrode in a CCP source.

**PS-TuP-39 Control of Radical Density Through Modulation of Electron Energy Probability Function in a Dual-Frequency (2/27.12 MHz) Inductively Coupled Plasma,** *Yeong Jae Jeong*, Department of Electrical Engineering, Hanyang University, Seoul, Republic of Korea; *U. Jung, C. Chung*, Department of Electrical Engineering, Hanyang University, Republic of Korea

The effects of 2 MHz and 27.12 MHz power on the electron energy probability functions (EPPFs), electron temperature ( $T_e$ ), absorbed power of plasma, and radical density were experimentally investigated in a dual frequency inductively coupled oxygen plasma. The RF powers are simultaneously applied to two parallel connected antennas. The EPPFs are investigated as a function of pressure and power. Experimentally, it was observed that electron heating and the EPPFs change with pressure and driving frequency. Through the effect of each driving frequency on the EPPFs, we achieved control over the radical density. These results have the potential to control radical density by changing the dual frequency RF power.

**PS-TuP-40 Effects of a Non-Sinusoidal Rf Field on Multipactor Discharge in a Parallel Plate Geometry,** *Asif Iqbal, D. Wen, J. Verboncoeur, P. Zhang*, Michigan State University

Multipactor [1] is a nonlinear discharge phenomenon occurring in RF and microwave components and systems in which a high frequency RF field creates an electron avalanche sustained through secondary electron emission [2] from metallic or dielectric surfaces. It can be detrimental to RF devices creating problems [1,3] such as the breakdown of dielectric windows, erosion of metallic structures, melting of internal components, etc. In addition, multipactor can often detune RF systems, cause multi-tone coupling and signal distortion, limit the transmission or delivery of RF power [1,3].

This work presents a study of two-surface multipactor discharge in a parallel plate geometry induced by a non-sinusoidal Gaussian-type RF field waveform [4,5]. We employ 3D electromagnetic Particle in Cell (PIC)

simulations using Computer Simulation Technology (CST) Particle Studio [6,7], and Monte Carlo (MC) simulations [6,7] to examine the effects of RF amplitude and the half peak width of the Gaussian-type electric field on multipactor susceptibility and time dependent physics [4-7].

The threshold peak RF voltage and the threshold time-averaged RF power per unit area for multipactor development increase with a Gaussian-type electric field compared to those with a sinusoidal electric field. The threshold peak RF voltage and RF power for multipactor increase as the full width at half maximum and/or half minimum (FWHM) of the Gaussian profile decreases. Expansion of multipactor susceptibility bands is observed compared to the sinusoidal RF operation. A high initial seed current density is found to shrink the multipactor susceptibility bands in the presence of space charge. The effect of space charge on multipactor susceptibility decreases as the FWHM of the Gaussian profile decreases.

65. J. R. M. Vaughan, IEEE Trans. Electron Devices, vol. 35, no. 7, pp. 1172–1180, 1988.
66. J. R. M. Vaughan, IEEE Trans. Electron Devices, vol. 36, no. 9, pp. 1963–1967, 1989.
67. A. Iqbal, D.-Q. Wen, J. Verboncoeur, and P. Zhang, “Recent Advances in Multipactor Physics and Mitigation,” High Voltage, 2023 (in the press), <https://doi.org/10.1049/hve2.12335>.
68. D.-Q. Wen, A. Iqbal, P. Zhang, and J. P. Verboncoeur, Physics of Plasmas 26, 093503 (2019).
69. D.-Q. Wen, A. Iqbal, P. Zhang, and J. P. Verboncoeur, Appl. Phys. Lett., vol. 121, no. 16, p. 164103, 2022.
70. A. Iqbal, J. Verboncoeur, P. Zhang, Phys. Plasmas 29, 012102 (2022).
71. A. Iqbal, D.-Q. Wen, J. Verboncoeur, and P. Zhang, “Two Surface Multipactor with Non-Sinusoidal RF Fields,” 2023 (under review).

This work was supported by the Air Force of Scientific Research (AFOSR) MURI Grant Nos. FA9550-18-1-0062 and FA9550-21-1-0367.

**PS-TuP-41 Field Reversals in High Voltage-Driven Low Pressure Capacitively Coupled Plasmas,** *De-Qi Wen*, Michigan State University; *J. Krek*, KLA Corporation; *J. Gudmundsson*, University of Iceland; *E. Kawamura, M. Lieberman*, University of California at Berkeley; *P. Zhang, J. Verboncoeur*, Michigan State University

Low pressure capacitively coupled plasmas (CCPs) are widely used in plasma processing, such as etching, sputtering, cleaning. In recent work, we presented the important role of realistic electron-induced secondary electron emission (SEE), metastable atom and photon-induced secondary electrons from electrodes on the plasma density in low pressure capacitive argon discharges at 13.56MHz. Including the surface processes, the plasma density from the kinetic particle-in-cell (PIC) simulations shows good agreement with experimental measurements [Schulenberg et al Plasma Sources Sci. Technol. 30 (2021) 105003] at low pressure (1-10 Pa). In this work, we investigated the high voltage-driven capacitive discharges at low pressure via the validated PIC model and studied the reversed electric field pointing from the electrode towards the bulk plasma. The reversed field is induced by the strong secondary electron emission during the phase of sheath collapse. Especially, we explored the transition behavior of the formation of field reversal as a function of driving voltage amplitude and found the field reversal starts to be formed at around 750 V for CCP with an electrode spacing of 4 cm at 10 mTorr argon and 13.56 MHz. Accordingly, the electron energy distribution function incident on the electrode shows peaks from around 3 eV to 10 eV while spanning the driving voltage from 150V to 2000 V, showing potentially favorable effects in plasma processing where directional electrons are preferred to solely thermal diffusion electrons. The field reversals found at macroscale will also be examined for microplasmas considering a similarity law.

This work was supported by the Air Force Office of Scientific Research (AFOSR) MURI Grant FA9550-21-1-0367 and NSF-DOE Partnership Grant for DE-SC0022078. The Icelandic Research Fund Grant Nos.163086 and 217999, and a gift from the Applied Materials Corporation, AKT Display Division.

## Advanced Surface Engineering Division Room Oregon Ballroom 203-204 - Session SE-TuP

### Advanced Surface Engineering Poster Session

**SE-TuP-1 Characterizations and Drill Performance of AlCrCN Coatings Deposited by High-Power Impulse Magnetron Sputtering.** *F. Yang*, National Taiwan University of Science and Technology, Taiwan; *B. Lu, J. Tsao*, Ming Chi University of Technology, Taiwan; *Y. Kuo*, National Taiwan University of Science and Technology, Taiwan; **Chi-Lung Chang**, Ming Chi University of Technology, Taiwan

In recent years, the production capacity of printed circuit boards (PCBs) has increased significantly resulting in an increase in the demand for micro drills, especially in the requirements of wear-resistant properties. Therefore, various PVD technologies are applied, especially the high power pulsed magnetron sputtering (HiPIMS) technology has the most potential for application, which due to the high ionization rate leads to high density and high mechanical properties of the thin film.

In this study, AlCrCN coatings were prepared via HiPIMS with four Al70Cr30 targets and two Cr targets, with a focus on the effects of carbon content and substrate bias on the microstructure, mechanical properties, and drill performance of the coatings. FE-SEM revealed the interlayers designed to improve adhesion strength from 10 N up to 58N. The highest hardness (3045 Hv) and highest adhesion force (58 N) were obtained by increasing the bias voltage (-75 V) with a carbon content of 9.4 at%. The drill test results showed better wear resistance and useful lifetime than CrAlN coating for PCBs application.

**SE-TuP-2 Fabrication of FeCrAlY-Al<sub>2</sub>O<sub>3</sub> Composite for Additive Manufacturing.** *Hsin-Mei Kao, K. Son, S. Yang, N. Ghanadi, S. Pasebani, B. Paul, C. Chang*, Oregon State University

FeCrAlY is commonly utilized because of its exceptional oxidation resistance, whereas alumina ceramics are valued for their high fracture toughness, resistance to wear, and corrosion<sup>1</sup>. Therefore, developing Al<sub>2</sub>O<sub>3</sub>-FeCrAlY composites is a promising approach for engineering applications requiring high temperature and strength, such as engines, solid oxide fuel cells, thermal barrier coatings, and catalytic supports<sup>1,2</sup>. The production of these composite powders involves using multiple materials or phases subjected to physical or chemical treatments such as ball milling and fluidized bed chemical vapor deposition to synthesize homogeneous powders. These fabrication processes have produced many functional materials, such as ceramics, metals, and composites, which possess improved mechanical, thermal, or electrical properties<sup>1</sup>. However, these methods are very time-consuming and expensive.

In this study, we investigated a new method to synthesize spherical composite powders consisting of FeCrAlY powders with Al<sub>2</sub>O<sub>3</sub> coatings, which are used as feedstock materials for metal additive manufacturing. Chitosan is used as a binder to hold FeCrAlY and Al<sub>2</sub>O<sub>3</sub> together, and then the mixture is spray-dried into spherical composite powders. We tailored the sizes and microstructures of the FeCrAlY-Al<sub>2</sub>O<sub>3</sub> composite by controlling various parameters such as material content, mixing, flow rates, and reaction temperature. By engineering these composite powders, we can improve the uniformity of material distribution and reduce powder denudation while printing complex structures using metal additive manufacturing technologies. This approach creates a bi-continuous FeCrAlY and Al<sub>2</sub>O<sub>3</sub> structure after laser melting and annealing. Furthermore, Al<sub>2</sub>O<sub>3</sub> acts as a templating material, which can be selectively etched away, resulting in a highly porous FeCrAlY structure with a large surface area. The composite powders' and printed structures' structure and surface properties were characterized using X-ray diffraction, X-ray 3D tomography, Brunauer-Emmett-Teller analysis, Scanning Electron Microscopy, and Energy Dispersive X-ray Spectroscopy techniques.

#### References

- (1)Li, J., et al. "Al<sub>2</sub>O<sub>3</sub>-FeCrAl Composites and Functionally Graded Materials Fabricated by Reactive Hot Pressing." *Composites Part A: Applied Science and Manufacturing*, vol. 38, no. 2, Feb. 2007, pp. 615-620.
- (2)Kim, Do Hyung, et al. "A Study on FeCrAl Foam as Effective Catalyst Support under Thermal and Mechanical Stresses." *Surface and Coatings Technology*, vol. 209, Sept. 2012, pp. 169-176.

**SE-TuP-3 Avoiding Mistakes During the Nanoindentation of Coatings,** *Esteban Broitman*, SKF B.V. - Research and Technology Development, Netherlands

Nowadays, nanoindentation has become a routinely technique for the mechanical characterization of thin films and small-scale volumes. Thanks to the development of friendly analysis software and advances in high sensitive instrumentation, it feels like the measurement and calculation of hardness and elastic modulus can be easily done by just "the pushing of one button." However, the consequences of easy procedures have led many researchers to multiple publications with erroneous data.

Recently, we have reviewed the nanoindentation hardness of materials at macro, micro, and nanoscale (E. Broitman, *Tribology Letters*, vol. 65, 2017, p. 23). Some misconceptions in the nanoindentation technique were highlighted, and solutions to errors were proposed. In this presentation, five typical mistakes in the measurement and data analysis during the nanoindentation of thin films will be critically reviewed, and the possible ways to avoid them will be discussed: 1) the wrong area selection to calculate instrumented indentation hardness; 2) the wrong data conversion from Vickers microindentation to Berkovich nanoindentation; 3) the confusion of thermal drift with creep and viscoelastic effects; 4) the wrong correlation of hardness with tip penetration; 5) the preconceptions about a direct relationship between elastic modulus and hardness.

The origins of the aforementioned mistakes will be elucidated from the lack of understanding on contacts mechanics theory, the limits and validation of the Oliver and Pharr's method, and preconceptions transmitted from generation to generation of nanoindenter users. At the whole, it will be stressed that it is not enough to know "how to push the start button of the nanoindenter" in order to measure the nanoscale mechanical properties of coatings.

**SE-TuP-4 Plasma Deposited Si-Rich Silicon Nitride: Deposition, Characterization, thickness scaling limitation and applications in Cap/Passivation of Advanced nano Devices,** *Son Nguyen, V. Pai*, IBM Research Division, Albany, NY; *Y. Yao*, IBM Corporation, East Fishkill Facility; *M. Rizzolo, A. Dutta, D. Canaperi*, IBM Research Division, Albany, NY; *U. Sharma*, IBM Research Division, Albany, NY (IBM Intern\*\*)

Most current nano-electronic devices are using final composited SiNx-SiO<sub>2</sub> layer to prevent moisture penetration in final devices prior to chip packaging (1). Silicon nitride (SiNx) as a dielectric plays an important role in the semiconductor industry for many years. Si-Rich SiN have been evaluated over the years in electronic device application (2,3). With device scaling to sub-5nm dimension, both passivation and capping layers also needs to scale down to the sub-5nm thickness without compromising the following properties: 1) Excellent Oxidation and diffusion Barrier. 2) High Electrical Breakdown and Low Leakage Current. 3) High stability under thermal stress with low Hydrogen content. 4) Positive performance impacts to the passivating electronic devices including electrical and mechanical properties. 5) Conformal step coverage over high topological structure at low deposition temperature.

This work is focusing on the Si-rich SiNx as an encapsulation film and its ultrathin thickness limitation as oxidation barrier and encapsulation layers. Low-temperature (200<sup>o</sup> C -300<sup>o</sup>C) plasma enhanced chemical vapor deposition (PECVD) process was used to deposit Si-rich SiNx for encapsulation/capping of temperature sensitive nano-electronic devices. Deposition temperature impact on the Si-Rich SiNx capping film's electrical, conformality, oxidation and barrier properties of the films are evaluated with completed material compositional analysis vs film's performance. To obtain a good process at low temperature for encapsulation/capping of temperature sensitive nano-device, novel cyclic multilayers deposition/plasma treatment approach was developed. Ultrathin (3-4 nm) Si-Rich Silicon Nitride film with excellent conformality, oxidation barrier and passivation performance are achieved for passivation/capping with novel cyclic multilayer deposition/plasma treatment approach at low deposition temperature of 200 C and with > 80% conformality over high aspect ratio nanodevice structures. Carbon doped ultrathin (4 nm) SiN (SiCN) was also evaluated and achieved similar robust cap performance for nanodevice fabrication. These high-performance Si-Rich SiN and SiCN films have excellent potential for logic and memory nanodevice as passivation and capping layers.

- (1)Sean King; *Journal of Vacuum Science & Technology A* **29**, 041501 (2011); doi: 10.1116/1.3584790
- (2)Son.V. Nguyen and S. Fridmann; *J. of Electrochemical Society*, V. 134, No# 9, p.2324-2329 (1987).

(3)H. Kim et al ; Journal of Vacuum Science & Technology A **35**, 01A101 (2017); <https://doi.org/10.1116/1.4964889>

**SE-TuP-5 Multifunctional Optical Surfaces Using Scalable Nanostructuring**, *Iliyan Karadzhev, J. Rombaut, C. Graham, A. Mezzadrelli, J. Arres Chillon*, Institute of Photonic Sciences (ICFO), Spain; *W. Senaratne, R. Bellman, D. Thelen, P. Mazumder*, Corning Research and Development Corporation; *V. Pruneri*, Institute of Photonic Sciences (ICFO), Spain

Current optoelectronic applications such as touchscreen displays, photovoltaic cells or lenses require surfaces that can possess multiple functions, for example, easy optical and/or electrical tunability, high transparency, self-cleaning properties, and antimicrobial properties, to name a few. Borrowing from designs found in nature such as the eyes of nocturnal insects or the lotus leaf, much progress has been made towards bio-inspired surfaces. Yet developing mass-scalable, and cost-efficient methods for fabricating multifunctional optical surfaces is still a major challenge due to the limitation of the existing nanofabrication methods that rely on traditional optical and e-beam lithography. In this talk, we review recent efforts from our group in developing optical surfaces based on the use of ultrathin metal films (UTMF) and solid-state dewetted nanoparticles (DNPs) as a scalable and lithography-free approach to confer functionalities such as high transparency, broadband and omnidirectional antireflection effect, self-cleaning properties, and antimicrobial properties.

Solid-state thermal dewetting of ultrathin metal films (Ag, Cu, Ni) has emerged as a viable strategy to obtain features down to few nanometers, therefore, it has great potential to be implemented as a fast and low-cost method in industrial scale nanofabrication. The dewetted nanoparticles on glass surfaces serve as a mask in creating nanopillars or nanoholes using dry etch process. Initial metal films thickness, temperature, and duration of the dewetting, and dry etching times are the parameters that give us morphological and optical control on the nanostructures. The structured surfaces present omnidirectional broadband antireflection effect with low scattering and have self-cleaning properties. Importantly, structures maintain their optical and wetting properties after repeated abrasion making them attractive to be used in consumer display devices. Moreover, when high aspect ratio nanopillars in fused silica are fabricated, we observe increase of the optical emissivity in the infrared range, which can be exploited for passive radiative cooling. The versatility of dewetted nanoparticles is also shown by using Cu DNPs to make transparent, antimicrobial surface.

**SE-TuP-9 Investigating the Microstructure and Mechanical Behavior of the Particle-Particle and Substrate-Particle Interfaces in Cold Sprayed Coatings**, *Tanvi Ajantwalay, S. Niverty, R. Kalsar, V. Joshi, A. Devaraj*, Pacific Northwest National Laboratory

During cold spray, powder particles undergo severe plastic deformation upon impact with the substrate. This results in particle flattening, oxide breakage, and metallurgical bond formation at particle-particle and substrate-particle interfaces. At smaller length scales, heterogeneity of the bond coating can create property differences, which are yet to be explored. Thus, a comprehensive understanding of local interfacial bond strength at this heavily deformed interface would assist in designing optimal cold spray processes. In this study, we investigated the microstructure and mechanical properties of zinc (Zn) cold sprayed on AZ91 magnesium (Mg) substrates via correlative microscopy and in situ micro-tensile testing. Micro-tensile dogbones fabricated using Plasma Focused Ion Beam (PFIB) were tested in a displacement-controlled mode to estimate the interfacial strength and live deformation behavior.

**SE-TuP-10 Icephobic Coating Using Polymers/Silica Nanoparticles Composite via Self-Formation of Superhydrophobic Surface**, *Aravind H. Patil*, Incheon National University/ Korea Polar Research Institute, Korea (Democratic People's Republic of); *N. Trinh*, Incheon National University, Korea (Democratic People's Republic of); *H. Do*, Korea Polar Research Institute, Korea (Democratic People's Republic of); *G. Seo, J. Wook Choi*, Seoul National University, Korea (Democratic People's Republic of); *Y. Kang*, Incheon National University, Korea (Democratic People's Republic of); *J. Lee, C. Chung*, Korea Polar Research Institute, Korea (Democratic People's Republic of); *H. Lee*, Incheon National University, Korea (Democratic People's Republic of)

The accretion of ice has resulted in adverse impact on a variety of household, industrial, and polar research station activities. Despite significant efforts being made to prevent ice adhesion with different surfaces by developing various passive anti-icing coatings, it is still essential to enhance overall performance and durability. Herein, we report the designing of icephobic coatings through self-formation of 3D porous micro-

nanostructure utilizing siloxane/fluoropolymer/silica nanoparticles (NPs). The spin coating method was used for coating PDMS/PTFE composite on aluminium (Al 6061) substrate. The excellent miscibility and adhesion in PDMS and PTFE were observed due to the secondary electrostatic interactions between H and F atoms. These interactions were supported by the density functional theory (DFT) calculations and structural studies. Moreover, the controlled addition of PTFE powder to PDMS improved the water-repelling properties, mechanical strength, and adhesion strength of the coating. The self-formation of superhydrophobic Cassie Baxter state of PDMS/PTFE composite was achieved by sprinkling SiO<sub>2</sub> NPs on it. The PDMS/PTFE/SiO<sub>2</sub> NPs composites, surface morphology images showed the formation of porous 3D micro-nanostructure that produces a highly textured surface with several trapped air pockets. These air pockets minimize the surface contact area with water droplets or ice, which enhanced the water contact angle (WCA) and reduced the ice adhesion strength (IAS). Additionally, we experimentally demonstrated that the freezing at low temperatures can be delayed by controlling the heat flow rate, interfacial contact area, and surface texture. These results suggest the feasibility of the method for a wide range of promising anti-icing applications.

\*Corresponding author: hbrlee@inu.ac.kr [mailto:hbrlee@inu.ac.kr]

**Keywords:** Superhydrophobicity, Icephobicity, PDMS/PTFE composite, SiO<sub>2</sub>NPs, freezing delay time

## Theory for Surface Processes and Spectroscopies Focus Topic

Room Oregon Ballroom 203-204 - Session TH-TuP

## Theory for Surface Processes and Spectroscopies Poster Session

**TH-TuP-1 Evaluation of Covalent Bonding in Ionic Compounds**, *Paul S. Bagus*, University of North Texas; *C. Nelin*, Consultant; *T. Vitova*, Karlsruhe Institute of Technology, Institute for Nuclear Waste Disposal, Germany; *B. Schacherl*, Karlsruhe Institute of Technology, KIT, INE, Germany

The extent of covalent bonding in ionic compounds like oxides and halides is of considerable importance for their chemical properties; see, for example Refs. [1-2]. It is often estimated from population analyses either based on the original Mulliken formalism [3] or on more modern variants. [4-5] However, population analyses may have artifacts and be misleading. In contrast, we will be using a set of three criteria to estimate covalent character of orbitals in cluster models of compounds. [6] The methods are based on: (1) variation of orbital energies for different symmetry frontier orbitals; (2) estimates of the size of the orbitals as measured by an effective radius; and (3) projection of atomic orbitals. We examine the changes in covalency for two sets of compounds. The first set includes three nominally Ni(II) compounds: NiO, Ni(OH)<sub>2</sub>, and NiCO<sub>3</sub>. The second set are nominally oxidation state IV actinide dioxides UO<sub>2</sub>, NpO<sub>2</sub>, and PuO<sub>2</sub>. As well as the covalency for ground state WFs, we also consider the different covalent character of cations where a core electron has been ionized or excited. The wavefunctions are obtained as fully relativistic *ab initio* solutions of Dirac Hartree-Fock and many body configuration interaction solutions. It is shown that there are surprising departures from the nominal oxidation states and that the changes are not always consistent with intuitive views of the changes in the covalent character of the different compounds.

PSB acknowledges support by the U.S. Department of Energy, Office of Science, Office of Basic Energy Sciences, Chemical Sciences, Geosciences, and Biosciences (CSGB) Division through its Geosciences program at Pacific Northwest National Laboratory (PNNL). TV and BS acknowledge funding from the ERC Consolidator Grant 2020 under the European Union's Horizon 2020 research and innovation programme (grant agreement No. 101003292).

1. P. A. Cox, *Transition Metal Oxides: An Introduction to their Electronic Structure and Properties* (Clarendon Press, Oxford, 1992).
2. J. S. Griffith, *The Theory of Transition-Metal Ions* (Cambridge Press, Cambridge, 1971).
3. R. S. Mulliken, *J. Chem. Phys.*, 1955, **23**, 2343-2346.
4. J. Hernandez-Trujillo and R. F. W. Bader, *J. Phys. Chem. A*, 2000, **104**, 1779-1794.

5. A. E. Reed, R. B. Weinstock, and F. Weinhold, *J. Chem. Phys.*, 1985, **83**, 735-746.

6. P. S. Bagus, B. Schacherl, and T. Vitova, *Inorg. Chem.*, 2021, **60**, 16090.

## Vacuum Technology Division

### Room Oregon Ballroom 203-204 - Session VT-TuP

#### Vacuum Technology Poster Session

**VT-TuP-1 Measurements of NEG Pumping Performance at Cryogenic Temperatures**, *Sam Lodge, P. Smith, A. Chew, N. Burch*, Edwards Ltd, UK; *D. Clement, Gamma Vacuum; P. Jones, P. Lamb, E. Lucchetta, P. Milner*, Edwards Ltd, UK; *T. Sinha*, Gamma Vacuum

Non-evaporable Getter (NEG) pumps are well established as a passive pumping technique in UHV and XHV applications. Recent studies comparing pumping speeds, sticking probabilities and capacities of Ti-V-Zr-Hf alloys at ambient and LN<sub>2</sub> temperatures will be reported.

Comparisons will be made with reported increased single element Ti and Ti alloy getters pumping performance at reduced operating temperatures.

**VT-TuP-3 Boosting Pumping Speed Simulations of Sticky Vacuum Components**, *Stefan Kiesel, A. Trützscher, K. Bergner*, VACOM Vakuum Komponenten & Messtechnik GmbH, Germany

Transmission probabilities of gaseous species through vacuum components are commonly studied using molecular flow Monte-Carlo simulation software, like Molflow+ [1]. Particle transmittance depends on the sticking coefficient between particle and wall. Since the sticking coefficient is only roughly known and varies e.g. with temperature, wall surface materials, and surface coverage, a simulation is typically repeated for different sticking coefficients. Our recent publication has shown, the amount of necessary simulations may be reduced to one by counting the amount of wall hits of transmitted particles [2].

In the presented study, we have employed this novel technique to several geometries and developed simple calculations to evaluate NEG coated tubes.

[1] Recent developments of Monte-Carlo codes MolFlow+ and SynRad+, M. Ady, R. Kersevan, 10th Int. Particle Accelerator Conf., Melbourne, Australia - doi:10.18429/JACoW-IPAC2019-TUPMP037, <https://accelconf.web.cern.ch/ipac2019/papers/tupmp037.pdf>

[2] Boosting sticking-dependent transmission studies to a single TPMC simulation, S. Kiesel et al., *Vacuum*, Volume 210, April 2023, 111744 – doi: 10.1016/j.vacuum.2022.111744

**VT-TuP-4 Present Status of the SuperKEKB Accelerator Vacuum System**, *Yusuke Suetsugu, K. Shibata, T. Ishibashi, M. Shirai, S. Terui*, High Energy Accelerator Research Organization (KEK), Japan; *M. Yao*, High Energy Accelerator Research Organization (KEK), Taiwan; *K. Kanazawa, H. Hisamatsu*, High Energy Accelerator Research Organization (KEK), Japan

The vacuum system of the SuperKEKB main ring (MR) consisting of 7-GeV electron ring (HER) and 4-GeV positron ring (LER), and the damping ring (DR) for 1.1 GeV positrons in the middle of the injector linac have been working well as a whole since the first commissioning in 2016. The maximum stored beam currents of MR are 1.46 A and 1.14 A for the LER and HER, respectively, and that of DR is approximately 30 mA, as of June 2022. The pressure rises per unit beam current are decreasing steadily. The new vacuum components developed for the SuperKEKB have been working as expected. No clear electron cloud effect has been observed in the LER so far after applying magnetic fields in the beam direction to the beam pipes at drift spaces in 2017. The recent behavior of the LER pressure against the beam current is explained by considering thermal gas desorption induced by the beam as well as photon-stimulated gas desorption. The beam lifetime is mostly limited by the Touschek effect due to a narrow dynamic aperture rather than the vacuum pressure, that is, the Rutherford scattering and Coulomb scattering. The challenges followed by high beam currents, such as damages of beam-collimator heads, excess heating of beam pipes at wiggler sections and so on, have recently become prominent. During the long shutdown time since July 2022 (called LS-1), we are installing a new non-linear beam collimator to reduce the beam impedances of collimator systems, exchanging the damaged collimator heads, replacing a beam pipe for the HER injection region to improve the injection efficiency, and installing the bellows chambers with photon masks in the wiggler section, together with maintenance works of the Belle II detector. The operation of the SuperKEKB will resume at the end of 2023.

Here we will report the present status of the SuperKEKB vacuum system and the main works during the LS-1.

**VT-TuP-6 Complex Bend Vacuum Chamber for NSLSII-U**, *Robert Todd, M. Seegitz, P. Palecek*, Brookhaven National Laboratory; *M. Ferreira*, European Spallation Source, Sweden; *D. Hidas, A. Khan, V. Smaluk, T. Shaftan, S. Sharma*, Brookhaven National Laboratory

While the NSLSII synchrotron is a third-generation light source providing outstanding brightness and flux, there is a robust R&D program in place to upgrade to a fourth generation, or beyond, facility. Inherent in the so-called complex-bend magnet and lattice designs are significant limitations on the beam and exit slot apertures of the vacuum chamber. These restrictions and the need for the vacuum chamber to be mechanically aligned and decoupled from the magnets impose unique challenges. As part of the design process, a thorough survey of existing fourth generation machines was completed to look at existing design solutions for accommodating beam and for providing adequate conductance and pumping. For our chamber, the selected solution is not novel and utilizes an aluminum split clamshell design that has been done in many machines past and present. The adaptation of this design along with improved machining and welding should provide the most cost-effective solution. The geometrical and impedance solutions and structural and thermal modeling will be shown along with dynamic pressure simulations generated by Synrad and Molflow modeling code. With continuing changes in lattice and magnet parameters, a systematic, iterative approach to vacuum design has been implemented and will be presented.

# Wednesday Morning, November 8, 2023

## 2D Materials Technical Group

### Room C123 - Session 2D-WeM

#### 2D-Materials: Defects, Dopants, and Modifications

**Moderators:** Jin Myung Kim, University of California, Irvine, Stuart Parkin, MPI Halle

#### 8:00am 2D-WeM-1 Developing Quantum Photon Sources from 2D Semiconductor Materials, *Xuedan Ma*, Argonne National Laboratory INVITED

Optical photons are ubiquitous in quantum communication and storage applications due to their long coherence times and ease to travel over long distances. On-demand quantum photon sources that may emit single photons as quantum information carriers are especially sought after for quantum-related applications. In this talk, I will present our recent effort in the development of solid-state quantum photon sources based on low-dimensional semiconductor materials. By atomic defect creation [1,2] and local strain field engineering,[3-7] we demonstrate versatile approaches for efficient single photon generation and modulation.

References:

- [1] W. Wang et al, *ACS Nano*, 16, 21240 (2022)
- [2] Q. Qian et al. *ACS Nano*, 16, 7428 (2022)
- [3] M. I. B. Utama et al. *Nat. Commun.* 14, 2193 (2023)
- [4] X. Li et al. *J. Phys. Chem. C* 126, 20057 (2022)
- [5] D. J. Morrow et al. *Phys. Rev. B* 104, 195302 (2021)
- [6] W. Wang et al. *ACS Photon.* 7, 2460 (2021)
- [7] L. Peng et al. *Nano Lett.* 20, 5866 (2020)

#### 8:40am 2D-WeM-3 Bandgap Modulation of Graphene by Boron Nitride Doping, *Sergi Campos Jara*, Leiden University, The Netherlands; *L. Caputo*, Université Catholique de Louvain, Belgium; *T. Roorda*, *T. Benschop*, *A. Mozes*, Leiden University, The Netherlands; *V. Calvi*, *R. van Rijn*, Delft University of Technology, Netherlands; *M. P. Allan*, *I. M.N. Groot*, Leiden University, The Netherlands

Since its discovery, graphene has shown to exhibit remarkable electronic properties.<sup>1</sup> Numerous techniques have been devised to create high-performance devices by manipulating the bandgap in order to enhance their semiconducting properties.<sup>2</sup>

Doping has proven to be one of the most effective methods for bandgap engineering. Experimental and theoretical studies on graphene doping show the possibility of making p-type and n-type semiconducting graphene by substituting C atoms. Boron and nitrogen have been specifically studied during the last years due to the interesting insulating behavior of h-BN. Boron, nitrogen, and carbon can be atomically mixed to form various semiconducting, hexagonal, layered structures. Experimental and theoretical studies have indicated that BNC nanostructures show semiconducting properties with small bandgaps.<sup>2,3</sup> Low concentrations of borazine rings within the graphene structure can modify graphene's electronic properties to form a 2D semiconductor material with homogeneous patterns.<sup>4,5</sup> The intercalation of hexagonal BN (h-BN) within the graphene lattice has already been successfully achieved, however, segregation of both materials has been the main issue. Recent research has demonstrated that incorporating borazine-like molecules with carbon structures into graphene can result in reduced segregation of h-BN domains.<sup>5,6</sup> Herrera Reinoza et al. demonstrated a notable example by depositing hexamethylborazine onto Ir(111), which yielded numerous boron-nitrogen-carbon (BNC) domains exhibiting low BN segregation and an estimated bandgap ranging between 1.4 and 1.6 eV.<sup>6</sup>

To grow our boron nitride-doped graphene nanomaterial (Figure 1a) we first synthesized graphene via chemical vapor deposition (CVD) by cyclic exposures to 10<sup>-5</sup> mbar of ethylene for 10 minutes with subsequent annealing at 1100 K for 10 minutes. We have successfully doped our graphene by exposing it to hexamethylborazine right after the 3<sup>rd</sup> cycle of graphene synthesis. Auger electron spectroscopy depicted in Figure 1b demonstrated the presence of B, C and N in the sample. As depicted in Figure 1c, a bandgap was opened on our BN-doped graphene, forming a semiconductor material.

#### 9:00am 2D-WeM-4 Wafer-Scale Photoluminescence Enhancement for MoS<sub>2</sub> Monolayers Through Simple Wet-Chemical Defect Passivation in Acidic Hydrogen Peroxide Solution, *Dennis H. van Dorp*, IMEC Belgium; *L. van der Krabben*, Radboud University Nijmegen, Netherlands; *A. Brady-Boyd*, Aberystwyth University, UK; *C. Gort*, TU Darmstadt, Germany; *S. Arnauts*, *T. Nuytten*, *H. Medina Silva*, *E. Altamirano Sanchez*, IMEC Belgium; *J. Hofmann*, TU Darmstadt, Germany; *S. Brems*, IMEC Belgium

It is expected that in the 2030 timeframe, CMOS technology nodes could include not only Si based transistors, but also possible 'Beyond-CMOS' devices that are co-integrated with the classical CMOS-based solutions. The alternative devices could be used along CMOS for specific functions. For instance, devices are being explored that have two-dimensional transition-metal dichalcogenides (2D TMDCs) as their conduction channel.

While device processing strategies for conventional CMOS technologies are well established, the use of TMDCs as atomic channel material poses new problems. In such applications, both dry and wet etching are essential processing steps for nanodevice fabrication, e.g. for patterning, contacting, layer selective etching, and surface engineering purposes. In contrast to dry etching, that may induce surface damage in the form of chalcogenide vacancies, wet-chemical methods provide an attractive alternative that avoids the problem of surface damage. However, the atomic scale dimensions of the 2D layer require ultimate selectivity and control to maintain and/or improve the electronic and optical properties at wafer-scale level. To meet these goals, in-depth insight is needed in the compatibility of TMDC's with wet-chemical solutions.

In this work, we will show the first semiconductor ICP-MS results on the atomic-scale etching kinetics of MoS<sub>2</sub> in acidic solutions. Despite the very small dimensions of TMDC atomic layers, a surprisingly high chemical stability is demonstrated for both multilayer and monolayer MoS<sub>2</sub>. Controlled wet etching of the layers was achieved for dilute HCl/H<sub>2</sub>O<sub>2</sub> solutions without significantly modifying the surface chemistry. In addition, it was found that wet-chemical treatment of MoS<sub>2</sub> can dramatically enhance the photoluminescence properties on wafer-scale level using simple acidic solutions that contain a strong oxidizing agent.

We will show that wet-chemical processing can be utilized to significantly lower defect related non-radiative decay in the monolayers through passivation of sulphur vacancies. Room temperature PL measurements were used to optimize the passivation step. PL enhancements of up to 3 orders of magnitude were consistently achieved. Wafer-scale PL mapping showed good uniformity across the 2-inch wafer. Cryo-PL measurements confirmed effective defect passivation through the quenching of the bound exciton peaks.

The data presented indicate a good wet-chemical compatibility of the atomic layer TMDC material which is highly relevant for future developments in the CMOS industry.

#### 9:20am 2D-WeM-5 Metal-to-Semiconductor Transition Observed in the Surface Density of States of Ti-Te Layered Monoclinic Crystals via Forced Atmospheric Exposure, *Bishal Pokhrel*, *J. Quarnstrom*, *S. Shrestha*, *H. Helfrich*, *E. Echeverria*, *D. McIlroy*, *M. Borunda*, *A. Yost*, Oklahoma State University

Transition metal chalcogenides are promising 2D materials due to their unique properties and emerging phenomena such as charge density waves, superconductivity, ferroelectricity and ferromagnetism. Specifically the transition metal trichalcogenides of the form AX<sub>3</sub> (A=Ti, Zr, Hf, X=S, Se, Te) exhibit a quasi 1-D nature with anisotropic bandstructure which leads to preferential charge transport along the chain direction and minimal edge scattering effects suitable for fabricating high-performance devices. In this study, we examine the surface sensitivity of a high pressure grown Ti-Te transition metal chalcogenide using the chemical vapor transport (CVT) technique and study the surface changes in the sample upon exposure to air. The high-pressure growth results in the formation of silvery mirror-like sheets and nanowhiskers atypical of bulk 1T-TiTe<sub>2</sub> growth, which is usually black and non-reflective. The silvery materials are capable of mechanical

# Wednesday Morning, November 8, 2023

exfoliation via the scotch tape method and if left in atmosphere turn a darker color within a few hours. The crystal structure and size of the sheets are examined using X-Ray Diffraction (XRD), transmission electron microscopy (TEM), and select area electron diffraction (SAED). The material adopts a preferential (001) single crystalline nature with monoclinic structure and P2 1/m space group symmetry. Additionally, the SAED patterns show signs of a superlattice formation at the surface of the exposed layer. The local density of states (LDOS) of the in-situ exfoliated sample surface, measured using scanning tunneling spectroscopy (STS), exhibits a metallic to semi-conducting transition, with narrow gap, when exposed to atmosphere, suggesting the surface rapidly decomposes. The STM topography indicates a decrease in surface roughness after exposure to atmosphere reminiscent of ad-layer/s formation at the surface. X-ray photoemission spectroscopy confirms the surface of the exposed sample contains -OH, O<sub>2</sub>, -H, H<sub>2</sub>O ad-atom species. Stability and reactivity of such layered materials has been a field of interest to researchers lately as these materials have the ability for extreme sensitivity when incorporated into a gas sensor device. In the interest of optical and gas sensing we fabricate simple FET devices and measure the opto-electronic properties while exposing to different wavelengths of light and gases (CO<sub>2</sub>, H<sub>2</sub>, H<sub>2</sub>O, and N<sub>2</sub>).

9:40am **2D-WeM-6 Correlated KPFM and TERS Imaging to Elucidate Defect-induced Inhomogeneities in Oxygen Plasma Treated 2D MoS<sub>2</sub> Nanosheets**, *Sanju Gupta*, Penn State University

Modulating physical and chemical properties of two-dimensional (2D) transition metal dichalcogenides (TMDC) by defect-engineering induced by oxygen plasma is actively pursued. In this work, exfoliated 2D MoS<sub>2</sub> layers treated by medium power oxygen plasma for different times (0, 10, 20, 40, and 60 s) are investigated using Kelvin Probe Force microscopy and tip-enhanced Raman spectroscopy (TERS) besides micro-Raman and photoluminescence (PL) spectroscopy. Under oxygen plasma, defects (mono- and di-sulfur vacancies) and chemical oxidation is predominant from 0s (native defects) up to 40s, while etching becomes dominant beyond 40 s, for mono- (1L), bi- (2L), and tri- (3L) layer MoS<sub>2</sub> with optimal defect density for four- (4L) and more layers. While Raman spectra exhibited lattice distortion (broadening of phonon bands) and surface oxidation by the presence of sub-stoichiometric molybdenum trioxide MoO<sub>3</sub> (*i.e.*, MoO<sub>3-x</sub> or MoS<sub>x</sub>O<sub>2-x</sub>) the increased spectral weight of trions and quenching in PL spectra are observed with treatment time. The localized nanodomains (~20-40 nm) and aggregated vacancies as nanovoids and intermixed MoS<sub>2</sub>/MoO<sub>3-x</sub> alloy are identified in near-field Raman spectra. The atomic force microscopy also showed defects aggregation and Kelvin probe force microscopy revealed the work function (WF) increase from 4.98 eV to 5.56 eV, corroborating the existence of MoO<sub>3-x</sub> phase which enables doping and shift Fermi level. We also highlight the unique interaction between the gold substrate and the formed MoO<sub>3-x</sub> facilitating Mo<sup>6+</sup> cation reduction to lower oxidation (*i.e.*, Mo<sup>4+</sup>) thereby yielding intermediate oxidation states responsible for lower WF (*ca.* theoretical 6.3 eV for stoichiometric MoO<sub>3</sub>). Strong correlations among the work function, vibrational and optical responses are established while exploring the oxygen plasma-induced defects and changing the landscape on oxygen doping at the nanoscale with varying MoS<sub>2</sub> layers, which are useful for heterogeneous electrocatalysis and applicable to other 2D TMDCs.<sup>1</sup>

<sup>1</sup>S. Gupta, A. Johnston, and S. Khondaker, *J. Appl. Phys.* **131**, 164303 (2022) and references therein.

Corresponding author: [sgup77@gmail.com](mailto:sgup77@gmail.com) [<mailto:sgup77@gmail.com>]

11:00am **2D-WeM-10 Imaging Carrier Motion in Graphene Using Scanning Tunneling Potentiometry**, *V. Brar, Zachary Krebs*, University of Wisconsin - Madison

INVITED

In this talk I will show how scanning tunneling potentiometry (STP) can be used to directly image the motion of charge carriers in graphene, revealing the manner that they scatter off defects, pass through potential barriers, and generate Hall voltages. In the ballistic regime, STP imaging allows for the semi-classical motion of graphene quasiparticles to be visualized over large lengthscales, and for their incoming/scattered wavefunctions to be imaged locally. Near potential barriers, this allows for the direct observation of Landauer residual resistivity dipoles and scattering processes involving quasibound states. When magnetic fields are applied, the carriers generate a Hall field that can be quantified using STM, and near potential barriers they are observed to take a spiral-like trajectory in low fields, and form bound states around the potentials in the quantum hall regime. We also probe the carrier motion as the graphene is heated and the electrons enter a hydrodynamic phase. In this regime, STP can be used to image the new

fluid-like flow patterns of the electrons and quantify how those new flow properties reduce the macroscopic resistivity of the sample.

11:40am **2D-WeM-12 Interfacial Design of 2D Materials for Energy-Efficient Nanoelectronics**, *Huamin Li*, University at Buffalo

With the rise of graphene (Gr) since 2004, two-dimensional (2D) have been extensively explored for energy-efficient nanoelectronics due to their novel charge transport properties compared to conventional three-dimensional (3D) bulk materials. However, there are still challenges and issues for the practical implementation of 2D materials. Here from the perspective of interfacial design, we take 2D semiconducting MoS<sub>2</sub> as an example to review our recent research on energy-efficient nanoelectronics, ranging from synthesis, metal contact, and device demonstration. First, at the interface between MoS<sub>2</sub> and substrates, an interfacial tension can be induced during high-temperature chemical vapor deposition (CVD) synthesis. Due to a mismatch of thermal expansion coefficients, the interfacial tension creates an anisotropy of in-plane charge transport and leads to a self-formed nanoscroll structure [DRC 2019]. Second, at the interface between MoS<sub>2</sub> and metal contact, a monolayer h-BN decoration can enable novel manipulation of charge transport through quantum tunneling, in contrast with conventional thermionic emission [IEEE NMDC 2018; Adv. Mater. 2019]. Third, at the interface between MoS<sub>2</sub> and other 2D materials, band-to-band Zener tunneling and cold-source charge injection can be enabled, giving rise to a superior transport factor (<60 meV/decade) in transistor configurations. These novel charge transport can overcome the fundamental limitations of "Boltzmann tyranny", and realize tunnel transistors and cold-source transistors with sub-60-mV/decade subthreshold swings [IEEE IEDM 2020; ACS Nano 2020]. Fourth, at the interface between MoS<sub>2</sub> and ferroelectric or ionic dielectrics, excellent electrostatic gating leads to a superior body factor (<=1), and also improves the energy efficiency for transistor operation [Nano Express 2023].

12:00pm **2D-WeM-13 Substrate Van Der Waals Force Effect on the Stability of Violet Phosphorous**, *Sarabpreet Singh*, University of Georgia; *M. GhafariAsl*, University of Georgia; *H. Ko*, Cornell University; *S. Gamage*, University of Georgia; *R. Distasio Jr.*, Cornell University; *M. Snure*, Air Force Research Laboratory; *Y. Abate*, University of Georgia

The weak van der Waals (vdWs) forces between monolayers has been a unique distinguishing feature of exfoliable materials since the first isolation of graphene. However, the vdWs interaction of exfoliable materials with the substrate and how this interface force influences the interaction of vdWs materials with the surroundings have yet to be well understood. Here, we experimentally and theoretically unravel the role of vdWs forces between the recently rediscovered wide band gap p-type vdW semiconductor violet phosphorus (VP), with various substrates (including, SiO<sub>2</sub>, mica, Si, Au) and quantify how VP stability in air and its interaction with its surroundings is influenced by the interface force. Using a combination of infrared nanoimaging and theoretical modeling we find the vdWs force at the interface to be a main factor that influences how VP interacts with its surroundings. In addition, the hydrophobicity of the substrate and the substrate surface roughness modify the vdWs force there by influencing VP's stability. We found that VP can maintain its stability for a prolonged period if it is exfoliated on SiO<sub>2</sub> substrate, followed by mica and Au substrates, and is least stable when placed on a Si substrate. Our results could guide in the selection of substrates when vdW materials are prepared and more generally highlight the key role of interface force effects that could significantly alter physical properties of vdWs materials. Our findings can assist in the choice of substrates to exfoliate vdWs materials and emphasize the crucial impact that interface forces can have on altering the physical properties of exfoliable materials.

**Actinides and Rare Earths Focus Topic  
Room C124 - Session AC+AS+TH-WeM**

**Nuclear Safeguards, Forensics, Environmental Science, and Stewardship**

**Moderators:** *Paul Roussel*, AWE, *David Shuh*, Lawrence Berkeley National Laboratory, *Evgeniya Tereshina-Chitrova*, Charles University, Prague, Czech Republic

8:00am **AC+AS+TH-WeM-1 Simulation Tools for Improvement of the Fission Track Analysis Method for Nuclear Forensics**, *Itzhak Halevy*, Nuclear Engineering, Ben Gurion Uni. Be'er Sheva, Israel INVITED  
To answer nuclear forensics questions, we are developing new innovative techniques and approaches to make this analysis more reliable and

# Wednesday Morning, November 8, 2023

accurate. Currently, only trained researchers can analyze microscope images. Since this analysis is dependent on the researcher's own abilities and skills, it is obvious that different researchers will produce results that are slightly distinct. A new worker's certification period is quite long, and it must cover numerous examples from previously measured data as well as some that we can only predict. A good simulation software can aid with training and provide a tool for grading new researchers. [1] The fission tracks were simulated by Monte-Carlo software, GEANT4, which uses all the physics behind the nuclear fission tracks, such as thermal neutrons flux, fission cross-section, radiation time, particle size, enrichment, etc. In this study, our Trainer2.0 software calculates the tracks on our Lexan detector and its projection, according to the physical parameters like neutron flux, size of the particle, the isotope, and radiation time. The result is a "star" centered on the simulated particle. Our full software is written with MatLab code.

We can simulate an extreme condition and learn new aspect in the fission track technique. From the simulation we can learn about the proper amount of material to use as a sample in the FTA technique.

The simulation can predict and compared to the mini-bulk and the micro-bulk analysis.

New idea of using penetrating fluorescent colors give as the ability to scan our detector in 3D instead of 2D. In this case we used the Dapi marker as a first shoot, this marker is well known for biomedical research.

This new idea to investigate the FT Star more than just by his projection.

Identifying the length of the tracks and their distribution allow us to determine the element source isotope be the shape of "fission products distribution" and the density of the impurities in the source.

## References

[1] Halevy I., Admon U., Chinea-Cano E., Weiss A.M., Dzigal N., E. Boblil, Dagan M., Orion I. and Radus R. Investigations, Progress in Nuclear Science and Technology, 2018, v. 5; p. 175-178 3.3.

8:40am **AC+AS+TH-WeM-3 Characterizing Actinides in Subsurface Sediments for Contaminant Remediation, Carolyn Pearce, H. Emerson, Pacific Northwest National Laboratory; C. Delegard, TradeWind Services LLC**

**INVITED**

The nuclear weapons fuel cycle consists of front-end steps to produce, extract, purify, and engineer plutonium, and back-end steps to safely manage, prepare, and dispose of radioactive wastes. Waste processing has resulted in the release of actinides to the subsurface worldwide, including the release of ~200 kg of plutonium and ~7 Kg of americium from process waste solutions to unconfined soil structures at the Hanford Site in Washington State. The subsurface mobility of actinides is influenced by complex interactions with sediments, groundwater, and any co-contaminants within the waste stream. Developing efficient remediation strategies for released actinides requires a complete understanding of retardation processes and mass flux, including the different mechanisms by which actinides are immobilized in the subsurface, and the effect of localized subsurface conditions. Here, sediments from Hanford waste disposal sites have been selected, based on historical information and sediment composition, for characterization of actinide (plutonium, americium, and uranium) immobilization mechanisms. Results show that the actinides are present in these samples as micron-sized particles, intrinsic and pseudo-colloids, and dissolved species, and that they have been significantly affected by the chemistry of the actinide-bearing waste source term. Spectroscopic characterization of actinides has also proved essential to understand their migration in the deep, unsaturated, vadose zone sediments at the Hanford Site, due to the significant variability in solubility and mobility with speciation and oxidation state.

9:20am **AC+AS+TH-WeM-5 Changes in Oxidation Mechanism with Relative Humidity: Application to Uranium Dioxide Powders, Scott Donald, L. Davisson, Lawrence Livermore National Laboratory**

**INVITED**

It is of interest in nuclear forensic science to understand the relationship between an interdicted sample's history and the resulting chemical and physical characteristics. It may be possible to glean information on the environmental characteristics experienced by uranium dioxide from variations in the chemistry and structure of a powder sample. The reaction between high purity, stoichiometric  $UO_2$  powder over a range of nominal conditions at room temperature was studied using a range of techniques, including XPS, SEM, and TEM, to interrogate changes to both the surface and bulk properties of the material. Oxidation resulting from the interaction of the surface with the local environment was observed and quantified. A

change in the reaction mechanism between low and high relative humidity has been proposed to describe the observed results.

The work was performed under the auspices of the U.S. Department of Energy by Lawrence Livermore National Laboratory under Contract DE-AC52-07NA27344 and funded by the Office of Defense Nuclear Nonproliferation Research and Development within the U.S. Department of Energy's National Nuclear Security Administration. LNLN-ABS-848427

11:00am **AC+AS+TH-WeM-10 Spatially Resolved Morphological and Chemical Analysis of Nuclear Materials, Brandon Chung, A. Baker, S. Donald, T. Li, R. Lim, U. Mehta, D. Rosas, S. Sen-Britain, D. Servando-Williams, N. Cicchetti, Lawrence Livermore National Laboratory; A. Ditter, D. Shuh, Lawrence Berkeley National Laboratory (LBNL)**

Nuclear forensics requires accurate identification of distinguishing material characteristics of interdicted nuclear materials. Local morphological and chemical variations in nuclear materials are nearly ubiquitous due to the varying provenance, process, and pathways. We will describe our efforts to strengthen operational and scientific methodologies to employ the focused ion beam-scanning electron microscopy (FIB-SEM) on uranium (U) and plutonium (Pu) materials for direct three-dimensional (3D) morphological analysis or to prepare site-specific material features to obtain spatially resolved characterizations using transmission electron microscopy (TEM) and X-ray synchrotron spectromicroscopy. Both U and Pu materials show variations in the internal chemical composition and morphology from their production processes and storage environments. This information is of potential use in discriminating material signatures to identify the origin and history of interdicted nuclear materials

11:20am **AC+AS+TH-WeM-11 Soft and Tender Spectromicroscopy for Nuclear Forensics at the Advanced Light Source, David Shuh, A. Ditter, Lawrence Berkeley National Laboratory (LBNL); N. Cicchetti, University of Nevada Las Vegas; R. Lim, S. Sen-Britain, D. Rosas, D. Servando-Williams, A. Baker, S. Donald, B. Chung, Lawrence Livermore National Laboratory**

The development of new methods and signatures is crucial to ensure that nuclear forensics activities remain effective. Synchrotron radiation analysis offers one way to extend the scope of forensics investigations in elemental, chemical, and structural analysis which all can be done in imaging modes that in some cases, reaches to the nanoscale. X-ray techniques are particularly useful because of their elemental specificity and non-destructive nature. The ability to use tunable, focused beams makes synchrotron radiation sources a potentially key tool for addition into the array of characterization techniques currently employed, particularly when it comes to the investigation of particles or areas of interest in smaller specimens. Recent efforts at the Advanced Light Source conducting tender and soft spectromicroscopy using x-ray fluorescence (XRF; Beamline 10.3.2) and a scanning transmission x-ray microscope (STXM; Beamline 11.0.2). The XRF measurements provide elemental analysis at the micron scale, whereas the STXM can probe chemical speciation with a spatial resolution of better than 25 nm. Several uranium and plutonium specimens have been investigated using these techniques and the potential signatures from this data, as well as its utility, will be demonstrated. The outlook for synchrotron radiation within nuclear forensics including the strengths and drawbacks of these techniques will also be discussed.

## Atomic Scale Processing Mini-Symposium

### Room A107-109 - Session AP+PS+TF-WeM

#### Plasma Deposition and ALD Processes for Coatings and Thin Films

**Moderators:** Silvia Armini, IMEC, Belgium, Jessica Kachian, Intel Corporation

8:00am **AP+PS+TF-WeM-1 Recent Progress in Analysis of the Conformality of Films by Atomic Layer Deposition, Riikka Puurunen, Aalto University, Finland**

**INVITED**

Conformality is a fundamental characteristic of atomic layer deposition (ALD) thin film growth technique. "Conformal" film refers to a film that covers all surfaces of a complex three-dimensional substrate with everywhere the same thickness and properties. ALD - invented independently by two groups in 1960s and 1970s - has since late 1990s been transformational in semiconductor technology. Apart from semiconductors, conformal ALD films find applications and interest in widely varied fields such as microelectromechanical systems,

# Wednesday Morning, November 8, 2023

pharmaceutical powder processing, optical coatings, battery technologies and heterogeneous catalysts.

Conformality follows directly from the “ideal ALD” principles: growth of material through the use of repeated separate self-terminating (i.e., saturating and irreversible) gas-solid reactions of at least two compatible reactants on a solid surface. Obtaining conformality in practice is not self-evident, however. Reasons for deviation from conformality are multiple, ranging from mass transport limitations to slow reaction kinetics and various deviations from ideal ALD (e.g., by-product reactivity or a continuous chemical vapor deposition (CVD) component through reactant decomposition or insufficient purging). Incomplete conformality can also be intentional: a saturation profile inside a feature can be exposed, to enable an analysis of kinetic parameters of the reactions.

This invited talk will explore recent progress especially by the author and collaborators in understanding ALD conformality and kinetics, obtained via experiments and simulations. Experiments have been made with the recently commercialized (chipmetrics.com) silicon-based PillarHall™ lateral HAR test chips (channel height ~500 nm) and spherical mesoporous high-surface-area materials (average pore diameter ~10 nm, sphere diameter ~1 mm). Simulations are presented for 1d feature-scale models and optionally a recently developed 3d code for spheres. Two codes are available on GitHub: DReaM-ALD (diffusion-reaction model, DRM) and Machball (ballistic transport-reaction model, BTRM). Often it is assumed that diffusion during an ALD process in HAR features is by Knudsen diffusion and free molecular flow conditions prevail ( $Kn \gg 1$ ). If so, a characteristic “fingerprint saturation profile” can be obtained, and the slope method (derived for DRM-ALD-Arts, GitHub) can be used to back-extract the lumped sticking coefficient. When diffusion is in the transition flow ( $Kn \sim 1$ ) or continuum flow ( $Kn \ll 1$ ), the shape of the saturation profile depends on process conditions and the slope method is not applicable.

**8:40am AP+PS+TF-WeM-3 ALD Temperature Cycling for Uniform Infilling of Macroscopic Nanoporous Solids, Benjamin Greenberg, K. Anderson, A. Jacobs, J. Wollmershauser, B. Feigelson, U.S. Naval Research Laboratory**  
Uniform ALD infilling of macroscopic nanoporous solids with aspect ratio greater than  $10^4$  can require precursor dose times on the order of  $10^3$  seconds, at least four orders of magnitude longer than typical dose times for ALD on wafers. For ALD processes based on relatively stable precursors and straightforward chemistries, such as ALD of  $Al_2O_3$  from trimethylaluminum (TMA) and  $H_2O$ , very long doses are generally harmless, but for some ALD processes, precursor decomposition and other side reactions are significant concerns. For example, at a deposition temperature of 180 °C, which has been chosen previously for ZnO ALD infilling to ensure rapid removal of  $H_2O$  from nanopores during purging,<sup>1</sup> diethylzinc (DEZ) decomposition<sup>2</sup> and surface Zn deethylation<sup>3</sup> may be substantial on the  $\sim 10^3$  s timescale.

In this work, we investigate the potential of temperature cycling as a route toward rapid yet controlled infilling of macroscopic nanoporous solids. We infill  $Al_2O_3$  nanoparticle compacts of  $\sim 1.5$  mm thickness and  $\sim 100$  nm pore size (aspect ratio  $> 10^4$ ) with ZnO using DEZ and  $H_2O$  as precursors, and we cycle the substrate temperature between  $\sim 160$  °C (during  $H_2O$  purges) and  $\sim 120$  °C (during all other steps). DEZ infiltration is accomplished via static dosing, wherein DEZ vapor is held in the ALD chamber for  $> 10^3$  seconds with the pump valve closed so that, in principle, diffusion/reaction and saturation are observable as a rise (due to byproducts) and flattening of the ALD chamber pressure, respectively. The 120/160 °C cyclical-temperature process produces clear saturation signals in the pressure trace, whereas fixed-temperature processes carried out entirely at 120 or 160 °C do not, apparently due to incomplete  $H_2O$  removal at 120 °C and DEZ decomposition and/or other side reactions at 160 °C. We use a variety of characterization techniques, including SEM/EDS, XRD, and electrical conductivity measurements, to assess the uniformity and purity of the ZnO infills.

1. A. Cendejas, D. Moher, and E. Thimsen, *J. Vac. Sci. Technol.* A **39**, 012406 (2021).
2. J. D. Ferguson, A. W. Weimer, and S. M. George, *J. Vac. Sci. Technol.* A **23**, 118 (2005).
3. T. Weckman and K. Laasonen, *J. Phys. Chem. C* **122**, 7685 (2018).

**9:00am AP+PS+TF-WeM-4 Plasmonic Plasma Process for Room Temperature Growth of High-quality Ultra-thin Dielectric Films, Takeshi Kitajima, M. Miyake, National Defense Academy, Japan; K. Watanabe, National Defense Academy, Japan; T. Nakano, National Defense Academy, Japan**

Catalytic surface reactions utilizing gold nanoparticle plasmons have been utilized in various applications in recent years.<sup>1</sup> We have applied hot electrons supplied from gold nanoparticles to plasma surface reactions to use them to form high-quality ultrathin dielectric films at room temperature.<sup>2</sup> We focused on the mixed effect of visible light for plasmon excitation and plasma VUV emission and discovered the effect of green light excitation that promotes radical nitriding. Due to the mercury probe measurement and TEM imaging, the film grown have superior dielectric feature and uniformity with less plasma induced damage in spite of nonuniform formation of gold nanoparticles.

In the growth sequence, Au was vapor-deposited on a  $SiO_2 / Si$  (100) substrate in an ultra-high vacuum chamber with an average thickness of 0.4 nm by electron beam deposition to form Au nanoparticles (C) on the surface. A 30 mTorr  $N_2$ -inductively coupled plasma was generated in the attached chamber, and the sample was irradiated with N radicals (R) that passed through a 30 line/inch SUS304 single mesh with the configuration shown in Fig. 1 (a) for 5 minutes. A filter and a white LED controlled the wavelength of light (L), and VUV light from  $N_2$  plasma was mixed. The reaction condition consisting of the above is RLC. Figure 1 (b) shows the dielectric characteristics of the SiON film (leakage current and EOT (equivalent oxide film thickness) when 1 V is applied). In green light suitable for Au plasmons, the hot electrons ( $\sim 4$  eV) generated by the deexcitation of plasmons enabled the bond conversion from Si-O to Si-N in the ultra-thin SiON shows the same characteristics as the ideal SiON film. By mixing VUV, it is possible to increase the film thickness further and reduce leakage.

Cross-sectional TEM image of SiON film after plasmonic process is shown in Fig. 1 (c). Beneath the Au particle SiON film with wide range of uniformity is confirmed and the single crystal lattice of Si substrate is clearly identified.

From the above, it is considered that the reaction between the adsorbed N radicals and Si proceeded, and a quality SiON film was formed by superimposing the photoelectron emission from the VUV light on the hot electron injection from the gold nanoparticles by green light irradiation.

1 C. Clavero, *Nat. Photonics* **8**, 95 (2014).

2 T. Kitajima, M. Miyake, K. Honda, and T. Nakano, *J. Appl. Phys.* **127**, 243302 (2020).

**9:20am AP+PS+TF-WeM-5 Time Resolved Energy Diagnostics of HiPIMS Discharges With Positive Cathode Reversal, Zachary Jeckell, T. Choi, M. Hassain, D. Kepekyan, N. Vishnoi, University of Illinois at Urbana Champaign; B. Jurczyk, Starfire Industries; D. Ruzic, University of Illinois at Urbana Champaign**

This work investigates the temporal evolution of a high-power impulse magnetron sputtering (HiPIMS), with a positive cathode reversal, discharge by using the Hidden ANALYTICAL PSM probe that can measure the ion energies as well as perform charge to mass (q/m) measurements. This work builds off other diagnostic work done on the chamber such as time resolved electron energy distribution functions from our time resolved Langmuir probe technique, previous work with measuring ion energy distribution functions using the SEMION probe, as well as preliminary measurements taken with the PSM probe. This work was performed on several different target materials such as Ag, Ti, ZnTe, and W. The diagnostic capabilities of the PSM allows for differentiation between the working gas and target material ions which enables us to calculate the ratio of target ions for a given condition. Previous work we have done has shown that at early stages of the positive cathode reversal there is an elevated population of metal ions and that the overall fraction of metal to working gas fraction is at its highest. Time and energy resolved mass spec data was collected on this system for a variety of conditions such as pulse lengths, pressures, and target material with the objective of developing a better understanding for the energetics at play. Additionally, by running the PSM with the filament on and a properly set repelling voltage it was possible to get a sense of the neutral energies as well. This required a deconvolution of the energy that the neutrals gain from the ionization from the filament. The goal was to use the results of those experiments to build a framework of understanding and

# Wednesday Morning, November 8, 2023

to use that information to deposit better films, such as increasing the hardness of TiN, reducing the resistivity of N doped ZnTe, improving the crystallinity of W films or improving the optical properties of a Ag thin film.

9:40am **AP+PS+TF-WeM-6 Electron-Enhanced ALD of TiO<sub>2</sub>, TiN, and TiCN at Low Temperature Using TDMAT Together with O<sub>2</sub> and NH<sub>3</sub> Reactive Background Gas**, Z. Sobell, A. Cavanagh, Steven George, University of Colorado Boulder

Electron-enhanced atomic layer deposition (EE-ALD) was utilized for the growth of TiO<sub>2</sub>, TiN, and TiCN films at T < 70 °C. Three Ti-based films were grown using sequential exposures of tetrakis(dimethylamido) titanium (TDMAT) precursor and electrons together with a continuous reactive background gas (RBG) (Figure 1). The electrons accelerated across a grid bias of 100 V desorb surface species by electron stimulated desorption. The electrons also dissociate the RBG as they travel to the substrate. The RBGs utilized to tune the film composition were oxygen (O<sub>2</sub>) for TiO<sub>2</sub> and ammonia (NH<sub>3</sub>) for TiN and TiCN.

TiO<sub>2</sub> EE-ALD was performed at T < 70 °C using TDMAT together with an O<sub>2</sub> RBG at ~1 mTorr. O<sub>2</sub> is believed to be dissociated by the electron beam, creating O radicals that add oxygen to form TiO<sub>2</sub> and remove N and C from the TDMAT precursor. XPS showed no detectable C or N in the TiO<sub>2</sub> films and a slightly O-rich stoichiometry. Oxygen-rich TiO<sub>2</sub> films may be more photochemically active due to bandgap narrowing and could be useful in photocatalysis.

TiN EE-ALD was conducted at T < 70°C using TDMAT together with an NH<sub>3</sub> RBG at a pressure of ~1 mTorr. NH<sub>3</sub> is believed to be dissociated by the electron beam, liberating H and NH<sub>x</sub> radicals that facilitate Ti nitridation and C removal from the film. Electron exposures for 20 seconds led to the rapid nucleation of TiN films with purities of > 96% and ultralow resistivities of < 120 μΩ-cm. These films may be useful as diffusion barriers in backend interconnects.

Incomplete C removal resulted from shorter electron exposures during TiN EE-ALD using TDMAT with NH<sub>3</sub> RBG. This carbon residual provides a pathway for the deposition of TiCN, an important amorphous ternary nitride diffusion barrier. TiCN EE-ALD film growth and properties were explored for electron exposure lengths from 20 seconds to 0.5 seconds. Shorter electron exposures led to an increase of the C:Ti ratio from ~0.03 to ~0.33 as measured by x-ray photoelectron spectroscopy (XPS) (Figure 2). Shorter electron exposures also produced a decrease in film density from ~5.3 g/cm<sup>3</sup> to ~3.3 g/cm<sup>3</sup>. In addition, shorter electron exposures yielded an increase in the film resistivity from < 120 μΩ-cm to ~2000 μΩ-cm as measured by ex situ spectroscopic ellipsometry (SE). Consequently, the enhanced diffusion barrier properties of TiCN EE-ALD films will be accompanied by higher film resistivities and lower film densities than TiN EE-ALD films.

11:00am **AP+PS+TF-WeM-10 A Non-Violent Approach to Remove SiN:H Surface Impurities (HCl) at Room Temperature**, Tsung-Hsuan Yang, T. Wang, G. Hwang, University of Texas at Austin; P. Ventzek, J. Zhao, Tokyo Electron America, Inc.

Our research presents a non-violent approach to remove H<sup>+</sup>/Cl<sup>-</sup> pairs, a common reaction byproduct, after depositing chlorosilane-type Si precursors (such as dichlorosilane, SiH<sub>2</sub>Cl<sub>2</sub>) on a SiN surface. While previous studies have suggested the use of H radicals in NH<sub>3</sub> and CH<sub>3</sub>NH<sub>2</sub> plasma to remove Cl impurities, these methods have limitations in high-aspect-ratio structures. The recombination rate of radicals may be too fast to reach the bottom of the trench, resulting in the accumulation of Cl and possibly the formation of a salt layer that inhibits further film growth. Through first-principles calculations, we propose an alternative solution by introducing polar molecules, such as NH<sub>3</sub>, N<sub>2</sub>H<sub>4</sub>, CH<sub>3</sub>NH<sub>2</sub>, and (CH<sub>3</sub>)<sub>2</sub>NH. When these polar molecules are dosed onto the surface, they can first abstract the H<sup>+</sup> from the H<sup>+</sup>/Cl<sup>-</sup> pair to form a complex with Cl<sup>-</sup>. Adjacent polar molecules then solvate the complex, forming a stable "microsolvation cluster." This cluster effectively captures Cl<sup>-</sup> while weakening the interactions between Cl<sup>-</sup> and surface amine groups, providing a pathway for HCl desorption with a lower energy barrier. Our calculations of free energy surface show that when the surface is saturated with CH<sub>3</sub>NH<sub>2</sub> molecules, the energy barrier for HCl desorption can be significantly reduced at 300K. Based on these promising findings, we propose a novel and non-aggressive atomic layer deposition (ALD) scheme to grow SiN at low temperatures while achieving a higher growth rate.

11:20am **AP+PS+TF-WeM-11 Influence of Plasma Species on the Growth Kinetics and Properties of Epitaxial InN Films Grown by Plasma-Enhanced Atomic Layer Deposition**, Jeffrey Woodward, D. Boris, U.S. Naval Research Laboratory; M. Johnson, Huntington Ingalls Industries; S. Walton, U.S. Naval Research Laboratory; S. Rosenberg, Lockheed Martin Space Advanced Technology Center; J. Hite, M. Mastro, U.S. Naval Research Laboratory

The controlled co-delivery of reactive and energetic plasma species during plasma-enhanced atomic layer deposition (PEALD) enables the growth of epitaxial layers at significantly reduced temperatures which are prohibitive to other methods. However, this capability is challenged by the complexity which arises from the reliance on plasma-surface interactions, and it is thus necessary to understand the influence of the plasma properties on the growth kinetics and resultant film properties. Among the III-nitride binary compounds, indium nitride (InN) is particularly well-suited for the investigation of the roles of reactive and energetic plasma species, as high-quality crystalline films can be achieved using trimethylindium (TMI) and a relatively simple N<sub>2</sub>/Ar plasma rather than N<sub>2</sub>/Ar/H<sub>2</sub> or NH<sub>3</sub>/Ar plasmas which generate greater varieties of species. This was explored in recent studies of InN PEALD on gallium nitride (GaN) using *in situ* synchrotron x-ray scattering, which revealed that the growth mode is correlated with the relative density of atomic N, while coarsening behavior is influenced by ion flux.[1]

In this work, epitaxial InN films are grown by PEALD on GaN (0001) at approximately 320 °C using TMI and N<sub>2</sub>/Ar plasma within various regimes of plasma species generation in order to investigate the influence on the resultant film properties. Optical emission spectroscopy and Langmuir probe measurements are used to correlate the production of atomic N and ions with the N<sub>2</sub> and Ar gas flows into the inductively coupled plasma (ICP) source. The InN films are characterized by atomic force microscopy (AFM), x-ray reflectivity (XRR), high-resolution x-ray diffraction (HRXRD), in-plane grazing incidence diffraction (IP-GID), synchrotron grazing incidence wide-angle x-ray scattering (GIWAXS), and x-ray photoelectron spectroscopy (XPS). The films are found to exhibit wurtzite phase and sixfold rotational symmetry with a clear epitaxial relationship to the GaN. Low fluxes of atomic N are found to promote larger domains, increased crystalline order, and smoother morphology compared to films grown with high atomic N fluxes. For the high atomic N flux condition, increasing ion flux is found to promote a very rough morphology containing large cluster-like features and decreased in-plane crystalline order, but increased out-of-plane crystalline order and a reduction in mosaic twist.

[1] J. M. Woodward *et al.*, J. Vac. Sci. Technol. A **40**, 062405 (2022)

11:40am **AP+PS+TF-WeM-12 One Step Synthesis of Patterned Coatings Using Immobilized Filaments in an Atmospheric Pressure Dielectric Barrier Discharge. Effect of Gap and Power Pulsing**, M. Brabant, Annaëlle Demaude, D. Petitjean, Université Libre de Bruxelles, Belgium; K. Baert, T. Hauffman, Vrije Universiteit Brussel, Belgium; M. Gordon, University of California Santa Barbara; F. Reniers, Université Libre de Bruxelles, Belgium

Deposition of patterned coatings to generate hybrid surface properties often require a multi-step process, such as the use of masks or lithography [1]. We proposed recently a simple scalable method for the deposition of patterned coatings (morphological and chemical contrasts) [2]. As a case study, the deposition of propargyl methacrylate (PMA) based-coatings was realized, as, due to its structure (one double and one triple bond), this molecule allows very fast deposition, and can lead to hydrophobic coatings, without the need of fluorinated atoms. Moreover, we showed that, depending on the deposition conditions, one could obtain hybrid hydrophilic/hydrophobic patterns.

To test the flexibility and the limits of the method, we now investigate further this route and try to understand better the effects of the gap between the electrodes and of the pulsed/non pulsed injection of the power. The deposited coating was characterized using μ-XPS, FTIR and contact angle measurements, whereas the discharge was characterized using a high intensity camera, electrical measurements (oscilloscope and Rogowski coil), and mass spectrometry. Due to the DBD configuration, the coating exhibits two distinct areas : the spot (S) area, corresponding to the coating deposited under the filament position, and the between spot (BS) area, corresponding to the coating deposited outside the filament position.

Filaments are immobilized thanks to beads fixed to one of the dielectrics, reducing locally the gap and therefore igniting specifically the discharge at these locations. Here the gap was fixed at 2, 2.5 and 3 mm. It is shown (using a high intensity camera, and electrical measurements) that an increase in gap leads to more energetic discharges inside the filaments. As shown by XPS, this leads to a lower preservation of the precursor structure

# Wednesday Morning, November 8, 2023

for the “S”area coating. In parallel, due to higher voltages needed to light up the discharge, surface discharges take place between the filaments leading to subsequent deposition also between the spots located under the filaments.

Pulsing the power (in the ms range) leads to more localized filaments, to a global change in the plasma behavior and to a change in the coating chemistry [3].

References :

- [1]. A. Demaude *et al.*, *Langmuir*, 2019, 35 (30), 9677–9683
- [2] A. Demaude *et al.*, *Advanced Science*. 2022, 9 (15), 2200237
- [3] A. Demaude *et al.*, *Plasma Chemistry and Plasma Processing*, submitted.

12:00pm **AP+PS+TF-WeM-13 Effect of Bias Pulsed Plasma Enhanced Atomic Layer Deposition for Void-Free SiO<sub>2</sub> Gap-Fill of High Aspect Ratio Trench Structures**, *Ye Ji Shin, H. Kim, G. Yeom*, Sungkyunkwan University, Korea

In 3-dimensional (3D) device structures, cells are getting thinner and higher to increase the density of devices which resulted in High Aspect Ratio (HAR) structures. Gap-fill process is one of the processes that could affect the device performance of HAR trench structures. Void and seam are observed after the gap-fill process and they allow penetration of the chemical etchant used in subsequent processes, and which degrades isolation performance and increases leakage currents. To solve this issue, various processes such as thermal ALD processes with inhibitors, plasma enhanced ALD with substrate biasing, etc. have been used but, with increasing the aspect ratio of the structure, it is found to be difficult to fill the gap completely without void or seam in the trench. In this study, bias power with pulsing was introduced to PEALD processes for void and seam free SiO<sub>2</sub> gap-filling. Pulsed bias power with various pulse duty ratio from 30 to 75% were used and compared with continuous wave (CW) bias power and no bias power to identify the effect of bias pulsing. The results showed that, as the bias pulse duty ratio was decreased, void and seam were decreased and disappeared at HAR trench structures even with negative bowing. The pulse biasing with low duty ratio appeared to open the opening of the trench top while the pulse biasing with high duty ratio and CW biasing operation appeared to close the opening of the trench top possibly due to differences in combined effect of ion bombardment flux and deposition. Eventually, void-free SiO<sub>2</sub> gap-fill for HAR trench structures were obtained with bottom-up filling under the pulsed bias conditions. Detailed experimental results and analysis data will be shown in the presentation.

## Applied Surface Science Division

Room **B117-119** - Session  
**AS+2D+CA+EL+EM+MS+NS+SE+SS+TF-WeM**

### Multi-Modal & Multi-Dimensional Analysis

**Moderators:** *Gustavo Trindade*, National Physical Laboratory, UK, *Paul Mack*, Thermo Fisher Scientific, UK, *Tim Nunney*, Thermo Fisher Scientific, UK

8:00am **AS+2D+CA+EL+EM+MS+NS+SE+SS+TF-WeM-1 Growth and Characterization of Large-Area 2D Materials**, *Glenn Jernigan*, US Naval Research Laboratory **INVITED**

Nothing could be more coupled than Growth and Characterization. When two dimensional (2D) materials appeared on the radar of the scientific community (with the amazing properties of graphene), it was immediately obvious that large area samples would be needed. Exfoliating flakes was insufficient for the demands of scientific studies, in addition to not being viable should a commercial application be developed. Thus, the search began for growth methods to produce large-area 2D materials for large scale testing and development.

The Naval Research Laboratory has, over the past 15 years, pursued research programs in producing large areas of graphene, transition metal dichalcogenides (TMDs), boron nitride (BN), and other 2D materials. In every one of those programs, they began with surface analysis of composition, chemistry, and morphology of the grown films. The uniquely sensitive nature of x-ray and ultraviolet photoelectron spectroscopy (XPS and UPS) and scanning tunneling and atomic force microscopy (STM and AFM) to 2D materials was necessary to measure the electrical, chemical, and physical properties obtained in the large area films and to understand what was observed in the exfoliated flakes. The production of large areas allowed “mass-scale” optical and electrical characterization, which then became a feedback loop in the search for new and interesting properties

Wednesday Morning, November 8, 2023

and relevant applications. In this presentation, I will show how we developed large-area graphene, by both epitaxial growth and chemical vapor deposition methods, TMDs, and other 2D materials for characterization and device utilization.

8:40am **AS+2D+CA+EL+EM+MS+NS+SE+SS+TF-WeM-3 Using a Correlative Approach with XPS & SEM to Measure Functionalized Fabrics for Antimicrobial Applications**, *Tim Nunney, H. Tseng*, Thermo Fisher Scientific, UK; *D. Marković, M. Radetić*, University of Belgrade, Serbia

Medical textiles are an indispensable component for a wide range of hygienic and healthcare products, such as disposable surgical gowns and masks, or personal protection equipment, with opportunities to provide further protection by engineering textiles with suitable medical finishing. While antibiotics are considered a viable option for their efficiency in treating bacterial infections, their abuse can result in adverse effects, e.g., bacteria resistance. Nanocomposites have emerged as a promising alternative to antibiotics, as the large surface-to-volume ratio and high activity helps attain the targeted antimicrobial efficiency by using tiny amounts of nanocomposites, and their biocompatibility and scalability are particularly advantageous for medical applications [1]. Thus, developing processing methods to integrate nanocomposites in the fabrics is essential for exploiting their properties for medical textiles.

In this study, polypropylene fabrics, alginate and copper oxides, were selected to develop novel antimicrobial nanocomposites based on various surface treatments, i.e. corona discharge and alginate impregnation, which led to improved fabrics hydrophilicity with functional groups introduced as binding sites for Cu(II), a precursor that formed Cu nanoparticles when reacted with reducing agents, i.e. NaBH<sub>4</sub> and ascorbic acid. The composition of the fabrics after being treated with corona discharge and impregnation observed by XPS indicates the materials formed mainly consisted of C and O, attributed to the presence of a thin, hydrophilic layer and alginate, respectively, consistent with depth profiling measurements. Following Cu reduction, XPS mapping of the fabrics finds that, reacting with ascorbic acid resulted in formation of nanocomposites containing a mixture of Cu and Cu (II) oxides across the surface, which could be visualised by using SEM in the same locations. Excellent anti-microbial activity against Gram-negative bacteria *E. coli*, Grampositive bacteria *S. aureus* and yeast *C. albicans* was observed for the treated fabrics[2]. This result not only demonstrates a cleaner, and healthier approach for developing novel nanocomposites, but more importantly highlights the role of surface techniques in uncovering challenges in designing and engineering functional textiles.

References:

- [1] D. Marković, J. Ašanin, T. Nunney, Ž. Radovanović, M. Radoičić, M. Mitrić, D. Mišić, M. Radetić, *Fibers. Polym.*, 20, 2317–2325 (2019)
- [2] D. Marković, H.-H. Tseng, T. Nunney, M. Radoičić, T. Ilic-Tomic, M. Radetić, *Appl. Surf. Sci.*, 527, 146829, (2020)

9:00am **AS+2D+CA+EL+EM+MS+NS+SE+SS+TF-WeM-4 Multi-Modal Analysis in Photoelectron Spectroscopy: From High-Resolution Imaging to Operando Experiments**, *Olivier Renault*, CEA-Leti, France; *A. Benayad*, CEA, France; *N. Gauthier*, CEA-Leti, France; *R. Charvier*, ST Microelectronics, France; *E. Martinez*, CEA-Leti, France

Over the past years, the field of surface and interface analysis has been greatly expanded by new developments made possible by lab-scale instruments enabling higher excitation energies. These new developments are directly serving technological advances especially in the area of technologies in renewable energies and nanoelectronics, which are addressing more and more complex system requiring to go beyond traditional ways of characterizing surfaces and interfaces. Different dimensions are to be explored in multi-modal surface analysis : the depth dimension, the lateral dimension, and the dynamic dimension.

After a short review of some of the achievements towards enhancing the depth dimension by lab-scale hard X-ray photoelectron spectroscopy (HAXPES) and the lateral dimension using X-ray PEEM, we will present different application cases of *operando* HAXPES. Here, the material is analyzed as being part of a device operated *in situ* during the experiment, in conditions that are as close as possible to the final applications and

# Wednesday Morning, November 8, 2023

where the interfaces can be studied in dynamic conditions. We will first review some results of *operando* HAXPES on resistive memories obtained with synchrotron radiation [1, 2] before presenting various lab-scale experiments [3, 4] and the current limitations to such approaches.

[1] B. Meunier, E. Martinez, O. Renault et al. *J. Appl. Phys.* **126**, 225302 (2019).

[2] B. Meunier, E. Martinez, O. Renault et al., *ACS Appl. Electron. Mater.* **3** (12), 5555–5562 (2021).

[3] O. Renault et al., *Faraday Disc.* **236**, 288–310 (2022).

[4] A. Benayad et al., *J. Phys. Chem. A* 2021, 125, 4, 1069–81.

9:20am **AS+2D+CA+EL+EM+MS+NS+SE+SS+TF-WeM-5 Multi-Modal Analyses of Ultrasonic-Spray-Deposited Ultrathin Organic Bathocuproine Films**, *J. Chen, Juliet Risner-Jamgaard, T. Colburn, A. Vaillonis, A. Barnum, M. Golding*, Stanford University; *K. Artyushkova*, Physical Electronics; *R. Dauskardt*, Stanford University

Bathocuproine (BCP) is a small organic molecule that is typically used as an ultrathin hole blocking interlayer (< 10 nm thickness) in organic solar cells and perovskite solar cells. The film is typically deposited via low-throughput vacuum thermal evaporation with an *in-situ* Quartz Crystal Monitor to measure film thickness. Open-air ultrasonic spray deposition for low-cost and large-scale deposition is an attractive alternative method for solution processing of BCP films, but the process lacks a comparable *in-situ* metrology. Given that the BCP film is transparent to visible light and ultrathin, it is important to utilize a multi-modal approach to evaluate optoelectronic and physical properties of the sprayed film.

A suite of characterization techniques that span a range of equipment complexity, measurement time, and measurement sensitivity are used to analyze the BCP films. We begin by demonstrating the limitations of the singular ellipsometry model<sup>1</sup> for BCP found in literature and motivate a need to rely on other techniques. Multi-modal analyses including X-Ray Reflectivity, Angle-Resolved X-ray Photon Spectroscopy (AR-XPS), Auger Spectroscopy, Scanning Electron Microscopy, and Transmission Electron Microscopy with EELS are then performed on the sprayed BCP film. The advantages and disadvantages of each characterization technique are compared and discussed. We conclude that AR-XPS provides the most distinctive determination of individual layer thicknesses for a sample architecture consisting of silicon substrate/native SiO<sub>2</sub>/BCP across the applicable range of AR-XPS from ~ 1–10 nm.

<sup>1</sup>Liu, Z.T., et al. The characterization of the optical functions of BCP and CBP thin films by spectroscopic ellipsometry. *Synthetic Materials*. 150(2):159–163. (2005)

9:40am **AS+2D+CA+EL+EM+MS+NS+SE+SS+TF-WeM-6 Combinatorial Synthesis and High-Throughput Characterization of Pt-Au Thin Films Fabricated by Confocal Magnetron Sputter Deposition**, *David Adams, R. Kothari, M. Kalaswad, C. Sobczak, J. Custer, S. Addamane, M. Jain, E. Fowler, F. DelRio, M. Rodriguez, R. Dingreville, B. Boyce*, Sandia National Laboratories

A few binary metal alloys are predicted to form thermally stable, compositionally segregated structures owing to the thermodynamic preference for minority species to collect and remain at grain boundaries established within the solid. (J.R. Trelewicz et al., PRB, 2009) When produced as a nanocrystalline thin film, these stable structures afford the potential to maintain excellent mechanical properties (e.g., high hardness) even after annealing to elevated temperature. Indeed, several systems, including Pt<sub>3</sub>Au<sub>1</sub> thin films, are reported to develop thermally-stabilized, hard, nanocrystalline structures attributed to solute segregation at grain boundaries. (P. Lu et al., *Materialia*, 2019)

Future studies that seek optimal stoichiometry and/or preferred synthesis processes require access to a wide range of composition as well as an ability to vary key deposition parameters. Toward this end, our team reports on the challenges and the benefits of combinatorial synthesis for expediting the discovery of improved binary metal thin films. Our study utilized confocal sputter deposition wherein Pt and Au targets were individually sputtered via pulsed DC magnetron methods. Substrates (150 mm diameter wafers) were fixed in order to gain access to a wide compositional range for each deposition. The sputter power and cathode tilt orientation were then varied in subsequent depositions to access the nearly full binary metal compositional range. The binary collision Monte Carlo program SiMTra (D. Depla et al., *Thin Solid Films* 2012), which simulates the transport of sputtered atoms within the process gas, helped guide the selection of these process parameters in order to achieve compositional goals in relatively few depositions. Notably, the binary

compositions predicted by SiMTra closely matched (within a few molar %) the measured compositions determined by Wavelength Dispersive Spectroscopy completed in 112 different areas across each wafer. The various combinatorial Pt-Au films were further characterized by high-throughput Atomic Force Microscopy, automated X-ray Diffraction, fast X-ray Reflectivity, mapping four-point probe sheet resistance, and automated nanoindentation. These studies reveal how hardness, modulus, film density, crystal texture, and resistivity of combinatorial films varied with composition as well the atomistics of film deposition. Attempts to correlate key film characteristics with the kinetic energies and incident angles of arriving metal species (estimated by SiMTra) are discussed with a goal of improving fabrication processes.

Sandia National Laboratories is managed and operated by NTESS under DOE NNSA contract DE-NA0003525.

11:00am **AS+2D+CA+EL+EM+MS+NS+SE+SS+TF-WeM-10 Optical and X-Ray Characterization and Metrology of Si/Si(1-X)Ge(X) Nanoscale Superlattice Film Stacks and Structures**, *Alain Diebold*, SUNY Polytechnic Institute  
**INVITED**

As traditional scaling of transistors comes to end, transistor channels and capacitors are being stacked to form new 3D transistor and memory devices. Many of these devices are fabricated using films stacks consisting of multiple Si/Si(1-x)Ge layers known as superlattices which must be fabricated with near atomic precision. In this talk, we discuss how Optical and X-Ray methods are used to measure the feature shape and dimensions of these structures. The use of X-Ray methods such as  $\omega$ -2 $\theta$  scans and reciprocal space maps provide layer thickness and stress characterization. We will use simulations to show how a buried layer with a different thickness or Ge concentration alters the data. Recent electron microscopy studies have quantified the stress at the interfaces of these superlattices. We will also discuss how Mueller Matrix spectroscopic ellipsometry (MMSE) based scatterometry is used to measure feature shape and dimension for the nanowire/nanosheet structures used to fabricate nanosheet transistors and eventually 3D DRAM. The starting point for optical scatterometry is determining the optical properties of stressed pseudomorphic Si(1-x)Ge. MMSE can be extended into the infra-red and into the EUV. In addition, small angle X-Ray scattering has been adapted into a method known as CDSAXS which can be used to characterize these structures. This talk will be an overview of these methods.

11:40am **AS+2D+CA+EL+EM+MS+NS+SE+SS+TF-WeM-12 Non-Destructive Depth Differentiated Analysis of Surfaces Using Ion Scattering Spectroscopy (ISS), XPS and HAXPES**, *Paul Mack*, Thermo Fisher Scientific, UK

Recently there has been renewed interest in probing deeper into surfaces using HAXPES in addition to the more surface sensitive (soft X-ray) XPS. On modern XPS systems, with high sensitivity, the total sampling depth may be somewhere between 10nm and 15nm but HAXPES enables the analyst to look deeper, without having to destructively sputter the surface with ions. For a complementary, more comprehensive analysis, XPS and HAXPES can be combined with Ion Scattering Spectroscopy (ISS). ISS is far more surface sensitive than XPS, typically being thought of as a technique to analyse the top monolayer of a sample for elemental information.

In this work, the combination of XPS, HAXPES and ISS on a single tool has been used to give a non-destructive depth differentiated analysis of a range of samples, including a perovskite and an industrially relevant material containing multiple transition metals. The combination of all three techniques provides insight into the depth distributions of elements and chemical states, from the top monolayer to beyond 20nm into the surface.

12:00pm **AS+2D+CA+EL+EM+MS+NS+SE+SS+TF-WeM-13 Towards Measurement of Molecular Shapes Using OrbiSIMS**, *Gustavo F. Trindade, J. Vorng, A. Eyres, I. Gilmore*, National Physical Laboratory, UK

An OrbiSIMS [1] instrument features a dual analyser configuration with a time-of-flight (ToF) mass spectrometer (MS) and an Orbitrap<sup>TM</sup> MS, which confer advantages of speed and high-performance mass spectrometry, respectively. The ability to combine the MS performance usually found in a state-of-the-art proteomics and metabolomics MS with 3D imaging at the microscale and from nanolayers of <10 nm of material has proved popular in a broad field of application from organic electronics to drug discovery. For secondary ions to be efficiently transferred to the Orbitrap analyser, the sample is biased by a target voltage  $V_T$  necessary to match the acceptance window of the Orbitrap. Furthermore, the ions kinetic energy from the SIMS collision process must be reduced. Therefore, in the OrbiSIMS, a

# Wednesday Morning, November 8, 2023

transfer system with helium gas at a pressure  $P_{He}$  slows the ions and reduces their kinetic energy distribution through inelastic collisions with gas atoms. Usually, an Orbitrap is used with an ambient pressure ion source and so here an extra gas flow of nitrogen is introduced that leads to an increase of pressure  $P_{N_2}$  to compensate.

We conducted a systematic assessment of  $V_T$  and  $P_{He}$  and  $P_{N_2}$  on the transmitted secondary ion intensities [2] and revealed a complex behaviour, indicating the possibility for additional separation of ions based on their shape, stability, and kinetics of formation. We showed that the  $V_T$  for maximum transmission of secondary ions will not be the same for all molecules of the same material and that sometimes multiple maxima exist. Here, we present recent progress towards the understanding of these phenomena and how we are leveraging it to measure molecular shape by using reference trisaccharides raffinose, maltotriose and melizitose [3].

[1] M. K. Passarelli *et al.*, "The 3D OrbiSIMS—label-free metabolic imaging with subcellular lateral resolution and high mass-resolving power," *Nat. Methods*, no. november, p. nmeth.4504, 2017, doi: 10.1038/nmeth.4504.

[2] L. Matjacic *et al.*, "OrbiSIMS metrology part I: Optimisation of the target potential and collision cell pressure," *Surf. Interface Anal.*, no. November 2021, pp. 1–10, 2021, doi: 10.1002/sia.7058.

[3] G.F. Trindade *et al.*, In preparation.

## Electronic Materials and Photonics Division Room B116 - Session EM-WeM

### Advancements in Microelectronics and Nanotechnology by Early and Mid Career Professionals

**Moderators:** Erica Douglas, Sandia National Laboratories, Stephen McDonnell, University of Virginia

8:00am **EM-WeM-1 Assessment and Benchmarking of Nonvolatile Memory Devices for Analog In Memory Computing**, **Matthew Marinella**, Arizona State University; *C. Bennett, P. Xiao, W. Wahby, S. Agarwal*, Sandia National Laboratories **INVITED**

Deep neural networks (DNNs) have garnered significant recent attention due to the revolutionary new capabilities they are enabling. These advancements have been made possible by the exponential increase in performance and energy efficiency of digital computing hardware over the past several decades. However, digital DNN accelerators are hitting ultimate limits of around 1-10 teraoperations per second per watt (TOPS/W) – and for progress to continue, new computing paradigms are needed. Analog in-memory computing (AIMC) is an architecture which promises to enable > 100 TOPS/W by efficiently processing the analog vector matrix multiply (VMM) operation at the heart of DNN algorithms – enabling capabilities well beyond what is possible with digital systems. The VMM operation is performed using an array of nonvolatile memory devices, which are programmed to represent a matrix of network weights through their conductance states. An input to this array is scaled to represent a vector, and each multiply is carried out using ohms law, followed by the accumulation of currents down each column. Many devices are under consideration for use with AIMC, including the flash memory cell (charge trapping and floating gate), and emerging resistive memory (ReRAM), conducting bridge memory (CBRAM), and electrochemical memory (ECRAM). The use of these devices for AIMC represents a significant departure from using the same devices for digital memory in that the neural network classification accuracy depends directly on the nuanced device-level behavior of nonvolatile memories. Device properties such as programming variability, read noise, drift, write linearity, and symmetry must be characterized in detail to form a dataset that can be used to model the accuracy of a DNN algorithm, when executed on an AIMC processor using that particular nonvolatile memory. For example, we have electrically characterized SONOS and ReRAM devices and simulated the classification accuracy for an AIMC accelerator running ImageNet on ResNet50 – which is a common machine learning benchmark. This talk will overview the process of benchmarking nonvolatile memory devices for AIMC, including electrical characterization, dataset generation, and process of modeling DNN accuracy based on this data. SNL is managed and operated by NTESS under DOE NNSA contract DE-NA0003525.

8:40am **EM-WeM-3 AVS Peter Mark Memorial Award Talk: Heterostructures for Low-Power Logic and Memory Devices**, **Deep Jariwala**<sup>1</sup>, University of Pennsylvania **INVITED**

The isolation of a growing number of two-dimensional (2D) materials has inspired worldwide efforts to integrate distinct 2D materials into van der Waals (vdW) heterostructures. While a tremendous amount of research activity has occurred in assembling disparate 2D materials into "all-2D" van der Waals heterostructures and making outstanding progress on fundamental studies, practical applications of 2D materials will require a broader integration strategy. I will present our ongoing and recent work on integration of 2D materials with 3D electronic materials to realize logic switches and memory devices with novel functionality that can potentially augment the performance and functionality of Silicon technology. First, I will present our recent work on gate-tunable diode<sup>1</sup> and tunnel junction devices<sup>2</sup> based on integration of 2D chalcogenides with Si and GaN. After that I will present phase control growth and integration strategies for 2D In chalcogenides at back end of line (BEOL) compatible temperatures.<sup>3</sup>

Following this I will present our recent work on non-volatile ferroelectric memory devices based on AlScN.<sup>4</sup> First, I will present on Ferroelectric Field Effect Transistors (FE-FETs) made using a heterostructure of MoS<sub>2</sub>/AlScN<sup>5,6</sup> and also introduce our work on Ferroelectric Diode (FeD) devices also based on thin AlScN.<sup>7</sup> In addition, I will also present how FeDs provide a unique advantage in compute-in-memory (CIM) architectures for efficient storage, search as well as hardware implementation of neural networks.<sup>8</sup>

#### References:

72. Miao, J.; et al....Jariwala, D. *Nano Letters* **2020**, *20*, (4), 2907-2915.

2. Miao, J.; et al.... Jariwala, D. *Nature Electronics* **2022**, 10.1038/s41928-022-00849-0.

3. Song, S.; et al.... Jariwala, D. *arXiv preprint arXiv:2303.02530* **2023**.

4. Kim, K.-H.; Karpov, I.; Olsson III, R.; Jariwala, D. *Nature nanotechnology* **2023**, DOI: 10.1038/s41565-023-01361-y.

5. Liu, X.; et al.... Jariwala, D. *Nano Letters* **2021**, *21*, (9), 3753-3761.

6. Kim, K.-H.; et al.... Jariwala, D. *Nature nanotechnology* **2023**, (in press).

7. Liu, X.; et al....Jariwala, D. *Applied Physics Letters* **2021**, *118*, (20), 202901.

8. Liu, X.; et al.... Jariwala, D. *Nano Letters* **2022**, *22*, (18), 7690-7698.

9:20am **EM-WeM-5 BeyondFingerprinting – Materials Discovery via High-Throughput, Low Cost, AI-Guided Materials Science**, *B. Boyce, R. Dingreville, Elliott Fowler, N. Trask, D. Adams, J. Coleman, K. Johnson*, Sandia National Laboratories

In 1957 Richard Bellman first introduced the 'Curse of Dimensionality' – describing how the number of samples needed to estimate an arbitrary function with a given level of accuracy grows exponentially with respect to the number of input variables [1]. Almost 70 years later, the field of Materials Science is still grappling with the Curse. Despite significant advances in capability and speed in materials synthesis and characterization since Bellman's observation, most materials discovery challenges are far too high dimensional in terms of both inputs and material properties to brute force through with high throughput experimentation alone [2]. Thus, artificial intelligence (AI) and machine learning (ML) are increasingly being utilized because they allow for the rapid development of process-structure-property-performance relationships across a vast material domain. These AI/ML frameworks are designed to take high dimensional search spaces and significantly reduce them into strongly correlated latent spaces. The core question motivating Sandia's BeyondFingerprinting Grand Challenge is: *How do you merge scientific data with a range of dimensionalities and uncertainties from multiple disparate sources (both experiments and high-fidelity simulations) to extract the most meaningful information through advanced machine learning algorithms?* In this talk, I will discuss how BeyondFingerprinting is addressing this question with a two-fold approach, including development of high throughput, low-cost data streams and Himulaya (Hybrid-Informed Multi-Layered Algorithms), across three distinct material exemplars: Laser Powder Bed Fusion, Electrodeposition and Physical Vapor Deposition. Furthermore, I will show how this framework is enabling the acceleration of material discoveries across each of these three domains through discussion of combinatorial synthesis (100s of samples per day) and high-throughput characterization (1000s of measurements per week) strategies, as well as data management and AI/ML approaches.

<sup>1</sup> Peter Mark Memorial Award Winner

# Wednesday Morning, November 8, 2023

Perspective will be provided on how advances in *BeyondFingerprinting* might impact the development of Electronic Materials and Devices.

[1] L. Chen, "Curse of Dimensionality," in *Encyclopedia of Database Systems*, L. Liu and M. T. Özsu Eds. Boston, MA: Springer US, 2009, pp. 545-546.

[2] E. J. Amis, X.-D. Xiang, and J.-C. Zhao, "Combinatorial materials science: What's new since Edison?," *MRS bulletin*, vol. 27, no. 4, pp. 295-300, 2002.

9:40am **EM-WeM-6 Tunability of the Thermal and Photophysical Properties of Blue-Emitting Fluoranthene Chromophores**, *Christopher Brewer, J. Wheeler, A. Pynch, F. Castellano*, North Carolina State University

Designing organic blue-emitting chromophores with properties suitable for applications in devices, such as OLEDs, is a challenging task. Organic blue-emitting chromophores often have broad emission profiles and do not sublimate cleanly for device fabrication. Consequently, organometallic blue emitters are more readily used in device applications due to their desirable thermal and photophysical properties. Despite these drawbacks, fluoranthene is a potential organic scaffold for designing blue-emitting organic chromophores. Fluoranthene's modular synthetic approach allows for nearly limitless functional group modification. Additionally, modifying its functional groups can tune fluoranthene's thermal and photophysical properties. Most notably, the volatility of the fluoranthene can be increased by installing trifluoromethyl substituents, while the volatility decreases when substituents such as methoxy are utilized. To date, our deepest blue-emitting fluoranthene chromophore (CIE 1931: 0.156, 0.111) incorporates trifluoromethyl and methoxy substituents while retaining desirable thermal properties. Ultimately, the vast array of synthetic modifications available with the fluoranthene scaffold makes this organic chromophore suitable for device fabrication, as both the emission and volatility can be controlled. This talk will discuss the photoluminescence of fluoranthene derivatives in both the solid and solution state, as well as the substituent influence on the volatility of the molecule.

11:00am **EM-WeM-10 Hf-Doping of Polycrystalline Gallium Oxide Thin-films**, *Seth King*, University of Wisconsin - La Crosse

Hafnium (Hf) doping of Ga<sub>2</sub>O<sub>3</sub> single crystals has shown that Hf occupies an octahedrally coordinated Ga site and behaves as an n-type dopant [1-3]. However, these reports have only studied a single concentration of Hf incorporated into melt grown Ga<sub>2</sub>O<sub>3</sub> single crystals. To gain insight into how Hf concentration impacts the optical, structural, and morphological properties of the material, polycrystalline Hf-doped Ga<sub>2</sub>O<sub>3</sub> were deposited by RF-sputtering onto silicon and fused silica substrates at room temperature. Deposited films, with varying concentrations of Hf, were subsequently characterized by spectroscopic ellipsometry, UV-Vis spectrophotometry, x-ray diffraction, x-ray photoelectron spectroscopy, and atomic force microscopy both in the as-deposited state and upon subsequent, ex-situ annealing.

Results show that all films, regardless of Hf concentration, are initially amorphous, but crystallize as β-Ga<sub>2</sub>O<sub>3</sub> upon annealing. Spectroscopic ellipsometry measurements show that the index of refraction of the film is altered by Hf incorporation, while UV-Vis measurements show that the optical bandgap is not significantly altered. These results suggest that Hf-doped Ga<sub>2</sub>O<sub>3</sub> may find use in optoelectronic devices and applications.

[1] <https://iopscience.iop.org/article/10.1088/1361-6641/ab75a6>

[2] <https://aip.scitation.org/doi/10.1063/5.0062739>

[3] <https://doi.org/10.1063/5.0062739>

11:20am **EM-WeM-11 Composition of Chemically Treated (111) Surfaces of Cd<sub>0.9</sub>Zn<sub>0.1</sub>Te by X-Ray Photoelectron Spectroscopy**, *H. Yuan, T. Nguyen, Thomas Tiedje*, University of Victoria, Canada; *B. Aitchison, Y. Song, M. Jackson*, Redten Technologies, Canada; *J. Chen, H. Wang*, University of Saskatchewan, Canada

Cd<sub>0.9</sub>Zn<sub>0.1</sub>Te (CZT) x-ray detectors have enabled high performance medical x-ray imaging systems. The surface properties of CZT are important in x-ray detector applications as they influence performance through their effects on electron-hole injection and collection. In this work, the composition of 111A surfaces of CZT single crystals were investigated following chemical etching with Br<sub>2</sub>/methanol and HCl, vacuum annealing, ozone oxidation and H<sub>2</sub>S exposure. Both synchrotron and lab-based X-ray photoelectron spectroscopy (XPS) were used to investigate changes in the surface composition and interfacial band alignment of treated CZT surfaces. Chemical etching with Br<sub>2</sub>/methanol was used to remove polishing damage, and leaves 4-6 monolayers of excess Te on the surface depending on the etch time and composition of the etch. HCl etching removes surface oxides formed by air exposure or by exposure to UV-generated ozone, leaving

elemental Te (Te<sup>0</sup>) on the surface. Residual Te<sup>0</sup> was removed by vacuum annealing at 250°C for one hour. XPS and Raman spectroscopy measurements on the vacuum annealed samples confirm the formation of a stoichiometric CZT surface. We were able to grow a mixed CZT-oxide about 8 nm thick by UV ozone exposure in air at room temperature for 1 hr. Depth profiles of the surface composition were obtained from the energy dependence of the photoelectron escape depth, accessible with the tunable x-ray energy available from the synchrotron source. We found a non-uniform vertical composition profile with CdO on the surface and Te<sup>0</sup> and TeO<sub>2</sub> underneath, suggesting that Cd out diffuses during oxidation.

Vacuum annealed and ozone oxidized surfaces were exposed to 500 ppm H<sub>2</sub>S in N<sub>2</sub> in a tube furnace at 250 °C and 280 °C for 0.5-2 hr. SEM/EDX imaging and ellipsometry measurements indicate that a 50-60 nm CdS layer is formed after 2 hr exposure to H<sub>2</sub>S at 280 °C. The ozone oxidized starting surface was found to be more reactive with H<sub>2</sub>S than the vacuum annealed surface. Sulfided surfaces were depleted in Te and O leaving a surface layer rich in CdS similar to the results of Nelson and Levi [1] with H<sub>2</sub>S plasma treatment. We are exploring the effect of the various surface treatments on x-ray detector performance.

[1] A. J. Nelson, D. Levi, Novel method for growing CdS on CdTe surfaces for passivation of surface states and heterojunction formation, *JVST A*, 15, 1119 (1997).

11:40am **EM-WeM-12 High Throughput Design of 2D Electronic Materials and Heterostructures**, *Nicholas Glavin*, Air Force Research Laboratory, Materials and Manufacturing Directorate, USA **INVITED**

2D materials represent an exciting opportunity to create tunable heterostructures for next generation electronic applications. In this talk, strategies and processes to enable high throughput design and customization of 2D materials which enable novel, multifunctional properties is presented. These techniques include rapid laser-manufacturing approaches, where high throughput structure/property evaluation can allow for rapid device design. This same process can be implemented in a roll-to-roll configuration to allow for manufacturing of ultralow cost 2D devices at scale for detection of a host of different sensing environments including detection of pathogens. Additionally, a two-step metal conversion process will be discussed that allows for direct synthesis of 2D transition metal dichalcogenide superlattices which can result in 3D heterostructures of interest to future applications.

**Fundamental Discoveries in Heterogeneous Catalysis Focus Topic**

**Room B113 - Session HC+SS-WeM**

**Origins of Single Atom Catalysis**

**Moderators: Rachael Farber**, University of Kansas, **Gareth Parkinson**, TU Wien

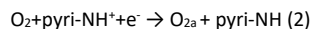
8:00am **HC+SS-WeM-1 Role of Pyridinic Nitrogen in the Mechanism of the Oxygen Reduction Reaction on Carbon Electrocatalysts**, *Kotaro Takeyasu*, University of Tsukuba, Japan; *S. Singh*, Shiv Nadar University, India; *K. Homma, K. Hayashida*, University of Tsukuba, Japan; *S. Ito, T. Morinaga*, National Institute of Technology, Tsuruoka College, Japan; *Y. Endo, M. Furukawa*, University of Tsukuba, Japan; *T. Mori*, National Institute for Materials Sciences (NIMS), Japan; *H. Ogasawara*, SLAC National Laboratory; *J. Nakamura*, International Institute for Carbon-Neutral Energy Research, Kyushu University, Japan

Nitrogen doped carbon catalysts are promising Pt-free catalysts for the oxygen reduction reaction (ORR) in polymer electrolyte fuel cells owing to the high durability and the high activity in alkaline media. The primary active site in N-doped carbon catalysts is the pyridinic nitrogen (pyri-N), which is bound to two carbon atoms with negative charge.[1] However, a large barrier of N-doped carbon catalysts for the commercial usage is the decreased activity in acidic media. Hence, we investigated this deactivation phenomenon to widen the applicability of N-doped carbon catalysts. In acidic media, the protonation of pyri-N (pyri-NH<sup>+</sup>) occurs as the first step owing to the basicity of pyri-N.

pyri-N + H<sup>+</sup> → pyri-NH<sup>+</sup> (1)

As the following process, we have demonstrated the electrochemical reduction of pyri-NH<sup>+</sup> coupled with thermal O<sub>2</sub> adsorption on carbon atoms near pyri-NH<sup>+</sup> using model catalysts:

# Wednesday Morning, November 8, 2023



In this reaction, the thermal adsorption of O<sub>2</sub> let the electrochemical reduction of pyri-NH<sup>+</sup> to pyri-NH thermodynamically favorable due to the adsorption energy of O<sub>2</sub>. Although the formation of pyri-NH<sup>+</sup> is a cause of the decrease in ORR activity, but pyri-NH<sup>+</sup> itself is essential for the formation of pyri-NH and the adsorption of O<sub>2</sub>. A key point is that a dope electron into π\* orbital of π-conjugative system near pyri-NH promotes the adsorption of O<sub>2</sub>. However, the hydration of pyri-NH<sup>+</sup> forming pyri-NH<sup>+</sup> · (H<sub>2</sub>O)<sub>n</sub> causes a lower shift in the redox potential and consequently, Eq. 2 becomes the rate-determining step (RDS). Therefore, we consider that the hydration of pyri-NH<sup>+</sup> is the main cause of the decrease in ORR activity in acid electrolytes.[2] Thus, we hypothesize an enhanced ORR activity by the introduction of hydrophobicity in the vicinity of pyri-NH<sup>+</sup>, suppressing the extent of hydration.

Introducing the hydrophobic cavity prevented the hydration of pyri-NH<sup>+</sup> but inhibited the proton transport. We then increased proton conductivity in the hydrophobic cavity by introducing SiO<sub>2</sub> particles coated with ionic liquid polymer/Nafion® which kept the high onset potentials with an increased current density even in acidic media.[3]

## References

- [1] D. Guo, J. Nakamura et al., *Science*, 2016, 351, 361-365.  
[2] K. Takeyasu, J. Nakamura et al., *Angew. Chem. Int. Ed.* 60, 5121 (2021).  
[3] S. K. Singh, K. Takeyasu, J. Nakamura et al., *Angew. Chem. Int. Ed.* 61, e202212506 (2022).

8:20am **HC+SS-WeM-2 Atomic-Level Studies of Mono-Carbonyl and Gem-Dicarbonyl Formation on Rh-Decorated Fe<sub>3</sub>O<sub>4</sub>(001)**, *Panukorn Sombut, C. Wang, L. Puntscher, M. Meier, J. Pavelec, Z. Jakub, M. Schmid, U. Diebold*, TU Wien, Austria; *C. Franchini*, University of Vienna, Austria; *G. Parkinson*, TU Wien, Austria

Understanding the interaction between reactant molecules and “single atom” active sites is important for comprehending the evolution of single-atom catalysts in reactive atmospheres. Here, we study how Fe<sub>3</sub>O<sub>4</sub>(001)-supported<sup>1</sup> Rh<sub>1</sub> monomers and Rh<sub>2</sub> dimer species interact with CO using density functional theory (DFT), combined with temperature-programmed desorption, x-ray photoelectron spectroscopy, and in-situ scanning tunneling microscopy techniques. Our results show that stable Rh<sub>1</sub>(CO)<sub>1</sub> monocarbonyls are the exclusive product of CO adsorption at both 2-fold and 5-fold coordinated Rh<sub>1</sub> sites, but the different coordination environment leads to different adsorption energies. The DFT calculations reveal that the Rh<sub>1</sub>(CO)<sub>1</sub> formed at the 5-fold coordinated Rh<sub>1</sub> site adopts an octahedral structure, while the Rh<sub>1</sub>(CO)<sub>1</sub> formed at the 2-fold coordinated Rh<sub>1</sub> site forms an additional bond to a subsurface oxygen atom of the support, leading to a pseudo-square planar structure. The direct addition of a second CO molecule to Rh<sub>1</sub>(CO)<sub>1</sub> at the 2-fold coordinated Rh<sub>1</sub> site to form a Rh<sub>1</sub>(CO)<sub>2</sub> gem-dicarbonyl is energetically favorable according to DFT; however, this process is not observed in experiments under UHV conditions. Instead, we observe the formation of limited Rh<sub>1</sub>(CO)<sub>2</sub> exclusively via the CO-induced breakup of Rh<sub>2</sub> dimers, in agreement with DFT results, which suggest an unstable Rh<sub>2</sub>(CO)<sub>3</sub> intermediate.

73. Bliem, R. *et al.* Subsurface cation vacancy stabilization of the magnetite (001) surface. *Science* **346**, 1215–1218 (2014).

8:40am **HC+SS-WeM-3 A Few Questions About Single Atom Catalysts: When Theory Helps**, *Gianfranco Pacchioni*, University of Milano-Bicocca, Italy **INVITED**

In the past, single atom catalysts (SACs) could not be clearly visualized and characterized due to the limitations associated with instrumental resolution. Today this is a new frontier in heterogeneous catalysis due to the high activity and selectivity of SACs for various catalytic reactions. This has opened various questions for theory. One is where are the atoms and what is the stability of SACs in working conditions. In order to address these questions, we will discuss the nature of isolated metal species deposited on oxide surfaces (TiO<sub>2</sub> and ZrO<sub>2</sub> in particular). These systems have been characterized experimentally using high-resolution scanning transmission

electron microscopy (STEM), Fourier transform infrared spectroscopy (FTIR), and temperature programmed desorption (TPD) spectra of adsorbed CO probe molecules. Combining these data with extensive Density Functional Theory (DFT) calculations one can provide an unambiguous identification of the stable single-atom species present on these supports and of their dynamic behavior.

The other question that can be addressed by theory is the prediction of the behavior of SACs in electrocatalytic processes such as the oxygen reduction (ORR), the oxygen evolution (OER) and the hydrogen evolution (HER) reactions. In this context we assist to a rapidly growing number of DFT studies and of proposals of universal descriptors that should provide a guide to the experimentalist for the synthesis of new catalysts, in particular related to graphene-based SACs. We will critically analyze some of the current problems connected with these DFT predictions: accuracy of the calculations, neglect of important contributions in the models used, physical meaning of the proposed descriptors, inaccurate data sets used to train machine learning algorithms, not to mention some severe problems of reproducibility. It follows that the “rational design” of a catalyst based on some of the proposed universal descriptors or on the DFT screening of large number of structures should be considered with some caution.

9:20am **HC+SS-WeM-5 A Multi-Technique Study Of Ethylene and H<sub>2</sub> Adsorption on Rh<sub>1</sub>/Fe<sub>3</sub>O<sub>4</sub>**, *Gareth Parkinson, C. Wang, P. Sombut, L. Puntscher*, TU Wien, Austria

The hydroformylation of alkenes has emerged as one of the most interesting applications of “single-atom” catalysis. Nevertheless, there have been relatively few fundamental studies into how the reactants (CO, alkene, and H<sub>2</sub>) bind at the active site. In this talk I will show STM, XPS, TPD and DFT results to illustrate how C<sub>2</sub>H<sub>4</sub> and H<sub>2</sub> interact with a Rh<sub>1</sub>/Fe<sub>3</sub>O<sub>4</sub>(001) model catalyst. Ethylene binds strongly at the Rh<sub>1</sub> sites, but there is very little evidence for the formation of di-ethylene species under UHV conditions. H<sub>2</sub> adsorbs as a dihydride at the Rh<sub>1</sub> sites, and desorbs close to room temperature in TPD experiments without spilling over onto the oxide support. Evidence for the co-adsorption of the different reactants will be discussed in the context of the hydroformylation reaction.

9:40am **HC+SS-WeM-6 Remote Activation of H–H bonds by Platinum in Single-Atom Alloy Catalysts**, *Francisco Zaera*, University of California Riverside

With heterogeneous catalysts, chemical promotion takes place at their surfaces. Even in the case of single-atom alloys (SAA), where a reactive metal is atomically dispersed in small quantities within the main host, it is assumed that both elements are exposed and available to bond with the reactants. Here we show, on the basis of *in situ* x-ray absorption spectroscopy data, that the Pt atoms in Cu-Pt SAA catalysts are located at the inner interface between the metal nanoparticles and the silica support instead. Kinetic experiments indicated that these catalysts still display better selectivity for the hydrogenation of unsaturated aldehydes to unsaturated alcohols than the pure metals. Quantum mechanics calculations not only corroborated the particular stability of Pt at the metal-support interface, but also explained the catalytic performance improvement as due to a remote lowering of the activation barrier for the scission of the H–H bond in molecular hydrogen at Cu sites by the internal Pt atoms.

11:00am **HC+SS-WeM-10 Electrifying Industrial Chemistry at the Molecular Level: Controlling the Electrocatalytic Transformation of Alcohols and Alkanes to Valuable Products**, *Marcel Schreier*, University of Wisconsin-Madison **INVITED**

Producing fuels and chemicals using renewable electricity holds the promise to enable a truly sustainable circular economy based on sustainably produced carriers of electrical energy and sustainably produced chemicals. To date, the vast majority of electrocatalytic reactions are limited to the transformation of small inorganic molecules such as CO<sub>2</sub>, H<sub>2</sub>O, N<sub>2</sub>, as well as the oxidation and reduction of alcohols. However, comprehensive electrification of the chemical industry will require electrocatalytic reactions that can promote the transformations of C(sp<sup>3</sup>)-H and C(sp<sup>3</sup>)-C(sp<sup>3</sup>) bonds, which are central to today’s industry.

In this presentation, I will show how fundamental understanding of the interfacial processes occurring in electrocatalytic reactions can be exploited to expand the reaction scope of electrocatalysis to the transformation of complex substrates involving the controlled activation of C-H and C-C bonds. In a first step, I will show how this approach allows us to transform ethanol to ethylene oxide, an important plastic precursor. Subsequently, I

# Wednesday Morning, November 8, 2023

will discuss methods to electrocatalytically transform inert alkanes such as methane and ethane at room temperature.

## 11:40am HC+SS-WeM-12 Probing Elementary Steps and Catalyst Structure Evolution: Insights into Formic Acid Conversion on Rh/Fe<sub>3</sub>O<sub>4</sub>(001) Model Catalysts, *Zdenek Dohnalek*, Pacific Northwest National Laboratory

Single-atom catalysis represents an exciting area of research due to the potential to qualitatively transform the activity and selectivity of supported metal catalysts. However, our fundamental understanding of their stability under reaction conditions is limited. To address this gap, we employed scanning tunneling microscopy (STM), X-ray photoelectron spectroscopy (XPS), and temperature programmed desorption (TPD). We prepared well-characterized model Rh/Fe<sub>3</sub>O<sub>4</sub>(001) catalysts with distinct types of Rh single-atom sites. In model catalytic studies, we investigated the effect of reactants on the structure and activity of such Rh/Fe<sub>3</sub>O<sub>4</sub>(001) catalysts. Formic acid, which deprotonates to surface formate and hydroxyl species, is employed as a model to follow the fate of dehydration and dehydrogenation reaction channels. We demonstrate that small amounts of Rh adatoms induce a shift from the dehydration pathway yielding CO on bare Fe<sub>3</sub>O<sub>4</sub>(001) to dehydrogenation yielding CO<sub>2</sub> on Rh<sub>ad</sub>-Fe<sub>3</sub>O<sub>4</sub>(001). Multiple turnovers are achieved on each Rh<sub>ad</sub> during the single TPD sweep. As Rh adatoms are highly unstable, we further studied the Rh stabilized in octahedral iron sites within the Fe<sub>3</sub>O<sub>4</sub>(001) surfaces that are stable on high surface area Rh/Fe<sub>3</sub>O<sub>4</sub> catalysts. A similar shift from dehydration to dehydrogenation is observed, but much higher coverages of Rh are required. We showed that adsorbed species transiently destabilize Rh<sub>oct</sub> and lead to the formation of Rh<sub>ad</sub>, which is only present during the reaction. Independent studies of hydroxylated surfaces reveal that surface OHs are responsible for the Rh<sub>oct</sub> destabilization and conversion to active Rh<sub>ad</sub> species. Studies of elementary reaction steps and catalyst dynamics on well-defined model systems are critical for the future design of catalysts with maximum activity and selectivity.

## 12:00pm HC+SS-WeM-13 Hydrogen and Hydrocarbon Reactions on Single-Atom RhCu(100), *Laurin Joseph, M. Powers, J. Rosenstein, A. Utz*, Tufts University

A class of catalysts called single-atom alloys allow for the combination of a more reactive, more expensive dopant metal dispersed within a less active, more selective, and cheaper base metal. These catalysts have been well characterized and studied using techniques such as temperature programmed desorption (TPD), scanning tunneling microscopy (STM), and reflection absorption infrared spectroscopy (RAIRS). However, the detailed, molecular-level bond activation energetics and kinetics have not yet been experimentally interrogated for high-barrier reactions on these catalysts—a region where more efficient catalysts are most sorely needed.

We will present recent results that first characterize the dissociation and spillover of H resulting from both atomic and molecular H<sub>2</sub> adsorption on base Cu(100) and RhCu(100) single atom alloy, and then describe results from energy resolved molecular beam studies of CH<sub>4</sub> dissociation that quantify reaction probability as a function of energy distribution among reactant and surface degrees of freedom. We expect these studies will reveal new insights into the molecular mechanism for an important class of heterogeneously catalyzed reactions and provide new benchmarks for computational studies of single atom catalysts.

## MEMS and NEMS Technical Group Room C120-122 - Session MN1-WeM

### MEMS Processes, Materials, and Fabrication

Moderators: *Benjamín Alemán*, University of Oregon, *Jaesung Lee*, University of Central Florida

## 8:00am MN1-WeM-1 Additive Manufacturing for 3D Metal Microsystems, *Robert Roberts*, The University of Texas at El Paso

INVITED

Recent developments in precision additive manufacturing technology offer a new dimension in microfabrication design and fabrication. In this talk, the

use of additive manufacturing for the realization of three-dimensional metal microsystems is explored via micro laser sintering (MLS). MLS is able to directly fabricate metal features from precursor metal powder with lateral resolutions of 15µm and layer heights of 5µm, making it well suited for the applications of MEMS, BioMEMS, and microsystems packaging.

An overview of the micro laser sintering fabrication process will be detailed, along with developments in new materials for MLS use. Multiple microsystems fabricated via this technology will then be highlighted including microelectrode arrays, high-temperature microfluidic reactors, and electrostatic relays. The use of metal additive manufacturing for the fabrication of metal microsystems packaging is presented. These system-in-packages (SiP) feature embedded microfluidic thermal management structures towards heterogeneous integration microsystems applications with high-power electronics. The additively manufactured devices were able to decrease the thermal resistance to 1.57°C/W, compared to 5.25°C/W for a conventional packages design.

## 8:40am MN1-WeM-3 Epitaxial Materials and Devices for High Performance RF Acoustics, *Vikrant Gokhale, B. Downey, D. Katzer, M. Hardy, J. Roussos, S. Mack, J. Champlain, A. Lang*, US Naval Research Laboratory; *P. Dhagat, A. Jander*, Oregon State University; *E. Jin*, US Naval Research Laboratory; *N. Nepal, V. Wheeler, D. Meyer*, US Naval Research Laboratory

INVITED

Thin film piezoelectric materials are crucial for creating acoustic micromechanical systems (MEMS) for RF signal processing applications. Conventionally, the metal-piezoelectric-metal transducer materials have been deposited via sputtering, which generally lead to well-textured polycrystalline films. Recent advances in the epitaxial growth of Group III-Nitride (III-N) piezoelectrics, and transition metal nitrides (TMNs) electrodes have enabled all-epitaxial RF acoustic devices with crystalline, lattice-matched and acoustic impedance-matched layers. Such heterostructures are capable of direct integration with GaN RF electronics. In this talk, we shall discuss new opportunities provided by epitaxial RF acoustics, as well as constraints on materials selection, heterostructure growth, and fabrication processes.

Epitaxial RF acoustic devices developed at NRL include surface acoustic wave (SAW) devices, and epitaxial high overtone bulk acoustic wave resonators (epi-HBARs) with a III-N/SiC and III-N/TMN/SiC heterostructure, respectively. Epitaxial SAW devices are used as resonators and delay line filters for low-loss RF signal processing while epi-HBARs are multi-mode phonon cavities with a comb-like RF spectrum capable of extending beyond 40 GHz (Ka band) with extremely low intrinsic loss, which results in record ( $f \times Q$ ) values and long cavity phonon lifetimes [1, 2]. Cryogenic experiments verify that epi-HBARs approach the fundamental limits of intrinsic anharmonic phonon loss [3] and may be well suited for applications such as RF oscillators and in quantum acoustodynamic systems. The near lattice-matched epitaxy of these heterostructures on 4H-SiC results in void-free films with high crystallinity, well-controlled phase and orientation, low defect density, and low surface/interface roughness [1, 4].

74. *Epitaxial bulk acoustic wave resonators as highly coherent multi-phonon sources for quantum acoustodynamics*. Nature Communications, 2020. **11**(1): p. 2314.
75. *X – Ka Band Epitaxial ScAlN/AlN/NbN/SiC High-Overtone Bulk Acoustic Resonators*. IEEE Electron Device Letters, 2023: p. 1-1.
76. *Temperature evolution of frequency and anharmonic phonon loss for multi-mode epitaxial HBARs*. Applied Physics Letters, 2020. **117**(12): p. 124003.
77. *Control of phase purity in high scandium fraction heteroepitaxial ScAlN grown by molecular beam epitaxy*. Applied Physics Express, 2020. **13**(6): p. 065509.

## 9:20am MN1-WeM-5 Slanted Wire Diffraction Gratings Fabricated by Two-Photon Polymerization for Micro-Mechanical Applications, *V. Paige Stinson, U. Subash, M. Poutous, T. Hofmann*, University of North Carolina at Charlotte

The use of diffraction gratings in communication and sensing technology is expansive, ranging from their use in integrated optics and spectral analysis to quantum electronics [1]. Their effectiveness in these applications depend on the manipulation of reflected and transmitted efficiencies by the principles of interference and diffraction. Slanted wire gratings are a particularly useful grating geometry as they can be operated at normal incidence. The transmitted diffraction efficiencies of slanted wire gratings

# Wednesday Morning, November 8, 2023

are sensitive to changes in slant angle [1]. In this study, this slant angle sensitivity is used to design a mechanically tunable diffractive grating. Motivated by the successful fabrication of infrared optics as well as micro-mechanical structures by two-photon polymerization, a resin compatible for fabrication by this approach (IP-Dip) is selected for modeling [2,3]. A rigorous coupled wave approach is used to determine a geometry which optimizes sensitivity to changes in slant angle. A geometry is selected such that the diffraction efficiency is transferred between the 0<sup>th</sup> and +1<sup>st</sup> orders. The efficiency transferred modulates between 0% and 75% for changes in slant angle between 45° to 35°. Realistically, this change in slant angle can be achieved by applying compression to the grating. The mechanical capabilities of the grating are investigated using finite-element method simulations. A prototype slanted wire grating is fabricated by two-photon polymerization and the quality is characterized using scanning electron microscopy. The results of the numerical modeling are presented and potential micro-mechanical applications for their use as transmissive pressure sensors and tunable beam splitters are discussed.

[1] T.K. Gaylord, M. Moharam, *Proceedings of the IEEE*, **73**, 894-937 (1985).

[2] V.P. Stinson, N. Shuchi, M. McLamb, G.D. Boreman, T. Hofmann, *Micromachines*, **13**, 2248 (2022).

[3] V.P. Stinson, N. Shuchi, D. Louisos, M. McLamb, G.D. Boreman, T. Hofmann, *Optics*, **4**, 300-309 (2023).

9:40am **MN1-WeM-6 Very High Frequency Stability of Single-Crystal Silicon Thermal-Piezoresistive Resonators with Phase-Locked Loop**, C. Watkins, University of Florida, Gainesville; **Jaesung Lee**, University of Texas at El Paso; **J. McCandless**, Cornell University; **H. Hall**, Air Force Research Laboratory; **P. Feng**, University of Florida, Gainesville

The Si piezoresistive MEMS heat engine first reported in 2011 [1] marked the start of research to examine the effects of self-sustained thermal-piezoresistive resonators (TPR) in applications such as sensing [2] and signal amplification [3]. TPRs are among a new class of actively transduced devices that offer performance benefits, specifically low motional resistance [4]. Besides, TPRs have the advantage of reduced thermal control needs thanks to the thermal-piezoresistive effect inherent to their operation and thus they could offer very high frequency stability. This paper reports a single-crystalline silicon (Si) TPR achieving very high frequency stability with phase-locked loop (PLL) measurement. A pair of resonators operating in a balanced-bridge configuration is presented, with one device being driven at resonance and the other used to systematically null the undesirable background response. The resonance frequency of the single Si TPR is collected over 40 hours in closed-loop tracking by PLL and yields an Allan deviation of  $\sigma_A \approx 2.66$  ppb for averaging time of  $\tau \approx 4.95$  seconds - the lowest ever reported among all Si TPRs studied to date. This result is significant because it suggests that such Si TPRs can potentially achieve frequency stabilities comparable to, or better than, existing state-of-the-art resonators used in oscillator circuits, with significantly reduced thermal control requirements (ovenization) and subsequent power demands. In this work we examine the potential impact of utilizing the Si TPR to generate an ultra-stable frequency source. We hypothesize that the intrinsic internal feedback offers enhanced quality (*Q*) factor which could contribute to a higher frequency stability. Additionally, an external DC power feedback loop could improve Si TPR stability by removing the linear long-term background frequency drift that is present in all of our PLL measurements.

[1] P. G. Steeneken, *et al.*, *Nat. Phys.* **7**, 354-359, (2011).

[2] A. Zope, *et al.*, *Front. Mech. Eng.* **8**, 898668, (2022).

[3] A. Ramezany, *et al.*, *Nano. Lett.* **18**, 2551-2556, (2018).

[4] A. Rahafruz, *et al.*, *Trans. Elec. Dev.* **59**, 3587-3593, (2012).

## MEMS and NEMS Technical Group

### Room C120-122 - Session MN2-WeM

#### Nanomechanics

**Moderators:** **Vikrant Gokhale**, US Naval Research Laboratory, **Robert Roberts**, The University of Texas at El Paso

11:00am **MN2-WeM-10 Spatial Mapping and Analysis of Graphene Nanomechanical Resonator Networks**, **Benjamin Alemán**, University of Oregon

**INVITED**

Networks of nanoelectromechanical (NEMS) resonators are useful analogs for a variety of many-body systems and enable disruptive applications in sensing, phononics, and mechanical information processing. A challenge toward realizing practical NEMS networks is the ability to characterize the constituent resonator building blocks and their coupling. In this work, we demonstrate a scalable optical technique to spatially map graphene NEMS networks and read out the fixed-frequency collective response as a single vector. Using the response vectors, we introduce an efficient algebraic approach to accurately quantify the site-specific elasticity, mass, damping, and coupling parameters of network clusters. In a departure from multiple regression, our algebraic analysis uses just two measured response vectors to fully characterize the network parameters, and does so without any a priori parameter estimates or iterative computation. We apply this suite of techniques to single-resonator and coupled-pair clusters, and find excellent agreement with expected parameter values and broader spectral response. Our approach offers a new, non-regressive means to accurately characterize a range of classical and quantum resonator systems and fills in a vital gap for programming NEMS networks.

11:40am **MN2-WeM-12 Nonlinear Stiffness and Nonlinear Damping in Atomically Thin MoS<sub>2</sub> Nanomechanical Resonators**, **Tahmid Kaisar**, University of Florida, Gainesville; **J. Lee**, University of Texas at El Paso; **D. Li**, **S. W. Shaw**, Florida Institute of Technology; **P. Feng**, University of Florida, Gainesville

Resonant micro/nanoelectromechanical systems (MEMS/NEMS) exhibits rich nonlinear responses because of their relatively small size and high vibration amplitude [1]. In this work, we provide experimental results and a quantitative study of nonlinear dynamics in atomically-thin nanomechanical resonators made of single-layer, bi-layer, and tri-layer (1L, 2L, and 3L) molybdenum disulfide (MoS<sub>2</sub>) vibrating drumheads. For these two-dimensional (2D) MoS<sub>2</sub> resonators operating in the very high-frequency band, a synergistic study with calibrated measurements and analytical modeling on the observed nonlinear responses have resulted in nonlinear damping and cubic and quintic order nonlinear stiffness. We find that the *quintic* force can be ~20% of the Duffing force at larger amplitudes, and thus it generally cannot be ignored in a nonlinear dynamics analysis. Though the nonlinear stiffness of 2D NEMS has been studied in literature, to date, there has been no experimental demonstration and investigation of nonlinear damping in 2D semiconductor NEMS resonators. This study provides the first quantification of nonlinear damping and frequency detuning characteristics in 2D semiconductor nanomechanical resonators and elucidates their origins and dependency on engineerable parameters, setting a foundation for future exploration and utilization of the rich nonlinear dynamics in 2D nanomechanical systems.

[1] Cross, M.C.; Lifshitz, R. In *Review of Nonlinear Dynamics and Complexity*; Schuster, H., Ed.; Wiley: New York, **2008**; Chapter 1.

## Plasma Science and Technology Division

### Room A106 - Session PS-WeM

#### Exploring Boundaries of Plasma Science (ALL-INVITED SESSION)

**Moderators:** **Michael Gordon**, University of California at Santa Barbara, **Mingmei Wang**, Lam Research Corporation

8:00am **PS-WeM-1 Electron Beam Driven Plasmas: Development and Use for Ultra Low T<sub>e</sub> Processing**, **Scott Walton**, Naval Research Laboratory

**INVITED**

The advantages of plasma-based materials processing techniques are numerous. The capability to rapidly and uniformly modify large areas (> 10<sup>3</sup> cm<sup>2</sup>) with high precision is one reason plasmas are widely used in the materials and surface engineering communities. However, with the ever-evolving demand for new materials and single nanometer-scale device

# Wednesday Morning, November 8, 2023

dimensions across a variety of applications, some of the limitations of conventional plasma sources are becoming apparent. The lack of process control and excessive ion energies in the development of atomic layer processing strategies are examples.

The Naval Research Laboratory (NRL) has developed a processing system based on an electron beam-generated plasma. Unlike conventional discharges produced by electric fields (DC, RF, microwave, etc.), ionization is driven by a high-energy ( $\sim$  keV) electron beam, an approach that can overcome many of the problems associated with conventional plasma processing systems. Electron beam-generated plasmas are generally characterized by high charged particle densities ( $10^{10}$ -  $10^{12}$  cm<sup>-3</sup>), low electron temperatures (0.3 - 1.0 eV), and in reactive gas backgrounds, a relatively low radical production rate compared to discharges. These characteristics allow the ability to precisely control the flux of charged and reactive neutrals as well as ion energy at adjacent surfaces. This provides the potential for controllably etching, depositing, and/or engineering the surface chemistry with monolayer precision.

An overview of NRL's research efforts in developing this technology will be presented, with a focus on source development and operation, plasma characterizations, and how the system can be advantageously applied to the processing of select materials. Examples include graphene, where erosion and damage is a major concern and the etching of semiconductor materials, such as Si, SiN and SiO<sub>2</sub>, where the focus is on etch rates and selectivity at low ion energy. This work is supported by the Naval Research Laboratory base program.

**8:40am PS-WeM-3 My Path to AVS Fellow: Non-Volatile Memory Processing from Fundamental Understanding to the Promise of Atomic Layer Etching and Sustainable Etch Precursors, Eric Joseph, IBM T. J. Watson Research Center** **INVITED**

Non-volatile memory technologies such as phase change memory (PCM) and magnetoresistive memory (MRAM) have seen various levels of success in manufacturing over the past decade. Intel/Micron's Optane PCM memory and Everspin's MRAM are just a few examples of recent products, while in more recent research, these same materials are also being explored as accelerator technologies for AI hardware applications. However, to enable these memory technologies, a significant understanding of plasma processing is required to achieve high fidelity pattern transfer while maintaining device performance. In this talk I will walk through first data highlighting the challenges of material volatility for both PCM and MRAM etching and how process induced modification of the material leads to deleterious device performance. Furthermore, we will review the promise of atomic layer etching in enabling new avenues to address patterning issues for MRAM and PCM and demonstrate how ALE can lead to new opportunities for sustainable future non-volatile memory processing applications.

**9:20am PS-WeM-5 VHF Plasma Enhanced Atomic Layer Deposition of SiN<sub>x</sub> using Aminosilane Precursors, Y. Ji, S. Choi, J. Kang, Sungkyunkwan University, Republic of Korea; A. Ellingboe, Dublin City University, Ireland; C. Lee, Merck Korea; H. Chandra, EMD Electronics; Geun Young Yeom, Sungkyunkwan University, Republic of Korea** **INVITED**

In this study, we investigated the plasma enhanced atomic layer deposition (PEALD) of silicon nitride (SiN<sub>x</sub>) using the VHF-CCP N<sub>2</sub> plasma and different aminosilane precursors at the process temperature range of 100–300 °C. The combinations of VHF-CCP plasma source instead of conventional HF-CCP plasma source and an adequate aminosilane precursor allowed a high growth rate and high quality films as well as excellent conformality close to 100% at substrate temperature of 300 °C. In addition, when external magnetic field was added during the VHF CCP N<sub>2</sub> plasma generation during the PEALD of SiN<sub>x</sub> film, the magnetized VHF CCP N<sub>2</sub> plasma allowed better film quality and higher conformality at low temperature of 200 °C.

**11:00am PS-WeM-10 PSTD 2022 Young Investigator Awardee Talk: Plasma Processing Challenges for Emerging Memory Technology, Luxherta Buzi<sup>1</sup>, IBM Research, T. J. Watson Research Center; N. Marchack, S. Engelmann, R. Bruce, IBM Research Division, T.J. Watson Research Center** **INVITED**

Continuously shrinking feature size in patterning imposes non-volatile memory processing challenges, particularly for phase change memory (PCM) materials, where damage mitigation is imperative. Optimization of etch process and chemistry in minimizing or eliminating structural or compositional damage is key for the success of this technology. Use of halogens is often needed for a better profile control, reduce redeposition, selective metal etching etc., but it can cause structural damage and elemental depletion of PCM materials leading to an increase in the recrystallization time. Ion sputtering with inert gases on the other hand, can cause material re-deposition on the sidewall, poor profile control and worse etch selectivity.

In addition to ion bombardment which is typically responsible for physical sputtering and increased roughness, plasma can generate short wavelength irradiation due to electron-neutral collisions. UV/VUV photons emitted in a plasma can reach high fluxes and thus become important in terms of plasma-surface interaction processes. Elemental depth profiling with ion beam analysis and time resolved laser reflectivity was done to study the phase transition behavior of GST when exposed to different chemistries, temperatures, plasma duration, and various reactor configurations.

Surface oxidation of PCM materials can substantially alter switching properties therefore, in-situ plasma enhanced CVD encapsulation has been viewed as a favorable solution. It is imperative that RIE and encapsulation mitigate damage and oxidation of PCM material during integration. In-situ encapsulation of GST and tuning of plasma parameters, caused controlled SiN film deposition with simultaneous selective etching and damage removal from GeSbTe-based PCM materials.

**11:40am PS-WeM-12 How Can Machine Learning Help Process Development?, Satoshi Hamaguchi, Osaka University, Japan** **INVITED**

The recent development in data science and technology such as machine learning (ML) and artificial intelligence (AI) is now changing the way we perform various tasks, including research and development. Process development for semiconductor manufacturing is so complex that there is much room for improvement in its efficiency by ML and AI. Often one of the major problems in applying ML and AI for process development is the lack or insufficiency of experimental data. One possible remedy is to form "digital twins," i.e., numerical simulation models of plasmas and plasma-interacting surfaces, and generate a large amount of data that can augment the shortage of experimental data. Even if the simulation results do not agree with experimental observations quantitatively, as long as the simulation data are correlated with experimental observations, such augmented data help us search optimal process conditions and perform a design of experiments. In this presentation, the recent development of data-driven plasma science [1] for low-temperature plasmas and their applications to material processing will be briefly reviewed. Then, more specifically, the prediction of sputtering yields/etch rates of materials by ion beams and the construction of plasma surrogate models will be discussed, which could allow real-time simulation of plasma processing systems for process control and fast survey of optimized process conditions.

[1] R. Anirudh, et al., "2022 Review of Data-Driven Plasma Science" IEEE Trans. Plasma Sci. (2023) to appear/ arXiv:2205.15832

## Quantum Science and Technology Mini-Symposium Room B110-112 - Session QS+VT-WeM

### Vacuum Technology for Quantum Applications

**Moderators: Ekta Bhatia, NY CREATES, Freek Molkenboer, TNO Science and Industry, the Netherlands**

**9:20am QS+VT-WeM-5 Stand-Alone Vacuum Cells for Compact Ultracold Quantum Technologies, Oliver Burrow, A. Arnold, P. Griffin, E. Riis, University of Strathclyde, UK** **INVITED**

Compact vacuum systems are key enabling components for cold atom technologies, facilitating extremely accurate sensing applications. There has been important progress toward a truly portable compact vacuum system; however, size, weight, and power consumption can be prohibitively large, optical access may be limited, and active pumping is often required. We have been developing centilitre-scale vacuum chambers with He-

<sup>1</sup> PSTD 2022 Young Investigator Awardee

# Wednesday Morning, November 8, 2023

impermeable viewports and an integrated diffractive optic, enabling robust laser cooling with light from a single polarization-maintaining fibre. With these devices, a cold atom demonstrator based on the vacuum cell delivers 107 laser-cooled 87Rb atoms per second, using minimal electrical power.

Pressure measurements in these compact systems are made from cold-atom loading curves, and pressure evolution have been studied in a ceramic based vacuum chamber. With continuous Rb gas emission, active pumping yields a 10–7 mbar equilibrium pressure, and passive pumping stabilizes to 3×10–6 mbar with a 17 day time constant. With no Rb dispensing and only passive pumping, a ceramic based vacuum chamber has currently kept a similar pressure for more than 500 days. The passive-pumping vacuum lifetime is several years, which is estimated from short-term He throughput with many foreseeable improvements.

Progress is also reported, including new cell materials, mobile cold-atom demonstration and adaptation of the fabrication technique into a cold-atom gravimeter vacuum system. This technology enables wide-ranging mobilization of ultracold quantum metrology.

Oliver S. Burrow, Paul F. Osborn, Edward Boughton, Francesco Mirando, David P. Burt, Paul F. Griffin, Aidan S. Arnold, Erling Riis; Stand-alone vacuum cell for compact ultracold quantum technologies. *Appl. Phys. Lett.* 20 September 2021; 119 (12): 124002. <https://doi.org/10.1063/5.0061010>

11:00am **QS+VT-WeM-10 Hybrid Quantum-HPC Computing Clouds in Europe**, *Richard Versluis*, TNO Science and Industry, the Netherlands  
**INVITED**

Quantum computing technology holds great promises for the long future but requires large investments in the near future as an enabler. Not only in terms of money and human resources such as talent, but also in infrastructure. This ranges from clean room infrastructure for QPU development, such as dedicated processing lines for quantum chip development to dedicated software and testing equipment for the screening and validation of quantum chips, to full stack system prototypes to demonstrate and validate crucial interfaces, but also to enable early adaptors to start implementing and exploring the potential of these new compute paradigms. Since a couple of years, some full stack demonstrators have been built, some in-house in a lab environment and some in an environment that is already a bit more market-orientated, such as a private cloud or a public cloud. Notably, some US companies like IBM, Google, Rigetti, IonQ and the Canadian company Dwave have set standards for online access to quantum computers. In Europe, the first publicly available cloud service for quantum computing, giving access to European quantum computers was Quantum Inspire, implemented by QuTech in The Netherlands. Since its launch in 2020, more online quantum computers have been launched in Europe, such as Quandel cloud.

With the necessity to get the most out of these early systems, hosting QPU's with still noisy and small numbers of qubits, a connection to HPC systems is crucial. It is anticipated that early advantage will be reached by combining classical and quantum algorithms, where the QPU could outperform an HC on some specific tasks, such as efficiency of the calculation in terms of wall clock time or energy used, the accuracy of the calculation, or simply by providing a different method of calculation that could not be done with a classical system. Integration of these, relatively immature systems, in an HPC workflow requires quite some effort. First of all, the language used to program quantum computers cannot be compared to high level classical programming languages like Python, C++, Rust etc. Secondly the integration of (runtime) compilers in the workflow is non-trivial. Hybrid classical-quantum algorithms, therefore require systems that can handle multiple languages, compiler services. Thirdly, the workflow management is not-standard: where the integration of classical accelerators like GPU's is based on standard-predefined interfaces such as scrum, these workflow interfaces for QPUs have not been defined yet.

In this talk I will highlight the goals and some first results of European activities on the integration of HPC and Quantum Computers in European projects such as the EuroHPC projects, OpenSuperQ plus and Quantum Large Scale Integration.

11:40am **QS+VT-WeM-12 Design Considerations of an XHV System for an Ion Trap Quantum Computer**, *Paul Smith*, N. Burch, A. Chew, P. Jones, P. Lamb, E. Lucchetta, S. Lodge, P. Milner, Edwards Ltd, UK; D. Clement, T. Sinha, Gamma Vacuum; A. Abolghasemi, L. Earl, J. Randall, Universal Quantum, UK

The design and configuration of an XHV system for an ion trap quantum computer is presented. A target operating pressure of 10<sup>-12</sup> mbar has been

identified to increase ion lifetime. Contributions to the residual gas load from leaks, permeation and outgassing will be evaluated as will the pumping strategies employed for each. The relative pumping performance of two combined NEG-IGP pumps will be reported. Other factors will be discussed including conductance optimization, limitations on component bakeout and NEG activation temperatures, vibrations, and shielding of magnetic fields and radiant heat loads.

12:00pm **QS+VT-WeM-13 Chances and Challenges: Aluminum Vacuum Components for Quantum Technology**, *Stefan Kiesel*, A. Trützschler, J. Hertel, K. Bergner, VACOM Vakuum Komponenten & Messtechnik GmbH, Germany

Quantum technology currently experiences a huge push towards commercialization, since it promises a variety of attractive applications, including quantum sensors, quantum computers, and quantum clocks. Many of these systems require a vacuum to isolate quantum objects or devices from the surrounding environment and to create stable conditions. In addition, signal paths into the vacuum are necessary to manipulate quantum objects, facilitated by hermetically sealed electrical and optical feedthroughs. The most advanced modern systems are built up from large and expensive laboratory equipment. However, the needs of commercially usable applications drive the development of quantum systems towards transportable, durable, and standardized solutions. To meet these challenging demands, better materials, novel manufacturing technologies and innovative designs are issues of today's development projects. As an example, aluminum Con-Flat (CF) components offer the possibility of providing customized solutions with high geometrical accuracy, reduced weight, low outgassing rates as well as vanishing magnetic permeability. As a manufacturer of vacuum components, VACOM is actively collaborating in several publicly funded projects to promote the development of quantum technology. In this talk we show goals and results of these projects regarding the development of vacuum systems and vacuum components for quantum technology.

## Surface Science Division

### Room D136 - Session SS+2D+AS+HC-WeM

#### Surface Science of 2D Materials

**Moderators:** Irene Groot, Leiden University, The Netherlands, Bo-Hong Liu, National Synchrotron Radiation Research Center

8:00am **SS+2D+AS+HC-WeM-1 Heterogeneous Photocatalysis: Alcohols on Bare and Metal-loaded TiO<sub>2</sub>(110) and Fe<sub>2</sub>O<sub>3</sub>(012)**, *Moritz Eder*, TU Wien, Austria; P. Petzoldt, M. Tschurl, Technical University of Munich, Germany; J. Pavelec, M. Schmid, U. Diebold, TU Wien, Austria; U. Heiz, Technical University of Munich, Germany; G. Parkinson, TU Wien, Austria

We investigated the (photo)chemistry of alcohols on TiO<sub>2</sub>(110) and Fe<sub>2</sub>O<sub>3</sub>(012) in ultra-high vacuum. Our studies focused on the role of the metal co-catalyst in the photocatalytic reaction by comparing the reactivity of bare and metal-loaded surfaces. We show that photocatalytic reactions are not merely a couple of redox reactions, but an interplay of thermal and photon-driven surface reactions.

Our results demonstrated that the co-catalyst plays a crucial role in the outcome of the reaction. On TiO<sub>2</sub>(110), alcohols are oxidized to the aldehyde/ketone and hydrogen surface species upon illumination. The hydrogen surface species were thermally converted to H<sub>2</sub> by the co-catalyst, allowing for a steady-state photocatalytic conversion of alcohols and the continuous production of molecular hydrogen. Using mass spectrometry, we determined turnover frequencies and rate constants. The identification of surface mechanisms on Fe<sub>2</sub>O<sub>3</sub> is less advanced, but there seem to be strong parallels in the photochemistry.

Our studies shed light on the fundamental processes involved in photocatalytic reactions on metal-loaded surfaces and contribute to the development of sustainable energy technologies.

8:20am **SS+2D+AS+HC-WeM-2 Factors Governing the Reactivities of Transition Metal Carbides at Vapor/Solid and Liquid/Solid Interfaces**, S. Alhowity, A. Ganesan, M. Gharraee, O. Omolere, *Qasim Adesope*, K. Balogun, P. Chukwunenye, F. D'Souza, T. Cundari, J. Kelber, University of North Texas

Transition metal carbides are of broad interest for both heterogeneous and electro-catalysis. However, fundamental understanding of chemical factors governing reactivities and selectivities at the vapor/solid and liquid/solid

# Wednesday Morning, November 8, 2023

interfaces remain sparse. Herein, *in situ* XPS results, electrochemical measurements, and DFT-based calculations are presented regarding the reactivities of NbC and TaC in the presence of O<sub>2</sub> vapor, and reactivity in solution towards the reduction of N<sub>2</sub> to NH<sub>3</sub>. NbC and TaC films were prepared by DC magnetron sputtering deposition, then exposed to O<sub>2</sub> vapor at room temperature, and analyzed by *in situ* XPS without exposure to ambient. Similarly prepared samples were also analyzed by *ex situ* XRD. These data show that, although Nb and Ta have similar oxophilicities, (a) deposited NbC films contain significant amounts of Nb oxide phases throughout the film, whereas TaC films deposited under similar conditions do not, and (b) the exposure of NbC films to O<sub>2</sub> at 300 K results in significant Nb oxide formation, but that TaC films remain inert towards O<sub>2</sub> under these conditions. DFT calculations indicate that this significant reactivity difference towards O<sub>2</sub> is due in large part to the greater Ta-C bond strength compared to Nb-C, and in part due to the relative energetic stabilities of the corresponding oxides. Electrochemical studies show that ambient-exposed NbC, with a Nb<sub>2</sub>O<sub>5</sub> surface layer, becomes reactive towards N<sub>2</sub> reduction to NH<sub>3</sub> under acidic conditions, but only after etching in NaOH to remove the surface oxide layer. Additionally, chronoamperometric data indicate that this reactive NbC surface is eventually modified under electrochemical conditions and becomes relatively inert towards N<sub>2</sub> reduction with time. Experiments involving *in situ* sample transfer between UHV and electrochemistry environments demonstrate that electrochemically active NbC surfaces in solution comprise Nb sub-oxide surface layers, in line with previous studies showing that effective NRR catalysts contain surface transition metal ions in intermediate oxidation states, supporting both N<sub>2</sub> lone pair attraction and pi-backbonding to bind and activate the NN triple bond.

**Acknowledgement** This work was supported in part by the UNT College of Science through COS grants 1600089 and RSG-2023-002 and in part by the NSF under grant no. DMR 2112864.

8:40am **SS+2D+AS+HC-WeM-3 Tunable Interfacial Electrochemistry at Moiré Material Interfaces**, *D. Kwabena Bediako*, University of California at Berkeley **INVITED**

At electrode–electrolyte interfaces, crystallographic defects are frequently implicated as active sites that mediate interfacial electron transfer (ET) by introducing high densities of localized electronic states (DOS). However, conventional defects can be challenging to deterministically synthesize and control at an atomic level, challenging the direct study of how electronic localization impacts interfacial reactivity. Azimuthal misalignment of atomically thin layers produces moiré superlattices and alters the electronic band structure, in a manner that is systematically dependent on the interlayer twist angle. Using van der Waals nanofabrication of two-dimensional heterostructures, scanning electrochemical cell microscopy measurements, and four-dimensional scanning transmission electron microscopy, we report a strong twist angle dependence of heterogeneous charge transfer kinetics at twisted bilayer and trilayer graphene electrodes with the greatest enhancement observed near the ‘magic angles’. These effects are driven by the angle-dependent engineering of moiré flat bands that dictate the electron transfer processes with the solution-phase redox couple, and the structure of the relaxed moiré superlattice. Moiré superlattices therefore serve as an unparalleled platform for systematically interrogating and exploiting the dependence of interfacial ET on local electronic structure.

9:20am **SS+2D+AS+HC-WeM-5 Growth of Ultrathin Silica Films on Pt(111) and Rh(111): Influence of Intermixing with the Support**, *Matthias Krininger*, Technical University of Munich, Germany; *F. Kraushofer*, Technical University of Munich, Austria; *N. Refvik*, University of Alberta, Canada; *F. Esch*, Technical University of Munich, Germany; *B. Lechner*, Technical University of Munich, Austria

Silica is a widely used catalyst support material for clusters and nanoparticles. Understanding the relationship between these clusters and the support is challenging, however, because SiO<sub>2</sub> is insulating, and in most applications not crystalline which drastically limits the use of experimental techniques to those that work on insulating samples and are not diffraction-based. Several previous studies have investigated ultrathin, quasi-2D silica films on a variety of metal supports [1], which can then be measured by scanning tunneling microscopy (STM), XPS and most other surface science methods. Previous work on Pt(111) did not result in closed films, which was attributed to lattice mismatch [2]. We show that closed films can in fact be grown on Pt(111) when silica is deposited in excess, likely due to formation of a platinum silicide layer with slightly expanded lattice constant at the interface. We also report results of film growth on

Rh(111), which is a near-perfect match to the lattice constant of freestanding SiO<sub>2</sub> films as calculated by theory. However, no high-quality films were achieved on Rh due to thermodynamic competition with a silicide.

References:

- [1] C. Büchner, M. Heyde, Two-dimensional silica opens new perspectives, *Prog. Surf. Sci.*, **92** (2017) 341-374.
- [2] X. Yu, B. Yang, J. A. Boscoboinik, S. Shaikhutdinov, and H.-J. Freund, *Appl. Phys. Lett.* **100** (2012), 151608.

9:40am **SS+2D+AS+HC-WeM-6 CO<sub>2</sub> Adsorption on Graphitic-Like Bilayer ZnO Film Studied by NAP-XPS**, *Bo-Hong Liu, S. Cheng*, National Synchrotron Radiation Research Center, Taiwan

CO<sub>2</sub> activation is a fundamental process in heterogeneous catalysis. ZnO-based catalyst has been extensively used in commercial methanol synthesis from CO<sub>2</sub> gas and the reverse water gas shift reaction. The adsorption behavior of CO<sub>2</sub> on the catalyst surface is pivotal to the reactivity. Whereas ZnO(0001)-Zn physisorbed or weakly chemisorbed CO<sub>2</sub>,<sup>1</sup> strong chemisorption of the molecule happens on non-polar surfaces, such as ZnO(10-10), resulting in a tridentate carbonate.<sup>2</sup> In Operando TEM investigation during methanol synthesis shows that ZnO single atomic layer stacks distortedly around Cu nanoparticles via strong metal-support interaction. The lack of interlayer ordering between the layers suggests a weak interlayer interaction; therefore, each layer resembles a free-standing sheet.<sup>3</sup> DFT modeling concluded that free-standing ZnO(0001) layer adopts an graphitic-like co-planner structure. The co-planner feature was verified experimentally for the bi-layer ZnO(0001) supported on Ag(111) and Au(111).<sup>4</sup> On Au(111) substrate, TPD shows that CO<sub>2</sub> adsorbs on the low coordinate sites at the layer edges.<sup>5</sup> In the present study, we investigate the CO<sub>2</sub> adsorption on bi-layer ZnO/Ag(111) film using NAP-XPS to extend the pressure condition towards reality. We found a more considerable CO<sub>2</sub> chemisorption at elevated pressure. The presentation will also address how the surface hydroxyl group influences CO<sub>2</sub> adsorption.

78. Wang, J.;Hokkanen, B.; Burghaus, U., Adsorption of CO<sub>2</sub> on pristine Zn–ZnO (0 0 0 1) and defected Zn–ZnO (0 0 0 1): A thermal desorption spectroscopy study. *Surf. Sci.* **2005**,*577* (2-3), 158-166.
79. Schott, V.;Oberhofer, H.; Birkner, A.;Xu, M.;Wang, Y.;Muhler, M.;Reuter, K.; Wöll, C., Chemical activity of thin oxide layers: strong interactions with the support yield a new thin-film phase of ZnO. *Angewandte Chemie International Edition* **2013**,*52* (45), 11925-11929.
80. Lunkenbein, T.;Schumann, J.;Behrens, M.;Schlögl, R.; Willinger, M. G., Formation of a ZnO overlayer in industrial Cu/ZnO/Al<sub>2</sub>O<sub>3</sub> catalysts induced by strong metal–support interactions. *Angewandte Chemie* **2015**,*127* (15), 4627-4631.
81. Tusche, C.;Meyerheim, H.; Kirschner, J., Observation of depolarized ZnO (0001) monolayers: formation of unreconstructed planar sheets. *Phys. Rev. Lett.* **2007**,*99* (2), 026102.
82. Deng, X.;Sorescu, D. C.; Lee, J., Enhanced adsorption of CO<sub>2</sub> at steps of ultrathin ZnO: the importance of Zn–O geometry and coordination. *Phys. Chem. Chem. Phys.* **2017**,*19* (7), 5296-5303.

11:00am **SS+2D+AS+HC-WeM-10 Investigation of Nitride Spintronic and Kagome-Structured Intermetallic Topological Materials Using Molecular Beam Epitaxy and Scanning Tunneling Microscopy**, *Arthur R. Smith*, Ohio University Physics and Astronomy Department

Owing to the overwhelming interest in topological [1] and spintronic materials [2], it is imperative to investigate these down to the atomic scale for their possible use in advanced devices. Many promising properties discovered among nitride materials, such as chemical stability and wide band gaps [3], may be combined with the equally promising aspects of topological materials, such as the topological Hall and Nernst effects [4]. Very recent work illustrates that spin-polarized scanning tunneling microscopy is a powerful tool for exploring topological band-structured Kagome antiferromagnets [5]. In our current work, we investigate both nitride material systems grown using molecular beam epitaxy as well as the growth of topological systems such as Kagome antiferromagnetic materials. Ongoing work in our group encompasses the investigation of Mn<sub>3</sub>Sn, FeSn, CrSn, Mn<sub>3</sub>Ga, and as a spintronic and topological nitride, Mn<sub>3</sub>GaN. These materials are grown in combined UHV MBE and scanning tunneling microscopy chamber systems in which the grown samples are first

# Wednesday Morning, November 8, 2023

fabricated using MBE and after that investigated for their structural, electronic, and magnetic properties including using STM and tunneling spectroscopy. Our goal is also to investigate these materials using spin-polarized STM as a function of temperature and applied magnetic field. Our current results show that these materials can be fabricated effectively using molecular beam epitaxy and investigated using various *in-situ* techniques such as reflection high energy electron diffraction and STM. Results from multiple on-going investigations will be presented with a birds-eye view of the progress. Especially to be presented will be STM and STS results in these Kagome systems grown using MBE.

This work is supported by the U.S. Department of Energy, Office of Basic Energy Sciences, Division of Materials Sciences and Engineering under Award No. DE-FG02-06ER46317.

- [1] P. Liu *et al.*, "Topological nanomaterials," *Nat. Rev. Mater.* **4**, 479 (2019).
- [2] A. Hirohata *et al.*, "Review on spintronics: Principles and device applications," *Journal of Magnetism and Magnetic Materials* **509**, 166711 (2020).
- [3] M. Xu *et al.*, "A review of ultrawide bandgap materials: properties, synthesis and devices," *Oxford Open Materials Science* **2**(1), itac004 (2022).
- [4] S. Roychowdhury *et al.*, "Giant Topological Hall Effect in the Noncollinear Phase of Two-Dimensional Antiferromagnetic Topological Insulator  $\text{MnBi}_4\text{Te}_7$ ," *Chemistry of Materials* **33**, 8343 (2021).
- [5] H. Li *et al.*, "Spin-polarized imaging of the antiferromagnetic structure and field-tunable bound states in kagome magnet  $\text{FeSn}$ ," *Scientific Reports* **12**, 14525 (2022).

11:20am **SS+2D+AS+HC-WeM-11 Molecular Beam Epitaxial Growth and Investigations of  $\text{FeSn}$  on  $\text{LaAlO}_3$** , Tyler Erickson, S. Upadhyay, H. Hall, D. Ingram, S. Kaya, A. Smith, Ohio University

Kagome antiferromagnetic and ferromagnetic materials provide an interesting avenue for research through the investigation of frustrated magnetism, band topology and electronic correlations [1-4].  $\text{FeSn}$  is a layer-wise antiferromagnetic Kagome structured material with characteristic dispersion-less flat bands and Dirac cones at the Brillouin zone boundaries. Li *et al.* have presented exciting spin-polarized scanning tunneling microscopy results revealing surface electronic and magnetic properties of *in-situ* cleaved bulk  $\text{FeSn}$  [1]. Zhang *et al.* reported strain engineering of  $\text{FeSn}$  on  $\text{SrTiO}_3$  (111) with precise control of the stanene layers [2]. Kawakami *et al.* reported  $\text{Fe}_3\text{Sn}_2$  growth on Pt buffer layers on top of  $\text{Al}_2\text{O}_3$  and studied various topological phenomena of this topological Kagome material [3,4]. Bhattarai *et al.* studied the magnetotransport properties of  $\text{FeSn}$  grown on silicon substrates [5]. Here, we study the growth of  $\text{FeSn}$  directly on  $\text{LaAlO}_3$  and report the successful growth of high-quality crystalline thin-films of  $\text{FeSn}$ . Reflection high-energy electron diffraction and x-ray diffraction are used to discover the *in-plane* and *out-of-plane* lattice constants, while atomic force microscopy and Rutherford backscattering provide topographical and stoichiometric characterization. Preliminary results indicate *in-plane* and *out-of-plane* lattice constants of 5.290 Å and 4.56 Å compared to the expected results of 5.297 Å and 4.481 Å, respectively. Besides discussing the thin film  $\text{FeSn}$  growth results, we also plan to present scanning tunneling microscopy results on the MBE-grown surfaces.

This work is supported by the U.S. Department of Energy, Office of Basic Energy Sciences, Division of Materials Sciences and Engineering under Award No. DE-FG02-06ER46317.

- [1] H. Li *et al.*, *Scientific Reports*, **12** 14525 (2022)
- [2] H. Zhang *et al.*, *Nano Lett.* **23**, 239 – 2404 (2023)
- [3] I. Lyalin *et al.*, *Nano Lett.* **21**, 6975 – 6982 (2021)
- [4] S. Cheng *et al.*, *APL Mater.* **10**, 061112 (2022)
- [5] N. Bhattarai *et al.*, *Phys. Status Solidi A*, **220**: 2200677 (2023)

11:40am **SS+2D+AS+HC-WeM-12 AVS Graduate Research Awardee Talk: Molecular Beam Epitaxial Growth, Structural Properties, and Surface Studies of  $a$ -Plane-Oriented  $\text{Mn}_3\text{Sn}$  on  $C$ -Plane  $\text{Al}_2\text{O}_3$** , Sneha Upadhyay<sup>1</sup>, T. Erickson, Ohio University; J. Hernandez, Universidad Autonoma de Puebla, Mexico; H. Hall, K. Sun, Ohio University; G. Cocoltzi, Universidad Autonoma de Puebla, Mexico; N. Takeuchi, Universidad Nacional Autonoma de Mexico, Mexico; A. Smith, Ohio University

Recently, Chen *et al.* reported the observation of tunneling magnetoresistance in an all-antiferromagnetic tunnel junction consisting of  $\text{Mn}_3\text{Sn}/\text{MgO}/\text{Mn}_3\text{Sn}$ .<sup>1</sup> Furthermore, Bangar *et al.* demonstrated a technique for engineering the spin Hall conductivity of  $\text{Mn}_3\text{Sn}$  films by changing the Mn: Sn composition.<sup>2</sup> These works show the potential of studying this Kagome antiferromagnetic material and the importance of being able to grow smooth films. This work uses molecular beam epitaxy to investigate the growth of  $\text{Mn}_3\text{Sn}$  (11 $\bar{2}$ 0) on  $\text{Al}_2\text{O}_3$  (0001). The growth is monitored *in-situ* using reflection high energy electron diffraction and measured *ex-situ* using X-ray diffraction, Rutherford backscattering, and atomic force microscopy. In our previous work, we carried out a single-step growth at 450°C, which resulted in a crystalline but discontinuous *a-plane-oriented* (~43% 11 $\bar{2}$ 0)  $\text{Mn}_3\text{Sn}$  film with a mix of other orientations including 0002.<sup>3</sup> Leading from this work, changes were made to the growth recipe, which involved carrying out a two-step growth procedure at room temperature, resulting in a contiguous, epitaxial  $\text{Mn}_3\text{Sn}$  film with up to ~82% 11 $\bar{2}$ 0-orientation. We are also exploring the effect of varying the Mn: Sn flux ratio and the film thicknesses (in the range of 5 – 200 nm) on the film crystallinity and orientation. We observe that varying the Mn: Sn flux ratio leads to a change in the RHEED patterns from pointy to streaky, and the XRD shows that the 11 $\bar{2}$ 0 peak can be varied between ~82% to ~38% of all the peaks' total intensity. We also plan to present the first results on ultra-high vacuum scanning tunneling microscopy imaging of the (11 $\bar{2}$ 0)  $\text{Mn}_3\text{Sn}$  surface.

## Acknowledgments:

The authors acknowledge support from the U.S. Department of Energy, Office of Basic Energy Sciences, Division of Materials Sciences and Engineering under Award No. DE-FG02-06ER46317. The authors would like to thank Dr. Eric Stinoff and his students for back-coating the sapphire (0001) substrates.

<sup>1</sup> X. Chen *et al.*, "Octupole-driven magnetoresistance in an antiferromagnetic tunnel junction." *Nature* **613**, 490 (2023).

<sup>2</sup> H. Bangar *et al.*, "Large Spin Hall Conductivity in Epitaxial thin films of Kagome Antiferromagnet  $\text{Mn}_3\text{Sn}$  at room temperature", *Adv. Quantum Technol.* **6**, 2200115 (2023).

<sup>3</sup> S. Upadhyay *et al.*, "Molecular beam epitaxy and crystal structure of majority *a-plane* oriented and substrate strained  $\text{Mn}_3\text{Sn}$  thin films grown directly on sapphire (0001)", *Journal of Vacuum Science and Technology A*, to be published (2023).

## Thin Film Division

### Room A105 - Session TF1+PS-WeM

#### Emerging and Advanced Materials and Processes

Moderators: Subhadra Gupta, University of Alabama, April Jewell, Jet Propulsion Laboratory

8:00am **TF1+PS-WeM-1 Modified Reactive Sputter Deposition of Titanium Nitride Thin Films via HIPIMS with Kick-Pulse**, A. Miceli, D. Santavicca, Stephen Stagon, University of North Florida **INVITED**

Direct current (DC) and radio frequency (RF) sputtering methods have been commonplace in industry for several decades and widely studied in the literature. Hard films of nitrides, such as titanium nitride (TiN), have been deposited using reactive DC sputtering onto cutting tools and medical devices extensively as well. For these applications, the films require excellent adhesion, high density, and high hardness. High-Power Impulse Magnetron Sputtering (HIPIMS) has emerged over the last several years as a method to produce films with increased density and mechanical properties. Process-structure-property relationships for reactive HIPIMS are not well developed. Additionally, conventional HIPIMS suffers from relatively low deposition rates, which become a challenge or barrier to adoption for applied TiN coatings that are typically greater than several microns in thickness. This work aims to look at increasing this deposition rate while maintaining the beneficial effects of HIPIMS by utilizing the short duration

<sup>1</sup> AVS Graduate Research Awardee

# Wednesday Morning, November 8, 2023

“kick-pulse” in the voltage/current cycle, leading to higher instantaneous deposition rates and increased adatom energy level. TiN films are deposited onto silicon (Si) wafers under varied reactive sputtering conditions, including DC, HIPIMS, and HIPIMS with kick-pulse. Structural characterizations are performed using scanning electron microscopy (SEM) and X-ray diffraction (XRD). Optical and electrical properties of the resulting films are also characterized using reflection UV-Vis spectroscopy and 4-point probe techniques. The deposition rate, morphology, and chemical composition of the films are highly affected by the processing conditions, with the kick-pulse producing significant increase in deposition rate and observed grain size. Further investigation will aim to develop a modified structural zone model to include HIPIMS with and without kick-pulse.

8:40am **TF1+PS-WeM-3 Time-Resolved ALD Reaction Heat**, *Ashley Bielinski, E. Kamphaus, L. Cheng, A. Martinson*, Argonne National Laboratory **INVITED**

Atomic layer deposition (ALD) is a surface synthesis technique that consists of sequential self-limiting surface reactions between molecular precursors and a substrate. Differences in the substrate surface as well as the precursor ligands can have a significant influence on the properties of the deposited film and the formation of interfaces, even within a given material system. ALD processes are often empirically optimized with only a simplified chemical understanding of the surface reactions. While this is sufficient for some applications, emerging technologies such as area-selective ALD and site-selective ALD seek to leverage the chemical selectivity between precursor molecules, inhibitors, and the substrate surface. To better understand and direct ALD surface reactions, we must improve our fundamental understanding of the surface reaction mechanisms and energetics.

Pyroelectric calorimetry enables in situ, time-resolved measurements of the heat generated by ALD surface reactions. We present a pyroelectric calorimeter optimized to operate under standard ALD conditions with resolution down to  $0.1 \mu\text{J}/\text{cm}^2$  and 50 ns. This process of ALD calorimetry was used to measure the heat generation rates from trimethylaluminum (TMA), tetrakis(dimethylamino)zirconium (TDMAZr) and water to form  $\text{Al}_2\text{O}_3$  and  $\text{ZrO}_2$ . The aerial heat generation rates were combined with in situ spectroscopic ellipsometry and ex situ Rutherford backscattering measurements to calculate the reaction thermodynamics on a per atom basis. These results were then compared with computational first principles models as well as calculations of the standard reaction enthalpies. The total measured heat was in good agreement with the standard enthalpies, but the computational models showed greater deviation. Pyroelectric calorimetry provides a unique opportunity to validate and provide benchmarks for computational models, helping to evaluate the accuracy of proposed models and mechanisms.

The heat generation rates were also analyzed to compare reaction kinetics. For example, the water reaction occurred at significantly different speeds on the TMA and TDMAZr saturated surfaces. Due to the high time-resolution, we were able to resolve, for the first time, a multi-step reaction for TDMAZr reacting with hydroxylated  $\text{ZrO}_2$ . Heat generation rates provide new insight into ALD processes, helping us to untangle the thermodynamics, kinetics, and mechanisms of these heterogeneous surface reactions.

9:20am **TF1+PS-WeM-5 Reducing Hysteresis in Atomic Layer Deposited  $\text{VO}_2$  Thin Films**, *V. Wheeler, Peter Litwin, S. Bennett, M. Currie*, US Naval Research Laboratory

$\text{VO}_2$  is a phase change material that undergoes a first order crystalline phase transition at a critical temperature ( $T_c = 68^\circ\text{C}$ ), resulting in significant changes in intrinsic electrical and optical properties, especially in the infrared. Optical and electrical variations associated with this phase transition are of particular interest as passive and active components of electronic and optoelectronic devices, including RF limiters, thermal regulation, and modulated signaling. Realizing this type of device often requires the integration of thin, conformal  $\text{VO}_2$  films with complex, non-planar structures (like metamaterials). Thus, atomic layer deposition (ALD) is an ideal deposition method in these cases.

While ALD is useful for integrating highly uniform and stoichiometric films with dissimilar materials, the low deposition temperature results in amorphous films that do not exhibit the required phase change for device applications. Thin  $\text{VO}_2$  films deposited by many methods, including ALD, typically require a post-deposition anneal to induce the crystallization necessary for large, abrupt, usable changes in properties during the phase transition. This anneal can be accomplished in many ways such as a slow traditional anneal in specific partial oxygen environments or using

environmentally independent laser processes to rapidly crystallize the film. However, the microstructure and resulting phase change properties are highly dependent on the method of crystallization and can lead to deleterious effects like large hysteresis windows ( $> 10^\circ\text{C}$ ) during heating and cooling through the phase transition of these films. For optimum performance in device applications, the hysteresis needs to be reduced or even eliminated.

In this work, we will discuss developing novel processes towards achieving crystalline ALD  $\text{VO}_2$  films and the impact they have on reducing hysteresis, including the introduction of nucleation layers and tailoring of plasma properties during plasma enhanced ALD. As an example, we have found that hysteresis can be reduced to a few degrees using ALD  $\text{TiO}_2$  films, independent of crystallinity, phase, or thickness of the  $\text{TiO}_2$  film itself, but ALD  $\text{Al}_2\text{O}_3$  or  $\text{HfO}_2$  buffer layers do not impact the hysteresis at all. When possible, we will discuss the possible causes and mechanisms behind hysteretic performance improvements.

9:40am **TF1+PS-WeM-6 Magnetron Sputtering Deposition and Stabilization of the Bismuth Sesquioxide ( $\text{Bi}_2\text{O}_3$ ) High-Temperature Equilibrium Phase**, *Sandra E. Rodil, A. Martinez, O. Depablos-Rivera*, Universidad Nacional Autónoma de México

Bismuth sesquioxide ( $\text{Bi}_2\text{O}_3$ ) exhibits a dynamic polymorphism characterized by two thermodynamically stable phases. The first is the monoclinic ( $\alpha$ ) phase, which remains stable from room temperature (RT) up to  $730^\circ\text{C}$ , while the second is the defect-fluorite cubic ( $\delta$ ) phase, stable above  $730^\circ\text{C}$  and up to the material's melting point ( $830^\circ\text{C}$ ). Additionally, during the cooling/heating process, two metastable phases ( $\beta$ -tetragonal and  $\gamma$ -bcc) are formed, and their transformation temperature depends on factors such as the cooling rate, ambient conditions (vacuum or air), and oxygen concentration.

The production of the  $\delta$ - $\text{Bi}_2\text{O}_3$  phase as a thin film date back to 1999, when it was first demonstrated using electrodeposition, followed by magnetron sputtering. The crystallographic structure of the films has been analyzed through X-ray diffraction patterns and visible Raman spectra. However, caution must be exercised when interpreting Raman spectra, as the broadband at  $600 \text{ cm}^{-1}$  associated with the defect-fluorite cubic ( $\delta$ ) phase can also be observed in other phases. To address this issue, we critically analyzed the assignments provided in the literature for this broad Raman mode and proposed an alternative explanation consistent with its observation in all films. Our proposal attributes the  $600 \text{ cm}^{-1}$  band to the presence of residual-weakly bonded [ $\text{BiO}_n$ ] units located at the grain boundaries of the nanocrystalline films. This band is not exclusive to the defective fluorite cubic structure of  $\text{Bi}_2\text{O}_3$ . Interestingly, we found a similar signal in the Raman spectra of the  $\text{Bi}_4\text{O}_7$  phase, which had not been reported before, suggesting possible incorrect assignments to the  $\delta$ -phase. We employed a density functional approximation of the  $\text{Bi}_4\text{O}_7$  molecular structure to gain further insights to calculate the Raman active bands. The theoretical estimations showed excellent agreement with experimental data, reinforcing the validity of our proposed explanation.

Finally, our investigations revealed that doping with heterovalent ions allows for stabilizing films exhibiting the  $\delta$ - $\text{Bi}_2\text{O}_3$  phase within a temperature range from room temperature to  $600^\circ\text{C}$ . This exciting discovery opens new possibilities for using these films as ionic conductors, potentially finding applications in various technological fields.

## Thin Film Division

### Room A105 - Session TF2+AP+SE+SS-WeM

#### Controlling Microstructure and Accessing Non-Equilibrium Phases in Thin Films

**Moderators: Robert Grubbs**, IMEC Belgium, **Richard Vanfleet**, Brigham Young University

11:00am **TF2+AP+SE+SS-WeM-10 Stabilizing Polar Polymorphs of Scandium Ferrite for Photovoltaics**, *M. Frye, Lauren Garten*, Georgia Institute of Technology **INVITED**

Metastability is no longer synonymous with unstable or unattainable, but further work is needed to enable the next generation of electronics and photovoltaics. In this talk I will discuss the development of a stabilization route for the P63cm phase of  $\text{ScFeO}_3$  through precursor control and interface engineering. The P63cm phase has potential for lead-free piezoelectric, photo-ferroic, and ferroelectric applications. Unfortunately, this phase is in competition with four other known polymorphs that are similar in structure and energy and there is not a well matched epitaxial

# Wednesday Morning, November 8, 2023

substrate. So we took a different approach by controlling the atomic layering of the precursor structure and the deposition timing to stabilize the P63cm phase under conditions that previously lead to the ground state. The film structure is verified by transmission electronic microscopy and x-ray diffraction. Ab initio calculations confirm that layered growth stabilizes the metastable phase and highlights the importance of the variable oxidation state of iron, the high activation energy against diffusion, and the surface termination of the substrate in designing a stabilization approach. This work highlights routes to access similar polymorphs on an array of different substrates, opening up new materials and new device architectures.

11:40am **TF2+AP+SE+SS-WeM-12 The Role of Thermal Vibrational Disorder in the Structural Phase Transition of VO<sub>2</sub> Probed by Raman Spectroscopy**, *Aminat Oyiza Suleiman*, Institut National de la Recherche Scientifique, Canada; *S. Mansouri*, Institut National de la Recherche Scientifique, Canada; *N. Émond*, Massachusetts Institute of Technology, Canada; *T. Bégin*, *J. Margot*, Université de Montréal, Canada; *C. Mohamed*, National de la Recherche Scientifique, Canada

Vanadium dioxide (VO<sub>2</sub>) is a typical correlated electron material which exhibits a first-order metal–insulator transition (MIT) at a near-room temperature of about 340 K. Upon heating, VO<sub>2</sub> switches from an insulating monoclinic phase (M1 or M2) to a metallic tetragonal rutile phase (R). The mechanism behind the MIT in VO<sub>2</sub> is still controversial: Is it a structure driven Peierls transition mechanism or a Mott transition where strong electron–electron correlations drive charge localization and collapse the lattice symmetry? By directly comparing the electrical and lattice–dynamic properties of VO<sub>2</sub>, useful information about the MIT/SPT in VO<sub>2</sub> can be obtained.

Herein, we therefore present a detailed Raman study of undoped (M1) and Cr-doped (M2) VO<sub>2</sub> thin films as a function of temperature. The studied VO<sub>2</sub> films with different thicknesses are deposited on c- and r-sapphire substrates. While their structural properties and morphology are examined by XRD and AFM techniques, respectively, Raman measurements are correlated to four-point probe resistivity measurements, giving an insight into the coupling between VO<sub>2</sub> structural phase (SP) and MI transitions. By distinctively combining the Raman data with information from reported EXAFS data, a relationship between the Raman intensities and the mean Debye–Waller factors ( $\sigma^2$ : the mean-square relative displacements) is established. The temperature dependence of the vanadium dimers Waller factor ( $\sigma_R^2(V-V)$ ), as calculated from the Raman intensity, was found to follow the temperature profile of the  $\sigma_{EXAFS}^2(V-V)$  obtained from the reported EXAFS data. These findings provide an evidence on the critical role of the thermal vibrational disorder in VO<sub>2</sub> phase transitions, demonstrating that by correlating Raman data with EXAFS analysis, both lattice and electronic structural dynamics can be probed.

12:00pm **TF2+AP+SE+SS-WeM-13 Interplay of Lattice Distortion and Electronic Structure in Metastable Brookite TiO<sub>2</sub>**, *Pritha Biswas*, Oregon State University; *M. Choi*, *K. Koirala*, *M. Bowden*, *L. Strange*, Pacific Northwest National Laboratory; *H. Zhou*, Argonne National Laboratory; *J. Tate*, Oregon State University; *Y. Du*, *T. Kaspar*, *D. Li*, *P. Sushko*, Pacific Northwest National Laboratory

Controlling the coupling between lattice distortions and electronic properties is one of the promising routes toward enhancing the performance of materials used in energy technologies, such as photocatalysis, photovoltaics, and energy storage. Oxide semiconductors that exhibit polymorphism represent a convenient class of systems to study this coupling by investigating the effect of external stimuli on transition pathways between polymorphs. Among the oxide semiconductors, earth-abundant TiO<sub>2</sub> exists in several polymorphic forms, including rutile, anatase, and brookite, with distinctly different structural symmetries. Compared to the common rutile and anatase polymorphs, metastable brookite TiO<sub>2</sub> is the least studied one due to the difficulties associated with its synthesis in a phase pure form. At the same time, mechanisms of its transformation to the more stable anatase and rutile polymorphs are promising to provide a rich insight into the relationships between the character of the lattice deformations, defect content, and electronic structure. We have developed a recipe for phase selective TiO<sub>2</sub> polymorph formation, where tuning of oxygen vacancy concentration drives the crystallization of amorphous TiO<sub>2</sub> thin films towards a specific polymorphic structure. In this study, thermal treatment was used to control the evolution of as-deposited, sputtered amorphous TiO<sub>2</sub> thin films towards the brookite lattice. The crystallinity and phase purity of the resulting structures were investigated by lab-based grazing incidence XRD, synchrotron XRD, and transmission electron

microscopy. The dependence of structural variations present in the sample on the details of the annealing treatments was evaluated using Rietveld refinement analysis. X-ray photoelectron spectroscopy (XPS), confocal Raman spectroscopy, and high-resolution transmission electron microscopy (HRTEM) were used to understand the effect of local deformation on the electronic structure of brookite. We found a correlation between the degree of lattice parameter deviation, shifts of the Raman vibrational modes, and the position of the brookite valence band. The effect of these lattice distortions at the atomic scale on the photocatalytic activity of brookite will be discussed.

# Wednesday Afternoon, November 8, 2023

## 2D Materials Technical Group

### Room C123 - Session 2D-WeA

#### 2D-Materials: Electronic/Magnetic/Optical Properties

**Moderators:** Zachary Krebs, University of Wisconsin - Madison, Xuedan Ma, Argonne National Lab

#### 2:20pm 2D-WeA-1 Josephson Diode Effect via Proximity Induced Superconductivity in 2D Materials, *Stuart Parkin*, Max Planck Institute for Microstructure Physics, Germany **INVITED**

Recently we have discovered a non-reciprocal Josephson diode effect in several Josephson junctions, both lateral and vertical, formed from conventional superconducting electrodes (Nb, NbSe<sub>2</sub>) separated by several non-superconducting metals including the 2D van der Waals metals, NiTe<sub>2</sub> [1] and WTe<sub>2</sub> [2], as well as sputtered layers of platinum that are magnetically proximitized via a magnetic insulator (YIG) [3]. Each of these materials becoming superconducting by proximity to the conventional superconducting electrodes. The superconductivity can be sustained over long distances of, in some cases, up to ~1 micron. The critical supercurrent densities for current flowing in opposite directions within the junction are distinct and can vary by up to 40% or more. For the van der Waals metals the non-reciprocity is only observed in the presence of a small magnetic field oriented perpendicular to the supercurrent, whereas for the Pt based junctions the diode effect is observed in zero field. For vertical Josephson junctions formed from WTe<sub>2</sub> we show that the non-reciprocity depends on the orientation of the magnetic field with respect to the crystal structure of the WTe<sub>2</sub>, proving thereby the intrinsic origin of the Josephson diode effect. We also show how the magnitude of the asymmetry increases with the thickness of the WTe<sub>2</sub> barrier [2]. Finally, we discuss our recent work on spin-triplet supercurrent spin valves using 2D chiral Kagome antiferromagnets [4].

[1] B. Pal *et al.*, "Josephson diode effect from Cooper pair momentum in a topological semimetal," *Nat. Phys.*, vol. 18, pp. 1228-1233, 2022.

[2] J.-K. Kim *et al.*, "Intrinsic supercurrent non-reciprocity coupled to the crystal structure of a van der Waals Josephson barrier," *arXiv:2303.13049*, 2023.

[3] K.-R. Jeon *et al.*, "Zero-field polarity-reversible Josephson supercurrent diodes enabled by a proximity-magnetized Pt barrier," *Nat. Mater.*, vol. 21, pp. 1008-1013, 2022.

[4] K.-R. Jeon *et al.*, "Chiral antiferromagnetic Josephson junctions as spin-triplet supercurrent spin valves and d.c. SQUIDs," *Nat. Nanotechnol.*, 2023.

#### 3:00pm 2D-WeA-3 Behavior of Excited States in 2H and 3R Bilayer WSe<sub>2</sub>, *Kathleen McCreary, M. Phillips, H. Chuang, D. Wickramaratne, M. Rosenberger, C. Hellberg, B. Jonker*, Naval Research Laboratory

Transition metal dichalcogenide bilayers exhibit improved stability and higher carrier mobility compared to their monolayer counterparts, and may be attractive for a variety of applications. Both 2H and 3R bilayers are energetically stable and are expected to exhibit semiconducting behavior. However, 2H has received the bulk of attention due to its ready availability in the form of mechanically exfoliated flakes. Here, we detail the energies and temperature dependent behaviors of the ground and the first excited excitonic states in both 2H and 3R WSe<sub>2</sub> bilayers. Samples are obtained through chemical vapor deposition, encapsulated with hBN, and reflectance contrast (RC) is measured to identify 1s and 2s excitonic states. At cryogenic temperatures, a splitting of approximately 17 meV is experimentally observed in both the 1s and 2s states of 3R bilayers. This splitting is consistent with our DFT calculations and is due to lack of inversion symmetry, with the two peaks corresponding to distinct excitonic transitions in the upper and lower layers of the 3R WSe<sub>2</sub>. As temperatures increase, excitonic states broaden and RC intensity decreases, preventing detection of 2s states above 100 K. The 1s state is evident at all temperatures between 4 K and 300 K, and splitting of the 1s state in 3R samples is detectable to approximately 250 K. This work provides much needed insight into bilayer systems and demonstrates that interlayer interactions are strong enough to significantly modify the optical properties in WSe<sub>2</sub> samples.

#### 3:20pm 2D-WeA-4 2D SnO/MoO<sub>3</sub> van der Waals Heterojunction with Tunable Electronic Behaviors for Multi-functional Applications: DFT Calculations, *Junyu Lang*, ShanghaiTech University, China; *Y. Ma*, Shanghai Jiao Tong University, China; *Y. Yang*, ShanghaiTech University, China

Introduction

Following the advent of graphene in the late 1940s, two-dimensional (2D) materials, such as MXenes, transition-metal dichalcogenides (TMDs), black phosphorene, etc., have attracted extensive attention. Among various 2D materials, transition-metal oxides (TMOs) possess exceptional advantages, such as tunable redox property, high chemical stability, environmental friendliness and earth-abundant characteristic. Metal oxide van der Waals (vdW) heterostructures have attracted extensive attention in fundamental research and new-device design. The remarkable advantage of their tunable energy band structure makes it particularly important to develop versatile metal-oxide heterojunctions and to explore their mechanisms. Herein, 2D SnO/MoO<sub>3</sub> vdW heterojunction is successfully constructed by first-principles calculations. The electronic structure of the SnO/MoO<sub>3</sub> vdW heterojunction has been systematically investigated, and the underlying physical mechanism responsible for its band alignment has been further revealed. A Z-scheme charge transfer mechanism has been demonstrated in SnO/MoO<sub>3</sub> with remarkable photocatalytic CO<sub>2</sub> reduction capability. Most importantly, the band alignment can be efficiently tuned by varying the external electric field, indicating its multifunctional potential. Furthermore, the CO<sub>2</sub> reduction reaction pathway and product selectivity occurring at the surface of 2D SnO/MoO<sub>3</sub> vdW heterojunction can be optimized by adjusting the applied electric field.

#### Results and Discussion

The vdW heterojunction, SnO/MoO<sub>3</sub> has been designed by first-principles calculations. The formation of 2D SnO/MoO<sub>3</sub> vdW heterojunctions is not limited by the relative horizontal displacements between the different layers, which greatly facilitates fabrication processes and functional applications. In addition, a Z-scheme charge transfer mechanism has been demonstrated in SnO/MoO<sub>3</sub>, exhibiting remarkable photocatalytic CO<sub>2</sub> reduction capability. Possible reduction reaction pathways for CO<sub>2</sub> on the surface of the SnO/MoO<sub>3</sub> vdW heterojunction were further explored and it was shown that CH<sub>4</sub> and CH<sub>3</sub>OH are the main products. Furthermore, we found that the electronic properties of 2D SnO/MoO<sub>3</sub> vdW heterojunction can be efficiently modulated by applying an external electric field, which is beneficial for optimizing the reaction path and improving the product selectivity of CO<sub>2</sub> reduction reactions. Most importantly, transitions between type-III and type-II band alignments are observed in the 2D SnO/MoO<sub>3</sub> vdW heterojunction at negative electric fields. These findings will provide a strong theoretical support for designing novel tunneling field-effect transistors and photocatalysts.

#### 4:20pm 2D-WeA-7 2D Materials Explored Using nanoARPES, *A. Bostwick, C. Jozwiak, Eli Rotenberg*, Lawrence Berkeley Lab, USA **INVITED**

Angle-resolved photoemission is a premiere technique for measuring the electronic structure of materials, as represented by momentum-resolved electronic bands. Furthermore, with modern high-resolution instrumentation it is possible to access the single-particle spectral function  $A(k, \omega)$ , which gives important information on the renormalization of excited state energies and lifetimes due to many-body interactions and defect scattering.

NanoARPES machines capable of spatially-resolving the ARPES spectrum on the mesoscopic scale are coming online at synchrotrons around the world, with spatial resolution in the range 100-1000nm. Combining these new small probes with arbitrary stacking orders of diverse materials assembled micromechanically, nanoARPES can obtain information on new materials far faster than in the past, when probe sizes limited us to wafer-scale, epitaxially grown heterostructures. Using small x-ray probes, nanoARPES can also study naturally or spontaneously-formed heterogenous materials. Most if not all nanoARPES machines are accessible through proposals to international user facilities, and the community specializing in these experiments is growing rapidly.

Most excitedly, nanoARPES offers the possibility to measure 2D materials and heterostructures at true device scales, and can thus enable for the characterization of materials under *in operando* conditions. In this talk I will review recent developments and pioneering experiments at the MAESTRO beamline at the Advanced Light Source in Berkeley, CA. These capabilities include the application of external fields (electrical, magnetic, and optical) and current. Prospects for the application of magnetic fields to create a new "MagnetoARPES" technique will be presented.

#### 5:00pm 2D-WeA-9 Probing Many-body Effects in 2D Materials using nanoARPES, *Jyoti Katoch*, Carnegie Mellon University, United States Minor Outlying Islands (the)

Two-dimensional (2D) materials provide unprecedented opportunity to engineer their physical properties by modification to the electronic structure utilizing external perturbations- strain, gating, adsorbates,

# Wednesday Afternoon, November 8, 2023

defects, twist-angle, and interface engineering. This is expected to cause changes to the Hamiltonian describing the system and has resulted in exotic phenomena such as superconductivity, bound quasiparticles, topological states as well as magnetic phases, with implications for novel electronics and spin-device applications. In this talk, I will present our work on directly visualizing (without any assumption) the electronic structure of atomically thin systems utilizing *in-operando* angle-resolved photoemission spectroscopy with nanoscale spatial resolution (nanoARPES) on 2D heterostructures and their fully functional devices [1,2,3,4,5]. I will present the experiments which demonstrate on-demand tuning of the electronic band structure in atomically thin systems, such as transition metal dichalcogenides (TMDCs) and graphene, by varying the twist-angle between the atomic layers and external dopants. Specifically, I will discuss the electric field tuning of the electronic interactions that result in van Hove singularity and flat bands in twisted bilayer graphene and twisted double bilayer graphene heterostructures. In addition, I will show our recent results where we observe the formation of quasiparticle polarons due to many-body interactions in graphene/TMDC heterostructures.

## References:

- [1] Katoch et. al., Nature Physics 14, 355-359 (2018).
- [2] Ulstrup  
[<https://arxiv.org/search/?searchtype=author&query=Ulstrup%2C+S>], et. al., Science Advances, Vol. 6, no. 14, eaay6104, (2020).
- [3] Jones, et. al., 2D Mater., 9 015032 (2022).
- [4] Muzzio, et. al., Physical review B Rapid Communications 101, 201409(R) (2020).
- [5] Jones, et. al., Adv. Mater., 32, 2001656 (2020).

5:20pm **2D-WeA-10 Electrical Transport of High-Quality CVD-Grown MoSe<sub>2</sub> Nanoribbons**, *Y.-J. Leo Sun*, Laboratory for Physical Sciences; *O. Ambrozaite, Z. Zhang, T. Kempa*, Johns Hopkins University; *T. Murphy*, University of Maryland, College Park; *A. Friedman, A. Hanbicki*, Laboratory for Physical Sciences

Two-dimensional (2D) materials such as transition metal dichalcogenides are excellent candidates for creating novel nano-electronic and photonic devices. Previous research indicates that the edge states of MoSe<sub>2</sub> could strongly influence its conductivity, and the 2D honeycomb structure enables different electronic performance along the zigzag and armchair edges. Understanding and controlling the conductivity is essential in devices like field effect transistors that use MoSe<sub>2</sub> as the channel. To date, transport along edge states of MoSe<sub>2</sub> nanoribbons, which have substantially reduced dimensionality relative to 2D crystals, has not been explored. In this project, we used chemical vapor deposition (CVD) to synthesize MoSe<sub>2</sub> nanoribbons through a particle-seeded approach. This approach yields directed growth of monolayer MoSe<sub>2</sub> to form high aspect ratio (>7) nanoribbons. Tip-enhanced photoluminescence (TEPL) is used to probe the optical properties of the edge and surface of the MoSe<sub>2</sub> nanoribbons. To perform electronic transport measurements, we used e-beam lithography to pattern contacts on the nanoribbons in a Hall bar configuration with the side contacts at the edges and tips of the nanoribbons. The influence of edge states on the electrical performance of MoSe<sub>2</sub> nanoribbons was investigated by conductivity and Hall transport measurements. Current flow in the transverse and longitudinal directions of the nanoribbon was compared to analyze the importance of edge states on MoSe<sub>2</sub> nanoribbon conductivity.

5:40pm **2D-WeA-11 Strain-Exciton Coupling in Two-dimensional Semiconductors**, *Jin Myung Kim, S. Nam*, University of California, Irvine, USA **INVITED**

In this talk, I will present our work on deterministic manipulation and confinement of excitons in two-dimensional (2D) semiconductors. I will discuss predictable and reconfigurable strain modulation in 2D transition metal dichalcogenides (TMDs) via wrinkle architectures. Strain exerted on wrinkled 2D TMDs was periodically modulated to tensile and compressive strain at peaks and valleys of the wrinkles, respectively. Furthermore, owing to the deformable nature of the wrinkle architecture, the applied strain can be tuned reconfigurably with the optical gap of TMDs dynamically modulated. We also observed exciton transport across apex and valley of strained TMDs as well as exciton localization at the apex due to strain gradient induced energy modulation of wrinkled TMDs. Finally, I will discuss an extension of our strain modulation approach to interlayer excitons in TMD vertical heterostructures where strain is used to tune both optical gap as well as interlayer coupling between the heterobilayers. I will share our

perspectives on strain-exciton engineering toward quantum and optoelectronic devices.

**Actinides and Rare Earths Focus Topic**  
**Room C124 - Session AC+AS+MI+TH-WeA**

**Emerging Topics and Methods in Actinide/Rare Earth Sciences**

**Moderators:** Edgar Buck, PNNL, Krzysztof Gofryk, Idaho National Laboratory, Liane Moreau, Washington State University

2:20pm **AC+AS+MI+TH-WeA-1 Chemical Imaging and Applications Using High Energy Resolution Fluorescence Detection for the Actinides**, *Samuel Webb, N. Edwards, V. Noel*, SLAC National Accelerator Laboratory **INVITED**  
Microscale synchrotron radiation-based x-ray fluorescence (SR-XRF) chemical analyses can provide a unique capability for chemical signature recognition and classification capabilities for actinide micro-particle analysis. SR-XRF is well suited to forensic type analyses of small particles because it is rapid, non-destructive, highly sensitive, has good spatial resolution, and can provide chemical information on the elements that are present when combined with x-ray absorption spectroscopy (XAS). The combination of spatially resolved distribution and chemical information, often known as chemical imaging, effectively provides a "chemical morphology" of the sample of interest and can show how chemical states are distributed within and among a series of particles. This type measurement is critical for understanding particle origin and history, as the spectroscopy, and its spatial distribution, can provide unique and complementary chemical signatures that may not be elucidated with other forms of measurement.

However, the conventional XAS capability in the near edge region as commonly implemented is often inadequate for systems that require high sensitivity or require a higher detail of spectroscopic information. This can be overcome with the combination of traditional micro SR-XRF and XAS, integrated with a high energy resolution fluorescence detector (HERFD) crystal analyzer. This has been recently implemented at BL 6-2b at SSRL and applied in the determination of the micron-scale oxidation state of uranium in particles. A discussion of the image and data processing techniques that can be applied using spatially resolved HERFD to obtain chemical and structural information, as well as the distribution of phases across different particles at the micro-scale, will also be presented.

3:00pm **AC+AS+MI+TH-WeA-3 High Energy X-Ray Characterization of Microstructure at Macroscopic Depths in Pu Alloys**, *Donald Brown*, Los Alamos National Laboratory; *T. Carver, R. Pakharel*, Los Alamos National Laboratory; *A. Smith*, Los Al; *P. Kenesei, J. Park*, Argonne National Laboratory **INVITED**

High energy (95keV) X-rays were utilized to characterize the microstructure of six PuGa alloy samples. The samples had different gallium content, age, and history (i.e. thermomechanical processing). The crystallographic textures, phase fractions, lattice parameters and dislocation densities of each sample were evaluated through distinct analysis techniques. The textures of the samples were modest. In each case, the dislocation densities were relatively high, comparable to cold worked metals, with some attributable to mechanical work and some likely due to self-irradiation damage (aging). The lattice parameters determined in the predominantly single-phase samples were larger than expected based on the nominal Ga concentration. The lattice parameter increase is attributed to self-irradiation induced Ga segregation leaving the matrix Ga lean. Finally, measurements of the lattice parameter were completed as a function of temperature to determine the crystallographic thermal expansion of the material.

4:20pm **AC+AS+MI+TH-WeA-7 Native Oxide Growth of Pu-Ga Alloys**, *Kasey Hanson, S. Hickam, D. Olive, A. Pugmire*, Los Alamos National Laboratory

Plutonium corrosion has proven to be an intricate area of research that garners considerable attention. In particular, understanding plutonium oxidation is significant to the safe handling and storage of plutonium metal, which is known to readily oxidize under ambient conditions. In order to mitigate this, plutonium metal is commonly stored in inert atmospheres. These include

# Wednesday Afternoon, November 8, 2023

gloveboxes as well as ultra-high vacuum (UHV) chambers used for materials characterization.

The objective of this work is to measure oxidation rates of plutonium metal in various storage environments. To achieve this, spectroscopic ellipsometry was selected due to its prevalence in a variety of industries to measure thin-film thickness. A non-destructive technique, ellipsometry exposes the sample to polarized light, and through changes in the amplitude ratio and phase difference of the reflected vs. incident light, one can generate a material's optical properties that can be used to determine oxide thicknesses.

Building upon previous work, this presentation will present the optical constants of plutonium metal, achieved through the use of ion sputtering under UHV, and plutonium oxide formed on plutonium metal in various storage and exposure conditions. These results will then be used to model oxide thickness values directly from ellipsometry measurements as well as provide additional insights into the nature of the oxide films relevant to plutonium storage and handling.

4:40pm **AC+AS+MI+TH-WeA-8 Molecular Beam Epitaxy of Ternary Nitrides: From Transition Metals to Actinoids**, *Kevin Vallejo*, Idaho National Laboratory; *S. Gutierrez Ojeda*, Universidad Nacional Autonoma de Mexico; *G. Hernandez Cocoltzi*, Benemerita Universidad Autonoma de Puebla, Mexico; *S. Zhou, K. Gofryk, B. May*, Idaho National Laboratory  
The exceptional properties of transition metal nitrides for coatings, as well as photo- and electrochemical applications have opened the doors for more detailed studies of their structure and synthesis. Mn- and Cr- nitrides are strong candidates to showcase the application of spintronic and magnetic sensing applications partially because of their ability to form several different metastable phases. Similarly, rare-earth nitrides have been studied for over 50 years due to their optical properties and strong electron correlations, leading to behaviors that range from insulating to metallic. This study uses molecular beam epitaxy to synthesize epitaxial thin films of different Mn-, Cr-, Ga-, and Ce-nitride phases. The electrical and magnetic properties of these films are investigated with the rocksalt MnN and CrN both showing metallic behavior, with the latter showing a magnetic transition ~280K. However, when combining these materials at similar growth conditions, instead of maintaining the rocksalt structure, a new ternary cubic phase of  $Mn_xCr_yN$  is obtained which shows narrow-gap semiconducting behavior. Additionally, density functional theory calculations show potential new phases where lanthanoid ternary phases are experimentally realizable. This work presents an avenue for the epitaxial integration of metallic, magnetic, and semiconductor materials via transition metal and lanthanoid compounds, en route to the synthesis of actinoid compounds.

5:00pm **AC+AS+MI+TH-WeA-9 Formation and Electronic Properties of Uranium Tellurides: A Thin Films Study**, *Evgenia Tereshina-Chitrova*, *S. Alex*, Institute of Physics CAS, Prague, Czechia; *O. Koloskova, L. Horak*, Charles University, Prague, Czechia; *O. Romanyuk, Z. Soban*, Institute of Physics CAS, Prague, Czechia; *T. Gouder, F. Huber*, JRC Karlsruhe, Germany  
Understanding the interaction of 5f electrons with other electrons in actinide compounds presents a significant challenge. Factors such as relativistic effects, strong electron correlations, and hybridization with ligands contribute to the complexity of observed effects. This complexity is exemplified in the case of the recently discovered unconventional superconductor  $UTe_2$  [1]. The ongoing debate surrounding  $UTe_2$  revolves around understanding its unconventional superconductivity, the nature of its electronic correlations [2,3], and the character of the 5f electrons. While it's evident that  $UTe_2$  exhibits intermediate occupancy of the 5f states at ambient pressure, there are two localizing interpretations of experimental findings regarding the degree of localization of the 5f electrons: the model based on  $5f^26d^1$  states with singlet crystal field states [4,5], and a  $5f^3$ -based model with atomic Kramers doublet and greater 5f itinerancy [6,7]. Interestingly enough, ab-initio calculations considering the  $4f^2$  U-ion ground state multiplet reproduce bulk experimental observations, such as the Schottky anomaly and magnetic anisotropy at low temperatures [8].

To contribute to this subject, we provide a comprehensive and detailed investigation of thin films of uranium tellurides with various compositions

$U_xTe_y$ , by means of X-ray Photoelectron Spectroscopy (XPS) and Ultra-violet Photoelectron Spectroscopy (UPS). We also explore the structural and bulk properties of the films, including their magnetic and transport characteristics. This comprehensive approach allows us to correlate the changes in XPS spectra across different compositions and crystal structures with resultant bulk properties, contributing to our understanding of the nature of the 5f electrons within uranium tellurides.

The work by E.A. T.-Ch. is supported by the Czech Science Foundation (GAČR) under the grant number 22-19416S. E.A. Ch.-T. is a recipient of the L'Oreal-UNESCO for Women in Science prize.

- [1] S. Ran et al., *Science* 365, 684 (2019).
- [2] I. M. Hayes et al., *Science*, 373, 797 (2021).
- [3] C. Duan et al., *Phys. Rev. Lett.* 125, 237003 (2020).
- [4] L. Miao et al., *Phys. Rev. Lett.* 124, 076401 (2020).
- [5] S. Liu et al., *Phys. Rev. B* 106, L241111 (2022).
- [6] S. Fujimori et al., *J. Phys. Soc. Jpn.* 88, 103701 (2019).
- [7] F. Wilhelm, *Commun. Phys.* 6, 96 (2023).
- [8] S. Khmelevsyi et al., *Phys. Rev. B* 107, 214501 (2023).

5:20pm **AC+AS+MI+TH-WeA-10 Nanoscale Uranium and Thorium Oxides for Applications in Advanced Nuclear Fuels**, *Matthew Heaney, L. Moreau, X. Guo*, Washington State University  
Nanomaterials of uranium and thorium oxides and their mixtures are of significance to the development of advanced nuclear fuels with properties such as self-healing and greater fission gas retention. They also serve as a means for furthering our understanding of spent nuclear fuel behaviors. Furthermore, thorium incorporation into the uranium sublattice induces changes in oxidation behavior, which would be a promising means to provide additional redox resistance. Coupling this with the possible application in fast neutron reactors presents a potential fuel for the Th fuel cycle, which is inherently proliferation resistant. However, these possible applications are purely hypothetical given that, compared to nanomaterials from the rest of the periodic table, actinide nanomaterials are heavily understudied. Therefore, it will be imperative to interrogate the properties of these nanomaterials. This work aims to explore three key areas. (1) How careful kinetic control through variations in synthetic methods can be used to produce particles with different sizes, shapes, and heterogeneities of mixing. (2) Elucidation of the structural and thermodynamic properties of these nanomaterials and how characteristic size, shape, and heterogeneity of mixing affect them through a variety of X-ray characterization and calorimetry techniques. X-ray characterization techniques such as X-ray absorption spectroscopy (XAS) is used to evaluate the heterogeneity of mixing, local structure, and oxidation state of particles while small-angle X-ray scattering (SAXS) is used to determine statistical values on particle size, shape, and polydispersity. Calorimetry techniques like high temperature drop calorimetry are used to determine enthalpies of formation for nanoparticles and the contribution surface effects have on the thermodynamics or thermogravimetric analysis-differential scanning calorimetry (TGA-DSC), which can be used to evaluate oxidation behaviors. (3) How sintered nanoparticles behave in *in-situ* reactor conditions as nuclear fuels and how particle characteristics can be chosen to achieve more desirable radiation-resistance and thermal properties for nuclear fuel, through irradiation studies performed at the 1-MW TRIGA reactor on the campus of Washington State University. Overall, the work presented provides initial evidence for the benefits of nanomaterials in the production of advanced reactor fuels and outlines important fundamental properties of actinides on the nanoscale.

# Wednesday Afternoon, November 8, 2023

## Applied Surface Science Division

### Room B117-119 - Session AS+CA+EL+EM+SE+SS+TF-WeA

#### Quantitative Surface Analysis I

**Moderators:** David Cant, National Physical Laboratory, UK, Peter Cumpson, University of New South Wales, Christopher Moffitt, Kratos Analytical Inc, Lev Gelb, University of Texas at Dallas

2:20pm **AS+CA+EL+EM+SE+SS+TF-WeA-1 Status of Efforts to Upgrade the Quality of Surface Analysis Data in the Literature, Donald Baer**, Pacific Northwest National Laboratory

Multiple efforts are being undertaken to address a growing presence of faulty surface analysis data and/or analyses appearing in the literature. Issues include bad data, incorrect analysis, and highly incomplete reporting of instrument and analysis parameters. This talk describes the status of four efforts to address some of the issues. Recognition of this problem within the surface analysis community has increased with an understanding that both inexperienced users and increased use of surface analysis methods outside the surface analysis community contribute to the problem. The current efforts build upon decades of development and efforts by standards committees, excellent books and journal publications, websites, short courses, and other efforts. A collection of guides, protocols and tutorials addressing reproducibility issues with a significant focus on XPS was published in JVSTA in 2020/21. A second collection, *Reproducibility Challenges and Solutions II*, with a more general focus on Surface and Interface Analysis was initiated in 2022 and is being finalized. The second collection addresses several techniques, including SIMS, SPM, and UPS, and includes topics such as theoretical modeling and machine learning in data analysis. A second effort focuses on a part of the community less interested in general understanding but needs to answer specific surface analysis questions. A new type of paper called Notes and Insights is being published in the journal Surface and Interface Analysis with the objective to provide incremental bits of useful information of importance to non-expert analysts. Two additional activities are underway to assist with reporting issues. Examination of papers in multiple journals found that instrument and analysis related information needed to assess or reproduce data is often incomplete or absent. To assist authors in reporting instrument parameters, papers describing in some detail related families of commercial instruments are being prepared for Surface Science Spectra. These papers describe the instrument, major components, geometry and provide example data related to common data collection modes. Authors will be able to reference these papers and identify specific modes of instrument operation used in their research. Another parameter reporting activity concerns sample handling before analysis. ISO Technical Committee 201 is developing a series of documents (ISO 20579 parts 1 to 4) on what needs to be reported regarding sample handling, storage, processing, and mounting for analysis. These standards describe what needs to be reported and contain informative annexes that provide information regarding the needs and challenges to proper sample handling to produce reliable useful surface analysis data.

2:40pm **AS+CA+EL+EM+SE+SS+TF-WeA-2 The behavior of the Shirley background of the Ti 2p spectra across the Ti 1s edge, Dulce Maria Guzman Bucio**, CINVESTAV-Unidad Queretaro, Mexico; *D. Cabrera German*, Universidad de Sonora, Mexico; *O. Cortazar Martinez*, *J. Raboño Borbolla*, CINVESTAV-Unidad Queretaro, Mexico; *M. Vazquez Lepe*, Universidad de Guadalajara, Mexico; *C. Weiland*, *J. Woicik*, National Institute of Standards and Technology; *A. Herrera Gomez*, CINVESTAV-Unidad Queretaro, Mexico  
A wide variety of photoemission spectra display a step-shaped background, called the Shirley-type background, which should be accounted for in the total background signal for reliably assessing chemical composition. However, it cannot be modeled with any method based on extrinsic processes like the inelastic dispersion of the photoelectrons (e.g., Tougaard-type backgrounds). Although its physical origin is still unknown, experimental data suggest that the Shirley-type background is due to phenomena occurring inside the atom [1,2]. To gain insights into those phenomena, we studied the behavior of the Shirley-type background for the Ti 2p photoemission spectra.

In this work, Ti 2p photoemission spectra were acquired with Synchrotron light (at Beamline 7-2 at the Brookhaven National Laboratory) from a clean metallic titanium film (sputtered on a Si (100) substrate) capped with an ultra-thin aluminum layer. The spectra were collected with 44 excitation energies around the Ti 1s edge. By simultaneously fitting Ti 2p

photoemission spectra obtained with excitation energies higher than the Ti 1s edge, we robustly determined the peak structure of the Ti 2p spectra. Outstandingly, the parameter of the Shirley-type background associated with the Ti 2p peak structure is modulated as the photon energy crosses the Ti 1s edge. The relation of this phenomenon with the physical origin of the Shirley background will be discussed. The KVL<sub>2,3</sub> Auger peaks—which overlap with the Ti 2p peaks—do not have a step-shaped background for most of the excitation energies.

Acknowledgments:

Use of the Brookhaven National Laboratory is supported by the U.S. Department of Energy's (DOE) Office of Science.

This work was partially financed by CONACyT Project Fronteras 58518, Mexico.

References:

- [1] A. Herrera-Gomez, D. Cabrera-German, A. Dutoi, M. Vazquez-Lepe, S. Aguirre-Tostado, P. Pianetta, D. Nordlund, O. Cortazar-Martinez, A. Torres-Ochoa, O. Ceballos-Sanchez, L. Gomez-Muñoz, Intensity modulation of the Shirley background of the Cr 3p spectra with photon energies around the Cr 2p edge, Surf. Interface Anal. 50 (2018) 246–252. <https://doi.org/10.1002/sia.6364>.
- [2] A. Herrera-Gomez, Interchannel Coupling with Valence Band Losses as the physical origin of the Shirley background in photoemission spectra (Old title: The unresolved physical origin of the Shirley background in photoemission spectra), Queretaro, 2015. <http://www.qro.cinvestav.mx/%0A~aherrera/reportesInternos/unknownOriginShirley.pdf>.

3:00pm **AS+CA+EL+EM+SE+SS+TF-WeA-3 Chemical Analysis of Multilayer System by Photoemission: The Binding Energy Reference Challenge, Thierry Conard**, A. Vanleenhove, IMEC Belgium; *D. Desta*, *H. Boyen*, University of Hasselt, Belgium

XPS is a well-established technique used for non-destructive analysis of the chemical composition of thin layers and interfaces. It is most commonly performed using Al K $\alpha$  radiation (1486.6 eV), which limits the analysis to the top 5-10nm. The recently developed laboratory-based hard X-ray photoelectron spectrometers (HAXPES) provide new analysis options. They enable the analysis of thicker film structures and interfaces buried down to 20-50 nm depending on the photon energy and facilitate the analysis of fragile buried layers without ion-induced chemical damage.

Increasing the number of analyzed (insulating) layers enhances the risk of significant vertical differential charging and makes the repeatability of binding energy determination more challenging. While charging has to be taken into account for XPS, the analysis of most XPS spectra is quite straightforward as long as the surface charge is stable and the lateral distribution of surface charge is uniform within the area of analysis. For HAXPES however vertical charge distribution comes into the game for a large group of structures whose development can benefit from HAXPES analysis. Vertical charge build-up can be complex, especially if examined structures exist of multiple layers and hence multiple interfaces, containing a large variety of materials. But even in 'simple' non-conducting one-layer structures a vertical charge gradient builds up when exposed to X-rays and small changes in the parameters of standard surface charge neutralization techniques - as the use of e-beam flood guns - can influence the nature of the charge gradient.

In this work, we will examine the influence of measurement conditions in single and multiple layers systems relevant to the microelectronic industry on the determination of precise binding energies.

HAXPES spectra of technologically relevant samples will be discussed to demonstrate the challenge of determining exact binding energy values. The set of examined samples comprises oxide layers Si samples and metal/high-k/Si stacks including high-k materials as HfO<sub>2</sub> and Al<sub>2</sub>O<sub>3</sub>. The surface potential will be precisely set and monitored in situ by depositing a metallic layer (such as Ag) on top of the stack and applying an external potential instead of using an electron neutralization source. All experiments are performed in a PHI Quantes system and/or a Scienta Omicron HAXPES Lab, both equipped with two monochromatic X-ray sources: an Al K $\alpha$  (1486.6 eV) and a Cr K $\alpha$  (5414.8 eV - Quantes) or Ga K $\alpha$  (9252.1 eV - HAXPES lab) X-ray source.

# Wednesday Afternoon, November 8, 2023

3:20pm **AS+CA+EL+EM+SE+SS+TF-WeA-4 Where Are We on the Road-Map to Artificially Intelligent Interpretation of X-ray Photoelectron Spectra?**, C. Moffitt, Kratos Analytical Inc; A. Roberts, J. Counsell, C. Blomfield, Kevin Good, K. Macak, Kratos Analytical Limited, UK

Robust peak identification is crucial for accurate sample analysis using X-ray photoemission spectroscopy (XPS). Automation of peak ID enhances this process by minimizing user error and bias. Current acquisition software offers improved computer-derived peak identification from unknown samples, instilling confidence in the correct identification of elements. Moreover, this forms the foundation for an automated sample analysis workflow known as Data-dependent Analysis (DDA). DDA involves identifying peaks in a survey spectrum and subsequently acquiring high-resolution spectra from major components. A recent User survey revealed that a significant majority of users rely on the large area survey acquisition mode as a starting point for analysis.

To provide a metric for confidence in the DDA process, existing spectral analysis data, which includes the element composition information, is used to generate reference spectra for testing purposes. These reference spectra serve as the basis dataset against which the performance of the automated analysis algorithm can be evaluated. By comparing the results of the algorithm with the reference spectra, statistical parameters can be calculated to assess the algorithm's precision, sensitivity, specificity, and accuracy in identifying elements of unknown spectra.

For experienced analysts, DDA serves as a time-saving acquisition method, while for inexperienced analysts, it provides assurance in accurate peak identification and appropriate high-resolution spectra acquisition. Here we highlight current status of automated XPS data acquisition in relationship to the 'expert system', championed in the early 2000's and full AI interpretation of XPS spectra of the future.

4:20pm **AS+CA+EL+EM+SE+SS+TF-WeA-7 Thin Film Analysis by XPS: Quantitative Analyses Using Physics-Based and Machine-Learning Approaches**, Lev Gelb, N. Castanheira, A. Walker, University of Texas at Dallas

We present progress towards quantitative analysis of XPS data using both model-based "fitting" approaches and machine learning methods. Two separate applications are considered.

The first concerns the simultaneous extraction of both compositional profiles and sputtering parameters from XPS sputter depth-profiles of multilayer films. Depth-profile data are routinely processed to provide "fractional composition vs ion dose" profiles, but such analyses typically assume the sample is homogeneous in the probed region, which is not true near interfaces, and cannot precisely convert between units of ion dose and depth without extensive calibration data. Our approach is to first construct analytical models for both the sample structure and for the sputtering process, and then to determine the model parameters (layer thicknesses, interfacial widths, material removal rates, etc.) that are most likely given the observed apparent fractional composition profiles. This is done numerically, by iteratively comparing simulated and observed apparent composition profiles. The only additional required inputs are the inelastic mean free paths for each tracked peak in each material present. The efficacy of this approach is demonstrated using both synthetic and experimental data sets, and various model improvements (sputter-induced mixing, *in situ* chemical reactions) are discussed.

The second application concerns the application of machine-learning tools to remove the inelastic scattering background from XPS spectra in order that accurate peak areas can be obtained. Our approach here is to generate a training data set which consists of a thousands of simulated XPS spectra with and without inelastic scattering included. This is accomplished using the SESSA software package[1]. This data set is then used to train a neural network algorithm to output a "no-background" spectrum from an input "with-background" spectrum; this output spectrum can then be used to compute peak areas for compositional analysis. The training set generation methodology and network structure are discussed, and application of the tool to both simulated and experimental spectra is demonstrated.

[1] Werner, W., Smekal, W., Powell, C. and Gorham, J. (2021), *Simulation of Electron Spectra for Surface Analysis (SESSA) Version 2.2 User's Guide*, Natl Std. Ref. Data Series (NIST NSRDS), <https://doi.org/10.6028/NIST.NSRDS.100-2021>.

4:40pm **AS+CA+EL+EM+SE+SS+TF-WeA-8 Room Temperature Ionic Liquids as Reference Materials for Photoelectron Spectrometers**, Benjamin Reed, National Physical Laboratory, U.K.; J. Radnik, BAM Berlin, Germany, UK; A. Shard, National Physical Laboratory, U.K.

Room-temperature ionic liquids (RTILs) are materials consisting of organic salts that are liquid below temperatures of 100°C and are used in several fields including electrochemistry,<sup>1</sup> pharmaceuticals, and medicine.<sup>2</sup> RTILs have several notable properties that make them ideal for X-ray photoelectron spectroscopy (XPS) analysis. They have an extremely low vapor pressure and high surface tension, and so can be analysed using conventional XPS under ultrahigh vacuum without the need for near-ambient pressure instrumentation. Also, when deposited in a recessed sample holder, the meniscus of an RTIL will be perfectly flat meaning that there are no contributions from sample topographic effects. Finally, and most importantly, they are highly homogeneous and have well-defined stoichiometries.<sup>3</sup>

These properties make RTILs potential reference materials for validating the intensity calibration of a photoelectron spectrometer. RTILs with non-coordinating bistriflimide (NTf<sub>2</sub>) anions (e.g. PMIM<sup>+</sup>NTf<sub>2</sub><sup>-</sup>) or dimethyl phosphate (DMP) anions (e.g. MMIM<sup>+</sup>DMP<sup>-</sup>) are such candidates, with core levels up to ~800 eV binding energy, making them apt for verifying the quantification of light elements, especially for organic materials.<sup>4,5</sup>

To accurately determine peak areas, however, requires the principal and secondary photoelectron signals to be deconvolved. Previous attempts by multiple laboratories using different quantification methods give a mean atomic composition within 1 at.% of the known stoichiometry, but some individual elements (such as fluorine) exhibit differences greater than 1 at.% because the elastic and inelastic secondaries are not suitably deconvolved. Attention must be paid to the energy loss function that defines the inelastic background over the full energy range of an XPS spectrum so that a suitable Tougaard background subtraction can be applied.<sup>6</sup> Here we present a study on several RTILs and discuss how they may be used to validate an XPS intensity calibration and provide confidence in measurements to XPS instrument operators.

<sup>1</sup>M. Armand, F. Endres, D. R. MacFarlane et al., *Nat. Mater.* **8**, 621 (2009).

<sup>2</sup>K. S. Egorova, E. G. Gordeev, and V. P. Ananikov, *Chem. Rev.* **117**, 7132 (2017).

<sup>3</sup>E. F. Smith, I. J. Villar Garcia, D. Briggs et al., *Chem. Commun.* **45**, 5633 (2005).

<sup>4</sup>B.P. Reed, J. Radnik, and A.G. Shard, *Surf. Sci. Spectra* **29**, 014001 (2022).

<sup>5</sup>X. Knigge and J. Radnik, *Surf. Sci. Spectra* **30**, 014006 (2023).

<sup>6</sup>M. P. Seah, I. S. Gilmore, and S. J. Spencer, *Surf. Sci.* **461**, 1 (2000).

5:00pm **AS+CA+EL+EM+SE+SS+TF-WeA-9 Fractional Coverage Analysis of Monolayers with XPS and Non-Destructive Depth-Profiling with Combined Soft and Hard X-Rays**, Norbert Biderman, K. Artyushkova, D. Watson, Physical Electronics USA

X-ray photoelectron spectroscopy (XPS) is a well-established technique for non-destructive analysis of the chemical composition of thin layers and interfaces. Angle-resolved XPS (AR-XPS) has been used to determine composition of depth profiles and layer thicknesses, traditionally with Al K $\alpha$  (1486.6 eV) X-ray beams for depths up to 5-10 nm below the surface. In recent years, new AR-XPS capabilities have been added to Physical Electronics XPS scanning microprobe instruments including Cr K $\alpha$  (5414.8 eV) hard X-ray photoelectron spectroscopy (HAXPES) that can probe buried interfaces up to 15-30 nm below the surface. Coinciding with the HAXPES development, the StrataPHI analysis software was developed to reconstruct quantitative, non-destructive XPS/HAXPES depth profiles from angle-dependent and single-angle photoelectron spectra.

In this talk, we will show that the StrataPHI software has been further developed to combine Al K $\alpha$  and Cr K $\alpha$  XPS and HAXPES data within a single depth profile to enhance extracted analytical information from various depths below the surface. We will explore the method of the combined technique as well as its application to multilayered thin film samples. The updated StrataPHI software also includes a fractional coverage analysis mode, relevant in situations where ultra-thin films exist as discrete islands – commonly observed in early thin-film deposition stages on the substrate rather than as a continuous, uniform film. A model system of discrete molybdenum sulfide (MoS<sub>2</sub>) monolayer triangles deposited on SiO<sub>2</sub>/Si substrate will be discussed.

# Wednesday Afternoon, November 8, 2023

Such added StrataPHI capabilities allow for scientists and engineers in metrology and research & development to analyze multi-layered thin films and ultra-thin films rapidly and non-destructively without potentially damaging ion beam sputtering that might otherwise be required to depth-profile or sputter-clean adventitious contamination off the surface.

5:20pm **AS+CA+EL+EM+SE+SS+TF-WeA-10 Reassessing the Reduction of Ceria in X-Ray Photoelectron Spectroscopy, David Morgan**, Cardiff University, UK

Given its excellent redox abilities, the use of cerium dioxide ( $\text{CeO}_2$ , ceria) and related materials in catalysis is widespread [1]. This  $\text{Ce}^{3+}/\text{Ce}^{4+}$  redox shuffle allows for great catalytic ability and a method of correlation of catalytic activity to the state of ceria [2–4]. Given that catalysis is a surface mediated process, XPS is critical in the analysis of pre- and post-mortem materials.

Over the years there has been debate on the degree of reduction of  $\text{CeO}_2$  during XPS analysis. Therefore, in continuation of our work on understanding the reduction of materials in modern spectrometers [5], we have investigated different cerium oxide preparations and shown that not only is the rate of reduction dependent on instrument type and experimental configuration (and hence appropriate analysis protocols should be implemented), but is also related to the morphology of the cerium which may, at least in part, account for the discrepancies in the degree of reduction in the literature. It is postulated that reduction rates could be used to indicate likely ceria morphology where other analysis is unavailable.

## References

[1] Catalysis By Ceria And Related Materials, 2nd Edition.; Trovarelli, A., Fornasiero, P., Eds.; Imperial College Press: London, 2013.

[2] Smith, L. R.; Sainna, M. A.; Douthwaite, M.; Davies, T. E.; Dummer, N. F.; Willock, D. J.; Knight, D. W.; Catlow, C. R. A.; Taylor, S. H.; Hutchings, G. J. "Gas Phase Glycerol Valorization over Ceria Nanostructures with Well-Defined Morphologies". *ACS Catal*, 2021, 11 (8), 4893–4907.

[3] Qiao, Z.-A.; Wu, Z.; Dai, S. "Shape-Controlled Ceria-Based Nanostructures for Catalysis Applications". *ChemSusChem*, 2013, 6 (10), 1821–1833.

[4] Ziemba, M.; Schilling, C.; Ganduglia-Pirovano, M. V.; Hess, C. "Toward an Atomic-Level Understanding of Ceria-Based Catalysts: When Experiment and Theory Go Hand in Hand". *Acc Chem Res*, 2021, 54 (13), 2884–2893.

[5] Morgan, D. J. "XPS Insights: Sample Degradation in X-ray Photoelectron Spectroscopy". *Surface and Interface Analysis*, 2023. (In Press)

## Acknowledgements

This work acknowledges the EPSRC National Facility for XPS ('HarwellXPS'), operated by Cardiff University and UCL, under contract No. PR16195, and C.M.A. Parlett and X. Zhou for provision of nanostructured ceria materials.

5:40pm **AS+CA+EL+EM+SE+SS+TF-WeA-11 Using High Sensitivity – Low Energy Ion Scattering Spectroscopy (LEIS) to Unravel the Complex Nature of High Entropy Alloys, Matthias Kogler, C. Pichler**, Centre for Electrochemistry and Surface Technology (CEST GmbH), Austria; *M. Valtiner*, Vienna University of Technology, Austria

Complex metallic materials such as Multi-Principal Alloys (MPEAs) and High Entropy Alloys (HEAs) have emerged as a promising class of materials given their unique inherent characteristics. Excellent mechanical, thermal, and corrosion properties allow for a broad spectrum of applications. However, due to the multi-element nature of these alloys, characterisation of the composition and microstructure proves to be a challenging task.

Especially with regard to corrosion-protective passivation films, the complex correlations with the corrosion behaviour are fully unclear to date, and require an in-depth atomic level characterisation and rationalisation. However, the precise layer by layer structure of such passive films is particularly demanding to assess, since traditional techniques such as XPS (X-ray photoelectron spectroscopy) or AES (Auger electron spectroscopy) have analysis penetration depths of several nanometres and cannot reach

atomic layer resolution. However, to fully understand and quantify the passivation layer structure, such an atomic layer resolution of the surface region is necessary, due to the complexity of HEAs.

In order to obtain an exact understanding of the atomistic mechanism at the monoatomic layer level, High-Sensitivity - Low Energy Ion Scattering Spectroscopy (HS-LEIS), was applied, which provides the required monolayer sensitive resolution to study the passivation layers of such complex multi-component alloys. The unique surface sensitivity combined with the implementation of in-situ treatment methods enabled the real-time study of oxide layer growth, as well as the analysis of temperature-dependent changes in the elemental surface composition. Due to the high resolution achieved by static and dynamic sputter depth profile modes, we could determine the exact composition of the HEA passivation layer with resolution on atomic monolayer scale.

The findings provide the potential to significantly advance the current understanding of the passivation behaviour of MPEAs and HEAs, and the development of novel metallic materials with superior properties. Valuable insights for understanding the material characteristics for those highly advanced materials could thereby be generated.

## Biomaterial Interfaces Division

### Room Exhibit Halls A-B Booth 1003 - Session BI-WeA

#### Biointerphases: Emerging Young Scientists Focus Session (ALL INVITED)

**Moderators: Caitlin Howell**, University of Maine, **Tobias Weidner**, Aarhus University, Denmark

2:20pm **BI-WeA-1 Mycelium's Dynamic Functionality Across Material Systems: Insights and Research Challenges, Wenjing Sun**, EPFL, Switzerland  
The surge in using fungal mycelium as a sustainable material aligns with global sustainability goals. Mycelium exhibits diverse functionality that varies across different forms of materials. This presentation explores past research, emphasizing differences in mycelium's roles and properties based on material types, fungal species, hypha types, and growing conditions. We also address research challenges in this domain.

2:40pm **BI-WeA-2 Breaking Protein-Membrane Chemistry to Understand the Molecular Origins of Adult-Onset Muscular Dystrophies, Andrew Carpenter, J. Baio**, Oregon State University

Dysferlinopathies are a class of adult-onset muscular dystrophies related by a similar disruption to the dysferlin mediate membrane repair of damaged muscle sarcolemmas. Dysferlin possesses a modular structure with 7 C2 domains, where the N-terminal C2A domain is believed to carry out the initial steps of the membrane repair process. Missense mutations within the C2A domain, as well as outside the domain, have been identified in patients with dysferlinopathies suggesting these mutations are disrupting the proper membrane repair function of dysferlin. In this talk we describe our recent progress towards understanding of how dysferlin interacts with cellular membranes and the impact missense mutations exert on this normal function. We utilize vibrational sum-frequency spectroscopy to identify several dysferlin C2A binding mechanisms at biomimetic membrane surfaces and test how missense mutations alter the normal membrane binding function. Further work that will be discussed extends our studies beyond the C2A domain to study how interactions between multiple C2 domains at membrane surfaces contributes to the full-length dysferlin-membrane membrane repair function.

3:00pm **BI-WeA-3 Understanding Adsorption, Adhesion, and Cohesion Phenomena at the Solid/Liquid Interface, Pierluigi Bilotto**, Centre for Electrochemistry and Surface Technology GmbH, Austria; *D. Barragan*, University of Calabria, Italy; *L. Mears, M. Valtiner*, TU Wien, Austria; *B. Zappone*, CNR/University of Calabria, Italy

Marine invertebrates such as mussels and barnacles exhibit an impressive ability to adhere in sea water onto wave-swept rocks, moving ship hulls, submerged metal infrastructures and even anti-adhesive Teflon coatings. On one hand, marine biofouling is a concern for maritime industries, aquaculture, water, and waste treatment industries, as it increases the weight and drag of ships and infrastructures and accelerates surface degradation (corrosion). On the other hand, biofouling is a source of inspiration to solve an outstanding challenge in surface and material science: How to control adsorption (on one surface), adhesion (between two different surfaces) and cohesion (between two equal surfaces) underwater. A large body of literature has been devoted to the aromatic

# Wednesday Afternoon, November 8, 2023

amino acid 3,4-dihydroxy-L-phenylalanine (DOPA), which is exceptionally abundant in mussel adhesive proteins. DOPA is able to bind to a wide variety of substrates and create protein cross-links in salty water using a diverse array of molecular interactions. However, it is becoming increasingly clear that DOPA is neither necessary nor sufficient to ensure underwater surface-attachment and tissue cross-linking. [1] Surface forces apparatus (SFA) and atomic force microscopy (AFM) are preferential tools to investigate forces at the solid/liquid interface when electrolytes are in play. [2] During this talk, I will review our current understanding on the role of DOPA in mussel adhesion, [3] and show our preliminary results in employing tropocollagen type I and type III nanofibrils as model systems to reveal adhesion, adsorption, and cohesion of macromolecules on different substrates. The expected outcomes of this project will shed light on a possible collagen-based biocompatible and biodegradable adhesive.

[1] P. Bilotto, C. Labate, M. P. De Santo, K. Deepankumar, A. Miserez, and B. Zappone, *Adhesive Properties of Adsorbed Layers of Two Recombinant Mussel Foot Proteins with Different Levels of DOPA and Tyrosine*, *Langmuir* **35**, 15481 (2019).

[2] P. Bilotto, A. M. Imre, D. Dworschak, L. L. E. Mears, and M. Valtiner, *Visualization of Ion|Surface Binding and In Situ Evaluation of Surface Interaction Free Energies via Competitive Adsorption Isotherms*, *ACS Phys. Chem. Au* **1**, 45 (2021).

[3] L. L. E. Mears, J. Appenroth, H. Yuan, A. T. Celebi, P. Bilotto, A. M. Imre, B. Zappone, R. Su, and M. Valtiner, *Mussel Adhesion: A Fundamental Perspective on Factors Governing Strong Underwater Adhesion*, *Biointerphases* **17**, 058501 (2022).

3:20pm **BI-WeA-4 Plasma and Beyond: Expanding the Horizons of Naturally-derived Polymers as Biomaterials Through Surface Modification**, **Morgan Hawker**, California State University Fresno **INVITED**

Naturally-derived polymers hold important utility in biomedical materials, ranging in applications from suturing to biosensors to tissue engineering scaffolds to drug delivery vehicles. Naturally-derived polymers are advantageous for use in biological settings owing to their non-immunogenic nature and favorable mechanical properties. Several naturally-derived polymers also degrade via enzymatic hydrolysis into non-toxic byproducts in vivo. All biomedical applications, however, require specific interactions between the naturally-derived polymer and biological species. These polymers universally lack the necessary surface cues required to facilitate such precise interactions. Thus, further modification is required to tailor naturally-derived polymer surface properties and enhance their applications as biomaterials. Although synthetic wet-chemical approaches have been used to this effect, these strategies introduce complex processing conditions that pose challenges to naturally-derived polymers (e.g., high temperatures and solvents).

Plasma treatment represents a promising alternative to control how naturally-derived polymer constructs interact with biological environments. This talk will highlight several recent thrusts toward better understanding fundamental interactions between plasma and three different naturally-derived polymers. In the first thrust, we seek to evaluate water vapor and nitrogen gas plasma-treated silk fibroin stability upon aging to better understand the shelf life of plasma-modified silks. Water contact angle goniometry findings demonstrate remarkable stability of modified silk materials after aging for 42 days under both ambient and elevated temperatures. In the second thrust, we explore immobilizing three different antioxidants on chitosan films via plasma activation. This thrust aims to target oxidants in burn wounds to enhance healing, and 2,2-diphenyl-1-picrylhydrazyl assay results demonstrate promising antioxidant activity for all modified surfaces. In the final thrust, we describe efforts in coating commercially-available wound dressing materials with an antibacterial film using plasma-enhanced chemical vapor deposition (contrasting pulsed and continuous power conditions). Surface analyses reveal differences in surface chemistry and wettability for plasma-treated dressings compared to untreated dressings. Collectively, these projects demonstrate how plasma modification can be harnessed to enhance the utility of naturally-derived polymers in the biomedical space.

## CHIPS Act Mini-Symposium

### Room C120-122 - Session CPS+CA-WeA

#### CHIPS Act: Interfaces and Defects

**Moderators:** **Tina Kaarsberg**, U.S. Department of Energy, Advanced Manufacturing Office, **Andrei Kolmakov**, National Institute of Standards and Technology (NIST)

2:20pm **CPS+CA-WeA-1 Future Needs and Current Trends in Interfacial Metrology for the Development of Reliable Ultra-Wide Bandgap Electronics**, **Luke Yates**, *A. Jarzembki, W. Hodges, M. Bahr, W. Delmas, Z. Piontkowski, A. McDonald, M. Smith, B. Rummel, C. Glaser, A. Binder, J. Steinfeldt, A. Allerman, A. Armstrong, B. Klein, G. Pickrell*, Sandia National Laboratories; *D. Morissette*, Purdue University; *J. Cooper*, Sonrisa Research Inc.; *R. Kaplar*, Sandia National Laboratories **INVITED**

Recent advancements in epitaxial growth and substrate development continue to inspire the next generation of wide-bandgap (WBG) semiconductor devices. In the last decade, the silicon carbide (SiC) and gallium nitride (GaN) material systems have seen extraordinary advancements that allow an increased commercial device adaptation. However, there still exists many reliability concerns that directly impact device manufacturing. These concerns manifest in our inability to accurately quantify and mitigate interface charge effects and material defects that exist within device structures due to growth conditions and processing limitations. Commercial endeavors will continue to address such concerns for WBG devices, but it is crucial that the research community complements and promotes these efforts through advanced interfacial metrology methods that can be applied to both current WBG devices and future ultra-wide-bandgap (UWBG,  $E_g > 3.4\text{eV}$ ) materials and devices, thus enabling the next leap forward in electronic device performance. These include materials such as high-Al-content AlGaN/AlN,  $\text{Ga}_2\text{O}_3$ , cubic BN, diamond, and others. Due to device performance scaling approximately as  $E_g^6$ , there exists substantial potential that has yet to be fully embraced in UWBG devices.

Interfacial metrology is a broad topic area that encompasses numerous thermal, mechanical, chemical, optical, and electronic properties at (dis)similar material interfaces. It is inextricably linked to our ability to develop devices that fully exploit the electronic capabilities of a given material system. This talk discusses current optical, acoustic, and electrical characterization efforts at Sandia and within the broader community to visualize and quantify interfacial properties, defects, and undesirable electronic charges within (U)WBG materials and devices. Specifically, a coupled hyper-spectral frequency-domain thermoreflectance/laser doppler vibrometry (FDTR/LDV) system that allows for enhanced understanding of thermal/mechanical properties of buried interfaces with a sensing depth greater than standard FDTR approaches has been implemented. Additionally, an improved quasi-static capacitance analysis method has been developed to more accurately evaluate interface traps at dielectric/(U)WBG material interfaces. Direct optical and photoemission approaches are becoming increasingly difficult to effectively utilize as larger bandgap devices are developed, necessitating the need for advanced thermal, vibrational, and electronic analysis methods. Future interfacial metrology efforts will require non-destructive methods that are capable of highly resolved in-situ full-field monitoring of buried interfaces within a device.

*SNL is managed and operated by NTESS under DOE NNSA contract DE-NA0003525*

3:00pm **CPS+CA-WeA-3 Diamond/h-BN Heterostructures for High-Performance Electronics**, **Yamaguchi Takahide**, National Institute for Materials Science, Japan **INVITED**

Diamond is an ultra-wide bandgap semiconductor displaying a high breakdown electric field, high thermal conductivity, and high carrier mobilities. These intrinsic properties are suitable for creating power conversion and communications devices. In order to utilize its full potential, however, the properties of its surfaces and interfaces to other materials used in combination are important. Hydrogen-terminated diamonds (diamonds with their surface carbon atoms covalently bonded with hydrogen atoms) are widely used to make field-effect transistors (FETs). They show p-type surface conductivity even when the diamonds are not doped intentionally. The surface conductivity is attributed to surface transfer doping; electrons in the valence band of diamond are transferred to acceptors in an adjacent coating material, thereby forming holes in the diamond surface. The acceptor material includes adsorbed water,  $\text{NO}_2$  gas,

# Wednesday Afternoon, November 8, 2023

and oxides such as  $\text{Al}_2\text{O}_3$ ,  $\text{MoO}_3$ , and  $\text{V}_2\text{O}_5$ , and coating the diamond surface with an acceptor material has been thought to be necessary to generate the surface conductivity. However, the surface transfer doping is accompanied by negatively charged acceptors, which cause carrier scattering and reduce hole mobility. It also leads to normally-ON operation, a finite conductivity at zero gate bias, which is undesirable particularly in power electronics.

In this presentation, I will present current trends in diamond electronics and our recent work on the creation of high-performance hydrogen-terminated diamond FETs without surface transfer doping [1]. We transferred a cleaved single crystal of hexagonal boron nitride (h-BN) on hydrogen-terminated diamond and used it as a gate insulator. This is useful for avoiding the formation of defects, which occurs in conventional deposition techniques and can cause acceptor states [2]. In addition, the transfer was made without exposing the diamond surface to air, using a vacuum suitcase and an Ar-filled glove box, which reduced the density of atmospheric acceptors. Our FETs exhibited excellent ON-state characteristics such as a room-temperature mobility of  $680 \text{ cm}^2\text{V}^{-1}\text{s}^{-1}$ , sheet resistance of  $1.4 \text{ k}\Omega$  and gate-length-normalized ON current of  $1600 \mu\text{m mA mm}^{-1}$ . These are among the best among p-channel wide-bandgap FETs. The FETs also exhibited normally OFF behavior with an ON/OFF ratio of  $10^8$ . Our new approach for making diamond FETs could lead to the development of high-performance wide-bandgap p-channel devices for power electronics and communications.

[1] Sasama et al. *Nature Electronics* **5**, 37 (2022).

[2] Sasama et al. *APL Materials* **6**, 111105 (2018); *Phys. Rev. Materials* **3**, 121601(R) (2019); *J. Appl. Phys.* **127**, 185707 (2020).

4:20pm **CPS+CA-WeA-7 Hydrogenation of a  $\text{Cu}_{2-x}\text{O}$  Confined Under Hexagonal Boron Nitride**, *J. Trey Diulus*, *E. Strelcov*, NIST Center for Nanoscale Science and Technology; *Z. Novotny*, Empa (Swiss Federal Laboratories for Materials Science and Technology), Switzerland; *N. Comini*, University of Zurich, Switzerland; *A. Naclerio*, *P. Kidambi*, Vanderbilt University; *J. Osterwalder*, University of Zurich; *A. Kolmakov*, NIST Center for Nanoscale Science and Technology

Hexagonal boron nitride (h-BN) exhibits a wide array of unique chemical and electrical properties that presents itself useful in numerous applications, such as a gate dielectric for high mobility diamond transistors,<sup>1</sup> increasing corrosion resistance,<sup>2</sup> or a device encapsulating material.<sup>3</sup> h-BN can be epitaxially grown by chemical vapor deposition (CVD) on copper surfaces with any orientation, and a near perfect lattice match on the Cu(111) surface, making Cu an ideal substrate to study intercalation.<sup>4,5</sup> Intercalation of  $\text{O}_2$  through h-BN to monitor oxidation of the Cu substrate can be studied during exposure to near ambient oxygen partial pressures (1-100 Pa),<sup>6</sup> or following exposure to atmosphere.<sup>5</sup> The oxidation occurs predominately at defects and/or grain boundaries in the h-BN, and occurs even at room temperature if the pressure is high enough (atm pressure), leading to a lifetime of a few weeks at these conditions for use of pristine unoxidized h-BN/Cu heterostructures.<sup>5</sup> To better understand this intercalation behavior, we studied the intercalation of  $\text{H}_2$  to observe the extent of recovery of the original metallic surface/interface after the h-BN/ $\text{Cu}_{2-x}\text{O}$  interface is formed. Using polycrystalline Cu foils with CVD grown h-BN after exposure to atmosphere for ~1 month as a model system, we assessed the reduction of the surface via two hydrogenation methods: (i) simple  $\text{H}_2$  exposure of 10 Pa followed by annealing in vacuum (sequentially) and during  $\text{H}_2$  exposure (simultaneously) (ii) exposure to a low power (75 W)  $\text{H}_2$  remote plasma also using 10 Pa, allowing for H radicals to interact with the surface. With *in situ* x-ray photoelectron (XPS) and Auger electron spectroscopy (AES), we track the changes in surface chemistry following each hydrogenation attempt. Additionally, *in situ* scanning electron microscopy provides morphological maps of the foil surface. To further study this hydrogenation mechanism from a fundamental perspective, we utilized h-BN grown on single crystalline Cu(111) and collected *in situ* ambient pressure XPS for the reduction of an ordered cuprous oxide confined beneath h-BN. Ultimately, H-radicals and ions can attack the confined oxide and partially reduce the surface, yet we were unable to fully recover metallic Cu. Our results indicate the original metallic interface might be repaired without damaging the overlying h-BN, which is of practical importance for development of h-BN encapsulated devices and interfaces.

<sup>1</sup>Sasama, Y. et al. *APL Mater* **6** (2018)

<sup>2</sup>Li, L. H. et al. *Adv Mater Interfaces* **1** (2014)

<sup>3</sup>Lo, C.-L. et al. *J Appl Phys* **128** (2020)

<sup>4</sup>Naclerio, A. E. et al. *Adv Mater*, 2207374 (2022)

<sup>5</sup>Kidambi, P. R. et al. *Chem Mater* **26**, 6380-6392 (2014)

<sup>6</sup>Diulus, J. T. et al. Towards 2D-confined catalysis on oxide surfaces. *ACS Nano Submitted* (2023)

4:40pm **CPS+CA-WeA-8 A Proven Model for Workforce Development**, *David Ruzic*, *D. Andruczyk*, University of Illinois at Urbana-Champaign

At the University of Illinois at Urbana-Champaign we have set up two complimentary structures to enable workforce development in the field of semiconductor manufacturing. The first is a relatively new degree program, a "Masters of Engineering in Plasma Engineering". This is a non-thesis master's degree which specializes in plasma technology and science related to making the machines which make the chips. The flagship class is a plasma laboratory where the students operate and analyze the experiments themselves in Vacuum Technology, DC Plasmas, RF Plasmas, Langmuir Probes, Spectroscopy, Plasma Etching, Plasma PVD Deposition, Atmospheric Pressure Plasmas and Fusion Plasmas. The program can usually be finished in three semesters and is open to students from all fields of engineering and science.

This program can be coupled with sponsored research at the University, particularly through the Illinois Plasma Institute. Companies who are sponsoring research at Illinois can use the Masters program to recruit, retain or re-train employees. In the case of a current employee, that person goes to Illinois while still working for the company, perhaps being paid less than 100%. Their work role at Illinois is to help work on the research project that is being sponsored, and do other remote work. Their school role is to take the courses in the degree program which includes classes directly related to their work for the company itself. If the company pays for the tuition, the student is required to continue working for the company upon graduation for a limited time, or pay back the tuition. The company is ensured a better-trained more-educated employee. The student is ensured of a job.

Examples will be described, and a program outlined that could be set-up at any major University.

5:00pm **CPS+CA-WeA-9 Characterization of Buffer Layers for Remote Plasma-Enhanced Chemical Vapor Deposition of Germanium-Tin Epitaxial Layers**, *Bridget Rogers*, Vanderbilt University; *S. Zollner*, *C. Armenta*, New Mexico State University; *G. Grzybowski*, KBR; *B. Clafin*, Air Force Research Lab

Germanium-tin alloys are of interest for infrared light detectors and lasers to increase capabilities in image and data capture and transmission, because they can have a direct band gap with more than about 7% tin. Remote plasma-enhanced chemical vapor deposition (PE-CVD) is particularly attractive for growth of Ge-Sn alloys because it enables low-temperature epitaxy directly on Si using common precursors  $\text{GeH}_4$  and  $\text{SnCl}_4$ . The growth of such epilayers can be optimized with an initial high-temperature buffer layer. This presentation will focus on the characterization of this buffer layer using atomic force microscopy, ellipsometry, thin-film powder x-ray diffraction, and x-ray photoelectron spectroscopy (XPS) for different growth conditions.

Thin Ge and Ge-Sn buffer layers with 10-20 nm thickness were deposited on Si (100) substrates for one minute at temperatures from 360°C to 500°C varying the  $\text{SnCl}_4$  flow. Ellipsometry spectra for all films show critical point structures in the  $E_{-1}$ ,  $E_1+\Delta_1$ , and  $E_2$  region of Ge, indicating that all layers are crystalline. A layer grown at 360°C without  $\text{SnCl}_4$  is well described as an 11 nm thick layer of crystalline germanium with 2 nm of roughness. Adding  $\text{SnCl}_4$  to the gas flow significantly reduces the height of the  $e_2$  maximum at  $E_2$ , indicating that the layer is rough. In addition, a new broad peak appears near 1.3 eV, which is attributed to plasmonic effects arising from metallic  $\beta$ -tin inclusions. The plasmon peak disappears in the layers grown at 490°C with the same  $\text{SnCl}_4$  flow. We conclude that depositing the buffer layer with  $\text{SnCl}_4$  at low temperatures leads to  $\beta$ -Sn precipitates, where plasmon oscillations can be excited, which are not present for high-temperature growth.

The tin contents in the layers were also estimated by x-ray photoelectron spectroscopy. While XPS measures the total amount of tin in the layers, the presence of substitutional tin in  $\text{Ge}_{1-x}\text{Sn}_x$  alloy buffers is best determined with x-ray diffraction. The (002) diffraction peak is absent in our buffers grown without  $\text{SnCl}_4$  or at high temperature. The (004) XRD peak position in these layers is also very similar to pure Ge. The  $\text{Ge}_{1-x}\text{Sn}_x$  (002) peak does appear in buffers grown at temperatures lower than 460°C. From the position of the (004) XRD peak, we estimate the tin content to be below

# Wednesday Afternoon, November 8, 2023

7%. Tin content determined from XRD shifts is much lower than the total tin content of about 20% estimated by XPS.

In summary, the substitutional tin content in thin  $\text{Ge}_{1-x}\text{Sn}_x$  buffer layers grown by PE-CVD is modulated by temperature and  $\text{SnCl}_4$  flow rates. Excess tin is present in  $\beta$ -tin precipitates, which lead to plasmonic resonances in ellipsometry spectra.

5:20pm **CPS+CA-WeA-10 Comparative Study of Mechanical and Corrosion Behaviors on Heat Treated Steel Alloys**, *Moe Rabea*, California State Polytechnic University, Pomona

This research examines the effects of heat treatment processes on the mechanical properties and corrosion resistance of 1045 and 4140 Steel Alloys for industrial applications. Heat treatment processes of full annealing, normalizing, quenching, and tempering are carried out on the alloy samples. The mechanical and corrosion resistance tests of the heat treated samples are carried out and the results obtained are related to their morphologies analysis. The results show that the heat treatment processes have an effect on the tensile strength, impact, and a significant effect on the corrosion resistance of the alloy samples. With respect to the strain characteristics, significant improvement in the ductility of the samples is recorded in the full annealing and alloy tempered samples. Thus, for application requiring strength and ductility such as in aerospace industries, this tempered heat treated alloy could be used. In addition, the quenched sample shows a significant improvement in hardness.

## Electronic Materials and Photonics Division

### Room B116 - Session EM-WeA

#### Advanced Materials for Electronic and Photonic Applications

**Moderators:** Parag Banerjee, University of Central Florida, Jason Kawasaki, University of Wisconsin - Madison, Stephen McDonnell, University of Virginia

2:20pm **EM-WeA-1 Mind the Gap: Integrating Materials and Engineering Research to Enable Advanced Electronics**, *Paul Lane*, National Science Foundation

INVITED

Continued advances in computing, communications, and energy technologies present tremendous challenges and opportunities. Underpinning developments have often progressed independent of the intended embodiment, delaying incorporation into next-generation technologies. This presentation will present a broad overview of NSF efforts to address challenges involved with integrating materials research with technological advances, focusing on semiconductors. Research is supported at the level of individual investigators and small teams through topical materials and engineering research programs and at a larger scale through centers and facilities. I will emphasize cross-directorate programs that play a critical role in these efforts, such as Designing Materials to Revolutionize and Engineer Our Future (DMREF), Future of Semiconductors (FuSE), and Future Manufacturing.

3:00pm **EM-WeA-3 Atomic Layer Deposition Defect Engineering of Step Tunneling MIIM Diodes**, *Shane Witsell*, *J. Conley*, Oregon State University

Asymmetric electrode metal/insulator/metal (MIM) tunnel diodes can perform as ultra-fast rectifiers for applications in THz energy harvesting and IR detection, but require low turn on voltage ( $V_{ON}$ ) and low zero bias resistance (ZBR) as well as current-voltage asymmetry ( $f_{asym}$ ) and non-linearity ( $f_{NL}$ ). Combining bilayer insulators as tunnel barriers (MIIM diodes) can improve performance over conventional MIM diodes via asymmetric resonant tunneling or "step" tunneling [1]. Utilizing insulating materials with *intrinsic* defects can further improve  $\eta_{asym}$  and  $f_{NL}$  as defect levels in the smaller band gap insulator can provide additional conduction pathways [2]. Finally, it has also been demonstrated that intentionally introduced *extrinsic* defect levels, precisely introduced into the insulator using atomic layer deposition (ALD) [3] can be used to engineer MIM diode performance. In this work, we investigate the use of ALD to intentionally introduce impurity defect levels into the large bandgap insulator of dual insulator MIIM diodes.

Three Al/HfO<sub>2</sub>/Al<sub>2</sub>O<sub>3</sub>/Pt MIIM diodes were investigated: (i) Ti doped: in which a two ALD cycle Ti defect layer was positioned within the middle of the Al<sub>2</sub>O<sub>3</sub>, and (ii) Ni doped: in which a two ALD cycle Ni defect layer was also positioned within the middle of the Al<sub>2</sub>O<sub>3</sub>, and (iii) an undoped control. ALD of HfO<sub>2</sub>, Al<sub>2</sub>O<sub>3</sub>, NiO, and Ti<sub>2</sub>O<sub>5</sub> was performed using TEMA/Hf/H<sub>2</sub>O, TMA/H<sub>2</sub>O, Ni(tBu<sub>2</sub>DAD)<sub>2</sub>/O<sub>3</sub>, and TTIP/H<sub>2</sub>O. For all devices, ALD

was performed onto a bottom Pt electrode. After ALD, Al was e-beam evaporated through a shadow mask with 250  $\mu\text{m}$  diameter holes to form top electrodes.

The Ni doped diodes were found to have improved maximum  $f_{asym}$  over the undoped control, but increased  $V_{ON}$ , likely due to suppression of conduction by to negative charge trapped at Ni defect levels lying energetically near or below the equilibrium Fermi level ( $E_{F,equl}$ ) [4]. The Ti doped diodes showed slightly reduced leakage current, likely due to positive trapped charge in Ti defect levels near or above the  $E_{F,equl}$ , and also increased maximum  $f_{asym}$ . However  $V_{ON}$  was not reduced. Compared to the undoped control, introducing either Ni or Ti defect levels resulted in an increase in  $f_{asym}$  at higher fields, but a slight decrease at low fields due to charge induced band bending. Ni doped devices also demonstrated a slight increase in breakdown field strength. Additional results will be presented at the meeting including capacitance-voltage measurements. This work shows that ALD can be an effective tool for engineering device behavior.

83. Alimardani et al. Appl. Phys. Lett. **102**, 143501 (2013)

84. Alimardani et al. Appl. Phys. Lett. **105**, 082902 (2014).

85. Holden et al. J. Appl. Phys. **129**, 144502 (2021).

86. Ichimura, *J. Electron. Mat.* **48**, 583 (2019).

3:20pm **EM-WeA-4 Silicon-Doped Titanium Nitride with Near-Zero Temperature Coefficient of Resistivity (0.05 ppm/K) in the Temperature Range, 80 K - 420 K**, *S. Novia Berriel*, *C. Feit*, University of Central Florida; *M. Islam*, University of Virginia; *J. Shi*, University of Central Florida; *A. Dhamdhare*, *H. Kim*, Eugenius, Inc.; *P. Hopkins*, University of Virginia; *D. Le*, *T. Rahman*, *P. Banerjee*, University of Central Florida

We demonstrate a materials system where the temperature coefficient of resistivity (TCR) can be effectively "dialed" to near zero ( $\sim 0.05$  ppm/K) across a wide temperature range spanning from 80 K to 420 K. Materials that show this behavior are referred to as near-zero temperature coefficient of resistivity (nz-TCR) materials. nz-TCR materials are instrumental for applications such as wearable strain sensors, automobile electronics, and microelectronics.

Our strategy to achieve nz-TCR is to atomically combine materials of opposing TCR's. Metals exhibit positive TCR, while semiconductors and insulators exhibit negative TCR. Atomic layer deposition (ALD) is well-suited for the task of tuning composition between metallic and insulating phases. To this end, we fabricate  $\text{Ti}_{100-x}\text{Si}_x\text{N}$  thin films *via* ALD where the TiN (metal) and  $\text{Si}_3\text{N}_4$  (insulating) are varied systematically across various sample sets. The TCR accordingly varies from positive (metallic and TiN rich) to negative (insulating and  $\text{Si}_3\text{N}_4$  rich).

$\text{Ti}_x\text{Si}_{100-x}\text{N}$  films are deposited on a Eugenius® 300 mm commercial QXP mini-batch system. The ratio of precursor pulses are varied from  $\text{TiCl}_4$  and dichlorosilane (DCS), with  $\text{NH}_3$  as a co-reactant as described in our previous work<sup>1</sup>. Specifically, Si content is varied for this work between  $2.0 \leq x \leq 3.9$  at%. All  $\text{Ti}_{100-x}\text{Si}_x\text{N}$  films are  $\sim 140$  nm thick. The films are investigated *via* temperature-dependent van der Pauw and temperature-dependent Hall measurements, thermal conductivity measurements, x-ray diffraction, x-ray photoelectron spectroscopy, high-resolution transmission electron microscopy combined with electron energy loss spectroscopy.

Our results indicate the films are nanocrystalline in nature with Si segregating at the grain boundaries. The Si appears to "getter" residual oxygen. Supported by density functional theory (DFT) calculations, we show a loss in electron mean free path upon Si addition to TiN. The electron mean free path is approximately  $\sim$  lattice parameter for TiN thus, satisfying the Mooij rule<sup>2</sup> – a universal basic criteria for establish nz-TCR behavior in materials.

1.C. Feit, S. Chugh, A. R. Dhamdhare, H. Y. Kim, S. Dabas, S. J. Rath, N. Mukherjee and P. Banerjee, Journal of Vacuum Science & Technology A **38**, 062404 (2020).

2.J. H. Mooij, *physica status solidi (a)* **17**, 521-530 (1973).

# Wednesday Afternoon, November 8, 2023

4:20pm **EM-WeA-7 An Auric Goldfinger Inspired Search for Copper Replacement Conductors**, *Sean King*, Intel Corporation **INVITED**

In the spy film "Goldfinger", MI6 agent James Bond's nemesis Auric Goldfinger plotted to corner the world gold market by radioactively contaminating Fort Knox's gold bullion supply. This presentation will examine the inverse scenario where present-day geopolitical tensions and supply chain constraints have the potential to limit the semiconductor industry's ability to implement platinum group metals as potential copper conductor replacements. We will begin by first describing the interconnect resistivity scaling challenges that motivate the consideration of non-copper conductors and how certain platinum group metals offer the potential to outperform copper at nanometer wire dimensions (specifically Ruthenium, Iridium, and Rhodium). To further motivate consideration of platinum group metal conductors, we share a benchmarking Meta-analysis of thin film and nanowire resistivities reported in the scientific literature for these metals along with numerous other metals also in consideration (i.e. Cobalt, Tungsten, Molybdenum). We will conclude by examining the supply chain challenges that may ultimately play a role in the selection of future copper replacement conductors and discuss research needed to address these challenges.

5:00pm **EM-WeA-9 Chalcogenide p-Type Transparent Conductors**, *Andriy Zakutayev*, 15013 Denver W pkwy **INVITED**

Transparent conductors (TCs) are unusual materials that are optically transparent to visible light like insulating glass yet have electrical conductivity like opaque metals. The TCs are useful for a broad range of applications including flat panel displays, light-emitting diodes, solar cells, Particularly rare but useful for optoelectronic energy conversion devices are transparent materials that have p-type electrical conductivity with holes rather than electrons (n-type) as majority charge carriers. In contrast to n-type TCs that are usually oxides, some of the top performing p-type TCs are nitrides (e.g. Mg:GaN) or chalcogenides (i.e. sulfides, selenides, tellurides).

In this presentation, I will focus on wide band gap chalcogenide materials as p-type transparent conductors for photovoltaic and photoelectrochemical solar cells. First, I will give an overview desired physical properties of TCs besides transparency and conductivity, and present high-throughput research workshop that can be used to experimentally and theoretically screen candidate materials for TC applications [1]. Then I will give two examples of how these design principles and research methods can be used to synthesize and characterize Zn<sub>1-x</sub>Cu<sub>x</sub>S [2] and ZnTe<sub>1-x</sub>Sex [3] chalcogenide p-type transparent conductors, and integrate them in CdTe thin film photovoltaic devices [4].

[1] Chem. Rev. 2020, 120, 4007; [2] Matter 1 862 (2019); [3] J. Mater. Chem. C, 10, 15806 (2022); [4] ACS Applied Energy Materials 3 5427 (2020)

5:40pm **EM-WeA-11 Strain Manipulation of Ferroelectricity and Flexoelectricity**, *Harold Hwang*, Stanford University and SLAC National Accelerator Laboratory **INVITED**

The ability to create and manipulate materials in two-dimensional form has repeatedly had transformative impact on science and technology. We have developed a general method to create freestanding complex oxide membranes and heterostructures using epitaxial water-soluble buffer layers, with millimeter-scale lateral dimensions and nanometer-scale thickness. This facilitates many new opportunities we are beginning to explore; here we will focus on the use of tensile strain and strain gradients to control the ferroelectric and flexoelectric response of oxide membranes.

**Fundamental Discoveries in Heterogeneous Catalysis Focus Topic**

**Room B113 - Session HC+SS-WeA**

**Advances in Complex Catalytic Systems**

**Moderators: Zdenek Dohnalek**, Pacific Northwest National Laboratory, **Dan Killelea**, Loyola University Chicago

2:20pm **HC+SS-WeA-1 Computational Studies of Selective Reduction Reactions on Metal and Metal Compounds Electrocatalysts**, *J.R. Schmidt*, UW Madison **INVITED**

Understanding and controlling the factors that govern selectivity in electrocatalysis is key to enabling a wide range of electrochemical transformations. I will highlight efforts from two ongoing collaborative studies, focusing on the selective 2e<sup>-</sup> reduction of oxygen to hydrogen

peroxide over a series of transition metal dichalcogenides; and the selective reduction of highly functionalized biomass molecules using traditional metallic electrocatalysts. In both cases, I will demonstrate how emerging computational electrocatalysis approaches yield a rich picture for the factors that govern catalytic selectivity in these systems. In addition, I will briefly discuss recent work focused on increase the long-term stability of these electrocatalysts, opening the doors to potential commercial applications.

3:00pm **HC+SS-WeA-3 Metal Atom Chemical Potential: A Key Descriptor for Predicting Particle Size Effects on Catalyst Performance, and How to Estimate It**, *Charles T. Campbell*, *K. Zhao*, *N. Janulaitis*, University of Washington

Many important catalysts and electrocatalysts for energy and environmental technologies involve late transition metal nanoparticles dispersed across the surface of some oxide or carbon support. The activity and long-term stability of these materials depend strongly on particle size below 7 nm, and, in this size range, upon the composition and atomic-level structure of the support surface. We show here that the chemical potential of the metal atoms in such supported catalysts provides a convenient descriptor of their performance as heterogeneous catalysts that captures many of the effects of particle size, metal-metal alloying and support on catalyst performance. Based on microcalorimetric measurements of metal adsorption energies, the metal chemical potential is shown to be predictable as a function of metal particle size and the adhesion energy of the particle to the support. For oxide supports, this adhesion energy correlates predictably with metal oxophilicity, as we defined based on heats of oxide formation from gaseous metal atoms. For carbon supports, this adhesion energy correlates predictably with metal carbophilicity, as we defined based on DFT estimates of C atom adsorption energies. These correlations provide predictions of metal chemical potential that can enable catalyst design.

Work supported by DOE-OBES under Grant Number DE-FG02-96ER14630.

3:20pm **HC+SS-WeA-4 Size-Dependent Properties of Cobalt Nanoclusters on CeO<sub>2</sub>(111)**, *M. Rahman*, Louisiana State University; *T. Ara*, University of Wyoming; *Ye Xu*, Louisiana State University; *J. Zhou*, University of Wyoming  
Cobalt is a versatile catalytic metal. It has been used to catalyze many reactions of technological importance, including Fischer-Tropsch synthesis, reforming, and ammonia synthesis, where oxidic Co and metallic Co lead to different catalytic pathways. Meanwhile, ceria offers a desirable set of properties as catalyst support, including the abilities to stabilize nanoclusters, undergo redox interaction with metals, and enhance oxygen availability. Nanoparticles of Co supported on ceria have therefore been the mainstay of many heterogeneous catalysis studies. We have carried out an investigation of Co nanoclusters supported on stoichiometric CeO<sub>2</sub>(111) using computational modeling and scanning tunneling microscopy (STM). Various sizes up to ca. 20 Co atoms have been optimized using a minima hopping algorithm combined with density functional theory (DFT) calculations, which identifies many compact, symmetric structures as minimum-energy for the sizes that are considered. Theory predicts that in this size regime, the Co clusters prefer to be notably wider than they are high. A significant fraction of the Co atoms in each cluster are oxidized, and most of those are located on the periphery between the clusters and ceria. Co atoms that are not directly in contact with the surface are effectively screened and remain neutral. The large aspect ratios and high fractions of oxidic Co in small clusters at low Co metal coverages are corroborated by STM studies of Co deposited on CeO<sub>2</sub>(111) thin film surfaces at ambient temperature. Our findings shed light on atomic-level characteristics of Co nanoclusters on ceria that are relevant to catalytic applications.

4:20pm **HC+SS-WeA-7 on-Surface Synthesis of Porous Planar-Carbon-Lattices: Fundamental Properties and Applications**, *Abner de Siervo*, INSTITUTE of Physics Gleb Wataghin, University of Campinas (UNICAMP), Brazil **INVITED**

Materials science in the nanoscale domain has become a reality for several applications, from integrated circuits, sensors, catalysts, medicines, and data-storage devices, among others [1]. We achieved the ability to understand materials and, more importantly, command the materials' properties at the atomic level using precise synthesis and growth methods. Therefore, during the last decades, enormous efforts have been made to develop new processes for the fabrication, characterization, and manipulation of materials in complex nanoarchitectures with atomic precision, making it possible to express emergent new chemical, electronic, photonic, magnetic, and structural properties. On-surface synthesis becomes a powerful bottom-up technique to fabricate such nanostructures

# Wednesday Afternoon, November 8, 2023

using organic and organometallic precursors as molecular building blocks [2]. In this talk, I will present some strategies we have adopted to produce planar carbon lattices nanostructures, for example, porous nanoribbons and nanomembranes [3-5]. For a complete understanding of the atomic and electronic properties of the materials, we have combined scanning tunneling microscopy and spectroscopy (STM/STS), X-ray photoelectron spectroscopy (XPS), and numerical simulations based on density functional theory (DFT) calculations.

Acknowledgments:

FAPESP, CNPq, and CAPES from Brazil have financially supported this work.

References:

[1] G Ali Mansoori and TA Fauzi Soelaiman. Nanotechnology—An introduction for the standards community. ASTM International, 2005.

2005.

[2] Johannes V. Barth. Annual Review of Physical Chemistry, 58(1):375–407,

2007.

[3] Alisson Ceccatto dos Santos, et al., Chemistry of Materials 32 (5), 2114–2122 (2020).

[4] Nataly Herrera-Reinoza, et al., Chemistry of Materials 33, 2871–2882 (2021).

[5] Alisson Ceccatto dos Santos, et al., J. Phys. Chem. C 125, 31, 17164–17173 (2021).

**5:00pm HC+SS-WeA-9 2D Surface Optical Reflectance for Surface Studies in Harsh Environments**, A. Larsson, Lund University, Sweden; S. Pfaff, Sandia National Laboratories; L. Rämisch, S. Gericke, A. Grespi, J. Zetterberg, Edvin Lundgren, Lund University, Sweden

During recent years, 2D Surface Optical Reflectance (2D-SOR) [1,2] microscopy [3] has emerged as a valuable surface characterization tool for model catalysts or electrodes [4] when performing operando investigations in harsh environments. In particular, 2D-SOR microscopy is favorably used as a complementary technique to other photon-in-photon-out techniques which do not carry direct information on the surface 2D morphology. In this presentation we will present the development and examples of 2D-SOR instrumentation and investigations from single and poly-crystalline samples in combination with Planar Laser Induced Fluorescence (PLIF) [2, 3], High Energy Surface X-Ray Diffraction (HESXRD) [5,6,7] and Polarization Modulation-Infrared Reflection Absorption Spectroscopy (PM-IRRAS) [8] coupled to Mass Spectrometry (MS) and Cyclic Voltammetry (CV) in thermal catalysis, electrocatalysis and corrosion. Illustrating examples of the versatility of the technique will be shown including reflectance changes during the thermal CO oxidation over Pd(100) and Pd polycrystalline surfaces. We show that reflectance changes during the reaction can be associated with the formation of thin Pd oxides by the combination of 2D-SOR and Surface X-Ray Diffraction (SXRD). The combined measurements demonstrate a sensitivity of 2D-SOR to the formation of a 2-3 Å thin Pd oxide film. During Cyclic Voltammetry (CV) in an acidic electrolyte using a Au(111) surface as an electrode, we show that the differential of the change in 2D-SOR reflectance correlate to various current features in the CV curve. This observation can be used to differentiate current features in the CV curve from a polycrystalline Au surface, demonstrating that the different grains contribute to the current at different potentials due to the different surface orientations. Finally, we show that 2D-SOR is a cheap and useful technique to investigate the corrosion of applied materials such as duplex stainless steels and Ni alloys.

[1] W. G. Onderwaater et al Rev. Sci. Instrum., **88** (2017) 023704.

[2] J. Zhou et al, J. Phys. Chem. C **121** (2017) 23511.

[3] S. Pfaff et al, ACS Appl. Mater. Interfaces **13** (2021) 19530.

[4] W. Linpe, et al, Rev. Sci. Instrum., **91** (2020) 044101.

[5] S. Pfaff, et al Rev. Sci. Instrum. **90** (2019) 033703.

[6] S. Albertin, et al, J. Phys. D: Appl. Phys. **53** (2020) 224001.

[7] W. Linpé, et al J. Electrochem. Soc. **168** (2021) 096511.

[8] L. Rämisch et al, Appl. Surf. Sci. **578** (2022) 152048

**5:20pm HC+SS-WeA-10 Interrogating Reactive Sites with Intrinsic Kinetics Over Well-Defined Supported Pt Nanoparticles**, T. Kim, C. O'Connor, Christian Reece, Harvard University

The chemical industry is the primary consumer of energy and fossil fuels in the industrial sector and relies almost entirely on complex heterogeneous catalytic systems. Yet our ability to employ these systems far outweighs our understanding. While a detailed understanding of heterogeneous catalysts does exist for model systems (e.g., 2D single crystals) at ultra-high vacuum, our understanding of applied catalytic materials (e.g., metal nanoparticles deposited on a metal oxide support) under reaction conditions is still lacking. Herein we utilise the Temporal Analysis of Products (TAP) technique to precisely resolve the intrinsic kinetics of CO oxidation of size selected 2nm Pt nanoparticles supported on SiO<sub>2</sub>. Using Diffuse Reflectance Infrared Fourier Transform Spectroscopy (DRIFTS) we identify multiple types of well-coordinated, undercoordinated, and bridge-bound CO sites exist on the Pt nanoparticles. However, through a combination of isotopic labelling and microkinetic modelling, we find that only two pathways for CO oxidation exist over the catalyst surface under the entire range of reaction conditions studied: a fast and a slow pathway. The fast pathway follows typical catalytic behaviour and shows a strong temperature dependence and a linear dependence on CO coverage, but the slow pathway is independent of both temperature and CO coverage which is unexpected for a slow catalytic process. This study demonstrates the importance of being able to precisely resolve kinetics over applied catalytic materials using techniques such as TAP. Further, it also hints that under reaction conditions the highly dynamic nature of catalytic surfaces implies that our classical understanding of structure-activity-relationships may not hold as strong as originally hoped.

**5:40pm HC+SS-WeA-11 The Effects of Catalytic Cluster Size on Catalysis and Electrocatalysis**, Scott Anderson, University of Utah **INVITED**

Supported sub-nano clusters are potentially a metals-efficient approach to catalysis, where all the expensive catalytic atoms (Pt, Pd, etc.) are exposed in the surface layer. In addition, because the properties of small clusters are highly size dependent, varying the cluster size provides a parameter that can be used to tune activity and selectivity. The problem with small clusters is that they tend to sinter and poison easily, and much of our work is in developing approaches to stabilize the supported clusters under thermal or electro-catalytic conditions.

Deposition of mass-selected clusters in UHV is used to prepare model catalysts and electrocatalysts with catalytic centers that all start out being the same size. We have developed an in-vacuum ALD-like self-limiting reaction approach to dope or alloy the clusters with elements like B, Sn, or Ge, with the goal of stabilizing the clusters against both poisoning and sintering. Two types of catalysis experiments will be described.

Gas-surface catalysis is studied in the UHV system by mass spectrometric methods, but we also have new microreactor system that allows clusters deposited on alumina or silica surfaces to be exposed to reactant flows at pressures up to 1 atm, with mass spectrometric product detection. This part of the talk will focus on using Ge doping to stabilize small Pt clusters against deactivation by both carbon deposition (coking) and sintering at temperatures up to 700 K. To goal is to make stable and selective alkane dehydrogenation and cracking catalysts.

Electrocatalysis is studied either *in situ*, using an electrochemical cell housed in an antechamber to the UHV system, or in conventional benchtop electrochemical cells. The *in situ* experiments allow us to study aqueous electrochemistry with minimal air exposure, while the *ex situ* setups allow more elaborate types of electrochemical measurements. Results for the hydrogen evolution reaction (HER), oxygen evolution reaction (ORR), and alcohol electro-oxidation will be presented for catalytic Pt<sub>n</sub> clusters deposited on indium tin oxide (ITO), fluorine tin oxide (FTO), and graphite (HOPG). For ITO/FTO, electrodes were prepared by soft landing the clusters. For HOPG, the effects of deposition energy on electrocatalytic activity and stability, and on physical properties measured by XPS and ISS will be discussed.

# Wednesday Afternoon, November 8, 2023

## Magnetic Interfaces and Nanostructures Division

Room B110-112 - Session MI+2D+TF-WeA

### Special Symposium on Coupling Phenomena in Magnetism

Moderator: Hendrik Ohldag, Lawrence Berkeley National Laboratory

2:20pm **MI+2D+TF-WeA-1 Coupling Spin-Orbit and Exchange Interaction in a Low-Dimensional Magnet**, *Pascal Jona Grenz<sup>1</sup>, M. Donath, P. Krüger*, University of Münster, Germany

Coupling exchange interaction (SOI) and spin-orbit interaction (XCI) provides the foundation for many prospective spin-based information technology applications. For example, it was suggested that the strength of SOI at a ferromagnet/heavy-metal (FM/HM) interface is decisive for the efficiency of writing magnetic bits in spin-orbit-torque MRAM devices [1].

Exploring the electronic structure is the key to access the factors underlying the coupling of SOI and XCI. We use spin- and angle- resolved inverse photoemission to study the interplay of SOI and XCI in the unoccupied electronic structure at the interface of a low-dimensional FM on a HM substrate. The prototypical FM/HM hybrid system Ni/W(110) exhibits exchange-split Ni-related states that become strongly influenced by SOI. A balanced ratio of SOI and XCI results in a magnetization- and k-dependent quenching or enhancement of the spin splitting. This remarkably large interplay of SOI reflected in the adlayer states contrasts previous studies of the occupied electronic structure of the same system, where the observations were attributed solely to either SOI or XCI [2].

Using density-functional-theory (DFT) calculations, we investigate the underlying drivers responsible for the experimentally observed coupling of SOI and XCI. We find that hybridization between adsorbate and substrate states, along with the strongly localized wave functions at the heavy W nuclei, cause the strong influence of SOI within the Ni-related exchange-split states.

[1] I.M. Miron *et al.*, *Nature*, **476** 189 (2011)

[2] A. Nuber, PhD Thesis (University of Würzburg, Germany, 2011)

2:40pm **MI+2D+TF-WeA-2 AVS Graduate Research Awardee Talk: Temperature Dependent Magnetic and Electronic Properties of NiCo<sub>2</sub>O<sub>4</sub> Thin Film Surfaces**, *Arjun Subed<sup>2,3</sup>*, University of Nebraska-Lincoln; *D. Yang, C. Mellinger, X. Xu*, University of Nebraska-Lincoln; *P. Dowben*, University of Nebraska-Lincoln

Although NiCo<sub>2</sub>O<sub>4</sub> thin film is shown to possess perpendicular magnetic anisotropy [1], we have observed in-plane spin polarization of NiCo<sub>2</sub>O<sub>4</sub> thin film in spin polarized inverse photoemission spectroscopy (SPIPES). The unoccupied states of NiCo<sub>2</sub>O<sub>4</sub>, above Fermi level, were observed to have unequal density of states for spin majority and spin minority carriers in SPIPES, and the spectra obtained from the SPIPES have spectral features that can be compared to the XMCD spectra. The in-plane spin polarization of NiCo<sub>2</sub>O<sub>4</sub> is found to decrease with increasing temperature, as expected. In addition to the temperature dependent change in spin polarization, we observed that there is change in the surface electronic properties of NiCo<sub>2</sub>O<sub>4</sub> from conducting to insulating when the temperature is increased. X-ray photoemission spectroscopy (XPS) studies show that there exist no appreciable binding energy changes of Ni 2p<sub>3/2</sub> and Co 2p<sub>3/2</sub> core levels with change in temperature (T) when the NiCo<sub>2</sub>O<sub>4</sub> film exists in conducting phase. However, when the NiCo<sub>2</sub>O<sub>4</sub> films became insulating, the core level binding energies changed reversibly with change in temperature during annealing and cooling cycles. The core level binding energy (BE) change with temperature (T) is found to closely follow a modified Arrhenius type model. The proposed model is also followed by Co 2p<sub>3/2</sub> and Fe 2p<sub>3/2</sub> core levels in temperature dependent XPS of insulating CoFe<sub>2</sub>O<sub>4</sub> thin films. Our studies indicate that thermal effects and oxygen defects should play the roles in changing both magnetic and electronic properties of NiCo<sub>2</sub>O<sub>4</sub> thin films with temperature.

[1] C. Mellinger *et al.*, *Phys. Rev. B* **101**, 014413 (2020).

3:00pm **MI+2D+TF-WeA-3 Antiferromagnetic Real-Space Configuration Probed by Dichroism in Scattered X-Ray Beams with Orbital Angular Momentum**, *Sophie Morley, M. McCarter, A. U. Saleheen, A. Singh*, Lawrence Berkeley Lab; *R. Tumbleson*, University of California Santa Cruz; *J. Woods*, Argonne National Laboratory; *A. Tremsin*, UC Berkeley; *A. Scholl*, Lawrence Berkeley Lab; *L. de Long, J. Hastings*, University of Kentucky; *S. Roy*, Lawrence Berkeley Lab

INVITED

X-ray beams with orbital angular momentum (OAM) are a promising tool for x-ray characterization

techniques. Beams with OAM have an azimuthally varying phase, and new material properties can

potentially be probed by utilizing this unique phase structure. Here, we show how OAM beams are

created through resonant diffraction from an artificial antiferromagnet with a topological defect. The

scattered OAM beams have circular dichroism whose sign is coupled to the phase of the beam [1]. Using

magnetic scattering calculations, we show that this dichroism is related to the real-space configuration

of the antiferromagnetic ground state. Thermal cycling of the artificial antiferromagnet can change the

ground state, as indicated by the changing dichroism. These results exemplify the potential of OAM

beams to probe matter in a way that is inaccessible using currently available x-ray techniques.

[1] M. R. McCarter *et al.*, *Phys. Rev. B* **107**, L060407 (2023)

5:00pm **MI+2D+TF-WeA-9 Spin-dependent Hybridization of Image-potential States with TI States in TI/Ag(111)**, *Sven Schemmelmann<sup>4</sup>*, Universität Münster, Germany; *P. Härtl*, Universität Würzburg, Germany; *P. Krüger*, Universität Münster, Germany; *M. Bode*, Universität Würzburg, Germany; *M. Donath*, Universität Münster, Germany

The BiAg<sub>2</sub> and PbAg<sub>2</sub> surface alloys exhibit giant Rashba splittings [1-4]. The related TI/Ag<sub>2</sub> surface alloy is expected to show states with smaller but still large Rashba splittings due to the lower atomic number of TI. However, this alloy forms only small patches with long-range structural order [5]. For higher coverages of TI on Ag(111), a smooth and stable wetting layer forms with a moiré superstructure due to the lattice mismatch between TI and Ag. We present a study of the unoccupied electronic structure of this superstructure by spin- and angle-resolved inverse photoemission. The experimental results are accompanied by DFT calculations. We observe surface states and an image-potential resonance located several Å in front of the surface. Surprisingly, one surface state exhibits almost no Rashba splitting even though it is located around the TI atoms. This result is explained by the orbital symmetry of the respective state. For the image resonance, we find hybridization with a downward dispersing TI state leading to spin-dependent spectral intensities that vary strongly close to the hybridization point. This observation, both in experiment and bandstructure calculations, is supported by charge distribution calculations showing an expeditious change from the image resonance to the TI-induced surface state depending on k<sub>||</sub>.

[1] C. R. Ast *et al.*, *Phys. Rev. Lett.* **98**, 186807 (2007)

[2] G. Bihlmayer, S. Blügel, and E. V. Chulkov, *Phys. Rev. B* **75**, 195414 (2007)

[3] S. Wissing *et al.*, *Phys. Rev. Lett.* **113**, 116402 (2014)

[4] L. El-Kareh *et al.*, *New J. Phys.* **16**, 045017 (2014)

[5] P. Härtl, S. Schemmelmann, P. Krüger, M. Donath, and M. Bode, submitted to *Phys. Rev. B*

<sup>1</sup> Falicov Student Award Finalist

<sup>2</sup> AVS Graduate Research Awardee

<sup>3</sup> Falicov Student Award Finalist

<sup>4</sup> Falicov Student Award Finalist

# Wednesday Afternoon, November 8, 2023

5:20pm **MI+2D+TF-WeA-10 Distinct Tamm and Shockley Surface States on Re(0001) Mixed by Spin-Orbit Interaction – A Photoemission Study**, **Marcel Holtmann**, P. Krüger, University of Münster, Germany; K. Miyamoto, T. Okuda, HiSOR, Japan; P. Grenz, University of Münster, Germany; K. Shimada, HiSOR, Germany; M. Donath, University of Münster, Germany

Tamm and Shockley states, these two paradigmatic concepts are used to describe surface states not only in electronic systems but also in photonic and phononic crystals. The Re(0001) surface was found to host both types of electronic surface states in neighboring, but qualitatively different gaps [1]. Interestingly, spin-orbit interaction generates a double W-shaped energy vs  $k_{||}$  dispersion by mixing both types of states and lifting their spin degeneracy. We employ a combination of spin- and angle-resolved photoemission, tight-binding model calculations, and density functional theory that accounts for the photoemission process to establish reliable criteria for distinguishing between the two types of surface states. Our approach leads to a coherent understanding of the mechanism of spin-orbit interaction in such a situation.

From a detailed investigation of the Re(0001) surface along the  $\Gamma M$  and  $\Gamma K$  high-symmetry directions [2], we obtain Rashba parameters of 0.32 and 0.34 eVÅ along the two respective directions. This indicates a slight warping of the surface state. Regarding the aforementioned state's spin polarization: at variance with theoretical predictions for a perfect hcp(0001) of rhenium [3], we do not find any out-of-plane spin polarization. This is attributed to monatomic steps of a real Re(0001) surface with alternating terminations, leading on average to an effective sixfold surface symmetry and vanishing net out-of-plane spin polarization.

[1] M. Holtmann *et al.*, Phys. Rev. B **105**, L241412 (2022)

[2] M. Holtmann *et al.*, Phys. Rev. B **107**, 165420 (2023)

[3] A. Urru and A. Dal Corso, Surf. Sci. **686**, 22 (2019)

5:40pm **MI+2D+TF-WeA-11 Coupling between Spin Order and Orbital Order in 2D-Superlattice Perovskite Film**, **Bin Hu**, University of Tennessee Knoxville **INVITED**

The coupling between spin order and orbital order presents a fundamental request to develop advanced multifunctional materials. 2D-superlattice perovskite films, known as solution-processing semiconductors, possess strong orbital order within non-degenerate Rashba band structures under the concurrent influence of spin-orbital coupling and symmetry breaking. This provides a fundamental condition to dynamically couple spin order and orbital order through multiferroic interface design. Here, we combine ferroelectric 2D-superalattice perovskite (4,4-DFPD<sub>2</sub>PbI<sub>4</sub>) film and ferromagnetic cobalt (Co) film to form multiferroic perovskite/Co interface. By using this multiferroic interface design, we found that the circularly polarized orbitals with right and left handedness ( $s^+$  and  $s^-$ ) in Rashba band structures can selectively interact with spin-up and spin-down spin dipoles on the Co surface, leading to a mutually selectivity between spin order and orbital order. Particularly, this selective interaction between spin order and orbital order can enable spin-switchable phenomena towards developing emerging functionalities in these solution-processing hybrid metal halide perovskites. When the ferromagnetic spins on the Co surface are altered between positive and negative magnetic field directions (**+B** and **-B**), the circularly polarized luminescence (CPL) in 2D-superlattice perovskite can be switched between  $s^+$  and  $s^-$  polarizations, leading to spin-switchable phenomena at room temperature. More interestingly, our polarized neutron reflectometry (PNR) studies found that circularly polarized photoexcitation generates a static magnetization within 2D-superlattice perovskite film prepared on the Co surface. This presents an optically induced magnetization phenomenon. Essentially, this optically induced magnetization reveals a long-range coupling between the spin order on the Co surface and the orbital order within Rashba band structures in 2D-superlattice perovskite film. This presentation will discuss the fundamental coupling between spin order and orbital order through Rashba band structures in 2D-superlattice perovskite film.

**Plasma Science and Technology Division**

**Room A106 - Session PS1+AS-WeA**

**Plasma Chemistry, Catalysis and Applications for the Environment and Sustainability**

**Moderators: Michael Gordon**, University of California at Santa Barbara, **Kenji Ishikawa**, Nagoya University

2:20pm **PS1+AS-WeA-1 Synthesis of Hydrogen and Structural Carbon Materials from Methane Using Radiofrequency Nonequilibrium Plasma**, **Elijah Thimsen**, Washington University in St. Louis **INVITED**

The production of hydrogen from methane by dehydrogenation of carbon is up to 6 times less energy intensive than water splitting and involves no intrinsic CO<sub>2</sub> byproduct. If hydrogen were used as a fuel at societal scale, billions of tons per year of carbon co-product would be produced. Steel and concrete are manufactured goods that are used at a scale of billions of tons per year, for structural applications. To avoid massive waste, the carbon co-product from hydrogen production could be used in structural applications, perhaps to displace concrete and steel. In this talk, I will focus on the use of radiofrequency capacitively coupled electrodeless discharges in a tubular flow-through configuration for methane dissociation. The plasma step of our process currently operates in the pressure range from 0.025 to 0.125 bar, and the goal is to synthesize an equimolar mixture of C<sub>2</sub>H<sub>2</sub> + HCN from CH<sub>4</sub> + N<sub>2</sub>. The mixture of C<sub>2</sub>H<sub>2</sub> + HCN is an intermediate between the plasma and a downstream thermocatalytic reactor. The downstream thermocatalytic reactor synthesizes acrylonitrile, which is a critical precursor to structural carbon fiber, from the C<sub>2</sub>H<sub>2</sub> + HCN mixture that elutes from the plasma. Remarkably, the plasma synthesis of C<sub>2</sub>H<sub>2</sub> + HCN from CH<sub>4</sub> + N<sub>2</sub> is highly selective. We have been able to achieve >95% methane conversion with >90% nominal yield of a stoichiometric mixture of C<sub>2</sub>H<sub>2</sub> + HCN. Downstream of the plasma in the thermocatalytic reactor, selectivity is somewhat challenging, but yields of the desired acrylonitrile in the range from 20 to 40% based on C<sub>2</sub>H<sub>2</sub> + HCN have been achieved at the time of writing. For technoeconomic context, the results will be compared against the industrial standard SOHIO ammoxidation process for the synthesis of acrylonitrile. Furthermore, I will take this opportunity to reflect on the prospect of running a gas-phase synthesis process at a reduced pressure of approximately 0.1 bar and a production rate of minimum 10,000 tons per year.

3:00pm **PS1+AS-WeA-3 Kinetics of Hydrocarbon Decomposition in Plasmas Operating Up to 5 bar**, **Norleakvisoth Lim**, M. Gordon, University of California at Santa Barbara

Hydrogen is a promising energy carrier to replace fossil fuels in response to the rise in global warming from CO<sub>2</sub> greenhouse gas emissions. Unfortunately, hydrogen is predominantly produced industrially via steam methane reforming, where the reaction itself and process heating requirements generate CO<sub>2</sub>. Direct methane pyrolysis for hydrogen generation has recently regained interest due to its potential for net zero CO<sub>2</sub> emission. This process requires high operating temperatures due to high C–H bond energies (4.55 eV for methane) and collateral issues such as catalyst poisoning via coking. As an alternative, plasma-based conversion of methane to hydrogen and carbon (as well as other hydrocarbons) is an attractive process due to its potential ability to generate reactive species that can overcome activation barriers, improve CH<sub>4</sub> conversion, and use less energy than required for water electrolysis. Thus, understanding the mechanism and kinetics of CH<sub>4</sub> dissociation in thermal and non-thermal plasmas is a crucial step to evaluate the efficacy of plasma conversion of hydrocarbons.

This talk will highlight conversion, selectivity, and kinetics measurements of plasma-based decomposition of CH<sub>4</sub> and C<sub>2</sub> hydrocarbons using various plasma excitation schemes (AC arc and nanopulse) at pressures up to 5 bar in a batch configuration with different electrode gaps. H<sub>2</sub> selectivities up to 80% were observed in AC-excited thermal arcs, with specific energy requirements (SER) decreasing with increasing pressure to ~300 kJ/mol CH<sub>4</sub>. In general, plasma-based conversion has fast rates and seems to not encounter the typical pseudo-equilibrium limit, i.e., due to hydrocracking of products back to CH<sub>4</sub>, that is typically encountered with thermal pyrolysis of CH<sub>4</sub> at temperatures from 900-1300 °C. Other CH<sub>4</sub> decomposition products (<30 mol %) observed include C<sub>2</sub>H<sub>2</sub> and C<sub>2</sub>H<sub>4</sub>, and plasma-decomposition of C<sub>2</sub>H<sub>4</sub> was also studied. Product distribution with pressure and various CH<sub>4</sub>:H<sub>2</sub> ratios will be discussed, along with characterization and management of the solid C product. This work suggests that higher operating pressures can potentially improve the efficiency of plasma conversion of hydrocarbons.

# Wednesday Afternoon, November 8, 2023

3:20pm **PS1+AS-WeA-4 Plasma Pyrolysis of Liquid Hydrocarbons to Produce H<sub>2</sub> and Solid Carbon**, *N. Lim, Michael Gordon*, University of California at Santa Barbara

Understanding and engineering reacting systems that enable more sustainable use of our natural resources is central to both reducing the risks associated with CO<sub>2</sub> emissions and making the long-term transition to a more circular, sustainable, and electrified economy. Moreover, developing technologies to leverage the energy density of liquids to produce clean H<sub>2</sub> and solid carbon without CO<sub>2</sub>, could be game changing. In this work, we investigate the potential of directly exciting plasmas in liquid hydrocarbons to create unique, multi-phase reaction environments, i.e., environments where plasma (ionized gas), gaseous H<sub>2</sub>, gaseous and liquid hydrocarbons, and solid carbon are all present simultaneously, to produce clean H<sub>2</sub> and carbon. The ultimate target is direct transformation of liquid hydrocarbons to gaseous H<sub>2</sub> and solid, easy-to-separate carbon using electricity that can be provided from any source and/or points of use.

As a proof of concept, we have recently demonstrated that it is indeed possible to strike and sustain plasma discharges in liquid hydrocarbons such as hexane, to simultaneously generate gaseous H<sub>2</sub> and solid carbon at high rates. Significant H<sub>2</sub> generation along with small amounts of other light hydrocarbons was observed. Initial, un-optimized experiments have been promising: a single pin-to-pin AC-driven, high voltage plasma discharge running at ~18 W (estimated from the plasma current-voltage transient) in liquid hexane produced ~80-100 sccm of H<sub>2</sub>, which is equivalent to an energetic input of ~240 kJ/mol H<sub>2</sub> = 33 kW\*hr/kg H<sub>2</sub>. This energy requirement for an un-optimized system is considerably lower than for water electrolysis (40 kW\*hr/kg H<sub>2</sub> (theoretical), but 60 kW\*hr/kg H<sub>2</sub> in practice), and promisingly competitive with other plasma-based hydrocarbon conversion processes. Preliminary experiments show that (i) the plasma is not simply vaporizing the liquid - so the system's specific energy input (SEI) is preferentially driving hydrocarbon cracking; (ii) small amounts of C<sub>2</sub>-C<sub>4</sub> products are also produced, where selectivity depends on plasma operating conditions; and (iii) the liquid hydrocarbon phase immediately turns yellow and then quickly black due to rapid formation of suspended carbon particulates. Hydrocarbon conversion, reaction rates, and characterization of the gas (MS), liquid (GC/MS), and solid (C/H analysis, SEM, Raman) phase products as a function of plasma operating conditions and hydrocarbon source will be discussed.

4:20pm **PS1+AS-WeA-7 Plasma-Surface Interaction in CO<sub>2</sub> Containing Plasmas**, *Olivier Guaitella, E. Baratte*, Ecole Polytechnique - CNRS, France; *V. Guerra*, Instituto Superior Técnico, Portugal; *D. Sadi, S. Bravo, C. Garcia-Soto*, Ecole Polytechnique - CNRS, France; *T. Silva*, Instituto Superior Técnico, Portugal

**INVITED**

The use of Non Thermal Plasmas to convert CO<sub>2</sub> is a very promising way of meeting environmental challenges. However, there are two main obstacles to their use and optimisation:

- i) the complexity of the kinetics of these plasmas makes it very difficult to predict their chemical reactivity,
- ii) while it is relatively easy to dissociate the CO<sub>2</sub> molecule in a plasma, it is difficult to avoid reverse reaction mechanisms that reduce the energy efficiency of conversion.

To address the first point, complementary experimental set-ups have been developed in this work to enable step-by-step validation of OD kinetic models including electronic, vibrational and chemical kinetics. This systematic approach relies on discharges as simple as pulsed glow discharge and radiofrequency discharges in batch reactor, monitored with in situ time resolved absorption spectroscopy. Thanks to these studies, models of pure CO<sub>2</sub> but also, CO<sub>2</sub>/N<sub>2</sub>, CO<sub>2</sub>/H<sub>2</sub> and CO<sub>2</sub>/CH<sub>4</sub> have been thoroughly validated against a large range of experimental conditions. Once these plasma sources have been well characterized, they can be used to study the fundamental mechanisms of plasma-catalyst interaction. The combination of a cold plasma and a catalyst is indeed the solution most often proposed to overcome reverse reaction processes and improve selectivity and energy efficiency. However, the design of materials truly capable of benefiting from the vibrationally or electronically excited species of the plasma relies on an understanding of these mechanisms.

In addition to plasma-catalysis, new concepts are currently emerging for continuously shifting chemical equilibria in the plasma phase, thereby improving yields. The use of ionic membranes (perovskite or Yttrium Stabilized Zirconia) or water used as solvent opens up new routes for improving plasma CO<sub>2</sub> conversion processes, but once again raises the

question of how these plasmas interact with complex surfaces. Examples of these approaches will be given.

5:00pm **PS1+AS-WeA-9 Study of Plasma-Catalyst Surface Interactions for Methane Dry Reforming**, *Michael Hinshelwood, G. Oehrlein*, University of Maryland, College Park

Plasma enhanced dry reforming of methane (DRM) at atmospheric pressure is a promising technique for converting greenhouse gases (CH<sub>4</sub> and CO<sub>2</sub>) into syngas (H<sub>2</sub> and CO), which can be further used for producing fuels and chemicals. The exact mechanism of enhancement of DRM due to plasma is not fully understood, however plasma-generated reactive species are thought to play an important role. Enhancement in DRM can take the form of increased product formation or reduced carbon coking which can deactivate the catalyst. We use a remote plasma-catalysis setup that enables the study of certain plasma-catalyst interactions by infrared spectroscopic methods [1]. Species adsorbed on the catalyst surface are analyzed in-situ using Diffuse Reflectance Infrared Fourier Transform Spectroscopy (DRIFTS), while gas phase products from the interaction are analyzed with Fourier Transform Infrared Spectroscopy (FTIR). The catalyst used is Ni, commonly used for dry reforming reactions, on a SiO<sub>2</sub>/Al<sub>2</sub>O<sub>3</sub> support. The catalyst is exposed to either Ar/CO<sub>2</sub> or Ar/CH<sub>4</sub> plasma, while other gas mixtures are introduced into the reaction chamber downstream from the plasma. This allows for evaluation of the effect of reaction species specific to either gas. DRIFTS measurements reveal that exposure to CH<sub>4</sub> plasma results in the buildup of CH<sub>2</sub> (2930 cm<sup>-1</sup>) and CH<sub>3</sub> (2960 cm<sup>-1</sup>, 2860 cm<sup>-1</sup>) containing species on the catalyst surface. Build-up of such species also occurs during catalyst coking and deactivation. Exposure to CH<sub>4</sub>/Ar plasma may be able to replicate coking at low temperatures where reaction rates are lower and surface mechanisms easier to resolve. If CH<sub>n</sub> (n=1-3) buildup at room temperature is followed by Ar plasma exposure, the CH<sub>2</sub> and CH<sub>3</sub> surface coverages are reduced at similar and temporally decreasing rates, but not eliminated. Comparing the effect of Ar plasma and Ar/CO<sub>2</sub> plasma on surface CH<sub>n</sub>, is used to evaluate the potential of Ar/CO<sub>2</sub> plasma to reduce catalytic deactivation during dry reforming. Our setup allows for variation of the catalyst temperature to test the impact of plasma on DRM at various degrees of catalyst activity. Increased understanding of the time-dependent relationship between downstream products (FTIR) and surface adsorbed species (DRIFTS) will shed light on the plasma enhancement of DRM to inform development of future systems.

This material is based upon work supported by the U.S. Department of Energy, Office of Science, Office of Fusion Energy Sciences under award number DE-SC0020232.

1.Y. Li, J. Jiang, M. Hinshelwood, S. Zhang, P. J. Bruggeman, and G. S. Oehrlein, "Characterization of plasma catalytic decomposition of methane: role of atomic O and reaction mechanism," *J. Phys. D: Appl. Phys.*, 55, 155204, (2022). doi: 10.1088/1361-6463/ac4728.

5:20pm **PS1+AS-WeA-10 Silver Nanoparticle Synthesis in Low-Pressure Plasmas: The Roles of Free Electrons and Photons**, *Chi Xu, J. Held, H. Andaraarachchi, U. Kortshagen*, University of Minnesota

The interactions of plasmas with liquids enable considerable electron and vacuum ultraviolet (VUV) photon fluxes to the solution surface, contributing to subsequent reduction processes and emerging as a novel technique of nanomaterials synthesis. To date, the solvated electrons were mostly proposed to be the critical reducing agent while the effect of photon-driven reactions on nanoparticle synthesis has not been fully understood. In this work, we use glycerol, a major co-product of biodiesel production as the solvent. Using this solvent, we investigate the silver nanoparticle formation in silver nitrate (AgNO<sub>3</sub>)-glycerol solutions delivered as droplets to a low pressure nonthermal plasma, opening new synthetic pathways over previous bulk reactions. We demonstrate that this system allows the formation of monodispersed sub-20 nm silver nanoparticles. By inserting crystal filters having various cut-on wavelengths between the plasma and the glycerol droplet, UV radiation from the plasma-liquid emission at wavelength ranges between 150 and 280 nm is differentiated, while plasma-generated electrons are prevented from reaching the droplet. To quantify the nanoparticle yield, the final silver ion concentration was measured using a colorimetric method. We find that UV radiation contributes ~70% of the integral plasma effect in reducing silver ions to atoms, likely driven by H radicals attributed to the photodissociation of glycerol with an energy threshold of ~5 eV. The UV emission was traced to originate from carbon species released into the plasma from the glycerol solvent. The effects of aldehydes are minimal, which was evaluated by

# Wednesday Afternoon, November 8, 2023

scavenger study and colorimetric assay kit, respectively. Using water as the solvent instead, silver nanoparticle formation in aqueous solutions instead of glycerol does not exhibit a strong dependence on UV emission under the same operating conditions.

The research was sponsored by the Army Research Office and was accomplished under Grant No. W911NF-20-1-0105.

5:40pm **PS1+AS-WeA-11 Plasma Synthesis of Hydrogen from Ethanol Solution**, *D. Lojen*, Université libre de Bruxelles, Belgium; *T. Fontaine*, Université libre de Bruxelles/ University of Mons, Belgium; *L. Nyssen*, Université libre de Bruxelles/Ghent University, Belgium; *D. Petitjean*, Université libre de Bruxelles, Belgium; *R. Snyders*, University of Mons, Belgium; *N. De Geyter*, Ghent University, Belgium; **Francois Reniers**, Université libre de Bruxelles, Belgium

In the quest for green energy sources, hydrogen is often presented as the fuel of the future. However, as such, hydrogen must be synthesized. Among the many synthesis routes, those which don't directly produce CO<sub>2</sub> are privileged. In this regard, water electrolysis, plasma splitting or pyrolysis of methane are intensively explored, sometimes already at the industrial or preindustrial scale. However, all routes present advantages and drawbacks. For instance, plasma splitting of methane has to deal with the removal of solid carbon from the reactor, and water electrolysis suffer from the high intrinsic energy cost to break the water molecule into H<sub>2</sub> and O<sub>2</sub>. In this paper, we present preliminary results of the plasma induced splitting of liquid ethanol, using a nanopulsed generator, as this route could be an intermediate between the high energy cost of water splitting, and the solid carbon problem evidenced in CH<sub>4</sub> plasma. Moreover, ethanol could be from renewable sources origin, and according to previous studies, its main oxygenated degradation product could be CO, which is useful for the chemical industry. The plasma reactor consists of a pin-to-plate electrode geometry, with the plate electrode being submerged in ethanol. The gases produced are quantified using atmospheric mass spectrometry (Hiden), and the discharge is characterized using a high speed photron camera, and electrical measurements. The main body of the reactor is glass-based, with selected entries for OES, mass spectrometry, gas inlet and outlet. Results show that the thickness of the liquid ethanol layer over the plate electrode plays a tremendous role as it generates two plasma regimes: up to 2.5 mm, the plasma is hot, with a high current and a reasonable peak voltage, whereas above 2.5 mm, the plasma changes to a DBD-like configuration, with ethanol playing probably the role of a dielectric. This induces an increase in voltage and a drop in current. Hydrogen production is directly related to the current injected in the discharge. In the hot plasma configuration, hydrogen is produced with 55% selectivity, dropping to <50 % at higher ethanol thicknesses. A change in the byproducts selectivities is also observed (C<sub>2</sub>H<sub>4</sub>, C<sub>2</sub>H<sub>2</sub>, CH<sub>4</sub>, C<sub>2</sub>H<sub>6</sub>, CO), with the change in plasma regime. Results also show the effect of the nanopulse duration and frequency and the electrode polarity.

Acknowledgements:

This project is funded by the EoS PlaSynH2 project (FNRS-FWO Excellence of Science program, Belgium).

## Plasma Science and Technology Division

### Room A107-109 - Session PS2+MS-WeA

#### Plasma-Surface Modeling

**Moderators:** *Emilie Despiauw-Pujo*, Univ. Grenoble Alpes, CNRS, LTM, **Jun-Chieh Wang**, Applied Materials

2:20pm **PS2+MS-WeA-1 Modeling and Simulation of Plasma-Surface Interactions in Nanofabrication**, *David Graves*, Princeton University  
**INVITED**

Plasma-enhanced atomic layer deposition (ALD) and etching (ALE) in principle offer an unprecedented opportunity to control surface composition and structure. By modulating process time, frequency, energy, and chemistry, it is possible to vastly increase the range of conditions and surface modification effects at surfaces. ALE/ALD can simplify the process by separating, for example, a chemical surface modification step from addition of energy through rare gas ion bombardment. It might be possible to design novel etch and/or deposition precursor molecules to take advantage of ALE/ALD modulation-oriented approaches. However, process modulation introduces the complexity of having the surface state change in time during the exposure. To understand and control these processes, an atomic scale plasma-surface interaction simulation is essential. In this talk, I briefly review the use of molecular dynamics (MD) simulations in plasma-

surface interactions and how they have been used to help understand conventional plasma etching and deposition. I then use our recent studies of PEALD to highlight both successes and limitations of the current state of the art when used for modulated atomic layer processes. The key issues of interatomic force fields for many new chemistries and materials; using MD to simulate an intrinsically multi-timescale process; and the need to couple well-diagnosed experiments with atomistic simulations are emphasized.

3:00pm **PS2+MS-WeA-3 Mechanisms of Phosphorus Halides Gas Boosting Cryogenic Dry Process Etch Rate: A Quantum Chemistry Investigation**, *Yu-Hao Tsai*, *D. Zhang*, TEL Technology Center, America, LLC; *T. Orui*, *T. Yokoyama*, *R. Suda*, Tokyo Electron Miyagi Limited, Japan; *T. Hisamatsu*, TEL Technology Center, America, LLC; *Y. Kihara*, Tokyo Electron Miyagi Limited, Japan; *P. Biolsi*, TEL Technology Center, America, LLC

3D-NAND fabrication requires ultrafast etch rate (E/R) of the dielectric material stacks to deliver the high-aspect-ratio contact (HARC) etch with an economical fashion. In a separate report submitted about the cryogenic dry etch process development, we introduce the results of the drastically higher E/R of Ox/SiN (ONON) than the room temperature ones. We also reveal the catalytic etching reaction which enables the fast-etch process. We then identify the E/R booster gases: phosphorus halide, which brings the E/R to a higher level. To advance the booster-process development, a fundamental understanding of how the performance enhancing gases work is unavoidably crucial. This paper focuses on the mechanisms of phosphorus halides booster making the ONON E/R faster than the non-boosted cryogenic etch processes. Using the density functional theory (DFT), we identify the major chemical reactions behind the E/R enhancement. Based on the findings, we highlight the major properties required for the booster gases to function. The experimental results verify the mechanisms built upon the DFT study. In addition, we discuss the impact from the halogen atoms of the molecules on the etch performance. The paper does not only provide the insight toward an even higher E/R but also shed a light on the synergy of combining the experiments and atomistic modeling for the advanced node manufacturing technology developments.

3:20pm **PS2+MS-WeA-4 Molecular Dynamics Simulations of Diamond Surface Processing via Low-Energy Hydrogen and Argon Ion Bombardment**, *Jack Draney*, Princeton University; *J. Vella*, Princeton University Plasma Physics Lab; *A. Panagiotopoulos*, *D. Graves*, Princeton University

Nitrogen-vacancy (NV) centers in diamond are promising for multiple applications in quantum information processing and sensing [1,2]. NV centers can locally detect and measure physical quantities such as magnetic and electric fields. However, these devices are currently limited by surface defects that compromise charge stability and spin coherence [1,2]. In this work, we explore plasma-assisted atomic layer etching of diamond using classical molecular dynamics (MD) simulations. We performed MD simulations of low-energy hydrogen (<50 eV) and argon (<200 eV) ion bombardment of diamond surfaces. Argon ion bombardment can be used to locally smooth initially rough diamond surfaces via the formation of an amorphous C layer, the thickness of which increases with argon ion energy. Subsequent exposure with hydrogen ions (or fast neutrals) will selectively etch this amorphous C layer, leaving the underlying diamond layer intact if the H energy is maintained between ~2–5 eV. The simulations suggest that combining Ar<sup>+</sup> smoothing with selective H removal of amorphous C could be an effective strategy for diamond surface engineering, leading to more reliable and sensitive NV center devices.

[1] Sangtawesin, S., Dwyer, B. L., Srinivasan, S., Allred, J. J., Rodgers, L. V., De Greve, K., ... & De Leon, N. P. (2019). Origins of diamond surface noise probed by correlating single-spin measurements with surface spectroscopy. *Physical Review X*, 9(3), 031052.

[2] Stacey, A., Dontschuk, N., Chou, J. P., Broadway, D. A., Schenk, A. K., Sear, M. J., ... & Hollenberg, L. C. (2019). Evidence for primal sp<sup>2</sup> defects at the diamond surface: candidates for electron trapping and noise sources. *Advanced Materials Interfaces*, 6(3), 1801449.

# Wednesday Afternoon, November 8, 2023

4:20pm **PS2+MS-WeA-7 Yesterday, Today, and Tomorrow for High-Aspect-Ratio Contact Etching: Unraveling the Mysteries of Plasma-Surface Interactions with Modeling and Simulations**, *Du Zhang, Y. Tsai*, TEL Technology Center, America, LLC; *M. Iwata, M. Yokoi, K. Tanaka*, Tokyo Electron Miyagi Limited, Japan; *T. Hisamatsu*, TEL Technology Center, America, LLC; *Y. Kihara*, Tokyo Electron Miyagi Limited, Japan; *P. Biolsi*, TEL Technology Center, America, LLC

INVITED

The ever-growing demand for big data storage and processing has driven advancements in both the design and process technologies of advanced memory devices. In particular, the fabrication of high-aspect-ratio contacts (HARC) is a key process step. Etch throughput and profile control are crucial for reducing manufacturing cost and ensuring device performance. To meet these challenges, multiscale mechanistic understandings are essential for driving process and design optimization.

In this paper, we will discuss the fundamental etch mechanisms of plasma-surface interactions for HARC etching assisted by atomistic / plasma / profile modeling. We will review the underlying surface reaction mechanisms of the conventional fluorocarbon gas chemistry. We will also discuss the typical process challenges with etch rate and profile control, as well as various possible mitigation methods. Moreover, we will introduce how hydrogen admixture into the fluorocarbon chemistry can alter the behavior of dielectric etch rate and surface chemistry in a way that breaks conventional wisdom, especially at lower wafer temperatures. By unraveling and utilizing these underlying mechanisms derived from multi-scale simulations, we have been able to design new processes to achieve enhanced performance.

5:00pm **PS2+MS-WeA-9 Optimization of Model Parameters in Simulations of High Aspect Ratio Plasma Etching**, *Florian Krüger*, University of Michigan, Ann Arbor; *D. Zhang, M. Park, A. Metz*, TEL Technology Center, America, LLC, USA; *M. Kushner*, University of Michigan, Ann Arbor  
Computational investigations of feature evolution during plasma etching of micro- and nano-electronics devices are highly dependent on a robust reaction mechanism and precise knowledge of reaction probabilities and coefficients to accurately represent the physical behavior of these processes. The increased complexity of the structures and use of novel gas compositions coupled with the necessarily reduced reaction set used by numerical investigations of feature evolution makes it difficult to choose these critical parameters from first principles. This problem is exacerbated by the fact that many of the physical and chemical processes occurring during plasma etching are based on different fundamental principles - i.e., physical sputtering, chemical sputtering, chemisorption, physisorption, spontaneous etching – that have different functional forms.

The aim of this work was to accelerate the development of reaction mechanisms for feature profile evolution during plasma etching. This is accomplished by selecting a subset of reaction rates and angular dependencies and matching the predictions of feature profiles to experimental data using autonomous optimization methods. To that end a series of etches of high aspect ratio (HAR) SiO<sub>2</sub> features using a C<sub>4</sub>F<sub>6</sub> / C<sub>4</sub>F<sub>8</sub> / Ar / O<sub>2</sub> plasma was performed and relevant quantities such as etch depth, etch rate, aspect ratio as well as critical widths at several depths were determined using scanning electron microscopy.

The same process was reproduced using gas phase and profile scale simulation tools, HEPM (Hybrid Plasma Equipment Model) and MCFPM (Monte Carlo Feature Profile Model), respectively. Some of the input parameters used by the MCFPM were coupled to a multi variate 2-step optimizer that adjusted relevant input parameters in to achieve the best match between simulation and experiments. Thus, the profile etch simulation effectively acts as an objective function on which the optimization is based. Due to the specific nature of the data and objective function with respect to spatial discretization, the 2-step approach – a combination of gradient descent and Nelder-Mead optimization - proved most effective.

The outcome and development this optimization process will be discussed. The resulting reaction mechanism was used to simulate features using similar but quantitatively different processing conditions to demonstrate how broadly the mechanism can be applied.

\* Work supported by Tokyo Electron, Samsung Electronics and the National Science Foundation.

5:20pm **PS2+MS-WeA-10 Prediction of Surface Morphology and Composition Evolution during Atomic Layer Deposition via Combined Ab-Initio and Monte Carlo Approach**, *Ting-Ya Wang, G. Hwang*, University of Texas at Austin

Atomic layer deposition (ALD) has been proposed as a method for achieving greater precision and control over film thickness, conformality, and impurity levels as compared to traditional chemical vapor deposition. It uses alternating cycles of two half-cycle reactions to achieve sequential and self-limiting deposition. However, finding the optimal conditions for the desired film properties and surface states for a certain material has largely relied on a trial-and-error approach. To expedite the search process, understanding the underlying mechanisms that influence surface chemistry and structure is crucial. However, currently available experimental methods may be limited in their ability to non-invasively observe surfaces at the atomic level or hindered by overlapping signals.

Theoretical methods have their own set of limitations. First-principles calculations, such as density functional theory (DFT), can be used to study the electronic structure of atoms and have been applied extensively to study surface reaction pathways. However, they are generally limited to a few hundred atoms and do not consider temperature and pressure effects. Ab-initio molecular dynamics (AIMD) simulations allow for studying dynamic processes, but they are similarly limited by both length and time scales. Monte Carlo (MC) simulations provide a way to study the thermodynamic properties of larger systems, and kinetic MC (KMC) allows for real-time simulation of system evolution. However, without a description of potential for each atom, both MC methods rely on predetermined lists of allowed events, which limit their accuracy and applicability.

Combining MC with DFT can potentially enhance the accuracy and applicability of simulations. However, in order to make these methods more reliable in describing various systems and include unknown reaction mechanisms, streamlining the integration of these two methods and the auto-generation of required information for MC simulations is important. In our work, we have applied this approach to investigate the evolution of surface structure and film morphology during plasma-enhanced ALD. Film morphology is a critical factor affecting film properties such as refractive index and wet etching rate, while surface structure determines the surface chemistry and thus affects deposition kinetics. We have examined the effects of plasma and different types of precursors on ALD processes and film properties, as well as the impact of process conditions, such as temperature and pressure.

5:40pm **PS2+MS-WeA-11 Modeling Reaction and Diffusion at a Plasma-Liquid Interface**, *Sean Peyres*, University of Illinois at Urbana-Champaign; *N. Üner*, Middle East Technical University, Turkey; *N. Abuyazid, R. Sankaran*, University of Illinois at Urbana-Champaign

Low-temperature, atmospheric-pressure plasmas can promote reactions at a liquid surface for various applications including nanoparticle synthesis, water purification, treatment of skin wounds, and chemical production. At the core of these processes, plasma-produced species, such as electrons and hydroxyl radicals, cross the gas-liquid boundary and rapidly react with solution-phase species, including the solvent, within a few nanometers to micrometers distance of the interface. A key consequence of the highly localized reactions is that the reaction rates are limited by mass transport of the solution species from the bulk liquid to the plasma-liquid interface. Previous experimental studies have observed such mass transport limitations, but a fundamental description of the mass transport has yet to be developed.

Here, we present a simple reaction-diffusion model for the reaction of plasma-produced species at a gas-liquid interface. The model consists of a set of nonlinear differential equations describing the reaction and diffusion of a single plasma species (referred to as a radical) and a single solution-phase species (referred to as a scavenger). The plasma-produced radical reacts both with the scavenger and itself in the solvent via recombination. To solve the equations analytically, simplifying assumptions were necessary. First, quasi-steady state was assumed, where the radical and scavenger concentrations quickly obtain a profile that can be solved for a given time. Then, various assumptions were made to solve the equations under limiting cases. Examples include negligible radical-scavenger reaction, uniform scavenger concentration, and fast reaction with the scavenger (compared to radical recombination). These results could be summarized by using dimensionless numbers that relate the competition between the radical-scavenger and radical recombination reactions along with the transport freedom of the scavenger.

# Wednesday Afternoon, November 8, 2023

Furthermore, we solved the full set of equations numerically and compared with the analytical solutions for the limiting cases. Finally, by adding a boundary condition for the diffusive layer, the bulk scavenger concentration could be calculated as a function of time and compared with previous experimental reports. We show that the model can be used to quantitatively predict and explain mass transport effects on reaction yields and selectivity.

6:00pm **PS2+MS-WeA-12 Integrated Modeling of Diamond Growth and the Surface Composition in CH<sub>4</sub>/H<sub>2</sub> Plasma**, *Y. Barsukov*, Princeton University Plasma Physics Lab; *A. Khrabry*, Princeton University; *Igor Kaganovich*, Princeton University Plasma Physics Lab

Microwave plasma generated in a mixture of CH<sub>4</sub> highly diluted in H<sub>2</sub> is typically used to grow diamonds. According to the broadly accepted mechanism, most of the surface of the growing diamond is unreactive because it is covered by hydrogen atoms. At a small fraction of the surface, hydrogen is removed by the so-called hydrogen-atom abstraction mechanism resulting in the formation of reactive sites (surface activation). Radical species produced in the CH<sub>4</sub>/H<sub>2</sub> plasma are adsorbed on the reactive surface sites, changing the surface composition and promoting the diamond film growth. Atomic H radicals play a key role in the surface activation, allowing for the CH<sub>3</sub> radicals to be adsorbed on the reactive sites which leads to the growth of diamond. Nevertheless, the main by-product of CH<sub>4</sub> decomposition in the plasma is C<sub>2</sub>H<sub>2</sub>, but its role in the growth process is still debated. A complex kinetic model which links fluxes of gaseous reactants from the plasma to the surface composition is needed to identify the role of each reactant.

To consider complex plasma-surface chemistry we performed a 0D kinetic modeling, where 83 surface reactions between CH<sub>4</sub>, CH<sub>3</sub>, H, H<sub>2</sub> and C<sub>2</sub>H<sub>2</sub> gaseous species are considered. The rates of all 83 reactions were calculated under the same approach, namely, we used WB97XD DFT functional and transition state theory. The DFT functional was validated for gaseous reactions, for which rate constants were measured. The following processes were considered in the model: 1) surface activation/passivation by H, H<sub>2</sub>, CH<sub>3</sub> and CH<sub>4</sub>, 2) adsorption/desorption of CH<sub>3</sub> and C<sub>2</sub>H<sub>2</sub> on the reactive surface sites, 3) hydrogen abstraction from the adsorbates, 4) incorporation of C atom from the adsorbate into the diamond network (sp<sup>3</sup> phase), and 5) formation of sp<sup>2</sup> phase from C<sub>2</sub>H<sub>2</sub> adsorbate.

The model reproduces the experimental observation that the rate of diamond growth strongly depends on the substrate temperature and has a peak near 1200 K. Detailed analysis of the surface composition shows that the growth is suppressed at low temperature due to formation of sp<sup>2</sup> phase. (The mechanism of sp<sup>2</sup> phase formation is similar to the mechanism of soot growth). At temperatures higher than 1200 K, the growth is suppressed due to reverse reactions leading to separation of C atoms from the diamond network into the adsorbed state and their subsequent desorption. Thus, our 0D kinetic model allows to link fluxes of plasma reagents with the surface composition and growth rate. The model will be expanded with reactions leading to doping of diamond, which are critical for the synthesis of sensors and qubits.

## Surface Science Division

### Room D136 - Session SS-WeA

#### A Special Session Honoring Wilson Ho: 25 Years of Single-Molecule Vibrational Spectroscopy and Microscopy

Moderators: *Xi Chen*, Tsinghua University, *Xiaohui Qiu*, Nanocenter

2:20pm **SS-WeA-1 Development of Single-Molecule Spectroscopy Inspired by STM-IETS**, *Yusoo Kim*, RIKEN, Japan **INVITED**

The scanning tunneling microscope (STM) is a versatile and powerful tool for investigating and controlling the chemistry of individual molecules on solid surfaces, mainly due to its extremely high spatial resolution. Using tunneling electrons from an STM tip, it is possible to excite various quantum states of single molecules on a surface, providing insights into the mechanisms of surface chemical reactions. Inspired by the pioneering work of Wilson Ho's group on single-molecule vibrational spectroscopy by inelastic electron tunneling spectroscopy combined with STM, we have been able to establish a dynamic approach to explore vibrational mode-selective chemistry in single-molecule reactions based on action spectroscopy with STM. Later, we developed an optical STM that combines the STM with light illumination and detection systems to probe molecular energetic processes such as energy transfer, conversion, and dissipation. In this talk, I will discuss some of our long-standing efforts to develop single-

molecule spectroscopy using local excitation sources, such as tunneling electrons and localized surface plasmon, generated at the STM junction.

2:40pm **SS-WeA-2 Unraveling Orbital Magnetism Contributions to Landau Levels in Moiré Quantum Matter**, *Joseph Strosio*, NIST **INVITED**

Flat and narrow band physics in moiré quantum matter (MQM) has proven to be extremely rich with new emergent quantum phases which can be tuned with applied electric and magnetic fields. The topological properties of the eigenstates of the moiré Hamiltonian are critical for establishing the quantum phase of the system. In this talk, we use the quantum ruler of Landau levels to unravel the energy-resolved valley-contrasting orbital magnetism and large magnetic susceptibility that contribute to the energies of Landau levels of twisted double bilayer graphene. These orbital magnetism effects lead to significant deviations from the standard Onsager relation, which manifests as a breakdown in scaling of Landau level orbits. These substantial magnetic responses emerge from the nontrivial quantum geometry of the electronic structure and the large length scale of the moiré lattice potential. We show that this breakdown of the original Onsager relation is unique in MQM due to the typical superlattice length scales in these systems. Going beyond traditional measurements, STM-based Landau level spectroscopy offers a complete "quantum ruler" resolving the full energy dependence of orbital magnetic properties in moiré quantum matter.

3:00pm **SS-WeA-3 Sub-Nanometer Resolved Single-Molecule Optical Imaging**, *Z. Dong*, University of Science and Technology of China; *Shaowei Li*, University of California, San Diego **INVITED**

Aspirations for reaching atomic resolution with light have been a major force in shaping nano-optics, whereby a central challenge is to achieve highly localized optical fields. The plasmonic nanocavity defined by the coinage-metal tip and substrate in a scanning tunneling microscope (STM) can provide highly confined and dramatically enhanced electromagnetic fields upon proper plasmonic resonant tuning, which can modify both the excitation and emission of a single molecule inside the nanocavity and produce intriguing new optoelectronic phenomena. In this talk, I shall demonstrate two recent STM-based phenomena related to single-molecule optical spectroscopy. The first is single-molecule Raman scattering closely associated with molecular vibrations. The spatial resolution of tip enhanced Raman spectroscopy (TERS) has been further driven down to the Angstrom scale at the single-bond level. Such a capability not only yields a new methodology called scanning Raman picoscopy for structural reconstruction and tracking bond breaking and forming of surface reactions, but also enables to clarify the chemical enhancement mechanism in TERS through well-controlled local contact environments. The second phenomenon is single-molecule electroluminescence. Through managements over molecular quenching and energy level alignment, we demonstrate clear single-molecule electroluminescence and even single-photon emission. Furthermore, by precisely controlling intermolecular distances, we can not only demonstrate coherent dipole-dipole coupling in homodimers, but also reveal intriguing transitions from incoherent hopping-like Forster energy transfer to coherent wavelike electronic energy transfer in donor-acceptor heterodimers. In addition, the wavelike quantum-coherent transfer channel is found three times more efficient than the incoherent channel in a one-step transfer process, highlighting the advantage of coherent channels in electronic energy transfer processes in large molecular networks. Our results provide new routes to optical imaging, spectroscopy and engineering of light-matter interactions and intermolecular coupling at the sub-nanometer scale.

3:20pm **SS-WeA-4 Magnetic Resonance Imaging of Individual Organic Radicals with sub-Molecular Resolution Using a Scanning Tunneling Microscope**, *Christopher Lutz*, *G. Czap*, IBM Almaden Research Center **INVITED**

Scanning tunneling microscopy (STM) gives atomic-resolution detection of properties such as the electronic density of states, spin polarization, and spin and vibrational excitations. Electron spin resonance (ESR) of individual atoms and small molecules has extended these capabilities to give very high energy resolution and quantum control, transforming individual adsorbed atoms into sensitive detectors of the local magnetic field. Here we present spin resonance of individual organic radical molecules adsorbed on an ultra-thin MgO film grown on a silver crystal. We find that several nearly-planar fluorenone derivatives become charged to anions upon adsorption on the insulating film. This spontaneous charging quenches the spin of the radicals, and transforms stable molecules into radical anions. These radicals are driven spin-resonantly by the radio-frequency electric field from the tip and sensed locally by magnetoresistance. We found a g-

# Wednesday Afternoon, November 8, 2023

factor of nearly 2 for each species and visualized the delocalized unpaired electron in these molecules by magnetic resonance imaging. We used conventional Fe-terminated tips as well as halogen-functionalized Fe tips in a 1-Kelvin microscope. Potential applications include the investigation of coupled molecular spins and graphene nanoribbon edge states, and the transfer of a spin-resonant molecule to the microscope tip in order to provide a versatile scanning ESR sensor.

## 4:20pm SS-WeA-7 Revealing the Local Band Structures of Sharp $WS_2/MoS_2$ Heterojunction and Graded $W_xMo_{1-x}S_2$ Alloy by Near-Field Optical Imaging, *Chi Chen*, Academia Sinica, Taiwan **INVITED**

With the development of various chemical vapor deposition (CVD) methods [1], many artificial 2D semiconductors have been synthesized, which increase the chances of forming disrupted interfaces and non-periodic or small-sized systems (defects and grain boundaries). All such systems create local electronic band structures within a finite scale, which cannot be readily explained by solid-state band theory nor be probed easily by confocal microscopes and macroscopic transport.

In this study, we investigated abrupt heterojunctions and graded alloys between two transition metal dichalcogenides (TMD), which involve non-periodic band structures and require high spatial resolution. We employed near-field photoluminescence (NF-PL) imaging to study the atomically sharp 1D interfaces between  $WS_2$  and  $MoS_2$ . With an optical resolution of 68 nm, a 105 nm-wide region for quenched PL was confirmed using NF-PL imaging [2]. Our NF-PL imaging resolved the narrowest quenching width and sharpest strain mapping because of the superior spatial resolution and stability of our home-built SNOM [3].

We further developed a near-field broadband absorption (or transmittance, NF-tr) imaging method to overcome the limitations of NF-PL for low-quantum-yield materials. The NF-tr technique provides abbreviation-free and nanoscale-resolution imaging capability of the entire conduction band over highly lateral inhomogeneity. We utilized NF-tr microscopy to investigate the varying bandgap and bowing factor of a single-layered  $W_xMo_{1-x}S_2$  alloy [4]. For the bilayer  $W_xMo_{1-x}S_2$  alloy, the energy contour maps present the bandgap evolution in the alloy and reveal bilayer coupling between the top and bottom layers. We can conclude that the bottom layer has an alloy nature, whereas the top layer is composed of pure  $WS_2$ . High-spatial-resolution spectral capability is essential for analyzing compositional and location-dependent bandgap evolutions.

- [1] K.-C. Chiu and Y.-H. Lee *et al.*, *Adv. Mater.* 30, 1704796 (2018)
- [2] H.-C. Chou and C. Chen *et al.*, *Nanoscale* 14, 6323 (2022)
- [3] J.-R. Yu and C. Chen *et al.*, *Rev. Sci. Instrum.* 91, 073703 (2020)
- [4] P.-W. Tang and C. Chen *et al.*, *ACS Nano*, 16, 5, 7503 (2022)

## 4:40pm SS-WeA-8 On-Surface Chemical Dynamics Probed with Concurrent In Situ STM, Infrared Spectroscopy, and Supersonic Molecular Beams, *Steven Sibener, J. Wagner, R. Edel, T. Grabnic, S. Brown, J. Saylor, J. Brown*, University of Chicago **INVITED**

We have developed the capability to elucidate interfacial reaction dynamics using an arguably unique combination of supersonic molecular beams combined with in situ STM and AFM visualization. These capabilities have been implemented in order to reveal the complex spatio-temporal correlations that govern heterogeneous reactions at their most fundamental level spanning atomic, nano, and meso length-scales. For example, time-lapse visualization of reacting interfaces is allowing us to probe the reactivity of specific sites at interfaces and how the presence of a reacted site or local region influences the subsequent reaction probability at proximal sites. Such correlations are important in chemisorption, catalysis, materials oxidation and erosion, and film processing. This capability also opens up a new view for interfacial reaction dynamics where incident beam kinetic energy and angle of incidence can be used for reaction control parameters with outcomes such as site-specific reactivity, changes for overall time-evolving mechanisms, and where the on-surface fate of chemisorbed species can be definitively ascertained. In this work the time-evolving interface can be probed either in real-time or, for reactions occurring under extreme thermal conditions, using time-lapse sequential imagery. This presentation will give illustrative examples from our recent work on the atomic and multiscale oxidative reactivity of HOPG graphite, H reactivity with SAMs, atomic oxygen interactions with single and multilayer graphene including moiré superlattices, and the energy disposal and geometric endpoint for molecular nitrogen chemisorption on Ru. Most recently, the ability to visualize single-molecule nitrogen dissociation events provides a new approach for assessing the importance of adiabatic vs. non-adiabatic interactions in chemisorption by examining the rate of energy disposal and ultimate atomic resting adsorption sites for the dissociatively

adsorbed atoms from each individual molecular scattering event. Taken together, these results provide a direct and information-rich complement to traditional gas-surface scattering experiments which monitor volatile products, especially with respect to uncovering the important on-surface chemical events that inform multiscale spatio-temporal correlations that influence interfacial reaction pathways.

## 5:00pm SS-WeA-9 Unravelling the Mysteries of Water and Ice: A Journey Starting from Single Water Molecule, *Ying Jiang*, International Center for Quantum Materials, School of Physics, Peking University, China **INVITED**

Despite its ubiquity in nature, water is one of most complicated condensed matters. The understanding of water structure and phase transition is far from satisfactory, and many unusual properties of water remain as puzzles. The main reason arises from the many-body hydrogen (H)-bonding interaction between the water molecules. Moreover, the light H nuclei can exhibit prominent quantum effects, in terms of tunneling and zero-point motion. The so-called nuclear quantum effects (NQEs) add additional complexity to water and ice. Therefore, it would be ideal to directly access the degree of freedom of H in water/ice. To this end, we have steadily continued to improve accuracies of imaging and spectroscopic methods based on scanning probe microscopy (SPM) (tip-enhanced inelastic electron tunneling spectroscopy and higher-order electrostatic force microscopy) [1,2], which acquire unprecedentedly high sensitivity to the H of single water molecule in a nearly non-invasive manner. In this talk, I will showcase the application of those techniques to probe water clusters, ion hydrates, 2D ice and even bulk ice surface [3-6], with increasing complexity. The possibility of combing SPM with quantum sensing technology to perform nanoscale NMR measurement of protons in ambient water will be also briefly discussed [7].

### References:

- [1] Guo *et al.*, *Science* 352, 321 (2016)
- [2] Peng *et al.*, *Nature Communications* 9, 122 (2018)
- [3] Meng *et al.*, *Nature Physics* 11, 235 (2015)
- [4] Peng *et al.*, *Nature* 557, 701 (2018)
- [5] Ma *et al.*, *Nature* 577, 60 (2020)
- [6] Tian *et al.*, *Science* 377, 315 (2022)
- [7] Zheng *et al.*, *Nature Physics* 18, 1317 (2022)

## 5:20pm SS-WeA-10 Probing Chemistry at the Angstrom-Scale via Tip-Enhanced Raman Spectroscopy, *Nan Jiang*, University of Illinois Chicago **INVITED**

The chemical interrogation of individual atomic adsorbates on a surface significantly contributes to understanding the atomic-scale processes behind on-surface reactions. However, it remains highly challenging for current imaging or spectroscopic methods to achieve such a high chemical spatial resolution. Tip-enhanced Raman spectroscopy (TERS), which couples scanning tunneling microscopy (STM) and surface-enhanced Raman spectroscopy, provides such a powerful capability to concurrently harvest topographic and chemical information with single-bond sensitivity at the angstrom-scale. Herein, we use ultrahigh vacuum (UHV) TERS to measure the angstrom-scale interfacial interactions of a vertical Van der Waals heterostructure of borophene with tetraphenylidibenzoperiflanthene (DBP) molecules. TERS reveals subtle ripples and compressive strains of the borophene lattice underneath the molecular layer. The induced interfacial strain is demonstrated to extend in borophene by  $\sim 1$  nm beyond the molecular region by virtue of 5 Å chemical spatial resolution. Furthermore, we use our method to probe the local chemical properties of oxidized borophene. The results show that single oxygen adatoms on borophene can be identified and mapped with  $\sim 4.8$  Å spatial resolution and single bond (B-O) sensitivity. In addition to offering atomic-level insights into the above-mentioned systems, our studies demonstrate UHV-TERS as a powerful tool to probe the local chemistry of surface adsorbates and interfacial structures in the atomic regime with widespread utilities in heterogeneous catalysis, on-surface molecular engineering, and low-dimensional materials.

## 5:40pm SS-WeA-11 Single Molecule Characterization of Cobalt Phthalocyanine $Co_2$ Reduction Catalysts, *X. Wang*, Yale University; *P. Zahl*, Brookhaven National Laboratory; *H. Wang, Eric Altman, U. Schwarz*, Yale University

Immobilized cobalt phthalocyanine (CoPc) derivatives have been identified as promising catalysts for  $CO_2$  electroreduction to methanol. The support as well as side chains attached to CoPc have a large effect on the activity and selectivity to methanol.  $CO$  adsorption strength is considered a key descriptor for  $CO_2$  reduction activity and selectivity. Therefore, we have begun to study  $CO$  interactions with individual supported CoPc molecules using scanning probe methods. This talk focuses on a combined scanning

# Wednesday Afternoon, November 8, 2023

tunneling microscopy, non-contact atomic force microscopy, and Kelvin probe force microscopy characterization of CoPc molecules on Ag(111) with CO functionalized tips. In addition to resolving the atomic structure, the data provides the three-dimensional force field acting between the tethered CO and supported CoPc molecules and the charge distribution across the CoPc that is responsible for it. Analysis of the force field yielded maps of the catalytically relevant equilibrium potential energy between the tethered CO and specific locations within the CoPc molecule. Surprisingly, the maps show that the strongest interaction is not directly above the Co atom, but rather in four nodes surrounding it. The results are being compared with amino-substituted CoPc where the amino groups have been shown to enhance catalytic activity.

6:00pm **SS-WeA-12 Switching Chemical Bonds by Mechanical Load at Single Molecule Level via Qplus Atomic Force Microscope, A.M. Shashika D. Wijerathna, M. Zirnheld**, Old Dominion University; **Z. Win**, City University of Hong Kong, Hong Kong Special Administrative Region of China; **Y. Li**, Center for Nanoscale Materials, Argonne National Laboratory; **R. Zhang**, City University of Hong Kong, Hong Kong Special Administrative Region of China; **S. Hla**, Center for Nanoscale Materials, Argonne National Laboratory; **Y. Zhang**, Old Dominion University

Switching Chemical Bonds by Mechanical Load at Single Molecule Level via Qplus Atomic Force Microscope

A.M. Shashika D. Wijerathna<sup>1</sup>, Markus Zirnheld<sup>1</sup>, Zaw Myo Win<sup>2</sup>, Yang Li<sup>3</sup>, Ruiqin Zhang<sup>2</sup>, Saw Wai Hla<sup>3</sup>, Yuan Zhang<sup>1</sup>

Affiliation: 1. Department of Physics, Old Dominion University, Norfolk, VA, 23529, USA.

2. Department of Physics, City University of Hong Kong, Hong Kong SAR, China.

3. Center for Nanoscale Materials, Argonne National Laboratory, Lemont, IL, 60439, USA.

Abstract: Mechanical properties of molecules adsorbed on materials surfaces are increasingly vital for the applications of molecular thin films. Here, we induce molecule conformational change by switching chemical bonds on a single molecule by mechanical load, and quantify the force and energy required for such switch via a low temperature (~ 5K) Scanning Tunneling Microscope (STM) and Qplus Atomic Force Microscope (Q+AFM). Molecule TBrPP-Co (a cobalt porphyrin) deposited on an atomically clean gold substrate typically has two of its pentagon rings tilted upward and the other two downward. An atomically sharp tip of the STM/Q+AFM, which vibrates with a high frequency (~ 30kHz), is employed to run over single TBrPP-Co molecule at different heights with 0.1Å as increment and meanwhile to record tip-molecule interaction strength in the form of tip frequency change. When tip approaches to the threshold distance to the molecule, mechanical load by the tip becomes large enough to switch chemical bonds of the molecule and cause pentagon rings flip their direction. Due to the sensitive nature of tip-molecule interaction, the rings flipping can be directly visualized by STM, as rings tilting upward exhibit two bright protrusions in contrast to rings downward in image. By processing frequency change, we obtain a three-dimensional mechanical potential and force map for the single molecule TBrPP-Co with the resolution of angstrom level in three dimensions. Our preliminary results indicate that an energy barrier of ~67meV for switching between covalent and coordinated bonds to cause rings flipping of TBrPP-Co.

## Thin Film Division

### Room A105 - Session TF+QS-WeA

#### Thin Films for Space and Electronic Applications

Moderators: **John Hennessy**, Jet Propulsion Laboratory, **Richard Vanfleet**, Brigham Young University

2:20pm **TF+QS-WeA-1 From Space Thrusters to Exoplanets Research, Christine Charles, R. Boswell, M. Davoodianidalik, J. Machacek, D. Tsifakis, M. Shadwell, H. Punzmann**, Australian National University, Australia; **K. Takahashi**, Tohoku University, Japan; **J. Lecomte, N. Suas-David, L. Rutkowski, E. Dudas, A. Benidar**, Université de Rennes, France; **S. Kassi**, Université de Grenoble-Alpes, France; **R. Georges**, Université de Rennes, France; **N. Smith, P. Tesch**, Oregon Physics

INVITED

Thousands of nano and micro-satellites are expected to be launched over the next decade, many in constellations, and rideshare opportunities are increasing. The Space Plasma, Power and Propulsion (SP3) laboratory works on a range of projects dealing with fundamental physics in astrophysical

plasmas (infrared spectroscopy of exoplanet atmosphere) as well as physics and engineering challenges related to space propulsion systems (geometric and plasma nozzles, the “Bogong” Naphthalene cold gas thrusters). The scalability in geometry and power of radiofrequency plasma devices has allowed the development of a range of electrodeless thrusters such as the low pressure (~1 mTorr) Helicon thruster and the higher pressure (~1 Torr) Pocket Rocket thruster. These have yet to be flown but have surprisingly been wonderful training platforms and opened doors to new areas of research. Expanding nearly collisionless plasmas (i.e. Helicon thrusters) can be used to investigate out-of-equilibrium thermodynamics via polytropic index studies both in the laboratory and in space. Expanding collisional plasmas (i.e. Pocket Rocket thruster) can be used to investigate plasma fluid flows in nozzle. As an example, the development of the Pocket Rocket thruster into a laminar nozzle capable of producing high vibrational temperatures for molecular gases, “Platypus”, was carried out for implementation onto the SMAUG exoplanet research apparatus (Spectroscopy of Molecules Accelerated in Uniform Gas flows) which produces non-LTE (Local Thermodynamic Equilibrium) spectra of various molecules characterised using cavity ringdown spectroscopy yielding successful acquisition of absorption spectra in the infrared using naphthalene/argon plasmas. Naphthalene is also our propellant of choice for the cost-effective green and safe “Bogong” thruster, co-developed by Boswell Technologies and SP3, fully space qualified and deployed in Low Earth Orbit on the 4th of January 2023 by a Space X Falcon 9 rocket (Transporter-6 Mission, 300 kg Skykraft satellite stack). Similar radiofrequency plasma technologies are used for our various thruster concepts and for our focused ion beam (FIB) studies using the Hyperion source developed by Oregon Physics. The use of such FIB applies to materials characterisation, forensic studies and bio-medical applications. SP3 is collaborating with Oregon Physics to develop an O<sub>3</sub><sup>-</sup> negative ion source. It is interesting that the mature ion gridded thruster technology (in operation on many commercial satellites including the deep space Bepi Colombo spacecraft on its way to Mercury) share technical similarities with focused ion beam sources.

3:00pm **TF+QS-WeA-3 Photodegradation of Self-Immolating Polymers as a Potential Solution to Optical Scattering, Alexandra Stapley, S. McFarland, J. Vawdrey, K. Mitchell, W. Paxton, D. Allred**, Brigham Young University  
Starshades and other optical devices that are sensitive to scattered light require dust mitigation techniques to provide low-scatter surfaces and edges. Poly(olefine) sulfones have been shown to photodegrade with the assistance of a photobase generator when exposed to deep UV light (254 nm) and heat (120°C). These may be applicable in minimizing dust on optical surfaces for space applications. Their behavior in vacuum was not investigated, however. We synthesized Poly(2-methyl 1-pentene) sulfone (PMPS) and Poly(1-hexene) sulfone (PHS) with and without a photobase generator. We studied the photodegradation (172 nm or 254 nm) of thin films in vacuum. Spectroscopic ellipsometry was used to quantify film thickness over time. The PMPS film with photobase generator fully degraded when exposed to 172 nm light in vacuum. A significant finding was that heat was not required to produce this result. PMPS film degradation without the photobase generator was slower and incomplete. The results of our PHS studies are also promising. This study shows that a PMPS film could potentially be used to protect optical surfaces until their deployment in space.

3:20pm **TF+QS-WeA-4 Enhancement of the Bifacial Absorber of Silver Antimony Sulfur Selenide Photovoltaic Devices, Sanghyun Lee**, University of Kentucky; **M. McInerney**, Rose-Hulman Institute of Technology  
Silver Antimony Sulfur Selenide, AgSb(S<sub>x</sub>Se<sub>1-x</sub>)<sub>3</sub> thin-film solar cells have promising properties such as tunable bandgap (0.7 - 1.9 eV), good doping concentration (10<sup>16</sup> cm<sup>-3</sup>), and high absorption coefficient (>10<sup>4</sup> cm<sup>-1</sup>). The efficiency of AgSb(S<sub>x</sub>Se<sub>1-x</sub>)<sub>3</sub> thin-films with x=0.53, 0.58, and 0.61 has been studied with >2.77 %. Since Antimony Sulfur Selenide, Sb(S<sub>x</sub>Se<sub>1-x</sub>)<sub>3</sub> thin-films have shown good optical and electronic properties as an absorber layer, further optimization of thin-film absorber layers could be achieved by utilizing both Sb(S<sub>x</sub>Se<sub>1-x</sub>)<sub>3</sub> and AgSb(S<sub>x</sub>Se<sub>1-x</sub>)<sub>3</sub> thin-films for bifacial devices. Furthermore, substituting Ag in Sb(S<sub>x</sub>Se<sub>1-x</sub>)<sub>3</sub> thin-films tends to increase the bandgap of the absorber layer by lowering the valence band based on studies of other thin-film absorber layers (CIGS, CZTSSe).

In this contribution, we have theoretically studied bifacial photovoltaic devices by combining thin-film absorbers of AgSb(S<sub>x</sub>Se<sub>1-x</sub>)<sub>3</sub>, Sb(S<sub>x</sub>Se<sub>1-x</sub>)<sub>3</sub>, and the combination of AgSb(S<sub>x</sub>Se<sub>1-x</sub>)<sub>3</sub> and Sb(S<sub>x</sub>Se<sub>1-x</sub>)<sub>3</sub> thin-films from the electronic band structure perspective. To fully utilize the promising properties of both Sb<sub>2</sub>(S<sub>x</sub>Se<sub>1-x</sub>)<sub>3</sub> and AgSb(S<sub>x</sub>Se<sub>1-x</sub>)<sub>3</sub> films, we investigated

# Wednesday Afternoon, November 8, 2023

different compositions and concentrations of Sulfur and Selenium with proposed empirical equations for electron affinity and bandgap energy through modeling and simulations.

Four different structures of thin-film absorbers have been studied above Molybdenum metal thin-films. For both  $\text{AgSb}(\text{S}_x\text{Se}_{1-x})_3$  and  $\text{Sb}(\text{S}_x\text{Se}_{1-x})_3$  thin-films, the electron affinity and bandgap energy increase as Sulfur (x) composition increases. However, the increased bandgap is not directly translated into improved solar cells efficiency due to the alignment of thin-film electronic structures. The best efficiency was achieved with 2  $\mu\text{m}$   $\text{AgSb}(\text{S}_{0.4}\text{Se}_{0.6})_3$  thin-film devices (18.4 %) at sulfur concentration,  $x = 0.4$ . However, once we combine two  $\text{AgSb}(\text{S}_x\text{Se}_{1-x})_3$  and  $\text{Sb}(\text{S}_x\text{Se}_{1-x})_3$  thin-films while keeping a total thickness, 2  $\mu\text{m}$  (1  $\mu\text{m}/1 \mu\text{m}$ ), an interface between  $\text{AgSb}(\text{S}_{0.4}\text{Se}_{0.6})_3/\text{Sb}_2(\text{S}_{0.4}\text{Se}_{0.6})_3$  and Molybdenum metal thin-films is preferably formed due to reduced effective Schottky hole barrier. If we assume the same amount of defect states at the interface, the improved effective Schottky hole barrier is 128 mV due to the favorable band alignment, which is approximate 4.3 times better than a  $\text{AgSb}(\text{S}_{0.4}\text{Se}_{0.6})_3$  thin-film structure. With a bi-layer  $\text{AgSb}(\text{S}_{0.4}\text{Se}_{0.6})_3/\text{Sb}_2(\text{S}_{0.4}\text{Se}_{0.6})_3$  thin-film absorber, we studied various doping concentrations impact on device efficiency based on the modified electronic band structure of each thin-film. The doping concentration of  $\text{AgSb}(\text{S}_{0.4}\text{Se}_{0.6})_3$  thin-film mainly increases the photogenerated current while  $\text{Sb}_2(\text{S}_{0.4}\text{Se}_{0.6})_3$  thin-film improves open voltage.

## 4:20pm TF+QS-WeA-7 Atomic Scale Processing and Surface Engineering to Maximize Microdevice Performance for Remote Sensing and Imaging Applications, Frank Greer, Jet Propulsion Laboratory (NASA/JPL) INVITED

Future UV, X-ray, infrared, and sub-millimeter telescopes and spectrometers have the potential to revolutionize our understanding of the formation and habitability of the modern universe, Earth, and other planetary bodies. [1-4] Star formation, dark energy, and the composition of the intergalactic medium are only some of the key scientific topics that can be addressed by UV astronomy and astrophysics. Sub-millimeter astronomy can probe the fine structure of the cosmic microwave background, giving glimpses into the early universe immediately following the Big Bang. [5] Remote observation in the infrared is critically important for the understanding of many aspects of Earth Science and Exoplanet atmospheres.

Unfortunately, harnessing the full potential of these missions is often constrained by performance of the available detectors and optical elements (the eyes of the instruments) that make the measurements and take the images. The limitations of these key components are frequently due to non-idealities in the materials and interfaces that are imbedded in or form these devices. Thus, the state-of-the art in materials science, thin films, and semiconductor processing can limit what we can know and learn because it constrains what we can "see". To improve our ability to "see" (by making new types of observations or observations with greater sensitivity), effort is required to improve the specialized materials that impact space-based instruments.

While bulk materials are important, many of the critical challenges in materials science for space applications occur at the nanoscale. Nanoscale coatings deposited by techniques such as atomic layer deposition (ALD) can be used in a variety of ways, including, but not limited to: anti-reflective coatings for UV detectors, passivation layers for infrared detectors, wiring layers in superconducting circuits, or superconducting sensing elements. Nanoscale surface engineering through atomic scale processes can substantially improve the optoelectronic properties of III-V sensors and optical elements such waveguides, especially in shorter wavelength ranges where surface roughness is particularly important.

This presentation will detail the fundamental materials science, surface engineering, and ALD/ALE approaches we have used in the fabrication of a variety of devices in multiple different wavelength ranges, demonstrating the boost in performance that is obtained with atomic level precision at key steps in the fabrication process.

[1] Barth, C. A. *Appl. Optics* 8, 1295, (1969).

[2] Hendrix, A. R., et al. *Icarus* 206, 608-617, (2010).

[3] Nicasastro, F., et al. *Science* 319, 55-57, (2008).

[4] Martin, D. C. et al. *Nature* 448, 780-783, (2007).

[5] de Bernardis, P. et al. *Nature* 404, 955-959, (2000).

5:00pm TF+QS-WeA-9 Advances in Plasma-Based Atomic Layer Processing of  $\text{AlF}_3$  for the Passivation of FUV Mirrors, Virginia Wheeler, D. Boris, US Naval Research Laboratory; L. Rodriguez de Marcos, J. del Hoyo, NASA Goddard Space Flight Center; N. Nepal, A. Lang, M. Sales, S. Walton, US Naval Research Laboratory; E. Wollack, M. Quijada, NASA Goddard Space Flight Center

Efficient ultraviolet mirrors are essential components for UV astronomy. While aluminum mirrors with fluoride-based passivation layers are commonly used in this application space due to their proven stability and reliability, the optical performance is still insufficient for systems where several reflections are required. In previous work, we demonstrated the feasibility of a new, room temperature plasma process based on electron beam-generated plasma in a benign  $\text{SF}_6$  environment to simultaneously remove the native oxide and form an  $\text{AlF}_3$  layer with tunable thickness [1]. This process has been used to demonstrate Al-mirrors with high FUV reflectivity ( $R \approx 90\%$  at  $\lambda = 121\text{nm}$ ), large area uniformity of the fluoride coating layer, low coating-induced polarization aberration, and improved durability. Plasma-enhanced atomic layer deposition (PEALD) is a known low temperature, highly conformal coating process which has previously been shown to produce  $\text{AlF}_3$  films [2], though little has been reported on their performance in FUV applications. In this work, we focus on optimizing PEALD  $\text{AlF}_3$  films and compare both the materials properties as well as the FUV performance with those produced through self-fluorination electron beam generated plasma process.

PEALD  $\text{AlF}_3$  films were deposited using trimethylaluminum and  $\text{SF}_6$  plasma precursors in a Veeco Fiji G2 reactor equipped with a turbo pump and substrate biasing. This reactor has also been customized to include a similar planar electron beam generated plasma if required to etch the native oxide from substrates prior to deposition of  $\text{AlF}_3$  films. ALD windows were optimized using an *in situ* ellipsometer to monitor the growth rate directly on Al substrates and supplemented with post-deposition x-ray photoelectron spectroscopy and atomic force microscopy to elucidate process-structure-property relationships. Plasma diagnostics, including optical emission spectroscopy and Langmuir probe measurements, were also conducted on the reactor to correlate plasma properties, such as fluence and ion energy, to resulting film properties. Initial plasma characterization showed that there was high atomic fluorine present at the substrate surface using a 1:1 Ar/ $\text{SF}_6$  plasma at 10mTorr but that this concentration was slightly reduced from that measured within the remote ICP plasma. Additionally, it was found that the fluorine density within the plasma increases linearly with  $\text{SF}_6$  flow fraction and RF power but only subtle differences were seen with increasing pressure. The influence of these parameters on the  $\text{AlF}_3/\text{Al}$  interface and FUV performance will also be discussed.

[1] L.V. Rodriguez de Marcos, et al. *Opt. Mater. Express* 11, 740-756 (2021)

[2] M.F.J. Vos, *Appl. Phys. Lett.* 111, 113105 (2017)

## 5:20pm TF+QS-WeA-10 Thin Film Processes for UV Detector Technologies for Next Generation NASA Missions, Robin Rodríguez, A. Jewell, J. Hennessy, M. Hoenk, T. Jones, S. Nikzad, Jet Propulsion Laboratory (NASA/JPL)

Galileo was the first deep space mission to fly a silicon charge-coupled device (CCD) for imaging; since then, silicon-based photodetectors have been used for imaging and/or spectroscopy on nearly every NASA mission. JPL's Advanced Detectors and Nanomaterials Group utilizes thin-film processing and nanoscale interface engineering methods to fabricate advanced detector technologies with improved stability and sensitivity. Our research is largely focused on the use of molecular beam epitaxy (MBE) for band structure engineering and passivation of silicon-based photodetectors. Developments in recent years has been geared toward wafer-scale processing as well as improving the space worthiness of MBE-passivated detectors. We also use atomic layer deposition (ALD) processes to engineer new coatings for advanced optics or detectors, including the customization of detector response over a broad wavelength range. The performance objectives for our technologies are defined to meet the objectives of a variety of NASA research programs with the ultimate goal of flight instrument and mission infusion. This presentation will provide an overview of recent advances in detector optimization for ultraviolet (UV) imaging and spectroscopy applications. Copyright 2023. All Rights Reserved.

## 5:40pm TF+QS-WeA-11 Commercializing Nanowire LEDs, David Laleyan, B. Le, G. Frolov, NS Nanotech Canada; M. Stevenson, S. Coe-Sullivan, NS Nanotech

MicroLED display technology consists of many carefully arranged microscopic light-emitting diodes (LEDs) to directly create color pixels.

# Wednesday Afternoon, November 8, 2023

MicroLED displays thus have the potential brightness, efficiency, and response time of inorganic LEDs, but suffer from the high cost of epitaxy, as well as the challenges of creating red, green, and blue emitters on a single material and substrate. Furthermore, conventional approaches of growing planar LEDs and then etching them into micron-scale devices cause a fundamental loss of efficiency, especially for the smallest devices. In this regard, nanowire-based LEDs for microLED applications have been of great interest and a topic of extensive research for over a decade. This is due to their unique ability to maintain high efficiencies as the LED size becomes quite small, even into the sub-micron regime, contrary to conventional thin-film LEDs. Another valuable benefit is the ability to form photonic crystal arrangements, such that the formation of a photonic bandgap leads to highly directional and narrow bandwidth emission. Most recently, reports have shown nanowire LEDs in the green with >25% external quantum efficiency (EQE) and red with >8% EQE, competitive with the best direct green and InGaN red LEDs ever fabricated – despite being sub-micron in size.

These structures were obtained by molecular beam epitaxy (MBE) using a selective area epitaxy (SAE) technique, where nanostructures can be controllably grown on a thin-film template. Novel development and engineering efforts are required for such nanowire LEDs to become commercially viable. This work presents a pathway towards the wafer-scale production of nanowire LEDs for displays. This talk will explain how breakthrough academic research can be made manufacturable by studying run-to-run variability, understanding the process windows, targeting yield-limiting steps, and ensuring process scalability. Focusing on the reproducibility and uniformity of nanowire growth by SAE is the first critical step toward the large-scale deployment of these highly efficient LED that are perfectly suited for the next generation of microLED displays.

## 2D Materials Technical Group

### Room C123 - Session 2D-ThM

#### 2D-Materials: Microscopy

Moderator: David Cobden, University of Washington

8:00am **2D-ThM-1 In and Ex Situ (S)TEM Manipulation of 2D Materials, J. Kotakoski, Harriet Åhlgren**, University of Vienna, Austria **INVITED**

Heteroatom implantation in 2D materials requires a delicate balance between being able to displace atoms from the target material while at same time stopping the incoming ion [1]. An additional problem is imposed by momentum and energy conservation, which fundamentally limits ion implantation of graphene to elements between Li and Ti. Nevertheless, some success has been made for light elements [2,3,4]. Unfortunately, even in the case of successful implantation, the samples suffer from surface contamination. Here, we describe how all of these issues can be overcome combining vacancy-mediated heteroatom implantation [5,6] with efficient sample cleaning [7] in a vacuum system shared with an atomic-resolution scanning transmission electron microscope [7].

#### References

87. Phys. Rev. B 83, 115424 (2011)
88. Nano Lett. 13, 4902 (2013)
89. 2D Mater. 4, 021013 (2017)
90. ACS Nano 12, 4641 (2018)
91. J. Phys. Chem. C 123, 13136-13140 (2019)
92. 2D Mater. 9, 025011 (2022)
93. Nano Lett. 21, 5179-5185 (2021)

8:40am **2D-ThM-3 Synthesis of Quantum-Confined Borophene Nanoribbons, Qiucheng Li, M. Hersam**, Northwestern University

Borophene refers to synthetic two-dimensional (2D) boron, which has attracted significant attention due to its anisotropic metallic, correlated electron phenomena, and diverse superlattice structures.<sup>[1]</sup> Reducing the dimensionality of nanomaterials imposes additional quantum confinement effects that unlock new physical phenomena, such as one-dimensional (1D) confined plasmons, spin-polarized edge states, and Luttinger liquid behavior. However, the realization of quantum-confined borophene nanoribbons (BNRs) is hampered by limited boron precursor options for bottom-up synthesis. In this work, we present a substrate mediation strategy to synthesize quantum-confined BNRs on vicinal Ag(977) substrates. The resulting BNRs inherit the high degree of polymorphism present in borophene, resulting in  $v_{1/5}$  and  $v_{1/6}$ -BNR lattice configurations in addition to phase intermixing.<sup>[2]</sup> Through atomic-scale imaging, spectroscopy, and first principles calculations, the edge structures of BNR polymorphs are shown to possess reconstructed armchair edges for  $v_{1/6}$ -BNRs and sawtooth zigzag edges for  $v_{1/5}$ -BNRs. The confined electron wave functions in 1D BNRs lead to the observation of energy level quantization and spatial nodes characteristic of quantum-well states.

#### Acknowledgement:

This work was supported by the Office of Naval Research (ONR N00014-17-1-2993) and the National Science Foundation Materials Research Science and Engineering Center (NSF DMR-1720139).

#### References:

- [1] Mannix, A. J., *et al.*, Synthesis of borophenes: Anisotropic, two-dimensional boron polymorphs. *Science*, **2015**, 350 (6267), 1513-1516.
- [2] Liu, X., *et al.*, Intermixing and periodic self-assembly of borophene line defects. *Nature Materials*, **2018**, 17 (9), 783-788.

9:00am **2D-ThM-4 Formation of Multilayer Bismuthene on Hexagonal Manganese Nitride, Ashok Shrestha, A. Abbas, A. Smith**, Ohio University

Bismuthene, a two-dimensional (2D) topological material, has attracted considerable attention due to its large bandgap compared to other 2D topological materials [1]. The structure and electronic properties of the single layer bismuthene have been studied by many authors [2, 3], but the growth, structure, and electronic properties of multilayer bismuthene have not yet been reported. We have successfully grown the multilayer of bismuthene on the hexagonal  $\zeta$ -phase  $Mn_2N$  surface using molecular beam epitaxy.

In this presentation, we will briefly discuss the growth of the thin layer of  $\zeta$ -phase  $Mn_2N$  in the first part, and the formation of a multilayer of

bismuthene in the second part. Initially, the  $Mn_2N$  film is prepared on MgO (001) substrate under nitrogen-rich conditions at 510 °C. The correct phase of  $Mn_2N$  is confirmed using various *in-situ* techniques such as reflection high energy electron diffraction, scanning tunneling microscopy, and Auger electron spectroscopy. Once a high-quality  $Mn_2N$  surface is achieved, an ultra-thin layer of bismuth is deposited on its top at 150 °C.

The STM investigations reveal atomically flat multiple terraces and steps of bismuthene with a step height of 1.60 Å, which agrees well with the height of bismuthene reported by Sun *et al.* (2022) [2], although the atomic resolution STM image shows the nearly rectangular structure. Some other interesting features of bismuthene, such as “quantum islands”, are also observed. The *ex-situ* X-ray diffraction clearly shows the Bi 0002 peak, giving an interplanar spacing of 3.20 Å. This measurement is consistent with twice the step height observed in the STM image. This work is supported by the U.S. Department of Energy, Office of Basic Energy Sciences, Division of Materials Sciences and Engineering under Award No. DE-FG02-06ER46317.

#### References:

- [1] F. Reis, G. Li, L. Dudy, M. Bauernfeind, S. Glass, W. Hanke, R. Thomale, J. Schafer, R. Claessen, *Science* **357**, 287-290 (2017).
- [2] S. Sun, J. Yang, S. Duan, J. Chen, and W. Chen, *ACS Nano* **16**, 1463-1443 (2022).
- [3] J. Gou, K. Longjuan, H. Xiaoyue, Y. L. Haung, J. Sun, S. Meng, K. Wu, L. Chen, A. S. Wee, *Sci. Adv.* **6**, eaba2773 (2020).

9:20am **2D-ThM-5 A Combined NAP-XPS and NAP-STM Study on 2D MoS<sub>2</sub>-based Catalysts for Hydrodeoxygenation of Organic Feedstocks, Lars Mohrhusen, M. Hedevang, J. Lauritsen**, Aarhus University, Denmark

For the technological utilization of sustainable feedstocks such as pyrolysis oils from biomass, oxygen removal via hydrodeoxygenation (HDO) is one of the most essential steps.<sup>[1]</sup> Metal-promoted MoS<sub>2</sub>-based catalysts are well-established for hydrode-sulphurization (HDS) of crude oil components, and thus a promising material for HDO catalysts.<sup>[2-4]</sup> This is already proven technology for simple feedstocks such as vegetable oils, but more complex compounds with high oxygen content and multiple oxygen functionalities such as bio-oils remain challenging, and thus gain increasing interest.

In contrast to the established use in (virtually oxygen free) HDS, the sulphide catalyst will be exposed to water or organic oxygenates in the herein desired HDO process. Thus, in the presence of oxygen, sulphur atoms may be partially exchanged. Thereby, active sites can become blocked, which triggers strong catalyst degradation on the long term. <sup>[5,6]</sup>

To gain an atomistic understanding of such processes, herein two-dimensional MoS<sub>2</sub> particles on Au (111) surfaces exposed to H<sub>2</sub> and/or oxygenate containing atmospheres were investigated combining microscopic (scanning tunneling microscopy (STM), see fig. 1) and spectroscopic insights (photoelectron spectroscopy (XPS)) under various conditions mimicking HDO from UHV level to the near-ambient-pressure regime (few mbar, NAP-STM, NAP-XPS).

9:40am **2D-ThM-6 NanoFrazor Technology - Fabricating Advanced 2D and Grayscale Structures for 2D Materials Using Thermal Scanning Probe Lithography and Direct Laser Sublimation, Nicholas Hendricks, A. Ubezio, M. Käppeli, J. Vergés, J. Chaaban, E. Çağın**, Heidelberg Instruments Nano, Switzerland

Thermal scanning probe lithography (t-SPL), enabled by the NanoFrazor technology, is establishing itself as a mature and reliable direct-write nanolithography technique for generating nanoscale structures [1-4]. The NanoFrazor technology offers an alternative or complementary process for conventional lithography techniques of electron-beam lithography (EBL) or focused-ion beam (FIB). t-SPL generates patterns by scanning an ultrasharp tip over a sample surface to induce local changes with a thermal stimulus. By using thermal energy as the stimulus, it is possible to perform various modifications to the sample via removal, conversion, or addition of/to the sample surface. Along with an ultrasharp tip, the t-SPL cantilever contains several other important functions such as an integrated thermal height sensor and an integrated heating element both of which are advantageous for fabricating devices for nanoelectronics, photonics, molecular sensing, and quantum computing.

To complement the sub-100 nm patterning capabilities of t-SPL, a direct laser sublimation (DLS) module has been incorporated into the NanoFrazor platform. The DLS module allows for increased throughput by patterning larger structures, e.g. > 500 nm, with a continuous wave (CW) laser operating at a wavelength of 405 nm. Over the last several years, further developments of the NanoFrazor technology have been realized that are

# Thursday Morning, November 9, 2023

enhancing the application space of nanofabrication. Such developments include the integration of the t-SPL and DLS modules into gloveboxes, active field stitching to allow seamless large area patterning with both t-SPL and DLS, and automated overlay to allow for precise nano and micropatterning on top of pre-existing structures.

Within this presentation, the background and workings of t-SPL will be introduced as well as the nanolithography and processing capabilities of both t-SPL and DLS will be presented, with a focus on patterning on topography. A workflow for detecting and correcting intentional topography (flakes of 2D materials, pre-patterned contacts, nanowires), and unintentional defects (impurities, folds in 2D material flakes) will be introduced. Device performance examples achieved using the damage-free lithography techniques will be included, in order to provide a comparison between conventional and novel nanolithography methods.

[1] S. Howell et al., *Microsystems & Nanoengineering*, 6, 21 (2020); [2] N. Lassaline et al., *Nature*, 582, 506-510 (2020); [3] X. Liu et al., *APL Materials*, 9, 011107 (2021); [4] M. Giordano et al., *Advanced Material Interfaces*, 10, 2201408 (2023)

## 11:00am 2D-ThM-10 Phase Transformations in 2D Van der Waals Materials: Insights from Cryogenic Atomic Resolution STEM and EELS, Miaofang Chi, Oak Ridge National Laboratory INVITED

Two-dimensional (2D) van der Waals (vdW) materials and their heterostructures offer a remarkable platform for investigating intriguing physical phenomena and implementing diverse applications. A key advantage of these materials is their tunable quantum behavior, which varies with the number of layers. Notably, samples with different thicknesses, particularly in the range from monolayer to several nanometers, exhibit distinct and exotic properties such as magnetism, electronics, and optoelectronics. While it is recognized that lattice structural transformations often accompany changes in electronic and spin structures, leading to the emergence of exotic quantum phenomena, it remains uncertain whether the same structural transformations observed in bulk materials occur in thin flake samples. Consequently, a comprehensive understanding of the structure-property relationship in several-layer thick 2D vdW materials is often lacking. In this presentation, we unveil the thickness-dependent phase transformation and exciton state changes in several model 2D vdW materials using cryogenic atomic resolution scanning transmission electron microscopy (STEM) and monochromated electron energy loss spectroscopy (EELS). Through our findings, we provide precise insights into the layer-number-dependent properties that are crucial for harnessing the unique quantum characteristics of thin layer 2D vdW materials for device applications.

## 11:40am 2D-ThM-12 Intercalation of Transition Metals in between Bilayer VSe<sub>2</sub>, V. Pathirage, K. Lasek, S. Lisenkov, University of South Florida; I. Ponomareva, University South Florida; Matthias Batzill, University of South Florida

Modifications of transition metal dichalcogenides (TMD) can be achieved by metal insertion into the van der Waals gap. Those metals covalently bond to the chalcogen atoms and thus form a 3D crystal structure. For ultrathin TMD films, however, insertion of excess metals will result in pseudo-2D nanolayers that may be incorporated with other van der Waals materials. In this talk we discuss modifications of bilayer VSe<sub>2</sub> by insertion of different transition metals (V, Cr, Mn) to modify its magnetic properties. The excess transition metals are inserted by sequential vapor deposition onto the VSe<sub>2</sub> bilayer film. DFT simulations indicate that excess metals diffuse readily through the VSe<sub>2</sub> layer to occupy energetically favorable inter-layer sites. Different ordered arrangements of excess metals are obtained with a maximum occupation close to half a monolayer (here one monolayer refers to the amount of metal atoms in a TMD layer). The ordering of the inserted atoms is probed by scanning tunneling microscopy. Magnetic properties are identified by x-ray magnetic circular dichroism studies and show strong magnetic moments on dilute inserted Cr or Mn atoms. However, as ordered superstructures are formed the measured average magnetic moment per atom decreases, possibly suggesting antiferromagnetic order in the insertion layer.

## 12:00pm 2D-ThM-13 Atomically Resolved Imaging of CVD-Grown Thin $\alpha$ -Mo<sub>2</sub>C Crystals, Saima Sumaiya, Columbia University; I. Demiralglu, Eskisehir Technical University, Turkey; O. Caylan, G. Buke, TOBB University of Economics and Technology, Turkey; C. Sevik, Eskisehir Technical University, Turkey; M. Baykara, University of California Merced

Transition metal carbides (TMCs) have been used in bulk form in a variety of applications for decades due to their attractive mechanical and chemical

properties. With the advent of nanotechnology, there is renewed interest in synthesizing these materials in thin form, with precise control of thickness for potential applications in fields such as energy storage and electromagnetic shielding. Consequently, it is of utmost importance to investigate the quality of these materials in terms of the presence of defects and their influence on properties, down to the atomic scale. Here, we present an atomic-resolution investigation of defects on thin crystals of molybdenum carbide ( $\alpha$ -Mo<sub>2</sub>C) grown via chemical vapor deposition (CVD), by way of conductive atomic force microscopy (C-AFM) measurements under ambient conditions. In particular, we observe a periodic modulation in the surface conductivity landscape with a periodicity that is  $\sim 5$  times higher than the periodicity of the atomic lattice of the (100) surface. It is additionally observed that this electronic super-structure is rotationally misaligned with the underlying atomic lattice. Atomic-resolution imaging additionally reveals the presence of defects on the crystals, with a defect density that is similar to that reported for natural two-dimensional transitional metal dichalcogenides. We characterize defects based on the type (enhancement / attenuation) and spatial extent (compact / extended) of the effect they have on the conductivity landscape of the crystal surfaces. While some have localized influence on conductivity over several unit cells, other defects extend over ten nanometers and more. In addition to surface defects, we are also able to quantify the influence of defects that are present sub-surface. *Ab initio* calculations performed by way of density functional theory (DFT) are employed to gather clues about the identity of the defects. The findings presented here provide insights for defect engineering aimed at achieving tailored electronic properties of TMCs in thin form.

## Applied Surface Science Division

### Room B117-119 - Session AS+CA+EL+EM+SE+SS+TF-ThM

#### Quantitative Surface Analysis II

**Moderators:** Samantha Rosenberg, Lockheed Martin, Thierry Conard, IMEC, Belgium, Benjamen Reed, National Physical Laboratory, UK

#### 8:00am AS+CA+EL+EM+SE+SS+TF-ThM-1 OrbiSIMS: Signal, Noise and Transmission Are Three Sides of a Metrology Triangle, G. Trindade, Y. Zhou, A. Eyres, National Physical Laboratory, UK; M. Keenan, Independent; Ian Gilmore, National Physical Laboratory, UK

In metrology, the science of measurement, a "metrology triangle" approach is used to provide a secure foundation. For example, the Quantum Metrology Triangle links Voltage, Resistance and Current through the Josephson Effect and the Quantum Hall Effect.

The OrbiSIMS<sup>1</sup>, introduced in 2017, has become increasingly popular for biological and material sciences studies owing to its ability to give high confidence in molecular identification (mass resolving power > 240,000 and mass accuracy < 2 ppm) simultaneously with high confidence in localisation (micrometre scale spatially and nanoscale in depth). With a growing number of instruments internationally there is an increased need for metrology for reproducible measurements. We will show how Signal, Noise and Transmission form three sides of a metrology triangle that combine to enable better measurement. In a recent comprehensive study of the noise in an Orbitrap mass spectrometer, a probabilistic model was developed.<sup>2</sup> A region of the intensity scale is described by Poisson statistics allowing the scaling parameter,  $A$ , that relates ion current to the number of ions in the trap to be determined. A true signal intensity scale is then established which allows the useful yield of atoms in an implant layer to be measured. Through comparison with time-of-flight and magnetic sector instruments the fractional ion transmission is determined.<sup>3</sup> We will discuss how Signal and Transmission combine to understand matrix effects in biological sample preparation and how understanding Signal and Noise are important for data analytical methods.

94. M. K. Passarelli. et al, I. S. Gilmore, *Nat. Methods*, 14(2017)12, 1175-1183.
95. M R. Keenan, G. F. Trindade, A. Pirkl, C. L. Newell, K. Ayzikov, J. Zhang, L. Matjacic, H. Arlinghaus, A. Eyres, R. Havelund, J. Bunch, A. P. Gould, A. Makarov and Ian S. Gilmore, in preparation.
96. Y. Zhou, A. Franquet, V. Spampinato, G. F. Trindade, P. van der Heide, W. Vandervorst and I S Gilmore, in preparation.

# Thursday Morning, November 9, 2023

8:20am **AS+CA+EL+EM+SE+SS+TF-ThM-2 Contribution of Imaging X-Ray Photoelectron Spectroscopy to Characterize Chrome Free Passivation Nano-Layer Deposited on Food-Packaging Tinplate: Composition and Chemical Environment**, *E. Ros, Vincent Fernandez*, CNRS, France; *N. Fairley*, CASAXPS, UK; *B. Humbert, M. Caldes*, CNRS, France

To protect metal from corrosion, passivation layer are widely used in food-packaging industry. Those Nano-metric protections create a thin oxide Nano-layer on the metal surface, making it less oxidisable. Common passivation are composed by chromium oxide[1], using hexavalent chromium as a reagent and reducing it. However, because of the toxicity of Cr(VI), European Union is gradually forbidding. Chromium Free Passivation Alternative is based on transitions metal oxides (Sn, Ti, Zr, Mn) and polymers. These samples present some roughness in few micron range observed by Atomic Force Microscopy. XPS Imaging were perform at different binding energy to allow extracting spectrum in each pixel over the eight (Mn 2p, O 1s, Sn 3d, Ti 2p, N 1s, C 1s, P 2s and Zr 3d) XPS core level process. This study show an anti-correlation between atomic concentration of Titanium and Tin Fig(1). We observe a ratio Sn oxide Sn metal homogeneous and independent of the Ti, Sn ratio More over using the vector method [2], [3] concurrently to height XPS core, we could extract two different chemical environments spectrum. The linear Least Square combination of these 2 spectrum allow us to model 131072 regions. To extract information form XPS data on heterogynous sample the combination of XPS imaging energy scan measurement with the vector method is a promising way. These results bring the useful information about different thin layer deposition steps. Imagerie XPS results are in agreement with Raman imagerie analysis

[1] R. Sandenbergh, M. Biermann, and T. von Moltke, 'Surface Analytical Characterization of Chromium Passivation on Tinplate', in *Passivation of Metals and Semiconductors, and Properties of Thin Oxide Layers*, P. Marcus and V. Maurice, Eds., Amsterdam: Elsevier Science, 2006, pp. 143–148. doi: 10.1016/B978-044452224-5/50024-X.

[2] J. Baltrusaitis *et al.*, 'Generalized molybdenum oxide surface chemical state XPS determination via informed amorphous sample model', *Applied Surface Science*, vol. 326, pp. 151–161, Jan. 2015, doi: 10.1016/j.apsusc.2014.11.077.

[3] M. d'Halluin *et al.*, 'Graphite-supported ultra-small copper nanoparticles – Preparation, characterization and catalysis applications', *Carbon*, vol. 93, pp. 974–983, Nov. 2015, doi: 10.1016/j.carbon.2015.06.017.

8:40am **AS+CA+EL+EM+SE+SS+TF-ThM-3 Cryo-Xps for Surface Characterisation of Nanomedicines**, *David Cant*, National Physical Laboratory,, UK; *Y. Pei*, National Physical Laboratory, UK; *A. Shchukarev, M. Ramstedt*, University of Umea, Sweden; *S. Marques, M. Segundo*, University of Porto, Portugal; *J. Parot, A. Molska, S. Borgos*, SINTEF, Norway; *C. Minelli, A. Shard*, National Physical Laboratory, UK

Nanomedicines are an area of great interest for current and future pharmaceutical development. The use of nanoparticles to act as carriers for a therapeutic load has the potential to significantly improve medical outcomes, for example by allowing a therapeutic agent to circulate within the body for longer, or by allowing targeted delivery of a drug to a specific site. Such nanomedicines often rely on specific functional coatings to achieve their desired impact; for example the majority of nanomedicines currently available on the market utilise a poly-ethylene glycol (PEG) surface coating for its 'stealth' properties, helping nanomedicines evade the body's clearance mechanisms. Accurate measurement of the surfaces of such nanomaterials is therefore of great importance, yet direct, quantitative surface chemistry measurements are not commonly available, and vacuum-based analysis methods such as XPS are unlikely to provide a representative measurement of the particles in their hydrated state.

Here we present to the best of our knowledge the first use of Cryo-XPS to provide direct, quantitative measurements of the surface chemistry of nanomedicines in a hydrated state. Two nanomedicine systems were measured: a drug-carrying polymer nanoparticle; and an mRNA loaded lipid nanoparticle. Both systems possessed a supposedly PEG-terminated surface, and were measured using XPS in both aqueous cryogenic state, and dry drop-cast onto a substrate. The results of these measurements clearly demonstrate that while the PEG surface cannot readily be observed in the dry state, the cryogenic measurements exhibit spectra that are consistent with the particle being measured in a hydrated condition.

9:00am **AS+CA+EL+EM+SE+SS+TF-ThM-4 Redox XPS as a Means to Address Some XPS Reproducibility Challenges**, *Peter Cumpson*, University of New South Wales, Australia

The challenge of better understanding of increasingly-complex specimens in surface analysis has been highlighted recently[1,2,3,4]. Especially at a time of high throughput XPS instruments and broadening of the (non-specialist) user community. An AVS survey conducted in 2018 found that 65% of those responding identified reproducibility as a significant issue [5].

There is an analogy to be made with some radically-different technologies. Machine Learning makes more sense of a moving image than a single snapshot, even if the snapshot were to come from a larger, better calibrated camera. Yet somehow we expect greater calibration precision, reference data and rigorous procedures to be the only route to reliable understanding of single spectra.

Generating a sequence of spectra from a progressively chemically-modified surface can remove many ambiguities that can otherwise cause misinterpretation. Such sequences thereby help with rapid understanding of the unmodified surface. On the theme of "Two is Better than One: Breaking Barriers with Coupled Phenomena" we present results from coupled stepwise oxidation/reduction of the surface and XPS to resolve such ambiguities for a wide range of materials and problems. Gas-phase oxidation agents are used to move through the redox states of a specimen in a controllable way, taking advantage of the logarithmic growth of oxide thickness. What is more, this oxidation is easy to implement in the entry-locks of modern XPS instruments through the use of vacuum ultraviolet light (VUV) and the *in situ* generation of ozone and gas-phase hydroxide free radicals. In the past there have been many studies of how particular materials react to ozone exposure at their surfaces, often employing XPS. Here we reverse this, and use ozone (and VUV) exposure to simplify the interpretation of spectra from a wide range of unknown materials, we think for the first time.

[1] D R Baer *et al.*, *J. Vac. Sci. Technol. A* 39, 021601 (2021); <https://doi.org/10.1116/6.0000873>

[2] G. H. Major *et al.*, *J. Vac. Sci. Technol. A* 38, 061204 (2020); <https://doi.org/10.1116/6.0000685>

[3] G. H. Major *et al.*, *J. Vac. Sci. Technol. A* 38, 061203 (2020) <https://doi.org/10.1116/6.0000377>

[4] D R Baer and M. H. Engelhard, *Journal of Surface Analysis* Vol. 26, No.2 (2019) pp. 94-95.

[5] D R Baer, J F Watts, A Herrera-Gomez, K J Gaskell, *Surf Interface Anal.* 2023; 1- 9. doi:10.1002/sia.7194

9:20am **AS+CA+EL+EM+SE+SS+TF-ThM-5 Sub-Nanometer Depth Profiling of Native Metal Oxide Layers Within Single Lab-XPS Spectra**, *Martin Wortmann*, *N. Frese*, Bielefeld University, Germany; *K. Viertel*, Bielefeld University of Applied Sciences and Arts, Germany; *D. Graulich, M. Westphal, T. Kuschel*, Bielefeld University, Germany

Many metals form nanometer-thin self-passivating native oxide layers upon exposure to the atmosphere, which affect their interfacial properties and corrosion behavior. Such oxide layers are commonly analyzed by X-ray photoelectron spectroscopy (XPS). Here we propose a simple and accessible depth profiling approach for oxide layers with sub-nanometer depth resolution from single lab-XPS spectra. Metals and their oxides can be distinguished by a binding energy shift to quantify their distinct signal contributions. Analogous to the widely used Hill equation we utilize the known photoelectron's inelastic mean free path to calculate the characteristic oxide layer thickness. However, in contrast to the Hill equation we analyze not only one, but all orbital energies in the XPS spectrum to develop a model that accounts for a depth-resolved concentration profile at the oxide-metal interface. The proposed model not only improves the accuracy and reproducibility of earlier methods but also paves the way for a more holistic understanding of the XPS spectrum.

# Thursday Morning, November 9, 2023

9:40am **AS+CA+EL+EM+SE+SS+TF-ThM-6 A Tag-and-Count Methodology Based on Atomic Layer Deposition (ALD) and Low Energy Ion Scattering (LEIS) for Quantifying the Number of Silanols on Fused Silica, Josh Pinder, Brigham Young University**

The concentration of surface silanols governs many of the properties of glass and fused silica surfaces including surface wetting, surface contamination rates, and thin film adhesion. Indeed, the concentration of surface silanols is impactful for diverse fields such as atomic layer deposition (ALD), chromatography, catalysis, and displays. Accordingly, various analytical and theoretical methods have been employed to determine the number of silanols on surfaces, including density functional theory, FTIR, thermogravimetric analysis, and temperature programmed desorption mass spectrometry. However, many of these methods are better applied to particulate materials than surfaces. In this presentation, we discuss a method for directly

measuring the concentrations of surface silanols on silica-containing surfaces via a tag-and-count methodology. This approach is based on tagging surface silanols by ALD via a single pulse of dimethylzinc or diethylzinc and then quantifying the number of tags (zinc atoms) using high

sensitivity-low energy ion scattering (HS-LEIS). Our method yielded the literature value for both fully hydroxylated fused silica and also fused silica that had been heated to 500, 700, and 900 C. We see this capability as enabling for all who work with glass, fused silica, and silicon wafers,

including for ALD.

11:00am **AS+CA+EL+EM+SE+SS+TF-ThM-10 ASSD Peter M. A. Sherwood Mid-Career Professional Awardee Talk: Providing Fundamental Mechanistic Insights Into Single-Site Catalytic Reactions, Jean-Sabin McEwen<sup>1</sup>, Washington State University INVITED**

The single atom limit achieves the ultimate degree of material efficiency for supported metal catalysts. To this end, the ability to create highly dispersed, single-site catalysts, which are highly efficient and have low cost, is very much desirable. While single atom sites can be created, there is still disagreement over whether the single atom sites are indeed catalytically active or if the observed catalytic activity of single-site catalysts is due to metal nanoparticles either unobserved during initial microscopy studies or formed upon exposure to catalytic conditions. Such disagreements create a crucial need for the development of well-defined single-site catalysts with an accurate theoretical model in order to correctly determine the chemical nature of the catalytically active sites. To this end, we provide new atomistic insights regarding the “44” Cu surface oxide through the integration of synchrotron-based X-ray Photoelectron Spectroscopy (XPS) measurements, Synchrotron X-ray Diffraction measurements (SXRD), Scanning Tunneling Microscopy (STM) and Density Functional Theory (DFT) techniques. We also quantify the low-temperature CO oxidation kinetics on Pt single-site catalysts supported on the “29” Cu surface oxide. The “29” Cu surface oxide is a high coverage chiral structure that arises when we further oxidize the “44” structure. Using STM, CO temperature programmed desorption (TPD), and DFT techniques, we determine that an accurate model for the “29” Cu oxide surface is formed from the growth of a Cu<sub>x</sub>O layer formed from 6 fused hexagonal rings above the Cu (111) surface where 5 oxygen adatoms are added at the center of the Cu<sub>x</sub>O rings. Furthermore, we determine the state of the Pt single atoms before, during, and after reaction through a combination of theoretical and experimental techniques. We also correlate ambient pressure experiments, surface science measurements and first principles-based calculations to demonstrate that Pt/Cu(111) single-atom alloys (SAAs) oxidized with varying degrees of O<sub>2</sub> exposure can be reduced with H<sub>2</sub> with reasonable kinetics (hours). This is in contrast to oxidized pure Cu(111) where such reduction is very slow (days). We further contrast the catalytic properties of Rh/Cu(111) SAAs with varying degrees of O<sub>2</sub> exposure to the those of Pt/Cu(111) SAAs. Finally, we report the effects of a copper oxide thin film toward the segregation of noble metal single-atoms on Cu (111) using DFT.

11:40am **AS+CA+EL+EM+SE+SS+TF-ThM-12 Beyond the Physical Origin of the Shirley Background in Photoemission Spectra: Other Predictions of the Interchannel Coupling with Valence Band Losses Mechanism, Alberto Herrera-Gomez, CINVESTAV-Unidad Queretaro, Mexico**

The physical mechanism proposed in our 2017 paper about the origin of the Shirley background in photoemission spectra<sup>1</sup> is based on interchannel

coupling<sup>2</sup> but with the important addition of energy losses in the valence band.<sup>3</sup> Besides the Shirley background, it is possible to derive other predictions of the interchannel Coupling with Valence Band Losses mechanism (ICLM). Two of them are discussed in this paper: 1) the quantitative relation between Auger peaks and the Shirley background and 2) the conduction-band-like structure of the extended region of the Shirley background.

<sup>1</sup> A. Herrera-Gomez et al. Surface and Interface Analysis 50(2), 246–252 (2018).

<sup>2</sup> E.W.B. Dias et al. Phys Rev B 78(2), 4553–4556 (1997).

<sup>3</sup>

<http://www.qro.cinvestav.mx/~aherrera/reportesInternos/unknownOriginShirley.pdf>

12:00pm **AS+CA+EL+EM+SE+SS+TF-ThM-13 Aging of Hydrophilicity in a Nano-Textured SS316 Thin Film Fabricated by Magnetron Sputtering, Pakman Yiu, Ming Chi University of Technology, Taiwan; J. Chu, J. You, National Taiwan University of Science and Technology, Taiwan**

According to the structural zone model by J.A. Thornton[1], we may manipulate the surface morphology of a thin film by altering the deposition temperature and vacuum. Therefore in this study, we prepared a series of SS316 thin film by magnetron sputtering under different Argon working pressure. Resultant thin film possessed a pressure dependent nano-textured surface which was dependent on working pressure. Furthermore, we discovered that the textured surface was highly hydrophilic (water contact angle <15 degrees). The hydrophilicity could be attributed to the combinatorial contribution of surface roughness and capillary effect. However, we also discovered that the hydrophilicity aged with time, where after 21 days the surface turned hydrophobic with water contact angle >90 degrees. XPS studies on both as-deposited and 21-days stored sample films revealed that there was a Carbon-rich surface layer on the surface which grew with time. Interestingly when we tried to clean the surface with Argon atmospheric plasma, the hydrophilicity was almost fully restored. Results revealed that the aging of hydrophilicity may due to the fact that nano-surface texture gathers hydrocarbons in the atmosphere, which eventually formed an extra film that altered the surface wetting property. Understanding the aging mechanism and method of recovery may contribute to the development of a long-lasting hydrophilic surface, which is very useful in applications such as self-cleaning surface and medical apparatus[2,3]

[1] J.A. Thornton, Ann. Rev. Mater. Sci. 7 (1977) 239–260.

[2] A. Syafiq, B. Vengadaesvaran, A.K. Pandey, Nasrudin Abd. Rahim, J. Nanomater. 2018 (2018) 6412601.

[3] M. Xiao, Y.M. Chen, M.N. Biao, X.D. Zhang, B.C. Yang, Mater. Biol. Appl. 70 (2017) 1057–1070.

## CHIPS Act Mini-Symposium

### Room C120-122 - Session CPS+MS-ThM

#### Chips and Science Act Implementation for Microelectronics (Including Workforce)

Moderators: **Alain Diebold**, SUNY Polytechnic Institute, **Tina Kaarsberg**, U.S. Department of Energy, Advanced Manufacturing Office

8:00am **CPS+MS-ThM-1 The Goals for the CHIPS and Science Act of 2022, D. Lavan, Jay Lewis**, National Institute for Science and Technology (NIST) INVITED

The goals for the CHIPS and Science Act of 2022 are to strengthen American manufacturing, supply chains, and national security, and invest in research and development, science and technology, and the workforce of the future to keep the United States the leader in the industries of tomorrow, including nanotechnology, clean energy, quantum computing, and artificial intelligence. An update on progress implementing the CHIPS and Science act will be provided, focusing on R&D Programs including the NSTC, the NAPMP, Manufacturing USA and the Metrology Program.

8:40am **CPS+MS-ThM-3 U.S. CHIPS Act and Semiconductor R&D Centers: Accelerating American Innovation, David Anderson**, NY CREATES INVITED  
This presentation by David Anderson, President of the New York Center for Research, Economic Advancement, Technology, Engineering, and Science

<sup>1</sup> ASSD Peter Sherwood Award

# Thursday Morning, November 9, 2023

(NY CREATES), details the latest updates on the U.S. CHIPS and Science Act and discusses semiconductor R&D centers as key drivers for stimulating innovation, enhancing domestic chip manufacturing capabilities, and bolstering the United States' position in the global semiconductor industry. Through an analysis of the CHIPS Act's key components and the vision put forth by the Federal government, Mr. Anderson will highlight its unprecedented opportunities for accelerating semiconductor R&D and cultivating a robust ecosystem within the U.S. Additionally, this presentation showcases the pivotal role of semiconductor R&D centers in harnessing collaborative research efforts, fostering public-private partnerships, and nurturing talent. Drawing upon his decades of experience in the industry, Anderson demonstrates the positive impact of semiconductor R&D centers on industry growth, job creation, and national security. Attendees will gain insights into the innovative research initiatives, cross-sector collaborations, and technology roadmaps that these centers facilitate, and how the CHIPS Act will help to propel the U.S. to the forefront of the semiconductor industry.

9:20am **CPS+MS-ThM-5 A View on the 1000x Performance Efficiency Goal,** **Steve Pawlowski,** Intel **INVITED**

Over the last two decades, large HPC machine efforts have become a procurement exercise. A large set of applications have been unable to leverage the additional computational power of newly-procured machines without significant additional software development. The machine architectures need to evolve: new systems architectures and innovations require a deep understanding of application use cases and their needs. Memory and storage, as foundational elements, will be at the center of future innovative systems, driving both greater performance and increased energy efficiency. We have a performance efficiency goal of achieving 1000x over the next 20 years. This talk posits that  $\geq 100x$  of the 1000x gain can be realized through repartitioning/packaging changes. The  $< 10x$  that remains can come from re-architecting the system based on a detailed understanding of the targeted applications.

11:00am **CPS+MS-ThM-10 Re-Shoring and Re-Energizing Microelectronics: the Workforce Challenge,** **M. Lundstrom, Vijay Raghunathan,** Purdue University **INVITED**

The CHIPS and Science Act is a bold initiative designed to re-shore semiconductor manufacturing, secure our supply chain, re-gain the lead in leading-edge chip technology, bolster our leading positions in design and semiconductor manufacturing equipment, and accelerate the pace of innovation. Accomplishing these ambitious objectives will require the kinds of mission-driven, deep university-industry-government partnerships that we have not seen since the Manhattan Project and Space Race. The semiconductor workforce is a key challenge – not just a larger workforce, but one educated to advance electronics in the new era we are entering. This talk will present the author's perspective on the magnitude of the challenge, the intimate connection between research, teaching, and innovation that must be maintained, the educational needs for new era electronics, how companies and universities should work together, and the role of international partnerships.

11:40am **CPS+MS-ThM-12 Saving Power with New Designs and Chiplets in the New Era of Advanced Packaging,** **Jan Vardaman,** TechSearch International, Inc. **INVITED**

Energy saving through new designs and package architectures including chiplets are driving developments and options in high-performance computing. An increasing number of companies are turning to chiplets, not only to achieve the economic advantages lost with expensive monolithic scaling, but also to meet the power savings requirements for datacenters and other high-performance computing applications. Co-packaged optics holds promise and is under development by a number of companies. Design with chiplets is one approach under consideration. A chiplet is not a package, but it is a new approach to system, package, and chip design. There are many package options that can be adopted and careful consideration is required to select the most appropriate options for the application. Options include the emerging 3DIC format with microbumps or hybrid bonding, laminate substrate package, fan-out on substrate, and silicon interposer. Challenges include design, test, assembly, and thermal. This presentation focuses on the move to energy savings and design and package methods being introduced to achieve power and performance goals.

## Electronic Materials and Photonics Division

### Room B116 - Session EM+TF-ThM

#### Wide- and Ultra-Wide Band Gap Materials and Devices

**Moderators:** **Erica Douglas,** Sandia National Laboratories, **Seth King,** University of Wisconsin - La Crosse, **Daniel Pennachio,** Naval Research Laboratory

8:00am **EM+TF-ThM-1 Ga<sub>2</sub>O<sub>3</sub> and AlN for Power and RF Electronics,** **Grace Xing,** Cornell University **INVITED**

It's of little surprise that there has been a consistent drive toward the use of wider bandgap materials for power and RF electronics. After all, the wider the bandgap, the greater the breakdown field, opening the door to making devices with a higher breakdown voltage for the same material thickness. Furthermore, the saturation velocity of mobile carriers in ultra-scaled devices tends to be about  $1-2 \times 10^7$  cm/s in most semiconductors.

However, nature is not always that generous. Typically, a move to a wider bandgap is accompanied by more challenging doping, point defect control, ohmic contacts, quality junctions, along with difficulty in making high-quality native substrates. Ga<sub>2</sub>O<sub>3</sub> and AlN are among the promising contenders, given their large bandgaps, availability of large-size bulk substrates ( $> 2$  inches), and heterojunctions. But both lack p-type. AlN possesses high thermal conductivity – slightly worse than that of copper but Ga<sub>2</sub>O<sub>3</sub> has a low thermal conductivity – worse than that of sapphire.

Given all these promises and obstacles, is it possible to harvest all the benefits in AlN and Ga<sub>2</sub>O<sub>3</sub> and demonstrate devices that are superior to those made from SiC and GaN? I will reflect on our efforts in seeking answers to these questions in the past many years researching on power and RF devices with a focus on Ga<sub>2</sub>O<sub>3</sub> and AlN [1-6].

References:

- [1] Z. Hu *et al.*, Appl. Phys. Lett. 92 85111 (2015) Near unity ideality factor and Shockley-Read-Hall lifetime in GaN-on-GaN p-n diodes with avalanche breakdown.
- [2] W. Li *et al.*, IEEE Trans. Electron Dev. (2020) Guiding principles for trench Schottky barrier diodes based on ultrawide bandgap semiconductors: a case study in Ga<sub>2</sub>O<sub>3</sub> [<https://doi.org/10.1109/TED.2020.3003292>]
- [3] A. Hickman *et al.*, SST (2021) Next generation electronics on the ultrawide-bandgap aluminum nitride platform.
- [4] A. Green *et al.*, APL Materials (2022) Beta-gallium oxide power electronics.
- [5] E.K. Kim *et al.*, APL (2023) N-polar GaN/AlGaN/AlN HEMTs on single-crystal bulk AlN substrates.
- [6] W. Zhao *et al.*, IEEE EDL (2023) 15-GHz epitaxial AlN FBARs on SiC substrates.

8:40am **EM+TF-ThM-3 Deep UV Photoluminescence Mapping of Gallium Oxide,** **Matthew McCluskey,** Washington State University

Photoluminescence (PL) spectroscopy is an important method to characterize dopants and defects in gallium oxide. Features in the PL spectrum include the intrinsic UV band, blue and green bands that involve donor-acceptor pairs, and red emission due to Cr<sup>3+</sup> impurities. PL mapping with excitation wavelengths as short as 266 nm reveals the spatial distribution of these features with submicron resolution. In Czochralski-grown  $\beta$ -Ga<sub>2</sub>O<sub>3</sub>:Fe, the Cr<sup>3+</sup> emission intensity shows striations that are attributed due to inhomogeneities during growth. In addition to defects in the bulk, PL microscopy has revealed several specific defects on the surface. Some of these localized centers are very bright UV emitters. Raman scans of these bright emitters revealed hydrocarbon peaks, which may point toward the origin of the light emission. Samples damaged by high-intensity laser pulses show significant changes in the intensity and energy of the intrinsic UV band.

9:00am **EM+TF-ThM-4 Spatially Resolved Polymorph Conversion in Ga<sub>2</sub>O<sub>3</sub>,** **U. Bektas, P. Chekhonin, R. Heller, R. Hübner, M. Liedke, N. Klingner, Gregor Hlawacek,** Helmholtz Zentrum Dresden-Rossendorf, Germany  
Monoclinic galliumoxide ( $\beta$ -Ga<sub>2</sub>O<sub>3</sub>) is a promising wideband gap semiconductor with a bandgap of 4.7 eV and a high breakdown voltage. However, the existence of several metastable polymorphs and the immature fabrication technology limits its applications. The research is based on the recent observation that  $\beta$ -Ga<sub>2</sub>O<sub>3</sub> can reliably be converted into  $\gamma$ -Ga<sub>2</sub>O<sub>3</sub> using high energy ion beams [1,2]. It could also be shown that

the resulting  $\gamma$ -Ga<sub>2</sub>O<sub>3</sub> layer exhibits an exceptional tolerance towards high fluence ion beam irradiation [3].

Here, we use focused ion beam (FIB) induced processing to convert  $\beta$ -Ga<sub>2</sub>O<sub>3</sub> into  $\gamma$ -Ga<sub>2</sub>O<sub>3</sub> in a spatially controlled way. We employ focused Ne ions from a helium ion microscope (HIM) and liquid metal alloy ion sources (LMAIS) based FIB with Co, Si, and In to induce the polymorph conversion. Electron backscatter diffraction (EBSD), transmission electron microscopy (TEM) and atomic force microscopy (AFM) are used to confirm, in a spatially resolved way, the successful polymorph conversion. From the obtained EBSD data the orientation relationship between the irradiated and unirradiated material is resolved. Broadbeam irradiated reference samples have been used to corroborate these results with channeling Rutherford backscattering spectrometry (c-RBS), X-ray diffraction (XRD) and Doppler broadening variable energy positron annihilation spectroscopy (DB-VEPAS) results. The obtained crystal structure and defect distribution data supports the model suggested for the conversion mechanism [3].

This research is supported by the tax funds on the basis of the budget passed by the Saxonian state parliament in Germany and the COST Action CA19140 FIT4NANO <https://www.fit4nano.eu/>.

[1] A. Azarov, C. Baziotti, Disorder-Induced Ordering in Gallium Oxide Polymorphs, *Phys. Rev. Lett.* **128** (2022), 015704.

[2] J. Garcia-Fernandez, S.B. Kjeldby, Formation of  $\gamma$ -Ga<sub>2</sub>O<sub>3</sub> by ion implantation: Polymorphic phase transformation of  $\beta$ -Ga<sub>2</sub>O<sub>3</sub>, *Appl. Phys. Lett.* **121** (2022), 191601.

[3] A. Azarov, J. G. Fernández, J. Zhao, F. Djurabekova, H. He, R. He, Ø. Prytz, L. Vines, U. Bektas, P. Chekhonin, N. Klingner, G. Hlawacek, A. Kuznetsov, Universal radiation tolerant semiconductor (2023), doi:10.48550/ARXIV.2303.13114.

9:20am **EM+TF-ThM-5 Low-Temperature Epitaxy and in-situ Doping of Ultrawide Bandgap Ga<sub>2</sub>O<sub>3</sub> Films via Hollow-Cathode Plasma-ALD**, *S. Ilhom, A. Mohammad, N. Ibrahimli, J. Grasso, B. Willis*, University of Connecticut; *A. Okyay*, OkyayTech Inc; *Necmi Biyikli*, University of Connecticut  
Wide and ultrawide bandgap (WBG/UWBG) semiconductors make the backbone of high-power high-frequency electronics, used in electric vehicles, 5G and beyond wireless communication systems, and smart power grids. Gallium oxide (Ga<sub>2</sub>O<sub>3</sub>) is an emerging UWBG semiconductor showing superior material properties particularly ideal for harsh environments (high temperature, high-energy radiation, corrosion) applications. Reducing the growth and doping process temperatures for Ga<sub>2</sub>O<sub>3</sub> would potentially enable a wider integration platform towards post-CMOS integration and flexible electronics.

Herein, we report on the low-temperature as-grown crystalline  $\beta$ -Ga<sub>2</sub>O<sub>3</sub> films on Si, glass, and sapphire via hollow-cathode plasma-assisted atomic layer deposition (HCP-ALD). The films were deposited using triethylgallium (TEG) and Ar/O<sub>2</sub> plasma as metal precursor and oxygen co-reactant, respectively. Additionally, we have employed *in situ* atomic layer doping to n-type dope Ga<sub>2</sub>O<sub>3</sub> films where tris-dimethylaminosilane (TDMAS) and tetrakis-dimethylaminotin(IV) (TDMASn) were utilized as the dopant precursors. Growth experiments have been performed at 240 °C under 50 W rf-plasma power. The doping process was carried out via both supercycle (ABC-type ALD-cycle) and co-dosing methods. Additionally, each unit ALD-cycle was followed by an *in-situ* Ar-plasma annealing treatment, which consisted of Ar-plasma exposure for 20 seconds at 250 W rf-power. Both *in-situ* and *ex-situ* ellipsometry were employed to measure the thickness and optical properties of the Ga<sub>2</sub>O<sub>3</sub> samples. X-ray diffraction (XRD) of the sample on sapphire revealed epitaxial Ga<sub>2</sub>O<sub>3</sub> films with monoclinic *b*-phase, while GIXRD analyses of the samples grown on Si and glass displayed *b*-phase polycrystalline films. HR-STEM imaging and EDX elemental analysis confirmed the epitaxial relationship of the films grown on sapphire substrates and displayed successful incorporation of dopant elements. Preliminary electrical conductivity measurements showed highly resistive samples. Therefore, *ex-situ* thermal annealing studies are carried out to explore dopant activation processes. Further studies from our XPS characterizations will provide additional insight about the chemical bonding states of the dopant species. A significant effort will be devoted for the comparison of Si and Sn-doping strategies and potential suggestions will be provided to overcome the challenges in achieving device quality undoped and doped Ga<sub>2</sub>O<sub>3</sub> layers at low processing temperatures.

9:40am **EM+TF-ThM-6 Growth of Metastable Ga<sub>2</sub>O<sub>3</sub> Epitaxial Films Using Metalorganic Chemical Vapor Deposition and Halide Vapor Phase Epitaxy**, *Jingyu Tang, K. Jiang, M. Weiler, M. Moneck, R. Davis, L. Porter*, Carnegie Mellon University

Gallium oxide (Ga<sub>2</sub>O<sub>3</sub>) is an ultra-wide bandgap semiconductor of interest for electronics that can operate in extreme conditions, such as high power, high temperature and radiation exposure.  $\beta$ -Ga<sub>2</sub>O<sub>3</sub> is thermodynamically stable at atmospheric conditions up to its melting point and is the phase produced in melt-grown, single-crystal substrates. However, epitaxial films of metastable polymorphs of Ga<sub>2</sub>O<sub>3</sub> are also of interest because they possess unique properties – such as piezoelectricity, ferroelectricity, or ferromagnetism – that could lead to new types of heterostructure devices. We report here the growth and characterization of both mixed-phase and phase-pure epitaxial films of each of the metastable polymorphs:  $\kappa(\epsilon)$  and  $\gamma$  using metalorganic chemical vapor deposition (MOCVD); and  $\alpha$ ,  $\kappa$  and  $\gamma$  using halide vapor phase epitaxy (HVPE). The effect of variables, such as substrate temperature, will be reported, as will the use of different substrates / orientations to produce phase-pure epitaxial films of  $\alpha$ -,  $\kappa$ -, and  $\gamma$ -Ga<sub>2</sub>O<sub>3</sub> in the same grown runs. The microstructure, composition, and morphology of the films and film/substrate interfaces were characterized using x-ray diffraction (XRD)  $\theta$ -2 $\omega$  scans, rocking curves, and  $\phi$  scans; scanning electron microscopy (SEM); and high-resolution cross-section transmission electron microscopy (TEM) with energy dispersive x-ray (EDX) analysis.

11:00am **EM+TF-ThM-10 AlGaIn/GaN HEMTs with Submicron Gates for High-Frequency Operation in Harsh Space Environments**, *Isabel Harrysson Rodrigue, M. Rais-Zadeh*, Jet Propulsion Laboratory, California Institute of Technology

Indium aluminum nitride/gallium nitride high electron mobility transistors (AlGaIn/GaN HEMTs) offer excellent properties such as high electron mobility and wide bandgap, making them ideal for high-frequency and high-power applications, in harsh environments. The wide band gap of the AlGaIn/GaN heterostructure infers inherent radiation tolerance compared to traditional Si microelectronics. Owing to the advantageous two-dimensional electron gas, AlGaIn/GaN HEMTs can provide increased sensitivity, fast response time, and low noise levels while withstanding extreme temperatures, radiation, and vibrations found in space. Its robustness and reliability make it ideal for long-term missions, ensuring accurate and uninterrupted sensing and detection in difficult space conditions. DC operation has been achieved for AlGaIn/GaN HEMTs with various larger gate dimensions. Separate studies have shown successful operation of AlGaIn/GaN HEMTs at high temperatures reaching 1000 °C. However, in achieving high-frequency operation, the device geometry must be size-optimized from large-area to scaled gate lengths in the submicron regime. RF analysis at both room temperature and high temperature is a necessary next step to determine the merits of these devices for extreme environment applications where these devices have advantages over other semiconductor technologies. In this work, the performance of AlGaIn/GaN HEMTs are optimized by reducing the gate length toward high-frequency operation in harsh space environments, with specific applications in on-board rover communications and for in situ readout of sensor data. The geometry schemes were chosen during the design phase, and the microfabrication process, metallization, and passivation materials were carefully evaluated. These results are promising for further testing, e.g., radiation tolerance, high temperatures, and monolithic circuit integration. The presented devices have an advantage over traditional heterogeneous integration strategies for GaN devices which requires silicon ASICs that, without cooling, cannot operate in high-temperature environments.

11:20am **EM+TF-ThM-11 Selected-Area P-Type Doping of GaN Using Focused-Ion Beams**, *Sam Frisone*, University of Michigan; *M. Titzte, A. Katzenmeyer*, Sandia National Lab; *B. Li*, Yale University; *A. Flores*, Sandia National Lab; *Y. Wang*, Los Alamos National Laboratory; *R. Goldman*, University of Michigan; *E. Biejelec*, Sandia National Lab; *J. Han*, Yale University

Due to their potential for high breakdown voltage and low on-resistance, GaN-based electronic devices are promising for high-power and high-frequency electronics. Vertical GaN p-i-n devices are expected to offer improved thermal management and reduced leakage current in comparison to their lateral counterparts; however, typical etching and regrowth processes introduce interfacial impurities that limit control of dopant profiles. Thus, a strategy for both vertical and lateral dopant selectivity, without the need for etching and regrowth, is essential for the development of high-quality vertical GaN devices. Here, we report on Mg doping using a liquid-metal ion source (LMIS) in a mass-selecting focused-

ion-beam (FIB) column. For these studies, an unintentionally doped (UID) 3.6 $\mu\text{m}$  GaN layer is grown by metalorganic chemical vapor deposition on n-type GaN. In preparation for FIB implantation, the UID GaN layer was patterned with an array of Au/Ti markers. Checkerboard patterns consisting of alternating 70x70 and 50x50 $\mu\text{m}$  squares, with and without Mg FIB implantation, were prepared using a Mg-doped AuSi eutectic as the LMIS. The ion energies were set to 70keV, resulting in a most probable ion implantation depth of 70nm; seven ion fluences ranging from  $10^{12}$ - $10^{15}$   $\text{cm}^{-2}$ , corresponding to Mg concentrations of  $10^{16}$ - $10^{19}$   $\text{cm}^{-3}$ , were used. To examine the activation of Mg dopants in GaN, we compare the pristine and implanted regions before and after rapid-thermal processing (RTP). A distinct checkerboard pattern is observed in secondary electron (SE) images, with reduced SE image intensities in the implanted regions compared to the pristine regions. Following removal of the Au/Ti markers and 30 seconds of RTP at 1100°C, the checkerboard pattern is reduced in the vicinity of the four lowest ion fluences. For all regions, cathodoluminescence (CL) spectroscopy reveals GaN near-band edge (NBE) emissions at 3.4eV. The intensity of NBE emission is highest in the pristine regions, especially those in the vicinity of the two lowest ion fluences. Furthermore, in pristine regions adjacent to the two lowest ion fluences we observe CL emissions at 2.85eV and 2.2eV. As discussed in [1], we attribute these emissions to impurity-related donor-acceptor pairs and yellow luminescence, respectively. The reduced SE image intensity and limited CL emission in the vicinity of the highest ion fluences suggest incomplete Mg dopant activation. The influence of additional RTP on the dopant activation will be discussed. [1] 10.1016/j.nanoen.2022.107689

11:40am **EM+TF-ThM-12 Epitaxial Growth and Characterization of High ScN Fraction ScAlN on NbN and SiC**, *Matthew Hardy, S. Katzer, A. Lang, E. Jin, N. Nepal, B. Downey, V. Gokhale, V. Wheeler*, U.S. Naval Research Laboratory

ScAlN thin films have attracted significant attention due to their factor of five increase in piezoresponse over AlN for  $\text{Sc}_{0.43}\text{Al}_{0.57}\text{N}$ . Integration of metallic epitaxial NbN with ScAlN using molecular beam epitaxy (MBE) enables a pathway towards a highly conductive lower electrode while preserving high crystal quality even in relatively thin ScAlN films suitable for use at or above X-band frequencies. Maintaining phase-pure and high crystal quality  $\text{Sc}_x\text{Al}_{1-x}\text{N}$  at high x is critical to improve resonator bandwidth and reduce insertion loss.

In this work, we show the importance of the ScAlN nucleation layer to the final crystal quality and anomalously oriented grain (AOG) density of MBE-grown ScAlN films on SiC and NbN/SiC. Starting the ScAlN growth with a  $\text{Sc}_{0.32}\text{Al}_{0.68}\text{N}$  layer can suppress the rock-salt ScAlN material at the nucleation interface, as seen by reflection high-energy electron diffraction (RHEED) and transmission electron diffraction (TEM). Nucleation using a linear composition grade from  $\text{Sc}_{0.32}\text{Al}_{0.68}\text{N}$  to  $\text{Sc}_{0.40}\text{Al}_{0.60}\text{N}$  over 100 nm leads to further improvements in the RHEED pattern, including a narrowing of the spots early in the growth, as well as elimination of remaining ring-like character in the final RHEED pattern after an additional 40 nm of growth, resulting in an X-ray diffraction (XRD) FWHM as low as  $1.22^\circ$  for ScAlN films grown on SiC. TEM shows near elimination of cubic grains that otherwise form in the initial layers of the  $\text{Sc}_{0.40}\text{Al}_{0.60}\text{N}$ . The grade thickness can be reduced to 25 nm (with the remaining 125 nm  $\text{Sc}_{0.40}\text{Al}_{0.60}\text{N}$ ) without degrading the XRD FWHM or RHEED pattern, increasing the average ScN fraction from 0.373 to 0.393. Finally, a 500-nm-total-thickness sample (100 nm  $\text{Sc}_{0.32}\text{Al}_{0.68}\text{N}$   $\rightarrow$   $\text{Sc}_{0.40}\text{Al}_{0.60}\text{N}$ , 400 nm  $\text{Sc}_{0.40}\text{Al}_{0.60}\text{N}$ ) was grown to show the impact of defect annihilation in thicker films, resulting in a reduction of XRD FWHM to  $0.89^\circ$ . The improved layer initiation shows that more gradual changes in surface energy and strain reduces the nucleation of undesirable cubic grains, and may point to a general strategy for elimination of anomalous grains in high ScN fraction ScAlN.

Employing a similar growth approach and using a novel two-step AlN interlayer enables integration of ScAlN on a NbN epitaxial metal lower electrode. Growth conditions to first encapsulate the NbN layer, and then provide a smooth surface for ScAlN nucleation are critical to minimize degradation in XRD FWHM or AOG density. ScAlN on NbN structures enable characterization of the ScAlN dielectric constant and electromechanical coupling coefficient ( $k_t^2$ ). A dielectric constant of 25 and  $k_t^2$  of 27% was extracted for  $\text{Sc}_{0.32}\text{Al}_{0.68}\text{N}$  from a  $\text{Sc}_{0.32}\text{Al}_{0.68}\text{N}/\text{AlN}/\text{NbN}/\text{SiC}$  sample.

12:00pm **EM+TF-ThM-13 Novel Graphene and SiC Epitaxy to Enable Film Transfer**, *Daniel Pennachio, J. Hajzus, A. Lang*, US Naval Research Laboratory; *R. Stroud*, Former employee of US Naval Research Laboratory; *R. Myers-Ward*, US Naval Research Laboratory

Remote epitaxy (RE) is a promising technique for epitaxial film transfer that utilizes graphene as a release layer [1]. Graphene grown on SiC(0001) substrates through Si sublimation or through propane chemical vapor deposition (CVD) is an ideal platform for remote epitaxy of wide bandgap (WBG) semiconductors as there is no need for a graphene transfer step, mitigating contamination or defects that can complicate the remote epitaxy process. In addition, the graphene/SiC materials system is compatible with commercially-viable WBG semiconductor growth and processing, making it a suitable choice for scalable future development. A challenge to utilizing SiC is that CVD growth is typically conducted using high-temperature hydrogen-based chemistries that could damage or remove graphene. This study investigates the effect of alternative low- $\text{H}_2$  CVD growth conditions on SiC/graphene/SiC(0001) remote epitaxy that may reduce damage to the graphene barrier. In addition, graphene preparation and associated surface morphology is varied to explore its effect on SiC epilayer formation.

For this work, the effects of Ar: $\text{H}_2$  process gas flow ratio, growth precursor C/Si ratio, and growth temperature on hot-wall CVD SiC RE crystalline quality were investigated. Both semi-insulating nominally on-axis 6H-SiC(0001) and n-type 4° off-axis 4H-SiC(0001) substrates were used to produce different surface morphologies and graphene layer numbers. Nomarski optical microscopy, scanning electron microscopy, and atomic force microscopy found CVD deposition at 1620°C with Ar/ $\text{H}_2$  ratios <20/5 slm, and C/Si ratios <1.55 to have the smoothest surface morphology and fewest polytype inclusions. Substrates with offcuts <0.1° from SiC(0001) exhibited lower epilayer macrostep density but showed evidence of polytype impurities and 3D growth at C/Si ratios > 1.0. RE on EG/4H-SiC(0001) substrates with a 4° off-cut from SiC[0001] had a wider parameter range resulting in single-crystalline growth compared to growth on the nominally on-axis substrates despite growth of >1 monolayer EG on these substrates. This study found smooth, single-crystalline polytype-pure SiC(0001) epilayers on EG substrates could be grown using predominantly Ar carrier gas, with  $\text{H}_2$  concentrations as low as ~2%. Through this study, optimal SiC RE growth conditions are suggested for a balance of EG survivability and SiC film morphology.

[1] Kim, Y., Cruz, S., Lee, K. et al. Nature 544, 340–343 (2017).

## Fundamental Discoveries in Heterogeneous Catalysis Focus Topic

### Room B113 - Session HC+SS-ThM

#### Dynamics and Mechanisms in Heterogeneously Catalyzed Reactions

**Moderators:** Arthur Utz, Tufts University, Jason Weaver, University of Florida

8:00am **HC+SS-ThM-1 Dehydration and Dehydrogenation of Formate on  $\text{Fe}_3\text{O}_4$ (001)**, *Marcus Sharp*, Pacific Northwest National Laboratory / Washington State University; *C. Lee, S. Smith, B. Kay, Z. Dohnálek*, Pacific Northwest National Laboratory

Interest in improving the activity and selectivity of catalysts has been persistent due to their importance in numerous chemical industries. Yet the mechanistic understanding of the active site structure, coordination environment, and stability is often lacking. Using a combination of temperature programmed reaction spectroscopy (TPRS), molecular beam scattering (MBS), and X-ray photoelectron spectroscopy (XPS) we investigate the reactivity of formic acid on the  $\text{Fe}_3\text{O}_4$ (001) that serves as a model reducible oxide support for single-atom catalysts. XPS shows that formic acid deprotonates at low temperature (~80 K), forming a formate intermediate and a protonated lattice oxygen (hydroxyl). At higher temperatures (400–600 K), the formate undergoes dehydration to CO and  $\text{H}_2\text{O}$  via two desorption channels, while dehydrogenation to  $\text{CO}_2$  is a minor channel. Angle-resolved TPRS and MBS experiments show that CO leaves the surface with excess kinetic energy closely focused along the surface normal. Surprisingly, not all formate species can react through the low-temperature channel. XPS, however, does not indicate a change in surface species throughout reaction temperatures. The addition of isotopically labeled formic acid (DCOOD) after the depletion of the low-temperature

reaction channel show a complete mixing of all surface formate species. Similarly, the addition of atomic hydrogen after the depletion of the low-temperature reaction shows that surface hydroxyls are important in guiding the decomposition reaction to various reaction channels. Fe deposition on top of Fe<sub>3</sub>O<sub>4</sub>(001) reveals that Fe based-structures also act as the active sites for the high-temperature desorption of CO. This study illustrates the complexity of reaction intermediates at catalyst surfaces where changes in surface morphology can lead to differences in product selectivity and activity.

**8:20am HC+SS-ThM-2 The Effect of No and Co on the Rh(100) Surface at Atmospheric Pressure, D. Boden, J. Meyer, Irene Groot, Leiden University, Netherlands**

Rhodium is used in automotive catalysis to reduce NO and CO emissions in the exhaust by catalyzing the reduction of NO to N<sub>2</sub> and the oxidation of CO to CO<sub>2</sub>. This means the rhodium nanoparticles in the catalyst are exposed to high pressures of NO and CO, both known to be highly corrosive gases, which leads to disintegration and sintering of the rhodium catalyst. It is important to understand the effect high pressures of NO and CO have on the rhodium surface at the nano scale, in order to design strategies to impede catalyst deactivation. Here, one of the most active rhodium facets, Rh(100), is studied at atmospheric pressures of NO and CO with scanning tunnelling microscopy (STM), in order to observe the roughening of the surface *in situ*. Additionally, atomistic thermodynamics, based on density functional theory (DFT) calculations, is used in combination with *ex situ* ultrahigh vacuum techniques (low-energy electron diffraction and Auger electron spectroscopy) to understand the behavior of adsorbates on the surface during the STM experiments, at the atomic scale. The formation of rhodium islands on the (100) terraces is observed at high CO pressures, in conjunction with roughening of the step edges. Interestingly, roughening does not occur at the same pressures of NO. The surface roughening is also less severe when co-dosing NO and CO, even at identical CO partial pressures. The results from atomistic thermodynamics show that NO likely inhibits CO adsorption by blocking the CO adsorption sites, thereby preventing carbonyl formation and decreasing surface roughening.

**8:40am HC+SS-ThM-3 Sustainable Production of Aromatics via Methane Dehydroaromatization: Role of Dynamic Carbon Accumulation, M. Hossain, Virginia Tech; M. Rahman, Southwest Research Institute, San Antonio Texas; D. Maiti, E. Sobchinsky, M. Kunz, R. Fushimi, Idaho National Laboratory; Sheima Khatib, Virginia Tech**

**INVITED**

Natural gas, mainly composed of methane, constitutes an available and cheap resource that can be used as a building block to produce chemicals. Methane dehydroaromatization (MDA) is a reaction capable of directly converting methane to value-added aromatics, without an intermediate syngas step. The reaction happens in non-oxidative conditions, producing mainly benzene and hydrogen,  $6 \text{ CH}_4(\text{g}) \rightarrow \text{C}_6\text{H}_6(\text{g}) + 9\text{H}_2(\text{g})$ . Zeolite-supported Mo catalysts have so far been the most widely studied catalysts in MDA, but they do not fulfill the conversion and stability requirements for commercialization. During the reaction induction period, Mo oxide species gradually reduce to Mo carbides, which are responsible for methane activation and subsequent conversion to aromatics. We have developed a strategy to improve benzene yield and catalyst stability by controlling the activation of the Mo species to optimize their reduction and dispersion before exposure to reaction conditions. Our results indicate that when activation of catalysts is performed by reduction in pure hydrogen under temperature-controlled conditions, the carbides formed (*ex situ*) lead to more selective catalysts that deactivate more slowly compared to carbides formed during reaction (*in situ*). To explain this difference, we studied the dynamic carbon accumulation kinetics on varying redox states of MoOx/HZSM-5 catalyst via strategic molecular probe experiments in the Temporal Analysis of Products (TAP) reactor. Incremental pulse-by-pulse TAP investigation helps to distinguish different surface reactions and paves the way for elucidating the role of catalyst state towards preferential soft coke formation, as opposed to hard coke that results in catalyst deactivation. These intrinsic kinetic fingerprints of the catalyst will provide guidance towards better MDA reaction protocols for sustained high aromatics production from waste greenhouse gas, methane.

**9:20am HC+SS-ThM-5 Mechanistic Understanding of Methanol Synthesis on an In<sub>2</sub>O<sub>3</sub> Catalyst, Yong Yang, ShanghaiTech University, China**

Indium oxide (In<sub>2</sub>O<sub>3</sub>) became a very promising catalyst in recent years for its high selectivity of CO<sub>2</sub> hydrogenation to methanol, an ideal fuel for green energy. The reaction normally requires elevated temperature from 220 to 330°C and relative high pressure around 50 bar. Deep mechanistic insight with experimental evidence is still in demand for effective development in

catalyst rational design. The widely applied direct kinetics investigation by *in situ* IR of this reaction is difficult due the formation of In<sub>2</sub>O<sub>3</sub> black under H<sub>2</sub> reduction condition.

Here based on a recent optimized c-In<sub>2</sub>O<sub>3</sub> catalyst, we investigate methanol synthesis reactivity correlated spectroscopic and kinetics properties at up to 16 bar and 270°C by online MS isotope kinetics measurements, *in situ* time resolved FT-IR and XPS (ThermoFisher ESCALab250Xi), in both in steady-states and transients. In all kinetics experiments reported here, the input total flow rate is controlled around 15 sccm with H<sub>2</sub>/D<sub>2</sub>:CO<sub>2</sub>:Ar ratio at 10.5 sccm:3.5 sccm:1.4 sccm and the resulted gas hour space velocity is around 17 L/g/Hr.

Both steady-states and transients isotope input results clearly indicate a normal kinetic isotope effect (KIE). In addition pressure dependence study indicates that the reaction rate is nearly proportional to the input pressure and Arrhenius plot yield activation energies with both inputs remain almost constant at different pressures, with a higher activation energy (E<sub>a</sub>) for D<sub>2</sub>/CO<sub>2</sub> than H<sub>2</sub>/CO<sub>2</sub> (120 vs. 100 kJ/mol). The KIE and pressure dependence behaviors are essentially different from Cu based catalyst in the same reaction, although E<sub>a</sub> values are close. A universal reaction rate equation with parameters of pressure and temperature is thus provided. Based on results from two series of isotope switching transients experiments from D<sub>2</sub>/CO<sub>2</sub> to H<sub>2</sub>/CO<sub>2</sub>, quantitative transient products analysis of exchanged D/H isotopic species reveals that there are up to 2.5 monolayers of dissociated deuterium involves in the D isotopomer methanol products. This indicates that the active surface is highly reduced with a high efficiency of surface hydrogenation to methanol. The surface species characterization by *in situ* FT-IR and XPS investigate sample *in situ* prepared as pre-oxidized, pre-reduced and further exposed with water vapor or CO<sub>2</sub>. The combined results provide key evidence for main XPS features assignments.

These results helps elucidating the kinetics and spectroscopic fundamentals in this reaction and hopefully will provide useful information toward the rational design of active and stable catalysts based on In<sub>2</sub>O<sub>3</sub> for CO<sub>2</sub> hydrogenation to methanol.

**9:40am HC+SS-ThM-6 The Strong Metal-Support Interaction Under Reactive Conditions and Its Influence on the Hydrogen Evolution Reaction Over Pt/TiO<sub>2</sub>(110), Philip Petzoldt, Technical University of Munich, Germany; M. Eder, TU Wien, Austria; M. Blum, Lawrence Berkeley National Laboratory (LBNL); T. Kratky, Technical University of Munich, Germany; S. Günther, Technical University Munich, Germany; M. Tschurl, B. Lechner, U. Heiz, Technical University of Munich, Germany**

Covering reactive nanoparticles with thin metal oxide films is a promising strategy to improve their stability and catalytic selectivity. Reductive heating of noble metal particles supported on reducible oxides initiates their encapsulation due to the strong metal-support interaction (SMSI). This phenomenon has been studied under well-defined UHV conditions on single crystals and on more applied, structurally inhomogeneous catalysts. However, only few studies provide insight at the atomic scale under reactive conditions which is crucial for the systematic optimization of catalytic systems.

In this contribution, we investigate the dynamic behavior of the SMSI state on Pt-loaded TiO<sub>2</sub>(110) under reactive conditions and its influence on the catalyst's activity in the photocatalytic hydrogen evolution reaction. Employing near ambient pressure XPS, we show that the SMSI kinetics may be tuned by choosing the oxygen pressure. Monitoring the hydrogen evolution reaction by mass spectrometry, we further demonstrate that the impact of the noble metal encapsulation on the catalyst's chemistry depends on the complex interplay of reaction conditions and catalyst preparation.

Our results provide new mechanistic insights into the interaction of noble metal particles with the support and may foster the development of catalysts with improved stability and selectivity.

**11:00am HC+SS-ThM-10 Rotational Orientation Effects in Hydrogen-Surface Scattering, Helen Chadwick, Y. Alkoby, G. Alexandrowicz, Swansea University, UK**

**INVITED**

The interaction of hydrogen with surfaces plays an important role in many heterogeneously catalysed reactions, for example converting ortho-hydrogen to para-hydrogen for the safe storage of liquid H<sub>2</sub> fuel, in the Haber Process for making ammonia and in the Fischer-Tropsch synthesis for making longer chain hydrocarbons. Carefully controlled, quantum state resolved experiments play a pivotal role in providing benchmarks which can be used to help develop accurate, predictive theoretical models of these important interactions. The influence of the rotational orientation

# Thursday Morning, November 9, 2023

projection quantum state of the molecule ( $m_j$ ), which can be considered classically to describe whether the hydrogen is rotating like a helicopter or cartwheel when it collides with the surface, has been less well characterised due to the challenges associated with preparing these quantum states, particularly in closed shell, ground state molecules. Here I will present a unique magnetic manipulation interferometry technique [1] that allows us to control and manipulate the rotational orientation and nuclear spin projection ( $m_j$ ) quantum states of small molecules both before and after they collide with a surface. Using the elastic scattering of  $H_2$  from LIF as an example [2], I will demonstrate that we can extract empirical scattering matrices from the data which can be compared directly to those from theoretical calculations. I will also show new results for  $H_2$  scattering from the stepped Cu(511) surface, where signals for several different diffraction channels have been measured which exhibit different dependencies on the rotational orientation states, as well as observations which suggest that  $H_2$  can dissociate when it collides with the surface. All of these results combined, provide very stringent experimental benchmarks which will help develop accurate theoretical models.

**Acknowledgments:** This work was supported by the Horizon 2020 Research and Innovation Programme Grant Number 772228 and an EPSRC New Horizons Grant Number EP/V048589/1.

## References

- [1] O. Godsi et al., Nat. Comm. 8, 15357 (2017).
- [2] Y. Alkoby et al., Nat. Comm. 11, 3110 (2020).

11:40am **HC+SS-ThM-12 Studies of Pt-Sn Catalysts for Methylcyclohexane Dehydrogenation to Toluene**, *Donna Chen*, University Of South Carolina; *M. Qiao, A. Ahsen, A. Heyden, J. Monnier*, University of South Carolina

The use of  $H_2$  as an energy carrier has emerged as an attractive alternative to fossil fuels, but a major challenge for the  $H_2$ -based economy lies in the efficiency of storage and transportation. The use of liquid organic hydrogen carriers (LOHC) would allow for the reversible storage of  $H_2$  through hydrogenation-dehydrogenation reactions. The toluene-methylcyclohexane (MCH) pair is ideal for this purpose because MCH has a relatively high gravimetric storage density, and both compounds are widely available, low-toxicity liquids at ambient temperature. While catalytic hydrogenation of LOHCs is exothermic and facile, a major problem with using LOHCs for hydrogen storage is that catalytic dehydrogenation is endothermic and not always reversible due to side reactions. Pt catalysts are active for dehydrogenation of MCH to toluene, but undesirable C-C bond breaking reactions also lead to coking and deactivation. In this work, model Pt-Sn bimetallic surfaces are studied for MCH dehydrogenation in order to understand the role of Sn in preventing the deactivation of Pt surfaces. Pt-Sn alloy surfaces were prepared by depositing Sn on Pt(111) and annealing to various temperatures to form ordered overlayers, which were characterized by low energy electron diffraction, scanning tunneling microscopy (STM), and X-ray photoelectron spectroscopy (XPS) in an ultrahigh vacuum (UHV) chamber. The model surfaces were then transferred into a flow reactor coupled directly to the UHV chamber for kinetic studies under realistic pressure conditions; after MCH reaction, the surfaces were transferred back to the UHV chamber for characterization by XPS and STM. The activity of the model single-crystal surfaces are also compared with the conventional catalysts consisting of supported Pt-Sn particles. Computational work will help identify the role of the various active sites and determine reaction mechanisms, as well as the rate and selectivity controlling steps at the active sites.

12:00pm **HC+SS-ThM-13 Platinum@Hexaniobate Nanopeapods: A Directed Photocatalytic Architecture for Dye-Sensitized Semiconductor  $H_2$  Production Under Visible Light Irradiation**, *Clare Davis-Wheeler Chin*, Sandia National Laboratories, USA; *P. Fontenot*, Tulane University; *T. Rostamzadeh*, University of New Orleans; *L. Treadwell*, Sandia National Laboratories, USA; *R. Schmehl*, Tulane University; *J. Wiley*, University of New Orleans

Platinum@hexaniobate nanopeapods (Pt@HNB NPPs) are a nanocomposite heterogeneous photocatalyst that was selectively engineered to increase the efficiency of hydrogen production from visible light photolysis. Pt@HNB NPPs consist of linear arrays of high surface area Pt nanocubes encapsulated within scrolled sheets of the semiconductor  $H_xK_{4-x}Nb_6O_{17}$ , and were synthesized in high yield via facile one-pot microwave heating method that is fast, reproducible, and more easily scalable than multi-step approaches required by many other state-of-the-art catalysts. The Pt@HNB NPPs unique 3D architecture enables physical separation of the Pt catalysts from competing surface reactions, promoting electron efficient delivery to the isolated reduction environment along directed charge transport

pathways that kinetically prohibit recombination reactions. Pt@HNB NPPs catalytic activity was assessed in direct comparison to representative state-of-the-art Pt/semiconductor nanocomposites (extPt-HNB NSCs) and unsupported Pt nanocubes. Photolysis under identical conditions exhibited superior  $H_2$  production by the Pt@HNB NPPs, which exceeded other catalyst  $H_2$  yields ( $\mu\text{mol}$ ) by a factor of 10. Turnover number (TON) and apparent quantum yield (AQY) values showed similar dramatic increases over the other catalysts. Overall, the results clearly demonstrate that Pt@HNB NPPs represent a unique, intricate nanoarchitecture among state-of-the-art heterogeneous catalysts, offering obvious benefits as a new architectural pathway towards efficient, versatile, and scalable hydrogen energy production. Potential factors behind the Pt@HNB NPPs superior performance are discussed below, as are the impacts of systematic variation of photolysis parameters and the use of a non-aqueous reductive quenching photosystem.

## Funding Statement

This material is based upon work supported by the National Science Foundation under grants CHE-1412670 (C.D.-W.C., T.R., J.B.W) and CHE-2004178 (J.B.W). Work is also supported by the Laboratory Directed Research and Development program at Sandia National Laboratories (C.D.-W.C., L.J.T.), a multimission laboratory managed and operated by National Technology and Engineering Solutions of Sandia LLC, a wholly owned subsidiary of Honeywell International Inc. for the U.S. Department of Energy's National Nuclear Security Administration under contract DE-NA0003525. (This paper describes objective technical results and analysis. Any subjective views or opinions that might be expressed in the paper do not necessarily represent the views of the U.S. Department of Energy of the United States Government).

## Advanced Focused Ion Beams Focus Topic Room A107-109 - Session IB-ThM

### Advances in FIB Instrumentation, Source, Optics, and Surface Analysis

**Moderators:** Alex Belianinov, Sandia National Laboratory, Armin Goelzhaeuser, Uni Bielefeld

8:00am **IB-ThM-1 TIBUSSII - the First Triple Beam Single Ion Implantation Setup for Quantum Applications**, *Nico Klingner, G. Hlawacek, S. Facsko*, Institute of Ion Beam Physics and Materials Research, Helmholtz-Zentrum Dresden - Rossendorf (HZDR), Germany; *J. Silvent, A. Delobbe*, Orsay Physics, France

**INVITED**

The ongoing miniaturization has reached a point where dopants, impurities or active impurities reach the quantum limit, making deterministic single ion implantation (SII) indispensable. Moreover, applications in quantum computing, spintronics, and magnonics require at the same time, a very precise spatial placement of these implants. Other requirements for such an implantation system would be a wide range of available ion species, the ability to implant at extremely low fluence as well as low voltage operation.

Our new system, named TIBUSSII, is expected to address all of these requirements. It will be the first UHV system to include a liquid metal alloy ion source (LMAIS) focused ion beam (FIB) column, a plasma FIB, and a scanning electron microscope (SEM). The 4-nm SEM will be used for damage-free navigation, orientation and inspection. Both FIB columns are mass-separated columns with three Einzel lenses, a chicane for neutral particles, and additional blankers and features optimized for single ion implantation.

We will show the current status of the system, which is currently being installed and further developed by HZDR and Orsay Physics. To verify the implantation of single ions, we are currently developing a secondary electron (SE) detection system with a sensitivity close to unity. It will be based on a semiconductor detector and is expected to surpass the detection efficiency of existing systems based on electron multiplication, such as channeltrons or microchannel plates.

8:40am **IB-ThM-3 A New Tool for Single Ion Implantation and Nanoscale Materials Engineering: System Design and Source Development**, *Gianfranco Aresta, K. Stockbridge, K. McHardy, P. Blenkinsopp*, Ionoptika Ltd., UK

Quantum computing is the next great frontier of science. It has the potential to revolutionize many aspects of modern technology, including digital communications, "quantum-safe" cryptography, and incredibly accurate time measurements.

# Thursday Morning, November 9, 2023

Single impurity atoms in semiconductors are receiving attention as potential quantum technologies, and proof-of-concept devices have shown promise. However, such devices are incredibly challenging to manufacture, as single atoms must be placed within ~ 20 nm of each other within a pure  $^{28}\text{Si}$  matrix.

All working devices thus far have been fabricated using hydrogen lithography with an STM followed by atomic layer deposition. This is labour-intensive and requires several days of meticulous preparation to create just a single quantum bit (qubit). Real-world devices will require arrays of hundreds or thousands of impurity atoms, highlighting the requirement for a scalable method of positioning single atoms with nanometer precision.

We report on a new commercial instrument for the fabrication of quantum materials and devices via single ion implantation.

The instrument features a high-resolution mass-filtered focused ion beam (FIB), a high-sensitivity deterministic implantation system, 6-inch wafer handling, and a high-precision stage. The deterministic implantation system allows single ion implantation with confidence levels as high as 98%.

The ion dose delivered to the sample can be adjusted across a wide range, providing many nanoscale materials engineering capabilities in a single tool, from single ion implantation to direct-write capabilities such as isotopic enrichment and targeted ion-implantation of nanomaterials.

The liquid metal alloy ion sources, coupled with a mass filtered column will enable the implantation of many different elements with isotopic resolution. Available sources include silicon, erbium, gold, and bismuth, while many others of technological interest are in development. We will report on the LMIG source development carried out at Ionoptika in collaboration with our partners.

9:00am **IB-ThM-4 ToF-SIMS on a Plasma FIB: Dos and Dont's, Jamie Ford**, University of Pennsylvania

While time-of-flight secondary ion mass spectrometry (ToF-SIMS) is a well-established analytical technique on dedicated instrumentation, it is uncommon to perform it on a Xe plasma focused ion beam microscope. Introducing a new technique to a central user facility with a novice user base has provided valuable lessons along the way. In this talk I will share some of those lessons, best practices for introducing novel techniques to users along with setting reasonable expectations, how ToF-SIMS can complement more traditional FIB-SEM analytical techniques, and results from the wide variety of polymers, metals, and ceramics investigated in a central academic facility.

9:20am **IB-ThM-5 Multimodal Characterization of Biological Samples on FIB Instruments Combining Nano-Scale SIMS, SE and STIM Imaging Under Ambient or Cryogenic Conditions, Antje Biesemeier, T. Taubitz, O. De Castro, J. Audinot, H. Hoang, P. Philipp**, Luxembourg Institute of Science and Technology (LIST), Luxembourg

**INVITED**

Focused Ion Beam (FIB) based Secondary Ion Mass Spectrometry (SIMS) is a potent technique for imaging and chemical analysis at the ultrastructural level. In a plethora of life and materials science domains, it already proved excellent sensitivity, dynamic range and mass resolution. In this regard and together with leading manufacturers of FIB instrumentation, LIST is developing tailored and compact double focusing magnetic sector mass spectrometers for multimodal analysis at high spatial resolution (< 20 nm, [1]). The advantages over time-of-flight (TOF) systems include the ability of working in the DC mode (providing significantly higher SI counts for a given analysis duration) and higher overall transmission. Moreover, our magnetic sector system is equipped with a continuous focal plane detector, allowing parallel detection of all masses for each scanned sample pixel over the selected mass range. Depending on the FIB platform the SIMS is installed on, the users can correlate SIMS with secondary electron imaging (SE, [1-4]), back-scattered electron imaging (BSE, [2]), and/or scanning transmission ion microscopy-based analysis (STIM, [3, 4]) within the same instrument. The range of primary ions that have been used for magnetic sector FIB-SIMS include  $\text{He}^+$ ,  $\text{Li}^+$ ,  $\text{Ne}^+$ ,  $\text{Ga}^+$ ,  $\text{Bi}^+$  and  $\text{Cs}^+$ .

As a close to native state sample preparation is mandatory for many biomedical research questions, we recently designed and built a new cryo FIB-SIMS platform that is based on an ultra-high brightness Gas Field Ion Source and that is equipped with a custom-made piezo-driven 5-axis cryo-stage along with sub-systems for cryo transfer and sample preparation (such as a specialised low humidity nitrogen atmosphere glovebox). The platform includes detection systems for SIMS, SE and STIM imaging by  $\text{He}^+/\text{Ne}^+$ , which combined with the cryo-capabilities result in an ideal tool for in-situ correlative studies on cryo lamella or other beam sensitive materials like battery materials [5].

Here, we will present an overview of our most recent developments and exemplary data sets from the field of nanotoxicology, demonstrating sub-cellular distribution and chemical identification of individual metal nanoparticles embedded in biological matrices after exposure.

[1] Rep. Prog. Phys. 84 (2021) p. 105901.

[2] Anal. Chem. 94, 30 (2022), p. 10754.

[3] Anal. Chem. 93, 43 (2021), p. 14417.

[4] J. Nanotechnol. 11 (2020), p. 1854.

[5] This work has received funding from the EU's Horizon 2020 Research and Innovation Programme (grant agreement no. 720964) and was supported by the Luxembourg National Research Fund via the projects INTER/DFG/19/13992454 and FNR CORE C21/BM/15754743.

11:00am **IB-ThM-10 Mobile and Non-Mobile Hydrogen in Hydrogen-Charged Zirconium Alloy, Edward Gillman**, Naval Nuclear Lab

Zirconium alloys are widely used for nuclear fuel cladding due to their mechanical behavior, resistance to corrosion, and low thermal neutron absorption cross-section. Over time, hydrogen is absorbed into zirconium alloys and exists as a solid solution so long as the concentration remains within the solubility limit for the alloy. Hydrogen migrates in the alloy and the migration depends on energy-dependent diffusional processes. When the concentration of hydrogen exceeds its solubility in zirconium alloy a non-mobile, brittle hydride phase can form. Embrittlement of zirconium alloy can result in reduced fracture toughness and in a phenomena known as Delayed Hydride Cracking (DHC). Hydrogen in solid solution is quite mobile within zirconium alloys at reactor operating temperatures requiring methods to predict hydrogen migration through the life of the zirconium alloy component. The dissolution and precipitation solvi for zirconium hydrides from zirconium in solid solution is an important aspect in hydrogen migration models. Here we use Time-of-Flight Secondary Ion Mass Spectroscopy (TOF-SIMS) to determine mobile and non-mobile hydrogen in hydrogen-charged zirconium alloys based on the hydrogen concentration in an uncharged commercial standard and LECO analysis for total hydrogen in hydrogen-charged zirconium alloy.

11:20am **IB-ThM-11 Visualization of the Pore Formation in Carbon Microspheres by Charge-compensated Helium Ion Microscopy, Natalie Frese, M. Wortmann, M. Westphal**, Bielefeld University, Germany; E. Diestelhorst, B. Brockhagen, University of Applied Sciences and Arts, Germany; K. Sattler, University of Hawaii; A. Gölzhäuser, Bielefeld University, Germany

Hydrothermal carbonization of aqueous saccharide solutions yields carbonaceous microspheres, which can be post-carbonized by high-temperature pyrolysis to enhance their electrochemical properties for applications in energy storage devices. The pyrolysis leads to the formation of hierarchical porosity, i.e. micro-, meso- and macropores. The underlying mechanism of the pore formation was revealed for the first time using charge-compensated helium ion microscopy. It was shown that oxygen-rich nanoclusters gradually aggregate at the sphere surface, which then disintegrate in a narrow temperature range, leaving behind equally sized mesopores. The observed mechanism sheds light on the formation of hierarchically porous hard carbon materials more broadly.

11:40am **IB-ThM-12 3D Volume and Surface Imaging Applications using Focused Ion Beams from LMAIS, Alexander Ost, A. Nadzeyka, L. Bruchhaus, T. Richter**, Raith GmbH, Germany

State-of-the-art Focused Ion Beam (FIB) technologies are in high demand nowadays as they allow not only to perform nanoscale patterning, but also ion imaging at high spatial resolution and analytical surface measurements with Secondary Ion Mass Spectrometry (SIMS). The liquid metal alloy ion source (LMAIS) technology, including the GaBiLi and AuGeSi sources, has been established for nanofabrication in the recent years [1]. Its excellent beam current stability, patterning and also imaging resolution [2], as well as fast adjusting of the sputtering yield with switching from one ion to the other within a few seconds allow a versatile use of this source technology.

Visualization of nanoscopic samples in 3D is of high interest in various domains, including nanotechnology, life and materials sciences, since it allows to study the surface and internal structure of the material compared to a simple 2D image. While a common method for 3D volume reconstruction consists of slice-wise imaging and milling of the sample involving stage tilt, the new GaBiLi source paves the way for a new approach to obtain 3D volume information. The GaBiLi source has the advantage to alternately analyze the sample by imaging with  $\text{Li}^+$  primary ions at high spatial resolution (down to 1.5 nm) in secondary electron (SE)

# Thursday Morning, November 9, 2023

mode and switching quickly to milling mode with Bi<sup>+</sup> primary ions at a high sputtering rate. Using this Mill&Image workflow the ion beam is always perpendicular to the sample surface and no sample tilt is needed. The set of SE images can be compiled into a 3D stack and cross-sectional views allow to visualize interior structures of the sample (Figure 1 a).

An alternative approach for 3D reconstruction, limiting surface sputtering and fully taking into account the surface topography, has been developed recently. Therefore, series of electron or ion microscopy images [3,4] are acquired around a region of interest (ROI). The images are implemented into a photogrammetry software used to obtain a 3D surface model (Figure 1 b) allowing detailed observation at all possible angles and magnifications, and even further numerical analysis [4].

In this contribution, we will demonstrate the capabilities of the Raith VELION FIB-SEM system equipped with GaBiLi/AuGeSi sources for 2D and 3D imaging workflows and give an outlook for combining in-situ 3D topographical information with analytical surface information from SIMS using these sources.

[1] L. Bischoff et al. *Appl.Phys.Rev.* 2016, 3(2),021101.

[2] N. Klingner et al. *Beilstein J.Nanotechnol.* 2020,11,1742–1749.

[3] F. Vollnhals, T. Wirtz. *Anal.Chem.* 2018, 90(20),11989–11995.

[4] A. D. Ost et al. *ES&T* 2021, 55(13),9384-9393.

**12:00pm IB-ThM-13 Application of Helium Ion Microscope in Site Specific Material Radiation Studies, Vaithiyalingam Shutthanandan, S. Lambeets, A. Devaraj,** Pacific Northwest National Laboratory

Helium ion microscopy (HIM) enables not only the imaging of materials with Helium ions but also the irradiation of materials with a focused Helium beam (0.25 nm diameter beam spot) to achieve controlled displacement damage and Helium dosing. In the past, several different ODS steels, nanostructured ceramic materials, and nanolayered thin films have been investigated to understand the fundamental mechanism of radiation damage. In many of these investigations, high-energy He ion irradiations were carried out in a large area over the entire specimen, followed by the characterization of radiation damage. The spot size of ion irradiation beams from conventional sources was in the order of 100s of microns or larger, preventing site-specific irradiation damage investigation of individual microstructural features. In such cases, often the overall irradiation damage evolution in the material would be a cumulative response of the entire material microstructure (grain boundaries, interphase interfaces, second phase precipitates, nano-crystalline regions, and other preexisting defects) to the ion beam irradiation. A nanoscale site-specific He ion irradiation method can aid in decoupling and individually analyzing the He ion irradiation response of different microstructural features in a mutually exclusive manner. We have developed methods to use the helium ion microscope (HIM) to irradiate specific sites (i.e., near grain interiors vs. grain boundaries or near and on precipitates) of metallic materials using helium ions in a controlled manner and to characterize these materials in combination with focused ion beam scanning electron microscopy (FIB/SEM), TEM, XPS, and APT. In this talk, recent studies utilizing HIM as a radiation tool will be discussed in detail.

## Light Sources Science Mini-Symposium

### Room C124 - Session LS+AC+LX+MI+TH-ThM

#### Tender X-ray Science and Time Resolved Studies

**Moderators: Alison Pugmire,** LANL, **David Shuh,** Lawrence Berkeley National Laboratory, **James G. Tobin,** University of Wisconsin-Oshkosh

**8:00am LS+AC+LX+MI+TH-ThM-1 Developments of High Resolution X-Ray Spectroscopic Tools for Probing Structural Properties of Actinide System from the Metal and Ligand Perspective, Tonya Vitova,** Karlsruhe Institute of Technology, Institute for Nuclear Waste Disposal, Germany **INVITED**

High energy resolution X-ray absorption and emission spectroscopic techniques became indispensable methods in actinide and radionuclide research.<sup>1-5</sup> One important motivation is studies concerning the mobilization and retention of long-lived actinides and fission products in geochemical processes relevant for safety studies of a potential deep geological nuclear waste repository.<sup>3-4</sup> In-depth insights into the actinide-ligand binding properties is a main application of these novel experimental techniques too.<sup>6</sup> Development at the ACT experimental station of the CAT-ACT wiggler beamline at the Karlsruhe Institute of Technology (KIT) Light Source will be discussed. One experimental technique especially powerful

to differentiate oxidation states of actinides (An) is the An M<sub>4,5</sub>-edge high-energy resolution X-ray absorption near-edge structure (HR-XANES).<sup>4</sup> This presentation highlights the latest technological developments at the ACT station enabling the HR-XANES spectroscopic technique for samples with low radionuclide loading down to 1 ppm in combination with a cryogenic sample environment reducing beam-induced sample alterations.<sup>7-8</sup> It paves the way for the examination of coupled redox/solid-liquid interface reactions.<sup>8</sup> Examples of applications of An M<sub>4,5</sub> edge core-to-core and valence band resonant inelastic X-ray scattering (CC-RIXS and VB-RIXS) for probing the electronic structure and binding properties of the actinide elements will be illustrated.<sup>6</sup> First results obtained using a newly developed versatile chamber for soft X-ray spectroscopy at the X-SPEC beamline at the KIT Light Source will be discussed.

*This work has received funding from the European Union's Horizon 2020 research and innovation program under grant agreement No. 847593. We also acknowledge funding from the ERC Consolidator Grant 2020 under the European Union's Horizon 2020 research and innovation program (grant agreement No. 101003292).*

#### References

1. Vitova, T. et al., *Inorganic Chemistry* **2020**,59 (1), 8-22.

2. Vitova, T. et al., *Chem Commun* **2018**,54 (91), 12824-12827.

3. Vitova, T. et al., *Nature Communications* **2017**,8, 16053.

4. Pidchenko, I. et al., *Environ Sci Technol* **2017**,51 (4), 2217-2225.

5. Bagus, P. S. et al., *Inorganic Chemistry* **2021**,60 (21), 16090-16102.

6. Vitova, T. et al., *Chem Sci* **2022**,13 (37), 11038-11047.

7. Schacherl, B. et al., *J Synchrotron Radiat* **2022**,29 (1), 80-88.

8. Schacherl, B. et al., *Anal Chim Acta* **2022**,1202, 339636.

**8:40am LS+AC+LX+MI+TH-ThM-3 High-Energy-Resolution X-Ray Spectroscopy and Actinides Research at SLAC, Dimosthenis Sokaras,** SLAC National Accelerator Laboratory **INVITED**

Nowadays, high-energy-resolution x-ray spectroscopy is a well-established and powerful tool available in state-of-the-art synchrotron facilities. The suppression of the core-hole lifetime contribution within the conventionally broad spectroscopic features of actinide series has revitalized the role of x-ray spectroscopy in the study of actinide complexes and intermetallics. Numerous studies have leveraged the fine structure of M or L absorption edge resonances to sensitively probe and quantify the oxidation state, 5f delocalization, and ligation of the actinides species. The increasing availability of large solid angle instruments coupled with high flux beamlines is quickly enabling such advanced studies for dilute samples or samples under special sample environments. In this presentation we will summarize the high-resolution tender and hard x-ray spectroscopy advances at SLAC and the actinides research program that these capabilities have enabled during the last decade.

**9:20am LS+AC+LX+MI+TH-ThM-5 New Insight Into Excited-State Chemical Dynamics Using Ultrafast X-Rays:Recent Highlights, Future Opportunities & Development Plans at LCLS, Robert Schoenlein,** Linac Coherent Light Source - SLAC National Accelerator Laboratory **INVITED**

Ultrafast X-rays from free-electron lasers (XFELs) are driving a qualitative advance in our understanding of condensed-phase chemical dynamics and catalysis. Ultrafast soft X-rays provide element-specific mapping of chemical bonds, charge distributions, oxidation states and frontier orbitals. Ultrafast hard X-ray pulses reveal the atomic scale structural dynamics of excited-state dynamics – revealing relaxation pathways, and the coupling of atomic structure, electronic structure, and solvent dynamics. This talk will highlight recent results from the Linac Coherent Light source (LCLS) using advanced ultrafast X-ray methods to track excited-state charge-transfer and relaxation pathways, and reveal the influence of molecular structural dynamics, and solvent coupling. Notably, multi-modal methods combining time-resolved X-ray scattering and spectroscopy represent a powerful approach for linking X-ray experimental observables with theory to achieve a deeper understanding of excited-state dynamics to advance the development of design principles for creating molecules, complexes, and assemblies with desired functions.

In addition, new science opportunities enabled by the nearly-completed upgrade of LCLS (LCLS-II) coupled with advanced instrumentation and methods will be discussed. LCLS-II will provide tunable soft X-ray pulses (0.25 to 5.0 keV) at high repetition rate (up to 1 MHz) and hard X-rays up to

# Thursday Morning, November 9, 2023

25 keV (at 120 Hz). This unprecedented capability will support powerful new methods such as time-resolved resonant inelastic X-ray scattering (RIXS). The new ChemRIXS instrument is optimized for studying solvated complexes with C, N, O (K-edges), 3d transition metals (L-edges), and rare-earth elements (M-edges) – where 2D RIXS maps of excited-state dynamics coupled with quantum chemical calculations will reveal the evolution of frontier orbitals. The Tender X-ray Instrument (TXI, 2.1-5.0 keV), now under development for LCLS-II, will support time-resolved tender X-ray spectroscopy (spanning the 4d transition metal L-edges and key functional ligands including P, S, and Cl), coherent scattering, and novel nonlinear X-ray pump / X-ray probe methods - combining X-rays from two independently tunable XFEL sources.

11:00am **LS+AC+LX+MI+TH-ThM-10 Attosecond Studies of Radiolysis at XFELs**, **Linda Young**, Argonne National Laboratory **INVITED**

We report the first attosecond x-ray pump/x-ray probe transient absorption study in condensed phases using a pure liquid water target. With tunable two-color attosecond x-ray pulses, the pump ionizes the valence band of water and the probe scans the oxygen K-edge absorption region. Theory establishes the nature of the detected transient absorption and models the observed signal for sub-femtosecond delay times.

**Acknowledgements:** This work supported in part by the US Department of Energy, Office of Science, Basic Energy Sciences, Chemical Sciences, Geosciences, and Biosciences Division under award # DEAC02-06CH11357. Use of the Linac Coherent Light Source (LCLS), SLAC National Accelerator Laboratory, is supported by the U.S. Department of Energy, Office of Science, Office of Basic Energy Sciences under Contract No. DE-AC02-76SF00515.

critical importance for fields ranging from cancer therapy to the longevity of nuclear reactors to space travel. In these applications, radiolysis is initiated by a high-energy particle that leads to the ejection of energetic primary electrons followed by inelastic and non-adiabatic processes that produce damaging low energy electrons and reactive radical species. A microscopic understanding of reaction mechanisms, especially in complex systems, is missing as typical techniques used to detect prominent species, EPR and UV spectroscopies, lack either time resolution or spectral clarity. Tunable ultrafast x rays can dissect the radiolysis process. That is, x-ray pump/x-ray probe studies can systematically either peel electrons from valence, or eject them from core orbitals and follow the ensuing dynamics on a site-specific basis.

11:40am **LS+AC+LX+MI+TH-ThM-12 First Real-Time Tracking of Oxidation States During Fast Redox of UO<sub>2</sub> Using a Microfluidic Electrochemical Cell and HR-XANES**, **Jennifer Yao**, Pacific Northwest National Laboratory; **B. Schacherl**, Karlsruhe Institute of Technology (KIT), Germany; **B. McNamara**, Pacific Northwest National Laboratory; **C. Vollmer**, Karlsruhe Institute of Technology (KIT), Germany; **N. Lahiri**, **E. Ilton**, **E. Buck**, Pacific Northwest National Laboratory; **T. Vitova**, Karlsruhe Institute of Technology (KIT), Germany

Real-time tracking of the oxidation states of a UO<sub>2</sub> electrode during electrochemical oxidation and reduction was achieved using operando high-resolution X-ray absorption near-edge structure (HR-XANES) spectroscopy at the ACT station of the CAT-ACT beamline at the KIT Light Source, Karlsruhe, Germany. This was made possible by utilizing a particle-attached microfluidic electrochemical cell (PAMEC) developed at PNNL, and employing KIT's advanced actinide M-edge HR-XANES technique.<sup>1-2</sup> The PAMEC is a three-electrode system consisting of a working electrode (WE) made of the materials of interest a platinum (Pt) reference electrode, and a Pt counter electrode.<sup>3</sup> The electrochemical analyzer connected to the PAMEC device controlled the redox process, e.g., applying constant potential on the UO<sub>2</sub> WE to reduce (-1.1 V vs Pt) or oxidize it (0.5 V vs Pt), while HR-XANES simultaneously scanned its surface chemistry. The U M-edge HR-XANES spectra revealed the evolution of U from U(IV) to U(V) and finally to U(VI) during the oxidation process. We were able to demonstrate the reversibility of this process by reducing the same electrode back to pure U(IV), as confirmed by HR-XANES. To our knowledge, this study reports the first in-situ and operando measurement of real-time oxidation state changes of UO<sub>2</sub>. The spectra obtained also provided insight into the electronic structure of U(VI) in the UO<sub>2</sub> alteration process. This successful international scientific collaboration showcases the potential of a PAMEC for in-situ and operando experiments with UO<sub>2</sub> and highlights its promising broad application for characterization of spent nuclear fuel systems.

References:

(1) Vitova, T.; Pidchenko, I.; Fellhauer, D.; Bagus, P. S.; Joly, Y.; Pruessmann, T.; Bahl, S.; Gonzalez-Robles, E.; Rothe, J.; Altmaier, M.; Denecke, M. A.; *Thursday Morning, November 9, 2023*

Geckeis, H., The role of the 5f valence orbitals of early actinides in chemical bonding. *Nature Communications* **2017**,*8*, 16053. 10.1038/ncomms16053  
(2) Schacherl, B.; Prüssmann, T.; Dardenne, K.; Hardock, K.; Krepper, V.; Rothe, J.; Vitova, T.; Geckeis, H., Implementation of cryogenic tender X-ray HR-XANES spectroscopy at the ACT station of the CAT-ACT beamline at the KIT Light Source. *Journal of synchrotron radiation* **2022**,*29*, 80-88. 10.1107/s1600577521012650

(3) Yao, J.; Lahiri, N.; Tripathi, S.; Riechers, S. L.; Ilton, E. S.; Chatterjee, S.; Buck, E. C., A microfluidic electrochemical cell for studying the corrosion of uranium dioxide (UO<sub>2</sub>). *RSC Advances* **2022**,*12*, 19350-19358. 10.1039/D2RA02501A

12:00pm **LS+AC+LX+MI+TH-ThM-13 Use of Artificial Intelligence Techniques To Analyze Materials Characterization Data From Actinide Containing Materials**, **Jeff Terry**, Illinois Institute of Technology

We have developed artificial intelligence (AI) based methodology that can be utilized to reliably analyze experimental results from Extended X-ray Absorption Fine Structure (EXAFS), Nanoindentation, and core level photoemission. Specifically, we use a genetic algorithm to extract the relevant structural parameters through fitting of the measured spectra. The current approach relies on a human analyst to suggest a potential set of chemical compounds in the form of feff.inp input files that may be present. The algorithm then attempts to determine the best structural paths from these compounds that are present in the experimental measurement. The automated analysis looks for the primary EXAFS path contributors to the potential compounds. It calculates a goodness of fit value that can be used to identify the chemical moieties present. The analysis package is called EXAFS Neo and is open source written in Python. I will illustrate the use of this package with fits of actinide species in the barrier layer of Tristructural-isotropic (TRISO) encapsulated nuclear fuel particles. The current particle design consists of a two-phase uranium-oxide/uranium-carbide kernel of 19.74% <sup>235</sup>U enrichment, a porous carbon buffer layer, and consecutive layers of pyrolytic carbon, silicon carbide (SiC) and pyrolytic carbon. The SiC layer provides the main barrier to fission product release. Much work has gone towards studying metallic fission product interaction in the SiC containment layer due to the propensity of metallic fission product release as a function of high temperature (safety) testing. Here, I will show how the interaction dynamics of plutonium and uranium within this layer have been determined through EXAFS measurements that have been fit with AI. One of the major benefits of using this technology is that actinide containing materials often have edges from higher Z-elements that limit the usable range of the spectrum. Our method fits momentum space data which does not suffer from transformation artifacts of real space over a small momentum range.

**Magnetic Interfaces and Nanostructures Division**  
**Room B110-112 - Session MI+2D+TF-ThM**

**2D Magnetism and Superconductivity**

**Moderators:** **Markus Donath**, Muenster University, Germany, **Valeria Lauter**, Oak Ridge National Laboratory

8:00am **MI+2D+TF-ThM-1 Heterostructures for Tunneling and Point-Contact Spectroscopy of Two-Dimensional Superconductors**, **Benjamin Hunt**, **Q. Cao**, Carnegie Mellon University; **E. Telford**, **C. Dean**, Columbia University **INVITED**

Tunneling spectroscopy is an indispensable experimental tool of modern condensed matter physics. Vertical planar tunneling, which uses a fixed-width tunnel barrier, offers advantages over other spectroscopic tools such as scanning tunneling microscopy (STM). One such advantage is the ability to tunnel in reorientable and very large ( $\geq 40$  T) magnetic fields at dilution refrigerator temperatures ( $\leq 30$  mK), a capability that has application in, for example, determining the order parameter symmetry of novel two-dimensional (2D) superconductors. We demonstrate a novel vertical planar tunneling architecture for van der Waals heterostructures based on via contacts, namely, metallic contacts embedded into through-holes in hexagonal boron nitride (hBN). This via-based architecture overcomes limitations of other planar tunneling designs and produces high-quality, ultra-clean tunneling structures from a variety of 2D materials. The physical area of our via-based tunnel contacts is limited only by nanofabrication techniques, and we demonstrate a crossover from diffusive to point contacts in the small-contact-area limit by studying the spectrum of a 2D superconductor, NbSe<sub>2</sub>. We show that our tunneling technique may enable highly-sought measurements of newly-discovered 2D superconductors such

# Thursday Morning, November 9, 2023

as monolayer 1T'-WTe<sub>2</sub>, rhombohedral trilayer graphene, twisted trilayer graphene, and twisted bilayer BSCCO.

8:40am **MI+2D+TF-ThM-3 Ghost States and Topography Inversion in 2D Materials**, *Mina Yoon*, Oak Ridge National Laboratory, USA **INVITED**

In this talk, I will discuss the challenges associated with characterizing the surface structures of single-atom thick materials, such as graphene and boron nitride, on metallic substrates or the surface of bulk systems, including quantum topological Kagome systems, using scanning tunneling microscopy (STM). The understanding of fundamental properties of two-dimensional (2D) materials and surface properties depends critically on the presence of "ghost" states, which arise due to different decay lengths in the wave function of the underlying layers and surfaces.

The existence of these ghost states, in conjunction with long-lived substrate states or underlying layers, plays a crucial role in interpreting and understanding the surface properties of 2D materials. These ghost states can originate from various sources, such as the bulk or the substrate, and can even arise from the boundary on the opposite side. The appearance of ghost states due to different decay lengths leads to unexpected results in surface structure measurements, including the intriguing phenomenon of topography inversion. Topography inversion refers to the counterintuitive result where the observed topography in STM images is opposite to the expected atomic geometry, as discussed in our recent study [1,2]. This inversion occurs as a consequence of the pervasive substrate states overshadowing the intrinsic states of the 2D materials. As a result, the measurement of the intrinsic properties of 2D materials becomes complicated, with the ghost and substrate states dominating the observed topography. To address these challenges, we employ a combination of first-principles density functional theory calculations and analytical modeling. Through our investigations, we demonstrate the critical role played by these ubiquitous substrate and ghost states in the observed topography inversion in STM images. By unraveling the influence of these states on STM measurements, we provide crucial insights for the accurate interpretation of STM topographies of atomically thin materials.

Our findings not only shed light on the phenomenon of topography inversion, but also contribute to the further development of 2D materials in (opto)electronic and quantum applications. Understanding and characterizing the ghost and substrate states is essential to unlock the full potential of 2D materials and enable their use in various technological advancements.

[1] "Spatially resolved on-dimensional boundary states in graphene-hexagonal boron nitride planar heterostructures", J. Park et al., Nat.Com. 5, 5403 (2014).

[2] "Topography inversion in scanning tunneling microscopy of single-atom-thick materials from penetrating substrate states", C. Park and M. Yoon, Sci. Reports 12, 7321 (2022).

11:00am **MI+2D+TF-ThM-10 Spatially-Resolved Photoemission Studies of Magnetic Weyl Semimetals**, *S. Sreedhar*, University of California, Davis; *M. Staab*, *R. Prater*, University of California at Davis; *A. Rossi*, Italian Institute of Technology, Italy; *V. Ivanov*, Lawrence Berkeley Lab; *Z. Shen*, University of California at Davis; *G. Conti*, Lawrence Berkeley Lab; *V. Taufour*, *S. Savrasov*, University of California at Davis; *S. Nemsak*, Lawrence Berkeley Lab; *Inna Vishik*, University of California-Davis **INVITED**

Co<sub>3</sub>Sn<sub>2</sub>S<sub>2</sub> is a magnetic Weyl semimetal below its Curie temperature (T<sub>c</sub>) of 177K. I will discuss spatial and temperature-dependent angle-resolved photoemission spectroscopy (ARPES) and x-ray photoelectron spectroscopy (XPS) studies in this system. Across T<sub>c</sub>, we observe signatures of a topological phase transition, but also observe changes in bulk bands which are inconsistent with a simple lifting of exchange interactions, suggesting enhanced electronic correlations in the regime without long-range magnetic order. I will also discuss spatial-dependent ARPES and XPS data which quantify the characteristic differences between Sn- and S-terminated surfaces, with relevance for interpreting surface-dominated phenomena.

11:40am **MI+2D+TF-ThM-12 High-Temperature Superconductor FeSe Films Enabled Through Temperature and Flux Ratio Control**, *Maria Hilse*, *H. Yi*, *C. Chang*, *N. Samarth*, The Pennsylvania State University; *R. Engel-Herbert*, Paul-Drude-Institut für Festkörperelektronik, Germany

FeSe, a bulk superconductor with a T<sub>c</sub> of 9 K has attracted a high level of attention since a skyrocketing boost in TC was reported for a single unit cell (UC) layer of FeSe grown on SrTiO<sub>3</sub>(001) by molecular beam epitaxy (MBE) to as high as 100 K. FeSe-SrTiO<sub>3</sub> heterostructures have since been fabricated by many groups but the record TC proved difficult to reproduce

and thus the mechanism behind it remains concealed. After extensive work in the past, the field appears to agree on certain key "ingredients" in the heterostructure sample preparation that are believed essential for the boost in TC. Those are; 1. an ultra-clean substrate surface of a double TiO<sub>2</sub> termination realized by a chemical and thermal *ex-situ* and/or thermal *in-situ* substrate preparation; 2. ultra-thin – one UC thickness – limit of FeSe; 3. a high number of Se vacancies in the FeSe film ensured through post-growth annealing steps in ultra-high vacuum (UHV) for several hours; 4. followed by a capping layer growth protecting FeSe against oxidation during *ex-situ* characterization.

We present our findings on FeSe thin film growth by MBE and present a roadmap for high-T<sub>c</sub> – 222 % higher than the reported bulk value in *ex-situ* transport measurements – circumventing above mentioned steps 1, 2, and 3 by simple *in-situ* Se/Fe flux ratio and temperature control during FeSe growth. FeSe films of 20-UC-thickness grown at varying temperatures and Se/Fe flux ratios and the structural and morphological properties of the obtained uncapped FeSe films were analyzed. The morphology of the films showed a sensitive dependence on the growth temperature and flux ratio spanning from perfectly smooth and continuous films with atomic terraces at 450 °C growth temperature and a low flux ratio of 2.5 to exclusively disconnected island growth of large height but smooth top surfaces at lower temperatures and/or higher flux ratios. Surprisingly, the tetragonal P4/nmm crystal structure of beta-FeSe was maintained for all investigated films and the *in-situ* observed diffraction pattern in reflection high energy diffraction also maintained the streaky pattern characteristic for smooth FeSe films even for the samples with the most pronounced island growth resulting in a root mean square atomic force microscopy roughness of more than 18 nm. Smaller flux ratios than 2.5 resulted in mixed – beta-FeSe/elemental Fe – phase samples. FeSe films grown under optimized conditions at 450 °C and a flux ratio of 2.5 (but without any post-growth UHV anneal) and capped with the commonly used FeTe (300 °C) and elemental Te (room temperature) layers yielded superconducting onset temperatures of about 30 K and a TC of 20 K.

12:00pm **MI+2D+TF-ThM-13 Unraveling Picosecond Dynamic Material Processes on the Mesoscale by X-Ray Microscopy**, *Thomas Feggeler*, University of California, Berkeley; *J. Lill*, *D. Guenzing*, *R. Meckenstock*, *D. Spoddig*, *B. Zingsem*, University of Duisburg-Essen, Germany; *M. Efremova*, Eindhoven University of Technology, Netherlands; *S. Pile*, *T. Schaffers*, Johannes Kepler University, Austria; *S. Wintz*, Max Planck Institute for Intelligent Systems, Germany; *M. Weigand*, Helmholtz Center Berlin, Germany; *A. Ney*, Johannes Kepler University, Austria; *M. Farle*, *H. Wende*, *K. Ollefs*, University of Duisburg-Essen, Germany; *D. Shapiro*, Lawrence Berkeley National Laboratory; *R. Falcone*, University of California, Berkeley; *H. Ohldag*, Lawrence Berkeley National Laboratory

Dynamic processes govern a multitude of phenomena in physical, chemical and material sciences. Time- and spatially resolved element-specific monitoring of such processes is crucial in the understanding of phenomena like magnetization dynamics, battery charging and discharging, and phase transitions of several kinds. Time-Resolved Scanning X-ray Microscopy (TR-STXM) [1] is a versatile tool fulfilling these demands on the mesoscopic scale, offering element-specific observations with sub 50 nm spatial resolution and picosecond time sampling. By introducing a phased-locked-loop excitation synchronization scheme, TR-STXM also allows to sample dynamics originating from continuous wave excitations. This presentation introduces the TR-STXM technique and its principle of operation, and the setup developed at the Advanced Light Source at Lawrence Berkeley National Laboratory. The presentation is complemented by examples of dynamic magnetic measurements, which allow for local monitoring of magnetization dynamics in fields such as spintronics, magnonics, biomedical and energy related applications. Here we demonstrate TR-STXM results on Py/Co microstructures [2], Py stripe ensembles [3] and magnetite nanoparticle chains inside magnetotactic bacteria *Magnetospirillum Magnetotacticum* [4,5], showcasing localized uniform and non-uniform resonant magnetic responses, supplemented by micromagnetic simulations in good agreement.

This work is funded by German Research Foundation projects OL513/1-1, 321560838, 405553726 TRR 270, and the Austrian Science Fund project: I 3050-N36. Lawrence Berkeley National Laboratory is acknowledged for funding through LDRD Award: Development of a Continuous Photon Counting Scheme for Time Resolved Studies. T.F. and R.F. acknowledge support from STROBE: A National Science Foundation S&T Center, under Grant No. DMR-1548924. This research used resources of the Advanced Light Source, a U.S. DOE Office of Science User Facility under contract no. DE-AC02-05CH11231. The use of the Stanford Synchrotron Radiation

# Thursday Morning, November 9, 2023

Lightsource, SLAC National Accelerator Laboratory, is supported by the US Department of Energy, Office of Science, Office of Basic Energy Sciences under Contract No. DE-AC02-76SF00515. We thank HZB for the allocation of synchrotron radiation beamtime.

- [1] T. Feggeler, A. Levitan, et al. *J. Electron Spectrosc. Relat. Phenom.* 2023. **267**: 147381.
- [2] T. Feggeler, R. Meckenstock, et al. *Sci. Rep.* 2022, **12**:18724.
- [3] S. Pile, T. Feggeler, et al. *Appl. Phys. Lett.* 2020, **116**(7): 072401.
- [4] T. Feggeler, R. Meckenstock, et al. *Phys. Rev. Res.* 2021, **3**(3): 033036.
- [5] T. Feggeler, J. Lill, et al. *New J. Phys.* 2023, **25**(4): 043010.

## Plasma Science and Technology Division Room A106 - Session PS1+MS-ThM

### AI/ML in Plasma Applications

**Moderators:** Robert Bruce, IBM Research, T. J. Watson Research Center, Yu-Hao Tsai, TEL Technology Center, America, LLC

8:00am **PS1+MS-ThM-1 Approaches to Accelerate Etch Process Optimization by Using Virtual Experiment**, *Tetsuya Nishizuka, R. Igosawa, T. Yokoyama, K. Sako, H. Moki, M. Honda*, Tokyo Electron Miyagi, Ltd., Japan  
**INVITED**

High Aspect Ratio Contact (HARC) hole etching is one of the processes which require a lot of efforts to optimize etch condition. As the aspect ratio increases, some issues such as “distortion” and “twisting” which are hole circularity degradation and deviation from vertical etch respectively, have been critical. Since they cause asymmetric profile along hole axis, not only vertical but also horizontal cross section is necessary to observe 3D profile image, it takes more time to conduct a series of experiments, and then it makes the optimization more difficult.

In this study, we created a model for a topography simulation which is based on Monte Carlo method, so that we can conduct “virtual experiment” on the simulator and expect to reduce the number of experiments by understanding etch mechanism. With respect to practicability for model building, we employed a procedure that representative ion and radical parameters which associate with etching behavior are carefully fitted to actual experimental results [1].

As the result, while this kind of asymmetric distortion profile is supposed to come from stochastic variation and charging in the hole [2], we found there is another systematic factor that is an interaction between re-deposition of sputtered etch material and initial mask profile by analyzing Amorphous Carbon Layer (ACL) etching precisely [3]. This model is consisted with the fact that the distortion deteriorates under low temperature condition. It was also applied to oxide-nitride (ON) layers etch and well reproduced twisting profile on the simulator.

Additionally, we attempted an automatic parameter fitting by using ML optimization for the purpose to minimize efforts in case of converting the model to the other applications than HARC.

- [1] Ohmine et. al., *Jpn. J. Appl. Phys.* 50 (2011)
- [2] Huang et. al., *J. Vac. Sci. Technol. A* 37 (2019)
- [3] Igosawa et. al., Proceedings of international symposium on dry process 2022

8:40am **PS1+MS-ThM-3 Recipe Optimization for Plasma Etching with Machine Learning Model Trained by Initial Dataset Using D-Optimal Design**, *Ryo Morisaki, T. Ohmori*, Hitachi, Ltd., Japan

The development of semiconductor fabrication processes is becoming more difficult due to a growing need for the miniaturization of semiconductor devices to the nano-scale level. Furthermore, growing demands for cutting-edge semiconductor devices of superior performance necessitate the swift development of the fabrication processes.

Plasma etching is a pivotal technique for semiconductor processes. Machine learning (ML) methods have been applied to optimize the recipe for these processes, which is a control parameter set including items such as plasma generation power, wafer bias power, gas species for plasma generation, and the flow rate of gases[1][2]. Datasets for training the ML model consist of recipes and their corresponding etching profiles. Generally, the recipes are curated by expert process engineers to reduce the cost of the etching experiments. On the other hand, design of experiments (DoE) methods can be utilized to obtain the training datasets without expert knowledge. Therefore, DoE has the potential to increase of the number of engineers who can optimize recipes for difficult etching processes.

In this work, two distinct approaches for creating an initial dataset for the training are compared to evaluate the efficiency of recipe optimization using an ML model. In the first approach, the initial dataset is created on the basis of the plasma etching knowledge of expert engineers, as has been conventionally practiced, and in the second approach, it is created on the basis of elementary knowledge for etching tool operations and a DoE method with the D-optimal criterion is used[3]. In the latter approach, a preliminary range of values for the recipe parameters, in which plasma generation and etching can occur, is established on the basis of fundamental knowledge of plasma etching. Subsequently, D-optimization is conducted on the recipe parameters within the specified range to generate a high-quality and diverse initial dataset that can improve the ML model for optimizing the recipes and profiles. In contrast to the conventional DoE with orthogonal array, this DoE with the D-optimal criterion method has no limitation on the number of experiments, thus making it suitable for creating small initial datasets to reduce the cost of the etching experiments. We report detailed comparison results of the efficiency of the etching optimization using each approach.

- [1]T. Ohmori et al., in Proc. Int. Symp. Dry Process, pp. 9–10 (2017).
- [2]H. Nakada et al., in Proc. Int. Symp. Dry Process, pp. 53–54 (2019).
- [3]J. Keifer, *Journal of the Royal Statistical Society. Series B (Methodological)*, vol. 21, no. 2, pp. 272–319 (1959).

9:00am **PS1+MS-ThM-4 Digital Twin Model to Compensate for Variations in Plasma Etching Process**, *T. Nakayama, T. Ohmori*, Hitachi, Ltd., Japan; *Naoto Takano*, Hitachi High-tech America, Inc.

The miniaturization of semiconductor devices based on Moore's Law has necessitated increasingly demanding precision in the mass production of devices. To achieve a target etching profile with nano-scale accuracy during the manufacturing process, plasma etching systems must be equipped with technologies to minimize variations of the etching. A set of parameters for the control function of the etching system is called a recipe, which is used as input data for the system. While the same recipe is used for all systems in mass production, the etching profiles are varied due to the drift of etching chamber conditions or differences in the conditions of the inner chamber parts replaced at the time of chamber maintenance. Etching rate (ER) data are often utilized to check the variations of chamber conditions and construct a compensation model, but a large ER dataset is required for the model, which is time consuming.

Therefore, we have been investigating a compensation method that requires only a small amount of data. In our method, first, a reference digital twin (DT) model utilizing neural networks is trained by sufficient data. A large amount of the training data consisting of recipes and ER can be prepared in advance by experiments using a reference chamber. Further, in addition to the experimental ER, simulation data of ion and radical fluxes correlating with ER (calculated by a plasma simulator) are used for the training data [1]. The simulation data can also be prepared in advance. Next, a small amount of ER data is obtained from a target chamber that has a different ER from that in the reference chamber. A target DT model is

# Thursday Morning, November 9, 2023

obtained by additionally training the reference DT using the small amount of ER data. Finally, a recipe that compensates for the ER difference is predicted using the target DT.

We prepared several hundred experimental ER data and calculated fluxes data using the reference chamber and the plasma simulator, respectively. Several tens of ER data were obtained as a small amount of data using a target chamber. Predicted recipes by the trained target DT model for ER compensation were experimentally verified in the target chamber. As a result, the ER difference used to check the variation of chamber conditions was decreased by our compensation method using DT models.

[1] T. Nakayama et al., Proc. Gaseous Electronics Conf., Sendai (2022).

9:20am **PS1+MS-ThM-5 Deep Learning-Enabled Plasma Equipment Design Optimization in Semiconductor Manufacturing**, S. Ahn, Jinkyu Bae, S. Yoo, S. Nam, Samsung Electronics, Republic of Korea

In plasma reactors, a focus ring which surrounds the wafer plays an important role in improving uniform fluxes and energy across the wafer. To ensure the uniformity and consistent processes, sophisticated design for the focus ring is necessary. However, focus ring design is very challenging due to the complexity of the design space and the high-dimensional geometry of the focus ring. Furthermore, the multi-scale and multi-physics nature of low-temperature plasmas (LTPs) makes it difficult to develop accurate simulation models that can capture the dynamics of plasma discharges. Simulating LTPs is the need to consider multiple physical and chemical processes that occur simultaneously, such as ionization, recombination, excitation, and attachment. These processes can be highly nonlinear and require a large range of integrating time scales from picosecond to millisecond. In this study, we present a Deep Neural Network framework employing the DeepONet, which is pre-trained deep neural operators between each physical quantities on behalf of physical governing equations. The training data is generated using HPEM (The Hybrid Plasma Equipment Model) plasma simulation solver. The framework involves two network types. The first network reduces the dimensions of the focus ring geometries to a latent representation. We used a geometric attention mechanism in Variational-Auto-Encoder (VAE) allowing us to discover the latent geometric features of focus ring parts. The high-dimensional design space was effectively reduced by the neural network model. We proposed the concept of using this latent representation in combination with the pre-trained neural networks. We pre-trained deep neural operators that can predict independently physical quantity fields, given general inputs. It is an efficient way of incorporating the plasma physics without embedding the partial differential equations into the loss function of the neural network. The proposed framework is shown to be efficient and effective in optimizing the focus ring design for different objectives, and the effects of variations in the design are thoroughly investigated based on very few measurements using pre-trained deep neural operators. This paper aims to develop framework for predicting plasma dynamics and carrying out focus ring design in reactors.

9:40am **PS1+MS-ThM-6 Wafer Arcing Detect Algorithm Using LSTM Autoencoder in Hardmask Strip Equipment with CCP Source**, Heewoong Shin, PSK, Republic of Korea

“Wafer arc” is one of the phenomenon that occur in semiconductor manufacturing equipment that utilizes plasma, rather than being limited to arc discharge in plasma science. In this study, we discuss the possibility of successfully classifying normal manufacturing process of semiconductor equipment using CCP and the abnormal data by using deep learning methodology. In general, since wafer arcs data have an obvious characteristics that engineers can easily notice, it is thought that they can also easily be detected by general SPC methodology. But in some cases, there are pattern anomalies that cannot be detected by SPC, or there are problems such as requiring the subjectivity of engineers for determining the data is normal or not because it is hard to find common in each abnormal data. Because wafer arcs might cause serious malfunctions in most equipment and are a major cause of yield reduction, so a function that can diagnose abnormalities in advance is required. However, wafer arcs are generally known to be difficult to reproduce to make abnormal data, and there are problems such as requiring high-resolution optical equipment to detect the arc phenomenon which also costs additional charge. In this study, we used specific parameters in lotlog of CCP equipment as an input of DL model. By training with LSTM-autoencoder, it shows the possibility of classifying normal and abnormal data successfully through simple learning. When the result of this research can be applied in mass-production, it is highly expected that it will effectively detect and

predict wafer arcs and other anomaly related to electrical/plasma parameters, and will greatly benefit the yield of semiconductor equipment.

## Plasma Science and Technology Division Room A106 - Session PS2+AS+SS-ThM

### Plasma-Surface Interactions I

**Moderators:** Lei Liu, Lam Research Corporation, Pingshan Luan, TEL Technology Center America

11:00am **PS2+AS+SS-ThM-10 Remote Plasma-Activated and Electron Beam-Induced Etching of Ruthenium and Its Comparison to Tantalum**, Yudong Li<sup>1</sup>, University of Maryland College Park; C. Preischl, M. Budach, H. Marbach, D. Rhinow, Carl Zeiss SMT, Germany; G. Oehrlein, University of Maryland College Park

Refractory metals are of importance in microfabrication, which necessitates patterning of these materials. One issue is to reduce near-surface modifications of materials during processing, which is often due to ion bombardment and atomic mixing. Recently, we have developed a novel technique of combining electron beam (ebeam) and remote plasma (RP) for materials processing [1, 2]. Material damage is significantly reduced since energetic ion bombardment is prevented. The RP generates reactive neutral precursors and the ebeam provides energy deposition to enable further precursor-materials interactions.

Here we investigate the effects of ebeam and RP on Ru and Ta with the goal of selective etching. The simultaneous irradiation of ebeam and RP with Ar and O<sub>2</sub> as the feed gas induces Ru etching. The Ru ER increases with emission current, electron energy, and O<sub>2</sub> flow rate, while it shows less dependence on RP power. A pretreatment step by ebeam/RP or RP only with Ar/O<sub>2</sub>/CF<sub>4</sub> significantly enhances the subsequent Ru ER induced by ebeam/RP with Ar/O<sub>2</sub>. This effect is likely associated with the reactor wall passivation by the introduction of CF<sub>4</sub> through RP, which reduces recombination of O atoms on reactor surfaces. For Ta, RP with fluorine-rich Ar/O<sub>2</sub>/CF<sub>4</sub> induces Ta etching at a high rate. If instead an O<sub>2</sub>-rich gas mixture is used, we observe Ta oxidation. The RP sustains the spontaneous Ta etching by generating F which interacts with Ta and forms volatile tantalum fluoride. Contrary to the Ru metal, where the ebeam induces etching, the ebeam is found to promote oxidation of Ta. The opposite roles of ebeam on Ru and Ta and the sensitive dependence on CF<sub>4</sub> flow rate of Ta etching provides the opportunity to achieve Ru over Ta etching selectivity.

We gratefully acknowledge the financial support of this work by Carl Zeiss SMT GmbH

References:

1. Lin, K.-Y., et al., SiO<sub>2</sub> etching and surface evolution using combined exposure to CF<sub>4</sub>/O<sub>2</sub> remote plasma and electron beam. *Journal of Vacuum Science & Technology A*, 2022. 40(6).
2. Lin, K.-Y., et al., *Electron beam-induced etching of SiO<sub>2</sub>, Si<sub>3</sub>N<sub>4</sub>, and poly-Si assisted by CF<sub>4</sub>/O<sub>2</sub> remote plasma*. *Journal of Vacuum Science & Technology A*, 2022. 41(1).

11:20am **PS2+AS+SS-ThM-11 Plasma Surface Ionization Wave Interaction with Single Channel Structures**, Joshua Morsell, S. Shannon, North Carolina State University

The interaction of atmospheric pressure plasma jets (APPJ) with materials has found promising applications in the fields of plasma medicine, catalysis, and material treatment. One area of interest is the surface ionization waves (SIW) present in these plasmas. SIWs interactions with complex interfaces is critical to these applications and require further study. A complex interface is any target with non-uniform electrical properties and/or non-planar surface morphology. The focus of this work is to study how surface ionization waves interact with single channel structures in dielectric media. The results show that the fraction of the SIW that escapes the channel is dependent on both driving voltage and channel width.

The plasma source in this study is an APPJ powered by a nanosecond DC pulse of positive polarity with helium as the working gas as used in [J. Morsell et al., *J. Phys D: Appl. Phys.* 56 (2023), 145201]. Voltage and current data are collected via integrated current and high voltage probes at the source head. Time resolved ICCD imaging is used to image SIW propagation. The single channel targets consist of a 25 x 50 mm glass slide which has had a single channel etched across its minor axis. There are six total channel samples with different widths and depths. These samples are mounted to a

<sup>1</sup> PSTD Coburn & Winters Student Award Finalist

# Thursday Morning, November 9, 2023

target stage, which has another glass slide with an optically transparent conductor acting as a ground plane allowing imaging through the substrate.

SIW velocities in the system have been measured. The first is the SIW velocity within the channel, the second is the radial velocity of the portion of the SIW that escapes the channel. Both velocities increase with increasing voltage but show no significant trends with channel geometry. Velocity magnitudes for radial surface waves are 40-70 km/s and in-channel velocities are determined to be 60-130 km/s. Total light emission from the discharge is used to determine the fraction of the SIW escaping the channel. There exists a strong dependence of SIW portioning with channel geometry and driving voltage. As voltage increases the SIW is less confined and the fraction of the SIW escaping the channel increases. As channel width increases less of the SIW is allowed to escape the channel. No conclusive trends are observed with respect to channel depth. Observation also reveals that the fraction of the escaping SIW relates to the sample area exposed to the discharge. A smaller area of the substrate is exposed to the SIW for low voltages and large geometry channels.

This work is supported by the U.S. Department of Energy, Office of Science, Office of Fusion Energy Sciences under Award Number DE-SC0020232.

11:40am **PS2+AS+SS-ThM-12 Plasma-wall Interactions: Implications for Advanced Chamber Materials Requirements**, *John Daugherty*, Lam Research Corporation **INVITED**

In semiconductor device fabrication, plasma-assisted processes dominate both the deposition and etching of materials. Over 50 years of successive technology nodes have motivated innovations and continuous improvements in plasma reactor technology, and the semiconductor industry now employs a sophisticated portfolio of plasma reactors that use a wide variety of chemistry and operating approaches. Today, many aspects of the fabrication process must achieve process variations of ~1% and often must contribute particle contamination of less than one particle per wafer pass. Despite dramatic improvement in reactor design and in chamber materials, it remains challenging to achieve current variation requirements because plasma reactors still suffer from process drift, molecular contamination, and particulate contamination that originate from plasma-modification of the chamber materials. The first consideration in choosing a chamber material is the expected maximum ion bombardment energy. The plasma conditions within a single chamber are quite nonuniform, and the ion energy may fall into several ranges. Some parts experience <20 eV ions, and while these parts can be engineered for very long lifetime, challenges remain in meeting performance requirements. Other parts experience ion energies >100 eV (sometimes >1 keV in etch processes). These parts are almost always cost-sensitive consumables. There is an intermediate range of ~50 to 100 eV where there is considerable materials design complexity because of the desire to maintain process stability for thousands of wafers while operating very near the energy thresholds for ion-enhanced chemical modification of the wall material. Another design consideration is that the chamber materials must withstand a repeating sequence of multiple chemistries and plasma conditions followed by *in situ* plasma cleans using still different chemistry. The variety of chemically reactive molecules and free radicals include mixtures containing multiple halogens, hydrogen, oxygen, and depositing species from fluorocarbons, hydrocarbons, complex deposition precursors, and etch products. Recently we have adapted sophisticated materials metrology to examine the materials modifications that occur throughout the lifecycle of real production parts. We have also performed control experiments that allow us to infer the dominant plasma processes that cause the materials modifications we observe on production parts used in various applications. The implications for what types of materials are suitable for different parts of a plasma reactor are explored in this presentation.

## Surface Science Division

### Room D136 - Session SS1+AS-ThM

#### Molecular Organization at Surfaces

Moderators: *Eric Altman*, Yale University, *Zdenek Jakub*, CEITEC

8:00am **SS1+AS-ThM-1 Supramolecular Self-assembly and Metal-Ligand Redox Assembly at Surfaces**, *Steven Tait*, Indiana University **INVITED**

The selection and positioning of specific functional groups will direct packing and stacking of organic building blocks, which determine the electronic and chemical properties of molecular thin films and semiconductors. Design of molecular ligands for metal-organic complexation at surfaces can address the long-standing grand challenge of

high selectivity in heterogeneous catalysis. Our group is working to develop principles of on-surface molecular self-assembly<sup>1</sup> and of metal-organic complexation<sup>2</sup> to gain new insight into molecular layers and new chemical activity at metal single-site catalysts.<sup>3</sup> This work involves close collaboration with multiple research groups to synergistically combine talent in design, synthesis, sample preparation, characterization, analysis, theory, and computational modeling. We use a range of surface characterization tools to interrogate these systems under well-controlled environments, including scanning probe microscopy, photoelectron spectroscopy, vibrational spectroscopy, and mass spectrometry. We investigate systems under a variety of conditions: solution/solid interface, ultra-high vacuum, and flow reactor conditions at high temperature and high pressure. Here, I will report on recent results in several aspects of this work. We have demonstrated the impact of conformational entropy in impeding self-assembly, but that this can be overcome with appropriate selection of co-solutes. Metal-organic complexes at surfaces can be designed to achieve single-site metal centers in which we can observe redox isomerism, control of metal oxidation state, transmetalation, and chemical spillover to the support. We have transferred this design concept for single-site catalysts to high-surface-area powder oxide supports and shown that these can operate as effective catalysts in solution and under gas flow conditions. Ongoing work will seek to extend understanding of these systems to achieve molecular thin films and single-site catalysts of greater complexity.

#### References

- [1] D. L. Wisman, H. Kim, C. Kim, T. W. Morris, D. Lee, and S. L. Tait, *Chemistry – A European Journal* **27**, 13887-13893 (2021). DOI: 10.1002/chem.202101611 [https://doi.org/10.1002/chem.202101611]
- [2] T. W. Morris, D. L. Wisman, N. Ud Din, D. Le, T. S. Rahman, S. L. Tait, *Surface Science* **712**, 121888 (2021). DOI: 10.1016/j.susc.2021.121888 [https://doi.org/10.1016/j.susc.2021.121888]
- [3] E. Wasim, N. Ud Din, D. Le, X. Zhou, M. S. Pape, G. E. Sterbinsky, T. S. Rahman, S. L. Tait, *Journal of Catalysis* **413**, 81-92 (2022). DOI: 10.1016/j.jcat.2022.06.010 [https://doi.org/10.1016/j.jcat.2022.06.010]

8:40am **SS1+AS-ThM-3 Self-Assembly Controlled at the Level of Individual Functional Groups**, *Benjamin Heiner*, *A. Pittsford*, *S. Kandel*, University of Notre Dame

Molecular self-assembly is a process that occurs when component molecules spontaneously organize into a specific arrangement due to the intermolecular interactions between them. These interactions are influenced by the functional groups present on the component molecules. By understanding the effects that different functional groups have on the self-assembly process, we can predict and control it. To do this, we study "families" of molecules that have a common backbone but differ in the functional groups they possess. We use a combination of experimental techniques, such as pulse deposition for scanning tunneling microscopy (STM), and a variety of computational methods to investigate the changes in self-assembly behavior that result from small modifications to the functional groups. In this talk/poster, I will present our work on a family of molecules with an indole backbone, including indol carboxylic acids, multiple isatin derivatives, and proline. By studying these molecules, we are able to gain a deeper understanding of the various intermolecular interactions that drive self-assembly in these systems.

9:00am **SS1+AS-ThM-4 Atomically-Defined, Air-Stable 2D Metal-Organic Frameworks on Graphene: How the Support Defines the System Properties**, *Zdenek Jakub*, *A. Kurowska*, *J. Planer*, *A. Shahsavari*, *P. Prochazka*, *J. Cechal*, CEITEC - Central European Institute of Technology, Czechia

The functionality of 2D metal-organic frameworks (MOFs), crucially depends on the local environment of the embedded metal, and such details are best ascertained on 2D MOFs supported on atomically flat surfaces. Here, we present three systems which are well-defined at the atomic-scale, decoupled from the metal support and stable both in ultrahigh vacuum and in ambient conditions: M-TCNQ (M = Ni, Fe, Mn) supported on epitaxial graphene/Ir(111). We show that these systems are monophasic with M<sub>2</sub>(TCNQ)<sub>2</sub> stoichiometry, and we demonstrate their remarkable chemical and thermal stability. Furthermore, by a combined experimental and computational approach we study the differences between 2D MOF systems supported on graphene and on Au(111), the prototypical surface for on-surface synthesis. We show that the Fe-TCNQ on graphene is non-planar with iron in quasi-tetrahedral sites, but on Au(111) it is planarized by stronger van-der-Waals interaction. Combined with the distinct energy level alignment with the supports, this results in significant differences in the 2D

# Thursday Morning, November 9, 2023

MOF properties on these two surfaces. Our results outline the limitations of common on-surface approaches using metal supports and show that the intrinsic 2D MOF properties can be partially retained on graphene. The modular M-TCNQ/graphene system combines the atomic-scale definition required for fundamental studies with the robustness and stability needed for applications, thus we consider it an ideal model for research in single atom catalysis or spintronics.

9:20am **SS1+AS-ThM-5 Using 2D COFs to Stabilize Single-Atom Catalysts on Model Surfaces: From Ultra-High Vacuum System to Ambient Conditions**, *Yufei Bai*, Indiana University; *D. Wisman*, NAVSEA Crane; *S. Tait*, Indiana University

Single-atom catalysts (SACs) combine the advantages of homogeneous and heterogeneous catalysts by limiting the reaction sites to isolated single metal atoms with well-defined chemical characters. Our group has developed a metal-ligand coordination method to stabilize SACs using 1,10-phenanthroline-5,6-dione (PDO) to coordinate with metal atoms such as Pt, Fe, and Cr. In order to further improve the stability of SACs and increase metal loading, we have synthesized single-layered covalent organic frameworks (SCOFs) on model surfaces under ultra-high vacuum (UHV) conditions or under ambient conditions. These two-dimensional (2D) networks with high thermal and chemical stability were used to confine single Pt atoms coordinated with ligands into SCOF pores. Under UHV conditions, the successful formation of the SCOF with regular hexagonal pores on the Au(111) surface was achieved by surface-mediated Ullmann radical coupling of 1,3,5-tris-(4-bromophenyl)benzene (TBB) and characterized by scanning tunneling microscopy (STM). Further sequential deposition of PDO ligand and Pt on the TBB-SCOF surface allowed the formation of single-site Pt catalysts by coordination interaction. STM images have proved the confinement of PDO in the SCOF pores, while X-ray photoelectron spectroscopy (XPS) has proven the oxidation state of Pt, which is an indication of the single atom character. Under ambient conditions, a 2D imine-linked SCOF was formed on the highly oriented pyrolytic graphite (HOPG) surface by a solid-vapor interface mechanism, which allows for a high quality SCOF with long-range order. STM characterization has shown that regular SCOF networks with negligible defects were formed on the HOPG surface with domain sizes greater than  $1\ \mu\text{m} \times 1\ \mu\text{m}$ . These systems which combine the COF and metal-ligand coordination strategy to stabilize SACs offer the possibility to achieve higher stability and greater loading in SACs.

9:40am **SS1+AS-ThM-6 Protein Adsorption on Mixed Self-Assembled Monolayers: Influence of Chain Length and Terminal Group**, *Rebecca Thompson*, St. Edward's University

Mixed self-assembled monolayers (SAMs) are often used as highly tunable substrates for biomedical and biosensing applications. It is well documented, however, that mixed SAMs can be highly disordered at the molecular level and do not pack as closely or homogeneously, particularly when the chain lengths and head groups of the SAM thiol components are significantly different. In the current study, we explore the impact of SAM structure and mixing ratio on the weak physisorption behavior of bovine serum albumin (BSA), which adsorbs more readily to hydrophobic, methyl-terminated SAMs. Our results suggest that once the mixture includes 50% or more of the methyl terminus, mixing ratio alone is a relatively good predictor of adsorption, regardless of the relative chain lengths of the thiols used in the mixture. This trend persists at any mixing ratio for SAMs where methyl- and hydroxyl-terminated groups are the same length or where the hydroxyl-terminated thiol is longer. The only variance observed is at low mixing ratios (<50% methyl-terminated) for a mixed SAM where the methyl-terminated component has a longer chain length. Relative protein adsorption increases on these mixtures, perhaps due to the disordered exposure of the excess alkane backbone. Taken together, however, we do not find significant evidence that varying chain lengths for mixed SAMs prepared on polycrystalline substrates and analyzed in air have an outsized influence on nanoscopic adsorption behavior, despite molecular-level disorder in the SAM itself.

Surface Science Division

Room D136 - Session SS2+AS+TF-ThM

Thin Film Surface Chemistry

Moderators: Eric Altman, Yale University, Zdenek Jakub, CEITEC

11:00am **SS2+AS+TF-ThM-10 Ultrafast Exciton Dynamics of Phthalocyanine Films with Different Molecular Orientations**, *Hui Ung Hwang*, *S. Kim*, *J. Kim*, Korea Research Institute of Standards and Science (KRISS), Republic of Korea

Organic semiconductors (OSCs) have enormous potential in advanced optoelectronic devices, such as organic light-emitting diodes and organic solar cells. To achieve higher performance and functional versatility for these applications, a deeper understanding of the generation and relaxation mechanism of photoexcited excitons in molecular films is essential. In this study, we investigate the ultrafast dynamics of excitons in planar-shape molecules of phthalocyanines (Pc), which can adopt a lying-down or standing-up orientation depending on the substrate used, as shown in Fig. 1.<sup>1</sup> The distinct ionization-energy difference of more than 0.5 eV measured by photoelectron spectroscopy confirms that the Pc thin film on HOPG substrate grows in the lying-down direction and the Pc on ITO grows in the standing-up direction. Exciton energy and population from the molecules with these two different orientations are measured by time-resolved two-photon photoemission (tr-2PPE) with time resolution of 85 fs. In this measurement, we first pump a singlet exciton population in the Pc with a femtosecond pulse and probe its evolution as a function of delay time with an ultraviolet pulse. Singlet excitons have a variety of relaxation pathways, including diffusion between molecules, intersystem crossing to triplet states, and dissociation at the interface with metals. The tr-2PPE experiments show that the exciton relaxation in Pc molecules with the standing-up geometry is dominated by exciton diffusion in the direction perpendicular to the substrate, resulting in relatively slow exciton relaxation. However, for Pc molecules in the lying-down geometry, the excitons undergo faster transfer to the metal interface due to aligned  $\pi$ -orbital overlap with neighboring molecules toward the substrate. These results imply that OSCs exhibit different exciton relaxation dynamics depending on their orientation and suggest that for planar molecules like Pc, the lying-down geometry is more favorable for exciton transfer and dissociation to the metal interface.

11:20am **SS2+AS+TF-ThM-11 Understanding the Surface Chemistry of Oxide Thin Films by Isotope Labeling**, *Yingge Du*, Pacific Northwest National Laboratory **INVITED**

Isotopic engineering is developing into a key approach to study the nucleation, diffusion, phase transition, and reaction of materials at an atomic level to reveal transport pathways, kinetics, and working/failure mechanisms of functional materials and devices. Understanding these phenomena leads to deeper insights into relevant physical processes, such as the transport and intercalation of ions in energy conversion and storage devices, and the role of active sites and supports during heterogeneous catalytic reactions. Likewise, isotopic engineering is being pursued as a means of modifying functionality to enable future technological applications. In this talk, I will present our work employing isotope labeling (e.g., <sup>18</sup>O and <sup>2</sup>H) during complex oxide thin films' (e.g., WO<sub>3</sub>, SrFeO<sub>2.5</sub>, and La<sub>1-x</sub>Sr<sub>x</sub>FeO<sub>3</sub>) synthesis and post-growth processing to track the distribution and redistribution of the isotope tracers. Isotope-resolved analysis techniques with high spatial resolution, such as time-of-flight secondary ion mass spectrometry and atom probe tomography, facilitate the accurate quantification of isotopic placement and concentration in well-defined heterostructures with precisely positioned, isotope-enriched layers. These studies allow us to better understand the growth mechanisms, surface chemistry, and elemental diffusion under working and extreme conditions.

12:00pm **SS2+AS+TF-ThM-13 Interaction of Self-Assembled Monolayers with Atomic Oxygen During Area-Selective Atomic Layer Deposition**, *Silvia Armini*, IMEC Belgium; *A. Brady Boyd*, School of Physical Sciences, Dublin City University, Ireland

Utilising self-assembled monolayers (SAMs) to achieve area-selective atomic layer deposition (AS-ALD) as an approach to bottom-up nanofabrication has recently gained significant attention from the nanoelectronics industry.

With the continued downscaling of feature sizes, top-down processing can no longer reach the challenging demands of the industry which requires conformal coating of high aspect ratio vias and a reduction in misalignment errors in multi-layered devices. In this work we attempt to imitate the effects of the ALD oxidation pulse experienced by the SAMs during the AS-

# Thursday Morning, November 9, 2023

ALD process by exposing two SAMs of different chain lengths and different functional groups, (3-trimethoxysilylpropyl)diethylenetriamine (DETA) and octadecyltrimethoxysilane (OTMS), to numerous controlled in-vacuo atomic oxygen exposures with subsequent characterisation by X-ray photoelectron spectroscopy (XPS). We monitor the sequential removal of the deposited monolayers with each successive atomic oxygen exposure for both SAMs. The etch rate is observed to be distinct for the different SAMs, the amino-terminated short chain DETA SAM reveals a linear etch rate while the longer chain OTMS SAM reveals an exponential etch rate. The results presented provide some insights into what characteristics are important for choosing the correct SAM for AS-ALD applications.

## Thin Film Division

### Room A105 - Session TF-ThM

#### Creating Organic-Inorganic Hybrid Materials

**Moderators:** Devika Choudhury, ASM, Robin Rodriguez, Jet Propulsion Laboratory

8:00am **TF-ThM-1 Functional Ceramic Heterostructures via Vapor and Liquid Phase Infiltration of Polymer Templates**, *Diana Berman*, University of North Texas **INVITED**

Robust and efficient process for synthesis of various composition inorganic coatings with controlled nanoporosity and structure is highly desirable for design of efficient catalytic, purification, and detection systems. Recently, infiltration of a nanoporous polymer template with inorganic precursors using sequential infiltration synthesis with inorganic vapor precursors followed by oxidative annealing was proposed as a new and efficient approach to create porous inorganic structures with tunable porosity and composition. The major limitations of the original water-based thermal sequential infiltration synthesis, though, are the thickness of the patterned structure being limited by vapor penetration depth of the precursors into the polymer template and the resulting material selection being restricted by the availability of high vapor pressure precursors. Here, we propose a swelling-based modification to the polymer infiltration process that allows to overcome these limitations. We summarize the basics of the multi-step infiltration approach, the structure and properties of the resulting materials, and their functional potential for practical applications. We report ultra-high accessibility of the pores when porous films are prepared via the polymer swelling-based infiltration synthesis (SBI). Using a quartz crystal microbalance (QCM) technique, we demonstrate increased solvent absorbing capabilities of highly porous ceramic films as a result of high interconnectivity of the pores in such structures. Our results show that the approach can be extended toward preparing conformal coatings, freestanding membranes, and powders consisting of metal or metal oxide nanoparticles embedded in a porous oxide matrix.

8:40am **TF-ThM-3 Effect of Polymer Templates on Nanoporous Inorganic Coatings Synthesized by Polymer Infiltration**, *Khalil Omotosho, D. Berman*, University of North Texas

Polymer templates infiltration synthesis of all-inorganic metal oxide architectures provides control over their thickness, porosity, and composition. In this study, we provide insights into the synthesis of nanoporous zinc oxide films as a model system via infiltration of polymers such as polymer of intrinsic microporosity (PIM-1) and representative of the block-copolymers family (polystyrene-polyvinyl pyridine block copolymer) that have different mechanisms of interaction with metal oxide precursors. We investigated the polymer infiltration process with both gas (diethyl zinc, DEZ, and water vapors) and solution (zinc acetylacetonate, Zn(acac)<sub>2</sub>, dissolved in ethanol) phase precursors. We systematically studied the effect of polymer template and the form of the metal oxide precursors on the properties of synthesized metal oxide thin coatings using the quartz crystal microbalance (QCM), X-ray diffraction (XRD), and X-ray photoelectron spectroscopy (XPS) analyses. Our study prove that the infiltration of polymer templates can be efficiently achieved using both gas phase and solution phase precursors. Furthermore, we show that the crystallinity of the synthesized ZnO films is mainly affected by the state of the precursor (gas or solution phase) and is independent of the polymer template type. In turn, the polymer type affects the surface termination of ZnO films. In addition, our findings demonstrate that the surface of porous ZnO coatings synthesized with BCP (here PS-P4VP) is more accessible than the surface of ZnO synthesized with PIM; however, despite the lower surface accessibility for ethanol molecules, ZnO synthesized via infiltration of PIM-1 with solution-phase precursors demonstrates the largest change in resistivity upon its exposure to ethanol vapor at room temperature.

Thursday Morning, November 9, 2023

9:00am **TF-ThM-4 Alkylation of Esters by TiCl<sub>4</sub> Vapor Phase Infiltration (VPI) and the Resulting Chemical and Thermophysical Properties of the Hybrid Materials**, *Shuaib Balogun*, Georgia Institute of Technology, USA; *S. Yim*, Georgia Institute of Technology; *B. Jean, T. Yom*, Georgia Institute of Technology, USA; *A. Steiner*, Sandia National Laboratories; *M. Losego*, Georgia Institute of Technology, USA

Vapor phase infiltration (VPI) is a post-processing modification technique used to imbue inorganic materials into polymers to create organic-inorganic hybrid materials with new properties. In VPI, inorganic material can become entrapped by reaction with the polymer functional group, by reacting with a co-reactant or by physical entrapment due to loss of volatility. While several VPI precursor-polymer chemistries have been explored and their chemical mechanisms have been noted, a lack of chemical intuition remains for fully understanding the chemical mechanisms that govern VPI processes. This study seeks to continue to build this knowledge by examining the chemical reaction mechanisms that occur during TiCl<sub>4</sub> infiltration into esters namely PMMA and PLA. In this research, the poly-methyl methacrylate / TiO<sub>x</sub> and poly-lactic acid / TiO<sub>x</sub> hybrid materials are prepared using VPI. The chemical states of the atoms in the polymers pre & post infiltration are studied using x-ray photoelectron spectroscopy (XPS) and Fourier-transform infrared (FTIR) spectroscopy. The chemical mechanism of infiltration appears to occur via an acid catalyzed SN<sub>2</sub>-alkylation reaction. As infiltration occurs in PMMA, there is an increase loss of methyl groups in the PMMA ester, whereas, in PLA there is an observed cleavage of the main chain at the methoxy bond, resulting in degradation of the polymer. The kinetics of this reaction and consequently the TiCl<sub>4</sub> infiltration increases with both VPI process temperature and TiCl<sub>4</sub> exposure time. Interestingly, the resulting hybrid materials offer new properties due to the reaction with TiCl<sub>4</sub>. Increased titanium loading leads to up to 100% chemical stability in PMMA. Additionally, films infiltrated with up to 6% Ti have a 50 % and 70 % reduction in coefficients of thermal expansion (CTE) below and above T<sub>g</sub> respectively. CTE continually reduces with increased titanium loading. In this talk, we will discuss how these chemical and physical changes could be used for various applications.

This project is supported by the Laboratory Directed Research and Development program at Sandia National Laboratories, a multimission laboratory managed and operated by National Technology and Engineering Solutions of Sandia LLC, a wholly owned subsidiary of Honeywell International Inc. for the U.S. Department of Energy's National Nuclear Security Administration under contract DE-NA0003525.

9:20am **TF-ThM-5 Free and Simple Simulations of Vapor-Phase Infiltration Process Kinetics Using Google Colab**, *Mark Losego*, Georgia Institute of Technology

Vapor-phase infiltration (VPI) is a post-polymerization chemical modification technique that exposes organic polymers to gas-phase inorganic precursors that sorb and become entrapped within the polymer to create organic-inorganic hybrid materials. The process kinetics for VPI are a complicated convolution of sorption, non-Fickian diffusion, and reaction processes. We recently introduced a reaction-diffusion model to capture many of the VPI process kinetics phenomena, and recent experimental work has demonstrated the validity of this model's process predictions. This talk will introduce our publication of this model on Google Colab, a free, web-based environment for running Python codes without any need for installing or configuring a Python platform on your personal computer. This web-based platform makes it free and simple for anyone to now run our reaction-diffusion VPI process simulation model. This talk will include how to access and run these simulations, defining the important model variables as well as how they relate to physical process parameters. Example simulations will be run and then compared to experimental data we and others have published to demonstrate how this reaction-diffusion model can be used to interpret and help predict VPI process phenomena.

9:40am **TF-ThM-6 High-Throughput Molecular Layer Deposition for the Discovery of Organic-Inorganic EUV Photoresists**, *Duncan Reece*, University of Washington, UK; *E. Crum*, University of Washington; *Y. Choe*, University of Washington, Republic of Korea; *D. Bergsman*, University of Washington

Continued progress in information and communication technologies requires sustained innovations in memory and storage devices' architecture and production processes. However, scaling technology to sub-5nm features may require Extreme Ultraviolet (EUV) sources, which necessitates new photoresist materials that are highly adsorbing of EUV while meeting the formal requirements of a photoresist. Such materials must also be environmentally conscious and abundantly available. One potential solution

162

8:00 AM

# Thursday Morning, November 9, 2023

is a hybrid inorganic-organic thin film produced through molecular layer deposition (MLD), the organic equivalent of atomic layer deposition. However, the discovery process for new MLD materials is typically slow and needs improvement.

Here, we present a high-throughput multi-chamber MLD reactor that can quickly screen hybrid MLD processes for their EUV compatibility. In the reactor, films are deposited with one shared inorganic reactant and six independent counter-reactants in parallel, simultaneously producing multiple potential resist materials. In this work, inorganic reactants consisted of highly and non-highly EUV absorbing metals, like diethyl zinc, trimethylaluminum, and tin(IV) t-butoxide, while the organic counter-reactants included ethylene glycol, 1,2,4-trihydroxybenzene, 1,5-hexadiene-3,4-diol, 2-butyne-1,4-diol, cis-2-butene, and 2-methylenepropane-1,3-diol. The resulting films were tested for solvent, developer, and etchant stability before and after exposure to deep UV, electron beam, or X-rays. Promising resists were further characterized and could be used for patterning. Results showed that the inorganic and organic linkers exhibited a range of stabilities and light sensitivities, which could be used to optimize the performance of thin film EUV resists. In addition, this method provides a much faster screening process for potential photoresist materials in a scalable system, allowing for the continued improvement of processor efficiency and progress.

**11:00am TF-ThM-10 Understanding the Physicochemical Properties and Structural Evolution of Sequential Infiltration Synthesis Derived Indium Oxyhydroxide Clusters for CO<sub>2</sub> Absorption, *Thabiso Kunene, A. Martinson,* Argonne National Laboratory**

Sequential infiltration synthesis (SIS) is a versatile route to hybrid organic-inorganic materials. While SIS is inspired ALD and often utilizes the same precursors and tools, SIS requires infiltration of these vapor phase precursors into a polymer film that includes reversible or irreversible interactions with polymer functional groups. In a second step, the infiltration of an oxygen source (e.g. H<sub>2</sub>O) affords reaction to form an inorganic oxyhydroxide that may be chemisorbed at the functional site or physically trapped within the polymer matrix. However, the atomic structure of the first few-atom clusters and the evolution of local coordination environment remain unresolved. Therefore, a more fundamental and detailed understanding of the growth mechanism and structural evolution of indium clusters during SIS is necessary to inform the synthetic design of target clusters for various applications. This talk will discuss the experimental and theoretical efforts to elucidate the growth and structure of indium oxyhydroxide clusters from trimethyl indium (TMIn) during SIS in PMMA polymers. FTIR, UV-vis and DFT calculations suggest the existence of octahedrally coordinated [In]<sup>3+</sup> species where water ligands complete the coordination sphere. The spectroscopic observations also indicate that the weak adducts formed between trimethyl indium precursor and the Lewis basic carbonyl and ester groups in PMMA are central to the oxyhydroxide growth pathways during SIS. Considering the traditional, solution phase organometallic properties and chemistry of trimethyl indium, we demonstrate a link between solution phase organometallic synthesis and the vapor phase SIS process. DFT calculations and In K-edge EXAFS with PDF analysis suggest the formation of dimeric indium oxyhydroxide species in the very first SIS cycle which is driven by the hydrolysis pathways of TMIn. The talk will also present refined SIS process conditions in which nucleation is only feasible in the first SIS cycle, in order to favor only indium oxyhydroxide cluster growth in subsequent cycles. Furthermore, the nature of SIS-derived InO<sub>x</sub>H<sub>y</sub>(H<sub>2</sub>O)<sub>z</sub> clusters as a function size (i.e., SIS cycle number) is examined by vibrational and UV-vis absorption signatures and compared to simulated spectra from DFT simulations. The SIS grown indium oxyhydroxide in PMMA presents opportunities to improve the CO<sub>2</sub> absorption capacity and gas selectivity of inexpensive polymers. The SIS-grown clusters provide a platform for use as a model system to study indium (oxy)hydroxide surface reactivity towards environmentally important transformations such as CO<sub>2</sub> capture and conversion.

**11:20am TF-ThM-11 Optimizing Aluminum Oxyhydroxide Vapor Phase Infiltration for the Vapor Phase Mordanting of Natural Dyes to Polyester Fabrics, *M. Losego, Nicole McClelland, E. McGuinness,* Georgia Institute of Technology**

Industrial textile dyeing and finishing processes are a significant environmental concern producing large quantities of wastewater that require significant treatment to remove unused synthetic chemicals.

Polyester fabrics in particular utilize high temperatures and chemical carrier agents in their dyeing processes. In this work, we present a method for attaching natural dye materials derived from madder root to polyethylene terephthalate fabrics via the introduction of aluminum oxyhydroxides through vapor phase infiltration. Vapor phase infiltration (VPI) is an emerging polymer modification technique that exposes a polymer to metalorganic precursors that diffuse into the polymer and become entrapped as inorganic clusters. The resulting hybrids have unique properties of both organic and inorganic materials. The VPI process has found significant use in modifying the properties of textile materials including their mechanical and optical properties. In this study, we examine the use of VPI to act as a mordant for natural dye adsorption and how the inorganic loading can be optimized for both dyeability and mechanical performance. Specifically we examine VPI of trimethylaluminum (TMA) into polyethylene terephthalate (PET) fabrics. Inorganic loading is controlled by varying the dose pressure of TMA (moles of TMA) and fabric mass (moles of carbonyl functional group) during VPI and quantified using thermogravimetric analysis (TGA). The resulting hybrid AlO<sub>x</sub>-PET fabrics have various inorganic loadings from 1 wt% aluminum oxyhydroxide to >20 wt%. The hybrid fabrics were then dyed with alizarin (derived from madder root) and the dye absorbance was quantified with UV-Vis spectroscopy. At low inorganic loadings the strength of color varied with inorganic content, but a steady-state absorbance was reached at around 1.8 wt% inorganic loading. At these low inorganic loadings, hybrid fabrics maintain key mechanical behaviors such as stiffness (as measured by drape) which is seen to increase significantly with additional inorganic loading. This change in texture was quantified using the Cusick drape test to determine shear and bending stiffness changes as a result of higher inorganic loading. By exploring dye saturation curves for different inorganic loadings, kinetics information was gathered to further optimize this dyeing process for industrialization. Overall, using VPI as a vapor phase mordanting process to fix natural dyes to PET fabrics illustrates the impact that even small quantities of the vapor deposited inorganic can have on approving dyeability, highlighting the practical use of these fabrics in the field of textile sustainability.

**11:40am TF-ThM-12 Tuning the Thermal Stability of Vapor Phase Infiltrated Polyacrylonitrile Fabrics, *Téa Cook, B. Jean, E. McGuinness, A. Gonzalez, M. Losego,* Georgia Institute of Technology**

VPI creates hybrid organic-inorganic materials by infiltrating polymers with vapor phase metalorganic precursors that sorb and permeate into the bulk of the polymer. Polyacrylonitrile (PAN) is a polymer previously unexplored in VPI. PAN is used in textiles and filtration, but one of its most common applications is as a precursor to carbon fiber. The metalorganic precursor trimethyl aluminum (TMA) has been shown to form a reversible adduct with the nitrile functional group, which is found on the backbone of PAN polymer chains. The VPI process has been shown to alter numerous properties of materials and, specifically, to reduce the thermal stability of hybrid materials. This work will discuss the role of VPI in modifying the thermal properties of infiltrated PAN fabrics as a function of VPI processing conditions such as exposure time, desorption time, and processing temperature. To explore the effects of inorganic loading on the thermal properties of this system, PAN is infiltrated with TMA and co-reacted with water vapor under varied processing conditions to tune the inorganic in each hybrid PAN/AlO<sub>x</sub> fabric. PAN infiltrates with high quantities of inorganic loading that can be tuned from 1% to 17% inorganic by weight, as measured by thermogravimetric analysis (TGA). TGA is further used to study the thermal degradation profile of the hybrid PAN/AlO<sub>x</sub>, and the kinetics of degradation via the Flynn-Wall-Ozawa analysis method. Through this analysis, the thermal stability of the PAN fabric is shown to decrease after infiltration. The temperatures of the first degradation event in the hybrid fabrics are about 100°C lower than the temperatures of the first degradation event of neat PAN fabric. The activation energy to degrade a PAN/AlO<sub>x</sub> hybrid of 7.5 wt % alumina is 67% of that required to degrade a PAN/AlO<sub>x</sub> hybrid of 15 wt % alumina. While infiltration reduces the activation energies of each degradation event relative to neat PAN, the change in activation energy varies with loading, suggesting that the thermal stability of hybrid PAN fabrics can be tuned by altering VPI processing conditions which may prove advantageous in the energy-intensive carbon fiber manufacturing process. Overall, this work explores a new VPI system: infiltration of TMA into PAN. Additionally, this work explores the vapor phase modification of PAN fabrics and how processing conditions can be used to tune the inorganic loading of AlO<sub>x</sub>/PAN hybrid fabrics and their thermal stability.

# Thursday Afternoon, November 9, 2023

## 2D Materials Technical Group

### Room C123 - Session 2D1-ThA

#### 2D-Materials: Topological and Quantum Properties

**Moderators:** Harriet Åhlgren, University of Vienna, Miaofang Chi, Oak Ridge National Laboratory

2:20pm **2D1-ThA-1 2D Transition Metal Chalcogenide Semimetals**, *David Cobden*, University of Washington **INVITED**

Graphite (graphene) is a 2D semimetal that after nearly two decades still continues to surprise. Only one other 2D semimetal,  $\text{WTe}_2$ , has been studied in detail down to the monolayer limit, where it too exhibits diverse properties including topological edge conduction, superconductivity, ferroelectricity, and probable excitonic order. The indications are therefore that 2D semimetals in general form an extraordinarily rich class of materials that deserves more exploration. We will talk about our ongoing work to understand the properties of monolayer  $\text{WTe}_2$  better, to investigate the hybrid semimetal system of graphene/ $\text{WTe}_2$ , and to isolate and study other semimetallic 2D transition-metal chalcogenides.

3:00pm **2D1-ThA-3 Artificial Graphene Nanoribbons with Tailored Topological States**, *Nathan Guisinger*, *P. Darancet*, Argonne National Laboratory, USA

Low-dimensional materials functioning at the nanoscale are a critical component for a variety of current and future technologies. From the optimization of light harvesting solar technologies to novel electronic and magnetic device architectures, key physical phenomena are occurring at the nanometer and atomic length-scales and predominately at interfaces. In this presentation, I will discuss low-dimensional material research occurring in the Quantum and Energy Materials (QEM) group at the Center for Nanoscale Materials. Specifically, the synthesis of artificial graphene nanoribbons by positioning carbon monoxide molecules on a copper surface to confine its surface state electrons into artificial atoms positioned to emulate the low-energy electronic structure of graphene derivatives. We demonstrate that the dimensionality of artificial graphene can be reduced to one dimension with proper "edge" passivation, with the emergence of an effectively-gapped one-dimensional nanoribbon structure. Remarkably, these one-dimensional structures show evidence of topological effects analogous to graphene nanoribbons. Guided by first-principles calculations, we spatially explore robust, zero-dimensional topological states by altering the topological invariants of quasi-one-dimensional artificial graphene nanostructures. The robustness and flexibility of our platform allows us to toggle the topological invariants between trivial and non-trivial on the same nanostructure. Our atomic synthesis gives access to nanoribbon geometries beyond the current reach of synthetic chemistry, and thus provides an ideal platform for the design and study of novel topological and quantum states of matter.

3:20pm **2D1-ThA-4 Critical Materials: Fine Tuning Electronic and Structural Properties of Rare-Earth Based 2-D Structures at the Atomic Limits**, *Kyaw Zin Latt*, Nanoscience and Technology Division, Argonne National Laboratory;

*T. Ajayi*, Nanoscience and Technology Division, Argonne National Laboratory; Nanoscale and Quantum Phenomena Institute, and Department of Physics & Astronomy, Ohio University; *X. Cheng*, Department of Chemistry and Biochemistry, Ohio University; *N. Dandu*, Materials Science Division, Argonne National Laboratory; *A. Ngo*, Materials Science Division, Argonne National Laboratory; Chemical Engineering Department, University of Illinois; *E. Masson*, Department of Chemistry and Biochemistry, Ohio University; *S. Hla*, Nanoscience and Technology Division, Argonne National Laboratory; Nanoscale and Quantum Phenomena Institute, and Department of Physics & Astronomy, Ohio University

Rare-earth metals have many important applications including quantum information, energy up-conversion, emission, and catalysis. In the rare-earth based molecules, the interaction between the metal atom and local electronic states plays a vital role in determining its properties. This can be exploited by engineering molecular ligands to tailor for desired applications. These molecular ligands not only protect the rare-earth metal atoms from the surrounding environment but also influence electronic and magnetic properties [1,2]. Thus, they can be used to tailor the properties of rare-earth ions. Based on the design of the ligands, it can form different types of self-assembled structures which further opens the opportunity to fine tune the properties. In our research, we have designed a variety of rare-earth (Eu,Tb,La) based molecular systems which are deposited onto noble metal surface such as Au(111) under ultrahigh vacuum(UHV) environment to form self-assembled 2D layers. Using a low temperature scanning tunneling microscope, atomic level characterizations of electronic

and structural properties of rare-earth complexes absorbed on metal surfaces are performed. Furthermore, tunneling spectroscopic mapping of a self-assembled cluster reveals the spatial variation of electronic orbitals. The experimental results are supported by density functional theory calculations.

[1]. T.M. Ajayi, V. Singh, K.Z. Latt, S. Sarkar, X. Cheng, S. Premarathna, N.K. Dandu, S. Wang, F. Movahedifar, S. Wieghold, N. Shirato, V. Rose, L.A. Curtiss, A.T. Ngo, E. Masson, & S.-W. Hla. *Atomically precise control of rotational dynamics in charged rare-earth complexes on a metal surface*. *Nat. Commun.* **13**, 6305 (2022).

[2]. T. M. Ajayi, N. Shirato, T. Rojas, S. Wieghold, X. Cheng, K. Z. Latt, D. J. Trainer, N. K. Dandu, Y. Li, S. Premarathna, S. Sarkar, D. Rosenmann, Y. Liu, N. Kyritsakas, S. Wang, E. Masson, V. Rose, X. Li, A. T. Ngo, & S.-W. Hla. *Characterization of just one atom using synchrotron x-rays*. *Nature* (2023) in press.

3:40pm **2D1-ThA-5 Quantum Sensing with Spin Qubits in Hexagonal Boron Nitride**, *Tongcang Li*, Purdue University **INVITED**

The recent discovery of spin qubits in hexagonal boron nitride (hBN), a van der Waals (vdW) layered material, has opened up exciting possibilities for quantum sensing. Owing to its layered structure, hBN can be easily exfoliated and integrated with various materials and nanostructures for in-situ quantum sensing. In this talk, I will provide a brief overview of recent advancements in quantum sensing and imaging using spin defects in hBN [Advances in Physics: X, 8, 2206049 (2023)] and discuss our contributions to this emerging field. We have demonstrated high-contrast plasmon-enhanced spin defects in hBN for quantum sensing [Nano Letters 21, 7708 (2021)] and investigated their excited-state spin resonance [Nature Communications, 13, 3233 (2022)]. Additionally, we achieved optical polarization and coherent control of nuclear spins in hBN at room temperature [Nature Materials 21, 1024 (2022)], paving the way for manipulating nuclear spins in vdW materials for quantum information science and technology applications. Finally, we will discuss our work on sensing paramagnetic ions in water using hBN spin defects [arXiv:2303.02326], which demonstrates the potential of ultrathin hBN quantum sensors for chemical and biological applications.

## 2D Materials Technical Group

### Room B110-112 - Session 2D2-ThA

#### 2D-Materials: Surface and Interface Effects

**Moderators:** Huamin Li, University at Buffalo-SUNY, Cristina Satriano, University of Catania

2:20pm **2D2-ThA-1 Two-dimensional van der Waals Materials and Their Mixed Low-Dimensional Hybrids for Electrochemical Energy Applications**, *Fei Yao*, University at Buffalo-SUNY

Compared with their 3D counterparts, two-dimensional (2D) van der Waals (vdW) materials exhibit quantum confinement where charge carriers are spatially confined at the physical boundaries. Particularly, when mixing 2D materials with other low-dimensional (LD) materials, they exhibit enormous potential in electrochemical energy applications due to the unique properties arising from reduced dimensionality and, more importantly, material integration synergy. In this work, 2D transition metal dichalcogenides and their mixed low-dimensional hybrids (MLDHs) are introduced with an emphasis on innovations covering 2D-based hybrid structure construction and electrochemical applications. Fundamental insight into the synergistic effect of the MLDHs integration for advancing the development of Li-ion batteries and electrocatalytic hydrogen evolution reaction will also be discussed. Leveraging the unique microreactor platform based on the 2D vdW platform, a mechanistic understanding of charge transport dynamics at the electrified interface will be highlighted. The knowledge gained on how mixed-dimensional physics and chemistry will shed light on the design principle of the electrode materials and deepen the understanding of the process-structural-property-performance (PSP) relationship of the vdW-based hybrid structures.

2:40pm **2D2-ThA-2 Influences of Fe Vacancy and Te Vacancy on Magnetic Domains on  $\text{Fe}_3\text{GeTe}_2$  Surfaces**, *TeYu Chien*, University of Wyoming; *D. Baral*, University of Arkansas; *Z. Fu*, *J. Tian*, University of Wyoming; *H. Chen*, Colorado State University

$\text{Fe}_3\text{GeTe}_2$  (FGT) is a van der Waals (vdW) ferromagnetic metallic material with Curie temperature around 230 K. Despite the central symmetric crystal structure, magnetic skyrmions and various magnetic domain textures have

# Thursday Afternoon, November 9, 2023

been reported in FGT. The magnetic domain textures can be widely tuned with thickness, temperature and magnetic field. Several ideas regarding the origin of the wild magnetic domain textures have been proposed, including oxidized layer induced DMI, Fe defect vacancy etc. Here, by utilizing spin polarized scanning tunneling microscopy (SPSTM), we revealed that, compared to Fe vacancies, the Te vacancies have stronger effects on altering the magnetic domains in the otherwise ferromagnetic system. A theoretical model will also be discussed to explain the difference between the Te vacancies and the Fe vacancies on the magnetic domain wall pinning.

**3:00pm 2D2-ThA-3 Emergent Moiré Phonons Due to Zone Folding in  $WSe_2$ - $WS_2$  Van Der Waals Heterostructures, Hsun Jen Chuang, B. Jonker, Naval Research Laboratory**

Bilayers of 2D materials offer opportunities for creating devices with tunable electronic, optical, and mechanical properties. In van der Waals heterostructures (vdWHs) where the constituent monolayers have different lattice constants, a moiré superlattice forms with a length scale larger than the lattice constant of either constituent material regardless of twist angle. Here, we report the appearance of moiré Raman modes from nearly aligned  $WSe_2$ - $WS_2$  vdWHs in the range of  $240\text{ cm}^{-1}$  -  $260\text{ cm}^{-1}$ , which are absent in both monolayers and homobilayers of  $WSe_2$  and  $WS_2$  and in largely misaligned  $WSe_2$ - $WS_2$  vdWHs. Using first-principles calculations and geometric arguments we show that these moiré Raman modes are a consequence of the large moiré length scale which results in zone-folded phonon modes that are Raman active. These modes are sensitive to changes in twist angle, but notably, they occur at identical frequencies for a given small twist angle away from either the 0-degree or 60-degree aligned heterostructure. Our measurements also show a strong Raman intensity modulation in the frequency range of interest, with near 0 and near 60-degree vdWHs exhibiting a markedly different dependence on excitation energy. In near 0-degree aligned  $WSe_2$ - $WS_2$  vdWHs, a nearly complete suppression of both the moiré modes and the  $WSe_2$   $A_{1g}$  Raman mode ( $\sim 250\text{ cm}^{-1}$ ) is observed when exciting with 532 nm CW laser at room temperature. Temperature-dependent reflectance contrast measurements demonstrate the significant Raman intensity modulation arises from resonant Raman effects.

**3:20pm 2D2-ThA-4 Stabilizing Metastable Constituent Structures via 2D Interlayer Interactions in Heterostructures, Fischer Harvel, D. Johnson, University of Oregon**

The interactions between constituent layers in heterostructures provide an opportunity to stabilize 2D compounds not found in equilibrium phase diagrams. Utilizing 2D layers of 3D structures like rock-salt structured PbSe, commonly found in thermodynamically stable heterostructures known as misfit compounds, phenomena such as charge transfer to and surface stabilization can be used to stabilize new structures. In the iron-selenide system  $\beta$ -FeSe exhibits high-temperature superconductivity ( $T_c \sim 107\text{ K}$ ) when grown in a monolayer on a  $SrTiO_3$  substrate. This motivation sparked our interest in investigating possible Fe-Se phases when layers of controlled composition are spatially confined between adjacent layers of PbSe. Using a computational "island" approximation, potential candidate Fe-Se structures were placed between bilayers of PbSe and were relaxed in DFT calculations to assess stability of different structures. Of the trialed candidates,  $(PbSe)_{1+n}(FeSe)_n$  with Fe in octahedral coordination (1T) maintained its structure when relaxed. Using the predicted densities of the relaxed model, precursors that mimic the nanoarchitecture of the heterostructure were prepared and annealed at low temperatures to prepare the heterostructures  $(PbSe)_{1+n}(FeSe)_n$  where  $n = 1, 2,$  and  $3$ . To probe the effect of different adjacent layers on the stability of the 1T  $FeSe_2$  layers, we successfully stabilized 1T- $FeSe_2$  in  $(PbSe)_{1+n}(NbSe_2)(PbSe)_{1+n}(FeSe_2)$ . These systems provide insights into interfacial interactions between constituent layers in 2D heterostructures that can be used to prepare layers with structures not found in the phase diagrams of the constituent elements.

**3:40pm 2D2-ThA-5 Comparative Study of How Growth Parameters Affect the Optoelectronic Properties of  $MoSe_2$  and  $WS_2$  on Sapphire Substrates Grown by Chemical Vapor Deposition (CVD), Selena Coye, Department of Physics, Clark Atlanta University; K. Johnson, Morehouse College, Department of Dual Degree Engineering; I. Matara Kankanamge, M. D. Williams, Department of Physics, Clark Atlanta University**

Two-dimensional molybdenum diselenide ( $MoSe_2$ ) and tungsten disulfide ( $WS_2$ ) exhibit remarkable properties that make them ideal for various applications in nanoelectronics, spintronics, valleytronics, and optoelectronics. The bandgap of these materials increases as their thickness decreases. Specifically, when reduced to a monolayer, the bandgap changes from indirect to direct. The bandgap of  $MoSe_2$  is  $1.1\text{ eV}$

for the bulk layer and  $1.5\text{ eV}$  for the few layers. On the other hand, monolayer  $WS_2$  has a direct bandgap of  $2.15\text{ eV}$ , whereas bulk  $WS_2$  has an indirect bandgap of  $1.3\text{ eV}$ . These materials are grown on different substrates however, sapphire is an excellent substrate for growing these materials due to its remarkable mechanical and thermal properties and chemical stability. Consequently, it produces a mechanically robust and thermally stable film, making it indispensable for devices requiring durability and the ability to withstand high temperatures. By growing  $WS_2$  on a sapphire substrate, it can achieve epitaxial growth by reducing the lattice mismatch between sapphire and  $WS_2$ . This leads to a high-quality  $WS_2$  film with fewer defects, thus enhancing the material's overall structural quality. Chemical vapor deposition (CVD) is the widely used technique to grow these materials. However, the quality of the layers (including their crystallinity, crystallite size, and coverage area) grown by CVD depends on factors such as growth temperatures, growth time, precursors, flow rate, and substrate nature. Our research will study the effect of carrier gas flow rate and growth time on the bandgap, lattice structure, optical properties, and structural quality of  $MoSe_2$ /sapphire and  $WS_2$ /sapphire layers grown by CVD. We will analyze the properties of these films using Raman/PL, FTIR spectroscopy, and confocal microscopy.

**4:00pm 2D2-ThA-6 Imaging Spin Filter for NanoESCA Based on Au/Ir or Oxide Passivated Fe, M. Escher, N. Weber, T. Kuehn, Marten Patt, FOCUS GmbH, Germany**

The energy-filtered photoelectron microscope NanoESCA [1,2] is a powerful tool for various application including work-function mapping, imaging XPS and in the last years more prominently for momentum microscopy on 2D materials (e.g. see [3]).

This analyzer can be used with an efficient spin filter that enables to image a 2D-distribution of the electron spin polarization by scattering the electrons at a polarizing target. We will show results from the first commercial build Au/Ir Imaging Spin Filter. Sherman functions of +68% and -58% were found at a reflectivity of more than 1% (also see literature [4]).

Spin-filtered images of magnetic domains show that along the diameter of the field of view more than 100 separate image points can be resolved. This increases the effective 2D figure-of-merit of this analyzer by nearly four orders of magnitude compared to single-channel spin detectors. We also present proof of principal measurements of an Imaging Spin Filter with oxide passivated Fe as scattering target [5]. Oxide passivated Fe allows for an easy switch of the polarization detection direction, like it is known from FERRUM detectors [6] for ARPES.

## References

- [1] M. Escher et al., J. Phys. Cond. Matter **17** (2005)
- [2] B. Krömkner et al., Rev. Sci. Instrum. **79** (2008)
- [3] A. Polyakov et al., Nature Comm. **13** (2022) 2472
- [4] C. Tusche et al., Ultramicroscopy **159** (2015) 520–529
- [5] M. Escher et al., Ultramicroscopy **253** (2023) 113814
- [6] M. Escher et al., e-J. Surf. Sci. Nanotech. Vol. **9** (2011) 340–343

## Electronic Materials and Photonics Division Room B116 - Session EM-ThA

**Theme: CMOS+X: Piezoelectrics, Ferroelectrics, Multiferroics, and Memory**

**Moderators: M. David Henry, Sandia National Labs, Stephen McDonnell, University of Virginia**

**2:20pm EM-ThA-1 Factors That Stabilize the Ferroelectric Phase of Hafnia, Jon Ihlefeld, S. Jaszewski, S. Fields, M. Lenox, B. Aronson, University of Virginia; T. Cai, B. Sheldon, Brown University; S. Calderon, Carnegie Mellon University; K. Kelley, Oak Ridge National Laboratory; T. Beechem, Purdue University; M. Henry, Sandia National Laboratories; E. Dickey, Carnegie Mellon University**

**INVITED**

Just over a decade ago, ferroelectricity – the presence of a permanent reorientable dipole – was reported in doped hafnium oxide thin films. This report generated a great deal of excitement as the inherent silicon compatibility of  $HfO_2$ , coupled with the extreme thinness of the films that exhibited the ferroelectric response promised to overcome a number of technological hurdles limiting utilization of ferroelectrics in microelectronics. In spite of the great promise and significant worldwide research efforts, this material has not yet been mass deployed owing to a number of challenges. These include: 1) performance variability for

nominally identical materials and devices produced by different research groups, 2) performance variability as films are used in devices – i.e. polarization changes with use. Virtually all of these issues can be traced to phase impurities in the films – i.e. the ferroelectric phase co-exists with non-ferroelectric phases. In this presentation, I will highlight our group's efforts to better understand this potentially game changing material and to overcome some of these challenges. Two major phase stabilizing mechanisms will be discussed, including: 1) oxygen vacancies, which in pure HfO<sub>2</sub> will be shown to exist in concentrations >20% and whose impact on phase stability appears to be greater than crystallite size and 2) mechanical stress, particularly the role of the top electrode, which serves as an out-of-plane rather than in-plane mechanical constraint. It will be shown that often-cited thermal expansion mismatch of the electrodes and hafnia layers is not consistent with the hafnia film stresses measured and is not a valid explanation of the so-called electrode capping effect. Finally, using synchrotron-based diffraction and spectroscopy, we will show how the phases evolve as the ferroelectric is poled and cycled and how this leads to performance instabilities. Finally, it will be shown that the presence of the non-ferroelectric tetragonal phase may be overstated and that an antipolar (e.g. truly antiferroelectric) orthorhombic phase with space group *Pbca* is common in hafnium zirconium oxide films and can better explain the observed electrical, vibrational, and mechanical behaviors.

**3:00pm EM-Tha-3 Internal Photoemission (IPE) Spectroscopy Measurement of Interfacial Barrier Heights in Pristine and Poled Ferroelectric ALD Hafnium-Zirconium-Oxide Metal/Oxide/Semiconductor (MOS) Devices, Jessica Haglund**, Oregon State University; *T. Mimura*, Gakushuin University, Japan; *J. Ihlefeld*, University of Virginia; *J. Conley*, Oregon State University

Ferroelectric Hf<sub>0.5</sub>Zr<sub>0.5</sub>O<sub>2</sub> (HZO) has attracted much attention for non-volatile memory applications since HfO<sub>2</sub> is already used as a gate dielectric. For efficient integration, knowledge about how HZO interacts with electrode materials is necessary. IPE provides a method to observe interfacial energy barrier heights "in-situ" in working devices. We previously reported the barrier heights in as-deposited HZO in metal insulator metal structures (MIM) [2]. However, both post deposition/metallization annealing, "waking", and "poling" are necessary to stabilize and exploit the ferroelectric behavior [1]. To date, there have not been reports of IPE barrier measurement on woken and poled HZO in metal oxide semiconductor (MOS) structures.

In this study, atomic layer deposition was used to deposit 20 nm HZO on a degenerately doped p-Si using 102 supercycles of TDMAH (HfO<sub>2</sub>) and TDMAZ (ZrO<sub>2</sub>). Next, a blanket 20 nm TaN film was deposited and annealed for 30 seconds at 600°C. This TaN layer was then stripped and replaced by an optically transparent electrode of 5nm TaN and 5 nm Pd. Waking was done using a 5000 cycle 1 kHz square wave with magnitude +/- 5V. Once a device was woken, it was poled using a single voltage pulse of +4V. IPE measurements were done by focusing a single wavelength of light on the device surface while applying a voltage (V<sub>app</sub>) between the Si and grounded top electrode and sweeping photon energy from 1.7 eV to 5.5 eV while measuring IPE current. The measurement is repeated at 0.1V increments from -1.5 to 1.5 V. IPE current thresholds were extracted at each applied voltage, V<sub>app</sub>, and plotted vs. V<sub>app</sub><sup>1/2</sup>. This plot was extrapolated to zero voltage to obtain the band offsets between the TaN and the Si conduction band (CB) and valence band (VB) and the HZO VB.

For pristine devices the TaN, Si CB, and Si VB barriers were measured at 2.5 eV, 3.5 eV, and 4.4 eV, respectively. Following waking, the TaN barrier was reduced to 2.1 eV, possibly indicating redistribution of oxygen defects toward the TaN interface. The Si CB and VB remained roughly the same at 3.4 and 4.6eV, respectively. The barriers of positive poled devices were within error of the woken devices, but the negative poled devices showed an increase in the TaN barrier to 2.8 eV and a decrease in the Si CB and VB barriers to 3.1 and 4.4 eV respectively. This suggests oxygen vacancy movement away from the TaN interface. IPE measurements give new insight into HZO devices operation. C-V and I-V measurements will be discussed at conference.

[1]E. D. Grimley *et al.*, *AEM2* 1600173, (2016)

[2]M. A. Jenkins *et al.*, *ACS AMI* 13, 14634–14643, (2021)

**3:20pm EM-Tha-4 Phase Transformations Driving Biaxial Stress Reduction During Wake-Up of Hafnium Zirconium Oxide Thin Films, Samantha Jaszewski**, Sandia National Laboratories; *S. Fields*, University of Virginia; *S. Calderon*, Carnegie Mellon University; *B. Aronson*, University of Virginia; *T. Beechem*, Purdue University; *K. Kelley*, Oak Ridge National Laboratory; *E. Dickey*, Carnegie Mellon University; *J. Ihlefeld*, University of Virginia

Biaxial stress has been identified to play an important role in the stability of the ferroelectric phase in hafnium oxide-based thin films. However, thus far, the stress state during wake-up has not been quantified. In this work, the stress evolution with electric field cycling in hafnium zirconium oxide capacitors is evaluated. The remanent polarization of a 20 nm thick hafnium zirconium oxide thin film increases from 13.8 μC/cm<sup>2</sup> in the pristine state to 17.6 μC/cm<sup>2</sup> following 10<sup>6</sup> field cycles at 2.5 MV/cm. This increase in remanent polarization with field cycling is accompanied by a decrease in relative permittivity of approximately 1.5, which could indicate that a phase transformation has occurred. The presence of a phase transformation is confirmed by nano-Fourier transform infrared spectroscopy measurements that show an increase in the ferroelectric phase after wake-up. Using an X-ray diffractometer with a collimated source and a two-dimensional detector, diffraction patterns from individual devices electric field-cycled from 0 to 10<sup>6</sup> cycles are collected and stress quantified using the sin<sup>2</sup>(ψ) technique. The biaxial stress was measured in several stages of wake-up and was observed to decrease from 4.3 ± 0.2 to 3.2 ± 0.3 GPa. This work provides new insight into the mechanisms associated with polarization wake-up in hafnium zirconium oxide.

**3:40pm EM-Tha-5 AVS Russell and Sigurd Varian Awardee Talk: Novel Chalcogenide Superlattice-Based Energy-Efficient Phase-Change Memory for 3D Heterogeneous Integration, Asir Intisar Khan<sup>1</sup>**, *X. Wu*, *A. Daus*, *H. Kwon*, *K. Goodson*, *H. Wong*, *E. Pop*, Stanford University

Today's nanoelectronics are reaching limits of energy and speed with conventional materials and traditional layouts that separate logic and memory. For tackling this grand challenge, phase-change memory (PCM) holds promise for both digital memory and brain-inspired computing.<sup>1,2</sup> However, PCM based on traditional phase-change materials like Ge<sub>2</sub>Sb<sub>2</sub>Te<sub>5</sub> (GST) suffers from high switching power and resistance drift, limiting its potential.<sup>1</sup>

Here, using novel chalcogenide superlattices (SL) and leveraging their unique structural and electro-thermal properties, we realize ultralow-power PCM both on rigid and flexible substrates. Using SLs of alternating thin layers of Sb<sub>2</sub>Te<sub>3</sub> and GeTe or GST, we achieved ~8-10x lower switching current density in superlattice-PCM on rigid silicon substrates, compared to conventional GST PCM.<sup>3</sup> Our SLs are sputter-deposited at low temperatures (200 °C), compatible with CMOS back-end-of-line processing. Electro-thermal confinement in the superlattice material enhances the heating efficiency, enabling a dramatic reduction of switching energy in such PCM, as confirmed by our transport measurements and electro-thermal simulations.<sup>4</sup>

We also uncovered a key correlation between the SL interfaces and PCM device performance. We found that both switching current and resistance drift decrease as the SL period thickness is reduced, however, SL interface intermixing increases both.<sup>5</sup> As the SL period thickness is reduced, a greater number of van der Waals (vdW) interfaces limits cross-plane thermal transport, but if the SL interfaces are intermixed, the thermal conductivity can increase, due to the loss of vdW gaps.

We also integrated these superlattices directly onto flexible polyimide substrates in a confined memory cell, achieving further energy efficiency. Our flexible SL-PCM devices show record-low switching current density<sup>6</sup> of 0.1 MA/cm<sup>2</sup>, ~100x lower than commercial PCM. This memory also shows multi-level operation, promising for Internet-of-Things devices on flexible substrates.

In summary, we achieved ultralow-power switching in nanoscale phase-change memory based on chalcogenide superlattices. Our results demonstrate how combining versatile material functionalities and their transport fundamentals can unlock decade-spanning advances in energy-efficient memory for heterogeneously integrated nanoelectronics.

**Refs:** 1. S. Raoux *et al.*, *MRS Bull.* **39**, 703 (2014); 2. A. Sebastian *et al.*, *Nat. Nanotech.* **15**, 529 (2020); 3. A.I. Khan, E. Pop *et al.*, *IEEE EDL* **43**, 204 (2022); 4. H. Kwon, E. Pop *et al.*, *Nano Lett.* **21**, 5984 (2021); 5. A.I. Khan, E. Pop *et al.*, *Nano Lett.* **22**, 6285 (2022); 6. A.I. Khan, E. Pop *et al.*, *Science* **373**, 1243 (2021).

<sup>1</sup> AVS Russell and Sigurd Varian Awardee

# Thursday Afternoon, November 9, 2023

## Fundamental Discoveries in Heterogeneous Catalysis Focus

### Topic

#### Room B113 - Session HC+SS-ThA

#### Closing in on Reality & HC Discovery Reception

**Moderators:** Liney Arnadottir, Oregon State University, Ashleigh Baber, James Madison University, Dan Killelea, Loyola University Chicago

2:20pm **HC+SS-ThA-1 Ion Imaging applied to Heterogeneous Catalysis on Metals**, *Theofanis Kitsopoulos*, University of Southern Mississippi **INVITED**  
I will discuss how to implement ion imaging methods to measure the kinetics and dynamics of elementary reaction on metal surfaces. I will discuss the recombination of H atoms on Pt and Pd, followed by a discussion on the kinetics of formic acid adsorption on Pt and Pd

3:00pm **HC+SS-ThA-3 Structure-Sensitive Metal-Support Interactions – Applications to Selective Hydrogenation Reactions**, *Helena Hagelin Weaver, H. Zhao, M. Lapak, L. Hsiao, D. Choi, C. Bowers*, University of Florida **INVITED**

Producing hyperpolarized molecules is important for increasing signal intensities in nuclear magnetic resonance (NMR) or magnetic resonance imaging (MRI) applications, and one efficient strategy is to add a parahydrogen molecule, where the nuclei have antiparallel spins, to an unsaturated substrate. The requirements for the production of a hyperpolarized molecule are that the added hydrogens must come from the same hydrogen molecule, i.e. a pairwise addition, the spins must be preserved, and the hydrogens in the generated product must be inequivalent. While this is efficient over homogeneous organometallic catalysts, heterogeneous catalysts would be preferred to facilitate separation of hyperpolarized product from the catalyst and allow continuous operation. However, over typical heterogeneous catalysts, i.e. oxide-supported metal nanoparticles, the pairwise addition of parahydrogen is challenging due to facile and reversible dissociation of dihydrogen, rapid diffusion of hydrogen atoms across the metal surface, step-wise addition of hydrogen atoms to the unsaturated molecule, and spillover of hydrogen from the active metal to the oxide support, as these are all mechanisms that can lead to a rapid loss in the singlet spin-correlation of the original parahydrogen molecule. Therefore, the pairwise selectivity in hydrogenation reactions over supported metal catalysts is often very low (< 1%).

To limit diffusion of hydrogen across the metal surface and improve the pairwise selectivity in the hydrogenation of propene, the metal particle size was first reduced to the limit, i.e. single atoms on the support. Single atoms on an oxide support are indeed more selective to pairwise addition of parahydrogen than larger nanoparticles of the same metal, but the activity is low and stability is an issue during reaction conditions. Another approach is to limit diffusion by blocking metal sites with an oxide overlayer. This was done by inducing strong metal-support interactions via a high-temperature reduction of titania-supported catalysts. The structure of the titania support, anatase versus rutile, influenced the metal-support interactions, and active metals, such as Rh and Ir, exhibited different behavior in the pairwise selective addition of parahydrogen to propene. However, in all cases, the high temperature reduction increased the pairwise selectivity regardless of whether geometric (migration of titania over metal) or electronic metal-support interactions were induced. Preliminary data reveal that oxide layers deposited by ALD can also improve the pairwise selectivity in hydrogenation reactions.

3:40pm **HC+SS-ThA-5 High Activity and Selectivity of Dilute Ti-Cu(111) Alloys Toward the Deoxygenation of Ethanol to Ethylene**, *J. Shi*, University of Florida; *H. Ngan, P. Sautet*, University of California at Los Angeles; *Jason Weaver*, University of Florida

Alloys comprised of an early transition metal dispersed in a coinage metal can provide opportunities for effecting selective chemical transformations of organic oxygenates and other compounds. In this talk, I will discuss our recent work to synthesize dilute Ti-Cu(111) surface alloys in ultrahigh vacuum and characterize their structural and chemical properties using experiments and DFT. We find that Cu-capped, Ti-containing islands are preferentially generated on step edges of Cu(111) during Ti deposition below ~500 K, whereas Ti atoms alloy into the step edges during deposition above 500 K. These dilute Ti-Cu(111) surfaces are highly selective for the deoxygenation of ethanol, resulting in the production of only C<sub>2</sub>H<sub>4</sub> and H<sub>2</sub> near 400 K during temperature programmed reaction spectroscopy. DFT calculations corroborate the high selectivity of metallic Ti-Cu(111) surfaces toward ethanol deoxygenation and predict that C<sub>2</sub>H<sub>4</sub> production becomes

significantly favored as the Ti ensemble size is increased from monomer to trimer, and that the O released to Ti during C-O bond cleavage promotes desorption of the C<sub>2</sub>H<sub>4</sub> product by destabilizing its adsorbed state.

## Advanced Focused Ion Beams Focus Topic

### Room A107-109 - Session IB-ThA

#### In Situ FIB Applications

**Moderators:** Valerie Brogden, University of Oregon, Shida Tan, Intel Corporation

2:20pm **IB-ThA-1 Surface Near Helium Damage in Materials Studied with a High Throughput Implantation Method**, *Peter Hosemann*, University of California at Berkeley, Lawrence Berkeley National Laboratory; *M. Baloocha, S. Stevenson, Y. Xie*, University of California at Berkeley **INVITED**  
Helium damage in materials is of interest to the nuclear fusion, fission and spallation community. Helium generation in bulk material can cause embrittlements and swelling while Helium implantation in surface near areas can lead to blistering, fuzz formation and spalling. All phenomena listed are based on the accumulation of Helium into nanosized bubbles as a function of temperature and external stress states. Studying these phenomena traditionally requires ion beam accelerators and large samples. In this work we introduced nanobeam ion implantation methods which enable rapid multi dose ion beam implantation in surface near regions to enable basic scientific studies in single crystal and polycrystal materials such as Cu, Si, W. The combination of Helium ion beam implantation using the Helium Ion Beam Microscope, Atomic Force Microscopy, Nanoindentation and Transmission Electron Microscope allows to bring insight into the formation of blisters, the linking up of Helium bubbles and the associated deformation and cracking mechanism. We were able to confirm previously posed hypothesis in tungsten blistering as well as show the dose threshold for silicon amorphization.

3:00pm **IB-ThA-3 Modes of Strain Accommodation in Cu-Nb Multilayered Thin Film on Indentation and Cyclic Shear**, *Mayur Pole, A. Devaraj, T. Ajantiwalay, S. Tripathi, M. Olszta, T. Wang*, PNNL; *B. Gwalani*, North Carolina State University; *Z. Lu, H. Mehta*, PNNL

Two-phase layered thin films with a high density of semi-coherent interfaces exhibit excellent mechanical properties and thermal stability. In this study, a magnetron-sputtered Cu-Nb dual-layered thin film (~500nm for Cu and ~150nm for Nb) having an amorphous interface between Cu and Nb with a high density of aligned growth twins in Cu is subjected to severe surface deformation. The material is loaded using indentation and cyclic shear under tribological testing. The strain accommodation in the subsurface microstructure after deformation varies based on the local structure and deformation mode. Grain refinement and crack formations in the stressed region of the Nb layer and localized crystallization of the amorphous interface are observed after indentation and scratch testing. Pronounced detwinning of growth twins in the Cu layer under the cyclic shear strain leaves large dislocations sites and loops which are observed both by high-resolution transmission electron microscopy and experiment-guided molecular dynamic (MD) simulations. Our simulations provided insights into understanding the pathway for the detwinning process under cyclic shear loading.

3:20pm **IB-ThA-4 Investigating the Site-Specific Mechanical Properties of Advanced Aluminum Alloys via in-Situ Micromechanical Testing Inside the Plasma FIB**, *Tanvi Ajantiwalay, A. Devaraj*, Pacific Northwest National Laboratory

Plasma focused ion beam (PFIB) has the potential to fabricate large damage-free specimens for various analytical applications. The use of heavier xenon (Xe) ions instead of conventional gallium (Ga) ions provide faster-milling rates and no ion-implantation. In this work, we demonstrate the utilization of PFIB to fabricate site-specific specimens for micromechanical testing of various aluminum (Al) alloys processed via advanced techniques such as friction stir, and additive manufacturing. Both these techniques modify the local microstructure of the base material to achieve grain refinement and hence optimum mechanical properties. A correlation between the microstructure and mechanical properties is thus established through in situ micromechanical testing inside the PFIB/SEM, which, is eventually beneficial to improve the process parameters and the overall performance of these alloys.

# Thursday Afternoon, November 9, 2023

3:40pm **IB-ThA-5 Evolution of Stress Fields During Crack Growth and Arrest in Micro-Cantilevers During *In Situ* Bending**, *Michael Meindlhuber, M. Alfreider*, Montanuniversität Leoben, Austria; *M. Burghammer, M. Rosenthal*, ESRF, The European Synchrotron, France; *R. Daniel, A. Hohenwarter, C. Mitterer, J. Todt, D. Kiener, J. Keckes*, Montanuniversität Leoben, Austria **INVITED**

In order to improve our understanding of the fracture behaviour in micro-cantilevers it is necessary to elucidate the multiaxial stress and strain fields throughout their irreversible deformation, especially in the regime where simplified homogeneous linear elastic assumptions are not valid anymore. In this contribution, cross-sectional X-ray nanodiffraction (CSnanoXRD) with a resolution of 200nm was used for the detection of the multi-axial strain fields associated with crack growth during *in situ* stepwise deformation of (i) a notched clamped cantilever prepared from a multi-layered thin film composed of four alternating brittle CrN and semi-ductile Cr layers on high-speed steel and (ii) a freestanding cantilever fabricated from a nanocrystalline FeCrMnNiCo alloy. Both cantilevers were manufactured by focused ion beam milling. The Cr/CrN clamped cantilever was loaded stepwise to 150 and 460 mN and multi-axial stress distributions were retrieved in a region of interest of  $40 \times 30 \mu\text{m}^2$ .

An effective negative stress intensity of  $-5.9 \pm 0.4 \text{MPa} \cdot \text{m}^{1/2}$  accompanied by a plastic zone around the notch tip arose in the notched Cr sublayer as a consequence of residual stress in the thin film. The *in situ* experiment indicated a strong influence of the residual stresses on the cross-sectional stress fields evolution and crack arrest capability at the CrN-Cr interface. In detail, crack growth in the notched Cr layer to the adjacent CrN-Cr interface occurred at a critical stress intensity of  $2.8 \pm 0.5 \text{MPa} \cdot \text{m}^{1/2}$ .

The freestanding FeCrMnNiCo cantilever was loaded to 22, 45 and 34mN loads, which corresponds to conditions where elastic loading, crack tip blunting and void formation and coalescence with the crack front are the governing mechanisms, respectively. In that case, CSnanoXRD data were evaluated in a region of  $30 \times 35 \mu\text{m}^2$  centered around the crack tip. At a load of 22mN, a bending stress up to  $\pm 1$  GPa was evaluated, while directly in front of the notch the crack opening stress raised to 4GPa. In a 200nm circular zone around the notch the measured stress distributions deviated evidently from the linear-elastic fracture mechanics assumptions. At 45mN, crack opening stresses increased to 4.5GPa and a  $1 \mu\text{m}$  wide distinct plastic zone formed. Further loading lead to a breakdown of the commonly assumed crack tip singularity and a significant decrease of the evaluated stress magnitude.

The quantitative experimental stress results provide unprecedented insights into the gradual stress evolution at the crack tip and across the cantilevers as well as associated fracture processes in nanocrystalline materials.

## Light Sources Science Mini-Symposium

### Room C124 - Session LS+AC+AS+LX+MI+TH-ThA

#### Facility Upgrades and Recent Capability Development

**Moderators:** *David Shuh*, Lawrence Berkeley National Laboratory, *James G. Tobin*, University of Wisconsin-Oshkosh, *Gertrud Zwicknagl*, Technical University Braunschweig

2:20pm **LS+AC+AS+LX+MI+TH-ThA-1 The Impact of Upgraded High-Brightness Synchrotron Lightsources on the Chemical Speciation of Nanoscale Heterogeneous Aggregates and Transformations**, *Andreas Scholl*, Advanced Light Source, Lawrence Berkeley National Laboratory **INVITED**

ALS-U is an ongoing upgrade of the Advanced Light Source (ALS) at Berkeley Lab that will endow the ALS with revolutionary x-ray capabilities. The new storage ring will enable the production of highly focused beams of soft x-ray light that are at least 100 times brighter than those of the existing ALS. Applying this technology at the ALS will help us better understand and develop new materials and chemical systems needed to advance our research needs in energy science, environmental systems research, and biosciences in the 21st century. This will create a world-leading platform for next-generation soft x-ray and tender x-ray instrumentation.

Four beamlines with new and upgraded capabilities will become available after the upgrade. The FLEXON beamline (Fluctuation and Excitation of Orders in the Nanoscale), a high-brightness coherent soft x-ray beamline, will provide x-ray photon correlation spectroscopy and diffraction imaging techniques to study electronic, chemical, and magnetic fluctuations in quantum materials with nanosecond temporal and nanometer spatial

resolution. A new ALS-U developed tender x-ray beamline is designed to address challenges at the frontiers of diverse scientific areas, ranging from soft condensed matter and biomaterials to energy science and Earth and environmental sciences. It will offer state-of-the-art nanometer-resolved chemical imaging and resonant scattering nanoprobe, enabling operando and in situ studies of materials of K-edges of elements (Na through Ca) and the M and L edges of lanthanides and actinides. These two beamlines will be complemented by two upgraded beamlines for nanometer 3D chemical tomography based on ptychography of light elements and first-row transition metals and for high-resolution ARPES.

The high coherent flux of the upgraded ALS will drastically improve the speed, sensitivity, and spatial resolution of nanoprobe, enabling the speciation and forensic study of nanoscale constituents and contaminants via x-ray absorption spectroscopy and fluorescence detection. Chemical signatures can be correlated with morphology and compared with chemical standards. Operando experiments, for example, of liquid phase systems and studies under ambient conditions, will be enabled by specially designed sample holders and liquid cells using the high penetration of tender x-rays.

3:00pm **LS+AC+AS+LX+MI+TH-ThA-3 The Advanced Photon Source Upgrade: A transformative tool for understanding material structure**, *Jonathan Lang, J. Lang*, Argonne National Laboratory **INVITED**

The APS is currently undergoing a major upgrade of the facility that will increase the brightness of the x-ray beams by factors of up to 500. This upgrade will provide transformational capabilities for examining the nanoscale structure and electronic configuration of materials and their evolution with external stimuli. This presentation will provide an update on the current status of the APS-U project, and discuss the new opportunities for imaging actinide and rare-earth compounds with this new source

3:40pm **LS+AC+AS+LX+MI+TH-ThA-5 Combining Focused Ion Beam Sectioning, Soft X-ray Spectromicroscopy, and Non-Negative Matrix Factorization to Reveal Actinide Chemical Speciation at the Nanoscale**, *Alexander Ditter, D. Smiles, J. Pacold, D. Lussier*, Lawrence Berkeley National Laboratory; *Z. Dai*, Lawrence Livermore National Laboratory; *A. Altman*, Lawrence Berkeley National Laboratory; *M. Bachhav*, Idaho National Laboratory; *B. Chung*, Lawrence Livermore National Laboratory; *C. Degueldre*, Lancaster University, UK; *S. Donald*, Lawrence Livermore National Laboratory; *L. He*, Idaho National Laboratory; *M. Mara, S. Minasian, D. Shuh*, Lawrence Berkeley National Laboratory **INVITED**

Spectromicroscopy methods, combining the chemical insight of spectroscopy with microscopy imaging, can give a unique and informative view of a sample of interest. Scanning Transmission X-ray Microscope (STXM) spectromicroscopy is one such method, utilizing synchrotron radiation to probe electronic structure with a spatial resolution in the tens of nanometers. Specialized methods like ptychography can push the spatial resolution even lower into the single nanometer range.

Discussed here, STXM spectromicroscopy is applied to two actinide samples: spent nuclear fuel, which offers a unique insight into the complex environment of nuclear fuel undergoing burnout, and uranium oxide allowed to age in a humid environment, which serves as a demonstration of the power of this technique for nuclear forensics investigations. These samples are created by focused ion beam (FIB) sectioning to generate cross-sections of ideal thickness for soft x-ray measurements (100-200 nm). The FIB method of sample preparation also allows for the measurement of highly radioactive spent fuel without containment due to the extremely small amount of material present.

Data analysis is a key component to the understanding of spectromicroscopy results for varied samples like these. Non-negative matrix factorization (NMF) is employed to identify key components and recent efforts to improve NMF to work with noisy individual STXM spectra are outlined here. Reproducibility of the analysis is a concern (as with similar methods like multivariate curve regression) and methods to enhance both reproducibility and interpretability of the results are discussed.

Combining STXM spectromicroscopy, FIB sectioning, and NMF analysis has allowed for unique insights into actinide materials. Potential future developments utilizing this method for other samples and with advanced techniques like ptychography are also discussed.

# Thursday Afternoon, November 9, 2023

## Manufacturing Science and Technology Group

Room C120-122 - Session MS+AP+AS+TF-ThA

### Machine Learning for Microelectronics Manufacturing Process Control

**Moderator:** Tina Kaarsberg, U.S. Department of Energy, Advanced Manufacturing Office

2:20pm **MS+AP+AS+TF-ThA-1 Human-Machine Collaboration for Improving Semiconductor Process Development, Keren Kanarik, LAM Research** **INVITED**

Although chips have been designed by computers for decades, the processes used to manufacture those chips are mostly developed manually – a costly endeavor using highly trained process engineers searching for a combination of tool parameters that produces an acceptable result on the silicon wafer. To assess whether AI could be beneficial in accelerating process engineering innovation and reducing costs, humans and machine algorithms were benchmarked on a virtual high aspect ratio plasma etch process [Kanarik, et al. Nature 616, 707–711 (2023)]. This talk will review results and take a behind-the-scenes look at the study, which showed a “human first, computer last” approach could reach process engineering targets dramatically faster and at half the cost compared to today’s approach. While human expertise and domain knowledge are essential for the foreseeable future, the results point us to a path to foundationally change the way processes are developed for manufacturing chips.

3:00pm **MS+AP+AS+TF-ThA-3 Machine Learning-based Atomic Layer Deposition, Kanad Basu, University of Texas at Dallas** **INVITED**

Atomic Layer Deposition (ALD) is dependent on a host of process parameters. These independent parameters can be set to a particular value to create customized recipes for growing films. Although they are considered to significantly influence the ALD process, existing research does not provide a methodology to quantify the impact of these parameters on growth rate and final thickness of a film. Moreover, process parameter-based thickness estimation is a resource- and time-intensive approach, requiring numerous experiments. To address these challenges, we propose a machine learning (ML)-aware strategy that generates “feature importance maps” to determine the most critical process parameters. In our study, we utilize a Veeco® Fiji Gen2 ALD system to grow a CeO<sub>2</sub> film. Specifically, our study is associated with 78 process parameters, which include chuck temperatures, chamber temperatures, line temperatures, precursor temperatures, gas flow rates, among others. Our approach utilizes a random forest classifier, which identifies the top-10 features (parameters) that affect ALD processes. The proposed approach furnishes promising results of up to 99% thickness prediction accuracy using the deduced top-10 features. These results are subsequently validated using in-situ spectroscopic ellipsometry, thereby advocating its effectiveness in generating the feature importance maps. We posit that only these ten features can be utilized to monitor and control ALD processes. Furthermore, in this analysis, we demonstrate the robustness of our solution, which is independent of the type of ALD process considered – standard ALD process or temperature-dependent Temperature-Time-Thickness (TTT) ALD processes. Moreover, by monitoring just ten of the 78 process parameters, the proposed approach has implications of reduced data dimensionality (up to 87.2% reduction in feature space).

3:40pm **MS+AP+AS+TF-ThA-5 Rapid Optimization of Gap-Fill Recipes Using Machine Learning, Sebastian Naranjo, L. Medina de Oliveira, M. Chopra, Sandbox Semiconductor**

Creating and optimizing deposition recipes for nanostructured devices is costly and time-consuming. A major source of defects and device performance degradation is the formation of interior voids. These voids can have a number of causes, including non-uniform deposition rates along the substrate surface due to imperfect seeding and/or mass transport and reaction kinetics factors, as well as critical dimension variations in the initial profile due to imperfections in preceding processing steps. For example, during electroplating, the substrate surface is seeded before material deposition is set to fill the gap. Non-conformal seedings can cause the deposited material to accumulate at different rates and lead to localized voids. Void defects can also occur in highly conformal processes such as atomic layer deposition or chemical vapor deposition due to critical dimension variations such as bowing or tapering in the pre-deposition profile. Current methods for optimizing process performance rely largely on trial and error. Here we present a cost-effective and systematic computational approach to optimize recipe conditions using Sandbox Studio AI, which employs a combination of feature scale modeling and

machine learning to rapidly predict process outcomes for a given electroplating system using a minimal number of experiments. In this approach, we first use critical dimension information about the fill height and void defects from a set of experiments to calibrate a feature scale model. We then use the calibrated model to predict critical dimension outcomes for thousands of possible process parameter combinations. These predictions are used to maximize process window stability and provide recipe recommendations that minimize the formation of voids even in the presence of seeding or initial profile imperfections. The showcased approach demonstrates how computational modeling can be used to accelerate learning cycles, improve process quality, and reduce development costs.

## Plasma Science and Technology Division

Room A106 - Session PS1-ThA

### Plasma-Surface Interactions II

**Moderators:** Lei Liu, Lam Research Corporation, Pingshan Luan, TEL Technology Center America

2:20pm **PS1-ThA-1 A Pseudo-Wet Plasma Etching Mechanism for SiO<sub>2</sub> at Cryogenic Temperature Using Hydrogen Fluoride Gas within-Situ Surface Monitoring, Shih-Nan Hsiao, M. Sekine, Nagoya University, Japan; Y. Iijima, R. Suda, Y. Ohya, Y. Kihara, Tokyo Electron Ltd., Japan; T. Tsutsumi, K. Ishikawa, Nagoya University, Japan; M. Hori, nagoya University, Japan**

The mainstream of every platform requiring data storage for mobile device applications is the 3D NAND flash memory, which boasts increased data capability. Despite its promising properties, the increasing number of stacking layers to enhance data capability poses various challenges, not only in terms of manufacturing process but also from a fundamental scientific perspective. The intensive development of the stacking number has led to significant advancements in deep hole etching, such as high-aspect-ratio contact (HARC) etching, for the stacking layers. Recently, an ultra-high speed etch process at cryogenic temperature for 3D NAND has been presented [1]. To explore the etching mechanism, the SiO<sub>2</sub> cryogenic etching using hydrogen fluoride (HF) plasma was investigated with *in situ* monitoring techniques including spectroscopic ellipsometry and attenuated total reflectance Fourier transformation infrared spectroscopy (ATR-FTIR). A dual frequency capacitively coupled plasma reactor was used to etch the PECVD-prepared SiO<sub>2</sub>. The T<sub>s</sub> was controlled from 20 to –60 °C by circulating a coolant through the bottom electrode. The etch rate (ER) of the SiO<sub>2</sub> dramatically increased by a factor of approximately 8, from 1.4 to 10.6 nm/s, as T<sub>s</sub> was decreased from 20 to –60 °C (see supplemental document for details). The presence of physisorption of HF and H<sub>2</sub>O at lower temperature was confirmed by the results obtained using the *in-situ* ATR-FTIR. The absorbance spectra acquired at different T<sub>s</sub> clearly display that the HF-related molecules were generated by the HF plasma and absorbed on the surface of the SiO<sub>2</sub> film. The ER exhibiting the increasing trend is consistent with the absorbance intensity of the HF-related molecules (also see supplemental document). This indicates that the absorption of HF and the incorporation of HF-related molecules contribute great impact on etching of SiO<sub>2</sub> at low temperature. Based on these results, a “pseudo-wet” etching model and surface reactions of SiO<sub>2</sub> using HF plasma at low temperature is proposed.

[1] Y. Kihara et al., VLSI symposium T3-22023.

2:40pm **PS1-ThA-2 Coalescence/De-Coalescence Plasma Patterns on a Plasma-Liquid Interface, Jinyu Yang, O. Dubrovski, P. Rumbach, H. Chang, D. Go, University of Notre Dame**

Self-organized anode patterns in plasma electrolysis have recently gained substantial interest, yet a comprehensive fundamental mechanistic understanding of the pattern formation and self-organization remains elusive. Here, we report observations of a distinct mode consisting of coalescence and de-coalescence oscillations (CDO) between plasma patterns when operating the cathodic glow discharge at a moderate current of ~26 mA. Fast-imaging measurements resolve a liquid conductivity- and viscosity-dependent CDO frequency of ~200 Hz, indicating a potential transport-limited process as the frequency is far lower than any reaction timescales inherent to plasma processes. We therefore propose that advective transport of liquid phase ions (cations) due to surface capillary waves that arise from the electrostatic Maxwell pressure on the plasma-liquid interface is responsible for the observed CDO plasma patterns. A

# Thursday Afternoon, November 9, 2023

theoretical model for viscous capillary waves, coupled with the electrostatic Maxwell stress, is developed. Both the theoretical and the experimental data collapse onto a single universal curve, suggesting a strong correlation between the measured CDO frequency and the induced capillary waves. Further experimental investigation using laser-assisted visualization reveals the existence of surface capillary waves when CDO plasma patterns are being generated, confirming the hypothesized connection between the unexpected dynamics of the plasma and the dynamic liquid behavior.

**3:00pm PS1-ThA-3 Plasma-Surface Interactions at Atmospheric Pressure: From Liquids to Catalytic Surfaces, Peter Bruggeman, University of Minnesota INVITED**

The unique non-equilibrium conditions of low temperature atmospheric pressure plasmas enable the delivery of highly reactive plasma species to substrates at (near) ambient temperatures which is beneficial for a broad range of applications. For example, plasmas interfacing with liquids enable plasma-aided decomposition of recalcitrant organic pollutants in water, decontamination of liquids and material synthesis. In addition, the interaction of plasmas with catalysts offers a sustainable electrically driven route to synthesize chemicals such as ammonia, a molecule that is vital for sustaining global food production or can be used to enhance catalytic reactors used for the removal of trace compounds like VOCs and NO<sub>x</sub> from polluted air streams.

In this presentation, we will discuss advances in our understanding of the underpinning mechanisms of plasma-induced liquid phase chemistry in the context of plasma-driven liquid phase redox reactions for nanomaterial synthesis and chemical conversions and gas phase plasma-catalyst interactions enabling the formation of NH<sub>3</sub> from N<sub>2</sub> and H<sub>2</sub> at near ambient conditions. We will show that a detailed experimental characterization of well-designed reactors allows us to develop simplified models of the complex plasma-substrate interactions leading not only to a conceptual but also quantitative understanding of the key species involved in the interactions and the rate limiting processes. We will for example show that a detailed knowledge of the gas phase OH and electron densities, allows us to quantitatively explain liquid phase plasma-induced redox reactions [1] and a detailed measurement of gas phase reactive species fluxes to the catalytic substrate enables one to conclude that NH<sub>3</sub> formation by plasma-catalysis is consistent with surface reactions involving N radicals [2].

## References

[1] Y. Yue, S. Exarhos, J. Nam, D. Lee, S. Linic, and P. J. Bruggeman, *Plasma Sources Sci. Technol.* **31**(2022) 125008

[2] B. Bayer, P. Bruggeman and A. Bhan., *ACS Catal.* **13** (2023) 2619-2630

## Acknowledgements

This work was partially supported by the US Department of Energy under Award Number DE-SC-0016053, the National Science Foundation under Award Number CBET-2234270 and the Army Research Office under Grant Number W911NF-20-1-0105.

**3:40pm PS1-ThA-5 Enabling Dry Etching of sub-10 Nm Features at Cryogenic Temperature, S. Srinivasan, J. Li, X. Yang, S. Jashi, T. Liu, Sumit Agarwal, Applied Materials, Inc.**

As the DRAM density scaling continues, there is an ever-increasing challenge in shrinking pattern space to sub-10 nm to enable higher pattern density. Sub-10 nm features induce considerable challenges for ICP based dry etching since the etching needs to be highly directional and spontaneous chemical etching needs to be minimized. With sub-10 nm space, however, the chemical etching is inevitable at room temperature and we observe tapered profile and top space enlargement even with extensive process optimization. To tackle this challenge, we evaluate carbon and oxide etch at cryogenic temperature, and observe significant improvement. For both carbon and oxide etch, cryogenic temperature was able to improve profile angle, shrink space CD as well as reduce defectivity by orders of magnitude, which were hardly achievable at room temperature. We attribute these improvements to the unique cryogenic temperature regime which have (1) stronger sidewall passivation due to higher radical sticking coefficient, (2) less spontaneous chemical etching due to lower reactivity and (3) unique reaction regime to enable new catalyst and passivation. The higher sticking coefficient at cryogenic temperature also allows leaner chemistry to be used, which reduces passivation at etch front and further increases etch rate and selectivity. We expect these process differentiations will benefit other applications with small features and high aspect ratios as well.

**4:00pm PS1-ThA-6 Study of Nonequilibrium Electron and Vibrational Response During Plasma Excitation, Sara Makarem, P. Hopkins, University of Virginia**

Plasmas have long been used for the synthesis and manipulation of materials because of their unique ability to deliver both energy and chemically active species to the surface of plasma exposed materials - an attribute that separates them from other approaches to materials processing. Indeed, that feature provides the ability to drive the surface out of thermal equilibrium with the bulk material thus enabling local physicochemical processes that can be harnessed to establish unique material properties. Traditionally, our understanding of energy delivery from these energetic species is developed using a variety of ancillary plasma diagnostics, temperature measurements, models, and perhaps post-treatment, ex situ surface characterizations to "re-construct" energy deposition and absorption. While certainly of value, none of these approaches provide a direct measure of the localized, transient response associated with the energy flux at the surface.

In this study, with the use of in-situ ultrafast optical detection and sub-picosecond laser systems, we resolve the influence of the various energetic species in an atmospheric plasma on the resulting electronic and thermal response of materials in real time. Through the development of new plasma diagnostics with sub-picosecond to microsecond temporal resolution, we measure the optical response of material surfaces subjected to various types, intensities, and temporal profiles of atmospheric pressure plasma excitations. Through control over both the photon energy and temporal resolution of the laser probe using sub-picosecond and continuous wave lasers of various wavelengths, we selectively probe the optical response of the plasma excited surface, which in turn is related to the electronic structure, scattering dynamics, thermal transport, and elastic and mechanical properties of the lattice. Thus, by utilizing these novel in situ laser-based probes of the electronic, mechanical, and thermal properties of plasma-excited surfaces, we investigate highly non-equilibrium states and properties of materials during plasma exposure.

**Plasma Science and Technology Division  
Room B117-119 - Session PS2-ThA**

## Plasma Modeling and Characterization

**Moderators: Catherine Labelle, Intel Corporation, Du Zhang, TEL Technology Center America**

**2:20pm PS2-ThA-1 Control of the Ion Angle and Energy Distribution by an Embedded Electrode in a Focus Ring for a Capacitively Coupled Rf Plasma, Seoi Choi, H. Lee, Pusan National University, Republic of Korea**

With the recent advancements in semiconductor processes reaching the nanoscale, research is underway to enhance the uniformity of plasma in plasma etching reactors. The non-uniformity of the etch process is noticeable at the edge of the wafer due to inhomogeneous electrical characteristics. We investigate a mechanism to control the plasma sheath above the wafer edge for a uniform etching process over the dielectric focus ring by changing the electric field and ion flux uniformly across the wafer surface using a two-dimensional particle-in-cell simulation parallelized with a GPU. An appropriate waveform on the electrode inserted inside the focus ring changes the sheath oscillation and ion flux to improve the ion energy and angular distributions (IEADs) to achieve a better etch rate.

**2:40pm PS2-ThA-2 Plasma Etch Chemistries for High Aspect Ratio Application with Low Emission, Phong Nguyen, C. Jennings, S. Biltek, N. Stafford, Air Liquide**

In recent years, several countries and semiconductor manufacturing companies have announced targets for net-zero carbon emission by 2050. Plasma etch processes are responsible for a high percentage of emission for chip manufacturing especially in high aspect ratio (HAR) dielectric etch. Such an etch process involves employment of high global warming potential (GWP) fluorocarbon gasses such as C<sub>4</sub>F<sub>8</sub>, CH<sub>2</sub>F<sub>2</sub>. In the past decades, Air Liquide R&D has developed multiple alternative chemistries in HAR applications with very low GWP. However, while the gas entering the plasma etch chamber may be high or low GWP, it is difficult to predict the emission gases post plasma due to the complexities of the breakdown and recombination processes within the plasma.

In this study, we demonstrate that the plasma etch chamber emission gas stream can be analyzed and quantified by Fourier Transform Infrared Spectroscopy (FTIR). Complementary to FTIR analysis, Quadrupole Mass

# Thursday Afternoon, November 9, 2023

Spectrometry (QMS), a powerful tool, is implemented to help identify emission species in the chamber via studying positive ion fragments present inside the plasma. In addition, these Air Liquide novel chemistries have shown improved etch performance with lower CO<sub>2</sub> equivalent emission as compared to that of current baseline in HAR etch processes.

3:00pm **PS2-ThA-3 Two and Three-Dimensional Kinetic Modeling of Capacitively Coupled Plasma Discharge in Cylindrical and Cartesian Geometry**, *Willca Villafana*, A. Powis, Princeton University Plasma Physics Lab; S. Rauf, Applied Materials; I. Kaganovich, Princeton University Plasma Physics Lab

In a Capacitively Coupled Plasma (CCP) discharge, the processing rates and uniformity of the wafer depend on key parameters such as the ion flux, ion energy distribution function (IEDF), and plasma homogeneity. The non-Maxwellian nature of the IEDF requires a kinetic treatment, which can be achieved with Particle-In-Cell (PIC) simulations.

In this work, we develop a procedure to control the plasma uniformity and its dynamics using a weak magnetic field with a 2D cylindrical axisymmetric model. The present investigation takes leverage of PIC modeling and uses the explicit EDIPIC-2D code [1]. A detailed analysis of the sheath structure, the ion flux, and IEDF at the wafer will be performed. Additionally, we will also report recent examples and progress regarding 3D PIC modeling using the in-house LTP-PIC code [2].

<sup>1</sup> <https://github.com/PrincetonUniversity/EDIPIC-2D>

<sup>2</sup> T. Charoy, et al, "2D axial-azimuthal particle-in-cell benchmark for low-temperature partially magnetized plasmas," *Plasma Sources Sci. Technol.* **28**(10), 105010 (2019).

## Acknowledgments:

This Research was funded by the US Department of Energy through CRADA agreement with AMAT.

3:20pm **PS2-ThA-4 Effect of Feed Gas Content and Substrate Temperature on RIE of SiN<sub>x</sub> with Ar/C<sub>4</sub>F<sub>6</sub>/O<sub>2</sub> Plasma**, *Xue Wang*, Colorado School of Mines, USA; R. Gasvoda, Lam Research Corporation, Tualatin; E. Hudson, P. Kumar, Lam Research Corporation, Fremont; S. Agarwal, Colorado School of Mines

**Effect of feed gas content and substrate temperature on RIE of SiN<sub>x</sub> with Ar/C<sub>4</sub>F<sub>6</sub>/O<sub>2</sub> plasma**

*Xue Wang*<sup>1</sup>, *Ryan J. Gasvoda*<sup>2</sup>, *Eric A. Hudson*<sup>3</sup>, *Prabhat Kumar* \*<sup>3</sup>, *Sumit Agarwal* \*<sup>1</sup>

<sup>1</sup>Colorado School of Mines, Chemical and Biological Engineering, Golden, CO, USA

<sup>2</sup>Lam Research Corporation, Tualatin, OR, USA

<sup>3</sup>Lam Research Corporation, Fremont, CA, USA

In reactive ion etching (RIE) with fluorocarbon-based plasmas, the etch selectivity of SiO<sub>2</sub> relative to SiN<sub>x</sub> is controlled by tuning the F to C ratio in fluorocarbon feed gas, and by tuning the ion energy. Previously, we showed that the substrate temperature is one potential process knob to control the etch selectivity for SiO<sub>2</sub> over SiN<sub>x</sub> during C<sub>4</sub>F<sub>6</sub>/Ar plasma RIE. Our *in situ* optical diagnostics show that increasing the substrate temperature during RIE of SiN<sub>x</sub> from 70 to 120 °C creates an etch-stop layer and lowers the etch rate of SiN<sub>x</sub>, with no noticeable effect over the same temperature range during RIE of SiO<sub>2</sub>. *In situ* infrared spectroscopy and *ex situ* X-ray photoelectron spectroscopy (XPS) show that the fluorocarbon layer on the SiN<sub>x</sub> surface is more defluorinated at 120 °C, likely forming a graphitic etch stop layer which lowers the etch rate.

In this work, we explore the substrate temperature dependence on RIE of SiN<sub>x</sub> as a function of O<sub>2</sub> dilution of a C<sub>4</sub>F<sub>6</sub>/Ar plasma. Using *in situ* four-wavelength ellipsometry, we measured the steady-state etch rate of SiN<sub>x</sub> over 200 s. In our experiments, we varied the O<sub>2</sub> to C<sub>4</sub>F<sub>6</sub> flow ratio over the range of 0.29 to 1.75. Consistent with previous studies, the etch rate of SiN<sub>x</sub> increased with increasing O<sub>2</sub> to C<sub>4</sub>F<sub>6</sub> flow ratio in the feed gas at both substrate temperature of 70 and 120 °C. High-resolution spectra of the C 1s and F 1s regions were measured for SiN<sub>x</sub> surfaces after 200 s of RIE with *ex situ* XPS for O<sub>2</sub> to C<sub>4</sub>F<sub>6</sub> flow rate ratios of 0.29, 0.75, and 1.75. Analysis of the XPS data shows that addition of O<sub>2</sub> results in a thinner CF<sub>x</sub> layer, which enhances the etch rate of SiN<sub>x</sub>. More interestingly, we found that the etch rate of SiN<sub>x</sub> is higher at 120 °C than that at 70 °C at low O<sub>2</sub> to C<sub>4</sub>F<sub>6</sub> ratios (< 1.25). This temperature dependence flips for O<sub>2</sub> to C<sub>4</sub>F<sub>6</sub> ratios >1.25. We speculate the thickness of CF<sub>x</sub> layer and mixing layer are influenced by the substrate temperature, which leads to this temperature dependent etch

behavior.

## Oral Presentation Requested

3:40pm **PS2-ThA-5 Characterization of Ion and Reactive Species in Perfluorocarbon Gas (C<sub>4</sub>H<sub>2</sub>F<sub>6</sub>-Z) Plasma for Mitigating Global Warming Potential**, *Minsu Choi*, Chungnam National University (CNU), Republic of Korea; Y. Lee, Institute of Quantum Systems (IQS), Chungnam National University (CNU), Republic of Korea; C. Cho, Chungnam National University (CNU), Republic of Korea; S. Kim, Institute of Quantum Systems (IQS), Chungnam National University (CNU), Republic of Korea; I. Seong, W. Jeong, B. Choi, S. Seo, Chungnam National University (CNU), Republic of Korea; Y. Seol, Institute of Quantum Systems (IQS), Chungnam National University (CNU), Republic of Korea; H. Tak, Sungkyunkwan University (SKKU), Republic of Korea; G. Yeom, Sungkyunkwan University (SKKU), SKKU Advanced Institute of Nano Technology (SAINT), Republic of Korea; S. You, Institute of Quantum Systems (IQS), Chungnam National University (CNU), Republic of Korea

In semiconductor and display manufacturing, Perfluorocarbon (PFC) gases are widely used for cleaning post-etching and deposition. With the adoption of advanced patterning like Double Patterning Tech (DPT) and Quadruple Patterning Tech (QPT), PFC gas consumption is rising. However, PFC gases are chemically stable, leading to a high Global Warming Potential (GWP). Reducing PFC gas emissions is essential due to their long-lasting global climate impact.

Transitioning to alternative gases requires understanding ion and active species distribution and plasma density, critical factors dependent on the plasma source. This study focuses on the comprehensive characterization of ion and active species in C<sub>4</sub>H<sub>2</sub>F<sub>6</sub>-Z gas and compares it to the conventional process gas, CHF<sub>3</sub>. Additionally, an essential plasma parameter, plasma density, is measured using a cut-off probe. Experiments in uniform chambers with Capacitively Coupled Plasma (CCP) and Inductively Coupled Plasma (ICP) sources reveal changes in ion and active species with power, pressure, gas ratio, and pulsing frequency.

Comparative data between the conventional and new gases are discussed. This research contributes to the development of alternative precursors to reduce the impact of global warming.

4:00pm **PS2-ThA-6 Cryogenic Aspect Ratio Etching of SiO<sub>2</sub> at CF<sub>4</sub>/H<sub>2</sub>/Ar Plasma in a Cryogenic Reactive Ion Etch System**, *Hee Tae Kwon*, I. Bang, J. Kim, H. Kim, S. Lim, S. Kim, S. Jo, J. Kim, W. Kim, G. Shin, G. Kwon, Kwangwoon University, Republic of Korea

In the manufacturing processes of 3D NAND, the high aspect ratio contact (HARC) etching process, which is one of the most critical steps, has encountered a significant challenge. HARC, typically performed at room temperature, has become increasingly difficult to achieve the desired high aspect ratio while maintaining high productivity. This challenge is expected to become harder when considering devices with highly stacked alternating layers of silicon-containing materials, such as SiO<sub>2</sub> and SiN. Therefore, cryogenic HARC technology has emerged as a promising solution to overcome this challenge, as it offers advantages in terms of productivity and better etch profile. Consequently, we conducted cryogenic aspect ratio etching of SiO<sub>2</sub> at CF<sub>4</sub>/H<sub>2</sub>/Ar plasma in a cryogenic reactive ion etch system. Overall, our results revealed that cryogenic aspect ratio etching of SiO<sub>2</sub> showed a higher etch rate and a higher aspect ratio under the experimental conditions. With these conditions, we conducted the cryogenic aspect ratio contact etching of SiO<sub>2</sub> for the comparison with the etching of SiO<sub>2</sub> at RT as well.

## Surface Science Division

### Room D136 - Session SS+HC-ThA

#### Alloys and Complex Surfaces

**Moderators:** Arthur Utz, Tufts University, Zhenrong Zhang, Baylor University

2:20pm **SS+HC-ThA-1 Single-Atom Alloy Catalysts: Born in a Vacuum, Tested in Reactors, and Understood In Silico**, *E Charles Sykes*, Tufts University **INVITED**

In this talk I will discuss a new class of heterogeneous catalysts called *Single-Atom Alloys* in which precious, reactive metals are utilized at the ultimate limit of efficiency. These catalysts were discovered by combining atomic-scale scanning probes with more traditional approaches to study surface-catalyzed chemical reactions. This research provided links between

# Thursday Afternoon, November 9, 2023

atomic-scale surface structure and reactivity which are key to understanding and ultimately controlling important catalytic processes. In collaboration with Maria Flytzani-Stephanopoulos these concepts derived from our surface science and theoretical calculations have been used to design *Single-Atom Alloy* nanoparticle catalysts that are shown to perform industrially relevant reactions at realistic reaction conditions. For example, alloying elements like platinum and palladium with cheaper, less reactive host metals like copper enables 1) dramatic cost savings in catalyst manufacture, 2) more selective hydrogenation and dehydrogenation reactions, 3) reduced susceptibility to CO poisoning, and 4) higher resistance to deactivation by coking. I go on to describe very recent theory work by collaborators Stamatakis (UCL) and Michaelides (Cambridge University) that predicts reactivity trends for a wide range of *Single-Atom Alloy* combinations for important reaction steps like H-H, C-H, N-H, O-H, and CO<sub>2</sub> activation. Overall, I hope to highlight that this combined surface science, theoretical, and catalyst synthesis and testing approach provides a new and somewhat general method for the a priori design of new heterogeneous catalysis.

**3:00pm SS+HC-ThA-3 Heterogeneities in Early Oxide Evolution on Ni-Cr Alloys Studied with a Combination of XPEEM and Data Analytics Methods, Keithen Orson**, University of Virginia; *W. Blades*, University of Arizona; *Y. Niu*, *A. Zakharov*, Max IV Laboratory, Sweden; *P. Reinke*, University of Virginia

The Ni-Cr alloy system is coveted for its mechanical properties and its resistance to degradation in high-temperature, corrosive environments. This resistance comes primarily from a chemically complex passive film composed of nanometers-thin layer of oxides and hydroxides, but many questions remain about the early stages of passive film growth. Studying this early regime gives insights into how surface orientation and features like grain boundary influence oxide nucleation and growth. The early regime is also where competition between Ni and Cr oxidation occurs on the surface. We studied oxide growth on Ni<sub>22wt%Cr</sub> using the XPEEM techniques  $\mu$ -XAS and  $\mu$ -XPS, giving chemical specificity with a pixel size of 50 nm. We conducted a controlled oxidation on a clean surface with up to 65 L of oxygen at 773 K which records oxide evolution with video rate focused on a region with (212) and (104) surfaces and the corresponding grain boundary. To address the size and complexity of the hyperspectral images we use Principal Component Analysis (PCA) and Non-Negative Matrix Analysis (NNMA) to identify the various spectral components and thus bonding states in the image with spatial and temporal resolution. The Ni L-edge spectra change little over the oxidation process and are characteristic for Ni(0) in line with the known preponderance of Cr oxidation under these conditions. All XAS images include image artifacts mostly seen as modulation of background intensity and slope. Valence band spectra ( $h\nu=95$  eV) reveal grain-dependent work function shifts and appear characteristic of the bonding state for O<sub>ads</sub>. The Cr L-edge shows strong spatial heterogeneities, with NNMA revealing the emergence of chromia nuclei. PCA, while less directly interpretable, gives good qualitative agreement with the NNMA. NNMA analysis informs segmentation of movies taken at a single energy in the Cr-L edge characteristic of oxide. Island nucleation begins between 5 and 20 L of exposure and a logistic growth behavior up to 65L of exposure consistent with Avrami-type nucleation. Chromium oxide particle density and distribution varies widely across the two grains, while particle size remains nearly constant. 21% of the (212) grain is covered evenly by oxide particles, while particle density on (104) is only 11% at the endpoint of the oxidation experiment. A region in the vicinity of the grain boundary on (212) is nearly devoid of chromia particles. In summary, early-stage Ni-Cr oxidation is grain- and texture-specific with chromia island growth dominating in the 0-65 L oxidation regime. Work function shifts and O adsorbates possibly play a role in these heterogeneities behavior.

**3:20pm SS+HC-ThA-4 The Impact of Crystallographic Orientation on the Oxidation of Ni-Cr Alloys, Petra Reinke**, University of Virginia, USA; *W. Blades*, Arizona State University; *D. Jessup*, *J. St.Martin*, *K. Orson*, University of Virginia, USA

Ni-Cr alloys in the FCC random solid solution structure are coveted for their mechanical properties combined with a superb corrosion resistance and thermal stability. The corrosion resistance in aqueous solution, specifically pitting resistance, can be further improved by addition of a third alloying element such as Mo or W. [1] The role of alloy composition and temperature is well studied but significant knowledge gaps exist in our understanding of the initial oxidation steps until complete oxide layers have formed and Cabrera-Mott type growth models can be applied. The competition between Ni and Cr oxidation plays out at < 873 K of relevance

for many energy applications. This regime is highly sensitive to the specifics of surface reactions but also impacted by alloy microstructure. The crystallographic orientation of the surface varies significantly between adjacent grains, and reaches deep into the crystallographic triangle with complex terrace and kink structures. Ni-Cr(100) and Ni-Cr(111) surfaces show highly distinct oxidation pathways modulated by the interfacial epitaxy between NiO and the alloy surface. [2,3] Recent work demonstrated that the pitting resistance in acidic solution is strongly grain orientation dependent. [4] It can be assumed that the orientation of oxide grains in the protective layer leads to contact potentials which influence reactant and vacancy diffusion across the oxide layer as the growth continues.

We will present combined STM, in-situ and operando XPS studies which resolve the oxidation process as a function of crystallographic orientation. We will introduce our approach to identify, and study individual grains with wide variability in surface (h k l) through a combination of metallurgical processing, EBSD, and SEM. The oxidation of individual grains is then be studied and significant variation in oxidation rate and oxide composition are isolated. Thermally induced faceting adds to the complexity of orientation dependent oxidation. It is generally assumed that the epitaxial relation between Ni-Cr and NiO drives its rapid nucleation and layered growth mode. We are extending this assessment beyond the well-studied singular surfaces and calculate structural interfacial models which will also include several chromia surfaces albeit chromia tends to nucleate as sub-oxide surface clusters. [2] The role of interfacial energies in the initial oxidation steps will be assessed for the singular and higher index surfaces.

[1] C. Volders *et al.* npj Materials Degradation **6**, 52 (2022).

[2] W. H. Blades *et al.* ACS Applied Materials & Interfaces **10**, 43219-43229 (2018).

[3] W. H. Blades *et al.* Corrosion Science **209**, 110755 (2022).

[4] K. Gusieva *et al.* The Journal of Physical Chemistry C **122**, 19499-19513 (2018).

**3:40pm SS+HC-ThA-5 Structure of Electrochemical Electrode/Electrolyte Interfaces from First Principles, Axel Groß**, University of Ulm, Germany

Our knowledge about structures and processes at electrochemical electrode-electrolyte interfaces is still rather limited, in spite of its technological relevance in energy conversion and storage. First-principles simulations can help to elucidate these structures in spite of the fact that these simulations are hampered by the complexity of these interfaces together with the fact that the dependence of these interfaces on the electrode potential needs to be properly taken into account. In this contribution, I will first show which insights first-principles calculations can provide with respect to halide and sulfate adsorbate structures at electrochemical interfaces [1,2] using grand-canonical approaches yielding reliable Pourbaix diagrams of the stable adsorbate phases. Furthermore I will demonstrate how ab initio molecular dynamics simulations can contribute to a better understanding of the structure of electric double layers at metal electrodes [3,4]. The presentation will conclude with some general remarks about remaining challenges in our understanding of electrochemical electrolyte/electrode interfaces [5].

## References

[1] F. Gossenberger, F. Juarez, and A. Groß, *Front. Chem.* **8**, 634 (2020).

[2] A. Groß, *J. Phys. Chem. C* **126**, 11439 (2022).

[3] S. Sakong and Axel Groß, *Phys. Chem. Chem. Phys.* **22**, 10431 (2020).

[4] A. Groß and S. Sakong, *Chem. Rev.* **122**, 10746–10776 (2022).

[5] A. Groß, *Curr. Opin. Electrochem.* **40**, 101345 (2023).

**4:00pm SS+HC-ThA-6 Surface Characteristics of Flexible Carbon-Doped Oxide Thin Films Under Reactive Ion Etching Process Using Fluorocarbon-Based Plasma, Seonhee Jang, T. Poche, R. Chowdhury**, University of Louisiana at Lafayette

The microelectronics industry is increasing research on flexible electronics. Instead of the traditional rigid Si-based electronics, flexible electronics utilize polymer substrates that allow stretching, bending, and folding of the device, which drastically expand its applications. A wide variety of inorganic materials, semiconductors, dielectrics, and metals have been integrated for the fabrication of flexible electronic devices. One of the dielectric materials employed in semiconductor devices is carbon-doped silicon oxide (SiCOH). In this study, flexible low-k SiCOH films were produced by plasma-enhanced chemical vapor deposition (PECVD) of tetrakis(trimethylsilyloxy)silane (C<sub>12</sub>H<sub>36</sub>O<sub>4</sub>Si<sub>5</sub>) precursor onto flexible indium tin oxide/polyethylene

# Thursday Afternoon, November 9, 2023

naphthalate (ITO/PEN) substrates using a set of different plasma powers, yielding the films with varying material properties. The physical properties including refractive index, extinction coefficient, surface morphology and roughness, and surface wettability were determined. The surface structures were analyzed by Fourier transform infrared (FTIR) and X-ray photoelectron (XPS) spectra. Four prominent peaks of Si-O-Si stretching, Si-CH<sub>3</sub> bending, Si-(CH<sub>3</sub>)<sub>x</sub> stretching, and CH<sub>x</sub> stretching modes were observed in the FTIR spectra. High-resolution XPS spectra of Si2p, C1s, and F1s were analyzed for the chemical bond structure and elemental composition. Mechanical properties including elastic modulus and hardness were measured using nanoindentation. The pristine SiCOH films were then subjected to an inductively coupled plasma-reactive ion etching (ICP-RIE) process. The etching properties of the flexible SiCOH films were characterized under a set of fluorocarbon (CF<sub>4</sub>)-based plasmas such as CF<sub>4</sub>, CF<sub>4</sub>+O<sub>2</sub>, and CF<sub>4</sub>+Ar. The CF<sub>4</sub> flow rate was maintained at 35 sccm while the O<sub>2</sub> and Ar flow rates were both at 24 sccm. The RF plasma at 13.56 MHz was maintained at 200 W and the ICP power at 40 W. The operating pressure and temperature were 10.0 Pa and ambient temperature, respectively. The duration for etching process was 30 s. Using deconvolution of FTIR and XPS spectra, the surface structures of the SiCOH films after etching process were compared with those of the pristine film. The fraction ratios of the deconvoluted peaks in each prominent peak in the FTIR spectra depended on the deposition plasma power and RIE etching gas composition. In the XPS spectra analysis, each Si2p and C1s peak showed a depressed peak intensity after etching process. With additional etchants of O<sub>2</sub> and Ar, the F1s peak shifted to higher binding energy for lower deposition plasma power and lower binding energy for higher deposition plasma power. Surface properties of flexible SiCOH films after etching were changed according to composition of etchants.

## Thin Film Division

### Room A105 - Session TF-ThA

#### Organic and Polymeric Materials

**Moderators:** Mark Losego, Georgia Institute of Technology, Matthias Young, University of Missouri

2:20pm **TF-ThA-1 Chemical, Biological, and Topological Control Using Chemical Vapor Deposition Polymerization, Joerg Lahann**, University of Michigan, Ann Arbor

**INVITED**

Chemical vapor deposition (CVD) polymerization is a highly effective method for producing conformal, defect-free, and precisely adjustable organic thin films. CVD is particularly advantageous for barrier coatings due to its ability to eliminate the environmental, health, and safety risks associated with solvents, while also providing a wide range of post-polymerization modification options. In this presentation, I will discuss the use of poly-p-xylylene (PPX) and its functional derivatives for modifying the chemical and biological properties of surfaces.

Beyond film deposition, anisotropic liquids, such as liquid crystalline (LC) phases, offer an intriguing possibility for templating materials due to their unique long-range alignment and elastic properties. By combining the benefits of CVD with LCs, we were able to synthesize end-attached nanofiber arrays supported by a solid surface using LC-templated CVD polymerization. Upon rinsing the LC template with organic solvents, we observed that the alignment of the resulting nanofibers correlated with the molecular ordering of the LC template. For example, when a nematic LC film with homeotropic (vertical) anchoring to the substrate was used, the resulting nanofibers were straight, whereas a cholesteric LC film induced helical nanofibers. We further manipulated the morphology of the nanofibers to form enantiomerically pure nanohelices by using a precursor with a chiral center.

T.M. Hafshejani, X. Zhong, J. Kim & J. Lahann, Chemical and Topological Control of Surfaces using Functional Polyene Coatings. *Organic Materials* **2023**, (in press).

X. Zhong, R. Jordan, J.-R. Chen, J.E. Raymond, J. Lahann, Mechanistic studies into the area-selectivity of chemical vapor deposition polymerization, *ACS Applied Materials and Interfaces* **2023** (in press).

D. Varadharajan, K. Nayani, C. Zippel, E. Spuling, K.C. Cheng, S. Sarangarajan, S. Roh, J. Kim, V. Trouillet, S. Bräse, N.L. Abbott, J. Lahann, Surfaces decorated with enantiomorphically pure polymer nanohelices via hierarchical chirality transfer across multiple length scales, *Advanced Materials* **2022**, *34*, 2108386.

K.C.K. Cheng, M.A. Bedolla-Pantoja, Y.-K. Kim, J.V. Gregory, F. Xie, A. de France, C. Hussal, K. Sun, N.L. Abbott, J. Lahann, Templated Nanofiber Synthesis via Chemical Vapor Polymerization into Liquid Crystalline Films, *Science* **2018**, *362*, 804–808.

3:00pm **TF-ThA-3 On the Mechanism of Oxidative Molecular Layer Deposition, Matthias Young, Q. Wyatt, K. Brathwaite, M. Mehregan, M. Ardiansyah, N. Paranamana, K. Brorsen**, University of Missouri

Oxidative molecular layer deposition (oMLD) was first reported in 2014 to form poly(3,4 ethylenedioxythiophene) (PEDOT) thin films using sequential gas-phase exposures of ethylenedioxythiophene (EDOT) monomers and an MoCl<sub>5</sub> chemical oxidant. In the last few years, the number of oMLD polymer chemistries has expanded to include at least four additional monomers, with successful demonstrations using at least three different chemical oxidants. These advances have laid the foundation for oMLD to potentially access a large library of polymers and copolymers with molecular-level precision of thickness and composition. However, within this broad landscape it has been unclear which polymer chemistries will and will not be accessible by oMLD. Here, we report on work to establish fundamental insights into the oMLD growth mechanism to guide further oMLD research. We examine oMLD growth using EDOT, pyrrole (Py), paraphenylenediamine (PDA), thiophene (Thi), and furan (Fu) monomers. We specifically identify (a) the importance of surface monomer-oxidant complexes that lead to self-limiting oMLD surface reactions and (b) the necessity for a two-electron chemical oxidant in these reactions, which must have sufficient oxidation strength to oxidize both a surface and a gas-phase monomer to enable oMLD growth. The mechanistic insight from these studies provides a conceptual framework to predict which oMLD chemistries are accessible using current known oxidants and identify opportunities to develop new chemical oxidants to access a broader range of oMLD chemistries. We report on studies testing the limits of these mechanistic principles by examining oMLD of various monomers and oxidants, as well as oMLD of copolymers. Interestingly, we also identify that molecularly assembled copolymer structures formed by oMLD provide improved electrochemical properties over the corresponding isolated homopolymers. The insights from these studies (1) help establish a roadmap for promising future directions in oMLD research, (2) provide a pathway to address previously intractable questions regarding the molecular origins of polymer properties, and (3) provide an opportunity to control and optimize polymer structure and properties for electrochemical applications including energy storage, water desalination, and sensors.

3:20pm **TF-ThA-4 Adsorbed Polymer Crystals in ICVD: Prevention and Control, Simon Shindler, R. Yang**, Cornell University

Initiated chemical vapor deposition (iCVD) is a technique used to fabricate polymer thin films from the vapor phase. For most applications, films produced in iCVD are practically defect free. However, as the technique is used more often in precision applications like membrane synthesis and even at an industrial scale, quality control and defect prevention will become critical. In this study, we address an important knowledge gap in iCVD by investigating defect formation, a topic that has received little attention to date. We show for the first time that polymer chains which accumulate in the reactor during normal operation can cause defects by forming aggregates on the sample surface. To study these defects in a controlled environment, we mimic the conditions under which they form. Nucleation and growth of defects are measured using optical microscopy over a range of temperatures and in the presence and absence of adsorbed monomer to better understand what drives aggregation. With this understanding we propose a method by which aggregates (and by extension, defects) can be prevented without restricting the domain of potential deposition conditions or stage temperatures used. Our investigation provides a better understanding of the factors driving polymer aggregation in iCVD, which may lead to further improvements in the deposition process.

3:40pm **TF-ThA-5 Area-Selective Initiated Chemical Vapor Deposition (AS-iCVD) for Non-Lithographic Patterning of Polymer Thin Films, Junjie Zhao<sup>1</sup>**, Zhejiang University, China

Patterning of polymer thin films is key to device fabrication and surface engineering. Developing non-photolithographic strategies such as area selective deposition (ASD) could bypass the need for complex optical systems and provide versatile routes for producing polymeric nanostructures. While previous attempts to achieve area selectivity for condensation polymerization and ring-opening metathesis polymerization

<sup>1</sup> TFD Paul Holloway Award Winner

# Thursday Afternoon, November 9, 2023

have been reported, strategies are yet to be explored for initiated chemical vapor deposition (iCVD) which involves free radical polymerization. In this talk, we will present a plasma surface treatment method to enable area-selective initiated chemical vapor deposition (AS-iCVD) for poly(1,3,5-Trivinyl-1,3,5-trimethylcyclotrisiloxane) (pV<sub>3</sub>D<sub>3</sub>). Using HBr/Ar and O<sub>2</sub> plasma, we were able convert Cu regions to high oxidation states, creating radical inhibitors in the non-growth area for iCVD. Our plasma surface treatment resulted in a nucleation delay of ca. 30 min, and enabled a deposition selectivity of ca. 90% on SiO<sub>2</sub> surface. We will discuss how plasma processing time affects the composition of surface Cu species and the resulting area selectivity for iCVD pV<sub>3</sub>D<sub>3</sub>. We will also show the application of our AS-iCVD process to pre-patterned Cu/SiO<sub>2</sub> substrates as a demonstration for self-aligned polymer patterning.

## 2D Materials Technical Group

Room Oregon Ballroom 203-204 - Session 2D-ThP

### 2D-Materials: Poster Session

#### 2D-ThP-1 Multi-MOF-Based Chemical Gas Sensors with Enhanced Selectivity and Sensitivity via Quartz Crystal Microbalances, *Tzer-Rung Su, J. Dhas, C. Pan, M. Paul, C. Simon, C. Chang*, Oregon State University

Metal-organic frameworks (MOFs) have emerged as promising materials for gas sensing applications due to their high surface area, chemical stability, and absorbent selectivity. In this work, we study the combination of thin film MOFs, including Zeolitic Imidazolate Framework (ZIF)-4, ZIF-7, ZIF-8, and ZIF-71 on Quartz Crystal Microbalances (QCM) as chemical sensors. ZIF thin films with controllable thickness were deposited using chemical bath deposition. ZIF films' physical and chemical properties were characterized by X-ray diffraction, Scanning Electron Microscopy, Brunauer-Emmett-Teller analysis, Fourier-transform infrared spectroscopy, and X-ray Photon Spectroscopy. The sensing response of MOFs/QCM sensors depends strongly on the pore properties of sensing material and molecular chemical properties<sup>1</sup>. The physical properties of each MOF, including its pore size, pore volume, and surface area, result in different uptake and release dynamic responses to various gas species, such as Ammonia, Carbon Dioxide, Water, and Volatile Organic Compounds. By simultaneously testing these MOFs/QCM sensors, we obtain different sensing responses to mixtures of gases; these data, combined with a data analytics tool, improve the overall selectivity of the sensing arrays.

Our results demonstrate that the MOF/QCM-based chemical sensing arrays can detect and distinguish a mixture of gas species, enabling the identification and quantification of different gas species.

#### References:

97. Li, X., Zhang, Y., & Guo, L. (2021). Metal-organic frameworks for QCM-based gas sensors: A review. *Sensors and Actuators B: Chemical*, 329, 129200. doi: 10.1016/j.snb.2021.129200

#### 2D-ThP-2 Graphene/Noble Metal Nanoparticles Nanocomposites at the Biointerface with a Blood Brain Barrier Model to Scrutinize Brain Wound Healing, *A. Foti, L. Cali, A. Agafonova, A. Cosentino, C. Anfusio, G. Lupo, Cristina Satriano*, University of Catania, Italy

Graphene-based nanomaterials represent an emerging aspect of regenerative medicine, and graphene oxide (GO) has been especially exploited to overcome the blood-brain barrier (BBB). Noble metal nanoparticles (NPs), including gold (Au), silver (Ag), and palladium (Pd), have the properties of adjustable size, optical properties, flexible surface modification, and biocompatibility, which makes them very attractive for nanomedicine of brain diseases. NPs are able to cross the BBB, therefore can be used as drug delivery carriers or, given their intrinsic anti-inflammatory properties, as theranostic platforms.

In this work, we prepared Au, Ag, and Pd NPs, 20-100 nm in size, and their respective hybrid systems with GO (NP@GO), aiming to investigate wound healing, a complex process involving cell adhesion, migration, and proliferation processes. The wound healing is critically affected by hypoxia, which inhibits endothelial wound repair as a result of decreased migration and proliferation. A derangement of brain wound healing may cause some cases of Alzheimer's disease, leading to an impairment of BBB integrity and function.

The physicochemical characterization was assessed by UV-visible spectroscopy, AFM, DLS and zeta potential, to investigate the plasmonic response thus estimating the NP optical diameter, the morphology, the hydrodynamic size and the surface charge, respectively.

In order to mimic *in vitro* the condition of hypoxia related to pathological situations, we used human brain microvascular endothelial cells (BMECs), the principal components of the BBB together with pericytes and astrocytes, and human umbilical vein endothelial cells (HUVECs). The cytotoxicity and/or proliferation were inspected via MTT assay, and cell migration by the wound scratch assay, while the cellular uptake and the organelle perturbation were scrutinized by confocal microscopy. Moreover, the levels of inflammatory cytokines such as IL-1 $\beta$ , IL-6, IL-8, TNF- $\alpha$ , and HIF1- $\alpha$  and VEGFA were detected at protein and mRNA levels, evaluating the reduction/increase of inflammatory cytokines/anti-inflammatory IL-10.

#### 2D-ThP-4 Performance and Reliability Improvement of IGTO TFTs via Co-Sputtering, *Seung Jin Kim, B. Choi*, Sungkyunkwan University, Korea

In this study, highly improved positive bias stress (PBS) and negative bias stress (NBS) stability of IGTO (InGaSnO) thin film transistor is achieved by simultaneous co-sputtering of HfO<sub>2</sub> and IGTO target. Channel doping via co-sputtering has been extensively studied, and its effect on improving reliability under bias stress has been confirmed through several studies. However, side effects such as decrease in on/off ratio or mobility degradation have also been observed. In this study, we fabricated TFTs with a 2-layer structure, where the bulk channel material was deposited separately after thin co-sputtering deposition of HfO<sub>2</sub> and IGTO at the interface the gate oxide and channel material, instead of co-sputtering the entire channel material. The threshold voltage shift under positive bias and negative bias stress at a stress time of 3000s was improved from 11.5V to 5.8V, and 2.9V to 1.2V respectively. In result, this study suggests an ultimate device fabrication method that can improve the reliability issues due to stress, which is an inherent problems in oxide semiconductors.

#### 2D-ThP-5 NanoFrazor Technology: Enabling Unique Nanowire and 2D Material Device Fabrication, *Nicholas Hendricks, A. Ubezio, M. Käppeli, J. Vergés, J. Chaaban, E. Çağın*, Heidelberg Instruments Nano, Switzerland

Thermal scanning probe lithography (t-SPL), enabled by the NanoFrazor technology, is a nanolithography technique particularly suitable for patterning, contacting, and modifying 2D materials and nanowires [1-5]. t-SPL generates patterns by scanning a heated ultrasharp tip over a sample surface to induce local changes. By using thermal energy as a stimulus, it is possible to perform various modifications to the sample via removal, conversion, or addition of/to the sample surface. Along with an ultrasharp tip, the t-SPL cantilever contains several other important functions such as an integrated thermal height sensor and an integrated heating element both of which are advantageous for generating devices from nanowires and 2D materials.

Nanowires and 2D materials have been the focus of intense academic and industrial research as these materials provide great promise as next generation electronic devices. However, when patterning electrical contacts to nanowires and 2D materials with conventional fabrication techniques (photolithography, electron beam lithography), the fabrication process becomes challenging and time consuming due to overlay requirements. These techniques can also lead to less than desired device performance due to damage from charged particles or ultraviolet irradiation, as well as contamination from residual resist. The issue of time intensive processing comes from the random positioning of nanowires and 2D material flakes on substrates which makes overlay challenging. This point of overlay is addressed with t-SPL by having an integrated thermal height sensor that allows for a non-invasive, in-situ measurement technique to detect buried nanowires or 2D materials prior to patterning. Such capabilities allow for real-time imaging and markerless overlay with high precision [6].

Within this presentation, the background and workings of t-SPL will be briefly introduced, nanostructuring on nanowires and 2D materials will be discussed along with electrical and optical device performance for nanowire and 2D material-based devices fabricated using t-SPL.

- [1] C. Rawlings et al., *ACS Nano*, 9, 6188-6195 (2015); [2] X. Zheng et al., *Nature Electronics*, 2, 17-25 (2019); [3] S. Howell et al., *Microsystems & Nanoengineering*, 6, 21 (2020); [4] A. Conde-Rubio et al., *ACS Applied Materials & Interfaces*, 14, 37 (2022); [5] X. Liu et al., *APL Materials*, 9, 011107 (2021); [6] H. Wolf et al., 2019 Pan Pacific Microelectronics Symposium (Pan Pacific), 1-9 (2019)

#### 2D-ThP-6 Synthesis of 2D-WS<sub>2</sub> on c-sapphire using H<sub>2</sub>S gas-source CVD, *Kun-An Chiu, W. Chen, H. Chen, Y. Lin, C. Chen, H. Chen, F. Chen*, Taiwan Instrument Research Institute, National Applied Research Laboratories, Taiwan

Two-dimensional materials are considered one of the key materials for next-generation semiconductor devices and industrial applications. In recent years, semiconductor devices based on two-dimensional electronic channel materials have shown their feasibility in transistor applications, in order to continue Moore's law [1]. WS<sub>2</sub> is one of the representative materials in two-dimensional transistors. WS<sub>2</sub> exhibits excellent properties, such as high carrier mobility, large on/off ratio, high optical excitation intensity, low response time, and good compatibility with other two-dimensional materials such as graphene [2, 3]. The development of growth processes for rapid and large-scale production of 2D transition metal dichalcogenides (TMDs) are receiving increasing attention in the fields of nanophotonics, flexible electronics, and sensors. Chemical vapor deposition

(CVD) is the most promising method for obtaining high-quality large-area 2D-TMDs. However, current equipment and technology make it difficult to effectively produce large-area, high-quality two-dimensional materials. Most two-dimensional material processes use powder as a precursor. The vapor pressure of metal and sulfur powders is not easily and stably controlled. Although some studies use a mixed H<sub>2</sub>S gas (Ar + H<sub>2</sub>S), it is difficult to effectively control the H<sub>2</sub>S concentration during the process due to the difference in gas density.

In this study, WS<sub>2</sub> was synthesized on a (0001) sapphire substrate using WO<sub>3</sub> powder and pure H<sub>2</sub>S gas as precursors in a hot-wall CVD furnace. The experiment was carried out at a process temperature of 950°C, a pressure of 10–50 torr, and a H<sub>2</sub>S/Ar flow ratio of 0.5–5%. The synthesized WS<sub>2</sub> flakes were characterized by using optical microscopy, Raman spectroscopy, in-plane X-ray diffraction, and transmission electron microscopy. The in-plane GIXRD results showed that the WS<sub>2</sub> flakes were heteroepitaxially grown on the (0001) sapphire substrate with two sets of orientation relationships: (100)<sub>WS2</sub> // (110)<sub>Al2O3</sub>, (110)<sub>WS2</sub> // (100)<sub>Al2O3</sub>, and (110)<sub>WS2</sub> // (110)<sub>Al2O3</sub>, (100)<sub>WS2</sub> // (100)<sub>Al2O3</sub>. This indicates that the WS<sub>2</sub> flakes have a consistent orientation. Furthermore, the TEM observation revealed that the WS<sub>2</sub> film thickness was ~ 7 Å, suggesting that the process can synthesize the WS<sub>2</sub> monolayer.

## References

- [1] T-E Lee, I. Radu, C-C Cheng, and Y-C Su. IEDM 2022, paper 7.4 (2022).
- [2] S. Cadot, O. Renault, D. Rouchon, *et al.*. J. Vacuum Sci. Tech. A 35 061502 (2017).
- [3] B. Yorulmaz, A. Özden, H Şar, *et al.*. Mater. Sci. Semicond. Process. 93 158-163 (2019).

## 2D-ThP-8 Polarization Sensitive Frequency Selective Metasurface for the Infrared Spectral Range, *Micheal McLamb, P. Stinson, N. Shuchi, D. Louisos, T. Hofmann*, University of North Carolina at Charlotte

Metasurfaces, in the form of perfect reflectors, have received attention for their sensing and filtering capabilities. Plasmonic metasurfaces allow for frequency filtering by controlling the input polarization. We demonstrate a frequency filtering metasurface composed of an array of subwavelength metallic pluses fabricated using two-photon polymerization.

## 2D-ThP-9 *In-situ* X-ray Absorption Spectroscopy Study of Monodispersed Cobalt Phthalocyanine on Carbon Nanotubes as Electrocatalyst for Carbon Dioxide Reduction to Methanol, *Mason Lyons*, Oregon State University; *C. Rooney, H. Wang*, Yale University; *Z. Feng*, Oregon State University

Carbon dioxide (CO<sub>2</sub>) is accumulating in the atmosphere, causing entrapment of thermal energy and more chaotic weather. To sustainably decumulate the atmospheric CO<sub>2</sub> and sequester future emissions, it must be utilized in a circular economy. Upcycling of CO<sub>2</sub> to value added products such as hydrocarbons and alcohols requires the use of catalysts, among which molecular catalysts are the most promising due to their product selectivity and high utilization of metals. Unlike many other catalysts which primarily produce the undesired carbon monoxide (CO) intermediate, cobalt phthalocyanine (CoPc) non-covalently anchored on carbon nanotubes (CNTs) exhibits preferential formation of methanol (MeOH) from CO<sub>2</sub> due to a modified Co electronic structure. To investigate the electronic and geometric arrangements of CoPc-CNTs during CO<sub>2</sub> reduction, *in-situ* X-ray absorption spectroscopy (XAS) was employed. The pre-edge peaks at 7710 eV related to orbital mixing increased while the 7715 eV peak related to bonding centro-symmetry decreased, when scanning from open circuit voltage to -1.1 V vs Reference Hydrogen Electrode (RHE) indicating a higher density of states in Co 3d<sup>2</sup> and axial coordination from CNT as well as C adsorbate, respectively. An absorption edge shift associated with Co reduction to Co(I) was also observed and persisted at MeOH producing conditions, previously only reported for CO producing systems. Fitting of the extended X-ray absorption fine structure (EXAFS) spectra confirmed the CoPc coordination and bond lengths with theoretical calculations as well as the presence of a carbon adsorbate at potentials more negative than -0.5 V vs RHE, enabling further CO reduction to MeOH. The rich information from *in-situ* XAS elucidated the structure-property relationship of this catalyst to explain the superior performance of CoPc dispersed on CNTs for CO<sub>2</sub> upgrade.

## 2D-ThP-10 A Method for creating Single Atom Catalysts through Vapor-phase Synthesis of Covalent Organic Frameworks, *Siamak Nejati*, University of Nebraska–Lincoln; *S. Gnani Peer Mohamed*, University of Nebraska - Lincoln

The process of synthesizing thin films of covalent organic frameworks (COFs) in situ, without the use of solvents, is an attractive route for the

creation of single-atom catalysts (SACs) based on metal-N<sub>4</sub> motifs. This one-step synthesis and integration approach makes it suitable for incorporating the materials into the architecture of electrode devices. Compared to traditional SACs preparation methods, this approach allows for an increase in the number of active sites and improved synthetic precision, resulting in highly desirable electrocatalytic performance. In this study, we employed porphyrins as precursors and demonstrated the feasibility of using vapor phase deposition to create COFs with metal-porphyrins. In recent decades, the improved electrocatalytic properties of porphyrin-based COFs with two or three dimensions have garnered significant attention. However, their covalent networks and organic nature make solution-based COF synthesis challenging for creating thin films, which limits their widespread use in various applications. We demonstrate a solvent-free vapor phase synthesis of crystalline and porous porphyrin-based COFs (POR-COFs) using 5,10,15,20-tetra(4-aminophenyl)porphyrin (TAPP) and its transition metal complex (MTAPP, M = Cu<sup>2+</sup>, Co<sup>2+</sup>) through pulse-assisted oxidative chemical vapor deposition (oCVD). Pyridine, a co-crystallizing agent, is used to enhance the crystallinity and structure of the MPOR-COF. We observed varying electrocatalytic activity towards different reactions depending on the occupancy of the porphyrin center. The synthesized MPOR-COFs exhibit excellent electrochemical performance for nitrate electroreduction to ammonia (Faradaic efficiency of ~86% at 1.7 V vs Ag/AgCl), oxygen reduction and evolution reaction in aprotic media, and as a cathode material for Li-Oxygen battery. This synthetic approach offers a sustainable and scalable method for thin film COF production and opens up new opportunities for their application in energy storage and conversion systems. The measured electrocatalytic activities proved that our approach to synthesizing catalysts from COFs is a viable path to realize the next generation of SACs catalysts.

## 2D-ThP-11 Real-Time Machine Learning Enhanced Defect Engineering in Ceria Nanostructures, *U. Kumar*, University of Central Florida; *A. Arunachalam*, University of Texas at Dallas; *C. Feit, N. Berriel*, University of Central Florida; *K. Basu*, University of Texas at Dallas; *P. Banerjee, S. Seal*, University of Central Florida; *Yifei Fu*, University of Central Florida, Orlando

Ceria nanostructures have been employed in diverse applications due to their distinctive defect structure, which grants them regenerative oxidative properties. The redox activity of ceria depends on its surface defect structure and is generally determined by its Ce<sup>3+</sup>/Ce<sup>4+</sup> oxidation state ratio, often measured by ex-situ X-ray photoelectron microscopy (XPS). Numerous studies have demonstrated that defect engineering strategies, such as size and morphology manipulation or introduction of doping, are effective in altering ceria nanostructures for various applications. However, despite the success achieved by these methods, it is still challenging to have precise and reversible control over ceria defect structures. To address this challenge, we propose the use of Machine Learning (ML) techniques to enhance defect engineering in ceria nanofilms.

Deposition conditions, such as temperature, pressure, and the number of cycles, play an important role in the ALD process. Our previous work<sup>1</sup> has demonstrated that well-optimized ALD processes can be achieved with the help of *in-situ* spectroscopic ellipsometry (SE). Therefore, the desired thickness of ceria thin film can be rapidly developed without the ex-situ characterization usually required by conventional approaches. In the current work, data collected through *in-situ* SE and ex-situ XPS has been correlated using ML algorithms. Two approaches have been studied to exert better control over the defective structure of ceria thin film. The first method involves an indirect approach of thickness prediction using an ML algorithm, followed by Ce<sup>3+</sup>/Ce<sup>4+</sup> estimation using an experimental calibration curve. The second method, with a more direct approach, involves Ce<sup>3+</sup>/Ce<sup>4+</sup> prediction using real-time ellipsometry data (amplitude ratio  $\psi$  and phase difference  $\Delta$ ) using Gradient Boost and Random Forest Regressor. Overall, in the present work, an ML algorithm trained by *in-situ* ES data was shown to be an effective approach to control the thickness and defect level of Ceria ALD films.

1. U. Kumar, C. Feit, S. N. Berriel, A. Arunachalam, T. S. Sakthivel, K. Basu, P. Banerjee and S. Seal, Journal of Vacuum Science & Technology A 39, 060405 (2021).

## 2D-ThP-12 Investigating the Fate of Nanoplastics in Aquatic Environments, *Tycho Roorda, I. Groot*, Leiden University, The Netherlands

Plastic particles in the ocean have become a contaminant of emerging concern due to their damage to humans and marine life[1,2]. Of all plastic production, which is increasing still, it has been shown that more than 99% of plastic waste which ends up in the oceans can not be accounted for[2,3]. The belief is that part of all this missing plastic degrades to a micro-

and nano-sized scale which had not yet been detected[4,5]. Nanoplastics have also been shown to promote the spreading of toxins, such as heavy metals, which would otherwise sink to the ocean floor at their source[6,7]. In order to understand the fate of nanoplastics in aquatic environments, we must have a better understanding of the degradation mechanisms at an atomic and chemical level. In this project, we have successfully deposited nanoplastics onto a substrate in UHV by physical vapor deposition for degradation studies and to investigate their binding mechanism to other toxins in the ocean. The deposition of nanoplastics is confirmed by mass spectrometry, Auger electron spectroscopy and X-ray photoelectron spectroscopy. The degradation mechanisms which will be studied are oxygenation, hydrogenation, UV exposure and thermal annealing which will be investigated in ultra-high vacuum with atomic force microscopy and combined scanning tunneling microscopy. This combination allows for the identification of individual particles by conductivity making it possible to study the binding mechanism between nanoplastics and certain toxins. In this project, we aim to investigate the binding mechanism between nanoplastic particles and heavy metals as well as the nanoplastics' degradation by operando dosing of gases and heating to real world conditions.

**2D-ThP-13 Plasma-Induced Energy Band Evolution for Two-Dimensional Heterogeneous Junctions**, A. Ahmed, A. Cabanillas, A. Chakravarty, F. Yao, Huamin Li, University at Buffalo

With the rise of two-dimensional (2D) materials and nanoelectronics, compatible processes based on existing Si technologies are highly demanded to enable new and superior device functions. In this work, we exploit the CMOS-compatible  $O_2$  plasma treatment as an effective anionic substitution doping approach for 2D  $WSe_2$ , and demonstrate a heterogeneous  $WSe_2/MoS_2$  junction as an anti-ambipolar field-effect transistor (FET) with outstanding performance. Specifically, novel plasma-induced oxidation and doping were performed to achieve a controllable enhancement of hole transport in  $WSe_2$  through moderate or even degenerate doping. By incorporating with 2D  $MoS_2$  dominated by electron transport as well as the applied in-plane and out-of-plane electric fields, an evolution of the energy band structure of the 2D heterogeneous junction can be obtained, and the corresponding charge transport, dominated by the Fowler-Nordheim (FN) tunneling, is comprehensively elucidated. As an anti-ambipolar FET, our prototype device exhibits outstanding and balanced performance including a superior peak-valley ratio (PVR,  $2.4 \times 10^5$ ) and a high current density (55 nA/ $\mu m$ ). This work demonstrates the great potential of 2D materials and their doping engineering to feasibly integrate with the existing CMOS technology and eventually improve the efficiency of future nanoelectronics.

**2D-ThP-14 in-situ Electronic structure monitoring of 2D TMDC-field effect transistor by operando-XPS**, Seungwook Choi, Korea Research Institute of Standards and Science (KRISS), Republic of Korea; G. Oh, T. Kim, Jeonbuk National University, Republic of Korea; A. Kim, Korea Research Institute of Standards and Science (KRISS), Republic of Korea

Two-dimensional transition metal dichalcogenide material-based field effect transistor (2D TMDC-FET) could be one of next-generation transistors because they have novel material properties including high on-off ratio above  $10^6$ , subthreshold swing of 140 mV/dec, Hall mobility around 10  $cm^2/Vs$ , and tunable bandgap depending on the number of layers. "Operando", which means under working conditions, analysis method has been proposed to investigate the correlation between devices and materials and observe intermediate state of material while the device is working. To examine chemical and electrical properties at the channel interface of thin film FET under working condition, operando X-ray photoelectron spectroscopy (XPS) should be studied due to its surface-sensitive performance.

In this study, we will introduce a lab-source operando XPS system specially for commercial XPS system including a transistor probe stage and a special sample holder. Here, we present the change of electronic structure of TMDC-FET depending on a gate voltage using our lab-source operando-XPS system. The results reveal that the quantitative band bending of the FET channel can be observed during operating FET (switching on/off). Furthermore, the quality of active channel/insulator interface can be monitored during FET operation. We provide the strategy to minimize beam-damage attributed by the use of micro-focused x-ray beam during operando analysis. Furthermore, this operando-XPS analysis results enable to provide the optimized material and device structure of 2D TMDC-FET.

**2D-ThP-15 Atomic Layer Deposition of  $Al_2O_3$  on Monolayer  $MoS_2$  with Mild  $NF_3$  Remote Plasma Treatment**, Kwangwuk Park, J. Kang, H. Lee, M. Leem, G. Yeom, H. Kim, Sungkyunkwan University (SKKU), Republic of Korea  
**Keywords:** Plasma treatment, atomic layer deposition, two-dimensional crystals, molybdenum disulfide, surface functionalization.

**Abstract.** Considering the expected superior immunity to short-channel effects while maintaining high electron mobility even at a few monolayer thicknesses [1, 2], molybdenum disulfide ( $MoS_2$ ), with a two-dimensional structure, is emerging as a promising alternative to ultrathin Si channels in future sub-nanometer transistors. Nevertheless, from a device integration standpoint, there remains a critical challenge: forming continuous dielectric films with a thickness of less than a few nanometers on  $MoS_2$  via atomic layer deposition (ALD) due to the limited number of active sites on the  $MoS_2$  surface [3]. Although various approaches have been explored to activate the  $MoS_2$  surface for facile chemical interaction with ALD precursors [4], several challenges remain unresolved. These include achieving thickness scalability of  $MoS_2$  down to a monolayer, ensuring thickness scalability of the gate dielectric, and adapting the process to three-dimensional device structures.

In this presentation, we introduce the use of  $NF_3$  remote plasma treatment on the  $MoS_2$  surface prior to ALD of an  $Al_2O_3$  film at 200 °C. Without treatment, direct thermal ALD of  $Al_2O_3$  on  $MoS_2$  results in island-like growth characterized by numerous incomplete boundaries. In contrast,  $MoS_2$  treated with  $NF_3$  remote plasma facilitates the deposition of continuous and pinhole-free  $Al_2O_3$  films, even at a thickness of 2 nm. We confirmed the minimal physical damage of the pretreatment to the monolayer  $MoS_2$  through Raman and photoluminescence spectroscopy. Finally, we will discuss the electrical characteristics of  $MoS_2$  field-effect transistors incorporating  $NF_3$  remote plasma pretreatment.

#### References

- [1] S. Ahmed, J. Yi, *Nano-Micro Lett.* 9, 50 (2017).
- [2] B. Liu, A. Abbas, C. Zhou, *Adv. Electron. Mater.* 3, 1700045 (2017).
- [3] S. McDonnell et al., *ACS Nano* 7, 10354–10361 (2013).
- [4] E. Schilirò et al., *Appl. Sci.* 11, 11052 (2021).

**2D-ThP-16 AgNFs Supported on Graphene Based Materials as Multi-Wavelength SERS Active Platforms**, A. Brancato, M. Condorelli, S. Sciacca, C. Bonaccorso, M. Barcellona, M. Fragalà, C. Satriano, G. Compagnini, Luisa D'Urso, University of Catania, Italy

Surface Enhanced Raman Spectroscopy (SERS) has been successfully employed in several fields of interest such as plasmonic sensing and biosensing, in-situ photocatalysis studies, single molecule detection, and many others real-world applications. Usually, the greatest contribution to the Raman enhancement is explained by an electromagnetic mechanism. To further potentiate the SERS effect, several research studies reported the employ of peculiar plasmonic nanostructures that allow the creation of hot-spots on characterized by strong electromagnetic fields. Moreover, the possibility to amplify Raman signals is strongly linked to the excitation wavelength of the employed laser interacting with the SER active substrate. In order to explore novel functional nanomaterials with a high enhancement in a wide range of excitation wavelengths, in this work we propose Silver Nanoflowers (AgNFs), anchored to reduced thiolated graphene oxide (r-GOSH) nanosheets. The success of the coupling preparation procedure was verified by comparing the Raman and IR spectra of the materials, before and after coupling metal nanostructures with the 2D layers, and by UV-vis spectroscopy analyses. Furthermore, a morphological characterization of the new materials was carried out using scanning electron and atomic force microscopies. Thanks to the NFs morphology and to the extended surface of 2D materials is possible create numberless hot spot regions between silver petals and in the nanogaps area of the 2D material, exhibiting significant plasmonic effects as well as unique optical feature in the overall visible range. The SERS properties of the 2D hybrid material were studied using a standard molecule 4-mercaptobenzoic acid (4-MBA) as probe analyte at the nanomolar concentration. As the AgNFs extinction spectra cover the entire visible range, we were able to study the enhancement in a laser wavelength range between 532 and 785 nm, finding very high enhancement factors. This suggests that AgNF could be an excellent SERS substrate on the entire visible and near infrared spectral region and demonstrates that such nanomaterial can be easily used to study analytes at low concentrations with any exciting wavelength, opening the possibility to investigate several biological and medical interest analytes without the interference of not desired optical phenomena such as luminescence.

# Thursday Evening, November 9, 2023

This work has been partially funded by the European Union (NextGeneration EU), through the MUR- PNRR project SAMOTHRACE (ECS0000022).

**2D-ThP-17 Angiogenin-Tailored Graphene Oxide Nanosheets to Target Prostate Cancer, Diego La Mendola, T. Marzo, University of Pisa, Italy; O. Hansson, University of Goteborg, Sweden; C. Satriano, University of Catania, Italy**

Angiogenin (ANG), an ubiquitous protein with a potent angiogenic power, is able to stimulate new vessel growth and cell self-renewal under both physiological and pathological conditions, including neuroprotection, inflammation and immune response. Anovel platform for modulating angiogenic processes in cancer therapies was developed based on graphene oxide (GO) functionalized with ANG. The new GO@ANG nanocomposite was characterized by means of UV-visible and fluorescence spectroscopies. The GO@ANG nanotoxicity was assessed by *in vitro* cellular experiments on human prostatic cancer cells (PC-3 line). Laser confocal microscopy (LSM) cell imaging evidenced an enhanced internationalization of the 2D nanomaterial functionalized with the protein rather than the bare nanosheets. Furthermore, significant changes in cell cytoskeleton organization compared to the cell treatments with free protein in different environmental conditions were detected. These results pointed to the modulating capability by the hybrid nanocomposite for different cellular biochemical response.

**2D-ThP-18 Defect Inventory of CVT Grown TaS<sub>2</sub> Crystals, Dejia Kong, R. Peckham, University of Virginia; Z. Mao, S. Lee, Pennsylvania State University; K. Burns, I. Harrison, P. Reinke, University of Virginia**

Defects are critical to the use and function of transition metal dichalcogenides (TMD), necessitating the study of the defect inventory from point defects to dislocations. The defect inventory sensitively modulates device performance metrics such as electron and phonon conductivity and exciton lifetimes. TMD layers exfoliated from bulk TMD crystals continue to serve as the main vehicle for experiments, and prototype devices. In this work, we present a scanning tunneling microscopy (STM) study at 293 K of the defect inventory in metallic 2H-TaS<sub>2</sub> which is a candidate for contacts in TMD devices. The 2H-TaS<sub>2</sub> bulk crystal was grown by chemical vapor transport (CVT) with an iodine transport agent and high crystalline quality is confirmed with XRD. We capture different groups of defects formed during the CVT process across length scales from point defects to screw dislocation. One of the most prominent surface defects are line vacancies that resemble drainage system patterns in geomorphology maps (Figure 1) and are interpreted as remnants of the flux agent reaction at the growth surface. These line defects are closed and overgrown. The subsurface line defects can be resolved in STM as they imprint electronic and structural inhomogeneities on the subsequent layers. TEM analysis will elucidate the structure and composition across the buried line defects. We will include a discussion of recent electrical measurements.

In addition to mapping the defect inventory, we studied tip-induced nanolithography which affords nanoscale control of vacancy island formation in 2H-TaS<sub>2</sub> and is initiated at point defects. A tip-induced reaction allows selective removal of the top layer (Figure 2) with nanometer precision creating well-defined and faceted "holes", respectively vacancy islands (v-island). The selective area removal of 2H-TaS<sub>2</sub> initiated by SPM probes has been reported previously, but the mechanism of such degradation is still discussed. We propose that it is related to the presence of traces of water at the tip or surface and present a detailed kinetic analysis of the etching process.<sup>1-3</sup> We studied the v-island growth over extended times and will discuss the feasibility of targeted etching of structures within the 2H-TaS<sub>2</sub> as a highly selective and high-resolution lithography process.

(1) Parkinson, B. *J Am Chem Soc* 1990, 112 (21), 7498-7502.

(2) Yamaguchi, W. et al. *Appl Surf Sci* 1997, 119 (1-2), 67-75.

(3) Zheng, H. S. *Nano Lett* 2018, 18, 2179-2185.

**2D-ThP-19 Advance in Momentum Microscopy with NanoESCA MARIS, Marten Patt, N. Weber, M. Escher, T. Kuehn, FOCUS GmbH, Germany**

Since its introduction in 2005, the energy-filtered photoelectron microscope NanoESCA [1,2] has been used for various application including work-function mapping, imaging XPS and in the last years more prominently for imaging the reciprocal space, i.e., momentum microscopy or orbital tomography (e.g., at the NanoESCA at synchrotron Elettra, Trieste [3]).

The latest revision of the analyzer, called NanoESCA MARIS, has a new

microscope lens. It was designed to achieve a better angular / momentum resolution while keeping the same good real space resolution < 35 nm from its predecessor. In momentum space mode, the instrument achieves a resolution of 0.005 Å<sup>-1</sup>. We will show the performance on the Rashba split surface state of a Au (111) single crystal (Fig. 1,b). In addition, new working modes, like off-axis zoom, double dispersive imaging mode and an energy dispersion snapshot mode were introduced with the new analyzer and will be presented. Developments in the Imaging Spin Filter for NanoESCA [4] will be discussed.

References

[1] M. Escher et al., *J. Phys. Cond. Matter* 17 (2005)

[2] B. Krömker et al., *Rev. Sci. Instrum.* 79 (2008)

[3] M. Wießner et al., *Nature Comm.* 5 (2014) 4156

[4] M. Escher et al., *Ultramicroscopy* 253 (2023) 113814

**2D-ThP-20 A Novel Method to Measure Cross-plane Resistivity of Ultra-Thin Films, S. Weng, University of Southern California; Y. Wang, Stanford University; Celsey Price, H. Blackwood, M. Choffel, A. Miller, University of Oregon; R. Li, M. Chen, University of Southern California; D. Johnson, University of Oregon; A. Majumdar, Stanford University; S. Cronin, University of Southern California**

Two-dimensional van der Waals heterostructures are of great interest because they are ideal for fundamental studies and diverse device applications. By vertically stacking 2D materials, you introduce the ability to control, manipulate, and generate the transport and confinement of charge carriers, excitons, phonons, and photons. Understanding and characterizing charge carrier transport across van der Waals interfaces is critical to the fundamental understanding and application of 2D van der Waals heterostructures. Measuring the cross-plane properties of a heterostructure is difficult, however, due to the measurements being intrinsically 2-probe, with the measured total cross-plane resistance including the lead and contact-sample interface resistances in addition to the resistance of the sample. Here we present a novel method to determine the bottom and top sample-contact and lead resistances through in-plane measurements, modeling the extent of current crowding in the end voltage as a function of contact width. The cross-plane sample resistance is obtained by subtracting these resistances from the measured total cross-plane resistance. This opens a unique opportunity to investigate the nature of charge transport across van der Waals interfaces. Temperature-dependent data for the PbSe(VSe<sub>2</sub>) heterostructure is used to demonstrate this approach. The dominant contributor to in-plane transport is the metallic VSe<sub>2</sub> layers. The cross-plane carrier transport is expected to be dominated by the semiconducting PbSe layers. A several order of magnitude difference between cross-plane and in-plane resistivities over the 5.5 – 300 K temperature range has been measured.

**2D-ThP-21 Evaluating the Impact of Defects, Interfaces and Boundaries on Thermal Transport in 2D Materials Using a Novel Opto-Thermal Metrology Technique with Sub-Micron Resolution, John Gaskins, A. Jones, P. Hopkins, B. Foley, Laser Thermal**

Two-dimensional materials offer unprecedented, often record setting thermal properties with seemingly robust potential to structurally and chemically manipulate phonon scattering and thermal transport. These phonon scattering events in 2D systems arise from the plethora of defects and interfaces that arise from both growth and post processing that also are routinely used to manipulate the 2D materials functionalities. The thermal transport properties of 2D materials at and around these defect phonon scattering sites, which often have length scales and spacings on the order of nanometers to 10's of nanometers, are difficult to isolate and measure individually with thermal measurement techniques. For example, optical based techniques for measuring thermal properties of 2D materials (e.g., Raman, TDTR) are ultimately diffraction limited and thus restricted to areal spatial resolution on the order of single micrometers. Techniques using lasers coupled with AFM-tips (e.g., Nano-FTIR) have shown promise in achieving sub-diffraction limited areal resolution to qualitatively interrogate optically excited surfaces, but lack the opto-thermal transduction power afforded by thermoreflectance-based methods to ensure accurate measurement of local temperature and thermal wave modulation.

Here, we introduce a new platform capable of characterizing the thermal properties of 2D materials with ~10 nm areal spatial resolution. Thermal maps of CVD-grown molybdenum disulfide (MoS<sub>2</sub>) and exfoliated hexagonal boron nitride (hBN) flakes (both on SiO<sub>2</sub>/Si supporting substrates) are presented, highlighting both (a) the higher in-plane thermal conductivity of the hBN compared to MoS<sub>2</sub>, as expected per the literature,

but more importantly (b) the direct visualization of how the thermal resistance increases near wrinkle defects, adlayer nucleation sites, and flake boundaries. These local increases in resistance are attributed to the impact of the defect on phonon transport. As a result, this new capability enables the direct visualization and estimation of the length scales over which various defect structures exert influence over phonon transport in these 2D materials.

**2D-ThP-22 Site-Specific Synthesis of Molybdenum Dichalcogenide Using Chemical Vapor Deposition Technique, *Chu Te Chen, A. Butler, Y. Fu, A. Cabanillas, A. Ahmed, A. Chakravarty, S. Jadeja, H. Hui, L. Samson, H. Zeng, A. Yadav, H. Li, The State University of New York, Buffalo; K. Wong, Applied Materials; F. Yao, The State University of New York, Buffalo***

Two-dimensional (2D) semiconducting transition metal dichalcogenides (TMDs) have been extensively explored for their potential as channel materials in electronic devices. The device performance has been significantly improved over the years due to the advancements in understanding of TMD materials, device design, and fabrication process. Despite the early success in demonstrating proof-of-concept devices, scalable and single-crystal growth of TMD films on suitable substrates remains a formidable roadblock to the development of commercially viable TMD-based nanoelectronics. To mitigate this problem, there is a pressing need for the precise growth of high-quality TMD layers at desired locations in the device architecture with consistent layer characteristics.

In this study, we introduce a novel approach for the direct and site-selective synthesis of MoS<sub>2</sub> flakes, a representative type of TMD materials, on silicon substrates using the chemical vapor deposition (CVD) technique. This achievement is enabled through seed layer patterning using E-beam lithography, facilitating site-specific nucleation and growth. By systematically exploring the CVD synthesis parameter space, critical process parameters that govern the sublimation and diffusion processes of the Mo-containing intermediates have been identified. To validate the success of the selective growth of MoS<sub>2</sub> and unveil the structure-property-performance relationship, a series of microscopic and spectroscopic characterizations coupled with electrical measurements are employed to determine the microstructural and transport properties of the obtained flakes. Our results represent technological innovation for direct, scalable synthesis of TMDs in a location-selective manner which has potential to advance the development of next-generation nanoelectronics based on TMD materials.

## Applied Surface Science Division

### Room Oregon Ballroom 203-204 - Session AS-ThP

#### Applied Surface Science Poster Session

**AS-ThP-1 Low-Energy Ion Scattering Intensities from Supported Nanoparticles: The Spherical Cap Model to Determine Number Density, Size, and Contact Angle, *Kun Zhao, University of Washington; D. Auerbach, Max Planck Institute for Multidisciplinary Science, Germany; C. Campbell, University of Washington***

Supported nanoparticles are of great importance to many technologies such as fuel processing, and catalyzed chemical synthesis, energy storage and generation, thin film fabrication, etc. Low energy ion scattering spectroscopy (LEIS) with noble gas ions like He<sup>+</sup> is a powerful tool for the characterization of nanoparticles dispersed across flat support surfaces due to its ability to probe the elemental composition in the topmost atomic layer of a surface, providing quantitative information regarding the size and number density of nanoparticles. Here, we present a derivation of the LEIS intensities expected from nanoparticles and the support material as a function of the average particle size, their number per unit area and their contact angle with the support when modeled as spherical caps of the nanoparticle material dispersed over the surface of a support. The model assumes that the ion intensities are determined only by the physical blocking of linear ion trajectories, and independent of the tilt angle of the local surface relative to the incident and scattered ion directions, an assumption we support by quantitative modelling of published data which tested tilt-angle effects. The model is a generalization to arbitrary contact angles of the hemispherical cap model which assumes 90° contact angle and has been widely used to model spectroscopic signals from nanoparticle arrays in LEIS (and also in Auger and photoelectron spectroscopies). This new model quantitatively reveals how LEIS signals are sensitive not only to the diameter and number density of the nanoparticle, but also to their contact angle (or height : diameter ratio). With the use of additional data

(e.g., from microscopies or adsorption microcalorimetry), the model presented here will enable more accurate determination of the average size, shape and number density of supported nanoparticles based on LEIS intensity measurements.

**AS-ThP-2 Work Function Measurement by Ultraviolet Photoelectron Spectroscopy: Versailles Project on Advanced Materials and Standards Interlaboratory Comparison, *Jeong Won Kim, A. Kim, H. Hwang, J. Kim, S. Choi, KRISS, Republic of Korea; N. Koch, D. Shin, Humboldt University Berlin, Germany; Z. Zhao, F. Liu, CAS, China; M. Choi, SK Hynix, Korea; K. Lee, Y. Park, Kyung Hee University, Republic of Korea***

Since the introduction of the work function (WF) through Einstein's photoelectric effect, it has become an important parameter for characterizing material surfaces. The WF governs charge injection/collection efficiency and charge transfer at material interfaces, making WF control and measurement crucial in many electronic and optical devices. Ultraviolet photoelectron spectroscopy (UPS) has been the primary method for measuring WF over several decades. However, reported WF values strongly depend on surface treatment and measurement conditions, even for the same material. Thus, it is necessary to develop a well-prepared guide to report reliable WF values.

To address this issue, we devised an interlaboratory comparison for WF measurement by UPS and present the results of a study conducted under the Versailles Project on Advanced Materials and Standards (VAMAS). Two samples, a gold film deposited on a flat Si wafer and highly oriented pyrolytic graphite (HOPG), were distributed to six international laboratories. Prior to the UPS measurements, the samples underwent common treatment processes, including instrumental settings for energy-scale calibration and bias optimization. The Au sample exhibited a WF of 5.40±0.12 eV after Ar<sup>+</sup> sputtering in vacuum, while the HOPG sample showed a WF of 4.61±0.09 eV after mechanical peeling-off. The narrow deviation in data among the laboratories for both high and low WF values will provide a basis for establishing a new international standard for UPS in the surface chemical analysis community.

**AS-ThP-3 Effect of Soft X-Ray Beam on Channel Properties of 2D-Field Effect Transistor During *operando* X-ray Photoelectron Spectroscopy, *Ansoon Kim, S. Choi, Korea Research Institute of Standards and Science (KRISS), Republic of Korea; G. Oh, T. Kim, Jeonbuk National University, Republic of Korea***

"*Operando*", meaning under working conditions, analysis method has been developed to investigate the relationship between device performance and material properties. To examine chemical and electrical properties at the channel interface of thin film field-effect transistor (FET) under working condition, *operando* X-ray photoelectron spectroscopy (XPS) should be studied due to its surface-sensitive performance. Synchrotron radiation has been used for most *operando*-XPS studies [1,2] due to its good spatial resolution (~70 nm) compared to lab-based X-ray source (usually 10 μm). Nevertheless, synchrotron-based XPS has a limitation to perform *operando* analysis of soft materials because its high photon flux may cause sample damage. However, regarding 2D materials, in-depth researches about changes in chemical or electrical property induced by micro- or nano-focused X-ray have not been published despite of high demands and lots of interests for its *operando*-XPS studies.

In this presentation, we demonstrate whether there is a change in chemical and electrical properties of partially oxidized MoTe<sub>2</sub> and MoS<sub>2</sub> flakes induced by micro-focused lab-X-ray. In addition, we also verify whether the X-ray induced chemical changes can be accelerated by high gate voltage during conducting *operando* FET measurements. As a result of this study, we suggest a method to minimize the photon-induced damage for *operando*-XPS using lab-source that a lot of analytical researcher will use in the future.

[1] N. Nagamura et al, "Chemical potential shift in organic field-effect transistors identified by soft X-ray *operando* nano-spectroscopy," *Appl. Phys. Lett.* **106**, 251604, 2015

[2] I. J. T. Jensen et al, "Direct Observation of Charge Transfer between NO<sub>x</sub> and monolayer MoS<sub>2</sub> by *Operando* Scanning Photoelectron Microscopy," *ACS Appl. Nano Mater.* **4**, 3319-3324, 2021

**AS-ThP-4 Transient Grating Time-Resolved PEEM to Study Charge-Carrier Transport, *Chandni Babu, D. Zigmantas, Lund University, Sweden***  
Understanding the transport of charge carriers on surfaces enables us to get insights into a material's fundamental properties, which is also important from an application point of view. Time-resolved photoemission

# Thursday Evening, November 9, 2023

electron microscopy (TR-PEEM) has gained popularity in the study of ultrafast photocarrier dynamics in different materials. Here we present a novel approach for measuring the transport of photoexcited electrons at surfaces - transient grating time-resolved PEEM. In this approach, the sample is simultaneously excited by two pump pulses whose interference leads to a periodic spatial modulation of the excited electrons (1). These electrons are then photoemitted by the probe pulse and are imaged in the PEEM. The gradual decay of the spatial modulation due to transport processes can be observed, providing insights into diffusion and other transport phenomena over the short length and time scales. We are using this technique to study wurtzite InP platelets which is less explored than its thermodynamically stable counterpart- zinc blende InP. Understanding the transport properties of wurtzite InP will help in developing novel electronic and optoelectronic devices.

Reference

[1] Eichler, H.J., Günter, P., Pohl, D.W. (1986). Diffraction and Four-Wave Mixing Theory. In: Laser-Induced Dynamic Gratings. Springer Series in Optical Sciences, vol 50. Springer, Berlin, Heidelberg.

**AS-ThP-5 Comparison of Commercially Available as-Received Lithium Metal Surfaces Using XPS and FTI, Harry Meyer, R. Sahore, A. Westover, Oak Ridge National Laboratory**

Lithium metal is used extensively a variety of battery applications. Like all alkali metals, Li-metal is reactive with ambient air to the point of being flammable. Li-metal must be stored in either vacuum or an inert atmosphere. The Department of Energy (DOE) sponsors a wide range of battery materials related projects because of their continued and growing importance to our society. One of these projects, sponsored by the Vehicle Technology Office (VTO) of DOE, is titled "Control of Li Surfaces for Solid-State Batteries". In this project, our goal is to understand the role of native and engineered surface layers on the cycling behavior of lithium metal in solid-state batteries. An initial step of the project was to examine native surface layers of various commercial lithium which are used by most researchers in the field. Li-metal obtained from four commercial sources was compared to Li-metal films prepared in our laboratory using thermal evaporation.

The as-prepared Li-metal film and the as-received Li-metal samples were stored in an inert Ar-filled glovebox prior to surface characterization using x-ray photoelectron spectroscopy (XPS) and Fourier transform infra-red spectroscopy (FTIR). FTIR analysis was done within the glovebox and so were never exposed to air. Samples for XPS were prepared in the Ar-filled glovebox by removing small sections from the as-received Li-metal materials and placing in a vacuum transfer holder (VTH). The VTH was sealed under vacuum in the load-lock of the glovebox, moved to the XPS laboratory, and unsealed by placing it in the vacuum load-lock of the XPS. The as-received surfaces were initially analyzed. Depth profiles were done to measure the composition as a function of depth. All samples showed a mix of Li-carbonate, Li-hydroxide, Li-oxide, and Li-carbide, but showed different distributions of each for each sample. This poster will compare the as-received surface compositions and compositions as a function of depth. This abstract has been authored by UT-Battelle, LLC under Contract No. DEAC05-00OR22725 with the U.S. Department of Energy.

**AS-ThP-6 Silver and Aluminum by X-ray Photoelectron Spectroscopy (XPS), Braxton Kulbacki, S. Jafari, A. Dean, S. Ko, M. Linford, Brigham Young University**

Silver (Ag) and aluminum (Al) are important technological materials. They have also been extensively analyzed by x-ray photoelectron spectroscopy and other material characterization methods. Ag is used to calibrate the ThermoFisher K alpha XPS instrument. When calibrating the instrument using Ag, the 3d5/2 peak is placed at a binding energy of 368.21 eV. Calibration of the instrument should be performed every six months. In this poster, I show and discuss the Ag calibration peak (Ag3d5/2) as well as the Ag 3d3/2, Ag 3p3/2, Ag 3p1/2, Ag 3s, Ag 4p, Ag MNN and Ag survey scans. The sample for analysis was prepared by sputtering a silver surface. The C 1s, O 1s and Ar 2p scans are included in this poster to demonstrate both the low level of contamination and the presence of ion implanted Ar. As revealed in the C1s and O1s narrow scans, argon sputtering removed carbon and oxygen contamination from the silver surface. This poster will also show and discuss XPS of aluminum metal obtained by sputtering aluminum foil. The Al 2p peak will be shown, along with its peak fitting using asymmetric peaks that appropriately account for its spin-orbit splitting.

**AS-ThP-7 Copper and Gold by X-ray Photoelectron Spectroscopy (XPS), Annika Dean, S. Jafari, B. Kulbacki, S. Ko, M. Linford, Brigham Young University**

X-ray photoelectron spectroscopy (XPS) is a surface-sensitive analytical technique used to study the characteristics of different materials. We analyzed sputtered copper and gold using a ThermoFisher Scientific K-Alpha XPS instrument. Copper is often used in the calibration of XPS instruments, particularly the Cu 2p<sub>3/2</sub> and Cu 2p<sub>1/2</sub> peaks. The Au 4f<sub>7/2</sub> peak is also used as a binding energy reference. While spectra for copper and gold are available using a variety of X-ray sources and instruments, the ThermoFisher Scientific K-Alpha XPS instrument is growing in use and popularity in the XPS community. As such, access to reference spectra taken with this instrument are an important resource. Elemental survey spectra are also useful for comparison when studying copper and gold-containing compounds, revealing changes in chemical and electronic states. Peak fitting of various signals is demonstrated, which suggests appropriate functional/mathematical forms for these signals.

**AS-ThP-8 Xps Investigation of Monoatomic and Cluster Argon Sputtering of Zirconium Dioxide, Michael Burrell, Naval Nuclear Laboratory, Knolls Atomic Power Laboratory; E. Gillman, Naval Nuclear Laboratory, Bettis Atomic Power Laboratory**

The surfaces of zirconium dioxide and yttria-stabilized zirconia (YSZ) have been analyzed using x-ray photoelectron spectroscopy (XPS) after ion sputtering with monoatomic Ar<sup>+</sup> or an argon gas cluster ion beam (GCIB). The O/Z ratio and new components in the Zr 3d lines show reduction to lower oxidation states when sputtered with monoatomic Ar<sup>+</sup>, but significantly less damage is observed when GCIB sputtering is used. The damaged surface layer caused by Ar<sup>+</sup> sputtering can be removed by subsequent GCIB sputtering. However, the depth resolution observed in depth profiles of thin YSZ films was significantly better when Ar<sup>+</sup> sputtering is used. Differences in the Sn content in the oxidized Zr-4 specimen were also observed when comparing Ar<sup>+</sup> and GCIB sputtering, suggesting preferential sputtering. Interestingly, for YSZ the Y 3d lines showed no reduced species when sputtered with either source.

**AS-ThP-10 Unlocking the Potential of Critical Rare Earth Minerals: Advanced Characterization and Analysis with XPS and RBS for Sustainable Resource Management, Sage Buchanan, Western University, Canada**

As the only recognized critical mineral common to over 37 nations, rare-earth elements (REE's) have garnered increasing attention for their indispensable role in clean energy and sustainable modern living practices. As essential components of permanent magnets, light-emitting phosphors, catalytic converters, and various other materials, REE's underpin high-tech consumer electronics, green energy, and advanced medical and defense systems. The critical status of REE's stems from the growing demand for these applications, as well as the clear geopolitical significance threatening their supply chain. In order to maintain responsible resource management strategies and promote the sustainable use and disposal of REE's, it is crucial to have a comprehensive understanding of the properties and quality of REE-containing materials. In an effort to advance current methodologies surrounding the analysis and characterization of REE-containing materials, this work presents preliminary results from an in-depth X-ray Photoelectron Spectroscopy (XPS) and Rutherford backscattering (RBS) study on several REE-containing minerals of significance.

To establish robust characterization and analysis procedures, several standard samples of relevant REE-containing minerals such as monazite, bastnaesite, and xenotime, as well as the metals and their oxides will be examined via XPS. Comprehensive characterization and analysis procedures will be developed to serve as valuable reference data for future characterization of REE-containing materials. In parallel, RBS and photoluminescence studies will be utilized to develop known pure standards and investigate the depth distribution of REE implantations onto silicon wafers. Together, these techniques will provide a strong foundation for understanding the composition, electronic structure, and surface chemistry of these reference materials which can serve as benchmarks for future works and industrial applications. Understanding the role of REE's in these materials is critical for optimizing extraction and recycling processes, enhancing material performance, and identifying potential substitutes or alternatives if needed. This comprehensive approach will contribute to more efficient and sustainable use of REE's, alleviating geopolitical pressure

while minimizing the environmental impact associated with the extraction and importation of REE's within and into North America.

**AS-ThP-11 Computer-Readable Image Markers for Automated Registration in Correlative Microscopy, Peter Cumpson**, University of New South Wales, Australia; *J. Sherriff*, University of Newcastle-upon-Tyne, UK  
We present a newly developed methodology using computer-readable fiducial markers to allow images from multiple imaging modalities to be registered automatically. This methodology makes it possible to correlate images from many surface imaging techniques to provide an unprecedented level of surface detail on a nanometre scale that no one technique can provide alone.

This methodology provides the capability to navigate to specific areas of interest when transferring samples from machine to machine seamlessly. Then taking data acquired from scanning electron microscope (SEM), helium-ion microscopy (HIM), secondary ion mass spectrometry (SIMS), x-ray photoelectron spectroscopy (XPS), atomic force microscopy (AFM) and optical inspection tools and combining all the data acquired to then generate a 3D data representative model of a surface.

**AS-ThP-12 Surface Restructuring and Stability of Perovskite Oxide Electrocatalysts Studied by Surface X-ray Diffraction and Grazing Incidence X-ray Absorption Spectroscopy, Alvin Chang, R. Jana, K. Stoerzinger, Z. Feng**, Oregon State University

In recent years, the trend towards clean and renewable energy sources has led to an increased interest in water-based electrocatalysis (i.e., producing green hydrogen from water as fuels and chemicals) for energy conversion and storage, but a key barrier for efficient water splitting is the high overpotential of the sluggish oxygen evolution reaction (OER). To overcome this, earth-abundant perovskite oxides of chemical formula  $AMO_3$  with compositional substitutions have shown drastically improved OER activities and are particularly attractive due to their high activity, low cost, high tunability of composition, and controllable electronic structures. For many metal oxides it was discovered that the surface can reconstruct under the oxidative conditions imposed by OER, forming (hydr)oxides prior to the onset of the reaction, and resulting in a different surface termination than that expected from the bulk. This restructuring is varied among materials and plays a critical role in determining the stability and activity of an electrocatalyst material during and after electrochemical cycling. Thus, understanding the drivers of transformation at electrocatalyst interfaces towards the development of materials design is a key research direction in many fields. In this work we examine the impact of electrochemical cycling on surface reconstruction of Lanthanum Nickel Iron Oxide ( $LaNi_{1-x}Fe_xO_{3-x}$ :  $x=0-0.375$ ) and Lanthanum Strontium Nickel Iron Oxide ( $La_{0.5}Sr_{0.5}Ni_{1-x}Fe_xO_3$ :  $x=0-0.625$ ) epitaxial thin films. Surface X-ray diffraction (SXRD) is employed to investigate the relationship between complex oxide bulk composition and terminal surface OER activity and stability. X-ray reflectivity (XRR) is used to probe the electron density of surface layers and crystal truncation rod (CTR) is used to study atomic reconstruction at the surface. In select compositions, in-situ XRR and CTR illuminate the reconstruction and amorphization process during cycling under OER conditions. Furthermore, grazing incidence X-ray absorption spectroscopy (GIXAS) is performed to capture the evolution of local coordination environments with increasing compositional substitutions and soft XAS is used to explore local electronic structures. Our findings uncover the role of underlying bulk descriptors in modulating OER performance through cycling-induced restructuring and unearth the fundamental driving forces behind surface transformations in perovskite oxide materials which will provide invaluable understanding to aid in the development of electrocatalytic surfaces under OER conditions for effective materials design towards high-performance electrolyzers and batteries for renewable energy storage and conversion.

**AS-ThP-13 XPS and ToF-SIMS Depth Profile Comparison of Si Heterojunction Solar Cells, Tae Kyong John Kim**, Case Western Reserve University; *K. Davis*, University of Central Florida; *I. Martin*, Case Western Reserve University

X-ray Photoelectron Spectroscopy (XPS) is one of the most widely used analysis techniques for probing surface composition as well as the composition variation with depth (e.g. depth profile). Even though XPS offers quantitative analysis, limitations do exist when using the technique for depth profiling measurement of Si Heterojunction (SHJ) Solar Cells: probe depth (7-10 nm), detection limit (0.1 atomic %), peak overlaps, inability to measure Hydrogen. Such limitations can be overcome by utilizing another surface analysis technique: Time of Flight – Secondary Ion

Mass Spectrometry (ToF-SIMS). ToF-SIMS offers a shallower probe depth (< 2 nm), more compatible with carrying out fine depth profile measurements (e.g. sputter segment of 2-3 nm); the technique also offers a higher detection limit (ppm-ppb), no peak overlap issue, and ability to measure Hydrogen. This work investigates the benefits and limitations of the two techniques when probing for differences in three SHJ Solar cells: Control, Good, Degraded. Even though XPS was able to monitor changes in Indium, Oxygen, and Silicon amounts, only ToF-SIMS was able to reveal the finer differences in the profiles of all of the elements considered (Sn, In, O, B, P, N, H): 1) Indium segregation at the ITO and a-Si:H interface, 2) difference in Boron distribution, 3) difference in the relative amounts of H, B, P, N.

**AS-ThP-14 Surface Analysis of Ru and Ir Thin Films after Device Fabrication Processing Techniques, Randall Wheeler, S. Antar, A. Valenti, C. Ventrice**, SUNY Polytechnic Institute; *M. Strohmayer, J. Brewer, C. Nassar, C. Keimel*, Menlo Microsystems, Inc.

Microelectromechanical systems (MEMS) are micron scale devices with moving parts. In particular, MEMS devices can be used for radio frequency (RF) switches. Ruthenium is often used as the electrical contact material of these MEMS-based RF switches because of its resistance to oxidation at elevated temperatures. In addition, the most stable stoichiometry of ruthenium oxide is  $RuO_2$ , which is an electrically conductive oxide. As the power density of MEMS devices is increased, the rate of metal oxide formation on the surface of the metallic Ru contacts is expected to increase, which may adversely affect the performance of the device. Since iridium resists oxidation at high temperatures and also has an electrically conductive native oxide, it may be an alternative to Ru for higher temperature applications. Measurements have been made to determine the stoichiometry and thickness of the surface oxide on Ru and Ir films after typical semiconductor fabrication processing techniques such as reactive ion etch (RIE), plasma ashing processes, and annealing in air. The metal thin films are deposited on  $SiO_2/Si(100)$  substrates, and the primary analysis techniques used for this study are angle-resolved XPS and AFM.

**AS-ThP-17 In-Depth Morphology/Evolution Characterization of an Obliquely Sputtered Micro/Mesoporous Si/SiO<sub>2</sub> Thin Film, Behnam Moeini**, Department of Chemistry and Biochemistry, Brigham Young University; *D. Shollenberger, D. Bell*, Restek Corporation; *D. Fullwood*, Mechanical Engineering Department, Brigham Young University; *R. Vanfleet*, Department of Physics and Astronomy, College of Physical and Mathematical Sciences, Brigham Young University; *M. Linford*, Department of Chemistry and Biochemistry, Brigham Young University

In this study, we evaluate the morphology/evolution of obliquely sputtered micro/mesoporous Si/SiO<sub>2</sub> thin films. We utilize various microstructure characterization metrics relying on physical descriptors, and statistical functions (such as two-point correlation functions) to assess the films. Morphological analyses were performed on scanning transmission electron microscopy (STEM) images. To examine film evolution/growth, we employ contrast-enhanced STEM images. Prior to imaging, films were infiltrated with ZnO using atomic layer deposition (ALD). Our analysis of the two-point correlation function reveals a simple ellipse/spherical local pore geometry, which differs from the long-range irregular arrangement of pores. Furthermore, by analyzing the internal structure of the pores using homology metrics, we find a good correlation with the theoretical models of morphological evolution in obliquely sputtered films.

**AS-ThP-18 Benefits of Cryo-XPS for Battery Analysis, Jonathan Counsell, A. Roberts**, Kratos Analytical Limited, UK; *C. Moffitt*, Kratos Analytical Inc., UK; *C. Blomfield*, Kratos Analytical Limited, UK; *D. Surman*, Kratos Analytical Inc.

Lithium-sulfur batteries (LSBs) are attractive because of their high theoretical energy density and low cost of raw materials. However, their commercialization has been hindered by several challenges, including the volume expansion of the sulfur electrode during cycling and the shuttle effect of polysulfide intermediates. To address these issues, it is crucial to have a deep understanding of the underlying mechanisms and the chemistry of the Li-S system. In the case of LSBs, XPS can be used to determine the oxidation states of sulfur and carbon in the anode material. Sulfur can exist in a range of oxidation states, from -2 to +6. The most commonly observed oxidation states of sulfur in LSBs are +2 and 0, corresponding to elemental sulfur and lithium sulfide, respectively. The presence of higher oxidation states, such as +4 and +6, can indicate the formation of polysulfide intermediates and the shuttle effect. The oxidation state of carbon can also be probed with XPS. Carbon can exist in various chemical environments, such as sp<sup>2</sup> hybridized carbon in graphene-like structures or sp<sup>3</sup> hybridized carbon in amorphous carbon. The presence of sp<sup>2</sup> hybridized carbon can indicate the formation of conductive carbon

networks, which can improve electron transport and enhance the performance of the LSB.

However, it is important to note that XPS can also introduce spectral artefacts and alter the surface chemistry of the sample. XPS can cause damage to the sample surface, leading to the formation of new chemical species that may not represent the true surface chemistry. To mitigate these effects, cryo-XPS can be used, which involves cooling the sample to cryogenic temperatures during analysis. This can stabilize the surface and reduce the formation of artefacts, providing a more accurate representation of the true surface chemistry.

## **AS-ThP-19 Analysis of Buried Interfaces for Device Technology by Soft and Hard X-ray Photoelectron Spectroscopy, Jennifer Mann, K. Artyushkova, S. Zaccarine, N. Biderman, Physical Electronics**

Due to its accuracy and reliability in determining nm-thick overlayers on Si, X-ray photoelectron spectroscopy (XPS) has been utilized as a metrology technique for many years. Performing surface-sensitive XPS is more challenging with a soft X-ray source because the interfaces of interest are frequently hidden beneath metal electrodes or oxide layers. Higher energy X-ray beams have made it possible to detect photoelectron signals from deeper in the material, however most of this analysis was performed at sites with synchrotron radiation. The recent development of lab-based hard X-ray photoelectron spectrometers (HAXPES) has created new, accessible opportunities for routine analysis of technologically significant devices.

This poster will showcase the current state of the art and potential future directions for integrating HAXPES and XPS in the study of semiconductors and nanoelectronics. It will highlight the advantages of using hard X-ray sources with a lab-based high throughput fully automated spectrometer. These benefits include the ability to analyze buried interfaces, such as electronic layers located below a surface capping layer, and compositional studies in the bulk of materials and interfaces beyond the sampling depth of soft X-rays. Deeper sampling also reduces the impact of surface contamination on the photoelectron signal and enables exploration beyond the potential depth of ion sputtering-induced damage. Additionally, eliminating the overlap between Auger and major photoemission peaks is crucial, particularly for transistor devices based on GaN technology, where quantification using XPS is impossible due to the overlap between Ga Auger peaks and N 1s photoelectron peaks.

Thin films of various types are critical components of modern microelectronic products. Conducting films form the interconnect layers in all chips, and dielectric films provide electrical insulation. Angle-resolved or angle-dependent XPS and HAXPES (ADXPS/ADHAXPES) is a powerful, non-destructive method that provides a quantitative chemical composition depth profile for thin film structures with thicknesses within the XPS sampling depth - under 5-10 nm for an Al K alpha soft X-ray source and ~15-30 nm for a Cr K alpha hard X-ray source. StrataPHI can be used for metrological applications in devices to estimate the structure of thin-film stacks from this angle-dependent data.

## **AS-ThP-20 X-ray Photoelectron Spectroscopy Analysis of PEMWE Catalyst Layers with Focus on Catalyst-Ionomer Interface, Jayson Foster, Colorado School of Mines, USA; X. Lyu, Oak Ridge National Laboratory, USA; E. Padgett, S. Mauger, National Renewable Energy Laboratory; A. Serov, Oak Ridge National Laboratory, USA; S. Pylypenko, Colorado School of Mines, USA**

Polymer exchange membrane water electrolyzers (PEMWEs) are an increasingly attractive clean energy technology for producing H<sub>2</sub> for transportation fuel. Low-temperature electrolysis systems need to make significant improvements in affordability, durability, and efficiency as well as in manufacturing scalability to meet the goal of decreasing the cost of clean hydrogen to \$1/kg by 2030. Development of the next generation of PEMWEs depends on further improvements of the catalyst to achieve better activity and stability, and optimization of catalyst layer structure. This study focuses on investigating PEMWE catalyst layers with focus on catalyst-ionomer interface using x-ray photoelectron spectroscopy (XPS) as it is highly surface sensitive in identifying subtle chemical differences. XPS is a powerful technique for investigation of catalyst layers. We have previously demonstrated its ability to detect small variations in fuel cell catalyst layer composition as a function of various parameters, including catalyst ink composition and electrode fabrication. However, the ionomer is typically susceptible to X-ray induced damage during data acquisition, thus analysis was conducted with a recently developed procedure in an effort to mitigate instrumental artefacts. In this talk, we use XPS to determine spatial homogeneity of the catalyst layers to evaluate the quality of the coating methods and to compare composition of catalyst layers prepared by

different fabrication methods. Next, XPS is used to probe small variations in catalyst layer composition as a function of ink shelf life. And finally, differences in the catalyst layer composition are evaluated as a function of durability testing conditions. Across these studies, elemental ratios of F to Ir were used to quantitatively track surface ionomer content relative to the amount of IrO<sub>2</sub> nanoparticles. Additionally, peak fitting of the O 1s spectrum was analyzed to provide further perspective on the catalyst-ionomer interface composition. This talk emphasizes the capabilities of XPS to advance our understanding of the catalyst-ionomer interface as related to catalyst ink properties, catalyst layer manufacturing, and catalyst layer durability.

## **AS-ThP-21 Correlative ToF SIMS and STEM-EDS Analysis of Platinum Coatings on Electrolyzer Porous Transport Layers, Genevieve Stelmacovich, L. van Eijk, M. Coats, Colorado School of Mines; S. Ware, J. Young, National Renewable Energy Laboratory; M. Walker, Colorado School of Mines; G. Bender, National Renewable Energy Laboratory; S. Pylypenko, Colorado School of Mines**

As the United States energy infrastructure moves towards integration of a hydrogen economy, advancing electrolyzer and fuel cell technologies has become increasingly important. In Proton Exchange Membrane Water Electrolyzers (PEMWE's), the anode catalyst layer (CL), the porous transport layer (PTL), and the interface between these two layers require further optimizations. To improve this interface and mitigate degradation involving oxide formation, titanium based PTLs are typically coated with a thin protective coating, usually platinum. It is essential to characterize PTL coatings and the CL/PTL interface to ensure limited platinum use while mitigating degradation effects.

We have recently demonstrated the capabilities of ToF SIMS as a characterization technique for PTLs, specifically its ability to differentiate coatings with different thicknesses and identify titanium and platinum oxide species at the CL/PTL interface through depth profile analysis. However, quantification of coating and oxide thickness is hindered due to the morphological nature of these materials as well as lack of standards. Our recent work focuses on correlations between Time-of-Flight Secondary Ion Mass Spectrometry (ToF-SIMS) and Scanning Transmission Electron Microscopy Energy-dispersive X-ray Spectroscopy (STEM-EDS) results for a series of Pt-coated samples with varied thicknesses of platinum. The same amount of time was used to coat flat titanium substrates and felt PTLs, providing samples with a range of coating thicknesses. Samples were cross-sectioned with Focused Ion Beam Scanning Electron Microscopy (FIB-SEM) for STEM-EDS analysis to determine thickness of Pt coatings and assess layer morphology. ToF-SIMS measurements were conducted on the same samples to obtain depth profiles, comparing measurements from three locations on each sample to understand the reproducibility of ToF-SIMS measurements and correlate them with TEM-EDS data. This talk will discuss reproducibility, sputter rates, and depth profile time conversions along with future directions of ToF SIMS on PTLs for investigation of degraded samples.

## **AS-ThP-22 Using X-Ray Photoelectron Spectroscopy (XPS) to Characterize Organo-Mineral Complexes in Environmental and Synthesized Samples, Qian Zhao, M. Engelhard, A. Bhattacharjee, Pacific Northwest National Laboratory; E. Rooney, University of Tennessee, Knoxville; E. Herndon, Oak Ridge National Laboratory; K. Bidas, University of Tennessee, Oak Ridge National Laboratory**

X-ray photoelectron spectroscopy (XPS) analysis is a powerful surface characterization approach to understanding the most dynamic interface of a material. The understanding of the interface of organics and minerals in soil is critical to global carbon (C) cycling as minerals play an important role in persisting soil organic matter (SOM). Yet mechanisms of the accumulation of organic matter (OM) by associating with minerals in soil are still unclear. Chemical characterization of OM that associate with minerals provides a mechanistic understanding of mineral-OM interactions. Surface characterization, such as XPS, allows us to probe the chemical states and speciation of OM on the surface of mineral particles. This work used both synthetic mineral-OM complexes and natural soil samples to investigate the chemistry of organics that associate with minerals. In the synthetic system, we employed synthetic soil habitat (SSH) platform that can simulate soil pore distribution and mineralogy, to probe OM-mineral interactions under changing biogeochemical conditions. Surface of SSH pores was pre-coated with ferrihydrite. Water extracted OM from soil flow through the SSH platform. Surface of SSH was measured before and after OM sorption by using XPS. XPS analysis found the relatively higher concentration of C in ferrihydrite-coated surface than control. Further, the deconvolution of C 1s spectra reveals that certain carbon functional groups

of SOM are preferentially adsorbed to ferrihydrite-coated surfaces. In the soil system, mesh bags (5  $\mu\text{m}$ ) containing ferrihydrite-coated quartz, hydrous Mn oxide-coated quartz, or quartz were buried in Toolik surface soils and incubated for 7, 14, and 28 days. The incubated mineral bags were analyzed via XPS to evaluate the quantity and composition of OM compounds that associate with specific minerals as well as spatially resolved changes in Fe and Mn speciation. We found higher organic contents in ferrihydrite-coated sand than Mn and quartz. The XPS data generated by the SSH experiments and Toolik buried mineral bag analyses are combined to provide a cross-scale understanding of organo-mineral interactions that develop in thawing permafrost soils under both redox conditions and increasing frequency of freeze-thaw cycles.

**AS-ThP-23 Do Different XPS Systems Give the Same Result?, Lyndi Strange, D. Baer, M. Engelhard, V. Shutthanandan,** Pacific Northwest National Laboratory; **A. Shard,** National Physical Laboratory, U.K.

Analyses of the literature indicate that there is growing use of XPS in multiple fields of research, and also a growing amount of faulty data analysis appearing in the literature. With the increasing number of XPS users, it is important that significant detail is paid toward data acquisition and analysis to ensure reproducible results. In our laboratory we have instruments from three vendors. Sometimes it is necessary to collect data from the instrument that is available at the time the analysis is needed. In addition, users often take the data away and analyze it using a variety of software packages. It is useful to know if data collected on "identical" samples produces the same results when collected on different systems and using "native" and other software packages for analysis. This paper describes a simple test of data collection on three different systems and analysis using the "native" software for each system and analysis when naively exported to CasaXPS. Our simple test sample was cleaned copper foil for on which we collected survey spectra and high-energy resolution Cu 3p and Cu 2p data using Kratos Axis DLD Ultra, Thermo-Fischer NEXSA, and Phi Quantera spectrometers. The following analyses and data comparison were conducted for both survey and narrow window data: i) comparison of Cu 3p and Cu 2p peak ratios, ii) Cu 3p and Cu 2p atom ratios using native software and iii) when exported to CasaXPS. In addition, we compared the full survey spectra shapes to the ideal Cu spectra provided by the National Physical Laboratory. We note that many software packages apply transmission function correction information to peak areas during analysis, not to collected data (although the NEXSA has an option of doing it either way). Good news is that using recently calibrated instruments and vendor supplied sensitivity factors, when the analysis is done consistently – using iterated Shirley background between 58.0 and 91.0 for the Cu 3p and 920.0 eV to 970.0 eV for the Cu 2p - the same quantity of Cu is indicated to better than 3% With attention to information transfer including transmission function information, and use of appropriate consistent sensitivity factors, similar results when using CasaXPS analysis. Thus, excellent consistency can be obtained in comparing data from different systems. However, consistent reporting of the steps needed for consistent data analyses are often not reported in publications thus the quality and consistency of the analyzed data is often unknown or incorrect.

**AS-ThP-25 Correlative Microscopy of SIMS, Helium Ion Microscopy and XPS, Jake Sheriff, I. Fletcher,** Newcastle University, UK; **P. Cumpson,** University of New South Wales, Australia

Secondary ion mass spectrometry (SIMS) is a widely used surface analytical technique to interpret surface composition. As a primary beam is raster-scanned across a surface it is possible to recreate a total ion image from the secondary ions ejected [1]. The Ionoptika J105 is equipped with two ion beams; C60 and GCIB, the resolution of the images generated by the J105 is dictated by the spot size of these beams.

The Helium ion microscope (HIM) developed by Zeiss uses a beam of He ions to generate a secondary electron image of a surface. The use of He ions as the imaging beam allows for a spot size down to  $<0.5\text{nm}$  [2]. This has allowed the HIM to take high resolution images on a submicron scale. Unusually, at Newcastle we use a magnetic-sector analyser to allow SIMS mapping of the surface as pioneered by LIST [3], giving potentially the highest spatial resolution of any SIMS instrument.

The Axis Nova X-ray photoelectron spectrometer (XPS) is capable of parallel imaging. This is done by illuminating the sample surface with x-rays then either electrostatically or magnetically projecting the electrons into the detector [4]. Using this type of imaging one can acquire a quantifiable image of the elemental distribution from a sample's surface.

All of these techniques only tell a part of a surface's story. The HIM is able to show an accurate picture of surface morphology with nanometre

resolution, while the SIMS is able to give the composition of the surface at the submicron scale and XPS can quantify the elemental distribution. By combining these techniques one can put these parts together and gain a better understanding of the surface structure, be it a bacterial colony or a piece of Martian rock.

We have developed a methodology to be able to co-localise areas of interest when transferring samples between multiple different surface techniques. Then automatically correlate all the images to form an accurate representation of a surface [5]. Correlative microscopy with SIMS, XPS, and HIM, allows an unprecedented level of surface detail to be found.

## References

- [1] J.C. Vickerman et al, *Surface Analysis The Principal Techniques*, 113-199, 2009
- [2] D.C. Joy *Helium Ion Microscopy Principles and Applications*, 9-15, 2013
- [3] T Wirtz et al *Nanotechnology* 26, 434001, 2015
- [4] P. Van der Heide *X-ray Photoelectron Spectroscopy An introduction to Principles and Practices*, p54-56 2012
- [5] J. Sheriff, *Ultramicroscopy*, 228, 113322, 2021

**AS-ThP-27 The Utility of Surface-Induced Dissociation in Molecular Identification, Gregory L. Fisher,** Physical Electronics; **S. Iida,** ULVAC-PHI, Japan

Kilo-electron volt collision-induced dissociation (keV-CID) enables the compositional identification and structural elucidation of molecules, metabolites and degradation products with 2D/3D visualization by mass spectrometry imaging (MSI). TOF-SIMS tandem MS imaging has been brought to bear for unambiguous molecular visualization in single cell-omics [1], natural product chemistry [2], metabolomics [3,4], surface modification [5], biocompatibility, high performance polymers and composites [6], 2D materials [7], electronic devices [8], catalysis [9], forensic and failure analysis, bio-medicine and pharmaceuticals [10-12]. Here, we will introduce and explore the advantages of surface-induced dissociation (SID) to assist molecular identifications together with the CID spectra. In contrast to the CID which promotes cleavage at every molecular bond, the SID is more subtle in that the bond cleavages result predominantly in the observation of functional group chemistry. While the SID and CID are generated at the same kinetic energy, the molecular energetics are distinct which can have a pronounced effect on the calibration and, hence, the putative peaks used for precursor identification.

## References

- [1] C.E. Chini, et al, *Biointerph.* **13** (2018) 03B409.
- [2] A. Mikhael, et al, *Rapid Comm. Mass Spectrom.* (2020) DOI: 10.1002/rcm.8740.
- [3] T. Fu, et al, *Anal. Chem.* **90** (2018) 7535-7543.
- [4] T. Fu, et al, *Nat. Sci. Rep.* **9** (2018) 1928-1938.
- [5] G.L. Fisher, et al, *Anal. Chem.* **88** (2016) 6433-6440.
- [6] S. Iida, et al, *Bunseki* **2018(2)** (2018) 52-57 (Japanese).
- [7] G.L. Fisher, et al, *Microscop. Microanal.* **23** (2017) 843-848.
- [8] S. Iida, et al, *Rapid Comm. Mass Spectrom.* (2019) DOI: 10.1002/rcm.8640.
- [9] S. Oh, et al, *Chem. Mater.* **32** (2020) 8512-8521.
- [10] A.L. Bruinen, et al, in *Imaging Mass Spectrometry: Methods and Protocols*, L.M. Cole, Ed. (Springer, 2017) p. 165-173.
- [11] N. Ogrinc Potočnik, et al, *Anal. Chem.* **89** (2017) 8223.
- [12] Y. Shi, et al, *J. Proteome Res.* **18** (2019) 1669-1678.

**AS-ThP-28 Unraveling the Temperature Induced Phase Transitions of PbOx Using Multi-Modal Characterization Approach, Ajay Karakoti, V. Shutthanandan, D. Bazak, D. Nguyen, V. Murugesan,** Pacific Northwest National Laboratory

Lead acid batteries are one of the oldest commercial batteries that have proven their reliability over the years in multiple battery applications such as starting-lighting-ignition (SLI) batteries, uninterruptible power supply (UPS), and emergency lighting etc. Despite its extensive use, limited research work in this battery technology have culminated into several research challenges that must be resolved for the further progression of this battery technology. Oxygen vacancy mediated transition of  $\text{PbO}_x$  phases (of varying stoichiometry) during electrode fabrication and during the

charge-discharge process is one such unresolved problems that have perplexed the researchers for many years. Prior investigations of the  $\text{PbO}_x$  phase evolution during thermal processing using spectroscopic and diffraction methods have shown that  $\text{PbO}_2$ - $\text{Pb}_3\text{O}_4$  transition passes through multiple stages though the exact stoichiometry and composition of the transition phases have never been fully understood. This study uses multimodal characterization approach to identify the structure and composition of  $\text{PbO}_x$  phases during the thermally induced phase transitions. Combined high temperature X-ray photoelectron Spectroscopy (XPS) and residual gas analysis (RGA) showed that initial surface of  $\text{PbO}_2$  is oxygen deficient, and that Pb oxidation state changes concurrently with oxygen release during heating. It is found that the oxygen evolution and corresponding oxidation state changes occur in continuous manner instead of demonstrating a transition at fixed temperature as observed using thermogravimetry analysis. XPS and RGA analysis also reveal that the phase transition can occur at a relatively lower temperatures in high vacuum conditions revealing a potential of vacuum and beam induced damage in Pb-based materials. The talk will also highlight the challenges in the quantitative XPS analysis of lead samples. Complimentary information from different characterization techniques such as Raman and NMR spectroscopy was combined to understand the thermally induced phase transition of  $\text{PbO}_x$  that could potentially relate to the evolution of  $\text{PbO}_x$  phases observed in lead acid batteries.

**AS-ThP-29 Quantitative Investigation of SiP and SiGe Layers using HAXPES and ToF-SIMS**, N. Gauthier, Olivier Renault, E. Martinez, J. Barnes, J. Richy, J. Kanyandekwe, CEA-LETI, France

Nowadays, “more Moore” and “more than Moore” device architectures have strongly increased the importance of novel materials thereby necessitating the availability of adequate characterization and metrology for reliable process control. For instance, the introduction of SiGe or SiP compounds used in MultiChannel Field Effect devices or raised sources and drain leads to the need for the determination of the exact composition of the resulting films. In this work, the quantification of binary materials such as SiP and SiGe has been investigated using mainly non-destructive HAXPES and ToF-SIMS. Indeed, while the main obstacle to the use of RBS is the characterization of thin films, techniques with appropriate quantification capabilities like Atom Probe Tomography and Transmission Electron Microscopy are both time consuming and suffer from a lack of sensitivity due to their highly localized analysis volume. For quantitative characterization, the conventional X-ray Photoelectron Spectroscopy (XPS) is a powerful tool. Yet, its low analysis depth remains a major limiting factor to study buried interfaces and especially in this study, since the obtained Si-based layers are oxidized in ambient conditions (or because they should be protected by metallic layers of a few nanometers). A novel lab-based hard x-ray sources (HAXPES) was used to investigate both the chemical composition at the binary material surface and the in-depth distribution of  $\text{SiO}_2$  within the layer thanks to the increase of the inelastic mean free path of electrons with increasing photon energy (Chromium  $K\alpha$ ,  $h\nu = 5414.7$  eV) [1]. To confirm the composition of the materials of interest obtained by HAXPES measurements and to calculate the adequate relative sensitive factor (RSF), the same films were characterized by ToF-SIMS. However, such as for HAXPES, Secondary Ion Mass Spectrometry (SIMS) characterization of SiP/SiGe layers often suffers from matrix effects due to the non-linear variation of ionization yields with P/Ge content. This limitation can be surpassed by analyzing reference samples, by following MCs<sup>2+</sup> secondary ions or using the full spectrum protocol [2]. Finally, the P and Ge (Si) compositions of the secondary ion beam were calculated and compared with the reference composition as determined by X-ray Diffraction. The repeatability of the measurements and the influence of the layer oxidation were also studied. To conclude, the in-depth composition of the layers and the thickness of surface oxide were accurately evaluated by coupling the HAXPES results with ToF-SIMS.

[1] O. Renault et al., *Faraday Disc.* **236**, 288-310 (2022).

[2] M. Py, et al., *Rapid Commun. Mass Spectrom.* 2011, 25, 629–638

**AS-ThP-30 ToF-SIMS Analyses in an H<sub>2</sub> Atmosphere: Improvements in Thin Films Depth Profiling and Reduction of Matrix Effect**, J. Ekar, Janez Kovač, Jozef Stefan Institute, Slovenia

ToF-SIMS is a very versatile and widely applicable method for precisely characterizing the molecular structure of surfaces. Still, it also has limitations, like nonquantitative analysis caused by the matrix effect, which limits the capabilities of depth profiling of thin films. Namely, chemically similar layers are challenging to distinguish in SIMS depth profiling of thin films, and interfaces between them are difficult to identify. The reason for

this is a change in the ionization yields caused by chemical composition varying from layer to layer. However, there are different ways of reducing the matrix effect. Most widely applied are laser or electron beam post ionization (SNMS), metal-assisted and matrix-enhanced SIMS, dynamic reactive ionization (DRI), and the introduction of different gases into the analysis chamber (gas flooding).

We applied the gas flooding approach to reduce the matrix effect and improve ToF-SIMS depth profiling, testing different atmospheres such as  $\text{H}_2$ ,  $\text{C}_2\text{H}_2$ , CO, and  $\text{O}_2$  in the 10-5 Pa pressure range during the analysis [1]. Gas flooding with  $\text{O}_2$  was previously used, while our group introduced the other three gases as a novelty. We achieved the best results with the  $\text{H}_2$  gas flooding during SIMS dual beam depth profiling.  $\text{H}_2$  atmosphere enables more straightforward and unambiguous differentiation of thin layers of metals (Cr, Al, Ti, Fe, Ni, Ag) and their oxides, different metals, and alloys with different compositions. Furthermore, the identification of interfaces becomes easier. We also did not observe a change in the sputter rate during  $\text{H}_2$  flooding. Surface roughening caused by the ion bombardment during depth profiling was also reduced in the  $\text{H}_2$  atmosphere [2]. This effect is more evident after longer sputtering and depends on the chemical composition of the layer of interest. We assume that this is due to surface amorphization during the sputtering process. Our recent SIMS results also show a correlation between the SIMS signals from metals in alloys when comparing alloys with different chemical compositions analyzed in the  $\text{H}_2$  atmosphere. The  $\text{O}_2$  atmosphere also gives better results than UHV conditions, but improvement is less pronounced than in the case of  $\text{H}_2$  flooding. These findings bring ToF-SIMS one step closer to becoming at least a semiquantitative method for surface chemical characterization.

[1] J. Ekar, P. Panjan, S. Drev, J. Kovač. ToF-SIMS Depth Profiling of Metal, Metal Oxide, and Alloy Multilayers in Atmospheres of  $\text{H}_2$ ,  $\text{C}_2\text{H}_2$ , CO, and  $\text{O}_2$ . *J. Am. Soc. Mass Spectrom.* 2022, 33, 31–44.

[2] J. Ekar, J. Kovač. AFM Study of Roughness Development during ToF-SIMS Depth Profiling of Multilayers with a Cs<sup>+</sup> Ion Beam in a  $\text{H}_2$  Atmosphere. *Langmuir* 2022, 38, 12871–12880.

**AS-ThP-34 Analysis of Defective Electrical Characteristics of Metal-Insulator-Metal(Mim) Capacitor and Improvement of Leakage Characteristics**, SUNG Gyu PYO, CAU, Republic of Korea

One of the most important characteristics required for RF capacitors is the minimization of the parasitic factor. The representative parasitic factor is the series resistance and the parasitic capacitance between the Si substrate and the MIM (Metal-Insulator-Metal) capacitor that can minimize this. Most compound semiconductors are equipped with MIM capacitors, and there is a trend to adopt MIM capacitors in the CMOS process. In general, when applying a PIP (Poly Insulator-Poly Si) capacitor, the distance from the Si substrate is 3000 to 5000 Å, and the parasitic capacitance accounts for 10 to 20% of the total capacitance, and is responsible for poly depletion at the interface between the insulator and the poly electrode. The voltage coefficient of the capacitance is also bad. Additionally, it is difficult to secure a high quality factor due to the parasitic resistance factor of Poly Si. Therefore, to overcome these problems, MIM capacitors using metal electrodes are being introduced. MIM capacitor uses a metallization layer with low resistance and no depletion as an electrode, so it can realize a high quality factor by greatly reducing the parasitic capacitance factor with the Si substrate. In the Al-based metal structure (Ti/Al/Ti/TiN or Ti/TiN/Al/Ti/TiN), silicon nitride has better interface characteristics with the metal electrode than silicon dioxide, so it can maintain stable capacitance, has low voltage dependence, and has low leakage. Current characteristics are also relatively good. In addition, compared to silicon nitride, the thickness of silicon dioxide to secure the same level of capacitance density is relatively thin, so the proportion of changes in interface properties or property degradation at pattern edges increases, so in terms of pattern size dependence, silicon dioxide In the case of the MIM top electrode etch process, dummy metal cannot be inserted during MIM patterning, so the pattern density is very low (~0.1%), and the topelectrode etch condition has good etch uniformity and a large selectivity for thin  $\text{Si}_3\text{N}_4$  films. Selection of the EPD (End Point Detection) signal and appropriate etch target is different for each reticle, so target control is not easy. Because metal-rich polymer occurs due to low pattern density, it is not easy to optimize post-processing conditions. In this study, we would like to present research results on the evaluation of electrical characteristics in this MIM structure and the influence and improvement of leakage current characteristics.

**AS-ThP-35 Assessment of Hafnium Oxynitride ( $\text{HfO}_{1-x}\text{N}_x$ ) and Silicon Hafnium Oxynitride ( $\text{SiHfO}_{1-x}\text{N}_x$ ) Components in Hf 4f XPS Spectra, M. Mayorga Garay, CINVESTAV-Queretaro, Mexico; J. Torres Ochoa, Universidad Politecnica de Juventino Rosas, Mexico; O. Cortazar Martinez, Dulce Maria Guzman Bucio, A. Herrera Gomez, CINVESTAV-Unidad Queretaro, Mexico**

Nitrided hafnium oxide is employed in CMOS devices. Annealing causes species migration and the growth of interface layers. A proper characterization of the chemical composition and depth profile of this type of multilayered nanofilms is essential; ARXPS is the tool of choice.

Using ARXPS, we characterized and explored the limits on hafnia nitridation through remote plasma. Hf 4f, Si 2p, O 1s, C 1s, and N 1s spectra were acquired before and after nitridation with various plasma power levels (500 W-2500 W). We discriminated the peak components using advanced tools such as Active Background and Simultaneous Fitting, both encompassed in the fitting software AAnalyzer®.

The Si 2p spectrum before nitridation shows a signal at 102.47 eV which is attributed to  $\text{Si}_{1-w}\text{Hf}_w\text{O}_2$  with high hafnium content. A byproduct of nitridation is oxidation of the substrate; a peak related to SiON appears at 102.65 eV. The Si 2p peak in  $\text{Si}_{1-w}\text{Hf}_w\text{O}_2$  shifts to lower binding energies after plasma treatment due to dipole effects. Silicon content increases in  $\text{Si}_{1-w}\text{Hf}_w\text{O}_2$  and one overlapped contribution related to  $\text{Si}_{1-w}\text{Hf}_w\text{O}_{2-x}\text{N}_x$  appears. Before nitriding, the Hf 4f spectra show peaks related to  $\text{HfO}_2$  (17.3 eV) and  $\text{Si}_{1-w}\text{Hf}_w\text{O}_2$  (17.8 eV). After nitriding, the fitting revealed two extra signals at 16.8 and 16.38 eV which are attributed to  $\text{SiHfO}_{1-x}\text{N}_x$  and  $\text{HfO}_{1-x}\text{N}_x$ .

**AS-ThP-36 A Novel Approach for Discriminating  $\text{Cu}^0$  and  $\text{Cu}^{1+}$  in Cu 2P Photoemission Spectra, A. Torres-Ochoa, Universidad Politecnica Juventino Rosas, Mexico; D. Cabrera-German, Universidad de Sonora, Mexico; O. Cortazar-Martinez, CINVESTAV-Unidad Queretaro, Mexico; M. Bravo-Sanchez, Universidad de Guadalajara, Mexico; G. Gomez-Sosa, Alberto Herrera-Gomez, CINVESTAV-Unidad Queretaro, Mexico**

The photoemission spectra of Cu 2p have been extensively examined because of the numerous uses of copper in electronics and catalysis. The Cu 2p spectra pose a particular challenge primarily since the  $\text{Cu}^0$  and  $\text{Cu}^{1+}$  peaks overlap and share almost identical shapes and are hard to distinguish by eye or peak-fitting analysis.  $\text{Cu}^{1+}$  and  $\text{Cu}^{2+}$  often coexist. This study reveals a subtle yet significant difference in the primary signal of the Cu 2p<sub>1/2</sub> branch. The variation in the Lorentzian width of the Cu 2p<sub>1/2</sub> branch enables the assessment of relative concentrations of  $\text{Cu}^0$  and  $\text{Cu}^{1+}$ . To achieve this level of analysis, advanced fitting techniques were employed, including the Block Method, Active Background, and SVSC background. The use of these tools allowed for closely fitting all the photoemission spectra. Through precise peak-fitting analysis, it was possible to quantify the relative ratio of  $\text{Cu}^{1+}$  to  $\text{Cu}^0$  states regardless of their significant overlap and the presence of  $\text{Cu}^{2+}$  signal.

**AS-ThP-37 Morphological and Chemical State Characterization of  $\text{Cu}_2\text{O}$  Nanoparticles and Thin Films, M. Kazi Haniun, Department of Physics, University of Dhaka, Bangladesh; S. Rodriguez Bonet, M. Bosco, Florencia Carolina Calaza, Instituto de Desarrollo Tecnológico para la Industria Química, Argentina**

In recent years, transition metal oxides thin films have gained a great attention from material scientists and engineers due to their different properties which in turn provide promising applications in various fields of technology.  $\text{Cu}_2\text{O}$  has been identified as promising materials for solar energy conversion. In addition to their favorable band gap energies that allow for the utilization of visible light, the low cost, earth abundance, and non-toxicity of Cu are additional advantages for developing Cu-based photoelectrodes. However, the poor-stability problem in the aqueous solution and low efficiency of  $\text{Cu}_2\text{O}$  thin films limit their final applications. The performance of the copper oxide thin films can be enhanced by improving the crystal quality and surface morphology of the material. Among different synthesis strategies for thin film fabrications, solution-processed methods, such as hydrothermal and electrophoretic deposition, are attractive in terms of their scalability, financial advantages and eco-friendliness. This work aims to provide a critical picture of the synthesis of  $\text{Cu}_2\text{O}$  thin films and nanoparticles by solution-processed methods. Precisely controlling the synthetic strategies will be our main focus which hopefully can contribute some useful information that helps to better understand the relation between synthetic process, final morphology, and the properties of corresponding  $\text{Cu}_2\text{O}$  thin films. In summary, results will be presented for  $\text{Cu}_2\text{O}$  nanoparticle synthesis where the materials were calcined at different temperatures ranging from 300 to 500 C, showing mainly  $\text{Cu}_2\text{O}$  chemical

composition and structure, but a hint to the presence of  $\text{Cu}_2\text{O}$  on the surface is observed by CO IR titration experiments. In the case of thin films deposited on glass by spin coating methods from copper chloride solutions, and then annealed to 300 and 400 C,  $\text{Cu}_2\text{O}$  micro sized needles are obtained but the presence of Cl ions is unavoidable even at the highest temperature of calcination.

## Electronic Materials and Photonics Division Room Oregon Ballroom 203-204 - Session EM-ThP

### Electronic Materials and Photonics Poster Session

**EM-ThP-1 Phase Transformation and Growth Mechanism of RF Sputtered Ferroelectric Lead Scandium Tantalate ( $\text{PbSc}_{0.5}\text{Ta}_{0.5}\text{O}_3$ ) Films for Thermal Management, Sanju Gupta, Penn State University**

Lead scandium tantalate ( $\text{PbSc}_{0.5}\text{Ta}_{0.5}\text{O}_3$ , PST), an order/disorder ferroelectric, is a potential candidate for electrocaloric cooling and pyroelectric IR detector. In this work, we report the phase transformation kinetics from two series of samples containing pure amorphous and mixture of amorphous and pyrochlore to desired perovskite phase using post-deposition rapid thermal processing (RTP) as well as growth mechanism of RF sputtered PST thin films using excess lead target on platinized silicon (Pt/Ti/SiO<sub>2</sub>/Si) substrates. We find that small changes in the temperature ramp have a large effect on the degree of perovskite conversion (ferroelectric phase), orientation (crystallographic texture), and long-range order parameter ( $\langle S_{111} \rangle$ ). Through isothermal annealing, we obtained optimal perovskite phase at  $\geq 700^\circ\text{C}$  temperature. The phase transformation is characterized by spontaneous formation of center-type in-plane radial rosette-like structures revealed by scanning electron microscopy. The PST perovskite crystallites were found to coexist with pyrochlore in RTP annealed films. The volume fractions for perovskite and pyrochlore phase were obtained from the analysis of "rosettes" and respective x-ray diffraction intensities which helped to determine various parameters associated with phase kinetics (n, k, and activation energy,  $E_a$ ) and accompanying growth. The effective activation energies of perovskite transition and growth were found to be  $332 \pm 11$  kJ/mol ( $345 \pm 11$  kJ/mol) and  $114 \pm 10$  kJ/mol ( $122 \pm 10$  kJ/mol), respectively, for pure amorphous only (and mixed amorphous and pyrochlore) phase following nucleation-growth controlled Avrami's equation. A linear growth rate ( $n \sim 1$ ) for the perovskite phase indicates predominant interface-controlled process and diffusion-limited phenomena thus inhibiting rosette size owing to reactant depletion and soft impingement at the grain boundary. However, the growth behavior is isotropic in two-dimension parallel to the plane of the substrates for both sample series. Lead loss was severe for in-situ growth and RTP combined with conventional furnace annealing than those of RTP only films, which were closer to stoichiometric *albeit* with excess lead and marginal oxygen vacancies ( $V_o$ ).<sup>1</sup>

<sup>1</sup>S. Gupta, J. Am. Cer. Soc. **106**, 2209-2224 (2023); <https://doi.org/10.1111/jace.18874>.

\*Corresponding author: [sgup77@gmail.com](mailto:sgup77@gmail.com)

**EM-ThP-2 Flexible Phototransistors Array based on Hybrid Channel composed of Tellurium nanowires and tellurium-film with High Optical Responsivity, Uisik Jeong, Sungkyunkwan University (SKKU), Republic of Korea; M. Naqi, Sungkyunkwan University (SKKU), Pakistan; S. Kim, Sungkyunkwan University (SKKU), Republic of Korea**

Tellurium (Te) has recently attracted substantial attention as a p-type channel material due to their favorable characteristics such as high transport properties, good photosensitivity, and piezoelectricity. Uniform and stable Te is important for the extensive applicability in terms of electronics and optoelectronics. Here, the novel hybrid channel of Te nanowires and Te-film for flexible p-type phototransistor arrays with highly linear photo-responsivity are reported for the first time. All the processes are conducted at a temperature lower than  $100^\circ\text{C}$  to reduce thermal budget on a flexible substrate. This paper includes optical properties of the TeNWs/Te-based FETs such as threshold voltage shift, photocurrent, responsivity, sensitivity, and time-domain behavior as well as electrical performance of those devices. The array consisting of 50 devices exhibits high mobility of  $> 5 \text{ cm}^2\text{V}^{-1}\text{s}^{-1}$  and  $I_{on}/I_{off}$  of  $> 10^4$  on average. More significantly, the stability of the devices is confirmed by the various tests such as positive/negative bias stress, illumination added bias stress, long-term stability response, and even mechanical bending stress, which exhibits stable and uniform characteristics of the devices.

**EM-ThP-3 Observation of Gapless Nodal-line States in NdSbTe**, *Sabin Regmi*, Idaho National Laboratory; University of Central Florida; *R. Smith*, *A. Sakhya*, *M. Sprague*, *M. Mondal*, *I. Bin Elius*, *N. Valadez*, University of Central Florida; *K. Gofryk*, Idaho National Laboratory; *A. Ptak*, *D. Kaczorowski*, Polish Academy of Sciences, Poland; *M. Neupane*, University of Central Florida

ZrSiS-type Lanthanide (*Ln*) based materials in the *LnSbTe* family bring the possibility of electronic correlations and magnetic ordering due to the presence of *Ln 4f* electrons in addition to the topology that the ZrSiS-type systems are well known for. Here, we carried out an angle-resolved photoemission spectroscopy (ARPES) study of Neodymium-based NdSbTe, supported by first-principles calculations and thermodynamic measurements. Thermodynamic measurements reveal a magnetic transition into an antiferromagnetic ground state at around 2 K. The paramagnetic phase ARPES results detect the presence of multiple gapless nodal lines, which is also supported by first-principles calculations. Two of such nodal lines reside along the bulk X-R high-symmetry direction and one lies across the  $\Gamma$ -M direction forming a diamond plane centered at the  $\Gamma$  point. Overall, this study reveals the topological electronic structure of NdSbTe and presents a new platform to understand how such electronic structure evolves with spin-orbit coupling tuning across the *LnSbTe* family.

\*This work is supported by the National Science Foundation under CAREER Award No. DMR-1847962 and the Air Force Office of Scientific Research MURI Grant No. FA9550-20-1-0322.

**EM-ThP-4 Growth of Mn-Doped Pb(In<sub>1/2</sub>Nb<sub>1/2</sub>O<sub>3</sub>)-Pb(Mg<sub>1/3</sub>Nb<sub>2/3</sub>O<sub>3</sub>)-PbTiO<sub>3</sub> Thin Films by Pulsed Laser Deposition**, *Da-Ren Liu*, Taiwan Instrument Research Institute, National Applied Research Laboratories, Taiwan

Because of their extraordinary large electromechanical coupling coefficient and piezoelectric coefficient, relaxor-based ferroelectric crystals Pb(In<sub>1/2</sub>Nb<sub>1/2</sub>O<sub>3</sub>)-Pb(Mg<sub>1/3</sub>Nb<sub>2/3</sub>O<sub>3</sub>)-PbTiO<sub>3</sub> (PIN-PMN-PT) and Mn-Doped Pb(In<sub>1/2</sub>Nb<sub>1/2</sub>O<sub>3</sub>)-Pb(Mg<sub>1/3</sub>Nb<sub>2/3</sub>O<sub>3</sub>)-PbTiO<sub>3</sub> (Mn:PIN-PMN-PT) with morphotropic phase boundary (MPB) have attracted extensive attention. The PIN-PMN-PT and Mn:PIN-PMN-PT not only have similar piezoelectric performance to that of the binary PMN-PT but also possesses higher phase transition temperature and coercive field. They also become important materials in the fabrication of high-performance electromechanical devices including transducers, actuators and sensors. In this study, highly textured thin films of the Mn:PIN-PMN-PT were grown on SrTiO<sub>3</sub> substrates by Nd:YAG pulsed laser deposition (PLD). According to the results of glancing-angle x-ray powder diffraction (GAXRD), the Mn:PIN-PMN-PT films are polycrystalline. The thickness and roughness of the films were characterized by grazing-incidence x-ray reflectivity (GIXR), and the piezoelectric constant  $d_{33}$  was measured by the piezoelectric force microscopy (PFM). The complex refractive indices were measured in the range from 1.5 to 4.0 eV by spectroscopic ellipsometry (SE). The average oscillator strength and its associated wavelength were estimated by using a Sellmeier-type dispersion equation.

**EM-ThP-5 Synthesis and Stability of MBE Grown NbSe<sub>2</sub>**, *C. Rogers*, University of Virginia; *A. Hasan*, The University of Virginia; *C. Jezewski*, *C. Naylor*, Components Research, Intel Corporation, Hillsboro, OR 97124, USA; *N. Shukla*, *Stephen McDonnell*, The University of Virginia

Metallic 2D materials offer a unique pathway to aggressive thickness scaling without sacrificing resistivity. Unlike conventional metals which see significant increases in resistivity, when the thickness is on the order of the electron mean free path, due to increase surface/interface scattering, for 2D materials the conduction is already largely confined to the individual layers with negligible transport across the van der Waals gaps. As such, when scaled into the nm regime, these materials see little or no increase in their resistivity.

Niobium diselenide (NbSe<sub>2</sub>) is a metal-like transition metal dichalcogenide that has a similar crystal structure to the well-studied 2H-MoS<sub>2</sub>. In our work, NbSe<sub>2</sub> is grown by molecular beam epitaxy and is shown to naturally deposit with self-intercalated Nb in the van der Waals gap. We demonstrate how the resistivity of NbSe<sub>2</sub> varies as a function of deposition temperature and flux ratio and then turn our focus to how the oxidation behavior of the thin films. Specifically, we show that the grown temperature of the thin films impacts their subsequent stability in air, likely due to differing grain sizes. In addition to this we show that some processing steps that are typically nanoelectronic device fabrication can also oxidize the material which suggests that due consideration must be taken if this material is to be integrated into any device architectures.

**EM-ThP-6 Hollow-Cathode Plasma-ALD of Titanium Nitride Films Using In-Situ Ellipsometry for Conductivity Analysis**, *D. Lefcort*, *S. Bin Hafiz*, *H. Mohammad*, *L. Antoine*, *N. Ibrahimli*, *S. Ilhom*, University of Connecticut; *A. Okyay*, OkyayTech Inc; *Necmi Biyikli*, University of Connecticut

Conducting TiN films are used in various CMOS device layers. As the trend towards highly complex and 3D device architectures continue along with continued scaling in the deep single-digit nanometer level, low-temperature and conformal deposition of precision thickness controlled TiN films are critically needed. Based on our achievements in crystalline III-nitride films using hollow-cathode plasma-assisted atomic layer deposition (HCP-ALD), in this study we have investigated TiN film deposition at 200 °C using the very same reactor. We have used *in-situ* ellipsometry to analyze the evolution of film resistivity using various fitting models including Drude-Lorentz and Drude dispersion models. We share our experimental findings on how the TiN film properties were impacted by the HCP-ALD process conditions as well as how the *in-situ* extracted film resistivity values compare with ex-situ measured resistivities.

The TiN films were deposited using metal-alkyl titanium precursor (tetrakis(dimethylamido)titanium – TDMAT) and various nitrogen/hydrogen plasma mixtures (N<sub>2</sub>/H<sub>2</sub> at various flow rates) at 200 °C substrate temperature and 50 – 100 W RF-power range. SiO<sub>2</sub>-coated Si(100) wafer and glass slide samples were utilized as substrates for TiN film deposition. Real-time *in-situ* ellipsometry data was recorded using a multiwavelength ellipsometer unit. TiN films grown at lower power values (50 vs 100 W) exhibited lower film resistivity values. The total N<sub>2</sub>/H<sub>2</sub> plasma gas flow and chamber pressure showed a significant impact on the film conductivity: When compared to 100/100 sccm plasma flow, 20/20 sccm samples grown on SiO<sub>2</sub>/Si(100) substrates displayed the lowest resistivity values reaching ~150 micro-ohm.cm. Grazing-incidence XRD (GIXRD) measurements revealed polycrystalline TiN films on SiO<sub>2</sub>/Si(100) substrates. The Drude-Lorentz and Drude dispersion model layer fitting results compare reasonably well with the Van der Waal sample measurements, verifying the effectiveness of *in-situ* ellipsometry for real-time film conductivity analysis.

**EM-ThP-7 A Statistical Design of Experiments and Structural Characterization of ITO for Perovskite Solar Cells**, *Firdos Ali*, Metallurgical and Materials Engineering, The University of Alabama; *D. Li*, Electrical and Computer Engineering, The University of Alabama; *S. Gupta*, Metallurgical and Materials Engineering, The University of Alabama

We have optimized the processing and annealing of sputtered indium-tin oxide (ITO) thin films for solar cell applications by DC magnetron sputtering. The effects of process parameters such as deposition power, reactive gas flow percentage, annealing temperature and time, as well as film thickness, on the sheet resistance and transmission of the ITO films was systematically studied, using a Design of Experiments. Additionally, structural characterization of the deposited films was performed using various techniques, including X-ray diffraction (XRD), transmission electron microscopy (TEM), scanning electron microscopy (SEM), four-point probe, UV-VIS spectrometry, and atomic force microscopy (AFM). TEM analysis revealed grain boundaries, crystallinity, and d-spacing of ITO thin film. The grain size was calculated with the help of the Scherrer equation. The XRD spectra of the ITO films revealed a polycrystalline structure with preferred (222) orientation of the ITO film. The SEM image of the ITO target gives information about the morphology of the racetrack after sputtering. The topography and surface roughness were evaluated by atomic force microscopy (AFM). A sheet resistance of 10 ohms/sq. and transmission of over 90% over 400-700 nm wavelengths was achieved. Perovskite solar cells fabricated with these optimized ITO electrodes showed promising properties.

**EM-ThP-8 Voltage Tunability in Foundry Produced Resonant PZT piezoMEMS**, *J. Evans*, *N. Montross*, *Sean Smith*, *S. Chapman*, *M. McDaniel*, Radiant Technologies Inc.

Radiant Technologies recently launched our Thin Film Foundry capable of producing a wide variety of structures. Radiant has been fabricating PZT thin films since 1990 while performing foundry services on a word-of-mouth basis. Over time our process has increased in capability and can now create released MEMS. We have also formalized our design rules and are now offering foundry services to the broader community.

# Thursday Evening, November 9, 2023

As a part of our process development, we demonstrated a variety of structures such as membranes and beams fixed at one or two ends, with and without tip masses. Released structures can have resonant modes ranging from 100s of Hz to 10s of kHz. These can be plugged into customer's projects or serve as a starting point for a custom design. We collaborate with customers to integrate our PZT capacitors into another stack/process or to deposit their unique sensor material/structure onto a piezoMEMS device.

In this presentation the voltage tunability of our released piezoMEMS structures will be demonstrated along with a brief overview of our foundry process and some examples of what our customers have been able to produce with it.

## EM-ThP-9 Enforcing $\pi$ - $\pi$ Stacking Using a 1D Perovskite Core, Raúl Castañeda, New Mexico Highlands University

During the past decade, hybrid organic-inorganic metal halides have attracted the attention of a broad group of institutions due to the many potential applications these materials can have, such as semiconductors, solar cells, and LEDs. More specifically, manganese-halide compounds have been studied for their emission properties and potential applications in X-ray detectors. In this work, four new manganese(II) chloride and manganese(II) bromide 1D coordination polymers were synthesized with 4-ethylpyridine (4-EtP) or 4-phenylpyridine (4PhP) and characterized by single-crystal X-ray diffraction. These materials have a manganese core surrounded by four edge-sharing halide atoms (MnX<sub>4</sub>) and the ligand coordinating from above and below the MnX<sub>4</sub> plane. Interestingly  $\pi$ - $\pi$  interactions are enforced by the 1D coordination polymer. Further studies on these types of materials can result in new molecular wires as semiconductor materials.

## EM-ThP-10 Modular until it's Not – Imaging Fast, Hard X-Rays at NIF, Mary Ann Mort, University of California at Davis; A. Carpenter, Lawrence Livermore National Lab; C. Hunt, University of California at Davis

The proposed multi-frame gated x-ray imager (MGXI) is a fast, hard x-ray imaging diagnostic for use in ICF and HED experiments at the National Ignition Facility (NIF), such as Compton radiography and hot spot imaging. MGXI has goals to image 10-100 keV x-rays with 100-1000 ps temporal resolution in 2-8 frames and >5% DQE. Modularity of the versatile testbed for initial MGXI component experimentation starts with testing microchannel plates (MCPs) under vacuum with an electron gun and a simple photodiode (PD) array. Simultaneously, MCPs will be modeled in Computer Simulation Technology (CST) to determine the effects an applied magnetic field has on the electron trajectories.

## Fundamental Discoveries in Heterogeneous Catalysis Focus Topic

### Room Oregon Ballroom 203-204 - Session HC-ThP

## Fundamental Discoveries in Heterogeneous Catalysis Poster Session

### HC-ThP-1 Insight into Synergistic Effect of Oxide-Metal Interface on Hot Electron Excitation, Eunji Lee, Korea National University of Education, Republic of Korea; B. Jeon, J. Park, Korea Advanced Institute of Science and Technology (KAIST), Republic of Korea; S. Lee, Korea National University of Education, Republic of Korea

Understanding the role of electron transfer by energy dissipation during chemical reactions on metal catalyst surfaces is significant for elucidating the fundamental phenomena at solid-gas and solid-liquid interfaces [1]. Electronic excitation by molecular interactions between reactants and catalyst surfaces generates a flow of excited electrons with an energy of 1–3 eV; these are called hot electrons [2]. To reveal the chemically induced electronic excitations on metal catalyst surfaces, metal-semiconductor catalytic nanodiodes can be used for real-time hot electron detector [3]. In addition, recently, it was found that when the metal-oxide interface is formed, the excitation of hot electrons can be amplified [4].

In this work, to understand the effect of the oxide-metal interface on hot electron excitation under exothermic chemical reactions, we employ advanced real-time detection of reaction-induced electronic excitation and report, for the first time, direct *in-situ* observations of hot electron transfer on metal-semiconductor Schottky nanodevices with well-controlled oxide-metal interfaces (CeO<sub>2</sub> nanocubes/Pt/TiO<sub>2</sub> Schottky nanodiodes). Direct measurement of the electron transfer according to the concentration of

interfacial sites (by controlling the coverages of deposited CeO<sub>2</sub> on Pt) allows us to investigate the effect of the oxide-metal interface on non-adiabatic electronic excitation during catalytic H<sub>2</sub> oxidation. Surprisingly, when compared according to the concentration of the CeO<sub>2</sub>/Pt interface, the efficiency of hot electron excitation appears to be the highest at a specific concentration of interfacial sites, proving that the inverse oxide-metal interface plays an important role in improving hot electron excitation under exothermic catalytic reactions. Our *operando* techniques using Schottky nanodiodes with well-controlled oxide-metal interfaces provide conclusive evidence about the promotional role of the inverse oxide-metal interfacial sites in heterogeneous catalysts, which contributes to the rational design of future hot electron-based catalysts [5].

## References

- [1] Jeong Young Park\* *et al.*, *Chemical Reviews*, **2015**, *115* (8), 2781
- [2] Si Woo Lee *et al.*, *Surface Science Reports*, **2021**, *76* (3), 100532
- [3] Si Woo Lee *et al.*, *ACS Catalysis*, **2019**, *9* (9), 8424
- [4] Si Woo Lee *et al.*, *Nature Communications*, **2021**, *12* (40), 1
- [5] Eunji Lee *et al.*, *in preparation*

### HC-ThP-2 Chemical Speciation and Structural Evolution of Rhodium and Silver Surfaces with High Oxygen Coverages, Dan Killelea, M. Turano, L. Jamka, M. Gillum, Loyola University Chicago; L. Juurlink, Leiden University, The Netherlands; T. Schäfer, University of Göttingen, Germany

The oxidation silver and rhodium surfaces are compared. In particular, I will discuss how the structures formed at high oxygen coverages differ for the metals and how their chemistries may be affected.

The interaction of oxygen with the surfaces of catalytically active transition metals has attracted much interest because of the relevance to heterogeneous catalysis. Recently, we have shown that oxygen coverages in excess of 1 ML are achievable using gas-phase atomic oxygen (AO) to dose the metal surfaces. This talk will discuss some recent results comparing the uptake of AO and O<sub>2</sub> on Ag(111), Rh(111), and curved Ag(111). On c-Ag(111) surfaces, the geometry of the monoatomic steps determines whether or not O will accumulate and the consequent surface reconstruction. Conversely, on Rh(111), subsurface oxygen readily forms from exposure to AO. Finally, the uptake of oxygen on Ag(111) is discussed; unlike Rh(111), where little surface reconstruction occurs, Ag(111) undergoes several phase transformations as the oxygen coverage is increased. These results using AO demonstrate that UHV compatible dosing can prepare the same surfaces resulting high pressure O<sub>2</sub> exposures, allowing for quantitative and structural analysis of the oxidized surfaces.

### HC-ThP-3 Exploring Field-Assisted Nitrogen Activation with Atom Probe Microscopy, Sten V Lambeets, M. Wirth, D. Perea, Pacific Northwest National Laboratory

Challenges in the development of green electricity and energy storage challenges are leading us to consider NH<sub>3</sub> as a promising future zero-carbon fuel. However, NH<sub>3</sub> production largely relies on the Haber-Bosch process requiring high temperature and pressure, making its production via this means responsible for approximately 1.5% of world CO<sub>2</sub> emissions. To unlock to full economic and environmental potential of NH<sub>3</sub>, it is critical to lower energy requirements and generate a zero-carbon NH<sub>3</sub> by coupling with renewable electricity<sup>1</sup>. The N<sub>2</sub> reduction reaction to NH<sub>3</sub> using electricity is extensively investigated with single atom electrocatalysts (SACs) recently showing promising results. Due to their morphology, the application of an electrical potential on SACs materials results in local High External Electric Fields (HEEFs) over the single atoms. If those effects present promising outcomes according to theoretical calculations<sup>2,3</sup>, the values of those HEEFs and the mechanisms involved remains largely unknown and unexplored.

Atom Probe Microscopy (APM) such as Field Ion Microscopy (FIM) and Operando Atom Probe (OAP) are ideal techniques to unravel those mechanisms at the nanoscale since they inherently rely on HEEFs for imaging. In this work, we will illustrate those capabilities with the room temperature N<sub>2</sub> dissociation over Ru single nanoparticle case imaged at the nanoscale using FIM and OAP.

We use the recently developed OAP technique<sup>4</sup> to effectively measure this dissociation over a 0001-oriented Ru specimen. After fixing a constant HEEF between 15 and 25 V/nm and the temperature at 300K,  $1.4 \times 10^{-7}$  mbar  $N_2$  pure gas is introduced in the analytic chamber. The electric field either directly ionize  $N_2$  or provoke its dissociation. Dissociated  $N(\text{ads})$  are mainly detected over the Ru{1012} facets while ionized  $N_2^{++}$  are detected on large areas in the periphery of the imaged apex. The occurrence of one or the other processes is intimately linked to the local surface structures and, subsequently, the local HEEFs.

APM are capable to observe and estimate the HEEF necessary to trigger specific chemical reaction steps such as the  $N_2$  dissociative adsorption (i.e. activation). With an accurate calculation of those HEEF, those values can be extrapolated to create new chemical and reactor system designed to perform  $N_2$  activation at relatively low energy cost. In a context of electrification of chemical processes, APM can help pave the way to a deeper understanding of the physical laws involved in electrochemistry, as well as in chemistry in general.

1. M.Wan *et al.* JACS Au 2,1338–1349(2022).

2. S.M.Kathmann, Phys.Chem.Chem.Phys.23,23836–23849(2021).

3. M.L.Karahka&H.J.Kreuzer, Surf.Sci.643,164–171(2016).

4. S.V.Lambeets *et al.* Top.Catal.1606-1622(2020)

## HC-ThP-4 Adsorption and Hydrogenation of 1,3-Butadiene on Cu (111) and a Pd/Cu (111) Single-Atom-Alloy, *Mohammad Rahat Hossain, M. Tenary*, University of Illinois - Chicago

A single atom alloy (SAA) is made by substituting catalytically active dopant metal atoms into the topmost atomic layer of a relatively inert host metal. Commonly, Pd and Pt are used for hydrogenation reactions due to their virtually zero barrier for  $H_2$  activation. Yet, these catalysts are easily coked by CO and their high activity often limits their selectivity. Industrially, these catalysts are often doped with a less active metal to prevent coking and enhance their selectivity. One of the most important steps in the refinement of alkene streams for the industrial-scale production of high-quality polymers is the selective hydrogenation of 1,3-butadiene. In the literature, Pd (111) shows higher selective control over hydrogenation of 1,3-butadiene to butene than Pt (111). Therefore, the presence of isolated Pd atoms on a Cu host surface can be a suitable SAA catalyst model for this particular reaction. In this study, we used reflection absorption infrared spectroscopy (RAIRS) and temperature programmed desorption (TPD) to investigate the adsorption of butadiene and butene, as well as the hydrogenation of butadiene on Cu (111) and a Pd/Cu (111) SAA. The TPD study shows butadiene binds strongly to the Cu (111) surface compared to 1-butene. The desorption peak in the 120-130 K temperature range indicates the production of 1-butene from the hydrogenation of butadiene on the Pd/Cu (111) SAA. Auger electron spectroscopy (AES) shows no accumulation of surface carbon demonstrating molecular desorption of butadiene from the surface under UHV. The observation of both in-plane ( $CH_2$ -wag at  $908 \text{ cm}^{-1}$ ) and out-of-plane (C-H bend at  $1023 \text{ cm}^{-1}$ ) modes with RAIRS at monolayer coverage indicates that butadiene is adsorbed neither parallel nor perpendicular to the surface. In addition, IR peaks at  $1464 \text{ cm}^{-1}$  for ( $-CH_3$ ) antisymmetric deformation and  $1412 \text{ cm}^{-1}$  for ( $=CH_2$ ) scissors modes are observed on the Pd/Cu (111) SAA, indicating 1-butene formation from butadiene hydrogenation. The ambient pressure RAIRS studies are currently underway to calculate the turnover frequency (TOF) of the above-mentioned catalyst for the hydrogenation of 1,3-butadiene.

## HC-ThP-5 Studying C-H Activation on RhCu Single-Atom Alloys Using Molecular Beams, *Molly Powers, J. Rosenstein, L. Joseph, A. Utz*, Tufts University

Single-atom alloys (SAAs) are a new class of heterogeneous catalysts drawing immense research interest due to their unique catalytic activity. An active dopant metal is atomically dispersed in a more inert, selective host metal to produce a catalyst that has a unique potential to simultaneously improve catalytic selectivity and activity compared to their single metal counterparts. To date, detailed surface science studies of SAAs have been limited to relatively low-barrier reactions. The poster will summarize recent work in our lab that extends the range of detailed mechanistic studies to higher barrier reactions, including C-H activation. Our study focuses on the reaction of simple hydrocarbons, such as methane, on a RhCu SAA catalyst.

While prior work has examined this system using reflection-absorption IR spectroscopy, temperature programmed desorption, and scanning tunneling microscopy, our supersonic molecular beam experiments permit the study of high energetic barriers to examine the dynamics, kinetics, and energetics of the initial C-H bond cleavage reaction, and the subsequent chemistry and diffusion of the surface-bound products of dissociative chemisorption.

## HC-ThP-6 Investigating the Dissociative Chemisorption of Methane on Ru(0001) via Supersonic Molecular Beam, *Matthew Kalan, Y. Li, A. Utz*, Tufts University

Recent theoretical studies have proposed the creation of a database of experimentally determined barrier heights for model reactions on transition metal surfaces as a tool for the development of chemically accurate computational methods for heterogeneously catalyzed reactions<sup>1</sup>. This approach has been effectively applied to the dissociative chemisorption of  $CH_4$  on Pt and Ni surfaces using semi-empirical specific reaction parameter density functional theory (SRP-DFT)<sup>2</sup>. Current work on SRP-DFT involves expanding its application to other surfaces, including Ru(0001). There is, however, substantial disagreement in the current literature as to the height of the barrier on Ru(0001), with experimentally determined values ranging from 0.38 to  $0.85^{3,4}$  eV. Our work applies supersonic molecular beam reactivity measurements to this system in order to provide an important experimental benchmark for additional SRD-DFT studies. By measuring reactivity across a wide range of translational energies, surface temperatures, and vibrational states, our data will also serve as a rigorous test of the theoretical predictions of any future first-principles methods. We will present the results from ongoing reactivity measurements of the dissociative chemisorption of  $CH_4$  on Ru(0001) and their implications for the dynamics of the reaction.

(1) Mallikarjun Sharada, S.; Bligaard, T.; Luntz, A. C.; Kroes, G.-J.; Nørskov, J. K. SBH10: A Benchmark Database of Barrier Heights on Transition Metal Surfaces. *J. Phys. Chem. C* **2017**, *121* (36), 19807–19815. <https://doi.org/10.1021/acs.jpcc.7b05677>.

(2) Migliorini, D.; Chadwick, H.; Nattino, F.; Gutiérrez-González, A.; Dombrowski, E.; High, E. A.; Guo, H.; Utz, A. L.; Jackson, B.; Beck, R. D.; Kroes, G.-J. Surface Reaction Barriometry: Methane Dissociation on Flat and Stepped Transition-Metal Surfaces. *J. Phys. Chem. Lett.* **2017**, *8* (17), 4177–4182. <https://doi.org/10.1021/acs.jpclett.7b01905>.

(3) Larsen, J. H.; Holmblad, P. M.; Chorkendorff, I. Dissociative Sticking of  $CH_4$  on Ru(0001). *7*.

(4) Mortensen, H.; Diekhöner, L.; Baurichter, A.; Luntz, A. C.  $CH_4$  Dissociation on Ru(0001): A View from Both Sides of the Barrier. *The Journal of Chemical Physics* **2002**, *116* (13), 5781–5794. <https://doi.org/10.1063/1.1456509>.

## HC-ThP-7 Size-Selected Pt Alloy Cluster Catalysts for the Dehydrogenation of Light Alkanes, *Autumn Fuchs, M. Malek, S. Anderson*, University of Utah

Size-selected  $Pt_n$ - $Ge_m$  clusters supported on alumina have been developed and are being investigated under ultra-high vacuum for the selective dehydrogenation of light alkanes. Surface analysis techniques such as temperature programmed desorption (TPD), x-ray photoelectron spectroscopy (XPS), and ion scattering spectroscopy (ISS), are used to characterize the clusters and probe binding sites and energies of small alkanes. TPD experiments have shown that the addition of Ge to  $Pt_n$  limits catalyst deactivation by carbon deposition (coking) and sintering. The number of Pt atoms in the cluster affects the number of available binding sites for ethylene on the surface. We will present a study of butane and isobutane dehydrogenation and cracking  $Pt_n$ /alumina and  $Pt_n/Ge_m$ /alumina. In addition to the surface science experiments, we will present data from a MEMS microreactor device that allows reactants to be flowed over a sample of deposited clusters at pressures up to 1 atm and temperatures to 1000 K. Reactions on clusters will be compared to reactions on Pt nanoparticles made via chloroplatinate drop-casting and reduction.

## HC-ThP-8 Switching between Hot Electron and Hot Hole Transfer during Chemical Reaction, *Hyekyung Kwon*, Korea National University of Education, Republic of Korea; *B. Jeon, J. Park*, Korea Advanced Institute of Science and Technology (KAIST), Republic of Korea; *S. Lee*, Korea National University of Education, Republic of Korea

Understanding hot carrier dynamics is crucial for the rapid development of nanocatalysts [1]. By observing the transfer of carriers quantitatively in real-time during a catalytic reaction, a correlation between catalytic performance and charge transfer can be identified [2]. When a chemical reaction occurs on a metal catalyst, electronic excitation is caused by the non-adiabatic dissipation of exothermic energy, leading to the generation of

electron-hole pairs (*i.e.*, hot carriers) [3]. In order to study the surface dynamics of these hot carriers, a metal/semiconductor Schottky (*i.e.*, catalytic nanodiode) needs to be coupled with heterogeneous catalysts [4].

In this work, we observed hot carriers excited in real time during the H<sub>2</sub>O<sub>2</sub> decomposition reaction using Pt/Si Schottky nanodiodes. When the Pt/Si nanodiode was immersed in the H<sub>2</sub>O<sub>2</sub> solution, the H<sub>2</sub>O<sub>2</sub> decomposition occurred on the Pt catalyst surface, and electron-hole pairs were excited. This could be detected as a current signal (*i.e.*, chemi-current; a current induced by a chemical reaction) flowing through the nanodevice. Interestingly, the flow of hot electrons was detected in the Pt/n-Si nanodiode, whereas the transfer of hot holes was observed in the Pt/p-Si nanodiode. The chemi-current caused by hot carrier transfer linearly depended on the concentration of the H<sub>2</sub>O<sub>2</sub> solution, confirming that the observed chemi-current was indeed a result of the H<sub>2</sub>O<sub>2</sub> decomposition occurring on the Pt catalyst. In order to electronically control the hot electron and hot hole transfers, we detected the currents while applying a reverse bias (*i.e.*, an electric field on the Schottky junction) to both the Pt/n-Si and Pt/p-Si nanodevices. In the Pt/n-Si nanodiode, through which hot electrons flowed, electron transfer was amplified under the reverse bias condition due to Schottky barrier lowering. However, when reverse bias was applied to the Pt/p-Si nanodevice, where hot hole transfer was dominant under open circuit, hot electron transfer surprisingly emerged instead of hot hole transfer. Accordingly, we can conclude that the movement of the hot hole in the Pt/p-Si nanodiode was due to the remaining holes after the electrons were consumed for inducing the chemical reaction. Our techniques to control and switch the transfer of hot carriers during a chemical reaction using metal-semiconductor Schottky junctions may shed light on potential applications of hot carriers in catalytic devices, energy conversion-based devices, or sensors.

## References

- [1] Si Woo Lee *et al.*, *Surface Science Reports*, **2021**, 76 (3), 100532
- [2] Si Woo Lee *et al.*, *ACS Catalysis*, **2019**, 9 (9), 8424
- [3] Si Woo Lee *et al.*, *Nano Letters*, **2023**, 23 (11), 5373
- [4] Si Woo Lee *et al.*, *Nature Communications*, **2021**, 12 (40), 1

**HC-ThP-9 Tracking Elementary Steps in Conversion of Carboxylic Acids on Single Crystalline and Nanofaceted TiO<sub>2</sub>(101)**, *Xingyu Wang*, Pacific Northwest National Laboratory; *W. Debenedetti*, Los Alamos National Laboratory; *C. O'Connor*, Harvard University; *Z. Dohnalek*, *G. Kimmel*, Pacific Northwest National Laboratory

In catalysis research, the material gap is one of several that the surface science community is trying to bridge, along with the pressure and temperature gaps. In the specific case of carboxylic acids on TiO<sub>2</sub>, previous studies discovered that for acetic acid reacting with anatase nanoparticles at ambient pressure, an environment very much like real world catalytic processes, acetone could be produced. However, under ultrahigh vacuum (UHV) conditions, with a few monolayers of acetic acid on anatase(101) single crystals, acetone was not observed as a product. In contrast, formic acid reactions with either nanoparticles or single crystals showed no evidence of C-C bond formation. Here, we prepared a sample with layers of synthesized anatase nanoparticles with mostly (101) facets in an UHV system and compared the reactivity of acetic acid with that on a anatase(101) single crystal, using TPD (temperature programmed desorption) and RAIRS (reflection absorption infrared spectroscopy) to track the elementary steps, with the goal to bridge this material gap and fully understand the reaction mechanisms of carboxylic acids on metal oxides.

**HC-ThP-10 ZnO Nanoparticles as an Effective Rhodamine B Dye Mineralization Under Direct Sunlight Irradiation**, *Jose Alberto Alvarado Garcia*, BENEMERITA UNIVERSIDAD AUTONOMA DE PUEBLA, Mexico; *G. ANAYA GONZALEZ*, Universidad Autónoma de Mexico; *R. PEREZ CUAPIO*, *H. JUAREZ SANTIESTEBAN*, BENEMERITA UNIVERSIDAD AUTONOMA DE PUEBLA, Mexico; *A. ARCE PLAZA*, INSTITUTO POLITÉCNICO NACIONAL, Mexico

In this research ZnO at different Zinc acetate concentration from 0.1-0.4 M was synthesized through colloidal synthesis and applied to mineralize Rhodamine B dye under direct sunlight irradiation, showing that this is strongly related to the particle size and defects presence at the particle. This relationship is well correlated to the UV-Vis absorbance spectrum and

photoluminescence (PL), showing up to 90 % of photocatalyst efficiency after 100 min for sample obtained at 0.3M, this behavior also is showed for those samples obtained at 0.1, 0.2 and 0.4 molar concentration. The XRD data analysis let the structure and crystallite average size (18- 27 nm) to be determined meanwhile the morphology and composition was obtained from HRSEM and EDS respectively. From the FTIR results the organic dye mineralization evolution was determined. Albeit the defects contribution was determined by PL.

**HC-ThP-11 Role of Vacancies and Absorbed Hydrogen Atoms on the Formation of Peroxides and Superoxides on CeO<sub>2</sub> Surfaces**, *M. Brites Helu*, *M. Vecchiotti*, *S. Collins*, Instituto de Desarrollo Tecnológico para la Industria Química, Argentina; *M. Calatayud*, Laboratoire de Chimie Théorique, Sorbonne Université, France; *Jorge Anibal Boscoboinik*, *D. Stacchiola*, Center for Functional Nanomaterials, Brookhaven National Laboratory; *F. Calaza*, Instituto de Desarrollo Tecnológico para la Industria Química, Argentina

It is well known that VOCs being recognized as major responsible for the increase in global air pollution. Catalytic combustion is an efficient technology for the abatement of VOC, which are oxidized over a catalyst at temperatures much lower than those of the thermal process. Specifically, gold supported catalysts on CeO<sub>2</sub> have shown a great performance in the oxidation of CO, methanol, toluene, etc. Besides, it is important to clarify the role of the support in such reaction. Ceria has the key property of high oxygen storage capacity which originates in its ability to rapidly switch from Ce to Ce oxidation states as the environment changes from reducing to oxidizing and vice versa. Its redox behavior is influenced by the substituent lattice groups that could be incorporated during different catalyst pretreatments and could affect the oxidation of VOC. This could be understood as the influence of oxygen vacancies and/or absorbed or coadsorbed H on the activation of oxygen molecules. The latter leads to the formation of superoxide and peroxide molecules on the surface, which could in principle be highly reactive towards oxidation of organic molecules.

In this context, we study, by IR spectroscopy and mass spectrometry, the interaction of O<sub>2</sub> with the modified CeO<sub>2</sub> based material, by creating vacancies following different reduction treatments. The possible role of the vacancies and/or presence of H atoms in the electron transfer from the surface to the oxygen molecule is discussed. Using AP-XPS we are able to prove that the surface/near surface of CeO<sub>x</sub> presents a charging effect which could be due to extra charge/electrons which then transfer to O<sub>2</sub> to form superoxide and peroxide species sequentially and presenting different thermal stabilities. Furthermore, the presence of different facets on the surface of the material could change the stability or amount of active species, thus comparison of results from polycrystalline ceria and CeO<sub>2</sub> nanocubes provide information about the structure-activity relationship for the rational design of catalytic materials.

**HC-ThP-12 Small Alcohol Reactivity Over TiO<sub>2</sub>/Au(111) Inverse Model Catalysts**, *Ashleigh Baber*, James Madison University

Gold-based catalysts have received tremendous attention as supports and nanoparticles for heterogeneous catalysis, in part due to the ability of nanoscale Au to catalyze reactions at low temperatures in oxidative environments. Surface defects are known active sites for low temperature Au chemistry, so a full understanding of the interplay between intermolecular interactions and surface morphology is essential to an advanced understanding of catalytic behavior and efficiency. Our undergraduate research lab uses ultrahigh vacuum temperature programmed desorption (UHV-TPD) to investigate the fundamental interactions between small alcohols on Au(111) and the reactivity of TiO<sub>2</sub>/Au(111) inverse model catalysts on small alcohol redox behavior. In a systematic study to better understand the adsorption and intermolecular behavior of small alcohols (C<sub>1</sub>-C<sub>4</sub>) on Au(111) defect sites, coverage studies of methanol, ethanol, 1-propanol, 1-butanol, 2-butanol, and isobutanol have been conducted on Au(111). These small alcohols molecularly adsorb on the Au(111) surface and high resolution experiments reveal distinct terrace, step edge, and kink adsorption features for each molecule. The desorption energy of small primary alcohols was shown to trend linearly with increasing C<sub>1</sub>-C<sub>4</sub> carbon chain length, indicating that the H-bonded molecular packing of 1-butanol resembles that of methanol, ethanol, and 1-propanol, while isobutanol and 2-butanol deviate from the trend. These energy insights are particularly interesting when studying the redox behavior of small alcohols over TiO<sub>2</sub>/Au(111). Depending on the surface preparation conditions, Au(111) supported TiO<sub>2</sub> nanoparticles react with small alcohols to form either reduced and oxidized products. The reactivity of the surface for ethanol oxidation was altered by controlling the oxidation

# Thursday Evening, November 9, 2023

state of  $\text{TiO}_x$  ( $x < 2$ ) and coverage of  $\text{TiO}_2$ . Low coverages of fully oxidized  $\text{TiO}_2$  nanoparticles on Au(111) are active for the selective oxidation of ethanol to form acetaldehyde, but not all small alcohols behave similarly.

## Advanced Focused Ion Beams Focus Topic Room Oregon Ballroom 203-204 - Session IB-ThP

### Advanced Focused Ion Beams Poster Session

**IB-ThP-1 Emission of Multiple Ion Species from a Single Ion Source: Top-Down FIB with LMAIS on a Lithography Platform, *Torsten Richter, A. Ost, A. Nadzeyka, P. Mazarov, L. Bruchhaus, F. Meyer***, Raith GmbH, Germany

Focused Ion Beams (FIB) technologies are broadly used in nanoscale science related applications, and they are inherently applied for direct nano-patterning, resist based processes [1] as well as ion microscopy [2]. FIB patterning has become a direct, versatile, and precise fabrication method of smallest features at high reproducibility. Therefore, high demands are made on the FIB in terms of beam stability, but also the sample stage requires a high degree of stability, accuracy and automation for nanoscale patterning and imaging.

The Liquid Metal Alloy Ion Source (LMAIS) is a versatile FIB source technology able to emit various ion species [3] at high stability. Light and heavy ions such as Silicon and Gold or Lithium and Bismuth are emitted simultaneously from a single ion source (AuGeSi or GaBiLi) [4] and separated using a downstream Wien filter. This source technology allows the optimization of lateral resolution as well as depth resolution, sputter yield or avoiding sample contamination by selecting the most suitable ion species. Combining the LMAIS with a high-precision laser interferometer stage, the Raith VELION FIB-SEM offers new process pathways reaching from nm-sized feature to wafer-scale patterning.

Besides nanofabrication, novel 3D ion microscopy imaging workflows have become possible thanks to the top-down FIB geometry on the VELION, becoming thus a powerful ion microscope for sample 3D reconstruction. Milling with bismuth allows a fast and homogeneous surface sputtering at highest depth resolution, while switching to Lithium ions enables 2D imaging at high lateral resolution (down to 1.5 nm).

In this contribution, we present the latest advances in LMAIS source technology along with related applications such as resist based ion beam lithography and introduce 3D ion microscopy using both light and heavy ions from LMAIS.

- [1] Lei Zhang et al., *Nanotechnology* 31 325301 (2020)
- [2] N. Klingner et al., *Beilstein J. Nanotechnology*. 11, 1742 (2020)
- [3] L. Bischoff et al., *Appl. Phys. Rev.* 3, 021101 (2016)
- [4] W. Pilz et al., *JVSTB* 37, 021802 (2019)

**IB-ThP-2 Roadmap for Focused Ion Beam Technologies, *K. Höflich***, Ferdinand Braun Institut, Germany; *G. Hobler*, TU Wien, Austria; *F. Allen*, University of California at Berkeley; *T. Wirtz*, LIST, Luxembourg; *G. Rius*, Institut de Microelectrónica de Barcelona, Spain; ***Gregor Hlawacek***, Helmholtz Zentrum Dresden-Rossendorf, Germany

This roadmap document comprises a review of the current state-of-the-art of advanced focused ion beam (FIB) processing and technology followed by an outlook on required future developments curated by a diverse group of stakeholders.

FIBs play an important role in scientific research in fields ranging from health and biology to quantum technology and nuclear fusion research. However, usually FIBs are perceived as tools for the preparation of samples for other methods such as transmission electron microscopy or atom probe tomography. The intention of this document is to show that this is a clear underestimation of the method by showcasing current and past applications as well as providing a guideline for academia, industry and funding agencies on necessary future developments. The roadmap starts with presenting the state-of-the-art of the FIB technology and instrumentation. The working principle of the FIB is described and an overview of additional instrumentation and detectors who widen the applicability of the method is given. In the second section the available instruments for the simulation and prediction of the focused ion implantation and milling process is given. This includes advanced simulation techniques such as DFT and MD but also computational efficient methods like BCA which can be used in the every day lab work by FIB users. The core part of the review describes the various applications which go beyond the preparation of TEM samples and include in addition to the above mentioned applications also the fields of spintronic and magnonics, Thursday Evening, November 9, 2023

super conductivity, photonics, micromechanics, MEMS/NEMS and many more.

In the last part the authors comprising the relevant stake holders give an overview of the required future development which will enable FIB technology to stay at the forefront of research in the discussed fields. This outlook part is partly based on a survey conducted within the European COST Action CA19140 FIT4NANO which unites more than 200 users, developers and manufacturers of FIB technology. The intention of this part is to act as a guideline for academic and commercial developers as well as funding agencies to steer the future developments in a direction agreed upon by the community. It is this aim supported by the divers group of contributors to the review which makes this roadmap relevant and timely for many fields of research.

**IB-ThP-3 A Multi-Scale Understanding of the Three-Dimensional Microstructure of the Cornea Using Oxygen Plasma Focused Ion Beam, Scanning Transmission Electron Microscopy and Micro-CT Techniques, *Valerie Brogden, M. Scanagatta-Long, H. Uehara, A. Lin***, University of Oregon

INVITED

The cornea is a transparent tissue of the eye which is used to focus light and consists of multiple layers including the epithelium, stroma, and endothelium. In certain genetic conditions, the endothelium deteriorates, leading to loss of pumping function and the formation of excrescences of collagen known as guttata. This condition describes Fuchs' endothelial corneal dystrophy (FECD), an inheritable disease which causes corneal fluid accumulation and eventual clouded vision. Since human corneal endothelial cells do not proliferate in vivo, the only treatment for advanced FECD is corneal transplantation. A shortage of donor corneas necessitates a new therapy for FECD.

Currently, the structural nature of guttata formation is not well understood. With a better understanding of guttata structure, new therapeutic methods may be developed. In order to investigate the three-dimensional structure of the endothelial layer on multiple length scales, we utilized Plasma Focused Ion Beam Scanning Electron Microscopy (PFIB-SEM) tomography in conjunction with Scanning Transmission Electron Microscopy (STEM) and Microcomputed Tomography ( $\mu$ -CT).

While xenon is the most commonly used PFIB species in materials sciences, oxygen is proving to be particularly useful for creating artifact-free cuts into biological tissue. Researchers have found that oxygen PFIB can be used to remove curtaining artifacts in organic samples significantly faster than xenon PFIB.

The above reasons make oxygen PFIB the ideal technique for understanding 3D volumes of biological structures where sub-micron resolution is necessary. However, due to the novelty of this technique, it has yet to be popularized. To demonstrate oxygen PFIB application to biological samples, a normal mouse cornea (C57BL6J) and an FECD mouse cornea (Col8a2<sup>Q455K</sup>) were examined as test samples.

Upon investigation of the 3D renderings of PFIB SnV data, we noted that the diseased cornea appears more topographical than the healthy cornea and the nanostructure of the guttata can be observed. This suggests that oxygen PFIB SnV with 3D rendering is a powerful technique for understanding the microstructure of the corneal endothelium. Paired with  $\mu$ -CT and STEM imaging, a correlative, three-dimensional, multiscale understanding of the cornea is possible.

**IB-ThP-5 Focused Ion Beam Implantation by Deceleration, *M. Titze***, Sandia National Laboratory; *J. Poplawsky*, Oak Ridge National Laboratory; *E. Bielejec*, Sandia National Laboratory; ***Alex Belianinov***, Sandia National Laboratories Ion implantation is a key capability for a growing number of scientific and industrial areas, including quantum information sciences, and the semiconductor industry. As devices become smaller, new materials and processes are introduced and quantum technologies transition to being mainstream, traditional implantation methods may fall short in terms of energy, species, and positional precision. In this talk we will show data demonstrating Au implants into Si at energies 10 eV–450 eV in a Raith Velion focused ion beam system by decelerating ions using bias and keeping the beam focused. The implants were validated using atom probe tomography. Our data reveal that standard implant modeling approaches fail to agree with experimentally measured depths, potentially due to surface sputtering and lattice enrichment. Finally, we discuss how our results pave a way to much lower implantation energies, while maintaining high spatial resolution.

## MEMS and NEMS Technical Group

Room Oregon Ballroom 203-204 - Session MN-ThP

### MEMS/NEMS Poster Session

#### MN-ThP-1 Ferroelectric and Photovoltaic Properties of $\text{Pb}_{0.95}\text{La}_{0.05}\text{Zr}_{0.54}\text{Ti}_{0.46}\text{O}_3$ Films as a Function of Film Thickness, *Sneha Kothapally, S. Kotru*, The University of Alabama

Ferroelectric materials are being extensively studied for optoelectronic, electrical, and photovoltaic applications. Ferroelectric photovoltaics (FEPV) are gaining research interest as their photovoltaic properties are tunable by controlling the ferroelectric polarization with the applied electric field. However, the low photocurrent obtained from FEPV materials is a significant problem that inhibits their practical applications. The surface quality and the crystalline structure of these films are shown to vary with the film thickness which can influence the photovoltaic response. In this work, ferroelectric  $\text{Pb}_{0.95}\text{La}_{0.05}\text{Zr}_{0.54}\text{Ti}_{0.46}\text{O}_3$  (PLZT) films of different thicknesses were prepared on platinumized silicon substrate using the sol-gel deposition technique. As-deposited films were annealed to promote crystallinity. The electrical measurements were taken using a capacitor structure (top electrode/PLZT/Pt), where the top electrodes were sputter deposited. The effect of the thickness of the PLZT layer on microstructure, ferroelectric, photovoltaic, and optical properties was investigated to find the optimal thickness for obtaining the best photo response. Enhanced photovoltaic properties coupled with ferroelectric properties exhibit potential applications for energy conversion in microelectromechanical systems (MEMS), and photovoltaic sensors such as UV sensors.

#### MN-ThP-2 An In-Situ Reflectometry Parylene Deposition Technique for Highly Accurate and Repeatable Film Thickness and Uniformity, *Steven Larson, K. Coombes, A. Mings, J. Norris*, Sandia National Laboratories

Parylene is a chemical vapor deposition (CVD) coating process used for conformal coating, energy harvesting, piezoelectric sensors, acoustic resonators, and many other application. Despite its use in a wide variety of applications, parylene deposition system manufacturers provide minimal methods to control film thickness. While methods have been developed for controlling parylene thickness, their widespread adoption has been limited by scalability, complexity, and cost. In this presentation we report a simple, scalable, and cost effective insitu reflectometry technique for parylene deposition that significantly increases the repeatability and accuracy of deposition thickness. We report film accuracy as a relative standard deviation of 2% as opposed to commercial parylene systems which we measure to a relative standard deviation of 17%. We then improve thickness uniformity with deposition flux modeling and a custom stage with planetary motion. Here we show a significantly improved wafer uniformity of 0.2%.

#### MN-ThP-3 The Effect of $\text{CH}_4/\text{H}_2$ Gas Admixture on the Selectivity Towards Pt in Dry Etching of PZT Thin-Films by ICP-RIE, *Madeleine Petschnigg, N. Andrianov, S. Azeem*, Silicon Austria Labs, Austria; *S. Trolier-McKinstry*, The Pennsylvania State University

Due to their high piezoelectric coefficients, ferroelectric thin-films based on lead zirconate titanate (PZT) are among the leading materials for active layers in actuator type microelectromechanical systems (MEMS) such as inkjet print heads, adaptive optics like micro mirrors or autofocus devices, and micromachined acoustic and ultrasonic transducers [1–3].

Well defined patterning of PZT films is crucial for the fabrication of MEMS based on this material. Inductively coupled plasma reactive ion etching (ICP-RIE) allows etching of deep trenches with high aspect ratios and anisotropic etch profiles. While Ti and Zr oxides can be etched chemically by the formation of volatile halides [4,5], the removal of PbO is mainly achieved by physical means, which limits the selectivity against masking and electrode materials. A selective patterning process is especially important for large diameter substrates due to typically radial non-uniformities.

This work illustrates the effect of introducing  $\text{CH}_4/\text{H}_2$  to the etch chemistry on the selectivity in dry patterning of PZT thin-films via ICP-RIE and discusses the potential chemical mechanism entailed. Figure 1 shows a significant increase in selectivity towards photoresist and Pt upon the addition of  $\text{CH}_4/\text{H}_2$  to a  $\text{CHF}_3/\text{Cl}_2/\text{BCl}_3$  gas mixture while the PZT etch rate remains approximately constant up to 25 vol% added  $\text{CH}_4/\text{H}_2$  as illustrated by Figure 2. This approach is expected to simplify the process flow and increase throughput in industrial PZT patterning by allowing a precise etch

stop while maintaining high etch rates and aspect ratios using only a single process.

### References

- [1] S. Trolier-McKinstry and P. Murali, *Thin Film Piezoelectrics for MEMS*, Journal of Electroceramics **12**, 7 (2004).
- [2] H. Bhurga and G. Piazza, *Piezoelectric MEMS Resonators*, (2017).
- [3] I. Kanno, J. Ouyang, J. Akedo, T. Yoshimura, B. Malič, and P. Murali, *Piezoelectric Thin Films for MEMS*, Appl. Phys. Lett. **122**, 090401 (2023).
- [4] T. Tillocher, *Deep Reactive Ion Etching of Bulk Titanium for Implantable Devices*, (unpublished).
- [5] R. d'Agostino, F. Fracassi, and C. Pacifico, *Dry Etching of Ti in Chlorine Containing Feeds*, Journal of Applied Physics **72**, 4351 (1992).

#### MN-ThP-4 Nanowatt Chemical Sensor for Unattended Sensing, *Mieko Hirabayashi, S. Yen*, Sandia National Laboratories; *O. Faruqe, B. Calhoun*, University of Virginia; *P. Miller, J. Moody*, Sandia National Laboratories

To detect sarin, a potent nerve agent, in unattended applications, we propose a sensor system pairing a sol gel-based transducer with a nanowatt readout circuit. Preliminary measurements demonstrate detection of a sarin surrogate producing a "wake up" signal output while consuming 380 nW of power. This work clears the path to future optimization of the sol gel transducer, use of the multiple channels, and development of the sensor packaging.

Sarin is nerve agent that, when inhaled, induces vomiting and diarrhea, miotic pupils, bradycardia, bronchorrhea, muscle spasms, weakness, flaccid paralysis, seizures, respiratory failure, and tachycardia [1]. For these reasons, sarin gas is notorious as a chemical weapon, and thus its detection at low concentrations is crucial.

Sarin sensors are often carbonnanotube (CNT)-based because this material enables a large surface area and unique electrical properties. These types of sensors are generally sensitive and operate at room temperature [2], but are often fabricated via drop coating, leading to less consistent and less suitable for mass production. By using spray coating of a based catalyzed sol-gel, we are facilitating wafer level sensor fabrication and system integration thereby increasing consistency between fabrication runs and decreasing the overall system size.

With a low power read-out circuit (nano-watt range), we enable unattended, battery-powered detectors for sensing at locations where a wired, full-powered sensor would be difficult to install. Our sensor demonstrates detection of a sarin surrogate using only 380 nW of power. The nW power consumption extends battery life to years for infrequent events [3]. Our results show a single-sensor result (for "waking up" a high-power analysis) with multiple channels for further development for applications and selectivity.

*SNL is managed and operated by NTESS under DOE NNSA contract DE-NA0003525*

- [1]N. M., Nurazzi. M. M. Harussani, ND Siti Zulaikha, A. H. Norhana, M. Imran Syakir, and A. Norli. *Polimery* 66, no. 2 (2021): 85-97.
- [2]J. Li, Y. Lu, Q. Ye, L. Delzeit, and M. Meyyappan. *Electrochemical and Solid-State Letters* 8, no. 11 (2005): H100.
- [3]R.H. Olsson, R.B. Bogoslovov, and C. Gordon. *IEEE Sensors*. 2016.

## Manufacturing Science and Technology Group Room Oregon Ballroom 203-204 - Session MS-ThP

### Manufacturing Science and Technology Poster Session

#### MS-ThP-1 Autonomous Synthesis in the MBE Using Real-Time Artificial Intelligence, *Tiffany Kaspar, L. Wang, J. Christudasjustus, M. Sassi, B. Helfrecht, J. Pope, A. Harilal, S. Akers, S. Spurgeon*, Pacific Northwest National Laboratory

Materials are the key components of nearly all advanced technologies, including quantum information systems, microelectronics, catalysis, and energy conversion and storage. Modern synthesis methods enable the fabrication of an ever-expanding array of novel, non-equilibrium, and/or metastable materials and composites that may possess unique and desirable functionality. Thin film deposition by molecular beam epitaxy (MBE) can produce atomically precise (or nearly so) materials with a wide range of functional electronic, magnetic, ferroelectric/multiferroic, optical, and/or ion-conducting properties. The current state of the art in precision design of functional materials is to manually explore the "growth phase

space” of the deposition technique to optimize the film properties of interest. Limitations of time and resources often result in incomplete exploration of the growth phase space and resulting properties. Faced with this lack of complete information, materials design and synthesis decisions are made based in part on intuition and luck, slowing both materials optimization and materials discovery. This current synthesis paradigm can be disrupted by employing artificial intelligence (AI)-accelerated analysis of *in situ* and *ex situ* data streams that will enable targeted synthesis of novel materials with desired structure, chemical stability, and functional properties. Here we present a preliminary implementation of such an AI-controlled MBE. We are integrating the control of key synthesis parameters (temperatures, gas flow rates, shutters) with AI-guided computer control. Guidance will be based on near-real-time analysis of reflection high energy electron diffraction (RHEED) patterns using sparse data analytics, with low-latency feedback to the control software. As an initial demonstration, we will control the morphology and phase purity of epitaxial anatase TiO<sub>2</sub> thin films.

**MS-ThP-2 Machine Learning Based Virtual Metrology for Effective Process Control in High Product Mix Manufacturing**, *Hyung Joo Lee, S. Choi*, Siemens EDA, Republic of Korea; *N. Greeneltch, S. Jayaram*, Siemens EDA

## 1. Introduction

The semiconductor foundry industry faces challenges with high product mix manufacturing, requiring increased flexibility in managing diverse customer demands. Coordinating multiple chambers and process steps with different designs and technology nodes is complex, resulting in reduced yields and increased costs.

## 2. CVD Process Challenges

The CVD process in semiconductor manufacturing experiences thickness variations due to device layout design and chamber condition drift. Lack of control across layouts affects transistor parameters and yield. Managing chamber-by-chamber variations is crucial for high-volume manufacturing, but current solutions hinder fab line management and throughput.

## 3. VM Approach and Modeling

Virtual metrology (VM) addresses the trade-off between metrology activities and cost by utilizing data from the process chamber (FDC) to predict metrology results. Design features are extracted and used for prediction across layouts and technologies, benefiting new layouts and production stages. Siemens' Calibre® software is employed for feature extraction, and ML methodologies construct the VM model. Results demonstrate the superiority of the VM model with design features and FDC.

## 4. APC System and Results

An APC system using the VM model for R2R control is proposed. It incorporates design features, FDC, and measurements to achieve the desired thickness target. The system triggers updates to the VM model based on prediction errors. The APC system significantly improves process capability and reduces film thickness variations. Control simulation confirms the effectiveness of the APC system in a high-mix product foundry fab setting.

## 5. Summary

The semiconductor foundry industry faces challenges in high product mix manufacturing. The CVD process experiences thickness variations from design features and chamber conditions, impacting yield. A VM approach, incorporating design features and FDC, improves process control. An APC system based on the VM model further enhances thickness control, demonstrating significant improvements in process capability and thickness variation reduction.

**MS-ThP-3 Experimental 3D Maintenance Work Measurement and Analysis for Maintenance Improvement and Enhancement of Productivity of Semiconductor Manufacturing Equipment**, *Takashi Numata, Y. Ogi, K. Mitani, R. Kawamata, N. Ikeda, T. Ege*, Hitachi, Ltd., Japan; *Y. Kadomoto, R. Ishibashi, Y. Shengnan, Y. Sakka, Y. Nakamura, K. Sato*, Hitachi High-Tech Corporation, Japan

Recently, high machine availability of semiconductor manufacturing equipment has become more important, and shortage of field service engineers has become serious. Therefore, maintenance improvement which enable to increase the capacity with inexperienced field engineers and realize productivity improvement of semiconductor manufacturing equipment has been needed.

Based on these circumstances, we have proposed maintenance work measurement and analysis technologies for maintenance improvement of

semiconductor manufacturing equipment. Our targets are to reduce durations of and maintenance work, and a rate of re-clean (failure of maintenance) especially focusing on periodical maintenance. Maintenance work measurement and analysis have a potential to enable us to extract work differences between skilled and unskilled maintenance workers, extract complex and difficult characteristics of maintenance work, and support and/or reduce such complex and difficult maintenance work.

In this study, we developed a measurement system with 3D sensors and motion sensors, experimentally measured maintenance work of semiconductor manufacturing equipment such as parts assembly and wiping by using the developed system, and extracted indicators of personal differences among workers. We extracted various indicators including task time, working posture, amount of head motion, change of eyesight, amount of hand motion. As a result, we demonstrated representative differences of extracted indicators between an experienced maintenance worker and an inexperienced maintenance worker.

From the result, it was suggested that application of maintenance work measurement and analysis system with results of maintenance enable us to extract important factors to cause re-clean, and standardize maintenance work based on skilled workers' movements and/or successful works. Then effective countermeasures for support and/or reduction of difficult task will be applied based on the results of maintenance work analysis.

## Surface Science Division

### Room Oregon Ballroom 203-204 - Session SS-ThP

#### Surface Science Poster Session

**SS-ThP-1 ESI Investigations of Melamine and Cyanuric Acid Clusters and Their Relationship to STM Experiments**, *Alex Walter, K. Handy, J. Soucek, S. Kandel*, University of Notre Dame

Pulse deposition, a novel sample deposition technique for scanning tunneling microscopy (STM), sprays molecules onto a surface through a process that forces non-equilibrium, high-energy structures. Electrospray ionization mass spectrometry (ESI-MS) is a “soft” ionization method; molecules of interest do not fully fragment, but instead can be observed whole, as can dimers, trimers, and other supramolecular structures, which is often seen as a limitation. However, this clustering of molecules allows for a “screening” of sorts for pulse-deposited STM experiments, which are significantly more time-intensive. ESI-MS and pulse deposition have similar sample delivery methods, and thus can be compared to each other and used to study molecules in tandem. For example, melamine and cyanuric acid together form highly toxic complexes in the body, but the precise crystallization and intermolecular forces that drive the creation of the toxic clusters is unknown. Using the ESI-MS as a precursor to investigation with pulse deposited STM imaging, we observed several stable noncovalent clusters of melamine and cyanuric acid, ranging from mixed dimers to mixed nonamers (four melamines and five cyanuric acids). In this presentation, I will discuss the results of our ESI-MS experiments on melamine and cyanuric acid as well as comment on STM experiments of different solution ratios and how ESI-MS and STM results can be jointly interpreted.

**SS-ThP-2 Scanning Tunneling Microscopy Study of the H<sub>2</sub>O-CO Co-Adsorbed Fe<sub>3</sub>O<sub>4</sub>(111) Surface for Understanding the Water-Gas Shift Reaction Mechanism**, *Asa Kiuchi, Y. Eda, T. Hirai, T. Shimizu*, Keio University, Japan

Magnetite (Fe<sub>3</sub>O<sub>4</sub>) is an attractive catalyst for the water-gas shift reaction (WGS), owing to its low cost and minimal environmental impact. However, the reaction path remains unclear despite extensive experimental and theoretical studies. This is partly due to the difficulty in conducting experiments and the complexity of analyzing data on co-adsorbed systems, which has resulted in a lack of clarity in the overall picture.

To clarify the mechanism of the WGS on magnetite, we performed scanning tunneling microscopy (STM) to observe CO exposed, H<sub>2</sub>O adsorbed, and H<sub>2</sub>O-CO co-adsorbed Fe<sub>3</sub>O<sub>4</sub>(111) surfaces. Our results confirmed that CO molecules do not adsorb on the bare surface at room temperature, agreeing with the previous study based on temperature programmed desorption[1]. Two types of adsorbate species appeared on the surface after the exposure to H<sub>2</sub>O, which we attribute to dissociated species, OH, and molecular water. We also found a larger adsorbate on the H<sub>2</sub>O-CO co-adsorbed surface, although it is unclear if this species is an intermediate of the WGS due to the complexity of the STM image. We are currently developing image analysis methods to identify and classify the

adsorbed species. Our study provides a new insight into the atomistic mechanism of the WGSR on Fe<sub>3</sub>O<sub>4</sub>(111).

[1]C. Lemire *et al.*, *Surf. Sci.* **572**, 103(2004).

## SS-ThP-3 Growth of Metal Nanoclusters on Thin Layer Moiré Pattern of Graphene and Feo on Single Crystal, *Shilpa Choyal, D. Liu, N. Jiang*, UIC

Graphene, a two-dimensional (2D) carbon crystal with sp<sup>2</sup> hybridization, has attracted much attention in recent years due to its novel chemical, electrical, and mechanical properties. Even materials that do not form cluster superlattices upon room temperature deposition may be grown into such by low-temperature deposition. A graphene monolayer was prepared on an Ir (111) single crystal, ethylene (C<sub>2</sub>H<sub>4</sub>) is pyrolytically cleaved on the surface. The resulting superstructure is examined using scanning tunneling microscopy (STM) and was identified as a well-aligned, incommensurate pattern known as moiré. This moiré pattern arises from overlapping the graphene lattice and the Ir (111) lattice, resulting in alternating bright and dark regions.

The moiré patterns in graphene act as nucleation sites for the growth of plasmonic metal nanoclusters. When Ag/Au metal is deposited on graphene, it nucleates at these sites to form nanoclusters on the surface. Through STM, we have examined the nucleation and growth of these nanoclusters, studying their shape, organization, and structural evolution. Additionally, we have also investigated the stability of these nanoclusters at different temperatures.

Moiré patterns are also found at iron oxide (FeO) thin layers on Au (111) surfaces. The FeO nanoislands are mostly truncated triangular and exhibit clear moiré superlattices. These superlattices result from the lattice mismatch between FeO and Au (111). In contrast to graphene, FeO demonstrates a preference for wetting by different metals, which imparts unique surface properties. FeO islands have two different growth sites one from Fe-edges and the other from O-edges. In addition to being located on top of FeO islands, different metal prefers to nucleate on the edge of FeO islands, where they selectively grow on the Fe-edges and O-edges.

## SS-ThP-4 Post-Synthesis Isotopic Purification of Oxygen in TiO<sub>2</sub> via Controllable Surface Injection of Interstitial Atoms, *H. Jeong, Nabil Hilmy Abuyazid, E. Seebauer*, University of Illinois at Urbana Champaign

Isotopically pure semiconductors have important applications for cooling electronic devices and for quantum computing and sensing. Raw materials of sufficiently high isotopic purity are rare and expensive, thereby creating special opportunities for post-synthesis methods that remove isotopic impurities. Through isotopic self-diffusion measurements of oxygen in rutile TiO<sub>2</sub> single crystals immersed in water, we demonstrate fractionation of <sup>18</sup>O by a factor of three below natural abundance in a near-surface region of 10 nm or more. The specially prepared and submerged surface injects large fluxes of O interstitials, which displace lattice <sup>18</sup>O deeper into the solid due to the statistics of interstitial-mediated diffusion combined with steep interstitial gradients. Multiscale modeling offers quantitative insights into how these physical effects work together and how they might be optimized. Both ultraviolet illumination and solution pH affect the experimental injection rate, and demonstrate that adjustments to the chemistry between the surface and fluid can be used to control chemistry between the surface and defects in the bulk. The benefits of such control extend beyond isotopic fractionation to defect engineering, as the injected O interstitials also remove O vacancies and compensate donor H impurities. Importantly, all these effects occur near room temperature. This accesses a regime wherein equilibrium concentrations of native defects become vanishingly small, and where kinetic effects dominate defect behavior. It thereby becomes possible to create materials whose properties circumvent thermodynamic constraints.

## SS-ThP-5 Analyses of Surface Structure and Chemical States of Carbon Black Nano Particles, *Mari Isagoda*<sup>1</sup>, Keio University, Japan; *T. Aoki*, Asahi Carbon Co., Ltd., Japan; *T. Shimizu*, Keio University, Japan

Carbon black (CB) is widely used as pigment and reinforcement material in tire production and is also expected to work as conductive auxiliaries of Lithium-ion batteries. To improve properties for these applications, precise control of the surface structure and chemical states of CB particles is critical. The crystallite model — particles made of small flakes of layered graphene — has been proposed based on transmission electron microscopy (TEM), and the edges of these graphene flakes are expected to be terminated with several types of functional groups [1]. However, the validity of the model and the exact types and locations of functional groups

are still in debate. In this study, we employed atomic force microscopy (AFM), scanning tunneling microscopy (STM), Raman spectroscopy, and x-ray photoelectron spectroscopy (XPS) to provide a comprehensive characterization of the surface structure and chemical states of CB particles.

In AFM and STM measurements of samples prepared by the drop-drying method, we observed that carbon black exists as aggregates of particles with a variety of sizes, ranging from approximately 10 nm to 300 nm. Our STM images of small-size particles less than 10 nm in diameter cannot be adequately explained by the crystallite model. Raman spectra of powdered samples showed two peaks centered at 1340 cm<sup>-1</sup> and 1590 cm<sup>-1</sup>, which correspond to D-band and G-band[2], respectively. By comparing the spectra with those of other carbon-based materials, we concluded that the carbon black consists of graphene sheets, as in the crystallite model, but it is rather close to amorphous. XPS suggests the existence of oxygen-containing species.

[1] S. Khodabakhshi, P. F. Fulvio, and E. Andreoli, *Carbon* **162**, 604-649 (2020).

[2] M. A. Pimenta, *et al.*, *Phys. Chem. Chem. Phys.* **9**, 1276-1291 (2007)."

## SS-ThP-6 Surface Chemistry of Zirconium Borohydride on Zirconium Diboride (0001), *Aoyele Ologun, M. Trenary*, University of Illinois - Chicago

Zirconium diboride ZrB<sub>2</sub> is an extremely hard material with a high melting point of 3246 °C; given these properties, ZrB<sub>2</sub> can be used for various applications, such as high-resistant coatings for body armors and tanks. In addition, it has also been explored as a diffusion barrier in microelectronics. Industrially, highly conformal thin films of ZrB<sub>2</sub> are grown via chemical vapor deposition (CVD), using zirconium borohydride Zr(BH<sub>4</sub>)<sub>4</sub> as a precursor. While surface chemistry plays a central role in the CVD of ZrB<sub>2</sub> from the Zr(BH<sub>4</sub>)<sub>4</sub> precursor, the surface mechanism is yet to be explored. In this study, we investigated the surface mechanism of Zr(BH<sub>4</sub>)<sub>4</sub> decomposition on a ZrB<sub>2</sub>(0001) surface with reflection absorption infrared spectroscopy (RAIRS), temperature-programmed desorption (TPD), and X-ray photoelectron spectroscopy (XPS). The RAIRS spectra obtained on exposing the ZrB<sub>2</sub>(0001) surface at 90K to Zr(BH<sub>4</sub>)<sub>4</sub> closely matched that of the pure compound, indicating adsorption of Zr(BH<sub>4</sub>)<sub>4</sub> without decomposition. However, new surface intermediates were formed upon heating to 280 K, as shown by the retention of the νB-Ht stretch (2569 cm<sup>-1</sup>) and δH-B-H bend (1228 & 1057 cm<sup>-1</sup>) in the RAIRS spectra. These surface intermediates were tentatively identified as either BH<sub>4</sub> or BH<sub>3</sub> and were found stable up to 330 K. Temperature-programmed desorption studies revealed the desorption of B<sub>2</sub>H<sub>6</sub> and H<sub>2</sub> at around 470 K.

## SS-ThP-7 An Annotated Compendium of X-Ray Photoelectron Spectroscopy (XPS) Spectra, *Samira Jafari, M. Linford, A. Dean, B. Kulbacki, S. Ko*, Brigham Young University

X-Ray photoelectron spectroscopy (XPS) is a powerful tool for studying surfaces, where, in its conventional embodiment, it is sensitive to the upper 5 – 10 nm of materials. XPS is widely used throughout science and technology. In XPS, photoemission of core electrons is a result of X-rays striking a surface. Two types of XPS spectra are collected: survey spectra and narrow scans. Survey spectra reveal the elements at surfaces. Narrow scans provide chemical/oxidation state information about those elements. XPS spectra are sometimes inappropriately acquired because of (a) contamination on the surface, (b) contamination in the instrument, e.g., due to a previously-analyzed fluorine-containing sample, and (c) poor method development, e.g., a failure to take a sufficient number of scans. For these reasons, it is important for analysts to have comparison spectra in their work. We intend to collect a number of XPS spectra of different materials and compile them into an annotated compendium that can help other XPS users. Spectral processing will largely be with CasaXPS. Data acquisition of narrow scans will be undertaken at low pass energies that will minimize peak FWHM values, while still providing good

statistics for the spectra. We hope this compendium will be a good resource for other researchers and scientists in their interpretation of their XPS spectra.

<sup>1</sup> SSD Morton S. Traum Award Finalist

**SS-ThP-8 Determination of Band Alignment in Semiconductor Heterojunctions by X-Ray Photoelectron Spectroscopy (XPS), Mohamed Nejib Hedhili, T. Ng, K. Lee, B. Ooi, KAUST, Saudi Arabia; O. Bakr, Kaust, Saudi Arabia**

Heterojunctions are widely used as an essential building block in advanced semiconductor devices because of their multiple functionalities. The electrical and optical properties of heterojunctions are strongly governed by their electronic band alignment.

High-resolution X-ray photoemission spectroscopy (HR-XPS) is proven to be a powerful way of measuring the valence band offsets in semiconductor heterojunctions. This study aims to determine the band alignment to different semiconductor heterojunctions by direct X-ray photoelectron spectroscopy (XPS) measurements. Type-I and Type-II band alignment were obtained.

Design of heterojunction based electronic/photonic devices requires an accurate determination of the band offset. This parameter is crucial to tailor heterojunction based devices as per the operating requirement.

**SS-ThP-9 Localized Plasmon-Controlled Chemistry at and Beyond the Nanoscale, Chamath Siribaddana, S. Rajak, S. Choyal, D. Liu, S. Mahapatra, L. Li, N. Jiang, University of Illinois Chicago**

Probing the effect of the local chemical environment of surface nanostructures is a challenge because the spatial resolution of conventional spectroscopic techniques is limited by the diffraction limit of light. Coupling light with plasmonic nano-objects creates highly localized surface plasmons (LSPs), which allows us to break this limit. Tip-enhanced Raman spectroscopy (TERS) is one such surface spectroscopic technique that uses the apex of the tip of a scanning tunneling microscope made from a plasmonic metal as a nano object to couple light to the near field. The Raman modes of the nanostructure underneath this tip are greatly enhanced which allows us to obtain chemical information with Angstrom scale spatial resolution. Thus, TERS can probe intermolecular interactions, molecule-substrate interactions, organic-2D material heterostructures, and the reactivity of 2-D materials to reveal how the local chemical environment affects the chemical and physical interactions of a molecule or a nanostructure on a surface. Apart from probing the local environment, the highly localized nature of LSPs can be used to drive energy-intensive and unselective thermally activated chemical reactions using light with a lower energy input and a site-selective manner. The controllability of LSPRs was demonstrated by dissociating a single bond inside a molecule in the presence of multiple equivalent bonds. The insights obtained into the local environment enable precise control of self-assemblies, on-surface reactions, and LSPRs and expand the ability to synthesize nanostructures with tailored electronic, optical, and magnetic properties required for next-generation nanodevices.

**SS-ThP-10 Heterostructured Nanomaterials Fabrication Using a Modular MBE Research Platform, Lukasz Walczak, Research and Development Division, PREVAC sp. z o.o., Raciborska 61, 44-362 Rogow, Poland; M. Florek, Research and Development Division, PREVAC sp. z o.o., Poland; M. Kwoka, Department of Microelectronics, Silesian University of Technology, Poland**

Many important processes such as energy conversion, electrochemical, corrosion, and biological processes take place at solid-gas and solid-liquid interfaces [1-3]. The molecular beam epitaxy (MBE) method is the one of powerful techniques for creating new nanomaterials and it is the key to improving the performance of novel battery generation or renewable energy sources such as solar, wind, or hydropower energy conversion devices. We would like to promote an original, modular ultra-high vacuum system for the fabrication of heterostructured nanomaterials by the molecular beam epitaxy (MBE) method. Its basic element is a vacuum installation, which consists of a sample loading chamber, a substrate preparation (cleaning) chamber, and a proper MBE chamber for the deposition of selected nanomaterials. All vacuum chambers are connected by appropriate vacuum locks and magnetic sample transfers between the above-mentioned chambers, which enables the implementation of all technological and research works without contact of deposited nanomaterials with the atmospheric environment. Vacuum conditions in all of the above-mentioned vacuum chambers are created using independent systems of various types of vacuum pumps. For the control of the substrate cleaning process, the deposition of nano-layers of selected electronic materials, and their initial characterization, the above-mentioned vacuum installation is equipped with electronic control systems and measurement data acquisition systems. Correct operation of the designed and the completed installation has been verified on the example of the deposition

of Mg nano-layers on the Si substrate. The conducted technological works and preliminary research works as well as the obtained results confirmed that the designed and assembled modular vacuum system can be very useful for the deposition of nanolayers of selected electronic materials using the MBE method, on the one hand on terms of their potential research applications, and on the other - in terms of their potential industrial applications, incl. for the production of photovoltaic renewable energy sources.

#### References:

- [1] S. Choudhury et al. C 2021, 7, 28.
- [2] A. Asyuda et al. Phys. Chem. Chem. Phys., 2020, 22, 10957-10967.
- [3] H. Aldahhak et al. J. Phys. Chem. C 2020, 124, 11, 6090-6102.

**SS-ThP-12 Angular and Velocity Distributions of NO<sub>2</sub> and O<sub>2</sub> Desorption from an Oxidized Ag(111) Surface, Arved Cedric Dorst, Georg-August Universität, Göttingen, Germany; R. Dissanayake, Max Planck Institute for Multidisciplinary Sciences, Germany; D. Schauer mann, Georg-August Universität, Göttingen, Germany; D. Killelea, Loyola University Chicago; T. Schäfer, Georg-August Universität, Göttingen, Germany**

Transition group metals are used as catalysts in various oxidation reactions. A common example is silver which found industrial usage in the epoxidation of ethylene to the ethylene oxide. To optimize such processes it is required to understand the dynamics and microscopic details.

In this talk, the velocity and angular distribution of NO<sub>2</sub> and recombinatively-desorbing oxygen from Ag(111) will be presented. Experimentally, we combined velocity-map imaging (VMI) and temperature-programmed desorption (TPD). NO<sub>2</sub> decomposes into NO and O after adsorption on silver. At 510 K, a clean  $p(4 \times 4)$ -O reconstruction with a maximum oxygen coverage of  $\vartheta_0 = 0.375$  ML forms on Ag(111).<sup>1</sup> The reaction probability  $S$  of NO<sub>2</sub> decomposition was studied at this temperature as a function oxygen coverage  $\vartheta_0$ .  $S$  is coverage-independent up to  $\vartheta_0 = 0.3$  ML which is a clear indication for a precursor-mediated mechanism.

In TPD spectra, the recombinative desorption of O atoms occurs as a defined O<sub>2</sub> desorption feature around 600 K. In contrast to NO<sub>2</sub> whose desorption appears thermal, these oxygen molecules exhibit a clearly hyper-thermal velocity distribution;  $\langle v \rangle$  is  $>200 \text{ m} \cdot \text{s}^{-1}$  above a flux-weighted, thermal velocity distribution. Compared to Rh(111),<sup>2</sup> we observe a significantly narrower  $\cos^2(\vartheta)$  angular distribution for the flux density of O<sub>2</sub> and the velocity distribution differs stronger from a thermal one. Finally, first results for the epoxidation of styrene to styrene oxide will be shown. We observe that the epoxide forms only at high oxygen coverage.

- [1] A. Michaelides, K. Reuter, and M. Scheffler, J. Vac. Sci. Technol. **A23**, 1487 (2005).
- [2] A.C. Dorst, F. Güthoff, D. Schauer mann, A.M. Wodtke, D.R. Killelea, and T. Schäfer, Phys. Chem. Chem. Phys. **24**, 26421 (2022).

**SS-ThP-14 Growth and Characterization of Bimetallic NiCo Particles on CeO<sub>2</sub>(111) Thin Film Surfaces, T. Ara, Nishan Paudyal, J. Zhou, University of Wyoming**

Ceria-supported Ni and Co have been of great interest as economical and promising catalysts for chemical reactions including CO oxidation, CO<sub>2</sub> hydrogenation, ethanol reforming, and dry reforming of methane. They can exhibit promising reactivity owing to the strong metal-support interaction. Bimetallic NiCo could provide interesting properties compared to individual metal counterparts due to the synergistic effects between two metals as well as the interaction between the metal and ceria. To elucidate the nature of the activity, we investigated the nucleation, growth, and sintering of metal particles of Ni, Co, and NiCo over well-ordered CeO<sub>2</sub>(111) thin films using scanning tunneling microscopy and x-ray photoelectron spectroscopy under ultrahigh vacuum conditions. Our results indicate that oxidation of the metal (Co, Ni) occurs at the cost of Ce<sup>4+</sup> reduction to Ce<sup>3+</sup> upon deposition of low coverages ( $< 0.2$  ML) of Co or Ni over CeO<sub>2</sub>(111) at room temperature. Both Ni and Co form small particles that are less than two-atomic layer high with no clear preferential nucleation at step edges, suggesting a strong metal-support interaction. Compared to Ni, Co forms relatively smaller particles with a higher particle density on CeO<sub>2</sub>(111) at 300 K that experiences less sintering with heating up to 800 K. Our studies show that bimetallic NiCo particles can be prepared by deposition of Ni followed by Co on CeO<sub>2</sub>. As demonstrated by scanning tunneling microscopy data, Co primarily deposits onto the pre-dosed Ni particles on CeO<sub>2</sub> at 300 K to produce NiCo bimetallic particles and addition of Co can

inhibit the sintering of Ni and enhance its thermal stability on ceria with heating.

**SS-ThP-15 DFT Calculations of Cyanuric Acid and Melamine from ESI-MS, Kaitlyn Handy, A. Walter, J. Soucek, S. Kandel, S. Corcelli,** University of Notre Dame

With the use of electrospray ionization mass spectroscopy (ESI-MS) we are able to observe clusters of cyanuric acid and melamine in solution. The clusters consist of homogenous and heterogenous mixtures with varying ratios of molecules. Several of these clusters are observed forming in high concentrations. Using density functional theory (DFT), calculations are run to model possible cluster structures. Both homogenous and heterogenous clusters arrange in a lattice structure. When there are clusters with disproportionality more cyanuric acid or melamine the molecular structure has variations leading to the molecule not lying flat. Larger clusters show increased stability when compared to smaller clusters.

**SS-ThP-17 Scanning Tunneling Microscopy Studies of Diarylethene Monolayer and Cluster Formation on Noble Metal Surfaces, Tomoko K. Shimizu, T. Kaneko,** Keio University, Japan; **K. Sagisaka,** National Institute for Materials Science, Japan

The supramolecular assembly on metal surfaces is governed by a subtle balance between intermolecular interaction and molecule-substrate interaction. Even on chemically similar metals, such as Cu, Ag, and Au, the deposition of the same molecule under the same condition may result in different types of assembled structures. We have observed such a case with a molecule called diarylethene, famous for its photochromism and expected to work as single molecule switching device.

After depositing molecular powder of the open-form isomer on metal surfaces at room temperature, scanning tunneling microscopy (STM) was performed in ultra-high vacuum at liquid helium temperature. Our STM images revealed the presence of both the open-form and closed-form isomers on all three metals. This is due to a stability reversal on metals compared to the gas phase, arising from charge transfer between molecules and metallic substrates[1]. Isolated adsorption was predominant on Cu(111) even after annealing. Co-deposition of NaCl was necessary to form a homogeneous monolayer, which was achieved via ion-dipole interaction[2]. On Au(111), closed-form isomers formed small clusters, such as trimers and tetramers, while the open-form remained isolated. In contrast, larger clusters made of both the open- and closed-form isomers were found on Ag(111), including chain-type clusters and three-fold symmetric chiral clusters. Mild annealing transformed all the open-form isomers to the closed-form isomers, and only three-fold symmetric clusters made of nine or more closed-form isomers were observed. The clusters found on Ag(111) have three-dimensional structures, suggesting local and weak intermolecular interaction. Theoretical analysis is underway to clarify the exact structures and interactions involved.

References

[1] T. K. Shimizu, et al., Chem. Commun. 49, 8710-8712 (2013).

[2] T. K. Shimizu, et al., Angew. Chem. Int. Ed. 53, 13729-13733 (2014).

**SS-ThP-18 Distinguishing Elements at the sub-Nanometer Scale on the Surface of a High Entropy Alloy, Lauren Kim, W. Scougale,** University of Wyoming; **P. Sharma,** Lehigh University; **N. Shirato, S. Wiegold,** Argonne National Laboratory; **W. Chen,** Northwestern University; **V. Rose,** Argonne National Laboratory; **G. Balasubramanian,** Lehigh University; **T. Chien,** University of Wyoming

High entropy materials, including high entropy alloys (HEAs), high entropy Van der Waals materials (HEX), and high entropy oxides (HEOs), have drawn the attention of scientists and engineers for their various functionalities and properties. While a wide variety of properties are being studied in these materials, a microscopic understanding is still missing. In this work, the spatial resolving power of scanning tunneling microscopy (STM) is combined with the elemental resolving X-ray absorption spectroscopy (XAS) to achieve this goal. With the unique X-ray assisted tunneling effect, the elemental distributions on the surface of a HEA at the sub-nm scale were revealed by a synchrotron X-ray scanning tunneling microscope (SX-STM). The elemental distribution at sub-nm scale was revealed by maximizing the correlation coefficient between the collected XAS mappings and the atomic scale elemental modeling. The results shown here demonstrate that SX-STM is a promising tool to reveal elements at the sub-nm scale, even for high entropy materials.

**SS-ThP-19 Soft X-Ray Spectro-Microscopy for Electrochemical Interfaces, Xiao Zhao, E. Carlson, T. Mefford, W. Chueh,** Stanford University

Most electrochemical reactions occur at interfaces. In response to applied voltage, electron and energy transfer between the first few atomic layers of electrochemical active materials and absorbates. Electrochemical reactions are also highly heterogeneous, as most electrochemical processes preferentially take place around active sites with certain facets, coordination structure and chemical environment. Characterizing these reactions requires a spectroscopic imaging platform with interfacial sensitivity and chemical sensitivity. **Direct characterization of electrochemical interfaces** is further complicated by the presence of liquid electrolyte, which requires the measurement performed *in-situ/operando*.

Here we are presenting the recent development of Scanning Total Electron Yield X-ray Microscopy (STEYXM) based on the Scanning Transmission X-ray Microscopy (STXM), which enables *in-situ* X-ray spectroscopic imaging of various electrochemical interfaces with **25nm spatial resolution and ~5nm surface sensitivity**. A custom electrochemical flow cell is used with three electrodes setup. The traditional transmission mode could provide complimentary bulk information of electrodes, while the electron yield mode maps the surface structure and oxidation state of electrodes, as well as the local electrochemical double layer structure. We anticipate that the development of STEYXM will enable the investigation of surface electrochemistry and advance our fundamental understanding of electrochemical reactions.

**SS-ThP-20 Effect of Heat Treatment on Silicon Carbide Reinforced Aluminum Matrix Composite Fabricated Through an Optimized Stir Casting Process, Conner Neely, D. Madiraju, M. Rabea,** California State Polytechnic University, Pomona

The purpose of this study is to determine the additional effect of heat treating on the hardness, corrosion resistance, and mechanical strength of cast aluminum matrix composites reinforced with SiC. The effects of heat treatment will be compared to an identical but untreated cast aluminum matrix composite reinforced by SiC, and additionally to pure aluminum. Accordingly, both composite samples were created from the same batch of matrix alloy in combination with SiC, melted and homogenized in an induction furnace to ensure stability and consistency of crystal structure. Microstructure and morphology analyses were conducted, the hardness was measured by the Micro Vickers hardness Tester (HM-200), corrosion of the samples was tested using salt spray chamber, and the tensile strength by a universal test machine. It was found that the heat treatment increased the hardness in the way of wear resistance of the Al-SiC composite, improved the corrosion resistance, the tensile strength, and showed more favorable material properties than the unaltered test sample of the Al-SiC composite.

**SS-ThP-22 Atomic-Scale Hydration Structures Visualized by Three-Dimensional Atomic Force Microscopy (3D-AFM), Keisuke Miyazawa,** Kanazawa University, Japan

Water molecules on a surface influence the chemical reactivity and molecular adsorption behavior of a surface. Given that these interfacial properties are influenced by local interactions between the material surface and water molecules, a deep understanding of the atomic-scale surface structures and their hydration structures is crucial for the design of surface functions. Recently, three-dimensional atomic force microscopy (3D-AFM) was developed as a method for investigating Subnanometer-scale hydration and flexible molecular structures on various surfaces. In 3D-AFM, an interaction force applied to an AFM tip is measured during the AFM tip 3D scanning at a solid-liquid interface to generate a 3D force image with atomic-scale local contrasts reflecting the local density distributions of molecules on a surface. Recent studies revealed the hydration structures of calcite (Fukuma et al., PRB 92 (2015) 155412), fluorite (Miyazawa et al., Nanoscale 8 (2016) 7334), sapphire and quartz (Nagai et al., Nanoscale 15 (2023) 13262). In this presentation, we present the recent studies of atomic-scale hydration structures investigations, and future prospects of 3D visualization of various solid-liquid interfacial phenomena using 3D-AFM.

## Thin Film Division

### Room Oregon Ballroom 203-204 - Session TF-ThP

#### Thin Film Poster Session

**TF-ThP-2 High Heat Resistant Y<sub>2</sub>O<sub>3</sub> Film on Quartz Prepared by Ion-Assisted Deposition, Naoto Kihara, S. Ogawa, K. Kawahara, R. Hayashi, T. Ogawa, AGC Inc., Japan; M. Tanimura, H. Okada, M. Ishikawa, Tsubasa Science Corporation, Japan**

#### Background

Along with the miniaturization of semiconductor devices, equipment using plasma processes such as dry etcher is required to have high plasma durability and low particle generation. Yttrium oxide (Y<sub>2</sub>O<sub>3</sub>) is used as a passivation film on the surface of the parts which are equipped in the chamber. In recent years, Y<sub>2</sub>O<sub>3</sub> films with high heat resistance are required to etch low-volatility or difficult-to-etch materials and developed for new plasma processes. In this study, we focused on the difference of thermal expansion between quartz substrate and Y<sub>2</sub>O<sub>3</sub> film, then report that Y<sub>2</sub>O<sub>3</sub> film with high heat resistance of 500°C was obtained introducing intermediate layer Y<sub>2</sub>O<sub>3</sub>-SiO<sub>2</sub>

#### Experiment

In this study, Y<sub>2</sub>O<sub>3</sub> and Y<sub>2</sub>O<sub>3</sub>-SiO<sub>2</sub> films were deposited on quartz substrate using the ion-assisted deposition method (IAD). The Y<sub>2</sub>O<sub>3</sub>-SiO<sub>2</sub> film which is the intermediate layer was formed by two-source co-evaporation of Y<sub>2</sub>O<sub>3</sub> and SiO<sub>2</sub>. Plasma resistance was evaluated by measuring the etched depth of the film using a profilometer after etching with CF<sub>4</sub> plasma. For heat resistance, the presence or absence of cracks was evaluated using an optical microscope after annealing in atmospheric environment. In addition, crystallinity and morphology were confirmed by X-ray diffraction measurement (XRD) and scanning electron microscopy (SEM), respectively.

#### Results and Discussion

On the basis of the XRD analysis results, the obtained Y<sub>2</sub>O<sub>3</sub> film crystal structure was a cubic crystal with the (222) orientation as the main peak. In addition, a uniform surface morphology without voids and pores was obtained from surface and cross-sectional SEM observation. The etching rate was 0.009 μm/hr, which was 1/100 of quartz. Moreover, in the heat resistance test results, there were no cracks at 400 °C, and cracks occurred at 500 °C. In the quartz/Y<sub>2</sub>O<sub>3</sub>-SiO<sub>2</sub>/Y<sub>2</sub>O<sub>3</sub> stacked film intended to improve heat resistance, there were no cracks at 500 °C, but cracks occurred at 600 °C. Thus, by introducing the intermediate layer, Y<sub>2</sub>O<sub>3</sub> stacked film having heat resistance at 500 °C was obtained. The reason for the improvement on heat resistance is presumed that the thermal expansion coefficient of Y<sub>2</sub>O<sub>3</sub>-SiO<sub>2</sub> has an intermediate value between quartz (0.5 ppm/°C) and Y<sub>2</sub>O<sub>3</sub> (7 ppm/°C), which reduces thermal strain and stress. The detailed mechanism is under analysis.

**TF-ThP-3 Improvement of Transparency and Electrical Conductivity of Ti-Doped ZnO Thin Films, Naoya Utsu, I. Takano, Kogakuin University, Japan**

In recent years, transparent conductive films have been used for touch panels, liquid crystal displays, solar cell electrodes, and other applications. Currently, indium tin oxide (ITO) or other oxide semiconductors are the mainstream materials that combine transparency and electrical conductivity. On the other hand, indium (In) is a rare metal with limited the production area, which limits its stable supply and causes significant price fluctuations. In this study, we focused on zinc oxide (ZnO) with sufficient resources and improved the transparency and electrical conductivity of ZnO by doping titanium (Ti).

The sample substrate was a slid glass with 15 x 10 mm in a size that ultrasonically cleaned with ethanol for 10 minutes. The oxide thin films were deposited by reactive sputtering using the multi-process coating system (BC5146, ULVAC Corp.). The deposition conditions were Zn sputtering input power of 20 W with an Ar gas flow rate of 20 sccm and an O<sub>2</sub> gas flow rate of 5 sccm to obtain a film thickness of 50 nm. At the same time, Ti was doped from 0 to 40 % with calculating from the Ti sputtering rate. For example, in the case of 10 % in the Ti doping, the sputtering rate of Zn is 0.085 nm/s (RF input power 20 W) and that of Ti is 0.0094 nm/s (DC input power 53 W).

For optical properties, transmittance was measured using a UV-visible spectrophotometer (UV-2550, Shimadzu Corp.). For electrical characteristics, the electrical conductivity was calculated from the resistance value of the deposited sample using a four-point probe (RG-5, NPS Corp.) with a pin spacing of 1.0 mm. Crystal structure analysis was performed by X-ray diffraction (SmartLab, Rigaku Co., Ltd.) at an X-ray incidence angle of 0.4 degrees.

Thursday Evening, November 9, 2023

The optimum condition for the transmittance and electrical conductivity was obtained at ZnO doped with Ti of 30 %. The transmittance and electrical conductivity of the film were 95.2 % and 739 S/m, respectively.

**TF-ThP-4 Improving Compositional Analysis of Copolymer Thin Films Using a Simple Density Correction, Simon Shindler, R. Yang, Cornell University**

When synthesizing copolymer thin films, accurate measurements of the polymer composition are essential to understanding and optimizing material properties. Determining the composition of thin films synthesized from the solution phase (e.g. spin coating, or spin casting) is straight forward, since researchers generally know the composition of the polymer before fabricating the film. In polymer vapor deposition of copolymers, the characterization of composition relies instead on techniques like Fourier transform infrared spectroscopy (FTIR) and x-ray photoelectron spectroscopy (XPS). While helpful in some applications, chain re-orientation at the polymer-air interface and adventitious carbon often bias XPS data – making it an unreliable tool for standalone film compositional measurement. FTIR transmission spectra are more commonly used to determine composition by comparing peak areas associated with known chemical functionality. This technique uses the Beer-Lambert law to relate composition to absorption and pathlength (film thickness). To obtain composition from this method, it is necessary to measure film thickness (generally using ellipsometry) and assume that all films being analyzed have equal density. For certain chemistries, copolymerization changes the polymer packing, causing density to vary significantly with composition. When uncorrected, the assumption of constant density leads to large errors and non-physical compositions. In the process of collecting film thickness from spectroscopic ellipsometry, the refractive index of the film is also measured. Because the density and refractive index are related through the Lorentz-Lorenz equation, film density is easily estimated. By applying a density correction, we demonstrate significant improvements to the measurement of composition from FTIR at essentially zero cost. Density correction improves the accuracy of compositional analysis using data that is already collected in many labs, making it a simple and cost effective improvement to existing methods.

**TF-ThP-5 Theoretical Prediction of Trisilylamine (TSA) Adsorption and Decomposition on Hydrogen-rich Silicon Nitride, Tsung-Hsuan Yang, T. Wang, G. Hwang, University of Texas at Austin; P. Ventzek, J. Zhao, Tokyo Electron America, Inc.**

The reactions of trisilylamine (TSA) precursor on silicon nitride (SiN) thin film in atomic layer deposition (ALD) process was investigated by density functional theory (DFT). A N-rich, H-terminated surface model was used to simulate the surface after NH<sub>3</sub> plasma treatment. Two reaction mechanisms were proposed depending on the abundance of excess hydrogens on the surface: (1) TSA reactions with primary amine (-NH<sub>2</sub>) and (2) TSA reactions with hydrogenated primary amine (-NH<sub>3</sub>). The source of excess hydrogen originates from the H radical from the NH<sub>3</sub> plasma which can survive on the SiN surface by being captured by the surface amine groups. Results show that in the first mechanism, the rate-determining step for TSA chemisorption is the TSA-adduct formation step which requires overcoming an energy barrier of 0.67eV predicted by climbing-image nudged elastic band (CI-NEB) method (*i.e.*, TSA(g) + -NH<sub>2</sub> → -NH-SiH<sub>3</sub> + (SiH<sub>3</sub>)<sub>2</sub>NH(g)). In the second mechanism, the rate-determining step is the hydrogen transfer step with a much lower energy barrier of 0.34eV (*i.e.*, TSA(g) + -NH<sub>3</sub> → •SiH<sub>3</sub>(g) + (SiH<sub>3</sub>)<sub>2</sub>NH(g) + -NH<sub>2</sub>).

**TF-ThP-6 Effects of Surface Morphology on the Phase Coexistence and Evolution in Li<sub>x</sub>CoO<sub>2</sub> Films Studied by PEEM, Elena Salagre, Dpto Física Materia Condensada, Universidad Autónoma de Madrid, Spain; E. Fuller, Sandia National Laboratories; M. González-Barrio, A. Mascaraque, Dpto Física de Materiales, Universidad Complutense de Madrid, Spain; T. Mentès, A. Locatelli, Elettra-Sincrotrone Trieste, Italy; I. Takeuchi, Materials Science and Engineering, Univ. Of Maryland; A. Talin, Sandia National Laboratories; P. Segovia, E. Garcia Michel, Dpto Física Materia Condensada, Universidad Autónoma de Madrid, IFIMAC, Spain**

The cathode material Li<sub>x</sub>CoO<sub>2</sub> (LCO) and related intercalation oxides are widely used in lithium-ion batteries and are now being investigated for applications in catalysis and neuromorphic computing[1][2][3], leading to great interest in their surface properties and mechanisms. The ability of LCO to change its composition from stoichiometric LiCoO<sub>2</sub> to Li<sub>x</sub>CoO<sub>2</sub> is the key feature for most technological applications. This process changes its atomic and electronic structures. Oriented islands and epitaxial thin films of Li<sub>x</sub>CoO<sub>2</sub> grown on SrTiO<sub>3</sub> (STO) have been studied at the Nanospectroscopy beamline of the Elettra storage ring using photoemission electron microscopy (PEEM) and low energy electron microscopy (LEEM)[4].

Different surface morphologies have been studied during Li deintercalation, including the phase coexistence regime. Stoichiometric LCO islands and films were delithiated *in situ* under UHV conditions by preferential Ne<sup>+</sup> sputtering followed by thermal treatment. Surface crystallinity and morphology were maintained throughout the experiments. The effects of delithiation on island size, distribution and the surrounding substrate and wetting layer were characterized. A shift in the valence band position towards the Fermi energy marks the IMT and is accompanied by a change in the surface conduction, observed as changes in the charge shift of the PEEM spectra. This has allowed us to relate the Li content to the metallization and therefore emergence and propagation of the IMT.

The spatial resolution of PEEM provides further and more detailed information on phase formation and evolution, as well as nucleation points and domain sizes. We were able to isolate the contribution of the different phases formed in the 0.5<x<1 region.

[1] N. Nitta, F. Wu, J. T. Lee, and G. Yushin, *Materials Today*, 18 (5), (2015).

[2] Z. Lu, H. Wang, D. Kong, K. Yan, P. C. Hsu, G. Zheng, H. Yao, Z. Liang, X. Sun, and Y. Cui, *Nature Communications* 5:1 5, 1 (2014).

[3] E. J. Fuller, F. el Gabaly, F. Léonard, S. Agarwal, S. J. Plimpton, R. B. Jacobs-Gedrim, C. D. James, M. J. Marinella, and A. A. Talin, *Advanced Materials* 29, 1604310 (2017).

[4] A. Locatelli, L. Aballe, T. O. Montes, M. Kiskinova, and E. Bauer, *Surface and Interface Analysis*, 38, 1554–1557 (2016).

## TF-ThP-7 Sorption-Vapor Synthesis of Zr-MOF, UiO-66-NH<sub>2</sub>, Sponge Composites, Jimmy Nguyen, G. Parsons, North Carolina State University

Metal-organic frameworks (MOFs) are materials of interest for their high surface area and chemical tuneability. MOF-Fabric, fiber, and sponge composites have been an area of research enhancing materials for applications like catalysis, separation, sensors, and energy storage. In comparison to other support matrices, sponges have greater molecular transport through their macroporous structure. The majority of current approaches for creating MOF-sponge/foam composites require multiple lengthy and resource consuming steps. These approaches often rely on either support pretreatment followed by MOF synthesis or support formation around premade MOF powder. The pretreatment method adds an additional hazardous step using high temperatures or heated acidic solutions. The support formation method requires more uncommon instruments like a high-pressure homogenizer and/or freeze-dryer. Here, a straight forward method for *in-situ* synthesis of a MOF film onto as-received commercially available sponges is reported. Sorption-vapor synthesis first involves the sponge absorbing precursor solution followed by a vapor-driven MOF nucleation and growth phase. The vapor phase exposure serves multiple roles including increasing the mobility of reactants to connect together, promoting crystalline behavior, and creating desired defects in the framework under specific conditions. This sorption-vapor synthesis technique enables the formation of plant fiber sponge@UiO-66-NH<sub>2</sub> composites retaining significant mechanical integrity capable of withstanding compressions. Through exploring different solvent systems, acidic vapors, and metal precursors, the conditions that maintain the most structural integrity was discovered. The conditions using a dimethyl formamide, ethanol, and water solvent system, acetic acid and water modulating vapor, and ZrCl<sub>4</sub> led to a crystalline MOF composite with a BET surface area of 114 ± 17 m<sup>2</sup>/g. The composite formed via sorption-vapor synthesis was found to be capable of catalyzing the hydrolysis of an organophosphate, dimethyl paraoxon, with a preliminary study exhibiting a half-life of < 20 mins. This work presents insight into a simple vapor driven mechanism for UiO-66-NH<sub>2</sub> film growth onto an as-received, commercial sponge.

## TF-ThP-8 Coating the Insides of Capillaries with a Flow-Through Atomic Layer Deposition (ALD) Reactor, Jacob Crossman, J. Pinder, D. Patel, Brigham Young University; D. Bell, RESTEK; M. Linford, Brigham Young University

Atomic layer deposition (ALD) is a process by which single or partial atomic or molecular layers are applied sequentially to a substrate. ALD often relies on a series of self-limiting half-reactions, where the number of these reactions applied to a surface is used to control the thickness of a deposited film to atomic dimensions. Ideally, ALD layers are consistent and conformal, which makes it an increasingly useful technique for semiconductor manufacturing. Traditionally, ALD is performed in a vacuum chamber that introduces and pumps away the precursors of the half-reactions. This approach is often effective on planar surfaces. However, it is not a viable method for coating high aspect ratio materials like the interior walls of

capillary columns that are 5 meters or longer. To resolve this limitation, we developed a flow-through, atmospheric pressure (AP) ALD reactor that relies on flowing nitrogen rather than diffusion in a vacuum to present a precursor to the substrate surface. Thin film growth with this reactor was confirmed with spectroscopic ellipsometry (SE), X-ray photoelectron spectroscopy (XPS), chromatography, and transmission electron microscopy (TEM). Indeed, our AP-ALD reactor includes two witness chambers containing planar silicon ‘witness shards’ placed before and after the capillary. The operation of this reactor was demonstrated with the well-known trimethylaluminum-water reaction. Reasonable ALD growth of Al<sub>2</sub>O<sub>3</sub> was confirmed by SE of witness shards and TEM of sections of a coated capillary. Little difference in film thickness was observed between witness shards in the two witness chambers and in the capillary itself. A chemical engineering analysis of our system suggested that a ca. 10-fold excess of reagent was present in the capillary, which explains the nearly uniform film growth at both ends of the capillary and in the witness chambers.

## TF-ThP-9 Surface studies and molecular beam epitaxy of Kagome Antiferromagnetic Mn<sub>3</sub>GaN grown on MgO (001), Ali Abbas, A. Smith, A. Shrestha, Ohio University

There have been very few studies of antiperovskite structure Mn<sub>3</sub>GaN in general although it was seen in molecular beam epitaxial growth as a second-phase precipitate when growing MnGaN [1]. And so, we grow thin films of Mn<sub>3</sub>GaN on MgO (001) substrates using rf N-Plasma MBE. In this abstract, we will discuss the growth recipe and surface study of Mn<sub>3</sub>GaN. To take advantage of noncollinear antiferromagnetic thin films in spintronics applications, it is important to study their spin structures using local probes like spin polarized scanning tunnelling microscopy. Initially we start with room temperature scanning tunneling microscopy of MBE-grown Mn<sub>3</sub>GaN surfaces and later will progress toward variable low temperature spin-polarized scanning tunnelling microscopy. In our work, Mn<sub>3</sub>GaN is deposited at 250 ± 10°C with a Mn: Ga: N flux ratio of 3:1:1. We keep the Ga:N ratio fixed using an RF plasma nitrogen source. The sample surface is continuously monitored throughout the growth using reflection high energy electron diffraction. During growth, the RHEED pattern was observed to be highly streaky, indicating an atomically smooth surface. In addition, we observed half-order fractional streaks (2x pattern) in the [100] direction. The calculated *in-plane* lattice constant based on RHEED is 3.89 ± 0.06 Å. This value is very close to the theoretical lattice constant *a* of Mn<sub>3</sub>GaN (3.898 Å) [3] and with the *in-plane* experimental value for sample growth by sputtering (3.896 Å); and in that work, the authors also observed a 2x pattern [2]. We also measure the *out-of-plane* lattice constant using X-ray diffraction. For the major 002 peak, the value calculated is 3.84 ± 0.06 Å which also agrees well with the theoretical value (3.898 Å) [3] and with the experimental reported *c* value (3.881 Å) [2]. Rutherford backscattering confirms a stoichiometry of 3:1:1.

This work is supported by the U.S. Department of Energy, Office of Basic Energy Sciences, Division of Materials Sciences and Engineering under Award No. DE-FG02-06ER46317.

References:

[1] KH. Kim, KJ. Lee, HS. Kang, FC. Yu, JA. Kim, DJ. Kim, KH. Baik, SH. Yoo, CG. Kim, YS. Kim, “Molecular beam epitaxial growth of GaN and GaMnN using a single precursor,” *Physica Status Solidi (b)* 241(7), 1458 (2004).

[2] T. Hajiri, K. Matsuura, K. Sonoda, E. Tanaka, K. Ueda, & H. Asano. “Spin-Orbit-Torque Switching of Noncollinear Antiferromagnetic Antiperovskite Manganese Nitride Mn<sub>3</sub>GaN,” *Physical Review Applied*, 16(2), 024003(2021).

[3] E. F. Bertaut, D. Fruchart, J. P. Bouchaud, and R. Fruchart. *Diffraction Neutronique de Mn<sub>3</sub>GaN*. *Solid State Commun.* 6, 251–256 (1968).

## TF-ThP-10 Improved Interface of Mo/Si Bilayers by Magnetron Sputtering, Chao-Te Lee, W. Chen, H. Chen, Taiwan Instrument Research Institute, National Applied Research Laboratories, Taiwan

The periodic Mo/Si bilayers were deposited on Si substrate by RF magnetron sputtering with cooling system. The effects of substrate temperature on the surface roughness and interface of Mo/Si bilayers were investigated by atomic force microscopy (AFM), and high resolution transmission electron microscopy (HRTEM). The AFM measurements showed the Mo/Si bilayers to have a uniform morphology with a very low surface roughness value under 0.2 nm. It was found that the Mo-on-Si and Si-on-Mo interfaces of Mo/Si bilayers were clearly observed by HRTEM in

# Thursday Evening, November 9, 2023

sputtering without using cooling system. The thickness of Mo-on-Si interface was almost 0.45 nm in the Mo/Si bilayers. However, the thickness of the Si-on-Mo interface was increased with increasing layers of Mo/Si bilayers. It was increased from 0.9 to 1.36 nm. After using cooling system in sputtering, the temperature was 15 °C, the Mo-on-Si and Si-on-Mo interfaces were all under 0.1 nm. The improved interface of Mo/Si bilayer was attributed to the interdiffusion of Mo/Si bilayer which was improved by sputtering by cooling system.

**TF-ThP-11 Optical Emission Spectroscopy Analysis of Self-limiting AlN Growth Process during Low-Temperature Plasma-Assisted ALD, Narmin Ibrahimli, R. Sultana, I. Saidjafarzoda, University of Connecticut; M. Kilinc, University at Buffalo; A. Okyay, OkyayTech; N. Biyikli, University of Connecticut**

This research aims to present the potential and advantages of implementing optical emission spectroscopy (OES) as a non-invasive technique to investigate and optimize the plasma-assisted atomic layer deposition (ALD) process for AlN thin films. OES enables the identification of species present in the plasma and analysis of the light emitted, rendering it as a crucial tool for evaluating the reactant species delivered to the surface and for gaining unique insights into the surface reaction products and possible mechanisms of the deposition process. The incorporation of time-resolved OES measurements allows for the determination of optimal precursor dosing and plasma exposure times necessary for saturating half-reactions, thereby enhancing the efficiency of the ALD process. Additionally, the versatility of time-resolved OES as a process monitoring tool for plasma-assisted ALD processes on production equipment provides the capability for real-time detection of process faults and monitoring of reactor wall conditions.

AlN thin films were deposited by employing trimethylaluminum (TMA) in combination with various nitrogen plasmas (N<sub>2</sub>/H<sub>2</sub>/Ar). The growth experiments were carried out in a hollow-cathode plasma-ALD reactor at 200 °C and 100 W RF plasma power. The light emission during the plasma half-cycle is coupled into a multimode fiber through one of the optical access ports via a collimating lens which feeds a compact spectrometer unit spanning from 300 to 1000 nm with a wavelength resolution of ~2 nm. The spectral data obtained from the AlN deposition procedure was assessed by examining the emission spectrum within the initial few milliseconds of a plasma half-cycle that followed a TMA dose, and contrasting it with the emission spectrum observed towards the end of the same half-cycle, when the plasma had become adequately saturated. The differences in the emission spectra are due to the reactions initiated by plasma species with precursor fragments adsorbed at the surface. At the end of the plasma step, when the surface reactions have saturated, the emission spectrum recorded during the ALD cycle resembles that of a steady-state plasma. The results indicate that time-resolved OES measurements can help determine optimal precursor dosing and plasma exposure times to enhance the efficiency of the ALD process. Future work involves a more detailed investigation of surface ligand-exchange reactions, plasma-surface interactions, and formed reaction byproducts in real-time to gain a deeper insight into the ALD process.

**TF-ThP-12 Oblique Angle Deposition on Porous Polymer Films, S. Bacheller, N. Welchert, Malancha Gupta, University of Southern California**  
Our group has developed a modified initiated chemical vapor deposition (iCVD) process in which frozen monomer is first captured on a cooled substrate, then polymerization occurs via a free radical polymerization mechanism, and finally the excess monomer is sublimated resulting in a porous polymer film. This talk will discuss applying oblique angle deposition to this modified iCVD process. We will demonstrate that delivering the monomer through an extension at an oblique angle results in porous films with three morphological regions: region 1 consists of porous polymer pillars, region 2 consists of densified pillars, and region 3 consists of dendritic structures. We will discuss the role of the substrate temperature, the extension angle, and the monomer deposition time on the growth process.

**TF-ThP-13 Fabrication and Characterizations of Aluminum Doped Cadmium Oxide (CdO:Al) Thin Film using Sol-Gel Spin-Coating Method, M. Syed, Krastin Harvey, LeMoyné Owen College; M. Syeda, J. Sultana, University of Memphis**

Aluminum-doped cadmium oxide (CdO:Al) thin films are deposited on silica substrates by the sol-gel spin-coating method as a function of spin coater's rpm (revolution per minute). Cadmium acetate dihydrate and Aluminum nitrate have been taken as the precursor material and a source of Al-dopant respectively. CdO:Al thin films are characterized by x-ray diffraction (XRD),

Fourier Transform Infrared (FT/IR), Field emission scanning electron microscopy (FE-SEM) and SEM-EDX. XRD result indicates the highest crystallinity at 6000 rpm with a crystallite size of 31.845 nm, cubic phase formation, and strain of ~1.6 X10<sup>-2</sup>. FE-SEM/SEM/EDX shows the well-faceted homogeneous surface structure at 6000 rpm having the average particle size of 130.05 nm. FT/IR confirms the presence of CdO:Al in the film with the peak position shifting to higher wavenumbers.

Keywords: Cadmium oxide, Thin Film, SEM, Crystallinity, Sol-gel process

**TF-ThP-14 Structural and Electronic Impact on Various Substrates of TiO<sub>2</sub> Thin Film Using Sol-Gel Spin Coating Method, Moniruzzaman Syed, T. Crosby, M. Frierson, J. Muhammad, LeMoyné Owen College; M. Syeda, J. Sultana, M. Azim, University of Memphis, USA**

Titanium dioxide (TiO<sub>2</sub>) thin film has been deposited on glass and silica substrates by using Sol-Gel spin coating method. The effect of annealing temperature on the structure, surface morphology, optical and electrical properties of these films are characterized by Raman, XRD, FT/IR, UVvis and four-point-probes measurements. XRD confirms the anatase phase of TiO<sub>2</sub>. Maximum crystal sizes are found to be ~31 nm on silica and ~23 nm on glass substrates at 500°C respectively. Electrical resistivity decreased with increasing annealing temperature having the higher value on glass substrates observed.

**TF-ThP-15 Thin Film Transformations with Spinodal Mechanisms, Rahul Basu, JNTU, India**

The topic of nucleation and growth in thin films traditionally has relied on the free energy barrier concept. In the present approach the growth of secondary phases is examined using a Moving Boundary analysis with heat transfer balances. The coupling of other components is not neglected. The possibility of spinodal breakup occurs within a miscibility gap and involves additional terms in the diffusion equation. These 4th order terms are modeled appropriately and included in the dominant Fickian diffusion model. The thin film approximation is used with a perturbation expansion. Although the spinodal model required two or more component alloys in a miscibility gap, the differential equations do not exclude a general one component model. It is shown that the onset of a nucleation regime is predictable from the MBP heat transfer analysis without the explicit use of Free Energy variables.

**TF-ThP-16 Optical Coating with High Hardness for MIR Optics Deposited by HIPIMS Deposition Technique, Bo-Huei Liao, Taiwan Instrument Research Institutes, Taiwan**

In this research, silicon nitride and silicon oxynitride multilayers are deposited by high power impulse magnetron sputtering. In order to increase the adhesion of the AR coating, plasma treatments in a rf discharge of Ar and O<sub>2</sub> are used to activate and clean the Ge substrate. Besides, Al<sub>2</sub>O<sub>3</sub> films are also deposited as the adhesion layer before the multilayers AR coating. The average transmittance from 3000 to 5000 nm was larger than 93.2%. The Mohs hardness scale was also larger than 8.

**TF-ThP-17 Thermal Atomic Layer Deposition of Er<sub>2</sub>O<sub>3</sub> Films from a Volatile, Thermally Stable Enaminolate Precursor, Chamod Dharmadasa, C. Winter, N. Jayakodiarachchi, Wayne State University; P. Evans, R. Liu, University of Wisconsin - Madison**

Lanthanide oxide films have many applications in optics, catalysis, and semiconductor devices. Er<sub>2</sub>O<sub>3</sub> films have useful properties that arise from its high dielectric constant, a large band gap energy, high refractive index, and thermodynamic stability at high temperatures. These properties have led to the investigation of Er<sub>2</sub>O<sub>3</sub> films for possible inclusion in CMOS devices, antireflective and protective coatings on solar cells, and passivation layers for III-V semiconductors. Er<sub>2</sub>O<sub>3</sub> films have been grown by many techniques, including PVD, CVD, and ALD. ALD is an important technique, since it gives Angstrom-level thickness control and can afford 100% conformal coverage in high aspect ratio features. ALD precursors reported to date for Er<sub>2</sub>O<sub>3</sub> films have problems that include low reactivity toward water as a co-reactant, oxidation of substrates when ozone is used as the co-reactant, and variable thermal stabilities. Recently, we described a series of volatile and thermally stable lanthanide(III) complexes that contain enaminolate ligands.<sup>1</sup> We report here detailed synthetic studies of the Er(L<sup>1</sup>)<sub>3</sub> precursor complex, its ALD precursor properties, and its use in the ALD of Er<sub>2</sub>O<sub>3</sub> films using water as the co-reactant. Depending upon the reaction conditions during precursor synthesis the compounds Er(L<sup>1</sup>)<sub>3</sub>, Er(L<sup>1</sup>)<sub>3</sub>(L<sup>1</sup>H), or K[Er(L<sup>1</sup>)<sub>4</sub>] can be isolated. The reaction conditions can be

# Thursday Evening, November 9, 2023

selected to provide high yields of  $\text{Er}(\text{L}^1)_3$ . The volatility and thermal stability characteristics of  $\text{Er}(\text{L}^1)_3$  are favorable for use as precursors for  $\text{Er}_2\text{O}_3$  and other rare-earth oxides. An ALD window in the growth of  $\text{Er}_2\text{O}_3$  films using  $\text{Er}(\text{L}^1)_3$  with water as the co-reactant was observed from 150 to 250 °C, with a growth rate of 0.25 Å/cycle. The films were characterized by electron microscopy, X-ray diffraction, X-ray photoelectron spectroscopy, and atomic force microscopy. Advantages of  $\text{Er}(\text{L}^1)_3$  include its simple synthesis, good volatility and high thermal stability, and high reactivity with water to afford  $\text{Er}_2\text{O}_3$  films. This class of new ALD precursors has the potential to enable more widespread use of the favorable properties of rare-earth oxide compounds and can be expanded to multi-component complex oxides containing rare earths.

## **TF-ThP-18 Highly Sensitive and Stable pH Sensor Electrodes of TiN Fabricated using HiPIMS with Kick, Lucas Mougeot, S. Stagon, J. Aceros, University of North Florida**

Titanium nitride deposition-sputtered sensors have been shown to function as sensitive pH sensors. The electrical conductivity and inertness of TiN advocates for this functionality. Literature has shown results only for DC-sputtered TiN pH sensors, however. This research identifies and analyzes the differences between DC-sputtered TiN sensors and those fabricated with HiPIMS and HiPIMS with Kick. The methods differ in their power source. Note that DC-sputtering involves a DC power signal. HiPIMS stands for High Power Impulse Magnetron Sputtering and uses a square wave power signal. HiPIMS with Kick also requires a square wave, but involves a short pulse before relaxing to the equilibrium voltage. For all sputtering methods, the power input to the titanium target averages at 250W. Additionally, the initial chamber pressures are all  $10^{-6}$  torr. Some settings differ to achieve consistent deposition rates between the techniques, such as the working pressure (3-5 mtorr). To create the sensors, TiN is deposited onto a ceramic screen-printed electrode (with gold metallic ink). There are four leads: active, counter, reference, and signal. The active and signal leads connect to the active electrode. The counter and reference leads connect to their own respective electrodes. TiN is deposited onto the active electrode. The reference electrode is composed of Ag/AgCl. In aqueous environments, a potential difference forms between the active and reference electrodes. This voltage is used to determine the pH of the solution. To compare the sensors, measured properties include sensitivity, hysteresis, response time, and drift. To measure sensitivity, the Nernst equation is employed to determine the linear relationship between voltage and pH. The slope of this graph directly relates with sensitivity, with steeper slopes denoting higher sensitivity (and vice versa). To measure hysteresis, the sensor measures a sequence of pH buffer solutions in time-contained steps (i.e. a pH sequence 4, 7, 10, 7, 4 limited to 240 seconds each). The voltage difference that exists between a first-stage measurement and a second-stage measurement of the same solution denotes hysteresis. For measuring response time and drift, the sensor is placed into a solution for a duration of time. Response time is the duration that exists between the initial exposure to the solution and the point when the output is first within 0.1 pH of the true value. Drift is longitudinal. Measured over the course of hours, drift is the output decay rate from the sensor's initial steady state. The Scanning Electron Microscope (SEM) and Atomic Force Microscope (AFM) are used to characterize the TiN depositions. The SEM characterizes the topographic features of the depositions. The AFM characterizes the film thickness.

## **TF-ThP-19 Temperature Dependent Thermal Conductivity Measurements of Thin Oxide Films Via Steady State Thermoreflectance, J. Gaskins, D. Olson, T. Bates, P. Hopkins, Laser Thermal; Ron Fisher, Laser Thermal, USA**

Continued dimensional scaling of materials in integrated circuits have resulted in major challenge in power dissipation and thermal management. These characteristic length scale reductions at all tiers of devices lead to temperature increases which accelerates the degradation of performance and reliability of very large scale integration. As technology nodes push to the <5 nm length scale, these thermal problems become more pronounced due to metal interconnect scaling resulting in reduced thermal conductivities, interfacial thermal resistances, and novel ultra-low-k amorphous dielectric layers that have intrinsically low thermal conductivities. Accurate understanding of these thermal properties will help guide the upcoming generations of interconnect and transistor technologies. Using Steady State Thermoreflectance in Fiber Optics (SSTR-F), we measure the thermal conductivity of a series of oxide thin films on silicon wafers. Prior to SSTR-F measurement, we coat the samples with a thin (~80 nm) film of Al to serve as an opto-thermal transducer. In practice, due to the steady state nature of the SSTR-F measurements, we are minimally sensitive to the thermal mass of the Al (heat capacity and

thickness) as compared to TDTR or FDTR, which is a typical major source of uncertainty in TDTR and FDTR. We report on the thermal conductivity of oxide films with thicknesses of 98, 229, 287, 431, and 867 nm. For the thinnest three samples, SSTR-F measures the thermal resistance of the oxide layer in addition to the ITR at each adjacent oxide layer interface (Al/oxide and oxide/Si). Thus, we measure the thermal conductivity by fitting the thermal resistance of this thickness skew as a function of thickness and fit a series thermal resistor model to these data to determine the thermal conductivity of these amorphous oxide films. This approach yields a thermal conductivity of 0.96 +/- 0.04 W/m/K. For the thickest two oxide samples, the thermal resistance is dominated by that of the oxide, and thus we report on direct measurements of the thermal conductivity of these films by dividing the thickness of the films by the measured thermal resistance and also come to a thermal conductivity of 0.96 +/- 0.04 W/m/K. The uncertainties in our measured values are calculated from spot to spot variation and propagation of uncertainty in the assumed parameters in our analysis. These SSTR-measured values agree well with prior measurements of the thermal conductivity of amorphous thin film dielectrics on silicon using TDTR that have been reported previously.

## **TF-ThP-20 Investigation on Atomic Layer Deposition Assisted Growth of Metal Organic Frameworksfilms and Their Sensing Performance, Zhe Zhao, Fudan University, China**

Weak interactions, non-uniformity and powdery assemblies limited the wide application of metal organic frameworks (MOFs) in devices<sup>[1, 2]</sup>. We report a new strategy for area-selective assembly of MOF particles to prepare a thin film with the assistance of atomic layer deposition (ALD)<sup>[3-5]</sup>. The mechanism of this strategy is utilizing ALD pretreatment to induce the growth of hydroxy double salt (HDS) nanosheets on substrates, and the HDS nanosheets are then chemically converted into a MOF structure<sup>[6]</sup>. Self-assembled hierarchically porous MOF films such as ZIF-67 (Co), ZIF-8 (Zn), Ni-MOF (Ni), PCN-333 (Fe), MIL-53 (Fe), etc. were formed on both flat and complex three-dimensional (3D) substrates at a combination of gas and liquid fabrication approaches, and can be precisely patterned by photolithography<sup>[7-10]</sup>. We demonstrate that the MOF film obtained possesses excellent electrochemical activity and can be applied in biosensor for ultra-high sensitivity and a low limit of detection towards glucose, lactic acid and dopamine<sup>[5-7]</sup>. This strategy is promising to prepare MOF film-based on-chip devices with advanced functions.

References:

- [1] Chem. Rev. 2012, 112, 933.
- [2] Adv. Mater. 2018, 30, 1802011
- [3] Zhe Zhao, et al. Adv. Funct. Mater. 2019, 29, 1906365.
- [4] Zhe Zhao, et al. J. Mater. Res. 2020, 35, 701.
- [5] Zhe Zhao, et al. Chem. Eng. J. 2021, 417, 129285.
- [6] Zhe Zhao, et al. J. Mater. Chem. A 2020, 8, 26119.
- [7] Zhe Zhao, et al. Nano Today 2022, 42, 101347.
- [8] Zhe Zhao, et al. J. Materiomics 2020, 6, 209.
- [9] Zhe Zhao, et al. Chin. Sci. Bull. 2021, doi: 10.1360/TB-2021-0093.
- [10] Zhe Zhao, et al. Electrochem. Energ. Rev., 2022, 5, 31.

## **TF-ThP-21 Vapor Phase Infiltration of Metal-Organic Framework for Electrocatalysis, Fan Yang, M. Cao, H. ren, R. Chen, Huazhong University of Science and Technology, China**

Abstract: Metal-organic frameworks (MOFs) with well-defined structures and uniformly arranged tunable pore sizes, large surface area attract lots of attentions for a wide range of application including catalysis, sensing and etc. Intrinsic MOFs, however, often suffers from low conductivity, reactivity, selectivity and etc. Vapor phase infiltration (VPI), as a gas-phase method modified from atomic layer deposition, assures an accurately infiltrated deposition of materials into porous materials like MOFs, due to the self-limiting characteristic. In our work, VPI were applied for MOFs as post-modification at organic ligands and metal nodes, respectively. Due to the modification accuracy both in position and amount altering the MOFs coordination environment, excellent electrochemical  $\text{CO}_2$  reduction reactivity of modified MOFs were obtained, showing promising reactivity and selectivity, comparing to pristine MOFs. The VPI strategy gives great implications for the precise and accurate construction of MOFs coordination environment.

References:

# Thursday Evening, November 9, 2023

1. Xueyang Han, Zhang Liu, Meng Cao, Haonan Ren, Chun Du, Fan Yang, Bin Shan, Rong Chen. "Atomic layer infiltration enabled Cu coordination environment construction for enhanced electrochemical CO<sub>2</sub> reduction selectivity: a case study of HKUST-1" *Chem. Mater.* 2022, 34, 6713-6722.

2. Yang, Fan;Hu, Wenhui;Yang, Chongqing;Patrick, Margaret;Cooksy, Andrew L.;Zhang, Jian;Aguiar, Jeffery A.;Fang, Chengcheng;Zhou, Yinghua;Meng, Ying Shirley;Huang, Jier;Gu, Jing. "Tuning Internal Strain in Metal-Organic Frameworks via Vapor Phase Infiltration for CO<sub>2</sub> Reduction" *Angewandte Chemie-International Edition*, 2020, 59, 4572-4580.

## Undergraduate Poster Session

### Room Oregon Ballroom 203-204 - Session UN-ThP

## Undergraduate Poster Session

#### **UN-ThP-2 Enhancing the Durability of Nitrogen Plasma-Treated PLA Films: Investigating Hydrophobic Recovery Reduction Methods, *Mina Abdelmessih, M. Hawker*, California State University, Fresno**

Poly(lactic acid) (PLA) is a promising eco-friendly biopolymer as it is produced from renewable feedstocks. The use of PLA in biomedical-related applications is increasing due to its non-toxicity *in vivo* and biodegradability. Nevertheless, the surface hydrophobicity of PLA limits its utility in the biomedical field, especially in applications related to tissue engineering. Although PLA scaffolds have potential for bone reformation and angiogenesis, a hydrophilic surface would further assist in developing *in vivo* applications. For instance, valuable properties such as cell adhesion and growth could be promoted on a hydrophilic PLA surface. Previous research has demonstrated promise in increasing hydrophilic surface properties on PLA utilizing radio frequency nitrogen plasma treatment. Nitrogen plasma-treated polymers, however, exhibit hydrophobic recovery where the plasma modified polymer surface is thermodynamically unfavorable, reverting back into its hydrophobic state with age. Hydrophobic recovery of treated PLA surfaces is detrimental, especially for biomedical applications. Methods of preventing this phenomenon in PLA are widely unexplored.

This work analyzed the effectiveness of different preservation methods in maintaining the hydrophilic character of nitrogen-plasma treated PLA. PLA films were prepared as model substrates and plasma-modified under optimized nitrogen plasma parameters (power, pressure, and treatment time). Following plasma treatment, samples were aged in different environments (e.g., cold temperature, under inert gas) for a period of one month. Samples exposed to different preservation environments (along with controls aged under ambient conditions) were subjected to multiple surface analyses throughout the aging period. Film surface wettability was analyzed utilizing water contact angle goniometry. X-ray photoelectron spectroscopy was utilized to determine plasma-treated PLA surface chemical composition as well as composition throughout the aging process. Expanding these preservation methods to PLA scaffolds has the potential to positively impact the use of PLA for tissue regeneration.

#### **UN-ThP-3 Applying Ammonia Plasma to the Surface of PTFE to Enhance Amine Content, *Sannad Jawad, A. O'Regan, M. Hawker*, California State University, Fresno**

The World Health Organization reports cardiovascular diseases to be among the most prevalent global health issues, with an estimated 17.9 deaths annually. Such diseases include congenital heart defects such as atrial or ventricular septal defects. Treatment options for these conditions include surgical intervention in which a patch made of a synthetic polymer or biological tissue is secured over the affected area. Among the most commonly used polymers is polytetrafluoroethylene (PTFE). This material is well known to be inert, exceedingly flexible, and highly resistant to wear. Although PTFE is widely recognized for its good qualities, it does have the potential to elicit a negative immune response that can be harmful to the body. This study aims to reduce the immune response by utilizing ammonia plasma to increase the concentration of amine groups on the surface of PTFE. Prior studies have shown success in introducing amine groups using different ammonia plasma parameters (e.g., power, pressure, and time). However, an optimized set of parameters that produce the maximum quantity of amine groups on the PTFE surface has yet to be realized.

This study focused on varying the ammonia plasma parameters in a systematic manner to establish the correlation between these parameters and the extent of amine group integration. A range of parameters was studied (pressure 70-500 mTorr, applied power 20-100 W, plasma exposure time: 0.5 - 5 min). After treating PTFE sheets with varying plasma exposure

times, applied powers, and feed gas pressures, surfaces were characterized to investigate the presence and quantity of amine groups. First, Fourier transform infrared spectroscopy (FTIR) was used to detect the presence of IR active functional groups. Then, X-ray photoelectron spectroscopy (XPS) was used to identify the elemental composition of the surface. Contact angle goniometry was then conducted to evaluate the polymer surface hydrophilicity. Lastly, the acid orange II colorimetric assay was performed to determine the quantity of primary amine groups.

#### **UN-ThP-4 Reporting of Parameters Related to Data Acquisition and Peak Fitting in XPS: A Further Evaluation of the Literature, *B. Maxwell Clark, G. Major*, Brigham Young University; *D. Baer*, Pacific Northwest National Laboratory; *M. Linford*, Brigham Young University**

X-ray photoelectron spectroscopy (XPS) is a widely used spectroscopic technique for analyzing thin films and materials. Because XPS peak widths and chemical shifts are often of about the same magnitude, spectra acquired in XPS typically require peak fitting. In recent years, significant challenges with reproducibility in XPS analyses have been identified. We recently surveyed about 400 papers from 2019 to understand the quality of peak fitting/data analysis in the literature. We have now surveyed an additional ca. 900 papers from 2021 to understand the reporting of important peak fitting and data acquisition information. Parameters investigated include X-ray source type, pass energy, spot size, vacuum level, and the types of baselines and synthetic fit components used in fits. In general, there is a severe lack of reporting of much of this essential information in the literature.

#### **UN-ThP-5 Analyzing the Surface Roughness and Surface Chemistry of Oxygen Plasma-Treated Silk Fibroin Films for Corneal Epithelial Tissue Regeneration, *Gurmeet Kaur, M. Hawker*, California State University, Fresno**

Corneal epithelial damage is common due to ocular surface injuries that prevent tissue regeneration. These corneal surface injuries could lead to corneal defects and potential blindness. Current treatments for corneal epithelial tissue regeneration are amniotic membrane implants, however, these have limitations regarding mechanical strength, transparency, and infectious disease transmission risk. A biomaterial that has similar bulk mechanical properties to those of the cornea is silk fibroin. Silk fibroin is biodegradable and optically transparent. Additionally, prior studies indicate that silk fibroin promotes corneal epithelial cell proliferation. Current research, however, indicates a decrease in initial cell attachment when compared to the amniotic membrane. We propose the use of oxygen plasma treatment to enhance epithelial cell adhesion. Notably, this strategy has proved successful for other polymers but has not been extended to silk surfaces. This study was inspired by conflicting evidence in previous literature about the roles of surface roughness and surface chemistry in epithelial cell attachment. In this work, silk fibroin films were fabricated and plasma treated with oxygen plasma to explore the impact of both film surface roughness and surface chemistry. First, silk fibroin films with high and low surface roughness values were fabricated by dissolving silk fibroin into water and hexafluoroisopropanol, respectively. Solutions were then dropcast onto glass slides and dried overnight. Films were then oxygen plasma treated using varied plasma parameters (e.g., exposure time, applied power). Surface wettability was analyzed using contact angle goniometry. Surface roughness was qualitatively and quantitatively measured using scanning electron microscopy and profilometry, respectively. Surface chemistry was analyzed by using x-ray photoelectron spectroscopy. Overall, findings demonstrate successful fabrication of a silk fibroin film library with systematically-varied surface roughness and surface chemistry. Future analysis of corneal epithelial cells attachment on these surfaces will be performed to evaluate efficacy for corneal epithelial tissue regeneration.

#### **UN-ThP-6 Exploring the Capabilities of Oxygen-Release Coatings on Collagen Films, *Haylee McFall, M. Hawker*, California State University, Fresno**

Common resective and regenerative periodontal surgeries leave tissues exposed during postoperative healing. These sites are hypoxic, prolonging tissue regeneration. An ideal postoperative patch would provide a sustained barrier to protect against infection and deliver oxygen for expedited healing. Collagen has recently been applied in postoperative healing due to its hemostatic advantages and physical barrier capabilities. However, collagen alone does not alleviate hypoxia through localized oxygen delivery. Oxygen release coatings through plasma-enhanced chemical vapor deposition (PECVD) have been used to control the release of drugs and other species from polymer surfaces. Although literature precedent reports the use of a 1,7-octadiene precursor for PECVD to

# Thursday Evening, November 9, 2023

encapsulate oxygen release coatings on polydimethylsiloxane, this strategy has yet to be applied to collagen for oral postoperative healing. We seek to extend this previously published approach to fabricate an oxygen-releasing collagen substrate.

In this work, collagen films were prepared as model substrates. Calcium peroxide powder was sieved to  $<37\mu\text{m}$  and applied to a collagen film. A hydrocarbon film was then deposited over the peroxide layer using PECVD with 1,7-octadiene as the plasma precursor. By manipulating exposure time, the plasma-deposited film thickness was altered. PECVD rate was measured using ellipsometry. A dissolved oxygen probe determined the flow of oxygen released from the prepared constructs in an aqueous environment, which was compared to exposure time. The relationship between film thickness and oxygen delivery was elucidated. With newly incorporated oxygen delivery capabilities, these plasma modified collagen films positively contribute to postoperative healing.

**UN-ThP-7 A Precise Measurement of Atomic Spacings in Rotated Hexagonal Mn Adatom Structures on a MnGaN-2D FM Substrate, Cherie D'Mello, Ohio University; Y. Ma, Ohio University, China; D. Hunt, M. Barral, V. Ferrari, CAC-CNEA, Argentina; A. Smith, Ohio University**

We precisely measured the atomic spacings between Mn adatoms composing two rotated hexagonal structures on a Mn/MnGaN-2D aFM/FM surface. The purpose of our study is to help verify possible theoretical structures proposed for the system.

The MnGaN-2D substrate used is ferromagnetic[1]. As measured using SQUID magnetometry, adding more Mn atoms on top results in a reduction of the overall surface magnetization, and this can potentially be understood as a partially compensated ferrimagnetic structure. But the precise nature of such a structure is in this case not yet understood. However, the Mn/MnGaN-2D structure was atomically resolved by *in-situ* scanning tunneling microscopy (STM). The images revealed two hexagonal Mn adatom structures (type A and type B) which differed in rotation by approximately 20 degrees. This was surprising given that the 2D MnGaN substrate used has a very regular hexagonal-like lattice structure. Three possible theoretical models of the rotated Mn hexagonal structures have been proposed, but none of them so far has been verified to be correct. What is needed is more precise and verified measurements of the spacings between the adatoms and the location of their precise geometrical positions. If this was done carefully, it would be important for ultimately being able to determine a successful model.

Therefore, we measured the spacings of the hexagonal structures seen in the STM images of the surface of the Mn/MnGaN-2D structure by first determining the STM image calibration using the well-known structure of the substrate and the known spacings between the substrate lattice sites as measured in the STM images. We performed first the drift corrections and after that the scanner asymmetry/scale corrections. After calibration, the results reveal the corrected spacings between the adatoms composing the two rotated hexagonal regions. Even the 20° rotation between the type A and B hexagons cannot easily be explained by a standard theoretical model involving adatoms resting in ideal surface substrate sites. The correct explanation will require additional theoretical modeling, possibly going beyond the standard methods.

Acknowledgements:

This work is supported by the U.S. Department of Energy, Office of Basic Energy Sciences, Division of Materials Sciences and Engineering under Award No. DE-FG02-06ER46317.

[1] Y. Ma *et al.*, "A Two-Dimensional Manganese Gallium Nitride Surface Structure Showing Ferromagnetism at Room Temperature," *Nano Letters* **18**, 158 (2018).

**UN-ThP-8 In-situ Spectroscopy Investigations of Methane Pyrolysis in Catalytic Molten Media, Phineas Lehan, O. Polonskyi, E. McFarland, M. Gordon, University of California at Santa Barbara**

The extensive use of fossil fuels as energy sources has raised serious concerns related to their limited supply as well as harmful greenhouse gas emissions. It is thus apparent that new, sustainable energy sources are needed, such as hydrogen. Current industrial approaches to produce hydrogen, e.g., steam and/or autothermal reforming of methane, are undesirable due to high CO<sub>2</sub> emissions. An interesting alternative to these processes is direct decomposition of methane to H<sub>2</sub> and solid carbon; moreover, this process can be made CO<sub>2</sub>-free by recycling part of the H<sub>2</sub> product for heating.

There has been recent strong interest in using molten media (metals or salts) both as thermochemical reaction media and for heat transfer to

efficiently carry out methane pyrolysis. In this process, CH<sub>4</sub> is typically bubbled through the molten media, reacting to form H<sub>2</sub> and low-density carbon that rises to the surface where it can be easily separated. However, traditional methods for analyzing gaseous products of methane decomposition involve ex-situ sampling, which cannot measure short-lived intermediates and potentially introduces discrepancies in results. Therefore, in-situ experiments are preferred to make time-resolved measurements to understand such processes.

In this study, we present results of in-situ infrared (IR) spectroscopy investigations of methane pyrolysis in molten media at temperatures between 800-1200°C. The primary focus is on melts composed of molten salts and their mixtures with catalytic, transition metal additives. We utilize an L-shaped quartz reactor configuration that allows analysis of an individual gas bubble as an isothermal batch reactor. In this configuration, conversion and reaction intermediates can be studied in real time and the molten salt environment wets the quartz reactor walls, preventing coking.

Methane conversion, obtained from the methane IR peak intensity as a function of time, temperature, and melt composition, was investigated. Results show that decomposition of methane in molten KBr has an activation energy of 333 kJ/mol, compared to 413 kJ/mol for gas phase thermal decomposition. Measurements with 3 wt % Fe in an FeCl<sub>3</sub> / KBr mixture suggest lower activation energies, and the presence of catalysis. Specifically, 90% conversion was achieved within 10 minutes at 850°C, which is comparable to conversion obtained in KBr melt at 1100°C under the same conditions. Additionally, multiple hydrocarbon intermediates within the infrared spectral range of 2800 cm<sup>-1</sup> to 3400 cm<sup>-1</sup> have been observed during early stages of pyrolysis at higher temperatures (~1200°C), which could provide additional insight into methane pyrolysis mechanisms.

**UN-ThP-9 Ultraviolet Photoelectron Spectroscopy as a Powerful Technique to Investigate the Synthesis - Electronic Properties - Optical Behavior Correlation of a Cu<sub>2</sub>O||TiO<sub>2</sub> Z-Scheme, Beatriz de la Fuente, T. Hauffman, Vrije Universiteit Brussel, Belgium**

Among the electronic properties, the positions of the electronic band edges and the work function are essential parameters for determining the potential of a photocatalyst and its ability to function in a solar conversion system. Oxidation and reduction reactions are greatly affected by the electrical characteristics of the material. In this concern, ultraviolet photoelectron spectroscopy (UPS), a highly surface-sensitive technique allowing the determination of work functions, ionization energies, and examination of valence levels, provided new synthesis – electronic property links of Cu<sub>2</sub>O||TiO<sub>2</sub> direct Z-schemes systems in combination with other surface characterization techniques such as field emission scanning electron microscopy (FE-SEM), energy-dispersive X-ray spectroscopy (EDX) and X-ray photoelectron spectroscopy (XPS). This study reveals that TiO<sub>2</sub> nanotubes modified with Cu<sub>2</sub>O nanoparticles exhibited a reduction in the value of the work function (WF = 3.67 ± 0.01 eV) and ionization potential (IP = 6.01 ± 0.04 eV) with respect to the TiO<sub>2</sub> substrate (WF = 4.29 ± 0.02 eV and IP = 7.65 ± 0.05 eV). By varying the deposition time, an optimized amount of Cu<sub>2</sub>O nanoparticles deposited led to a significant reduction in the WF and IP to facilitate the excitation of electrons, which later translated into a maximum absorbance in the visible wavelength range. This work provides a tool to tune the mentioned electronic parameters based on the electrodeposition time of Cu<sub>2</sub>O, which is beneficial for the improvement of TiO<sub>2</sub>||Cu<sub>2</sub>O catalyst design and fabrication.

**UN-ThP-10 Reduced Microbial Attachment with Increased Oil Infusion in Liquid-Infused Silicone Material, Emma Kunesh, C. Fong, C. Howell, University of Maine**

Silicone polymers infused with free liquid silicone are of interest in the biomedical materials community due to their ability to significantly reduce both protein and bacterial adhesion. However, the potential for free liquid on the surface to be lost into the environment is of concern. To enhance the safety of liquid-infused silicone in medical applications, we examined how reducing free liquid via partial infusion of the solid affected the adhesion of three different species of clinically important bacteria. To create the partially infused samples, controlled infusion duration was used, resulting in samples with infusion volumes ranging from 10–100% of maximum. The partially infused samples were then exposed to *Enterococcus faecalis*, *Escherichia coli* and *Pseudomonas aeruginosa* for 24 h. For all bacteria, increasing infusion levels correlated with progressive reductions in attachment and biofilm formation. Samples infused to 80% of their maximum value were able to resist *E. coli* and *E. faecalis* adhesion at levels statistically similar to fully infused controls. However, below this infusion percentage *E. coli* and *E. faecalis* adhesion increased significantly. In

contrast, samples infused to only 40% of their maximum values were able to resist adhesion by *P. aeruginosa* at levels similar to controls. Further tests with *P. aeruginosa* showed that significant differences were visible after only 4h of incubation. Together, our results demonstrate that partially infused silicone material can still effectively reduce microbial attachment, providing a potential avenue for enhancing the safety of liquid-infused silicone materials in medical applications.

## **UN-ThP-12 Exploring Thresholding Methods in Textured Surface UV-Vis Detection of Chemical and Biological Contamination in Liquids, Anna Folley, L. White, C. Howell, University of Maine**

Current commercial assessment of chemical and biological pollutants in liquids frequently requires labor-intensive manual collection and measurement, typically employing costly UV-Visible spectrometers. We have recently shown that a low-cost surface texture that functions as a diffraction grating can be used to get comparable results to a spectrometer; however, the system's sensitivity could be improved. Here, we describe how optimizing thresholding methods could increase the sensitivity and decrease the limit of detection of contaminants in liquid. We designed a method to image and capture changes in the diffraction pattern as a liquid containing biological and chemical pollutants passes over the diffraction surface. Various image thresholding methods were evaluated to determine their influence of overall detection sensitivity. The efficacy of distinct thresholding techniques for analyzing contaminants which scatter light as opposed to simply absorb light was also explored. The findings from our study demonstrate that thresholding plays a pivotal role in identifying liquid contaminants and suggest the potential for refining thresholding methods to enhance sensor sensitivity.

## **UN-ThP-13 Analyzing Diffraction Pattern Colors in Textured Surface UV-Vis Detection of Chemical and Biological Contamination in Liquids, Lindsay Pierce, L. White, C. Howell, University of Maine**

Conventional evaluation of chemical and biological pollutants within liquids entails manual collection and measurement procedures. We have developed an alternative approach to contaminant analysis that uses a textured surface as continuous, in-line diffraction grating sensor; however, systematic shifts in the color of the diffraction pattern as contaminant levels rise and fall have not yet been analyzed. Here, we explore the prospect of tracking systematic color shifts within the diffraction pattern to enhance the detection of liquid contaminants. Using images of the diffraction pattern under both static and continuous flow conditions, we investigated different hue thresholding methodologies. The colors exhibited clear, systematic shifts in the presence of contaminants within the liquid, demonstrating the potential to extract color information from the diffraction grating sensors to provide additional information about contaminants in liquid.

## **UN-ThP-14 A Density Functional Theory Analysis of an Acetone-Acetone Aldol Condensation on an Pt-Doped Fe<sub>3</sub>O<sub>4</sub> Surface, Jack Gordon, H. Nguyen, L. Árnadóttir, Oregon State University**

Aldol condensation reactions provide an efficient way to form carbon-carbon bonds, making them pivotal for processes in synthesis and polymerization. An Fe<sub>3</sub>O<sub>4</sub> surface acts to catalyze the process, but experimental data shows that an addition of Pt in small concentrations enhances the reaction rate, suggesting alterations in the reaction mechanism and/or a decrease in the activation energy. Due to the surface's promise in facilitating aldol condensations, a greater understanding of the mechanism is desired. Density Functional Theory (DFT) as implemented in VASP 6.2 was used to calculate and compare changes in energies and the activation barriers of elementary reaction steps of different reaction pathways. The calculations indicate that the platinum-doped surface does act as a more efficient catalyst than the non-platinum-doped alternative. Furthermore, the data suggests a plausible mechanism in which both an octahedral iron and platinum act as adsorption sites for acetone, while a surface oxygen acts as a recipient for hydrogen during enolate formation. Of the two co-adsorbed acetones, the acetone bound to the iron demonstrates a preference toward enolate formation.

## **UN-ThP-15 An STM Investigation of the Ambient Adsorption of L-Isoleucine on the Surface of Au(111), Dillon Dodge, University of Tulsa; R. Dirks, Columbia University; L. Hornbrook, E. Iski, University of Tulsa**

The role of surfaces in the molecular interaction between 2D layers of amino acids has become a recent topic of investigation concerning questions like homochirality and, by extension, the origin of life on Earth. Previous research has examined how metallic islands are formed on the surfaces of Cu(111) and Au(111) due to the immobilization of diffusing metal adatoms in ultra-high vacuum (UHV) and electro-chemical (EC) liquid

cells respectively, showing that the biological molecules drastically interact with the surface indicating that metallic surfaces do not act as static hosts during these molecular interactions.

This research used scanning tunneling microscopy (STM) to observe the interactions of L-Isoleucine on the surface of Au(111) scanning completely in air at room temperature following drop cast deposition of the amino acid. Similar to past research, we observed interactions with the surface including step edge deformations and the formation of metallic islands, though in notably different scales and frequencies. This indicates that results found from experiments in UHV and EC cells are at least partially analogous to those done in air, which is a potentially more realistic representation of conditions of early earth.

However, not all behaviors seen in our experiments done in air were perfectly correlated to ones in prior investigations. For example, whereas the metallic islands caused by the deposition of 0.55 mM L-Isoleucine in UHV and EC cells were frozen in place regardless of active observation by the tip, the deformations that we observed in air were quickly reconstructed as a result of tip-assisted reconstruction regardless of isoleucine concentration. Additionally, we imaged herringbones present next to sites of molecular interaction after hours of unprotected exposure to air following deposition. These findings indicate the need to study molecular adsorption at a wide variety of conditions in an effort to truly understand the interaction between biological molecules and model surfaces, like Au(111).

## **UN-ThP-16 Towards Plasma Enhanced Atomic Layer Deposition, Sivagya Kc, W. Jen, S. Hues, E. Graugnard, Boise State University**

The fabrication of microelectronics relies on thin film technologies. As the demand for improved performance of microchips continues to escalate, atomic layer deposition (ALD) has emerged as a crucial technique in enabling precise and controlled thin film deposition. Plasma-enhanced ALD in particular is an energy-enhanced method for synthesizing thin films with mono-layer resolution. Unlike conventional thermal ALD processes where chemical precursors react with a heated substrate to deposit the thin film, forming a plasma of the ALD precursors allows for alternate reaction paths, potentially leading to improved film density, crystallinity, and mechanical properties at lower deposition temperatures. Plasma exposure during ALD can also assist in the removal of surface contaminants during the deposition process.

In this project, a capacitively coupled plasma is generated by applying a direct current (DC) bias between the powered and grounded electrodes in a quartz chamber, inducing an electric field. This couples with the precursor gas to create a high-energy plasma that produces energetic reactive species, which can then be directed to the substrate, providing novel reaction pathways having a more desired thermal budget to achieve the desired film properties. This chamber will be integrated into an ALD system to enable plasma-enhanced ALD. The chemical, physical, and electrical properties of the resulting films will be characterized.

## **UN-ThP-17 Role of Post-Deposition Annealing on Defectivity in 2D Materials, Icelene Leong, W. Jen, A. Rode, J. Wilson, R. Clouse, D. Tenne, S. Hues, Boise State University; E. Graugnard, Boise State University and Center for Advanced Energy Studies**

With the increasing complexity of microelectronics, the development of new forward-looking materials and processes has become imperative to enable their functionality. Among the potential pathways to further miniaturize devices, two-dimensional (2D) materials offer great promise due to their outstanding electrical properties even at the atomic level. Molybdenum disulfide (MoS<sub>2</sub>) is a notable example of a 2D material that exhibits these desirable characteristics and can be synthesized through chemical vapor deposition (CVD) at elevated temperatures. For deposition temperatures below 300°C, atomic layer deposition (ALD) shows promise for synthesis of MoS<sub>2</sub> films, but film quality is generally lower than CVD films, and ALD films often employ post-deposition annealing (PDA) to improve their quality.

Ultimately, electrical performance of 2D materials is of primary interest, yet device fabrication can be time consuming and expensive. Thus, there arises a need for the ability to rapidly evaluate the quality of ALD thin films prior to test device fabrication. Raman spectroscopy, a powerful analytical technique widely employed for the characterization of 2D thin films, presents itself as a promising approach for efficient metrology. Variations in the crystallinity and defect density of MoS<sub>2</sub> can induce peak shifts or

# Thursday Evening, November 9, 2023

broadening in the corresponding Raman spectra. Establishing a quantitative correlation between these changes and the film properties would enable a swift and non-destructive method for characterizing thin films to evaluate which processing conditions produce films of sufficient quality for device fabrication. To establish this approach, ALD MoS<sub>2</sub> films will be deposited on a variety of substrates and subsequently subjected to various annealing conditions, including different temperatures, durations, and environments. The Raman spectra of the annealed samples will be evaluated using deconvolution of the phonon modes giving rise to the peaks in the spectra. These data, along with processing conditions, will be correlated with defect densities acquired through transmission electron and scanning probe microscopies and film conductivity. This approach will establish a quantitative relationship between Raman spectral features and film mobilities, which will enable high-throughput metrology for ALD process development of high quality 2D materials.

**UN-ThP-18 Plasma-Excited Nitrogen for Stabilization of GaN During High Temperature Annealing, Reilly Shanahan, E. Thimsen, D. Mohr,** Washington University in St. Louis

Gallium nitride (GaN) is a wide bandgap semiconductor material that can outperform silicon in power electronics applications. Activation of p-type Mg dopants embedded by ion implantation requires extreme annealing temperatures, at which elemental decomposition becomes a challenge. High N<sub>2</sub> pressures are usually required to prevent the decomposition of GaN during high temperature annealing, which leads to exorbitant production costs. In this work, we explore the hypothesis that the annealing process can be run at low pressure conditions (decreasing costs) by using N<sub>2</sub> plasma to provide the chemical potential required to stabilize GaN. Previous research has demonstrated that the presence of plasma results in the growth of GaN from Ga melt at unexpectedly high temperatures without high pressure. In this work, a comparative approach is used wherein thin film GaN samples deposited on sapphire substrates are annealed at high temperature with and without N<sub>2</sub> plasma. The samples are characterized specifically by looking for pits on the GaN surface. These pits are a hallmark of the early stage of decomposition. The results suggest that N<sub>2</sub> plasma improves stability of GaN during low-pressure, high-temperature annealing.

**UN-ThP-19 C<sub>3</sub> Oxidation Chemistry over CuO<sub>x</sub>/Cu(111), John Yoo, E. Schell, J. Loiselet, A. Baber,** James Madison University

The oxidation of C<sub>3</sub> compounds, propylene and 1-propanol (1-PrOH), yield important products including propylene oxide and hydrogen over copper-based catalysts. Gaining a better insight into the activity of the C<sub>3</sub> compounds over Cu and CuO<sub>x</sub> will help improve the understanding of which surface preparations are most reactive. The adsorption and reaction of propylene and 1-PrOH were studied over Cu(111), sputtered Cu(111), oxidized Cu<sub>2</sub>O/Cu(111), and partially oxidized CuO<sub>x</sub>/Cu(111) using temperature programmed desorption (TPD). TPD results showed the oxidized Cu(111) catalyzed the reaction of 1-PrOH but not propylene. Cu(111) was sputtered with Ar<sup>+</sup> ions to further identify and analyze the C<sub>3</sub> adsorption on defect sites. Sputtered Cu(111) introduced more adsorption sites compared to the clean and oxidized Cu(111) surfaces. These experiments help provide a fundamental understanding of the interactions that occur between C<sub>3</sub> compounds and the differently prepared Cu(111) surfaces. This will set the groundwork for future Cu-based model catalyst research.

**UN-ThP-20 Computationally Enhanced Experimental Investigation of Reactivity of Isomeric Butanol on TiO<sub>2</sub>/Au(111), Haley Frankovich, L. Garber, A. Galgano, E. Schell, K. Letchworth Weaver, A. Baber,** James Madison University

Biofuels can be used to reduce global dependence on fossil fuels while contributing to a carbon-neutral cycle. Biobutanol has low volatility and multiple transportation options which make it an attractive alternative fuel. Understanding the fundamental thermal catalysis processes of butanol over heterogeneous model catalysts can aid in the design of more efficient catalysts. To better understand the processes in play, temperature-programmed desorption (TPD), atomic force microscopy (AFM), density functional theory (DFT), and high-performance computing are used to investigate its reaction. This study aimed to examine the reactivity of different isomers of butanol, namely 1-butanol, 2-butanol, and isobutanol, when exposed to a TiO<sub>2</sub>/Au(111) surface. TPD was used to detect products, with 1-butanol showing little reactivity and elimination products, 2-butanol showing oxidation and elimination, and isobutanol yielding all products. The selectivity of the reaction was not altered during successive desorption experiments, indicating that the model catalyst was stable without

reoxidation between experiments. AFM highlighted the morphology of the surface and shows the Au(111) crystal has ~0.13ML and 0.27ML of TiO<sub>2</sub> with predominantly 1D wire like nanoparticles. Higher coverages of TiO<sub>2</sub> result in more particles distributed across the surface indicating that the reactivity was influenced by butanol proximity to TiO<sub>2</sub> nanoparticles rather than differences in size or shape. DFT calculations to investigate energetic trends and provide an atomic-scale understanding of the structure of butanol adsorbed on the surface are ongoing.

**UN-ThP-21 Effect of Thermal Annealing and Sputtering by Ion Bombardment on WSe<sub>2</sub> Adsorption Sites, Ava Galgano, E. Schell,** James Madison University; *J. St. Martin*, University of Virginia; *A. Baber*, James Madison University; *P. Reinke*, University of Virginia

Transition metal dichalcogenides (TMDs) are two dimensional materials gaining attention as catalysts for CO<sub>2</sub> hydrogenation and the hydrogen evolution reaction due to their unique properties at low dimensions. Defects, or surface irregularities, of the atomic structure of TMDs are suggested active sites; however, the link between defects, electronic structure, and activity is unknown, which limits the ability to control reactivity. To better understand the fundamental nature of defects on TMDs, WSe<sub>2</sub> was studied using temperature programmed desorption (TPD). The surface of WSe<sub>2</sub> was cleaved via mechanical exfoliation and the sample was mounted on a tantalum (Ta) sample holder. The WSe<sub>2</sub>/Ta sample was gently annealed and sputtered under ultrahigh vacuum (UHV) conditions to increase the defect inventory. Results shown here will highlight the reactivity of methanol as a probe molecule using UHV-TPD on WSe<sub>2</sub>/Ta. Methanol/Ta control experiments showed a shift to higher desorption temperature (192 to 237 K) after the sample anneal temperature was increased from 473 to 673 K. Similarly, on WSe<sub>2</sub>/Ta after annealing, methanol desorption temperatures increased from 168 to 200 K, indicating a potential alloying of WSe<sub>2</sub> with Ta. The WSe<sub>2</sub> surface was gently sputtered via Ar<sup>+</sup> bombardment and the desorption temperature of the methanol/WSe<sub>2</sub> peak (120-140 K) increased as sputter energy increased for similar methanol coverages. These results indicate that ion bombardment increased the defect inventory of WSe<sub>2</sub> without alloying. Future microscopy studies will link the geometric changes induced by sputtering WSe<sub>2</sub> to the shift in methanol binding energies, lending insight into the structure/stability relationships of TMD defects.

**UN-ThP-22 Enhancing the Selectivity of Acetaldehyde Formation Using a Copper-based Model Catalyst, Joseph Loiselet, E. Schell, A. Galgano, A. Baber,** James Madison University

Acetaldehyde is a common intermediate in many industrial chemical syntheses. Current methods of acetaldehyde formation are inefficient and wasteful, leading to low product yields and unwanted by-products. In order to improve acetaldehyde yield and minimize other products, the dry dehydrogenation and dehydration of ethanol was observed using temperature programmed desorption (TPD). These reactions occurred on flat, roughened, and oxidized Cu(111) surfaces under ultrahigh vacuum (UHV) conditions. The reaction of ethanol over each surface was studied, and the oxidized Cu(111) most readily formed acetaldehyde and hydrogen at 350 K. A second reaction pathway formed ethylene and water at 350 K. The selectivity for acetaldehyde production was maintained over 80% throughout consecutive TPDs, yet the yield decreased continuously as the surface became less oxidized. Future experiments will study the reactivity of a partially oxidized Cu(111) sample using UHV-TPD.

**UN-ThP-23 Understanding CO Binding Trends for CO<sub>2</sub> Reduction Catalyst Optimization, Erin Schell, J. Loiselet, A. Galgano, A. Baber,** James Madison University

In the past century, there has been a drastic increase of anthropogenic carbon dioxide in the Earth's atmosphere. The excess of this greenhouse gas has dramatic negative effects on the environment such as extreme weather patterns, poorer air quality, and a rise in global temperatures. Studying the thermodynamics of the formation of carbon dioxide (CO<sub>2</sub>) is a crucial component to combat this obstacle. Cu-based catalysts are the industrial standard for the reduction of CO<sub>2</sub>. One mechanism for CO<sub>2</sub> reduction first produces CO as an intermediate, however the binding of CO to metal sites inhibits further CO<sub>2</sub> reduction. Therefore CO binding must be minimized to promote the efficient reduction of CO<sub>2</sub>. This is a detailed study of the adsorption and reaction of CO on a Cu(111) surface. A clean Cu(111) sample was prepared under ultrahigh vacuum (UHV) conditions and exposed to varying pressures of carbon monoxide as well as a sputtered Cu(111) sample, and an oxidized Cu<sub>2</sub>O/Cu(111) sample. Temperature programmed desorption experiments were done on each of the prepared samples. Defects imposed by sputtering formed higher energy

CO adsorption sites, whereas oxidized surfaces decrease the stability of CO binding. Therefore the oxidized Cu(111) surfaces play an important role in minimizing CO poisoning on Cu catalysts.

**UN-ThP-24 Comparatively Testing CO Oxidation on Rh-Doped and Pt-Doped Copper-Based Catalysts**, *Maggie Rickman, G. Miller*, Washington State University; *V. Çinar*, Tufts University; *I. Waluyo*, Brookhaven National Laboratory; *E. Sykes*, Tufts University; *J. McEwen*, Washington State University

The production of carbon monoxide (CO) at low temperatures, from incomplete combustion, is a prominent issue due to its effects of acting as a poison. One way to counteract this is through single-site catalyst that aids in its conversion at low temperatures. Previous work in the literature has extensively investigated the use of precious metals for this reaction, but this becomes increasingly costly. The use of precious metal nanoclusters also binds CO too strongly at low temperatures, which causes the catalyst to deactivate. An alternative is to design a catalyst in which the precious metal is atomically dispersed. Such a catalyst has been shown to have low temperature catalytic performance when Pt is atomically dispersed and deposited on a Cu surface oxide support [1]. We have compared the mechanistic pathways of such a single-site catalyst to when Pt is incorporated into the underlying Cu(111) surface to form a single atom alloy [2]. The oxidation of CO is also tested where a cluster of Rh atoms forms an alloy with the underlying Cu(111) surface for which a Cu oxide layer is grown over it. We further test the activation of H<sub>2</sub> on such systems, where Rh is placed at its most energetically favorable position on the oxide layer. We compare the energetic pathways when Rh is adsorbed next to an oxygen adatom in the oxide layer to determine its effect on the dissociative adsorption of H<sub>2</sub>. The optimized versions of these structures were calculated via Density Functional Theory (DFT) calculations using the Vienna ab initio Simulation Package (VASP). We then used Nudged Elastic Band (NEB) calculations to model the kinetic barriers. Once the initial test of the Pt/Cu surface completes, we will be able to compare and contrast how it acts as a catalyst relative to Rh. We have been able to produce the kinetic pathways for Rh single atom alloys as well as Rh clusters to see which is more favorable for CO oxidation. This will allow us to move forward for the rational design of catalysts for the activation of CO in the presence of H<sub>2</sub>.

[1] Therrien, A. J. *et al.* An atomic-scale view of single-site Pt catalysis for low-temperature CO oxidation. *Nat Catal.* **1**, 192–198 (2018).

[2] Schilling, A. C. *et al.* Accelerated Cu<sub>2</sub>O Reduction by Single Pt Atoms at the Metal-Oxide Interface. *ACS Catal.* **10**, 4215–4226 (2020).

**UN-ThP-25 Deconvoluting information-rich Ga(I) X-ray adsorption near-edge spectroscopy features from first principles**, *Grace Miller*, Washington State University; *C. Huang*, Carleton College; *S. Scott*, University of California at Santa Barbara; *J. McEwen*, Washington State University, Pacific Northwest National Laboratory

Due to the high demand of propylene, it is appealing to look at replacing Pt- and Cu-based catalysts for propane dehydrogenation. In this regard, an attractive alternative are Ga-based compounds. X-ray Adsorption Near-Edge Spectroscopy (XANES) contains information about the coordination environment and the oxidation state of Ga under reaction conditions. In our previous work, we deconvoluted the experimental features of Ga(III) compounds [1]. Since Ga(I) and Ga(III) compounds are both involved in propane dehydrogenation, we benchmark the spectral features of Ga(I) compounds in this work. We compare the calculations derived from structures based on *Li et al.* [2] to three additional Ga(I) structures (Ga(Si(SiMe<sub>3</sub>)<sub>3</sub>)<sub>4</sub>), (Ga(C(SiMe<sub>3</sub>)<sub>3</sub>)<sub>4</sub>), ((Ga<sub>2</sub>Br<sub>3</sub>)<sub>6</sub>NET) to further deconvolute the XANES features. Based on the literature, the XANES features with higher intensities correspond to Ga(I) oxidation states while the XANES features with lower intensities correspond to Ga(III) oxidation states. Using the CASTEP code with a Perdew-Berkeby-Erzenhoff (PBE) functional, we simulate the XANES from first principles. We further compare the Ga(III) features of our compounds to what has been identified previously in the literature [1]. Interestingly, two bulk Ga(I) structures did not have the high-intensity feature as was identified in the other Ga(I) compounds. The study is ongoing where we are quantifying interaction energy between Ga(I) cations within these structures, where our initial results indicate that the interaction energy between them is attractive.

[1] Groden, K. *et al.* First-Principles Approach to Extracting Chemical Information from X-ray Absorption Near-Edge Spectra of Ga-Containing Materials. *J. Phys. Chem. C* **125**, 27901–27908 (2021).

[2] Li, L., Chalmers, J. A., Bare, S. R., Scott, S. L. & Vila, F. D. Rigorous Oxidation State Assignments for Supported Ga-Containing Catalysts Using

Theory-Informed X-ray Absorption Spectroscopy Signatures from Well-Defined Ga(I) and Ga(III) Compounds. *ACS Catal.* **13**, 6549–6561 (2023).

**UN-ThP-26 A Computational Investigation of the Urea Oxidation Reaction Mechanism Using Density Functional Theory: Promoting the NiOOH Active Phase by Introducing Effective Metal-Dopants**, *Matteo Garcia-Ortiz, Q. Jin, L. Árnadóttir*, Oregon State University

Urea electrochemical oxidation is of general interest for water treatment in agriculture, but also a possible fuel for urea fuel cells. Urea oxidation is also of fundamental interest for amide chemistry. The urea oxidation reaction (UOR) in alkaline medium neutralizes urea into relatively benign products including H<sub>2</sub>, N<sub>2</sub>, and CO<sub>2</sub>, rather than harmful NO<sub>x</sub> compounds. Previous studies have suggested direct and indirect reaction routes for this full oxidation. The presence of metallic ions such as Fe, Co, and Cu in the nickel hydroxide surface may improve selectivity towards the indirect pathway where the Ni(OH)<sub>2</sub>/NiOOH redox couple plays an important role. Since NiOOH is the active phase for UOR, the first step of transferring Ni(OH)<sub>2</sub> to NiOOH is crucial. In this work, we investigate the effect of Fe dopant on the Ni hydroxide transformation. Performing DFT calculations, as implemented in the Vienna Ab initio Simulation Package, the thermodynamics of the nickel dihydroxide to nickel oxyhydroxide mechanism was calculated. We found that doping the β-Ni(OH)<sub>2</sub> surface with Fe significantly reduces the free energy change for sequential surface dehydrogenation to β-NiOOH, from 2.27 eV to 0.93 eV, favoring the creation of UOR active sites. This indicates promising potential for the improvement of urea oxidation performance with Fe doping.

**UN-ThP-27 Advanced Scanning Probe Microscopy and Infrared Nanospectroscopy Characterization of Atomic Layer Deposited and Etched Thin Films**, *Benjamin Bailey, P. Davis*, Boise State University

Scanning probe microscopies are routinely employed for nanoscale materials characterization. In particular, atomic force microscopy (AFM) and associated advanced scanning probe microscopy (SPM) techniques can map nanoscale surface topography and morphology as well as provide insight into electrical, magnetic, and mechanical properties. More recently, with the development of AFM-IR, AFM can be combined with infrared (IR) spectroscopy to provide chemical identification with <10 nm resolution. Here, we report AFM characterization of atomically thin films created through metal-organic chemical vapor deposition (MOCVD), atomic layer deposition (ALD) of layered two-dimensional (2D) semiconductors such as MoS<sub>2</sub> and WSe<sub>2</sub>. High resolution AFM is used to characterize ALD film quality and morphology, while advanced SPM modes are employed to measure electrical properties of interest. Additionally, AFM-IR is brought to bear to provide insight into the use of atomic layer etching (ALE) for these materials. These results hold promise for advancing the characterization and integration of novel 2D materials into semiconductor device manufacturing.

**UN-ThP-28 Towards in-Situ Transmission FTIR of ALD Systems**, *Anthony Donegan, S. Hues, E. Graugnard*, Boise State University

An apparatus was constructed which allowed a Nicolet Magna 550 Fourier Transform Infrared Spectrometer (FTIR) to interface with an industrial Atomic Layer Deposition (ALD) furnace. Aluminum Zinc Oxide films were grown using ALD. The resulting films were characterized through in-situ FTIR. Significant noise was introduced by the method of interfacing the FTIR with the ALD furnace. The film produced little to no absorbance and the resulting signal showed no indication of chemical changes which could not be attributed to random noise. Guidelines to reduce noise and signal loss in future similar experiments were provided.

**UN-ThP-29 Gas-Phase Analysis of Plasma-Enhanced Modification of Silk Films**, *Mollie Corbett, B. Yashkus, J. Blechle*, Wilkes University

Silk fibroin's range of mechanical properties make it a viable option for use in tailored medical devices, but its uncontrolled biological lifespan poses a significant challenge in creating these various types of devices. To combat this issue, the wettability can be altered to promote or inhibit enzymatic interactions, resulting in predictable material degradation. Plasma-enhanced chemical vapor deposition (PECVD) has been shown to be an effective method in altering the wettability of silk films via water contact angle goniometry results. Because little is known about the chemical mechanisms which make these modifications possible, an improved understanding of gas phase interactions can aid in ensuring reproducible surface modifications.

One way to combat this issue is utilizing optical emission spectroscopy (OES), which is an effective way to monitor the plasma during the treatment process. Mechanistic information is gleaned by analyzing the gas

# Thursday Evening, November 9, 2023

phase species with and without the presence of silk. Specifically, density and temperature measurements can be determined from plasma emission and are used to provide better insight into the gas-surface interface.

Acrylic acid and pentane precursors are used, as they have been shown to successfully deposit hydrophobic or hydrophilic films on silk materials. For ease of comparison, all treatments lasted 30 s at 65 W with a total system pressure of 75 mTorr, utilizing a 10% (by pressure) argon addition to serve as both a carrier gas and actinometer.

Molecular nitrogen emission was observed in all plasmas containing silk, indicating possible etching of the surface. Additionally, molecular H<sub>2</sub> bands were observed in both pentane and acrylic acid spectra. Acrylic acid plasmas also contained molecular bands for CO, CO<sub>2</sub><sup>+</sup>, and OH. Excluding argon and hydrogen, all other expected atomic transitions (such as carbon and oxygen) remained absent through all pentane and acrylic acid plasmas. Density measurements indicate a slight increase in the concentrations of all observed species upon the addition of silk. The concentrations of all species, excluding nitrogen, were calculated to have increased by a factor of ~1.5 to 2.0. Vibrational temperature measurements of CO were determined to be 943 ± 13 K, while the temperature of H<sub>2</sub> increases by an order of magnitude.

Using gas phase measurements, we can gain insights to better understand the success demonstrated by PECVD in silk film modification. Recognizing the mechanisms of the changing surface chemistry can assist in making fine procedural adjustments, helping to achieve more consistent results in altering silk to control its lifetime without impacting its bulk properties.

## **UN-ThP-30 Quantifying Oxygen Diffusion in Epitaxial SrTiO<sub>3</sub> Thin Films, Sihang Hui, University of Florida, Gainesville**

Emerging technologies such as magneto-ionic memory devices, fuel cells, and resistive switches rely heavily on the oxygen migration through thin films [1,2]. Such a device's performance requires precise control and understanding of oxygen diffusion [3]. These diffusion mechanisms and oxygen barriers are imposed in part by the design of strain and interface symmetry of the heterostructures. However, due to the difficulty of measuring small concentrations of oxygen ions (~1 at%) moving through nanoscale distances, the diffusion rates of oxygen ions in these heterostructures are not well characterized. This project focuses on developing a method to better measure and understand the migration rates and barriers of oxygen ions in oxide thin films using X-ray reflectometry (XRR). While XRR methods for measuring diffusion exist for superlattice structures [4], the focus here is on enabling such measurements in single layer epitaxial films, which would greatly expand the utility and accessibility of the method.

Our approach uses a nanoscale diffusion couple composed of an epitaxial layer of perovskite SrTiO<sub>3</sub> (STO) thin film using the pulsed laser deposition (PLD) process and capped with a metal gettering layer (e.g., Ta) and an atmospheric protection layer (e.g., Pt). In-situ annealing experiments were conducted to promote diffusion. To quantify the diffusion at the interface, XRR measurements were collected and fit to one-dimensional chemical depth-profile models before and after the anneal. From there, a diffusion coefficient for each annealing condition can be calculated from a fit to the oxygen profile shape [5]. Figure 1a shows an example of an X-ray reflectivity (XRR) scan before and after an annealing procedure near our low-temperature-time bound. Post-annealing, there are changes in the reflectivity curve for  $Q \geq 0.15 \text{ \AA}^{-1}$  that can be fit to a small change in the Ta/STO interface roughness.

References [1] F. Zahoor, et al., *Nanoscale Res. Lett.* 15 (2020) 90 [2] M. Nichterwitz, et al., *APL Mater.* 9 (2021) 030903 [3] F. Gunkel, et al., *Appl. Phys. Lett.* 116 (2020) 120505 [4] F. Yang, et al., *ACS Omega* 8 (2023) 27776 [5] S. Brennan, et al. *Metall. Mater. Trans. A*, 43 (2012) 4043

## **UN-ThP-31 Understanding the Role of the Interface in Thermoelectric Materials, Eli Robinson, Z. Irving-Singh, J. Sanders, R. Brown, W. Kim, P. Hall, N. Coates, University of Portland; J. Heath, Reed College**

A thermoelectric material is able to convert waste heat into usable electricity. A typical thermoelectric consists of inorganic semiconductors. Newer classes of thermoelectrics are instead composed of organic-inorganic composites, which offer the advantage of being solution-processable for greater ease and lower cost of fabrication. Here, we studied how the interface of a composite thermoelectric comprising gold nanoparticles and PEDOT:PSS influences its thermoelectric figure of merit. In order to better understand this interfacial component, samples of Au nanoparticles were mixed with PEDOT:PSS in varying volume fractions.

These samples were then prepared for various analytical methods, with emphasis on SEM imaging and TGA analysis.

## **UN-ThP-32 Ex-Situ Synthesis and Characterization of PEDOT:PSS-Au NP Composite Thermoelectrics, Won Sung Kim, J. Sanders, E. Robinson, Z. Irving-Singh, R. Brown, P. Hall, N. Coates, University of Portland; J. Heath, Reed College**

Thermoelectrics offer significant promise in addressing society's demand for advancements in energy conversion and storage technologies. The interface between hybrid organic/inorganic films comprising poly(3,4-ethylenedioxythiophene):polystyrene sulfonate (PEDOT:PSS) and PSS-coated gold nanoparticles (AuNPs) plays a critical factor in thermoelectric properties. We hypothesize that the size, shape, and surface chemistry of the AuNPs influence the total interfacial area, energy, and thickness. To fine-tune these interfacial properties, we used an ex-situ approach to precisely control the shape (prisms, rods, spheres) and volume fraction of AuNPs in PEDOT:PSS@AuNP films. SEM images revealed that this method enables reproducible control over the volume fraction of AuNPs, and surface enhanced Raman spectroscopy (SERS) provided additional details about the chemical composition of the interface.

## **UN-ThP-33 Stabilization of Amidines and Imidoyl Amidine Ligands, A. Peoble, Michaela Martinez, R. Castañeda, New Mexico Highlands University**

Imodiamidines are prospective nitrogen-based ligand frameworks with the opportunity to adopt two chelate coordination modes, bidentate and tridentate. These coordination modes are advantageous for binding to various metal ions, by which multiple applications can be derived. Among such possible applications, imodiamidines can be used as a starting material in Magnetic Resonance Imaging (MRI) contrasting agents. Our research focuses specifically on the synthesis of N-2-pyridylimodyl-2-pyridylamidine (Py<sub>2</sub>ImAm), and N-2-pyrimidylimodyl-2-pyrimidylamidine (Pm<sub>2</sub>ImAm) and its metastable form N-2-pyrimidylamidine (Pm<sub>2</sub>Am). All three ligands have been successfully synthesized, however, only Py<sub>2</sub>ImAm is a stable compound. Pm<sub>2</sub>ImAm and Pm<sub>2</sub>Am decompose over time, which hinders the possibilities of large-scale production, long-term storage, and overall utilization. As such, we are currently investigating stabilization procedures for Pm<sub>2</sub>ImAm and Pm<sub>2</sub>Am, one of which is transforming the ligands into stable salts. Thus far, we have been successful in synthesizing a stable discrete-hydrogen bond dimer with trifluoroacetic acid and Pm<sub>2</sub>Am. Currently, we are attempting other possible anions for the stabilization of these ligands as salts, while also testing their solubility and stability.

# Friday Morning, November 10, 2023

## 2D Materials Technical Group

### Room C123 - Session 2D+EM-FrM

#### 2D-Materials: Device Application

**Moderators:** Maria Hulse, Pennsylvania State University, **Tongcang Li**, Purdue University

#### 8:20am 2D+EM-FrM-1 Stochastic Computing Enabled by 2D Memtransistors, **Saptarshi Das**, Pennsylvania State University **INVITED**

In the emerging era of artificial intelligence, deep learning, and Big-data, the energy and hardware investments required for conventional high-precision digital computing are becoming increasingly unsustainable. As a result, there is a growing need for a new paradigm that prioritizes energy and resource efficiency over precision for many computing applications. Stochastic computing (SC) is a promising alternative because it can perform basic arithmetic operations using simple logic gates, unlike digital computers that require many logic gates and a high transistor volume. However, the hardware investment necessary to generate stochastic bits (s-bit), the fundamental computing primitive for SC, has hindered its widespread adoption. While traditional silicon complementary metal oxide semiconductor (CMOS) technology can accelerate SC, it still requires extensive hardware investment. Memristor and spin-based devices offer natural randomness but rely on hybrid designs involving CMOS peripherals, which increase the area and energy burden.

To overcome these limitations, we have developed a standalone SC architecture embedded in memory based on two-dimensional (2D) memtransistors. This monolithic and non-von Neumann SC architecture requires only a tiny amount of energy (< 1 nano Joules) for s-bit generation and to perform arithmetic operations, and occupies a small hardware footprint, highlighting the benefits of SC. Additionally, the researchers demonstrate the acceleration of Bayesian inference using their SC platform.

#### 9:00am 2D+EM-FrM-3 Electrical Characteristics of Semi-Metallic 2H-NbSe<sub>2</sub> for Scalable Interconnects, **Abir Hasan**, T. Alem, C. Rogers, S. Stevenson, S. McDonnell, N. Shukla, University of Virginia

Despite Copper being the current material of choice for interconnect technology, it suffers from increased resistivity at scaled dimensions and the necessity for a barrier-liner to prevent diffusion. This has motivated the exploration of alternate materials that can overcome these limitations for scaled CMOS technology nodes. Metallic 2D materials can offer a promising option. In this work, we evaluate the properties of 2D semi-metallic material 2H Niobium diselenide (2H-NbSe<sub>2</sub>) as a candidate for realizing highly scalable interconnect technology without the need for barrier-liner. We performed detailed electrical characterization evaluating the dimensional scaling, dependence of the resistivity on temperature, device lifetime, effect of encapsulation layer etc. on ribbon devices fabricated with 2H-NbSe<sub>2</sub> material. 2H-NbSe<sub>2</sub> showed negligible change in resistivity compared to the bulk value when scaled down to thicknesses less than 15 nm. High current density transport measurements are performed on 2H-NbSe<sub>2</sub> ribbon devices with varied width (0.1-1um) at elevated temperature (>= 100°C) to assess the reliability and failure characteristics. Lifetime of the NbSe<sub>2</sub> ribbons improved when an Al<sub>2</sub>O<sub>3</sub> encapsulation layer was used. Our work provides critical insights into the potential of NbSe<sub>2</sub> for realizing scalable interconnects.

#### 9:20am 2D+EM-FrM-4 Magneto-Transport Measurement and Maximum Entropy Mobility Spectrum Analysis in Semiconductor Substrates for Graphene Growth, **Ruhin Chowdhury**, University of New Mexico; A. Majeed, Intel Corp.; E. Renteria, D. Ghosal, University of New Mexico; M. Arnold, M. Lagally, University of Wisconsin - Madison; F. Cavallo, University of New Mexico

Our study focuses on the multi-carrier electrical transport characterization of heat-treated bulk Ge near its melting point. Single-crystalline Ge has recently gained relevance as a substrate for the chemical vapor deposition (CVD) of high-quality graphene sheets, nanowires, and nanoscale wigglers.<sup>1,2</sup> Deposition of graphene on (110) Ge substrates allows integration of a 2D sheet with widely used semiconductors without the need for release and transfer processes, which may lead to the degradation of graphene's structural and functional properties. Determining the full potential of graphene/Ge for electronic applications requires understanding charge transport in this material combination. To date, quantitative models of lateral charge transport in graphene/Ge (i.e., transport of mobile carriers in the direction parallel to the graphene/Ge interface) are not available, primarily due to the overwhelming contribution of bulk Ge. In this work, we

isolated and identified all mobile carrier types undergoing drift in heat-treated Ge at the typical condition for CVD of monolayer graphene. We believe these results to be the basis for quantifying carrier mobilities, carrier concentrations, and carrier types in graphene/Ge.

We performed magneto-transport measurements of heat-treated Ge between 50 K and 400 K and a magnetic field spanning from -7T to 7T to extract the conductivity tensor of the material. The Ge substrates were nominally intrinsic before annealing. Next, we used maximum entropy mobility spectrum analysis (MEMSA)<sup>3</sup> to identify the carrier types contributing to transport in Ge (110). Our analysis consistently shows the contribution of heavy holes (HH) and light holes (LH) in bulk Ge. The excess holes in bulk Ge are attributed to the formation of acceptor-like vacancies during high-temperature annealing of Ge.<sup>4</sup> The trend of carrier mobility vs. temperature indicates that different scattering mechanisms are dominant for HH and LH in a given temperature range. In addition to the contribution of HH and LH in bulk Ge, we identified two additional carrier types, namely electron and ultra-low mobility holes. We attribute the electrons to donor-type interstitials and the low-mobility holes to accumulated HH near the native oxide/Ge interface.

**ACKNOWLEDGMENT.** This work was supported by the U.S. AFOSR and Clarkson Aerospace Corporation under award No. FA9550-21-1-0460/UNM 21-1-0460.

[1] B. Kiraly, et al. Nano Lett. 15, 11, 7414–7420 (2015)

[2] R.M. Jacobberger et al. Nat. Commun. 6, 8006 (2015)

[3] Kiatgamolchai, S., et al. Phys Rev E Stat Nonlin Soft Matter Phys 66(3 Pt 2B): 036705 (2002)

[4] S. Mayburg, Phys. Rev. 95, 38 (1954).

#### 9:40am 2D+EM-FrM-5 What Are 2D Materials Good for?, **E. Pop**, **Tara Pena**, Stanford University **INVITED**

This talk will present my (biased!) perspective of what two-dimensional (2D) materials could be good for. For example, they could be good for applications where their ultrathin nature gives them distinct advantages, such as flexible electronics [1] or light-weight solar cells [2]. They may not be good where conventional materials work sufficiently well, like transistors thicker than a few nanometers. I will focus on 2D materials for 3D heterogeneous integration of electronics, which presents major advantages for energy-efficient computing [3]. Here, 2D materials could be monolayer transistors with ultralow leakage [4] (due to larger band gaps than silicon), used to access high-density memory [5]. Recent results from our group [6,7] and others [8] have shown monolayer transistors with good performance, which cannot be achieved with sub-nanometer thin conventional semiconductors, and the 2D performance could be further boosted by strain [9]. I will also describe some unconventional applications, using 2D materials as thermal insulators [10], heat spreaders [11], and thermal transistors [12]. These could enable control of heat in “thermal circuits” analogous with electrical circuits. Combined, these studies reveal fundamental limits and some unusual applications of 2D materials, which take advantage of their unique properties.

**Refs:** [1]A. Daus et al., Nat. Elec. 4, 495 (2021). [2] K. Nassiri Nazif, et al., Nat. Comm. 12, 7034 (2021). [3] M. Aly et al., Computer 48, 24 (2015). [4]

# Friday Morning, November 10, 2023

C. Bailey et al., EMC (2019). [5] A. Khan et al. Science 373, 1243 (2021). [6] C. English et al., IEDM, Dec 2016. [7] C. McClellan et al. ACS Nano 15, 1587 (2021). [8] S. Das et al., Nat. Elec. 4, 786 (2021). [9] I. Datye et al., Nano Lett. 22, 8052 (2022). [10] S. Vaziri et al., Science Adv. 5, eaax1325 (2019). [11] C. Koroglu & E. Pop, IEEE Elec. Dev. Lett. 44, 496 (2023). [12] M. Chen et al., 2D Mater. 8, 035055 (2021).

10:40am **2D+EM-FrM-8 Effect of Temperature on the Surface Morphologies of Sulfurized-Grown WS<sub>2</sub>**, *Md Samim Reza, M. Singh*, Indian Institute of Technology Delhi, India

Tailored morphologies are essential for realizing the diverse applications of tungsten disulfide. This work reports on a successful growth of WS<sub>2</sub> that involves the sulfurization of a sputter-deposited (Angstrom Engineering Evovac) thin film of tungsten (150-300 Å with a rate of 0.4 Å/s) on a SiO<sub>2</sub> substrate (University Wafers) and the effect of temperature on the surface morphology of as-grown WS<sub>2</sub>. The as-deposited tungsten substrate was cut into 2cm x 2cm and placed inside a custom-design horizontal CVD system (Quazar Technologies). A sulfur (99.5% pure precipitated powder, 600-1000 mg, Sigma Aldrich) was placed upstream (20-40 cm) from the tungsten heating zone (700-1000 °C) to grow WS<sub>2</sub> under a carrier gas (Ar) flow of 0-400 sccm. Raman spectroscopy (514 nm laser source with a spot size of ~1 μm<sup>2</sup> for 100x objective, 1mW power, Renishaw inVia) revealed the peaks at ~350/cm and ~417/cm, confirmed the growth of WS<sub>2</sub> and the peak intensity ratio of in-plane and out-of-plane ( $E_{2g}^1/A_{1g}$ ) < 1, suggest a multilayer growth [1]. The X-ray diffraction (Rigaku Ultima IV) analysis indicates the growth of hexagonal-phased WS<sub>2</sub> (JCPDS: 08-0237) with a mixed plane to a (002)-dominated at higher temperatures. The field emission scanning electron microscopy (Magna LMU, Tescan) scans revealed the growth morphology from a planar to a nanoflower, forming a thin film of WS<sub>2</sub>. Different sulfurization temperatures result in distinct morphologies, with a thin film morphology obtained at 700-750°C, followed by the dominance of nanoflower-like WS<sub>2</sub> structures between 850°C and 950°C as observed by field emission scanning electron microscopy. At temperatures higher than 950°C, WS<sub>2</sub> nanoflowers with vertical alignment are grown on a SiO<sub>2</sub> substrate. Electron dispersive X-ray (EDX, Ametek) spectra show a stoichiometry close to 1:2 for W: S. The atomic force microscope analysis (Dimension Icon, Bruker) revealed that surface roughness (sputter-deposited tungsten roughness of ~80 nm) increased from ~5 to 80 nm with the growth temperature. The experimental results emphasize the importance of temperature in determining the surface morphologies of WS<sub>2</sub>. The ability to control the growth temperature offers customization of WS<sub>2</sub> morphologies that could allow the fabrication of WS<sub>2</sub>-based devices with the desired properties [2-3].

[1] Berkdemir et al., Scientific Reports, 3, 1755 (2013)

[2] Sebastian et al., Nature Communications 12, 693 (2021)

[3] Li et al., The Journal of Physical Chemistry C, 126(22), 9293-9303.

11:00am **2D+EM-FrM-9 The Study of Internal Ion Transport in Ionic CuiP<sub>2</sub>S<sub>6</sub>**, *Yujie Sun, B. Liu*, Tsinghua University, China

Memristor-based neuromorphic computing is promising for artificial intelligence. However, most of the reported memristors have limited linear computing states and consume large operation energy which hinder their applications. Herein, we report a memristor based on ionic two-dimensional CuiP<sub>2</sub>S<sub>6</sub> (2D CIPS), in which up to 1350 linear conductance states are achieved by controlling the migration of internal Cu ions in CIPS. In addition, the device shows a low operation current of ~100 pA. Cu ions are proven to move along the electric field by *in-situ* scanning electron microscopy and energy dispersive spectroscopy measurements. Furthermore, complex signal transport among multiple neurons in the brain is imitated by 2D CIPS-based memristor arrays. Our results offer a new platform to fabricate high-performance memristors based on ion transport in 2D materials for neuromorphic computing.

## Atomic Scale Processing Mini-Symposium

### Room C124 - Session AP+PS-FrM

#### Atomic Scale Processing Late Breaking Atomic Layer Etching and Area Selective Deposition

Moderator: Eric Joseph, IBM T.J. Watson Research Center

8:20am **AP+PS-FrM-1 Atomic Layer Etching of SiO<sub>2</sub> via H<sub>2</sub>/SF<sub>6</sub> Plasma and TMA**, *David Catherall, A. Minnich*, California Institute of Technology

The quality factor of ultrahigh Q silica microdisk resonators has reached values exceeding one billion but remains at around an order of magnitude

below intrinsic upper limits due to surface-roughness scattering. Atomic layer etching (ALE) has potential to mitigate this scattering because of its ability to smooth surfaces to sub-nanometer length scales. Here, we report an ALE process for etching of SiO<sub>2</sub> using sequential exposures of TMA and Ar/H<sub>2</sub>/SF<sub>6</sub> plasma. The Ar/H<sub>2</sub>/SF<sub>6</sub> plasma has been reported to enable *in-situ* production of HF, enabling HF exposures in the ALE process without the need for an external source of HF vapor. We observe etch rates up to 0.6 Å per cycle and examine the effect on surface roughness. This work advances a process of relevance to ultrahigh Q silica resonators which are fundamental elements of on-chip photonic devices such as frequency combs.

8:40am **AP+PS-FrM-2 Area Selective Deposition of HfO<sub>2</sub> on Oxide and Nitride Surfaces**, *ByungChan Lee*, Incheon National University, Republic of Korea; *C. Nguyen*, Incheon National University, Viet Nam; *S. Shim, Y. Kang, H. Lee*, Incheon National University, Republic of Korea

Due to the scaling down in the Si device fabrication, the aspect ratio and complexity of 3D device structures is rapidly increased, leading to the limitation of the conventional fabrication process including deposition, etching, lithography and so on. Area selective deposition (ASD) has received great attentions from the Si industry as one of the unit processes to overcome the limitations. ASD is developed based on the atomic layer deposition (ALD) which has the unique self-saturation surface reaction mechanism. The surface chemical properties are modified by using the promoter or inhibitor which promotes or inhibits the thin film growth, respectively. Accordingly, the ALD thin films are selectively deposited on the desired area. At the beginning of the ASD research, the self-assembled monolayers (SAMs) were commonly used as an inhibitor. But the inherent size of SAMs has potential problems for the pattern interference in nm-size scale. In this study, we investigated the ASD using a small molecule inhibitor (SMI). We selected the aldehyde molecules as SMI to inhibit the nitride surface but not on oxide surface. By using density functional theory (DFT) calculation, adsorption behaviors and energetics of the aldehydes was studied on nitride and oxide surfaces. From the experiments, it was observed that the aldehyde selectively adsorbs on only nitride surface but not on oxide surface and block the HfO<sub>2</sub> deposition until 15 cycles. The inhibition of nitride surface using SMI can contribute to many unit processes of Si device fabrication by simplifying the process scheme.

9:00am **AP+PS-FrM-3 Surface Functionalization of SiN<sub>x</sub> over SiO<sub>2</sub> with Aldehydes to Enable Area-Selective Atomic Layer Deposition**, *Andrew Kaye*, Colorado School of Mines, USA; *S. Agarwal*, Colorado School of Mines; *B. Zope, A. Derecskei, R. Pearlstein, X. Lei*, EMD Electronics, USA

As the semiconductor device dimensions continue to shrink, area-selective atomic layer deposition (AS-ALD), which is a bottom-up technique, can address the challenges associated with device fabrication. SiO<sub>2</sub> and SiN<sub>x</sub> are two of the most commonly used dielectrics in semiconductor devices, and deposition on one dielectric with minimal deposition on the other can simplify processing. For example, in 3D-NAND structures, there are alternating layers of SiO<sub>2</sub> and SiN<sub>x</sub>, and during processing, it is desirable to grow a metal oxide on SiO<sub>2</sub> with no growth on SiN<sub>x</sub>. In AS-ALD, inhibitor molecules can be used to functionalize SiN<sub>x</sub>, because very few ALD precursors have an inherent binding selectivity to SiO<sub>2</sub> over SiN<sub>x</sub>. Finding inhibitor molecules that selectively adsorb on SiN<sub>x</sub> over SiO<sub>2</sub> is also challenging since on SiO<sub>2</sub> films contain SiOH groups, which react readily with many compounds such as chlorosilanes, alkoxides, and aminosilanes. We have previously shown that aldehydes selectively adsorb on SiN<sub>x</sub> with minimal adsorption on SiO<sub>2</sub>.

This work focuses on the adsorption mechanisms of two aldehydes, 3,5,5-trimethylhexanal (TMH) and dodecanal (DDA), on plasma-deposited SiN<sub>x</sub> films characterized with *in situ* attenuated total reflection Fourier transform infrared spectroscopy. We show that TMH adsorbs on SiN<sub>x</sub> forming silyl ethers, amino alcohols, enamines, and imines with surface -SiH<sub>x</sub> and -NH<sub>x</sub> groups being the reactive sites. Reaction of DDA with SiN<sub>x</sub> leads to the formation of similar surface species except for enamines. Amino alcohols are reaction intermediates formed due to the reaction of surface amines with aldehydes — the complete reaction should result in the formation of imines with H<sub>2</sub>O as the byproduct. The presence of amino alcohols is not desirable since the -OH group may react with metal ALD precursors and reduce selectivity. We show that once the amino alcohols are formed on the surface, they cannot be converted to imines by increasing the substrate temperature. The surface composition of the underlying SiN<sub>x</sub> film greatly affects the uptake of the aldehyde and the relative ratio of the surface

# Friday Morning, November 10, 2023

species formed after adsorption of both aldehydes. The aldehydes desorb from the surface when the substrate temperature is increased, and further desorption occurs over time at elevated temperatures. After desorption at a constant temperature, TMH can be replenished by redosing. In practical applications the SiN<sub>x</sub> surface is partially oxidized upon exposure to the atmosphere. To understand the effect of surface oxidation, the plasma-deposited SiN<sub>x</sub> films were exposed to the atmosphere for several days. The atmosphere exposed SiN<sub>x</sub> films were then cleaned with D<sub>2</sub> plasma to possibly etch the surface oxide layer to enhance reactivity by restoring -SiD<sub>x</sub> and -ND<sub>x</sub> surface species.

9:20am **AP+PS-FrM-4 Surface Reactions During Atomic Layer Etching of Platinum by High-Density Nitrogen-Oxygen Plasma and Organic Acid Vapor**, *Thi-Thuy-Nga Nguyen*, Nagoya University, Japan; *D. Akagi, T. Uno, T. Okato*, AGC Inc., Japan; *K. Ishikawa, M. Hori*, Nagoya University, Japan  
Anisotropic patterning process of metal layers in complex nanostructures is a big challenge. Pt is a promising material, but it is a hard-to-etch material. Dry etching of Pt thin film has been developed by using halogen-based plasmas of SF<sub>6</sub>, CF<sub>4</sub>, or Cl<sub>2</sub> gas. However, the anisotropic etch profiles of Pt films in most cases have not achieved due to the redeposition of the etch residues that produces fences or tapered sidewall. Recently, non-halogen chemistry for noble metal etching has been developed using atomic layer etching (ALE) with surface modification by oxidation and removal of the oxide layer by vapor of organic compounds [1].

Our developed floating wire-assisted high-density plasma at medium pressure significantly increases the chemical reaction rate to the sample surface, that was applied in the reduction of SnO<sub>2</sub> [2] and dry etching of TiAlC [3]. Here, we have demonstrated ALE of Pt via high-density plasma oxidation and removal of the modified layer by organic acid vapor or organic acid plasma. High-density nitrogen-oxygen based plasma (N-O plasma) was generated to fully oxidize Pt surface and form a dominant oxidation state (Pt<sup>4+</sup>). Surface modifications after the reactions of Pt with N-O plasmas and the modified layer with organic acid vapor or plasma were analyzed by X-ray photoelectron spectroscopy. The film thickness was characterized by ellipsometry and X-ray reflectivity. Surface roughness was analyzed by atomic force microscopy, and patterning profiles were observed by transmission electron microscopy. The N-O plasmas and organic acid plasmas were diagnosed by high-resolution optical emission spectroscopy.

The formation and desorption of organometallic compounds on Pt surface are able to be atomic-level controlled at low temperature (less than 100 °C). A smooth surface of Pt film was obtained with the etch depth per cycle from 0.3 to 0.7 nm/cycle. The exposure of Pt film to N-O plasmas determines the dominant oxidation state, surface roughness, and thickness of the modified layers, that strongly affects to etching performance of Pt film. The non-halogen atomic layer etching of Pt has been successfully developed in this study.

- [1] J. Chang and J.P. Chang, *J. Phys. D: Appl. Phys.* 50, 25 (2017).
- [2] T.T.N. Nguyen et al., *Plasma Process. Polym.* 19, 6 (2022).
- [3] T.T.N. Nguyen et al., *Sci. Rep.* 12, 1 (2022).

9:40am **AP+PS-FrM-5 Isotropic Plasma-Thermal Atomic Layer Etching and in-Situ Atomic Layer Deposition Passivation of Aluminum Films for Superconducting Quantum Devices**, *Haozhe Wang*, Duke University; *I. Chen, D. Catherall, A. Hossain, A. Minnich*, California Institute of Technology  
Metallic and dielectric film surface imperfections negatively impact the performance of superconducting quantum devices, including qubits and microwave kinetic inductance detectors. Despite considerable exploration into the effects of these imperfections on decoherence and low-frequency fluctuations, contemporary microfabrication methodologies fall short in rectifying them. Here, we report an atomic layer etching and in-situ deposition (ALE/ALD) process that enables the etching of the native oxide and passivation of aluminum films, all in high vacuum. The process for both ALE and ALD involves sequential exposures to SF<sub>6</sub> plasma and TMA at temperatures around 300 °C; whether the exposures lead to deposition or etching is controlled by adjusting the duration of each dose at the selected temperature. The resulting films are characterized using x-ray photoelectron spectroscopy, high-resolution transmission electron microscopy, and energy-dispersive spectroscopy. The characterization methods indicate that the ~ 40 Å thick native oxide was removed and the resulting surface passivated with ~ 10 Å of AlF<sub>3</sub>. Using x-ray photoelectron spectroscopy, we confirmed that the films are resistant to re-oxidation after exposure to the atmosphere for nine months. Our approach to engineer

the surfaces of superconducting films at the atomic scale may enable superconducting quantum devices with improved performance.

## Applied Surface Science Division

Room **B117-119** - Session  
**AS+2D+CA+EM+MS+NS+SE+SS+TF-FrM**

### Industrial Applications

**Moderators:** Marko Sturm, University of Twente, Netherlands, Alan Spool, Western Digital Corporation, Yundong Zhou, National Physical Laboratory, UK

8:20am **AS+2D+CA+EM+MS+NS+SE+SS+TF-FrM-1 Correlative Analysis Using Time-of-flight Secondary Ion Mass Spectrometry for Beam Sensitive Samples**, *Jean-Paul Barnes, C. Guyot, P. Hirchenhahn, A. De Carvalho, N. Gauthier, T. Mairandron, B. Gilquin, D. Ratel, C. Gaude, O. Renault*, Univ. Grenoble Alpes, CEA, Leti, France; *A. Galtayries*, Chimie ParisTech, PSL University, CNRS, Institut de Recherche de Chimie Paris, France; *G. Fisher*, Physical Electronics USA; *C. Seydoux, P. Jouneau*, Univ. Grenoble Alpes, CEA, IRIG-MEM, France

**INVITED**

Time-of-flight Secondary Ion Mass Spectrometry (TOF-SIMS) is now widely used for materials analysis in domains such as semiconductor and energy applications. These challenging applications also provide access to well-controlled, custom made samples that have allowed the limits of TOF-SIMS analysis to be identified and helped in the development of correlative analysis approaches. Recent examples include combining AFM measurements with TOF-SIMS depth profiling to correct for sputter rate differences [1] or to measure mechanical or electrical properties and performing X-ray tomography prior to FIB-TOF-SIMS analysis to allow morphological and compositional data from the same volume to be visualized [2]. Currently we are working on two aspects. Firstly improving the quantification and chemical sensitivity of the technique by combining TOF-SIMS with photoemission techniques (XPS or XPEEM), and secondly trying to improve the lateral resolution by correlation with SEM and AFM measurements. Recent examples will be shown for the analysis of beam sensitive organic samples such as OLED devices, brain tissue samples after medical device implantation [3] and symbiotic microorganisms [4]. As well as the correlative aspects between techniques, we will show how tandem mass spectrometry can help in analyzing complex organic samples. In all cases the importance of sample preparation is paramount, especially for biological samples. For example, for the correlation between TOF-SIMS and XPS on OLED samples, a wedge crater protocol has been developed to allow analysis on exactly the same area of the sample whilst minimizing beam damage to the sample. Wedge crater preparation and transfer between instruments is performed under a protected environment (vacuum or inert gas) to avoid unwanted surface modifications.

Part of this work, carried out on the Platform for Nanocharacterisation (PFNC), was supported by the "Recherches Technologiques de Base" and the "CARNOT" program of the French National Research Agency (ANR).

- [1] M. A. Moreno *et al.* *JVST B*, vol. 36, MAY 2018.
- [2] A. Priebe *et al.* *ULTRAMICROSCOPY*, vol. 173, pp. 10-13, FEB 2017.
- [3] A. G. De Carvalho *et al.* *Biointerphases*, vol. 15, 2020.
- [4] C. Uwizeye *et al.* *PNAS*. Vol 118, e2025252118, 2021.

9:00am **AS+2D+CA+EM+MS+NS+SE+SS+TF-FrM-3 Secondary Ion Mass Spectroscopy of Battery Surface and Interface Chemistry – Metrology and Applications**, *Yundong Zhou, S. Marchesini, X. Yao, Y. Zhao, I. Gilmore*, National Physical Laboratory, UK

Batteries are very important to achieve carbon net zero. Understanding battery materials change, electrode surfaces, solid electrolyte interphase (SEI) evolution and novel solid-state electrolyte structures is very helpful for developing better batteries. Surface chemical analysis techniques such as X-ray photoelectron spectroscopy (XPS) and Raman spectroscopy are often used but they have their limitations. XPS analysis cannot always resolve overlapping binding energies for some key SEI elements. The SEI often has poor Raman signal intensity. These are all hurdles for battery applications.

Secondary ion mass spectrometry has great potential to study interfacial chemistry in batteries owing to high sensitivity and high-resolution imaging in 2D and 3D. In this study, we use an OrbISIMS instrument which is equipped with two complementary mass spectrometers (MS). A time-of-flight (ToF) MS has the capability for 2D and 3D imaging using a Bi<sub>3</sub><sup>+</sup> liquid metal ion gun with a spatial resolution of up to 200 nm but with modest mass resolving power. The Orbitrap MS offers high mass resolution and

# Friday Morning, November 10, 2023

mass accuracy ( $> 240,000$  at  $m/z$  200 and  $< 2$  ppm, respectively). The instrument is equipped with low energy Cs and O<sub>2</sub> sputter beams for high resolution depth profiling of inorganic materials. It also has a Leica docking station enabling samples to be transferred using a vacuum sample transfer chamber from an argon glove box without atmospheric exposure. To improve the quality of measurements on battery materials, we have used ion implanted materials to determine relative sensitivity factors for relevant elements. We have also conducted a systematic study to optimise the OrbiSIMS depth profiling capability. These findings along with recommendations to reduce effects of signal saturation will be discussed and examples of the application to batteries will be provided. We will provide examples of the application of ToF MS and Orbitrap MS. (1,2)

98. X. Yao et al., *Energy Environ. Sci.*, 2023, DOI: 10.1039/D2EE04006A.
99. S. Marchesini et al., *ACS Appl. Mater. Interfaces*, 14(2022)52779-52793.

9:20am **AS+2D+CA+EM+MS+NS+SE+SS+TF-FrM-4 Characterizing Ion Distribution at the Solid-Electrolyte Interface in Solid-State Lithium Ion Batteries with ToF-SIMS, Teodora Zagarac**, University of Illinois - Chicago; *M. Counihan, J. Lee, Y. Zhang*, Argonne National Laboratory, USA; *L. Hanley*, University of Illinois - Chicago; *S. Tepavcevic*, Argonne National Laboratory, USA

Interest in solid state lithium-ion batteries as the next generation of energy storage devices has led to intense study of the chemistry, structure, and manufacturing processes for polymer electrolytes. Lithium bis(trifluoromethanesulfonyl) imide (LiTFSI) salt is often used to introduce Li ions into the solid-state electrolyte. Lithium bis(fluorosulfonyl)imide salt (LiFSI) and lithium nitrate (LiNO<sub>3</sub>) are less expensive salts with the potential to improve performance characteristics over pure LiTFSI in certain electrolyte formulations. The differences in distribution and reactivity of these different salts are still unknown but are critical to battery performance. Time-of-flight secondary ion mass spectrometry (ToF-SIMS) imaging and depth profiling was performed to compare the distributions of Li<sup>+</sup> cations and TFSI<sup>-</sup>, FSI<sup>-</sup>, and NO<sub>3</sub><sup>-</sup> anions across the solid-electrolyte interface (SEI) formed between the polymer electrolyte and thin lithium metal electrode. Experiments were performed on ~600 nm salt-rich poly(ethylene oxide) electrolytes with ~10 nm overlayers of vapor-deposited Li metal. Samples were probed with 30 keV Bi<sub>3</sub><sup>+</sup> from a liquid metal ion gun while depth profiling with 10 keV Ar<sub>1400</sub> gas cluster ion beam to collect both positive and negative ion mass spectra. Ion distributions from the three salts and their 3D images will be presented and discussed in terms of the relative composition of their SEI layers. Chemical differences from ToF-SIMS analysis help explain the differences in electrochemical SEI formation and half cell cycling: LiTFSI and LiFSI are similar, but LiNO<sub>3</sub> presents much different electrochemical properties.

9:40am **AS+2D+CA+EM+MS+NS+SE+SS+TF-FrM-5 A Perspective on X-ray Photoelectron Spectroscopy (XPS) Peak Fitting, and Reporting of XPS Data Acquisition and Peak Fitting Parameters in the Literature, Matthew Linford**, *G. Major, J. Pinder*, Brigham Young University

We recently reported that a rather large fraction (ca. 40 %) of the XPS peak fitting in the literature is at best suspect. In a recent Perspective article (doi: 10.1116/6.0002437) we argue that the various stakeholders of the problem can act together to improve the current situation. This Perspective begins with representative examples of poor XPS peak fitting. The purpose of showing these examples is to demonstrate to the reader that we are not quibbling or arguing over subtle interpretations of the data. Increasingly, we see errors that might be classified as egregious. We argue that science is in a state of 'pre-crisis' more than in a state of 'crisis'. We suggest that if too much incorrect data analysis enters the literature it may cease to be self-correcting. We note the very large number of surface and material characterization techniques available today and how this presents a challenge for scientists. Consequently, it is likely that many manuscripts are incompletely reviewed today. Graduate students and post-docs at research institutions are often given minimal training on acquiring and analyzing XPS data. High fees for instruments can limit access to them and student training. Prisoner's dilemmas may help explain situations in science that lead to suboptimal outcomes for the community. Authors are primarily responsible for the quality of the research in their papers, not reviewers or editors. We question the wisdom of placing the names of reviewers and editors on papers. In some cases, staff scientists are not adequately recognized for their intellectual contributions to projects. Selective reviewing may allow more reviews to be performed without overtaxing the

community. Reviewing at some open access journals may be inadequate. Collaboration needs to be encouraged to a greater extent at some institutions.

10:00am **AS+2D+CA+EM+MS+NS+SE+SS+TF-FrM-6 Unsupervised and Supervised Machine Learning Applied to ToF-SIMS of an Organic Matter-Rich Mudstone with Molecular Biomarker**, *M. Pasterski*, University of Illinois Chicago; *M. Lorenz*, Oak Ridge National Laboratory; *A. Ilevlev*, Oak Ridge National Laboratory; *R. Wickramasinghe*, *Luke Hanley*, *F. Kenig*, University of Illinois Chicago

Time-of-flight secondary ion mass spectrometry (ToF-SIMS) imaging has been used to detect organic compounds including molecular biosignatures (biomarkers) in geologic samples (R.C. Wickramasinghe, *et al.*, *Anal. Chem.*, 2021, 93, 15949). The spatial distribution of these biomarkers can help determine when and how these organics were incorporated into the host rock. ToF-SIMS imaging can rapidly collect a large amount of data, but molecular and fragment ions of different species are mixed together in complex mass spectra that are difficult to interpret. Here, we apply unsupervised and supervised machine learning (ML) to help interpret the mass spectra obtained by ToF-SIMS of an organic-carbon-rich mudstone from the Middle Jurassic of England (UK). It was previously shown that the presence of sterane molecular biomarkers in this sample can be detected via ToF-SIMS (M.J. Pasterski, *et al.*, *Astrobiol.*, in press). We use unsupervised ML on field emission scanning electron microscopy – electron dispersive spectroscopy (SEM-EDS) measurements to define compositional categories based on differences in elemental abundances. We then test the ability of four ML algorithms - k-nearest neighbors (KNN), recursive partitioning and regressive trees (RPART), eXtreme gradient boost (XGBoost), and random forest (RF) - to classify the ToF-SIMS spectra using the categories assigned via SEM-EDS, using organic and inorganic labels, as well as using presence or absence of detectable steranes. KNN provided the highest predictive accuracy and balanced accuracy. The feature importance, or the specific features of the ToF-SIMS data used by the KNN model to make classifications could not be determined, preventing post-hoc model interpretation. However, the feature importance extracted from the other three models was useful for interpreting spectra. We determined that some of the organic ions used to classify biomarker containing spectra may be fragment ions derived from kerogen.

10:40am **AS+2D+CA+EM+MS+NS+SE+SS+TF-FrM-8 Probing Thin Film Interfaces at the Nanoscale by Low Energy Ion Scattering, Marko Sturm**, *A. Chandrasekaran, A. Valpreda, A. Zameshin, R. Van de Kruijs, A. Yakshin, F. Bijkerk, M. Ackermann*, University of Twente, Netherlands **INVITED**

The growth of thin films with nanometer range thickness is of great importance for application topics as nanoelectronics, oxidation protection of thin films and optical coatings for X-ray applications. The performance of these coatings often critically depends on the sharpness of the interfaces between different layers. In this talk I will outline how we use Low-energy ion scattering (LEIS) to study interface formation between layers of different transition metals (TMs) and between TMs and Si.

LEIS with noble gas ions as projectiles yields surface peaks that indicate the composition of the outermost atomic layer of a sample. This makes the technique excellently suited to study whether deposition of a thin film leads to a closed layer. However, deposition of an overlayer on top of an underlayer may result in surface segregation of underlayer atoms (driven by surface energy differences or stress), such that the surface composition is not directly representative for the in-depth concentration profile. We analyzed the evolution of surface coverage versus deposited thickness for a large set of TM/TM film combinations, deposited by magnetron sputtering in a system that allows LEIS analysis without vacuum break after deposition. By applying a model that takes into account surface segregation, the interface profiles were derived from these layer growth profiles, which we call deposition depth profile. In addition, we demonstrated that the sharpness of interfaces in TM/TM film systems can be predicted by a phenomenological model with the crystal structure and surface energy of the materials as input parameter. This model in principle predicts the sharpness of the interface in any TM/TM thin film combination! [1]

Apart from surface peaks, LEIS spectra typically also contain so-called tails, caused by projectiles that, after sub-surface scattering, are reionized when leaving the sample. It was demonstrated before that LEIS tails can be used to determine thickness of various thin film systems, when the stopping power of the projectiles is known. Here, we show that LEIS tails can also be used to determine the sharpness of interfaces of few nm Si-on-W and Si-on-Mo films, by comparing LEIS measurements with Monte Carlo simulations with the TRBS code, which takes into account multiple

# Friday Morning, November 10, 2023

scattering and stopping in the target. This approach allows interface characterization from a single sample, without the need to make a deposition depth profile.

References:

[1] A. Chandrasekaran, R.W.E. van de Kruijs, J.M. Sturm, A.A. Zameshin and F. Bijkerk, ACS Applied Materials & Interfaces **11**, 46311 (2019)

## 11:20am AS+2D+CA+EM+MS+NS+SE+SS+TF-FrM-10 The Effect of Instrument Settings, Sample Distance, and Tilt on TofsimsSecondary Ion Intensities, Alan Spool, L. Finney, Western Digital

Experiments were performed to explore the effects of various instrument settings and sample placements on secondary ion intensities to better understand what factors have the greatest effect on repeatability and replicability in TOF-SIMS. A batch of magnetic recording disks used in hard disk drive manufacture, natively flat and homogeneous, were used as test samples for the purpose. As expected, by far the largest variable altering raw intensities was the LMIG tip stability. LMIG tips can have stable emission currents while still producing variable pulsed LMIG beam currents with resultant variable secondary ion counts. This variability sometimes is seen in slow current drift, but is sometimes so rapid that measurements taken directly before each measurement are not close enough in time to properly scale the measurement results. In these cases, normalization is the only solution. Secondary ion intensities were remarkably insensitive to small variations in sample height (position relative to the extractor). Far more interesting were the changes to the secondary ion intensities that resulted from tilting the sample. These effects varied amongst the secondary ions detected such that normalization did not remove them. Secondary ion emission as a function of emission angle has long been understood to be like a cosine function and to vary somewhat from ion to ion. These different angular profiles explain the differences seen in ion detection as a function of tilt. Some of these differences proved to be asymmetrical, varying depending on whether the sample was tilted toward or away from the primary ion source, an indication that in some situations some residual momentum from the initial primary ion impact onto the surface is carried into the secondary ion emission. These results have implications for attempts to do quantitative analysis on any sample that is not completely flat.

## 11:40am AS+2D+CA+EM+MS+NS+SE+SS+TF-FrM-11 Evaluation of Unaltered and Irradiated Nuclear Graphite Surfaces through Integrated Traditional XPS and HAXPES Techniques, Jonathan Counsell, L. Soomary, K. Zahra, Kratos Analytical Limited, UK; B. Spencer, A. Theodosiou, University of Manchester, UK

Graphite-moderated reactors have been operational worldwide for several decades. There exists a substantial body of research in this domain, with particular emphasis on investigating the impact of irradiation damage on the graphite matrix. In order to satisfy the design and regulatory requisites of these advanced reactors, it becomes imperative to gain a deeper comprehension of the retention and transportation mechanisms of fission products within graphite.

This study outlines a technique for the precise assessment of the surface chemistry of highly-oriented pyrolytic graphite (HOPG), serving as a representative model akin to the current graphite grades utilized in the nuclear sector. We delve into the process of surface etching aimed at eliminating surface adsorbates and contaminants. This process involves the utilization of both monatomic and cluster ions, the former inadvertently causing undesirable damage to the graphite structure. Such damage is evidenced by a significant reduction in the sp<sup>2</sup> component of C 1s. We introduce the use of UPS analysis as a straightforward means of determining the presence of sp<sup>2</sup> characteristics in the uppermost atomic layers.

Moreover, we examine the consequences of high-energy ion implantation (Cs<sup>+</sup>) and the ensuing damage to the HOPG surface. This examination is carried out using XPS (1486eV) and HAXPES (2984eV), thereby showcasing the capability to characterize the resulting surface damage and the associated alterations within the probed depths.

## Electronic Materials and Photonics Division

### Room B116 - Session EM1+TF-FrM

#### Advanced Patterning and Fabrication for Device Scaling

Moderators: Stephen McDonnell, University of Virginia, Michelle Paquette, University of Missouri-Kansas City

## 8:20am EM1+TF-FrM-1 Thin Film Challenges and Opportunities in a 3D-Evolving Memory Landscape, Johan Swerts, imec, Belgium INVITED

Device architectures used in SRAM memory transitioned in the past decade from the historical 2D planar transistor to FINFET. The next innovation revealed for the 3nm node is a 3D stacked gate-all-around architecture in combination with a backside power delivery network. For further scaling, stacking nmos and pmos, the so-called complementary-FET (CFET) design, is envisaged to happen in 2030. New metallization schemes to tackle the RC challenge as device dimensions of the interconnects shrink, such as Cu replacements materials in a direct metal etch integration scheme. A broad variety of complementary deposition techniques and introduction of new materials will be needed to enable the above-mentioned novelties.

A similar trend towards stacking functional cells can be observed in various memories, such as the emerging memories that aim to bridge the gap between DRAM and NAND, thereby enabling fast data storage and retrieval for real-time processing in connected devices at low cost. These memories are based on phase change, filamentary, magnetic, or ferroelectric mechanisms and often use multi-element materials. They have been extensively explored in 2D capacitor or transistor based devices, but for further density scaling 3D device designs are needed where a conformal deposition technique such as ALD is required. Cell scaling challenges also hold for the traditional DRAM which lead to exploring 3DDRAM integration routes. One viable pathway for scaling implies the replacement of the typical Si-channel based transistor by a deposited semiconductor oxide channel. Ultimate 3DDRAM implementation would require a conformal deposition of that channel.

This presentation reviews key thin film opportunities and challenges, including but not limited to ALD, in a 3D-evolving memory landscape.

## 9:00am EM1+TF-FrM-3 Patterning Challenges in the Era of Vertical Scaling, Luciana Meli, IBM Research Division, Albany, NY INVITED

With the end of conventional device scaling, achieving higher compute power has relied on a combination of design and integration innovations, and material breakthroughs to keep up with scaling demands. While traditional dimensional scaling will only continue for the back end of the line, controlling pattern variability and placement remains a critical challenge from a lithography perspective.

Looking ahead, vertical scaling paths will be essential to enhance performance in traditional analog computing and to scale up qubits in quantum computing. This talk will focus on key patterning challenges associated with these vertical scaling pathways, including stacked FETs and chiplet-based architectures, and address opportunities for innovation.

## 9:40am EM1+TF-FrM-5 Plasma Etch Challenges and Innovations to Enable sub-26nm Pitch L/S Patterning with High-NA EUV, Nafees Kabir, Intel Corporation

Extreme ultraviolet (EUV) lithography has been a game changer for the semiconductor industry, enabling tight pitches of 36-40 nm for the 7nm logic technology node. Employing an extremely short 13.5nm wavelength, EUV lithography has surpassed 193i by improving resolution and thus the ability to print tighter features, as well as replacing the complex and expensive multiple-step patterning of 193i with single-patterning. However, despite achieving single-exposure 28nm pitch for the 5nm logic technology node, the current scanner is approaching its resolution limit.

As we prepare to embrace another litho evolution, **high-NA EUV lithography technology** is projected to enable 2nm and beyond logic technology nodes without requiring complex multi-step patterning. The key enabler to improve resolution is the numerical aperture (NA) of the lens. Hence, moving from current **0.33NA to 0.55NA** has the ultimate capability to enable 8nm resolution and patterning 16nm pitch with single-exposure. With this change in NA, the depth-of-focus (DOF) is reduced and pushes us towards the use of **thinner resists** (~20-25nm FT).

This brings us to a new process territory, not only for litho, but also for plasma etch. Need for etch innovation is at a premium to work hand-in-hand to enable pattern transfer of critical features in beyond-2nm logic nodes to further advance Moore's Law.

# Friday Morning, November 10, 2023

In this work, we will share some early innovative plasma etch techniques to demonstrate patterning of basic elements like lines/spaces, contact holes etc. and novel process integration schemes involving Chemically Amplified Resists (CAR) to enable more complex structures with high fidelity.

10:00am **EM1+TF-FrM-6 Area-Selective Deposition with Carborane and Aromatic Self-Assembled Monolayer Blocking Layers**, *Michelle Paquette, R. Bale*, University of Missouri-Kansas City; *B. Garland*, Lehigh University; *S. King*, Intel Corporation; *A. Molder, N. Oylar, S. Pinnepalli*, University of Missouri-Kansas City; *N. Strandwitz, V. Vemuri*, Lehigh University; *T. Vo*, University of Missouri-Kansas City

Area-selective deposition (ASD) is an important strategy in improving the fidelity of and/or reducing the complexity of current multi-pattern pitch-division processes. Dielectric on dielectric (DoD) deposition is of interest for fully self-aligned via flow; however known DoD processes are limited in terms of materials, selectivities, and processing ranges. A common strategy for achieving ASD is to use a blocking layer on the non-growth surface (e.g., a metal) to be able to deposit a target material selectively on the desired surface (e.g., a dielectric). The most well-established blocking layers are self-assembled monolayers (SAMs) based on long alkyl chains, such as dodecanethiol. While these have demonstrated extremely promising results, they do present limitations such as restricted processing windows (e.g., temperature), a typical requirement for solution-phase processing, long exposure times (e.g., 12–48 h), limited stability (temperature, time, chemical), and presence of defects (e.g., pinholes) resulting from disorder or alkyl chain distortions. We investigate two alternative classes of SAMs as blocking layers on metal: carborane thiols and aromatic thiols. Both classes possess several appealing features including the capacity for well-ordered packing (based on 3D symmetry and Van der Waals packing for carboranes and pi-stacking for aromatics), vapor phase deposition, and—importantly—cross-linking through a variety of mechanisms including heat, plasma, and radiation (e.g., UV, e-beam), thus potentially enabling fewer defects, greater stability (leading to wider/more flexible processing windows and/or higher selectivity), as well as the possibility of additional top-down patterning. We investigate the influence of SAM formation (substrate, derivative, deposition conditions, post-deposition treatment) on their resulting composition and structure as well as their blocking capability toward a selection of atomic layer deposition chemistries.

## Electronic Materials and Photonics Division

### Room B116 - Session EM2-FrM

#### Emergent Photonic Materials and Devices for Mid-IR Applications

**Moderators:** Parag Banerjee, University of Central Florida, Erin Cleveland, U.S. Naval Research Laboratory

10:40am **EM2-FrM-8 Enabling Novel Infrared (IR) Materials for Next-Generation Applications**, *Kathleen A. Richardson*, University of Central Florida, College of Optics and Photonics

INVITED

Technological advances in areas important to industry, defense and society are moving rapidly with requirements to *see and sense* in ways not thought possible before. To realize such advances, new materials with unique function can lead to new components for systems that are smaller, lighter in weight, requisite of less power and lower cost. Security and sensing systems must be versatile to work in a wide range of extreme environmental conditions such as in smoke, fog or in space. Other applications require more robust thermo-mechanical performance metrics, which must be evaluated in trade space to yield a viable solution for more rugged system needs. Materials that transmit light in the infrared portion of the electromagnetic spectrum allows one to 'see' in these regions, often when visible imaging is not possible, but also to serve as windows if they are robust 'enough'. How one transitions viable candidates from lab-scale demonstrators to commercial products takes an understanding of both science and engineering, manufacturability, and prioritization of attributes. This alignment with the end-customer needs must start early in the material design and development process, often well before the actual material solution is fully developed.

This talk reviews general aspects of how infrared glasses for bulk and planar film devices, glass ceramics as gradient refractive index (GRIN) media and alloys for optical phase change (O-PCM) have been designed, developed at prototype scale, and successfully transitioned from the university lab benchtop to the marketplace. These key outcomes suggest a methodology for how this could be done across other candidate optical material systems.

11:20am **EM2-FrM-10 Inverse Piezoelectric Effect in Reverse Biased High-Voltage GaN PN Diodes Observed by In-Situ Biased X-Ray Topography Imaging**, *Andrew Koehler, N. Mahadik*, U.S. Naval Research Laboratory; *M. Liao*, National Research Council Postdoctoral Fellow Residing at U.S. Naval Research Laboratory; *A. Jacobs*, U.S. Naval Research Laboratory; *G. Foster*, Jacobs Inc. Residing at U.S. Naval Research Laboratory; *S. Atwimah, P. Pandey, T. Nelson, D. Georgiev, R. Khanna*, EECS Department University of Toledo; *K. Hobart, T. Anderson*, U.S. Naval Research Laboratory

Next-generation power systems demand increasingly compact and efficient power conversion circuits, which can be delivered by wide bandgap gallium nitride (GaN) technology. Vertical GaN PN junction diodes are fabricated by growing GaN PN epitaxial layers by metal organic chemical vapor deposition (MOCVD) on native GaN substrates. Greater than 800 V reverse blocking voltage is achieved by implementation of nitrogen ion implanted edge termination for electric field management. The termination scheme consists of a hybrid of a shallow implanted junction termination extension (JTE), multiple deeper implanted guard rings (GRs), and implanted isolation that penetrates the PN junction. The implanted nitrogen selectively compensates the P-type doping of the anode layer. 1 mm<sup>2</sup> discrete diodes were singulated from a wafer and mounted in an open lid custom package with a silver glass die attach, to allow for in-situ biased high resolution X-ray topography (XRT) using  $g = [11-20]$  diffraction conditions. Without applied bias, a compressive uniaxial strain of 0.015% is observed, resulting from the die attach process. As illustrated by technology computer aided design (TCAD), the electric field in the diode, under reverse bias, is spread by the edge termination, from the edge of the anode into the termination region, where lattice strain is introduced via the inverse piezoelectric effect. The edge termination effectively operates by reducing the peak electric field at the anode edge; however, the guard rings induce localized nonuniformities in the electric field profile across the termination region, particularly near the surface. The reverse in-situ biased XRT measurements show a nonuniform strain profile in the termination region corresponding to the nonuniform electric field of the GaN diode under reverse bias, with a peak strain near the isolation edge. At a reverse bias of 500 V, the observed piezoelectric induced strain peaked near the isolation implanted edge with a significant (0.32%) amount of strain, which could potentially induce material degradation, causing long-term reliability concerns. In-situ biased XRT imaging can be used as an experimental method to map piezoelectric strain from electric field in GaN, or other piezoelectric material systems to facilitate devices with increased performance and robust operation.

## Fundamental Discoveries in Heterogeneous Catalysis Focus Topic

### Room B113 - Session HC+SS-FrM

#### Greatest Hits in Heterogeneous Catalysis

**Moderators:** Liney Arnadottir, Oregon State University, Ashleigh Baber, James Madison University, Dan Killelea, Loyola University Chicago

8:20am **HC+SS-FrM-1 CO Characterized Pt/Cu(111) Single Atom Alloy (SAA) for the Hydrogenation of Unsaturated Aldehydes**, *David Molina, M. Trenary*, University of Illinois - Chicago

The use of heterogeneous catalysts is of high importance in a vast number of industrial processes. A promising new type of heterogeneous catalyst known as single atom alloys (SAAs) greatly reduce the amount of precious metal (e.g. Pt, Pd, Rh, Ru) used and have shown enhancements in selectivity, when compared to their pure counterparts, in various types of reactions, including hydrogenation reactions. Hence, it is important to be able to quantify the amount of precious metal on the surface of these catalysts and understand their properties. We have used reflection absorption infrared spectroscopy (RAIRS) and temperature programmed desorption (TPD) of adsorbed CO were used to probe the properties of Pt/Cu(111) surfaces, ranging from a multilayer film of Pt on Cu(111) to 2% Pt/Cu(111). For Pt deposition on Cu(111) at room temperature, the Pt coverage was varied from a multilayer film to 0.23 monolayer (ML). As the Pt coverage decreased, a RAIR C–O stretch peak in the range of 2041-2050 cm<sup>-1</sup> showed isolated Pt atoms embedded in the Cu(111) surface. Pt islands were identified by a C–O stretch peak in the range of 2058-2067 cm<sup>-1</sup>, showing CO on top of Pt atoms. These islands also allowed for CO to bind at bridge sites between two Pt atoms and this was supported by the observed C–O stretch peak at 1852 cm<sup>-1</sup>. Deposition of low coverages of Pt at 380, 450 and 550 K formed SAAs in which surface Pt is only present as isolated atoms that had replaced Cu atoms in the topmost atomic layer, in agreement with previous studies with scanning tunneling microscopy.

# Friday Morning, November 10, 2023

Adsorption of CO on top of the Pt atoms of the SAAs leads to a C–O stretch in the range of 2041–2046  $\text{cm}^{-1}$ . Compared to the SAA formed by Pt deposition at 380 K, deposition at 450 and 550 K led to more dispersed Pt atoms as indicated by the lack of a shift of the C–O stretch peaks, indicating that the distance between CO molecules was not low enough for dipole-dipole coupling shifts to occur. In all cases, the C–O stretch of CO on the Pt atoms of Pt/Cu(111) was significantly redshifted relative to its value on Pt(111), which is a manifestation of how nearby Cu atoms alter the Pt–CO bonding. The well characterized Pt/Cu(111) SAA is currently being used to study the hydrogenation of model unsaturated aldehydes.

**8:40am HC+SS-FrM-2 Efficient Catalyst and Protection Layer of Ni/ $\alpha$ -Al<sub>2</sub>O<sub>3</sub> Catalysts for Improved H<sub>2</sub>O/CO<sub>2</sub> Reforming Reaction of CH<sub>4</sub> via Atomic Layer Deposition, Dae Woong Kim, H. Jeong, W. Hong, J. Park, S. Oh, J. Jang, Hyundai Motor Company, Republic of Korea**

Recently, production of synthetic gas by combined steam and CO<sub>2</sub> reforming reaction of CH<sub>4</sub> (CSCR) is proposed for dealing with the energy problem. In the CSCR process as methane reforming reaction, the synthesis of steam (H<sub>2</sub>O), CH<sub>4</sub>, and CO<sub>2</sub> occurs at high temperatures and pressures in the presence of metal catalysts.[1] In general, Ni-based catalysts are attractive materials because of their relatively high activity and low cost as compared to noble metal catalysts.[2] As a support structure, a thermally stable, acid-free and inert  $\alpha$ -Al<sub>2</sub>O<sub>3</sub> is a well-known material.[3] However, catalytic pellets through mixed powder sintering have low structural strength as well as poor catalytic utilization due to dead nickel volume. Therefore, atomic layer deposition (ALD) is proposed as a reliable and atomic scale-adjustable process for conformally growing NiO on  $\alpha$ -Al<sub>2</sub>O<sub>3</sub> surface with an exact thickness. In the case of ALD-based catalyst growth, the reaction efficiency can be maximized without a catalyst dead area because the catalyst is formed only on the active surface where the reforming reaction can occur.

In this work, ALD NiO film was grown on  $\alpha$ -Al<sub>2</sub>O<sub>3</sub> pellet supporter which is followed by reduction annealing for highly active CSCR reforming catalyst with a low Ni concentration. Furthermore, an ultra-thin Al<sub>2</sub>O<sub>3</sub> protection layer was proposed to enhance stability and coking resistant of Ni/ $\alpha$ -Al<sub>2</sub>O<sub>3</sub> catalyst during reforming reaction. Detailed experimental results will be presented.

[1] Energy Fuels 2015, 29, 1055–1065

[2] RSC Advanced 2015, 5, 7539–7546

[3] Journal of Energy Chemistry 22(2013)919–927

[4] Catalysis Science & Technology 2020, 10, 8283

**9:00am HC+SS-FrM-3 Complementary Outer Atomic Layer Analysis of Catalyst Materials Using LEIS, P. Brüner, IONTOF GmbH, Germany; J. Järvillehto, Department of Chemical and Metallurgical Engineering, Aalto University School of Chemical Engineering, Finland; S. Saedy, Chemical Engineering Department, Delft University of Technology, Netherlands; Thomas Grehl, IONTOF GmbH, Germany**

Performance of material in heterogeneous catalysis is dominated by the composition and chemical state of the outer atomic layer. A number of techniques successfully characterize the material at and close to the surface (e.g. XPS) or directly the interaction of the gas phase with the surface (operando techniques, e.g. IR). Also, physical properties like specific surface area are determined. However, Low Energy Ion Scattering (LEIS) is the only technique capable of determining specifically the elemental composition of the outer atomic layer. This opens a range of possibilities to learn about the materials and especially the preparation of catalysts. Due to the high sensitivity of LEIS, this can be performed on both model as well as industrial catalysts.

In this contribution, we will highlight a range of catalysis applications of LEIS on very different materials. This includes nanoparticles and their catalytically active phase on the surface of these particles, and how this surface changes depending on the environment, e.g. a calcination procedure. This can be a dispersed Pt phase and the prevention of sintering by ALD coating. Also industrial particles used for low cost catalysts are shown, specifically the behavior of the active Fe phase and reorganization of the surface under calcination. Another example is demonstrating the Pt deposition inside porous Al<sub>2</sub>O<sub>3</sub> beads using ALD [1], and how LEIS analysis can help to optimize the process.

Common to all examples is the specific view that LEIS allows due to its single atomic layer information depth, complementing the information gathered from the many other (surface) analytical techniques applied to catalyst materials.

[1] J. Järvillehto, Thesis, Aalto University, <https://aaltodoc.aalto.fi/handle/123456789/119352>

**9:20am HC+SS-FrM-4 Size-Selected Pt<sub>n</sub> Cluster Electrocatalysts for Alcohol Oxidation, Zihan Wang, University of Utah, China; T. Masubuchi, University of Utah, Japan; M. O'Brien, S. Anderson, University of Utah**

Alcohol oxidation is catalyzed by size-selected Pt<sub>n</sub> clusters deposited on indium tin oxide (ITO) and highly oriented pyrolytic graphite (HOPG) electrodes is being investigated. Clusters are generated in the gas phase, mass selected, then deposited on the electrode supports under controlled conditions, in UHV. Electrocatalysis is studied using a unique *in situ* system that allows aqueous electrochemistry to be studied in an antechamber on the UHV system, without exposure to air. Based on cyclic voltammetry (CV), the activity and selectivity for oxidation of 1- and 2-propanol are strongly dependent on cluster size, for Pt<sub>n</sub>/ITO, and the activity is correlated with Pt core level binding energies measured by XPS. For HOPG, high activity has been observed for both soft- and hard-landed clusters, and the challenge is to understand the nature of the Pt-HOPG binding for cluster prepared under different conditions. Preliminary data shows that even HOPG, which has weak bonding with Pt, can preserve the deposited cluster size long enough to give size-dependent electrocatalysis, if the clusters are deposited under conditions that pin them to the support. The results for propanol oxidation are expected to provide insight into primary vs. secondary alcohol oxidation in glycerol, which is important for upgrading biobased glycerol into commercial products.

**9:40am HC+SS-FrM-5 Calorimetric Energies of Metal Atoms within Nanoparticles on Oxide and Carbon Supports: Improved Size Dependencies, Adhesion Energies and Trends versus Metal Element with the Spherical Cap Model, Kun Zhao, University of Washington; D. Auerbach, Max Planck Institute for Multidisciplinary Sciences, Germany; C. Campbell, University of Washington**

The chemical potential of metal atoms in supported nanoparticles is an important descriptor of their catalytic performance that captures the effects of particle size and support. Previously, we used the hemispherical cap model (HCM), which assumes 90 degree contact angle of nanoparticles, to model the chemical potential versus size of the nanoparticles. The HCM has been successful in predicting the chemical potential increase with the decreasing of particle size and gives linear trends of adhesion energy with the metal oxophilicity or carbophilicity per unit area for the metal nanoparticles on oxide or carbon supports, respectively. However, the assumption of 90 degree contact angle in the HCM creates errors in the contact angle, particle size and adhesion energy when compared to the expectation of equilibrium shape.

Here, we will relax the assumption of hemispherical shape, and treat the more general case of spherical caps with any contact angle. We show that by simultaneously analyzing the data from metal vapor adsorption calorimetry (metal chemical potential versus coverage) and the data from He<sup>+</sup> low-energy ion scattering spectroscopy or LEIS (signal versus coverage) within this new spherical cap model (SCM), we can determine the only contact angle that is consistent with both these sets of data. We then apply that approach to reanalyze all the metal / support systems which we had previously analyzed using the HCM to determine this self-consistent contact angle and the corresponding adhesion energy. These analyses rely on our recently developed SCM model for analyzing LEIS signals versus coverage which accounts for blocking of ion trajectories by particle material for any contact angle.<sup>1</sup> The resulting adhesion energies and contact angles are more accurate in predicting chemical potential versus size for all the metal / support systems. The trends of adhesion energy versus metal oxophilicity (for each oxide support) and carbophilicity (for carbon support) per unit area are also improved compared to earlier reports, and now better explain the support effect on the adhesion of metal nanoparticles.

## Reference

1. Zhao, K.; Auerbach, D.; Campbell, C. T. Low Energy Ion Scattering Intensities from Supported Nanoparticles: The Spherical Cap Model. *J. Phys. Chem. C* 2023. <https://doi.org/10.1021/acs.jpcc.3c01175>

**10:00am HC+SS-FrM-6 Insights Into Adsorbate-Driven Surface Restructuring Using Size-Selected Pt/SiO<sub>2</sub> Nanoparticle Catalysts, Christopher O'Connor, T. Kim, C. Owen, Harvard University; N. Marcella, University of Illinois; A. Frenkel, Stony Brook University/Brookhaven National Laboratory; B. Kozinsky, C. Reece, Harvard University**  
Heterogeneous catalysts are complex, dynamic materials that can undergo restructuring under reaction conditions. A key aspiration in the rationale design of catalysts is to tune performance (activity, selectivity, and stability)

# Friday Morning, November 10, 2023

by using reactant conditions (composition, pressure, and temperature) and materials architecture to modify surface structure and composition. Herein, we investigate size-dependent catalyst restructuring under reactions conditions using a series of well controlled size-selected (1 – 8 nm) platinum nanoparticles supported on SiO<sub>2</sub> (Pt/SiO<sub>2</sub>) as a model system. Diffuse Reflectance Infrared Fourier Transform Spectroscopy (DRIFTS) measurements on 2 nm Pt/SiO<sub>2</sub> show that ~35% of CO adsorption sites are undercoordinated Pt under 1 mbar CO at 25 °C which is consistent with a regular truncated octahedral nanoparticle model. Under a CO environment, an incremental increase in temperature up to 350 °C induces restructuring to form a more undercoordinated surface indicated by a ~ 14% increase in total Pt sites for CO adsorption and ~ 75% undercoordinated surface sites. A thermal treatment at 350 °C under an inert atmosphere can reverse the catalyst structure to a well-coordinated surface, while cooling under a CO atmosphere can partially trap the surface in an undercoordinated structure. In contrast, 8 nm Pt/SiO<sub>2</sub> does not undergo significant restructuring from 25 to 350 °C under 1 mbar CO as evidenced by DRIFTS measurements. The experimental results are compared to theoretical calculations and molecular dynamics simulations to provide atomistic insight into the experimentally observed nanoparticle restructuring. This study clearly demonstrates that the adsorbate-driven surface restructuring of supported nanoparticle catalysts is strongly dependent on the reaction conditions (gas composition and temperature) and nanoparticle size, having broad implications for the structure of catalytically active surfaces under reaction conditions.

## Advanced Focused Ion Beams Focus Topic Room B110-112 - Session IB1-FrM

### Advances in FIB Specimen Preparation

**Moderators:** **Tanvi Ajantawalay**, Pacific Northwest National Laboratory, **Gregor Hlawacek**, Helmholtz-Zentrum Dresden - Rossendorf

8:20am **IB1-FrM-1 An Air-Free Transfer Mechanism For FIB SEM**, **Valerie Brogden**, **J. Garman**, **S. Wiemholt**, **K. Langworthy**, University of Oregon  
**INVITED**

Lithium-ion batteries are increasingly prolific in the landscape of modern technology. Analysis of lithium metals with techniques such as Scanning Electron Microscopy (SEM) and Focused Ion Beam (FIB) can reveal critical information about the microstructure and composition of these materials. However, a problem presents itself when loading lithium metals into SEM/FIB systems. Lithium and other battery materials react with oxygen and can be quickly contaminated by exposure to atmosphere. Therefore, samples must be manipulated in an oxygen-free glove box. There is not currently a solution for mounting lithium samples onto a SEM/FIB stage for analysis without exposing the samples to atmosphere.

In this paper, we present a prototype for a glove box load lock that addresses this problem directly. This device bolts directly onto a ThermoFisher Plasma FIB and allows researchers to remove samples from positive-pressure packaging and mount the samples directly on the stage in an oxygen-free environment, and then pump the tool down to vacuum without contamination by atmosphere.

## Advanced Focused Ion Beams Focus Topic Room B110-112 - Session IB2-FrM

### Advances in TEM and APT Specimen Preparation

**Moderators:** **Tanvi Ajantawalay**, Pacific Northwest National Laboratory, **Gregor Hlawacek**, Helmholtz-Zentrum Dresden - Rossendorf

9:00am **IB2-FrM-3 Correlative and In Situ TEM/APT Technique Reveals Insights into Early Oxide Film Formation in a High Entropy Alloy**, **Bharat Gwalani**, Engineering Bldg | 911 Partners Way  
**INVITED**

Oxide film formation is a critical process that occurs on the surface of materials when they come into contact with oxygen. In some cases, oxide films can help protect the material from further corrosion, but in other cases, they can lead to degradation of the material over time. Understanding the early stages of oxide film formation is therefore important for designing materials that are resistant to corrosion. This study employed a combination of correlative and in situ techniques, specifically transmission electron microscopy (TEM) and atom probe tomography (APT), to investigate the initial stages of oxide film formation in a high entropy alloy (HEA). The research aimed to gain insight into the

mechanisms of oxide film formation and the chemical changes that occur during the process. By analyzing the nano-scale chemical changes of the oxide film and the underlying HEA as a function of time, we observed the phase transformation pathway resulting from a single-layer to a multi-layer oxide film, which provided important insights into the process of oxide film formation. The study demonstrates the potential of these techniques in providing a deeper understanding of the processes involved in oxide film formation, enabling the design of materials with improved corrosion resistance and durability.

9:40am **IB2-FrM-5 Applications of Advanced Focused Ion Beam System to Energy Storage Materials**, **Yaobin Xu**, **X. Cao**, **W. Xu**, **J. Zhang**, **C. Wang**, Pacific Northwest National Laboratory

Battery technology has received considerable attention in recent decades due to the rapid growth of the electric vehicle and consumer electronics markets. An in-depth understanding of the electrode, interfacial structure, and chemical distribution of battery materials is essential to further advance battery technology. Focused ion beam-scanning electron microscope (FIB-SEM) is an analytical method combines ion beam for materials processing and electron beam for imaging. It enables both two-dimensional (2D) and three-dimensional (3D) imaging capability, combined with electron backscatter diffraction (EBSD) and energy dispersive X-ray spectrometry (EDS) detector, could also provide multimodal information collection, which is an effective and powerful analytical approach for battery structural analysis.

Lately, the plasma FIB-SEM (PFIB-SEM) technology has been developed with different ion source and higher ablation efficiency. It promises great potential for battery materials characterization, due to accessing representative 2D area and 3D volume via much faster (compared with traditional Ga<sup>+</sup> system) milling rate as well as enabling Ga<sup>+</sup> free sample preparation on advanced battery system through non-reactive ion source (Xe<sup>+</sup> and Ar<sup>+</sup> ion). Besides, for air and beam sensitive battery materials, like alkali metal electrode, sulfide based solid state electrolyte, combing cryogenic stage and inert gas transfer system, we could image and process them without air contamination during sample transfer and reduce ion/beam damage under cryogenic condition. In this presentation, cryogenic PFIB-SEM has been used to perform 2D microstructure and chemical analysis and 3D imaging/chemical analysis on different battery systems including Li metal anode, lithium nickel manganese cobalt oxide (NMC) cathode and solid-state electrolyte.

The successful demonstration of the cryogenic PFIB-SEM provides exciting possibilities for the investigation of both current and future generations of advanced battery technologies, and will be an important analytical approach for battery research and development.

10:00am **IB2-FrM-6 The Fabrication of Ruthenium single crystal specimen with Focused Ion Beam and Field Ion Microscopy for Atom Probe Tomography**, **Mark G Wirth**, **D. Perea**, **S. Lambeets**, Pacific Northwest National Laboratory

Metallic surfaces may undergo a series of surface and subsurface structural and chemical transformations while exposed to reactive gases that inevitably change the surface properties. Understanding such surface dynamics from a fundamental science point of view is an important requirement to build rational links between chemical/structural surface properties and design new catalysts with desired performance or new materials with enhanced resistance to corrosion. This is the case for Ruthenium (Ru), a relatively scarce precious material found in various large-scale applications such as chlorine, nitrates, and acetic acid production. Additionally, Ru shows promising properties for low temperature Haber-Bosch process to produce ammonium.

The imaging techniques of Field Ion Microscopy (FIM) and Atom Probe Tomography (APT), when combined, provide unique atomically resolved surface structure and compositional maps used to understand metal oxidation dynamics. FIM enables correlative atomic to nanoscale imaging of the surface of a very sharp metal needle revealing a complex network of crystallographic facets, the nanoscale apex size and hemispherical like shape of which models that of a metal nanoparticle. While APT and Operando Atom Probe (OAP) is used to track the chemical interaction between the complex surface with reactive gases such as O<sub>2</sub> or N<sub>2</sub> through composition mapping.

Compared to other metals, Ru specimen preparation is relatively challenging due to fragility related to its hexagonal close packed (HCP) crystal structure. This makes Ru particularly sensitive to mechanical stresses during FIM and APT experiments. Additionally, Ga implantation from a FIB-based needle specimen preparation approach can lead to the formation

# Friday Morning, November 10, 2023

surface defects, complicating the indexing of the atomically resolved surface structure. In this work we will focus on the Ru specimen fabrication by FIB and the surface imaging by FIM with the indexing of Miller indices mapped across various surface features.

## Advanced Focused Ion Beams Focus Topic Room B110-112 - Session IB3-FrM

### Beam Induced Defect and Material Engineering

**Moderators:** **Tanvi Ajantimalay**, Pacific Northwest National Laboratory, **Gregor Hlawacek**, Helmholtz-Zentrum Dresden - Rossendorf

10:40am **IB3-FrM-8 Modeling and Experimental Demonstrations of Ion-Solid-Gas and Photon Beam Interactions During Nanoscale Synthesis**, **Philip Rack**, University of Tennessee, United States Minor Outlying Islands (the) **INVITED**

We study focused ion beam (FIB) processing using the Monte Carlo based simulation code EnvizION. This code simulates ion-substrate interactions and evolves the substrate to elucidate nanoscale milling and substrate damage. Additionally, we extended the simulation to include ion beam etching with a reactive precursor. The use of precursor gas for etching can greatly enhance material removal, allowing for enhanced etching at a significantly lower dose, and consequently, with much less associated damage to the bulk material. At the same time, the achievable resolution of the etched valley is impacted by a number of factors, such as the competition between chemical etching and physical sputtering, and the impact of the etching shape on gas coverage, and platform level patterning artifacts. EnvizION has been designed as a purpose built FIB simulation code, accounting for changes in the substrate configuration due to physical sputtering, as well as the dynamics of the precursor gas, while maintaining sufficient speed to practically simulate ion doses on the order of millions of ions. We study the etching of SiO<sub>2</sub> using a XeF<sub>2</sub> precursor gas. Etching simulations are validated against experimental data, and are used to identify how gas flux, beam current distribution, and platform level artifacts combine to determine achievable nanoscale resolution. Etching is studied for both Ne<sup>+</sup> and Ga<sup>+</sup> ion beam species, and the effective beam current distribution of each, corresponding to the experimental data, is identified. We additionally study the effect of the competition between etching gas flux and the beam dwell time, and in order to optimize resolution, we identify an intermediate gas flux for which etching resolution is the lowest.

In this presentation we will overview the EnvizION Monte Carlo simulation details including the ion-solid-precursor interactions and various sub-routines including secondary electron generation, surface energy minimization, vacancy-interstitial recombination, subsurface damage accumulation, and various precursor dynamics including adsorption, desorption, surface diffusion, secondary electron induced dissociation and ion-solid energy transfer induced dissociation. For each we will highlight the impact that the physical/chemical property effects the evolving nanoscale resolution of ion beam induced sputtering/chemical etching.

11:20am **IB3-FrM-10 Displacement Damage and Total Ionizing Dose Response of Ga<sub>2</sub>O<sub>3</sub> MOSFETs**, **Michael Titze**, Sandia National Laboratories Gallium Oxide (here β-Ga<sub>2</sub>O<sub>3</sub>) is a promising material for compact high-voltage electronics due to its high breakdown voltage compared to Si. Introduction of Ga<sub>2</sub>O<sub>3</sub> devices in radiation environments however requires prior knowledge of their response to various types of radiation, most notably displacement damage (DD) from neutrons in reactor environments, and total ionizing dose (TID) as experienced in x-ray / gamma environments. Device testing in appropriate environments is typically expensive and requires very long exposures due to the small interaction cross section of neutrons / gammas. Instead, we use a dual-beam focused ion beam and scanning electron microscope system (FIB-SEM) to probe radiation effects through surrogate environments. The FIB is used to generate predominantly DD with a small amount of TID while the SEM generates exclusively TID.

We use SRIM and PENELOPE simulations to determine the amount of DD and TID for each beam and observe the drive current and threshold voltage shift in DD and TID environments. We find that DD degrades the drive current but does not alter the threshold voltage. TID does not alter the drive current but changes the device threshold voltage.

This work was performed, in part, at the Center for Integrated Nanotechnologies, an Office of Science User Facility operated for the U.S. Department of Energy (DOE) Office of Science. Sandia National Laboratories

Friday Morning, November 10, 2023

is a multimission laboratory managed and operated by National Technology & Engineering Solutions of Sandia, LLC, a wholly owned subsidiary of Honeywell International, Inc., for the U.S. DOE's National Nuclear Security Administration under contract DE-NA-0003525. The views expressed in the article do not necessarily represent the views of the U.S. DOE or the United States Government.

11:40am **IB3-FrM-11 Helium Ion Microscopy for Morphological Analysis of Thrombi Extracted via Thrombectomy for Acute Stroke**, **Michael Westphal**, **N. Frese**, University Bielefeld, Germany; **C. Sommer**, Institut für Neuropathologie, Universitätsklinik Mainz, Germany; **A. Kitsiou**, **W. Schäbitz**, Universitätsklinik für Neurologie, Evangelisches Klinikum Bethel gGmbH, Universitätsklinikum OWL, Germany; **A. Beyer**, **A. Götzhäuser**, University Bielefeld, Germany

Strokes are one of the leading causes of death in the aging Western society. Especially in elderly patients, strokes are frequently recurring events. An essential component of stroke management after acute therapy is to diagnose the cause of the stroke for secondary prevention. More than 50 thrombi extracted via thrombectomy were examined by chargecompensated helium ion microscopy to investigate possible correlations between their morphology and the origin.

## Manufacturing Science and Technology Group Room C120-122 - Session MS-FrM

### Microelectronics R&D for Life-Cycle Energy Efficiency

**Moderators:** **Nicholas Johnson**, Energetics, **Tina Kaarsberg**, U.S. Department of Energy, Advanced Manufacturing Office

8:20am **MS-FrM-1 Energy Efficient Scaling in Microelectronics: Enabling a New Era in Computing for a Sustainable Future**, **Sadasivan Shankar**, SLAC National Accelerator Laboratory **INVITED**

The geometrical scaling of integrated circuit technology (known by the moniker as Moore's law) has led to many of the computing-based innovations over the last half century. Given the slowing down of scaling, it is important that the energy efficiency of computing should increase to offset the increasing number of digital devices and growing ubiquity of computing in all aspects of the world economy. To understand energy limits for information processing, we explore energy associated with both human-made and natural systems.

Based on lessons from the nature and fundamental analysis, we propose a new paradigm is to double the energy efficiency of computation in every succeeding generation in addition to the ongoing technological scaling. Using examples of synapses from a mammalian brain and quantum information, we estimate the headroom available for energy reduction to be of the order of 1000X to a million or more depending on the metrics. This can be enabled by trade-offs of the performance at the single switch level, with that at the system level including communication and storage, and with the total compute operations needed at the application level.

The opportunities for this new trajectory in computing resides in combinations of architectures, materials, devices, and algorithms/software and application-specific information processing. This energy-based design and scaling in turn could lead to exponential use of computing in even more innovative ways from Artificial Intelligence-driven applications, driverless cars, and smart grids due to the resulting Rebound Effect. As computing is the foundation of new sustainable economy, the intent of this new era is to leverage innovations in science and technology to form a green framework for the planet.

9:00am **MS-FrM-3 Improving Asic Energy Efficiency from Systems to Silicon**, **Godwin Maben**, Synopsys, Inc **INVITED**

Improving Energy efficiency while designing an electronic product, includes considering power as one of the constraints from the beginning of chip design, Macro Architecture selection, power performance trade-offs, appropriate workload selection, defining a power efficient architecture from Hardware perspective and designing an efficient Firmware, System's software, Application Software....etc.

In this presentation, we will look into every aspect of design cycle, in developing a complete platform, which is energy efficient from Systems to Silicon and How EDA tools have emerged as one of the key component in addressing Energy Efficiency, in addition to traditional Performance.

# Friday Morning, November 10, 2023

9:40am **MS-FrM-5 Atomic Precision Advanced Manufacturing for Tunnel Field Effect Transistors, *Shashank Misra***, Sandia National Laboratories  
**INVITED**

The energy efficiency of microsystems improved by more than 1000x every 20 years under Dennard scaling, where shrinking the linear dimension of a transistor while maintaining a constant electric field scaled the frequency and the voltage of operation. Satisfying the continued demand for computing, when scaling is projecting a single doubling of energy efficiency over the next 15 years, will require innovation across algorithms, architectures, and devices. Sandia has established programs pursuing the basic research underlying probabilistic neuromorphic computing, reconfigurable architectures, energy-efficient AI at the edge, and material manipulation for fine-grained integration of sensing and computation. In this talk, I will focus on a specific transistor that circumvents the physical limitation that ended Dennard scaling, and lowers the operating voltage of a circuit.

Tunnel field effect transistors (TFETs) rely on band-to-band tunneling, and promise a 10x improvement in energy efficiency compared to metal oxide semiconductor transistors (MOSFETs), all while maintaining the same materials. They have not achieved this promise due to poor on:off current ratios, and smeared dopant profiles producing gradual turn-on currents. We have designed a TFET in a vertical geometry which uses atomic precision advanced manufacturing (APAM) to form the buried electrode and the intrinsic tunnel barrier. This design boosts current by scaling with the area of the device instead of a 1D edge and obviates limitations from the abruptness of the doping profile. However, APAM has traditionally only been used to fabricate qubits, and has little to do with microelectronics.

Here, we integrate APAM with conventional fabrication, providing a straightforward path both to advanced transistor devices that work in practical conditions, and to scaled manufacturing. We first demonstrate both the two halves of the vertical TFET device operating at room temperature. We show an APAM nanowire integrated with common back end of line processing, which reveals the APAM nanowire strongly confines carriers, leading to current densities that exceed that of copper. Next, we demonstrate the gated top half the TFET device, limiting processing to thermal budgets tolerated by APAM. The low-thermal budget MOS transistor is used to evaluate the quality of APAM material. Next, we demonstrate integration into a CMOS fabrication flow, complete with working hybrid APAM-CMOS circuits. Finally, we explore operational robustness by showing that CMOS features fail before APAM features in accelerated lifetime testing.

*SNL is managed and operated by NTESS under DOE NNSA contract DE-NA0003525.*

10:40am **MS-FrM-8 Materials, Devices, and Packaging Opportunities Towards a Super Energy Efficient Future, *Paul Fischer***, Intel Corp. **INVITED**

As highlighted in the SRC's decadal plan, the total energy consumption by microelectronics is doubling approximately every three years while the world's energy production is growing only linearly and at about 2% per year. Despite the efficiency gains from continued Moore's Law scaling, global hunger for compute is growing faster. At Intel we are committed to building a more Responsible, Inclusive, and Sustainable world Enabled by our collective actions and in 2020 laid out our RISE strategy and goals which include a 10x increase in product energy efficiency by 2030.

But what emerging technology options are in the research pipeline to enable product energy efficiency which could shape future opportunities consistent with the Department of Energy's Energy Efficiency Scaling over 2 decades (EES2) effort? Product energy consumption is ultimately the culmination of broad technology ingredients spanning applications, software, algorithms, architectures, circuits, materials, devices, and packaging. In this talk Dr. Fischer will discuss a subset of these ingredients best aligned with AVS conference themes: emerging materials, devices, and packaging technologies which could drastically alter the energy requirements of future microelectronic products.

11:20am **MS-FrM-10 EES2 Update—A Pledger's Perspective, *Steve Pawlowski***, Intel **INVITED**

**Plasma Science and Technology Division  
Room A107-109 - Session PS+NS-FrM**

**Advanced Patterning and Plasma-Engineered Materials  
Moderator: Angelique Raley, TEL US**

8:20am **PS+NS-FrM-1 EUV Lithography Patterning towards Devices Nano Scaling, *Danilo De Simone***, IMEC, Belgium **INVITED**

Nowadays, the device scaling driven by the Moore's law is continuing by the deployment of the 0.33NA extreme ultraviolet lithography (EUVL) in high volume manufacturing further driven by the need to improve cycle time and cost. To further simplify and improve EUV patterning reducing cost and enable 2nm technology and below, high NA EUV lithography (0.55NA) is under development. At the same time, as the nanoscale is pushed further down, the stochastic nature of the patterning process and the thinning down of the films become the major patterning roadblocks. To enable the high NA technology, new knobs and faster learning cycles on patterning process development are needed to improve the process window. This presentation will show the latest development on EUV patterning materials and their challenges and provide an insight status of overcoming these obstacles towards the devices scaling at nanometric level.

9:00am **PS+NS-FrM-3 Break Healing and LER Mitigation for Low Dose EUV Exposure, *Rémi Vallat, P. Bézard, B. Chowrira***, IMEC, Belgium; *A. Fathzadeh, W. Halim*, KU Leuven, Belgium; *F. Lazzarino, K. Ronse*, IMEC, Belgium

Challenges introduced with High NA EUV lithography will be defectivity management with ultra-thin resists while using low EUV dose<sup>1</sup>. Reducing the density of bridges and breaks is thus a major point of focus for its introduction<sup>2</sup>. Ultra-thin resists, at low EUV dose, may come with high bridge/ break density (positive/ negative-tone resist, respectively). In the case of bridges, a descum step is traditionally introduced, which creates breaks instead (in ultra-thin resists) and further reduces the resist budget for underlayer patterning. Therefore, recovering breaks is a strategic capability for defect reduction.

The proposed way to recover breaks is to use non-conformal PECVD deposition on top of spin-on-glass (SoG). Since, the resist budget is going to be ultra-thin, the underlayer beneath will also have to be ultra-thin, leading to its failing as an hard-mask (break creation) during transfer into an amorphous carbon layer. Depositing extra Silicon-based polymers on top of the ultra-thin underlayer addresses that issue, by increasing the hard-mask etch budget. However, the polymer must be deposited on SoG, selectively to amorphous carbon to prevent the formation of an etch-blocking layer. This approach is presented in figure 1.

The selectivity of deposition is successfully developed, and results are shown in figure 2. The underlayer budget is clearly increased using PECVD. Also, the reduction in break density is demonstrated in figure 3 using a radical ion etching and/or quasi-atomic layer etch into aC, designed to maximize the break density in order to easily observe any improvement brought by the PECVD. The line-edge roughness is improved as well, due to the reduced contribution of breaks.

[1] L. Meli et al, *Proc. SPIE* 11609, 116090P (2021)

[2] P. De Bisschop, *J. Micro/Nanolithogr. MEMS MOEMS* 16, 041013 (2017)

9:20am **PS+NS-FrM-4 Carbon Resist Microlens Etching in DF-CCP CF<sub>4</sub> Plasmas: Comparison between Modeling and Experiments, *P. Ducluzaux***, Univ. Grenoble Alpes, CNRS, LTM / STMicroelectronics, France; *D. Ristoïu*, STMicroelectronics, France; *G. Cunge, Emilie Despiou-Pujo*, Univ. Grenoble Alpes, CNRS, LTM, France

Over the past decade, the development of image sensors used in smartphones has focused on reducing pixel size to improve photography resolution. Microlenses are a key component of these sensors, as they focus the incident light on the photodiode, enhancing the sensor's quantum efficiency. However, the manufacture of resist microlenses requires an etching step in low-pressure fluorocarbon plasmas, in which complex chemico-physical reactions can lead to a final 3D shape that is difficult to control.

In this paper, we propose to investigate numerically the influence of tunable operating conditions (RF power, pressure, etc.) on the etching of carbon resist microlenses in CF<sub>4</sub> plasmas, to better understand the link between process parameters, plasma properties and the final microlens shape. Using a 2D hybrid model (Hybrid Plasma Equipment Model), we simulate the CF<sub>4</sub> plasma gas-phase in a dual-frequency capacitively coupled plasma reactor. We then use the plasma properties obtained from this

# Friday Morning, November 10, 2023

simulation (densities, fluxes, and energies of charged and neutral species) as entry parameters for an etching profile model (Monte Carlo feature profile module). First, we investigate numerically and experimentally (ellipsometry, TOF-SIMS) the impact of pressure (30-200 mT) and RF powers (100-1500 W) on the etch rate and on the cross-sectional structure (chemical composition, reactive layer thickness) of resist blanket wafers. Then, we analyze the impact of these parameters on the etching of spherical resist microlenses, comparing the simulated 3D final shape with experimental profiles (AFM, SEM) obtained in an industrial reactor.

Our results show that the low-frequency (13.56 MHz) power increases the F penetration in the resist due to an increase in the ion energy, while the high-frequency (40 MHz) power increases the etch rate due to an increase in the ion flux. The impact of operating conditions on the microlens profiles will be discussed in details during the presentation and provide insights into the chemico-physical mechanisms involved in carbon resist etching.

9:40am **PS+NS-FrM-5 Investigations of Surface Reaction Mechanisms in EuV Induced Hydrogen Plasmas**, *Tugba Piskin*, University of Michigan; *V. Volynets, S. Nam, H. Lee*, Samsung Electronics Co., Inc., Republic of Korea; *M. Kushner*, University of Michigan

The deployment of extreme ultraviolet lithography (EUVL) is enabling a few nm critical sizes in microelectronic processing. In one implementation, the EUV photon beams are produced by ablating and ionizing tin droplets with a pulsed laser. The ionized tin species emit photons with 13.5 nm wavelength—where these photons are collected by reflective optics and transferred to the scanner unit. The collector mirror is exposed to the tin plasma, which potentially results in a decrease in reflectivity and lifetime. Pumping H<sub>2</sub> through the EUV chamber can help resolve this problem as an in-situ cleaning technique of deposited tin on the mirror. The hydrogen slows down fast tin radicals by reacting with them in the gas phase and etching. Photoionization of the H<sub>2</sub> by the EUV produces a plasma which etches the deposited tin on the mirror by producing stannane.

EUV photons with 92 eV energy are capable of photo-dissociating and ionizing hydrogen gas while producing energetic electrons and H atoms. Ions, energetic electrons, and photons in turn produce secondary electron emission from surfaces, the latter of which can also produce energetic electrons. In this work, we computationally investigate the etch rate of tin and the redeposition of stannane in a generic EUV lithography tool by the EUV produced hydrogen plasma using a modified version of the Hybrid Plasma Equipment Model (HPEM). The consequences of secondary electron emission from the surfaces by electrons and photons will be discussed. The fluxes of hydrogen radicals and ions to the collector mirror are the most significant factor for the in-situ cleaning. The energy and angular distributions and fluxes to the collector mirror of hydrogen radicals and ions for pressures of a few to hundreds of Torr and hundreds of Watts EUV power will be discussed.

Work supported by Samsung Electronics and the US National Science Foundation.

10:00am **PS+NS-FrM-6 Area Selective Processing Based on Physisorption to Improve Functions of Extreme Ultraviolet Resist**, *Van Long Nguyen, N. Maldonado, G. Denbeaux, C. Vallee*, SUNY Polytechnic Institute, Albany  
In semiconductor manufacturing, ~10 nm critical dimensions are already in production by using EUV lithography [1]. The smaller critical dimensions require better line edge/width roughness (LER/LWR) or local critical dimension uniformity (LCDU) of EUV resists to ensure the quality of patterning features, as well as device performance. Furthermore, ultrathin EUV resists (20- to 40-nm) are currently utilized to minimize the risk of pattern collapse, which however results in poor etching selectivity to underlying layers for post-lithographic pattern transfer. Recently, employing area selective deposition as a post-treatment method on the EUV resist patterns has been reported as a promising strategy to improve the function of EUV resists [2]. In this research, we tried to improve the local roughness and thickness of the EUV resist by developing an area selective (AS) processing including both deposition and infiltration based on the physisorption mechanism, instead of the conventional chemisorption mechanism. We achieved AS physisorption based on the difference in Van der Waals interactions of surfaces/bulks with a specific gas molecule. The interaction of physisorbed molecules with samples is calculated based on a classical model. SO<sub>2</sub> gas was chosen based on the theoretical calculation to test its selective physisorption capability to the Sn-based resist versus SiO<sub>2</sub>. After SO<sub>2</sub> exposure, we observed a significant thickness increase in the case of Sn-based resist (Figure S1a) but not in the SiO<sub>2</sub> (Figure S1b), as shown in the supplemental document. The observed thickness increase suggested SO<sub>2</sub> could both selectively physisorb onto the surface and into the bulk of

the resist due to its porosity. These selective physisorbed molecules onto the surface and into the bulk of the resist are then converted to chemisorbed molecules by a dissociation process using energetic Ar plasma to complete a cycle of AS deposition and AS infiltration, respectively. Ellipsometry, angle-resolved X-ray photoelectron spectroscopy, and atomic force microscopy are employed as key techniques to characterize changes during and after the AS processing. This work is funded by Semiconductor Research Corporation (SRC).

[1] <https://irds.ieee.org/editions/2022/executive-summary> for International Roadmap for Devices and Systems (IRDS), 2022 Edition.

[2] Nye, Rachel A., et al. "Enhancing Performance and Function of Polymethacrylate Extreme Ultraviolet Resists Using Area-Selective Deposition." *Chemistry of Materials* 35.5 (2023): 2016-2026.

10:40am **PS+NS-FrM-8 Recent Advances in Ga<sub>2</sub>O<sub>3</sub> Material Development at AFRL**, *S. Mou, T. Asel, A. Neal, Y. Kim, Brenton Noesges, A. Charnas, J. Li, T. Back, K. Burzynski, B. Newton, A. Green, J. Blevins*, Air Force Research Laboratory, Materials and Manufacturing Directorate, USA **INVITED**

Ga<sub>2</sub>O<sub>3</sub> has been of interest due to its critical electric field (8 MV/cm)[1], its ability for native substrates to be grown from the melt, and the ability to controllably dope thin films of Ga<sub>2</sub>O<sub>3</sub> via growth methods such as molecular beam epitaxy (MBE) and metal-organic chemical vapor deposition (MOCVD). All of these properties make Ga<sub>2</sub>O<sub>3</sub> an attractive candidate for high power electronic applications and the ability to grow substrates from the melt make it economically feasible in this space when compared to other materials such as GaN and SiC. The Air Force Research Lab (AFRL) has invested into substrate development with Northrup Grumman Synoptics to provide a domestic source of substrates. Czochralski grown (010) Fe and Mg doped Ga<sub>2</sub>O<sub>3</sub> has been demonstrated up to 2 inch wafers by Northrup Grumman Synoptics and challenges in surface polishing have been overcome by using a 2 step process that removes subsurface damage and produces a surface that is ready for epitaxial growth. AFRL's in house research on epitaxial films via plasma assisted MBE has identified sources of unintentional doping during the growth of Ga<sub>2</sub>O<sub>3</sub>. It was demonstrated that both the oxidation of the Si doping source material and the quartz bulb used to provide the oxygen plasma during growth were contributing significant amounts of Si in the grown films. By adjusting the plasma power to reduce the etching of the quartz plasma bulb we were able to demonstrate epitaxial films with unintentional doping levels <1 × 10<sup>16</sup> cm<sup>-3</sup>. Control of the intentional Si doping was achieved in collaboration with Cornell University by modifying the Si doping source to include a "showerhead" to reduce the effect of the oxidation of the Si source material[2, allowing control from 8 × 10<sup>16</sup> cm<sup>-3</sup> to 1 × 10<sup>19</sup> cm<sup>-3</sup>. Additional thin film development was done in collaboration with Agnitron on MOCVD grown Ga<sub>2</sub>O<sub>3</sub> films. High purity Ga<sub>2</sub>O<sub>3</sub> films were demonstrated using trimethylgallium as the source for gallium during the growth. The MOCVD grown films' mobility and carrier concentration were measured via temperature dependent Hall Effect at AFRL and exhibited a record electron mobility of 23,400 cm<sup>2</sup>/Vs at 32 K, with a low acceptor concentration of 2 × 10<sup>13</sup> cm<sup>-3</sup>, further demonstrating the purity of the films grown via this method[3]. These results demonstrate the investment that AFRL has in Ga<sub>2</sub>O<sub>3</sub> and present the contributions that AFRL has made to the development to Ga<sub>2</sub>O<sub>3</sub> material system.

[1] M. Higashiwaki et al. *Appl. Phys. Lett.* **100**, 013504 (2012).

[2] J.P. McCandless et al. *Appl. Phys. Lett.* **121**, 072108 (2022).

[3] G. Seryogin et al. *Appl. Phys. Lett.* **117**, 262101 (2020).

# Friday Morning, November 10, 2023

11:20am **PS+NS-FrM-10 Reverse Lift-Off Process to Avoid Sidewall Artifacts Resulting from Dry Etching “Challenging” Materials**, *D. Lishan*, Plasma-Therm, LLC; *V. Genova*, Cornell University; *S. Norris*, Axoft; *K. Dorsey*, Physical Sciences, Inc.; *Sabrina Rosa-Ortiz*, Plasma-Therm LLC

This work explores a process to avoid sidewall redeposition issues when dry etching materials that do not readily form volatile and desorbing etching byproducts under common operating temperatures. Common dry patterning approaches for these challenging thin films use methods relying on physical mechanisms (i.e., sputtering with accelerated ions) and often result in material being redeposited on the sidewalls of the masking material. Upon removing the mask, the resputtered sidewall material remains and forms features projecting above the material. These features, sometimes referred to as rabbit or dog ears, fences, and veils, may fall over, break and cause particles, or penetrate over layers. We present an etching approach that avoids these issues. Materials such as Pt, Au, Ni, LiNbO<sub>3</sub>, Cu, Ni, Fe, Mn, Co, Mn, PZT, ScAlN, and perovskites fall in the category of “challenging” to etch materials and impact applications such as MRAM, PiezoMEMS, quantum devices and photonics.

Lift-off patterning requires line-of-sight deposition which is typically an evaporative process that constrains thermal budgets and materials that can be deposited. We discuss a technique derived from this well-known additive method of patterning thin metal layers but using a subtractive approach. In this “reverse -lift” off approach, a layered structure with an undercut in a sacrificial layer is also used. Following etching, the material that was sputter etched and redeposited on sidewalls is removed along with the sacrificial layer. Unwanted redeposition is avoided with the proper choice of sacrificial layer material, mask, and undercut structured or with familiar lift-off resist patterning (LOR). Importantly, the dry etching can be done in common parallel plate RIE and ICP configurations and does not require an ion gun source, thus making the method more accessible.

Results demonstrate physically etching a difficult material without the consequences of resputtered material. Pt was used as a test vehicle with film thicknesses up to 200 nm. Positive results were obtained with LOR patterning, with SiO<sub>2</sub> as the mask with a Si sacrificial layer, and with a Cr sacrificial layer. Both IBE and ICP configurations were used with similar results showing that the expected feature dimensions were maintained without the profile changes typically observed with tilt and rotation IBE. Modeling considered feature spacing, resputter distribution (cosine ejection), and incident ion angles to better understand the limits and dimensions of the lift-off structure. This work offers a process technique that can solve the issue of dog ears when plasma etching low or nonvolatile materials.

11:40am **PS+NS-FrM-11 Control of Ge/Si Core/Shell Nanoparticles Growth In Pulsed Nonthermal Plasmas**, *Yifan Gui*, *J. Polito*, *M. Kushner*, University of Michigan

Core/Shell nanoparticles (CSNPs) are a type of nanomaterial that has the characteristic structure of a core and an outer shell composed of distinct materials. CSNPs have received increasing attention over the past decade due to their tunable optical properties and wide applicability in the biomedicine, semiconductor and catalyst fields. The major challenges in synthesizing CSNPs with consistent specifications lie in the variation of size uniformity, core and shell purity as a result of diverse operating conditions. While continuous-wave nonthermal plasma approaches for synthesis of CSNPs have enabled crystalline growth at low reactor temperatures, pulsing the plasma could give an edge in CSNPs production by addressing these issues. Both computational and experimental prior works have demonstrated the capability of pulsed nonthermal plasma in synthesizing nanoparticles with improved size uniformity<sup>1,2</sup>.

The aim of this work is to computationally investigate the consequences of pulsed power nonthermal plasmas on size uniformity and core/shell purity of Si/Ge CSNPs using the Hybrid Plasma Equipment Model (HPEM) coupled with DTS Dust Transport Simulation Module (DTS). The test system is an inductively coupled plasma (ICP) having two plasma sources intended to enhance CSNP size uniformity while utilizing separate core and shell synthesis zones for better core/shell purity control. CSNPs are produced under operating conditions of a few Torr, 10 W of ICP power with pulse period of 50  $\mu$ s, with Ar/GeH<sub>4</sub> and Ar/SiH<sub>4</sub> gas mixtures flowing from top and middle inlets. The consequences of process parameters such as pulse period, duty cycle and ICP power, and the corresponding impacts on CSNP

properties will be discussed and compared to CSNP properties resulting from continuous-wave operation.

Work supported by Army Research Office MURI Grant W911NF-18-1-0240, the National Science Foundation (PHY-2009219), and the Department of Energy Office of Fusion Energy Science (No.DE-SC0020232).

<sup>1</sup>S. J. Lanham, et al. Journal of Applied Physics **132**, 073301 (2022)

<sup>2</sup>J. Schwan, B. Wagner, et al. J. Phys. D: Appl. Phys. **55**, 094002 (2022)

## Plasma Science and Technology Division Room A106 - Session PS+SE-FrM

### Atmospheric Pressure Plasmas and Their Applications

**Moderators:** **Michael Johnson**, Naval Research Laboratory, USA, **Floran Peeters**, LeydenJar Technologies

8:20am **PS+SE-FrM-1 Electrolyte Engineering for Nitrogen Fixation by Plasma Electrolysis**, *Brandon Kamiyama*, University of Illinois at Urbana Champaign; *M. Eslamisaray*, University of Illinois Urbana-Champaign; *R. Pierrard*, *R. Sankaran*, University of Illinois at Urbana Champaign

The fixation of nitrogen is critical to our most basic need, the growth of plants for food. Industrially, nitrogen is fixed to ammonia (NH<sub>3</sub>) by the Haber-Bosch process which has a large physical and environmental footprint. The development of alternative methods that are sustainable and deployable at a small scale has become one of the active areas of research. Among the different approaches being explored, plasma-based electrolytic reactors have shown the most promise, capable of activating nitrogen in air or with water as a source of hydrogen at atmospheric pressure and near room temperature without any catalyst and using only electricity which could in the future come from renewable sources. However, a key challenge is selectivity of products with typical processes producing NH<sub>3</sub>, nitrates (NO<sub>3</sub><sup>-</sup>), and nitrites (NO<sub>2</sub><sup>-</sup>).

In this work, we studied direct-current plasma in contact with an electrolyte solution. Various products were characterized in the liquid phase including NH<sub>3</sub>, NO<sub>3</sub><sup>-</sup>, NO<sub>2</sub><sup>-</sup>, as well as hydrogen peroxide (H<sub>2</sub>O<sub>2</sub>). To control the product selectivity, various conditions were mapped including gas feed, cathodic vs. anodic polarity, and pH. Our most promising result was that the pH and more generally, the electrolyte composition, was found to greatly influence the product distribution. At low pH, the product distribution shifted more to the reduced form, NH<sub>3</sub>, and at high pH, the distribution shifted more to the oxidized form, NO<sub>3</sub><sup>-</sup>. We also found a strong effect on the presence of O<sub>2</sub> (in air) and humidity. These results can be used to selectively synthesize nitrogen products, elucidate product formation mechanisms, or to inform scale up of similar plasma-liquid systems for sustainable nitrogen fixation.

8:40am **PS+SE-FrM-2 Two Atmospheric Pressure Plasma Jets Driven by Phase-Shifted Voltages: A Method to Control Plasma Properties at the Plasma-Surface Interface**, *Michael Johnson*, Huntington Ingalls Industries; *G. Brown*, University of Texas, Austin; *D. Boris*, *T. Petrova*, *S. Walton*, Naval Research Laboratory

Atmospheric pressure plasma jets project plasma away from their electrodes, enabling the treatment of remotely located surfaces, and making them appealing for a diverse range of surface treatment applications. However, their small effective areas pose a challenge to broader adoption and utilization. To circumvent this limitation, multiple plasma jets can be used in tandem to increase their effective area. The objective of this study is to examine the interactions between two plasma jets and leverage this relationship to manipulate plasma properties at the plasma-surface interface. The jets are positioned at a 130° angle from each other, converging at the surface of a glass substrate. Each jet is driven by an individual piezoelectric transformer, powered by identical but phase-shifted voltage waveforms, which provides precise control over their relative timing and influence plasma properties. As phase difference between the two jets is varied the jet behavior changes from a regime where the two jets repel each other to a regime of enhanced jet interaction, resulting in an expanded effective area for the plasma. Interestingly, increasing this phase difference led to reduced power consumption while simultaneously enhancing electron density at the intersection point. Consequently, this technique of utilizing phase-shifted jets presents a method for increasing the effective area of the plasma and controlling plasma properties at an interface, potentially benefiting a wide array of applications.

This work supported by the Naval Research Laboratory Base program

# Friday Morning, November 10, 2023

9:00am **PS+SE-FrM-3 Plasma Chemistry in Atmospheric Pressure Gases and Liquids: Fundamentals and Novel Applications**, *Alexander Fridman*, Drexel University, Nyheim Plasma Institute **INVITED**

The presentation is focused on fundamental and applied aspects of the non-equilibrium plasma chemical processes performed in high pressure gases and liquids. As an example of the gas-phase processes, the plasma synthesis of NO from atmospheric pressure air is considered, with especial attention on minimizing energy cost of the process. As an example of the plasma-chemical processes in liquid water, the PFAS abatement in considered with especial attention to complete mineralization of these important impurities. As an example of plasma chemistry in cryogenic liquids, the plasma synthesis of polymeric nitrogen is considered. The process is accomplished in liquid nitrogen using the nanosecond-pulsed discharges organized with creation of bubbles during the synthesis.

9:40am **PS+SE-FrM-5 Integrated Circuit Manufacturing with Plasma Activated Chemical Treatment (IMPACT): Effect of Plasmas on Photoresist and Cleaning Solutions in Semiconductor Processing**, *Christian Williams, S. Dubowsky, D. Curreli, M. Sankaran, D. Ruzic*, University of Illinois at Urbana-Champaign

Low-temperature, atmospheric-pressure plasmas open various chemical and material applications because of their ability to be in contact with temperature-sensitive surfaces such as plastics and liquids. In this work, we investigated the potential of plasmas to modify two key components of semiconductor processing [1]: the photoresist and cleaning solution used to remove the photoresist after lithographic exposure. Two different plasma sources were used in experiments, a dielectric-barrier discharge and a pulsed direct current discharge jet. Characterization of the gas phase was performed by optical emission spectroscopy (OES) and the chemical modification of the treated solutions was examined using ion chromatography (IC). Ultraviolet-visible (UV/Vis) spectroscopy was also used to measure OH radical concentrations in the treated samples. In parallel, a reaction network was constructed using CRANE, a MOOSE-based tool for plasma chemistry modeling. Simulations provided the concentrations of species which could then be compared to experiments to understand potential reaction mechanisms.

10:00am **PS+SE-FrM-6 Increasing Adhesion of Polyurethane Painting on Aluminum by Atmospheric Pressure Plasma Jet Treatment**, *Jorane Berckmans, C. Tubier*, Chemistry of Surfaces, Interfaces and Nanomaterials (ChemSIN), Faculty of Sciences, Université Libre de Bruxelles, Brussels, Belgium; *R. Revilla Castillo*, Research Group Electrochemical and Surface Engineering (SURF), Department of Materials and Chemistry, Vrije Universiteit Brussel, Brussels, Belgium; *C. Poleunis*, Unité Physico-Chimie et de Physique des Matériaux (PCPM), Université Catholique de Louvain, Louvain-la-Neuve, Belgium; *H. Terry*, Research Group Electrochemical and Surface Engineering (SURF), Department of Materials and Chemistry, Vrije Universiteit Brussel, Brussels, Belgium; *A. Delcorte*, Unité Physico-Chimie et de Physique des Matériaux (PCPM), Université Catholique de Louvain, Louvain-la-Neuve, Belgium; *F. Reniers*, Chemistry of Surfaces, Interfaces and Nanomaterials (ChemSIN), Faculty of Sciences, Université Libre de Bruxelles, Brussels, Belgium

Nowadays, industries are looking for replacement of chromium VI in aluminum pretreatment. In this quest, plasma treatments could represent an interesting approach. Indeed, atmospheric plasmas enable a wide range of possible modifications of materials (etching, grafting, surface functionalization) but also allow an easy industrial upscale.[1,2]

In this work, aluminum 99,99% surfaces were modified by an atmospheric pressure plasma jet (APPJ) and the effect on polyurethane paint adhesion was studied. The difference in wettability, chemistry and roughness induced by plasma treatments were investigated by water contact angle, X-ray photoelectron spectroscopy and atomic force microscopy respectively. In parallel, optical emission spectroscopy (OES) was used to characterize the plasma phase. The correlation between plasma species, identified by OES, and the resulting surface modification was investigated. Then, the adhesion of the polyurethane coatings on the plasma-modified surfaces was studied by a tape test according to ASTM D3359. The coating – aluminum substrate interface has been also characterized by ToF-SIMS, to identify specific fragments characteristics for bonding.

Different plasma sources were used, with different plasma conditions (PlasmaTreat Openair FG5001, 2 bars of dry air, at varying distances from 5 mm to 10 mm and treatment times of 0,5 to 60,0 s by tuning the number of scans and the scan rate of the APPJ over the surface, SurfX Atomflo 600, with 30,0 L/Min of Ar at varying flow of oxygen from 0,00 to 0,60 L/Min, distance from 5 mm to 30 mm and treatment times of 0,04 s to 25 s by

tuning the number of scans and the scan rate of the APPJ over the surface). Varying humidity containing in plasma, by water injection, was also studied with the SurfX Atomflo 600.

It is shown that, for most of the plasma treatments used, an increase of the adhesion of polyurethane coatings is observed (Fig. 1) and associated with the surface modification of the aluminum and with the plasma chemistry.

## References

- [1] H. Butt, K. Graf, M. Kappl, Phys. Chem. Interfaces 2013, 28,1379.
- [2] K. G. Kostov, T. M. C. Nishime, A. H. R. Castro, A. Toth, L. R. O. Hein, Appl. Surf. Sci. 2014, 314, 367.

## Acknowledgements

This work is partly supported by the ULB-VUB “joint research group” fund.

10:40am **PS+SE-FrM-8 Fundamentals of Atmospheric Pressure Discharges for Plasma Catalytic Applications**, *Judith Golda, D. Steuer, R. Labenski, H. van Impel, M. Böke, V. Schulz-von der Gathen*, Ruhr-University Bochum, Germany **INVITED**

A central challenge of our time is the energy transition from fossil energy sources to renewable ones. Plasma catalysis is one of the promising techniques that has been proposed to contribute to this transition. Research shows that synergies between classical catalysis and plasma processes can be obtained due to the distinct non-equilibrium character of atmospheric pressure plasmas and their interaction with surfaces. However, the underlying mechanisms are hard to entangle as typical reactor designs for plasma catalysis are packed bed reactors. While advantageous for industrial processes, the diagnostics of these reactors is challenging.

In this talk, we give an insight into the diagnostic challenges of plasmas for catalysis as well as possible approaches to overcome them. We will discuss alternative reactor designs for fundamental studies such as micro-structured surface dielectric barrier discharges. We will give an overview of global and local diagnostic techniques: Current-voltage characteristics for dissipated plasma power and estimation of electron densities, emission-based techniques for reactive species densities such as atomic oxygen (state-enhanced actinometry) or temperature (rotational bands), and electric field estimation (Stark splitting and shifting).

This research is funded by the German Research Foundation within CRC 1316 in project A6.

11:20am **PS+SE-FrM-10 Atmospheric Pressure Inductively Coupled Torus Torch System for 3D Printing the Silicon-Nanofiber (Si/CNF) Anodes for Li-ion Batteries**, *Yuri Glukhoy*, Nanocoating Plasma Systems Inc; *M. Ryaboy*, UC Berkeley

Our approach to environmentally-friendly manufacturing low-cost Si anodes with the core-shell heterostructure includes 3D plasma beam printing. Excitingly, because of the merits of low price, high doping content, and no toxic emission during the process, Si sawdust, which is a waste of the solar cell industry, can be a fascinating raw material for Si shells with well-tailored functions and electrical properties. However, the transition of the Si sawdust requires a long resident time in the high-temperature plasma and a high RF power to sustain it. We offer a new method of generation of Si vapor and the simultaneous lamination of CNF through the recirculation of both Si and CNF in the high-temperature torus plasma torch. It allows the incremental sublimation of Si particles, while Si vapor is deposited in the fly on the fibers' preheated surfaces. This torus torch recirculated in the high-temperature doughnut-like reactor is generated by two tangentially injected in the opposite direction axial atmospheric plasma beams in the swirling mode. Besides the high-temperature plasma species, these beams are designed to bring the liquid Si droplets from the melted Si powder injected into the high-temperature plasma discharge generating such a beam. Two inductors with transversal RF fields are positioned on the opposite sides of the doughnut and surround this profile. They boost this torus plasma torch, increasing the plasma density and current until its magnetic field pinches into the high-temperature plasma cord. But RF power applied to the inductor should be limited to avoid melting the CNF at 3550 °C. This recirculation process in the high-temperature plasma reactor should provide a conformal Si lamination of CNF in the fly to achieve the Si shell's thickness of around 1 µm. Two outlets are welded to this doughnut to extract the Si/CNF composites and generate the plasma sprays. Ended with the nozzles and directed to the opposite sides of the copper tape serving as a current collector, they provide 3D printing of the Si/CNF anodes in the roll-to-roll mode.

# Friday Morning, November 10, 2023

11:40am **PS+SE-FrM-11 Design and Functionality of a Low-Frequency Pulsed Plasma System**, *M. Gulan*, Technological University Dublin, Ireland; **Vladimir Milosavljevic**, Technological University Dublin, Ireland & Faculty of Physics, University of Belgrade, Serbia, Ireland

This study presents the design and functionality of a kHz pulsing plasma generator at atmospheric pressure, which can be used for a range of applications, such as sterilization in food processing or plasma-based treatments for biological samples. This next generation plasma system is developed to operate in ambient air or on an argon/helium/oxygen/nitrogen gas mixture at atmospheric pressure, making it suitable for a range of applications such as surface modification, plasma-based sterilization, and material processing. The system's unique design allows for improved efficiency, higher plasma density, and greater control over plasma parameters compared to previous systems. The plasma tool is particularly suitable for sensitive and fragile materials. This work describes the development and operation of a non-thermal, dielectric-free atmospheric plasma system designed for use in surface treatment and modification applications. The system was developed in-house to meet the specific technological needs, and includes detailed information on the design and operating parameters of the system. The new plasma system allows an increase in the plasma-surface interaction selectivity and reduces plasma induced damages to the surface. The innovative design of our plasma system led to the development of unique plasma parameters that are not currently available on the market. Specifically, the system allows for precise control of plasma temperature, density, and composition, which are essential for effective plasma treatment of a range of materials. These unique parameters were designed with the goal of simplifying plasma treatment in industrial applications such as surface modification, cleaning, and sterilization, where precision and efficiency are critical factors for success. The system creates a plasma discharge in gap from 5 to 60 mm in space of hundreds of cm<sup>2</sup>. The plasma source is based on a pulse resonance circuit which allows the creation of high voltage pulses with the ability to control and reduce a current of the plasma discharge. The study also includes different setting of plasma source to control the ion flux, the ion energy and the plasma chemistry. Plasma pulsing allows new domains of ion energy and radical fluxes to be reached, thereby extending the operating range of plasma generators. The plasma diagnostics in this work include the absorption spectra of oxygen and nitrogen based molecules and their dependence on the process parameters such as duty cycle, discharge frequency, pick-to-pick voltage, etc.

## Thin Film Division

### Room A105 - Session TF+SE-FrM

#### Metal-Organic Frameworks and Other Network Materials

**Moderators: Christophe Vallee**, SUNY College of Nanoscale Science and Engineering, **Junjie Zhao**, Zhejiang University

8:20am **TF+SE-FrM-1 Membrane Design by Atomic Layer Deposition**, **Mikhael Bechelany**, CNRS/European Institute of Membranes, France  
**INVITED**

Atomic layer deposition (ALD) is a technology offering the possibility to prepare thin films of high quality materials on high aspect ratio substrates with precise thickness control, high uniformity and excellent conformality, a unique capability. Therefore, this route is particularly suited for the structural modification and pore tailoring of synthetic membranes. ALD coatings have been prepared on a wide variety of membrane substrates, from inorganic templated supports to porous polymers. In this talk we aim to provide an extensive summary of the advances of ALD applied to membranes. A selected list of our studies will be used to illustrate how the ALD route can be implemented to improve the operational performance of different inorganic, organic, hybrid or composite membranes. We will show examples how ALD [1], could be used for the design of membranes in which the geometry can be tuned accurately and the dependence of the physical-chemical properties on the geometric parameters can be studied systematically in order to investigate their performances in renewable energy (gas separation [2,3] and osmotic energy harvesting [4]), environmental (water treatment [5], and sensors [6,7] as well as health applications.

Furthermore, the challenges and opportunities of the route for this specific membrane application are also discussed. This talk comprehensively shows the benefits of ALD and its application in various facets of membranes and membrane associated engineering processes, and will help exploiting the numerous prospects of this emerging and growing field.

100. Chemistry of Materials 2018, 30, 7368-7390
101. Journal of Membrane Science, 2015, 475, 39-46
102. Journal of membrane Science, 2020, 596, 117701
103. ACS Appl. Mater. Interfaces, 2017, 9, 16669-16678
104. Separation and Purification Technology, 2023, 312, 123377
105. Journal of Materials Chemistry A, 2019, 7, 8107-8116
106. Sensors and Actuators B: Chemical, 2021, 344, 130302

9:00am **TF+SE-FrM-3 Ultrathin Transferable MOF/Polymer Janus Thin Films with Tunable Turing Morphologies**, **Xinyu Luo<sup>1</sup>**, **J. Zhao**, Zhejiang University, China

Janus thin films are known for their distinct asymmetric structures that bring unique properties for energy harvesting, mist collection and membrane separation applications. Decorating Janus thin films with Turing patterns could enlarge the surface area and generate stretchability. However, these delicate structures are particularly difficult to synthesized by conventional methods and not easily transferable for integration of composites and devices. Here, we report a novel interfacial synthesis method using an atomic layer deposited (ALD) ZnO template and a nanoscale polymer topcoat for Janus thin films with the intricate Turing patterns. Through confining the reaction at the interface between the ALD ZnO layer and the polymer topcoat, a continuous micron-scale MOF film, acting as the Turing morphogen, was rapidly formed and anchored onto the bottom side of the polymer topcoat, thus leading to a Janus structure. We obtained Turing patterns in the MOF/polymer Janus thin films that agree well with the prediction by the Gray-Scott diffusion-reaction model. Our Turing Janus film remained flexible even with 96wt% MOF loading and can be transferred onto various substrates for membrane separation and sensing applications. Gas permeation tests confirm the absence of pinhole defects in the Turing Janus films transferred onto porous alumina support. Additionally, the Turing structures provide stretchability to the Janus films that allows repeated bending on flexible electrodes for gas sensors. The reported Turing Janus film demonstrated a proof-of-concept handy transferable thin film product for versatile functions.

9:20am **TF+SE-FrM-4 Growth of Metal-Organic Framework Thin Films by a Vapor-Assisted Conversion Method**, **D. Speed**, **A. Bajpai**, **Greg Szulczewski**, The University of Alabama

Metal-organic frameworks (MOFs) are a class of highly porous materials that can be synthesized using a variety of inorganic nodes and organic linkers, which enable MOFs for applications in gas sensing, gas storage, and gas separations. In this talk, we will describe the synthesis of MOFs thin films via a hot vapor-assisted conversion method on a variety of substrates. In general, the precursor components to the MOF are dissolved in an appropriate organic solvent and transferred to the substrate as a small droplet. The reaction is initiated by heating the droplet in the presence of the hot vapor from the organic solvent. Specifically, we describe the results for UiO-66 and UiO-67 thin films and Co-MOF-74 and Ni-MOF-74 thin films. The thin films were characterized by x-ray diffraction, IR/Raman spectroscopy and scanning electron microscopy. The growth of UiO-67 is interesting. Quasi-octahedral crystals appear to grow from the surface, which is in contrast to the other MOFs we studied. The role of precursor concentration appears to strongly effect the film growth mechanism. The porosity of the films was assessed by measurement adsorption isotherms using aromatic hydrocarbons as the probe molecules. In all cases the films show saturation adsorption uptake comparable to bulk samples. Overall, the vapor-assisted conversion method is a convenient way to grow thin films at low temperatures within a few hours.

9:40am **TF+SE-FrM-5 Enhancing the Electrical and Optical Properties of Thermochromic VO<sub>2</sub>: The Impact of Nanostructuring and Gold Nanoparticles**, **Gregory Savorianakis**, **S. Konstantinidis**, **M. Voué**, Université de Mons, Belgium; **N. Martin**, FEMTO-ST, France

Monoclinic VO<sub>2</sub> (m-VO<sub>2</sub>) exhibits a Metal-Insulator Transition (MIT) at approximately 67°C, making it a thermochromic material of interest. In this study, we initially show the optimization of magnetron sputtering using a vanadium target within an Ar/O<sub>2</sub> mixture to synthesize films that are 200 nm thick and contain m-VO<sub>2</sub> crystals. Our synthesis process involves precise control of the oxygen flow rate and subsequent annealing of the films in O<sub>2</sub> for 120 minutes at 500°C.

<sup>1</sup> TFD James Harper Award Finalist

# Friday Morning, November 10, 2023

In the first segment of our research, we validate our numerical findings obtained through the Cavity Modelling Framework (CAMFR) by comparing them to the optical properties of the synthesized films. Our simulations demonstrate how nanostructuring via ribbon-like structures can be adjusted to enhance film properties for potential applications in smart windows. By varying parameters such as the width of VO<sub>2</sub> nano-ribbons, periodicity, and film thickness, we can achieve improved energy efficiency and a less opaque appearance compared to a dense film with the same thickness.

Secondly, we conducted experimental research where we combined m-VO<sub>2</sub> films with gold nanoparticles (AuNPs) to achieve tunable plasmonic signals in response to temperature variations. Our study demonstrates the successful grafting of AuNPs onto the surface of the VO<sub>2</sub> film using (3-aminopropyl) trimethoxysilane (APTMS) linkers. We observed a noticeable shift in the wavelength of the plasmonic peak, which was quantified as a function of temperature for two distinct platforms: one with NPs positioned on top of the VO<sub>2</sub> film and another with NPs embedded within the film. Additionally, our investigations into resistivity and optical hysteresis revealed that the presence of AuNPs amplifies the resistivity drop by one order of magnitude and enhances the transmission drop by 15%. Furthermore, it reduces the critical temperature by 5°C and narrows the hysteresis width.

In a subsequent development, we have successfully synthesized thermochromic VO<sub>2</sub> nanostructures, including tilted nanocolumns, zig-zags, and helices, utilizing the Glancing Angle Deposition (GLAD) technique. Our optical and ellipsometry analyses have revealed a significant anisotropy that correlates with the sample's rotation during measurement. This unique type of sample introduces a new dimension of control beyond temperature alone, allowing us to fine-tune its optical response. By combining both factors, we can achieve multi-dimensional tunability.

The here-mentioned work may pave the way towards the elaboration of thin film materials with high optical accordability which can potentially be used in applications as colour display, protection against counterfeiting, opto-electronics chips or energy-saving smart windows.

10:00am **TF+SE-FrM-6 Atomic Layer Deposition of Sn-doped MoO<sub>2</sub> Electrode Films with Distorted Rutile Structure for High-performance TiO<sub>2</sub>-based DRAM Capacitors**, *Jae Hyeon Lee, J. Han, J. Shin, W. Kang*, Seoul National University of Science and Technology, Republic of Korea  
Traditional DRAM capacitor electrodes, typified by TiN, confront performance deterioration attributed to their low work function and the formation of low-k TiO<sub>x</sub>N<sub>y</sub> interfacial layers. As device scaling progresses, these issues become increasingly critical, driving recent research efforts to explore alternative electrode materials to replace TiN. Molybdenum dioxide (MoO<sub>2</sub>) emerges as a promising candidate, boasting a low resistivity of 150 μΩ-cm, a high work function (>5 eV), and excellent thermal stability, outperforming TiN. Furthermore, MoO<sub>2</sub> exhibits a distorted rutile structure similar to rutile-TiO<sub>2</sub> which is a next-generation DRAM capacitor high-k material, enabling the low-temperature growth of rutile-TiO<sub>2</sub> on MoO<sub>2</sub> bottom electrode. However, MoO<sub>2</sub> deposition presents challenges due to its metastable nature compared to the stable phase molybdenum trioxide (MoO<sub>3</sub>).

In this study, we successfully fabricated distorted rutile MoO<sub>2</sub> films through atomic layer deposition (ALD) by incorporating SnO into MoO<sub>3</sub>. The ALD process was performed using a super-cycle method consisting of the MoO<sub>3</sub> ALD sub-cycles and SnO ALD sub-cycles. The optimal sub-cycle ratio of MoO<sub>3</sub> to SnO was determined by varying the ratio from 100:1 to 100:5. After post-deposition annealing, MoO<sub>2</sub> films with resistivity of 0.254 Ω-cm and an RMS roughness of 0.48 nm were obtained. Finally, to assess the feasibility of Sn-doped MoO<sub>2</sub> films as DRAM capacitor electrodes, metal-insulator-metal capacitors were fabricated using Sn-doped MoO<sub>2</sub> as bottom electrodes. Through this, it was confirmed that ALD TiO<sub>2</sub> film was crystallized into the rutile phase on the Sn-doped MoO<sub>2</sub>, and a high dielectric constant of 130 was obtained despite the relatively low TiO<sub>2</sub> deposition temperature. Consequently, this study confirmed the viability of Sn-doped MoO<sub>2</sub> as a promising DRAM capacitor electrode material.

10:40am **TF+SE-FrM-8 Area Selectivity and Crystallographic Orientation of Zif-8 Films Deposited by Molecular Layer Deposition**, *Jorid Smets, V. Rubio-Giménez*, KU Leuven, Belgium; *S. Armini*, IMEC, Belgium; *R. Ameloot*, KU Leuven, Belgium

Integrating metal-organic frameworks (MOFs) into electronic devices would benefit from controlled vapor-phase thin film deposition. In this study, we

Friday Morning, November 10, 2023

investigate the molecular layer deposition (MLD) of zeolitic imidazolate framework 8 (ZIF-8). Thin films were deposited on various substrates through consecutive self-limiting reactions of diethyl zinc, water, and 2-methyl imidazole, employing an all-vapor-phase process in an atomic layer deposition reactor. Two-step ZIF-8 MLD was utilized in this study, in which an amorphous layer is first deposited via MLD, followed by crystallization during a linker post-treatment step.[1] The degree of crystalline orientation of the resulting MOF layers can be tuned by changing the surface termination of the substrate. Moreover, these surface groups influence the mobility of the building blocks on the surface, allowing control over the surface coverage. We exploited this phenomenon to perform direct area-selective deposition of ZIF-8. The mechanisms behind these observations were elucidated using various imaging techniques, synchrotron GIXRD, and in-situ ellipsometry.

[1] Smets, J.; Cruz, A. J.; Rubio-Giménez, V.; Tietze, M. L.; Kravchenko, D. E.; Arnauts, G.; Matavž, A.; Wauteraerts, N.; Tu, M.; Marcoen, K.; Imaz, I.; Maspoch, D.; Korytov, M.; Vereecken, P. M.; De Feyter, S.; Hauffman, T.; Ameloot, R. Molecular Layer Deposition of Zeolitic Imidazolate Framework-8 Films. *Chem. Mater.* 2023, 35 (4), 1684–1690.

11:00am **TF+SE-FrM-9 Electron-Beam Assisted Solvent-Free Bottom-Up Patterning of Zeolitic Imidazolate Frameworks**, *Dennis Lee, Y. Miao*, Johns Hopkins University; *M. Dorneles de Mello*, Brookhaven National Laboratory; *M. Ahmad*, Stony Brook University/Brookhaven National Laboratory; *M. Abdel-Rahman, P. Eckhert*, Johns Hopkins University; *A. Boscoboinik*, Brookhaven National Laboratory; *H. Fairbrother, M. Tsapatsis*, Johns Hopkins University

For many years, researchers have been trying to develop a way to create patterns in porous materials like metal-organic frameworks (MOFs) for use in electronic and optical devices.<sup>[1]</sup> Recent progress has been made in understanding how irradiation with X-rays<sup>[2]</sup> and electron beams (e-beams)<sup>[3,4]</sup> causes amorphization in MOFs and zeolitic imidazolate frameworks (ZIFs), a subclass of MOFs. Researchers have also found that certain types of ZIFs with halogen atoms on their structural linkers undergo a solubility switch when exposed to irradiation, allowing for selective removal of either the exposed or non-exposed regions to create ZIF patterns.<sup>[5]</sup>

In this presentation, I will describe our work on a bottom-up approach to patterning non-halogenated ZIFs using an e-beam-assisted solvent-free technique.<sup>[6]</sup> By pretreating metal oxide precursors (i.e., ZnO for ZIF-8 and CoO<sub>2</sub> for ZIF-67) with 2-methylimidazole (2mlm) linker vapor, we were able to sensitize the oxide surface to e-beam exposure, delaying the conversion of the oxides to ZIFs in irradiated areas while allowing growth in non-irradiated areas. This all-vapor phase technique resulted in well-defined patterns with features as small as 150 nm width and 150 nm gap, making it a promising method for micro and nanofabrication processes.

During the presentation, I will focus on our primary approach to enable the creation of ZIF patterns without solvents or masks. It will also be discussed in our systematic investigation of the 2mlm-sensitized oxide film, which involves the use of various characterization methods, such as atomic force microscopy, transmission electron microscopy, grazing incidence X-ray diffraction, and X-ray photoelectron spectroscopy.

## References

[1] I. Stassen, N. Burtch, A. Talin, P. Falcaro, M. Allendorf, R. Ameloot, *Chem. Soc. Rev.* **2017**, 46, 3185.

[2] R. N. Widmer, G. I. Lampronti, N. Casati, S. Farsang, T. D. Bennett, S. A. T. Redfern, *Phys. Chem. Chem. Phys.* **2019**, 21, 12389.

[3] S. Conrad, P. Kumar, F. Xue, L. Ren, S. Henning, C. Xiao, K. A. Mkhoyan, M. Tsapatsis, *Angew. Chemie Int. Ed.* **2018**, 57, 13592.

[4] Y. Miao, M. Tsapatsis, *Chem. Mater.* **2021**, 33, 754.

[5] M. Tu, B. Xia, D. E. Kravchenko, M. L. Tietze, A. J. Cruz, I. Stassen, T. Hauffman, J. Teyssandier, S. De Feyter, Z. Wang, R. A. Fischer, B. Marmiroli, H. Amenitsch, A. Torvisco, M. de J. Velásquez-Hernández, P. Falcaro, R. Ameloot, *Nat. Mater.* **2021**, 20, 93.

[6] Y. Miao, D. T. Lee, M. D. de Mello, M. Ahmad, M. K. Abdel-Rahman, P. M. Eckhert, J. A. Boscoboinik, D. H. Fairbrother, M. Tsapatsis, *Nat. Commun.* **2022**, 13, 420.

11:20am **TF+SE-FrM-10 Al<sub>2</sub>O<sub>3</sub> Atomic Layer Deposition on a Porous Matrix of Carbon Fibers (FiberForm) for Oxidation Resistance**, *Jack Widmer, S. George*, University of Colorado Boulder

Atomic layer deposition (ALD) was used to coat a porous matrix of carbon fibers known as FiberForm with Al<sub>2</sub>O<sub>3</sub> to improve oxidation resistance.

Static trimethylaluminum (TMA) and H<sub>2</sub>O exposures for Al<sub>2</sub>O<sub>3</sub> ALD were used to obtain the uniform coating of this high porosity material. The carbon surfaces were initially functionalized for Al<sub>2</sub>O<sub>3</sub> ALD by exposure to sequential exposures of nitrogen dioxide and TMA. A gravimetric model was developed to predict the mass gain per cycle under conditions when the ALD reactions reach saturation during each reactant exposure. The uniformity of the Al<sub>2</sub>O<sub>3</sub> ALD coating on FiberForm was confirmed by scanning electron microscopy (SEM) and energy dispersive X-ray spectroscopy (EDS) analysis. The SEM, EDS and gravimetric model were all consistent with a uniform Al<sub>2</sub>O<sub>3</sub> ALD coating on the porous carbon fiber network when the ALD reactions reach saturation on the entire surface area. In contrast, the profile of the Al<sub>2</sub>O<sub>3</sub> ALD coating on the FiberForm was also characterized using undersaturation conditions when the ALD reactions do not reach saturation throughout the FiberForm sample. These Al<sub>2</sub>O<sub>3</sub> coverage profiles were consistent with diffusion-limited Al<sub>2</sub>O<sub>3</sub> ALD. The oxidation of the FiberForm and the Al<sub>2</sub>O<sub>3</sub> ALD-coated FiberForm was also investigated by thermogravimetric analysis (TGA). TGA revealed that a 50 nm thick Al<sub>2</sub>O<sub>3</sub> coating deposited using 400 Al<sub>2</sub>O<sub>3</sub> ALD cycles enhanced the oxidation resistance. The Al<sub>2</sub>O<sub>3</sub> ALD coating increased the oxidation onset temperature by ~200 °C from 500 °C to 700 °C and decreased the oxidation rate by ~30%. The oxidation rate of the Al<sub>2</sub>O<sub>3</sub> ALD-coated FiberForm samples was also constant and independent of the thickness of the Al<sub>2</sub>O<sub>3</sub> ALD coating. This behavior suggested that the oxidation is dependent on the competing O<sub>2</sub> diffusion into the FiberForm and CO<sub>2</sub> diffusion out of the FiberForm.

11:40am **TF+SE-FrM-11 Mesoporous UiO-66-NH<sub>2</sub> Thin Film Growth on TiO<sub>2</sub> Coated Fabrics Using Atomic Layer Deposition (ALD) for Enhanced Organophosphate Degradation, *Mai Abdelmigeed*, North Carolina State University**

Nowadays, most of the UiO-66-NH<sub>2</sub> research focuses on the capabilities of the microporous UiO-66-NH<sub>2</sub>-fabric composites for organophosphate degradation via hydrolysis. Unfortunately, microporous UiO-66-NH<sub>2</sub> suffers from diffusion limitation of the bulky organophosphates accessing the active sites. As a novel solution, we are introducing the aqueous phase synthesized mesoporous UiO-66-NH<sub>2</sub> thin film on fabric coated with »20 nm TiO<sub>2</sub> using ALD. The mesoporous version of UiO-66-NH<sub>2</sub> overcomes the mass transfer limitation issues while the TiO<sub>2</sub> layer works as nucleation centers to form a dense, robust, and homogeneous MOF thin films. The mesoporosity of the solvothermally synthesized UiO-66-NH<sub>2</sub>-fabric composites is mainly due to the utilization of an amphoteric surfactant, CAPB, as a template to construct these mesochannels.<sup>[1]</sup> Fig.(1,a) shows the benign MOF synthesis process avoiding the common toxic solvents and highly acidic medium at elevated temperatures. Importantly, Fig.(1,b) shows the pore size distribution of mesoporous UiO-66-NH<sub>2</sub> has both characteristic pore width peaks corresponding to the microporous range and a new peak at »28 Å corresponding to the mesoporous range. The benign synthesis approach allows mesoporous UiO-66-NH<sub>2</sub> growth on a range of fabrics. Fig.(1,c) shows a MOF thin film on PP coated with TiO<sub>2</sub> using atomic layer deposition that achieves BET SA up to »360m<sup>2</sup>/g<sub>comp</sub>. Fig.(1,d) shows that these mesoporous UiO-66-NH<sub>2</sub> composite enhanced the paraoxon methyl (DMNP) degradation with a half-life time of less than a minute compared to a half-life time of 2.5 minutes for microporous UiO-66-NH<sub>2</sub>. Similar trends were found for live nerve agent degradation. To conclude, the benign synthesis process of the mesoporous UiO-66-NH<sub>2</sub> thin film improves the growth of this MOF on a large range of fabrics and enhances the organophosphates degradation, respectively. These thin film MOF-fabric composites have great potential in filtration, protection, and catalysis applications.

[1] K. Li, S. Lin, Y. Li, Q. Zhuang, J. Gu, *Angewandte Chemie - Int. Ed.* 57 (2018) 3439–3443.

**Bold page numbers indicate presenter**

— A —

A. Castro, F.: NS1+2D+BI+SS-MoM-1, **11**  
 Abate, Y.: 2D-WeM-13, 107  
 Abbas, A.: 2D-ThM-4, 145; TF-ThP-9, **197**  
 Abbondanza, G.: SS1+HC-MoM-6, 20  
 Abdelmessih, M.: UN-ThP-2, **200**  
 Abdelmigeed, M.: TF+SE-FrM-11, **221**  
 Abdel-Rahman, M.: TF+SE-FrM-9, 220  
 Abdul, E.: NS2+2D+EM-TuA-10, 73  
 Abdulagatov, A.: AP+PS+TF-MoM-10, **5**  
 Aboharb, L.: VT-TuM-4, **62**  
 Abolghasemi, A.: QS+VT-WeM-12, 119  
 Abraha, P.: PS-TuP-22, 99  
 Abroshan, H.: AP+PS+TF-MoM-8, **5**  
 Abuyazid, N.: PS+MS-TuA-7, **75**; PS2+MS-WeA-11, 139; SS-ThP-4, **193**  
 Aceros, J.: TF-ThP-18, 199  
 Ackermann, M.: AS+2D+CA+EM+MS+NS+SE+SS+TF-FrM-8, 209  
 Adams, D.: AS+2D+CA+EL+EM+MS+NS+SE+SS+TF-WeM-6, **112**; EM-WeM-5, 113  
 Addamane, S.: AS+2D+CA+EL+EM+MS+NS+SE+SS+TF-WeM-6, 112  
 Adesope, Q.: SS+2D+AS+HC-WeM-2, **119**  
 Adriaensens, P.: SS+HC-TuA-11, 79  
 Agafonova, A.: 2D-ThP-2, 175  
 Agarwal, S.: AP+PS-FrM-3, 207; EM-WeM-1, 113; PS1-ThA-5, **170**; PS2-ThA-4, 171  
 Åhlgren, H.: 2D-ThM-1, **145**  
 Ahmad, M.: LX+AS+HC+SS-MoM-8, 11; TF+SE-FrM-9, 220  
 Ahmed, A.: 2D-ThP-13, 177; 2D-ThP-22, 179  
 Ahmed, M.: CA2+AS+LS+NS+SS+VT+MoM-8, **8**  
 Ahmed, T.: TH2-TuA-7, 81  
 Ahn, C.: 2D-TuM-3, **44**  
 Ahn, S.: PS1+MS-ThM-5, 159  
 Ahsen, A.: HC+SS-ThM-12, 153  
 Ai, B.: BI+AS+EM+NS+SE+TF-TuA-1, 70  
 Ai, Q.: CA+AS+LS+NS+SS+VT-MoA-3, 27  
 Aitchison, B.: EM-WeM-11, 114  
 Aitken, M.: VT-MoM-3, 21; VT-TuA-4, 83  
 Ajantiwalay, T.: IB-ThA-3, 167; IB-ThA-4, **167**; SE-TuP-9, **104**  
 Ajayi, T.: 2D1-ThA-4, 164  
 Ajo, H.: AC-TuP-2, 85  
 Akagi, D.: AP+PS-FrM-4, 208  
 Akers, S.: MS-ThP-1, 191  
 Alaani, M.: EL1+TF-MoA-3, 29  
 Albrecht-Schoenart, T.: AC+MI+TH-TuA-7, 68  
 Alem, T.: 2D+EM-FrM-3, 206  
 Alemán, B.: MN2-WeM-10, **117**  
 Alemansour, H.: NS1+2D+BI+SS-MoM-4, 12  
 Alex, S.: AC+AS+MI+TH-WeA-9, 126  
 Alexander, M.: BI1-MoA-3, **25**; BI1-MoA-5, 26  
 Alexandrowicz, G.: HC+SS-ThM-10, 152  
 Alfonso, D.: SS1+HC-MoM-5, 20  
 Alfreider, M.: IB-ThA-5, 168  
 Alhowity, S.: SS+2D+AS+HC-WeM-2, 119  
 Ali, F.: EM-ThP-7, **186**; TF2-TuA-8, 80  
 Alipour, A.: NS1+2D+BI+SS-MoM-4, 12  
 Alkoby, Y.: HC+SS-ThM-10, 152  
 Allen, F.: IB-ThP-2, 190  
 Allen, J.: AC+MI+TH-TuM-10, 46  
 Allen, N.: EL-TuP-9, **90**  
 Allerman, A.: CPS+CA-WeA-1, 130  
 Allred, D.: TF+QS-WeA-3, 142  
 Al-Mahboob, A.: 2D+TF-TuA-10, **67**  
 Alonso-Mori, R.: AC+MI+TH-TuM-13, 47  
 Alsaeed, O.: PS-TuP-11, **97**  
 Altamirano Sanchez, E.: 2D-WeM-4, 106

Altman, A.: LS+AC+AS+LX+MI+TH-ThA-5, 168  
 Altman, E.: SS-WeA-11, **141**  
 Alvarado Garcia, J.: HC-ThP-10, **189**  
 Amann, A.: NS1+2D+BI+SS-MoM-4, 12  
 Amann, P.: LX+AS+HC+SS-MoM-3, **10**  
 Ambrozaite, O.: 2D-WeA-10, 125  
 Ameloot, R.: TF+SE-FrM-8, 220  
 Amend, A.: PS+TF-MoM-10, **15**  
 Amir, S.: PS-TuP-17, **98**  
 Amonette, E.: EL-TuP-8, **90**  
 An, R.: SS+HC-TuA-11, 79  
 ANAYA GONZALEZ, G.: HC-ThP-10, 189  
 Andary, S.: NS1+2D+BI+SS-MoM-5, 12  
 Andaraarachchi, H.: PS1+AS-WeA-10, 137  
 Andersen, M.: BI-TuP-11, 88  
 Anderson, D.: CPS+MS-ThM-3, **148**  
 Anderson, K.: AP+PS+TF-WeM-3, 109  
 Anderson, S.: HC+SS-FrM-4, 212; HC+SS-WeA-11, **134**; HC-ThP-7, 188  
 Anderson, T.: EM2-FrM-10, 211  
 Andersson, J.: BI2+AS+HC+SS-MoM-8, 7  
 Andreasson, J.: EL1-MoM-6, 10  
 Andrianov, N.: MN-ThP-3, 191  
 Andruczyk, D.: CPS+CA-WeA-8, 131  
 Anfuso, C.: 2D-ThP-2, 175  
 Angrick, C.: SS+AS+TF-MoA-8, **40**  
 Antar, S.: AS-ThP-14, 181  
 Antipov, S.: VT-TuM-2, 62  
 Antoine, L.: EM-ThP-6, 186  
 Antonelli, G.: EL-TuP-12, 91  
 Antonov, G.: AP+PS-MoA-3, 23  
 Aoki, T.: SS-ThP-5, 193  
 Applebee, Z.: BI-TuP-9, **87**  
 Ara, T.: HC+SS-WeA-4, 133; SS-ThP-14, 194  
 Arat, K.: NS1+2D+BI+SS-MoM-4, 12  
 ARCE PLAZA, A.: HC-ThP-10, 189  
 Ardiansyah, M.: TF-ThA-3, 173  
 Ardizzi, A.: AP+PS-MoA-11, 24  
 Aresta, G.: IB-ThM-3, **153**  
 Arias, S.: NS+2D+EM+MN+SS-TuM-11, 54  
 Armakavicius, N.: EL1+TF-MoA-1, **28**  
 Armenta, C.: CPS+CA-WeA-9, 131; EL1-MoM-6, **10**; EL-TuP-4, 89; EL-TuP-6, 90  
 Armini, S.: AP+EM+PS+TF-TuM-12, 49; SS2+AS+TF-ThM-13, **161**; TF+SE-FrM-8, 220  
 Armstrong, A.: CPS+CA-WeA-1, 130  
 Armstrong, G.: PS+MS-TuA-1, 74  
 Árnadóttir, L.: LX+AS+BI+HC+SS+TH-MoA-1, **30**; UN-ThP-14, 202; UN-ThP-26, 204  
 Arnauts, S.: 2D-WeM-4, 106  
 Arnold, A.: QS+VT-WeM-5, 118  
 Arnold, M.: 2D+EM-FrM-4, 206  
 Aronson, B.: EM-ThA-1, 165; EM-ThA-4, 166  
 Arres Chillon, J.: SE-TuP-5, 104  
 Artyushkova, K.: AS+2D+CA+EL+EM+MS+NS+SE+SS+TF-WeM-5, 112; AS+CA+EL+EM+SE+SS+TF-WeA-9, 128; AS-ThP-19, 182; CA1+AS+LS+NS+SS+VT-MoM-3, **7**  
 Arunachalam, A.: 2D-ThP-11, 176  
 Asel, T.: PS+NS-FrM-8, 216  
 Asmari, N.: NS1+2D+BI+SS-MoM-5, 12  
 Asnes, D.: EL-TuP-2, 89; EL-TuP-3, 89  
 Atoyebi, O.: BI2+AS+HC+SS-MoM-9, 7  
 Atwimah, S.: EM2-FrM-10, 211  
 Audinot, J.: IB-ThM-5, 154  
 Auerbach, D.: AS-ThP-1, 179; HC+SS-FrM-5, 212  
 Avdiaj, S.: VT-MoA-5, **42**  
 Aydin, K.: 2D-TuM-3, 44  
 Aydogan Gokturk, P.: TH2-TuA-11, **82**  
 Azamoum, Y.: PS-TuM-4, 55  
 Azeem, S.: MN-ThP-3, 191  
 Azim, M.: TF-ThP-14, 198

Azpiroz, N.: SE+TF-MoA-1, 38  
 — B —  
 Babayew, R.: AC-TuP-3, 85  
 Baber, A.: HC-ThP-12, **189**; UN-ThP-19, 203; UN-ThP-20, 203; UN-ThP-21, 203; UN-ThP-22, 203; UN-ThP-23, 203  
 Babu, C.: AS-ThP-4, **179**  
 Bacheller, S.: TF-ThP-12, 198  
 Bachhav, M.: LS+AC+AS+LX+MI+TH-ThA-5, 168  
 Bachmann, J.: AP1+2D+EM+PS+TF-TuA-7, 69  
 Back, T.: PS+NS-FrM-8, 216  
 Badouric, L.: SE1+TF-MoM-6, **18**  
 Bae, J.: PS1+MS-ThM-5, **159**  
 Baer, D.: AS+CA+EL+EM+SE+SS+TF-WeA-1, **127**; AS-ThP-23, 183; UN-ThP-4, 200  
 Baert, K.: AP+PS+TF-WeM-12, 110; SS+AS+TF-MoA-9, 40; SS+HC-TuA-11, 79  
 Bagus, P.: TH1+AS+SS-TuM-6, 61; TH2+AS+SS-TuM-12, 61; TH-TuP-1, **104**  
 Bahr, M.: CPS+CA-WeA-1, 130  
 Bai, Y.: SS1+AS-ThM-5, **161**  
 Bailey, B.: NSP-SuA-8, 3; UN-ThP-27, **204**  
 Bailey, L.: QS+EM+TF-MoM-2, 15  
 Baio, J.: BI+AS+EM+NS+SE+TF-TuA-10, 72; BI+AS+PS-TuM-12, 50; BI+AS+PS-TuM-4, **50**; BI-WeA-2, 129  
 Bajpai, A.: TF+SE-FrM-4, 219  
 Baker, A.: AC+AS+TH-WeM-10, 108; AC+AS+TH-WeM-11, 108  
 Bakr, O.: SS-ThP-8, 194  
 Balajka, J.: SS+2D+AS+HC-TuM-13, **59**  
 Balakrishnan, G.: QS+SS-TuA-4, 76  
 Balasubramanian, G.: SS-ThP-18, 195  
 Bale, R.: EM1+TF-FrM-6, 211  
 Ballard, J.: QS+SS-TuA-11, **77**  
 Balogun, K.: SS+2D+AS+HC-WeM-2, 119  
 Balogun, S.: TF-ThM-4, **162**  
 Baloocha, M.: IB-ThA-1, 167  
 Bamford, S.: CA1+AS+LS+NS+SS+VT-MoM-5, 8  
 Banerjee, P.: 2D-ThP-11, 176; EM-WeA-4, 132  
 Bang, I.: PS2-ThA-6, 171; PS-TuP-28, **100**; PS-TuP-29, 100; PS-TuP-34, 101  
 Bao, Y.: VT-MoM-4, 21  
 Baral, D.: 2D2-ThA-2, 164  
 Baratte, E.: PS1+AS-WeA-7, 137  
 Barcellona, M.: 2D-ThP-16, 177  
 Barker, D.: NS+EM+MN-MoA-1, 31; VT-MoA-9, 42; VT-MoM-4, **21**; VT-MoM-8, 22  
 Barnes, J.: AS+2D+CA+EM+MS+NS+SE+SS+TF-FrM-1, **208**; AS-ThP-29, 184  
 Barnum, A.: AS+2D+CA+EL+EM+MS+NS+SE+SS+TF-WeM-5, 112  
 Barone, M.: EL1+TF-MoA-4, 29  
 Barragan, D.: BI-WeA-3, 129  
 Barral, M.: UN-ThP-7, 201  
 Barrentine, E.: AP-TuP-4, 86  
 Barsukov, Y.: AP+PS-MoA-6, **24**; PS2+MS-WeA-12, 140  
 Barton, D.: EL1-MoM-5, 9; EL-TuP-11, 91  
 Barynova, K.: PS+SE-MoA-1, 34  
 Basu, K.: 2D-ThP-11, 176; MS+AP+AS+TF-ThA-3, **169**  
 Basu, R.: TF-ThP-15, **198**  
 Bates, T.: TF-ThP-19, 199  
 Batista, E.: TH1-TuA-3, **81**  
 Batista, V.: SS+HC-TuA-1, **78**  
 Batzill, M.: 2D-ThM-12, **146**  
 Baumbach, R.: AC+MI+TH-TuM-10, 46  
 Bavarian, M.: TF1-TuA-3, 79

## Author Index

- Baykara, M.: 2D-ThM-13, 146  
 Bazak, D.: AS-ThP-28, 183  
 Beasley, M.: BI2+AS+HC+SS-MoM-9, 7  
 Beaudoin, F.: QS+SS-TuA-11, 77  
 Beaux, M.: AC+MI+TH-TuA-12, **68**  
 Bechelany, M.: SE1+TF-MoM-6, 18; TF+SE-FrM-1, **219**  
 Bediako, D.: SS+2D+AS+HC-WeM-3, **120**  
 Beechem, T.: EM-ThA-1, 165; EM-ThA-4, 166  
 Bégin, T.: TF2+AP+SE+SS-WeM-12, 123  
 Bekman, H.: VT-MoM-10, 22  
 Bektas, U.: EM+TF-ThM-4, 149  
 Belianinov, A.: IB-ThP-5, **190**  
 Bell, D.: AS-ThP-17, 181; TF-ThP-8, 197  
 Bellido-Gonzalez, V.: VT-TuA-9, 83  
 Bellman, R.: SE-TuP-5, 104  
 Benayad, A.:  
   AS+2D+CA+EL+EM+MS+NS+SE+SS+TF-WeM-4, 111  
 Bender, G.: AS-ThP-21, 182  
 Benesova, M.: TH1+AS+SS-TuM-5, 60  
 Benidar, A.: TF+QS-WeA-1, 142  
 Bennett, C.: EM-WeM-1, 113  
 Bennett, S.: TF1+PS-WeM-5, 122  
 Benschop, T.: 2D-WeM-3, 106  
 Benzing, J.: NSP-SuA-8, 3  
 Bera, K.: PS+MS-TuA-12, 76; PS+MS-TuA-3, **74**; PS+MS-TuA-8, 75  
 BERARD-BERGERY, S.: PS-TuP-24, 99  
 Berckmans, J.: PS+SE-FrM-6, **218**  
 Berg, R.: SS+HC-TuA-10, **78**  
 Bergner, K.: QS+VT-WeM-13, 119; VT-TuA-3, **83**; VT-TuP-3, 105  
 Bergsman, D.: TF-ThM-6, 162  
 Berman, D.: TF-ThM-1, **162**; TF-ThM-3, 162  
 Bernien, M.: VT-TuA-10, 83  
 Berriel, N.: 2D-ThP-11, 176  
 Berriel, S.: EM-WeA-4, **132**  
 Besprozvanny, D.: QS+EM+TF-MoM-2, 15  
 Beyer, A.: IB3-FrM-11, 214  
 Bézard, P.: PS+NS-FrM-3, 215  
 Bhandari, G.: AP-TuP-4, **86**  
 Bhatia, E.: EL-TuP-1, 89; QS+EM+TF-MoM-10, **17**  
 Bhattacharjee, A.: AS-ThP-22, 182  
 Bidas, K.: AS-ThP-22, 182  
 Biderman, N.: AS+CA+EL+EM+SE+SS+TF-WeA-9, **128**; AS-ThP-19, 182  
 Biedron, A.: QS+EM+TF-MoM-10, 17  
 Bielejec, E.: EM+TF-ThM-11, 150  
 Bielejec, E.: AQS-SuA-1, 1; IB-ThP-5, 190  
 Bielinski, A.: TF1+PS-WeM-3, **122**  
 Biesemeier, A.: IB-ThM-5, **154**  
 Bijkerk, F.:  
   AS+2D+CA+EM+MS+NS+SE+SS+TF-FrM-8, 209  
 Bilotto, P.: BI-WeA-3, **129**; NS-TuP-8, **93**  
 Biltek, S.: PS2-ThA-2, 170  
 Bin Ali, A.: VT-TuA-10, **83**  
 Bin Elius, I.: EM-ThP-3, 186  
 Bin Hafiz, S.: EM-ThP-6, 186  
 Binder, A.: CPS+CA-WeA-1, 130  
 Biolsi, P.: PS2+MS-WeA-3, 138; PS2+MS-WeA-7, 139; PS-TuM-5, 56  
 Biswas, P.: TF2+AP+SE+SS-WeM-13, **123**  
 Biyikli, N.: EM+TF-ThM-5, **150**; EM-ThP-6, **186**; PS-TuP-25, 100; TF-ThP-11, 198  
 Biznarova, J.: QS-MoA-3, **36**  
 Black, C.: QS+EM+TF-MoM-10, 17; QS-MoA-4, 36  
 Blackwood, H.: 2D-ThP-20, 178  
 Blades, W.: SS+HC-ThA-3, 172; SS+HC-ThA-4, 172  
 Blanc, R.: PS+TF-MoM-1, **13**  
 Blank, K.: BP-SuA-11, **2**  
 Blanton, E.: 2D+TF-TuA-11, 67  
 Blechle, J.: UN-ThP-29, 204  
 Blenkinsopp, P.: IB-ThM-3, 153  
 Blevins, J.: PS+NS-FrM-8, 216  
 Blockhuys, F.: SS+HC-TuA-11, 79  
 Blomfield, C.: AS+CA+EL+EM+SE+SS+TF-WeA-4, 128; AS-ThP-18, 181  
 Blum, M.: HC+SS-ThM-6, 152  
 Bode, M.: MI+2D+TF-WeA-9, 135  
 Boden, D.: HC+SS-ThM-2, 152  
 Boespflug, R.: VT-TuM-2, 62  
 Boeyink, B.: SE+TF-MoA-8, 38  
 Boixaderas, C.: PS+TF-MoM-3, 14  
 Böke, M.: PS+SE-FrM-8, 218  
 Bolkenbaas, O.: AP+EM+PS+TF-TuM-5, **47**  
 Bollinger, A.: QS-MoA-4, 36  
 Bonaccorso, C.: 2D-ThP-16, 177; 2D-TuM-12, 45  
 Bonvalot, M.: AP1+2D+EM+PS+TF-TuA-1, **69**  
 Boosalis, A.: EL-TuP-12, **91**  
 Booth, J.: PS-TuM-4, 55  
 Bordoalvas, A.: EL1-MoM-1, 9  
 Borgos, S.: AS+CA+EL+EM+SE+SS+TF-ThM-3, 147  
 Boris, D.: AP+PS+TF-WeM-11, 110; AP-TuP-6, **86**; PS+SE-FrM-2, 217; TF+QS-WeA-9, 143  
 Borunda, M.: 2D-WeM-5, 106  
 Bosco, M.: AS-ThP-37, 185  
 Boscoboinik, A.: TF+SE-FrM-9, 220  
 Boscoboinik, J.: HC-ThP-11, **189**;  
   LX+AS+HC+SS-MoM-8, **11**  
 Bosnick, K.: NS+EM+MN-MoA-9, **33**; NS-TuP-2, **92**  
 Bostwick, A.: 2D-WeA-7, 124  
 Boswell, R.: TF+QS-WeA-1, 142; VT-MoA-8, **42**  
 Böttcher, S.: EW-TuL-5, **64**  
 Boulard, F.: AP+PS-MoA-9, 24  
 Bourgeois, G.: PS+TF-MoM-3, 14  
 Bowden, M.: TF2+AP+SE+SS-WeM-13, 123  
 Bowers, C.: HC+SS-ThA-3, 167  
 Boyce, B.:  
   AS+2D+CA+EL+EM+MS+NS+SE+SS+TF-WeM-6, 112; EM-WeM-5, 113  
 Boyen, H.: AS+CA+EL+EM+SE+SS+TF-WeA-3, 127  
 Brabant, M.: AP+PS+TF-WeM-12, 110; PS-TuP-30, **101**  
 Brady Boyd, A.: SS2+AS+TF-ThM-13, 161  
 Brady-Boyd, A.: 2D-WeM-4, 106  
 Brancato, A.: 2D-ThP-16, 177  
 Brar, V.: 2D-WeM-10, 107  
 Brathwaite, K.: TF-ThA-3, 173  
 Braun, J.: SS+AS+TF-MoA-8, 40  
 Bravo, S.: PS1+AS-WeA-7, 137  
 Bravo-Sanchez, M.: AS-ThP-36, 185  
 Breitenstein, D.: BI2-MoA-10, 26; BI-TuP-10, 88  
 Brems, S.: 2D-WeM-4, 106  
 Brenning, N.: PS+SE-MoA-1, 34  
 Bretaña, A.: AC+MI+TH-TuM-6, 46; AC-TuP-2, **85**  
 Brewer, C.: EM-WeM-6, **114**  
 Brewer, J.: AS-ThP-14, 181; NS+EM+MN-MoA-10, 33  
 Brgenhøj, M.: BI+AS+PS-TuM-2, 49  
 Briley, A.: BP-SuA-7, 2  
 Brindley, J.: VT-TuA-9, 83  
 Brites Helu, M.: HC-ThP-11, 189  
 Brockhagen, B.: IB-ThM-11, 154  
 Brodie, A.: NS+EM+MN-MoA-5, 32  
 Broer, R.: TH1-TuA-1, **81**  
 Brogden, V.: IB1-FrM-1, **213**; IB-ThP-3, **190**  
 Broitman, E.: SE+TF-MoA-5, **38**; SE-TuP-3, **103**  
 Brommesson, C.: BI+AS+EM+NS+SE+TF-TuA-4, 71  
 Brontvein, O.: NS1+2D+BI+SS-MoM-6, 13  
 Brorsen, K.: TF-ThA-3, 173  
 Brown, D.: AC+AS+MI+TH-WeA-3, **125**  
 Brown, G.: PS+SE-FrM-2, 217  
 Brown, J.: SS-WeA-8, 141  
 Brown, R.: UN-ThP-31, 205; UN-ThP-32, 205  
 Brown, S.: SS-WeA-8, 141  
 Brown-Tseng, E.: SS+AS+TF-MoA-9, 40  
 Bruce, J.: LX-TuP-2, **91**  
 Bruce, R.: PS-WeM-10, 118  
 Bruchhaus, L.: IB-ThM-12, 154; IB-ThP-1, 190  
 Brucker, G.: VT-MoM-3, **21**; VT-TuA-4, 83  
 Bruggeman, P.: PS1-ThA-3, **170**  
 Brugger-Hatzl, M.: NS+2D+EM+MN+SS-TuM-5, 54  
 Brundle, C.: TH2+AS+SS-TuM-12, **61**  
 Brune, H.: NSP-SuA-9, 3  
 Brüner, P.: HC+SS-FrM-3, 212  
 Buchanan, S.: AS-ThP-10, **180**  
 Buchine, I.: NS+2D+EM+MN+SS-TuM-4, 53  
 Buck, E.: LS+AC+LX+MI+TH-ThM-12, 156  
 Budach, M.: PS2+AS+SS-ThM-10, 159  
 Bui, T.: NS+EM+MN-MoA-1, 31  
 Buke, G.: 2D-ThM-13, 146  
 Burch, K.: QS+EM-TuM-12, **57**  
 Burch, N.: QS+VT-WeM-12, 119; VT-TuP-1, 105  
 Burger, J.: SE+TF-MoA-8, 38  
 Burghammer, M.: IB-ThA-5, 168  
 Burke, D.: VT-TuM-3, 62  
 Burke, P.: EW-TuL-7, 65  
 Burnham, N.: NS+2D+EM+MN+SS-TuM-10, **54**; NS-TuP-4, **92**  
 Burns, K.: 2D-ThP-18, 178  
 Burrell, M.: AS-ThP-8, **180**  
 Burrow, O.: QS+VT-WeM-5, **118**  
 Burzynski, K.: PS+NS-FrM-8, 216  
 Bushell, A.: EW-TuL-3, **64**  
 Butch, N.: AC+MI+TH-TuM-10, 46  
 Butera, R.: QS-MoA-1, **36**  
 Butler, A.: 2D-ThP-22, 179  
 Buturlim, V.: AC+MI+TH-TuM-11, **46**;  
   AC+MI+TH-TuM-4, 46  
 Buzi, L.: PS-WeM-10, **118**  
 Bylander, J.: QS-MoA-3, 36  
 — C —  
 Cabanillas, A.: 2D-ThP-13, 177; 2D-ThP-22, 179  
 Cabrera German, D.:  
   AS+CA+EL+EM+SE+SS+TF-WeA-2, 127  
 Cabrera-German, D.: AS-ThP-36, 185  
 Çağın, E.: 2D-ThM-6, 145; 2D-ThP-5, 175  
 Cahen, D.: NS+2D+EM+MN+SS-TuM-4, 53  
 Cai, T.: EM-ThA-1, 165  
 Cai, W.: SE+TF-MoA-3, **38**  
 Calatayud, M.: HC-ThP-11, 189  
 Calaza, F.: AS-ThP-37, **185**; HC-ThP-11, 189  
 Calderon, S.: EM-ThA-1, 165; EM-ThA-4, 166  
 Caldes, M.: AS+CA+EL+EM+SE+SS+TF-ThM-2, 147  
 Calegari Andrade, M.: SS+HC-TuA-7, **78**  
 Calhoun, B.: MN-ThP-4, 191  
 Cali, L.: 2D-ThP-2, 175; 2D-TuM-12, 45  
 Calvi, V.: 2D-WeM-3, 106  
 Campbell, C.: AS-ThP-1, 179; HC+SS-FrM-5, 212; HC+SS-WeA-3, **133**  
 Campos Jara, S.: 2D-WeM-3, **106**  
 Canaperi, D.: SE-TuP-4, 103  
 Canlas, J.: NS-TuP-2, 92  
 Cannon, A.: BI+AS+PS-TuM-13, 51  
 Cant, D.: AS+CA+EL+EM+SE+SS+TF-ThM-3, **147**  
 Canvel, Y.: PS-TuM-13, **57**

## Author Index

- Cao, M.: TF-ThP-21, 199  
 Cao, Q.: MI+2D+TF-ThM-1, 156  
 Cao, X.: IB2-FrM-5, 213  
 Caouette, M.: CA1+AS+LS+NS+SS+VT-MoM-3, 7  
 Caputo, L.: 2D-WeM-3, 106  
 Cardwell, N.: CA+AS+LS+LX+MN+SE+SS-TuM-4, 51  
 Carlson, E.: SS-ThP-19, 195  
 Caron, A.: SS2-MoM-9, 20  
 Carpena-Nuñez, J.: LX+AS+HC+SS-MoM-4, 11  
 Carpenter, A.: BI+AS+PS-TuM-4, 50; BI-WeA-2, **129**; EM-ThP-10, 187  
 Carrascon, R.: EL1+TF-MoA-1, 28  
 Carter, R.: TF2-TuA-11, 80  
 Cartier, J.: SE1+TF-MoM-6, 18  
 Carver, T.: AC+AS+MI+TH-WeA-3, 125  
 Cary, J.: PS+MS-TuA-9, 75  
 Castagna Ferrari, V.: TF2-TuA-9, **80**  
 Castañeda, R.: EM-ThP-9, **187**; UN-ThP-33, 205  
 Castanheira, N.: AS+CA+EL+EM+SE+SS+TF-WeA-7, 128  
 Castellano, F.: EM-WeM-6, 114  
 Catherall, D.: AP+PS-FrM-1, **207**; AP+PS-FrM-5, 208; AP+PS-MoA-11, 24  
 Cavallo, F.: 2D+EM-FrM-4, 206  
 Cavanagh, A.: AP+PS+TF-WeM-6, 110  
 Cawkwell, M.: TH1-TuA-3, 81  
 Caylan, O.: 2D-ThM-13, 146  
 Cechal, J.: SS1+AS-ThM-4, 160  
 Čekada, M.: SE+TF-MoA-6, 38  
 Celebi, A.: SS2-MoM-10, 20  
 Celis-Barros, C.: AC+MI+TH-TuA-7, 68  
 Centrone, A.: NS-TuP-6, 93  
 Ceratti, D.: NS+2D+EM+MN+SS-TuM-4, 53  
 Chaaban, J.: 2D-ThM-6, 145; 2D-ThP-5, 175  
 Chadwick, H.: HC+SS-ThM-10, **152**  
 Chaka, A.: TH2-TuA-7, **81**  
 Chakravarthi, S.: 2D+TF-TuA-11, 67  
 Chakravarty, A.: 2D-ThP-13, 177; 2D-ThP-22, 179  
 Challa, S.: NS+EM+MN-MoA-11, **33**  
 Champ, T.: SE+TF-MoA-8, 38  
 Champlain, J.: MN1-WeM-3, 116  
 Chanana, A.: NS+EM+MN-MoA-8, 33  
 Chandra, H.: PS-WeM-5, 118  
 Chandrasekaran, A.: AP+PS+TF-MoM-8, 5; AS+2D+CA+EM+MS+NS+SE+SS+TF-FrM-8, 209  
 Chang, A.: AS-ThP-12, **181**  
 Chang, C.: 2D-ThP-1, 175; MI+2D+TF-ThM-12, 157; SE-TuP-1, **103**; SE-TuP-2, 103  
 Chang, H.: PS1-ThA-2, 169  
 Chang, J.: AP+PS-MoA-1, 23; AP+PS-MoA-2, 23  
 Chang, T.: AP2+PS+TF-TuA-11, 70  
 Chapman, S.: EM-ThP-8, 186  
 Charles, C.: TF+QS-WeA-1, **142**; VT-MoA-8, 42  
 Charmette, C.: SE1+TF-MoM-6, 18  
 Charnas, A.: PS+NS-FrM-8, 216  
 Charvier, R.: AS+2D+CA+EL+EM+MS+NS+SE+SS+TF-WeM-4, 111; CA+AS+LS+NS+SS+VT-MoA-10, **28**  
 Chason, E.: SE+TF-MoA-2, 38  
 Chasse, B.: BP-SuA-7, 2  
 Chauvin, A.: PS-TuP-9, 97  
 Chavez, A.: SE+TF-MoA-1, 38  
 Chekhonin, P.: EM+TF-ThM-4, 149  
 Chen, C.: 2D-ThP-22, **179**; 2D-ThP-6, 175; AP-TuP-2, 85; NS-TuP-16, 95; SS-WeA-7, **141**  
 Chen, D.: HC+SS-ThM-12, **153**  
 Chen, F.: 2D-ThP-6, 175; NS-TuP-16, 95  
 Chen, H.: 2D+TF-TuA-8, 66; 2D2-ThA-2, 164; 2D-ThP-6, 175; TF-ThP-10, 197  
 Chen, I.: AP+PS-FrM-5, 208; AP+PS-MoA-11, **24**  
 Chen, J.: AS+2D+CA+EL+EM+MS+NS+SE+SS+TF-WeM-5, 112; EM-WeM-11, 114  
 Chen, M.: 2D-ThP-20, 178; AP2+PS+TF-TuA-11, 70  
 Chen, Q.: NS-TuP-9, 93  
 Chen, R.: TF-ThP-21, 199  
 Chen, S.: NS1+2D+EM+MN-TuA-3, 72  
 Chen, W.: 2D-ThP-6, 175; SS-ThP-18, 195; TF-ThP-10, 197  
 Chen, X.: BI+AS+EM+NS+SE+TF-TuA-1, 70  
 Cheng, B.: NS+EM+MN-MoA-10, **33**  
 Cheng, L.: TF1+PS-WeM-3, 122  
 Cheng, S.: SS+2D+AS+HC-WeM-6, 120  
 Cheng, X.: 2D1-ThA-4, 164  
 Chevolleau, T.: AP1+2D+EM+PS+TF-TuA-1, 69; PS+TF-MoM-3, **14**; PS-TuM-12, 56  
 Chew, A.: QS+VT-WeM-12, 119; VT-TuP-1, 105  
 Chi, M.: 2D-ThM-10, **146**  
 Chien, T.: 2D2-ThA-2, **164**; SS-ThP-18, 195  
 Chin-Wook, C.: PS-TuP-32, 101  
 Chiu, K.: 2D-ThP-6, **175**  
 Cho, C.: PS2-ThA-5, 171; PS-TuP-37, **102**; PS-TuP-38, 102  
 Cho, H.: PS-TuP-5, 96  
 Cho, N.: PS-TuP-15, **98**  
 Cho, S.: NS-TuP-14, **94**  
 Choe, Y.: TF-ThM-6, 162  
 Choffel, M.: 2D-ThP-20, 178  
 Choi, B.: 2D-ThP-4, 175; NS-TuP-7, 93; PS2-ThA-5, 171; PS-TuP-37, 102; PS-TuP-38, 102  
 Choi, C.: PS-TuP-13, 97; PS-TuP-4, 96  
 Choi, D.: HC+SS-ThA-3, 167  
 Choi, H.: NS1+2D+BI+SS-MoM-3, 12  
 Choi, K.: AP2+PS+TF-TuA-12, **70**  
 Choi, M.: AS-ThP-2, 179; PS2-ThA-5, **171**; PS-TuP-37, 102; PS-TuP-38, 102; SS+AS+TF-MoA-11, 41; TF2+AP+SE+SS-WeM-13, 123  
 Choi, S.: 2D-ThP-14, **177**; AS-ThP-2, 179; AS-ThP-3, 179; MS-ThP-2, 192; PS2-ThA-1, **170**; PS-TuP-35, **101**; PS-WeM-5, 118  
 Choi, T.: AP+PS+TF-WeM-5, 109  
 Chopra, M.: MS+AP+AS+TF-ThA-5, 169  
 Chopra, N.: PS+SE-MoA-4, **35**; PS-TuP-21, 99  
 Chowdhury, R.: 2D+EM-FrM-4, **206**; AP-TuP-3, 85; SS+HC-ThA-6, 172  
 Chowdhury, S.: AQS-SuA-3, **1**  
 Chowrira, B.: PS+NS-FrM-3, 215  
 Choyal, S.: SS-ThP-3, **193**; SS-ThP-9, 194  
 Christ, B.: TH2+AS+SS-TuM-12, 61  
 Christudasjustus, J.: MS-ThP-1, 191  
 Chu, J.: AS+CA+EL+EM+SE+SS+TF-ThM-13, 148; BI+AS+EM+NS+SE+TF-TuA-2, **70**  
 Chu, T.: NS1+2D+BI+SS-MoM-3, 12  
 Chuang, H.: 2D2-ThA-3, **165**; 2D-WeA-3, 124  
 Chuckwu, K.: LX+AS+BI+HC+SS+TH-MoA-1, 30  
 Chueh, W.: SS-ThP-19, 195  
 Chukwunonye, P.: SS+2D+AS+HC-WeM-2, 119  
 Chung, B.: AC+AS+TH-WeM-10, **108**; AC+AS+TH-WeM-11, 108; LS+AC+AS+LX+MI+TH-ThA-5, 168  
 Chung, C.: PS-TuP-31, 101; PS-TuP-33, 101; PS-TuP-39, 102; SE-TuP-10, 104  
 Chung, K.: PS+TF-MoM-5, **14**  
 Chung, T.: NS-TuP-16, 95  
 Cicchetti, N.: AC+AS+TH-WeM-10, 108; AC+AS+TH-WeM-11, 108  
 Cinar, V.: SS+AS+TF-MoA-3, 39  
 Çinar, V.: UN-ThP-24, 204  
 Cintron Figuero, D.: NSP-SuA-8, 3  
 Ciobanu, C.: NS+2D+EM+MN+SS-TuM-3, 53  
 Claflin, B.: CPS+CA-WeA-9, 131  
 Clark, A.: CA1+AS+LS+NS+SS+VT-MoM-1, **7**  
 Clark, B.: CA+AS+LS+NS+SS+VT-MoA-6, 27; CA-TuP-3, 89; UN-ThP-4, **200**  
 Clark, R.: AP+EM+PS+TF-TuM-11, 48  
 Clement, D.: QS+VT-WeM-12, 119; VT-TuP-1, 105  
 Clerix, J.: AP+EM+PS+TF-TuM-1, 47  
 Clingerman, D.: SS+AS+TF-MoA-9, 40  
 Clouse, R.: UN-ThP-17, 202  
 Coates, N.: UN-ThP-31, 205; UN-ThP-32, 205  
 Coats, M.: AS-ThP-21, 182  
 Cobden, D.: 2D1-ThA-1, **164**  
 Cochrane, K.: NS+EM+MN-MoA-5, 32  
 Coccoltzi, G.: SS+2D+AS+HC-WeM-12, 121  
 Coe-Sullivan, S.: TF+QS-WeA-11, 143  
 Cohen, B.: EW-TuL-7, 65  
 Cohen, H.: TH2-TuA-12, **82**  
 Cohen, S.: NS+2D+EM+MN+SS-TuM-4, **53**; NS1+2D+BI+SS-MoM-6, **13**  
 Colburn, T.: AS+2D+CA+EL+EM+MS+NS+SE+SS+TF-WeM-5, 112  
 Cole, C.: PS-TuM-3, 55  
 Coleman, J.: EM-WeM-5, 113  
 Coll, B.: EW-TuL-7, 65  
 Collins, R.: EL1+TF-MoA-3, 29; EL1-MoM-1, 9  
 Collins, S.: HC-ThP-11, 189  
 Collison, W.: QS+EM+TF-MoM-10, 17  
 Comini, N.: CPS+CA-WeA-7, 131  
 Compagnini, G.: 2D-ThP-16, 177  
 Conard, T.: AS+CA+EL+EM+SE+SS+TF-WeA-3, **127**  
 Concepcion, J.: LX-TuP-1, 91  
 Condorelli, M.: 2D-ThP-16, 177  
 Conley, J.: EM-ThA-3, 166; EM-WeA-3, 132  
 Connolly, N.: PS+SE-MoA-10, **35**; PS+SE-MoA-11, 35  
 Consiglio, S.: AP+EM+PS+TF-TuM-11, 48  
 Conti, A.: SS+2D+AS+HC-TuM-13, 59  
 Conti, G.: MI+2D+TF-ThM-10, 157  
 Cook, T.: TF-ThM-12, **163**  
 Coombes, K.: MN-ThP-2, 191  
 Coombs, R.: BI-TuP-11, 88  
 Cooper, J.: CPS+CA-WeA-1, 130  
 Copeland, C.: NS+EM+MN-MoA-5, 32; NS+EM+MN-MoA-8, **33**  
 Corbett, M.: UN-ThP-29, **204**  
 Corcelli, S.: SS-ThP-15, 195  
 Cortazar Martinez, O.: AS+CA+EL+EM+SE+SS+TF-WeA-2, 127; AS-ThP-35, 185  
 Cortazar-Martinez, O.: AS-ThP-36, 185  
 Cosentino, A.: 2D-ThP-2, 175  
 Couet, S.: PS+TF-MoM-1, 13  
 Counihan, M.: AS+2D+CA+EM+MS+NS+SE+SS+TF-FrM-4, 209  
 Counsell, J.: AS+2D+CA+EM+MS+NS+SE+SS+TF-FrM-11, **210**; AS+CA+EL+EM+SE+SS+TF-WeA-4, 128; AS-ThP-18, **181**  
 Coye, S.: 2D2-ThA-5, **165**  
 Crist, B.: SS+HC-TuA-12, **79**  
 Cristaudo, V.: SS+AS+TF-MoA-9, **40**  
 Cronin, S.: 2D-ThP-20, 178  
 Crosby, T.: TF-ThP-14, 198  
 Crossman, J.: TF-ThP-8, **197**  
 Crudden, C.: AP+EM+PS+TF-TuM-3, **47**  
 Crum, E.: TF-ThM-6, 162  
 Cumpson, P.: AS+CA+EL+EM+SE+SS+TF-ThM-4, **147**; AS-ThP-11, **181**; AS-ThP-25, 183

## Author Index

- Cundari, T.: SS+2D+AS+HC-WeM-2, 119  
 Cunge, G.: PS+NS-FrM-4, 215; PS-TuP-7, 96  
 Currelli, D.: PS+SE-FrM-5, 218  
 Currie, M.: TF1+PS-WeM-5, 122  
 Custer, J.:  
   AS+2D+CA+EL+EM+MS+NS+SE+SS+TF-  
   WeM-6, 112  
 Cyrille, M.: PS+TF-MoM-3, 14  
 Czap, G.: NSP-SuA-9, 3; SS-WeA-4, 140  
 — D —  
 D. Williams, M.: 2D2-ThA-5, 165  
 Dai, Z.: LS+AC+AS+LX+MI+TH-ThA-5, 168  
 Dandu, N.: 2D1-ThA-4, 164  
 Daniel, R.: IB-ThA-5, 168  
 Danilov, A.: NS2+2D+BI+EL+SS-MoM-10, **13**  
 Dannar, A.: SS+AS+TF-MoA-3, **39**  
 Darakchieva, V.: EL1+TF-MoA-1, 28; EL-TuP-  
 13, 91  
 Darancet, P.: 2D1-ThA-3, 164  
 Darlington, T.: NS2+2D+EM-TuA-8, **73**  
 Das, S.: 2D+EM-FrM-1, **206**; 2D+TF-TuA-9, **66**  
 Datta, A.: TF2-TuA-10, 80  
 Daugherty, J.: PS2+AS+SS-ThM-12, **160**  
 Daul, C.: AC+MI+TH-TuM-13, 47  
 Daus, A.: EM-ThA-5, 166  
 Dauskardt, R.:  
   AS+2D+CA+EL+EM+MS+NS+SE+SS+TF-  
   WeM-5, 112  
 Davanco, M.: NS+EM+MN-MoA-8, 33  
 Davis, K.: AS-ThP-13, 181  
 Davis, P.: NSP-SuA-8, **3**; UN-ThP-27, 204  
 Davis, R.: EL-TuP-9, 90; EM+TF-ThM-6, 150  
 Davisson, L.: AC+AS+TH-WeM-5, 108  
 Davis-Wheeler Chin, C.: HC+SS-ThM-13, **153**  
 Davoodianidalik, M.: TF+QS-WeA-1, 142; VT-  
 MoA-8, 42  
 Day, C.: VT-TuA-12, 84  
 Day, P.: QS+EM+TF-MoM-5, 16  
 De Carvalho, A.:  
   AS+2D+CA+EM+MS+NS+SE+SS+TF-FrM-1,  
   208  
 De Castro, O.: IB-ThM-5, 154  
 De Geyter, N.: PS1+AS-WeA-11, 138  
 de Graaf, C.: TH1-TuA-1, 81  
 de la Fuente, B.: UN-ThP-9, **201**  
 de Long, L.: MI+2D+TF-WeA-3, 135  
 de Marneffe, J.: AP+PS-MoA-1, 23  
 de Siervo, A.: HC+SS-WeA-7, **133**  
 De Simone, D.: PS+NS-FrM-1, **215**  
 De Yoreo, J.: BI+AS+PS-TuM-10, **50**  
 Dean, A.: AS-ThP-6, 180; AS-ThP-7, **180**; SS-  
 ThP-7, 193  
 Dean, C.: MI+2D+TF-ThM-1, 156  
 Debenedetti, W.: HC-ThP-9, 189  
 Degueldre, C.: LS+AC+AS+LX+MI+TH-ThA-5,  
 168  
 Deijkers, S.: 2D-TuM-4, **44**  
 del Hoyo, J.: TF+QS-WeA-9, 143  
 Delabie, A.: AP+EM+PS+TF-TuM-1, **47**;  
   AP+EM+PS+TF-TuM-12, 49  
 Delchambre, A.: PS-TuP-3, 96  
 Delcorte, A.: PS+SE-FrM-6, 218  
 Delegard, C.: AC+AS+TH-WeM-3, 108  
 Delmas, W.: CPS+CA-WeA-1, 130  
 Delobbe, A.: IB-ThM-1, 153  
 DelRio, F.:  
   AS+2D+CA+EL+EM+MS+NS+SE+SS+TF-  
   WeM-6, 112; NSP-SuA-8, 3  
 Demaude, A.: AP+PS+TF-WeM-12, **110**; PS-  
 TuP-30, 101  
 Demiroglu, I.: 2D-ThM-13, 146  
 Denbeaux, G.: PS+NS-FrM-6, 216  
 Denecke, R.: TH2-TuA-9, 81  
 Deng, X.: SS1+HC-MoM-5, **20**  
 Denlinger, J.: AC+MI+TH-TuM-10, **46**  
 Depablos-Rivera, O.: TF1+PS-WeM-6, 122  
 Derecskei, A.: AP+PS-FrM-3, 207  
 Despiau-Pujos, E.: PS+NS-FrM-4, **215**; PS-TuP-  
 7, 96  
 Desta, D.: AS+CA+EL+EM+SE+SS+TF-WeA-3,  
 127  
 Devaraj, A.: IB-ThA-3, 167; IB-ThA-4, 167; IB-  
 ThM-13, 155; SE-TuP-9, 104  
 Devereaux, Z.: AP2+PS+TF-TuA-9, 69  
 Deviere, J.: PS-TuP-3, 96  
 Dhagat, P.: MN1-WeM-3, 116  
 Dhamdhere, A.: EM-WeA-4, 132  
 Dharmadasa, C.: TF-ThP-17, **198**  
 Dhas, J.: 2D-ThP-1, 175; BI1-MoA-6, 26;  
   SS+AS+TF-MoA-11, 41  
 Dhinojwala, A.: BP-SuA-9, **2**  
 Dickey, E.: EM-ThA-1, 165; EM-ThA-4, 166  
 Dickie, M.: QS+EM+TF-MoM-5, 16  
 Diebold, A.:  
   AS+2D+CA+EL+EM+MS+NS+SE+SS+TF-  
   WeM-10, **112**  
 Diebold, U.: HC+SS-WeM-2, 115;  
   SS+2D+AS+HC-TuM-1, 58; SS+2D+AS+HC-  
   TuM-10, 59; SS+2D+AS+HC-TuM-13, 59;  
   SS+2D+AS+HC-TuM-2, 58; SS+2D+AS+HC-  
   WeM-1, 119  
 Diestelhorst, E.: IB-ThM-11, 154  
 Dietrich, P.: CA+AS+LS+LX+MN+SE+SS-TuM-  
 10, **52**; LX+AS+HC+SS-MoM-5, 11  
 Dimitrakellis, P.: LX+AS+HC+SS-MoM-8, 11  
 Dingreville, R.:  
   AS+2D+CA+EL+EM+MS+NS+SE+SS+TF-  
   WeM-6, 112; EM-WeM-5, 113  
 Dirks, R.: UN-ThP-15, 202  
 Dissanayake, R.: SS-ThP-12, 194  
 Distasio Jr., R.: 2D-WeM-13, 107  
 Ditter, A.: AC+AS+TH-WeM-10, 108;  
   AC+AS+TH-WeM-11, 108;  
   LS+AC+AS+LX+MI+TH-ThA-5, **168**  
 Diulus, J.: CA-TuP-2, **88**; CPS+CA-WeA-7, **131**  
 Divis, M.: AC+MI+TH-TuM-11, 46  
 Dixon, B.: BP-SuA-7, 2  
 Dixson, R.: NS+EM+MN-MoA-5, 32;  
   NS+EM+MN-MoA-8, 33  
 D'Mello, C.: UN-ThP-7, **201**  
 Do, H.: SE-TuP-10, 104  
 Dodge, D.: UN-ThP-15, **202**  
 Dogariu, A.: AP-TuP-2, 85  
 Dohnalek, Z.: HC+SS-WeM-12, **116**; HC-ThP-  
 9, 189  
 Dohnálek, Z.: HC+SS-ThM-1, 151  
 Doležal, P.: AC+MI+TH-TuM-11, 46  
 Dolia, K.: EL-TuP-8, 90  
 Domenichini, B.: CA+AS+LS+NS+SS+VT-MoA-  
 10, 28  
 Donald, S.: AC+AS+TH-WeM-10, 108;  
   AC+AS+TH-WeM-11, 108; AC+AS+TH-WeM-  
 5, **108**; LS+AC+AS+LX+MI+TH-ThA-5, 168  
 Donath, M.: MI+2D+TF-WeA-1, 135;  
   MI+2D+TF-WeA-10, 136; MI+2D+TF-WeA-9,  
   135; SS+AS+TF-MoA-8, 40  
 Donegan, A.: UN-ThP-28, **204**  
 Dong, W.: SS+HC-TuA-1, 78  
 Dong, Z.: SS-WeA-3, 140  
 Dorneles de Mello, M.: LX+AS+HC+SS-MoM-  
 8, 11; TF+SE-FrM-9, 220  
 Dorsey, K.: PS+NS-FrM-10, 217  
 Dorst, A.: SS-ThP-12, **194**  
 Douglass, K.: NS+EM+MN-MoA-1, 31; VT-  
 MoM-9, 22  
 Dowben, P.: MI+2D+TF-WeA-2, 135  
 Downey, B.: EM+TF-ThM-12, 151; MN1-  
 WeM-3, 116; SE1+TF-MoM-5, 18  
 Draney, J.: PS2+MS-WeA-4, **138**  
 Drnovšek, A.: SE+TF-MoA-6, **38**  
 Drobek, M.: SE1+TF-MoM-6, 18  
 D'Souza, F.: SS+2D+AS+HC-WeM-2, 119  
 du Rietz, A.: BI+AS+EM+NS+SE+TF-TuA-4, **71**  
 Du, X.: 2D+TF-TuA-11, 67  
 Du, Y.: SS+AS+TF-MoA-11, 41; SS2+AS+TF-  
   ThM-11, **161**; TF2+AP+SE+SS-WeM-13, **123**  
 Duan, X.: 2D+TF-TuA-1, **66**  
 Dubois, J.: PS+TF-MoM-3, 14  
 Dubowsky, S.: PS+SE-FrM-5, 218; PS+SE-  
   MoA-11, 35  
 Dubrovski, O.: PS1-ThA-2, 169  
 Duchon, T.: SS1+HC-MoM-1, 19  
 Ducluzaux, P.: PS+NS-FrM-4, 215  
 Dudas, E.: TF+QS-WeA-1, 142  
 Dudy, L.: AC+MI+TH-TuM-10, 46  
 Dulal, P.: EL1+TF-MoA-4, **29**; EL1-MoM-1, 9  
 Dumitrescu, E.: NS-TuP-11, 94  
 Duncan, J.: 2D+TF-TuA-7, 66  
 Dunkelberger, A.: BI2+AS+HC+SS-MoM-9, 7  
 Dunlap, M.: CA-TuP-4, **89**  
 Durand, D.: BI-TuP-11, 88  
 Duree, J.: PS-TuP-26, 100  
 D'Urso, L.: 2D-ThP-16, **177**; 2D-TuM-12, 45  
 Dussart, R.: AP+PS-MoA-3, **23**  
 Dutta, A.: SE-TuP-4, 103  
 Dwivedi, O.: AP+PS-MoA-6, 24  
 Dziadkowiec, J.: SS2-MoM-10, 20  
 — E —  
 Earl, L.: QS+VT-WeM-12, 119  
 Ebadollahi, N.: QS+EM+TF-MoM-1, 15; QS-  
   MoA-11, **37**  
 Ebong, A.: SE+TF-MoA-1, 38  
 Echeverria, E.: 2D-WeM-5, 106  
 Eckel, S.: VT-MoA-9, 42; VT-MoM-8, **22**  
 Eckhert, P.: TF+SE-FrM-9, 220  
 Eda, Y.: SS-ThP-2, 192  
 Edel, R.: SS-WeA-8, 141  
 Eder, M.: HC+SS-ThM-6, 152;  
   LX+AS+BI+HC+SS+TH-MoA-5, 31;  
   SS+2D+AS+HC-WeM-1, **119**  
 Edwards, N.: AC+AS+MI+TH-WeA-1, 125  
 Efremova, M.: MI+2D+TF-ThM-13, 157  
 Ege, T.: MS-ThP-3, 192  
 Ekari, J.: AS-ThP-30, 184  
 Elgad, N.: AC-TuP-3, 85  
 Eller, M.: CA+AS+LS+LX+MN+SE+SS-TuM-1,  
 51  
 Ellingboe, A.: PS-WeM-5, 118  
 Elliott, S.: AP+PS+TF-MoM-8, 5  
 Elstgeest, D.: VT-MoM-10, 22  
 Emerson, H.: AC+AS+TH-WeM-3, 108  
 Emmelkamp, J.: VT-MoM-10, 22  
 Emminger, C.: EL-TuP-6, 90  
 Émond, N.: TF2+AP+SE+SS-WeM-12, 123  
 Endo, Y.: HC+SS-WeM-1, 114  
 Engbrecht, K.: CA+AS+LS+NS+SS+VT-MoA-11,  
 28  
 Engelhard, M.: AS-ThP-22, 182; AS-ThP-23,  
 183  
 Engel-Herbert, R.: MI+2D+TF-ThM-12, 157  
 Engelmann, S.: PS-WeM-10, 118  
 Eparvier, F.: SS+HC-TuA-10, 78  
 Erickson, T.: SS+2D+AS+HC-WeM-11, **121**;  
   SS+2D+AS+HC-WeM-12, 121  
 Esch, F.: LX+AS+BI+HC+SS+TH-MoA-5, 31;  
   SS+2D+AS+HC-WeM-5, 120  
 Escher, M.: 2D2-ThA-6, 165; 2D-ThP-19, 178;  
   EW-TuL-2, 64  
 Eslamisaray, M.: PS+SE-FrM-1, 217  
 Espinoza, S.: EL1-MoM-6, 10  
 Ettouri, R.: AP+PS-MoA-3, 23  
 Evans, J.: EM-ThP-8, 186  
 Evans, P.: TF-ThP-17, 198  
 Eyres, A.:  
   AS+2D+CA+EL+EM+MS+NS+SE+SS+TF-

## Author Index

- WeM-13, 112; AS+CA+EL+EM+SE+SS+TF-ThM-1, 146  
— F —
- F. Trindade, G.:  
AS+2D+CA+EL+EM+MS+NS+SE+SS+TF-WeM-13, **112**
- Faase, R.: BI+AS+EM+NS+SE+TF-TuA-10, 72
- Facsko, S.: IB-ThM-1, 153
- Fairbrother, H.: TF+SE-FrM-9, 220
- Fairley, N.: AS+CA+EL+EM+SE+SS+TF-ThM-2, 147
- Falcone, R.: MI+2D+TF-ThM-13, 157
- Fan, X.: LX-TuP-4, 92
- Fangohr, H.: NS-TuP-11, 94
- Fantner, G.: NS1+2D+BI+SS-MoM-5, 12
- Farber, R.: QS+SS-TuA-9, 77
- Farle, M.: MI+2D+TF-ThM-13, 157
- Faruqe, O.: MN-ThP-4, 191
- Fassion, A.: PS-TuM-12, **56**
- Fathzadeh, A.: PS+NS-FrM-3, 215
- Faye, D.: VT-MoA-3, **42**
- Fears, K.: BI1+PS-MoM-6, 6; BI2+AS+HC+SS-MoM-9, **7**
- Fedchak, J.: VT-MoA-9, **42**; VT-MoM-8, 22
- Feggeler, T.: MI+2D+TF-ThM-13, **157**
- Feicht, J.: VT-TuM-6, 62
- Feigelson, B.: AP+PS+TF-WeM-3, 109
- Feit, C.: 2D-ThP-11, 176; EM-WeA-4, 132
- Felbinger, J.: QS-MoA-10, **37**
- Feldner, A.: BI+AS+EM+NS+SE+TF-TuA-7, 71; BI-TuP-4, **87**
- Femi-Oyetero, J.: QS+EM+TF-MoM-5, **16**
- Feng, P.: MN1-WeM-6, 117; MN2-WeM-12, 117
- Feng, Z.: 2D-ThP-9, 176; AS-ThP-12, 181
- Fernandez Velasco, L.: SS+HC-TuA-11, 79
- Fernandez, V.: AS+CA+EL+EM+SE+SS+TF-ThM-2, **147**
- Ferrari, V.: UN-ThP-7, 201
- Ferreira, M.: VT-TuM-13, 63; VT-TuP-6, 105
- Fields, S.: EM-ThA-1, 165; EM-ThA-4, 166
- Fillion, M.: VT-TuA-12, **84**
- Fini, E.: NS+2D+EM+MN+SS-TuM-10, 54
- Finney, L.:  
AS+2D+CA+EM+MS+NS+SE+SS+TF-FrM-10, 210
- Finzel, J.: SS+AS+TF-MoA-3, 39
- Fiorenza, R.: 2D-TuM-12, 45
- Fischer, D.: BI+AS+PS-TuM-12, 50
- Fischer, J.: PS+SE-MoA-1, 34
- Fischer, P.: MS-FrM-8, **215**
- Fisher, G.:  
AS+2D+CA+EM+MS+NS+SE+SS+TF-FrM-1, 208; AS-ThP-27, **183**; EW-TuL-4, **64**
- Fisher, R.: TF-ThP-19, **199**
- Flaemmich, M.: VT-TuA-3, 83
- Flavell, W.: LX+AS+HC+SS-MoM-10, **11**
- Fletcher, I.: AS-ThP-25, 183
- Fletcher, W.: VT-MoM-3, 21
- Florek, M.: SS-ThP-10, 194
- Flores, A.: EM+TF-ThM-11, 150
- Flores-Mireles, A.: BI-TuP-11, 88
- Foley, B.: 2D-ThP-21, 178
- Folley, A.: UN-ThP-12, **202**
- Fong, C.: BI-TuP-11, **88**; UN-ThP-10, 201
- Fontaine, B.: PS+TF-MoM-3, 14
- Fontaine, T.: PS1+AS-WeA-11, 138
- Fontenot, P.: HC+SS-ThM-13, 153
- Ford, J.: IB-ThM-4, **154**
- Forte, G.: 2D-TuM-12, 45
- Fortuna, C.: 2D-TuM-12, 45
- Foster, G.: EM2-FrM-10, 211
- Foster, J.: AS-ThP-20, **182**
- Foti, A.: 2D-ThP-2, 175; 2D-TuM-12, 45
- Foucher, M.: PS-TuM-4, 55
- Fowler, E.:  
AS+2D+CA+EL+EM+MS+NS+SE+SS+TF-WeM-6, 112; EM-WeM-5, **113**
- Fragalà, M.: 2D-ThP-16, 177
- Fraix, A.: 2D-TuM-12, 45
- Franceschi, G.: SS+2D+AS+HC-TuM-2, 58
- Franchini, C.: HC+SS-WeM-2, 115
- Frankovich, H.: UN-ThP-20, **203**
- Franz, K.: BI1+PS-MoM-6, 6
- Frenkel, A.: HC+SS-FrM-6, 212
- Frerichs, H.: NS1+2D+BI+SS-MoM-4, 12
- Frese, N.: AS+CA+EL+EM+SE+SS+TF-ThM-5, 147; IB3-FrM-11, 214; IB-ThM-11, **154**
- Freund, H.: TH1+AS+SS-TuM-1, **60**
- Fricke, C.: AC+MI+TH-TuA-10, **68**
- Fridman, A.: PS+SE-FrM-3, **218**
- Friedman, A.: 2D-WeA-10, 125
- Frierson, M.: TF-ThP-14, 198
- Frisone, S.: EM+TF-ThM-11, **150**
- Frolov, G.: TF+QS-WeA-11, 143
- Frost, H.: QS+EM+TF-MoM-10, 17
- Fruhmann, P.: BI+AS+EM+NS+SE+TF-TuA-11, 72; BI+AS+EM+NS+SE+TF-TuA-7, **71**; BI-TuP-4, 87
- Frye, B.: EL-TuP-5, **90**; EL-TuP-8, 90
- Frye, M.: TF2+AP+SE+SS-WeM-10, 122
- Fu, Y.: 2D-ThP-11, **176**; 2D-ThP-22, 179
- Fu, Z.: 2D2-ThA-2, 164
- Fuchs, A.: HC-ThP-7, **188**
- Fuchs, E.: QS+SS-TuA-11, 77
- Fuentes-Garcia, M.: VT-TuM-6, **62**
- Fukasawa, M.: AP+PS-MoA-5, 23
- Fuller, E.: SS+AS+TF-MoA-10, 41; TF-ThP-6, 196
- Fuller, J.: BI2-MoA-9, 26
- Fullwood, D.: AS-ThP-17, 181
- Furche, F.: LX-TuP-2, 91
- Furukawa, M.: HC+SS-WeM-1, 114
- Fushimi, R.: HC+SS-ThM-3, 152
- G —
- Gaiser, A.: AC+MI+TH-TuA-7, **68**
- Gajdek, D.: SS1+HC-MoM-6, 20
- Galais, M.: PS-TuP-9, 97
- Galvano, A.: UN-ThP-20, 203; UN-ThP-21, **203**; UN-ThP-22, 203; UN-ThP-23, 203
- Gallagher, A.: AC+MI+TH-TuM-10, 46
- Galtayries, A.:  
AS+2D+CA+EM+MS+NS+SE+SS+TF-FrM-1, 208
- Gamage, S.: 2D-WeM-13, 107
- Gamble, L.: BI1-MoA-1, 25
- Ganesan, A.: SS+2D+AS+HC-WeM-2, 119
- Ganta, S.: PS+MS-TuA-10, 75; PS+MS-TuA-3, 74; PS+MS-TuA-8, **75**
- Gaowei, M.: VT-MoA-1, **41**
- Garber, L.: UN-ThP-20, 203
- Garcia Michel, E.: SS+AS+TF-MoA-10, 41; TF-ThP-6, 196
- Garcia-Ortiz, M.: UN-ThP-26, **204**
- Garcia-Soto, C.: PS1+AS-WeA-7, 137
- Gardiner, J.: NS1+2D+BI+SS-MoM-4, 12
- Gardner, W.: CA1+AS+LS+NS+SS+VT-MoM-5, 8
- Garland, B.: EM1+TF-FrM-6, 211
- Garman, J.: IB1-FrM-1, 213
- Garten, L.: TF2+AP+SE+SS-WeM-10, **122**
- Garvey, S.: NS-TuP-8, 93
- Garza, R.: PS+SE-MoA-10, 35
- Gaskins, J.: 2D-ThP-21, **178**; TF-ThP-19, 199
- gassilloud, z.: AP1+2D+EM+PS+TF-TuA-1, 69
- Gasvoda, R.: PS2-ThA-4, 171
- Gaude, C.:  
AS+2D+CA+EM+MS+NS+SE+SS+TF-FrM-1, 208
- Gauthier, N.:  
AS+2D+CA+EL+EM+MS+NS+SE+SS+TF-WeM-4, 111;  
AS+2D+CA+EM+MS+NS+SE+SS+TF-FrM-1, 208; AS-ThP-29, 184
- Gelb, L.: AS+CA+EL+EM+SE+SS+TF-WeA-7, **128**
- Gelhar, A.: BI+AS+PS-TuM-3, 49
- Genova, V.: PS+NS-FrM-10, 217
- Geohegan, D.: 2D+TF-TuA-3, 66
- George, S.: AP+PS+TF-MoM-10, 5; AP+PS+TF-MoM-3, 4; AP+PS+TF-MoM-4, 4; AP+PS+TF-MoM-5, 4; AP+PS+TF-MoM-9, 5; AP+PS+TF-WeM-6, **110**; AP-TuP-7, 86; TF+SE-FrM-10, 220
- Georges, R.: TF+QS-WeA-1, 142
- Georgiev, D.: EM2-FrM-10, 211
- Gericke, S.: HC+SS-WeA-9, 134
- Gerling, J.: NS+EM+MN-MoA-5, 32
- Gewirth, A.: SS1+HC-MoM-3, **19**
- GhafariAsl, M.: 2D-WeM-13, 107
- Ghanadi, N.: SE-TuP-2, 103
- Gharaee, M.: SS+2D+AS+HC-WeM-2, 119
- Ghodsi, V.: AP+PS+TF-MoM-9, 5; AP-TuP-7, 86
- Ghosal, D.: 2D+EM-FrM-4, 206
- Giesen, M.: SS1+HC-MoM-1, 19
- Gil, H.: PS-TuP-14, 98; PS-TuP-16, 98; PS-TuP-19, 99
- Gill, H.: PS-TuP-12, 97
- Gillman, E.: AS-ThP-8, 180; IB-ThM-10, **154**
- Gillum, M.: HC-ThP-2, 187; NS-TuP-17, 95; SS+AS+TF-MoA-6, **40**
- Gilmore, L.:  
AS+2D+CA+EL+EM+MS+NS+SE+SS+TF-WeM-13, 112;  
AS+2D+CA+EM+MS+NS+SE+SS+TF-FrM-3, 208; AS+CA+EL+EM+SE+SS+TF-ThM-1, **146**
- Gilquin, B.:  
AS+2D+CA+EM+MS+NS+SE+SS+TF-FrM-1, 208
- Glaser, C.: CPS+CA-WeA-1, 130
- Glavin, N.: 2D+TF-TuA-11, 67; EM-WeM-12, **114**
- Glukhoy, Y.: PS+SE-FrM-10, **218**
- Gnani Peer Mohamed, S.: 2D-ThP-10, 176; TF1-TuA-3, **79**
- Go, D.: PS1-ThA-2, 169
- Gofryk, K.: AC+AS+MI+TH-WeA-8, 126; AC+MI+TH-TuM-11, 46; AC+MI+TH-TuM-6, 46; EM-ThP-3, 186; QS+EM+TF-MoM-8, 16
- Gohira, T.: PS+TF-MoM-6, 14
- Gokhale, V.: EM+TF-ThM-12, 151; MN1-WeM-3, **116**
- Golbek, T.: BI+AS+PS-TuM-2, 49; BI+AS+PS-TuM-5, 50
- Golda, J.: PS+SE-FrM-8, **218**
- Golding, M.:  
AS+2D+CA+EL+EM+MS+NS+SE+SS+TF-WeM-5, 112
- Goldman, R.: EM+TF-ThM-11, 150
- Goldstein, B.: QS+SS-TuA-12, 77
- Gofuński, M.: CA+AS+LS+LX+MN+SE+SS-TuM-1, 51
- Göhlhäuser, A.: IB3-FrM-11, 214; IB-ThM-11, 154
- Gomez-Sosa, G.: AS-ThP-36, 185
- Gonzalez, A.: TF-ThM-12, 163
- González-Barrio, M.: SS+AS+TF-MoA-10, 41; TF-ThP-6, 196
- Good, K.: AS+CA+EL+EM+SE+SS+TF-WeA-4, **128**
- Goodson, K.: EM-ThA-5, 166
- Gorb, S.: BI+AS+PS-TuM-12, 50
- Gordon, J.: UN-ThP-14, **202**

## Author Index

- Gordon, M.: AP+PS+TF-WeM-12, 110; PS1+AS-WeA-3, 136; PS1+AS-WeA-4, **137**; UN-ThP-8, 201
- Gorman, J.: VT-MoM-4, 21
- Gort, C.: 2D-WeM-4, 106
- Gostenčnik, Ž.: SE+TF-MoA-6, 38
- Goto, S.: VT-MoM-5, 21
- Göttlicher, J.: TH1+AS+SS-TuM-5, 60
- Gouder, T.: AC+AS+MI+TH-WeA-9, 126
- Gould, I.: CA+AS+LS+LX+MN+SE+SS-TuM-3, 51
- Gouraud, P.: PS+TF-MoM-3, 14
- Grabnic, T.: SS-WeA-8, 141
- Graham, C.: SE-TuP-5, 104
- Graham, D.: BI1-MoA-1, **25**
- Grasso, J.: EM+TF-ThM-5, 150; NS2+2D+EM-TuA-11, **73**
- Graugnard, E.: NSP-SuA-8, 3; UN-ThP-16, 202; UN-ThP-17, 202; UN-ThP-28, 204
- Graulich, D.: AS+CA+EL+EM+SE+SS+TF-ThM-5, 147
- Graves, D.: PS2+MS-WeA-1, **138**; PS2+MS-WeA-4, 138; PS-TuP-6, 96
- Greczynski, G.: SE1+TF-MoM-1, 17
- Green, A.: PS+NS-FrM-8, 216
- Greenberg, B.: AP+PS+TF-WeM-3, **109**
- Greeneltch, N.: MS-ThP-2, 192
- Greer, F.: AP+PS-MoA-11, 24; QS+EM+TF-MoM-5, 16; TF+QS-WeA-7, **143**
- Greer, R.: AC+MI+TH-TuM-6, 46
- Gregory, S.: TF1-TuA-4, 79
- Grehl, T.: HC+SS-FrM-3, **212**
- Grenouillet, L.: PS+TF-MoM-3, 14
- Grenz, P.: MI+2D+TF-WeA-1, **135**; MI+2D+TF-WeA-10, 136
- Grespi, A.: HC+SS-WeA-9, 134; SS1+HC-MoM-6, 20
- Griffin, P.: QS+VT-WeM-5, 118
- Groot, I.: 2D-ThP-12, 176; HC+SS-ThM-2, **152**
- Groß, A.: SS+HC-ThA-5, **172**
- Grzeskowiak, S.: PS-TuM-5, 56
- Grzybowski, G.: CPS+CA-WeA-9, 131
- Guaitella, O.: PS1+AS-WeA-7, **137**
- Gudmundsson, J.: PS+SE-MoA-1, **34**; PS-TuP-41, 102
- Guenzing, D.: MI+2D+TF-ThM-13, 157
- Guerra, V.: PS1+AS-WeA-7, 137
- Gui, Y.: PS+NS-FrM-11, **217**
- Guiheux, D.: CA+AS+LS+NS+SS+VT-MoA-10, 28
- Guisinger, N.: 2D1-ThA-3, **164**
- Gulan, M.: PS+SE-FrM-11, 219
- Gump, C.: SE+TF-MoA-8, **38**
- Günther, S.: HC+SS-ThM-6, 152; LX+AS+BI+HC+SS+TH-MoA-5, 31
- Guo, X.: AC+AS+MI+TH-WeA-10, 126
- Guo, Y.: NS+EM+MN-MoA-2, 31
- Gupta, A.: PS-TuM-13, 57
- Gupta, M.: TF-ThP-12, **198**
- Gupta, S.: 2D-WeM-6, **107**; EM-ThP-1, **185**; EM-ThP-7, 186; TF2-TuA-8, **80**
- Gutierrez Ojeda, S.: AC+AS+MI+TH-WeA-8, 126
- Guyot, C.: AS+2D+CA+EM+MS+NS+SE+SS+TF-FrM-1, 208
- Guzman Bucio, D.: AS+CA+EL+EM+SE+SS+TF-WeA-2, **127**; AS-ThP-35, **185**
- Gwalani, B.: IB2-FrM-3, **213**; IB-ThA-3, 167
- Gys, N.: SS+HC-TuA-11, **79**
- H —
- H. Patil, A.: SE-TuP-10, **104**
- Ha, C.: NS-TuP-11, 94
- Hachtel, J.: 2D+TF-TuA-3, 66
- Hadfield, R.: QS+EM+TF-MoM-9, 16
- Hagelin Weaver, H.: HC+SS-ThA-3, **167**
- Hagenhoff, B.: BI2-MoA-10, **26**; BI-TuP-10, 88
- Haglund, J.: EM-ThA-3, **166**
- Hahn, M.: LX+AS+BI+HC+SS+TH-MoA-10, **31**
- Haidu, F.: VT-TuA-3, 83
- Haines, A.: LX-TuP-2, 91
- Hajzuz, J.: EM+TF-ThM-13, 151
- Halasz, G.: NS-TuP-11, 94
- Halevy, I.: AC+AS+TH-WeM-1, **107**; AC-TuP-3, **85**
- Halim, W.: PS+NS-FrM-3, 215
- Hall, H.: MN1-WeM-6, 117; SS+2D+AS+HC-WeM-11, 121; SS+2D+AS+HC-WeM-12, 121
- Hall, J.: NS1+2D+EM+MN-TuA-3, 72
- Hall, P.: UN-ThP-31, 205; UN-ThP-32, 205
- Halls, M.: AP+PS+TF-MoM-8, 5
- Hamaguchi, S.: AP+PS-MoA-5, 23; PS-WeM-12, **118**
- Hammer, L.: SS+2D+AS+HC-TuM-1, 58
- Han, D.: NS-TuP-7, **93**
- Han, J.: EM+TF-ThM-11, 150; TF+SE-FrM-6, 220
- Han, S.: PS-TuP-26, 100; QS+SS-TuA-4, 76; SE+TF-MoA-1, **38**
- Hanbicki, A.: 2D-WeA-10, 125
- Handy, K.: SS-ThP-1, 192; SS-ThP-15, **195**
- Hanley, L.: AS+2D+CA+EM+MS+NS+SE+SS+TF-FrM-4, 209; AS+2D+CA+EM+MS+NS+SE+SS+TF-FrM-6, **209**; BI1-MoA-6, 26
- Hanson, K.: AC+AS+MI+TH-WeA-7, **125**
- Hansson, O.: 2D-ThP-17, 178
- Hao, Q.: NS-TuP-9, 93
- Hara, K.: PS+MS-TuA-2, **74**
- Hardy, M.: EM+TF-ThM-12, **151**; MN1-WeM-3, 116; SE1+TF-MoM-5, 18
- Hariharalakshmanan, R.: NS-TuP-1, **92**
- Harilal, A.: MS-ThP-1, 191
- Harlow, G.: SS1+HC-MoM-6, **20**
- Harrison, I.: 2D-ThP-18, 178
- Harrysson Rodrigues, I.: EM+TF-ThM-10, **150**
- Härtl, P.: MI+2D+TF-WeA-9, 135
- Harvel, F.: 2D2-ThA-4, **165**
- Harvey, K.: TF-ThP-13, **198**
- Harvey, S.: CA+AS+LS+LX+MN+SE+SS-TuM-3, **51**
- Harwood, D.: SE+TF-MoA-1, 38
- Hasan, A.: 2D+EM-FrM-3, **206**; EM-ThP-5, 186
- Hasbrook, A.: BI+AS+EM+NS+SE+TF-TuA-10, **72**
- Hastings, J.: MI+2D+TF-WeA-3, 135
- Hauffman, T.: AP+PS+TF-WeM-12, 110; SS+AS+TF-MoA-9, 40; SS+HC-TuA-11, 79; SS1+HC-MoM-2, **19**; UN-ThP-9, 201
- Havela, L.: AC+MI+TH-TuM-11, 46; AC+MI+TH-TuM-4, **46**
- Haverkort, M.: TH1+AS+SS-TuM-5, 60
- Hawker, M.: BI-WeA-4, **130**; UN-ThP-2, 200; UN-ThP-3, 200; UN-ThP-5, 200; UN-ThP-6, 200
- Hayashi, R.: TF-ThP-2, 196
- Hayashida, K.: HC+SS-WeM-1, 114
- Haye, M.: VT-MoM-10, 22
- He, L.: LS+AC+AS+LX+MI+TH-ThA-5, 168
- He, X.: TF2-TuA-10, 80
- Head, A.: LX+AS+HC+SS-MoM-4, **11**; LX-TuP-1, 91
- Heaney, M.: AC+AS+MI+TH-WeA-10, **126**
- Heath, J.: UN-ThP-31, 205; UN-ThP-32, 205
- Hedevang, M.: 2D-ThM-5, 145
- Hedhili, M.: SS-ThP-8, **194**
- Heil, P.: PS+SE-MoA-9, 35
- Heiner, B.: SS1+AS-ThM-3, **160**
- Heiz, U.: HC+SS-ThM-6, 152; LX+AS+BI+HC+SS+TH-MoA-5, 31; SS+2D+AS+HC-WeM-1, 119
- Held, J.: PS1+AS-WeA-10, 137
- Heldebrant, D.: CA+AS+LS+NS+SS+VT-MoA-8, 28
- Helfrecht, B.: MS-ThP-1, 191
- Helfrich, H.: 2D-WeM-5, 106
- Hellberg, C.: 2D-WeA-3, 124
- Heller, R.: EM+TF-ThM-4, 149
- Hemminge, J.: LX-TuP-2, 91
- Hendricks, J.: QS+SS-TuA-12, **77**; VT-MoM-9, 22
- Hendricks, N.: 2D-ThM-6, **145**; 2D-ThP-5, **175**
- Hennessy, J.: AP+PS+TF-MoM-1, **4**; TF+QS-WeA-10, 143
- Henry, M.: EM-ThA-1, 165; QS+SS-TuA-4, 76
- Her, J.: SE+TF-MoA-9, 39
- Herman, G.: LX-TuP-4, 92
- Herman, T.: NS+EM+MN-MoA-1, 31
- Hernandez Cocolletzi, G.: AC+AS+MI+TH-WeA-8, 126
- Hernandez, J.: SS+2D+AS+HC-WeM-12, 121
- Hernandez, S.: AC+MI+TH-TuA-10, 68
- Herndorf, E.: AS-ThP-22, 182
- Herr, A.: PS-TuM-13, 57
- Herr, Q.: PS-TuM-13, 57
- Herrera Gomez, A.: AS+CA+EL+EM+SE+SS+TF-WeA-2, 127; AS-ThP-35, 185
- Herrera-Gomez, A.: AS+CA+EL+EM+SE+SS+TF-ThM-12, **148**; AS-ThP-36, **185**
- Hersam, M.: 2D-ThM-3, 145; NS1+2D+EM+MN-TuA-7, 73
- Hertel, J.: QS+VT-WeM-13, 119
- Hettige, Y.: EL-TuP-1, 89; EL-TuP-4, **89**
- Heyden, A.: HC+SS-ThM-12, 153
- Hickam, S.: AC+AS+MI+TH-WeA-7, 125
- Hidas, D.: VT-TuP-6, 105
- Hilfiker, M.: EL1+TF-MoA-5, 29
- Hilse, M.: MI+2D+TF-ThM-12, **157**
- Hinshelwood, M.: PS1+AS-WeA-9, **137**
- Hirabayashi, M.: MN-ThP-4, **191**
- Hirai, T.: SS-ThP-2, 192
- Hirata, A.: AP+PS-MoA-5, 23
- Hirchhahn, P.: AS+2D+CA+EM+MS+NS+SE+SS+TF-FrM-1, 208
- Hirsch, R.: AP-TuP-7, 86
- Hisamatsu, H.: VT-TuP-4, 105
- Hisamatsu, T.: PS2+MS-WeA-3, 138; PS2+MS-WeA-7, 139
- Hite, J.: AP+PS+TF-WeM-11, 110
- Hla, S.: 2D1-ThA-4, 164; SS-WeA-12, 142
- Hlawacek, G.: EM+TF-ThM-4, **149**; IB-ThM-1, 153; IB-ThP-2, **190**
- Hoang, H.: IB-ThM-5, 154
- Hobart, K.: EM2-FrM-10, 211
- Hobler, G.: IB-ThP-2, 190
- Hodges, W.: CPS+CA-WeA-1, 130
- Hoenk, M.: TF+QS-WeA-10, 143
- Hoffenberg, L.: PS-TuP-6, **96**
- Höflich, K.: IB-ThP-2, 190
- Hofmann, J.: 2D-WeM-4, 106
- Hofmann, T.: 2D-ThP-8, 176; MN1-WeM-5, 116
- Hohenwarter, A.: IB-ThA-5, 168
- Hojoh, H.: VT-MoM-5, 21
- Holcomb, M.: AP-TuP-4, 86
- Holler, K.: BI+AS+PS-TuM-12, 50
- Holtmann, M.: MI+2D+TF-WeA-10, **136**
- Homma, K.: HC+SS-WeM-1, 114
- Honda, F.: AC+MI+TH-TuM-11, 46; AC+MI+TH-TuM-4, 46

## Author Index

- Honda, M.: PS+TF-MoM-2, 14; PS1+MS-ThM-1, 158
- Hong, J.: PS-TuP-15, 98; PS-TuP-5, **96**
- Hong, T.: AP2+PS+TF-TuA-12, 70
- Hong, W.: HC+SS-FrM-2, 212
- Hong, Y.: QS+EM+TF-MoM-1, 15; QS-MoA-11, 37
- Hopkins, P.: 2D-ThP-21, 178; EM-WeA-4, 132; PS1-ThA-6, 170; TF-ThP-19, 199
- Horak, L.: AC+AS+MI+TH-WeA-9, 126
- Hori, M.: AP+PS-FrM-4, 208; PS+TF-MoM-6, 14; PS1-ThA-1, 169
- Hornbrook, L.: UN-ThP-15, 202
- Hosemann, P.: IB-ThA-1, **167**
- Hossain, A.: AP+PS-FrM-5, 208; AP+PS-MoA-10, **24**; AP+PS-MoA-11, 24
- Hossain, M.: AP+PS+TF-WeM-5, 109; HC+SS-ThM-3, 152; HC-ThP-4, **188**; PS+SE-MoA-8, **35**
- Hosseini, N.: NS1+2D+BI+SS-MoM-5, 12
- Housley, C.: AC-TuP-2, 85
- Howell, C.: BI+AS+EM+NS+SE+TF-TuA-3, 70; BI-TuP-11, 88; BI-TuP-9, 87; BP-SuA-7, **2**; UN-ThP-10, 201; UN-ThP-12, 202; UN-ThP-13, 202
- Hoyer, C.: AC+MI+TH-TuA-1, **67**
- Hrabar, S.: CA+AS+LS+LX+MN+SE+SS-TuM-1, 51
- Hsiao, C.: NS-TuP-16, **95**
- Hsiao, L.: HC+SS-ThA-3, 167
- Hsiao, S.: PS+TF-MoM-6, 14; PS1-ThA-1, **169**
- Hu, B.: MI+2D+TF-WeA-11, **136**
- Hu, Z.: BI+AS+EM+NS+SE+TF-TuA-4, 71
- Huang, C.: UN-ThP-25, 204
- Huber, F.: AC+AS+MI+TH-WeA-9, 126
- Hubin, A.: SS1+HC-MoM-2, 19
- Hübner, R.: EM+TF-ThM-4, 149
- Hudson, E.: PS2-ThA-4, 171
- Hues, S.: NSP-SuA-8, 3; UN-ThP-16, 202; UN-ThP-17, 202; UN-ThP-28, 204
- Hui, H.: 2D-ThP-22, 179
- Hui, S.: UN-ThP-30, **205**
- Hulbert, S.: VT-TuM-13, 63
- Huli, L.: PS-TuM-5, 56
- Hultman, L.: SE1+TF-MoM-1, **17**
- Humbert, B.: AS+CA+EL+EM+SE+SS+TF-ThM-2, 147
- Hummel, M.: BI+AS+EM+NS+SE+TF-TuA-10, 72
- Huneycutt, S.: SE+TF-MoA-1, 38
- Hunt, B.: MI+2D+TF-ThM-1, **156**
- Hunt, C.: EM-ThP-10, 187
- Hunt, D.: UN-ThP-7, 201
- Hurley, D.: QS+EM+TF-MoM-8, 16
- Hurley, M.: NSP-SuA-8, 3
- Hussey, D.: NS+EM+MN-MoA-4, 32
- Hütner, J.: SS+2D+AS+HC-TuM-13, 59
- Hwang, G.: AP+PS+TF-WeM-10, 110; AP-TuP-5, 86; PS2+MS-WeA-10, 139; TF-ThP-5, 196
- Hwang, H.: AS-ThP-2, 179; EM-WeA-11, **133**; SS2+AS+TF-ThM-10, **161**
- Hyundong, E.: PS-TuP-32, 101
- I —
- Ibrahimli, N.: EM+TF-ThM-5, 150; EM-ThP-6, 186; PS-TuP-25, **100**; TF-ThP-11, **198**
- Ilevlev, A.: 2D+TF-TuA-3, 66; AS+2D+CA+EM+MS+NS+SE+SS+TF-FrM-6, 209
- Igosawa, R.: PS1+MS-ThM-1, 158
- Ihlefeld, J.: EM-ThA-1, **165**; EM-ThA-3, 166; EM-ThA-4, 166
- Iida, S.: AS-ThP-27, 183
- Iijima, Y.: PS+TF-MoM-6, 14; PS1-ThA-1, 169
- Ikeda, N.: MS-ThP-3, 192
- Ilhom, S.: EM+TF-ThM-5, 150; EM-ThP-6, 186
- Ilic, B.: NS+EM+MN-MoA-8, 33
- Ilton, E.: LS+AC+LX+MI+TH-ThM-12, 156
- Imai, M.: PS-TuM-1, **55**
- Imai, Y.: PS+TF-MoM-6, **14**
- Imre, A.: SS+2D+AS+HC-TuM-1, **58**
- Ingram, D.: SS+2D+AS+HC-WeM-11, 121
- Iqbal, A.: PS-TuP-40, **102**
- Irving-Singh, Z.: UN-ThP-31, 205; UN-ThP-32, 205
- Isagoda, M.: SS-ThP-5, **193**
- Ishibashi, R.: MS-ThP-3, 192
- Ishibashi, T.: VT-TuP-4, 105
- Ishihara, T.: VT-TuA-11, **84**
- Ishii, Y.: PS-TuM-1, 55; PS-TuM-10, 56
- Ishikawa, K.: AP+PS-FrM-4, 208; PS+TF-MoM-6, 14; PS1-ThA-1, 169
- Ishikawa, M.: TF-ThP-2, 196
- Iski, E.: UN-ThP-15, 202
- Islam, M.: EM-WeA-4, 132
- Islam, N.: NS2+2D+EM-TuA-10, **73**
- Isobe, M.: AP+PS-MoA-5, 23
- Ito, S.: HC+SS-WeM-1, 114
- Itzhak, N.: NS1+2D+BI+SS-MoM-6, 13
- Ivanov, V.: MI+2D+TF-ThM-10, 157
- Iwata, M.: PS+TF-MoM-6, 14; PS2+MS-WeA-7, 139
- J —
- Jackson, M.: EM-WeM-11, 114
- Jacobs, A.: AP+PS+TF-WeM-3, 109; EM2-FrM-10, 211
- Jadeja, S.: 2D-ThP-22, 179
- Jafari, S.: AS-ThP-6, 180; SS-ThP-7, **193**
- JAFARI, S.: AS-ThP-7, 180
- Jahan, C.: PS+TF-MoM-3, 14
- Jain, M.: AS+2D+CA+EL+EM+MS+NS+SE+SS+TF-WeM-6, 112
- Jakub, Z.: HC+SS-WeM-2, 115; SS1+AS-ThM-4, **160**
- Jalan, B.: QS+EM+TF-MoM-3, **16**
- Jamka, E.: SS+AS+TF-MoA-6, 40
- Jamka, L.: HC-ThP-2, 187
- Jana, R.: AS-ThP-12, 181
- Jander, A.: MN1-WeM-3, 116
- Jang, J.: HC+SS-FrM-2, 212
- Jang, S.: AP-TuP-3, **85**; SS+HC-ThA-6, **172**
- Jang, Y.: PS-TuP-12, 97; PS-TuP-14, 98; PS-TuP-16, 98; PS-TuP-19, 99
- Janssen, T.: AP+EM+PS+TF-TuM-6, **48**
- Janulaitis, N.: HC+SS-WeA-3, 133
- Jariwala, D.: 2D+TF-TuA-11, 67; EM-WeM-3, **113**
- Järvillehto, J.: HC+SS-FrM-3, 212
- Jarzembski, A.: CPS+CA-WeA-1, 130
- Jaszewski, S.: EM-ThA-1, 165; EM-ThA-4, **166**
- Jawad, S.: UN-ThP-3, **200**
- Jayakodiachchi, N.: TF-ThP-17, 198
- Jayaram, S.: MS-ThP-2, 192
- Jaye, C.: BI+AS+PS-TuM-12, 50
- Jayswal, N.: EL1-MoM-1, 9
- Jean, B.: TF-ThM-12, 163; TF-ThM-4, 162
- Jeckell, Z.: AP+PS+TF-WeM-5, **109**
- Jelezko, F.: QS+SS-TuA-1, **76**
- Jen, W.: UN-ThP-16, 202; UN-ThP-17, 202
- Jenkins, T.: PS+MS-TuA-9, 75
- Jennings, C.: PS2-ThA-2, 170
- Jennings, G.: VT-MoM-3, 21; VT-TuA-4, 83
- Jensen, D.: AP-TuP-2, 85
- Jensen, E.: SS+HC-TuA-9, **78**
- Jeon, B.: HC-ThP-1, 187; HC-ThP-8, 188
- Jeon, S.: 2D+TF-TuA-11, 67
- Jeong, H.: HC+SS-FrM-2, 212; SS-ThP-4, 193
- Jeong, U.: EM-ThP-2, **185**
- Jeong, W.: PS2-ThA-5, 171; PS-TuP-37, 102; PS-TuP-38, 102
- Jeong, Y.: PS-TuP-39, **102**; PS-TuP-5, 96
- Jernigan, G.: AS+2D+CA+EL+EM+MS+NS+SE+SS+TF-WeM-1, **111**
- Jessup, D.: SS+HC-ThA-4, 172
- Jewell, A.: AP+PS+TF-MoM-1, 4; TF+QS-WeA-10, 143
- Jezewski, C.: EM-ThP-5, 186
- Ji, D.: PS-TuP-15, 98
- Ji, Y.: PS-WeM-5, 118
- Jiang, K.: EM+TF-ThM-6, 150
- Jiang, N.: NS-TuP-5, 92; NS-TuP-6, 93; SS+2D+AS+HC-TuM-3, 58; SS-ThP-3, 193; SS-ThP-9, 194; SS-WeA-10, **141**
- Jiang, Y.: AP2+PS+TF-TuA-11, **70**; SS-WeA-9, **141**
- Jin, E.: EM+TF-ThM-12, 151; MN1-WeM-3, 116
- Jin, Q.: UN-ThP-26, 204
- Jo, S.: PS2-ThA-6, 171; PS-TuP-28, 100; PS-TuP-29, 100; PS-TuP-34, **101**
- Johns, J.: CA+AS+LS+LX+MN+SE+SS-TuM-13, **52**
- Johnson, C.: QS+EM+TF-MoM-10, 17
- Johnson, D.: 2D2-ThA-4, 165; 2D-ThP-20, 178; 2D-TuM-1, **44**; SS2-MoM-9, **20**
- Johnson, G.: CA+AS+LS+NS+SS+VT-MoA-8, 28
- Johnson, K.: 2D2-ThA-5, 165; EM-WeM-5, 113
- Johnson, M.: AP+PS+TF-WeM-11, 110; AP-TuP-6, 86; PS+SE-FrM-2, **217**
- Johnson, S.: VT-MoM-3, 21
- Jones, A.: 2D-ThP-21, 178; SS+HC-TuA-10, 78
- Jones, J.: CA1+AS+LS+NS+SS+VT-MoM-3, 7
- Jones, L.: BI+AS+EM+NS+SE+TF-TuA-1, 70
- Jones, P.: QS+VT-WeM-12, 119; VT-TuP-1, 105
- Jones, T.: TF+QS-WeA-10, 143
- Jonker, B.: 2D2-ThA-3, 165; 2D-WeA-3, 124
- Joselevich, E.: NS1+2D+BI+SS-MoM-6, 13
- Joseph, E.: PS-WeM-3, **118**
- Joseph, L.: HC+SS-WeM-13, **116**; HC-ThP-5, 188
- Joshi, S.: PS1-ThA-5, 170
- Joshi, V.: SE-TuP-9, 104
- Jouneau, P.: AS+2D+CA+EM+MS+NS+SE+SS+TF-FrM-1, 208
- Jousten, K.: VT-TuA-10, 83
- Joy, N.: PS-TuM-5, 56
- Jozwiak, C.: 2D-WeA-7, 124
- JUAREZ SANTIESTEBAN, H.: HC-ThP-10, 189
- Jubin, S.: AP+PS-MoA-6, 24
- Jugovac, M.: SS+AS+TF-MoA-10, 41
- Juhel, M.: CA+AS+LS+NS+SS+VT-MoA-10, 28
- Julbe, A.: SE1+TF-MoM-6, 18
- Jung, D.: PS-TuP-5, 96
- Jung, J.: SS+AS+TF-MoA-5, 40
- Jung, U.: PS-TuP-39, 102
- Junige, M.: AP+PS+TF-MoM-4, **4**; AP-TuP-7, **86**
- Jurczyk, B.: AP+PS+TF-WeM-5, 109
- Jusufagic, L.: BI+AS+EM+NS+SE+TF-TuA-9, **71**
- Juurlink, L.: HC-ThP-2, 187
- K —
- Kabir, N.: EM1+TF-FrM-5, **210**
- Kaczorowski, D.: AC+MI+TH-TuM-11, 46; AC+MI+TH-TuM-4, 46; EM-ThP-3, 186
- Kadomoto, Y.: MS-ThP-3, 192
- Kaganovich, I.: AP+PS-MoA-6, 24; PS+MS-TuA-12, 76; PS2+MS-WeA-12, **140**; PS2-ThA-3, 171; PS-TuP-6, 96
- Kaiser, T.: MN2-WeM-12, **117**
- Kaiser, S.: LX+AS+BI+HC+SS+TH-MoA-5, 31

## Author Index

- Kalan, M.: HC-ThP-6, **188**
- Kalasad, M.:  
AS+2D+CA+EL+EM+MS+NS+SE+SS+TF-WeM-6, 112
- Kalinin, S.: NS+2D+EM+MN+SS-TuM-1, **53**;  
NS+2D+EM+MN+SS-TuM-12, 54; NSP-SuA-1, 2
- Kalsar, R.: SE-TuP-9, 104
- Kamali, E.: NS-TuP-2, 92
- Kamiyama, B.: PS+SE-FrM-1, **217**
- Kamphaus, E.: TF1+PS-WeM-3, 122
- Kanarik, K.: MS+AP+AS+TF-ThA-1, **169**
- Kanazawa, K.: VT-TuP-4, 105
- Kandel, S.: SS1+AS-ThM-3, 160; SS-ThP-1, 192; SS-ThP-15, 195
- Kaneda, Y.: AP+EM+PS+TF-TuM-12, **49**
- Kaneko, T.: SS-ThP-17, 195
- Kang, J.: 2D-ThP-15, 177; AC+MI+TH-TuM-10, 46; PS-WeM-5, 118
- Kang, W.: TF+SE-FrM-6, 220
- Kang, Y.: AP+PS-FrM-2, 207; SE-TuP-10, 104
- Kangül, M.: NS1+2D+BI+SS-MoM-5, 12
- Kanjolia, R.: AP2+PS+TF-TuA-9, 69
- Kanté, B.: AQS-SuA-8, **1**
- Kanyandekwe, J.: AS-ThP-29, 184
- Kanzo, K.: PS-TuM-5, 56
- Kao, H.: SE-TuP-2, **103**
- Kapelyan, D.: PS+SE-MoA-8, 35
- Kaplar, R.: CPS+CA-WeA-1, 130
- Käppeli, M.: 2D-ThM-6, 145; 2D-ThP-5, 175
- Kar, S.: QS+EM+TF-MoM-10, 17
- Karabacak, T.: NS-TuP-1, 92
- Karadzhev, I.: SE-TuP-5, **104**
- Karagoz, B.: LX+AS+HC+SS-MoM-4, 11
- Karahashi, K.: AP+PS-MoA-5, 23
- Karakoti, A.: AS-ThP-28, **183**
- Kardish, M.: BI1+PS-MoM-6, 6
- Karthäuser, J.: BI+AS+PS-TuM-3, 49; BI-TuP-1, 86
- Kas, J.: TH2+AS+SS-TuM-10, 61
- Kaspar, T.: MS-ThP-1, **191**; TF2+AP+SE+SS-WeM-13, 123
- Kassi, S.: TF+QS-WeA-1, 142
- Katarivas Levy, G.: AC-TuP-3, 85
- Kato, S.: PS+SE-MoA-2, 34
- Katoch, J.: 2D-WeA-9, **124**
- Katzenmeyer, A.: EM+TF-ThM-11, 150
- Katzer, D.: MN1-WeM-3, 116
- Katzer, S.: EM+TF-ThM-12, 151
- Kauffman, D.: SS1+HC-MoM-5, 20
- Kaur, G.: UN-ThP-5, **200**
- Kaushik, V.: QS+EM+TF-MoM-10, 17
- Kawaguchi, M.: NS+EM+MN-MoA-3, 32
- Kawahara, K.: TF-ThP-2, 196
- Kawamata, R.: MS-ThP-3, 192
- Kawamura, E.: PS-TuP-41, 102
- Kay, B.: CA-TuP-4, 89; HC+SS-ThM-1, 151
- Kaya, S.: SS+2D+AS+HC-WeM-11, 121
- Kaye, A.: AP+PS-FrM-3, **207**
- Kazi Haniun, M.: AS-ThP-37, 185
- Kazuma, E.: SS+AS+TF-MoA-5, 40
- Kc, S.: UN-ThP-16, **202**
- Keckes, J.: IB-ThA-5, 168
- Keenan, M.: AS+CA+EL+EM+SE+SS+TF-ThM-1, 146
- Keimel, C.: AS-ThP-14, 181
- Kelber, J.: SS+2D+AS+HC-WeM-2, 119
- Kelley, K.: EM-ThA-1, 165; EM-ThA-4, 166
- Kelly, C.: PS+SE-MoA-8, 35
- Kempa, T.: 2D-WeA-10, 125
- Kenesei, P.: AC+AS+MI+TH-WeA-3, 125
- Kenig, F.: AS+2D+CA+EM+MS+NS+SE+SS+TF-FrM-6, 209
- Kenney, J.: PS-TuM-4, 55
- Kepelyan, D.: AP+PS+TF-WeM-5, 109
- Kerr, A.: NS-TuP-17, **95**
- Kersell, H.: LX-TuP-4, 92
- Kessels, E.: 2D-TuM-4, 44; AP+EM+PS+TF-TuM-5, 47; QS+EM+TF-MoM-9, 16
- Kessels, W.: AP+EM+PS+TF-TuM-10, 48; AP+EM+PS+TF-TuM-6, 48
- Khan, A.: EM-ThA-5, **166**; VT-TuP-6, 105
- Khanna, R.: EM2-FrM-10, 211
- Khatib, S.: HC+SS-ThM-3, **152**
- Khivantsev, K.: TH2-TuA-7, 81
- Khrabrov, A.: PS+MS-TuA-12, 76
- Khrabry, A.: PS2+MS-WeA-12, 140
- Kidambi, P.: CPS+CA-WeA-7, 131
- Kiener, D.: IB-ThA-5, 168
- Kiesel, S.: QS+VT-WeM-13, **119**; VT-TuP-3, **105**
- Kihara, N.: TF-ThP-2, **196**
- Kihara, Y.: PS+TF-MoM-2, 14; PS1-ThA-1, 169; PS2+MS-WeA-3, 138; PS2+MS-WeA-7, 139
- Kilic, U.: EL-TuP-10, 90
- Kilinc, M.: TF-ThP-11, 198
- Killelea, D.: HC-ThP-2, **187**; NS-TuP-17, 95; SS+AS+TF-MoA-6, 40; SS-ThP-12, 194
- Kim, A.: 2D-ThP-14, 177; AS-ThP-2, 179; AS-ThP-3, **179**
- Kim, D.: HC+SS-FrM-2, **212**; PS-TuP-12, 97; PS-TuP-13, 97; PS-TuP-14, **98**; PS-TuP-15, 98; PS-TuP-16, 98; PS-TuP-19, 99; PS-TuP-4, 96; PS-TuP-5, 96
- Kim, G.: 2D+TF-TuA-11, 67; PS-TuP-12, 97; PS-TuP-14, 98; PS-TuP-16, 98
- Kim, H.: 2D-ThP-15, 177; AP+PS+TF-WeM-13, 111; AP2+PS+TF-TuA-12, 70; EM-WeA-4, 132; PS+TF-MoM-5, 14; PS2-ThA-6, 171; PS-TuP-15, 98; PS-TuP-28, 100; PS-TuP-29, 100; PS-TuP-34, 101
- Kim, J.: 2D-WeA-11, **125**; AS-ThP-2, **179**; NS1+2D+BI+SS-MoM-3, 12; PS2-ThA-6, 171; PS-TuP-16, 98; PS-TuP-19, 99; PS-TuP-28, 100; PS-TuP-29, **100**; PS-TuP-34, 101; SS2+AS+TF-ThM-10, 161
- Kim, K.: PS-TuP-19, **99**
- Kim, L.: SS-ThP-18, **195**
- Kim, M.: PS-TuM-13, 57; PS-TuP-31, 101
- Kim, S.: 2D-ThP-4, **175**; EM-ThP-2, 185; PS2-ThA-5, 171; PS2-ThA-6, 171; PS-TuP-13, **97**; PS-TuP-28, 100; PS-TuP-29, 100; PS-TuP-34, 101; PS-TuP-37, 102; PS-TuP-38, 102; PS-TuP-4, 96; SS2+AS+TF-ThM-10, 161
- Kim, T.: 2D-ThP-14, 177; 2D-TuM-3, 44; AS-ThP-13, **181**; AS-ThP-3, 179; HC+SS-FrM-6, 212; HC+SS-WeA-10, 134
- Kim, W.: EL2-MoA-8, **30**; PS2-ThA-6, 171; PS-TuP-28, 100; PS-TuP-29, 100; PS-TuP-34, 101; UN-ThP-31, 205; UN-ThP-32, **205**
- Kim, Y.: EL-TuP-2, 89; EL-TuP-3, **89**; NS+EM+MN-MoA-4, 32; PS+NS-FrM-8, 216; SS+AS+TF-MoA-5, 40; SS-WeA-1, **140**
- Kimmel, G.: CA-TuP-4, 89; HC-ThP-9, 189
- King, S.: EM1+TF-FrM-6, 211; EM-WeA-7, **133**; EM-WeM-10, **114**
- Kirsch, K.: VT-MoM-2, **21**
- Kisslinger, K.: 2D+TF-TuA-11, 67
- Kißlinger, T.: SS+2D+AS+HC-TuM-1, 58
- Kitajima, T.: AP+PS+TF-WeM-4, **109**; PS-TuP-2, **95**
- Kitsiou, A.: IB3-FrM-11, 214
- Kitsopoulos, T.: HC+SS-ThA-1, **167**
- Kiuchi, A.: SS-ThP-2, **192**
- Klein, B.: CPS+CA-WeA-1, 130
- Klimov, N.: NS+EM+MN-MoA-1, **31**; NS+EM+MN-MoA-11, 33; NS+EM+MN-MoA-4, **32**
- Klingner, N.: EM+TF-ThM-4, 149; IB-ThM-1, **153**
- Knight, S.: EL1+TF-MoA-1, 28
- Knoops, H.: QS+EM+TF-MoM-2, 15; QS+EM+TF-MoM-9, 16
- Ko, A.: PS-TuM-5, 56
- Ko, H.: 2D-WeM-13, 107
- ko, S.: AS-ThP-7, 180
- Ko, S.: AS-ThP-6, 180; SS-ThP-7, 193
- Ko, W.: NS-TuP-11, 94; QS+SS-TuA-10, **77**; QS+SS-TuA-3, 76
- Koch, N.: AS-ThP-2, 179
- Koehler, A.: EM2-FrM-10, **211**
- Kogler, M.: AS+CA+EL+EM+SE+SS+TF-WeA-11, **129**
- Koirala, K.: TF2+AP+SE+SS-WeM-13, 123
- Kolel-Veetil, M.: BI2+AS+HC+SS-MoM-9, 7
- Kolmakov, A.: CA+AS+LS+LX+MN+SE+SS-TuM-1, 51; CA-TuP-2, 88; CPS+CA-WeA-7, 131; LX+AS+HC+SS-MoM-1, **10**
- Kolmer, M.: NS1+2D+EM+MN-TuA-3, **72**
- Kolorenc, J.: AC+MI+TH-TuM-5, **46**
- Koloskova, O.: AC+AS+MI+TH-WeA-9, 126; AC+MI+TH-TuM-11, 46
- Kondeti, V.: PS-TuP-21, **99**
- Könenkamp, R.: NS2+2D+EM-TuA-10, 73
- Kong, D.: 2D-ThP-18, **178**
- Konstantinidis, S.: TF+SE-FrM-5, 219
- Kopecz, R.: BI+AS+PS-TuM-3, 49; BI-TuP-1, **86**
- Korlacki, R.: EL1+TF-MoA-5, **29**; EL-TuP-10, 90; EL-TuP-13, 91
- Kortshagen, U.: PS1+AS-WeA-10, 137
- Kotakoski, J.: 2D-ThM-1, 145
- Kothapally, S.: MN-ThP-1, **191**
- Kothari, R.:  
AS+2D+CA+EL+EM+MS+NS+SE+SS+TF-WeM-6, 112
- Kotowska, A.: BI1-MoA-5, **26**
- Kotru, S.: MN-ThP-1, 191
- Kovac, A.: TH1+AS+SS-TuM-5, 60
- Kovač, J.: AS-ThP-30, **184**
- Kovarik, L.: TH2-TuA-7, 81
- Kovatch, L.: PS-TuM-10, 56
- Kozinsky, B.: HC+SS-FrM-6, 212
- Kratky, T.: HC+SS-ThM-6, 152; LX+AS+BI+HC+SS+TH-MoA-5, 31
- Kraushofer, F.: LX+AS+BI+HC+SS+TH-MoA-5, 31; SS+2D+AS+HC-TuM-1, 58; SS+2D+AS+HC-WeM-5, 120
- Krawicz, A.: PS-TuM-5, 56
- Krebs, Z.: 2D-WeM-10, **107**
- Krek, J.: PS-TuP-41, 102
- Kringle, L.: CA-TuP-4, 89
- Krinninger, M.: LX+AS+BI+HC+SS+TH-MoA-5, 31; SS+2D+AS+HC-WeM-5, **120**
- Krishnan, S.: EL2-MoM-8, **10**
- Kroll, T.: AC+MI+TH-TuM-13, 47
- Krüger, F.: PS2+MS-WeA-9, **139**
- Krüger, P.: MI+2D+TF-WeA-1, 135; MI+2D+TF-WeA-10, 136; MI+2D+TF-WeA-9, 135
- Kruger, S.: PS+MS-TuA-9, 75
- Krymski, D.: QS-MoA-11, 37
- Kuang, A.: VT-TuA-12, 84
- Kuboi, N.: AP1+2D+EM+PS+TF-TuA-3, **69**
- Kudlanov, E.: AP-TuP-2, 85
- Kuehn, T.: 2D2-ThA-6, 165; 2D-ThP-19, 178
- Kugler, D.: SS+2D+AS+HC-TuM-13, 59
- Kuh, B.: PS+TF-MoM-5, 14
- Kühn, T.: EW-TuL-2, 64
- Kuhne, P.: EL1+TF-MoA-1, 28; EL-TuP-13, 91
- Kulbacki, B.: AS-ThP-6, **180**; AS-ThP-7, 180; SS-ThP-7, 193
- Kumar, P.: 2D+TF-TuA-11, 67; PS2-ThA-4, 171
- Kumar, S.: NS+2D+EM+MN+SS-TuM-4, 53

## Author Index

- Kumar, U.: 2D-ThP-11, 176  
 Kummel, A.: AP2+PS+TF-TuA-9, **69**  
 Kundrata, I.: AP1+2D+EM+PS+TF-TuA-7, 69  
 Kunene, T.: TF-ThM-10, **163**  
 Kunesch, E.: BI-TuP-11, 88; UN-ThP-10, **201**  
 Kunz, M.: HC+SS-ThM-3, 152  
 Kunze, K.: LX+AS+HC+SS-MoM-5, 11  
 Kuo, L.: NS1+2D+EM+MN-TuA-7, **73**  
 Kuo, P.: NS+EM+MN-MoA-11, 33  
 Kuo, Y.: SE-TuP-1, 103  
 Kurahashi, M.: SS+AS+TF-MoA-1, **39**  
 Kurowska, A.: SS1+AS-ThM-4, 160  
 Kuschel, T.: AS+CA+EL+EM+SE+SS+TF-ThM-5, 147  
 Kushner, M.: PS+MS-TuA-11, 75; PS+NS-FrM-11, 217; PS+NS-FrM-5, 216; PS2+MS-WeA-9, 139  
 Kuwabara, H.: PS-TuP-22, **99**  
 Kuwahara, K.: PS+TF-MoM-10, 15; PS-TuM-1, 55; PS-TuM-10, 56  
 Kwak, H.: AP+PS+TF-MoM-8, 5  
 Kwansa, A.: BI+AS+PS-TuM-13, 51  
 Kwoka, M.: SS-ThP-10, 194  
 Kwon, G.: PS2-ThA-6, 171; PS-TuP-28, 100; PS-TuP-29, 100; PS-TuP-34, 101  
 Kwon, H.: EM-ThA-5, 166; HC-ThP-8, **188**; PS2-ThA-6, **171**; PS-TuP-12, 97; PS-TuP-14, 98; PS-TuP-16, 98; PS-TuP-19, 99; PS-TuP-28, 100; PS-TuP-29, 100; PS-TuP-34, 101  
 — L —  
 La Mendola, D.: 2D-ThP-17, **178**  
 Labenski, R.: PS+SE-FrM-8, 218  
 Lado, J.: QS+SS-TuA-10, 77; QS+SS-TuA-3, 76  
 Lagally, M.: 2D+EM-FrM-4, 206  
 Laha, P.: SS+AS+TF-MoA-9, 40  
 Lahann, J.: TF-ThA-1, **173**  
 Lahiri, N.: LS+AC+LX+MI+TH-ThM-12, 156  
 Laleyan, D.: TF+QS-WeA-11, **143**  
 LaManna, J.: NS+EM+MN-MoA-4, 32  
 Lamb, P.: QS+VT-WeM-12, 119; VT-TuP-1, 105  
 Lambeets, S.: CA+AS+LS+LX+MN+SE+SS-TuM-4, **51**; HC-ThP-3, **187**; IB2-FrM-6, 213; IB-ThM-13, 155  
 Lane, C.: QS+SS-TuA-3, 76  
 Lane, P.: EM-WeA-1, **132**  
 Lang, A.: EM+TF-ThM-12, 151; EM+TF-ThM-13, 151; MN1-WeM-3, 116; TF+QS-WeA-9, 143  
 Lang, J.: 2D-WeA-4, **124**; LS+AC+AS+LX+MI+TH-ThA-3, **168**  
 Langworthy, K.: IB1-FrM-1, 213  
 Lanham, E.: PS+MS-TuA-9, 75  
 Lapak, M.: HC+SS-ThA-3, 167  
 Larson, S.: MN-ThP-2, **191**  
 Larsson, A.: HC+SS-WeA-9, 134; SS1+HC-MoM-6, 20  
 Laschewsky, A.: BI-TuP-1, 86  
 Lasek, K.: 2D-ThM-12, 146  
 Latt, K.: 2D1-ThA-4, **164**  
 Lauhon, L.: NS1+2D+BI+SS-MoM-3, **12**  
 Lauritsen, J.: 2D-ThM-5, 145  
 Lavan, D.: CPS+MS-ThM-1, 148  
 LaVan, D.: CA-TuP-2, 88  
 Law, S.: QS+EM-TuM-10, **57**  
 Lawall, J.: VT-MoM-4, 21  
 Lawrie, B.: NS-TuP-11, 94  
 Lazzarino, F.: PS+NS-FrM-3, 215; PS+TF-MoM-1, 13; PS-TuM-13, 57  
 Le, B.: TF+QS-WeA-11, 143  
 Le, D.: EM-WeA-4, 132  
 Le, L.: EL1-MoM-3, **9**; EL-TuP-2, **89**; EL-TuP-3, 89  
 Lechner, B.: HC+SS-ThM-6, 152; LX+AS+BI+HC+SS+TH-MoA-5, **31**; SS+2D+AS+HC-WeM-5, 120  
 Lecomte, J.: TF+QS-WeA-1, 142  
 Leddy, J.: PS+MS-TuA-9, 75  
 Lederer, S.: VT-TuM-2, 62  
 LeDuc, H.: QS+EM+TF-MoM-5, 16  
 Lee, B.: AP+PS-FrM-2, **207**  
 Lee, C.: HC+SS-ThM-1, 151; PS-WeM-5, 118; TF-ThP-10, **197**  
 Lee, D.: LX+AS+HC+SS-MoM-8, 11; TF+SE-FrM-9, **220**  
 Lee, E.: HC-ThP-1, **187**  
 Lee, H.: 2D-ThP-15, 177; AP+PS-FrM-2, 207; MS-ThP-2, **192**; PS+MS-TuA-11, 75; PS+NS-FrM-5, 216; PS2-ThA-1, 170; PS-TuP-33, 101; PS-TuP-35, 101; SE-TuP-10, 104  
 Lee, J.: AS+2D+CA+EM+MS+NS+SE+SS+TF-FrM-4, 209; MN1-WeM-6, **117**; MN2-WeM-12, 117; PS-TuM-3, **55**; PS-TuP-12, **97**; PS-TuP-16, 98; SE-TuP-10, 104; TF+SE-FrM-6, **220**  
 Lee, K.: AS-ThP-2, 179; SS-ThP-8, 194  
 Lee, M.: EL2-MoA-8, 30; SS+AS+TF-MoA-5, **40**  
 Lee, P.: AP2+PS+TF-TuA-9, 69  
 Lee, S.: 2D-ThP-18, 178; CA+AS+LS+LX+MN+SE+SS-TuM-1, 51; HC-ThP-1, 187; HC-ThP-8, 188; PS-TuP-4, 96; SS+2D+AS+HC-TuM-4, **58**; TF+QS-WeA-4, **142**  
 Lee, W.: PS-TuP-37, 102; PS-TuP-38, 102  
 Lee, Y.: PS2-ThA-5, 171; PS-TuP-37, 102; PS-TuP-38, 102  
 Leem, M.: 2D-ThP-15, 177  
 Lefaucheux, P.: AP+PS-MoA-3, 23  
 Lefcort, D.: EM-ThP-6, 186  
 Leggett, G.: BI2+AS+HC+SS-MoM-10, **7**  
 Lehan, P.: UN-ThP-8, **201**  
 Lei, H.: BI1-MoA-1, 25  
 Lei, X.: AP+PS-FrM-3, 207  
 Lemishko, K.: PS+MS-TuA-1, 74  
 Lennon, C.: QS+EM+TF-MoM-9, 16  
 Lenox, M.: EM-ThA-1, 165  
 Lensen, H.: VT-MoM-10, 22  
 Leonard, E.: BI-TuP-11, 88; BI-TuP-8, **87**  
 Leong, I.: UN-ThP-17, **202**  
 Leslie, J.: VT-MoM-3, 21; VT-TuA-4, 83  
 Letchworth Weaver, K.: UN-ThP-20, 203  
 Leusink, G.: AP+EM+PS+TF-TuM-11, 48  
 Lewandowski, M.: SS+2D+AS+HC-TuM-5, **59**  
 Lewin, E.: SE1+TF-MoM-3, **18**  
 Lewis, F.: SS+AS+TF-MoA-6, 40  
 Lewis, J.: CPS+MS-ThM-1, **148**  
 Lezuo, L.: SS+2D+AS+HC-TuM-2, 58  
 Li, A.: QS+SS-TuA-4, 76  
 Li, B.: EM+TF-ThM-11, 150  
 Li, C.: AP+PS+TF-MoM-5, 4; NS2+2D+BI+EL+SS-MoM-11, 13  
 Li, D.: EM-ThP-7, 186; MN2-WeM-12, 117; TF2+AP+SE+SS-WeM-13, 123; TF2-TuA-8, 80  
 Li, H.: 2D-ThP-13, **177**; 2D-ThP-22, 179; 2D-WeM-12, **107**; BI+AS+EM+NS+SE+TF-TuA-1, 70  
 Li, J.: PS+NS-FrM-8, 216; PS1-ThA-5, 170  
 Li, L.: NS-TuP-5, 92; NS-TuP-6, 93; SS-ThP-9, 194  
 Li, Q.: 2D-ThM-3, **145**  
 Li, R.: 2D-ThP-20, 178; QS+EM+TF-MoM-1, **15**; QS-MoA-4, 36  
 Li, S.: SS-WeA-3, **140**  
 Li, T.: 2D1-ThA-5, **164**; AC+AS+TH-WeM-10, 108  
 Li, X.: AC+MI+TH-TuA-1, 67  
 Li, Y.: HC-ThP-6, 188; PS2+AS+SS-ThM-10, **159**; SS-WeA-12, 142; VT-TuM-3, **62**  
 Liao, B.: TF-ThP-16, **198**  
 Liao, M.: EM2-FrM-10, 211  
 Liaw, P.: LX-TuP-4, 92  
 Liddle, J.: NS+EM+MN-MoA-5, 32  
 Lieberman, M.: PS-TuP-41, 102  
 Lieberzeit, P.: BI+AS+EM+NS+SE+TF-TuA-11, 72; BI+AS+EM+NS+SE+TF-TuA-7, 71; BI-TuP-4, 87  
 Liedke, M.: EM+TF-ThM-4, 149  
 Lietz, A.: PS-TuP-11, 97; PS-TuP-17, 98; PS-TuP-18, 98  
 Lilje, L.: VT-TuM-2, 62  
 Liljeroth, P.: 2D-TuM-10, **44**  
 Lill, J.: MI+2D+TF-ThM-13, 157  
 Lill, T.: PS+TF-MoM-8, **15**  
 Lim, C.: PS-TuP-31, **101**  
 Lim, M.: SS+AS+TF-MoA-9, 40  
 Lim, N.: PS1+AS-WeA-3, **136**; PS1+AS-WeA-4, 137  
 Lim, R.: AC+AS+TH-WeM-10, 108; AC+AS+TH-WeM-11, 108  
 Lim, S.: AP+PS+TF-MoM-8, 5; PS2-ThA-6, 171; PS-TuP-28, 100; PS-TuP-29, 100; PS-TuP-34, 101  
 Lin, A.: IB-ThP-3, 190  
 Lin, J.: SE2+TF-MoM-8, **18**  
 Lin, Y.: 2D-ThP-6, 175  
 Lindblad, D.: AP+PS+TF-MoM-11, **5**  
 Linford, M.: AS+2D+CA+EM+MS+NS+SE+SS+TF-FrM-5, **209**; AS-ThP-17, 181; AS-ThP-6, 180; AS-ThP-7, 180; CA+AS+LS+NS+SS+VT-MoA-6, 27; CA-TuP-3, 89; EL-TuP-9, 90; SS-ThP-7, 193; TF-ThP-8, 197; UN-ThP-4, 200  
 Lisenfeld, J.: QS+SS-TuA-7, **77**  
 Lisenkov, S.: 2D-ThM-12, 146  
 Lishan, D.: PS+NS-FrM-10, 217  
 Litch, E.: PS+MS-TuA-11, **75**  
 Litwin, P.: TF1+PS-WeM-5, **122**  
 Liu, B.: 2D+EM-FrM-9, 207; SS+2D+AS+HC-WeM-6, **120**  
 Liu, D.: EM-ThP-4, **186**; NS-TuP-5, 92; SS+2D+AS+HC-TuM-3, **58**; SS-ThP-3, 193; SS-ThP-9, 194  
 Liu, E.: PS-TuM-3, 55; PS-TuM-5, **56**  
 Liu, F.: AS-ThP-2, 179  
 Liu, M.: LX-TuP-1, 91; QS+EM+TF-MoM-10, 17; QS-MoA-4, 36  
 Liu, R.: TF-ThP-17, 198  
 Liu, T.: PS1-ThA-5, 170  
 Liu, Y.: EL-TuP-12, 91; NS+2D+EM+MN+SS-TuM-12, **54**  
 Lizarbe, A.: CA+AS+LS+NS+SS+VT-MoA-6, **27**; CA-TuP-3, **89**  
 Locatelli, A.: TF-ThP-6, 196  
 Lodge, S.: QS+VT-WeM-12, 119; VT-TuP-1, **105**  
 Loidl, B.: NS-TuP-8, 93  
 Loiselet, J.: UN-ThP-19, 203; UN-ThP-22, **203**; UN-ThP-23, 203  
 Lojen, D.: PS1+AS-WeA-11, 138  
 Lopez Gonzalez, A.: EL-TuP-1, **89**  
 Lorenz, M.: AS+2D+CA+EM+MS+NS+SE+SS+TF-FrM-6, 209  
 Lorincik, J.: AC-TuP-3, 85  
 Losego, M.: TF1-TuA-4, 79; TF-ThM-11, 163; TF-ThM-12, 163; TF-ThM-4, 162; TF-ThM-5, **162**  
 Lou, J.: CA+AS+LS+NS+SS+VT-MoA-3, 27  
 Louisos, D.: 2D-ThP-8, 176  
 Love, C.: TF2-TuA-11, 80

## Author Index

- Love, J.: EL-TuP-1, 89; EL-TuP-4, 89; EL-TuP-6, 90
- Lu, B.: SE-TuP-1, 103
- Lu, Q.: BI2-MoA-9, 26
- Lu, W.: SS+HC-TuA-3, 78
- Lu, Z.: IB-ThA-3, 167
- Lucatorto, T.: SS+HC-TuA-10, 78
- Lucchetta, E.: QS+VT-WeM-12, 119; VT-TuP-1, 105
- Lufungula, L.: SS+HC-TuA-11, 79
- Lundgren, E.: HC+SS-WeA-9, **134**; SS1+HC-MoM-6, 20
- Lundin, D.: PS+SE-MoA-1, 34
- Lundstrom, M.: CPS+MS-ThM-10, 149
- Luo, D.: BI+AS+EM+NS+SE+TF-TuA-1, 70
- Luo, X.: TF+SE-FrM-3, **219**
- Lupo, G.: 2D-ThP-2, 175
- Lussier, D.: LS+AC+AS+LX+MI+TH-ThA-5, 168
- Lutz, C.: NSP-SuA-9, 3; SS-WeA-4, **140**
- Lynch, J.: 2D+TF-TuA-11, 67
- Lyons, M.: 2D-ThP-9, **176**
- Lyu, L.: NS+2D+EM+MN+SS-TuM-10, 54; NS-TuP-4, 92
- Lyu, X.: AS-ThP-20, 182
- Lyu, Z.: LX-TuP-4, 92
- M —
- M.N. Groot, I.: 2D-WeM-3, 106
- Ma, X.: 2D-WeM-1, **106**
- Ma, Y.: 2D-WeA-4, 124; UN-ThP-7, 201
- Maben, G.: MS-FrM-3, **214**
- Macak, K.: AS+CA+EL+EM+SE+SS+TF-WeA-4, 128
- Machacek, J.: TF+QS-WeA-1, 142
- Mack, P.: AS+2D+CA+EL+EM+MS+NS+SE+SS+TF-WeM-12, **112**; EW-TuL-3, 64
- Mack, S.: MN1-WeM-3, 116
- Mackus, A.: 2D-TuM-4, 44; AP+EM+PS+TF-TuM-10, 48; AP+EM+PS+TF-TuM-5, 47; AP+EM+PS+TF-TuM-6, 48
- maddaka, R.: NS+EM+MN-MoA-2, 31
- Madelat, N.: SS1+HC-MoM-2, 19
- Madiraju, D.: SS-ThP-20, 195
- Madison, A.: NS+EM+MN-MoA-5, **32**
- Maes, J.: 2D-TuM-4, 44
- Magis, T.: PS+TF-MoM-3, 14
- Mahadik, N.: EM2-FrM-10, 211
- Mahapatra, S.: NS-TuP-6, 93; SS-ThP-9, 194
- Maier, K.: PS-TuM-10, 56
- Main, D.: PS+MS-TuA-9, **75**
- Mainali, M.: EL1-MoM-1, 9
- Maindron, T.: AS+2D+CA+EM+MS+NS+SE+SS+TF-FrM-1, 208
- Maiti, D.: HC+SS-ThM-3, 152
- Majee, A.: 2D+EM-FrM-4, 206
- Major, G.: AS+2D+CA+EM+MS+NS+SE+SS+TF-FrM-5, 209; CA+AS+LS+NS+SS+VT-MoA-6, 27; CA-TuP-3, 89; UN-ThP-4, 200
- Majumdar, A.: 2D-ThP-20, 178
- Makarem, S.: PS1-ThA-6, **170**
- Maksymovych, P.: NS-TuP-11, **94**; QS+SS-TuA-10, 77; QS+SS-TuA-3, **76**
- Maldonado, N.: PS+NS-FrM-6, 216
- Malek, M.: HC-ThP-7, 188
- Malholtra, Y.: NS+EM+MN-MoA-2, 31
- Mamunuru, M.: PS-TuP-11, 97
- Mann, J.: AS-ThP-19, **182**; EW-TuL-4, 64
- Mansouri, S.: TF2+AP+SE+SS-WeM-12, 123
- Mao, Z.: 2D-ThP-18, 178
- Maple, M.: AC+MI+TH-TuM-10, 46
- Mara, M.: LS+AC+AS+LX+MI+TH-ThA-5, 168
- Marandi, A.: AP+PS-MoA-11, 24
- Marbach, H.: PS2+AS+SS-ThM-10, 159
- Marcella, N.: HC+SS-FrM-6, 212
- Marchack, N.: PS-WeM-10, 118
- Marchesini, S.: AS+2D+CA+EM+MS+NS+SE+SS+TF-FrM-3, 208
- Marcoen, K.: SS+HC-TuA-11, 79
- Margot, J.: TF2+AP+SE+SS-WeM-12, 123
- Marinella, M.: EM-WeM-1, **113**
- Marković, D.: AS+2D+CA+EL+EM+MS+NS+SE+SS+TF-WeM-3, 111
- Marques, E.: AP+EM+PS+TF-TuM-12, 49
- Marques, S.: AS+CA+EL+EM+SE+SS+TF-ThM-3, 147
- Marquis, K.: BP-SuA-7, 2
- Marschall, K.: VT-TuA-3, 83
- Martin, B.: PS+TF-MoM-3, 14
- Martin, I.: AS-ThP-13, 181
- Martin, N.: TF+SE-FrM-5, 219
- Martinez Celis, M.: AC+MI+TH-TuM-11, 46
- Martinez Guajardo, A.: BI-TuP-1, 86
- Martinez, A.: TF1+PS-WeM-6, 122
- Martinez, E.: AS+2D+CA+EL+EM+MS+NS+SE+SS+TF-WeM-4, 111; AS-ThP-29, 184
- Martinez, M.: UN-ThP-33, **205**
- Martinick, B.: QS+EM+TF-MoM-10, 17
- Martinson, A.: TF1+PS-WeM-3, 122; TF-ThM-10, 163
- Maruyuma, B.: LX+AS+HC+SS-MoM-4, 11
- Maryon, O.: NSP-SuA-8, 3
- Marzo, T.: 2D-ThP-17, 178
- Mascaraque, A.: SS+AS+TF-MoA-10, 41; TF-ThP-6, 196
- Massey, K.: VT-TuA-9, **83**
- Masson, E.: 2D1-ThA-4, 164
- Mastro, M.: AP+PS+TF-WeM-11, 110
- Mastugi, Y.: VT-TuA-11, 84
- Masubuchi, T.: HC+SS-FrM-4, 212
- Matara Kankanamge, I.: 2D2-ThA-5, 165
- Materise, N.: QS+EM+TF-MoM-11, **17**
- Matsui, M.: PS-TuM-1, 55; PS-TuM-10, **56**
- Matsushima, K.: PS+TF-MoM-2, 14; PS+TF-MoM-6, 14
- Mauger, S.: AS-ThP-20, 182
- Maurer, P.: AQS-SuA-6, **1**
- May, B.: AC+AS+MI+TH-WeA-8, 126; QS+EM+TF-MoM-8, **16**
- Mayorga Garay, M.: AS-ThP-35, 185
- Maza, W.: BI2+AS+HC+SS-MoM-9, 7
- Mazarov, P.: IB-ThP-1, 190
- Mazumder, P.: SE-TuP-5, 104
- McCallum, J.: QS-MoA-8, **37**
- McCandless, J.: MN1-WeM-6, 117
- McCarter, A.: EW-TuL-1, **64**
- McCarter, M.: MI+2D+TF-WeA-3, 135
- McClelland, N.: TF-ThM-11, **163**
- McCluskey, M.: EM+TF-ThM-3, **149**
- McCreary, K.: 2D-WeA-3, **124**
- McDaniel, M.: EM-ThP-8, 186
- McDonald, A.: CPS+CA-WeA-1, 130
- McDonnell, S.: 2D+EM-FrM-3, 206; EM-ThP-5, **186**
- McEwen, J.: AS+CA+EL+EM+SE+SS+TF-ThM-10, **148**; CA+AS+LS+LX+MN+SE+SS-TuM-4, 51; TH2-TuA-9, 81; UN-ThP-24, 204; UN-ThP-25, 204
- McFall, H.: UN-ThP-6, **200**
- McFarland, E.: UN-ThP-8, 201
- McFarland, S.: TF+QS-WeA-3, 142
- McGehee, M.: CA+AS+LS+LX+MN+SE+SS-TuM-3, 51
- McGillivray, S.: SS2-MoM-9, 20
- McGuinness, E.: TF-ThM-11, 163; TF-ThM-12, 163
- McHardy, K.: BI-TuP-7, **87**; IB-ThM-3, 153
- McHenry, T.: SS2-MoM-9, 20
- McIlroy, D.: 2D-WeM-5, 106
- McInerney, M.: TF+QS-WeA-4, 142
- McLamb, M.: 2D-ThP-8, **176**
- McLeod, A.: AP2+PS+TF-TuA-9, 69
- McNamara, B.: LS+AC+LX+MI+TH-ThM-12, 156
- McRae, C.: QS+EM+TF-MoM-11, 17
- Mears, L.: BI-WeA-3, 129; SS2-MoM-10, 20
- Mechielsen, T.: VT-MoM-10, 22
- Meckenstock, R.: MI+2D+TF-ThM-13, 157
- Medina de Oliveira, L.: MS+AP+AS+TF-ThA-5, 169
- Medina Silva, H.: 2D-WeM-4, 106
- Meeuwenoord, R.: SE+TF-MoA-5, 38
- Mefford, T.: SS-ThP-19, 195
- Mehregan, M.: TF-ThA-3, 173
- Mehta, H.: IB-ThA-3, 167
- Mehta, U.: AC+AS+TH-WeM-10, 108
- Meier, M.: HC+SS-WeM-2, 115
- Meindlumer, M.: IB-ThA-5, **168**
- Meisner, D.: PS-TuP-1, 95
- Meissner, U.: VT-TuA-4, 83
- Meli, L.: EM1+TF-FrM-3, **210**
- Mellinger, C.: MI+2D+TF-WeA-2, 135
- Mentes, T.: TF-ThP-6, 196
- Merkx, M.: AP+EM+PS+TF-TuM-5, 47; AP+EM+PS+TF-TuM-6, 48
- Merte, L.: SS1+HC-MoM-6, 20
- Mettler, J.: PS+SE-MoA-10, 35; PS+SE-MoA-11, **35**
- Metz, A.: PS2+MS-WeA-9, 139
- Metzler-Nolte, N.: BI+AS+EM+NS+SE+TF-TuA-9, 71
- Meyer, D.: MN1-WeM-3, 116; SE1+TF-MoM-5, 18
- Meyer, F.: IB-ThP-1, 190
- Meyer, H.: AS-ThP-5, **180**
- Meyer, J.: HC+SS-ThM-2, 152
- Meynen, V.: SS+HC-TuA-11, 79
- Mezzadrelli, A.: SE-TuP-5, 104
- Mi, Z.: NS+EM+MN-MoA-2, 31; SS+HC-TuA-1, 78
- Miano, D.: NS-TuP-8, 93
- Miao, Y.: LX+AS+HC+SS-MoM-8, 11; TF+SE-FrM-9, 220
- Miceli, A.: TF1+PS-WeM-1, 121
- Michielsen, B.: SS+HC-TuA-11, 79
- Mignot, Y.: PS-TuM-3, 55
- Miller, A.: 2D-ThP-20, 178; EL2-MoM-10, **10**
- Miller, E.: EL1+TF-MoA-4, 29; EL1-MoM-1, 9; EL-TuP-5, 90
- Miller, G.: UN-ThP-24, 204; UN-ThP-25, **204**
- Miller, P.: MN-ThP-4, 191
- Milner, P.: QS+VT-WeM-12, 119; VT-TuP-1, 105
- Milosavljevic, V.: PS+SE-FrM-11, **219**
- Mimura, T.: EM-ThA-3, 166
- Min, J.: NS+EM+MN-MoA-2, 31; PS+TF-MoM-5, 14
- Minasian, S.: LS+AC+AS+LX+MI+TH-ThA-5, 168
- Minelli, C.: AS+CA+EL+EM+SE+SS+TF-ThM-3, 147
- Mings, A.: MN-ThP-2, 191
- Minnich, A.: AP+PS-FrM-1, 207; AP+PS-FrM-5, 208; AP+PS-MoA-10, 24; AP+PS-MoA-11, 24
- Mirabella, F.: CA+AS+LS+LX+MN+SE+SS-TuM-10, 52; LX+AS+HC+SS-MoM-5, 11
- Miroshnik, L.: PS-TuP-26, **100**; QS+SS-TuA-4, **76**
- Mishra, A.: BI+AS+PS-TuM-1, **49**
- Misra, S.: MS-FrM-5, **215**

## Author Index

- Mitani, K.: MS-ThP-3, 192  
 Mitchell, K.: TF+QS-WeA-3, 142  
 Mittendorfer, F.: SS+2D+AS+HC-TuM-13, 59  
 Mitterer, C.: IB-ThA-5, 168  
 Miura, M.: PS-TuM-1, 55; PS-TuM-10, 56  
 Miyake, M.: AP+PS+TF-WeM-4, 109  
 Miyamoto, K.: MI+2D+TF-WeA-10, 136  
 Miyazawa, K.: SS-ThP-22, **195**  
 Mobberley, J.: CA+AS+LS+NS+SS+VT-MoA-11, 28  
 Moeini, B.: AS-ThP-17, **181**  
 Moffitt, C.: AS+CA+EL+EM+SE+SS+TF-WeA-4, 128; AS-ThP-18, 181; EW-TuL-6, **64**  
 Mohamed, C.: TF2+AP+SE+SS-WeM-12, 123  
 Mohammad, A.: EM+TF-ThM-5, 150  
 Mohammad, H.: EM-ThP-6, 186  
 Mohammed, A.: PS-TuP-25, 100  
 Mohgouk Zouknak, L.: CA+AS+LS+NS+SS+VT-MoA-10, 28  
 Mohite, A.: CA+AS+LS+NS+SS+VT-MoA-3, 27  
 Mohr, D.: UN-ThP-18, 203  
 Mohr, S.: PS+MS-TuA-1, **74**  
 Mohrhusen, L.: 2D-ThM-5, **145**  
 Moinpour, M.: AP2+PS+TF-TuA-9, 69  
 Moki, H.: PS1+MS-ThM-1, 158  
 Molder, A.: EM1+TF-FrM-6, 211  
 Molina, D.: HC+SS-FrM-1, **211**  
 Molkenboer, F.: VT-MoM-10, **22**  
 Molska, A.: AS+CA+EL+EM+SE+SS+TF-ThM-3, 147  
 Monaghan, D.: VT-TuA-9, 83  
 Mondal, M.: EM-ThP-3, 186  
 Moneck, M.: EM+TF-ThM-6, 150  
 Monnier, J.: HC+SS-ThM-12, 153  
 Montes, L.: NS1+2D+BI+SS-MoM-4, 12  
 Montross, N.: EM-ThP-8, 186  
 Moody, J.: MN-ThP-4, 191  
 Moody, M.: NS1+2D+BI+SS-MoM-3, 12  
 Morales, D.: CA+AS+LS+LX+MN+SE+SS-TuM-3, 51  
 Moras, P.: SS+AS+TF-MoA-10, 41  
 Moreau, L.: AC+AS+MI+TH-WeA-10, 126; AC+MI+TH-TuA-11, **68**; NS-TuP-12, 94  
 Morgan, D.: AS+CA+EL+EM+SE+SS+TF-WeA-10, **129**; CA+AS+LS+NS+SS+VT-MoA-6, 27; CA-TuP-3, 89  
 Mori, T.: HC+SS-WeM-1, 114  
 Morinaga, T.: HC+SS-WeM-1, 114  
 Morisaki, R.: PS1+MS-ThM-3, **158**  
 Morissette, D.: CPS+CA-WeA-1, 130  
 Morley, S.: MI+2D+TF-WeA-3, **135**  
 Morrison, G.: AC+MI+TH-TuM-6, 46; AC-TuP-2, 85  
 Morsell, J.: PS2+AS+SS-ThM-11, **159**  
 Mort, M.: EM-ThP-10, **187**  
 Mosley, Y.: BI+AS+EM+NS+SE+TF-TuA-1, 70  
 Motoyama, H.: VT-MoM-5, 21  
 Motoyama, K.: PS-TuM-3, 55  
 Mou, S.: PS+NS-FrM-8, 216  
 Mougeot, L.: TF-ThP-18, **199**  
 Mozes, A.: 2D-WeM-3, 106  
 Mucci, J.: QS+EM+TF-MoM-10, 17  
 Mueller, D.: SS1+HC-MoM-1, **19**  
 Muggli, K.: PS-TuP-27, 100  
 Muhammad, J.: TF-ThP-14, 198  
 Muhring-Salamone, S.: BI2-MoA-8, **26**  
 Mui, D.: NS+EM+MN-MoA-3, 32  
 Muir, B.: CA1+AS+LS+NS+SS+VT-MoM-5, 8  
 Mullens, S.: SS+HC-TuA-11, 79  
 Mulvany, O.: VT-TuA-12, 84  
 Muray, L.: NS+EM+MN-MoA-5, 32  
 Murphy, R.: NS+EM+MN-MoA-4, 32  
 Murphy, T.: 2D-WeA-10, 125  
 Murray, J.: BI+AS+EM+NS+SE+TF-TuA-1, 70  
 Murray, T.: QS+EM+TF-MoM-10, 17  
 Murugesan, V.: AS-ThP-28, 183  
 Myers-Ward, R.: EM+TF-ThM-13, 151  
 — **N** —  
 Na, B.: PS-TuP-37, 102  
 Nachtrieb, K.: BI2-MoA-9, 26  
 Naclerio, A.: CPS+CA-WeA-7, 131  
 Nadzeyka, A.: IB-ThM-12, 154; IB-ThP-1, 190  
 Nahm, H.: PS-TuP-33, **101**  
 Naikare, H.: BI+AS+EM+NS+SE+TF-TuA-1, 70  
 Nakakura, C.: PS-TuP-26, 100  
 Nakamura, J.: HC+SS-WeM-1, 114; SS+AS+TF-MoA-4, 40  
 Nakamura, K.: PS+SE-MoA-2, 34  
 Nakamura, Y.: MS-ThP-3, 192  
 Nakano, T.: AP+PS+TF-WeM-4, 109; PS-TuP-2, 95  
 Nakayama, T.: PS1+MS-ThM-4, 158  
 Nalaskowski, J.: QS+EM+TF-MoM-10, 17  
 Nam, S.: 2D-WeA-11, 125; PS+MS-TuA-11, 75; PS+NS-FrM-5, 216; PS1+MS-ThM-5, 159  
 Nambodiri, P.: QS+EM+TF-MoM-1, 15  
 Nanayakkara, T.: QS+EM+TF-MoM-10, 17; QS-MoA-4, **36**  
 Naqi, M.: EM-ThP-2, 185  
 Naranjo, S.: MS+AP+AS+TF-ThA-5, **169**  
 Nassar, C.: AS-ThP-14, 181  
 Navarro, G.: PS+TF-MoM-3, 14  
 Navid, I.: SS+HC-TuA-1, 78  
 Nawaz, A.: SS+HC-TuA-4, **78**  
 Naylor, C.: EM-ThP-5, 186  
 Neal, A.: PS+NS-FrM-8, 216  
 Neely, C.: SS-ThP-20, **195**  
 Nejati, S.: 2D-ThP-10, **176**; TF1-TuA-3, 79  
 Nelin, C.: TH-TuP-1, 104  
 Nelson, T.: EM2-FrM-10, 211  
 Nemsak, S.: CA+AS+LS+LX+MN+SE+SS-TuM-12, **52**; MI+2D+TF-ThM-10, 157  
 Nepal, N.: EM+TF-ThM-12, 151; MN1-WeM-3, 116; SE1+TF-MoM-5, **18**; TF+QS-WeA-9, 143  
 Neupane, M.: EM-ThP-3, 186  
 Newsome, E.: VT-MoA-9, 42  
 Newton, B.: PS+NS-FrM-8, 216  
 Ney, A.: MI+2D+TF-ThM-13, 157  
 Ng, T.: SS-ThP-8, 194  
 Ngan, H.: HC+SS-ThA-5, 167  
 Ngo, A.: 2D1-ThA-4, 164  
 Nguyen, A.: NS-TuP-3, **92**  
 Nguyen, C.: AP+PS-FrM-2, 207  
 Nguyen, D.: AS-ThP-28, 183  
 Nguyen, H.: LX+AS+BI+HC+SS+TH-MoA-1, 30; UN-ThP-14, 202  
 Nguyen, J.: TF-ThP-7, **197**  
 Nguyen, M.: CA+AS+LS+NS+SS+VT-MoA-8, **28**  
 Nguyen, P.: PS2-ThA-2, **170**  
 Nguyen, S.: SE-TuP-4, **103**  
 Nguyen, T.: AP+PS-FrM-4, **208**; EM-WeM-11, 114  
 Nguyen, V.: PS+NS-FrM-6, **216**  
 Nguyen-Phan, T.: SS1+HC-MoM-5, 20  
 Nijboer, D.: SE+TF-MoA-5, 38  
 Nikitin, A.: VT-MoM-3, 21  
 Nikolla, E.: TH2-TuA-9, 81  
 Nikzad, S.: TF+QS-WeA-10, 143  
 Nilsen, O.: TF1-TuA-1, **79**  
 Nishizuka, T.: PS1+MS-ThM-1, **158**  
 Niu, Y.: SS+HC-ThA-3, 172  
 Niverty, S.: SE-TuP-9, 104  
 Noel, V.: AC+AS+MI+TH-WeA-1, 125  
 Noesges, B.: PS+NS-FrM-8, **216**  
 Nonclercq, A.: PS-TuP-3, 96  
 Nordlund, D.: AC+MI+TH-TuM-13, 47  
 Norris, J.: MN-ThP-2, 191  
 Norris, S.: PS+NS-FrM-10, 217  
 Nos, J.: AP+PS-MoA-3, 23  
 Novotny, Z.: CPS+CA-WeA-7, 131  
 Nowak, S.: AC+MI+TH-TuM-13, 47  
 Numata, T.: MS-ThP-3, **192**  
 Nunnery, T.: AS+2D+CA+EL+EM+MS+NS+SE+SS+TF-WeM-3, **111**; EW-TuL-3, 64  
 Nuwayhid, R.: TF2-TuA-11, **80**  
 Nuytten, T.: 2D-WeM-4, 106  
 Nye, R.: AP+EM+PS+TF-TuM-1, 47  
 Nykpanchuk, D.: LX+AS+HC+SS-MoM-8, 11  
 Nyns, L.: AP+EM+PS+TF-TuM-1, 47  
 Nyssen, L.: PS1+AS-WeA-11, 138  
 — **O** —  
 O'Brien, M.: HC+SS-FrM-4, 212  
 O'Connor, C.: HC+SS-WeA-10, 134  
 O'Connor, C.: HC+SS-FrM-6, **212**; HC-ThP-9, 189  
 Odilinye, C.: LX-TuP-4, **92**  
 Oehrlein, G.: PS1+AS-WeA-9, 137; PS2+AS+SS-ThM-10, 159  
 Ogasawara, H.: HC+SS-WeM-1, 114  
 Ogawa, D.: PS+SE-MoA-2, **34**  
 Ogawa, S.: TF-ThP-2, 196  
 Ogawa, T.: TF-ThP-2, 196  
 Ogi, Y.: MS-ThP-3, 192  
 Oh, G.: 2D-ThP-14, 177; AS-ThP-3, 179  
 Oh, S.: HC+SS-FrM-2, 212  
 Oh, Y.: AP2+PS+TF-TuA-12, 70  
 Ohldag, H.: MI+2D+TF-ThM-13, 157  
 Ohmori, T.: PS1+MS-ThM-3, 158; PS1+MS-ThM-4, 158  
 Ohya, Y.: PS+TF-MoM-2, 14; PS+TF-MoM-6, 14; PS1-ThA-1, 169  
 Okada, H.: TF-ThP-2, 196  
 Okato, T.: AP+PS-FrM-4, 208  
 Okuda, T.: MI+2D+TF-WeA-10, 136  
 Okyay, A.: EM+TF-ThM-5, 150; EM-ThP-6, 186; TF-ThP-11, 198  
 Olander, J.: EL-TuP-13, 91  
 Olgiati, M.: CA-TuP-1, **88**; SS2-MoM-10, **20**  
 Olive, D.: AC+AS+MI+TH-WeA-7, 125  
 Ollefs, K.: MI+2D+TF-ThM-13, 157  
 Ologun, A.: SS-ThP-6, **193**  
 Olson, D.: TF-ThP-19, 199  
 Olson, S.: QS+EM+TF-MoM-10, 17  
 Olsson III, R.: 2D+TF-TuA-11, 67  
 Olszta, M.: IB-ThA-3, 167  
 Omolayo, S.: VT-TuM-5, **62**  
 Omolere, O.: SS+2D+AS+HC-WeM-2, 119  
 Omotosho, K.: TF-ThM-3, **162**  
 Ono, M.: VT-MoM-5, **21**  
 Onyango, I.: CA+AS+LS+LX+MN+SE+SS-TuM-4, 51  
 Ooi, B.: SS-ThP-8, 194  
 Op De Beeck, A.: PS-TuP-9, 97  
 O'Regan, A.: UN-ThP-3, 200  
 Orgiu, E.: 2D-TuM-13, **45**; NS-TuP-13, **94**  
 Orihuela, B.: BI1+PS-MoM-6, 6  
 Orion, I.: AC-TuP-3, 85  
 Orson, K.: SS+HC-ThA-3, **172**; SS+HC-ThA-4, 172  
 Orui, T.: PS2+MS-WeA-3, 138  
 Ost, A.: IB-ThM-12, **154**; IB-ThP-1, 190  
 Osterwalder, J.: CPS+CA-WeA-7, 131  
 Otto IV, I.: PS-TuM-2, **55**  
 Otzen, D.: BI+AS+PS-TuM-2, 49  
 Owen, C.: HC+SS-FrM-6, 212  
 Owen, J.: QS+SS-TuA-11, 77  
 Owens, A.: PS+MS-TuA-1, 74  
 Oyler, N.: EM1+TF-FrM-6, 211  
 Özcan, O.: BI+AS+PS-TuM-3, **49**  
 — **P** —  
 P. Allan, M.: 2D-WeM-3, 106

## Author Index

- Pacchioni, G.: HC+SS-WeM-3, **115**; TH2-TuA-10, **82**
- Pacold, J.: LS+AC+AS+LX+MI+TH-ThA-5, 168
- Padgett, E.: AS-ThP-20, 182
- Pai, V.: SE-TuP-4, 103
- Palecek, P.: VT-TuM-13, 63; VT-TuP-6, 105
- Palla, L.: NS-TuP-8, 93
- Palmstrom, A.: CA+AS+LS+LX+MN+SE+SS-TuM-3, 51
- Pan, C.: 2D-ThP-1, 175
- Panagiotopoulos, A.: PS2+MS-WeA-4, 138
- Pandey, A.: NS+EM+MN-MoA-2, 31
- Pandey, P.: EM2-FrM-10, 211
- Pandit, S.: QS+EM-TuM-5, **57**
- Papa Rao, S.: EL-TuP-1, 89; QS+EM+TF-MoM-10, 17
- Paquette, M.: EM1+TF-FrM-6, **211**
- Paranamana, N.: TF2-TuA-10, **80**; TF-ThA-3, 173
- Park, D.: PS-TuP-4, 96
- Park, J.: AC+AS+MI+TH-WeA-3, 125; HC+SS-FrM-2, 112; HC-ThP-1, 187; HC-ThP-8, 188; PS-TuP-31, 101
- Park, K.: 2D-ThP-15, **177**; SS+HC-TuA-3, 78
- Park, M.: PS2+MS-WeA-9, 139; PS-TuP-4, 96
- Park, S.: PS+TF-MoM-5, 14
- Park, Y.: AS-ThP-2, 179
- Parker, G.: BI1-MoA-6, **26**
- Parkin, S.: 2D-WeA-1, **124**
- Parkinson, G.: HC+SS-WeM-2, 115; HC+SS-WeM-5, **115**; SS+2D+AS+HC-TuM-10, 59; SS+2D+AS+HC-WeM-1, 119
- Parot, J.: AS+CA+EL+EM+SE+SS+TF-ThM-3, 147
- Parsons, G.: AP+EM+PS+TF-TuM-1, 47; TF-ThP-7, 197
- Partridge, J.: AP+PS+TF-MoM-10, 5; AP+PS+TF-MoM-3, 4; AP+PS+TF-MoM-5, 4
- Pasebani, S.: SE-TuP-2, 103
- Paskov, P.: EL1+TF-MoA-1, 28
- Pasterski, M.:  
AS+2D+CA+EM+MS+NS+SE+SS+TF-FrM-6, 209
- Patel, D.: TF-ThP-8, 197
- Pathirage, V.: 2D-ThM-12, 146
- Patriotis, M.: QS+SS-TuA-4, 76
- Patt, M.: 2D2-ThA-6, **165**; 2D-ThP-19, **178**; EW-TuL-2, **64**
- Paudel, B.: SS+AS+TF-MoA-11, 41
- Paudyal, N.: SS-ThP-14, **194**
- Paul, B.: SE-TuP-2, 103
- Paul, M.: 2D-ThP-1, 175
- Pavelec, J.: HC+SS-WeM-2, 115; SS+2D+AS+HC-TuM-10, **59**; SS+2D+AS+HC-WeM-1, 119
- Pawlak, B.: SS+HC-TuA-11, 79
- Pawlawski, S.: CPS+MS-ThM-5, **149**; MS-FrM-10, **215**
- Paxton, W.: TF+QS-WeA-3, 142
- Pearce, C.: AC+AS+TH-WeM-3, **108**
- Pearlstein, R.: AP+PS-FrM-3, 207
- Pearson, J.: SS+AS+TF-MoA-10, 41
- Peckham, R.: 2D-ThP-18, 178
- Pedersen, K.: BI+AS+PS-TuM-2, 49
- Peeters, S.: QS+EM+TF-MoM-9, **16**
- Pei, J.: NS+2D+EM+MN+SS-TuM-10, 54
- Pei, Y.: AS+CA+EL+EM+SE+SS+TF-ThM-3, 147
- Pena, T.: 2D+EM-FrM-5, **206**
- Penedo, M.: NS1+2D+BI+SS-MoM-5, 12
- Pennachio, D.: EM+TF-ThM-13, **151**
- Penny, C.: PS-TuM-3, 55
- Peoble, A.: UN-ThP-33, 205
- Perea, D.: CA+AS+LS+LX+MN+SE+SS-TuM-4, 51; HC-ThP-3, 187; IB2-FrM-6, 213
- PEREZ CUAPIO, R.: HC-ThP-10, 189
- Perez, D.: TH1-TuA-3, 81
- Perry, J.: PS-TuP-27, 100
- Petitjean, D.: AP+PS+TF-WeM-12, 110; PS1+AS-WeA-11, 138; PS-TuP-30, 101
- Petralia, S.: 2D-TuM-12, 45
- Petrillo, K.: PS-TuM-3, 55
- Petrov, I.: SE1+TF-MoM-1, 17
- Petrova, T.: PS+SE-FrM-2, 217
- Petruzza, P.: PS-TuM-11, **56**
- Petschnigg, M.: MN-ThP-3, **191**
- Petzoldt, P.: HC+SS-ThM-6, **152**; LX+AS+BI+HC+SS+TH-MoA-5, 31; SS+2D+AS+HC-WeM-1, 119
- Peyres, S.: PS+MS-TuA-7, 75; PS2+MS-WeA-11, **139**
- Pfaff, S.: HC+SS-WeA-9, 134
- Pham, T.: LX+AS+BI+HC+SS+TH-MoA-3, **30**
- Philipp, P.: IB-ThM-5, 154
- Philipsen, V.: AP+PS-MoA-1, 23
- Phillips, C.: NS2+2D+BI+EL+SS-MoM-11, 13
- Phillips, M.: 2D-WeA-3, 124
- Pichler, C.: AS+CA+EL+EM+SE+SS+TF-WeA-11, 129
- Pickrell, G.: CPS+CA-WeA-1, 130
- Pierce, L.: UN-ThP-13, **202**
- Pierrard, R.: PS+SE-FrM-1, 217
- Pigram, P.: CA1+AS+LS+NS+SS+VT-MoM-5, **8**
- Pile, S.: MI+2D+TF-ThM-13, 157
- Pinder, J.: AS+2D+CA+EM+MS+NS+SE+SS+TF-FrM-5, 209; AS+CA+EL+EM+SE+SS+TF-ThM-6, **148**; TF-ThP-8, 197
- Pinnepalli, S.: EM1+TF-FrM-6, 211
- Pintar, A.: NS+EM+MN-MoA-8, 33
- Piontkowski, Z.: CPS+CA-WeA-1, 130
- Pirch, A.: SS+HC-TuA-11, 79
- Pirkl, A.: BI2-MoA-10, 26
- Piskin, T.: PS+NS-FrM-5, **216**
- Pitten, J.: QS+EM+TF-MoM-11, 17
- Pittsford, A.: SS1+AS-ThM-3, 160
- Plakhotnyuk, M.: AP1+2D+EM+PS+TF-TuA-7, **69**
- Plambeck, N.: VT-TuM-2, 62
- Planer, J.: SS1+AS-ThM-4, 160
- Plank, H.: NS+2D+EM+MN+SS-TuM-5, **54**
- Planksy, J.: LX+AS+BI+HC+SS+TH-MoA-5, 31
- Plymale, A.: BI1-MoA-6, 26
- Poche, T.: AP-TuP-3, 85; SS+HC-ThA-6, 172
- Podraza, N.: EL1+TF-MoA-3, 29; EL1+TF-MoA-4, 29; EL1-MoM-1, **9**; EL-TuP-5, 90; EL-TuP-8, 90
- Pokharel, R.: AC+AS+MI+TH-WeA-3, 125
- Pokhrel, A.: PS-TuM-13, 57
- Pokhrel, B.: 2D-WeM-5, **106**
- Pokhrel, H.: 2D+TF-TuA-7, **66**
- Pole, M.: IB-ThA-3, **167**
- Poletto, S.: QS-MoA-5, **37**
- Poleunis, C.: PS+SE-FrM-6, 218
- Polito, J.: PS+NS-FrM-11, 217
- Pollard, S.: 2D+TF-TuA-7, 66
- Polly, R.: TH1+AS+SS-TuM-6, **61**
- Polonsky, O.: UN-ThP-8, 201
- Pomeroy, J.: QS+EM+TF-MoM-1, 15; QS-MoA-11, 37
- Ponomareva, I.: 2D-ThM-12, 146
- Pop, E.: 2D+EM-FrM-5, 206; EM-ThA-5, 166
- Pope, J.: MS-ThP-1, 191
- Poplawsky, J.: IB-ThP-5, 190
- Porcelli, T.: SE+TF-MoA-8, 38
- Porter, L.: EM+TF-ThM-6, 150
- Posseme, N.: AP+PS-MoA-9, 24; PS+TF-MoM-3, 14
- POSSEME, N.: PS-TuP-24, 99
- Possémé, N.: AP1+2D+EM+PS+TF-TuA-1, 69
- Postawa, Z.: CA+AS+LS+LX+MN+SE+SS-TuM-1, 51
- Potma, E.: NS2+2D+BI+EL+SS-MoM-8, **13**
- Potyrailo, R.: CA+AS+LS+LX+MN+SE+SS-TuM-5, **52**; NS+EM+MN-MoA-10, 33
- Poulidakos, L.: NS+2D+EM+MN+SS-TuM-10, 54; NS-TuP-4, 92
- Pourtois, G.: AP+EM+PS+TF-TuM-12, 49
- Poutous, M.: MN1-WeM-5, 116
- Powell, M.: QS+EM+TF-MoM-2, 15
- Powers, M.: HC+SS-WeM-13, 116; HC-ThP-5, **188**
- Powis, A.: PS2-ThA-3, 171
- Prabhakaran, V.: CA+AS+LS+NS+SS+VT-MoA-8, 28
- Prager, J.: PS-TuP-17, 98; PS-TuP-18, 98; PS-TuP-27, 100
- Prater, R.: MI+2D+TF-ThM-10, 157
- Prathibha Jasti, N.: NS+2D+EM+MN+SS-TuM-4, 53
- Prchal, J.: AC+MI+TH-TuM-11, 46
- Preischi, C.: PS2+AS+SS-ThM-10, 159
- Price, C.: 2D-ThP-20, **178**
- Prochazka, P.: SS1+AS-ThM-4, 160
- Pruneri, V.: SE-TuP-5, 104
- Ptok, A.: EM-ThP-3, 186
- Pugmire, A.: AC+AS+MI+TH-WeA-7, 125
- Puntscher, L.: HC+SS-WeM-2, 115; HC+SS-WeM-5, 115
- Punzmann, H.: TF+QS-WeA-1, 142
- Puretzky, A.: 2D+TF-TuA-3, 66
- Pursel, S.: PS+SE-MoA-9, 35
- Puurunen, R.: AP+PS+TF-WeM-1, **108**
- Pylypenko, S.: AS-ThP-20, 182; AS-ThP-21, 182
- PYO, S.: AS-ThP-34, **184**
- Pyrch, A.: EM-WeM-6, 114
- Pyun, D.: PS-TuP-16, **98**
- Q —
- Qiao, M.: HC+SS-ThM-12, 153
- Qu, C.: PS-TuP-11, 97
- Quarnstrom, J.: 2D-WeM-5, 106
- Quelhas, K.: NS+EM+MN-MoA-1, 31
- Quijada, M.: TF+QS-WeA-9, 143
- R —
- Raadu, M.: PS+SE-MoA-1, 34
- Rabea, M.: CPS+CA-WeA-10, **132**; SS-ThP-20, 195
- Raboño Borbolla, J.:  
AS+CA+EL+EM+SE+SS+TF-WeA-2, 127
- Rack, P.: IB3-FrM-8, **214**
- Radach, D.: EW-TuL-7, **65**
- Radetić, M.:  
AS+2D+CA+EL+EM+MS+NS+SE+SS+TF-WeM-3, 111
- Radnik, J.: AS+CA+EL+EM+SE+SS+TF-WeA-8, 128
- Raghunathan, V.: CPS+MS-ThM-10, **149**
- Rahaman, M.: 2D+TF-TuA-11, 67
- Rahman, M.: HC+SS-ThM-3, 152; HC+SS-WeA-4, 133
- Rahman, T.: EM-WeA-4, 132
- Rai, B.: AC+MI+TH-TuM-6, **46**; AC-TuP-2, 85
- Rais-Zadeh, M.: EM+TF-ThM-10, 150
- Raites, Y.: PS+SE-MoA-3, 34; PS+SE-MoA-4, 35; PS-TuP-21, 99
- Rajak, S.: NS-TuP-5, **92**; SS-ThP-9, 194
- Rajan, J.: EW-TuL-7, 65
- Ramach, U.: BI2+AS+HC+SS-MoM-8, 7
- Raman, A.: SS+HC-TuA-7, 78
- Raman, R.: NS2+2D+EM-TuA-11, 73
- Ramanantoanina, H.: AC+MI+TH-TuM-13, 47; TH1+AS+SS-TuM-5, 60
- Ramanujam, B.: EL1+TF-MoA-3, **29**
- Ramisch, L.: HC+SS-WeA-9, 134
- Ramstedt, M.: AS+CA+EL+EM+SE+SS+TF-ThM-3, 147

## Author Index

- Rananavare, S.: NS2+2D+EM-TuA-10, 73  
 Randall, J.: QS+SS-TuA-11, 77; QS+VT-WeM-12, 119  
 Rangnekar, S.: NS1+2D+EM+MN-TuA-7, 73  
 Rasmussen, M.: BI+AS+PS-TuM-12, 50  
 Ratel, D.: AS+2D+CA+EM+MS+NS+SE+SS+TF-FrM-1, 208  
 Rath, D.: SS+2D+AS+HC-TuM-10, 59  
 Rauf, S.: PS+MS-TuA-10, 75; PS+MS-TuA-12, 76; PS+MS-TuA-3, 74; PS+MS-TuA-8, 75; PS2-ThA-3, 171; PS-TuM-4, 55  
 Ravelli, F.: VT-TuA-12, 84  
 Ravichandran, J.: 2D+TF-TuA-8, 66  
 Rebarz, M.: EL1-MoM-6, 10  
 Reece, C.: HC+SS-FrM-6, 212; HC+SS-WeA-10, 134  
 Reece, D.: TF-ThM-6, 162  
 Reed, B.: AS+CA+EL+EM+SE+SS+TF-WeA-8, 128  
 Reekmans, G.: SS+HC-TuA-11, 79  
 Reeks, J.: SS2-MoM-9, 20  
 Refvik, N.: SS+2D+AS+HC-WeM-5, 120  
 Regmi, S.: EM-ThP-3, 186  
 Rehr, J.: TH2+AS+SS-TuM-10, 61  
 Reidy, K.: NS1+2D+EM+MN-TuA-1, 72  
 Reimann, A.: SS+AS+TF-MoA-8, 40  
 Reinke, P.: 2D-ThP-18, 178; SS+HC-ThA-3, 172; SS+HC-ThA-4, 172; UN-ThP-21, 203  
 Remy, A.: PS-TuP-3, 96  
 ren, H.: TF-ThP-21, 199  
 Renaud, V.: PS-TuM-13, 57  
 Renault, O.: AS+2D+CA+EL+EM+MS+NS+SE+SS+TF-WeM-4, 111; AS+2D+CA+EM+MS+NS+SE+SS+TF-FrM-1, 208; AS-ThP-29, 184; CA+AS+LS+NS+SS+VT-MoA-10, 28  
 Reniers, F.: AP+PS+TF-WeM-12, 110; PS+SE-FrM-6, 218; PS1+AS-WeA-11, 138; PS-TuP-3, 96; PS-TuP-30, 101; PS-TuP-9, 97  
 Renteria, E.: 2D+EM-FrM-4, 206  
 Renzas, R.: QS+EM+TF-MoM-2, 15  
 Revilla Castillo, R.: PS+SE-FrM-6, 218  
 Revzin, A.: CA+AS+LS+LX+MN+SE+SS-TuM-1, 51  
 Reza, M.: 2D+EM-FrM-8, 207  
 Rhee, D.: 2D+TF-TuA-11, 67  
 Rheinfrank, E.: SS+2D+AS+HC-TuM-2, 58  
 Rhinow, D.: PS2+AS+SS-ThM-10, 159  
 Ribaudou, T.: EL2-MoA-10, 30  
 Richardson, K.: EM2-FrM-8, 211  
 Richmond, J.: VT-MoA-8, 42  
 Richter, S.: EL1+TF-MoA-1, 28; EL-TuP-13, 91  
 Richter, T.: IB-ThM-12, 154; IB-ThP-1, 190  
 Richy, J.: AS-ThP-29, 184  
 Ricker, J.: VT-MoM-9, 22  
 Rickman, M.: UN-ThP-24, 204  
 Riis, E.: QS+VT-WeM-5, 118  
 Rindert, V.: EL-TuP-13, 91  
 RioPousa, D.: VT-MoM-3, 21  
 Risner-Jamtegaard, J.: AS+2D+CA+EL+EM+MS+NS+SE+SS+TF-WeM-5, 112  
 Rissanen, E.: QS-MoA-11, 37  
 Ristoiu, D.: PS+NS-FrM-4, 215  
 Rittschof, D.: BI1+PS-MoM-6, 6  
 Rius, G.: IB-ThP-2, 190  
 Riva, M.: SS+2D+AS+HC-TuM-1, 58; SS+2D+AS+HC-TuM-2, 58  
 Rivero Arias, M.: EL-TuP-6, 90  
 Rizzolo, M.: SE-TuP-4, 103  
 Roagelv, A.: AC+MI+TH-TuM-1, 45  
 Roberg, K.: BI+AS+EM+NS+SE+TF-TuA-4, 71  
 Roberts, A.: AS+CA+EL+EM+SE+SS+TF-WeA-4, 128; AS-ThP-18, 181  
 Roberts, R.: MN1-WeM-1, 116  
 Robinson, E.: UN-ThP-31, 205; UN-ThP-32, 205  
 Robinson, J.: NSP-SuA-8, 3  
 Robinson, S.: NS+EM+MN-MoA-1, 31; NS+EM+MN-MoA-4, 32  
 Rode, A.: UN-ThP-17, 202  
 Rodil, S.: TF1+PS-WeM-6, 122  
 Rodriguez Bonet, S.: AS-ThP-37, 185  
 Rodriguez de Marcos, L.: TF+QS-WeA-9, 143  
 Rodriguez, M.: AS+2D+CA+EL+EM+MS+NS+SE+SS+TF-WeM-6, 112  
 Rodriguez, R.: AP+PS+TF-MoM-1, 4; TF+QS-WeA-10, 143  
 Roeters, S.: BI+AS+PS-TuM-4, 50  
 Rogalskyj, S.: PS-TuM-5, 56  
 Rogers, B.: CPS+CA-WeA-9, 131  
 Rogers, C.: 2D+EM-FrM-3, 206; EM-ThP-5, 186  
 Roldan Cuenya, B.: SS+2D+AS+HC-TuM-4, 58  
 Romadanov, I.: PS+SE-MoA-3, 34  
 Roman, A.: PS+TF-MoM-3, 14  
 Romanyuk, O.: AC+AS+MI+TH-WeA-9, 126  
 Rombaut, J.: SE-TuP-5, 104  
 Romero Cedillo, J.: PS-TuP-7, 96  
 Ronco, A.: AP+PS-MoA-9, 24  
 Ronse, K.: PS+NS-FrM-3, 215  
 Rooney, C.: 2D-ThP-9, 176  
 Rooney, E.: AS-ThP-22, 182  
 Roorda, T.: 2D-ThP-12, 176; 2D-WeM-3, 106  
 Ros, E.: AS+CA+EL+EM+SE+SS+TF-ThM-2, 147  
 Rosa Ortiz, S.: PS-TuP-1, 95  
 Rosa-Ortiz, S.: PS+NS-FrM-10, 217  
 Rosas, D.: AC+AS+TH-WeM-10, 108; AC+AS+TH-WeM-11, 108  
 Rose, R.: SE+TF-MoA-9, 39  
 Rose, V.: SS-ThP-18, 195  
 Rosenberg, S.: AP+PS+TF-WeM-11, 110  
 Rosenberger, M.: 2D-WeA-3, 124  
 Rosenhahn, A.: BI+AS+EM+NS+SE+TF-TuA-9, 71; BI+AS+PS-TuM-3, 49; BI1+PS-MoM-1, 6; BI2-MoA-8, 26; BI-TuP-1, 86  
 Rosenhek-Goldian, I.: NS+2D+EM+MN+SS-TuM-4, 53; NS1+2D+BI+SS-MoM-6, 13  
 Rosenstein, J.: HC+SS-WeM-13, 116; HC-ThP-5, 188  
 Rosenthal, M.: IB-ThA-5, 168  
 Rossi, A.: MI+2D+TF-ThM-10, 157  
 Rostamzadeh, T.: HC+SS-ThM-13, 153  
 Rotenberg, E.: 2D-WeA-7, 124  
 Rouleau, C.: 2D+TF-TuA-3, 66  
 Roussel, P.: AC+MI+TH-TuA-9, 68; AC+MI+TH-TuM-13, 47  
 Roussos, J.: MN1-WeM-3, 116  
 Roy, D.: NS-TuP-12, 94  
 Roy, S.: MI+2D+TF-WeA-3, 135  
 Rubio-Giménez, V.: TF+SE-FrM-8, 220  
 Rubloff, G.: TF2-TuA-9, 80  
 Ruder, A.: EL-TuP-13, 91  
 Rudin, S.: AC+MI+TH-TuM-12, 47  
 Rudolph, M.: PS+SE-MoA-1, 34  
 Ruellan, A.: SE+TF-MoA-5, 38  
 Rumancev, C.: BI+AS+EM+NS+SE+TF-TuA-9, 71  
 Rumbach, P.: PS1-ThA-2, 169  
 Rummel, B.: CPS+CA-WeA-1, 130; QS+SS-TuA-4, 76  
 Rutkowski, L.: TF+QS-WeA-1, 142  
 Ruzic, D.: AP+PS+TF-WeM-5, 109; CPS+CA-WeA-8, 131; PS+SE-FrM-5, 218; PS+SE-MoA-10, 35; PS+SE-MoA-11, 35; PS+SE-MoA-8, 35  
 Ryaboy, M.: PS+SE-FrM-10, 218
- S —
- Sadi, D.: PS1+AS-WeA-7, 137  
 Sadowski, J.: 2D+TF-TuA-10, 67  
 Saedy, S.: HC+SS-FrM-3, 212  
 Saeed, K.: BI+AS+PS-TuM-5, 50  
 Sagisaka, K.: SS-ThP-17, 195  
 Sahin, O.: BI-TuP-2, 87  
 Sahore, R.: AS-ThP-5, 180  
 Saidjafarzoda, I.: PS-TuP-25, 100; TF-ThP-11, 198  
 Sakhya, A.: EM-ThP-3, 186  
 Sakka, Y.: MS-ThP-3, 192  
 Sako, K.: PS1+MS-ThM-1, 158  
 Salagre, E.: SS+AS+TF-MoA-10, 41; TF-ThP-6, 196  
 Saleh, I.: VT-TuM-13, 63  
 Sales, M.: TF+QS-WeA-9, 143  
 Salisbury, J.: SE+TF-MoA-9, 39  
 Salovich, N.: PS+SE-MoA-9, 35  
 Samarasingha, N.: EL-TuP-6, 90  
 Samarth, N.: 2D-TuM-5, 44; MI+2D+TF-ThM-12, 157  
 Samson, L.: 2D-ThP-22, 179  
 Sanchez-Mansilla, A.: TH1-TuA-1, 81  
 Sanders, J.: UN-ThP-31, 205; UN-ThP-32, 205  
 Sandoval, T.: AP+EM+PS+TF-TuM-5, 47  
 Sangwan, V.: NS1+2D+EM+MN-TuA-7, 73  
 Sankaran, M.: PS+SE-FrM-5, 218  
 Sankaran, R.: PS+MS-TuA-7, 75; PS+SE-FrM-1, 217; PS+SE-MoA-10, 35; PS2+MS-WeA-11, 139  
 Sano, N.: BI-TuP-7, 87  
 Santavica, D.: TF1+PS-WeM-1, 121  
 Sapkota, D.: EL1+TF-MoA-3, 29  
 Sarkar, S.: PS-TuM-13, 57  
 Sarrazin, A.: PS-TuM-12, 56  
 Sassi, M.: MS-ThP-1, 191  
 Sato, K.: MS-ThP-3, 192  
 Satriano, C.: 2D-ThP-16, 177; 2D-ThP-17, 178; 2D-ThP-2, 175; 2D-TuM-12, 45  
 Sattler, K.: IB-ThM-11, 154  
 Sautet, P.: HC+SS-ThA-5, 167  
 Sauvage, L.: PS-TuP-9, 97  
 Savorianakis, G.: TF+SE-FrM-5, 219  
 Savrasov, S.: MI+2D+TF-ThM-10, 157  
 Saylor, J.: SS-WeA-8, 141  
 Scanagatta-Long, M.: IB-ThP-3, 190  
 Schäbitz, W.: IB3-FrM-11, 214  
 Schacherl, B.: LS+AC+LX+MI+TH-ThM-12, 156; TH1+AS+SS-TuM-3, 60; TH1+AS+SS-TuM-5, 60; TH-TuP-1, 104  
 Schäfer, T.: HC-ThP-2, 187; SS-ThP-12, 194  
 Schaff, O.: LX+AS+HC+SS-MoM-5, 11  
 Schaffers, T.: MI+2D+TF-ThM-13, 157  
 Schaueremann, D.: SS-ThP-12, 194  
 Scheiner, B.: PS-TuP-11, 97  
 Schell, E.: UN-ThP-19, 203; UN-ThP-20, 203; UN-ThP-21, 203; UN-ThP-22, 203; UN-ThP-23, 203  
 Schemmelmann, S.: MI+2D+TF-WeA-9, 135  
 Scherer, B.: NS+EM+MN-MoA-10, 33  
 Scherschligt, J.: VT-MoA-9, 42; VT-MoM-4, 21; VT-MoM-8, 22  
 Schjøtt, B.: BI+AS+PS-TuM-2, 49  
 Schlom, D.: EL1+TF-MoA-4, 29  
 Schmehl, R.: HC+SS-ThM-13, 153  
 Schmid, M.: HC+SS-WeM-2, 115; SS+2D+AS+HC-TuM-1, 58; SS+2D+AS+HC-TuM-10, 59; SS+2D+AS+HC-TuM-13, 59; SS+2D+AS+HC-TuM-2, 58; SS+2D+AS+HC-WeM-1, 119  
 Schmidt, J.: HC+SS-WeA-1, 133  
 Schmitt, B.: TH2-TuA-7, 81  
 Schneider, C.: SS1+HC-MoM-1, 19  
 Schneider, J.: SE2+TF-MoM-10, 19

## Author Index

- Schoenlein, R.: LS+AC+LX+MI+TH-ThM-5, **155**
- Scholl, A.: LS+AC+AS+LX+MI+TH-ThA-1, **168**;  
MI+2D+TF-WeA-3, 135
- Schönemann, E.: BI-TuP-1, 86
- Schreier, M.: HC+SS-WeM-10, **115**
- Schroeder, M.: VT-TuM-2, 62
- Schroeder, S.: LX+AS+BI+HC+SS+TH-MoA-8, **31**
- Schubert, M.: EL1+TF-MoA-1, 28; EL1+TF-MoA-5, 29; EL-TuP-10, 90; EL-TuP-13, 91
- Schuck, P.: NS2+2D+EM-TuA-8, 73
- Schujman, S.: QS+EM+TF-MoM-10, 17
- Schultz, J.: NS-TuP-6, **93**
- Schulz-von der Gathen, V.: PS+SE-FrM-8, 218
- Schwab, C.: NS1+2D+BI+SS-MoM-4, **12**
- Schwarz, U.: SS-WeA-11, 141
- Schweikert, E.: CA+AS+LS+LX+MN+SE+SS-TuM-1, 51
- Sciaccia, S.: 2D-ThP-16, 177
- Scirè, S.: 2D-TuM-12, 45
- Scott, S.: UN-ThP-25, 204
- Scougale, W.: SS-ThP-18, 195
- Scurr, D.: BI1-MoA-2, 25; BI1-MoA-5, 26
- Seal, S.: 2D-ThP-11, 176
- Seebauer, E.: SS-ThP-4, 193
- Seegitz, M.: VT-TuM-13, 63; VT-TuP-6, 105
- Seewald, L.: NS+2D+EM+MN+SS-TuM-5, 54
- Seferai, V.: QS+EM+TF-MoM-9, 16
- Segovia, P.: SS+AS+TF-MoA-10, 41; TF-ThP-6, 196
- Segundo, M.: AS+CA+EL+EM+SE+SS+TF-ThM-3, 147
- Seibert, S.: NS1+2D+BI+SS-MoM-4, 12
- Seidel, R.: LX-TuP-2, 91
- Sejour, B.: BI-TuP-2, 87
- Sekine, M.: PS+TF-MoM-6, 14; PS1-ThA-1, 169
- Sekine, R.: AP+PS-MoA-11, 24
- Selloni, A.: SS+HC-TuA-7, 78
- SELMOUNI, A.: PS-TuP-24, **99**
- Seltenhammer, A.: NS-TuP-8, 93
- Senaratne, W.: SE-TuP-5, 104
- Sen-Britain, S.: AC+AS+TH-WeM-10, 108; AC+AS+TH-WeM-11, 108
- Seo, B.: PS-TuP-33, 101
- Seo, G.: SE-TuP-10, 104
- Seo, S.: PS2-ThA-5, 171; PS-TuP-37, 102; PS-TuP-38, 102
- Seol, Y.: PS2-ThA-5, 171; PS-TuP-37, 102; PS-TuP-38, 102
- Seong, I.: PS2-ThA-5, 171; PS-TuP-37, 102; PS-TuP-38, **102**
- Serov, A.: AS-ThP-20, 182
- Serra, T.: PS-TuP-3, 96
- Servando-Williams, D.: AC+AS+TH-WeM-10, 108; AC+AS+TH-WeM-11, 108
- Setina, J.: VT-TuA-10, 83
- Sevik, C.: 2D-ThM-13, 146
- Seydoux, C.: AS+2D+CA+EM+MS+NS+SE+SS+TF-FrM-1, 208
- Shabani, J.: QS+EM+TF-MoM-11, 17
- Shadwell, M.: TF+QS-WeA-1, 142; VT-MoA-8, 42
- Shaftan, T.: VT-TuM-13, 63; VT-TuP-6, 105
- Shahsavari, A.: SS1+AS-ThM-4, 160
- Shaikhutdinov, S.: SS+2D+AS+HC-TuM-4, 58
- Shan, A.: EL1+TF-MoA-3, 29; EL1-MoM-1, 9
- Shanahan, R.: UN-ThP-18, **203**
- Shankar, S.: MS-FrM-1, **214**
- Shannon, S.: PS+SE-MoA-5, **35**; PS2+AS+SS-ThM-11, 159
- Shapiro, D.: MI+2D+TF-ThM-13, 157
- Shaqfeh, E.: NS+EM+MN-MoA-3, 32
- Shard, A.: AS+CA+EL+EM+SE+SS+TF-ThM-3, 147; AS+CA+EL+EM+SE+SS+TF-WeA-8, 128; AS-ThP-23, 183
- Sharma, P.: SS-ThP-18, 195
- Sharma, S.: VT-TuP-6, 105
- Sharma, U.: SE-TuP-4, 103
- Sharp, M.: HC+SS-ThM-1, **151**
- Shaw, B.: VT-TuA-7, **83**
- Shchukarev, A.: AS+CA+EL+EM+SE+SS+TF-ThM-3, 147
- Sheldon, B.: EM-ThA-1, 165
- Shen, Z.: MI+2D+TF-ThM-10, 157
- Shengnan, Y.: MS-ThP-3, 192
- Sheriff, J.: AS-ThP-25, **183**
- Sherriff, J.: AS-ThP-11, 181
- Shi, J.: EM-WeA-4, 132; HC+SS-ThA-5, 167
- Shi, X.: PS+MS-TuA-10, 75; PS-TuM-4, **55**
- Shibata, K.: VT-TuP-4, 105
- Shim, S.: AP+PS-FrM-2, 207
- Shimada, K.: MI+2D+TF-WeA-10, 136
- Shimizu, T.: SS-ThP-17, **195**; SS-ThP-2, 192; SS-ThP-5, 193
- Shin, D.: AS-ThP-2, 179
- Shin, G.: PS2-ThA-6, 171; PS-TuP-28, 100; PS-TuP-29, 100; PS-TuP-34, 101
- Shin, H.: PS1+MS-ThM-6, **159**
- Shin, J.: TF+SE-FrM-6, 220
- Shin, Y.: AP+PS+TF-WeM-13, **111**
- Shindler, S.: TF-ThA-4, **173**; TF-ThP-4, **196**
- Shiota, T.: PS-TuM-1, 55
- Shirai, M.: VT-TuP-4, 105
- Shirato, N.: SS-ThP-18, 195
- Shoer, L.: PS+SE-MoA-9, 35
- Shollenberger, D.: AS-ThP-17, 181
- Shower, P.: SE+TF-MoA-9, 39
- Shrestha, A.: 2D-ThM-4, **145**; TF-ThP-9, 197
- Shrestha, B.: EL1-MoM-1, 9
- Shrestha, P.: QS-MoA-11, 37
- Shrestha, S.: 2D-WeM-5, 106
- Shuchi, N.: 2D-ThP-8, 176
- Shuh, D.: AC+AS+TH-WeM-10, 108; AC+AS+TH-WeM-11, **108**; LS+AC+AS+LX+MI+TH-ThA-5, 168
- Shukla, N.: 2D+EM-FrM-3, 206; EM-ThP-5, 186
- Shul, R.: PS-TuP-26, 100
- Shutthanandan, V.: AS-ThP-23, 183; AS-ThP-28, 183; IB-ThM-13, **155**
- Shykind, D.: PS+SE-MoA-9, **35**
- Shyner, S.: QS+SS-TuA-9, 77; SS-WeA-8, **141**
- Sidhik, S.: CA+AS+LS+NS+SS+VT-MoA-3, 27
- Sieg, S.: PS-TuM-3, 55
- Siemons, L.: SS+HC-TuA-11, 79
- Sigillito, A.: QS+SS-TuA-11, 77
- Silva, T.: PS1+AS-WeA-7, 137
- Silvent, J.: IB-ThM-1, 153
- Simka, H.: AP+PS-MoA-2, 23
- Simon, C.: 2D-ThP-1, 175
- Simpson, R.: EW-TuL-3, 64
- Singh, A.: MI+2D+TF-WeA-3, 135
- Singh, M.: 2D+EM-FrM-8, 207
- Singh, S.: 2D-WeM-13, **107**; HC+SS-WeM-1, 114
- Sinha, J.: AP+EM+PS+TF-TuM-1, 47
- Sinha, T.: QS+VT-WeM-12, 119; VT-TuP-1, 105
- Sinno, T.: QS+SS-TuA-4, 76
- Siribaddana, C.: SS-ThP-9, **194**
- Sirvinskaite, R.: VT-TuM-2, **62**
- Skogg, C.: BI2-MoA-9, 26
- Smaluk, V.: VT-TuP-6, 105
- Smets, J.: TF+SE-FrM-8, **220**
- Smiles, D.: LS+AC+AS+LX+MI+TH-ThA-5, 168
- Smit, M.: SS2-MoM-9, 20
- Smith III, C.: VT-TuM-12, 63
- Smith, A.: 2D-ThM-4, 145; AC+AS+MI+TH-WeA-3, 125; SS+2D+AS+HC-WeM-10, **120**; SS+2D+AS+HC-WeM-11, 121; SS+2D+AS+HC-WeM-12, 121; TF-ThP-9, 197; UN-ThP-7, 201
- Smith, M.: CPS+CA-WeA-1, 130
- Smith, N.: EL-TuP-12, 91; TF+QS-WeA-1, 142
- Smith, P.: QS+VT-WeM-12, **119**; VT-TuP-1, 105
- Smith, R.: CA-TuP-4, 89; EM-ThP-3, 186
- Smith, S.: EM-ThP-8, **186**; HC+SS-ThM-1, 151
- Smith, T.: AP+PS-MoA-1, **23**
- Snure, M.: 2D+TF-TuA-11, 67; 2D-WeM-13, 107
- Snyders, R.: PS1+AS-WeA-11, 138; PS-TuP-9, 97
- So, C.: BI2-MoA-9, **26**
- Soban, Z.: AC+AS+MI+TH-WeA-9, 126
- Sobchinsky, E.: HC+SS-ThM-3, 152
- Sobczak, C.: AS+2D+CA+EL+EM+MS+NS+SE+SS+TF-WeM-6, 112
- Sobell, Z.: AP+PS+TF-WeM-6, 110
- Socquet, C.: PS+TF-MoM-3, 14
- Soeda, M.: VT-TuA-11, 84
- Sokaras, D.: AC+MI+TH-TuM-13, 47; LS+AC+LX+MI+TH-ThM-3, **155**
- Solgaard, J.: AP+PS-MoA-11, 24
- Sombut, P.: HC+SS-WeM-2, **115**; HC+SS-WeM-5, 115
- Sommer, C.: IB3-FrM-11, 214
- Son, J.: CA+AS+LS+NS+SS+VT-MoA-11, **28**
- Son, K.: SE-TuP-2, 103
- Song, S.: 2D+TF-TuA-11, **67**; NS-TuP-11, 94; QS+SS-TuA-10, 77; QS+SS-TuA-3, 76
- Song, Y.: EM-WeM-11, 114
- Song, Z.: EL-TuP-8, 90
- Soomary, L.: AS+2D+CA+EM+MS+NS+SE+SS+TF-FrM-11, 210
- Sorensen, P.: EL-TuP-10, **90**
- Sotir, D.: EL1+TF-MoA-4, 29
- Soucek, J.: SS-ThP-1, 192; SS-ThP-15, 195
- Soulie, J.: PS-TuM-13, 57
- Souriau, L.: PS+TF-MoM-1, 13; PS-TuM-13, 57
- Sousa, C.: TH1-TuA-1, 81
- Spagna, S.: NS1+2D+BI+SS-MoM-4, 12
- Speed, D.: TF+SE-FrM-4, 219
- Spencer, B.: AS+2D+CA+EM+MS+NS+SE+SS+TF-FrM-11, 210
- Spiegelman, J.: AP2+PS+TF-TuA-9, 69
- Spoddig, D.: MI+2D+TF-ThM-13, 157
- Spool, A.: AS+2D+CA+EM+MS+NS+SE+SS+TF-FrM-10, **210**
- Sprague, M.: EM-ThP-3, 186
- Sprey, H.: 2D-TuM-4, 44
- Spurgeon, S.: MS-ThP-1, 191
- Sreedhar, S.: MI+2D+TF-ThM-10, 157
- Srinivasan, K.: NS+EM+MN-MoA-8, 33
- Srinivasan, S.: PS1-ThA-5, 170
- St. Martin, J.: UN-ThP-21, 203
- St. Martin, J.: SS+HC-ThA-4, 172
- Staab, M.: MI+2D+TF-ThM-10, 157
- Stacchiola, D.: HC-ThP-11, 189; LX+AS+HC+SS-MoM-4, 11; SS+2D+AS+HC-TuM-12, **59**
- Stach, E.: 2D+TF-TuA-11, 67
- Stafford, N.: PS2-ThA-2, 170
- Stagon, S.: TF1+PS-WeM-1, **121**; TF-ThP-18, 199
- Stan, G.: NS+2D+EM+MN+SS-TuM-3, **53**
- Stanishev, V.: EL1+TF-MoA-1, 28; EL-TuP-13, 91

## Author Index

- Stapley, A.: TF+QS-WeA-3, **142**
- Stavis, S.: NS+EM+MN-MoA-5, 32; NS+EM+MN-MoA-8, 33
- Stavitski, E.: LX-TuP-1, 91
- Steely, L.: SS+AS+TF-MoA-9, 40
- Steinbrück, A.: BI+AS+EM+NS+SE+TF-TuA-9, 71
- Steiner, A.: TF-ThM-4, 162
- Steinfeldt, J.: CPS+CA-WeA-1, 130
- Steininger, R.: TH1+AS+SS-TuM-5, 60
- Stelmacovich, G.: AS-ThP-21, **182**
- Steuer, D.: PS+SE-FrM-8, 218
- Stevens, T.: PS-TuP-26, 100
- Stevenson, M.: TF+QS-WeA-11, 143
- Stevenson, S.: 2D+EM-FrM-3, 206; IB-ThA-1, 167
- Stevenson, T.: AP-TuP-4, 86
- Stewart, D.: TF2-TuA-9, 80
- Stinson, P.: 2D-ThP-8, 176
- Stinson, V.: MN1-WeM-5, **116**
- Stockbridge, K.: IB-ThM-3, 153
- Stoerzinger, K.: AS-ThP-12, 181
- Stokey, M.: EL1+TF-MoA-5, 29
- Straatsma, T.: TH1-TuA-1, 81
- Strandwitz, N.: EM1+TF-FrM-6, 211
- Strange, L.: AS-ThP-23, **183**; TF2+AP+SE+SS-WeM-13, 123
- Strelcov, E.: CA-TuP-2, 88; CPS+CA-WeA-7, 131
- Strickland, W.: QS+EM+TF-MoM-11, 17
- Strohmayr, M.: AS-ThP-14, 181
- Stroschio, J.: SS-WeA-2, **140**
- Stroud, R.: EM+TF-ThM-13, 151
- Strunge, K.: BI+AS+PS-TuM-2, 49; BI+AS+PS-TuM-5, 50
- Strzhemechny, Y.: SS2-MoM-9, 20
- Stuehn, L.: NS1+2D+BI+SS-MoM-4, 12
- Sturm, M.: AS+2D+CA+EM+MS+NS+SE+SS+TF-FrM-8, **209**
- Su, T.: 2D-ThP-1, **175**; SE+TF-MoA-2, **38**
- Suas-David, N.: TF+QS-WeA-1, 142
- Subash, U.: MN1-WeM-5, 116
- Subedi, A.: MI+2D+TF-WeA-2, **135**
- Suda, R.: PS+TF-MoM-2, 14; PS1-ThA-1, 169; PS2+MS-WeA-3, 138
- Suetsugu, Y.: VT-TuM-1, **61**; VT-TuP-4, **105**
- Sugai, H.: PS+SE-MoA-2, 34
- Sugano, R.: PS-TuM-1, 55
- Suleiman, A.: TF2+AP+SE+SS-WeM-12, **123**
- Sultana, J.: TF-ThP-13, 198; TF-ThP-14, 198
- Sultana, R.: TF-ThP-11, 198
- Sumaiya, S.: 2D-ThM-13, **146**; BI-TuP-2, **87**
- Šumandl, P.: SE+TF-MoA-6, 38
- Sumiyoshi, A.: SS+AS+TF-MoA-4, **40**
- Sun, K.: NS+EM+MN-MoA-2, 31; SS+2D+AS+HC-WeM-12, 121
- Sun, R.: CA1+AS+LS+NS+SS+VT-MoM-5, 8
- Sun, W.: BI-WeA-1, **129**
- Sun, Y.: 2D+EM-FrM-9, **207**; 2D-WeA-10, **125**
- Sung-Joon, P.: PS-TuP-32, **101**
- Surendran, M.: 2D+TF-TuA-8, **66**
- Suresh Babu, S.: PS+SE-MoA-1, 34
- Surman, D.: AS-ThP-18, 181
- Surman, M.: AP+PS+TF-MoM-10, 5
- Sushko, P.: TF2+AP+SE+SS-WeM-13, 123
- Suzer, S.: SS2-MoM-8, 20; TH2-TuA-11, 82
- Svanidze, E.: AC+MI+TH-TuM-3, **45**
- Swain, P.: NS1+2D+BI+SS-MoM-5, **12**
- Swerts, J.: AP+EM+PS+TF-TuM-1, 47; EM1+TF-FrM-1, **210**
- Sydorenko, D.: PS+MS-TuA-12, 76
- Syed, M.: TF-ThP-13, 198; TF-ThP-14, **198**
- Syeda, M.: TF-ThP-13, 198; TF-ThP-14, 198
- Sykes, E.: SS+AS+TF-MoA-3, 39; SS+HC-ThA-1, **171**; UN-ThP-24, 204
- Szanyi, J.: TH2-TuA-7, 81
- Szuczewski, G.: TF+SE-FrM-4, **219**
- T —
- Tait, S.: SS1+AS-ThM-1, **160**; SS1+AS-ThM-5, 161
- Tak, H.: PS2-ThA-5, 171; PS-TuP-13, 97; PS-TuP-4, **96**
- Takahashi, K.: TF+QS-WeA-1, 142
- Takahide, Y.: CPS+CA-WeA-3, **130**
- Takano, I.: TF-ThP-3, 196
- Takano, N.: PS1+MS-ThM-4, **158**
- Takasaki, K.: PS-TuM-1, 55
- Takeuchi, I.: SS+AS+TF-MoA-10, 41; TF-ThP-6, 196
- Takeuchi, N.: SS+2D+AS+HC-WeM-12, 121
- Takeya, J.: SS+AS+TF-MoA-5, 40
- Takeyasu, K.: HC+SS-WeM-1, **114**
- Talin, A.: SS+AS+TF-MoA-10, 41; TF-ThP-6, 196
- Tallarek, E.: BI-TuP-10, **88**
- Tamura, M.: PS+TF-MoM-6, 14
- Tanaka, K.: PS+TF-MoM-2, 14; PS2+MS-WeA-7, 139
- Tang, J.: EM+TF-ThM-6, **150**
- Tanimura, M.: TF-ThP-2, 196
- Tapily, K.: AP+EM+PS+TF-TuM-11, 48
- Tarrio, C.: SS+HC-TuA-10, 78
- Tate, J.: TF2+AP+SE+SS-WeM-13, 123
- Taubitz, T.: IB-ThM-5, 154
- Taufour, V.: MI+2D+TF-ThM-10, 157
- TAVERNIER, A.: PS-TuP-24, 99
- Tchoubar, O.: VT-TuM-13, 63
- Telford, E.: MI+2D+TF-ThM-1, 156
- Tenne, D.: UN-ThP-17, 202
- Tennent, N.: CA2+AS+LS+NS+SS+VT+MoM-10, 8
- Tennyson, J.: PS+MS-TuA-1, 74
- Tenorio, J.: NSP-SuA-8, 3
- Tepavcevic, S.: AS+2D+CA+EM+MS+NS+SE+SS+TF-FrM-4, 209
- Tercero, J.: AP+PS-MoA-5, **23**
- Tereshina-Chitrova, E.: AC+AS+MI+TH-WeA-9, **126**
- Terlier, T.: CA+AS+LS+NS+SS+VT-MoA-3, **27**
- Terry, J.: LS+AC+LX+MI+TH-ThM-13, **156**
- Terryn, H.: PS+SE-FrM-6, 218; SS+AS+TF-MoA-9, 40; SS1+HC-MoM-2, 19
- Terui, S.: VT-TuP-4, 105
- Tesch, P.: TF+QS-WeA-1, 142
- Tezsevin, I.: AP+EM+PS+TF-TuM-10, 48
- Thelen, D.: SE-TuP-5, 104
- Theodosiou, A.: AS+2D+CA+EM+MS+NS+SE+SS+TF-FrM-11, 210
- Thepass, H.: 2D-TuM-4, 44
- Thibaut, S.: PS-TuM-3, 55
- Thimsen, E.: PS1+AS-WeA-1, **136**; UN-ThP-18, 203
- Thissen, A.: CA+AS+LS+LX+MN+SE+SS-TuM-10, 52; LX+AS+HC+SS-MoM-5, **11**
- Thompson, R.: SS1+AS-ThM-6, **161**
- Thum, M.: BI2-MoA-9, 26
- Tian, J.: 2D2-ThA-2, 164
- Tiedje, T.: EM-WeM-11, **114**
- Tillocher, T.: AP+PS-MoA-3, 23
- Tippens, J.: VT-TuM-12, **63**
- Titze, M.: EM+TF-ThM-11, 150; IB3-FrM-10, **214**; IB-ThP-5, 190
- Tobin, J.: AC+MI+TH-TuM-13, **47**
- Todd, R.: VT-TuM-13, **63**; VT-TuP-6, **105**
- Todt, J.: IB-ThA-5, 168
- Tokei, Z.: PS-TuM-13, 57
- Tokumasu, T.: AP+EM+PS+TF-TuM-10, 48
- Tomura, M.: PS+TF-MoM-2, 14
- Tong, X.: SS+2D+AS+HC-TuM-11, **59**
- Torres Ochoa, J.: AS-ThP-35, 185
- Torres-Ochoa, A.: AS-ThP-36, 185
- Trask, N.: EM-WeM-5, 113
- Travis, J.: SE+TF-MoA-8, 38
- Treadwell, L.: HC+SS-ThM-13, 153
- Tremsin, A.: MI+2D+TF-WeA-3, 135
- Trenary, M.: HC+SS-FrM-1, 211; HC-ThP-4, 188; SS+AS+TF-MoA-5, 40; SS-ThP-6, 193
- Tressler, J.: PS-TuP-1, 95
- Trindade, G.: AS+CA+EL+EM+SE+SS+TF-ThM-1, 146
- Tringides, M.: NS1+2D+EM+MN-TuA-3, 72
- Trinh, N.: SE-TuP-10, 104
- Tripathi, S.: IB-ThA-3, 167
- Tripp, R.: BI+AS+EM+NS+SE+TF-TuA-1, 70
- Trolier-Mckinstry, S.: MN-ThP-3, 191
- Trützschler, A.: QS+VT-WeM-13, 119; VT-TuP-3, 105
- Tsai, Y.: PS2+MS-WeA-3, **138**; PS2+MS-WeA-7, 139
- Tsao, J.: SE-TuP-1, 103
- Tsapatsis, M.: LX+AS+HC+SS-MoM-8, 11; TF+SE-FrM-9, 220
- Tschurl, M.: HC+SS-ThM-6, 152; LX+AS+BI+HC+SS+TH-MoA-5, 31; SS+2D+AS+HC-WeM-1, 119
- Tseng, H.: AS+2D+CA+EL+EM+MS+NS+SE+SS+TF-WeM-3, 111; EW-TuL-3, 64
- Tsifakis, D.: TF+QS-WeA-1, 142
- Tsutsumi, T.: PS+TF-MoM-6, 14; PS1-ThA-1, 169
- Tubier, C.: PS+SE-FrM-6, 218
- Tuck, S.: BI1+PS-MoM-6, **6**
- Tumbleson, R.: MI+2D+TF-WeA-3, 135
- Tumusange, M.: EL1-MoM-1, 9
- Turano, M.: HC-ThP-2, 187
- Turek, I.: AC+MI+TH-TuM-11, 46
- U —
- U. Saleheen, A.: MI+2D+TF-WeA-3, 135
- Ubezio, A.: 2D-ThM-6, 145; 2D-ThP-5, 175
- Uddi, M.: AP-TuP-2, **85**
- Ueda, S.: AP2+PS+TF-TuA-9, 69
- Uehara, H.: IB-ThP-3, 190
- Uene, N.: AP+EM+PS+TF-TuM-10, **48**
- Uner, N.: PS+MS-TuA-7, 75
- Üner, N.: PS2+MS-WeA-11, 139
- Uno, T.: AP+PS-FrM-4, 208
- Upadhyay, S.: SS+2D+AS+HC-WeM-11, 121; SS+2D+AS+HC-WeM-12, **121**
- Urban, F.: EL1-MoM-5, 9; EL-TuP-11, **91**
- Urdaneta, G.: AP-TuP-2, 85
- Utsu, N.: TF-ThP-3, **196**
- Utz, A.: HC+SS-WeM-13, 116; HC-ThP-5, 188; HC-ThP-6, 188
- Uvdal, K.: BI+AS+EM+NS+SE+TF-TuA-4, 71
- V —
- Vagos, P.: EL-TuP-12, 91
- Vailionis, A.: AS+2D+CA+EL+EM+MS+NS+SE+SS+TF-WeM-5, 112
- Valadez, N.: EM-ThP-3, 186
- Valenti, A.: AP+EM+PS+TF-TuM-11, **48**; AS-ThP-14, 181
- Valery, A.: CA+AS+LS+NS+SS+VT-MoA-10, 28
- Vallat, R.: PS+NS-FrM-3, **215**
- Vallee, C.: PS+NS-FrM-6, 216
- Vallée, C.: AP+EM+PS+TF-TuM-11, 48; AP1+2D+EM+PS+TF-TuA-1, 69; PS-TuM-2, 55
- Vallejo, K.: AC+AS+MI+TH-WeA-8, **126**; QS+EM+TF-MoM-8, 16

## Author Index

- Valpreda, A.: AS+2D+CA+EM+MS+NS+SE+SS+TF-FrM-8, 209
- Valtiner, M.: AS+CA+EL+EM+SE+SS+TF-WeA-11, 129; BI2+AS+HC+SS-MoM-8, 7; BI-WeA-3, 129; NS-TuP-8, 93; SS2-MoM-10, 20
- Van de Kruijs, R.: AS+2D+CA+EM+MS+NS+SE+SS+TF-FrM-8, 209
- van der Krabben, L.: 2D-WeM-4, 106
- Van Dongen, K.: AP+EM+PS+TF-TuM-1, 47
- Van Doorslaer, S.: SS+HC-TuA-11, 79
- van Dorp, D.: 2D-WeM-4, **106**
- van Duin, A.: AP+EM+PS+TF-TuM-10, 48
- van Eijk, L.: AS-ThP-21, 182
- van Impel, H.: PS+SE-FrM-8, 218
- Van Lint, C.: PS-TuP-9, 97
- van Rijn, R.: 2D-WeM-3, 106
- van Rüschen, J.: BI2-MoA-10, 26
- van Setten, M.: AP+EM+PS+TF-TuM-12, 49
- Vanfleet, R.: AS-ThP-17, 181; EL-TuP-9, 90
- Vanleenhove, A.: AS+CA+EL+EM+SE+SS+TF-WeA-3, 127
- Vardaman, J.: CPS+MS-ThM-12, **149**
- Varga, A.: AP1+2D+EM+PS+TF-TuA-7, 69
- Vasudevan, R.: NS+2D+EM+MN+SS-TuM-12, 54
- Vawdrey, J.: TF+QS-WeA-3, 142
- Vazquez Lepe, M.: AS+CA+EL+EM+SE+SS+TF-WeA-2, 127
- Vazquez-Miranda, S.: EL1-MoM-6, 10
- Vecchietti, M.: HC-ThP-11, 189
- Veis, M.: EL-TuP-4, 89
- Vella, J.: AP+PS-MoA-6, 24; PS2+MS-WeA-4, 138
- Vemuri, V.: EM1+TF-FrM-6, 211
- Vennemann, A.: BI-TuP-10, 88
- Ventrice, C.: AP+EM+PS+TF-TuM-11, 48; AS-ThP-14, 181
- Ventzke, P.: AP+PS+TF-WeM-10, 110; TF-ThP-5, 196
- Verboncoeur, J.: PS-TuP-40, 102; PS-TuP-41, 102
- Vergés, J.: 2D-ThM-6, 145; 2D-ThP-5, 175
- Verhaar, G.: CA2+AS+LS+NS+SS+VT+MoM-10, 8
- Verheijen, M.: QS+EM+TF-MoM-9, 16
- Verkhoturov, D.: CA+AS+LS+LX+MN+SE+SS-TuM-1, **51**
- Verkhoturov, S.: CA+AS+LS+LX+MN+SE+SS-TuM-1, 51
- Verma, A.: PS+MS-TuA-12, **76**; PS+MS-TuA-3, 74; PS+MS-TuA-8, 75
- Versluis, R.: QS+VT-WeM-10, **119**
- Vidal Muller, A.: LX-TuP-1, 91
- Vienes, J.: CA2+AS+LS+NS+SS+VT+MoM-10, 8
- Viertel, K.: AS+CA+EL+EM+SE+SS+TF-ThM-5, 147
- Villafana, W.: PS2-ThA-3, **171**
- Villarrubia, J.: NS+EM+MN-MoA-5, 32
- Visart de Bocarmé, T.: CA+AS+LS+LX+MN+SE+SS-TuM-4, 51
- Vishik, I.: MI+2D+TF-ThM-10, **157**
- Vishnoi, N.: AP+PS+TF-WeM-5, 109
- Vitova, T.: LS+AC+LX+MI+TH-ThM-1, **155**; LS+AC+LX+MI+TH-ThM-12, 156; TH1+AS+SS-TuM-5, **60**; TH-TuP-1, 104
- Vlachos, D.: LX+AS+HC+SS-MoM-8, 11
- Vo, T.: EL-TuP-1, 89; EM1+TF-FrM-6, 211; QS+EM+TF-MoM-10, 17
- Völkle, J.: BI+AS+EM+NS+SE+TF-TuA-11, **72**; BI+AS+EM+NS+SE+TF-TuA-7, 71
- Vollmer, C.: LS+AC+LX+MI+TH-ThM-12, 156
- Volynets, V.: PS+NS-FrM-5, 216
- von Jeinsen, N.: BI-TuP-7, 87
- Vora, G.: BI1+PS-MoM-6, 6
- Vorng, J.: AS+2D+CA+EL+EM+MS+NS+SE+SS+TF-WeM-13, 112
- Voué, M.: TF+SE-FrM-5, 219
- **W** —
- W. Shaw, S.: MN2-WeM-12, 117
- Wagner, J.: SS-WeA-8, 141
- Wagner, M.: NS2+2D+BI+EL+SS-MoM-11, **13**
- Wahby, W.: EM-WeM-1, 113
- Wajda, C.: AP+EM+PS+TF-TuM-11, 48
- Walczak, L.: SS-ThP-10, **194**
- Walker, A.: AS+CA+EL+EM+SE+SS+TF-WeA-7, 128; CA2+AS+LS+NS+SS+VT+MoM-10, **8**
- Walker, M.: AS-ThP-21, 182
- Wallace, A.: VT-TuA-4, 83
- Waller, H.: SS1+HC-MoM-6, 20
- Waller, G.: TF2-TuA-11, 80
- Walter, A.: SS-ThP-1, **192**; SS-ThP-15, 195
- Walton, S.: AP+PS+TF-WeM-11, 110; AP-TuP-6, 86; PS+SE-FrM-2, 217; PS-WeM-1, **117**; TF+QS-WeA-9, 143
- Waluyo, I.: UN-ThP-24, 204
- Wang, B.: NS-TuP-15, **95**
- Wang, C.: CA+AS+LS+NS+SS+VT-MoA-5, **27**; HC+SS-WeM-2, 115; HC+SS-WeM-5, 115; IB2-FrM-5, 213
- Wang, F.: CA+AS+LS+NS+SS+VT-MoA-1, **27**
- Wang, H.: 2D-ThP-9, 176; AP+PS-FrM-5, **208**; EM-WeM-11, 114; SS-WeA-11, 141
- Wang, J.: PS-TuM-4, 55
- Wang, L.: MS-ThP-1, 191
- Wang, T.: AP+PS+TF-WeM-10, 110; AP-TuP-5, **86**; IB-ThA-3, 167; PS+MS-TuA-10, 75; PS2+MS-WeA-10, **139**; TF-ThP-5, 196
- Wang, X.: HC-ThP-9, **189**; PS2-ThA-4, **171**; SS-WeA-11, 141
- Wang, Y.: 2D-ThP-20, 178; EL-TuP-12, 91; EM+TF-ThM-11, 150; QS+EM-TuM-5, 57
- Wang, Z.: HC+SS-FrM-4, **212**
- Wanka, R.: BI2-MoA-8, 26
- Ward, D.: BI-TuP-7, 87
- Ware, S.: AS-ThP-21, 182
- WARSONO, A.: PS-TuP-24, 99
- Watanabe, F.: NS-TuP-1, 92
- Watanabe, K.: AP+PS+TF-WeM-4, 109
- Watkins, C.: MN1-WeM-6, 117
- Watkins, O.: AP+PS-MoA-2, **23**
- Watson, D.: AS+CA+EL+EM+SE+SS+TF-WeA-9, 128
- Watts, J.: BI1-MoA-2, **25**
- Weaver, J.: HC+SS-ThA-5, **167**
- Weaver, S.: SE+TF-MoA-9, 39
- Webb, S.: AC+AS+MI+TH-WeA-1, **125**
- Weber, N.: 2D2-ThA-6, 165; 2D-ThP-19, 178; EW-TuL-2, 64
- Weides, M.: QS+EM+TF-MoM-9, 16
- Weidner, T.: BI+AS+PS-TuM-1, 49; BI+AS+PS-TuM-12, 50; BI+AS+PS-TuM-2, **49**; BI+AS+PS-TuM-4, 50; BI+AS+PS-TuM-5, 50
- Weigand, M.: MI+2D+TF-ThM-13, 157
- Weigandt, K.: NS+EM+MN-MoA-4, 32
- Weiland, C.: AS+CA+EL+EM+SE+SS+TF-WeA-2, 127
- Weiler, M.: EM+TF-ThM-6, 150
- Weiß, A.: BI+AS+EM+NS+SE+TF-TuA-11, 72
- Weiss, A.: AC-TuP-3, 85
- Welchert, N.: TF-ThP-12, 198
- Wells, I.: QS+EM+TF-MoM-10, 17
- Wen, B.: SS+HC-TuA-7, 78
- Wen, D.: PS-TuP-40, 102; PS-TuP-41, **102**
- Wende, H.: MI+2D+TF-ThM-13, 157
- Weng, S.: 2D-ThP-20, 178
- Weng, T.: AC+MI+TH-TuM-13, 47
- Westland, Y.: VT-MoM-10, 22
- Westly, D.: NS+EM+MN-MoA-5, 32; NS+EM+MN-MoA-8, 33
- Westover, A.: AS-ThP-5, 180
- Westphal, M.: AS+CA+EL+EM+SE+SS+TF-ThM-5, 147; IB3-FrM-11, **214**; IB-ThM-11, 154
- Wheeler, J.: EM-WeM-6, 114
- Wheeler, R.: AS-ThP-14, **181**
- Wheeler, V.: AP-TuP-6, 86; EM+TF-ThM-12, 151; MN1-WeM-3, 116; SE1+TF-MoM-5, 18; TF+QS-WeA-9, **143**; TF1+PS-WeM-5, 122
- White, F.: AC+MI+TH-TuA-7, 68
- White, L.: BI+AS+EM+NS+SE+TF-TuA-3, **70**; UN-ThP-12, 202; UN-ThP-13, 202
- Whitten, A.: TH2-TuA-9, **81**
- Wickramaratne, D.: 2D-WeA-3, 124
- Wickramasinghe, R.: AS+2D+CA+EM+MS+NS+SE+SS+TF-FrM-6, 209
- Widmer, J.: TF+SE-FrM-10, **220**
- Wiegold, S.: SS-ThP-18, 195
- Wiemann, M.: BI-TuP-10, 88
- Wiemholt, S.: IB1-FrM-1, 213
- Wijerathna, A.: SS-WeA-12, **142**
- Wiley, J.: HC+SS-ThM-13, 153
- Wilhelm, F.: AC+MI+TH-TuM-1, **45**
- Williams, C.: PS+SE-FrM-5, **218**
- Willis, B.: EM+TF-ThM-5, 150; NS2+2D+EM-TuA-11, 73
- Willson, S.: QS+SS-TuA-9, **77**
- Wilson, J.: UN-ThP-17, 202
- Wilson, M.: BI2-MoA-9, 26
- Win, Z.: SS-WeA-12, 142
- Winiarska, A.: VT-TuM-2, 62
- Winkler, D.: CA1+AS+LS+NS+SS+VT-MoM-5, 8
- Winkler, G.: BI2-MoA-10, 26
- Winkler, R.: NS+2D+EM+MN+SS-TuM-5, 54
- Winter, B.: LX-TuP-2, 91
- Winter, C.: AP2+PS+TF-TuA-9, 69; TF-ThP-17, 198
- Wintz, S.: MI+2D+TF-ThM-13, 157
- Wirth, M.: HC-ThP-3, 187; IB2-FrM-6, **213**
- Wirtz, T.: IB-ThP-2, 190
- Wisman, D.: SS1+AS-ThM-5, 161
- Witsell, S.: EM-WeA-3, **132**
- Woick, J.: AS+CA+EL+EM+SE+SS+TF-WeA-2, 127
- Wolf, C.: NS+EM+MN-MoA-4, 32
- Wollack, E.: TF+QS-WeA-9, 143
- Wollmershauser, J.: AP+PS+TF-WeM-3, 109
- Wong, H.: EM-ThA-5, 166
- Wong, K.: 2D-ThP-22, 179
- Wong, S.: CA1+AS+LS+NS+SS+VT-MoM-5, 8
- Wood, B.: LX+AS+BI+HC+SS+TH-MoA-3, 30
- Woods, J.: MI+2D+TF-WeA-3, 135
- Woodward, J.: AP+PS+TF-WeM-11, **110**; AP-TuP-6, 86
- Wook Choi, J.: SE-TuP-10, 104
- Word, R.: NS2+2D+EM-TuA-10, 73
- Worsch, C.: VT-TuA-3, 83
- Wortmann, M.: AS+CA+EL+EM+SE+SS+TF-ThM-5, **147**; IB-ThM-11, 154
- Wostyn, K.: PS+TF-MoM-1, 13
- Wouters, B.: SS1+HC-MoM-2, 19
- Wray, L.: AC+MI+TH-TuM-10, 46
- Wu, S.: QS+EM-TuM-3, **57**
- Wu, W.: PS+MS-TuA-1, 74
- Wu, X.: EM-ThA-5, 166
- Wu, Y.: NS+EM+MN-MoA-2, 31
- Wüest, M.: VT-MoM-1, **21**
- Wyatt, Q.: TF-ThA-3, 173
- Wyns, K.: SS+HC-TuA-11, 79

## Author Index

— X —

Xi, Z.: LX-TuP-1, 91  
 Xiao, K.: 2D+TF-TuA-3, **66**  
 Xiao, P.: EM-WeM-1, 113  
 Xiao, Y.: AP-TuP-2, 85; NS+EM+MN-MoA-2, **31**; NS-TuP-9, **93**; SS+HC-TuA-1, 78  
 Xie, Y.: IB-ThA-1, 167  
 Xing, G.: EM+TF-ThM-1, **149**  
 Xu, C.: PS1+AS-WeA-10, **137**  
 Xu, W.: IB2-FrM-5, 213  
 Xu, X.: MI+2D+TF-WeA-2, 135  
 Xu, Y.: HC+SS-WeA-4, **133**; IB2-FrM-5, **213**  
 — Y —  
 Yadav, A.: 2D-ThP-22, 179  
 Yadav, S.: EL-TuP-6, 90  
 Yaita, T.: AC+MI+TH-TuA-3, **67**  
 Yakshin, A.:  
   AS+2D+CA+EM+MS+NS+SE+SS+TF-FrM-8, 209  
 Yakushiji, M.: PS+TF-MoM-10, 15  
 Yamashita, Y.: PS+MS-TuA-2, 74  
 Yamauchi, T.: PS-TuP-22, 99  
 Yan, J.: NS-TuP-11, 94; QS+SS-TuA-10, 77; QS+SS-TuA-3, 76  
 Yan, Y.: EL-TuP-8, 90  
 Yang, C.: VT-TuA-4, **83**  
 Yang, D.: MI+2D+TF-WeA-2, 135  
 Yang, F.: SE-TuP-1, 103; TF-ThP-21, **199**  
 Yang, J.: PS1-ThA-2, **169**  
 Yang, K.: SS+HC-TuA-1, 78  
 Yang, P.: TH1-TuA-3, 81  
 Yang, R.: BI1+PS-MoM-3, **6**; TF-ThA-4, 173; TF-ThP-4, 196  
 Yang, S.: NS+EM+MN-MoA-2, 31; SE-TuP-2, 103  
 Yang, T.: AP+PS+TF-WeM-10, **110**; TF-ThP-5, **196**  
 Yang, X.: PS1-ThA-5, 170  
 Yang, Y.: 2D-WeA-4, 124; BI+AS+EM+NS+SE+TF-TuA-1, **70**; HC+SS-ThM-5, **152**  
 Yao, F.: 2D2-ThA-1, **164**; 2D-ThP-13, 177; 2D-ThP-22, 179  
 Yao, J.: LS+AC+LX+MI+TH-ThM-12, **156**  
 Yao, M.: VT-TuP-4, 105  
 Yao, X.: AS+2D+CA+EM+MS+NS+SE+SS+TF-FrM-3, 208  
 Yao, Y.: SE-TuP-4, 103  
 Yashkus, B.: UN-ThP-29, 204  
 Yates, E.: BI2-MoA-9, 26  
 Yates, L.: CPS+CA-WeA-1, **130**  
 Yatom, S.: PS-TuP-21, 99  
 Ye, Z.: SS+HC-TuA-1, 78  
 Yee, B.: PS-TuP-11, 97  
 Yehuda-Zada, Y.: AC-TuP-3, 85  
 Yen, S.: MN-ThP-4, 191  
 Yeo, Y.: PS-TuP-5, 96  
 Yeom, J.: PS-TuP-4, 96  
 Yeom, G.: 2D-ThP-15, 177; AP+PS+TF-WeM-13, 111; PS2-ThA-5, 171; PS-TuP-12, 97; PS-

TuP-13, 97; PS-TuP-14, 98; PS-TuP-15, 98; PS-TuP-16, 98; PS-TuP-19, 99; PS-TuP-5, 96; PS-WeM-5, **118**  
 Yeom, J.: TF2-TuA-11, 80  
 Yi, F.: CA-TuP-2, 88  
 Yi, H.: MI+2D+TF-ThM-12, 157  
 Yi, S.: AP2+PS+TF-TuA-11, 70  
 Yim, S.: TF-ThM-4, 162  
 Yingling, Y.: BI+AS+PS-TuM-13, **51**  
 Yiu, P.: AS+CA+EL+EM+SE+SS+TF-ThM-13, **148**  
 Yoda, Y.: VT-TuA-1, **82**  
 Yokoi, M.: PS+TF-MoM-2, **14**; PS2+MS-WeA-7, 139  
 Yokoyama, T.: PS1+MS-ThM-1, 158; PS2+MS-WeA-3, 138  
 Yom, T.: TF-ThM-4, 162  
 Yoo, J.: UN-ThP-19, **203**  
 Yoo, S.: PS1+MS-ThM-5, 159  
 Yoon, K.: PS+TF-MoM-5, 14  
 Yoon, M.: 2D+TF-TuA-3, 66; MI+2D+TF-ThM-3, **157**  
 Yoshida, H.: VT-MoA-6, **42**  
 Yost, A.: 2D-WeM-5, 106  
 You, J.: AS+CA+EL+EM+SE+SS+TF-ThM-13, 148  
 You, S.: PS2-ThA-5, 171; PS-TuP-37, 102; PS-TuP-38, 102  
 Young, J.: AS-ThP-21, 182  
 Young, L.: LS+AC+LX+MI+TH-ThM-10, **156**  
 Young, M.: TF2-TuA-10, 80; TF-ThA-3, **173**  
 Yu, K.: AP+EM+PS+TF-TuM-11, 48  
 Yu, P.: AP+EM+PS+TF-TuM-5, 47  
 Yu, S.: AC+MI+TH-TuM-13, 47  
 Yu, X.: BI1+PS-MoM-5, 6; BI1-MoA-6, 26; CA2+AS+LS+NS+SS+VT+MoM-11, **9**  
 Yu, Y.: 2D+TF-TuA-3, 66; LX-TuP-1, **91**  
 Yuan, H.: EM-WeM-11, 114  
 Yun, S.: AP2+PS+TF-TuA-9, 69  
 — Z —  
 Zaccarine, S.: AS-ThP-19, 182  
 Zaera, F.: HC+SS-WeM-6, **115**  
 Zagorac, T.:  
   AS+2D+CA+EM+MS+NS+SE+SS+TF-FrM-4, **209**  
 Zahl, P.: NS+2D+EM+MN+SS-TuM-11, **54**; SS-WeA-11, 141  
 Zahra, K.: AS+2D+CA+EM+MS+NS+SE+SS+TF-FrM-11, 210  
 Zahradnik, M.: EL1-MoM-6, 10  
 Zajo, Z.: NS+EM+MN-MoA-3, **32**  
 Zakharov, A.: SS+HC-ThA-3, 172  
 Zakharov, D.: LX+AS+HC+SS-MoM-4, 11  
 Zakutayev, A.: EM-WeA-9, **133**  
 Zamarripa, C.: EL-TuP-6, 90  
 Zameshin, A.:  
   AS+2D+CA+EM+MS+NS+SE+SS+TF-FrM-8, 209  
 Zappone, B.: BI-WeA-3, 129  
 Zeng, H.: 2D-ThP-22, 179

Zetterberg, J.: HC+SS-WeA-9, 134  
 Zhang, C.: SS+AS+TF-MoA-5, 40  
 Zhang, D.: PS2+MS-WeA-3, 138; PS2+MS-WeA-7, **139**; PS2+MS-WeA-9, 139  
 Zhang, H.: EL1+TF-MoA-1, 28  
 Zhang, J.: IB2-FrM-5, 213  
 Zhang, K.: SS+HC-TuA-11, 79  
 Zhang, L.: TF1-TuA-4, **79**  
 Zhang, P.: NS-TuP-15, 95; PS-TuP-40, 102; PS-TuP-41, 102  
 Zhang, R.: SS-WeA-12, 142  
 Zhang, Y.: AS+2D+CA+EM+MS+NS+SE+SS+TF-FrM-4, 209; BI1+PS-MoM-5, **6**; NS+2D+EM+MN+SS-TuM-11, 54; SS-WeA-12, 142  
 Zhang, Z.: 2D-WeA-10, 125; SS+HC-TuA-3, **78**  
 Zhao, H.: HC+SS-ThA-3, 167  
 Zhao, J.: AP+PS+TF-WeM-10, 110; TF+SE-FrM-3, 219; TF-ThA-5, **173**; TF-ThP-5, 196  
 Zhao, K.: AS-ThP-1, **179**; HC+SS-FrM-5, **212**; HC+SS-WeA-3, 133  
 Zhao, Q.: AS-ThP-22, **182**  
 Zhao, X.: SS-ThP-19, **195**  
 Zhao, Y.: AS+2D+CA+EM+MS+NS+SE+SS+TF-FrM-3, 208; BI+AS+EM+NS+SE+TF-TuA-1, 70  
 Zhao, Z.: AS-ThP-2, 179; TF-ThP-20, **199**  
 Zheng, W.: LX+AS+HC+SS-MoM-8, 11  
 Zhou, C.: QS+EM+TF-MoM-10, 17  
 Zhou, H.: TF2+AP+SE+SS-WeM-13, 123  
 Zhou, J.: HC+SS-WeA-4, 133; SS-ThP-14, 194  
 Zhou, P.: SS+HC-TuA-1, 78  
 Zhou, S.: AC+AS+MI+TH-WeA-8, 126  
 Zhou, Y.: AS+2D+CA+EM+MS+NS+SE+SS+TF-FrM-3, **208**; AS+CA+EL+EM+SE+SS+TF-ThM-1, 146  
 Zhu, H.: SS+HC-TuA-3, 78  
 Zhu, J.: NS+EM+MN-MoA-3, 32  
 Zhu, Z.: BI1-MoA-6, 26; NS1+2D+BI+SS-MoM-3, 12; SS+AS+TF-MoA-11, **41**  
 Ziatdinov, M.: NS+2D+EM+MN+SS-TuM-12, 54  
 Ziamba, T.: PS-TuP-17, 98; PS-TuP-18, 98; PS-TuP-27, **100**  
 Zigmantas, D.: AS-ThP-4, 179  
 Zingsem, B.: MI+2D+TF-ThM-13, 157  
 Zirnheld, M.: SS-WeA-12, 142  
 Zollner, S.: CPS+CA-WeA-9, 131; EL1-MoM-6, 10; EL-TuP-1, 89; EL-TuP-4, 89; EL-TuP-6, **90**  
 Zope, B.: AP+PS-FrM-3, 207  
 Zorn, G.: SE+TF-MoA-9, **39**  
 Zucker, M.: VT-TuM-10, **63**  
 Zulqarnain, S.: PS-TuP-17, 98; PS-TuP-18, **98**  
 zur Loye, H.: AC+MI+TH-TuM-6, 46; AC-TuP-2, 85  
 Zveny, J.: PS-TuP-3, **96**